STRUCTURE OF THE RED DOG DISTRICT, WESTERN BROOKS RANGE, ALASKA

Jose de Vera

A Thesis submitted in the fulfilment of the requirements of the University of London for the degree of Doctor of Philosophy

Department of Geology
Royal Holloway, University of London
Egham, Surrey TW20 0EX
United Kingdom

December 2005



A mis Padres

ABSTRACT

This thesis presents a structural and stratigraphic analysis of the Red Dog district, western Brooks Range, northwestern Alaska. The aims of the research were to define the structure and stratigraphic context of the Red Dog district and, in particular, of the giant Zn-Pb-Ag and barite deposits in the region, in order to develop new tectonostratigraphic models for the area and for the mineralization. The research programme involved extensive periods of regional fieldwork combined with detailed mapping of the Red Dog open pit together with structural analysis, reconstructions and tectonostratigraphic analyses. The research presented in this thesis has resulted in a new structural interpretation and a new tectonostratigraphy for the Red Dog district, western Brooks Range of Alaska. This has lead to a new model for the tectonostratigraphic evolution of the Red Dog district, for the mineralization and also for the western Brooks Range.

The Red Dog district of the western Brooks Range consists of two major allochthonous terranes, the Arctic Alaska and the Angayucham terranes. These form part of a telescoped Devonian through Jurassic continental passive margin and oceanic crust that are now preserved in seven stacked allochthon sheets bounded by regional sub-horizontal thrust systems. These were thrust northwestwards onto the passive margin of northern Alaska in the Mid-Late Jurassic - Late Cretaceous Brookian orogeny, forming a NE-SW- to WNW-ESE-trending and WNW-vergent thin-skinned foreland fold and thrust belt. The Arctic Alaska terrane of the western Brooks Range consists of the lower six allochthons formed by the telescoping of proximal and distal sedimentary sections of the southern passive margin of the ancestral Alaskan continent. The seventh and uppermost thrust sheet consists of the Misheguk Mountain allochthon of the Angayucham terrane. This is interpreted to have formed as Middle Jurassic oceanic crust south of the ancestral passive margin and subsequently obducted northwestwards onto the telescoped passive margin during the Brookian orogeny.

The Zn-Pb-Ag and barite mineralization of the Red Dog district is confined to the Red Dog thrust plate of the Endicott Mountains allochthon of the Arctic Alaska terrane of northern Alaska. The Red Dog plate exhibits a complex stratigraphy reflecting

emplacement into a foredeep basin where olistostromal units were being formed and incorporated into the thrust plate itself. The mineralization appears to be structurally controlled by the major NW-trending Wulik Peaks transverse zone within the dominant NE-SW-trending fold and thrust belt of the western Brooks Range. Late Devonian to Late Mississippian extensional faults associated with rifting and passive margin development of the Arctic Alaska terrane controlled the contraction of the passive margin during the Brookian orogeny that formed the western Brooks Range in this region. The Sooner River arch was a WNW-ESE trending basement high that controlled the formation of the Wulik Peaks transverse zone as well as probably localizing the Zn-Pb-Ag and barite deposits of the Red Dog district. These WNW-ESE-trending basement involved faults were also later reactivated by Middle Eocene to Present Day extension. This new tectonostratigraphic model for the world-class Red Dog Zn-Pb-Ag and barite mineralization has important implications for exploration of new deposits within the Red Dog district, as well as elsewhere in the Brooks Range of northern Alaska.

CONTENTS

		PAGE No.
Title Page		i
Dedication		ii
Abstract		iii
Contents		v
List of Figures		xii
List of Tables		xxvi
List of Enclosures		xxvii
List of Appendices		xxviii
CHAPTER 1	***INTRODUCTION***	**1**
1.1	Introduction	2
1.2	Location of the Red Dog district	4
1.3	Geology of the Red Dog district	5
1.4	Aims of research	10
1.5	Research methodology	11
1.6	Thesis Outline	12
1.7	Acknowledgements	13
CHAPTER 2	***REVIEW OF THE TECTONIC EVOLUTION OF THE BROOKS RANGE, ALASKA***	**15**
2.1	Introduction	16
2.2	Plate tectonic setting and evolution	17
2.3	The Brooks Range	29
2.3.1	Physiographic elements	29

2.3.2 Geological framework 30
2.3.3 Structure of the Brooks Range 32
2.3.4 Structural units of the Brooks Range 34
2.3.5 Orogenic events 35
2.4 Arctic Alaska Terrane 44
2.4.1 Tectonic affinity of the Arctic Alaska terrane 47
2.4.2 Origin of the Arctic Alaska terrane 49
2.4.3 Stratigraphy of the Arctic Alaska terrane 51
2.4.4 Structural units of the Arctic Alaska terrane 51
2.5 Angayucham terrane 63
2.5.1 Structural units of the Angayucham terrane 65
2.5.2 Tectonic affinity of the Angayucham terrane 66
2.5.3 Origin of the Angayucham terrane 67
2.5.4 Correlation with other terranes 69
2.5.5 Mechanics of ophiolite emplacement 70
2.6 Mineral deposits of the Brooks Range 70
2.6.1 Pre-accretionary mineral deposits 70
2.6.2 Accretionary and post-accretionary deposits 73
2.7 Summary 74

CHAPTER 3 REVIEW OF THE GEOLOGY OF THE RED DOG DISTRICT **76**

3.1 Introduction 77
3.2 History of exploration and discoveries 82
3.3 Regional stratigraphy 83
3.3.1 Stratigraphic units of the Red Dog district 86
3.3.2 Igneous rocks 97
3.4 Regional structure 98
3.4.1 Structure of the Red Dog district 98
3.4.2 Wrench Creek and Sivukat Mountain Faults 100

3.4.3 Structural Models 100
3.5 Sediment-hosted Zn-Pb-Ag deposits: An overview 102
3.5.1 Definitions 102
3.5.2 Classification and Nomenclature 102
3.5.3 Examples of sediment-hosted Zn-Pb-Ag deposits 106
3.5.4 General characteristics 106
3.5.5 Tectonostratigraphic setting 109
3.5.6 Temporal distribution of sediment-hosted Zn-Pb-Ag deposits 111
3.5.7 Morphology and structure of sediment-hosted Zn-Pb-Ag deposits 115
3.5.8 Genesis of sediment-hosted Zn-Pb-Ag deposits 118
3.6 Mineralization of the Red Dog district 121
3.6.1 Deposits of the Red Dog district 121
3.6.2 Ore genesis and timing of mineralization 132
3.7 Summary 137

CHAPTER 4 THRUST TECTONICS: A REVIEW **138**

4.1 Introduction 139
4.2 Basic Geometric Elements 141
4.2.1 Thrust faults 141
4.2.2 Thrust sheets 146
4.2.3 Thrust fault-related folds 149
4.2.4 Mechanics of thrust faulting 152
4.3 Thrust Systems 155
4.3.1 Duplexes 155
4.3.2 Imbricate thrust systems 160
4.3.3 Triangle zones and mountain fronts 169
4.3.4 Basement-involved thrust systems 174
4.4 3D thrust systems 177
4.4.1 Lateral ramps, tear faults and transverse zones 177
4.5 3D thrust belt geometries 189

4.6 Thrust Sequences 194
4.6.1 In-sequence thrusting 194
4.6.2 'Out-of-sequence' thrusting 196
4.6.3 Synchronous thrusting 198
4.7 Summary 201

***CHAPTER 5 STRATIGRAPHY OF THE RED DOG DISTRICT* 202**

5.1 Introduction 203
5.2 Nomenclature and rationale of description 203
5.3 Depositional megasequences 209
5.3.1 Ellesmerian stratigraphy (Late Devonian – Late Jurassic) 209
5.3.2 Brookian Stratigraphy (Early Cretaceous) 211
5.4 Stratigraphy of the Arctic Alaska terrane 212
5.4.1 Stratigraphy of the Endicott Mountains allochthon 212
5.4.2 Stratigraphy of the Picnic Creek allochthon 245
5.4.3 Stratigraphy of the Kelly River allochthon 249
5.4.4 Stratigraphy of the Ipnavik River allochthon 259
5.4.5 Stratigraphy of the Nuka Ridge allochthon 259
5.4.6 Stratigraphy of the Copter Peak allochthon 261
5.5 Stratigraphy of the Angayucham terrane 266
5.5.1 Igneous stratigraphy of the Misheguk Mountain allochthon 266
5.5.2 Tectonic affinity of the Angayucham terrane 271
5.6 Foreland basin stratigraphy 272
5.6.1 Early syn-orogenic megasequence 272
5.6.2 Late syn-orogenic megasequence 281
5.7 Summary 284

CHAPTER 6 STRUCTURAL ANALYSIS OF THE RED DOG DISTRICT **286**

6.1 Introduction 287
6.2 Structural nomenclature and hierarchy 287
6.2.1 Structural units 287
6.3 Arctic Alaska terrane 292
6.3.1 Endicott Mountains allochthon 292
6.3.2 Picnic Creek allochthon 348
6.3.3 Kelly River allochthon 357
6.3.4 Ipnavik River and Nuka Ridge allochthons 370
6.3.5 Copter Peak allochthon 370
6.4 Angayucham terrane 373
6.4.1 Misheguk Mountain allochthon 373
6.5 Structure of the thrust front 389
6.5.1 Amphitheatre Mountain triangle zone 392
6.5.2 The Wulik Peaks transverse zone 398
6.5.3 Amaruk River emergent thrust front 408
6.5.4 Structure of the North Slope parautochthon 414
6.6 Wrench Creek and Sivukat Mountain faults 420
6.6.1 Wrench Creek fault 425
6.6.2 Sivukat Mountain fault 427
6.6.3 Other late extensional faults 433
6.7 Thrust systems and kinematic analyses 438
6.7.1 Thrust systems 438
6.7.2 Kinematic analyses 439
6.7.3 Thrust sequences 442
6.8 Summary 444

CHAPTER 7 ***STRUCTURAL ANALYSIS OF THE Zn-Pb-Ag AND BARITE DEPOSITS OF THE RED DOG DISTRICT*** **446**

7.1 Introduction 447
7.2 Deposits of the Red Dog Creek area 450
7.2.1 Qanaiyaq deposits (formerly the Hilltop deposit) 458
7.2.2 Main deposit 460
7.2.3 Aqqaluk deposit 500
7.2.4 Paalaaq deposit 503
7.3 Deposits of the Anarraaq-Wulik area 503
7.3.1 Anarraaq deposit 503
7.3.2 Aktigiruq deposit 506
7.4 Deposits of the Su-Lik area 509
7.5 Summary 511

CHAPTER 8 ***DISCUSSION*** **513**

8.1 Introduction 514
8.2 Tectonostratigraphy of the Red Dog district 514
8.2.1 Introduction 514
8.2.2 Tectonostratigraphy of the Red Dog district 520
8.3 Structural analysis of the Red Dog district 529
8.3.1 Introduction 529
8.3.2 Tectonic events in the Red Dog district, Northwestern Brooks Range 529
8.3.3 Fold and thrust belt structures in the Red Dog district 531
8.3.4 Tectonostratigraphic model for the evolution of the Red Dog district 552
8.4 Tectonic evolution of the Western Brooks Range 558
8.4.1 Transverse zones and basement structural inheritance 558

8.4.2 Inherited basement-involved faults and lateral/oblique ramps 565
8.4.3 Tertiary regional strike-slip faults systems and Tertiary extensional fault systems 566
8.5 Implications for Zn-Pb-Ag and barite mineralization of the Red Dog District 566
8.5.1 Introduction 566
8.5.2 Structural controls on Red Dog mineralization 568
8.5.3 Tectonostratigraphic model for the formation of Red Dog district mineralization 572
8.5.4 Implications for exploration in the Red Dog district and in the Western Brooks Range 573
8.6 Summary 575

CHAPTER 9 CONCLUSIONS **576**

9.1 Introduction 577
9.2 Tectonostratigraphy of the Red Dog district 577
9.3 Regional structure of the Red Dog district 580
9.4 Zn-Pb-Ag and barite mineralization of the Red Dog district 584
9.5 Suggestions for future research 585

LIST OF REFERENCES **587**

APPENDIX 1 **633**

LIST OF FIGURES

PAGE No.

CHAPTER 1 INTRODUCTION

Figure 1.1 Location of the study area 3

Figure 1.2 Digital elevation model (DEM) of Alaska 6

Figure 1.3 LANDSAT 7 TM image of northwest Alaska 7

Figure 1.4 LANDSAT 7 TM image of the Red Dog district 8

Figure 1.5 Geomorphological features of the study area 9

CHAPTER 2 REVIEW OF THE TECTONIC EVOLUTION OF THE BROOKS RANGE, ALASKA

Figure 2.1 Plate tectonic setting of Alaska 19

Figure 2.2a Tectonic evolution of Alaska (570-360 Ma) 20

Figure 2.2b Tectonic evolution of Alaska (360-220 Ma) 21

Figure 2.2c Tectonic evolution of Alaska (230-160 Ma) 22

Figure 2.2d Tectonic evolution of Alaska (160-120 Ma) 23

Figure 2.2e Tectonic evolution of Alaska (120-84 Ma) 24

Figure 2.2f Tectonic evolution of Alaska (84-66 Ma) 25

Figure 2.2g Tectonic evolution of Alaska (66-50 Ma) 26

Figure 2.2h Tectonic evolution of Alaska (50-0 Ma) 27

Figure 2.3 Terrane map of the North American Cordillera 28

Figure 2.4 Geological map of northern Alaska 31

Figure 2.5 Brooks Range regional cross sections 33

Figure 2.6 Tectonic model for the Brookian orogeny 37

Figure 2.7 Two-stage model for the Brookian orogeny 38

Figure 2.8 Plate tectonic model of northern Alaska 40

Figure 2.9	Cross sections across the central Brooks Range and North Slope foreland basin	42
Figure 2.10	Tectonic events in northern Alaska (Jurassic-Tertiary)	45
Figure 2.11	Summary tectonostratigraphy of the Brooks Range	46
Figure 2.12	Palaeogeography and structure of Arctic Alaska	48
Figure 2.13	Restorations of the Arctic Alaska terrane	50
Figure 2.14a	Structural map of the western Brooks Range	53
Figure 2.14b	Simplified allochthon map of the western Brooks Range	54
Figure 2.15	Regional cross section across the Arctic Slope parautochthon	58
Figure 2.16	Relationships between the Brooks Range and the Lisburne Hills-Herald Arch thrust belts	59
Figure 2.17	Cross section across the Angayucham terrane	64
Figure 2.18	Alternative origin of the ultramafic rocks of the western Brooks Range	68
Figure 2.19	Mineral deposits in the Brooks Range	71

CHAPTER 3 REVIEW OF THE GEOLOGY OF THE RED DOG DISTRICT

Figure 3.1	Zn-Pb-Ag and barite belt of the western Brooks Range	78
Figure 3.2	Devonian-Jurassic margin of the Arctic Alaska terrane	79
Figure 3.3a	Summary chronostratigraphy of the Red Dog district	80
Figure 3.3b	Stratigraphy of the Red Dog sequence	81
Figure 3.4	Structural hierarchy of the Red Dog district	84
Figure 3.5	Allochthon map of the Red Dog district	85
Figure 3.6	Tectonic model for the De Long Mountains	99
Figure 3.7	Model for genesis of sediment-hosted Zn-Pb-Ag deposits	103
Figure 3.8	Late Devonian-Early Mississippian tectonic setting of the Canadian Cordillera	104

Figure 3.9	Map of mineral deposits of the Canadian Cordillera	105
Figure 3.10	Cross sections through the Canadian Cordillera	110
Figure 3.11	Temporal distribution of sediment-hosted Zn-Pb-Ag deposits	112
Figure 3.12	Worldwide distribution of sediment-hosted Zn-Pb-Ag deposits	113
Figure 3.13	Modern Zn-Pb hydrothermal systems	114
Figure 3.14	Idealized section through a sediment-hosted Zn-Pb-Ag deposit	116
Figure 3.15	Geologic map of the Red Dog Creek area	122
Figure 3.16	Thrust plate map of the Main deposit	128
Figure 3.17	Cross sections through the Main deposit	129
Figure 3.18	Cross sections through the Aqqaluk and Paalaaq deposits	130
Figure 3.19	Cross sections through the Su and Lik deposits	131
Figure 3.20	Cross sections through the Anarraaq deposit	133

CHAPTER 4 THRUST TECTONICS: A REVIEW

Figure 4.1	Worldwide distribution of foreland fold and thrust belts	140
Figure 4.2	Thrust fault elements	142
Figure 4.3	Thrust fault nomenclature	143
Figure 4.4	Elliot's 'bow & arrow' rule	145
Figure 4.5	Absaroka thrust sheet, Rocky Mountains, USA	147
Figure 4.6	Thrust sheet types	148
Figure 4.7	Fault-related folds	150
Figure 4.8	Coulomb wedge model	153
Figure 4.9	Thrust systems	156
Figure 4.10	Spatial distribution of thrust systems	157
Figure 4.11	Synoptic model for duplex development	159

Figure 4.12	Duplex example, Mount Crandell	161
Figure 4.13	Examples of duplexes	162
Figure 4.14	Pine Mountain thrust	163
Figure 4.15	Antiformal stack	164
Figure 4.16	Cross section across the Appalachians, eastern USA	165
Figure 4.17	Map of the central Alberta Foothills	166
Figure 4.18	Cross section through the Canadian Rocky Mountains	167
Figure 4.19	Cross section through the Cantabrian Mountains, Spain	168
Figure 4.20	Models for the structure of mountain fronts	171
Figure 4.21	Triangle zones in the Canadian Rocky Mountains	172
Figure 4.22	Passive roof thrust	173
Figure 4.23	Basement-involved thrust systems in orogenic belts	175
Figure 4.24	Inversion structures and thrust systems	176
Figure 4.25	3D thrust geometries	178
Figure 4.26	Transfer fault	179
Figure 4.27	3D geometry of thrust systems	180
Figure 4.28	3D frontal and lateral ramps	183
Figure 4.29	Influence of transverse structures on thrust displacement	184
Figure 4.30	3D duplex model	185
Figure 4.31	Eyelid window	186
Figure 4.32	Erosion of hinterland-dipping duplex	187
Figure 4.33	Klippe and window geometries in the Crowsnest Mountain	188
Figure 4.34	Map view thrust belt geometries	190
Figure 4.35	Geometry of thrust systems	192
Figure 4.36	Thrust sequences	195

Figure 4.37 Break-back thrust sequence, Southern Pyrenees, Spain 197

Figure 4.38 Synoptic model for synchronous thrusting 199

CHAPTER 5 STRATIGRAPHY OF THE RED DOG DISTRICT

Figure 5.1 Summary geological map of the Red Dog district 204

Figure 5.2 Summary chronostratigraphy of the Red Dog district 205

Figure 5.3 Chronostratigraphy of the Arctic Alaska terrane 206

Figure 5.4 Summary stratigraphy of the Endicott Mountain allochthon 213

Figure 5.5 Stratigraphy of the Wolverine Creek plate 214

Figure 5.6 Stratigraphy of the Red Dog plate 215

Figure 5.7 Stratigraphy of the Key Creek plate 216

Figure 5.8 Sedimentary features of the Hunt Fork Shale and the Noatak Sandstone 217

Figure 5.9 Sedimentary features of the Kanayut Conglomerate 220

Figure 5.10 Sedimentary features of the Kayak Shale 223

Figure 5.11 Sedimentary features of the Kivalina unit 226

Figure 5.12 Sedimentary features of the Ikalukrok unit 228

Figure 5.13 Mineralization in the Ikalukrok unit I 231

Figure 5.14 Mineralization in the Ikalukrok unit II 233

Figure 5.15 Sedimentary features of the undivided Lisburne Group 235

Figure 5.16 Sedimentary features of the Siksikpuk Formation 239

Figure 5.17 Sedimentary features of the Otuk Formation 240

Figure 5.18 Mineralization in the Etivluk Group 243

Figure 5.19 Summary stratigraphy of the Picnic Creek allochthon 246

Figure 5.20 Sedimentary features of the Akmalik Chert 248

Figure 5.21 Summary stratigraphy of the Kelly River allochthon 250

Figure 5.22	Sedimentary features of the Baird Group	251
Figure 5.23	Sedimentary features of the Utukok Formation	253
Figure 5.24	Sedimentary features of the Kogruk Formation	255
Figure 5.25	Local unconformities in the Utukok and Kogruk formations	256
Figure 5.26	Sedimentary features of the Etivluk Group	258
Figure 5.27	Summary stratigraphy of the Ipnavik River allochthon	260
Figure 5.28	Summary stratigraphy of the Nuka Ridge allochthon	262
Figure 5.29	Summary stratigraphy of the Copter Peak allochthon	263
Figure 5.30	Copter Peak volcanic unit	264
Figure 5.31	Igneous stratigraphy of the Misheguk Mountain allochthon	267
Figure 5.32	Rock units of the Misheguk Mountain allochthon	268
Figure 5.33	Rock units of the Misheguk Mountain allochthon	269
Figure 5.34	Early Cretaceous unconformity	273
Figure 5.35	Sedimentary features of the early Okpikruak Formation	275
Figure 5.36	Sedimentary features of the Okpikruak Formation olistostrome	276
Figure 5.37	Mechanisms of transport	280
Figure 5.38	Sedimentary features of the late Okpikruak Formation	282

CHAPTER 6 STRUCTURAL ANALYSIS OF THE RED DOG DISTRICT

Figure 6.1	Structural hierarchy and units of the Red Dog district	288
Figure 6.2a	Structural map of the Red Dog district	293
Figure 6.2b	Cross section I-I’	294
Figure 6.2c	Cross section II-II’	295
Figure 6.2d	Cross section III-III’	296
Figure 6.2e	Cross section IV-IV’	297

Figure 6.2f	Cross section V-V’	298
Figure 6.3	Structural map of the Mount Raven window	300
Figure 6.4	Cross section across the Mount Raven window	301
Figure 6.5	Structural features of the Mount Raven window	304
Figure 6.6	Structure of the eastern limb of the Mount Raven antiform	305
Figure 6.7	Structure of the western limb of the Mount Raven antiform	306
Figure 6.8	Structure of the plunging termination of the Mount Raven antiform	307
Figure 6.9	Field sketches showing the Mount Raven antiform	308
Figure 6.10	Detail of fault-related folds	310
Figure 6.11	Stereographic projections of structural data from the Mount Raven antiform	312
Figure 6.12	Structural features of the Wulik River window	314
Figure 6.13	Structural features of the Wulik River window	315
Figure 6.14	Structural features of the Wulik River window	316
Figure 6.15	Stereographic projections of structural data from the Wulik River window	317
Figure 6.16	Thrust subplates of the Red Dog plate	319
Figure 6.17	Structural features of the Red Dog plate	320
Figure 6.18	Detachment folds in the Red Dog plate	323
Figure 6.19	Detail of detachment folds in the Upper Wulik River area	325
Figure 6.20	Cleavages in the Red Dog plate	326
Figure 6.21	Structural map of the Alexander Ridges	327
Figure 6.22	Cross section across the Alexander Ridges	328
Figure 6.23	Sketch of the Alexander Ridges	329
Figure 6.24	Simplified structural map and sections of the Key Creek plate in the Husky Hills	332

Figure 6.25	Panoramic view of the Husky Hills from Deadlock Mountain	333
Figure 6.26	Structural features of the Key Creek plate in the Husky Hills	334
Figure 6.27	Fault-related folds in the Husky Hills	335
Figure 6.28	Detail of plunge termination of the Husky Hills antiform	336
Figure 6.29	Stereographic projection of structural data from the Husky Hills antiform	338
Figure 6.30	Husky Hills mineralization	340
Figure 6.31	Structural map of the Key Creek plate in the Deadlock Mountain area	342
Figure 6.32	Cross section across the Key Creek plate in the Deadlock Mountain area	343
Figure 6.33	Structural features of the Key Creek plate in the Deadlock Mountain area	344
Figure 6.34	Structural relationships in the Deadlock Mountain area	345
Figure 6.35	Detail of fault-related folds in the Deadlock Mountain area	346
Figure 6.36	Stereographic projection of structural data from the Deadlock Mountain area	347
Figure 6.37	Detachment folds in the Key Creek plate	349
Figure 6.38	Structural features of the Amaruk River plate	352
Figure 6.39	Map of the Chimneys area	353
Figure 6.40	Structural relationships in the Chimneys area	354
Figure 6.41	Structural features of the Puzzle Creek plate	355
Figure 6.42	Evidence of SE-verging thrusting	356
Figure 6.43	Structural features of the Chimneys plate	360
Figure 6.44	Structural features of the Amphitheatre	362
Figure 6.45	Structural features of the Wulik Peaks plate	364
Figure 6.46	Structural map of folded thrust	365

Figure 6.47	Sketch of folded thrust	366
Figure 6.48	Structural features of the Kelly plate	368
Figure 6.49	Stereographic projections of structural data from the Kelly River allochthon	369
Figure 6.50	Structural features of the higher allochthons	371
Figure 6.51	Structural map of the Misheguk Mountain allochthon	375
Figure 6.52	Structural features of the Misheguk Mountain allochthon	376
Figure 6.53	Cross section across the Misheguk Mountain allochthon	377
Figure 6.54	Panorama of the Avan Hills	378
Figure 6.55	Sketch of the Avan Hills	379
Figure 6.56	Structural features of the Angayucham thrust in the Avan Hills	381
Figure 6.57	Detailed sketches of tectonic fabrics of the Angayucham terrane	382
Figure 6.58	Stereographic projections of the Angayucham thrust	383
Figure 6.59	Structural features of the Misheguk Mountain allochthon at Iyikrok Mountain	387
Figure 6.60	Stereographic projections from Iyikrok Mountain	388
Figure 6.61	Thrust front	390
Figure 6.62	Panoramic view triangle zone	393
Figure 6.63	Cross section across the Amphitheatre Mountain triangle zone	394
Figure 6.64	Structural features of the Amphitheatre Mountain triangle zone	396
Figure 6.65	Detail of SE-verging folds	397
Figure 6.66	Structural styles in the hangingwall of the Amphitheatre Mountain backthrust	399
Figure 6.67	Stereographic projection of structural data Amphitheatre Mountain triangle zone	400
Figure 6.68	Sketches of the Amphitheatre Mountain triangle zone	401
Figure 6.69	Wulik Peaks transverse zone	402

Figure 6.70	Structural features of the Wulik Peaks transverse zone	404
Figure 6.71a	Cross section of the Wulik Peaks transverse zone	405
Figure 6.71b	Panorama across the Wulik Peaks transverse zone	406
Figure 6.72	Stereographic projection of the Wulik Peaks transverse zone	407
Figure 6.73a	Extensional faults along the Wulik Peaks transverse zone I	409
Figure 6.73b	Extensional faults along the Wulik Peaks transverse zone II	410
Figure 6.74	Detail of extensional faults	411
Figure 6.75	Structural features of the Amaruk River emergent thrust front	412
Figure 6.76	Cross section of the Amaruk River emergent thrust front	413
Figure 6.77	Structural features of the North Slope parautochthon	415
Figure 6.78	Stereographic projections of structural data from the North Slope parautochthon	416
Figure 6.79	Landsat 5 TM image showing the Wrench Creek and Sivukat Mountain faults	421
Figure 6.80	DEM showing the Wrench Creek and Sivukat Mountain faults	422
Figure 6.81	Topographic profile across the Wrench Creek and Sivukat Mountain faults	423
Figure 6.82	Structural features of the Wrench Creek fault	426
Figure 6.83	Cross sections across the Wrench Creek fault	428
Figure 6.84	Stereographic projections of structural data from the Wrench Creek fault	429
Figure 6.85	Structural features of the Sivukat Mountain fault	431
Figure 6.86	Cross sections across the Sivukat Mountain fault	432
Figure 6.87	Evidence for strike-slip	434
Figure 6.88	Stereographic projections of structural data from the Sivukat Mountain fault	435
Figure 6.89	Outcrop-scale extensional faults	436

Figure 6.90 Stereographic projection of minor extensional faults 437

Figure 6.91 Summary tectonic transport map 440

CHAPTER 7 STRUCTURAL ANALYSIS OF THE Zn-Pb-Ag AND BARITE DEPOSITS OF THE RED DOG DISTRICT

Figure 7.1 Geological map of the central part of the Red Dog district Showing the distribution of sediment-hosted Zn-Pb-Ag and barite deposits 448

Figure 7.2 Geologic map of the Red Dog Creek area 449

Figure 7.3 South-north cross section across the Red Dog Creek area 451

Figure 7.4 Southwest-northeast cross section across the Red Dog Creek area 452

Figure 7.5 Southwest-northeast cross section across the Red Dog Creek area 453

Figure 7.6 Photomosaic of the Red Dog Creek area 454

Figure 7.7 Pre-mining view of the Red Dog Creek area and deposits 455

Figure 7.8 Rose diagram showing the orientation of the deposits of the Red Dog area 457

Figure 7.9 Qanaiyaq deposit 459

Figure 7.10 Red Dog mine pit map 461

Figure 7.11 Detailed structural map of the east pit 462

Figure 7.12 Photomosaic and structural interpretation of the east pit wall 463

Figure 7.13 Examples of thrust faults 465

Figure 7.14 Photographs showing thrust faults 466

Figure 7.15 Sketches of thrust faults I 467

Figure 7.16 Sketches of thrust faults II 468

Figure 7.17 Sketches of thrust faults III 469

Figure 7.18 Stereographic projection of thrust faults 471

Figure 7.19 Outcrop-scale duplexes 472

Figure 7.20	Detachment folds	474
Figure 7.21	Sketches showing detachment folds I	475
Figure 7.22	Sketches showing detachment folds II	476
Figure 7.23	Stereographic projections of detachment folds	477
Figure 7.24	Sketches of fault-propagation folds	478
Figure 7.25	Photographs showing cleavage fabrics	480
Figure 7.26	Photographs showing spaced cleavage fabrics in the Kivalina unit	481
Figure 7.27	Photomicrographs showing cleavage fabrics	482
Figure 7.28	Stereographic projections of cleavage fabrics	483
Figure 7.29	Photographs of late extensional faults	487
Figure 7.30	Bench sections showing late extensional faults	488
Figure 7.31	Stereographic projections of late extensional faults	489
Figure 7.32	Photographs showing the Main deposit orebody	491
Figure 7.33a	Photographs showing ore veins	492
Figure 7.33b	Photographs showing ore breccias	493
Figure 7.34	Sketch of vein and stereographic projections of vein orientation	495
Figure 7.35	West pit wall photomosaic and interpretation	497
Figure 7.36	Structural features of the Red Dog west pit wall	498
Figure 7.37	Sketch of melange fabrics in the west pit wall	499
Figure 7.38	Stereographic projections of structural data from the west pit wall	501
Figure 7.39	Cross section across the Aqqaluk deposit	502
Figure 7.40	Cross section across the Anarraaq deposit	504
Figure 7.41	Structural features of the Anarraaq deposit	505
Figure 7.42	Mineralization of the Anarraaq deposit	507
Figure 7.43	Stereographic projection of structural data from the Anarraaq area	508

Figure 7.44 Cross section across the Su – Lik deposit 510

CHAPTER 8 DISCUSSION

Figure 8.1 Summary geological map of the Red Dog district 515

Figure 8.2 Tectonostratigraphy of the Red Dog district 516

Figure 8.3 Structural hierarchy of the Red Dog district 517

Figure 8.4 Summary structural map of the Red Dog district 518

Figure 8.5 Regional cross-sections across the Red Dog district 519

Figure 8.6 Chronostratigraphy of the Arctic Alaska terrane 522

Figure 8.7a Regional seismic line across the North Slope parautochthon 525

Figure 8.7b Line diagram interpretation of A showing the key tectonostratigraphic divisions 526

Figure 8.8 Diagrams of gravitational sliding and the development of olistostromes in submarine settings 527

Figure 8.9 Igneous stratigraphy of the Angayucham terrane 528

Figure 8.10 Model for the Franciscan Complex, California 534

Figure 8.11 Models for the development of accretionary wedge systems 535

Figure 8.12 Summary tectonic transport indicators Red Dog district 538

Figure 8.13 Summary structural data Red Dog district 539

Figure 8.14 Block diagram of thrust front structures and transverse zone, Ural mountains 541

Figure 8.15 Transverse zone geometries – comparable systems I 542

Figure 8.16 Transverse zone geometries - comparable systems II 543

Figure 8.17 Foreland basin geometry and regional Bouguer anomalies 545

Figure 8.18 Hope basin map and geoseismic section, Chukchi Sea 546

Figure 8.19 Landsat TM image and aeromagnetic contours, Red Dog district 547

Figure 8.20	Map of northwestern Alaska showing pre-existing basement structures	548
Figure 8.21	Models for the tectonostratigraphic development of the Red Dog thrust plate	553
Figure 8.22	Schematic model for the tectonostratigraphic evolution of the Red Dog district	554
Figure 8.23	Synoptic diagram of the Wulik Peaks transverse structures	555
Figure 8.24	Conceptual model for the inversion of the Uinta basin transverse zone	556
Figure 8.25	Control of the detachment level by extensionally fault-controlled stratigraphy	557
Figure 8.26	Synoptic plan view model for the evolution of the Wulik Peaks transverse zone	559
Figure 8.27	Synoptic 3D block diagram of the Wulik Peaks transverse zone	560
Figure 8.28a	Landsat TM image of the northwestern Brooks Range and the Lisburne Hills fold belt	561
Figure 8.28b	Interpretation of the Landsat TM image in A	562
Figure 8.29	Seismic section and interpretation of rift structures Hanna basin, northern Chukchi Sea	563
Figure 8.30	Tertiary strike-slip fault systems and Tertiary basin systems of northern Alaska	567
Figure 8.31	Landsat TM image showing alignment of mineralization along the Sooner River Arch – Wulik Peaks transverse zone	569
Figure 8.32	Tectonic model for North American Cordilleran ore deposits	570
Figure 8.33	Comparative examples of fault controlled SEDEX deposits	571
Figure 8.34	Schematic model for the structural control on the Red Dog deposits	574

LIST OF TABLES

PAGE No.

CHAPTER 3 REVIEW OF THE GEOLOGY OF THE RED DOG DISTRICT

Table 3.1 Inventory of sediment-hosted Zn-Pb-Ag and barite deposits 107-108

CHAPTER 6 STRUCTURAL ANALYSIS OF THE RED DOG DISTRICT

Table 6.1 Features of the allochthons of the Arctic Alaska terrane 290

Table 6.2 Features of the plates of the Endicott Mountains allochthon 299

Table 6.3 Features of the windows of the Wolverine Creek plate 302

Table 6.4 Features of the subplates of the Red Dog plate 321

Table 6.5 Features of the plates of the Picnic Creek allochthon 350

Table 6.6 Features of the plates of the Kelly River allochthon 358

Table 6.7 Features of the Misheguk Mountain allochthon 374

Table 6.8 Features of the thrust front in the Red Dog district 391

Table 6.9 Features of the North Slope parautochthon 418

Table 6.10 Features of the Wrench Creek and Sivukat Mountain faults 424

LIST OF ENCLOSURES

Enclosure I Geological map of the Red Dog district

Enclosure II Regional geological cross-sections

Enclosure III Bench sections - Red Dog mine East pit

LIST OF APPENDICES

Appendix 1 Table with coordinates of station points in east pit wall of the Red Dog mine

CHAPTER 1

INTRODUCTION

1.1 INTRODUCTION

1.2 LOCATION OF THE RED DOG DISTRICT

1.3 GEOLOGY OF THE RED DOG DISTRICT

1.4 AIMS OF RESEARCH

1.5 RESEARCH METHODOLOGY

1.6 THESIS OUTLINE

1.7 ACKNOWLEDGEMENTS

CHAPTER 1 *INTRODUCTION*

1.1 INTRODUCTION

This Ph.D thesis presents a field-based structural analysis of the Red Dog district of the western Brooks Range, Alaska. Research has resulted in new tectonostratigraphic, structural and tectonic evolutionary models for the district and the western Brooks Range foreland fold and thrust belt.

The Red Dog district (Fig. 1.1) forms part of a belt of high-grade sediment-hosted Zn-Pb-Ag and barite deposits that extends along strike for more than 200 km in the western Brooks Range of Alaska (e.g. Kelley *et al*. 1997; Kelley & Jennings, 2004; Young, 2004). The district contains one of the world's largest zinc reserves and resources (e.g. Jennings & King, 2002; King *et al.* 2002; Kelley & Jennings, 2004), the world's largest single zinc deposit (King *et al*. 2002), the world's largest zinc concentrate mine producer (King *et al.* 2002; Teck Cominco Ltd. 2005), and is a reference for the exploration of sediment-hosted Zn-Pb deposits (Koehler & Tikkanen, 1991; Jennings *et al*. 1998; Jennings & King, 2002; King *et al*. 2002; Kelley & Jennings, 2004; Young, 2004).

The Red Dog district (Fig. 1.1) remained virtually unexplored until the late 1960's, when early reconnaissance studies (e.g. Tailleur, 1970) showed the high potential for base metal exploration in the area. Despite having been studied and intensely explored over the last four decades (e.g. Martin, 1970; Tailleur, 1970; Plahuta, 1978; Lange *et al*. 1985; Moore *et al.* 1986; Mayfield *et al*. 1988; Ellersieck *et al.* 1990; Young, 1992; Jennings *et al*. 1998; Jennings & King, 2002; King *et al*. 2002; Young, 2004), the geology of the district, and particularly its complex structure, is still very poorly understood. (e.g. Martin, 1970; Moore *et al*. 1986; Mayfield *et al*. 1988; Ellersieck *et al*. 1990; Young, 1992). This thesis (and De Vera *et al*. 2004) is the first detailed structural study of the Red Dog district.

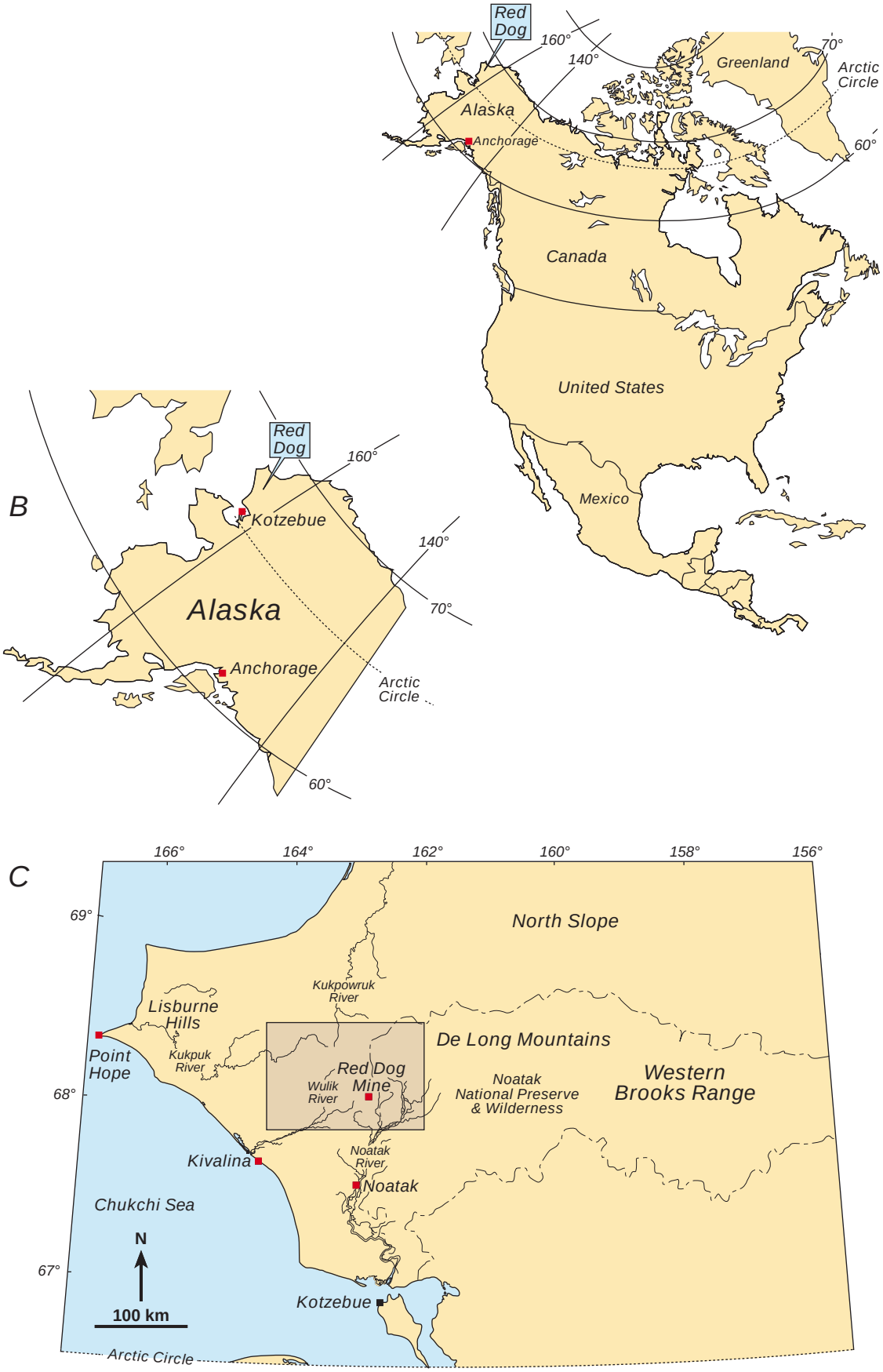


Figure 1.1. Location of the study area. **A.** Map of North America showing the location of the Red Dog district. **B.** Map of Alaska showing the location of the Red Dog district. **C.** Map of northwest Alaska showing the location of the Red Dog mine and outline of the study area.

1.2 LOCATION OF THE RED DOG DISTRICT

The Red Dog district is located approximately 1000 km northwest of Anchorage and 135 km north of Kotzebue, in the De Long Mountains of the western Brooks Range, in northwest Alaska (Figs. 1.1 – 1.3). The district lies entirely north of the Arctic Circle, extending approximately from latitude 67° 45' to 68° 30' N and from longitude 162° 10' to 164° 25' W (Figs. 1.1c & 1.4). The Red Dog district is located in one of the most remote parts of the North American continent (Fig. 1.1a & 1.2). The area is accessible by air and also by sea during a limited season in the summer, which spans approximately three months depending on the annual sea ice conditions.

The Red Dog mine (Figs. 1.1c, 1.3, 1.4 & 1.5a), located approximately at latitude 68° 04' 29" N longitude 162° 51' 19" W and 268 m above sea level, is the only year-round human habitation in the district. The nearest settlements are the Inupiat Eskimo villages of Noatak, approximately 70 km to the south on the Noatak River and Kivalina approximately 90 km to the southwest down the Wulik River on the Chukchi Sea coast (Figs. 1.1c & 1.3). The Red Dog mine is an open pit zinc-lead mine operation (Fig. 1.5a) owned by Teck Cominco Ltd and run by Teck Cominco Alaska Inc. The Red Dog mine is the world's largest producer of zinc, with an annual production capacity that exceeds $5x10^5$ tons of zinc concentrate (Teck Cominco Ltd. 2005).

The Red Dog district contains a range of geomorphologic terrains, which vary from extensive swampy tundra lowlands with broad braided river plains to treeless barren terrain with long rolling hills and rugged peaks (Fig. 1.5a – d). The average elevation is approximately 300 m, although higher ground locally attains elevations that exceed 1000 m above sea level. Mount Raven (Fig. 1.5d) is the highest point in the district with an elevation of 1190 m above sea level. The area is approximately 50% exposed, 80% of which consists of rubble outcrops (Fig. 1.5e) and only 20% of actual *in situ* intact outcrop. Lowland areas are poorly exposed because of an extensive tundra cover (Fig. 1.5a, e), whereas highland areas show the effects of mass wasting related to the continuous permafrost and the widespread occurrence of glacial, alluvial, and other Quaternary deposits, as well as the seasonal snow cover.

The climate of the area is that typical of Arctic to sub-Arctic conditions with annual temperatures that typically range from –45°C in the winter to 15°C in the summer. Annual precipitation is in the order of 50 to 80 cm a year. The area is normally snow and ice-free during July and August and is exposed to 24-hour daylight for most of June and July. Local fauna is rich and includes grizzly bear, wolverine, arctic wolf, fox, musk ox, caribou, moose, and mountain sheep. Sparse vegetation includes muskeg and tussock tundra, willows, mosses, and lichen.

1.3 GEOLOGY OF THE RED DOG DISTRICT

The Red Dog district is located in the external part of the Brooks Range orogenic belt (Fig. 1.3). It contains a number of strata-bound sediment-hosted Zn-Pb-Ag and barite deposits, including the Qanaiyaq, Main, Aqqaluk, Paalaaq, Anarraaq, Su, Lik deposits and the more recently discovered Aktigiruq deposit (e.g. Moore *et al*. 1986; Jennings *et al*. 1998; King *et al.* 2002; Young, 2004). The stratigraphy of the area consists of Late Devonian to Early Cretaceous sedimentary and igneous rocks (e.g. Moore *et al*. 1986; Mayfield *et al*. 1988; Young, 1992; Dumoulin *et al*. 2004; Young, 2004). The sediment-hosted Zn-Pb-Ag mineralization occurs in Mississippian to Pennsylvanian deep marine siliciclastic and carbonate strata of the Kuna Formation (Moore *et al.* 1986; Young, 1989; King *et al.* 2002; Kelley *et al*. 2004*a, b*; Young, 2004) and is interpreted to have formed in a third order basin of the ancient continental margin setting of Alaska (e.g. King *et al*. 2002; Young, 2004). The continental passive margin was subsequently deformed and incorporated into far-travelled allochthonous thrust sheets during the Cretaceous Brookian orogeny (e.g. Moore *et al*. 1986; Mayfield *et al*. 1988; Young, 2004). The mineralization is now preserved in complexly thrust faulted and folded thrust sheets of the Brooks Range allochthon (e.g. Moore *et al.* 1986; Jennings *et al*. 1998; King *et al*. 2002).

This thesis investigates the structure and tectonic evolution of the Red Dog district and its sediment-hosted Zn-Pb-Ag and barite deposits. Particular focus is placed upon the controls that pre-existing basin structures of the continental margin exerted on the development of thrust systems during the Brookian orogeny. The implications for the tectonic evolution of this part of the Brooks Range and for the genesis as well as subsequent deformation of the Zn-Pb-As and barite deposits are analyzed and discussed.

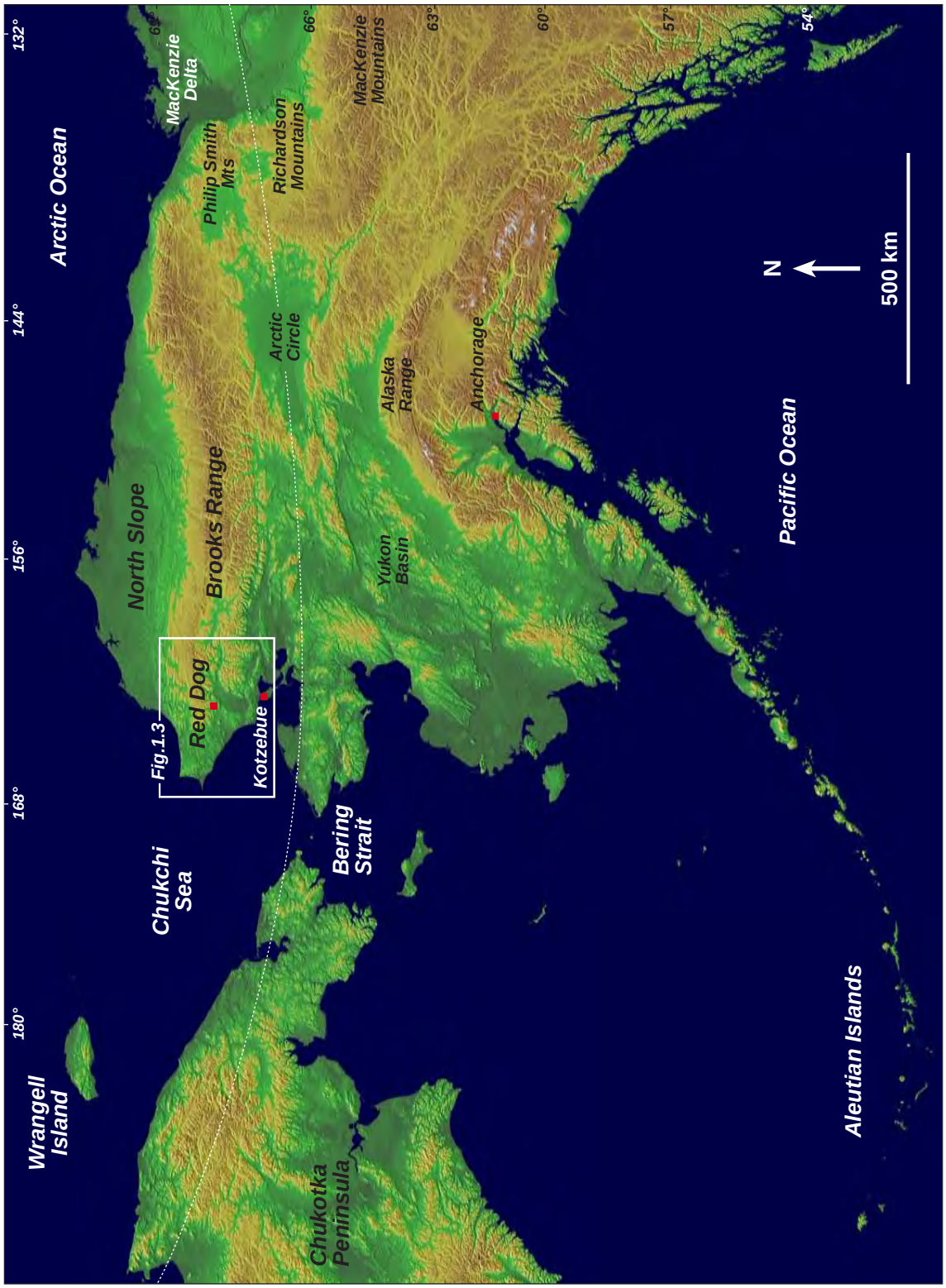


Figure 1.2. Digital elevation model (DEM) of Alaska and easternmost Russia showing the location of the Red Dog mine and the study area. (DEM imagery from National Geophysical Data Centre, 2005).

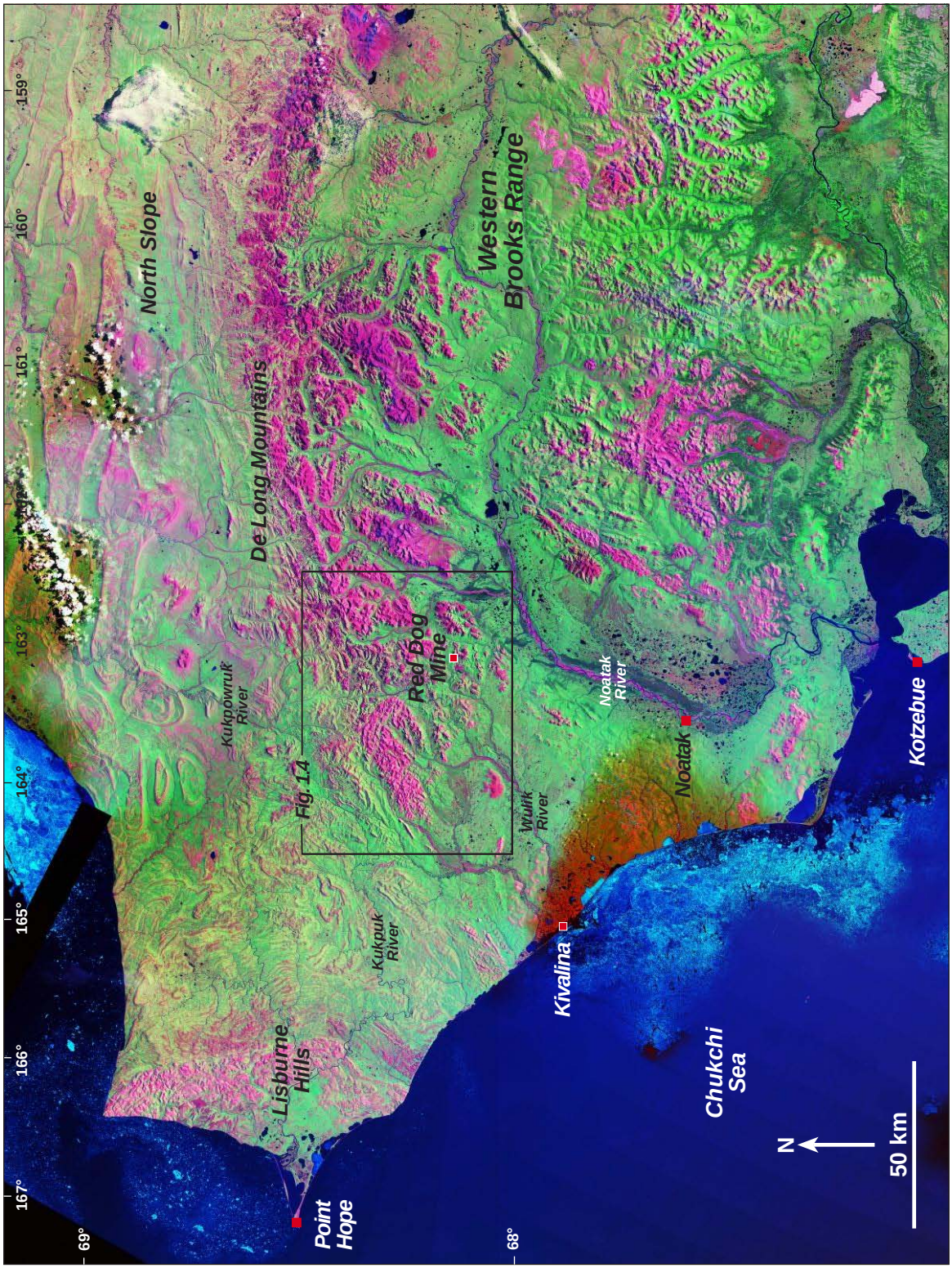


Figure 1.3. Landsat 7 TM mosaic (spectral bands 7, 4, 2) of the western Brooks Range showing the location of Red Dog mine and outline of the study area (imagery from National Aeronautics and Space Administration, 2005).

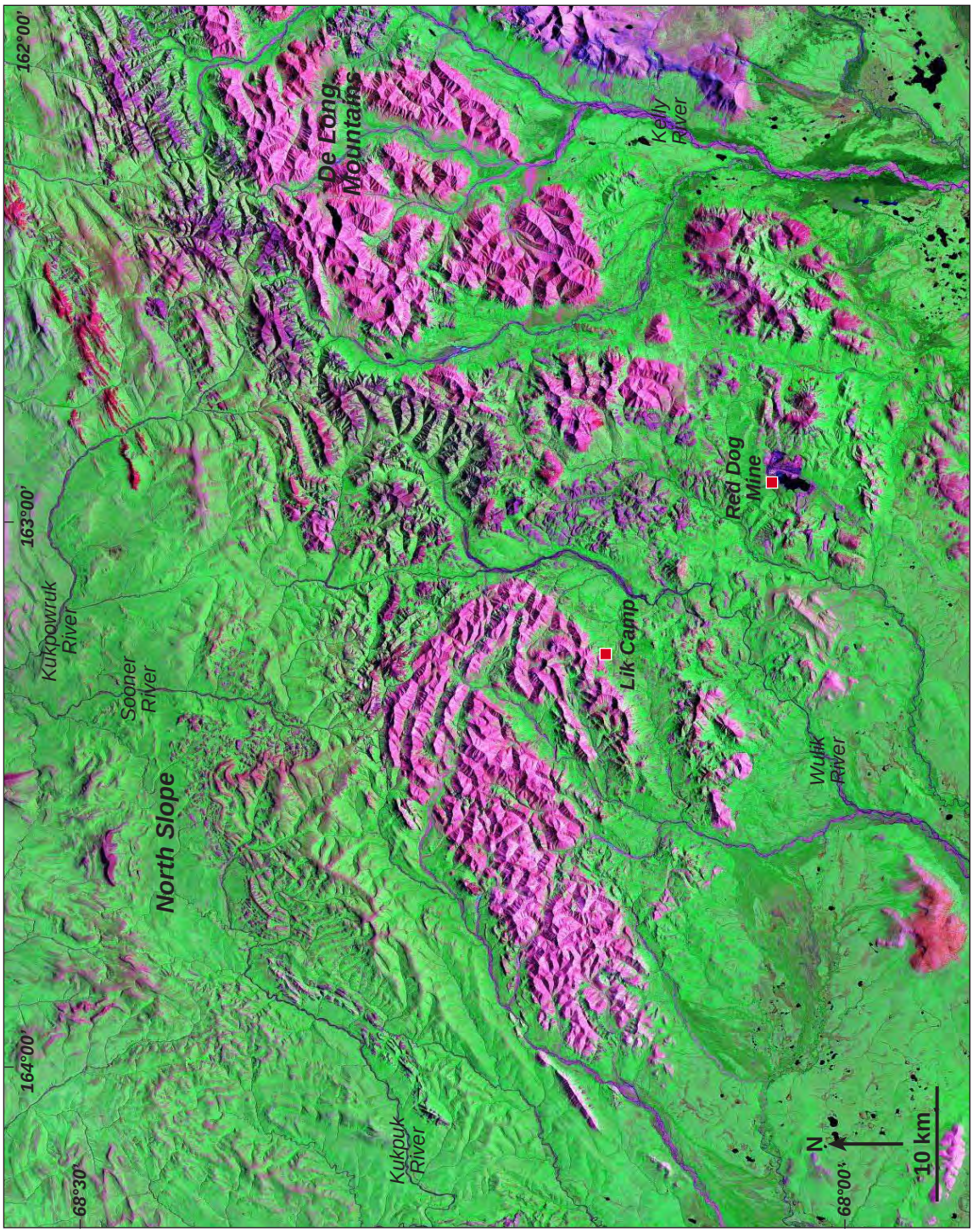


Figure 1.4. Landsat 7 TM image (spectral bands 7,4,2) of the Red Dog district showing the location of the Red Dog mine and Lik Camp (imagery from National Aeronautics and Space Administration, 2005).



Figure 1.5. Geomorphical features of the study area. **A.** WNW-looking view of the Red Dog mine and plant. **B**. NW-looking oblique aerial view of Lik Camp. **C.** Barren terrain in the Upper Wulik River area. **D.** W-looking oblique aerial view of rugged relief in the Mount Raven area. **E.** Extensive tundra cover. Wulik River area. Exploration drill rig is encircled for scale. **F.** The author examines a rubble outcrop in the North Basin area.

Understanding the structure and tectonostratigraphic evolution of the district is essential for current sediment-hosted Zn-Pb exploration and exploitation efforts in the area. The structural models derived from this study may be applicable for the exploration of sediment-hosted Zn-Pb-Ag elsewhere in the Brooks Range and in fold and thrust belts in other orogenic belts.

1.4 AIMS OF RESEARCH

The main aims of this Ph.D research are:

- To determine the structure of the Red Dog district of the western Brooks Range, Alaska.
- To determine the structural and tectonostratigraphic evolution of the Red Dog district.
- To determine the structure of the sediment-hosted Zn-Pb-Ag and barite deposits of the Red Dog district.
- To determine the structure and tectonic transport directions within the Red Dog district and the frontal thrust systems of the western Brooks Range foreland fold thrust belt in the region.
- To construct cross sections across the Red Dog district and the Zn-Pb-Ag and barite deposits of the district.
- To develop a comprehensive model for the structural development of the Red Dog district and for the deformation of the Zn-Pb-Ag and barite deposits.
- To identify new prospective areas for further exploration in the Red Dog district.

1.5 RESEARCH METHODOLOGY

The Ph.D research programme involved 16 months of intensive field studies in the Red Dog district and the Noatak National Preserve and Wilderness of the western Brooks Range (Figs. 1.1c, 1.3 & 1.4). Field work was carried out during the summer seasons of 2000, 2001, 2002, 2003 and 2004, and covered an area of approximately 10,000 km^2.

Field studies were based at the Red Dog mine (Figs. 1.1c, 1.2, 1.3, 1.4 & 1.5a) for seasons 2000 to 2004 and also partly based at Lik Camp (latitude 68° 10' 16"N, longitude 163° 11' 27"W) (Figs. 1.4 & 1.5a) during the summer of 2002. Field work was accomplished on foot and was also supported by helicopter, adopting a system that entailed daily 'drop-offs' and 'pick-ups' as well as reconnaissance flights over the study area.

Field studies involved mapping and collection of structural and stratigraphic data at a range of scales, from detailed (1:200 scale) structural mapping in the open pit of the Red Dog mine (Fig. 1.5a) and regional-scale (1:10.000, 1:50.000 & 1:100.000 scales) geological mapping and structural analysis of the western Brooks Range foreland fold and thrust belt. Additional studies involved collection of stratigraphic and structural data from 20 exploration drill holes and detailed logging of over 3000 m of NQ-size exploration diamond drill core. 700 samples were collected and studied under the microscope for petrographic and microstructural analyses. Field data collected by the author were supplemented with existing U. S. Geological Survey reconnaissance maps and unpublished Teck Cominco American Inc. Exploration geological maps, reports, and exploration drill hole data. Conventional aerial photographs, an orthorectified photomosaic (AEROMAP US), and remote sensing images (LANDSAT TM, LANDSAT ETM & MARS SLAR) were used during field mapping and also aided regional-scale structural analyses and map compilation.

1.6 THESIS OUTLINE

This Ph.D thesis consists of nine chapters, which are contained in five main sections:

- Chapter 1 introduces the context of the research and the location of the study area, the research aims, and the overall methodologies used.

- Chapters 2, 3 and 4, provide background information through comprehensive and critical reviews of the tectonic setting and evolution of the Brooks Range, the regional geology of the Red Dog district, sediment-hosted Zn-Pb deposits, and thrust tectonics.

- Chapters 5, 6, and 7 form the bulk of the thesis and document the stratigraphy and structure of the Red Dog district. Chapter 5 introduces the stratigraphy of the study area and sets a new tectonostratigraphic framework. Chapter 6 describes and analyses the regional structure of the Red Dog district. Chapter 7 focuses on the structure of the sediment-hosted Zn-Pb-Ag and barite deposits of the Red Dog district.

- The results of work presented in Chapters 5, 6, and 7 are summarized and discussed in relation to existing work in Chapter 8. This chapter proposes a new structural model for the tectonic evolution of the Red Dog district and addresses the implications of the results derived from this study for the regional tectonics of the western Brooks Range and exploration in the Red Dog district.

- Chapter 9 lists the conclusions of the research study and outlines avenues for further research.

1.7 ACKNOWLEDGEMENTS

First of all, I would like to thank my supervisor Professor Ken McClay for offering me the unique opportunity to carry out this Ph.D project and for his encouragement and patience in the last stages of completing this research programme.

Teck Cominco American Inc. (formerly Cominco American Inc.), George Cole, and John Thompson are gratefully acknowledged for funding throughout the research programme. Teck Cominco Alaska Inc. and the Northwest Alaska Native Association (NANA) are thanked for providing access to the Red Dog mine site and district.

Very many special thanks to Adrian King, Lorne Young, and all the people involved in exploration at Red Dog over the years, including Brigitte Dejou, Jeff Clark, Scott Jennings, John Robinson, Kathy Tureck, Kent Turner, Lou O'Connor, Gerry Booth, Michelle Pearson, Boris Lum, and Dan Delauder. I would also like to thank the Red Dog mine geologists Bob Robinson, Tom Krolak, Gary Coulter (now in the environmental department), and Marie Paré.

John Martinisko, Mark Thompson, Sam Hill, Jim Kulas, and the environmental group at Red Dog are gratefully thanked for all their help and invaluable helicopter support during the 2002 and 2003 field seasons. Chad Baker, Steve Lozano, Bob Shields and the surface operations crews are thanked for providing access and facilitating and making safe my work in the mine pit.

Brian Marten and Graeme Broadbent (Rio Tinto Exploration) and Russ Franklin (Kennecott Exploration) are gratefully acknowledged for helpful discussions, and very generous logistic support and helicopter time during the 2002 field season.

U. S. Geological Survey geologists Karen Kelley, Julie Dumoulin, John Slack, Chris Potter, Tom Moore, Bob Burruss, and Craig Johnson are thanked for support, helicopter time and providing access to the Noatak National Preserve and Wilderness during the 2003 and 2004 field seasons.

Gill Mull (formerly at Alaska Division of Geological and Geophysical Surveys), Paul O'Sullivan (formerly at Syracuse University) and Travis Hudson (Applied Geology) are thanked for insightful comments and discussions.

Thanks to all the helicopter pilots for their invaluable help, specially Walter Greaves (deceased), Bill Zeimann, Ken Wheeler, Doc, Jason, and Bob Mendenhall.

Special thanks to Covadonga Brime, Fernando Alvarez, Josep Poblet, Mayte Bulnes (Departamento de Geología, Universidad de Oviedo) and Martin Feely (Department of Geology, National University of Ireland, Galway) who together with Ken made all this possible.

The Society of Economic Geologists Foundation is gratefully acknowledged for awarding me with a Hickok-Radford Memorial Fund Award to support fieldwork at Red Dog in 2002. The Geology Department at Royal Holloway, University of London is also acknowledged for awarding me with the prize to the best paper written by a research student at the Geology Department in 2003.

Very many thanks to all my friends, colleagues at Royal Holloway and the Fault Dynamics Research Group, including Tim Dooley, April Harper, Paul Whitehouse, Alejandro Amilibia, Gianluca Grando, Frank Lehane, Badar Al-Barwani, Jorge Ginés, Juan Fernandez, Mario Vazquez, Mario Del Castello, Oscar Fernández, Rubén Domínguez, Katerina Vasileiadou, Ahmet Yildiz, Pablo Granado, Alice Ghiselli and everyone who in a way or another helped me through all these years.

Special thanks to Dr. Moral and all the neurology personnel at Hospital Valle del Nalón for all their help.

Finally, I would like to thank my parents and my sisters for their endless encouragement and support through the years.

CHAPTER 2

REVIEW OF THE TECTONIC EVOLUTION OF THE BROOKS RANGE, ALASKA

2.1 INTRODUCTION

2.2 PLATE TECTONIC SETTING AND EVOLUTION

2.3 THE BROOKS RANGE

2.4 ARCTIC ALASKA TERRANE

2.5 ANGAYUCHAM TERRANE

2.6 MINERAL DEPOSITS OF THE BROOKS RANGE

2.7 SUMMARY

CHAPTER 2 REVIEW OF THE TECTONIC EVOLUTION OF THE BROOKS RANGE, ALASKA

2.1 INTRODUCTION

This chapter presents a review of the tectonic setting and evolution of the Brooks Range and provides background information for the structural analysis conducted in this research programme. The aim of this chapter is to summarize the current understanding of the structure and evolution of the Brooks Range and to outline problems that currently subject of controversy.

The Brooks Range, the northernmost orogenic belt of Alaska (Figs. 1.2, 1.3 & 2.1), is key to the understanding of the tectonic evolution of Alaska and the surrounding Arctic landmasses (e.g. Grantz *et al*. 1991; Moore *et al*. 1994; Plafker & Berg, 1994; Young, 2004). It records a complex tectonic history of Late Devonian to Jurassic rifting and sedimentation on the ancient S-facing continental passive margin of Arctic Alaska (Tailleur & Brosgé, 1970; Mull, 1982; Moore *et al*. 1994; Young, 2004) followed by ophiolite obduction and arc-continent collision that resulted in the development of the Brooks Range orogenic belt in Cretaceous to Tertiary time (e.g. Tailleur & Brosgé, 1970; Roeder & Mull, 1978; Mull, 1982; Mayfield *et al*. 1988; Grantz *et al*. 1991; Moore *et al*. 1994; Young, 2004). The structure of the Brooks Range is characterized by far-travelled and regionally folded allochthonous thrust sheets (e.g. Tailleur & Brosgé, 1970; Mull, 1982; Mayfield *et al*. 1988; Moore *et al*. 1994; Young, 2004).

Prior to the development of the Brooks Range orogenic belt, the ancient rifted continental margin of Arctic Alaska was the site of development of a large number of Devonian and Carboniferous mineral deposits, including the Late Mississippian sediment-hosted Zn-Pb-Ag and barite deposits of the Red Dog district and Drenchwater Creek (e.g. Lange *et al*. 1981, 1985; Moore *et al*. 1986; Young, 1989; Schmidt, 1997*a*; Jennings *et al*. 1998; Jennings & King, 2002; King *et al*. 2002; Kelley & Jennings, 2004; Kelley *et al*. 2004*a, b*) as well as the Devonian to Carboniferous volcanogenic and carbonate-hosted Zn-Cu deposits of the Ambler district (e.g. Einaudi & Hitzman, 1986; Folger & Schmidt, 1986; Hitzman, 1986; Hitzman *et al*. 1986; Nokleberg *et al*. 1994; Schmidt, 1997*b*; Nokleberg *et al*. 2003).

2.2 PLATE TECTONIC SETTING AND EVOLUTION

Alaska spans the North American Plate from the continental passive margin of the Canada basin in the north to the tectonically active southern boundary with the subducting Pacific Plate in the south (Grantz *et al*. 1991; Moore *et al*. 1994; Plafker & Berg, 1994; Young, 2004) (Fig. 2.1). Alaska records a remarkable Proterozoic to Present Day tectonic history of extension, terrane accretion, subduction and related magmatism, strike-slip faulting, and oroclinal bending (e.g. Grantz *et al*. 1991; Plafker & Berg, 1994; Young, 2004).

The geologic history of Alaska is the result of the Palaeozoic to Present Day progressive southward growth of continental crust by accretion and imbrication of the continental passive margin together with oceanic sediments, magmatic arcs and ophiolites of southern and central Alaska against the more rigid lithospheric block of Arctic Alaska (e.g. Moore *et al.* 1994; Plafker & Berg, 1994; Klemperer *et al.* 2002; Young, 2004) (Fig. 2.2). Most of Alaska consists of terranes (Fig. 2.3) of dominantly island arc and oceanic affinities that have been accreted to, displaced from and/or rotated to varying degrees relative to autochthonous parts of the continental margin (Moore *et al*. 1994; Plafker & Berg, 1994; Silbering *et al*. 1994) (Fig. 2.3). These terranes are correlative to the collage of terranes described for the contiguous North American Cordillera (e.g. Coney *et al*. 1980; Jones *et al*. 1981; Jones, 1983; Silbering & Jones, 1984; Coney & Jones, 1985; Howell *et al*. 1985; Jones *et al*. 1987; Coney, 1989; Plafker & Berg, 1994; Silbering *et al*. 1994; Nokleberg *et al.* 1997; Price & Monger, 2003) (Fig. 2.3).

Terrane accretion in Alaska is believed to continue into the Present Day with the collision of the Yakutat terrane along the southern margin of Alaska (Grantz *et al*. 1991; Plafker & Berg, 1994; Plafker *et al*. 1994; Glen, 2004) (Figs. 2.1, 2.2e & 2.3). Terranes in Alaska are offset by a series of Cenozoic to Present Day dextral strike-slip fault systems that include the Denali, Tintina, Kaltag, and Kobuk faults (e.g. Grantz, 1966; Jones *et al*. 1987; Oldow *et al*. 1989; Gabrielse & Yorath, 1991; Grantz *et al*. 1991; Moore *et al*. 1994; Plafker & Berg, 1994; Avé Lallemant *et al*. 1998) (Figs. 2.1, 2.2h, 2.4 & 2.5). These strike-slip faults have a plan-view arcuate geometry (Figs. 2.1 & 2.2h) and are believed to have cumulative dextral strike-slip displacements of hundreds

of kilometres (Gabrielse & Yorath, 1991; Plafker & Berg, 1994). The Present Day plan-view arcuate geometry of terranes and strike-slip faults in Alaska (Figs. 1.2, 2.1 & 2.2h) is generally ascribed to oroclinal bending that resulted from Cenozoic collision of North America against a Eurasian backstop (Plafker & Berg, 1994; Glen, 2004; Young, 2004) (Fig. 2.2f – h) although alternative models that do not require oroclinal bending for the curved distribution of geologic belts in Alaska have been also proposed (e.g. Young *et al*. 1997). The Brooks Range orogen lies in northern Alaska, north of all these accreted terranes and strike-slip faults and records one of the earliest events of terrane accretion along the ancient continental margin of Alaska.

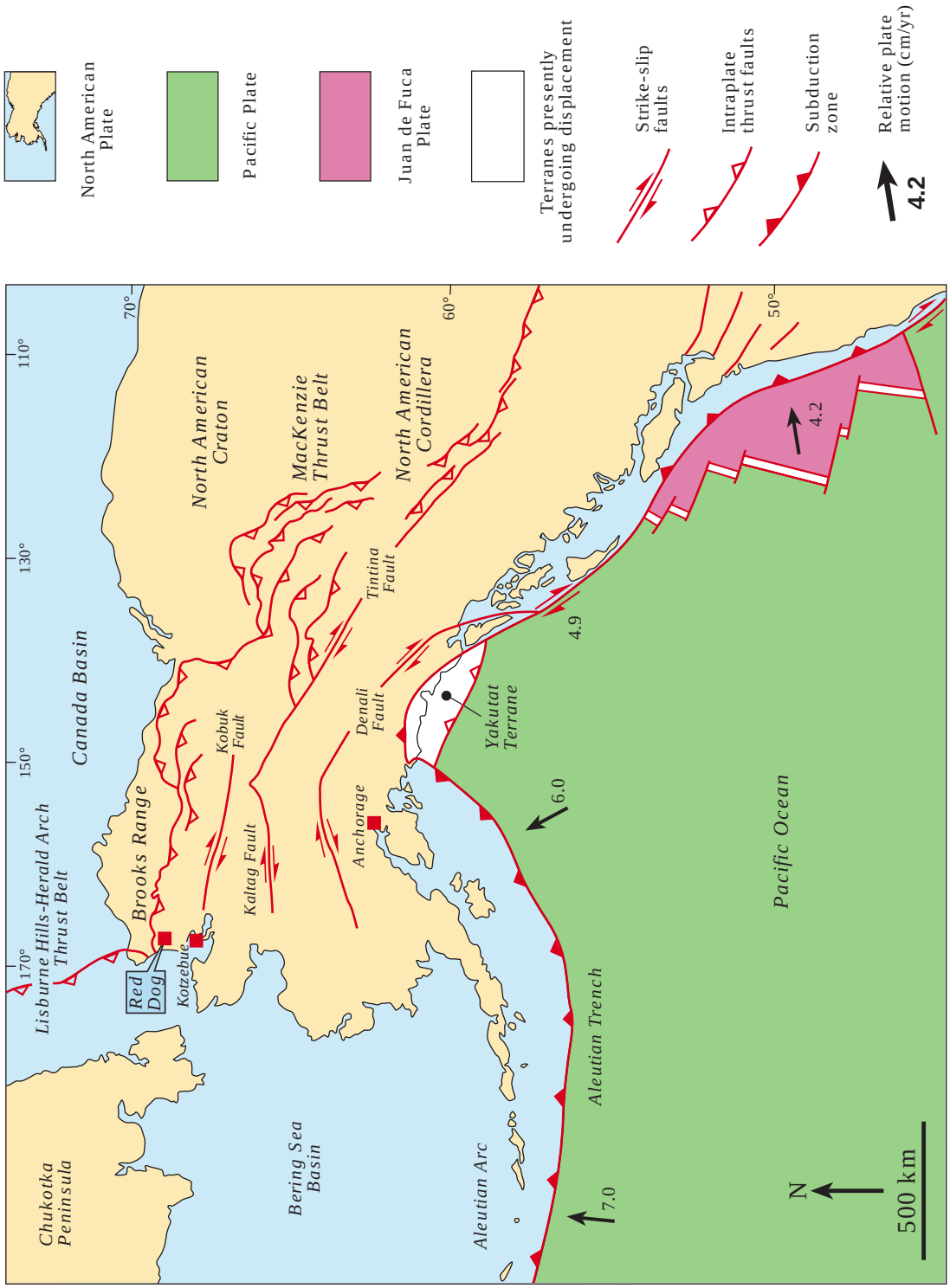


Figure 2.1. Plate tectonic setting of Alaska (modified from Moore *et al.* 1994; Plafker & Berg, 1994). The location of the Red Dog district is shown.

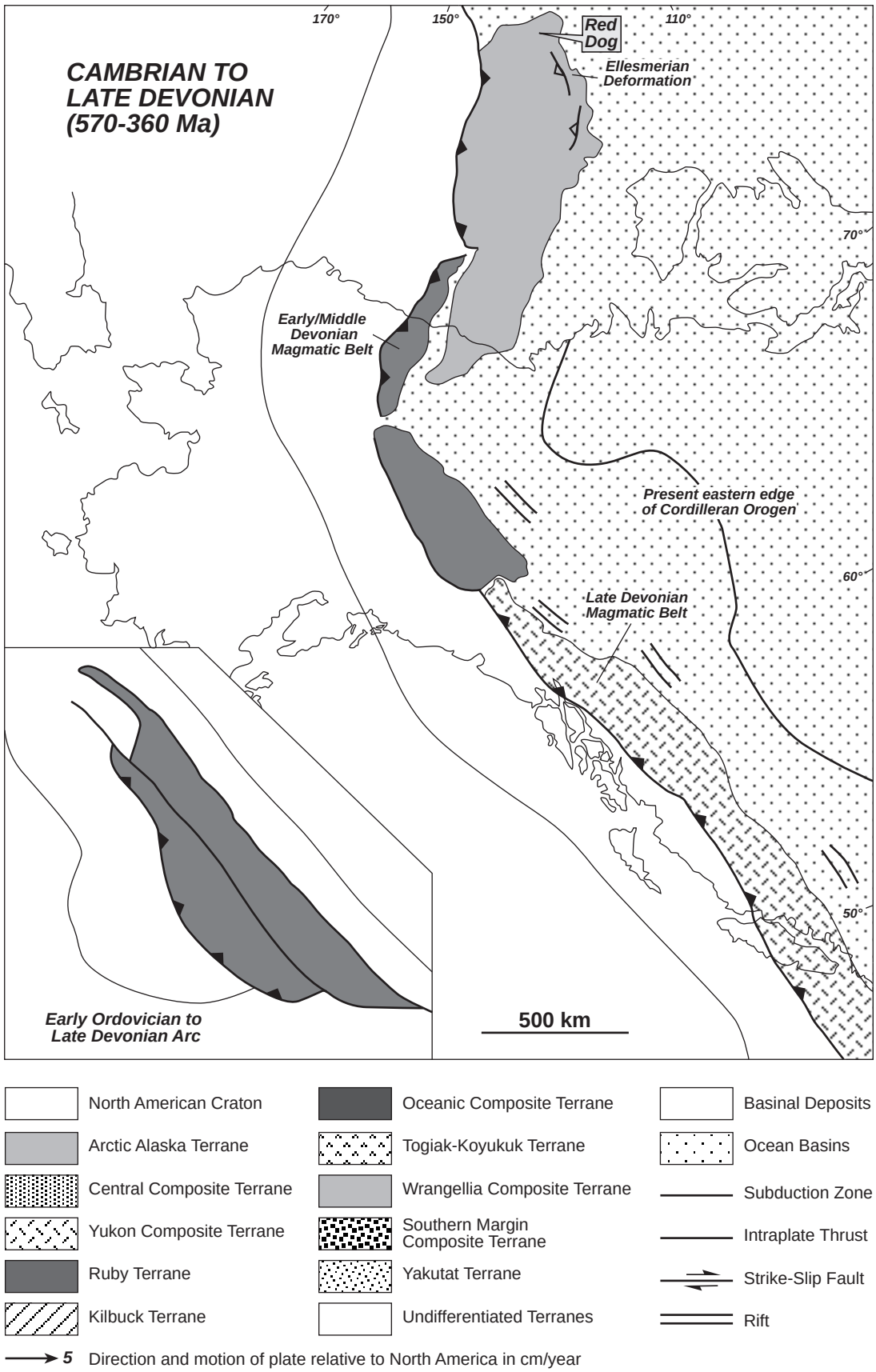


Figure 2.2a. Cambrian to Late Devonian inferred configuration of terranes in Alaska. Orientations of geological and geographic features are referred to Present Day geographic coordinates (modified from Plafker & Berg, 1994).

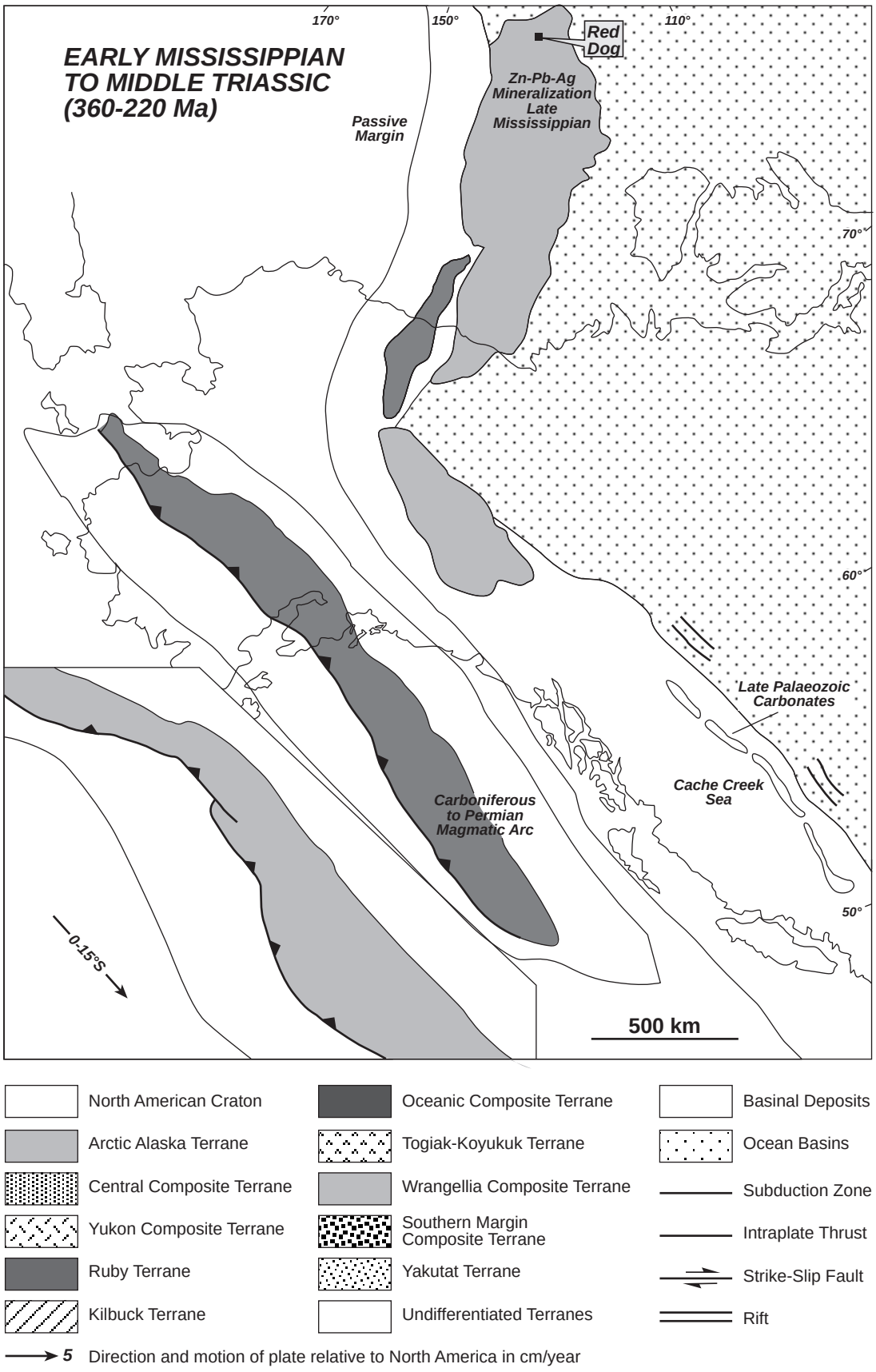


Figure 2.2b. Early Mississippian to Middle Triassic. Passive margin sedimentation on the Arctic Alaska terrane (modified from Plafker & Berg, 1994).

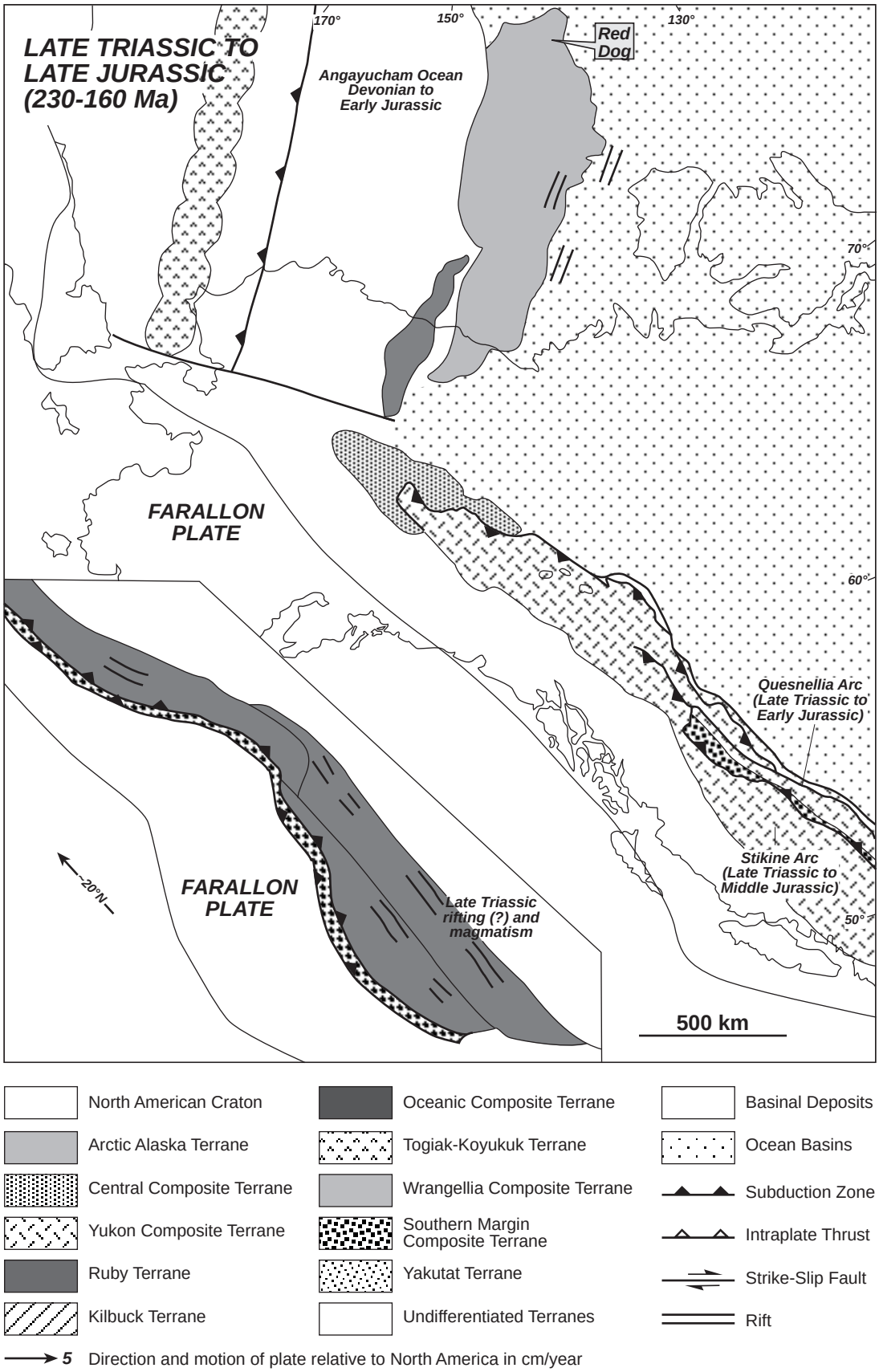


Figure 2.2c. Late Triassic to Late Jurassic (modified from Plafker & Berg, 1994).

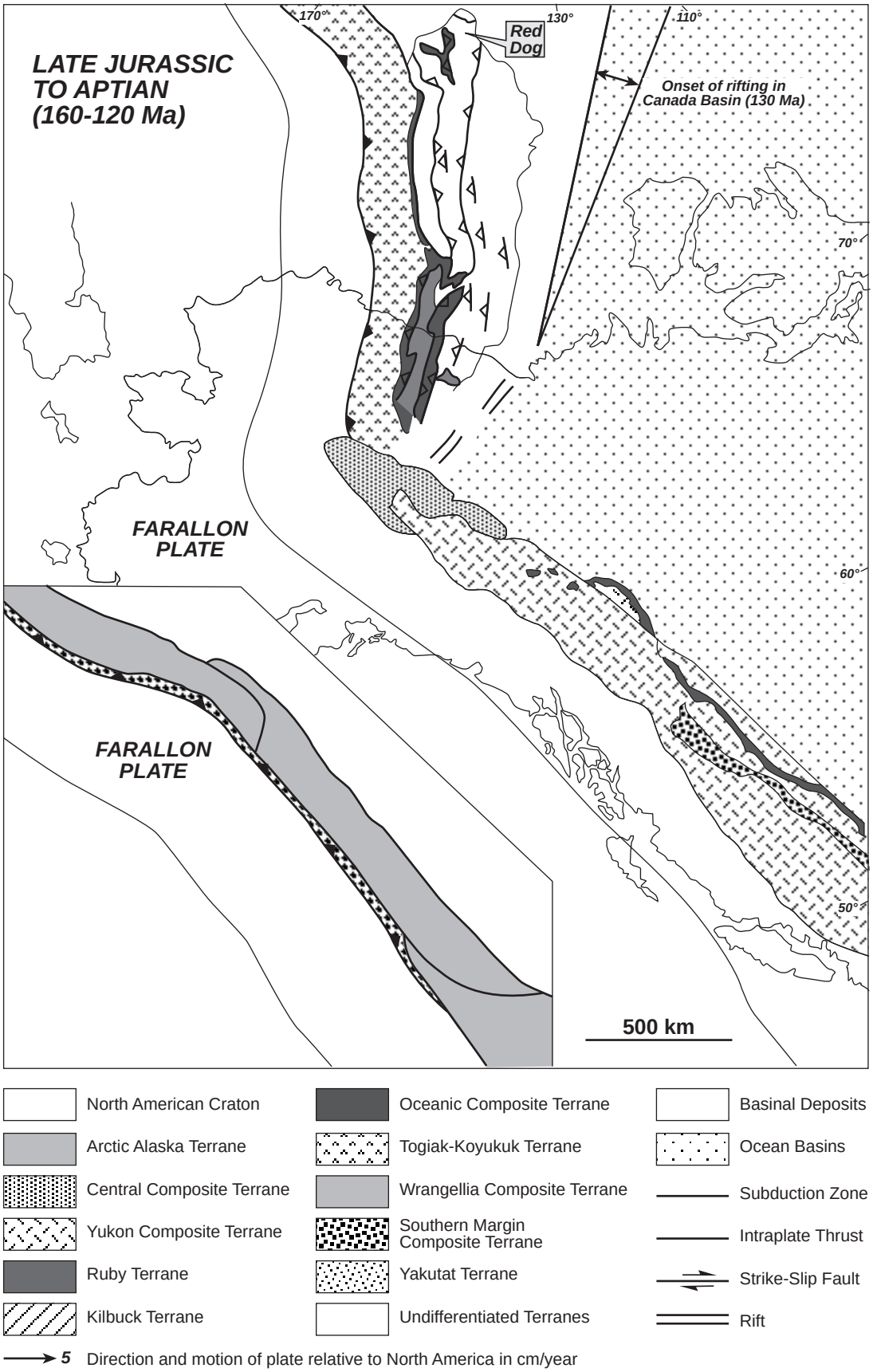


Figure 2.2d. Late Jurassic to Aptian. Onset of the Brookian orogeny in middle Jurassic time (modified from Plafker & Berg, 1994).

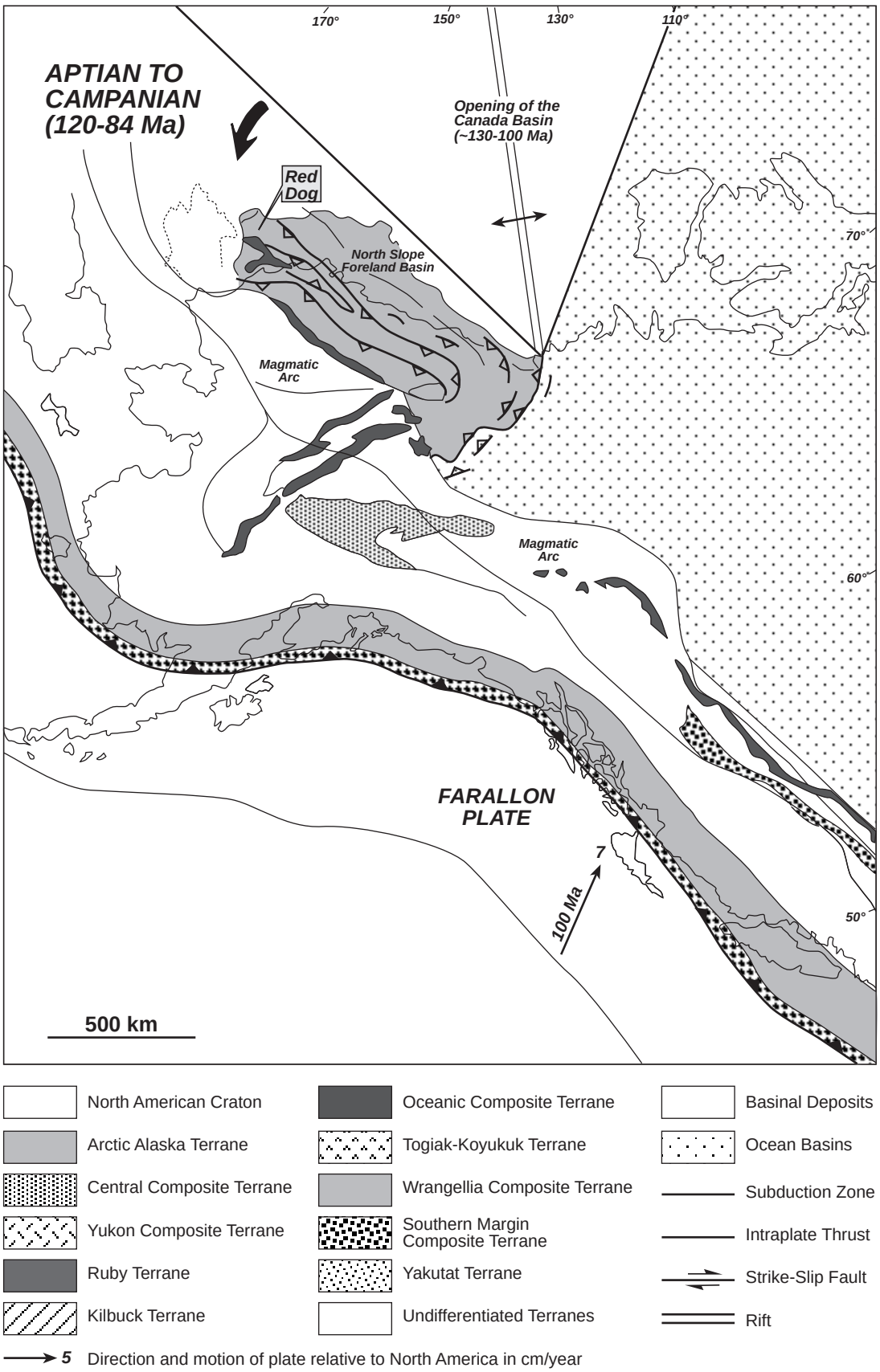


Figure 2.2e. Aptian to Campanian. The Canada Basin opened, driving counterclockwise rotation of northern Alaska. Magmatism was accompanied by thermal metamorphism throughout much of Alaska at this time (modified from Plafker & Berg, 1994).

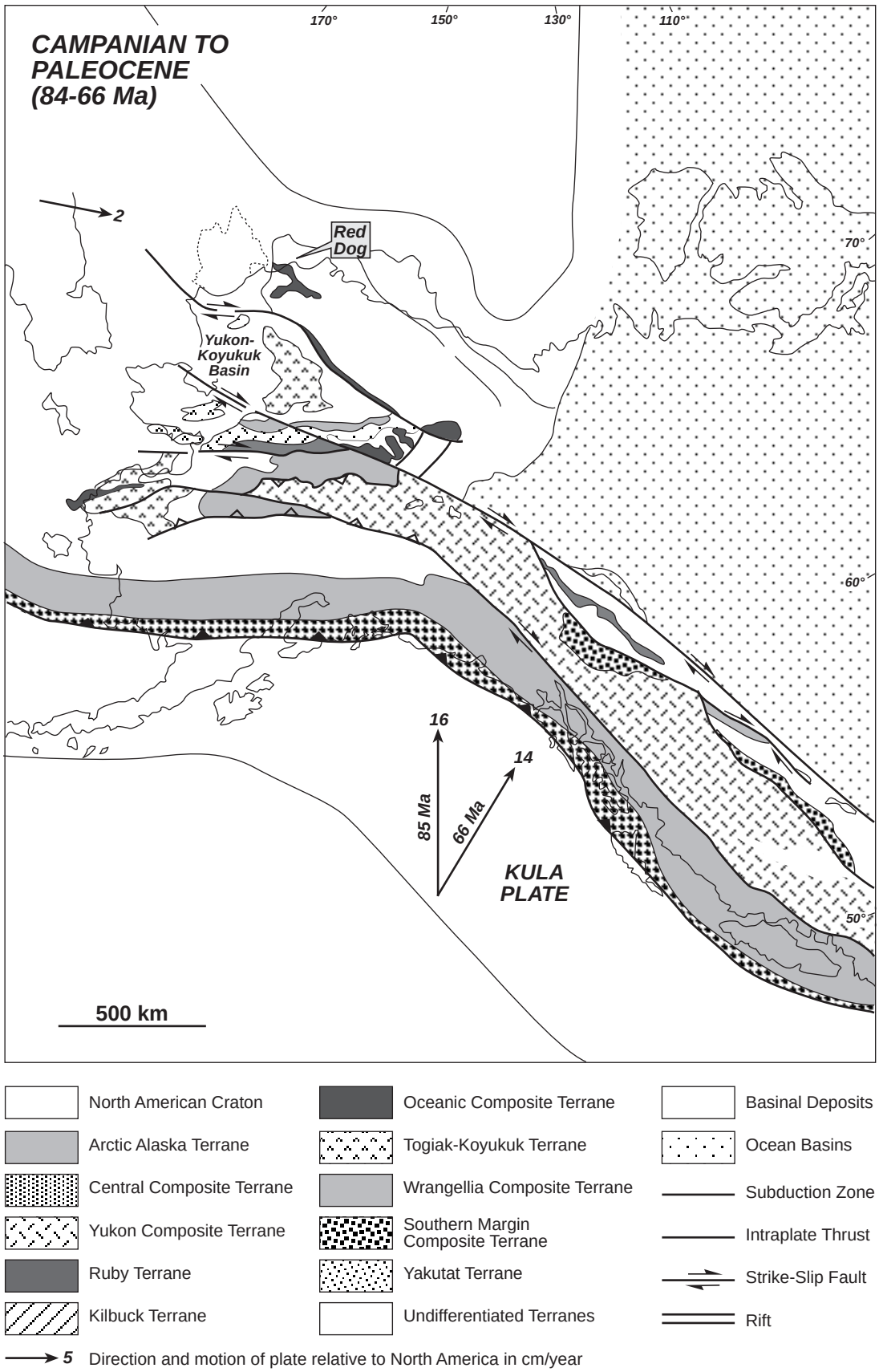


Figure 2.2f. Campanian to Paleocene. Dextral transpression along the continental margin resulted in northwestward movement of the Tukon composite terrane along the Tintina and related faults, driving further clockwise rotation of the Ruby terrane and attached Oceanic terrane to close the Yukon-Koyukuk basin (modified from Plafker & Berg, 1994).

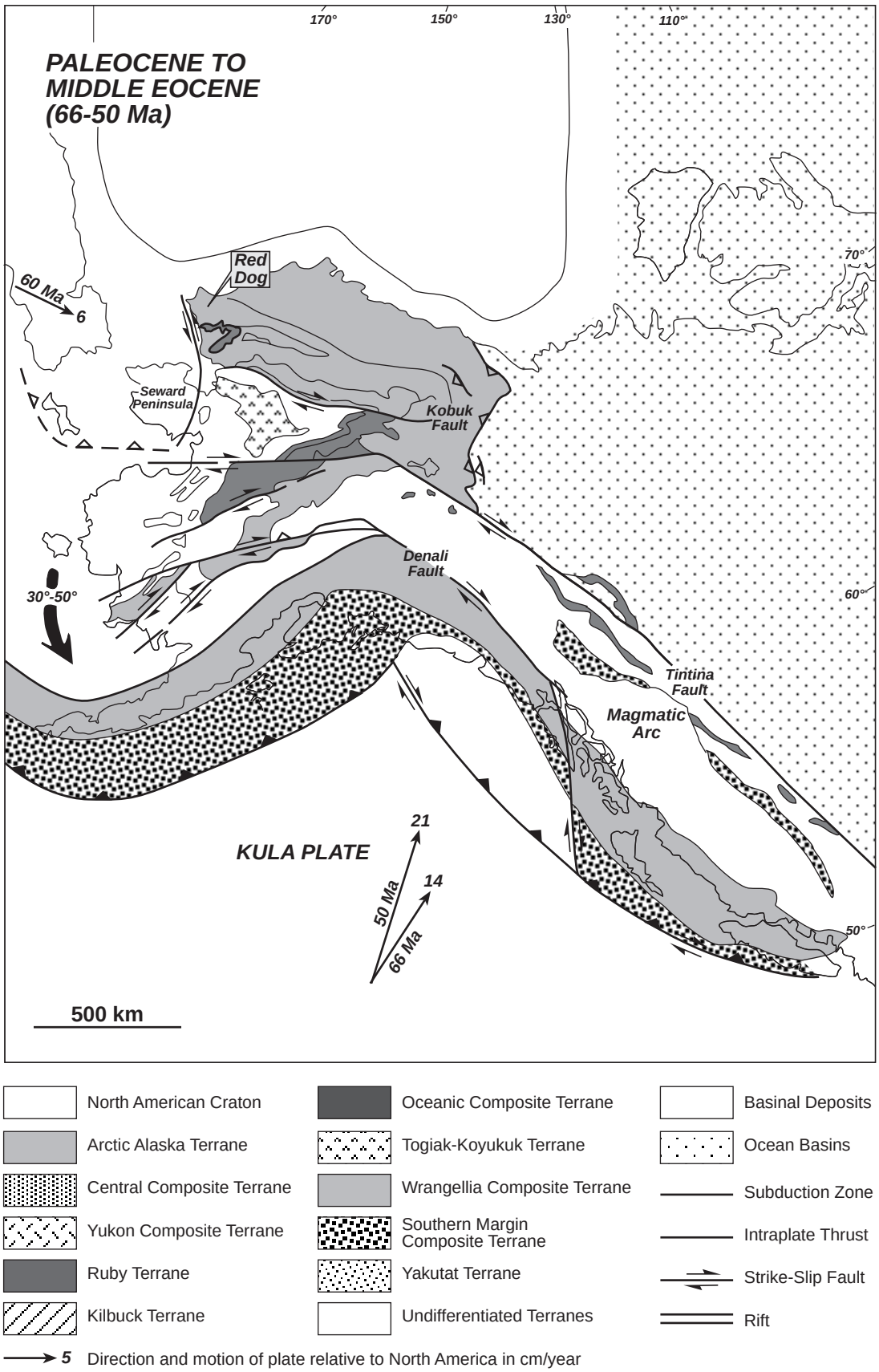


Figure 2.2g. Paleocene to Middle Eocene. Large-scale counterclockwise rotation of western Alaska and displacement of the western Arctic Alaska terrane (Seward Peninsula) was driven by compression between Eurasia and North America. Dextral displacement on the Denali fault (modified from Plafker & Berg, 1994).

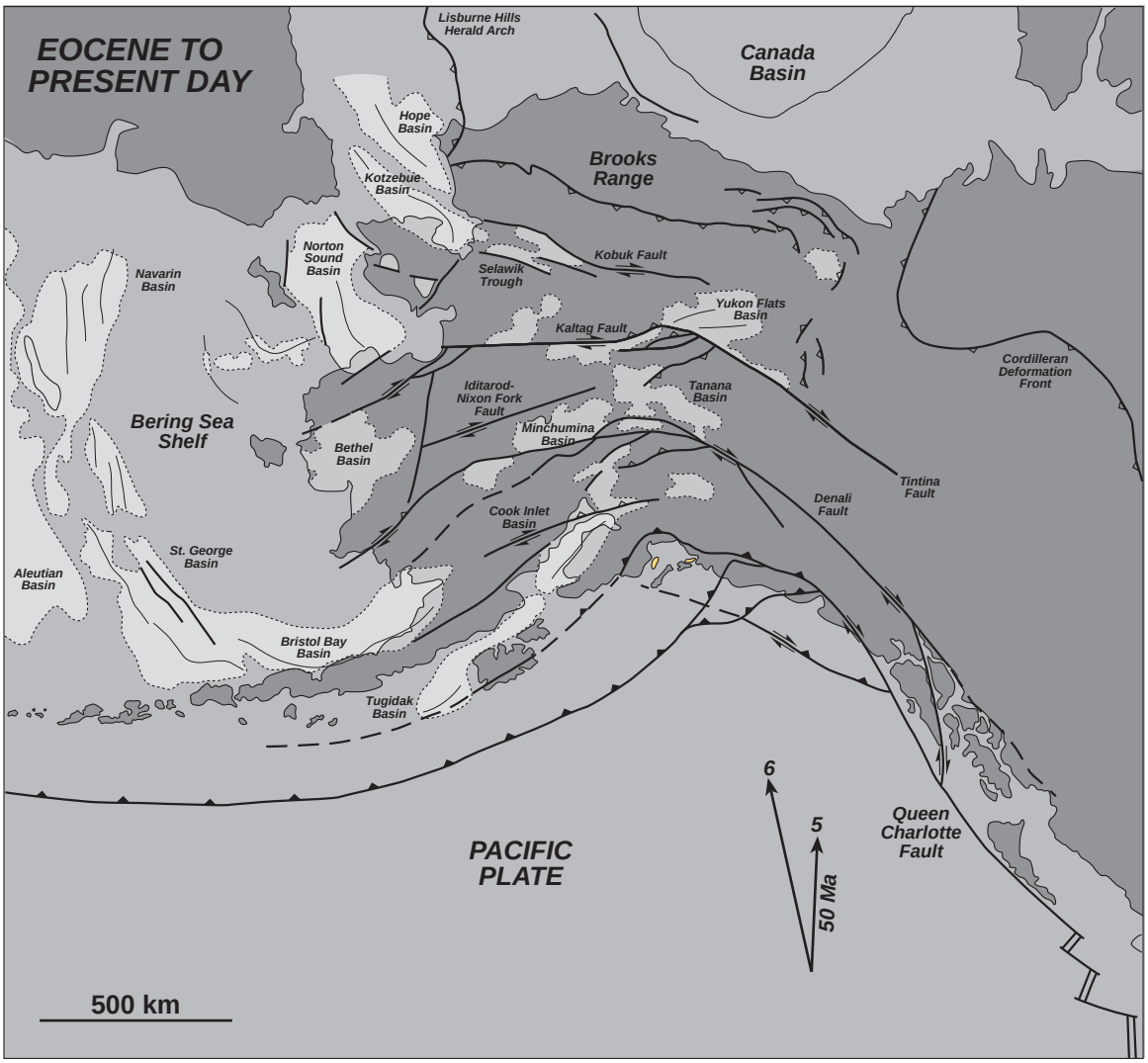


Figure 2.2h. Eocene to Present Day. Onset of northwestward Pacific plate relative motions resulted in the formation of the present Aleutian Arc, displacement on intraplate faults, and the formation of basins onland and on the contiguous continental shelves (modified from Plafker & Berg, 1994).

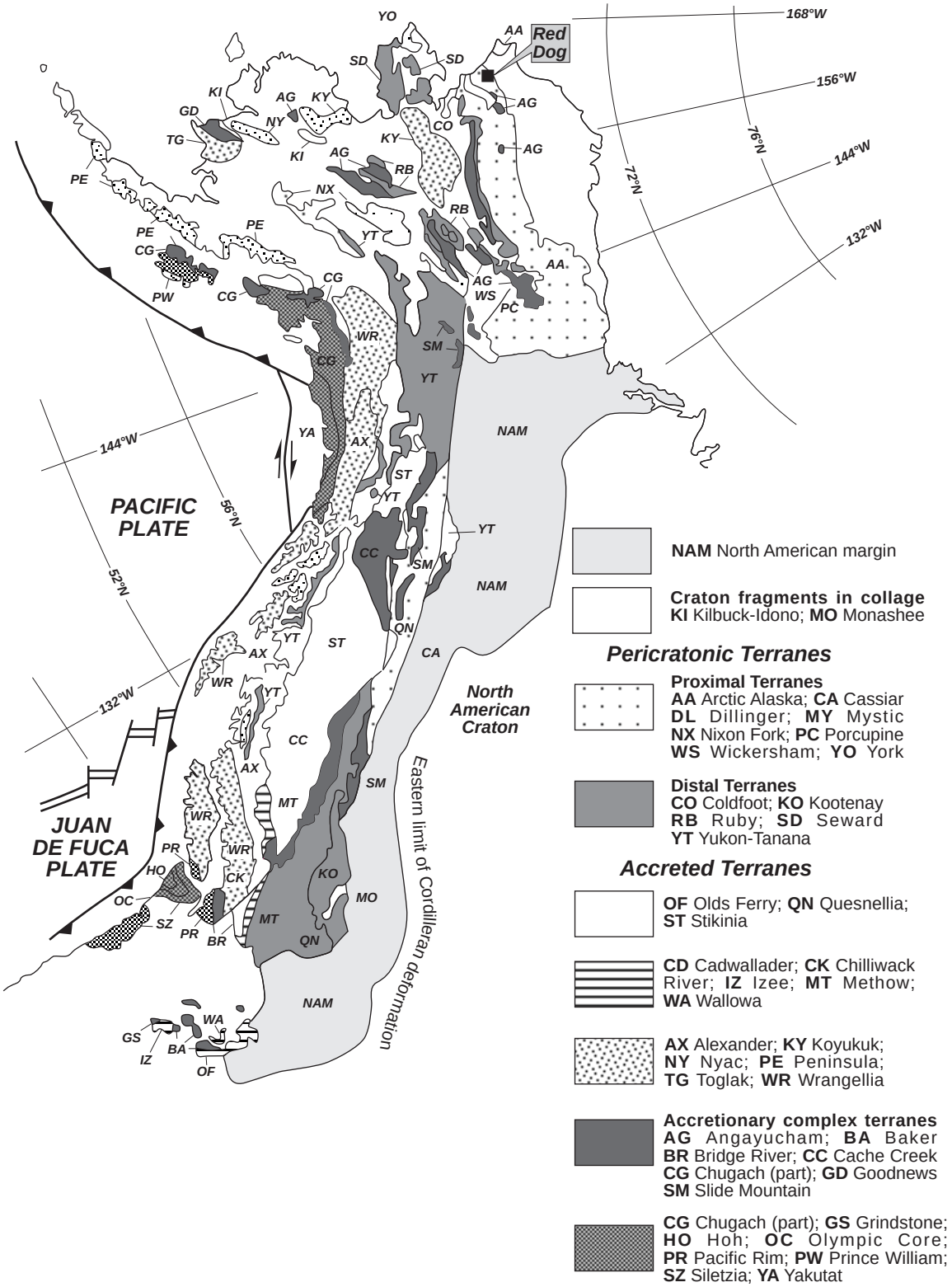


Figure 2.3. Terrane map of the North American Cordillera and Alaska. Patterns show the dominant tectonic affinity of individual terranes (modified from Monger & Nokleberg, 1996; Nokleberg *et al*. 1997; Price & Monger, 2003). The location of the Red Dog district is shown.

2.3 THE BROOKS RANGE

The earliest geologic studies of the Brooks Range date back to the early 1900's with the work of Brooks (1906), Smith (1913), Leffingwell (1919), and Smith (1939). A better understanding of the geology and tectonic evolution of the Brooks Range was acquired with the work of Brosgé *et al*. (1962), Tailleur *et al*. (1966), Martin (1970), Tailleur & Brosgé (1970), Tailleur (1973), Mull (1982), Moore *et al*. (1986), Mayfield *et al.* (1988), Grantz *et al*. (1991), Moore *et al*. (1994), Moore *et al*. (1997), O'Sullivan *et al*. (1997), and Young (2004) amongst others.

The Brooks Range orogenic belt encompasses important mineral and hydrocarbon reserves, including one of the world's largest zinc resources in the Red Dog district of the western Brooks Range (e.g. Kelley & Jennings, 2004), significant copper and zinc resources in the Ambler district of the southern Brooks Range (e.g. Einaudi & Hitzman, 1986; Nokleberg *et al.* 1994, 2003), the largest oil field in North America at Prudhoe Bay (e.g. Plafker & Berg, 1994), and one third of the potential coal reserves of the United States (e.g. Moore *et al*. 1994).

2.3.1 Physiographic Elements

The Brooks Range (Figs. 2.1 & 2.4) is the physiographic continuation of a series of mountain ranges that extend from the Canadian Rocky Mountains through the MacKenzie, Richardson and Philip Smith Mountains of the Yukon and Northwest Territories in Canada to northern Alaska (Grantz *et al*. 1991) (Figs. 1.2 & 2.1). The Brooks Range forms the drainage divide between waters that flow northward into the Arctic Ocean and those that flow southward into the Yukon River basin and the Pacific Ocean (Fig. 1.2). It is separated from the Arctic Ocean by the Arctic Foothills and the Arctic Coastal Plain (Grantz *et al.* 1990; Young, 2004) (Fig. 2.4). The Arctic Foothills and Arctic Coastal Plain are also referred to as the North Slope (Young, 2004) (Figs. 1.2 & 2.4). The Brooks Range is approximately 900 km long and as much as 300 km wide (Moore *et al*. 1994, 2002*a*; Young, 2004). It stretches across the entirety of northern Alaska, extending approximately from latitude 66° to 70° N and from longitude 141° to 167° W (Figs. 1.2, 2.1 & 2.4). The Brooks Range consists dominantly of rugged E-W- to NE-SW-trending ranges, ridges and hills that progressively decrease in elevation and relief to the west (Plafker & Berg, 1994) (Fig. 1.2). Elevations range from 500 to 1500

m in its western and central parts, and from 2100 to 2400 m in the eastern part, where the Brooks Range locally exceeds 2700 m (Plafker & Berg, 1994). The northern topographic edge of the Brooks Range is commonly called the range or mountain front (Young, 2004). North of the mountain front are the Arctic Foothills and the Arctic Coastal Plain, dominated by tundra-covered rolling hills, plateaus, long ridges and lowlands with decreasing relief to the north (Plafker & Berg, 1994) (Fig. 1.2).

2.3.2 Geological Framework

The Brooks Range is a Middle Jurassic-Late Cretaceous to Tertiary E-W- to NE-SW-trending and N- to NW-vergent, arc-continent collision orogenic belt formed by units that span from Late Proterozoic to Cenozoic in age (e.g. Tailleur & Brosgé, 1970; Mull, 1982; Moore *et al*. 1994; Young, 2004). The Brooks Range is located approximately 1000 km north of the Present Day convergent plate margin between the continental North American Plate and the subducting oceanic Pacific Plate (Moore *et al*. 1994) (Figs. 2.1, 2.2h & 2.3).

The Brooks Range is bounded to the north by the North Slope foreland basin and the opening Canada basin (e.g. Mull, 1982; Grantz *et al*. 1990, 1991; Moore *et al*. 1994; Young, 2004) (Figs. 2.1 & 2.4). To the south, the Brooks Range is separated from the Yukon-Koyukuk basin along the E-W-trending dextral strike-slip Kobuk fault (Dillon, 1989; Grantz *et al*. 1991; Moore *et al*. 1994; Avé Lallemant *et al*. 1998; Young, 2004) (Figs. 2.1, 2.2h, 2.4 & 2.5b). To the west it is bounded by the Lisburne Hills-Herald Arch thrust belt (Moore *et al*. 1994; Moore *et al*. 2002*a*; Young, 2004) and the Tertiary extensional Hope basin (Klemperer *et al*. 2002; Moore *et al*. 2002*a*) (Figs. 2.1 & 2.4). To the east it merges into the MacKenzie fold and thrust belt and the North American Cordillera (Tailleur, 1969; Aitken & Long, 1978; Moore *et al*. 1994; Plafker & Berg, 1994) (Figs. 2.1 & 2.4).

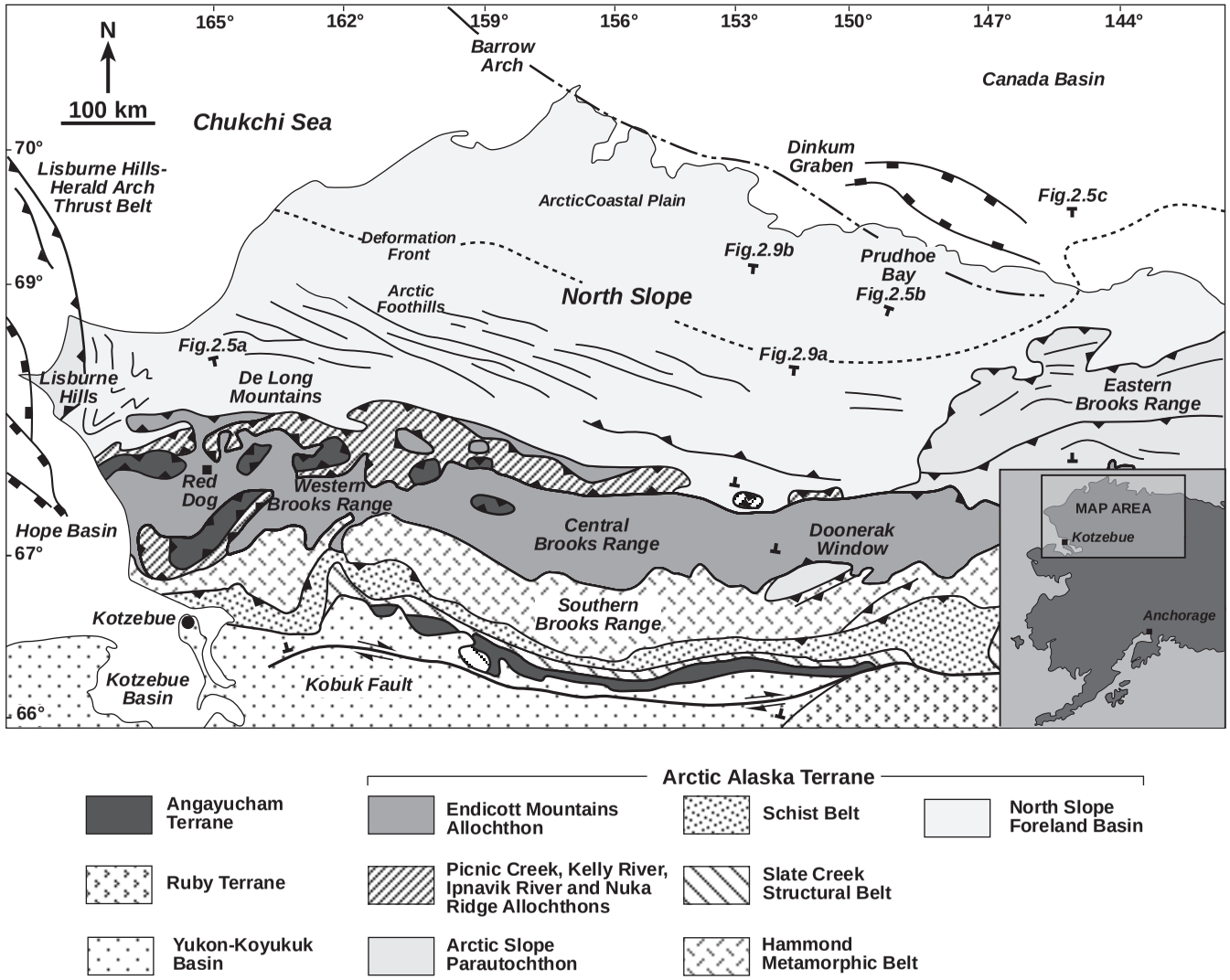


Figure 2.4. Geological map of northern Alaska (modified from Moore *et al.* 1994). The location of the Red Dog mine is shown.

2.3.3 Structure of the Brooks Range

The Brooks Range orogenic belt is zoned, with a hinterland of exhumed penetratively and poly-deformed, metamorphic and igneous rocks in the south, together with a northern foreland fold and thrust belt and a moderately deformed foreland basin (Mull, 1982, 1985, 1989; Grantz *et al*. 1991; Moore *et al*. 1994; Young, 2004) (Figs. 2.4 & 2.5). The Brooks Range orogen has a regional westward plunge so that progressively deeper structural levels are exposed to the east (Mull, 1982; Moore *et al*. 1994, 1997*b*; Young, 2004). The Brooks Range is considered unusual compared with most orogenic belts in that early synorogenic deep-marine strata of Early Cretaceous age and the highest structural levels of the orogen are extensively preserved (Moore *et al*. 1994). This has been interpreted as an indicator that the structural relief was relatively low during the period of greatest contraction (e.g. Moore *et al*. 1994).

The structural style of the Brooks Range foreland fold and thrust belt is dominated by complex thrust tectonics, with dominantly N- to NW-transported thrust sheets that expose successively younger rocks to the north (e.g. Mull, 1982; Mayfield *et al*. 1988; Moore *et al*. 1994). The large-scale structure of the Brooks Range orogen varies between the dominant NE-SW-trending arcuate western Brooks Range (Figs. 1.2, 1.3, 1.5 & 2.4), the dominantly E-W-trending central Brooks Range (Figs. 1.2 & 2.4), and the salient formed by the eastern Brooks Range (Moore *et al.* 1994; Young, 2004; Potter *et al*. 2004) (Figs. 1.2 & 2.4). The western and central Brooks Range share the same tectonic history of Middle Jurassic to Cretaceous deformation and show comparable structural styles (Moore *et al*. 1994) (Figs. 2.4 & 2.5). In contrast, the eastern Brooks Range has a markedly different structural style (Figs. 2.4 & 2.5) and distinct tectonic evolution characterized by basement-involved Cenozoic thrusting (Wallace & Hanks, 1990; Hanks 1993*a, b*; Wallace, 1993; Grantz *et al*. 1994; O'Sullivan *et al*. 1997; Wallace *et al*. 1997; O'Sullivan & Wallace, 2002; Wallace & Homza, 2004; Young, 2004). The regional structure of the Brooks Range fold and thrust belt has been described by Mull (1982, 1985), Mull *et al*. (1987*b*), Mull (1989), Mayfield *et al*. (1988), Wallace & Hanks (1990), Grantz *et al*. (1991), Hanks (1993*a*, *b*), Wallace (1993), Moore *et al.* (1994), Cole *et al*. (1997) and Moore *et al*. (1997*b*) amongst others. Because of its vast size many studies in the Brooks Range have been largely reconnaissance in style (e.g. Martin, 1970; Tailleur & Brosgé, 1970; Mull, 1982; Moore

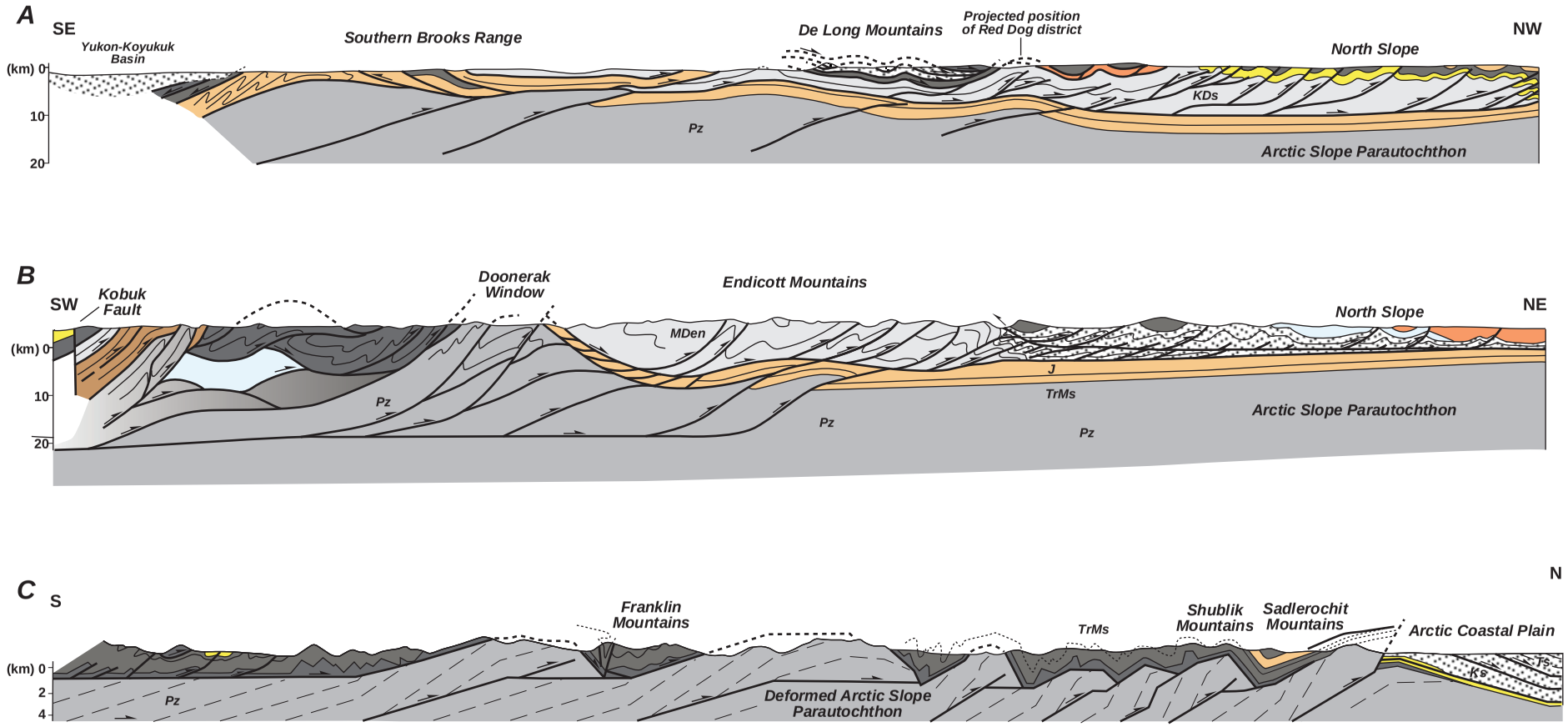


Figure 2.5. Regional cross-sections through the Brooks Range. **A.** Western Brooks Range (modified from Mayfield *et al.* 1988). Projected position of the Red Dog district is shown. **B.** Central Brooks Range (modified from Mull *et al.* 1989; Moore *et al.* 1994). **C.** Eastern Brooks Range (modified from Namson & Wallace, 1986; Wallace, 1993; Moore *et al.* 1994). Pz: Palaeozoic parautochthonous basement. TrMs: Undivided Mississippian to Triassic strata. MDen: Devonian to Mississippian. Ts: Tertiary sedimentary rocks. Refer to Figure 2.4 for location of individual cross sections.

et al. 1986; Mayfield *et al*. 1988; Curtis *et al*. 1990; Ellersieck *et al*. 1990*a*; Mayfield *et al*. 1990; Moore *et al*. 1994).

The amount of shortening in the Brooks Range fold and thrust belt has not been accurately determined, partly due to the stratigraphic and palaeogeographic uncertainties as well as the limitations given by the lack of detailed structural analyses (Mull, 1982; Mayfield *et al*. 1988; Moore *et al*. 1994; Young. 2004). Shortening estimates vary greatly depending on the specific region and on the inferred tectonic transport direction. Mull (1982) estimated shortening in a minimum of 96 km for the eastern Brooks Range (Fig. 2.5c) and a minimum of 580 km (Fig. 2.5a) for the western Brooks Range. Oldow *et al*. (1987) proposed approximately 540 km of shortening based on balanced cross sections across the central Brooks Range (Fig. 2.5b). Mayfield *et al*. (1988) estimated 700 to 800 km of shortening for the western Brooks Range (Fig. 2.5a) but suggested that shortening could exceed 1000 km. These large amounts of shortening were challenged by Kelley & Brosgé (1995), who have argued in favour of significantly lesser amounts of shortening in the Doonerak window (Figs. 2.4 & 2.5b) in the central Brooks Range. More recently, Wissinger *et al*. (1998), using seismic-constrained cross sections, have estimated 500 to 600 km of shortening across the central Brooks Range.

2.3.4 Structural Units of the Brooks Range

The Brooks Range orogen is commonly subdivided into linear zones that can be differentiated on the basis of stratigraphy, structural style, metallogenesis, and/or metamorphic grade. Structural nomenclature of the Brooks Range is complex and there are many assorted structural classifications (e.g. Mull, 1982; Moore *et al*. 1986; Mayfield *et al*. 1988; Moore *et al*. 1992; Karl & Mull, 1993; Moore *et al*. 1994; Young, 2004). The structural units have been variously described as terranes, subterranes, allochthons, sequences, belts, and domains (e.g. Tailleur & Brosgé, 1970; Mayfield *et al*. 1988; Moore *et al*. 1992; Karl & Mull, 1993; Moore *et al.* 1994; Young, 2004).

Unlike southern Alaska, the lateral continuity of belts suggests that northern Alaska and the Brooks Range are not composed of numerous accreted and unrelated terranes (Einaudi & Hitzman, 1986; Moore *et al*. 1994; Young, 2004) (Figs. 2.3 & 2.4).

Specifically, northern Alaska and the Brooks Range consist of two main terranes. These are the Arctic Alaska and Angayucham terranes (Karl & Mull, 1993; Silbering *et al*. 1994; Moore *et al*. 1994; Monger & Nokleberg, 1996; Nokleberg *et al*. 1997; Price & Monger, 2003; Young, 2004) (Figs. 2.3 & 2.4), which are described in detail in sections 2.4 and 2.5. The Koyukuk and Ruby terranes, partially covered by the Yukon-Koyukuk basin, lie south of the Brooks Range (Figs. 2.3 & 2.4).

2.3.5 Orogenic Events

Northern Alaska and the Brooks Range record the effects of the Palaeozoic Ellesmerian orogeny (Lerand, 1973), the Mesozoic Brookian orogeny (Mull, 1982; Moore *et al*. 1994; Young, 2004), and a series of Cenozoic episodic contractional events (e.g. Cole *et al*. 1997, Moore *et al*. 1997*b*; O'Sullivan *et al*. 1997; O'Sullivan & Wallace, 2002; Moore *et al*. 2004).

Ellesmerian Orogeny

The Ellesmerian orogeny (Lerand, 1973) refers to an Early Palaeozoic orogenic event (Fig. 2.2a) that is recognized over much of the Arctic region (Hubbard *et al*. 1987; Moore *et al*. 1994). The Ellesmerian orogen extends from Svalsbard along the northwest side of the Canadian Arctic Archipelago through the Brooks Range of Alaska and the Chukotka Peninsula in easternmost Russia, and also southward from east of the Mackenzie Delta to reappear in the Antler orogen of the western United States (Sweeney, 1982). Little is known about the Ellesmerian orogeny in northern Alaska and the timing of deformation is controversial (e.g. Anderson & Wallace, 1990; Moore *et al*. 1994). Anderson & Wallace (1990) recognize the Ellesmerian orogen of northern Alaska to be pre-Middle Devonian. In the Brooks Range, the effects of the Ellesmerian orogeny are solely recorded in the Arctic Slope parautochthon (Figs. 2.4 & 2.5), which is dominantly buried beneath strata of the North Slope foreland basin and only locally exposed across the Brooks Range fold and thrust belt (Moore *et al.* 1994; Young, 2004). The Ellesmerian orogeny involved Proterozoic to Early Palaeozoic rocks that are unconformably overlain by younger rocks (Lerand, 1973; Moore *et al*. 1994; Young, 2004).

Brookian Orogeny

The Brookian orogeny (Mull, 1982) refers to the orogenic event that resulted from the collision of the ancient S-facing (Present Day coordinates) continental passive margin of Alaska (Arctic Alaska terrane) with an island arc and a related oceanic crust assemblage (Koyukuk and Angayucham terranes, respectively) in the Middle Jurassic to Cretaceous (e.g. Roeder & Mull, 1978; Mull, 1982; Box, 1985; Mayfield *et al*. 1988; Patton & Box, 1989; Moore *et al*. 1994; Young, 2004) (Figs. 2.2c – e & 2.6). Box (1985), Harris *et al.* (1987) and Harris (1998) have compared underthrusting and subduction of the ancient continental margin of Arctic Alaska with the Cenozoic arc-continent collision and subduction of Australia beneath Timor and also with the subduction and collision of China beneath Taiwan.

During the Late Jurassic to Early Cretaceous partial underthrusting and attempted subduction of the more buoyant extended continental crust of the passive margin of Arctic Alaska beneath the oceanic crust-island arc assemblage resulted in the obduction of an ophiolite and the subsequent accretion, emplacement and stacking of allochthonous thrust sheets (Roeder & Mull, 1978; Mull, 1982; Box, 1985; Mayfield *et al*. 1988; Moore *et al*. 1994) (Fig. 2.6). This resulted in an abrupt change of sedimentation, from slow, northerly-derived shallow to deep marine sedimentation on the S-facing (Present Day coordinates) passive continental margin, to rapid syn-orogenic sedimentation from the south (Tailleur & Brosgé, 1970; Mull, 1982; Mayfield *et al*. 1988; Moore *et al.* 1994; Young, 2004) (Fig 2.7). Broadly synchronous with collision, rifting in the north produced counter-clockwise rotation of the Arctic Alaska terrane away from northernmost Canada (Carey, 1958; Tailleur, 1973; Rickwood, 1970; Mull, 1982; McWhae, 1986; Grantz *et al*. 1990, 1991) and resulted in the opening of the Canada Basin (Figs. 2.2c, d & 2.6d, e, f).

Tectonic Models for the Brookian Orogeny

Moore *et al*. (1994) proposed a model for the Brookian orogeny that is the most widely accepted (Fig. 2.6). In this model, Late Palaeozoic to Early Mesozoic subduction took place along the southern margin of the Angayucham Ocean. Coeval with subduction, sedimentation took place on the continental margin of Arctic Alaska (Moore *et al*. 1994). Initial subduction of Late Palaeozoic and Early Mesozoic oceanic crust took

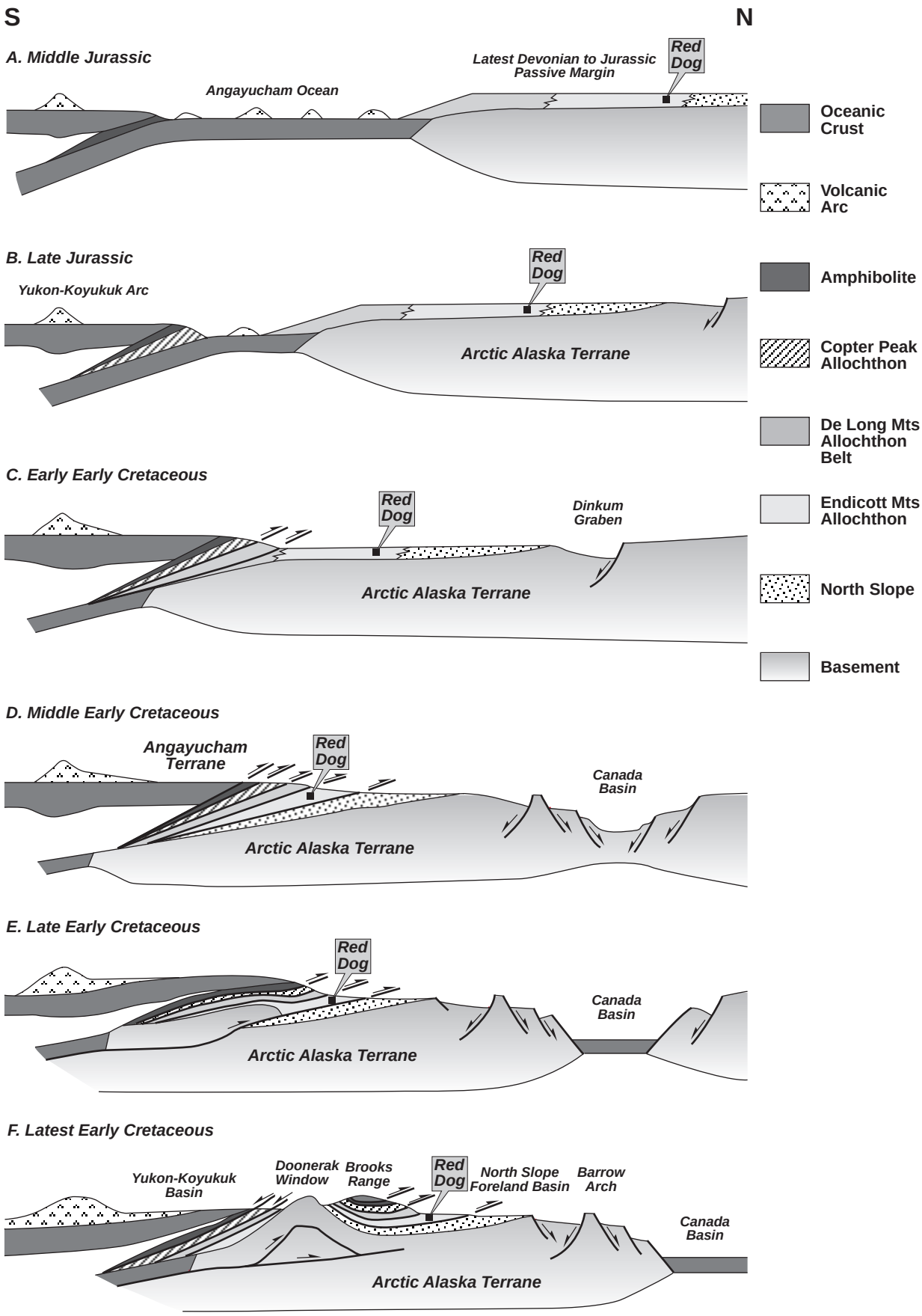


Figure 2.6. Tectonic model for the Brookian orogeny (modified from Moore *et al.* 1994). Location of the Red Dog district is shown schematically.

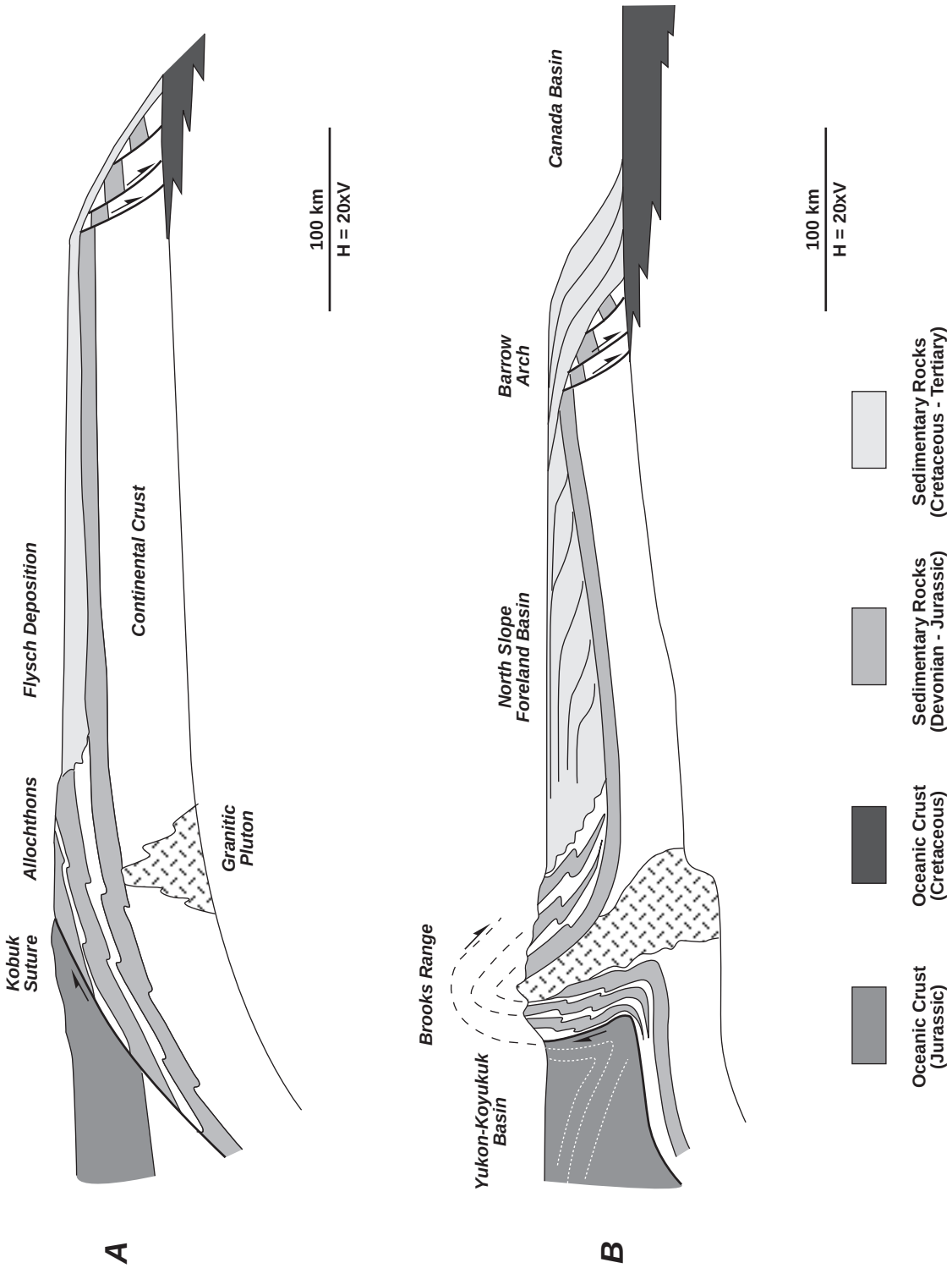


Figure 2.7. Two-stage model for the Brookian orogeny. **A.** Early Brookian event (Neocomian). **B.** Late Brookian event (Albian) (modified from Mull, 1982, 1989).

place in Middle Jurassic (Fig. 2.6a). Continued subduction resulted in underthrusting of the older oceanic crust beneath young and hot oceanic crust and related arc terranes (Koyukuk arc) producing amphibolite-grade metamorphism (Fig. 2.6b). By Late Jurassic time, subduction of the lower oceanic plate was nearly completed and the Angayucham Ocean was almost closed (Fig. 2.6b). A subduction complex, consisting mostly of seamounts and oceanic plateau fragments, detached from the subducted oceanic crust (Moore *et al*. 1994) (Fig. 2.6b). Broadly synchronously, failed rifting resulted in the opening of the Dinkum graben to the north (Present Day coordinates) (Fig. 2.6b). In latest Jurassic to earliest Cretaceous time, the Arctic Alaska terrane initiated subduction (Fig. 2.6c). The sedimentary cover was detached from the basement and imbricated into series of northward-transported allochthonous thrust sheets (Fig. 2.6c). Partial subduction of continental crust of the Arctic Alaska terrane in middle Early Cretaceous produced blueschist facies metamorphism (Moore *et al*. 1994; Till & Snee, 1995) (Fig. 2.6d). Telescoping and imbrication of the passive margin continued at the same time as rifting and break up occurred along the northern margin of the Arctic Alaska terrane resulting in the opening of the Canada basin. In late Early Cretaceous, middle to lower crustal rocks containing the blueschist facies assemblages were uplifted and emplaced at higher structural levels by large-scale, basement-involved, out of sequence thrusting and duplex development that resulted in thickening of lower crust (Fig. 2.6e). The Canada basin opened and the Barrow arch formed along the northern margin of the Arctic Alaska terrane (Moore *et al*. 1994) (Fig. 2.6e). Continued contraction in latest Early Cretaceous resulted in middle and lower crustal thickening. Coeval crustal attenuation took place in the southern Brooks Range along regional-scale extensional faults downthrown to the south (Fig. 2.6f). Resulting uplift and erosional unroofing shed large volumes of clastic detritus northward into the North Slope foreland basin to the north and southward into Koyukuk basin (Fig. 2.6f).

Evidence for southward subduction or underthrusting of the continental margin beneath and island arc and oceanic crust (Fig. 2.6) includes blueschist-facies metamorphism (Till, 1992; Till & Snee, 1995), N-directed emplacement of sedimentary allochthonous thrust sheets (Tailleur, 1969; Roeder & Mull, 1978; Mull, 1982, 1985; Mayfield *et al*. 1988; Moore *et al*. 1994) (Figs. 2.5, 2.6 & 2.8c), and the position of ophiolitic rocks above continental passive margin strata (Roeder & Mull, 1978; Grantz *et al*. 1991; Moore *et al*. 1994; Young, 2004). Although the arc-continent collision model for the

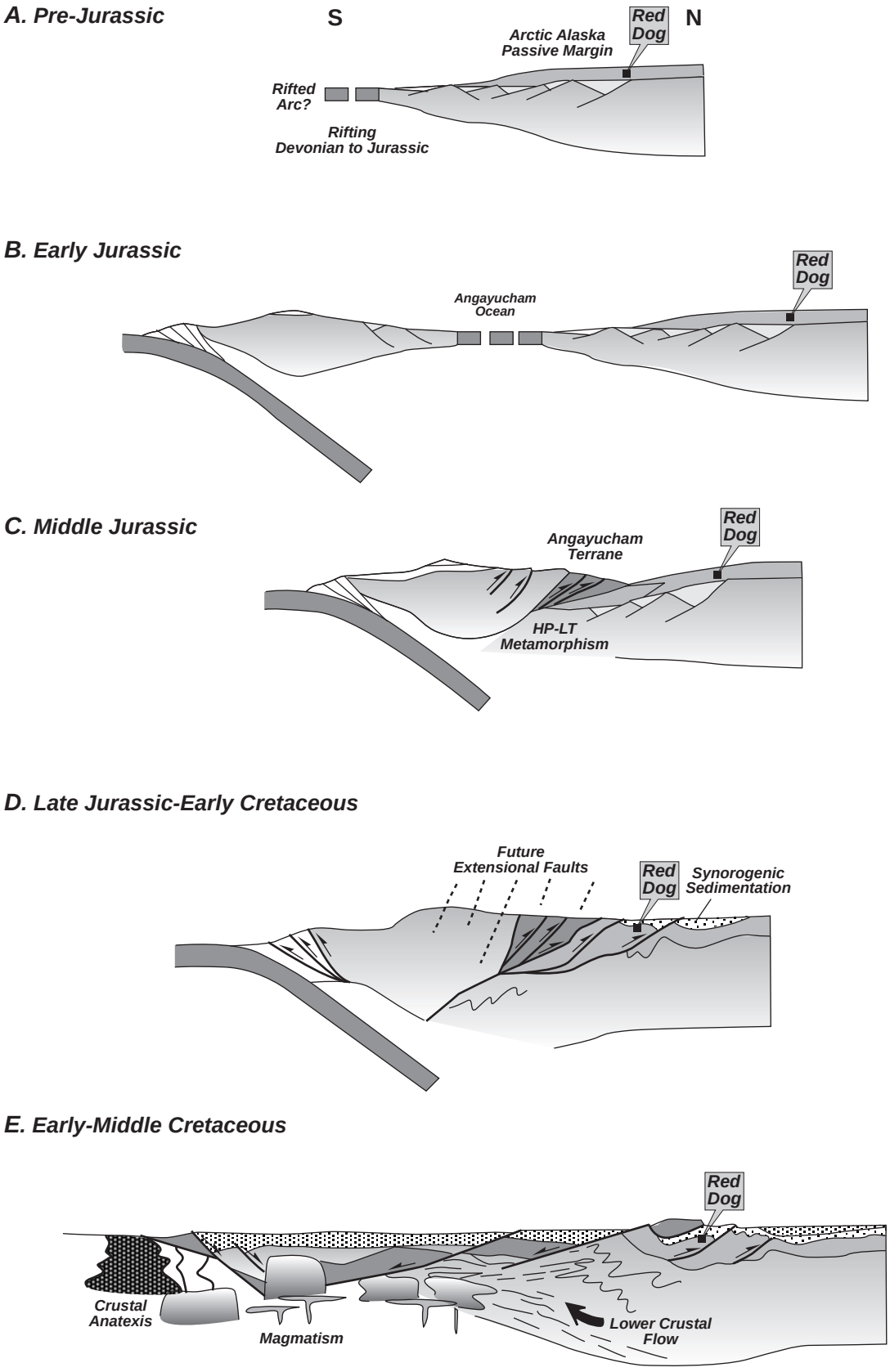


Figure 2.8. Schematic plate tectonic model of northern Alaska, showing a period of large-magnitude extension in Early to Middle Cretaceous (modified from Miller & Hudson, 1991). The location of the Red Dog district is shown schematically.

underthrusting of the ancient continental margin of Arctic Alaska (Fig. 2.6) explains most of the geologic relationships observed in the Brooks Range and northern Alaska, Ellersieck & Mayfield (1983), Mayfield *et al.* (1988), and Grantz *et al.* (1991) have pointed out several problems with this model. The arc-continent collision model requires subduction of more than 500 km of thick and relatively light continental crust beneath the thinner and denser oceanic crust (Ellersieck & Mayfield, 1983; Mayfield *et al.* 1988; Grantz *et al.* 1991). In addition, the Koyukuk arc is believed to have formed only after ophiolite obduction in Middle to Late Jurassic time (Grantz *et al.* 1991), and also only a small part of the Brooks Range faces the Koyukuk arc rocks.

Churkin *et al.* (1979, 1980) proposed an alternative model for the Brooks Range involving multiple phases of N- and S-verging thrusting and emplacement of allochthonous thrust sheets. This model was widely critiqued by Crane (1980), Dutro (1980), Mayfield (1980), Metz (1980), Mull (1980), Nelson (1980) and Mayfield *et al.* (1988). The arc-continent collision model of Tailleur (1970), Roeder & Mull (1978), Box (1985), Moore *et al.* (1994) amongst others, with subsequent modifications by Miller & Hudson (1991, 1993), O'Sullivan *et al.* (1997, 1998) and Moore *et al.* (2002, 2004) remains the most widely accepted.

Brookian Deformation Phases and Timing

The Brookian orogeny has been traditionally subdivided into two main deformation phases (e.g. Mull, 1982, 1985; Mull *et al.* 1987*b*; Mayfield *et al.* 1988; Mull, 1989; Moore *et al.* 1994; Young, 2004) (Fig. 2.7). The first phase is an early Brookian event, characterized by ductile deformation and metamorphism in the inner part of the orogen and thin-skinned thrusting and emplacement of allochthonous thrust sheets in the more external part during Middle Jurassic to Early Cretaceous time (e.g. Mull, 1982, 1985; Mull *et al.* 1987*b*; Mayfield *et al.* 1988; Mull, 1989; Moore *et al.* 1994) (Figs. 2.6a – e & 2.7a). The second phase (Figs. 2.6f, g & 2.7b) is a late Brookian event associated with deformation of Early Cretaceous (Albian) and younger strata of the North Slope foreland basin into complex tight antiforms and broad synforms (Mayfield *et al.* 1988; Mull, 1982, 1985; Mull *et al.* 1987*b*; Mull, 1989; Moore *et al.* 1994; Young, 2004). This latter event also included regional-scale folding and uplift of the previously

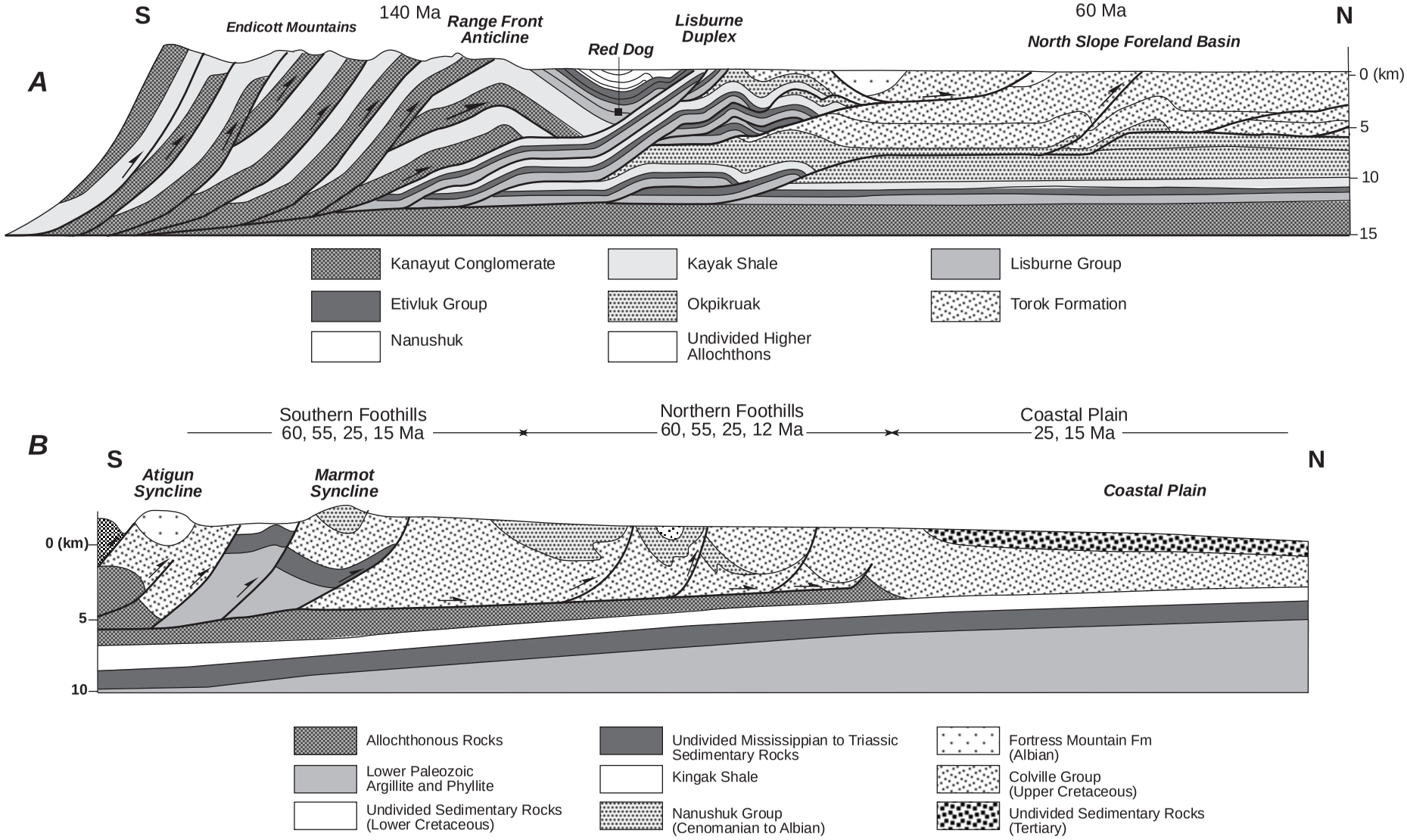


Figure 2.9. Cross sections across (A) the central Brooks Range and (B) the North Slope foreland basin. Projected apatite fission track data show exhumation events at 140, 60, 55, 25, and 15 Ma (modified from Cole *et al.* 1997; O'Sullivan *et al.* 1997). Projected position of the Red Dog district is shown in cross section A. Refer to Figure 2.4 for location of individual sections.

emplaced allochthon sheets (Mull, 1982, 1985; Mayfield *et al*. 1988; Moore *et al*. 1994; Young, 2004) (Fig. 2.9).

The relative and absolute timing of Brookian deformation has been widely discussed by Mull (1982), Mayfield *et al*. (1988), Gottschalk (1990), Miller & Hudson (1991, 1993), Till (1992), Till *et al*. (1993), Moore *et al*. (1997*b*), O'Sullivan *et al*. (1997, 1998), Cole *et al*. (1997) and more recently by Moore *et al*. (2002*a*, *b*), O'Sullivan & Wallace, (2002) and Moore *et al*. (2004). Gottschalk (1990) suggested that given that shortening in the North Slope foreland basin took place through the Eocene and possibly later, basement-involved thrusting and uplift of the hinterland may have been a continuous process, which spanned from Late Jurassic-Early Cretaceous to Early Tertiary and possibly later. Alternatively, Miller & Hudson (1991, 1993) proposed that a regional extensional event separated the early and late Brookian events and argued that northern Alaska was the site of orogenic collapse and extension from 130 to 90 Ma (Fig. 2.8). Extensional faults, such as those proposed by Miller & Hudson (1991) have been documented by Gottschalk & Oldow (1988) along the southern Brooks Range. However, Till (1992), Till *et al*. (1993), Till & Snee (1995), Mull *et al*. (1997) and Vogl (2002), based upon a series of thermochronology, radiometric and field studies in the southern Brooks Range, have provided compelling evidence for contraction and crustal thickening from 120 to 108 Ma that contradicts the model of Miller & Hudson (1991).

Cenozoic Tectonic Events

Recent apatite and zircon fission track thermochronology studies across the Brooks Range fold and thrust belt and the North Slope foreland basin have revealed a series of Tertiary km-scale regional exhumation and denudation events at 60 Ma, 45 Ma, and 25 Ma (e.g. O'Sullivan *et al*. 1993; Cole *et al*. 1997; Moore *et al*. 1997*b*; O'Sullivan *et al*. 1997, 1998; O'Sullivan & Wallace, 2002; Moore *et al*. 2002*b*, 2004) (Fig. 2.9). These episodic exhumation events are interpreted to reflect N-verging Tertiary contraction and uplift (Cole *et al*. 1997; Moore *et al*. 1997*b*; O'Sullivan *et al*. 1997). The effects of Tertiary contraction are more obvious in the eastern Brooks Range (e.g. O'Sullivan & Wallace, 2002; Potter *et al*. 2004), where the Brooks Range forms a prominent salient (Figs. 1.2, 2.1, 2.2h & 2.4) that exposes parautochthonous rocks that are elsewhere

buried beneath the North Slope foreland basin (Wallace, 1993; Moore *et al*. 1994; Wallace *et al*. 1997; Potter *et al*. 2004; Young, 2004) (Figs. 2.4 & 2.5).

Models for Cenozoic Tectonic Events

Cenozoic contraction in the Brooks Range has been ascribed to the far-reaching effects of Pacific-North American plate interactions and plate reorganization along the southern margin of Alaska (e.g. Wallace & Engebretson, 1984; Grantz *et al*. 1991; Moore *et al*. 1994; Blythe *et al*. 1996; O'Sullivan *et al*. 1997; O'Sullivan & Wallace, 2002; Moore *et al*. 2004). Grantz *et al*. (1991) argued that Cenozoic deformation in the eastern Brooks Range is a distal effect of convergence between the Pacific and North American plates at the Aleutian arc (Figs. 2.1, 2.2g & 2.2h). Alternatively, Blythe *et al.* (1996) and O'Sullivan *et al.* (1997) suggested that Tertiary contraction in the Brooks Range is the result of flat subduction of the Kula Plate underneath Alaska during the Eocene (Fig. 2.10). More recently, Moore *et al.* (2004) have argued that Tertiary events are the result of retroarc thrusting that resulted from subduction in southern Alaska, followed by collision of the Yakutat terrane (Fig. 2.3) with the southern Alaska continental margin in the Neogene. Contraction in the eastern Brooks Range is believed to continue into the Present Day (e.g. O'Sullivan & Wallace, 2002; Potter *et al.* 2004).

Moore *et al*. (2002*b*, 2004) proposed a complex tectonic model for the evolution of the Brooks Range that integrated the effects of the Brookian orogeny (e.g. Mull, 1982), the Middle Cretaceous extensional event of Miller & Hudson (1991), and Cenozoic episodic contraction of Moore *et al*. (1997*b)* and O'Sullivan *et al.* (1997). In this respect, Moore *et al*. (2002*b*, 2004) argued that the Brooks Range is the result of the superposition of two distinct orogenic events that included at least four distinct tectonic events, including both contraction and extension. Moore *et al*. (2002*b*, 2004) proposed that the structures at the deformation front of the Brooks Range resulted from a Tertiary contraction event unrelated to the Mesozoic Brookian orogeny.

2.4 ARCTIC ALASKA TERRANE

The Arctic Alaska terrane (Figs. 2.3, 2.4 & 2.6) is the most extensive terrane of northern Alaska and the Brooks Range. It consists mostly of Proterozoic to Cenozoic rocks with North American continental margin affinities (Plafker & Berg, 1994; Young, 2004)

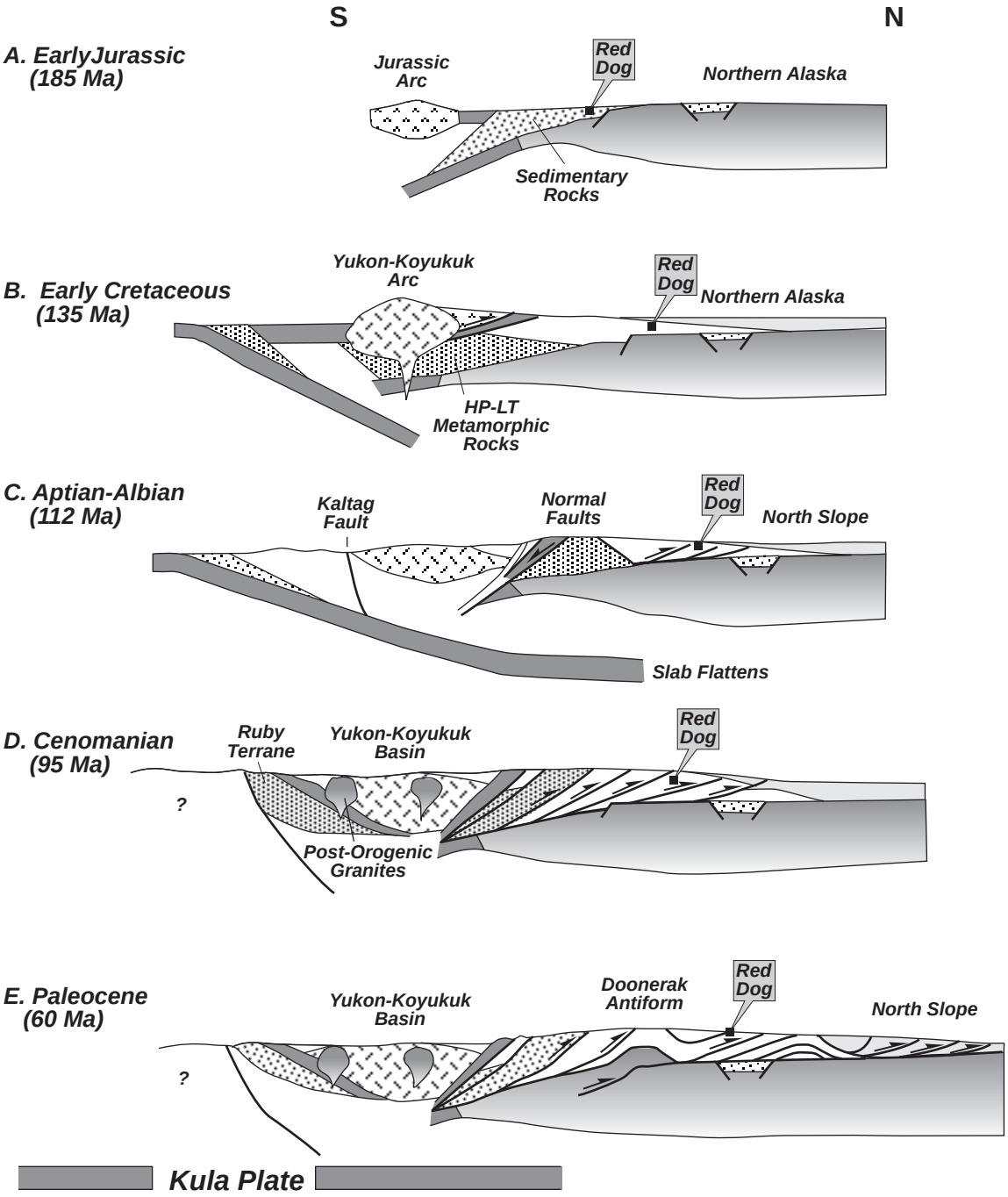


Figure 2.10. Sequence of tectonic events in northern Alaska from Jurassic to Tertiary (Paleocene) (modified from Blythe *et al.* 1996). **A.** By the Early Jurassic, an island arc had overriden the rifted continental margin of Arctic Alaska. **B.** Little or no further contraction occurred until *ca.* 135 Ma, when a N-dipping subduction zone and the Yukon-Koyukuk arc formed, causing renewed deformation in northern Alaska. **C.** At *ca.*113 Ma, the subduction zone flattened, causing uplift and erosion in the southern Brooks Range. Rapid deposition began in the North Slope and Yukon-Koyukuk basins. **D.** By *ca.* 95 Ma deformation had ceased in the Brooks Range, and post-orogenic granites intruded the Yukon-Koyukuk basin. **E.** At 60 Ma flat-slab subduction of the Kula Plate induced the development of the Doonerak antiform and thrust faulting and folding in the North Slope foreland basin. The projected location of the Red Dog district is shown schematically.

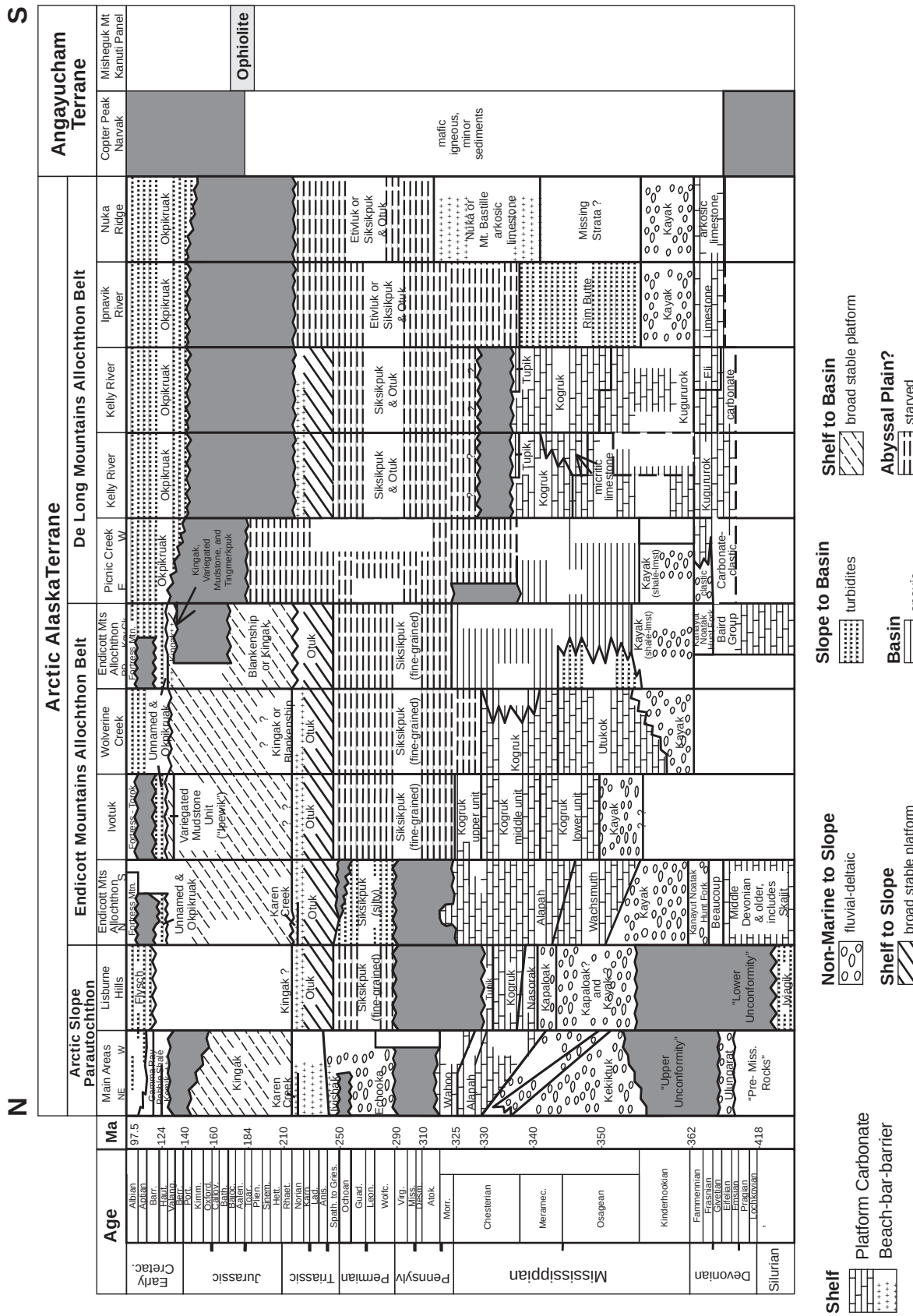


Figure 2.11. Summary tectonostratigraphy of the Brooks Range (modified from Young, 2004).

(Figs. 2.10 & 2.11) that were deposited upon a continental crust of unknown thickness and composition (Moore *et al.* 1994). The Arctic Alaska terrane is characterized by a collision orogen (Brooks Range fold and thrust belt) in its southern part (Fig. 2.5), a foreland basin (North Slope foreland basin) in the central part (Fig. 2.5), and by an Atlantic-type rifted continental margin (Barrow Arch and Canada Basin) in the northernmost part (Mull, 1982; Grantz *et al*. 1990, 1991, 1994; Moore *et al*. 1994; Young, 2004) (Figs. 2.4 & 2.6f). A large portion of the Arctic Alaska terrane is believed to be autochthonous to parautochthonous and lies north of, under and also possibly south of the Brooks Range fold and thrust belt (Young, 2004) (Figs. 2.5 & 2.6). Its extension to the west is not well constrained and it possibly extends under the Hope basin in the Chukchi Sea (Fig. 2.4) into the Chukotka Peninsula of easternmost Russia (Churkin & Trexler, 1981; Fujita & Newberry, 1982; Box, 1985; Moore *et al*. 1994; Klemperer *et al*. 2002; Amato *et al.* 2004). To the south, the Arctic Alaska terrane is separated from the Angayucham, Koyukuk and Ruby terranes, and the Yukon-Koyukuk basin along the E-W-trending dextral strike-slip Kobuk fault (Dillon, 1989; Moore *et al.* 1994; Avé Lallemant *et al*. 1998; Young, 2004) (Figs. 2.1, 2.2h & 2.4). To the east, the Arctic Alaska terrane is bounded by a complex and poorly understood deformation zone in the Yukon and Northwest Territories of Canada (Moore *et al*. 1994; Avé Lallemant *et al*. 1998) (Fig. 2.1).

2.4.1 Tectonic Affinity of the Arctic Alaska Terrane

The Arctic Alaska terrane has been interpreted as an ancient S-facing (Present Day coordinates) Atlantic-type continental passive margin (Tailleur, 1969; Tailleur & Brosgé, 1970; Mull, 1982; Moore *et al*. 1986; Mayfield *et al*. 1988; Moore *et al*. 1994; Young, 2004) developed to the south of an ancestral continental highland, which formed the source area for strata of the passive margin during Late Palaeozoic to Late Mesozoic time (Mayfield *et al*. 1988; Moore *et al*. 1994; Young, 2004) (Figs. 2.6a, 2.8a, b, 2.11 & 2.12). This continental passive margin is interpreted to be the tectonic setting in which the Mississippian sediment-hosted Zn-Pb-Ag and barite deposits of the Red Dog district formed (Moore *et al.* 1986; Young, 2004). The passive margin consisted of Late Devonian to Jurassic strata that were deposited in fluvial to deep marine environments (Tailleur & Brosgé, 1970; Mull, 1982; Moore *et al*. 1986; Mayfield *et al*. 1988; Moore *et al.* 1994; Young, 2004) (Fig. 2.11). The crustal structure of the passive

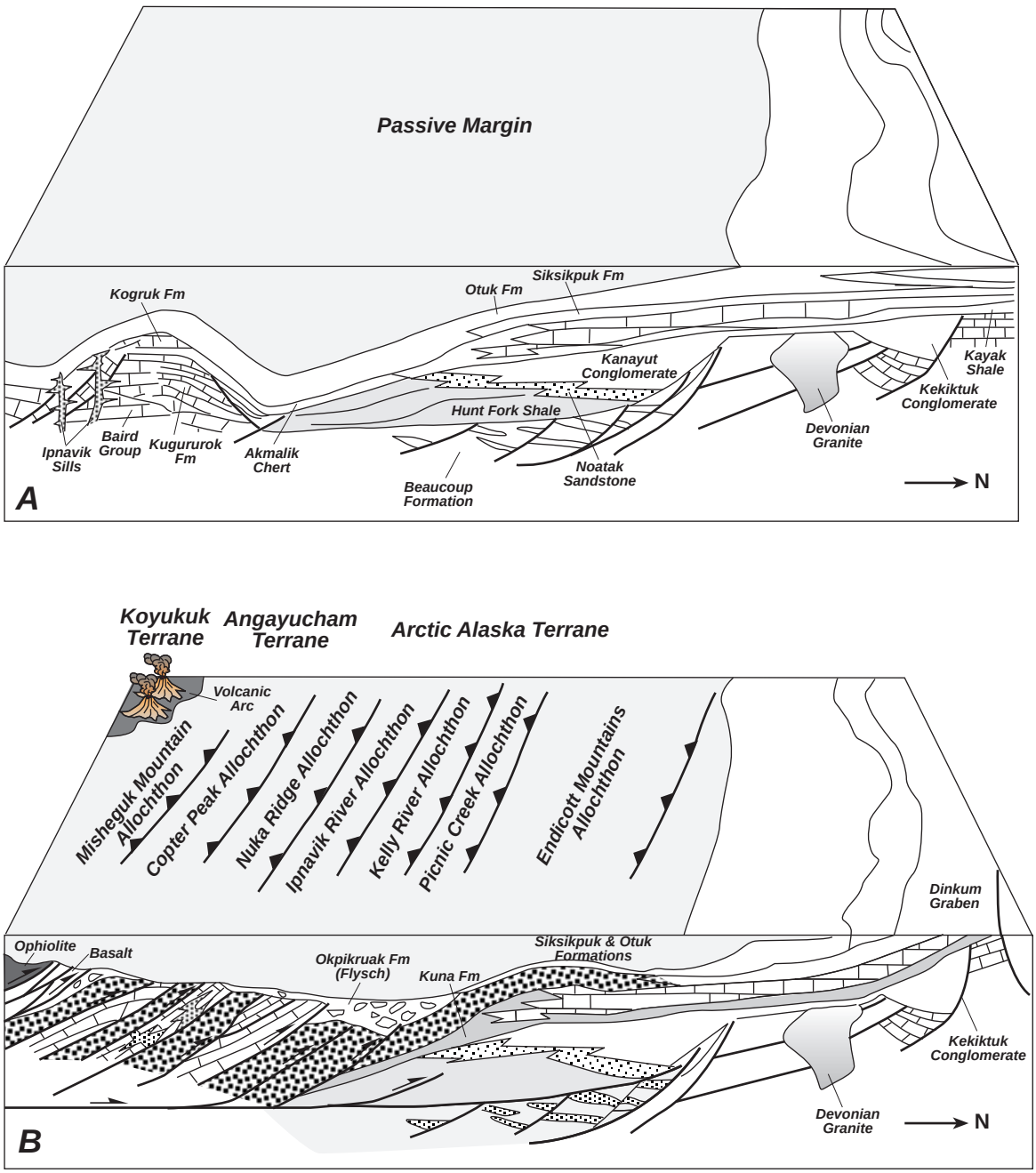


Figure 2.12. Paleogeography and structure of the continental margin of Arctic Alaska in (A) Jurassic time and (B) during the Brookian orogeny in Early Cretaceous (modified from Moore *et al.* 1994).

margin is unknown in that intense thrusting and folding and subduction of the basement (Fig. 2.6) have obscured many of the original geological relationships (e.g. Mull, 1982; Mayfield *et al*. 1988; Moore *et al.* 1994; Young, 2004).

Moore *et al*. (1986) proposed a horst-and-graben model, with carbonate platform sedimentation on basement highs and deep-water restricted and starved sedimentation in the grabens (Moore *et al*. 1986). This setting was characterized by local condensed sedimentation and deposition of black shales and pelagic strata in which the Zn-Pb-Ag and barite deposits of the western Brooks Range were hosted (Moore *et al*. 1986; Young, 2004). The passive margin was subsequently subducted and telescoped in Middle Jurassic to Early Cretaceous during the Brookian orogeny (Figs. 2.6, 2.8c, 2.10 & 2.11b) forming the Brooks Range foreland fold and thrust belt (Mull, 1982; Mayfield *et al*. 1988; Moore *et al*. 1994) (Figs. 2.4 & 2.5).

2.4.2 Origin of the Arctic Alaska Terrane

The site where the Arctic Alaska terrane originated is controversial (e.g. Moore *et al.* 1994; Lewchuk *et al*. 2004; Young, 2004). The Arctic Alaska terrane is considered a suspect terrane (Coney & Jones, 1985) in that its relation to the North American craton and neighbouring terranes is uncertain (Moore *et al*. 1994) (Fig. 2.3). Several models for the origin of the Arctic Alaska terrane and the opening of the Canada basin have been proposed (Carey, 1958; Bogdanov & Tilman, 1962; Tailleur, 1969; Rickwood, 1970; Tailleur, 1973; Herron *et al*. 1974; Churkin & Trexler, 1980; Jones, 1980; Churkin & Trexler, 1981; Dutro, 1981; Nilsen, 1981; Jones, 1982; Mull, 1982; McWhae, 1986; Oldow *et al*. 1987; Smith, 1987; Grantz *et al*. 1990; Moore *et al.* 1994; Plafker & Berg, 1994; Lane, 1997; Grantz *et al*. 1998; Lewchuk *et al*. 2004) (Fig. 2.13).

The most widely accepted model is that of rifting and counter-clockwise rotation of the Arctic Alaska terrane away from northernmost Canada about a pole of rotation located near the MacKenzie River Delta (*ca*. latitude 68°N longitude 137°W) during Late Jurassic to early Late Cretaceous time (Carey, 1958; Tailleur, 1969, 1973; Rickwood, 1970; Mull, 1982; McWhae, 1986; Grantz *et al*. 1990; Moore *et al*. 1994; Plafker & Berg, 1994; Grantz *et al.* 1998) (Figs. 2.2d, e & 2.13a). Rifting and the subsequent opening of the Canada basin (Fig. 2.6d – f) is believed to have taken place after a 100

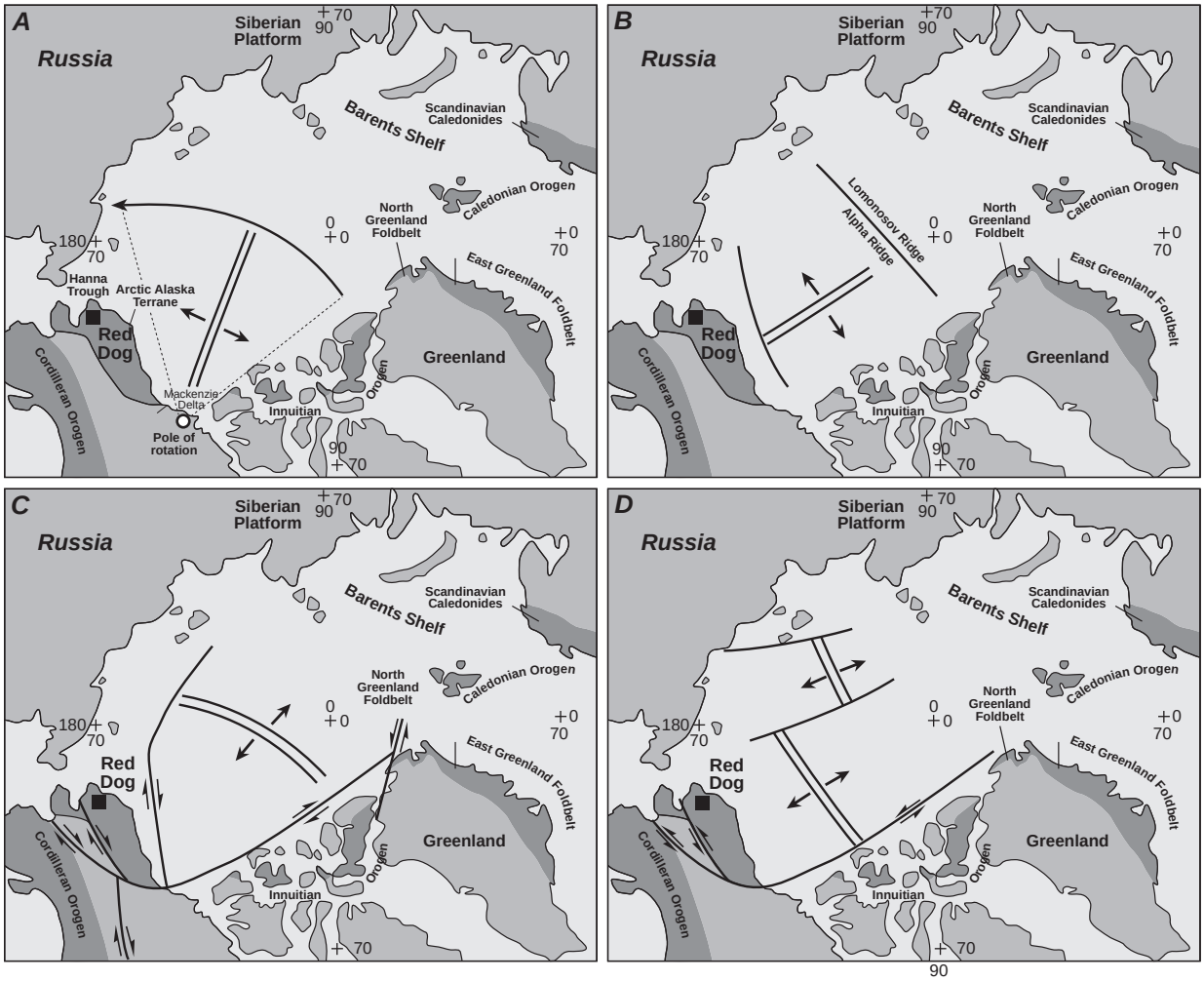


Figure 2.13. Palaeotectonic maps showing possible restorations of the Arctic Alaska terrane to positions in the Cordilleran, Innuitian, and Caledonian orogen (modified from Moore *et al.* 1994). **A.** Rotational origin. Arctic Alaska is rotated oroclinally from Innuitian orogen about a pole of rotation near the MacKenzie delta (Carey, 1958; Tailleur, 1969, 1973; Rickwood, 1970; Newman *et al.* 1977; Mull, 1982; Sweeny, 1982; McWhae, 1986; Howell & Wiley, 1987; Ziegler, 1988; Grantz *et al.* 1990; Grantz & May, 1993). **B.** In-situ origin (Bogdanov & Tilman, 1964; Herron *et al.*1974; Churkin & Trexler, 1980, 1981). **C.** Yukon origin. Arctic Alaska terrane is translated by large scale right slip along Tintina fault from position in northern Canadian part of Cordilleran orogen and is offset right laterally along Porcupine lineament (Jones, 1980, 1982). **D.** Barents shelf origin. Arctic Alaska is translated by large-scale left slip along transform fault parallel to Canadian Arctic Islands shelf edge from original position in northern Caledonian or Innuitian orogens (Dutro, 1981; Nilsen, 1981; Oldow *et al.* 1987; Smith,1987). The location of the Red Dog district is shown schematically.

Ma interval of extension and failed rifting (Grantz & May, 1983; Hubbard *et al.* 1987; Grantz *et al*. 1990) that resulted in the opening of the Dinkum Graben, north of the Barrow Arch (Grantz *et al*. 1994; Moore *et al.* 1994) (Figs. 2.4 & 2.6b, c). Alternative non-rotational models (Figs. 2.13b – d) have been proposed by Bogdanov & Tilman (1964), Herron *et al*. (1974), Churkin & Trexler (1980, 1981), Jones (1980, 1982), Dutro (1981), Nilsen (1981), Oldow *et al.* (1987), Smith (1987) and Lane (1997). Lane (1997) proposed a series of complex multiple rift-drift events that did not require rotation of northern Alaska. Mull (1982) discussed the implications of rotation of the Arctic Alaska terrane for the tectonic evolution of the Brooks Range and argued that the apparent increase in shortening from east to west supports the rotation hypothesis.

Palaeomagnetic studies have been used to test the possible rotational origin of the Arctic Alaska terrane (e.g. Newman *et al*. 1979; Halgedahl & Jarrard, 1987; Hillhouse & Grommé, 1988; Harbert *et al.* 1990; Hillhouse & Coe, 1994; Lewchuk *et al.* 2001, 2004). Halgedahl & Jarrard (1987) and Harbert *et al*. (1990) supported the rotation hypothesis. In contrast, Lewchuk *et al*. (2001, 2004) have proposed that the palaeomagnetic data possibly indicated that the Arctic Alaska terrane did not remain fixed in its current orientation with respect to the North American craton but also stated that the data were not sufficient to differentiate between the rotational and translational models.

2.4.3 Stratigraphy of the Arctic Alaska Terrane

The stratigraphy of the Arctic Alaska terrane has been summarized by Martin (1970), Tailleur & Brosgé (1970), Mull (1982), Moore *et al*. (1986), Mayfield *et al.* (1988), Moore *et al*. (1994) and Young (2004) amongst others. Stratigraphic nomenclature of the Brooks Range and in particular the Arctic Alaska terrane is complex (Dumoulin *et al*. 2004; Young, 2004). The Arctic Alaska terrane (Fig. 2.11) consists of Late Devonian to Cretaceous strata that were deposited during rifting and development of the ancient continental passive margin of Alaska and also during the Brookian orogeny.

2.4.4 Structural Units of the Artic Alaska Terrane

The Arctic Alaska terrane can be subdivided into seven distinct structural units, which are broadly coincident with structural domains of the Brooks Range orogenic belt (Karl

& Mull, 1993; Moore *et al*. 1994; Young, 2004). These are the Arctic Slope parautochthon, the allochthon belts and the North Slope foreland basin, which form the northern and external part of the orogen, and the Hammond metamorphic belt, Schist belt and the Slate Creek structural belt that form the southern and more internal part of the orogen (Mull, 1982; Karl & Mull, 1993; Moore *et al*. 1994, Young, 2004) (Fig. 2.4). The Hammond metamorphic belt, the Schist belt, and to a lesser extent the Slate creek structural belt show some evidence of linkage to the Arctic Slope parautochthon (L. E. Young, 2002, *pers. comm.*).

The Allochthon Belts

The allochthons of the Arctic Alaska terrane consist of thrust fault bounded units of Devonian through Cretaceous clastic and carbonate strata that have been stacked, gently folded and eroded forming numerous klippen and windows (Martin, 1970; Tailleur & Brosgé, 1970; Moore *et al*. 1986; Mayfield *et al*. 1988; Moore *et al*. 1994; Young, 2004) (Figs. 2.4, 2.5 & 2.14). These allochthon belts form the fold and thrust belt of the Brooks Range and are extensively preserved in the western and central Brooks Range (Figs. 2.4, 2.5 & 2.14). The allochthon belts are important for the purposes of this study as these occur in the Red Dog district.

Fault-bounded sedimentary successions of the Brooks Range were firstly recognized and described by Tailleur *et al*. (1966, 1967), Snelson & Tailleur (1968), Tailleur & Brosgé (1970), and Martin (1970). Tailleur & Brosgé (1970) firstly referred to the allochthon belts of as the ‘disturbed belt’ because of their discontinuity and structural complexity. These were first named ‘thrust tectonic units’ (Snelson & Tailleur, 1968; Tailleur & Brosgé, 1970) and subsequently referred to as ‘thrust sequences’ (Mayfield *et al*. 1978), allochthons (Mayfield *et al*. 1983, 1988; Moore *et al*. 1986; Mull *et al*. 1987*b*; Mull, 1989) and/or subterranes (Jones *et al*. 1987; Moore *et al*. 1992). A better understanding of the allochthons and stacking patterns was achieved with the studies of Dutro *et al.* (1976), Ellersieck *et al.* (1979), Mull (1979, 1982, 1985), Ellersieck *et al.* (1984), Moore *et al.* (1986), Mayfield *et al*. (1988), and Young (1992).

Each allochthon is interpreted as an almost coeval portion of the ancient continental passive margin of Arctic Alaska and as a group they are believed as having been deposited contiguously (Mayfield *et al.* 1988; Moore *et al.* 1994). The Brooks Range

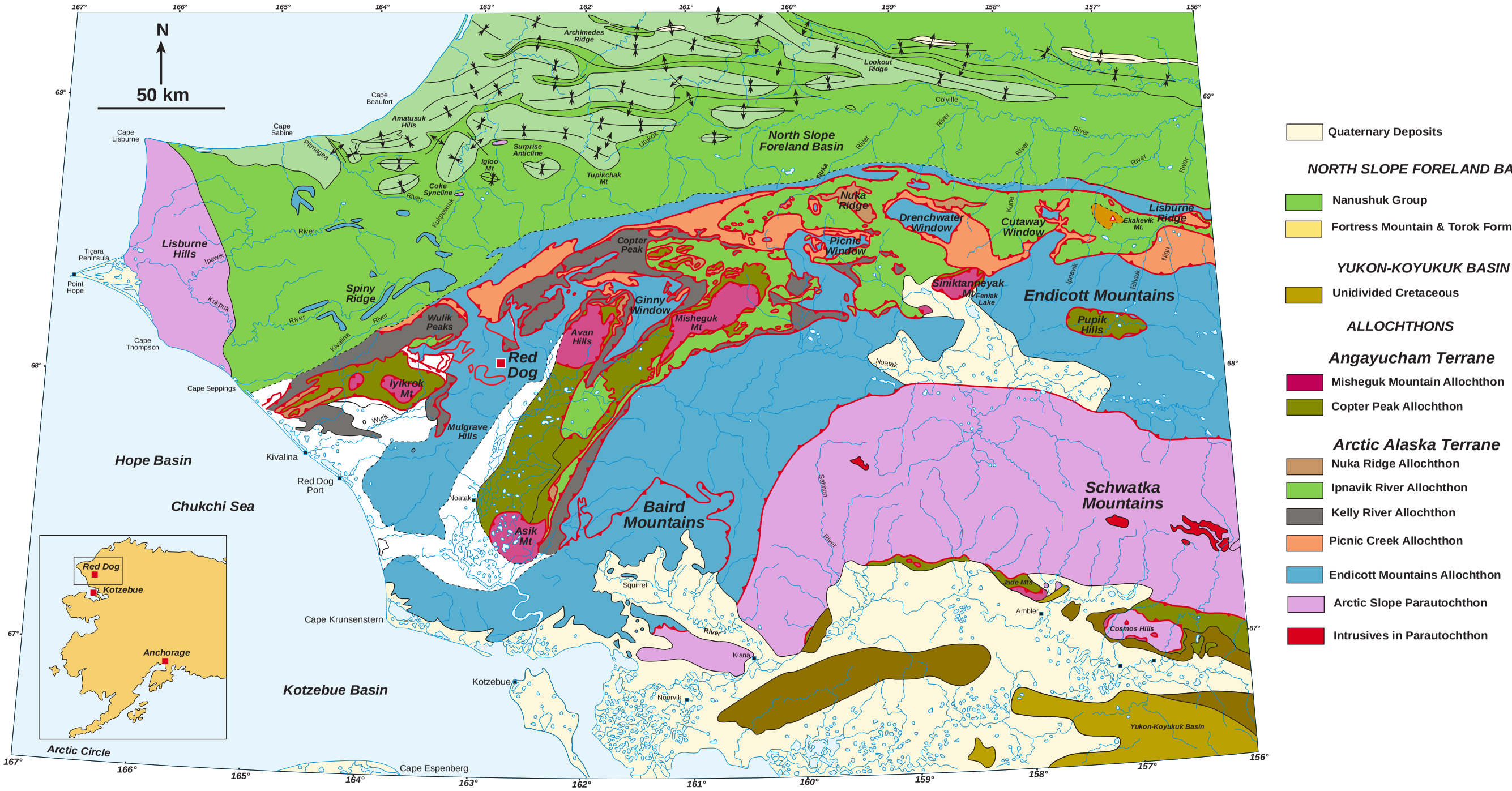


Figure 2.14a. Structural map of the western Brooks Range (modified from Mayfield *et al.* 1988; Moore *et al.* 1994). The location of the Red Dog mine is shown schematically.

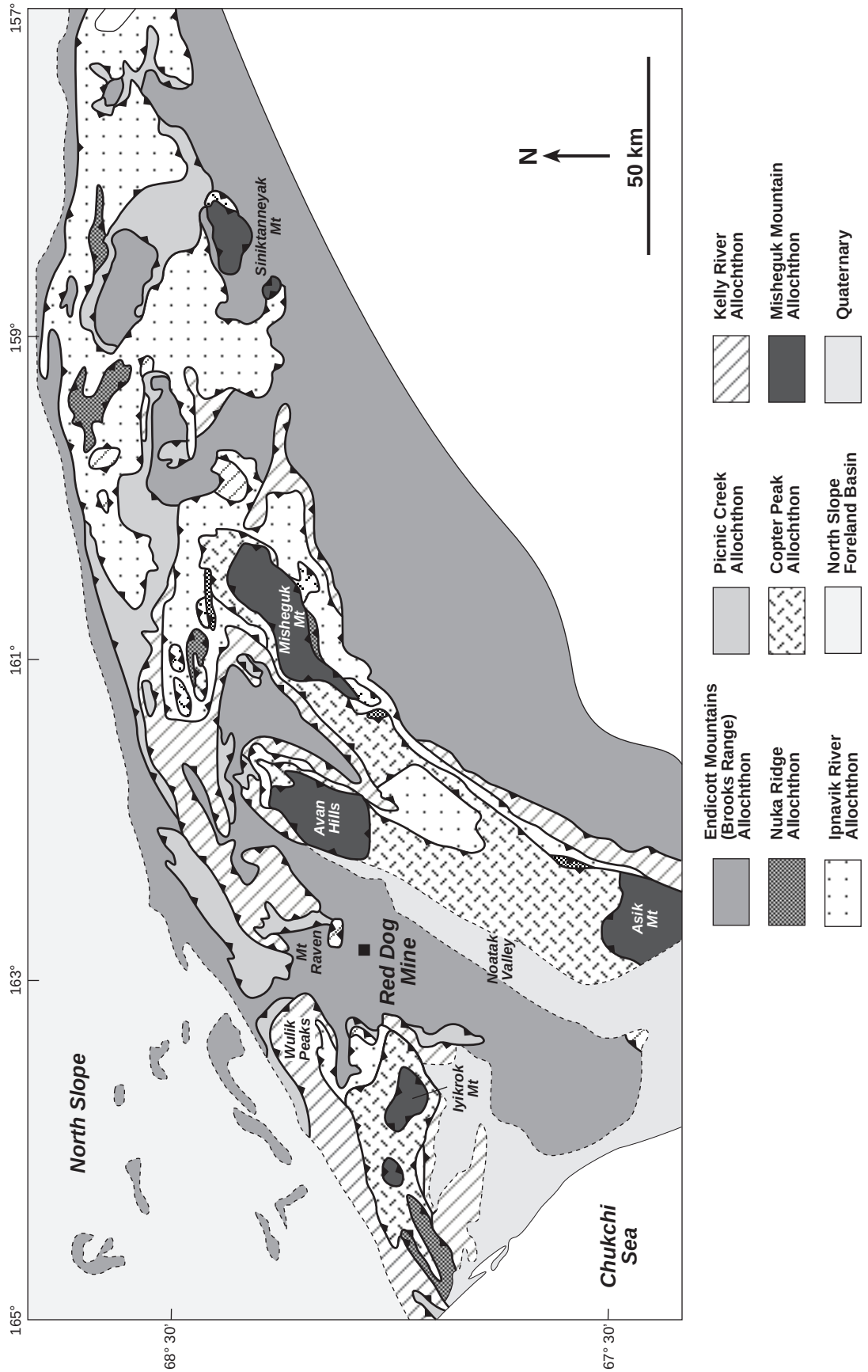


Figure 2.14b. Simplified allochthon map of the De Long Mountains of the western Brooks Range (modified from Mayfield *et al.* 1988; Moore *et al.* 1994). The location of the Red Dog mine is shown.

comprises two main allochthon belts. These are the Endicott Mountains allochthon belt and the De Long Mountains allochthon belt (Karl & Mull, 1993). The Endicott Mountains and the De Long Mountains allochthon belts have also been referred to as the Endicott Mountains subterrane (Moore *et al*. 1992, 1994; Young, 2004) and De Long Mountains subterrane, respectively (Moore *et al*. 1992, 1994). The De Long Mountains allochthon belt has also been referred to as the Sheenjek terrane in the eastern Brooks Range (Jones *et al*. 1987).

The Endicott Mountains allochthon belt consists of the Endicott Mountains allochthon (Mull, 1982; Moore *et al*. 1994) of the central Brooks Range, and the Brooks Range and Wolverine Creek allochthons of the western Brooks Range (Martin, 1970; Moore *et al*. 1986; Young, 1992). The De Long Mountains allochthon belt (Karl & Mull, 1993) contains the Picnic Creek, Kelly River, Ipnavik River, and Nuka Ridge allochthons (e.g. Moore *et al*. 1994; Young, 2004) (Fig. 2.14). These allochthons consist of Late Devonian to Early Cretaceous sedimentary successions (Moore *et al*. 1994) (Fig. 2.11). The allochthons of the De Long Mountains allochthon belt are stratigraphically similar to the Endicott Mountains allochthon belt and only differ in some of their Mississippian to Early Cretaceous stratigraphy (Moore *et al*. 1994; Young, 2004) (Fig. 2.11). The Endicott Mountains and De Long Mountains allochthon belts are of special significance in this study in that are widely exposed in the Red Dog district. Structural data for most of the allochthons are scarce and limited to reconnaissance style studies (e.g. Tailleur *et al*. 1967; Martin, 1970; Mayfield *et al*. 1988; Ellersieck *et al*. 1990*a*, *b*; Moore *et al*. 1994; Young, 2004)

Endicott Mountains Allochthon

The Endicott Mountains allochthon (Martin, 1970) is the most extensive of the Arctic Alaska terrane (Moore *et al*. 1994). It extends for about 900 km from the Chukchi Sea on the west to the easternmost Brooks Range in the east (Fig. 2.4). The thickness of the Endicott Mountains allochthon ranges from 1500 m in the western Brooks Range (Fig. 2.5a) to as much as 6 km in the central Brooks Range (Moore *et al*. 1994) (Fig. 2.5b). The Endicott Mountains allochthon hosts the sediment-hosted Zn-Pb-Ag and barite deposits of the Red Dog district (Moore *et al*. 1986; Young, 1989, 2004). The Endicott Mountains allochthon also includes the Brooks Range and Wolverine Creek allochthons

of Martin (1970), Moore *et al*. (1986) and Young (1992). The Endicott Mountains allochthon consists of Late Devonian to Early Cretaceous sedimentary and minor igneous rocks (Moore *et al*. 1994, Young, 2004). The Brooks Range allochthon of the western Brooks Range has traditionally been subdivided into two distinct stacked sequences. In ascending structural order, these are the Red Dog and Key Creek sequences. The Red Dog sequence is characterized by Early to Late Mississippian black shales that host the mineralization of the Red Dog district.

Picnic Creek Allochthon

The Picnic Creek allochthon (Ellersieck *et al*. 1979) was named for exposures in the Picnic Creek window in the eastern De Long Mountains. Information from the Picnic Creek allochthon is scarce (Mull *et al*. 1987*a*; Moore *et al*. 1994). The Picnic Creek allochthon contains Late Devonian to Early Cretaceous sedimentary rocks. The characteristic feature of the Picnic Creek allochthon is the presence of deep water Mississippian stratigraphy (Mull *et al.* 1987*a*).

Kelly River Allochthon

The Kelly River allochthon (Snelson & Tailleur, 1968) is found exclusively in the western Brooks Range (Martin, 1970; Moore *et al*. 1986; Mayfield *et al*. 1988; Moore *et al*. 1994; Young, 2004). The Kelly River allochthon has been subdivided into at least four lithostratigraphically distinct sequences (e.g. Moore *et al.* 1986; Mayfield *et al.* 1988; Young, 2004) and consists of Late Devonian to Early Cretaceous sedimentary rocks. The characteristic feature is extensive carbonate platform strata of Late Devonian and Carboniferous age.

Ipnavik River Allochthon

The Ipnavik River allochthon or Ipnavik Tectonic unit (Snelson & Tailleur, 1968) and the Nuka Ridge allochthon (Tailleur *et al*. 1966) form the structurally highest levels of the Arctic Alaska terrane (Fig. 2.14). The Ipnavik River allochthon is characterized by deep water Mississippian strata that are locally intruded by mafic sills (Moore *et al*. 1994; Young, 2004).

Nuka Ridge Allochthon

The Nuka Ridge allochthon (Tailleur *et al*. 1966) is locally exposed across the Brooks Range and is poorly understood. The Nuka Ridge allochthon is characterized by abundant arkose and arkosic limestone of Mississippian age.

Arctic Slope Parautochthon

The Arctic Slope parautochthon (Karl & Mull, 1993), also referred to as the North Slope terrane or North Slope subterrane (Jones *et al*. 1987; Moore *et al*. 1992; Moore *et al*. 1994), refers to the autochthonous to parautochthonous portion of the Arctic Alaska terrane that underlies the allochthons of the Brooks Range fold and thrust belt and strata of the North Slope foreland basin (Mull, 1982; Karl & Mull, 1993; Young, 2004) (Figs. 2.4, 2.5 & 2.15). Geologic information on the Arctic Slope parautochthon is scarce and comes primarily from petroleum-industry seismic reflection profiles, exploration wells (e.g. Bird, 1982; Bruynzeel *et al*. 1982; Grantz & May, 1983; Kirschner *et al*. 1983; Bird, 1998) and from limited exposures across the Brooks Range fold and thrust belt (Moore *et al*. 1994; O'Sullivan *et al*. 1998) (Figs. 2.4 & 2.5). The Arctic Slope parautochthon is exposed in the eastern Brooks Range, the Mount Doonerak window of the central Brooks Range, in the Lisburne Hills, and in the Swatchka Mountains of the southern Brooks Range (Mull, 1982; Mayfield *et al*. 1988; Moore *et al*. 1994; Young, 2004) (Figs. 2.4, 2.5, 2.14 & 2.16). The Arctic Slope parautochthon preserves the structure of the ancient continental margin of the Arctic Alaska terrane as a series of Paleozoic graben and half graben structures that include the Umiat and Ikpikpuk basins (Figs. 2.15 & 2.16).

The Arctic Slope parautochthon comprises three major megasequences. These are from oldest to youngest, the Franklinian, Ellesmerian, and Brookian megasequences (Lerand, 1973; Grantz & May, 1979; Hubbard *et al*. 1987; Moore *et al*. 1994; Young, 2004) (Fig. 2.13). The Franklinian Megasequence has traditionally been referred to as the 'Pre-Mississippian rocks' or the 'Pre-Mississippian sequence' (Bird & Molenaar, 1987; Moore *et al*. 1994) and is unconformably overlain by Mississippian strata over much of the Arctic Alaska terrane. The Ellesmerian Megasequence has been interpreted to record sedimentation on a subsiding fold and thrust belt (Nilsen, 1981; Hubbard *et al*.

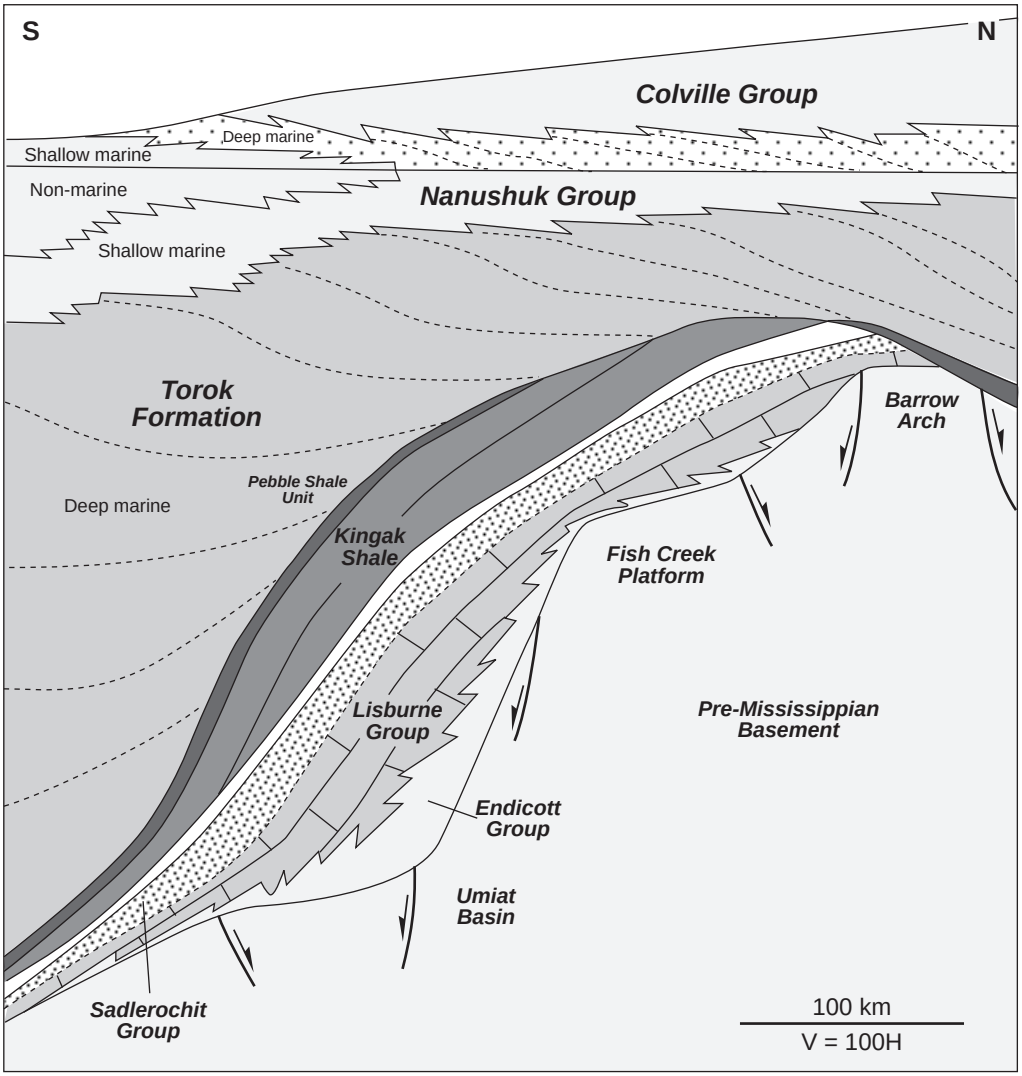


Figure 2.15. Regional cross section illustrating the stratigraphic relationships in the North Slope foreland basin, north of the Brooks Range (modified from Moore *et al.* 2002). Refer to Figure 2.4 for location of section. Note basement highs (Barrow arch) and basins filled with strata of the Endicott Group (Umiat basin).

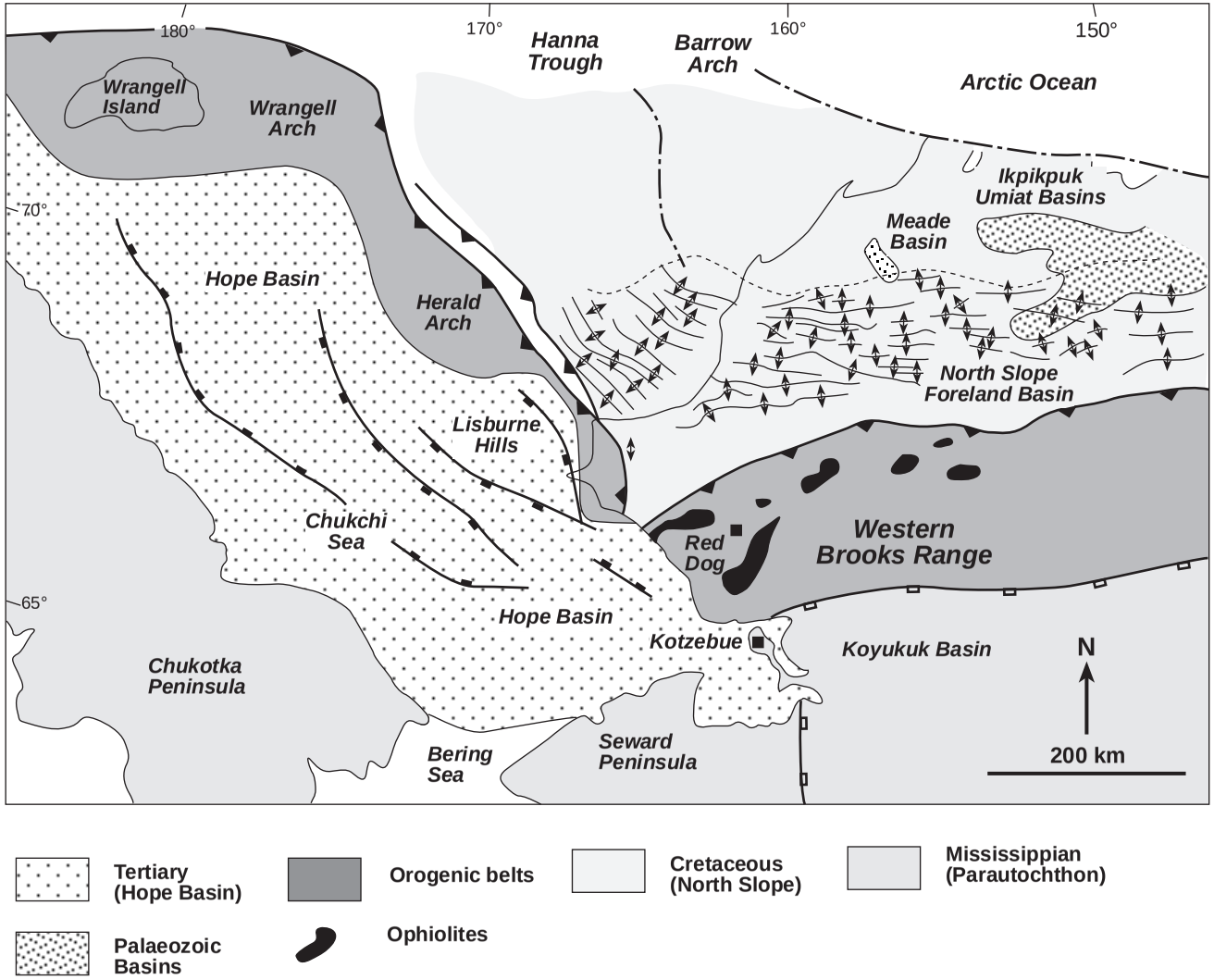


Figure 2.16. Map of northwestern Alaska showing the structural relationships between the Brooks Range and the Lisburne Hills-Herald Arch fold and thrust belts (modified from Moore *et al.* 2002). The location of the Red Dog district is shown.

1987) or alternatively Late Devonian to Jurassic sedimentation on a S-facing (Present-Day coordinates) passive continental margin (Mull, 1982; Moore *et al.* 1994).

The Brookian Megasequence records Early Cretaceous to Tertiary synorogenic sedimentation and the development of a foreland basin related to thrusting and formation of the Brooks Range (Hubbard *et al*. 1987; Grantz *et al*. 1991; Moore *et al*. 1994). Time transgressive correlative rocks to the Ellesmerian and Brookian megasequences of the Arctic Slope parautochthon are preserved in the allochthon belts of the Brooks Range fold and thrust belt (Fig. 2.11). Hubbard *et al*. (1987) identified a fourth megasequence between the Ellesmerian and Brookian Megasequence, referred to as the Beaufortian Megasequence. This is interpreted as sequences deposited during a Jurassic to Early Cretaceous (Early Neocomian) failed rift event that occurred in the north Beaufort shelf, and in the Dinkum Graben (Fig. 2.4) prior to the opening of the Canada Basin. The Beaufortian Megasequence is also known as the upper Ellesmerian beds (Grantz *et al.* 1990) or the Dinkum graben sequence (Moore *et al.* 1994).

The Lisburne Hills-Herald Arch Thrust Belt

The Lisburne Hills-Herald Arch thrust belt (Moore *et al*. 2002) is an uplifted portion of the Arctic Slope parutochthon (L. E. Young, 2002, *pers. comm*.). The Lisburne Hills-Herald Arch thrust belt is exposed in the Lisburne Peninsula, west of the De Long Mountains of the western Brooks Range (Fig. 2.4) and is interpreted to be the onland expression of an 800 km-long arcuate thrust belt that continues northwestward offshore along the Herald and Wrangell arches of the northern Chukchi Sea (Grantz *et al*. 1975; Moore *et al*. 2002*a*) (Figs. 2.4 & 2.16). Payne (1955) firstly introduced the term Tigara Uplift to refer to the onshore expression of this thrust belt in the Lisburne Peninsula. In the Lisburne Hills, the Lisburne Hills-Herald Arch thrust belt is a NNW- to N-trending and dominantly E-verging fold and thrust belt (Moore *et al.* 2002*a*; Young, 2004).

The age of deformation in the Lisburne Hills-Herald Arch thrust belt has not been determined precisely (Moore *et al*. 1994). It has been regarded as Late Cretaceous or Tertiary by Patton & Tailleur (1977) and Grantz *et al*. (1981), but Mull (1979, 1985, 2002, *pers. comm.*) based on stratigraphic relationships and palaeocurrent analyses suggests that the thrust belt was probably active in late Early Cretaceous (Albian) or even earlier. The minimum age of thrusting is solely constrained by undeformed

middle Eocene (Pre-41 Ma) strata of the Hope basin that unconformably overlie the Lisburne Hills-Herald Arch thrust belt south of Point Hope in the Chukchi Sea (Tolson, 1987; Moore *et al.* 1994; Klemperer *et al.* 2002; Moore *et al.* 2002*a*) (Figs. 2.4 & 2.16).

Lisburne Hills-Herald Arch – Brooks Range Relationship

The structural relationship between the Lisburne Hills-Herald Arch and western Brooks Range thrust belts and their relative timing of deformation remain controversial (Moore *et al*. 2002*a*). The Lisburne Hills-Herald Arch thrust belt has been interpreted as the structural continuation of the Brooks Range fold and thrust belt, either formed originally along a different trend or later bent oroclinally (Tailleur & Brosgé, 1970; Patton & Tailleur, 1977; Moore *et al.* 2002*a*). This has been referred to as the Chukchi syntaxis (Tailleur & Brosgé, 1970). Alternatively, Grantz *et al*. (1975, 1981) and Mayfield *et al*. (1988) suggested that the Lisburne Hills-Herald Arch formed in Late Cretaceous or Early Tertiary time by a contractional event unrelated to the Brookian orogeny. This implies that average northeast-southwest structural trend of the western Brooks Range (Figs. 2.4, 2.14 & 2.16), which broadly parallels the structural grain of the Lisburne Hills, was caused by a late event that did not involve oroclinal bending. Karl & Long (1990) ascribed the curvature of the western Brooks Range to E-verging thrusting superimposed on N- to NW-directed Brookian thrusting. L. E. Young (2002, *pers. comm.*) and C. G. Mull (2002, *pers. comm.*) argued that the Lisburne Hills-Herald Arch and western Brooks Range do not represent a syntaxis but two separate thrust belts. L. E. Young (2002, *pers. comm.*) suggested that the Lisburne Hills-Herald Arch is a separate thrust belt that was developed upon strata of the Arctic Slope parautochthon, now buried underneath synorogenic strata of the North Slope foreland basin. Moore *et al.* (2002*a*) suggested that the Lisburne Hills-Herald Arch thrust belt formed without oroclinal bending as the northward continuation of the Brooks Range fold and thrust belt. Moore *et al*. (2002*a*) argue that the Lisburne Hills-Herald Arch thrust belt could have not formed as a separate orogen in response to convergence between North America and Eurasia in Early Tertiary time but instead originated as a component of the Brooks Range orogen that was reactivated during Cenozoic contraction.

North Slope Foreland Basin

The North Slope foreland basin (Bird, 1982, 1988; Moore *et al*. 1994) (Figs. 2.4, 2.5 & 2.15), also referred to as the Colville basin (Mayfield *et al.* 1988; Cole *et al*. 1997; Young, 2004), spans the Arctic Foothills and Arctic Coastal Plain. It is filled with more than 10 km of Late Jurassic to Present Day deep marine to continental synorogenic strata (Grantz *et al*. 1991; Moore *et al*. 1994) that were deposited northward from the advancing Brooks Range fold and thrust belt (Mull, 1982; Bird, 1988; Molenaar, 1988; Grantz *et al*. 1991; Moore *et al.* 1994; Handschy, 1998*a*; Young, 2004) (Figs. 2.6f, 2.7a, b & 2.15). Synorogenic strata of the North Slope foreland basin overlie strata of the Arctic Slope parautochthon (Bird, 1982; Bird & Molenaar, 1987; Bird, 1988; Moore *et al*. 1994; Young, 2004) (Fig. 2.15). The northern extent of the North Slope foreland basin is delineated by the Barrow arch, a broad WNW-ESE-trending basement high that formed in the Palaeozoic and was subsequently reactivated during the opening of the Canada basin in Jurassic and Cretaceous time (Grantz & May, 1979; Grantz *et al*. 1990, 1991, 1994; Moore *et al.* 1994) (Figs. 2.4, 2.5, 2.6, 2.14, 2.15 & 2.16). Strata of the North Slope foreland basin have been gently folded into broad open synclines and tight anticlines with fold axial traces that are dominantly E-W-trending (Mull, 1982, 1985, 1989; Mayfield *et al*. 1988) (Figs. 2.4, 2.9 & 2.16). Deformation of the foreland basin strata has been ascribed to the late Brookian deformation event and/or subsequent episodic deformation in the Cenozoic (Mull, 1982, 1985; Moore *et al*. 1994, 1997*b*; O'Sullivan *et al*. 1997; Young, 2004).

Hammond Metamorphic Belt

The Hammond metamorphic belt (Karl & Mull, 1993), also referred to as the Hammond subterrane (Moore *et al*. 1994), extends for approximately 800 km along the southern Brooks Range (Fig. 2.4). It consists of an imbricated assemblage of thick carbonate and clastic units with phyllitic and schistose textures, greenschists and locally blueschists and amphibolite facies metamorphic mineral assemblages (Jones *et al*. 1987; Moore *et al*. 1994). The Hammond metamorphic belt shares common features with the Arctic Slope parautochthon, such as a well-developed pre-Mississippian unconformity (Mull, 1982). The Hammond metamorphic belt shares similarities with the Kootenay terrane and contained subterranes of the North American Cordillera, which form part of the

Yukon-Tanana terrane in Alaska (Silbering & Jones, 1984; Plafker & Berg, 1994) (Fig. 2.3).

Schist Belt

The Schist belt (Karl & Mull, 1993) (Fig. 2.4), also referred to as the Coldfoot terrane (Moore *et al*. 1994), is a 850 km long metamorphic belt (Gottschalk, 1990) that comprises Proterozoic to Devonian phyllites, mica-schists and amphibolites (Moore *et al*. 1994; Young, 2004) that is juxtaposed against the Hammond metamorphic belt (Moore *et al*. 1994) (Fig. 2.4). The Schist belt is interpreted to have undergone high-pressure and low-temperature metamorphism (blueschist to eclogite facies), followed by greenschist facies retrograde metamorphism (Gottschalk *et al*. 1998). The earlier blueschist – eclogite facies metamorphic event is believed to have taken place in the Middle to Late Jurassic (Fig. 2.8c) whereas the later retrograde event is interpreted to be Early Cretaceous in age (Gottschalk *et al*. 1998; Gottschalk & Snee, 1998). A link with the Arctic Slope parautochthon is suggested by the occurrence of Devonian intrusives in both belts (L. E. Young, 2002, *pers. comm.*). The Schist belt contains evidence for a Devonian arc, including an extensive belt of major volcanogenic Zn-Cu massive sulphide deposits of the Ambler district (Einaudi & Hitzman, 1986; Hitzman *et al*. 1986; Nokleberg *et al*. 1994; Schmidt, 1997*b*; L. E. Young, 2002, *pers. comm*.; Nokleberg *et al*. 2003)

Slate Creek Structural Belt

The Slate Creek structural belt (Karl & Mull, 1993), also referred to as the Slate Creek terrane (Moore *et al*. 1992) (Fig. 2.4), includes schist, phyllite, and a tectonic melange with blocks of diabase, mafic volcanic rocks, schist, and Mississippian to Triassic chert (Young, 2004) that extend along the southern margin of the Brooks Range (Fig. 2.17a). This tectonic melange has been referred to as the 'autoclastic melange' (Pallister *et al*. 1989) and represents the structural contact with the overlying Angayucham terrane (Moore *et al.* 1994) (Fig. 2.17a).

2.5 ANGAYUCHAM TERRANE

The Angayucham terrane (Jones *et al*. 1987) is an allochthonous unit that consists of ultramafic to felsic igneous rocks and minor siliceous pelagic and carbonate strata of

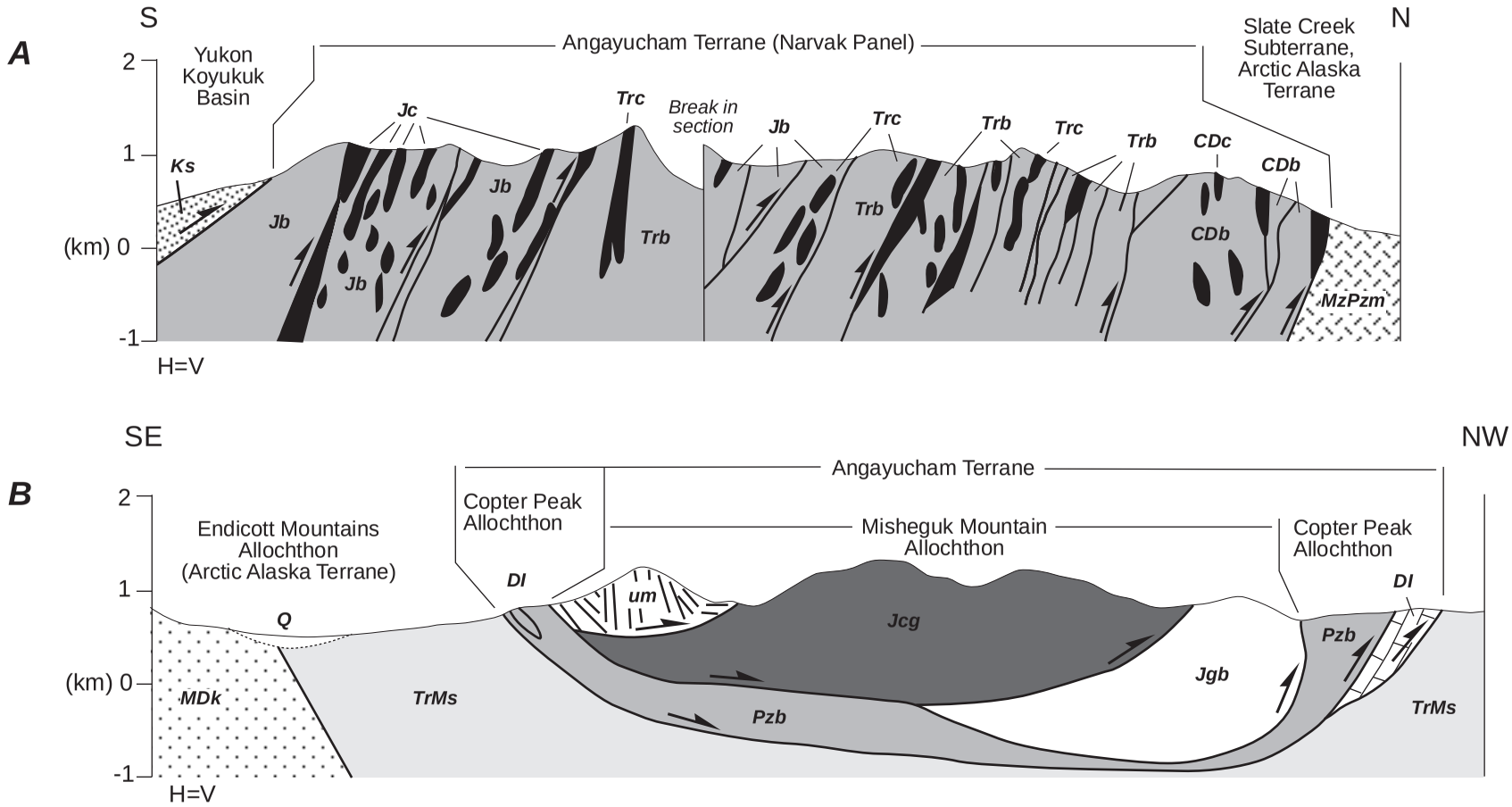


Figure 2.17. Cross sections showing structural relations of the Angayucham terrane. **A.** Angayucham terrane in the southern Brooks Range. Ks: Cretaceous sedimentary rocks; Jb: Jurassic pillow basalt, diabase and micrograbbro; Trc: Triassic chert; CDb: Devonian and Carboniferous pillow basalt, diabase and microgabbro; CDc: Devonian and Carboniferous chert; MzPzm: Autoclastic melange (modified from Pallister *et al*. 1989). **B.** Angayucham terrane at Siniktanneyak Mountain. Q: Quaternary deposits; Jcg: Jurassic (?) cumulate gabbro; Jgb: Jurassic (?) isotropic gabbro with plagiogranite dikes and stocks; TrMs: Mississippian to Triassic sedimentary rocks of undivided Kayak Shale, Lisburne and Etivluk groups; MDk: Devonian and Mississippian (?) terrigenous clastic rocks of the Kanayut Conglomerate; DI: Devonaian fossiliferous carbonate rocks; Pzb: Palaeozoic diabase and pillowed volcanic rocks; um: dunite, harzburgite and pyroxenite (modified from Nelson & Nelson, 1982).

Devonian through Jurassic age (Tailleur, 1968; Martin, 1970; Roeder & Mull, 1978; Moore *et al*. 1994; Harris, 1998, 2004; Young, 2004) (Fig. 2.4). The Angayucham terrane is exposed in a series of S-dipping sheets that extend for more than 500 km along the southern Brooks Range (Pallister *et al*. 1989; Moore *et al*. 1994) (Figs. 2.4, 2.5a, 2.14, 2.16 & 2.17a) and to the north in a series of discontinuous regional synforms in the western Brooks Range (Mull, 1982; Mayfield *et al*. 1988; Moore *et al*. 1994; Patton *et al*. 1994; Harris, 1998, 2004) (Figs. 2.4, 2.5b, 2.14, 2.16 & 2.17b). In the western Brooks Range, the Angayucham terrane crops out in five separate complexes. From west to east these are the Iyikrok Mountain, Avan Hills, Asik Mountain, Misheguk Mountain, and Siniktanneyak Mountain complexes (Martin, 1970; Mayfield *et al*. 1988; Moore *et al*. 1994; Patton *et al*. 1994; Harris, 1992, 1998, 2004; Young, 2004) (Figs. 2.4, 2.14 & 2.17b). The Angayucham terrane is believed to exceed 10 km in thickness in the southern Brooks Range (Pallister & Carlson, 1988; Pallister *et al*. 1989), and is inferred to be 8 to 11 km thick in the western Brooks Range (Barnes & Tailleur, 1970; Morin & Moore, 1996; Saltus *et al*. 2001*a*, *b*; Young, 2004). The contact between the Angayucham terrane and the Arctic Alaska terrane in the southern Brooks Range has been referred to as the Kobuk suture (Mull, 1982, 1989) (Fig. 2.7a) or the Angayucham thrust (Dillon, 1989).

2.5.1 Structural Units of the Angayucham Terrane

The Angayucham terrane consists of two distinct structural units that formed at different sites and were possibly tectonically assembled during the Brookian orogeny (Moore *et al*. 1994; Harris, 1998). A lower unit consists dominantly of imbricated metamorphosed mafic volcanic rocks (Moore *et al*. 1994). This unit is referred to as the Copter Peak allochthon in the fold and thrust belt (Ellersieck *et al*. 1979; Mull, 1982; Moore *et al*. 1986; Mayfield *et al*. 1988, Moore *et al*. 1994) (Figs. 2.4, 2.14 & 2.17b) or the Narvak thrust panel (Patton & Box, 1989) in the southern Brooks Range (Fig. 2.17a). The Copter Peak allochthon has been interpreted as an accretionary prism developed in a suprasubduction zone (Moore *et al*. 1994) (Fig. 2.6b) or a volcanic pile that formed in the distal part of the ancient continental margin of Arctic Alaska (Harris, 1998). The upper unit, which consists dominantly of ultramafic and mafic rocks (Roeder & Mull, 1978; Moore *et al*. 1994), is referred to as the Misheguk Mountain allochthon in the fold and thrust belt (Snelson & Tailleur, 1968; Mull, 1982; Mayfield *et*

al. 1988, Moore *et al*. 1994) (Figs. 2.4, 2.14 & 2.17b) or the Kanuti thrust panel in the southern Brooks Range (Patton & Box, 1989) (Fig. 2.17a). The Misheguk Mountain allochthon consists of tectonized harzburgites, dunites, as well as interlayered pyroxenites, layered and massive gabbros, and late-stage intrusive diorites and plagiogranites (Roeder & Mull, 1978; Moore *et al.* 1994; Harris, 1992, 1998, 2004) and is interpreted as an oceanic crust slab that was obducted on to the ancient continental passive margin of Arctic Alaska during the early stages of the Brookian orogeny (e.g. Roeder & Mull, 1978; Mull, 1982; Mayfield *et al*. 1988; Moore *et al*. 1994; Harris, 1992, 1998, 2004; Young, 2004) (Figs. 2.6 & 2.17b).

2.5.2 Tectonic Affinity of the Angayucham Terrane

Martin (1970) firstly interpreted the ultramafic and mafic rocks of the western Brooks Range as ultrabasic plutons that intruded the thrust sheets of the allochthon belts as lopoliths. Tailleur (1973) and Patton *et al.* (1977) alternatively argued that both the Copter Peak and Misheguk Mountain allochthons of the Angayucham terrane were part of a dismembered ophiolite, but later work by Roeder & Mull (1978), Mayfield *et al*. (1988), Wirth *et al.* (1993) and Harris (1998, 2004) has shown that the gabbroic and ultramafic rocks of the Misheguk Mountain allochthon differ from the oceanic and diabase assemblage of the Copter Peak allochthon and are not genetically related. The Copter Peak allochthon contains from Late Devonian to Early Jurassic rocks, whereas the Misheguk Mountain allochthon yields isotopic ages that indicate crystallization in the Middle Jurassic (Wirth *et al*. 1993; Moore *et al*. 1994; Harris, 1998, 2004). Trace element geochemistry of the Copter Peak allochthon indicates oceanic plateau and seamount basalts affinities, whereas geochemical data from the Misheguk Mountain allochthon show an island arc tectonic affinity (Moore *et al*. 1994). The ultramafic rocks of the Misheguk Mountain allochthon have been interpreted as remnants of a S-dipping allochthonous ophiolite thrust sheet that had its root along the northern edge of the Yukon-Koyukuk basin (e.g. Tailleur, 1973, Patton *et al.* 1977; Roeder & Mull, 1978; Moore *et al.* 1994; Young, 2004) (Fig. 2.7).

The Misheguk Mountain allochthon is generally interpreted as an ophiolite and has been referred to as the Brooks Range ophiolite (Harris, 1992, 1998, 2004). The base of the allochthon locally contains a well-developed metamorphic sole that consists of garnet-

bearing amphibolites and quartz-mica schists, greenschists, metabasalts, cherts, marbles and psammites (Harris, 1992, 1998 & 2004). The upper contact of the ophiolite is erosional (Wirth & Bird, 1992) and the top of the ophiolite sequence is commonly absent. However, Roeder & Mull (1978) recognized the presence of remnants of a small sheeted-dyke complex, and Harris (1992) has described a sheeted-dyke complex and a volcanic cover sequence (i.e. pillow lavas) for the Siniktanneyak complex (Figs. 2.14 & 2.16). The Brooks Range ophiolite is interpreted as a fragment of Jurassic oceanic lithosphere that formed along a NE-SW-spreading ridge above a subduction zone near the ancient continental margin of Arctic Alaska (Harris, 2004) (Fig. 2.8a, b). Harris (1998, 2004) argued that the ophiolitic rocks of the western Brooks Range once formed part of a single ophiolite thrust sheet as large as 350 km in strike length, 50 km in width and as much as 3 to 4 km thick.

Saltus *et al*. (2001*a, b*), T. L. Hudson (2002, *pers. comm.*) using modelling of limited gravity and magnetic data, proposed an alternative model in which the ultramafic rocks of the western Brooks Range are not allochthonous ophiolite thrust sheets (Fig. 2.18b) but rooted igneous bodies that intruded the sedimentary successions of the continental margin prior to the Brookian orogeny (Fig. 2.18c). Karl (1991) had previously arrived to a similar conclusion based upon the geochemistry and tectonic affinity of mafic rocks of the western Brooks Range. L. E. Young (2002, *pers. comm.*), Harris *et al*. (2003), and T. E. Moore (2004, *pers. comm.*) argued that the model of Saltus *et al*. (2001*a, b*) did not consider the fundamental age, structural relations and geochemical and tectonic affinity of the Copter Peak and Misheguk Mountain allochthons.

2.5.3 Origin of the Angayucham Terrane

The Angayucham terrane has oceanic and ophiolite affinities but the tectonic setting in which the terrane formed is still poorly understood. Interpretations are primarily based on the relative timing of crystallization and metamorphism at the base of the Misheguk Mountain allochthon (Wirth *et al*. 1993; Harris, 1998). Boak *et al*. (1985) first recorded K-Ar hornblende ages of 154 and 153 Ma from amphibolite and garnet-bearing biotite-hornblende gneiss collected from the base of the ophiolite at Iyikrok Mountain (Fig. 2.14). Wirth *et al.* (1993) reported $^{40}Ar/^{39}Ar$ hornblende ages for two complexes as 184-187 Ma and $^{40}Ar/^{39}Ar$ hornblende ages from their metamorphic soles range from

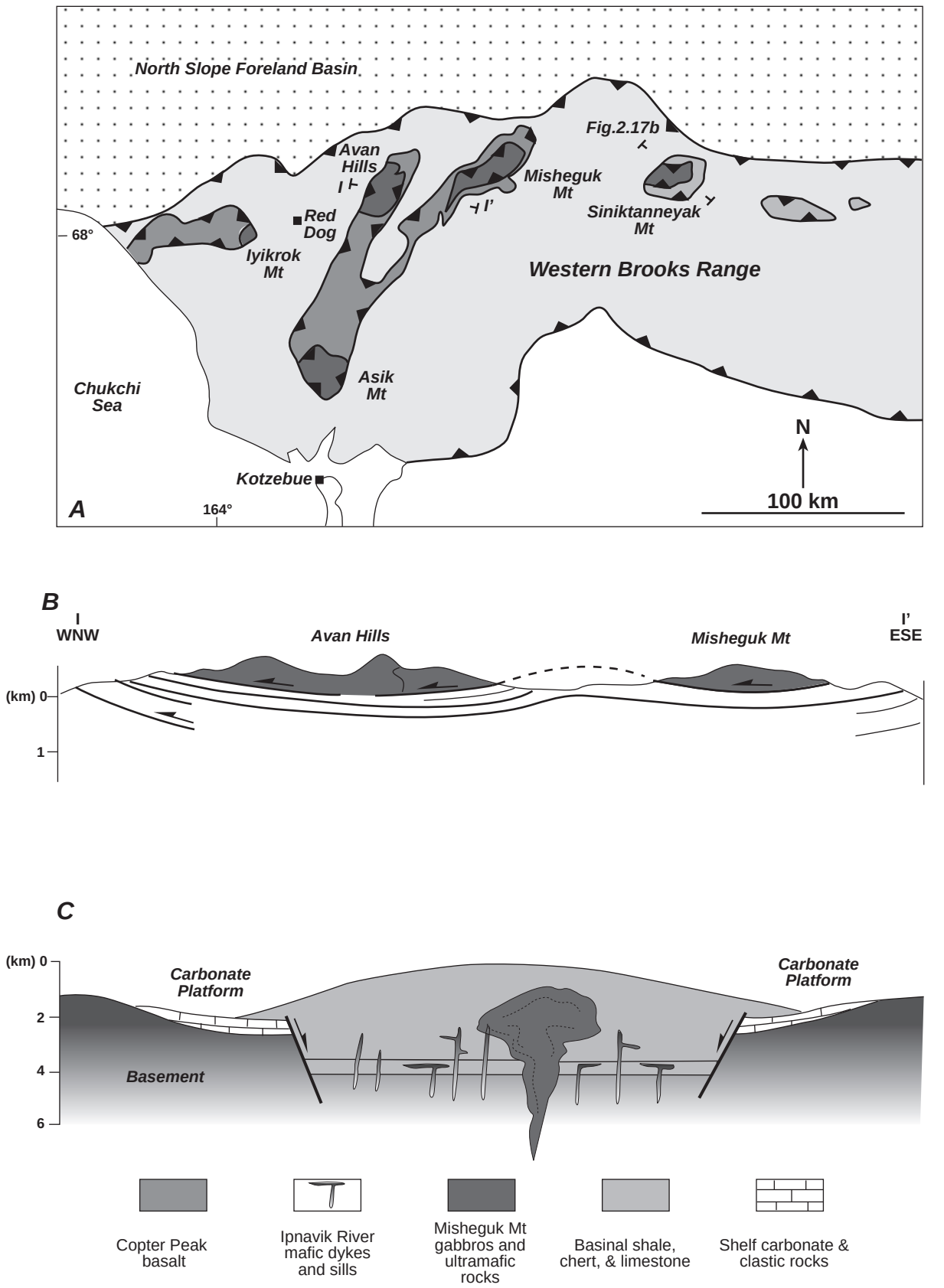


Figure 2.18. Alternative model for the origin of the ultramafic rocks of the western Brooks Range (modified from Saltus *et al*. 2001). **A.** Simplified map of the western Brooks range showing the distribution of ultramafic rocks. Location of the Red Dog mine is shown. **B.** Schematic cross section showing sub-horizontally stacked thrust sheets. **C.** Reconstruction of the Arctic Alaska basin in the Jurassic , showing an intrusive origin for mafic and ultramafic rocks.

163-169 Ma. Wirth *et al*. (1993) suggested that the long interval between the crystallization and emplacement of the ophiolite provides evidence for a long history of transport following intra-oceanic thrusting and proposed that the ophiolite formed in a setting far from the ancient continental margin of Arctic Alaska. Hacker *et al.* (1996) reinterpreted these ages and instead argued that the metamorphic sole and igneous rocks $^{40}Ar/^{39}Ar$ ages are indistinguishable, indicating emplacement of a young, hot ophiolite. Harris (1998) recorded a 165 Ma $^{40}Ar/^{39}Ar$ age from the metamorphic sole, whereas Moore *et al*. (1994) reported a 170 Ma U-Pb zircon age from a plagiogranite. Harris (1998, 2004) argued for a limited time between crystallization and tectonic emplacement and also suggested that compositional similarities between the metamorphic sole and continental margin material imply spatial and temporal proximity of the ophiolite with the Arctic Alaska passive margin prior to emplacement. Differences in geochemistry and age between ophiolite and metamorphic sole (Harris, 1992) rule out the classic model of intra-oceanic thrusting at a spreading centre proposed for many other Tethyan-type ophiolites (e.g. Moores, 2003; Dilek, 2003). The Brooks Range ophiolite is typical of ophiolites that are transitional between mid-ocean ridge basalts and arc-types (Harris, 1992, 1998, 2004).

2.5.4 Correlation with other Terranes

Possible equivalents of the Angayucham terrane in Alaska are found in the Tozitna and Innoko domains of the Ruby terrane of central Alaska (Patton *et al*. 1994; L. E. Young, 2002, *pers. comm.*). The Angayucham terrane is also interpreted to be correlative to the Slide Mountain terrane of the North American Cordillera (Silbering & Jones, 1984; Plafker & Berg, 1994; Nokleberg *et al.* 1997; Price & Monger, 2003) (Fig. 2.3) and forms part of the Oceanic composite terrane of Plafker & Berg (1994) (Fig. 2.2). Fujita & Newberry (1982) suggested that comparable ophiolite suites of the Chukotka Peninsula in easternmost Russia might have been emplaced by the same tectonic event as the western Brooks Range ophiolites. Although the Brooks Range ophiolites are similar to other Cordilleran-type ophiolites in terms of composition and inferred age of emplacement, the Brooks Range ophiolites bear more similarity to Tethyan-type ophiolites in that they were emplaced onto a passive continental margin instead of over an arc or a previously accreted terrane (Wirth *et al*. 1993; Moore *et al*. 1994; Harris, 1998, 2004). Harris (1992) suggested that the Brooks Range ophiolite is similar in

composition, geochemistry, and structural evolution to the Semail ophiolite of Oman and other Tethyan-type ophiolites thrust sheets.

2.5.5 Mechanics of Ophiolite Emplacement

Little is known about the mechanics of ophiolite emplacement in the Brooks Range. Most data come from reconnaissance-style work in the Misheguk Mountain and Avan Hills complexes (e.g. Harris, 2004). Kinematic indicators at the base of the ophiolite indicate a dominant northwest tectonic transport direction (Harris, 1998, 2004). Although the ophiolite is interpreted as having been emplaced by thrusting (e.g. Moore *et al*. 1994; Morin & Moore, 1996; Young, 2004), final emplacement of some or all of the Misheguk Mountain allochthon may have involved extensional faulting along N-dipping low-angle detachment faults (e.g. Miller, 1987; Gottschalk & Oldow, 1988; Gottschalk *et al*. 1998; Harris, 1998, C. J. Potter, 2003, *pers. comm.*; T. E. Moore, 2004, *pers. comm.*).

2.6 *MINERAL DEPOSITS OF THE BROOKS RANGE*

The Brooks Range orogenic belt contains a large number and a great variety of mineral deposits and prospects (e.g. Lange *et al*. 1985; Einaudi & Hitzman, 1986; Hitzman *et al*. 1986; Moore *et al*. 1986; Nokleberg *et al*. 1994; Schmidt, 1997*a, b*; Kelley *et al*. 1997; Nokleberg *et al*. 2003; Kelley & Jennings, 2004; Young, 2004) (Fig. 2.19). These define a series of distinct metallogenic belts that are dominantly parallel to the tectonic elements of the Brooks Range (Einaudi & Hitzman, 1986; Nokleberg *et al*. 2003) and commonly occur at the margins of individual geologic belts (Fig. 2.19). The tectonic setting and distribution of mineral deposits in the Brooks Range are similar to that found in the adjacent North American Cordillera and in other orogenic belts (e.g. Einaudi & Hitzman, 1986; Gabrielse & Yorath, 1991) with a consistent relationship between the tectonic affinity of the host terranes and the type of mineral deposits (Einaudi & Hitzman, 1986; Nokleberg *et al*. 1994, 2003).

2.6.1 Pre-Accretionary Mineral Deposits of the Palaeozoic Continental Margin

Pre-accretionary mineral deposits (Einaudi & Hitzman, 1986) formed during rifting and development of the Palaeozoic continental passive margin of ancient Arctic Alaska (Einaudi & Hitzman, 1986; Nokleberg *et al*. 2003). These deposits are predominantly

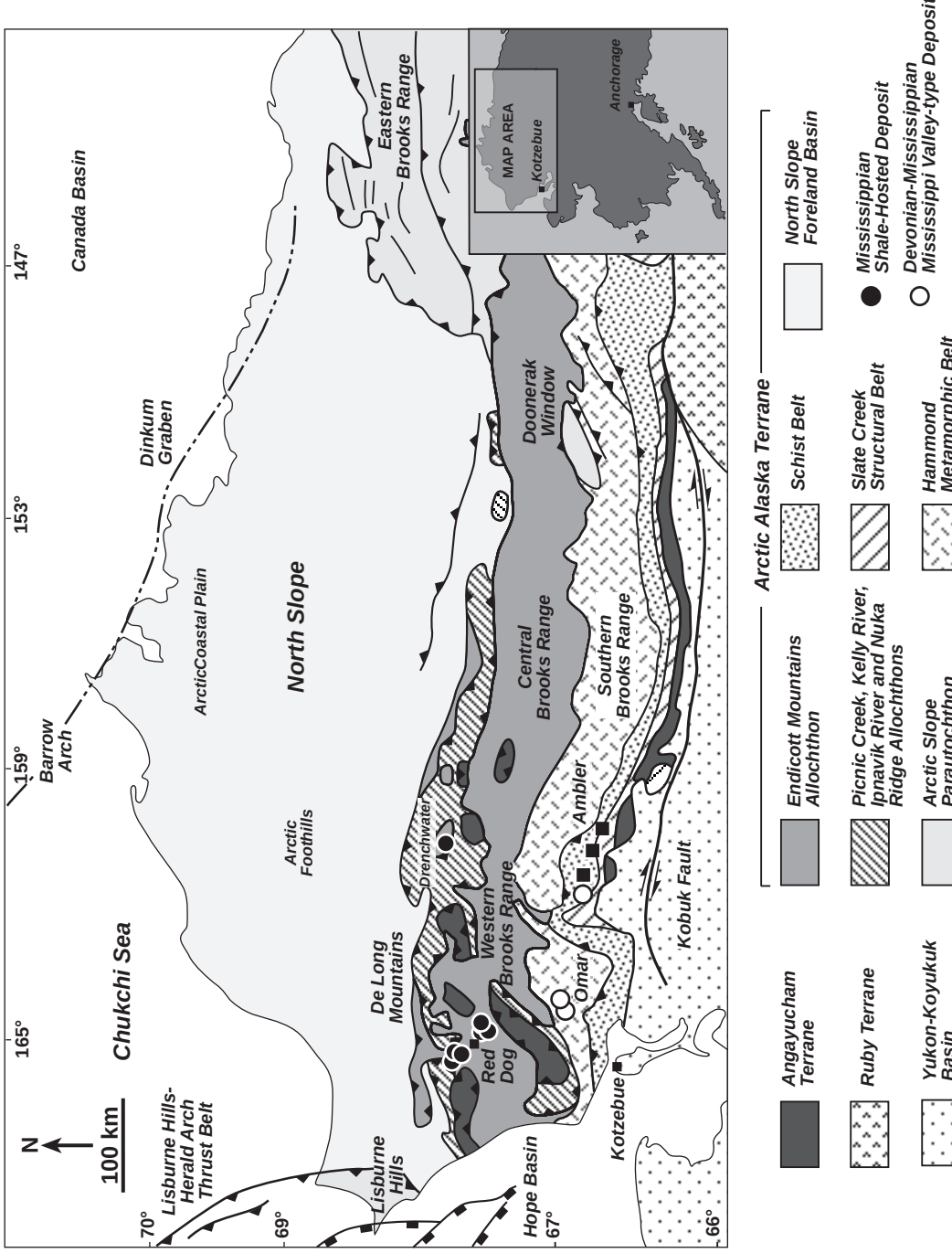


Figure 2.19. Map of the Brooks Range showing the distribution of mineral deposits (geology modified from Moore *et al.* 1994, deposits from Einaudi & Hitzman, 1986; Schmidt, 1997*a*, *b*; Nokleberg *et al.* 2003). The location of the Red Dog mine is shown.

stratiform and are hosted by Palaeozoic sedimentary and volcanic rocks (Nokleberg *et al*. 1994, 2003). In the Brooks Range, stratigraphic relationships, abrupt facies changes in sedimentary rocks of Devonian to Mississippian age (Mull *et al*. 1982; Moore *et al*. 1986; Mayfield *et al*. 1988; Young, 2004) combined with the presence of bimodal volcanic rocks of Late Devonian age (Moore *et al*. 1994; Young, 2004) indicate a continental passive margin setting. Mineralization includes sediment-hosted Zn-Pb-Ag and barite deposits (Moore *et al*. 1986; Kelley & Jennings, 2004), volcanogenic Cu-Zn deposits (Einaudi & Hitzman, 1986; Hitzman, 1986; Hitzman *et al*. 1986; Nokleberg *et al*. 2003), carbonate-hosted and Mississippi Valley-type deposits, and porphyry-type Cu deposits (Einaudi & Hitzman, 1986; Nokleberg *et al*. 1994, 2003)

Sediment-Hosted Zn-Pb-Ag and Barite Deposits

Sediment-hosted Zn-Pb-Ag and barite deposits occur along an approximately 300 km long extensively mineralized belt in the western Brooks Range, which includes the deposits of the Red Dog district and Drenchwater Creek (Lange *et al.* 1981, 1985; Forrest & Sawkins, 1987; Lange *et al*. 1985; Moore *et al*. 1986; Young, 1989; Jennings *et al*. 1998; King *et al*. 2002; Kelley & Jennings, 2004; Young, 2004) (Fig. 2.19). These deposits occur dominantly in Late Mississippian black shales that are contained in imbricated and complexly deformed thrust sheets of the Endicott Mountains allochthon or Brooks Range allochthon (Moore *et al*. 1986; Young, 1989, 2004) (Figs. 2.4, 2.5 & 2.19). The geology of the sediment-hosted Zn-Pb-Ag deposits of the Red Dog district is reviewed in detail in Chapter 3.

Carbonate-Hosted Cu and Zn-Pb-Ba Deposits

Carbonate-hosted Cu and Zn-Pb-Ba deposits include the carbonate-hosted Cu Ruby Creek deposit (Hitzman, 1986; Nokleberg *et al.* 1994, 2003) and a series of poorly understood WNW- to NNW-trending Pb-Ba veins and Mississippi Valley-type Zn-Pb-Ba deposits hosted in brecciated Devonian dolostones (Einaudi & Hitzman, 1986) in the western Brooks Range (Fig. 2.19). These include the Omar, Frost and Powder Milk Zn-Pb occurrences (Folger & Schmidt, 1986; Schmidt, 1997*b*). The Ruby Creek deposit is interpreted to have formed along a rifted continental margin in Late Devonian time (Hitzman, 1986) and occurs along a fault-controlled carbonate platform margin adjacent to a graben filled with basinal shales.

Volcanogenic Cu-Zn Deposits

Volcanogenic Cu-Zn deposits occur in the Ambler district of the southern Brooks Range (Fig. 2.4), which consists of a belt of Late Devonian metamorphosed basalts, rhyolites, carbonates, and black shales (Einaudi & Hitzman, 1986; Hitzman *et al*. 1986; Schmidt, 1986; Nokleberg *et al*. 1994; Schmidt, 1997*b*; Nokleberg *et al*. 2003). Volcanogenic Cu-Zn mineralization includes the Arctic (Schmidt, 1986), Smucker and Sun (Einaudi & Hitzman, 1986) and Ruby Creek (Hitzman, 1986; Bernstein & Cox, 1986) deposits. Hitzman (1986), based on palaeogeographic reconstructions, suggested that the volcanogenic Cu-Zn deposits and the carbonate-hosted deposits of the Ambler district formed on opposite sides of a major shale-filled graben. The Ruby Creek deposit (Hitzman, 1986; Bernstein & Cox, 1986) is inferred to have formed along a fault-controlled basin margin.

Porphyry-type and Skarn Deposits

Porphyry-type and skarn deposits occur related to Devonian plutonic rocks of the southern Brooks Range (Einaudi & Hitzman, 1986; Newberry *et al*. 1986; Nokleberg *et al*. 2003). These include Cu-Mo deposits, W-Mo deposits, and Sn skarns that occur associated to metaluminous granite and granodiorite.

2.6.2 Accretionary and Post-Accretionary Deposits

Accretionary and post-accretionary deposits formed during and immediately after the Brookian orogeny (Einaudi & Hitzman, 1986) and are related to Cretaceous plutonism and metamorphism that largely postdate the development of the Brooks Range foreland fold and thrust belt. These deposits include Au-bearing quartz veins, porphyry Cu-Mo deposits and Sn skarns amongst other occurrences (Einaudi & Hitzman, 1986).

2.7 SUMMARY

This chapter has reviewed the current understanding of the tectonic evolution of the Brooks Range and its main structural units. The main points arising from this chapter are summarized below.

- The Brooks Range is an E-W- to NE-SW-trending and N- to NW-verging arc-continent collision orogenic belt that consists of rocks that span from Late Proterozoic to Cenozoic age.

- The Brooks Range is the result of the Middle Jurassic-Late Cretaceous Brookian orogeny and has also experienced a series of Cenozoic episodic contractional events.

- The Brookian orogeny resulted from underthrusting of the ancient continental passive margin of Alaska (Arctic Alaska terrane) beneath an island arc and oceanic crust assemblage (Angayucham terrane).

- Broadly coeval with collision, Arctic Alaska was rifted away from the North American craton by counter-clockwise rotation, giving rise to the opening of the Canada basin.

- The Brooks Range consists of two terranes, the Arctic Alaska and Angayucham terranes.

- The Arctic Alaska terrane contains the Brooks Range foreland fold and thrust belt, which is the telescoped ancient continental margin. The Arctic Alaska terrane consists of at least five thrust sheets or allochthons dominated by sedimentary rocks.

- The Angayucham terrane comprises two assemblages of volcanic and igneous rocks that formed south (Present Day coordinates) of the ancient continental passive margin and were obducted and accreted during the Brookian orogeny.

- Mineral deposits of the Brooks Range include sediment-hosted Zn-Pb-Ag and barite deposits, carbonate-hosted Zn-Pb and volcanogenic Zn-Cu deposits that formed in Devonian and Mississippian time on the rifted continental passive margin of Arctic Alaska.

CHAPTER 3

REVIEW OF THE GEOLOGY OF THE RED DOG DISTRICT

3.1 INTRODUCTION

3.2 HISTORY OF EXPLORATION AND DISCOVERIES

3.3 REGIONAL STRATIGRAPHY

3.4 REGIONAL STRUCTURE

3.5 SEDIMENT-HOSTED Zn-Pb-Ag DEPOSITS: A REVIEW

3.6 MINERALIZATION OF THE RED DOG DISTRICT

3.7 SUMMARY

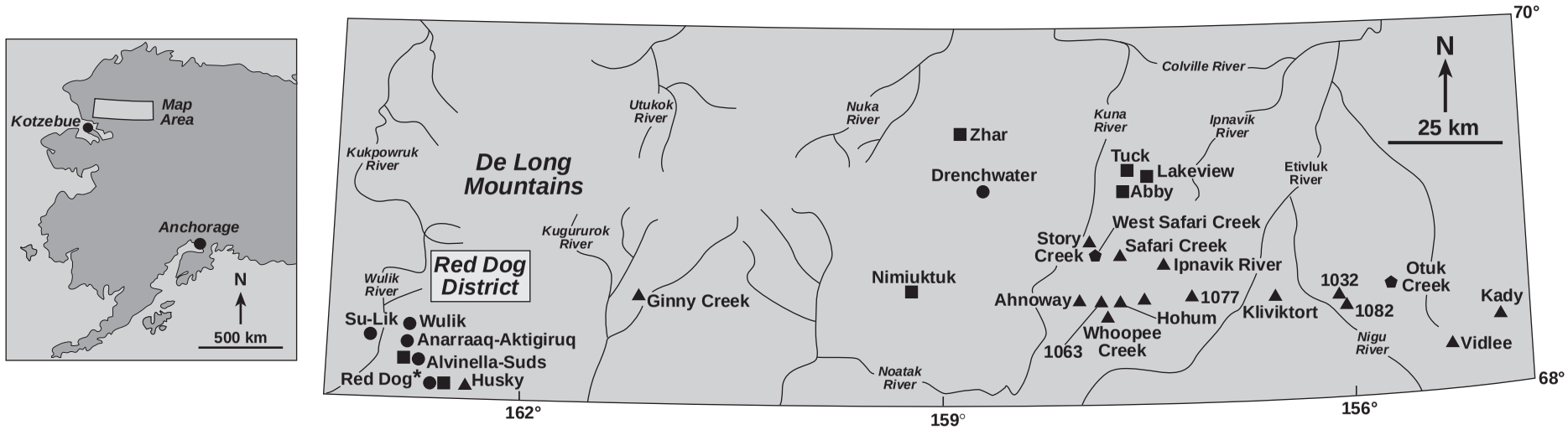
CHAPTER 3 REVIEW OF THE GEOLOGY OF THE RED DOG DISTRICT

3.1 INTRODUCTION

This chapter presents a review of the geology and the sediment-hosted Zn-Pb-Ag and barite mineralization of the Red Dog district of the western Brooks Range, Alaska (Fig. 3.1). It also provides an overview of sediment-hosted Zn-Pb-Ag deposits. The aim of this chapter is to introduce the geology of the Red Dog district.

The Red Dog district forms part of a 300 km-long, E-W-trending belt of sediment-hosted Zn-Pb-Ag and barite deposits in the western Brooks Range, Alaska (e.g. Kelley *et al*. 1997, 2000; Jennings & Kelley, 2004; Young, 2004) (Fig. 3.1). The Red Dog district contains one of the world's largest zinc reserves and resources, including the world's largest single zinc deposit (e.g. Jennings & King, 2002; King *et al.* 2002; Kelley & Jennings, 2004). The Red Dog mine is the world's largest zinc concentrate producer (Kelley & Jennings, 2004; Teck Cominco Ltd. 2005). In addition, the Red Dog district encompasses some of the world's largest barite accumulations (e.g. Johnson *et al.* 2004; Kelley *et al*. 2004*a*) as well as significant natural gas resources (G. G. Booth, 2001, *pers. comm.;* Nelson, 2001).

The Red Dog district consists of Late Devonian to Early Cretaceous siliciclastic and carbonate strata together with felsic to ultramafic rocks that formed on the ancient rifted continental margin of Arctic Alaska (e.g. Moore *et al*. 1986; Young, 2004) (cf. Chapter 2, Figs. 2.6a, 2.11 & 3.2). The continental margin was complexly thrust faulted and folding during the Mesozoic Brookian orogeny (Fig. 2.6) forming a series of regional allochthonous thrust sheets (e.g. Moore *et al*. 1986; Mayfield *et al*. 1988; Young, 2004) (Figs. 2.4, 2.5a, 2.6b – f). The sediment-hosted Zn-Pb-Ag and barite deposits of the Red Dog district occur in Late Mississippian black shales and carbonate strata of the Kuna Formation (e.g. Moore *et al*. 1986; Young, 1989; Kelley & Jennings, 2004) (Figs. 2.11, 3.1 & 3.3). The mineralization is believed to have formed in a extensional fault-controlled restricted basin of the ancient continental margin (Moore *et al*. 1986; Young, 2004) (Fig. 3.2). The origin of the deposits is poorly understood as mineralization shows textures that suggest both syn-sedimentary and replacement processes (e.g. Young, 1989; Sims, 1996; Jennings *et al.* 1998; King *et al*. 2002; Kelley & Jennings, 2004; Kelley *et al*. 2004*a, b*).



■ Barite deposit or occurrence. Host rocks: Mississippian limestones, cherts or shales and Permian cherts and mudstones of the Siksikpuk Formation

● Sediment-hosted Zn-Pb-Ag deposit. Host rocks: Late Mississippian black shales, cherts, and carbonates of the Kuna Formation

⬟ Sulphide-bearing concretions (Zn-Pb). Host rocks: Early Mississippian Kayak Shale

▲ Vein-breccia Zn-Pb-Ag, Cu, Au. Host rocks: Devonian-Mississippian clastic rocks including the Noatak Sandstone, Kanayut Conglomerate, and Kayak Shale

* Includes the Qanaiyaq, Main, Aqqaluk, and Paalaaq deposits

Figure 3.1. Sediment-hosted Zn-Pb-Ag and barite belt of the western Brooks Range (modified from Kelley *et al.* 1997; Kelley & Jennings, 2004; Werdon *et al.* 2004). The location of the Red Dog district is shown.

Figure 3.2. Schematic cross section (not to scale) showing the reconstructed Late Devonian to Jurassic continental margin of the Arctic Alaska terrane prior to the Cretaceous Brookian orogeny (modified from Moore *et al*. 1986). Minimum width of section is approximately 560 km. The location of the sediment-hosted Zn-Pb-Ag and barite deposits of the Red Dog district is shown.

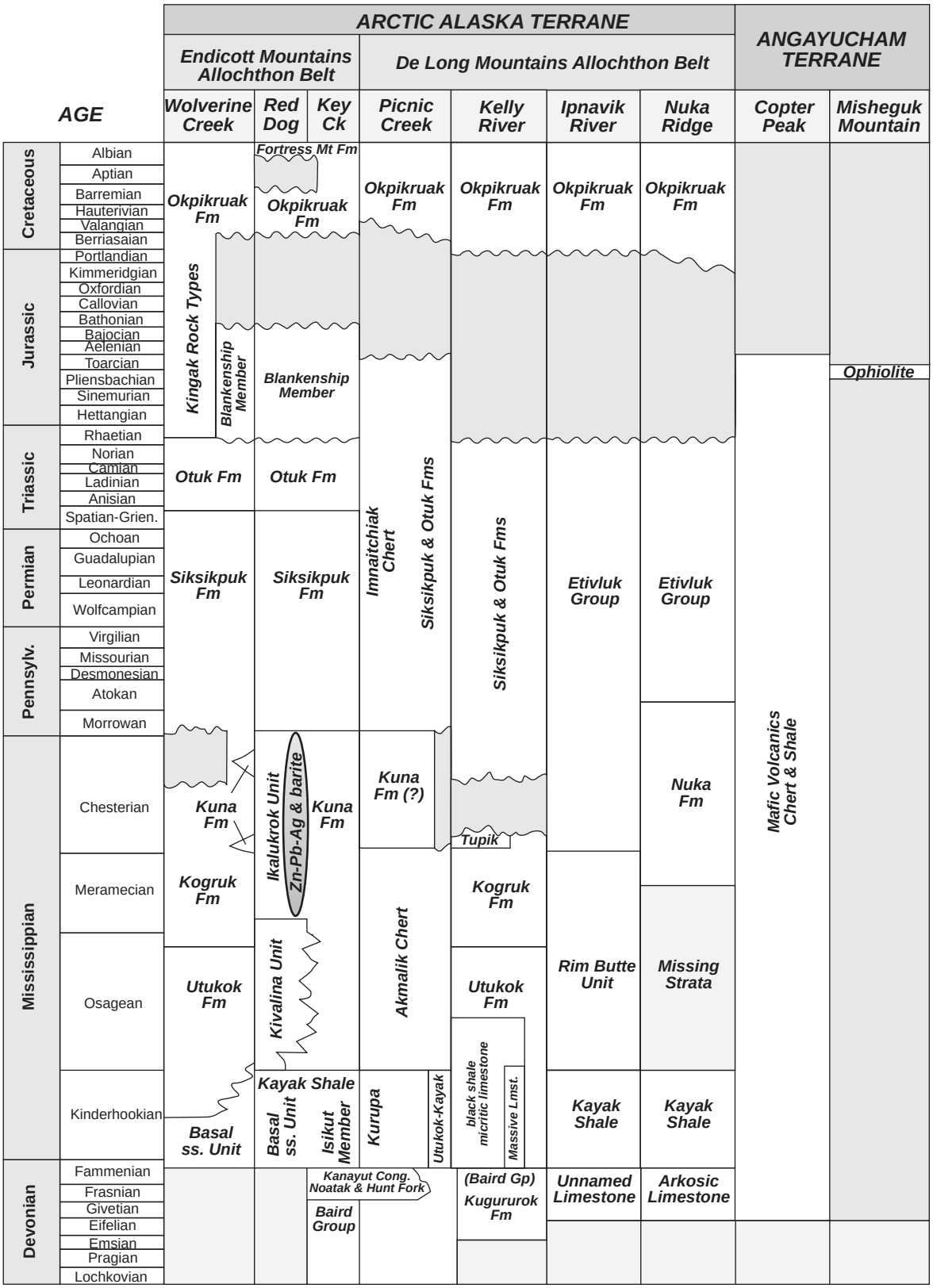


Figure 3.3a. Summary chronostratigraphy of the Red Dog district (modified from Young, 2004). The stratigraphic position of the sediment-hosted Zn-Pb-Ag and barite deposits is shown.

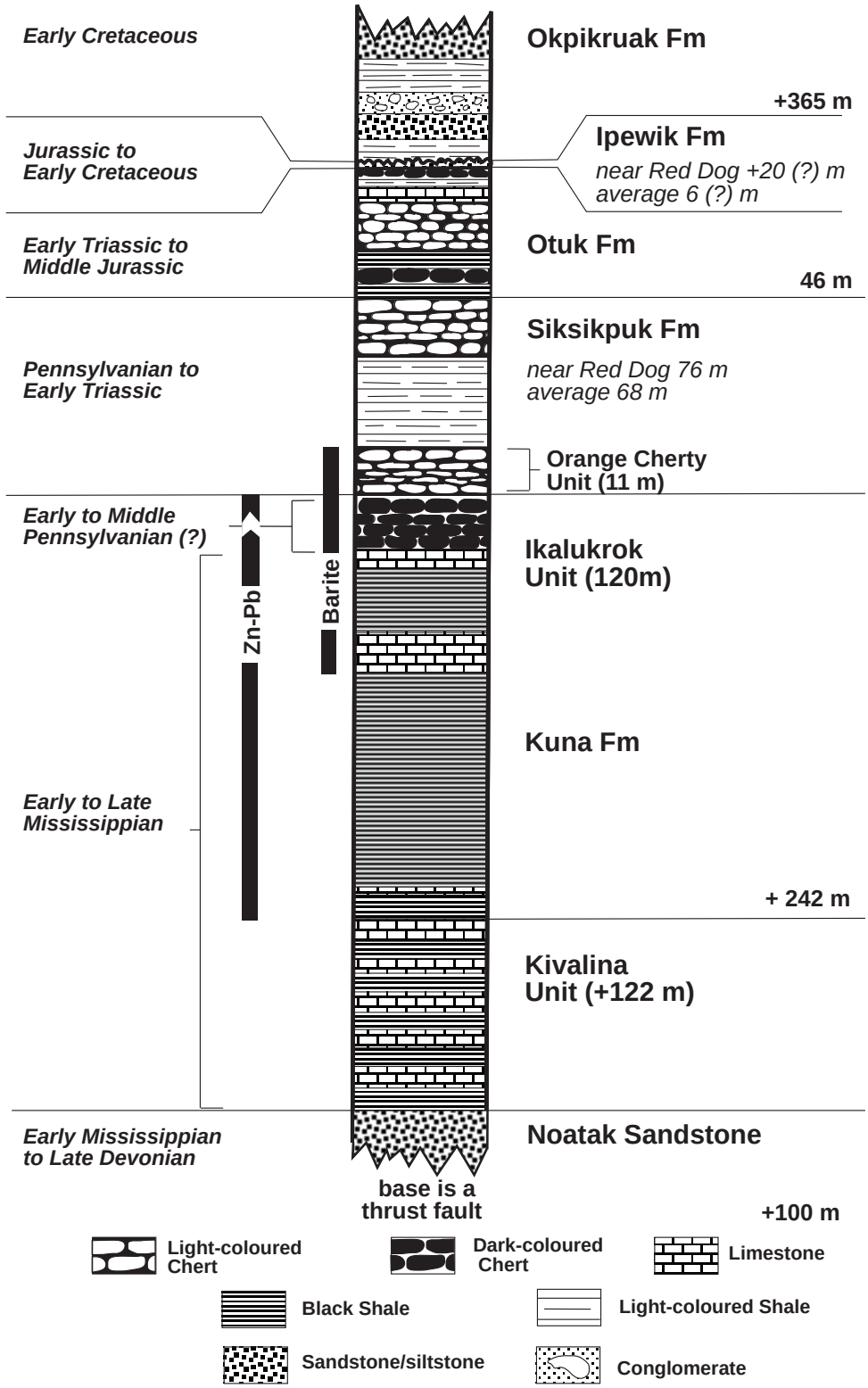


Figure 3.3b. Stratigraphy of the Red Dog sequence, Brooks Range allochthon (modified from Moore *et al*. 1986). The stratigraphic position of the sediment-hosted Zn-Pb and barite deposits of the Red Dog district is shown.

3.2 HISTORY OF EXPLORATION AND DISCOVERIES

The Red Dog district has been explored for sediment-hosted Zn-Pb-Ag deposits for the last four decades (e.g. Tailleur, 1970; Plahuta & Robinson, 1979; Moore *et al*. 1986; Koehler & Tikkanen, 1991; Jennings *et al*. 1998; Jennings & King, 2002; King *et al*. 2002; Kelley & Jennings, 2004).

The first reports of mineralization in the Red Dog region date back to 1955, when U. S. Geological Survey geologist Irvin Tailleur visited Ferric Creek (King *et al*. 2002), located approximately 13 km west-southwest of what is now the Red Dog mine. The significance of the mineralization of the Red Dog district was recognized in 1968, when Bob Baker, a bush pilot and part-time prospector from Kotzebue, brought the Red Dog Creek area to the attention of Tailleur (e.g. Moore *et al*. 1986, Koehler & Tikkanen, 1991; Kelley & Jennings, 2004). The red-stained colour of the creek, which cuts through the mineralization, had previously attracted the attention of Baker (Moore *et al*. 1986; Koehler & Tikkanen, 1991). Tailleur visited the area in 1968 and noticed signs of mineralization (Koehler & Tikkanen, 1991). Tailleur named the location Red Dog Creek after Baker's prospecting company, the Red Dog Mining Company, which was named after Baker's dog (Koehler & Tikkanen, 1991).

In December 1978 Cominco staked the ground of the Red Dog Creek area (Kelley & Jennings, 2004) and finally drilled the showings in May 1980, 'discovering' the Main deposit (e.g. Moore *et al*. 1986; Koehler & Tikkanen, 1991; King *et al*. 2002). In October 1982, Cominco and the Northwest Alaska Native Association (NANA) signed an agreement for the development of the Red Dog deposit (e.g. Koehler & Tikkanen, 1991; King *et al*. 2002). The Red Dog mine was developed and in December 1989 was put into production (e.g. Koehler & Tikkanen, 1991; Kelley & Jennings, 2004), remaining operative 365 days a year to this day (Teck Cominco Ltd. 2005). Post-mine development exploration in the district has successfully resulted in the discovery of other major sediment-hosted Zn-Pb-Ag and barite deposits, including the Aqqaluk, Paalaaq, Anarraaq, Wulik and Aktigiruq deposits together with numerous Zn-Pb showings and prospects (e.g. Jennings *et al*. 1998; Jennings & King, 2002; King *et al*. 2002; Kelley & Jennings, 2004; Young, 2004) (Fig. 3.1).

3.3 REGIONAL STRATIGRAPHY

The stratigraphy of the western Brooks Range including the Red Dog district records a complex palaeogeography and depositional history (e.g. Martin, 1970; Moore *et al.* 1986; Mayfield *et al.* 1988; Young, 1992; Dumoulin *et al.* 2004; Young, 2004) (Figs. 2.11 & 3.2). The Red Dog district exposes Late Devonian to Early Cretaceous sedimentary and igneous rocks of the ancient continental passive margin of Arctic Alaska (Figs. 2.11, 3.2 & 3.3) that are contained in seven fault-bounded distinct Late Devonian to Early Cretaceous stratigraphic successions that are interpreted as having been deposited coevally and contiguously (e.g. Moore *et al*. 1986; Mayfield *et al*. 1988; Young, 1989, 1992; Dumoulin & Harris, 1999; Dumoulin *et al*. 2004; Young, 2004) (Figs. 3.2 & 3.3). Each stratigraphic succession is separated by major thrust faults that bound allochthonous units of regional extent referred to as 'sequences' or 'allochthons' (e.g. Martin, 1970; Moore *et al*. 1986; Mayfield *et al.* 1988; Ellersieck *et al.* 1990) (Chapter 2, Figs. 2.15, 3.4 & 3.5). The allochthons are regionally arranged in such way that more distal parts of the ancient passive margin are stacked onto more proximal passive margin units (e.g. Moore *et al.* 1986; Mayfield *et al.* 1988; Young, 2004) (Figs. 3.2 & 3.4).

Interpretive palinspastic reconstructions indicate that the Late Devonian to Jurassic basin was approximately 600 km long and 200 km wide (e.g. Young, 2004) and had a 'horst-and-graben' geometry (Moore *et al.* 1986) (Fig. 3.2). Sedimentation is believed to have been largely controlled by N- to NW-trending extensional faults (Young, 2004). Deposition on basement highs was characterized by extensive platform carbonate sedimentation (Figs. 2.11 & 3.2), whereas deposition in grabens was characterized by starved deep water sedimentation and restricted water circulation that favoured development of sediment-hosted Zn-Pb-Ag and barite deposits (e.g. Moore *et al*. 1986; Young, 1989; Dumoulin *et al.* 2004; Young, 2004) (Figs. 2.11 & 3.2).

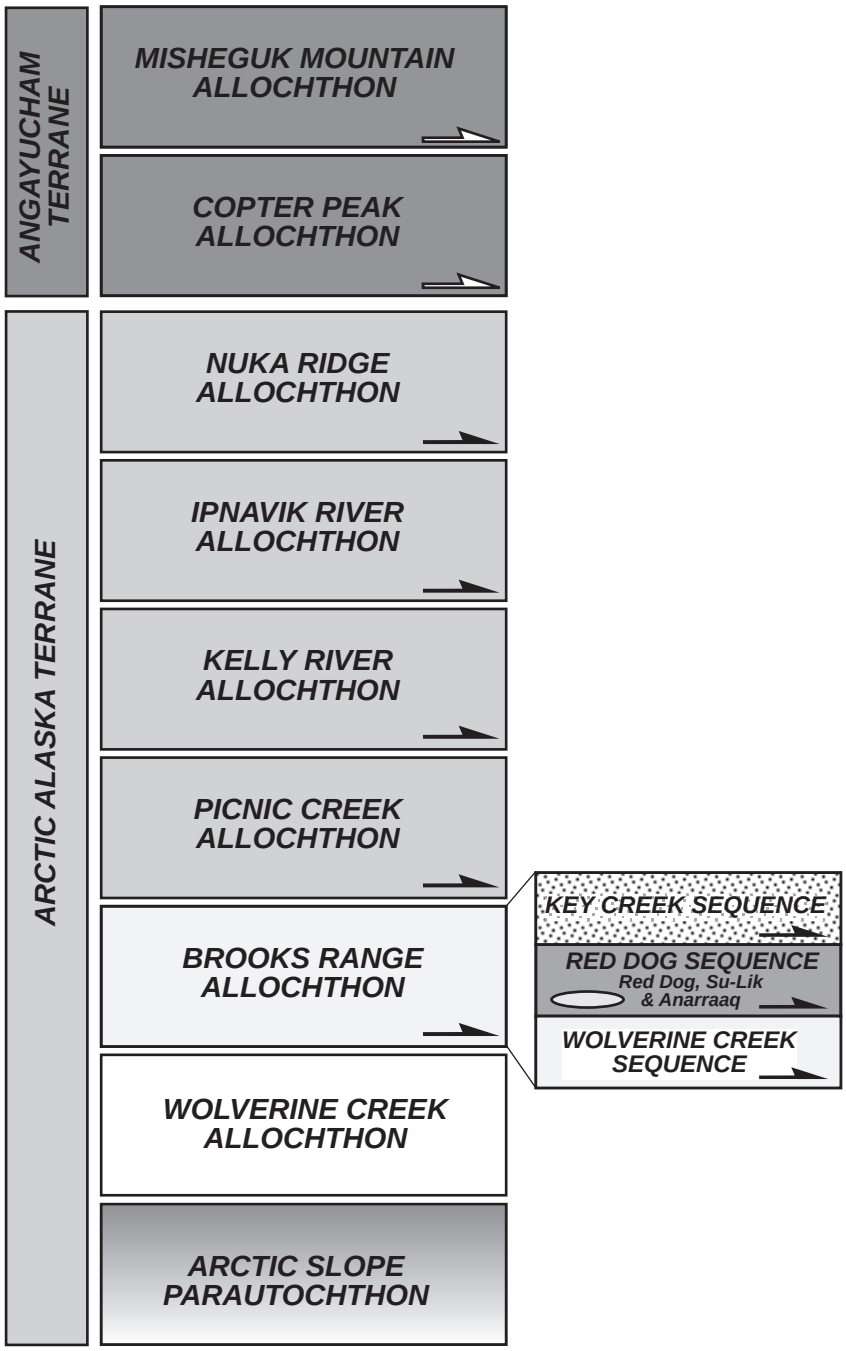


Figure 3.4. Structural hierarchy of the Red Dog district (modified from Moore *et al*. 1986; Young, 1992, 2004). The structural position of the sediment-hosted Zn-Pb-Ag and barite deposits is shown.

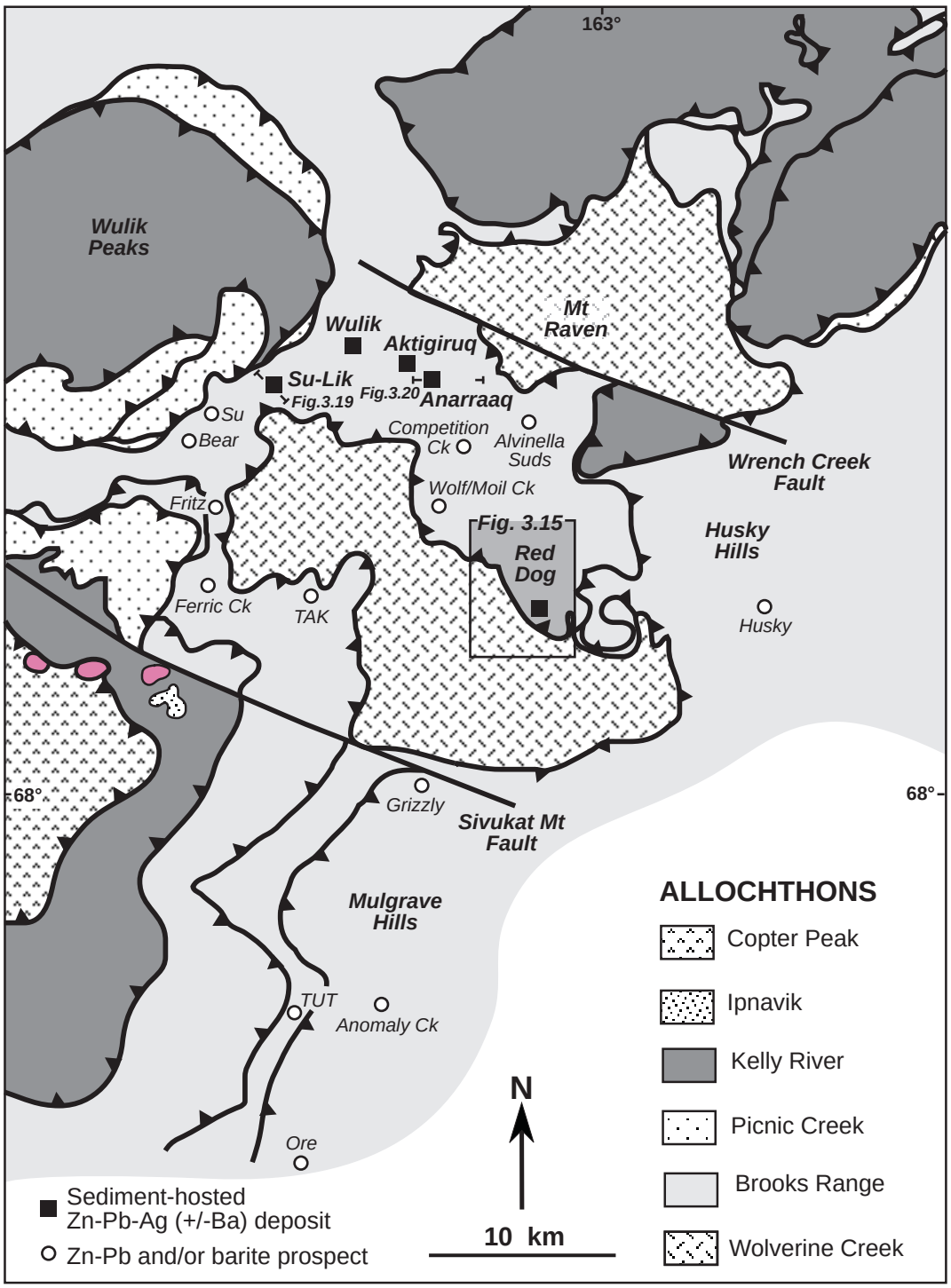


Figure 3.5. Allochthon map of the Red Dog district (modified from Moore *et al*. 1986; Wrench Creek and Sivukat Mountain faults from Martin, 1970; Young, 1992, 2004). Location of the sediment-hosted Zn-Pb-Ag and barite deposits of the Red Dog district is shown. Red Dog includes the Qanaiyaq, Main, Aqqaluk, and Paalaaq deposits. Zn-Pb mineral occurrences from Young (2004).

3.3.1 Stratigraphic Units of the Red Dog District

Stratigraphic nomenclature of the Red Dog district is complex (e.g. Dumoulin *et al.* 2004; Young, 2004) and consists of a number of groups, formations as well as informal and unnamed units that occur in distinct allochthons (Figs. 3.2, 3.3a & 2.11). The stratigraphy consists of Late Devonian to Early Cretaceous clastic and sedimentary rocks together with Devonian to Jurassic felsic to ultramafic igneous rocks (Young, 2004) (Figs. 3.2, 3.3 & 2.11).

Baird Group

The Baird Group (Tailleur *et al*. 1967) consists of Late Devonian and older carbonate rocks (Young, 2004), including the Skajit Limestone, the Kugururok Formation, the Eli Limestone, and a series of unnamed carbonate units that are extensively exposed in the Baird Mountains of the western Brooks Range (Dumoulin & Harris, 1987; Moore *et al.* 1994). The Kugururok Formation, which occurs in the Red Dog district, is described below.

Kugururok Formation

The Kugururok Formation (Dumoulin & Harris, 1987, 1992; Moore *et al*. 1994; Young, 2004) consists dominantly of light grey-weathering skeletal packstone and grainstone and mudstone grading to peloidal packstone deposited in a high energy, shallow-water carbonate platform environment (Dumoulin & Harris, 1992, 1999; J. A. Dumoulin, 2003, *pers. comm.*). The Kugururok Formation of the Red Dog district has yielded Late Emsian to Early Eifelian (late Early to early Middle Devonian) and Middle Givetian (late Middle Devonian) ages (Dumoulin & Harris, 1999). The Kugururok Formation is characteristic of the Kelly River allochthon but also occurs in the Picnic Creek allochthon (Young, 2004).

Endicott Group

The Late Devonian to Early Mississippian (?) Endicott Group (Tailleur *et al.* 1967) regionally overlies the early Middle Devonian Skajit Limestone, the Apoon Assemblage and the early Late Devonian Beaucoup Formation (e.g. Moore *et al*. 1994; Handschy, 1998*b*; Young, 2004). The Endicott Group consists of the Hunt Fork Shale, the Noatak Sandstone, the Kanayut Conglomerate, and the Kayak Shale (e.g. Bowsher & Dutro,

1957; Chapman *et al*. 1964; Mull *et al*. 1982; Moore *et al*. 1994; Young, 2000, 2004) (Fig. 3.3.a). The Endicott Group has been interpreted as having been deposited in a regressive to transgressive braided fluvial and deltaic environment (e.g. Nilsen, 1981; Nilsen & Moore, 1982*a*, *b*, 1984; Moore & Nilsen, 1984; Moore *et al*. 1994; Handschy, 1998*b*; Young, 2004). The Endicott Group is believed to be Frasnian to Fammenian and possibly Kinderhookian in age (e.g. Moore *et al*. 1989; Young, 2004).

Hunt Fork Shale

The early Late Devonian Hunt Fork Shale (Chapman *et al*. 1964) disconformably (?) overlies the Middle Devonian Beaucoup Formation (Dutro *et al*. 1979). The Hunt Fork Shale consists primarily of brown to grey phyllitic siltstones and shales, which are interpreted as having been deposited in a prodelta environment (e.g. Moore & Nilsen, 1984; Young, 2004). Fossils from the lower and upper parts of the Hunt Fork Shale have yielded Frasnian (early Late Devonian) and Famennian (late Late Devonian) ages, respectively (Brosgé *et al*. 1979; Young, 2004). The thickness of the Hunt Fork Shale in the Red Dog district is unknown (Young, 2004). Handschy (1998*b*) has reported a thickness of approximately 6 km in the central Brooks Range, where the unit is possibly structurally thickened.

Noatak Sandstone

The Late Devonian Noatak Sandstone (Smith, 1913) is transitional between the Hunt Fork Shale and the overlying Kanayut Conglomerate (Nilsen & Moore, 1984; Moore *et al*. 1994). It consists of approximately 200 to 300 m of trough-cross stratified carbonate-cemented bitoturbated quartzose sandstone interbedded with layers of brown-weathering fine to medium-grained sandstone and grey-weathering commonly pebbly coarse-grained sandstone (e.g. Nilsen & Moore, 1984; Moore *et al*. 1994; Young, 2004). The Noatak Sandstone has been interpreted to record deposition in an inner-shelf to shoreline environment during Famennian (late Late Devonian) time (e.g. Nilsen & Moore, 1984). The Noatak Sandstone and in lesser extent the overlying Kanayut Conglomerate hosts Zn-Pb vein-breccia mineralization (e.g. Ellersieck *et al*. 1990; Kelley & Mull, 1995; Werdon *et al*. 1996; Kelley *et al*. 1997; Werdon, 1999; Kelley *et al*. 2000; Werdon *et al*. 2004; Young, 2004). It has been proposed that the Noatak Sandstone (Fig. 3.3) represents a basin aquifer through which Zn-Pb-enriched fluids

moved prior to discharge and formation of the Zn-Pb-Ag deposits of the Red Dog district (e.g. Moore *et al*. 1986; Young & Moore, 1987; Young, 1989; Werdon, 1999; Werdon *et al*. 2004).

Kanayut Conglomerate

The Kanayut Conglomerate (Bowsher & Dutro, 1957; Porter, 1966) consists of thinning and fining upward cycles of fluvial conglomerates, sandstones and shales (e.g. Nilsen, 1981; Nilsen & Moore, 1982*a*, *b*; Moore & Nilsen, 1984; Nilsen & Moore, 1984; Moore *et al*. 1989, 1994; Young, 2004). Conglomerates and sandstones exhibit medium to large-scale cross-bedding sedimentary structures. Sandstones are mainly composed of detrital quartz, chert, and shale clasts (Young, 2000, 2004) with locally abundant wood and plant fragments. Young (2000, 2004) reported a thickness of approximately 150 to 185 m for the Kanayut Conglomerate of the Red Dog district. The Kanayut Conglomerate is probably correlative with the Kekiktuk Conglomerate (e.g. Moore *et al*. 1994; Handschy, 1998*a*, *b*; Young, 2004) that is preserved below strata of the North Slope foreland basin, north of the Red Dog district (Figs. 3.3a, 2.11 & 2.15). The Kanayut Conglomerate is interpreted as having been derived from a source area located to the north and/or northeast (e.g. Tailleur *et al*. 1967; Nilsen, 1981; Handschy, 1998*b*). Bogdanov & Tilman (1964) suggest that Devonian red beds on Wrangell Island (Fig. 1.2), located off the north coast of Russia, may be correlative with the Kanayut Conglomerate of the Brooks Range.

Kayak Shale

The Early to Late Mississippian Kayak Shale (Bowsher & Dutro, 1957) (Fig. 3.3) was named for exposures of black marine shale found between the Kanayut Conglomerate and the Lisburne Group in the central Brooks Range. The Kayak Shale is subdivided into two members. These are the Basal Sandstone unit and the Shale and Limestone unit (Bowsher & Dutro, 1957; Young, 2000, 2004).

The Basal Sandstone unit (Bowsher & Dutro, 1957), also referred to as the Isikut Member of the Kayak Shale (Mull *et al*. 1997), consists of thinly cross-stratified and ripple-marked fine-grained quartzose sandstone and highly-bioturbated sandstone, siltstone and shale that conformably overlie the Kanayut Conglomerate (Fig. 3.3a)

(Young, 2004). In the Red Dog district, the Basal Sandstone unit has yielded Late Hinderhookian (Early Mississippian) to Meramecian (Late Mississippian) ages (Dumoulin & Harris, 1999; Young, 2004).

The Shale and Limestone unit (Bowsher & Dutro, 1957) consists of non-calcareous black shale and brown to orange-weathering limestone and/or sandy limestone (Young, 2000, 2004). Fossils include crinoids, bryozoans and brachiopods. Septarian and or iron concretions are common (Young, 2000). In the Red Dog district, the Kayak Shale ranges in thickness from tens of metres to more than 245 m (Moore *et al*. 1986; Young, 2000, 2004).

Lisburne Group

The Lisburne Group (Schrader, 1902) is a Mississippian to Pennsylvanian succession that is widely exposed in the Red Dog district (Dumoulin *et al*. 2004). The Lisburne Group in the Red Dog district consists of the Kuna, Kogruk, Utukok and Tupik formations and a series of informal units that include the Akmalik Chert and the Rim Butte units (e.g. Mull *et al*. 1982; Moore *et al*. 1986; Mull *et al*. 1987*a*; Mayfield *et al*. 1988; Dumoulin *et al*. 1993; Moore *et al*. 1994; Dumoulin *et al*. 1997, 2004). These units were deposited in shallow marine to deep marine anoxic environments (e.g. Campbell, 1967; Armstrong, 1974; Armstrong & Bird, 1976; Armstrong & Mamet, 1977; Dumoulin *et al*. 1993; Moore *et al*. 1994; Dumoulin *et al*. 1997, 2004; Young, 2004). The term Lisburne Group has also been used to refer exclusively to Mississippian to Pennsylvanian platform carbonate strata (e.g. Kogruk Formation) (Young, 2004).

Kuna Formation

The Kuna Formation (Mull *et al*. 1982) hosts all known sediment-hosted Zn-Pb-Ag deposits of the Red Dog district (e.g. Jennings & King, 2002; King *et al*. 2002; Kelley & Jennings, 2004; Dumoulin *et al*. 2004; Young, 2004). The Kuna Formation was previously referred to as the ‘dark-coloured facies of the Lisburne Group’ (Tailleur *et al*. 1966) or ‘the black Lisburne’ (Tailleur & Brosgé, 1970; Plahuta & Robinson, 1979), which formed the base of the Kagvik sequence of Churkin *et al*. (1979, 1980). The

Kuna Formation consists dominantly of black shales and cherts together with minor amounts of micritic limestones and turbidites (e.g. Mull *et al*. 1982; Moore *et al*. 1986; Dumoulin *et al*. 1993; Dumoulin & Harris, 1999; Young, 2000; Dumoulin *et al*. 2004; Young, 2004). Conodont faunas indicate that the Kuna Formation of the Red Dog district is Middle Osagean (Early Mississippian) and Late Meramecian to Early Chesterian (Late Mississippian) (Dumoulin & Harris, 1999; Dumoulin *et al*. 2004; Young, 2004). The Kuna Formation is subdivided into two informal members or units. These are the Kivalina unit and the Ikalukrok unit (e.g. Moore *et al*. 1986; Young, 1989, 2000; Dumoulin *et al*. 2004; Young, 2004) (Figs. 3.3b & 2.11).

Kivalina Unit

The Kivalina unit (Moore *et al*. 1986) is characteristic of the Red Dog district and has not been identified elsewhere in the Brooks Range (Dumoulin *et al*. 2004; Young, 2004) (Figs. 3.2, 3.3b & 2.11). It consists of approximately 122 m of calcareous dark grey to black shales interbedded with graded laminations of fine-grained calcarenite that gradationally overlie the Kayak Shale of the Endicott Group (Moore *et al*. 1986; Young, 2000; Dumoulin *et al*. 2004; Young, 2004) (Fig. 3.3b). Coarse-grained skeletal grainstones and calcareous fine-grained sandstones to siltstones are also locally present (e.g. Dumoulin *et al*. 1993; Dumoulin & Harris, 1999; Dumoulin *et al*. 2004; Young, 2004). Fossils include widespread crinoids, bryozoans, foraminifera, and ostracods (e.g. Dumoulin & Harris, 1999; Dumoulin *et al*. 2004). The Kivalina unit has been interpreted to record deposition in an outer shelf to deep-water environment (e.g. Dumoulin *et al*. 1993; Dumoulin & Harris, 1999; Dumoulin *et al*. 2004; Young, 2004).

Ikalukrok Unit

The Ikalukrok unit (Moore *et al*. 1986) hosts the Zn-Pb-Ag and barite deposits of the Red Dog district (Moore *et al*. 1986; Young, 1989; Jennings *et al*. 1998; Jennings & King, 2002; King *et al*. 2002; Dumoulin *et al*. 2004; Kelley & Jennings, 2004; Young, 2004) (Figs. 3.3b & 2.11). It consists of approximately 123 m of black shales and cherts together with minor turbidites and carbonate strata (Moore *et al*. 1986; Young, 1989, 2000; Dumoulin *et al*. 2004; Young, 2004). The lower part of the Ikalukrok unit consists dominantly of dark grey to black shales together with calcareous radiolarites and calcareous to lithic turbidites (Moore *et al*. 1986; Dumoulin *et al*. 1993; Young,

2000; Dumoulin *et al.* 2004) (Fig. 3.3b). The upper part of the Ikalukrok unit contains medium to thick-bedded black cherts (Moore *et al.* 1986; Young, 1989, 2000; Dumoulin *et al.* 2004; Young, 2004) (Fig. 3.3b). The uppermost Ikalukrok unit contains 'mammiform' sedimentary structures (Young, 2000) that have been interpreted by Young (2004) as possible mud volcanoes. Conodonts and radiolarians indicate that the Ikalukrok unit in the Red Dog district is Osagean to Chesterian (early Late Mississippian) (Dumoulin *et al.* 1993; Dumoulin & Harris, 1999; Dumoulin *et al.* 2004).

Churkin *et al.* (1979, 1980), based on geological mapping, argued that the Kuna Formation was deposited on oceanic crust. Subsequent sedimentological, palaeontological, and geochemical studies by Mull *et al.* (1982), Moore *et al.* (1986), Young (1989, 1992), Dumoulin *et al.* (1993), Dumoulin & Harris (1999), Dumoulin *et al.* (2001, 2004), and Young (2004) suggested that the Kuna Formation was deposited in a continental margin basin and slope setting characterized by anoxic conditions with locally high organic productivity. Palinspastic reconstructions (e.g. Moore *et al.* 1986; Young, 2004) suggest that the Kuna Formation of the Red Dog district was bounded to the north and to the south by platform carbonates (e.g. Moore *et al.* 1986; Dumoulin *et al.* 2004; Young, 2004) (Figs. 3.2 & 3.3a).

Utukok Formation

The Early Mississippian Utukok Formation (Sable & Dutro, 1961) conformably or unconformably (?) (Kelley *et al.* 1998) overlies the Kugururok Formation of the Baird Group and grades upwards into the overlying Kogruk Formation (Figs. 3.2 & 3.3a). The Utukok Formation consists dominantly of orange-weathering impure bioclastic limestones (wackestones to grainstones) and shales together with minor sandstones and black shales (e.g. Dumoulin *et al.* 2004; Young, 2004). In the Red Dog district, the Utukok Formation has yielded Kinderhookian and Middle to Late Osagean (Early Mississippian) conodont ages (Dumoulin & Harris, 1999; Dumoulin *et al.* 2004), being time correlative with the Kayak Shale and the lower part of the Kuna Formation (Dumoulin *et al.* 2004) (Fig. 3.3a).

Kogruk Formation

The Early Mississippian Kogruk Formation (Sable & Dutro, 1961) consists of limestones (skeletal packstones and grainstones) (Dumoulin & Harris, 1999) and locally abundant dolostones and cherts (Young, 1992; Dumoulin *et al*. 2004; Young, 2004) (Figs. 3.2 & 3.3a). Fossils include corals, echinoderms, and brachiopods (Dumoulin *et al*. 2004). Conodont faunas indicate that the Kogruk Formation in the Red Dog district is Late Meramecian (Late Mississippian) (Dumoulin & Harris, 1999; Dumoulin *et al*. 2004; Young, 2004). The Kogruk Formation is interpreted as having been deposited in a carbonate platform setting, coevally with most or all of the Kuna Formation (Dumoulin *et al*. 2004; Young, 2004).

Tupik Formation

The Tupik Formation (Sable & Dutro, 1961) consists of approximately 45 m of thin-bedded, dark-grey limestones and nodular to well-bedded spiculitic black cherts (e.g. Moore *et al*. 1986; Young, 1992) that conformably overlie the Kogruk Formation (Young, 2004) (Fig. 3.3a). Foraminifera assemblages from the Tupik Formation of the Red Dog district have yielded Meramecian (Late Mississippian) ages (Dumoulin & Harris, 1999; Dumoulin *et al*. 2004), although the uppermost part of the unit could be Pennsylvanian (Young, 2004).

Akmalik Chert

The Akmalik Chert (Mull *et al*. 1987*a*) consists of approximately 87 m of thin-bedded, spiculitic and radiolarian-bearing black cherts, black shales together with minor siliceous black mudstones and rare dolostones that conformably overlie the Kayak Shale (Mull *et al*. 1987*a*; Moore *et al*. 1994) (Figs. 3.2 & 3.3a). Radiolarian and conodont faunas indicate that the Akmalik Chert of the Red Dog district is Morrowan (Early Mississippian) and Meramecian to Chesterian (Late Mississippian) (Dumoulin & Harris, 1999; Dumoulin *et al*. 2004), being time correlative with the Kuna Formation. Mull *et al*. (1987*a*) interpreted the Akmalik Chert as a deep-water equivalent of platform carbonate strata of the Lisburne Group, correlative to the Kuna Formation.

Rim Butte Unit

The Rim Butte unit (Dumoulin *et al*. 1993) consists of fine-grained siliceous shales, cherts, and fine-grained calcareous turbidites that are locally intruded by vesicular mafic igneous sills of uncertain age (Dumoulin *et al*. 1993; Moore *et al*. 1994; Young, 2004) (Figs. 3.2 & 3.3a). Dumoulin *et al*. (1993, 2004) have interpreted the Rim Butte unit as having been deposited in a slope to basin setting. The Rim Butte unit is interpreted to be broadly coeval with the Kuna Formation.

Nuka Formation

The Nuka Formation (Tailleur & Sable, 1963) is a succession of arkoses and arkosic limestones of Late Mississippian (Chesterian) to Early Pennsylvanian age (Mayfield *et al*. 1988; Moore *et al*. 1994; Young, 2004) (Figs. 3.2 & 3.3a). The Nuka Formation includes red beds as well as glauconitic units with brachiopod and crinoid faunas that were deposited in a shallow-water environment (e.g. Tailleur & Sable, 1963). The Nuka Formation is one of the least understood units of the Brooks Range (Young, 2004) and no detailed data have been published for that of the Red Dog district, where it is poorly exposed. Provenance analyses indicate that clastic detritus of the Nuka Formation were derived from an unrecognized Proterozoic (*ca.* 2.07 Ga) granitic source (Mayfield *et al*. 1988; Moore *et al*. 1994, 1997*a*; T. E. Moore, 2004, *pers. comm.*).

Etivluk Group

The Etivluk Group (Mull *et al*. 1982), also locally referred to as Imnaitchiak Chert (e.g. Mull *et al*. 1987*a*; Moore *et al*. 1994), consists of Pennsylvanian to Triassic thin-bedded cherts, shales, silicified shales, and silicified limestones that overlie the Kuna Formation (Fig. 3.2). The Etivluk Group is broadly time and facies transgressive with coarse clastic strata of the Sadlerochit Group (Young, 2004), which unconformably overlies the Lisburne Group in the Arctic Slope parautochthon north of the Red Dog district (e.g. Mayfield *et al*. 1988; Moore *et al*. 1994; Handschy, 1998*a*; Young, 2004) (Figs. 3.3b & 2.11). The Etivluk Group consists of the Siksikpuk and Otuk formations (e.g. Patton, 1957; Mull *et al*. 1982), which are widely exposed in the Red Dog district (e.g. Moore *et al*. 1986; Young, 2000, 2004).

Siksikpuk Formation

The Pennsylvanian to Lower Triassic Siksikpuk Formation (Patton, 1957) consists of a condensed succession of cherts and shales (Young, 2000, 2004) that is subdivided into the lower, middle, and upper Siksikpuk units (Moore *et al*. 1986; Young, 2000, 2004) (Fig. 3.3b). Patton (1957) and Mull *et al*. (1987*a*) regarded the Siksikpuk as Permian, whereas Mull *et al*. (1982) suggested a Pennsylvanian to Triassic age. Murchey *et al*. (1988), Moore *et al*. (1994), and more recently Young (2004) have suggested a possible Pennsylvanian age.

The lower Siksikpuk unit (Fig. 3.3b) consists approximately of 5 to 39 m of bright orange-weathering, thin to medium bedded grey chert and grey to whitish shale (Moore *et al*. 1986; Young, 2000, 2004). This unit has been informally referred to as the 'orange cherty unit' (e.g. Moore *et al*. 1986; Young, 1989, 2000) (Fig. 3.3b). Disseminated barite, barite beds, nodules, needles, rosettes and botroydal pyrite and marcasite are common (Young, 2000). Young (1992) identified approximately 24 m of siltstone in the lower Siksikpuk unit at one locality and argued that the Siksikpuk Formation possibly lies disconformably the Lisburne Group (Young, 2004). The middle Siksikpuk unit (Fig. 3.3b) consists of 23 to 46 m of laminated maroon, grey and green shales, and rare chert (Moore *et al*. 1986; Young, 2000, 2004). The upper Siksikpuk unit (Fig. 3.3b) consists approximately of 9 to 46 m of dominantly irregular, nodular, and wavy-bedded greenish, grey or less commonly red chert with minor and thin interbedded shales (Moore *et al*. 1986; Young, 2000, 2004). Young (2004) has inferred an Early Permian age the middle and upper units based upon correlation with regionally-dated sections (e.g. Murchey *et al*. 1988; Moore *et al*. 1994). The uppermost Siksikpuk Formation contains a transitional facies, characterized by approximately 10 m of laminated green-grey, sheared brown-grey, with lesser maroon shale and subordinate thin-bedded chert (Young, 2000, 2004). This unit has been informally referred to as the 'transitional subunit' (Young, 2000) or the 'transition facies' (Young, 2004).

Otuk Formation

The Lower Triassic to Middle Jurassic Otuk Formation (Mull *et al*. 1982), formerly known as the Shublik Formation (Leffingwell, 1919), consists of shales, cherts, and

dolostones that overlie the Siksikpuk Formation (Moore *et al*. 1986; Young, 2000, 2004) (Fig. 3.3b). The Otuk Formation is subdivided into four units or members. These are from oldest to youngest the Shale Member, the Chert Member, the Limestone Member, and the Blankenship Member (e.g. Mull *et al*. 1982; Young, 2004).

The Shale Member (Mull *et al*. 1982) consists of 9 to 26 m of laminated light grey, green grey and black shale with minor thin-bedded black and grey chert (Young, 2000, 2004). Laminated pyrite and/or marcasite, barite needles, rosettes and massive barite beds up to 1 m thick are locally present (Young, 2004). The Chert Member (Mull *et al*. 1982) consists approximately of 20 m of thin-bedded grey, greenish or black cherts interbedded with shale layers (Young, 2000, 2004). A distinctive marker horizon occurs central part of the chert Member (e.g. Moore *et al*. 1986; Young, 2000, 2004). It consists of 1 to 2.5 m of laminated to thin-bedded black chert with black shale partings (Young, 2000). Where severely deformed, strongly folded cherts grades abruptly to bodies of massive jasperoid with mottled translucent, white, grey, black, purple, red and orange colours (Young, 2000). The Limestone Member (Mull *et al*. 1982) consists of tan to buff-yellow weathering cherts, fossiliferous cherty dolomites and limestones. Fossils include *Monotis* sp. (Mull *et al*. 1982; Young, 2004). The Limestone Member is overlain by the Blankenship Member, which consists of 3 to 6 m of laminated black shale and chert (Young, 2000, 2004).

Ipewik Formation

The Early Jurassic to Early Cretaceous (Valangian) Ipewick unit (Crane & Wiggins, 1976) or Ipewik Formation (Moore *et al*. 1986) conformably (?) overlies the Otuk Formation (e.g. Moore *et al*. 1986; Young, 1989; Moore *et al*. 1994; Young, 2000) (Fig. 3.3a, b). The Ipewik Formation consists of maroon, red and grey shales together with coquinoid limestones, siltstones, and quartzitic sandstones (e.g. Crane & Wiggins, 1976; Ellersieck *et al*. 1983; Moore *et al*. 1986; Mayfield *et al*. 1988; Moore *et al*. 1994; Young, 2000). Quartzose sandstones found at the top of the Ipewik Formation have been referred to as the Tingmerkpuk Member (e.g. Curtis *et al*. 1983; Mayfield *et al*. 1988; Young, 2000, 2004).

Okpikruak Formation

The Early Cretaceous Okpikruak Formation (Gryc *et al*. 1951) unconformably overlies the Etivluk Group (e.g. Moore *et al*. 1986; Young, 2000, 2004) (Fig. 3.3a, b). Detailed information from the Okpikruak Formation is scarce (e.g. Crane, 1987; Wilbur *et al*. 1987; Siok, 1989; Dumoulin & Harris, 1999; Young, 2000, 2004) and no detailed data have been published from the Red Dog district or the western Brooks Range. The Okpikruak Formation consists dominantly of olistostromes, conglomerates, sandstones, siltstones, and shales that were deposited in a deep marine environment (e.g. Martin, 1970; Crane, 1987; Young, 2000, 2004). Sparse *Buchia* (Curtis *et al*. 1982) of dominantly Tithonian age (uppermost Jurassic) and *Buchia* cf. (Curtis *et al*. 1990) are the only fossils found in the Okpikruak Formation. The Okpikruak Formation is believed to be progressively older in higher allochthons and younger in lower allochthons (Mayfield *et al*. 1988; Moore *et al*. 1994; Young, 2004). The Okpikruak Formation is at least as old as Berriasian (earliest Early Cretaceous) in the Ipnavik River allochthon (Mayfield *et al*. 1988) but is no older than Valangian (Early Cretaceous) in the Endicott Mountains/Brooks Range allochthon (Fig. 2.11) (Mayfield *et al*. 1988; Moore *et al*. 1994; C. G. Mull, 2004, *pers. comm.*). The Okpikruak Formation has been interpreted as having been deposited during the Mesozoic Brookian orogeny in a N-migrating foredeep (e.g. Crane, 1987; Mayfield *et al*. 1988; Young, 2004) or possibly in a 'piggy-back' basin (e.g. Hubbard *et al*. 1987; Moore *et al*. 1994). The Okpikruak Formation of the Red Dog district is reported to be 365 m thick (e.g. Moore *et al*. 1986; Young, 2000, 2004)

Fortress Mountain Formation

The Early Cretaceous (Aptian) Fortress Mountain Formation (Patton, 1956) consists of approximately 3 km of conglomerates, sandstones, and shales (Molenaar *et al*. 1981, 1988). The Fortress Mountain Formation is interpreted to record deposition in a submarine fan complex setting developed at the front of the Brooks Range fold and thrust belt (e.g. Mull *et al*. 2000) during the early stages of filling of the North Slope foreland basin (e.g. Molenaar *et al*. 1988).

3.3.2 Igneous rocks

In the Red Dog district Early to Late Mississippian scattered and highly-altered small felsic to mafic alkaline hypabyssal intrusives occur spatially related to the sediment-hosted Zn-Pb-Ag and barite deposits (e.g. Moore *et al*. 1986; Young, 2000, A. R. King, 2002, *pers. comm.;* Young, 2004). These rocks commonly intrude strata of the Kuna Formation and are believed to have ascended along Mississippian to Pennsylvanian basement extensional faults during incipient continental rifting (A. R. King, 2002, *pers. comm.*; L. E. Young, 2004, *pers. comm.*). Early (?) Mississippian intermediate to mafic igneous rocks, consist of sills or dykes, as well as flows or tuffs (Young, 2004). Rhyolites locally occur associated to silicified and sulphide-veined Ikalukrok unit at the Red Dog mine (Werdon *et al*. 2004; Young, 2004).

Devonian to Jurassic mafic and ultramafic igneous rocks are extensively preserved in the structurally-higher thrust sheets of the Brooks Range (e.g. Martin, 1970; Moore *et al*. 1986; Mayfield *et al*. 1988; Young, 2004). The Ipnavik River allochthon contain diabase sills up to 100 m thick, which consist mainly of micrograbbro of tholeiitic or mildly alkaline composition (e.g. Ellersieck *et al*. 1984; Mayfield *et al*. 1988; Karl & Long, 1990; Young, 2004). Mafic sills have not been dated but Young (2004), based on stratigraphic relationships, has suggested a possible Late Mississippian to Pennsylvanian or Permian age. The Copter Peak and Misheguk Mountain allochthons contain Devonian to Jurassic basalt, whereas peridotites and gabbro characterizes the Misheguk Mountain allochthon (e.g. Moore *et al*. 1986; Mayfield *et al*. 1988; Young, 2004).

3.4 REGIONAL STRUCTURE

The structure of the Red Dog district is poorly understood and information comes largely from reconnaissance mapping of the De Long Mountains together with mining industry exploration drilling, mapping and unpublished reports (e.g. Martin, 1970; Moore *et al*. 1986; Mayfield *et al*. 1988; Curtis, 1990; Ellersieck *et al*. 1990; Mayfield *et al*. 1990; Young, 1992, 2000; Jennings *et al*. 1998; King *et al*. 2002).

3.4.1 Structure of the Red Dog District

The structure of the Red Dog district is dominated by a series of stacked and regionally folded thrust sheets or allochthons. The allochthons define NE-SW- and NW-SE-trending thrust faults and folds (Moore *et al*. 1986; Young, 1992, 2004). The allochthons and structures within them define two dominant structural trends, NE-SW- and NW-SE-trending thrust faults and folds (Moore *et al*. 1986; Young, 1992, 2000, 2004) (Fig. 3.5). Moore *et al*. (1986) and Young (1992) described eight allochthons (Fig. 3.4) or thrust sheets that were emplaced during the Brookian orogeny (Fig. 2.6). These are in ascending structural, the Wolverine Creek, Brooks Range, Picnic Creek, Kelly River, Ipnavik River, Nuka Ridge, Copter Peak, and Misheguk Mountain allochthons (Figs. 3.4 & 3.5). The six structurally lower allochthons contain Late Devonian to Early Cretaceous sedimentary rocks (Moore *et al*. 1986; Mayfield *et al*. 1988) and are assigned to the Arctic Alaska terrane (Young, 2004) (Fig. 2.11). The two uppermost allochthons consist largely of felsic to ultramafic igneous rocks and have been assigned to the Angayucham terrane (e.g. Young, 2004) (Fig. 2.11). The stratigraphy of individual allochthons is summarized in Figure 3.3a. Moore *et al*. (1986) further subdivided the Brooks Range allochthon into the Red Dog and Key Creek sequences. The Red Dog sequence (Fig. 3.5) of Moore *et al*. (1986) is of special significance for the purposes of this thesis in that it hosts all known Zn-Pb-Ag and barite deposits of the Red Dog district (e.g. Moore *et al*. 1986; Young, 1989, 2000; Kelley & Jennings, 2004; Young, 2004).

The allochthons of the Red Dog district are regionally stacked (Fig. 3.6 & Chapter 2) and gently folded into open synforms and antiforms that have been attributed to the Late Brookian deformation event and/or subsequent Cenozoic events (Young, 2004).

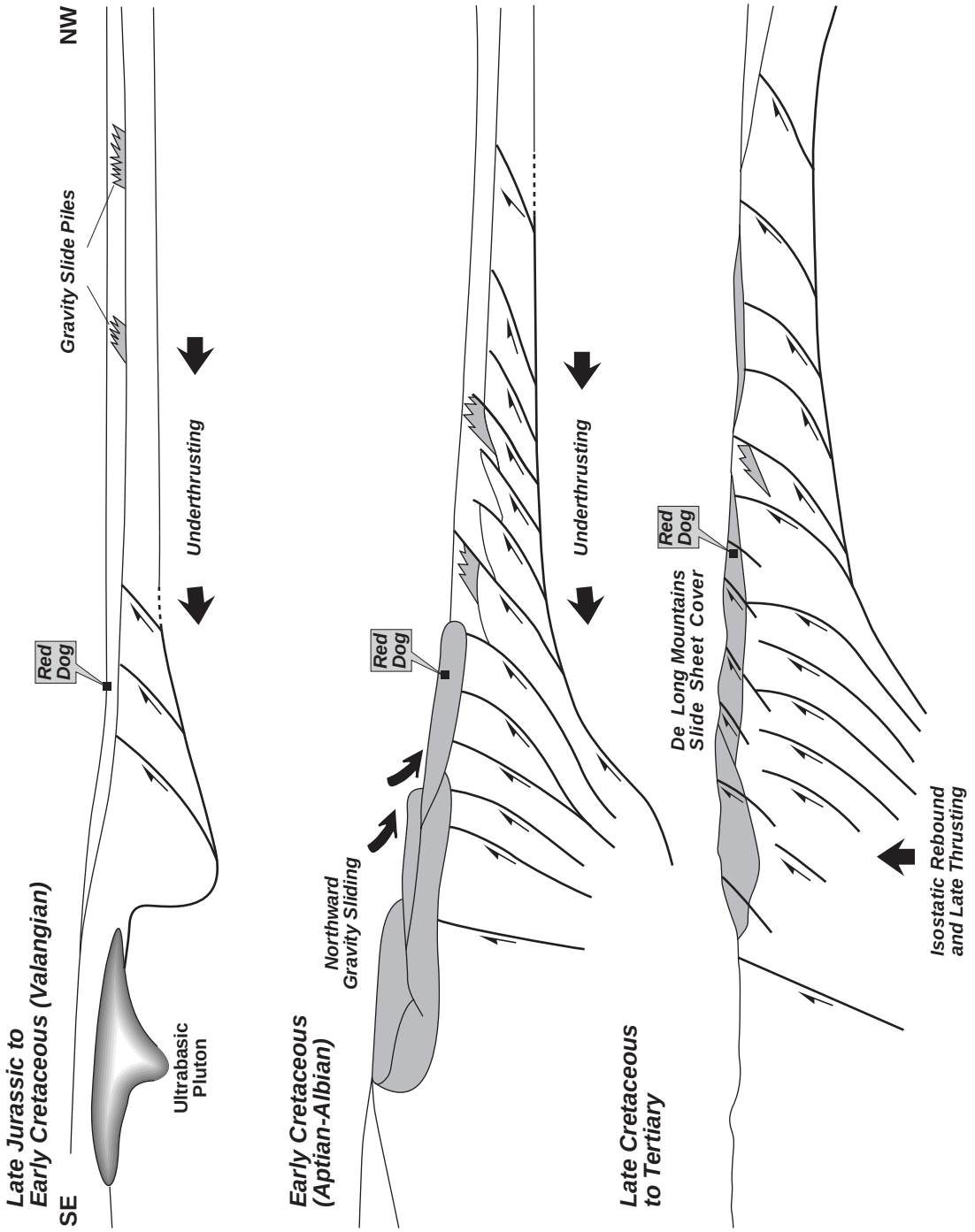


Figure 3.6. Tectonic model (not to scale) for the De Long Mountains, including the Red Dog district (modified from Martin, 1970). Emplacement of allochthonous thrust sheets (grey shaded units) is largely controlled by gravity sliding, whereas thrusting is restricted to deeper structural levels. Schematic location of the Red Dog district is shown.

3.4.2 Wrench Creek and Sivukat Mountain Faults

The allochthons of the Red Dog district are offset by two poorly understood regional-scale NW-SE-trending faults. These are the Wrench Creek and Sivukat Mountain transcurrent fault zones of Martin (1970) or Wrench Creek and Sivukat Mountain faults of Young (1992) (Fig. 3.5). The Sivukat Mountain fault has been also referred to as the Gertrude fault (Mayfield *et al*. 1990). The Wrench Creek and Sivukat Mountain faults have been interpreted as a dextral strike-slip fault system (e.g. Martin, 1970; Plahuta & Robinson, 1979), partly or entirely as thrust faults (e.g. Moore *et al*. 1986; Ellersieck *et al*. 1990; Mull *et al*. 1995; Kennecott Exploration, 2002, *pers. comm.*), or as dextral strike-slip faults with possible components of oblique and/or dip slip movement (e.g. Young, 1992). Martin (1970) inferred a combined dextral displacement on the faults of at least 13 km, whereas Young (1992) suggested an unknown amount of dextral strike-slip displacement with at least hundreds of metres of vertical displacement to the southwest. Martin (1970) proposed that the Wrench Creek and Sivukat Mountain faults were active in Late Cretaceous to Early Tertiary. Mayfield *et al*. (1990) and Young (1992), based on interpretation of map patterns, argued that movement on the Wrench Creek fault was Albian or younger and post-dated Brookian thrusting and folding.

3.4.3 Structural Models

Several models have been proposed for the tectonic evolution of the De Long Mountains, including the Red Dog district (e.g. Martin, 1970; Moore *et al*. 1986; Young, 1992). Martin (1970) proposed three main phases of deformation that included N-verging thrusting and dominant gravity sliding in Late Jurassic to Early Cretaceous, Middle Cretaceous (Albian) and Late Cretaceous to Early Tertiary (Fig. 3.6). L. E. Young (2002, *pers. comm.*) proposed a similar model in which the allochthons of the Red Dog district were emplaced by gravity sliding, showing attenuation and grading laterally into olistostrome sheets. Moore *et al*. (1986) recognized two separate contractional events with two directions of contraction in the western De Long Mountains and Red Dog district. Young (1992, 2000, 2004) has argued that the dominant NE-SW-trending structural grain defined by the allochthons of the Red Dog district (Figs. 3.5, 2.5 & 2.14) is disrupted by NW-SE-trending and NE-verging thrust faults in the area comprised between the Wrench Creek and Sivukat Mountain faults (Fig. 3.5). Young (2000) suggested that NE-verging thrust faults and folds are related

to the emplacement of the Lisburne Hills-Herald Arch thrust belt to the west (cf. Chapter 2; Figs. 2.1, 2.2h, 2.4, 2.14 & 2.16). Young (2000) informally referred to this tectonic event as 'Tigaran', after the Tigara uplift of Payne (1955). However, Young (2004) has most recently argued that the temporal relationships between these two events are ambiguous and contradictory and has proposed that NE-verging thrust faults and folds in the Red Dog district may have simply resulted from strike-slip movement on the Wrench Creek and Sivutak Mountain faults. In this respect, C. G. Mull (2004, *pers. comm.*) has argued that NW-SE-trending thrust faults north of the Red Dog mine simply reflect a drag effect of movement on the Wrench Creek fault (Fig. 3.5). Young (1992) proposed a more complex model with five phases of deformation that involved N-verging thrusting, N- to N-verging and folding of older thrust faults, dextral strike-slip faulting, NE-verging thrusting and northeast-southwest late extensional faulting.

O'Sullivan (1999), O'Sullivan *et al*. (2000), and P. B. O'Sullivan (2002, *pers. comm.*), based on limited apatite and zircon fission track studies in the Red Dog district, have proposed that deformation in the Brooks Range is largely or entirely of Cenozoic age. P. B. O'Sullivan (2002, *pers. comm.*) has suggested that NE-verging thrust faults resulted from Paleocene (*ca*. 60 Ma) reactivation of Early Cretaceous Brookian thrust faults, whereas NW-verging thrust faults formed in the Eocene (*ca*. 45 Ma). O'Sullivan (1999), O'Sullivan *et al*. (2000), and P. B. O'Sullivan *et al*. (2000), and O'Sullivan (2002, *pers. comm.*) also argued that fission track data indicated that the allochthons of the Red Dog district have undergone large amounts of shortening and were subjected to burial depths of *ca*. 9 km. This contrasts with thermal data from conodont alteration indices by Dumoulin & Harris, (1999) and Dumoulin *et al*. (2004). Conodont alteration indices from the Red Dog district indicate burial depths of 3.5 to 5.5 km (Dumoulin & Harris, 1999; Dumoulin *et al.* 2004).

3.5 SEDIMENT-HOSTED Zn-Pb-Ag DEPOSITS: AN OVERVIEW

This section provides an overview of sediment-hosted Zn-Pb-Ag deposits and the tectonostratigraphic setting in which they form. The aim of this section is to provide background for the understanding of the relationships between mineralization and the tectonic evolution of the Red Dog district.

3.5.1 Definition

Sediment-hosted Zn-Pb-Ag deposits are defined as sulphide deposits that form from the discharge of hydrothermal fluids by exhalative processes on the sea floor and/or by sulphide replacement and/or infill of sedimentary units below the sea floor (e.g. Goodfellow *et al*. 1993; Lydon, 1995; Large *et al*. 2002; Large, 2003). Sediment-hosted Zn-Pb-Ag deposits are an important mineral resource and constitute more than 50% of the world's zinc and lead reserves (Goodfellow, 1999).

3.5.2 Classification and Nomenclature

Sediment-hosted Zn-Pb-Ag deposits have been referred to a variety of terms, such as 'shale-hosted' (Maynard, 1991), 'stratiform sediment-hosted zinc-lead' (Gustafson & Williams, 1981; Abbott *et al*. 1986; Goodfellow *et al*. 1993; Goodfellow, 1999), 'stratabound sediment-hosted', 'sedimentary exhalative' or 'SEDEX' (Carne & Cathro, 1982; Briskey, 1986; MacIntyre, 1991; Lydon, 1995) and 'sediment-hosted massive sulphide' (Large, 2001). Classification and nomenclature of sediment-hosted Zn-Pb-Ag deposits remain however problematic, in particular when referring to descriptors such as 'exhalative' or 'stratiform' (Large, 2001; K. D. Kelley, 2004, *pers. comm.*). Sediment-hosted Zn-Pb-Ag deposits comprise the sedimentary exhalative (SEDEX), Mississippi Valley-type (MVT), Irish-type, Broken Hill-type, and sandstone-hosted lead deposits (Large, 2001). Geologic and isotopic data suggest that some of these deposit types may be genetically related (e.g. Goodfellow *et al*. 1993; Large, 2001; Nelson *et al*. 2002). For example, the close spatial relationships between SEDEX and Mississippi Valley-type deposits (Figs. 3.8 & 3.9) has been interpreted by MacIntyre (1991), Goodfellow *et al*. (1993) and more recently by Nelson *et al*. (2002) as permissive evidence for a genetic link between the two deposit types.

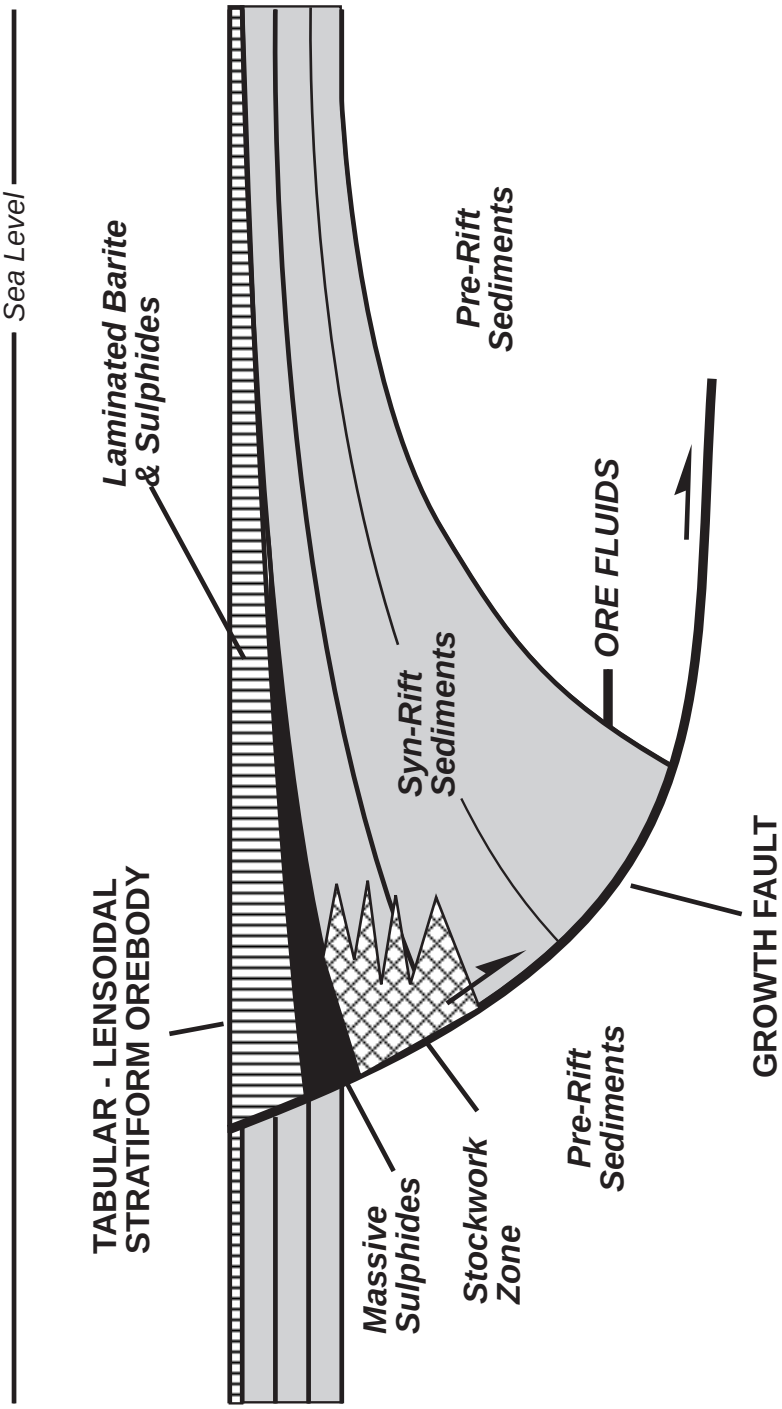


Figure 3.7. Synoptic model for formation of sediment-hosted Zn-Pb-Ag deposits during syn-rift extensional faulting (modified from McClay & Bidwell, 1987).

Figure 3.8. Schematic cross section showing the tectonic setting of sediment-hosted Zn-Pb-Ag, volcanic massive sulphide (VMS) and Mississippi Valley-type (MVT) deposits of the Canadian Cordillera in Late Devonian to Early Mississippian (modified from Nelson *et al.* 2002).

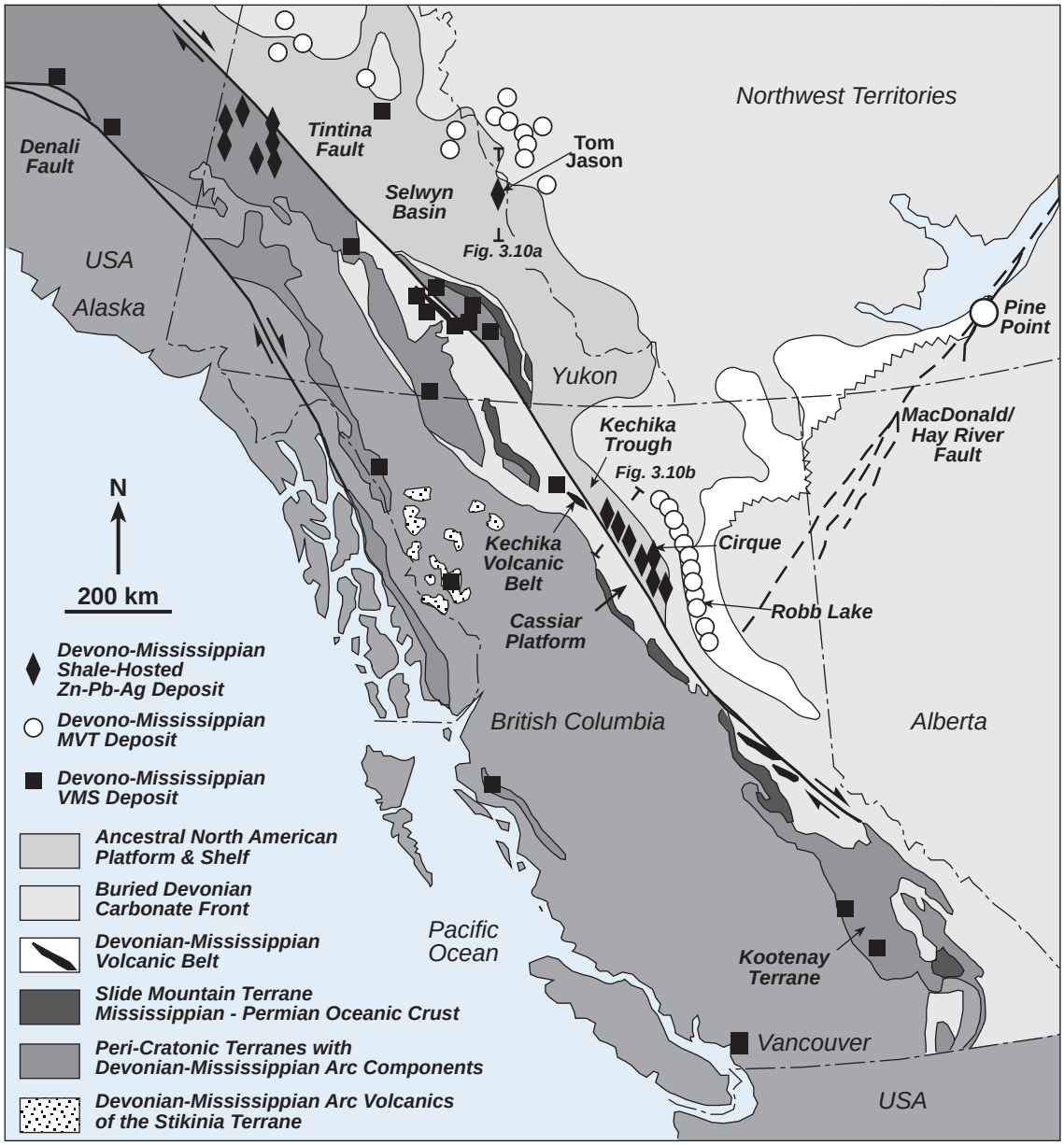


Figure 3.9. Mineral deposits of the Canadian Cordillera, showing the distribution of Devonian to Carboniferous sediment-hosted Zn-Pb-Ag deposits (modified from Nelson *et al.* 2002).

3.5.3 Examples of Sediment-Hosted Zn-Pb-Ag Deposits

Classic examples of sediment-hosted Zn-Pb-Ag deposits include the Middle Proterozoic Century, Dugald River, George Fisher, Hilton, HYC, Lady Loretta, McArthur River, and Mount Isa deposits of northeastern Australia (e.g. Broadbent, 1995; Broadbent *et al*. 1998; Bull & Rawlings, 1998; Large *et al*. 1998; McGoldrick *et al*. 1998; Perkins, 1998; Perkins *et al*. 1998; Perkins & Bell, 1998; Broadbent *et al*. 2002; Betts *et al*. 2003; Chapman, 2004), the Middle Proterozoic Sullivan deposit of British Columbia, Canada (e.g. Hamilton *et al*. 1982, 1983; McClay, 1983*a*, *b*; Hamilton *et al*. 2001), the Palaeozoic Anvil, Tom, Jason, Howard's Pass, Cirque, and Driftpile Creek deposits of the Selwyn basin and Kechika trough of northwest Canada (e.g. Abbott *et al*. 1986; McClay & Insley, 1986*b*; McClay & Bidwell, 1987; McClay *et al*. 1988, 1989; McClay, 1991; Goodfellow, 1998; Nelson *et al*. 2002), the Meggen and Rammelsberg deposits of Germany (e.g. Krebs, 1981), the Galmoy, Lisheen, Navan, Silvermines, and Tynagh deposits of Ireland (e.g. Hitzman & Large, 1986; Hitzman, 1999; Hitzman *et al*. 2002; Lee & Wilkinson, 2002) and the Qanaiyaq, Main, Aqqaluk, Paalaaq, Anarraaq, Su-Lik, Wulik, and Aktigiruq deposits of the Red Dog district in Alaska (e.g. Moore *et al*. 1986, Young, 1989; Jennings *et al*. 1998; Jennings & King, 2002; King *et al*. 2002; Kelley & Jennings, 2004; Kelley *et al*. 2004*a*, *b*; Young, 2004). An inventory of sediment-hosted Zn-Pb-Ag and barite deposits is presented in Table 3.1.

3.5.4 General Characteristics

Sediment-hosted Zn-Pb-Ag deposits are very diverse and show important variations in mineral parageneses, chemical compositions, textures, sizes, ore grades, association with magmatism and lithologies of the host rocks (e.g. Goodfellow *et al*. 1993, 1998; Goodfellow, 1999; Large, 2001). The main economic minerals of sediment-hosted Zn-Pb-Ag deposits are sphalerite and galena (e.g. Large, 1980, 1983; Goodfellow *et al*. 1993; Goodfellow, 1999). Associated minerals include pyrite, pyrrhotite, chalcopyrite, and barite (e.g. Briskey, 1986; Goodfellow *et al*. 1993). Barite typically occurs in large amounts, forming 25% or more of the total mineralization (e.g. Goodfellow *et al*. 1993). The most common gangue mineral is quartz, in part of hydrothermal origin, which typically occurs in the form of silica or chert (e.g. Goodfellow *et al*. 1993). Relative abundance of sulphide minerals varies from deposit to deposit and also within a single deposit (Large, 1983). Pb/Zn ratios commonly range from 1:1 to 1:8 (e.g. Large, 1983).

Deposit	Location	Zn (%)	Pb (%)	Cu (%)	Ag (g/T)	Au (g/T)	Barite	Size (Mt)	Age (Ma)
Jurassic									
Santa Lucia	Cuba	5.7	1.8	0.0	30.0	0.0	Yes	19.4	150
Gunga	Pakistan	5.0	1.0	0.0	0.0	0.0	Yes	10.0	150
Duddar	Pakistan	16.4	3.9	0.0	0.0	0.0	Yes	1.0	150
Filizchai	Azerbaijan	7.0	1.0	2.1	0.0		?	5.0	175
Carboniferous									
Red Dog (Qanaiyaq)	Alaska	18.0	5.0				Yes	9.0	~330
Red Dog (Main)	Alaska	19.0	5.0				Yes	48.0	~330
Red Dog (Aqqaluk)	Alaska	14.0	4.0				Yes	72.0	~330
Red Dog (Paalaaq)	Alaska	15.0	4.0				Yes	13.0	~330
Su-Lik	Alaska	8.8	3.0	0.0	28.0	0.0	Yes	25.0	~330
Anarraaq	Alaska	18.0	5.4		85.0		Yes	18.0	~330
Galmoy	Ireland	10.9	1.0				?	6.7	340
Lisheen	Ireland	12.0	1.5	0.0	32.0	0.0	?	20.0	340
Navan	Ireland	10.1	2.6	0.0	0.0	0.0	No	69.9	340
Silvermines	Ireland	6.4	2.5	0.0	23.0	0.0	Yes	17.7	340
Tynagh	Ireland	4.5	4.8	0.4	46.5	0.0	Yes	13.6	340
Walton	Nova Scotia	1.4	4.3	0.6	305.5	0.0	Yes	0.7	340
Late Devonian									
Tom	Yukon	7.0	4.6	0.0	49.1	0.0	Yes	15.7	350
Jason	Yukon	7.4	6.5	0.0	79.9	0.0	Yes	10.1	370
Cirque	BC Canada	8.0	2.0	0.0	0.0	0.0	Yes	52.2	370
Driftpile	BC Canada	11.9	3.1	0.0	0.0	0.0	Yes	2.4	370
Elura	Australia	8.4	5.6	0.0	139.0	0.0	Yes	27.0	370
Meggen	Germany	7.0	1.0	0.1	14.0	0.0	Yes	50.0	370
Rammelsberg	Germany	16.4	7.8	1.0	103.0	0.0	Yes	27.2	370
Zhairem	Khazakhstan	5.0	2.0	0.5	0.0	0.0	Yes	N/A	370
Tekeli	Khazakhstan	6.0	5.0	1.0	0.0	0.0	Yes	6.0	380
Early Silurian									
Howards Pass	Yukon	5.0	2.0	0.0	9.0	0.0	No	476.0	435
Howards Pass	Yukon	5.0	2.0	0.0	9.0	?	No	476.0	435
Peary Land	Greenland	8.0	1.0	0.0	?	0.0	No	12.0	435
El Aguilar	Argentina	8.5	6.5	0.1	100.0	0.0	No	30.0	450
Bleikvassli	Norway	7.5	3.0	0.4	0.0	0.0	No	6.0	460
Mofjellet	Norway	4.7	1.0	0.4	0.0	0.0	No	4.2	460
Early Cambrian									
Dy	Yukon	6.7	5.5	0.1	84.0	1.0	Yes	21.1	510
Faro	Yukon	5.7	3.4	0.0	36.0	0.0	Yes	57.6	510
Grum	Yukon	4.9	3.1	0.0	49.0	0.0	Yes	31.0	510
Swim	Yukon	4.7	3.8	0.0	42.0	0.0	Yes	4.3	510
Vangorda	Yukon	4.9	3.8	0.3	54.0	0.8	Yes	7.5	510
Koushk	Iran	15.0	3.0	0.0	0.0	0.0	?	5.0	510

Table 3.1. Inventory of sediment-hosted Zn-Pb-Ag deposits (modified from Goodfellow *et al*. 1993; Goodfellow, 1998. 1999). Tonnages and grades for the deposits of the Red Dog district are from King *et al*. (2002), Kelley & Jennnings (2004), and Kelley *et al*. (2004*a*).

Portel	Portugal	1.4	0.2	0.0	0.0	0.0	Yes	35.0	510
Fuenteheridos	Spain	2.0	0.2	0.0	0.0	0.0	Yes	100.0	510
Duncan	Canada	3.1	3.3	0.0	0.0	0.0	?	2.8	550
H.B	Canada	4.1	0.8	0.0	4.8	0.0	?	6.5	550
Jersey	Canada	3.5	1.7	0.0	3.1	0.0	?	7.7	550
Mel	Canada	5.6	2.1	0.0	0.0	0.0	Yes	4.8	550
Reeves-MacDonald	Canada	3.5	1.0	0.0	3.4	0.0	?	5.8	550
Late Proterozoic									
Aberfeldy	Scotland	1.2	0.4	0.0	0.0	0.0	Yes	N/A	600
Middle Proterozoic									
Kholodnina	Russia	7.0	1.5	0.0	0.0	0.0	?	N/A	1075
Rosh Pinah	Namibia	7.0	2.0	0.1	0.0	0.0	Yes	17.4	1100
Jiashengpan	China	3.8	1.3	0.0	0.0	0.0	No	N/A	1300
Balmat-Edwards	USA	10.1	0.3	0.0	0.0	0.0	No	17.4	1300
New Calumet	Canada	8.8	2.8	0.2	0.0	0.1	No	1.3	1300
Sullivan	Canada	5.5	5.8	0.0	59.0	0.0	No	170.0	>1468
Sargipali	India	0.4	2.0	0.0	65.0	0.0	?	N/A	1600
Big Syn	South Africa	2.5	1.0	0.1	12.9	0.0	Yes	101.0	1650
Black Mountain	South Africa	0.6	2.7	0.8	29.8	0.0	Yes	81.6	1650
Broken Hill	South Africa	1.8	3.6	0.3	48.1	0.0	Yes	85.0	1650
Gamsberg	South Africa	7.1	0.5	0.0	6.0	0.0	Yes	150.0	1650
Century	Australia	10.0	1.5	0.0	30.0	0.0	?	120.0	1670
Hilton	Australia	10.2	6.5	0.0	137.9	0.0	No	72.0	1670
Lady Loretta	Australia	14.0	8.0	0.0	110.0	0.0	Yes	9.0	1670
Mount Isa	Australia	6.0	7.0	0.1	160.0	0.0	No	125.0	1670
Dugald River	Australia	15.0	2.0	0.0	62.0	0.0	No	12.0	1670
HYC	Australia	9.5	4.1	0.0	40.0	0.0	No	227.0	1690
Broken Hill	Australia	12.0	13.0	0.2	175.0	0.0	No	300.0	1690
Balaria (Zawar)	India	5.6	1.1	0.0	0.0	0.0	No	19.0	1700
Baroi Magra	India	1.2	4.3	0.0	0.0	0.0	No	11.0	1700
Mochia (Zawar)	India	3.8	1.7	0.0	0.0	0.0	No	27.0	1700
Zarwarmala	India	3.7	2.1	0.0	0.0	0.0	No	18.0	1700
Dariba	India	7.3	2.0	1.0	5.0	0.0	No	13.0	1800
Dariba	India	1.2	4.0	0.3	200.0	0.0	No	31.6	1800
Dariba-Rajpura	India	5.1	1.2	1.1	122.0	0.0	No	51.0	1800
Rampura-Agucha	India	13.5	1.6	0.0	45.0	0.0	No	61.1	1800
Saladipura	India	1.0	0.0	0.0	0.0	0.0	No	115.0	1800
Sindesar	India	2.1	0.5	0.0	0.0	0.0	No	70.0	1800

Table 3.1. (continued). Inventory of sediment-hosted Zn-Pb-Ag deposits (modified from Goodfellow *et al*. 1993; Goodfellow, 1998. 1999). Tonnages and grades for the deposits of the Red Dog district are from King *et al*. (2002), Kelley & Jennnings (2004), and Kelley *et al*. (2004*a*).

The mineralization commonly occurs as stratiform, massive to disseminated sulphides in sheet-like or lens-like tabular bodies that are commonly interbedded with black shales, siltstones, limestones, evaporites, cherts, and sandstones (e.g. Large, 1980; Carne & Cathro, 1982; Lydon, 1983; Abbott *et al*. 1986; Briskey, 1986; Sangster, 1990; Goodfellow *et al.* 1993; Goodfellow, 1999; Large, 2001, 2003). Common depositional textures include fine-grained layered sulphides, framboidal and colloform pyrite with overgrowths together with granular sphalerite, galena and pyrite. Sulphide grain size typically ranges from 150 to 400 µm (e.g. McClay, 1983). In metamorphic and highly complexly deformed areas, metamorphism may partially or completely replace the original depositional textures and increases grain size through recrystallization and development of porphyroblastic textures (e.g. McClay, 1983).

3.5.5 Tectonostratigraphic Setting

Sediment-hosted Zn-Pb-Ag deposits form in a wide range of tectonostratigraphic settings (e.g. Sawkins, 1976; Large, 1980; Goodfellow *et al.* 1993; Goodfellow, 1999; Large, 2003). Most deposits are believed to have formed at either Atlantic-type rifted continental margins or long-lived failed intracontinental rift basins (e.g. Sawkins, 1976; Large, 1980, 1983; Briskey, 1986; Goodfelllow *et al.* 1993; Goodfellow, 1999; Large, 2001; Large *et al.* 2002) (Fig. 3.10). Betts *et al.* (2003) have recently proposed back arc basins as a favourable tectonic setting for the development of sediment-hosted Zn-Pb-Ag deposits. Passive margins, intracontinental rifts, and back arc basins are commonly characterized by a continuous sedimentary record that spans for hundreds of million of years (e.g. Goodfellow *et al*. 1993; Goodfellow, 1998, 1999; Betts *et al*. 2003). Examples of long-lived basins hosting sediment-hosted Zn-Pb-Ag deposits include the Selwyn basin and Kechika trough of northwest Canada (e.g. Abbott *et al.* 1986; McClay & Insley, 1986*b*; McClay & Bidwell, 1987; McClay *et al*. 1988, 1989; Goodfellow *et al*. 1993; Goodfellow, 1998, 1999) and the Mount Isa basin of northeastern Australia (e.g. Bull & Rawlings, 1998; Perkins, 1998; Betts & Lister, 2002; Betts *et al.* 2003). These basins commonly have horst and graben geometries characterized by abrupt facies or thickness changes with development of local unconformities (Goodfellow *et al*. 1993). Moderate magmatism including basaltic volcanic rocks or sills commonly accompany the rifting event (e.g. Goodfellow *et al.* 1993; Goodfellow, 1999) (Fig. 3.10). Most sediment-hosted Zn-Pb-Ag deposits appear to be spatially and genetically

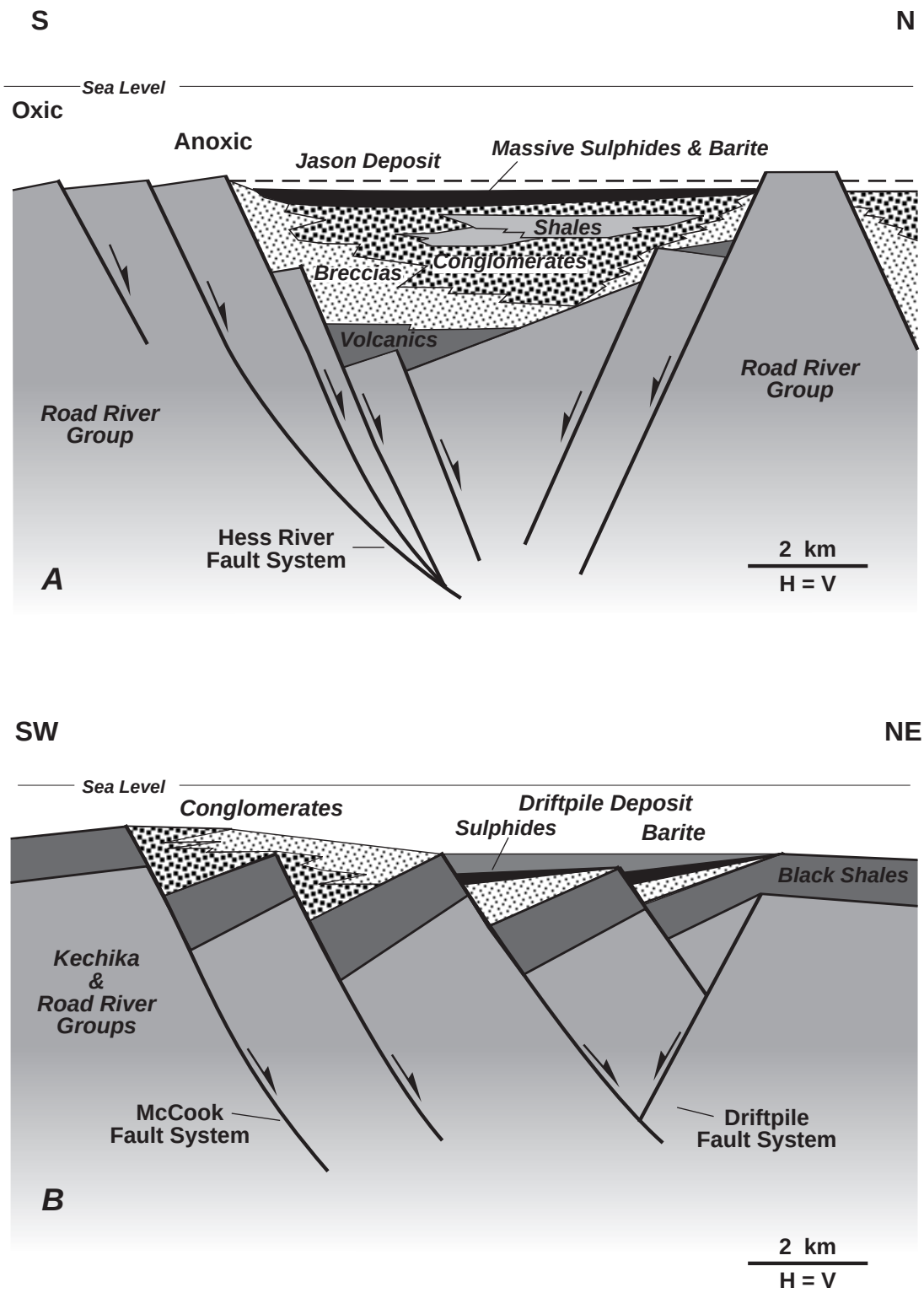


Figure 3.10. Cross sections through the Jason and Driftpile sediment-hosted Zn-Pb and barite deposits, northern Canadian Cordillera. **A.** MacMillan Pass graben system, Selwyn Basin, Yukon Territory (modified from McClay & Bidwell, 1987). **B.** Gataga graben system, Kechika Trough, northeast British Columbia (modified from McClay *et al*. 1988). Refer to Figure 3.9 for approximate location of cross sections.

related to syn-sedimentary extensional faults (e.g. Goodfellow *et al.* 1993; Hitzman, 1999) and commonly form in half-grabens near the down-faulted margins or in adjacent bathymetric depressions (e.g. Goodfellow *et al.* 1993) (Fig. 3.10). Mineralization is typically localized near or at the intersection between fault systems (e.g. Goodfellow *et al*. 1993; Goodfellow, 1998, 1999; Hitzman, 1999; Betts & Lister, 2002; Betts *et al.* 2003). Sediment-hosted Zn-Pb-Ag deposits are believed to have formed during syn-rift extensional faulting (e.g. McClay & Insley, 1986*b*; McClay & Bidwell, 1987; McClay *et al*. 1988, 1989), post-rift extensional reactivation of fault systems (e.g. Goodfellow *et al*. 1993) or during regional contraction and basin inversion (e.g. Broadbent *et al.* 1998).

3.5.6 Temporal Distribution of Sediment-Hosted Zn-Pb-Ag Deposits

Sediment-hosted Zn-Pb-Ag deposits appear in the Proterozoic and become rare after the Carboniferous (Goodfellow *et al.* 1993) (Fig. 3.11; Table 3.1). This contrasts with the temporal distribution of other Zn-Pb deposit types (e.g. volcanogenic massive sulphide deposits), which span for a larger portion of geological time (e.g. Goodfellow *et al.* 1993; Lydon, 1995; Goodfellow, 1999). Proterozoic sediment-hosted Zn-Pb-Ag deposits formed at the rifted continental margins of Rodinia (Fig. 3.12a). Phanerozoic sediment-hosted Zn-Pb-Ag deposits formed from Middle Devonian to Early Carboniferous (Mississippian) time and are spatially related to the rifted continental margins of Pangea (e.g. Goodfellow *et al.* 1993; Goodfellow, 1999) (Fig. 3.12b). Faunal assemblages and the association of the deposits with fossiliferous limestones indicate that most Phanerozoic sediment-hosted Zn-Pb-Ag deposits were deposited in palaeogeographic locations within 30° north and south of the Equator at water depths of approximately 500 m or more (e.g. Goodfellow *et al*. 1993; Goodfellow, 1999). Barite is common in Phanerozoic deposits but rare in deposits of Proterozoic age (Goodfellow *et al*. 1993) (Table 3.1). A less productive event of sediment-hosted Zn-Pb-Ag deposits occurred in Jurassic and Cretaceous time along the Tethyan continental margins (e.g. Large, 2001). Sediment-hosted Zn-Pb mineralization systems are believed to be forming in the Present Day. Examples include the Guaymas basin (northern Gulf of California), the Red Sea, and the Afar Rift (e.g. Lonsdale *et al.* 1980; Goodfellow & Blaise, 1988; Goodfellow & Franklin, 1994; Goodfellow, 1999) (Fig. 3.13).

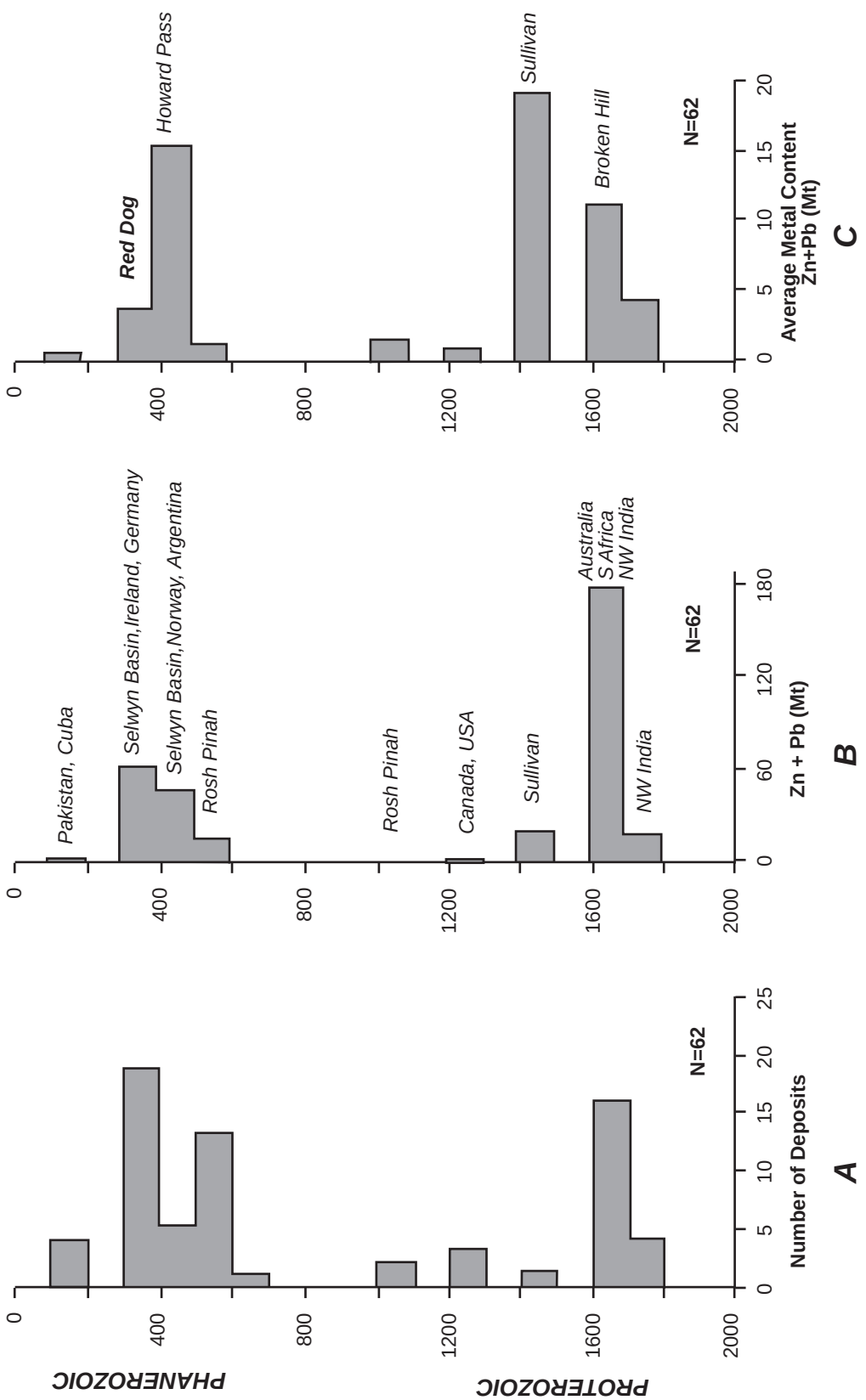


Figure 3.11. Temporal distribution of sediment-hosted Zn-Pb-Ag deposits. **A.** Number of deposits per 100 Ma interval. **B.** Tonnes of combined zinc and lead per 100 Ma interval. **C.** Average metal content of deposits per 100 Ma interval (from Lydon, 1995).

A. PROTEROZOIC



B. PHANEROZOIC

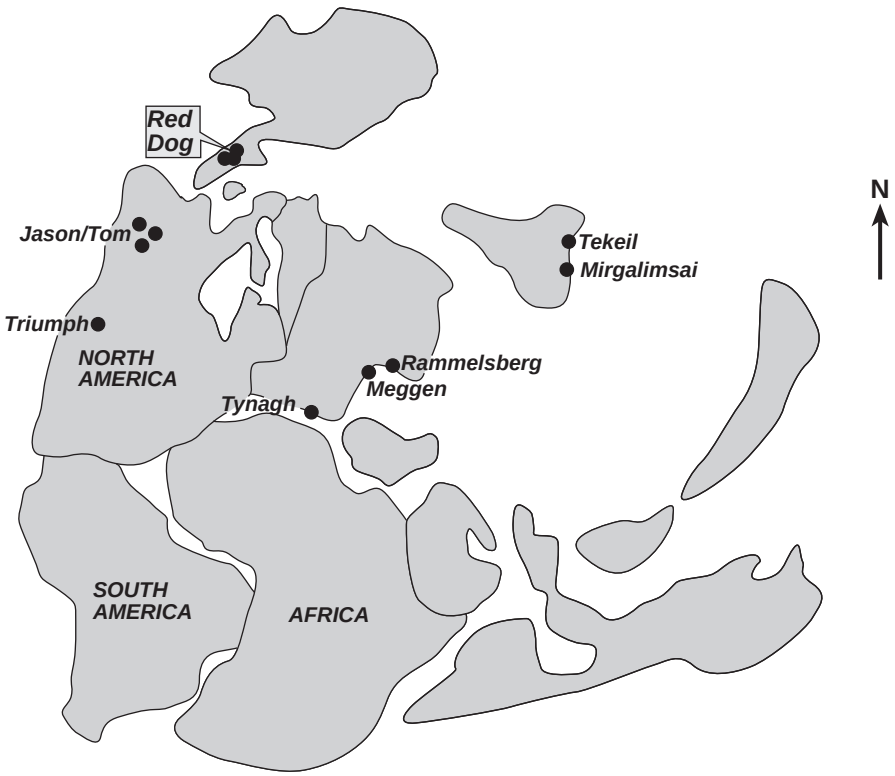


Figure 3.12. Temporal distribution of sediment-hosted Zn-Pb-Ag deposits (modified from Goodfellow, 1999). **A.** Proterozoic and Lower Cambrian deposits plotted on a Proterozoic paleogeographic reconstruction. **B.** Devonian and Carboniferous deposits plotted on the Late Devonian palaeogeographic reconstruction of Pangea. The location of the Red Dog district is shown.

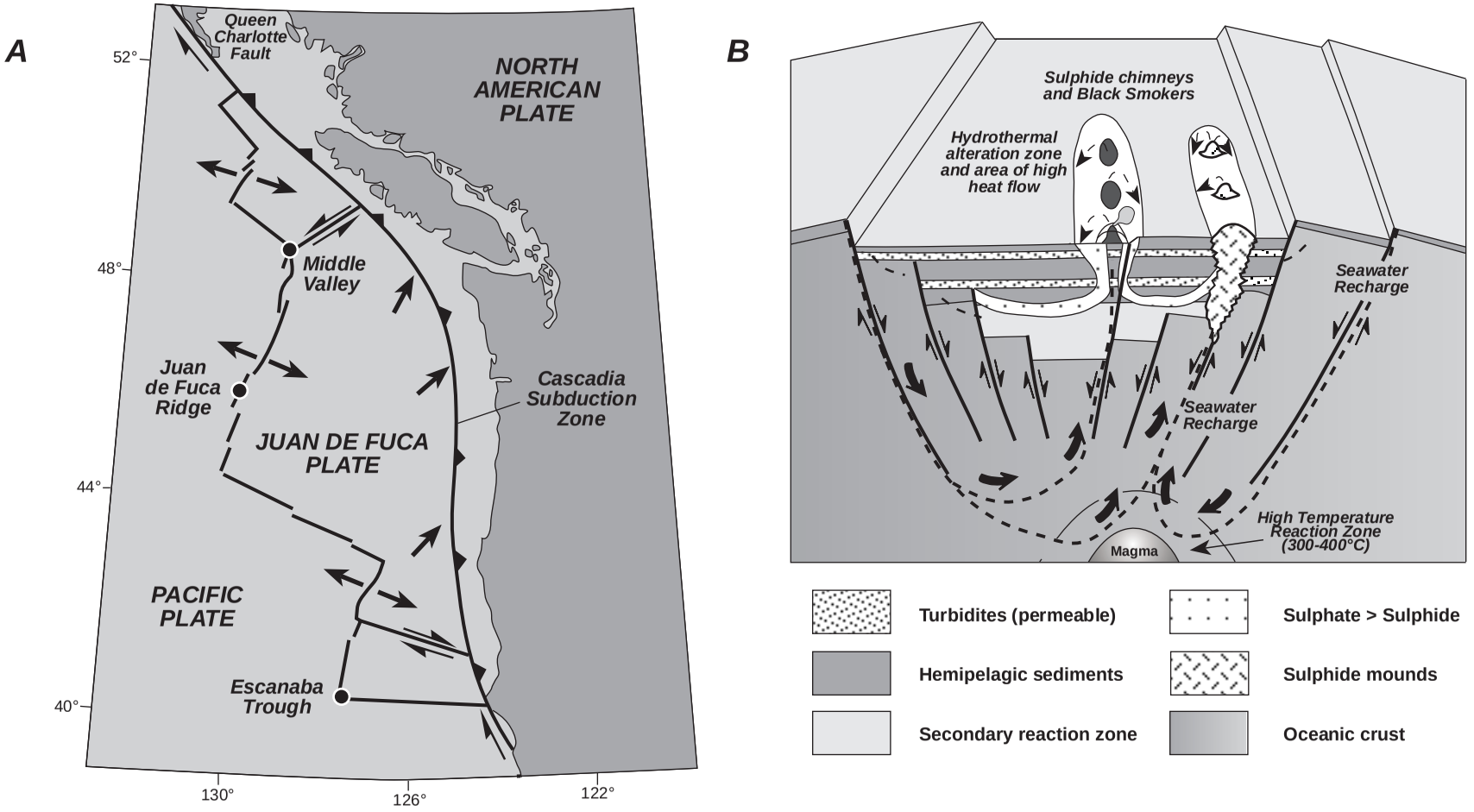


Figure 3.13. Modern Zn-Pb hydrothermal systems (modified from Goodfellow, 1999). **A.** Location of the Middle Valley, Juan de Fuca Ridge, and Escanaba Zn-Pb deposits in relationship with the major tectonic elements. Arrows indicate relative plate movement. **B.** Model for the formation of massive sulphide deposits, Middle Valley, northern Juan de Fuca Ridge.

3.5.7 Morphology and Structure of Sediment-Hosted Zn-Pb-Ag Deposits

Sediment-hosted Zn-Pb-Ag deposits are typically zoned about inferred vent systems (Goodfellow *et al*. 1993; Goodfellow, 1999) (Fig. 3.14). They commonly consist of a vent complex, bedded ore facies, and distal facies (Fig. 3.14). In addition, many deposits have a feeder pipe and a zone of hydrothermal alteration (Fig. 3.14). The bulk of the mineralization is contained in a stratiform body that typically has a high lateral extent-to-thickness ratio, approximately ≥20 (e.g. Large, 1983; Goodfellow *et al*. 1993; Goodfellow, 1999). They commonly occur as sheets or tabular lenses (Fig. 3.14) up to a few tens of metres thick and more than 1 km long (e.g. Large, 1983; Briskey, 1986; Goodfellow *et al*. 1993; Goodfellow, 1999).

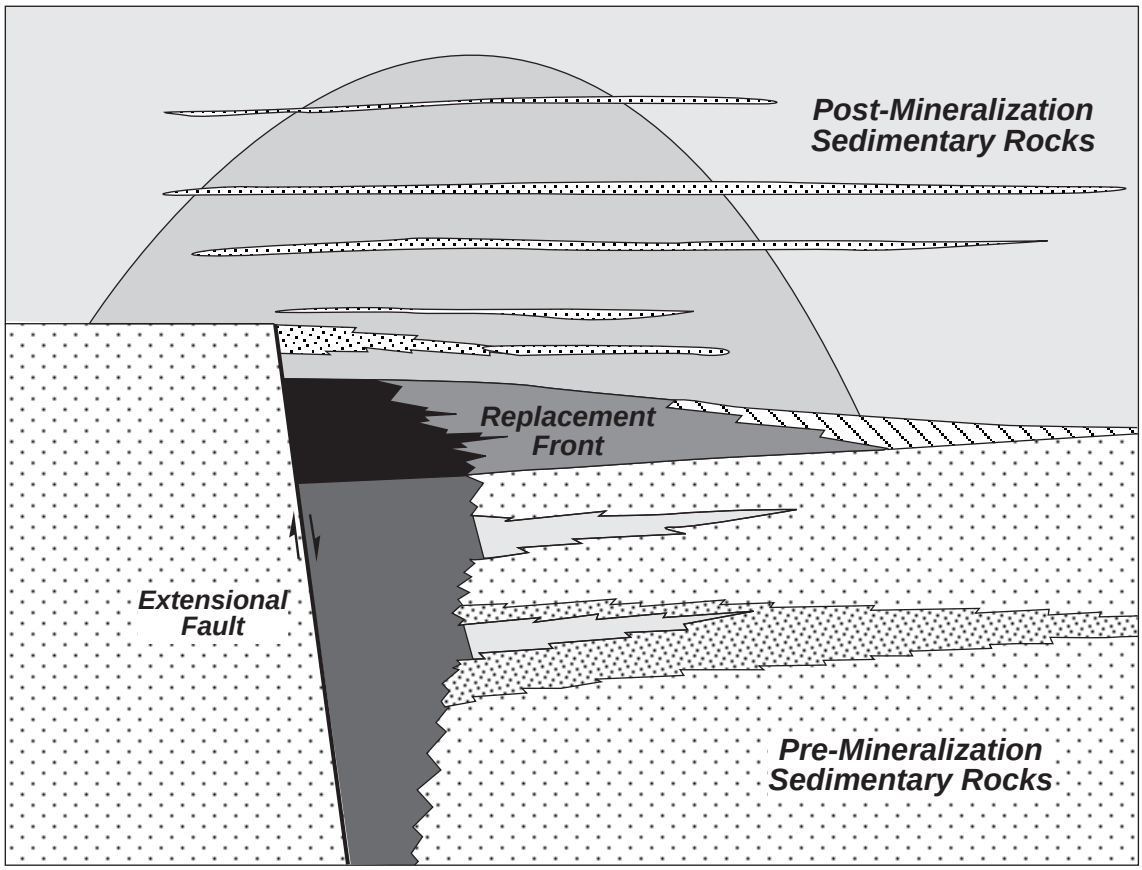
Sulphide minerals and textures grade and thickness of sediment-hosted Zn-Pb-Ag deposits are characteristically zoned with Zn/Pb ratios that increase away from the vent complex (Goodfellow *et al*. 1993; Goodfellow, 1999). Zonation has been documented for many deposits, including Sullivan (e.g. Hamilton *et al*. 1982), Red Dog (e.g. Moore *et al*. 1986; Young, 1989), and the deposits of the Selwyn basin and Kechika trough (e.g. Abbott *et al*. 1986; McClay & Insley, 1986*b*; McClay & Bidwell, 1987; McClay *et al*. 1988, 1989; McClay, 1991; Goodfellow, 1998, 1999).

Vent Complex

The vent complex is the zone of interaction between the ascending hydrothermal mineralizing fluids and the host sediments (Fig. 3.14). It is the most distinctive and economically important zone of most sediment-hosted Zn-Pb-Ag deposits and typically consists of massive zones, replacement patches, irregular veins and/or disseminations of sulphides together with varying amounts of carbonate and quartz (e.g. Goodfellow *et al*. 1993; Goodfellow, 1999) (Fig. 3.14). Sulphide minerals include pyrite, pyrrhotite, galena, sphalerite, ferroan carbonate, dolomite, quartz, tourmaline, lesser muscovite, chlorite, chalcopyrite, arsenopyrite, and sulphosalt minerals (Goodfellow *et al*. 1993; Goodfellow, 1999) (Fig. 3.14).

Bedded Ore Facies

The bedded ore facies consists of sulphides that are regularly interbedded with layers of the host rock (Goodfellow *et al*. 1993; Goodfellow, 1999) (Fig. 3.14). Host lithologies



Sedimentary-hydrothermal Facies (sphalerite, galena, pyrite, pyrrhotite, chalcopyrite, interbedded with barite, chert and pelagic/clastic sedimentary rocks)

Distal Sedimentary Facies
(barite, carbonates, Fe-oxides, phosphates, pyrite, minor sphalerite, chert)

Vent Complex (bedded sulphides brecciated, veined and variably replaced by a combination of chalcopyrite tetrahedrite, arsenopyrite, pyrrhotite, galena and sphalerite)

Feeder Pipe (footwall sedimentary rocks brecciated infilled and variably replaced by one or more combinations of quartz, carbonates, chlorite, sericite, tourmaline and minor sulphides)

Hydrothermal Alteration Zone
(albite, chlorite, carbonates, minor sulphides)

Fault-scarp Sedimentary Breccia

Strata-bound zones of infilling, replacement and alteration of permeable sedimentary units

Thin beds of hydrothermal minerals
(barite, apatite, pyrite, minor sphalerite)

Figure 3.14. Schematic section (not to scale) showing the main elements of sediment-hosted Zn-Pb-Ag and barite deposits (modified from Goodfellow *et al*. 1993; Goodfellow, 1999).

include cherts, limestones, organic matter, sedimentary breccias, shales, siltstones, sandstones and conglomerates of turbiditic origin (Goodfellow *et al*. 1993; Goodfellow, 1999). The most common minerals are pyrite, pyrrhotite, sphalerite, galena that are typically interlayered with cherts and carbonates (Goodfellow, 1999). Individual sulphide layers range in thickness from a few millimetres to centimetres (Goodfellow *et al*. 1993). Sulphide laminae are usually monomineralic, whereas thicker sulphide layers are commonly polimineralic and show a marked vertical compositional zonation (Goodfellow *et al*. 1993). Bedding contacts are normally sharp, particularly between sulphide-rich layers and the host lithologies.

Distal Sedimentary Facies

The distal sedimentary facies (Fig. 3.14) consist of low-grade bedded or layered sulphides (pyrite and minor sphalerite) together with other products (e.g. barite, carbonates, phosphates, cherts) that are deposited away from the centre of the vent complex (Goodfellow, 1999) (Fig. 3.14). The contact between the bedded ore facies and the distal sedimentary facies is in most cases gradational (Goodfellow *et al*. 1993).

Feeder Pipe

The feeder pipe underlies the vent complex and is the zone of reaction between the ascending mineralizing fluids and the sediments below the vent complex (Goodfellow *et al*. 1993; Goodfellow, 1999) (Fig. 3.14). The feeder zone is typically spatially associated with a syn-sedimentary extensional fault (Goodfellow, 1998, 1999) (Fig. 3.14). Fault-scarp breccias, debris flows, and abrupt facies changes suggest that extensional faulting was active before, during and after sulphide formation (Goodfellow *et al*. 1993; Goodfellow, 1999) (Fig. 3.14). Although feeder pipes are common in sediment-hosted Zn-Pb-Ag deposits they have not been identified for all deposits (e.g. Howards Pass, Cirque) (e.g. Goodfellow, 1998, 1999).

Hydrothermal Alteration Zone

A zone of hydrothermal alteration commonly overlies sediment-hosted Zn-Pb-Ag deposits (Fig. 3.14). Alteration commonly includes stockwork, and/or disseminated sulphides together with silica, albite, and chlorite (e.g. Briskey, 1986; Goodfellow *et al*. 1993; Goodfellow, 1999) (Fig. 3.14). Extensive hydrothermal alteration in the rock

overlying some sediment-hosted Zn-Pb-Ag deposits suggests that discharge continued after the formation of the main stratiform sulphide body (e.g. Goodfellow, 1998, 1999). Examples include the albite-chlorite alteration zones overlying the Sullivan deposit (e.g. Hamilton *et al*. 1982, 1983; Goodfellow *et al.* 1993; Goodfellow, 1999) and extensive silicification in the Red Dog deposits (e.g. Kelley *et al*. 1995) and the Meggen deposit (e.g. Kelley & Jennings, 2004).

3.5.8 Genesis of Sediment-Hosted Zn-Pb-Ag Deposits

The formation of sediment-hosted Zn-Pb-Ag deposits requires a sedimentary basin, the generation and migration of metalliferous hydrothermal fluids, and the fixation and preservation of the transported metals as sulphides on or near the sea floor (e.g. Large, 1980, 1983; Goodfellow *et al*. 1993; Goodfellow, 1999). Sediment-hosted Zn-Pb-Ag deposits have traditionally been interpreted as being the result of syn-sedimentary exhalative processes on the sea floor (e.g. Carne & Cathro, 1982; Large, 1983; Goodfellow *et al*. 1993; Lydon, 1995). Sedimentary exhalative models suggest that metalliferous fluids are expelled onto the sea floor and reacted with a reduced water column to precipitate sulphides coeval with sedimentation (e.g. Carne & Cathro, 1982; Goodfellow et al. 1993). Laminated sulphide textures typically reflect episodicity in the hydrothermal activity and sulphide deposition.

An alternative for the formation of sediment-hosted Zn-Pb-Ag deposits comes from the extensive research on the deposits of northeastern Australia (e.g. Broadbent, 1995; Broadbent *et al*. 1998; Bull & Rawlings, 1998; McGoldrick *et al*. 1998; Perkins, 1998; Perkins & Bell, 1998; Perkins *et al*. 1998; Betts & Lister, 2002; Broadbent *et al*. 2002; Betts *et al*. 2003), which are thought to have formed either by hydrothermal basin derived fluids that migrated during basin inversion into the post-rift strata or by wholesale replacement of reactive strata by hydrothermal fluids during regional deformation and metamorphism (e.g. Broadbent *et al.* 1998; McGoldrick *et al.* 1998; Perkins, 1998; Perkins & Bell, 1998; Perkins *et al*. 1998; Broadbent *et al*. 2002; Betts *et al*. 2003).

Replacement of sulphide minerals has been recognized in many sediment-hosted Zn-Pb-Ag deposits including Navan (e.g. Ashton, 1986), Broken Hill (e.g. Wright *et al.* 1987),

Tom (e.g. Goodfellow *et al*. 1993), Dugald River, Lady Loretta and McArthur River (e.g. Muir, 1983), Century (e.g. Broadbent *et al*. 1998; G. C. Broadbent, 2002, *pers. comm.*), Lisheen (Hitzman *et al*. 2002; Lee & Wilkinson, 2002), and the deposits of the Red Dog district (Young, 1989; Sims, 1996; Jennings *et al*. 1998; King *et al*. 2002; Kelley & Jennings, 2004; Kelley *et al*. 2004*a, b*).

Diagenetic models suggest that the discharge of metalliferous fluids occurs along permeable strata at shallow depths below the sea floor (Eldridge *et al*. 1993). In this model, laminated sulphides are commonly interpreted to reflect permeability contrasts in the host sediments. Epigenetic models (e.g. Broadbent *et al*. 1998) form commonly associated to events of basin inversion. Perkins & Bell (1998) suggest that sulphide deposition occurs as a result of fluid and wall rock interactions during late orogenic hydrothermal activity.

Despite the diversity of timing and processes involved in sulphide deposition, the various genetic models share a number of characteristics. All models are based on the migration of metalliferous hydrothermal fluids, a network of faults and permeable strata to act as aquifers and to focus the mineralization, and the involvement of anoxic sediments (Betts *et al*. 2003).

Fluid Flow

Several models have been proposed to explain the migration of hydrothermal fluids to the seafloor of sedimentary basins hosting sediment-hosted Zn-Pb-Ag deposits (Goodfellow *et al*. 1993). These include the stratal aquifer model of Lydon (1983), the seismic pumping model of Sibson *et al*. (1975) and the convection cell model of Russell (1983).

Stratal Aquifer Model

The stratal aquifer model of Lydon (1983) postulated that a syn-rift clastic succession overlain by a seal of impermeable basinal shales is the ideal setting for the development of a geothermal reservoir, regardless of the heat source (e.g. Lydon, 1983; Goodfellow *et al*. 1993). The low thermal conductivity and low permeability of the shales significantly reduces conductive and convective heat loss, providing elevated

temperatures in the syn-rift reservoir and capable of sustaining a hydrothermal system for a prolonged period (Lydon, 1983). The discharge of ore-forming fluids is believed to be spatially and temporally related to rupture by extensional faulting of the shale seal (e.g. Lydon, 1983; Goodfellow *et al*. 1993; Goodfellow, 1999).

Seismic Pumping Model

The seismic pumping model (Sibson *et al.* 1975) postulated that the migration of hydrothermal fluids is controlled by tectonic stresses. The seismic pumping model suggested that an increase in tectonic stress along a fault surface causes dilation in the adjacent rocks (Sibson *et al*. 1975). Fluids that migrate into the low-pressure areas are expelled along the fault surface when shear failure and fault movement occur (Sibson *et al*. 1975; Goodfellow *et al*. 1993). The seismic pumping model was originally developed to explain the formation of epigenetic deposits (e.g. Sibson *et al*. 1975) but Goodfellow *et al.* (1993) and Goodfellow (1999) have argued that seismic pumping may also significantly contribute to the migration of hydrothermal fluids that form sediment-hosted Zn-Pb-Ag deposits. In addition, Goodfellow *et al*. (1993) argued that the seismic pumping model of Sibson *et al.* (1975) provides an explanation for the spatial association of sediment-hosted Zn-Pb-Ag deposits with extensional faults.

Convection Cell Models

Convection cell models have been proposed by Russell (1983). These models assume that a downward-propagating convective cell along extensional faults that use the elevated heat in a rifted continental crust (Russell, 1983; Goodfellow, 1999).

Location of Hydrothermal System

Cross-stratal migration of hydrothermal fluids at a single vent requires an unusual set of conditions (Goodfellow *et al*. 1993). Two models have been proposed. The first model invokes dilatant fault zones that provide a cross-stratal zone of high hydraulic conductivity (Goodfellow *et al.* 1993). A second model invokes subsurface hydrothermal fluid diapirs above a heat source, for example a magmatic body (Goodfellow *et al.* 1993).

The spatial association with syn-sedimentary growth faults have been well documented for many ancient sediment-hosted Zn-Pb-Ag deposits (e.g. Gordey *et al*. 1982; McClay & Insley, 1986*b*; McClay & Bidwell, 1987; McClay *et al*. 1988, 1989; McClay, 1991; Goodfellow *et al*. 1993; Broadbent, 1995; Broadbent *et al*. 1998; Goodfellow, 1998, 1999; Hitzman, 1999; Broadbent *et al*. 2002; Betts *et al*. 2003) and also in modern systems (Fig. 3.13). In the Middle Valley, northern Juan de Fuca Ridge, Escanaba Trough hydrothermal discharge presently focuses at the intersection of extensional and transform faults (Goodfellow *et al*. 1993) (Fig. 3.11).

3.6 MINERALIZATION OF THE RED DOG DISTRICT

The sediment-hosted Zn-Pb-Ag and barite mineralization of the Red Dog district has been described by Tailleur (1970), Nokleberg & Winkler (1978), Plahuta (1978), Plahuta & Robinson (1979), Lange *et al*. (1981), Lange *et al*. (1985), Moore *et al*. (1986), Young (1989), Edgerton (1997*a, b*), Schmidt (1997*a*) and Jennings *et al*. (1998). Recent descriptions include Ayuso *et al*. (2004), Kelley *et al*. (2004*a, b*), Kelley & Jennings (2004), Johnson *et al*. (2004), Leach *et al*. (2004), Slack *et al*. (2004), Werdon *et al*. (2004), and Young (2004).

The Zn-Pb-Ag and barite deposits of the Red Dog district occur in Late Mississippian black shales and carbonate strata of the Kuna Formation (Moore *et al*. 1986; Young, 1989; Jennings & King, 2002; King *et al*. 2002; Young, 2004) (Figs. 3.1, 3.3 & 3.15). The deposits occur in the Red Dog plate or sequence of the Brooks Range allochthon of Moore *et al*. (1986, 1989) (Figs. 3.5 & 3.15). Moore *et al*. (1986) initially described the Zn-Pb mineralization of the Red Dog area as a Mississippian to Pennsylvanian black shale-hosted Zn-Pb-Ag deposit that formed in the early stages of a long-lived starved sedimentary basin. The sediment-hosted Zn-Pb-Ag deposits of the Red Dog area have been more recently referred to as hybrid SEDEX-replacement deposit or as strata-bound syn-sedimentary replacement deposits (e.g. Jennings *et al*. 1998; Jennings & King, 2002; King *et al*. 2002).

3.6.1 Deposits of the Red Dog District

Mineralization of the Red Dog district occurs in three areas. These are the Red Dog Creek area (Moore *et al*. 1986; Young, 1989; King *et al*. 2002; Kelley *et al*. 2004*b*), Su-

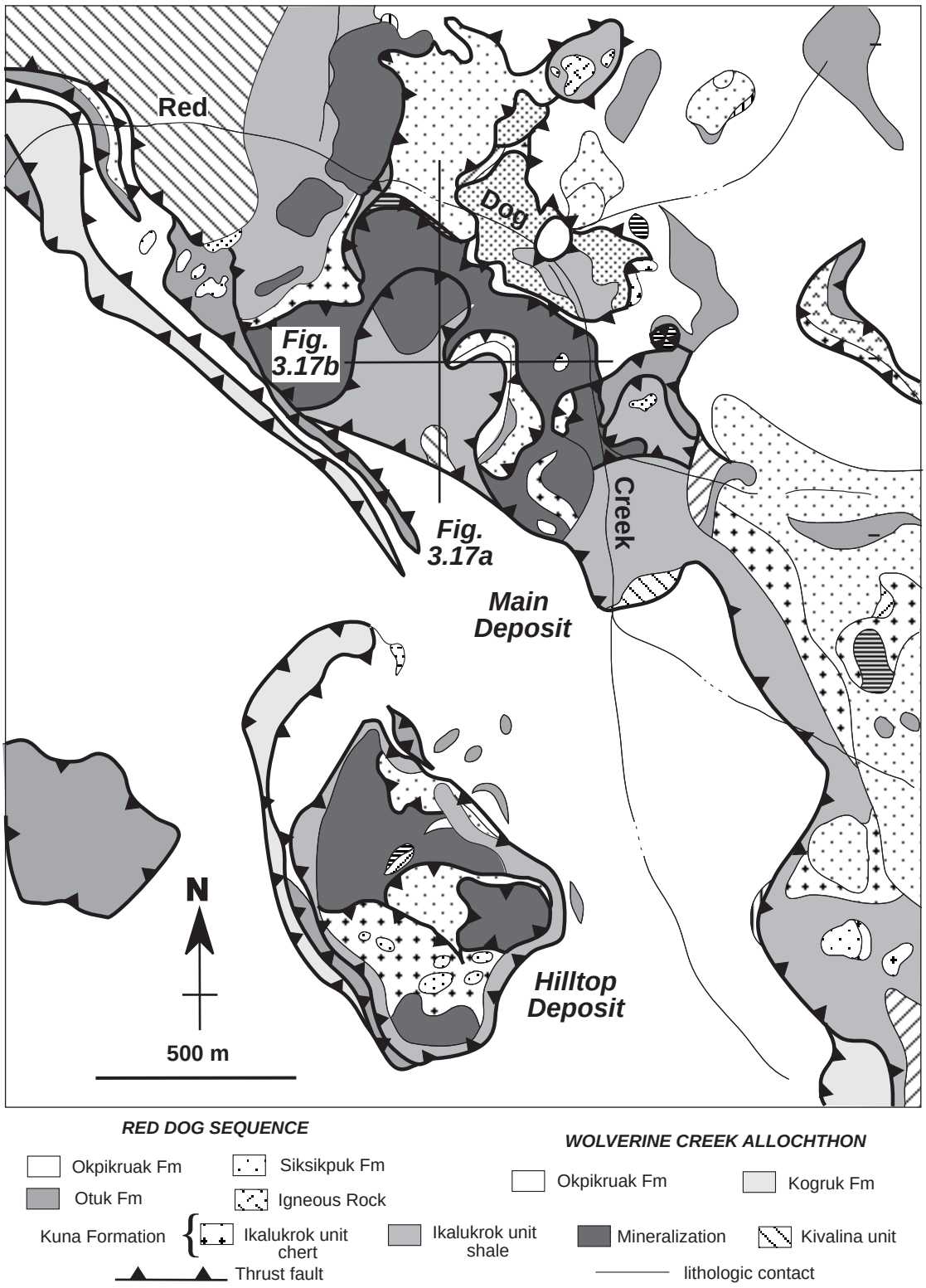


Figure 3.15. Geologic map of the Red Dog Creek area (modified from Moore et *al*. 1986).

Lik (Booth, 1983; Forrest, 1983; Forrest & Sawkins, 1987), and Anarraaq-Wulik (Jennings & King, 2002; King *et al*. 2002; Kelley *et al*. 2004*a*).

Deposits of the Red Dog Creek Area

The Red Dog Creek area contains four northerly-aligned deposits. From south to north, these are the Qanaiyaq, Main, Aqqaluk, and Paalaaq deposits (Moore *et al*. 1986; Young, 1989; King *et al*. 2002; Kelley *et al*. 2004*b*) (Fig. 3.5).

Qanaiyaq Deposit

The Qanaiyaq deposit (King *et al*. 2002), formerly known as Hilltop (Moore *et al*. 1986; Young, 1989) (Fig. 3.15), is approximately 90 m thick, 850 m long and 600 m wide (Nokleberg *et al*. 1994). It contains inferred resources of approximately 9 Mt at 18% Zn, 5% Pb (Moore *et al*. 1986; Young, 1989; King *et al*. 2002). The Qanaiyaq deposit, including a 10 m-thick interval at 3% Cu, is relatively rich in Cu compared with other deposits of the district (A. R. King, 2001, *pers. comm.*).

Main Deposit

The Main deposit (Fig. 3.15), originally referred to as the Red Dog deposit (e.g. Tailleur, 1970; Moore *et al*. 1986) contains 48 Mt at 19% Zn, 5% Pb (Moore *et al.* 1986; King *et al*. 2002; Kelley *et al*. 2004*b*). The Red Dog deposit is a stratabound accumulation of silica, barite rock, and sulphide rock. The Main deposit is vertically and laterally zoned (Moore *et al*. 1986). Most mineralization occurs in a massive Pb-Zn-rich vent complex below a silica and barite cap, and above a feeder zone characterized by sphalerite and galena veins that cut silicified black shale of the Ikalukrok unit (Moore *et al*. 1986; Goodfellow, 1999). Although sulphides are restricted to the Ikalukrok unit, significant barite occurs in the lower unit of the overlying Siksikpuk Formation. Sulphide vein mineralization is well developed in Ikalukrok unit host rocks, more commonly in silicified rock (e.g. Moore *et al*. 1986).

Aqqaluk Deposit

The Aqqaluk deposit is lens-shaped and has an approximate maximum thickness of about 180 m and is 700 to 900 m wide. The Aqqaluk deposit contain estimated resources of 72 Mt at 14% Zn and 4% Pb (Jennings *et al*. 1998; King *et al*. 2002).

Paalaaq Deposit

Paalaaq is the deepest and northernmost of the known deposits of the Red Dog Creek area. It lies at depths of 160 to 650 m and contains inferred resources of 13 Mt at 15% Zn and 4% Pb (Jennings *et al*. 1998; King *et al*. 2002).

Su and Lik Deposits

The Su and Lik deposits (e.g. Booth, 1983; Forrest, 1983; Forrest & Sawkins, 1983; Sterne *et al*. 1984), located approximately 19 km northwest of the Red Dog mine (Figs. 3.1 & 3.5), contain inferred resources of 34 Mt at 10% combined Zn and Pb (King *et al*. 2002). The Lik deposit consists of over 25 Mt at 8.8% Zn, 3% Pb and 38g/T silver (Booth, 1983) and hosted in Mississippian black shale of the Ikalukrok unit of the Kuna Formation (Forrest, 1983; Forrest & Sawkins, 1983; King *et al*. 2002). The Lik deposit is approximately 2 km long, 500 m wide and approximately 70 m thick (Forrest & Sawkins, 1983). Sulphide minerals include sphalerite, galena, pyrite, marcasite and tetrahedrite, which are present in four distinct textural associations that include laminar, complex, brecciated, and nodular ore (Forrest & Sawkins, 1983). The Su and Lik deposits lack the barite cap that characterizes the deposits of the Red Dog Creek area.

Deposits of the Anarraaq-Wulik Area

These include the recently discovered Anarraaq, Wulik, and Aktigiruq deposits (Jennings & King, 2002; Kelley & Jennings, 2002; King *et al*. 2002), which are located approximately 11 km northwest of the Red Dog mine.

Anarraaq Deposit

The Anarraaq deposit is located approximately 11 km north-northwest of the deposits of the Red Dog Creek area (Figs. 3.1 & 3.15) and has inferred resources of approximately 18 Mt at 18% Zn, 5.4% Pb, and 85 g/t Ag (King *et al*. 2002; Kelley *et al*. 2004*a*). The Anarraaq deposit lies approximately 700 m below surface and consists of strata-bound, banded to massive sphalerite, galena, and pyrite that occur in a lens-shaped orebody (Kelley *et al*. 2004*a*), approximately 530 m in length, 430 m in width and up to 100 m thick. The deposit is contained within a larger body of silicified and pyritic shales, approximately 900 m long, 700 m wide and 130 m thick and is overlain by a thick barite deposit (King *et al*. 2002; Kelley *et al*. 2004*a*) that is separated from the sulphides by

unmineralized black shales (King *et al*. 2002; Young, 2004). The Anarraaq deposit is estimated to contain approximately 1 Bt of barite and is one of the largest barite accumulations documented (King *et al*. 2002; Johnson *et al*. 2003, 2004; Kelley *et al*. 2004*a*).

The Anarraaq deposit shares many common characteristics with the deposits of the Red Dog area, such as the massive occurrence of barite and high-grade mineralization (King *et al*. 2002). The Anarraaq is however moderately less silicified than the deposits of the Red Dog Creek area (L. E. Young, 2001, *pers. comm*.), does not contain vein ore and has pyrite rich layered sulphides that does not occur in the deposits of the Red Dog Creek area (Kelley *et al*. 2004*a*).

Wulik and Aktigiruq Deposits

The Wulik deposit is poorly delineated (Kelley & Jennings, 2004) and may represent an extension or lateral equivalent of the Aktigiruq deposit. The Aktigiruq deposit is located approximately 4 km northwest of the Anarraaq deposit (Figs. 3.1 & 3.5). It lies 900 m below surface is still poorly delineated and open to further exploration (King *et al*. 2002). It contains high-grade intervals, including 23.8 m at 21 % Zn and 5.2 m at 46 % Zn (King *et al*. 2002). Drilling in 2004 intersected 35 m at 14.7% zinc (Teck Cominco Ltd., 2005). Mineralization extends to the west with grades as high as 30% Zn.

Other Mineral Occurrences

In addition to the major sediment-hosted Zn-Pb-Ag and barite deposits of the Red Dog Creek, Su-Lik, and Anarraaq-Wulik areas, the Red Dog district contains a number of sediment-hosted Zn-Pb and barite showings as well as Zn-Pb vein-breccia mineralization (e.g. Moore *et al*. 1986; Kelley *et al*. 1997, 2000; Young, 2000; Werdon *et al*. 2004; Young, 2004). These include the Anomaly Creek, Alvinella, Bear, Competition Creek, Ferric Creek, Fritz, Grizzly, Gull Creek, Husky, Moil-Wolf Creek, ORE, Su, Suds, TAK, TUT prospects amongst others (e.g. Sterne *et al*. 1984; Young, 2004) (Fig. 3.5).

Zn-Pb Vein-Breccia Mineralization

Zn-Pb vein-breccia mineralization consists of banded sulphides in veins and sulphide-bearing breccias (e.g. Kelley *et al*. 1997, 2000; Werdon *et al*. 2004; Young, 2004), which are sharply discordant with the host rocks (Werdon, 1999; Werdon *et al*. 2004). Vein-breccia mineralization occurs in Late Devonian to Early Mississippian clastic strata of the Noatak Sandstone and/or the Kanayut Conglomerate Endicott Group (Moore *et al*. 1986; Kelley & Mull, 1995; Kelley *et al*. 1997; Werdon, 1999; Kelley *et al*. 2000; Werdon *et al*. 2004; Young, 2004) (Fig. 3.1). Sulphide minerals include pyrite, galena and rare sphalerite, which occur as disseminations and/or intergranular replacements (e.g. Moore *et al*. 1986; Werdon, 1999, Kelley *et al*. 2000; Young, 2004). Zn-Pb vein-breccia mineralization has been interpreted as pathways for the mineralizing fluids that formed the deposits of the Red Dog district (e.g. Werdon, 1999; Kelley *et al*. 2000; L. E. Young, 2002, *pers. comm.*; Werdon *et al.* 2004; J. J. Wilkinson, 2004, *pers. comm*.) or as remobilization of disseminated sulphides along faults during the Mesozoic Brookian orogeny or younger Tertiary contractional episodes (e.g. Ellersieck *et al*. 1982, 1990; Kurtak *et al*. 1995; Werdon *et al*. 1996; T. E. Moore, 2004, *pers. comm*.).

Structure of the Deposits of the Red Dog District

The structure of the Zn-Pb-Ag and barite deposits of the Red Dog district is poorly understood due to the lack of exposure, except in the open pit of the Red Dog mine. Most information comes from exploration drilling in the Red Dog Creek (e.g. Moore *et al*. 1986; Sims, 1996; Edgerton, 1997*a, b*; Jennings *et al*. 1998).

Structure of the Main Deposit

Moore *et al*. (1986) proposed that the structure of the Main deposit is controlled by northerly-trending stacked thrust sheets that record two orthogonal contractional events created fold interference creating dome and basin patterns. This model derived primarily from interpretation of patterns in contour maps constructed from drill hole data (Moore *et al*. 1986) and is not well constrained. Moore *et al*. (1986) also suggested that reactivation of thrust faults as listric extensional faults may have taken place after thrusting ceased. The mineralized plates lie on a ‘tectonic melange’ (Moore *et al*. 1986).

Moore *et al*. (1986) proposed a model for the Red Dog deposit area and distinguished three different plates or structural panels (Figs. 3.16 & 3.17). These are in ascending structural order: the lower waste and ore plate, the upper waste and ore plate and the remnant mineralized plate (Figs. 3.16 & 3.17). These structural units are usually referred to as lower, median and upper plates.

More recently, Edgerton (1997*a, b*) has suggested a different structural model that consists of at least three deformational events. These include an early event related to the mineralization stage, a NNE-verging contractional event that emplaced the Brooks Range allochthon over the Wolverine Creek allochthon and a later event characterized by NW-verging thrusting and reactivation of pre-existing NNE-directed structures as dextral oblique reverse faults. Edgerton (1997*a, b*) also suggests that deformation style and kinematics associated with the onset of the Brooks Range orogeny were relatively persistent before and during the deposition of the Cretaceous Okpikruak Formation. More recently, O'Brien (2000) based on mapping in the Red Dog mine establish three local periods of deformation: 1) Northwest to north-northeast early thrust-related contractional deformation, 2) northwest-southeast and north-northeast—south-southwest regional dextral brittle shearing, and 3) north-south to north-northwest—south-southeast and NW-SE-trending late extensional tear faulting. Alternatively, Young (2000) proposes two main tectonic events.

Structure of the Aqqaluk and Paalaaq deposits

Little information has been published on the geology of the Aqqaluk and Paalaaq deposits (Jennings *et al*. 1998; King *et al*. 2002) (Fig. 3.18). The Aqqaluk and Paalaaq deposits are arranged in northerly-dipping thrust panels of the Red Dog sequence of the Brooks Range allochthon of Moore *et al*. (1986).

Structure of the Su-Lik Deposits

Information on the structure of the Su and Lik deposits is scarce. Forrest & Sawkins (1983) suggested that the deposits lie on a NW-dipping thrust sheet (Fig. 3.19) of the Red Dog sequence of the Brooks Range allochthon of Moore *et al*. (1986).

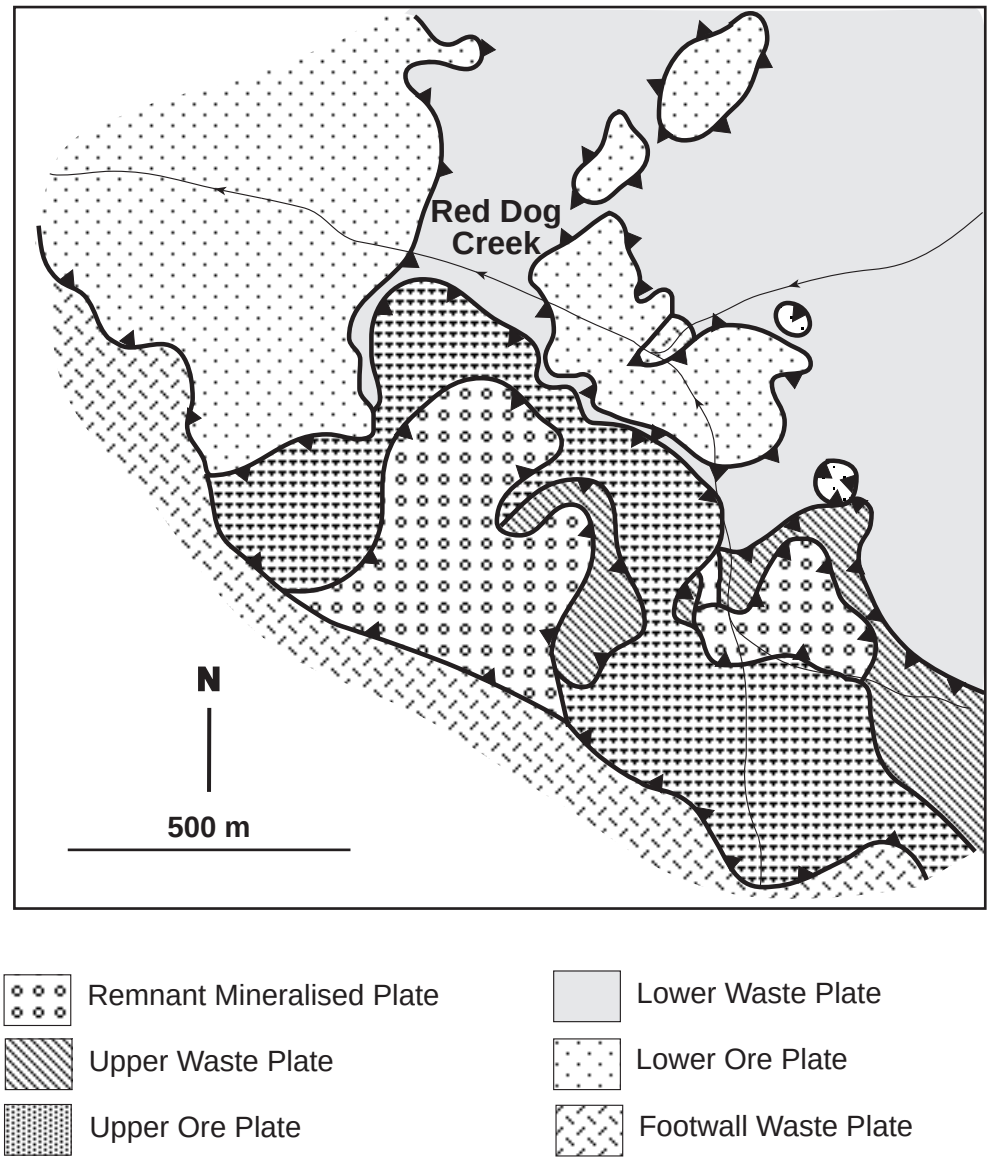


Figure 3.16. Thrust plate map of the Main deposit (modified from Moore *et al*. 1986).

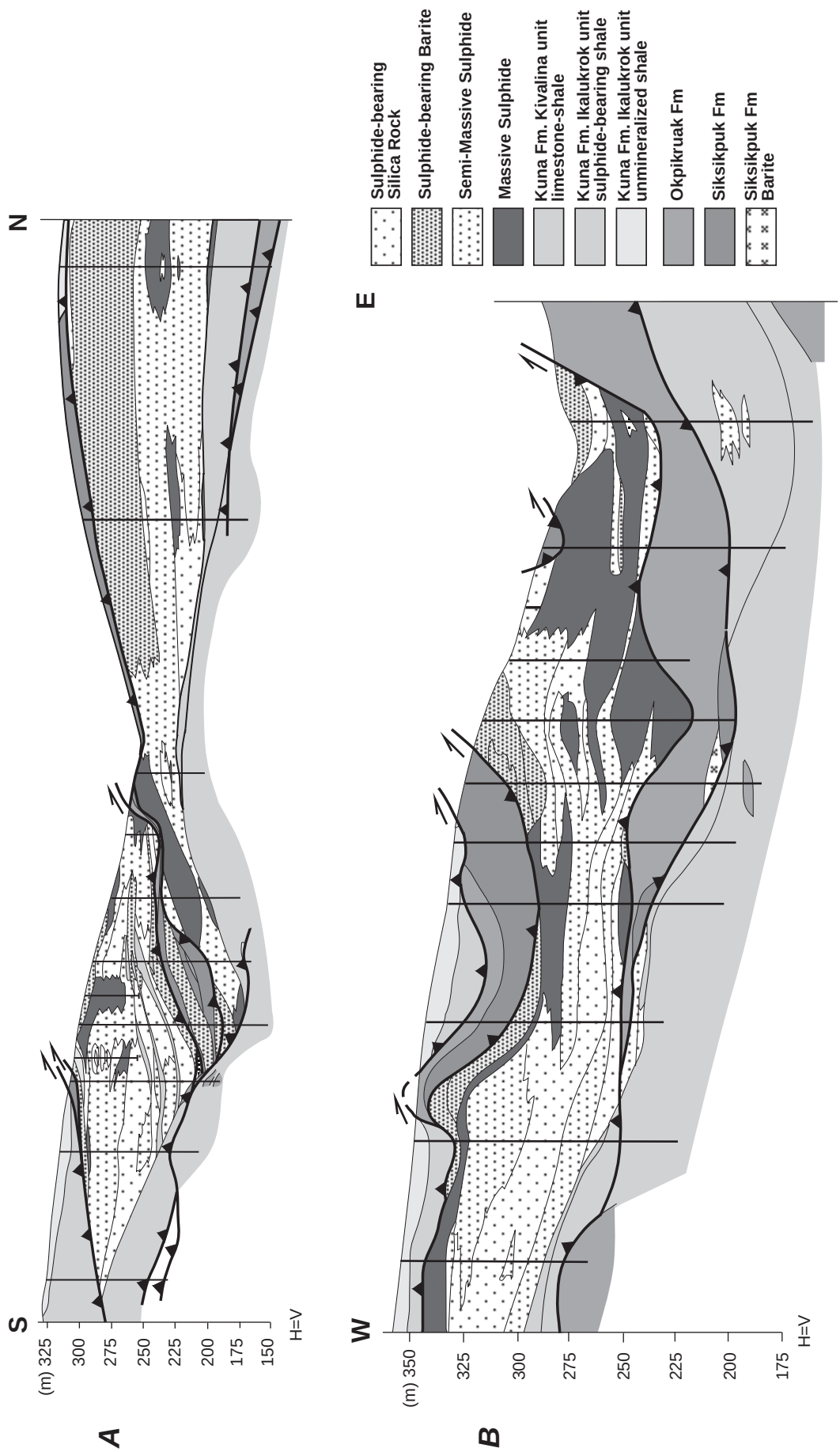


Figure 3.17. Geological cross sections through the Main deposit (modified from Moore *et al.* 1986). **A.** South-north cross section. **B.** West-east cross section. Refer to Figure 3.15 for location of individual sections.

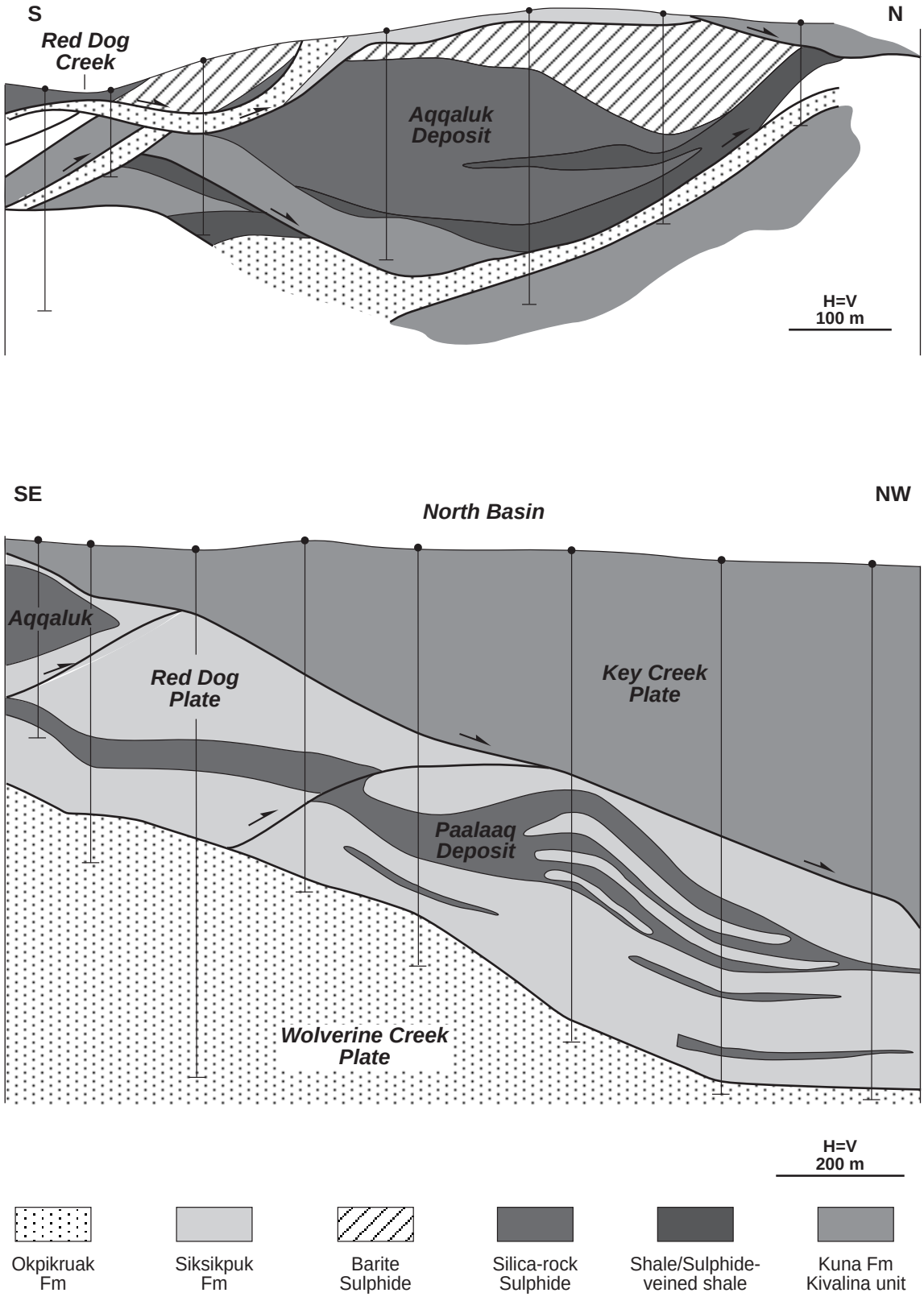


Figure 3.18. Schematic cross sections through the Aqqaluk and Paalaaq deposits (modified from Jennings *et al*. 1998).

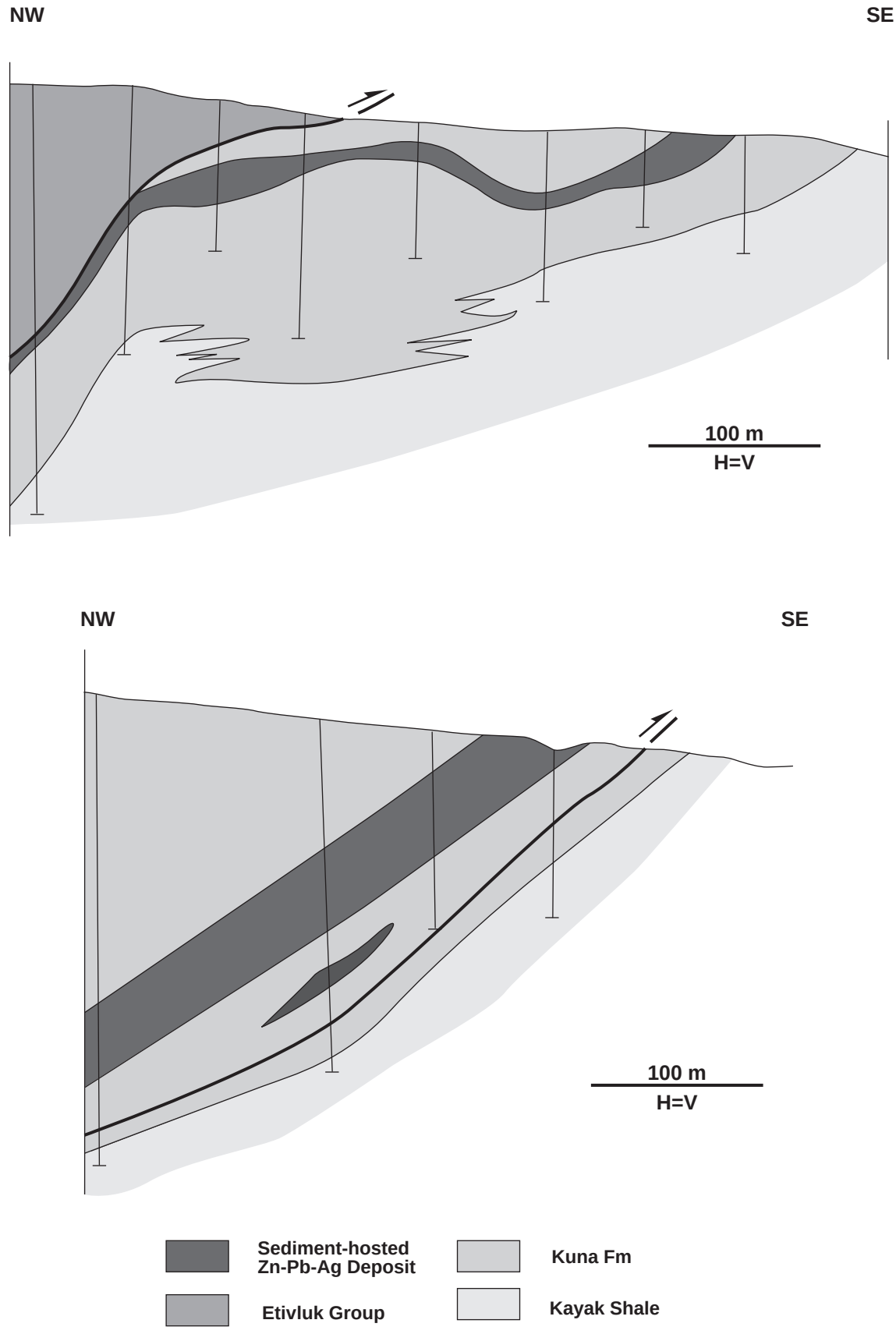


Figure 3.19. Cross sections of Su-Lik deposits (modified from Forrest & Sawkins, 1983). Refer to Figure 3.5 for location of sections.

Structure of the Anarraaq, Wulik and Aktigiruq deposits

Little is known about the structure of the Anarraaq, Wulik and Aktigiruq deposits. They lie at the base of a NE-verging thrust sheet of the Red Dog plate of the Brooks Range allochthon (Teck Cominco American Inc. 2000) (Fig. 3.20).

3.6.2 Ore Genesis and Timing of Mineralization

The mechanisms of metal transport and deposition, the source of metals, and mechanisms of fluid flow that formed the sediment-hosted Zn-Pb-Ag deposits of the Red Dog district are still poorly understood (Kelley & Jennings, 2004). The deposits of the Red Dog district show evidence for a syn-sedimentary and a replacement origin.

Tectonostratigraphic Setting

There has been controversy with regard to the geological setting in which the Kuna Formation and the Zn-Pb-Ag and barite deposits of the Red Dog district formed. Lange *et al*. (1985) and Lange & Nokleberg (1987) argued that petrologic, geochemical and isotopic data on igneous rocks together with regional stratigraphic and structural relationships indicated that the sediment-hosted Zn-Pb-Ag deposits of the Red Dog Creek area formed in an island arc setting. Moore *et al*. (1986), Young & Moore (1987) and Young (1989) alternatively suggested that the deposits of the Red Dog area formed in the early stages of a long-lived starved epicontinental basin. It is now widely accepted that the mineralization of the Red Dog district formed in a continental margin basin (e.g. Moore *et al*. 1986; Young, 1989; Dumoulin *et al*. 2004; Young, 2004) (Fig. 3.2).

Timing of Mineralization

The maximum age of the Ikalukrok host rocks, as determined from conodont and radiolarians, is late Meramecian to early Chesterian (340 to 330 Ma) (Dumoulin *et al*. 2004). Age constraints on the mineralization of the Red Dog district come primarily from radiometric data of igneous rocks associated to the deposits of the Red Dog Creek area (e.g. Werdon, 1999; Morelli *et al*. 2004; Werdon *et al*. 2004). These include a $^{39}Ar/^{40}Ar$ isotopic age of 344 Ma from an altered alkali gabbro sill north of the Aqqaluk deposit and a *ca*. 314 Ma age from an altered mineralized sill from the Main deposit (e.g. Werdon, 1999; Werdon *et al*. 2004). Morelli *et al*. (2004), based on Re-Os dating

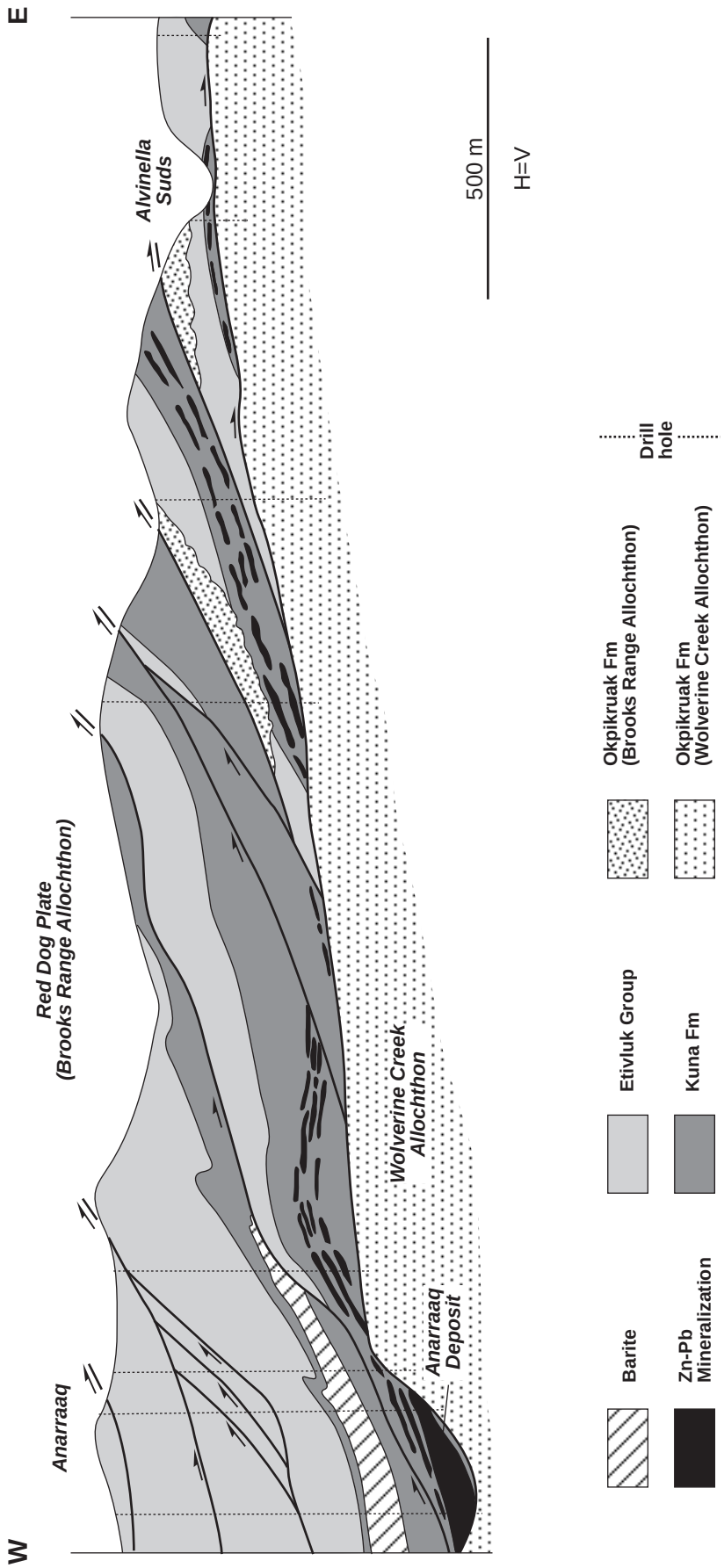


Figure 3.20. Cross section through the Anarraaq and Suds areas showing the Anarraaq deposit (modified from Cominco American Inc. Exploration, 2001). Refer to Figure 3.5 for location of section.

of pyrite from massive and vein ore from the deposits of the Red Dog Creek area, have suggested that the main mineralizing fluids were emplaced at 338±5.8 Ma. These ages imply that mineralization is Late Mississippian to Pennsylvanian in age (Werdon, 1999; Morelli *et al.* 2004; Werdon *et al.* 2004), and suggests that the main event of mineralization may largely post-date deposition of much of the Ikalukrok unit host rock (Young, 2004).

Mechanisms of Mineralization

The complex mineral parageneses of the Red Dog district are interpreted to reflect several pulses of mineralization and silicification (Jennings *et al.* 1998). Early, very fine-grained quartz and sphalerite are cut by veins of late stage sphalerite, galena, pyrite, and silica (e.g. Schmidt & Zierenberg, 1985). Moore et al. (1986) suggested that the deposits formed by a combination of sediment replacement and sulphide deposition on the sea floor. Young (1989) recognizes both syngenetic stratiform and epigenetic replacement features in the Main and Qanaiyaq deposits.

Evidence for Syn-sedimentary Mineralization

Evidence for a syn-sedimentary origin of the mineralization of the Red Dog district includes the presence of laminated sulphides and massive sulphide-bearing bedded barite-rock (e.g. Lange *et al.* 1985; Moore *et al.* 1986; Young & Moore, 1987; Young, 1989; Young, 2004), preservation of a possible vent fauna (e.g. Plahuta, 1978; Plahuta & Robinson, 1979; Moore *et al.* 1986; Jennings *et al.* 1998; Young, 2004) and the local presence of clastic-textured sulphides (e.g. Moore et al. 1986; Schmidt & Zierenberg, 1989; Schmidt, 1997*a*). Lewchuk (2001) and Lewchuk *et al.* (2004) based on palaeomagnetic dating of the mineralization at the Red Dog mine have argued in favour of a syn-sedimentary Zn-Pb-Ag origin for the deposits of the Red Dog Creek area.

Evidence for Replacement Mineralization

Evidence supporting replacement as the primary process involved in base metal sulphide deposition in the deposits of the Red Dog district includes abundant, well-documented replacement textures and the predominant massive texture of the sulphides (e.g. Moore *et al.* 1986; Jennings *et al.* 1998), multiple veining and brecciation events in sulphide and silica rock (e.g. Moore *et al.* 1986; Young, 1989) and the lack of typical

exhalative features (Kelley *et al*. 2004a, b). In addition, the mineralization of the Red Dog area has a well-developed replacement style beneath the barite (e.g. Young, 1989; Sims, 1996; Edgerton, 1997*a, b*; Jennings *et al*. 1998; King *et al*. 2002; Kelley *et al*. 2004*a, b*), which suggests that the ore-forming event may have been in part younger (Kelley *et al*. 2004*a*, Young, 2004).

It has long been recognized that sediment-hosted Zn-Pb-Ag mineralization of the Red Dog district may have replaced carbonate (e.g. Young, 1989; Schmidt & Zierenberg, 1989; Young, 2004). Barite at the Anarraaq deposit appears to be an early diagenetic replacement of carbonate (Dumoulin *et al*. 2004; Kelley *et al*. 2004*a*). Both sphalerite and quartz form pseudomorphs after euhedral barite crystals (Jennings *et al*. 1998). Pyrite and sphalerite have been identified replacing radiolarians in the Lik deposit (King *et al*. 2002). Replacement of carbonate nodules and layers in shale by barite and sulphides is common in the Anarraaq deposit (Kelley *et al*. 2004). Barite-replaced fossils have been also identified locally in the district (Young, 2004). Sulphide textures at Anarraaq indicate that mineralization probably replaced carbonate (Kelley *et al*. 2004).

The timing of mineralization for other deposits of the Red Dog district is unknown. Kelley *et al*. (2004*a*) suggested that the Anarraaq deposit possibly formed in Late Mississippian time, broadly coeval with the deposits of the Red Dog Creek area. Kelley *et al*. (2004*a*) have argued that the similar appearance and geochemistry of sphalerite in massive zones from Anarraaq to the vein ore at Red Dog suggests that sulphides at Anarraaq may have formed at the same time during the Late Mississippian.

Deposition of barite in unlithified black shale initiated mineralization at Red Dog. Subsequent sulphide- and silica-bearing fluids migrated through the same structurally controlled fluid paths but were trapped beneath the earlier barite, minimizing metal loss to the overlying water column (Young, 1989). Replacement of surrounding black shale and the overlying barite by sulphide and silica took place from below (Sims, 1996; Jennings *et al*. 1998; Jennings & King, 2002; King *et al*. 2002; Ayuso *et al*. 2004). New data obtained for the Red Dog district (Ayuso *et al*. 2004) show that the extensive silicification that accompanies and overprints some of the deposits of the Red Dog

district was probably produced at burial depths of 2 to 6 km during Mesozoic thrusting, and unrelated to sulphide deposition. In contrast, Slack *et al*. (2004) have suggested that silica was introduced by the same hydrothermal fluids that formed the Zn-Pb-Ag deposits. Mineralization at Anarraaq probably occurred in a fault-bounded Carboniferous basin during early diagenesis in the shallow subsurface (Kelly et al. 2004*a*). Large-scale replacement of carbonate by barite or sulphides has not been documented at Red Dog.

3.7 SUMMARY

This chapter has reviewed the geology of the Red Dog district and its sediment-hosted Zn-Pb-Ag. The key points from this chapter are summarized below:

- The Red Dog district forms part of a 200 km-long belt of sediment-hosted Zn-Pb-Ag and barite deposits in the western Brooks Range. The Red Dog district contains one of the world's largest zinc reserves and resources and the world's largest single zinc deposit.

- The Red Dog district consists of Late Devonian to Early Cretaceous sedimentary rocks and felsic to ultramafic rocks that were complexly deformed by thrust faulting and folding and incorporated into eight thrust sheets or allochthons.

- Regional studies have identified eight distinct thrust sheets or allochthons. These are in ascending structural order, the Wolverine Creek, Brooks Range, Picnic Creek, Kelly River, Ipnavik River, Nuka Ridge, Copter Peak, and Misheguk Mountain allochthons.

- The Zn-Pb-Ag and barite mineralization of the Red Dog district occurs in Late Mississippian black shales and carbonates of the Kuna Formation, which is characteristic of the Brooks Range allochthon. The Zn-Pb-Ag and barite deposit of the Red Dog district are believed to have formed in a basin the ancient continental margin of Arctic Alaska (Arctic Alaska terrane).

- Mineralization occurs in three areas and includes five major deposits. The Qanaiyaq, Main, Aqqaluk and Paalaaq deposits of the Red Dog Creek and the Su-Lik and Anarraaq deposits.

- The Zn-Pb-Ag and barite mineralization of the Red Dog district contains both characteristics of syn-genetic and replacement origin. The Zn-Pb-Ag and barite deposits of the Red Dog district exhibit mainly replacement rather than sedimentary exhalative characteristics.

CHAPTER 4

THRUST TECTONICS: A REVIEW

4.1 INTRODUCTION

4.2 BASIC GEOMETRIC ELEMENTS

4.3 THRUST SYSTEMS

4.4 3D THRUST SYSTEMS

4.5 3D THRUST BELT GEOMETRIES

4.6 THRUST SEQUENCES

4.7 SUMMARY

CHAPTER 4 THRUST TECTONICS: A REVIEW

4.1 INTRODUCTION

This chapter presents a review on thrust tectonics and the geometry, kinematics, and dynamics of foreland fold and thrust belts. The aim of this chapter is to introduce some basic concepts and terminology that is used in the structural analyses shown in Chapters 6 and 7.

Foreland fold and thrust belts (Fig. 4.1), found at the margins of orogenic belts formed either by continent-continent collision, arc-continent collision, or subduction, are excellent examples for the study of the structure and evolution of thrust systems. The earliest studies on thrust tectonics date back to the late 1800's and early 1900's with the work of McConnell (1887) in the Canadian Rocky Mountains, Peach *et al*. (1907) in the Moine thrust of northwest Scotland and Argand (1911) in the Alps. Since then, research into the geometries and dynamics of thrust systems has been widely published (e.g. Rich, 1934; Douglas, 1952; Bally *et al*. 1966; Dahlstrom, 1969, 1970; Price, 1981; Boyer & Elliot, 1982; Butler, 1982, 1983; Coward, 1983; Price & Fermor, 1985; Boyer, 1986; Mitra, 1986; Morley, 1986; Price, 1986; Butler, 1987; Mitra, 1988; Morley, 1988; Woodward *et al*. 1989; McClay, 1992; Fermor, 1999; McClay, 2004).

Foreland fold and thrust belts consist of an array of thrust faults that shorten a pre-orogenic sedimentary wedge (e.g. sediments deposited in a continental passive margin) during orogeny (e.g. Bally *et al*. 1966). The internal characteristics and structure of fold and thrust belts are remarkably varied and diverse (McClay, 2004). Classic examples include the fold and thrust belts of the Canadian Rocky Mountains (e.g. Bally *et al*. 1966; Dahlstrom, 1969, 1970; Price, 1981; Price & Fermor, 1985; Price, 1986; Fermor & Price, 1987; Fermor & Moffat, 1992, Fermor, 1999, Price & Monger, 2003), the Appalachians of the eastern United States (e.g. Mitra, 1988; Hatcher, 1989; Hatcher *et al*. 1990), the Pyrenees and Cantabrian Mountains of northern Spain (e.g. Pérez-Estaún *et al*. 1988; Muñoz, 1992; Alvarez-Marrón, 1995), and the Andes (e.g. Baby *et al*. 1992; Roeder & Chamberlain, 1995; Cristallini *et al*. 2004; Ramos *et al*. 2004) (Fig. 4.1).



Figure 4.1. Worldwide distribution of the main foreland fold and thrust belts (modified from Roeder & Boyer, 2001).

4.2 BASIC GEOMETRIC ELEMENTS

This section introduces some of the more widely used terms and concepts in thrust tectonics, which are essential in the description and analysis of foreland fold and thrust belts.

4.2.1 Thrust Faults

Thrust faults are the fundamental elements of foreland fold and thrust belts (Bally *et al.* 1966; Dahlstrom, 1969, 1970; Elliot, 1976; Boyer & Elliot, 1982; McClay, 1992). A thrust fault can be defined as a map-scale contractional fault that shortens a datum surface, usually bedding in upper crustal rocks or a regional foliation surface in more highly metamorphosed and strained rocks (McClay, 1992). The process of thrusting causes shortening in the form of repetition and thickening of the rock succession (Dahlstrom, 1970; Boyer & Elliot, 1982; McClay, 1992), altering the shape but not the amount of a rock volume according to the principle of least work (Dahlstrom, 1969, 1970; Elliot, 1976).

Thrust Fault Elements

Thrust faults are three-dimensional surfaces of finite extent (Elliot, 1976; Boyer & Elliot, 1982; Hossack, 1983) that have a slipped region or *Somigliana* dislocation (Eshelby, 1973; Price, 1988) surrounded by a ductile bead (e.g. a cleavage front or an anticline-syncline pair) (Elliot, 1976; Boyer & Elliot, 1982) (Fig. 4.2). Thrust faults terminate in tip lines where the fault displacement dies out to zero (e.g. Elliot, 1976; Boyer & Elliot, 1982; Woodward *et al*. 1989; Price & Cosgrove, 1990; McClay, 1992; Wilkerson *et al*. 2002) (Fig. 4.2). Thrust faults cut up section in the direction of tectonic transport bringing older rocks over younger rocks, commonly following a 'staircase' or 'stair-step' trajectory (e.g. Rich, 1934; Dahlstrom, 1970; Boyer & Elliot, 1982; Price & Cosgrove, 1990; McClay, 1992) (Fig. 4.3a). This produces 'ramp-flat' geometries (Dahlstrom, 1970; Boyer & Elliot, 1982; Woodward *et al*. 1989; McClay, 1992), in which long sub-horizontal and bedding-parallel fault segments, or flats, are separated by shorter and more steeply-dipping fault segments or ramps. Thrust faults commonly form flats in incompetent lithologies and ramps in more competent units (Boyer & Elliot, 1982; McClay, 1992) (Fig. 4.3a). Ramp angles typically range from 15° to 30° (Fermor, 1999). Steeper ramps rarely develop as they accommodate very

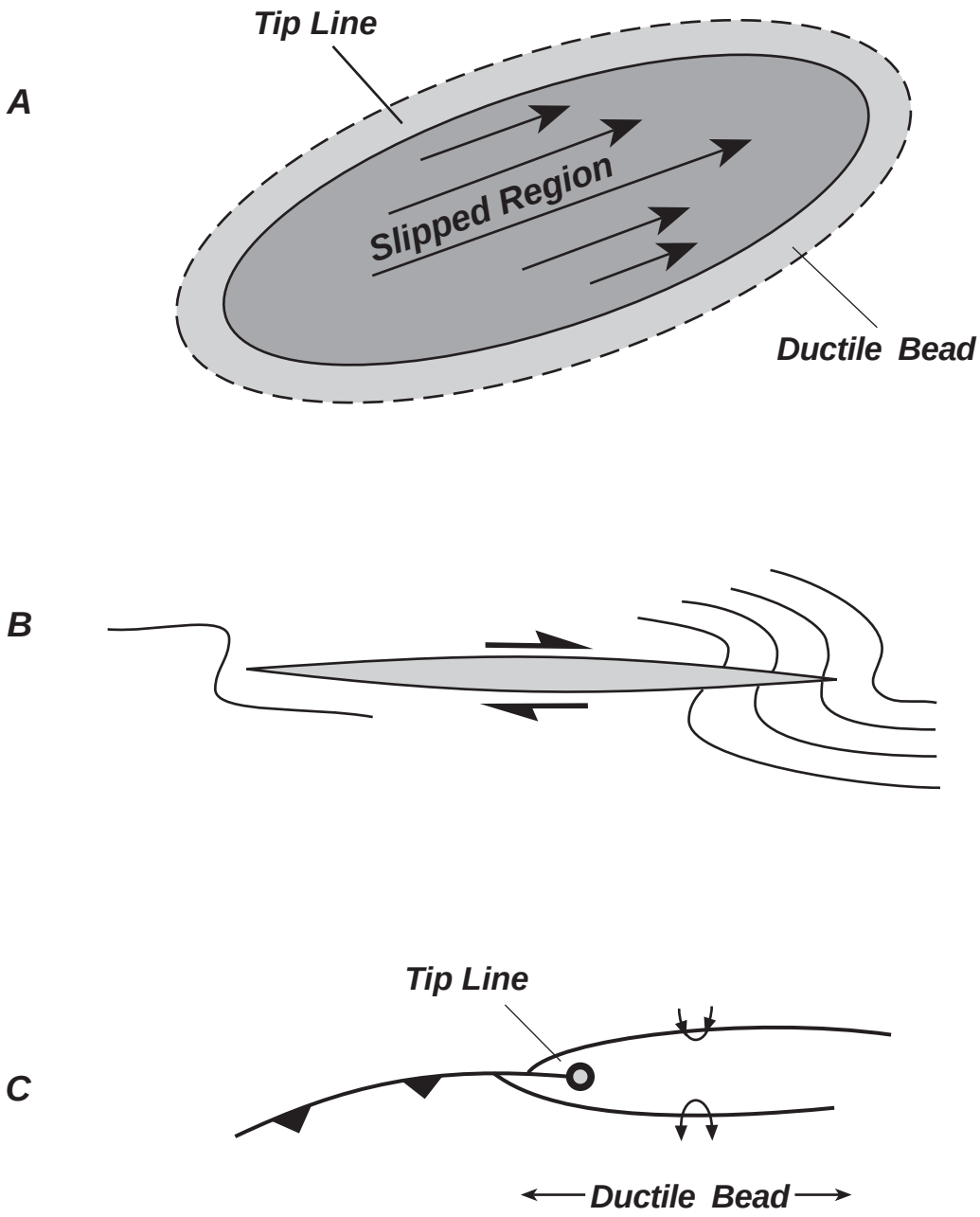


Figure 4.2. Thrust fault elements. **A.** Somigliana dislocation surrounded by a tip-line and a ductile bead. The slipped region of the fault is contained within the tip-line. **B.** Cross-section through a Somigliana dislocation with an anticline-syncline pair forming a ductile bead beyond the tip-line. **C.** Outcrop pattern of a tip-line in the Canadian Rocky Mountains (modified from Elliot, 1976).

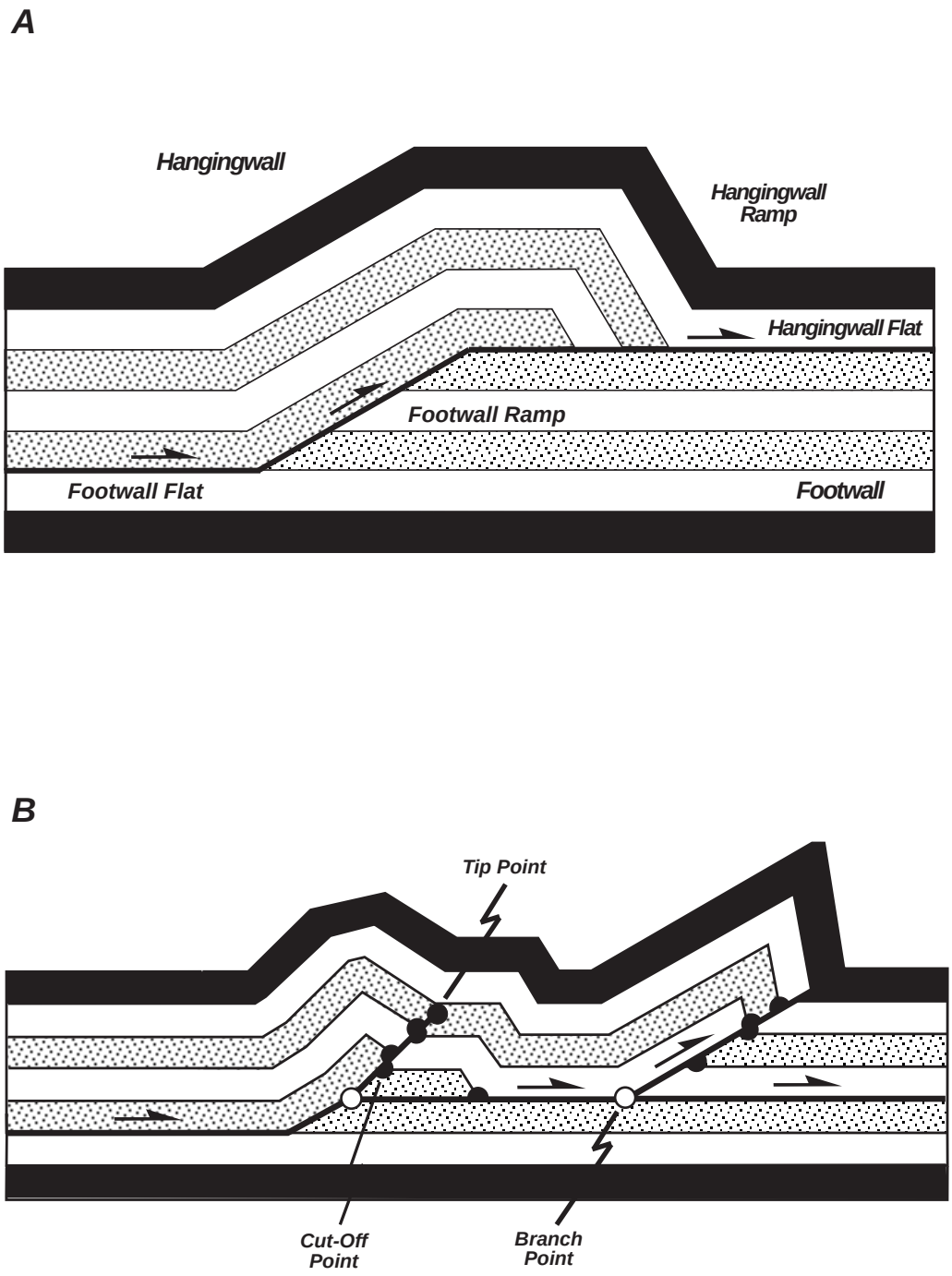


Figure 4.3. Thrust fault nomenclature. **A.** Thrust ramps in cross-section. **B.** Cross section illustrating branch points (white circles), cut-off points (black half-moons) and tip-points (black circles) (modified from McClay, 1992).

limited displacement and require large amounts of work (e.g. Coward, 1983; Apotria *et al*. 1992; Fermor, 1999; Wilkerson *et al*. 2002).

The fault blocks overlying and underlying a thrust surface are termed hangingwall and footwall, respectively (e.g. Boyer & Elliot, 1982; Butler, 1982; Price & Cosgrove, 1990) (Fig. 4.3a). The point of intersection of bedding with a fault surface is referred to as a cut-off and the point where two individual thrust faults merge is referred to as a branch point (Boyer & Elliot, 1982) (Fig. 4.3b). Several branch points and cut-offs form branch and cut-off lines, respectively (Boyer & Elliot, 1982) (Fig. 4.3b). Ramps and flats are often classified according to whether they are cut offs in the hangingwall or footwall of a given thrust fault surface (Boyer & Elliot, 1982) (Fig. 4.3a). Ramps that are cut offs in the hangingwall are termed hangingwall ramps (Fig. 4.3a) and those cut offs in the footwall are termed footwall ramps (Boyer & Elliot, 1982) (Fig. 4.3a).

Thrust Fault Displacements

Thrust faults are scale independent structures and can largely vary in size and displacement (Twiss & Moores, 1992; Hatcher, 2004). Individual thrust faults are documented to have lengths that exceed 700 km and fault displacements that range from 100 to 150 km (e.g. Lewis and Purcell thrusts of the Rocky Mountains and the Saltville and Whiteoak Mountain thrusts of the southern Appalachians) (Hatcher, 2004). The total displacement on a thrust fault is the cumulative result of small displacements (e.g. Price, 1988), each of which involves only a small part of the fault and propagates as a displacement discontinuity or dislocation at a velocity that is small relative to the length and width of the fault (Price, 1988, 1990). The most commonly described relationship between thrust fault length and displacement is referred to as the '*Bow and Arrow'* rule (Elliot, 1976; Boyer & Elliot, 1982) (Fig. 4.4). This rule postulates that the maximum displacement vector of a thrust fault is the normal bisector of a straight line joining the tip lines of a given thrust fault (Elliot, 1976; Boyer & Elliot, 1982). Elliot (1976) estimated the magnitude of such vector to be less than 10% of the strike length of the straight line (Fig. 4.4). The normal bisector of the straight line can also be used as an indicator of the tectonic transport direction (e.g. Elliot, 1976; Boyer & Elliot, 1982; Woodward *et al*. 1989) (Fig. 4.4). The '*Bow and Arrow*' rule, however, does not take in

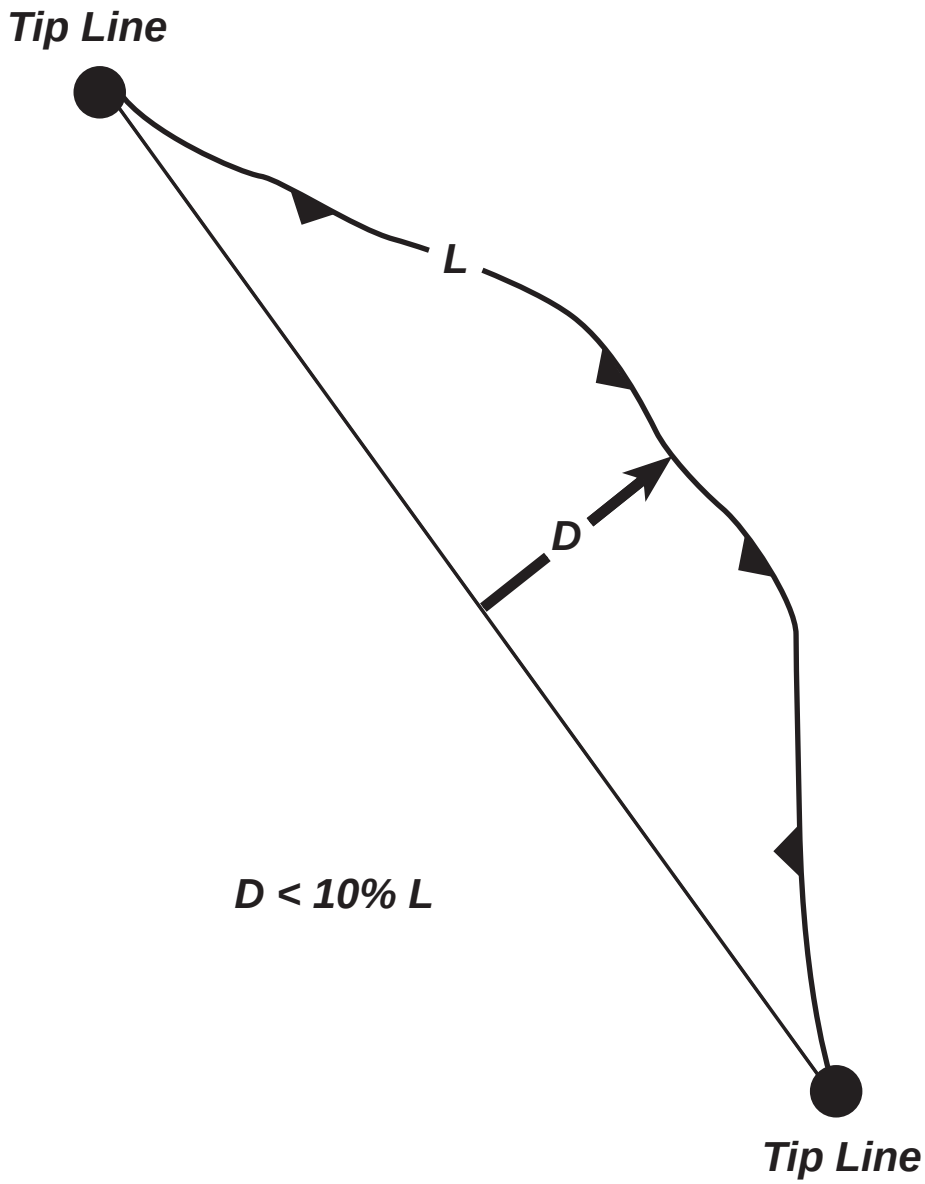


Figure 4.4. Elliot's 'Bow and Arrow' rule, showing the relationship between thrust fault displacement (D) and length (L) (modified from Elliot, 1976).

account factors such as the occurrence of intervening transverse or lateral structures, which are commonly responsible for considerable along-strike variations in thrust fault displacement and in the tectonic transport direction (e.g. Boyer & Elliot, 1982; Apotria *et al*. 1992; McClay, 1992; Wilkerson, 1992; Wilkerson *et al*. 1992; Apotria, 1995; Wilkerson *et al*. 2002).

4.2.2 Thrust Sheets

The volume of rock bounded by two individual thrust faults is commonly referred to as thrust sheet or thrust panel (e.g. Dahlstrom, 1970; Boyer & Elliot, 1982; McClay, 1992) (Fig. 4.5). Thrust sheets are bounded by low angle thrust faults and commonly have a lateral extent that is large compared with its thickness (Dahlstrom, 1970; Boyer & Elliot, 1982). Thrust sheet size is dependent on the thickness and strength of the rock units, as well as the mechanical properties of the evolving fold and thrust belt (e.g. Davis *et al*. 1983; Dahlen, 1990; Colleta *et al*. 1991; Liu *et al*. 1992; Marshak & Wilkerson, 1992; Marshak *et al*. 1992; Boyer, 1995; Mitra, 1997; Macedo & Marshak, 1999; Hatcher, 2004; Marshak 2004). Thrust sheets are commonly named after their sole or basal thrusts (Fig. 4.5).

Types of Thrust Sheets

Hatcher & Hooper (1992) and more recently Hatcher (2004) have proposed a classification of thrust sheets, which consists of three fundamental types. These are, foreland fold-thrust belt thrust sheets, Type C crystalline thrust sheets, and Type F crystalline thrust sheets (Hatcher & Hooper, 1992; Hatcher, 2004) (Fig. 4.6). Foreland fold-thrust belt thrust sheets shorten sedimentary wedges and are the dominant thrust sheets in the external parts of orogenic belts (Hatcher & Hooper, 1992; Hatcher, 2004) (Fig. 4.6a). Type C thrust sheets, the largest in orogenic belts, are crustal-scale thrust sheets that commonly detach along the brittle-plastic transition in either continental or oceanic crust (Hatcher, 2004) (Fig. 4.6b). Examples of Type C thrust sheets include the oceanic crust slabs obducted on to continental margins during the early stages of orogenic collision (e.g. Dewey, 1976; Moores, 2003). Type F thrust sheets or fold-related thrust sheets form below the ductile-brittle transition, or alternatively cool and evolve into smaller Type C thrust sheets (Hatcher, 2004) (Fig. 4.6c).

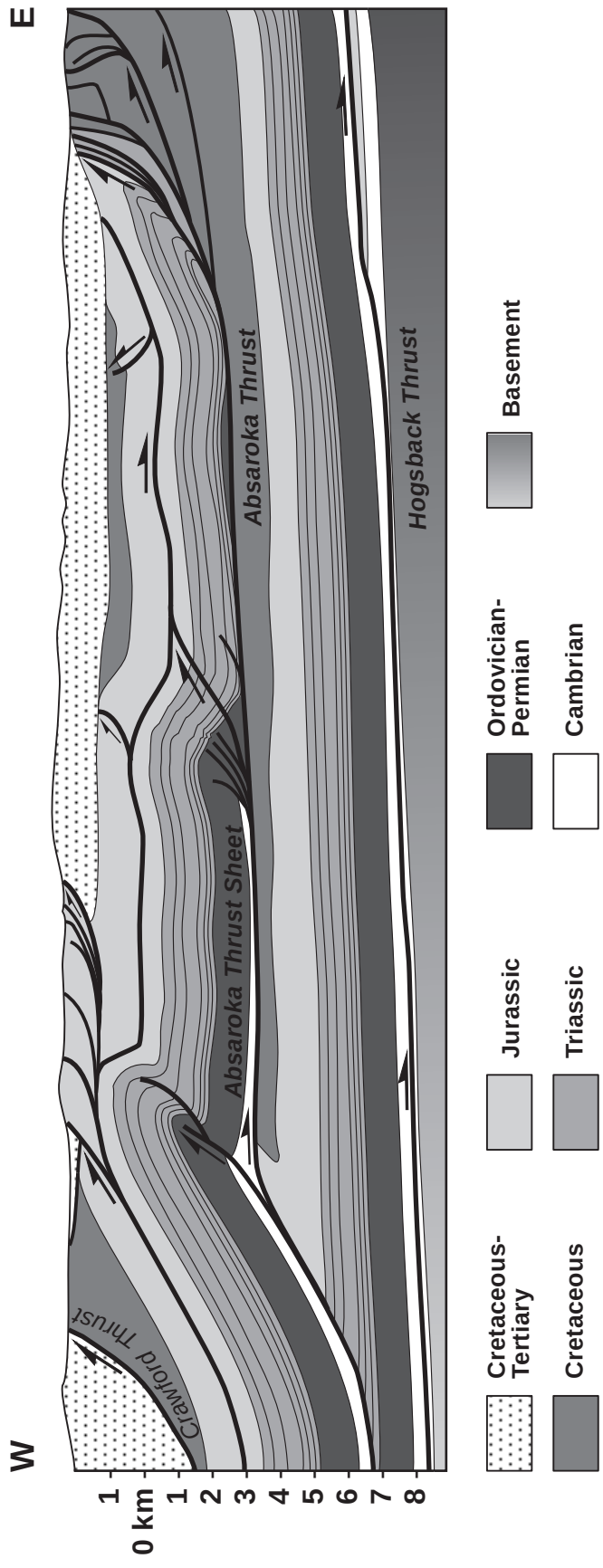


Figure 4.5. Absaroka thrust sheet, Rocky Mountains, United States (modified from Mitra, 1990).

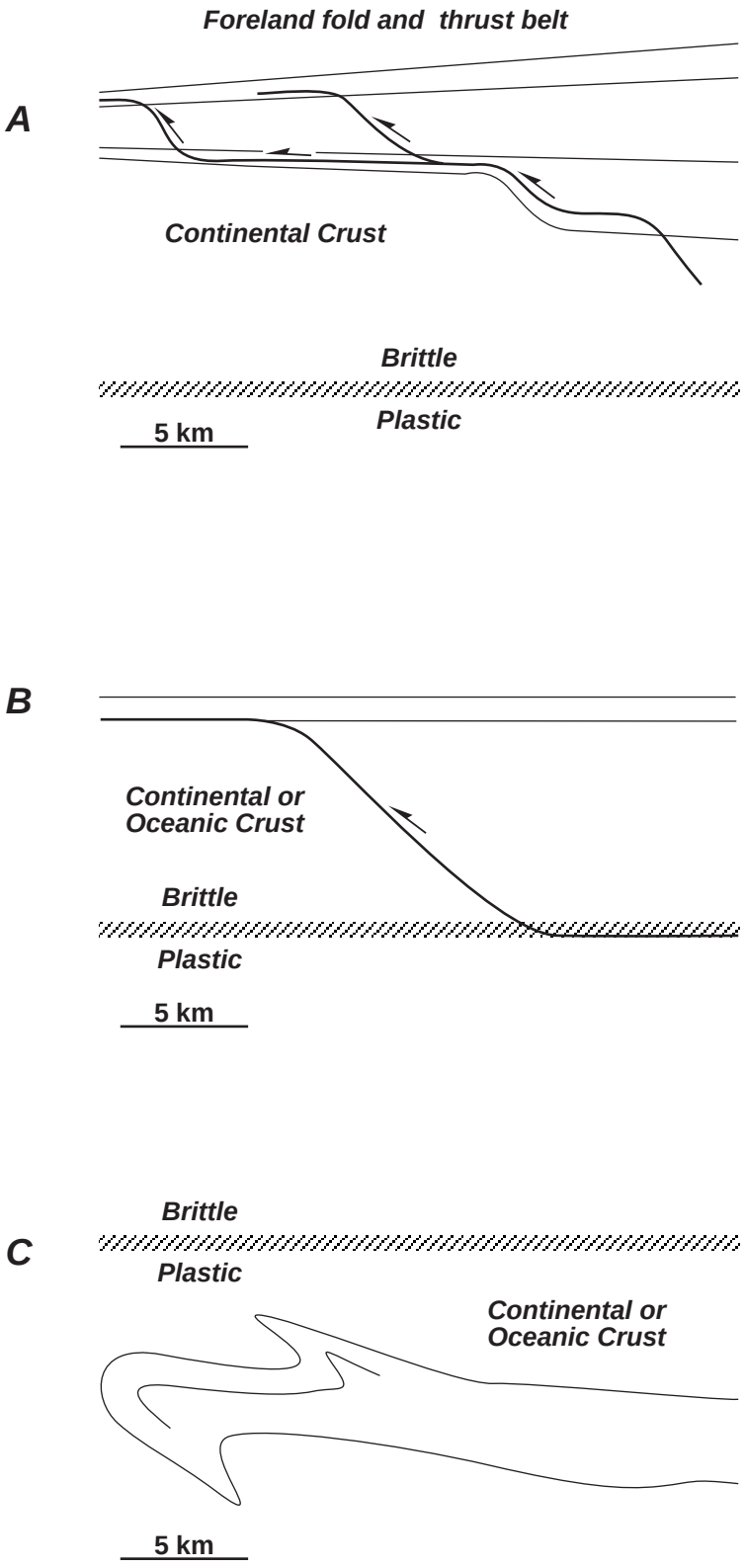


Figure 4.6. Types of thrust sheets. **A.** Foreland fold-thrust belt thrust sheets. Thrusts are generated by propagation into a wedge-shaped sedimentary succession with a weak basal unit and a strong structural lithic unit that influences the size of the imbricates. **B.** Type C thrust sheet. Crustal-slab thrust sheets detach along the plastic-brittle transition, transporting the entire crustal section. **C.** Type F or fold-related thrust sheets. Formed at deeper structural levels, below the plastic-brittle transition (modified from Hatcher, 2004).

Allochthons

Thrust sheets of regional extent that have been transported long distances from their original palaeogeographic positions are commonly referred to as allochthons (e.g. Davis & Reynolds, 1984; Ramsay & Huber, 1987*a*; Twiss & Moores, 1992) and their contained rocks are referred to as allochthonous (e.g. Endicott Mountains allochthon of the Brooks Range, cf. Chapter 2, Figs. 2.4 & 2.5). Allochthons are typically rootless and cannot be readily restored using conventional techniques (e.g. Dahlstrom, 1970; Woodward *et al*. 1989). A large region of rock that has not been moved relatively to the allochthonous thrust sheets (e.g. basement underlying a fold and thrust belt) and is at or near its palaeogeographic location is referred to as the autochthon or autochthonous (e.g. Davis & Reynolds, 1984; Ramsay & Huber, 1987*a*; Twiss & Moores, 1992). The term parautochthon (e.g. Arctic Slope Parautochthon of northern Alaska; cf. Chapter 2, Figs. 2.4 & 2.5) is also often introduced to refer to portions of the autochthonous basement that have an uncertain structural relationship (e.g. thrust involvement) with the allochthonous thrust sheets (Twiss & Moores, 1992). The term nappe or thrust nappe has also been used to refer to allochthonous thrust sheets, usually associated with regional-scale recumbent folds (McClay, 1981, 1992).

4.2.3 Thrust Fault-Related Folds

Foreland fold and thrust belts are characterized by a close interaction of thrust fault and fold structures, which are geometrically and kinematically linked (e.g. Suppe, 1983, 1985; Jamison, 1987; Mitra, 1990; McClay, 1992; Hardy *et al*. 1996; Poblet & McClay, 1996; McClay, 2004; Shaw *et al*. 2005). Three main types of thrust fault-fold interaction have been described. These are the fault-bend fold, fault-propagation fold and fault detachment fold (e.g. Rich, 1934; Dahlstrom, 1969; Suppe, 1983, 1985; Jamison, 1987; Mitra, 1990, 1992; Suppe & Medwedeff, 1990; Shaw *et al*. 2005) (Fig. 4.7). The relationships between fault slip, and fault and fold geometries for each of these type of structures have been quantified in a number of geometric models (e.g. Suppe, 1983; Suppe & Medwedeff, 1990) and these relationships used to constrain structural interpretations in natural examples from fold and thrust belts worldwide (e.g. Suppe, 1983, 1985; Mitra, 1988; Poblet & McClay, 1996; Mitra, 2002; Poblet *et al*. 2004).

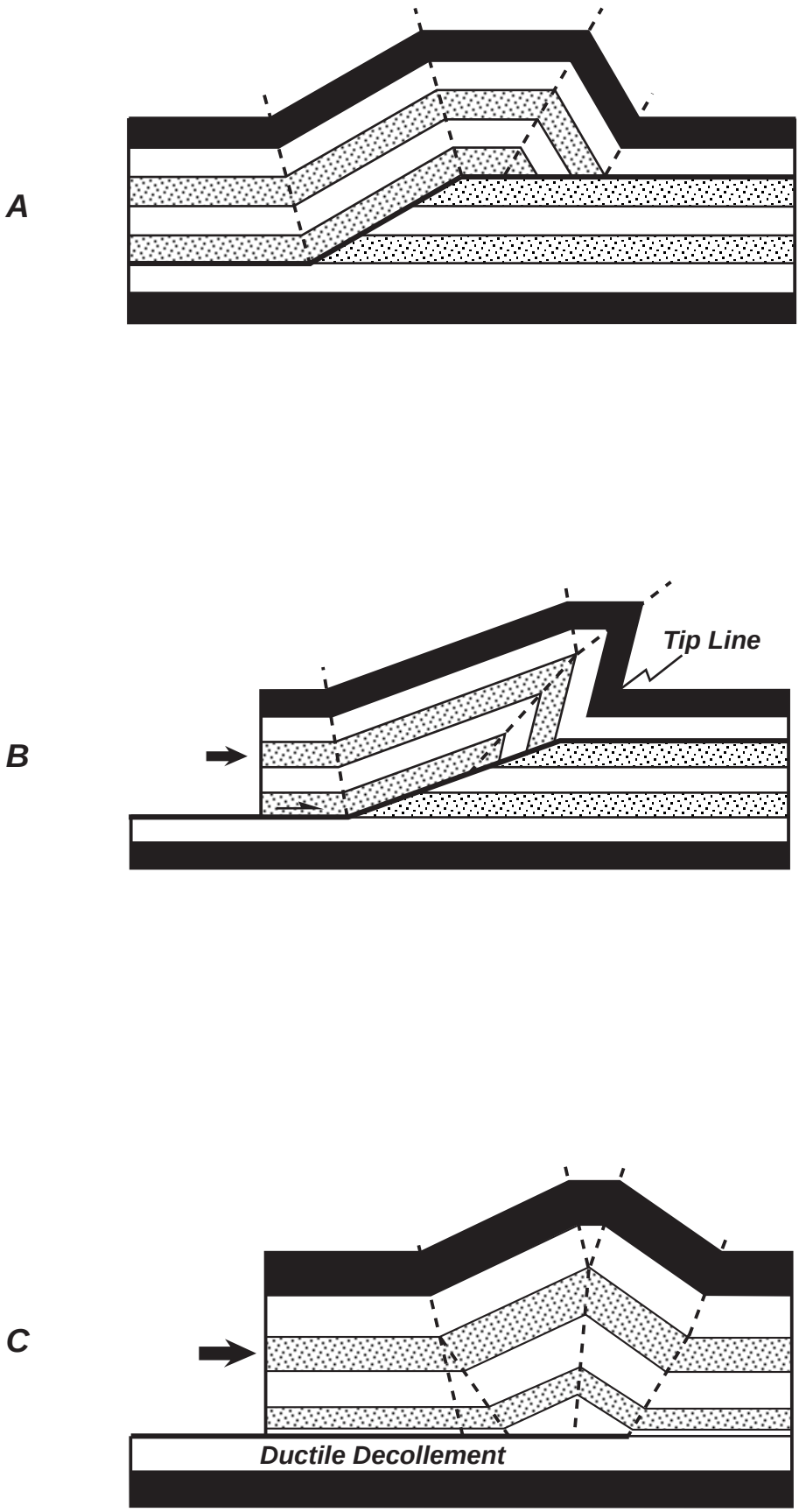


Figure 4.7. Fault-related folds. **A.** Fault-bend fold. **B.** Fault-propagation fold. **C.** Detachment fold (modified from McClay, 1992).

Fault-bend folds (Figs. 4.7a & 4.3a) occur where a detachment steps up along a ramp from one incompetent horizon to another (e.g. Rich, 1934; Suppe, 1983, 1985; Woodward *et al*. 1989). Movement over this ramp causes the rocks in the hangingwall to fold in a characteristic geometry, sometimes referred to as 'snake-head' geometry (Woodward *et al*. 1989) (Figs. 4.3a & 4.7a). Fault-propagation folds (Fig. 4.7b) are similar to fault-bend faults in that they occur where a ramp steps up from a lower *decollement*, but differ in that the thrust fault does not exist as a through-going structure from the start of deformation but gradually propagates with continued slip (Suppe, 1985; Suppe & Medwedeff, 1990). In a fault-propagation fold deformation beyond the fault tip is accommodated by folding (Dahlstrom, 1969; Woodward *et al*. 1989; McClay, 1992). In contrast, detachment folds (Fig. 4.7c) are not associated with a ramp in an underlying thrust fault, but result from buckling of a competent layer overlying a less competent layer, commonly shales or evaporites (e.g. Dahlstrom, 1969; Suppe, 1985; Woodward *et al*. 1989; McClay, 1992). Detachment folds may have a parallel geometry in their outer arc and disharmonic and non-parallel geometries in the core of the anticlines or may form by folding of strata above a basal *decollement*, which is isoclinally folded in the core of the anticline forming lift-off folds (McClay, 1992). A fold located at the tip of a blind thrust can be either a fault-propagation or a detachment fold. Jamison (1987) has suggested that the mechanical stratigraphy determines what type of fault-related fold is developed. A detachment fold is expected where the thrust rides low in a ductile unit, that underlies a more competent unit. In turn, in a layered sequence with more modest ductility contrast, the fault-propagation fold may be more probable (Jamison, 1987).

The three types of thrust fault-related folds are not mutually exclusive, either through time in a particular structure or spatially within a fold and thrust belt (Hardy *et al*. 1996). Alternative models for the evolution of fault-related folds include the 'break-thrust' model proposed by Willis (1983), Jamison (1987), Fisher *et al*. (1992), Woodward (1997) or faulted/transported detachment folds (e.g. Mitra, 2002; Wallace & Homza, 2004). According to this model, a detachment fold is later deformed by a thrust fault that breaches the frontal limb (e.g. Mitra, 2002). These models postulate that folding is the dominant mechanism involved and that the propagation of the thrust fault is a secondary process that accommodates discontinuities in the strain pattern associated

with folding. Mitra (2002) and Wallace & Homza (2004) have documented examples from the Zagros of Iran and the eastern Brooks Range of Alaska respectively. Mitra (2002) has suggested that hybrids of fault-detachment and fault-propagation folds are possibly common in nature.

Thrust fault-related folds in contractional settings do not extend indefinitely and are rarely cylindrical over large distances, but rather commonly terminate as plunging anticlines near the tips of the thrust fault (e.g. Dahlstrom, 1970; Elliot, 1976; Apotria *et al*. 1992; Fermor, 1999, Wilkerson *et al*. 2002) (Fig. 4.2c). The formation of such terminations is often ascribed to loss of slip on the underlying thrust fault (i.e. a displacement gradient), to changes in the fault geometry or to some combination of these mechanisms (e.g. Apotria *et al*. 1992; Wilkerson *et al*. 2002).

4.2.4 Mechanics of Thrust Faulting

Geologists have attempted to develop dynamic models for the mechanic behaviour and dynamic evolution of foreland fold and thrust belts. Wedge-type models were first analysed by Elliot (1976) and Chapple (1978). The critical taper or critical Coulomb wedge model (Fig. 4.8) incorporating brittle frictional rheology for the emplacement of accretionary wedges and foreland fold and thrust belts was first postulated by Davis *et al*. (1983); Dahlen (1984), and Dahlen *et al*. (1984). This model together with the subsequent modifications and developments (e.g. Davis & Engelder, 1985; Zhao *et al*. 1986; Davis & Von Huene, 1987; Dahlen & Barr, 1989; Dahlen, 1990; Koons, 1990, 1994; Willet *et al*. 1993) provides a convincing mechanical explanation for the overall shape of orogenic wedges, and for the sliding of a fold and thrust belt on a basal *detachment.*

The Critical Coulomb Wedge Theory

The critical Coulomb wedge theory assumes that a foreland fold and thrust belt or accretionary wedge has a triangular cross section, a characteristic surface slope α, and a basal *decollement* of dip $ß$ (Davis *et al*. 1983; Dahlen, 1984; Dahlen *et al*. 1984; Dahlen, 1990) (Fig. 4.8). The wedge, which is assumed to have a Navier-Coulomb rheology, forms by pushing an initially layered succession from the rear such that thrusts propagate in sequence towards the foreland until a critical taper $\alpha + ß$ is attained

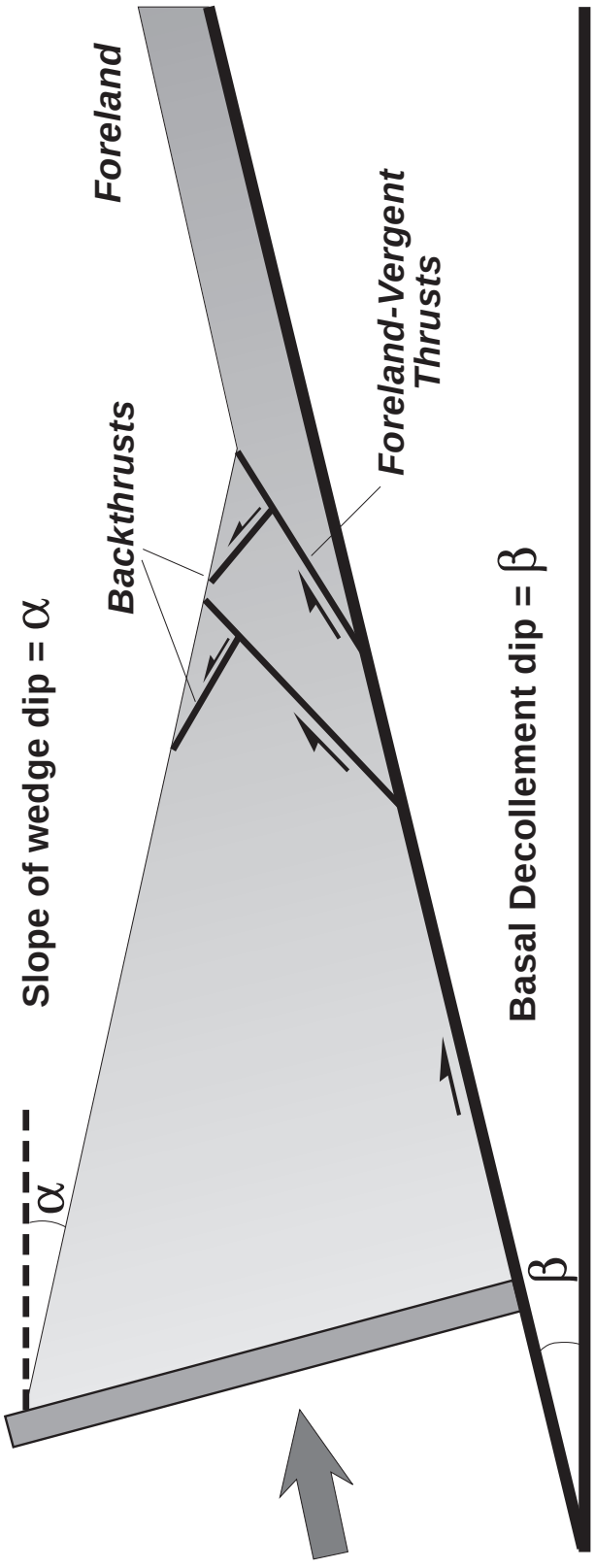


Figure 4.8. Coulomb wedge model for the development of accretionary wedges or foreland fold and thrust belts (modified from Davis *et al.* 1983; Dahlen, 1990).

(Davis *et al*. 1983; Dahlen, 1984; Dahlen *et al*. 1984). The critical taper is defined as the angle at the front of the wedge for which the wedge is on the verge of Coulomb failure everywhere including at its base where frictional sliding along a *decollement* is assumed to be occurring (e.g. Davis *et al*. 1983; Dahlen, 1984; Dahlen *et al*. 1984) (Fig. 4.8). Subsequent deformation involves transport of the wedge along the basal *decollement* or the wedge continues to grow in a self-similar fashion by addition of new material at the wedge toe but maintaining the critical taper (e.g. Davis *et al*. 1983; Dahlen, 1984; Dahlen *et al*. 1984).

The steady state wedge shape is primarily controlled by the relative magnitudes of the strength of the wedge material as well as the frictional strength of the basal detachment (Davis *et al*. 1983; Dahlen, 1984; Dahlen *et al*. 1984). Other factors that control the critical taper include pore fluid pressure, erosion, synchronous sedimentation at the top of the wedge and underplating of material at the base of the wedge (e.g. Platt, 1986; Dahlen & Suppe, 1988; Storti *et al*. 2000; McClay & Whitehouse, 2004). To maintain the critical taper, every increment in growth in the length of the wedge must be balanced by a proportional increment in height at every point along the length of the wedge (Davis *et al*. 1983; Dahlen, 1984; Dahlen *et al*. 1984). A way of maintaining the critical taper is to increase the angle of the basal detachment. This can be achieved if progressively deeper levels within the thrust belt become involved in thrusting (Morley, 1988; Mitra & Sussman, 1997). Increasing the basal friction increases the critical taper, whereas increasing the internal strength of the wedge material decreases the critical taper (Davis *et al*. 1983; Dahlen, 1984; Dahlen *et al*. 1984). The wedge taper can decrease due to erosion or simply due to foreland propagation of the thrust front (Morley, 1988).

The interaction between tectonics and sedimentation is known to play an important role in the dynamics of the orogenic wedge (e.g. Koons, 1990; Storti & McClay, 1995; Beaumont *et al*. 2000; Storti *et al*. 2000; McClay & Whitehouse, 2004). The addition of synorogenic strata in front and on top of a growing imbricate Coulomb wedge adds taper and lowers the topographic slope of the wedge as well as increasing the normal stress on the basal *decollement* surface. As a result, the Coulomb wedge grows vertically by concentrating deformation towards the rear of the wedge, and the amount

of lateral shortening in the wedge decreases in order to achieve a critical taper (Storti & McClay, 1995).

Critical wedge models have successfully explained the mechanics of development of foreland fold and thrust belts (e.g. Dahlen & Suppe, 1988; Dahlen, 1990; Willet, 1991), however, they have been also widely critiqued in the literature (e.g. Woodward, 1987; Price, 1988, 1990; Hatcher & Hooper, 1992; Bombolakis, 1994). Price (1988, 1990) argued that the critical tapered wedge model is too oversimplified to resolve details of the internal structure of orogenic wedges, including the kinematics of individual large thrust faults (e.g. Price, 1988). Price (1988, 1990) argued that the critical taper theory ignores a large amount of fundamental structural observations and data from earthquake seismology, which show that slip on thrust faults involves the propagation of dislocations, each of which affects only a small portion of the fault at any one time.

4.3 THRUST SYSTEMS

Thrust faults rarely occur isolated but rather commonly join up in arrays of thrusts faults referred to as thrust systems (e.g. Boyer & Elliot, 1982; Mitra, 1986; McClay, 1992), in which thrust faults are geometrically, kinematically and mechanically linked (McClay, 1992) (Figs. 4.9 & 4.10). Thrust systems are commonly subdivided into duplexes, imbricate thrust systems and triangle zones (Boyer & Elliot, 1982; Mitra, 1986; McClay, 1992) (Figs. 4.9 & 4.10). Duplexes and imbricate thrust systems are generally found at any structural position in orogenic belts, whereas triangle zones are characteristic of the frontal and most external parts of foreland fold and thrust belts (e.g. De Paor, 1988; Woodward *et al.* 1989; McClay, 1992; Jones, 1996) (Figs. 4.9 & 4.10).

4.3.1 Duplexes

Dahlstrom (1970) formally introduced the duplex concept to refer to an array of thrust sheets or 'horses' bounded at the top and the bottom by a roof and a floor thrust faults, respectively. Horse-bounding thrust faults are termed linking thrusts (e.g. Dahlstrom, 1970; Boyer & Elliot, 1982; McClay & Insley, 1986*a*; Mitra, 1986; McClay, 1992) (Figs. 4.9 & 4.10). Linking thrusts are usually described to be sigmoidal in shape and to ramp up through more competent units bounded by incompetent units, in which the roof and floor thrust faults are developed (Dahlstrom, 1970; Boyer & Elliot, 1982; McClay

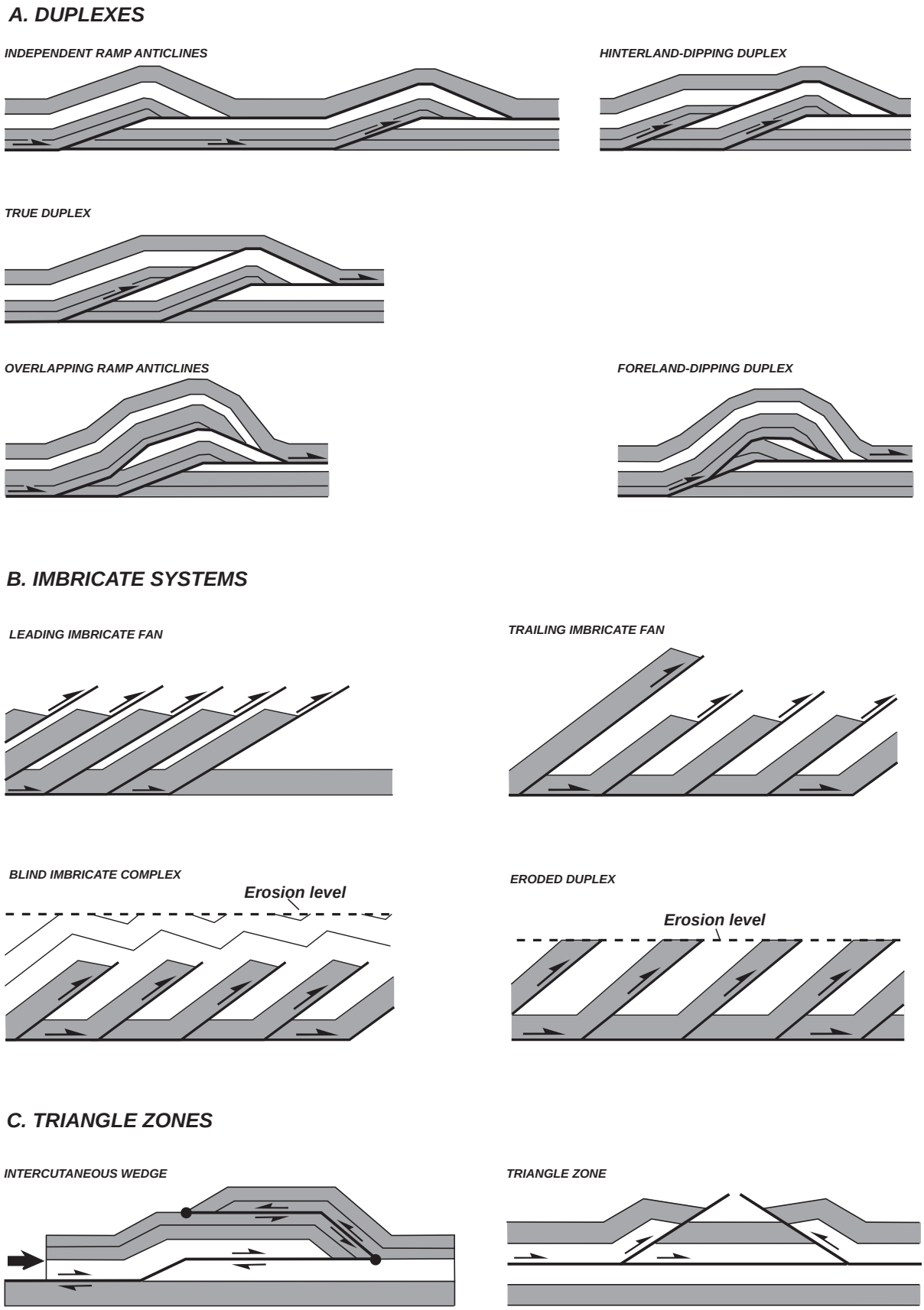


Figure 4.9. Thrust systems. **A.** Duplexes. **B.** Imbricate systems. **C.** Triangle zones. (modified from Boyer & Elliot, 1982; Mitra, 1986; Woodward *et al*. 1989; McClay, 1992).

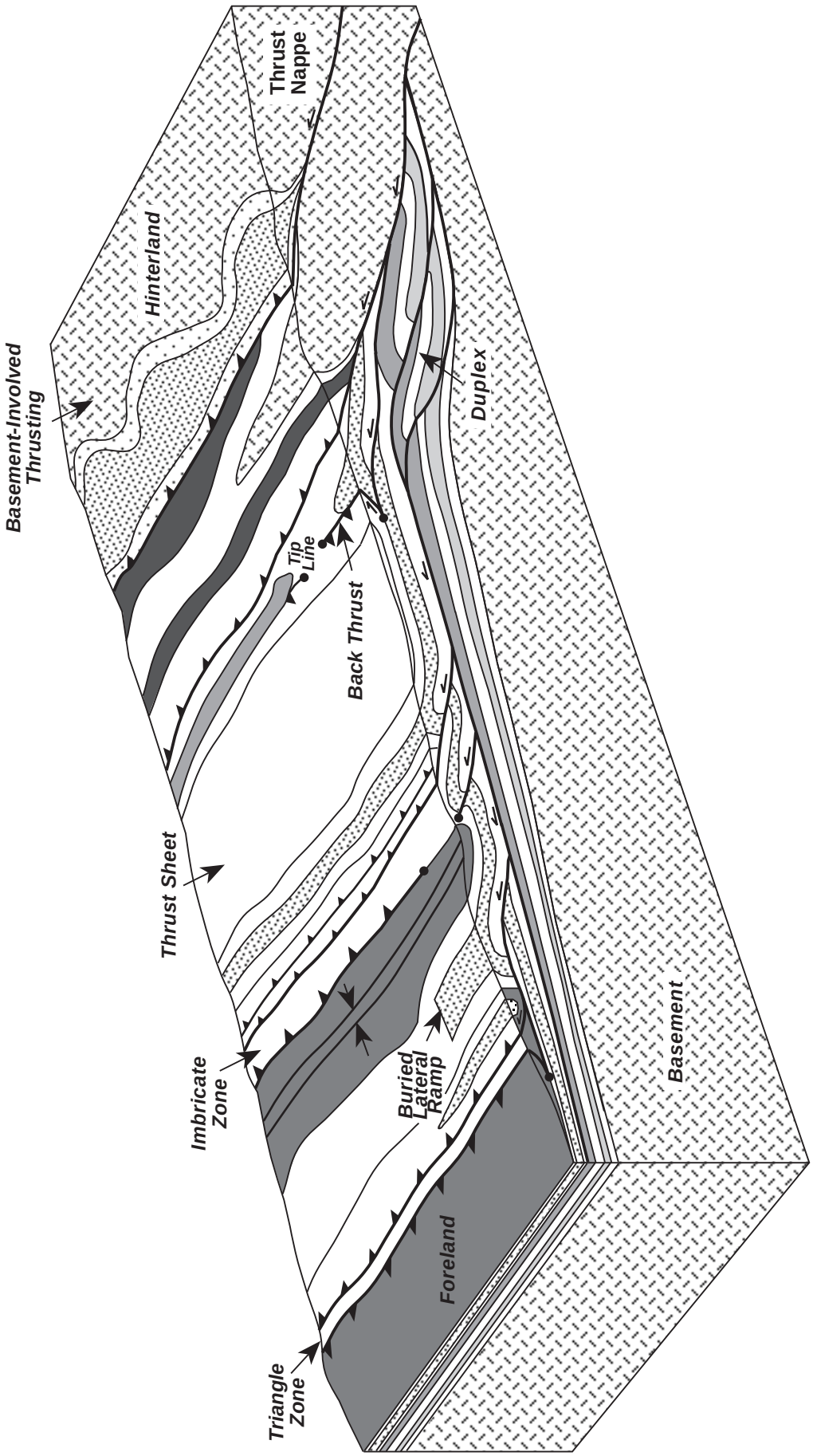


Figure 4.10. 3D diagram showing the spatial distribution of thrust systems in a foreland fold and thrust belt (modified from De Paor, 1988).

& Insley, 1986*a*; McClay, 1992). The term duplex is also commonly introduced as a descriptor to refer to a particular type of structure found at the frontal and most external part of foreland fold and thrust belts, the passive roof duplex (Banks & Warburton, 1986), which is described later in this chapter.

Based upon the relationship between fault spacing and displacement, Boyer & Elliot (1982) proposed a three-fold geometric classification of duplexes, later revised and modified by Mitra (1986), who identified the following types of duplexes (Fig. 4.9a). These are, independent ramp anticlines and hinterland-dipping duplexes, true duplexes, and overlapping ramp anticlines. All three types of duplexes form by the progressively footwall imbrication of a thrust ramp (Figs. 4.9a, 4.10 & 4.11). In the independent ramp anticlines the spacing between adjacent thrust faults is greater than the displacement involved. As a result, the ramp anticlines are separated from each other by broad synformal structures (Fig. 4.9a). Hinterland-dipping duplexes, those in which both the link thrusts and the bedding dip towards the hinterland, are formed where the initial spacing of thrust faults is small such that, at the contact between horses, the roof thrust dips towards the hinterland (Mitra, 1986). If the slip between the horses is very high, they can eventually slide completely over one another to produce an imbricate stack, which is known as a foreland-dipping duplex (Fig. 4.9a). True duplexes are formed by a particular combination of final thrust spacing, ramp angle and ramp height such that parts of all the link thrusts and roof thrust are parallel to the frontal ramp of the duplex (Fig. 4.9a). True duplexes of Boyer & Elliot (1982) were later revised by Mitra (1986), who divided them into three categories depending upon their position with respect to larger thrust faults. According to Mitra (1986), duplexes may occur in the footwall to a ramp anticline, in the hangingwall to a ramp anticline or in front of a ramp anticline. Then the terms ramp anticline footwall, ramp anticline hangingwall and frontal zone of ramp anticline (Mitra, 1986) are introduced. Hinterland-dipping duplexes contain faults that curve asymptotically into the roof and floor thrusts (McClay & Insley, 1986*a*; Mitra & Boyer, 1986). The curved fault geometry inside the duplex is a result of the deformation of older horses by slip on younger faults. This sequence can be recognized because the faults at the leading edge of the duplex have successively lower dips and less curvature (Groshong & Usdansky, 1988).

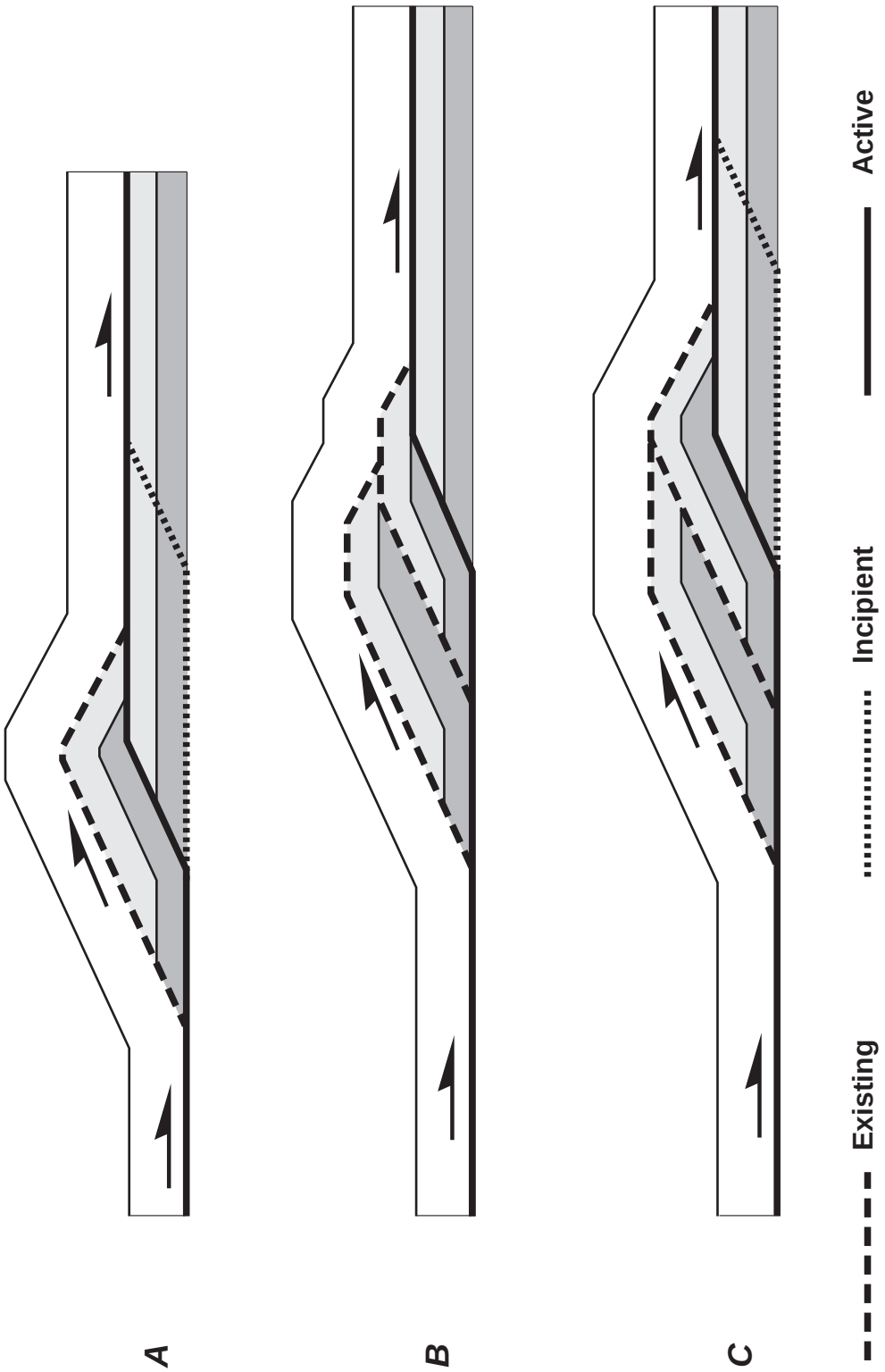


Figure 4.11. Conceptual model for duplex development (modified from Boyer & Elliot, 1982).

Overlapping ramping anticlines are formed where the crests of successive ramp anticlines partially or totally overlap (Fig. 4. 9a). A duplex formed by overlapping ramp anticlines that have coincident trailing branch lines is referred to as an antiformal stack (Boyer & Elliot, 1982; Mitra, 1986; McClay, 1992) (Fig. 4.12).

Duplex structures are common structures in foreland fold and thrust belts at a range of scales. Duplex geometries in nature are very diverse (e.g. Couzens-Schultz *et al*. 2003) (Figs. 4.12, 4.13, 4.14, 4.15 & 4.16) and may significantly differ from the conceptual models proposed by Boyer & Elliot (1982) and Mitra (1986) (Fig. 4.11). Examples include duplexes from the Lewis thrust of the Canadian Rocky Mountains (e.g. Douglas, 1952; Dahlstrom, 1970; McClay & Insley, 1986*a*) (Fig. 4.12) and the Mountain City window duplex (e.g. Boyer & Elliot, 1982; Diegel, 1986; Geiser, 1988) (Figs. 4.13 & 4.14).

4.3.2 Imbricate Thrust Systems

Imbricate thrust systems (Figs. 4.9b, 4.17, 4.18 & 4.19) are closely related branching arrays of thrust faults that are characteristic of the frontal parts of foreland fold and thrust belts (Boyer & Elliot, 1982). Imbricate thrust systems occur as imbricate fans (Figs. 4.9b, 4.17, 4.18 & 4.19), in which a series of linked gently- to steeply-dipping emergent thrusts diverge upwards from a sole or floor thrust (Boyer & Elliot, 1982; McClay, 1992). Thrust faults in imbricate thrust systems are often depicted to have listric fault geometries that merge with a basal detachment (e.g. Boyer & Elliot, 1982; Fermor & Moffat, 1992; Price & Monger, 2003).

Depending on where the amount of displacement is concentrated, imbricate fans are subdivided into leading and trailing imbricate fans (e.g. Dahlstrom, 1970; Boyer & Elliot, 1982; Mitra, 1986; McClay, 1992) (Fig. 4.9b). Leading imbricate fans accommodate most of the displacement on the leading and lowermost thrust fault (Fig. 4.9b), whereas in the trailing imbricate fans, the displacement is mainly concentrated on the trailing and structurally highest thrust fault (Fig. 4.9b).

Imbricate thrust systems do not necessarily crop out but may remain buried in that shortening at shallower structural levels may be accommodated by processes other than

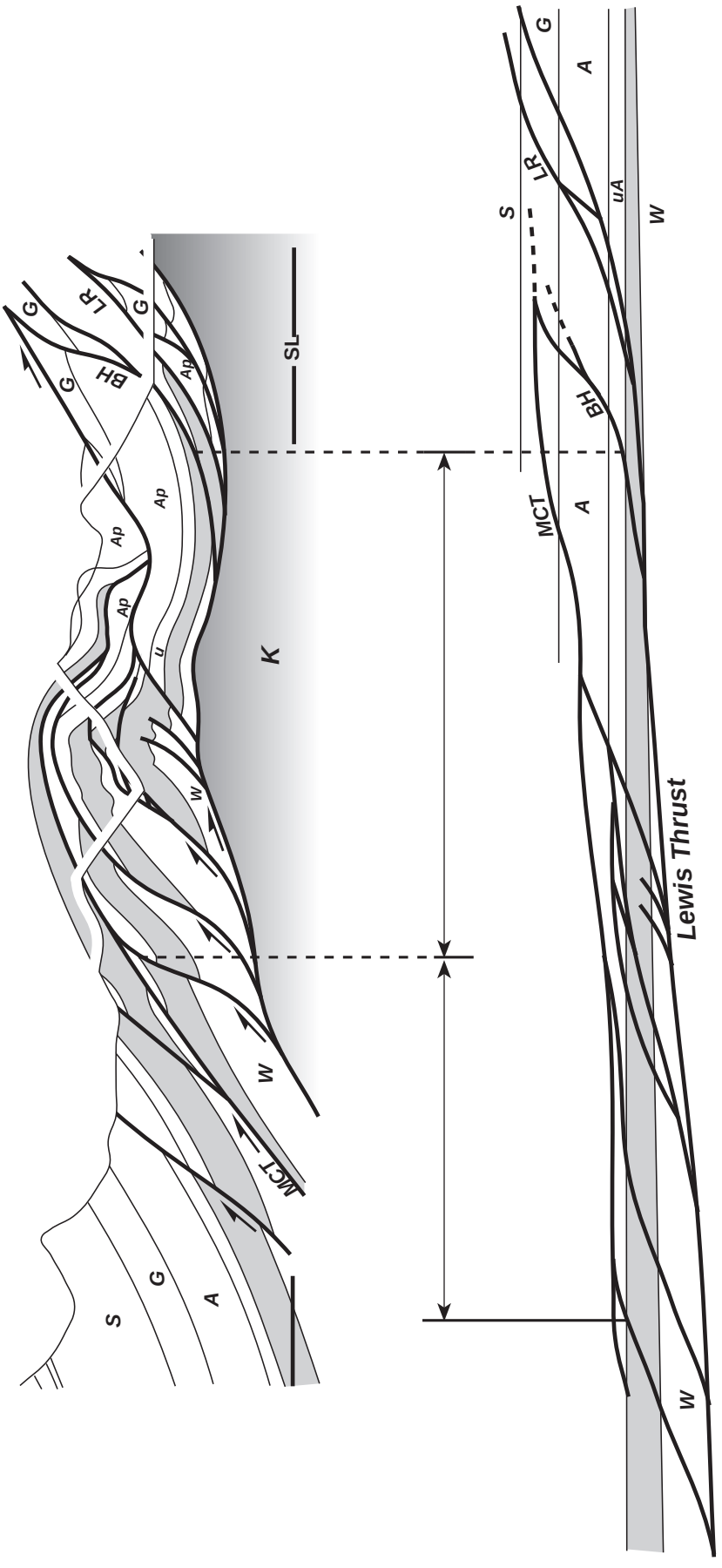


Figure 4.12. Mount Crandell duplex, Canadian Rocky Mountains. Precambrian Belt Supergroup, comprising Waterton (W), lower Altyn (fine stipple), mid and upper Altyn (uA), Grinnel (G), and Siyeh (S), is thrust over Cretaceous siliciastics (K) by Lewis thrust. Mount Crandell thrust (MCT) is roof and Lewis thrust is floor to duplex, and folded horse just northwest of Mount Crandell suggests that duplex developed toward foreland (modified from Douglas, 1952).

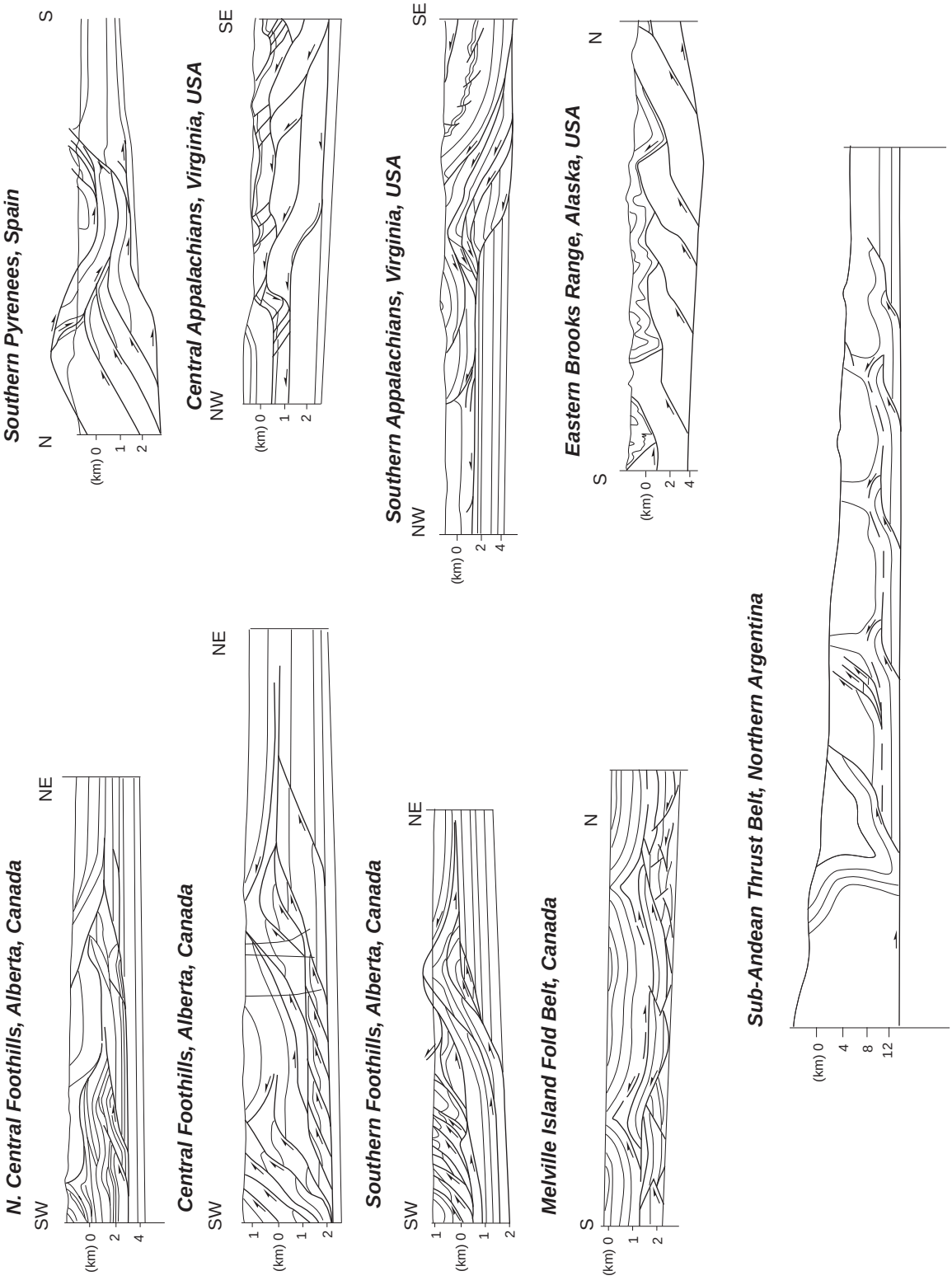


Figure 4.13. Examples of duplexes in foreland fold and thrust belts (modified from Couzens-Schultz *et al.* 2003).

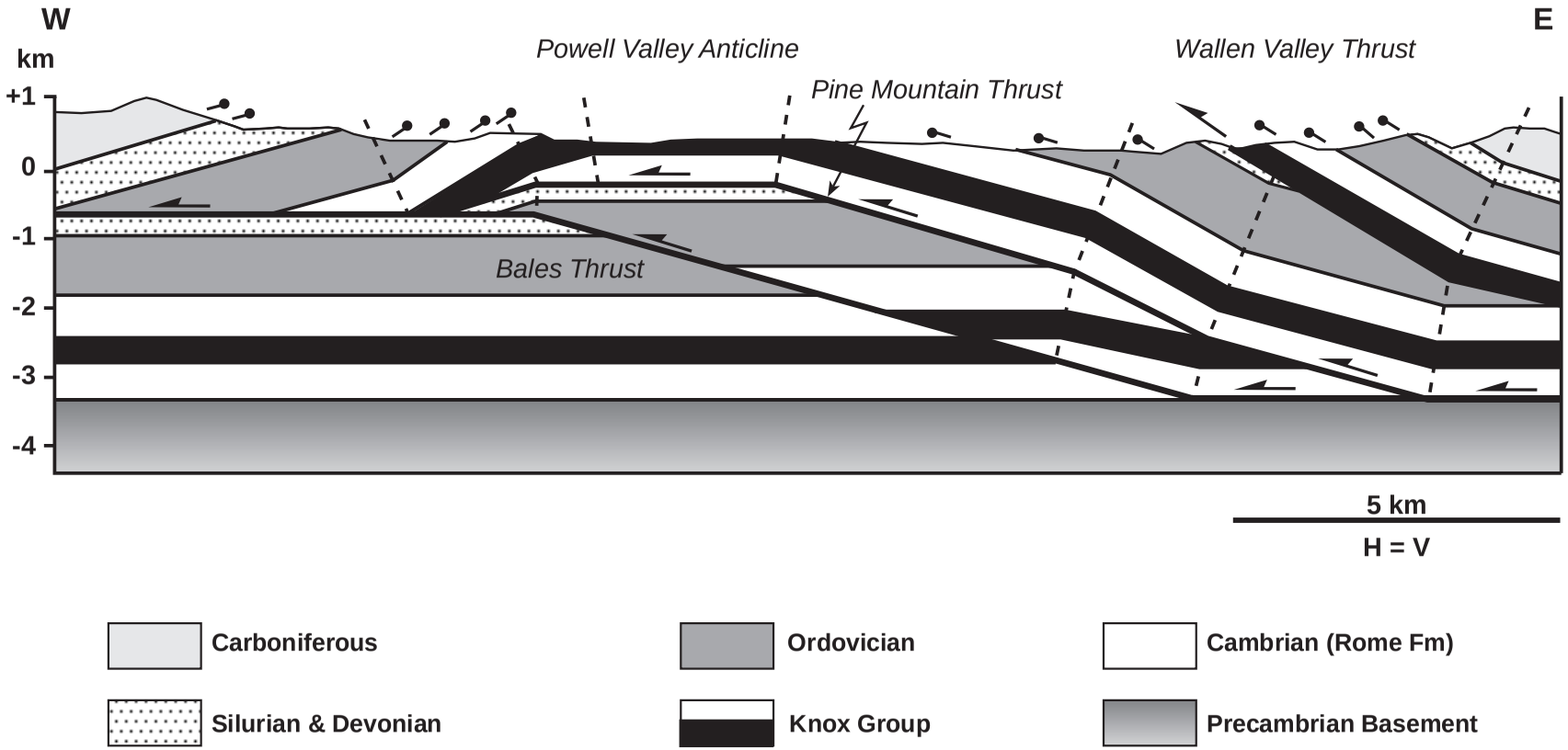


Figure 4.14. Cross section through the Pine Mountain thrust, Appalachians, eastern USA. Note that the Pine Mountain thrust sheet is folded by an underlying imbrication on the Bales thrust (modified from Suppe, 1983, 1985).

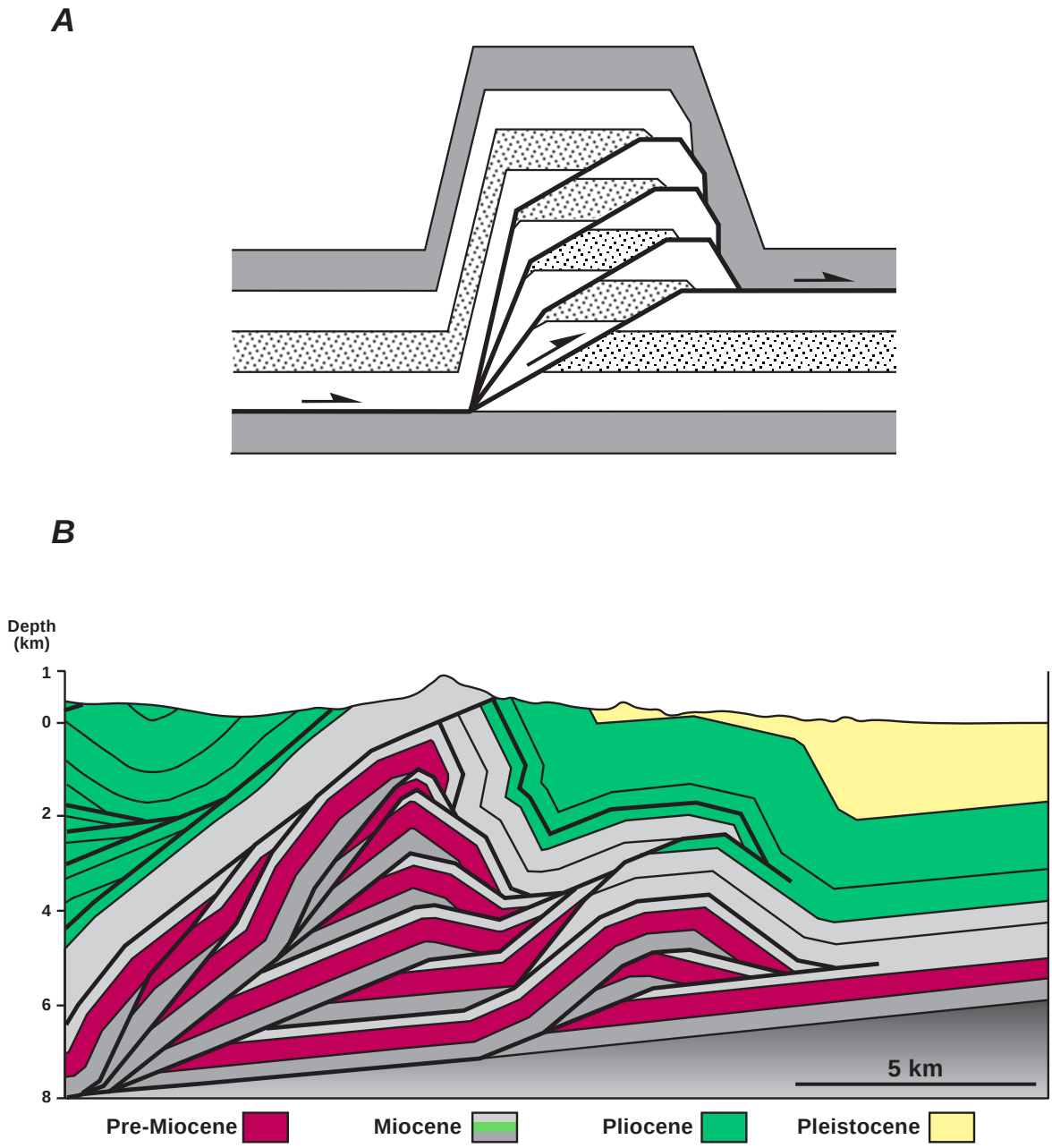


Figure 4.15. Antiformal stack. **A.** Synoptic conceptual model (modified from McClay, 1992). **B.** Natural example from the southern Taiwan thrust belt (modified from Suppe, 1983).

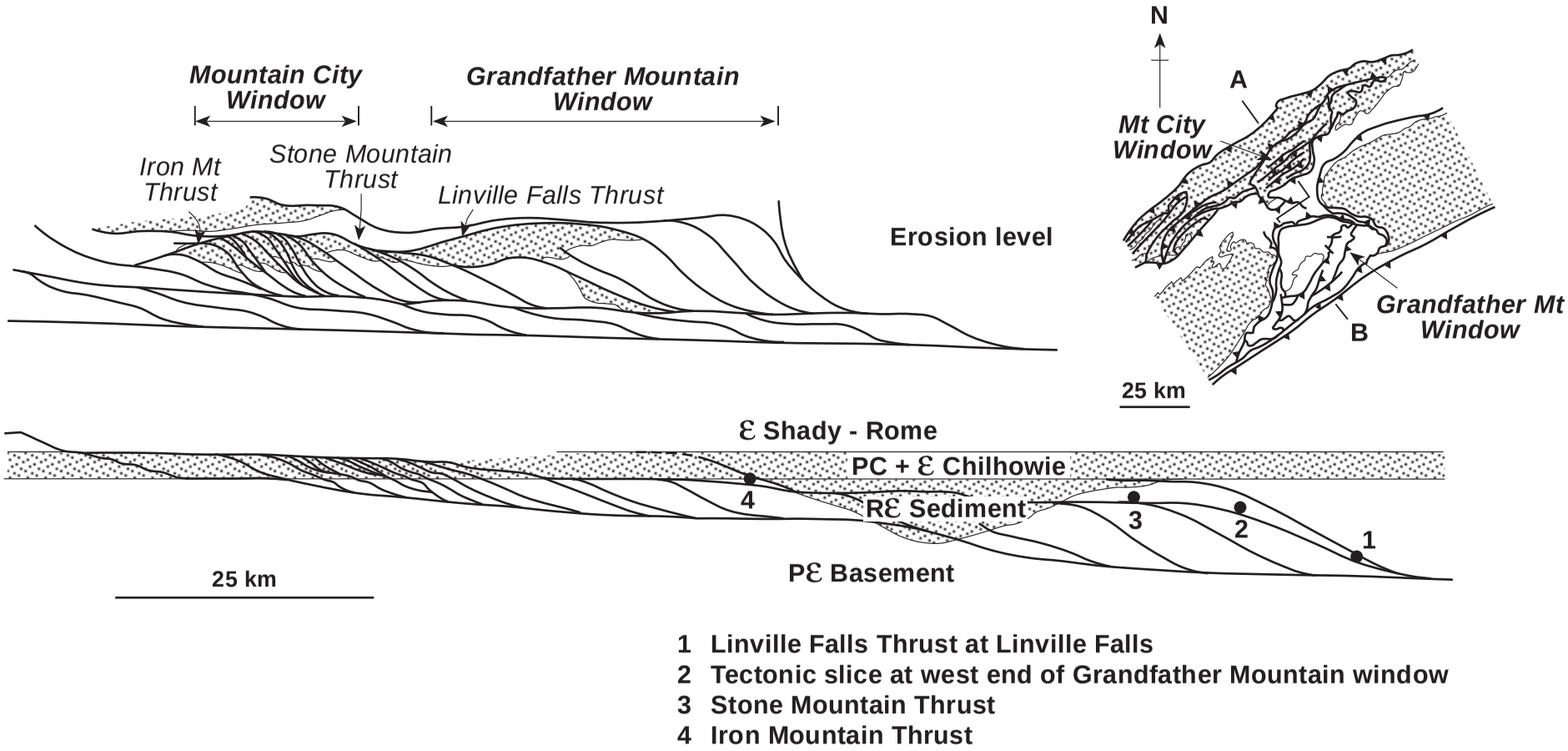


Figure 4.16. Cross section through the Grandfather and Mountain City windows. Appalachians. USA (modified from Geiser, 1988).

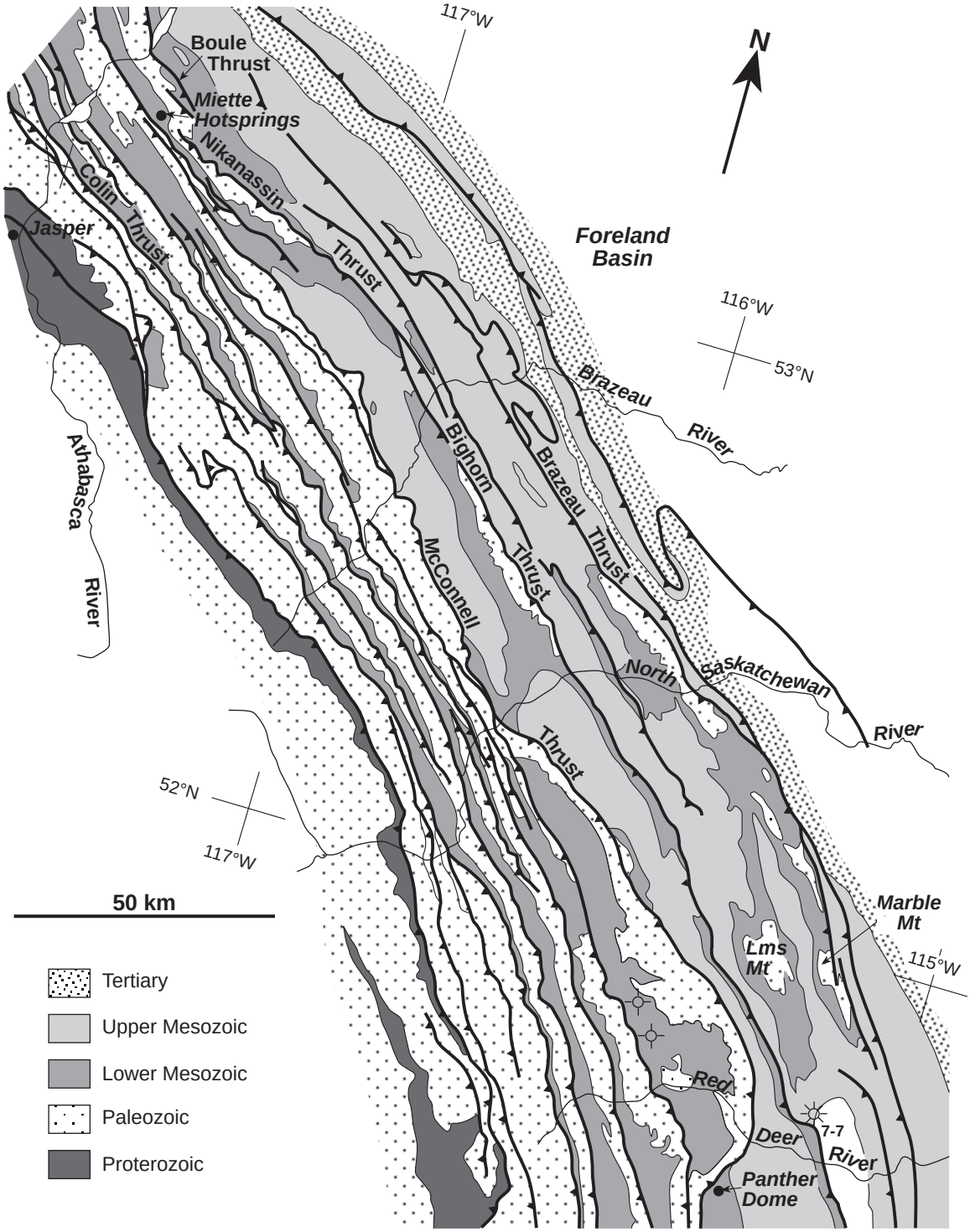


Figure 4.17. Geological map of the central Alberta Foothills and Front Ranges of the Canadian Rocky Mountains showing imbricate thrust systems (modified from Fermor, 1999). Note that younger rocks are progressively exposed towards the foreland.

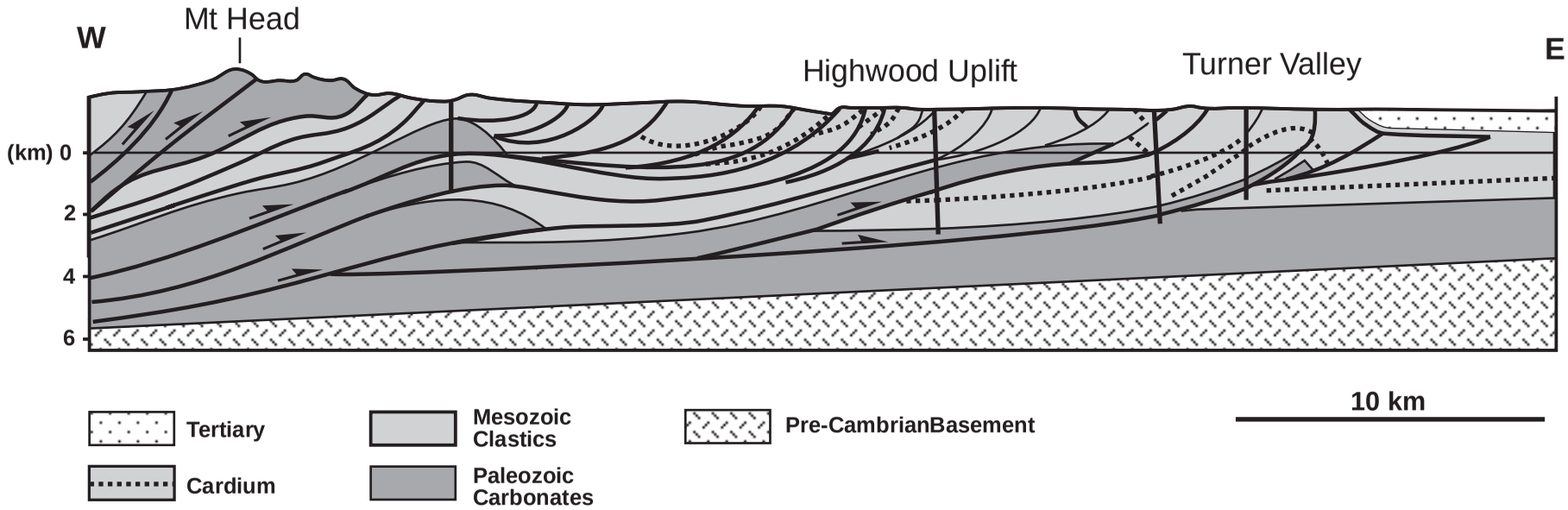


Figure 4.18. Cross section through Turner Valley-Higwood structure of the southern Canadian Rocky Mountains. Note imbricate stacks in the crest and frontal wall of the structural culmination developed east of Mount Head and in the Highwood Uplift area (modified from Bally *et al*.1966).

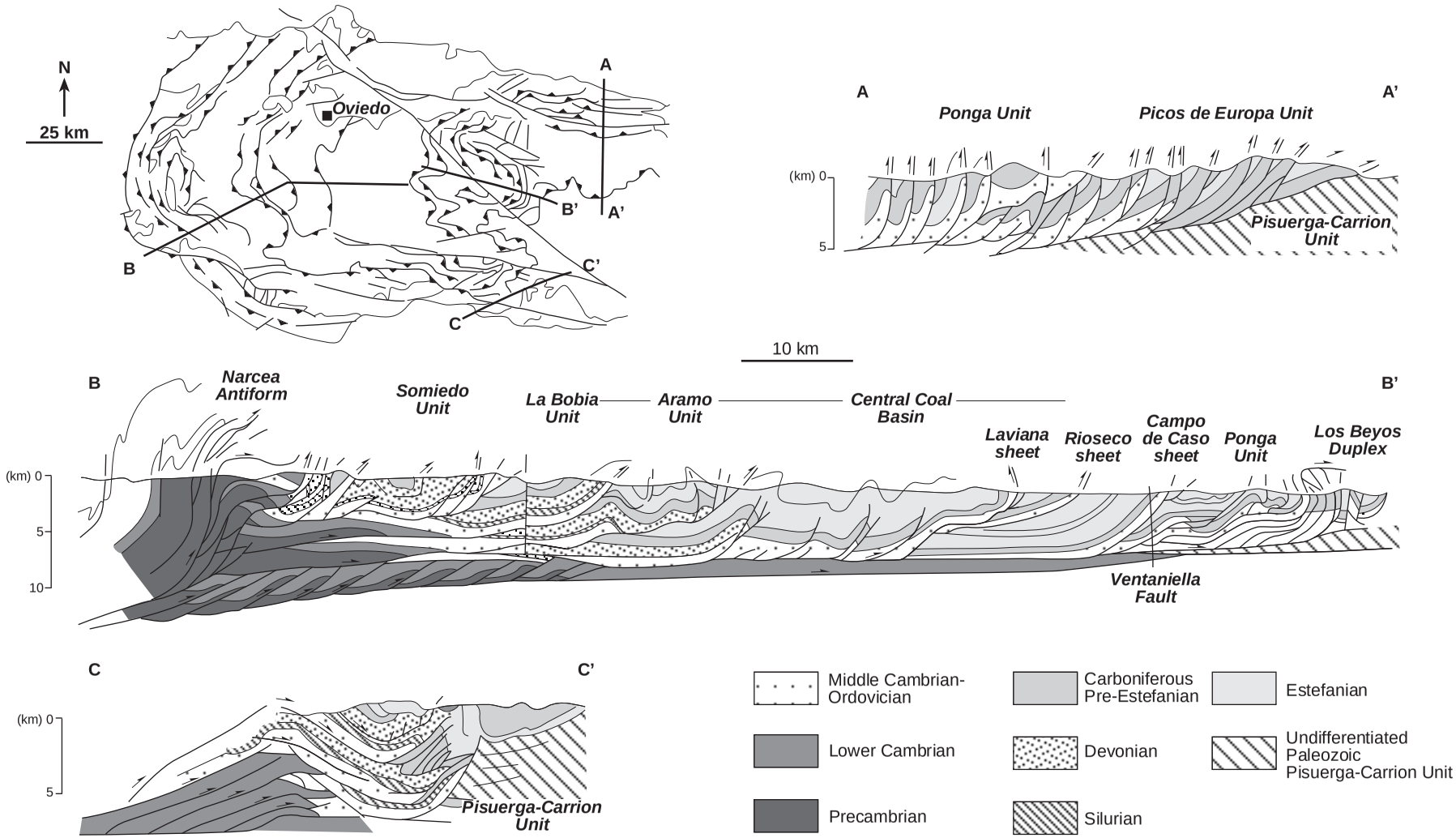


Figure 4.19. Cross sections through the Cantabrian Mountains, Variscan Belt of northwestern Spain illustrating the geometry of thrust systems (modified from Alonso, 1987; Perez-Estaun *et al.* 1988; Marquinez, 1989).

thrusting (e.g. detachment folding, penetrative deformation, zonation of structural styles) (Boyer & Elliot, 1982; McClay, 1992). These thrust systems are referred to as blind imbricate complexes (McClay, 1992) (Fig. 4.9b). In addition, since complete large-scale duplex structures are rarely preserved, imbricate thrust systems formed from a branching array of thrusts that die out into tip lines and which have been subsequently eroded away may become difficult to distinguish from duplexes that have had the leading branch lines eroded (Boyer & Elliot, 1982; McClay, 1992) (Fig. 4.9b).

The southern Canadian Rocky Mountains (e.g. Bally *et al*. 1966; Dahlstrom, 1970; Price, 1981, 1986; Fermor & Moffat, 1992; Price & Monger, 2003) (Figs. 4.17 & 4.18), the southern Appalachians of the eastern United States (e.g. Mitra, 1988; Hatcher *et al*. 1987, 1990), the Cantabrian Mountains of northern Spain (e.g. Perez-Estaún *et al*. 1988; Alvarez-Marrón, 1995; Bulnes, 2002) and the Magallanes fold and thrust belt of Patagonia (e.g. Alvarez-Marrón *et al*. 1993) are examples of fold and thrust belts with well-developed frontal imbricate thrust systems. Commonly, thrust faults in imbricate systems become rotated as younger thrust sheets are emplaced beneath them (e.g. Boyer & Elliot, 1982). This mechanism accounts for some geometric relationships and steeply-dipping thrust faults observed in the frontal part of thrust belts.

4.3.3 Triangle Zones and Mountain Fronts

The term triangle zone (e.g. Gordy *et al*. 1977) was firstly introduced to describe the structure of the eastern margin of the Cordilleran Foothills of the southern Canadian Rocky Mountains (e.g. Jones, 1996). Triangle zones (Fig. 4.9c), also referred to as tectonic wedges (Wentworth *et al*. 1984), are zones of opposed thrust dip and vergence that are found in frontal part of the fold and thrust belt, typically associated with a duplex or an antiformal stack structure (Jones, 1986; McClay, 1992) (Figs. 4.10 & 4.15). A secondary usage of the term triangle zone refers to a combination of two thrust faults that share a same basal *decollement* but have opposing dips and vergence such that they define a triangular shape between them (McClay, 1992) (Fig. 4.9c.).

Triangle zones are the result of tectonic wedging in the frontal part of foreland fold and thrust belts (Fig. 4.9c). The process of tectonic wedging implies that the section above a tectonic wedge has undergone less horizontal tectonic transport than the thrust section

beneath it (Lawton *et al*. 1994; Jones, 1996). Jones (1996) proposed that tectonic wedging occurs only at the frontal and most external part of a fold and thrust belt during the final episodes of an orogeny, by a process that is different from those which created the fold and thrust belt hinterland. Several classifications of triangle zones and thrust fronts have been proposed (e.g. Banks & Warburton, 1986; Morley, 1986; Price, 1986; Vann *et al*. 1986; Jones, 1996) (Fig. 4.20). Classic examples of triangle zone structures include the Highwood and Cabin Creek triangle zones of the frontal part of the southern Canadian Rocky Mountains foreland fold and thrust belt (e.g. Bally, 1983; Jones, 1996; MacKay *et al*. 1996; Price & Monger, 2003) (Fig. 4.21).

A particular type of triangle zone is the passive roof duplex (Banks & Warburton, 1986) (Fig. 4. 22). A passive roof duplex is defined as a duplex in which the roof thrust has a backthrust sense and the rocks lying above the roof thrust remain relatively stationary during foreland-directed propagation of the underlying horses (Banks & Warburton, 1986; Vann, 1986) (Fig. 4.22a). Passive roof duplexes have been described for the frontal parts of the Kirthar and Sulaiman thrust belts and the Potwar Plateau and Salt Range of Pakistan (e.g. Banks & Warburton, 1986; Morley, 1986; Jadoon *et al*. 1994; Jaswal *et al*. 1997; Grelaud *et al*. 2002), the Taiwan thrust belt (e.g. Suppe, 1980; Covey, 1986; Mugnier *et al*. 1997) (Fig. 4.15), and the northeastern Brooks Range (e.g. Namson & Wallace, 1986; Wallace, 1993; Wallace *et al*. 1997) (Fig. 4.22b). Mugnier *et al*. (1997) have suggested that development of passive roof duplex structures appears to be coeval with intense syn-orogenic erosion and sedimentation.

The structure of the frontal parts of fold and thrust belts is not always controlled by triangle zones or passive roof duplexes but is commonly characterized by emergent thrust fronts (Morley, 1986; Vann, 1986) in which the thrust sheets emerge to the surface and are thrust on to syn-orogenic strata of the foreland basin.

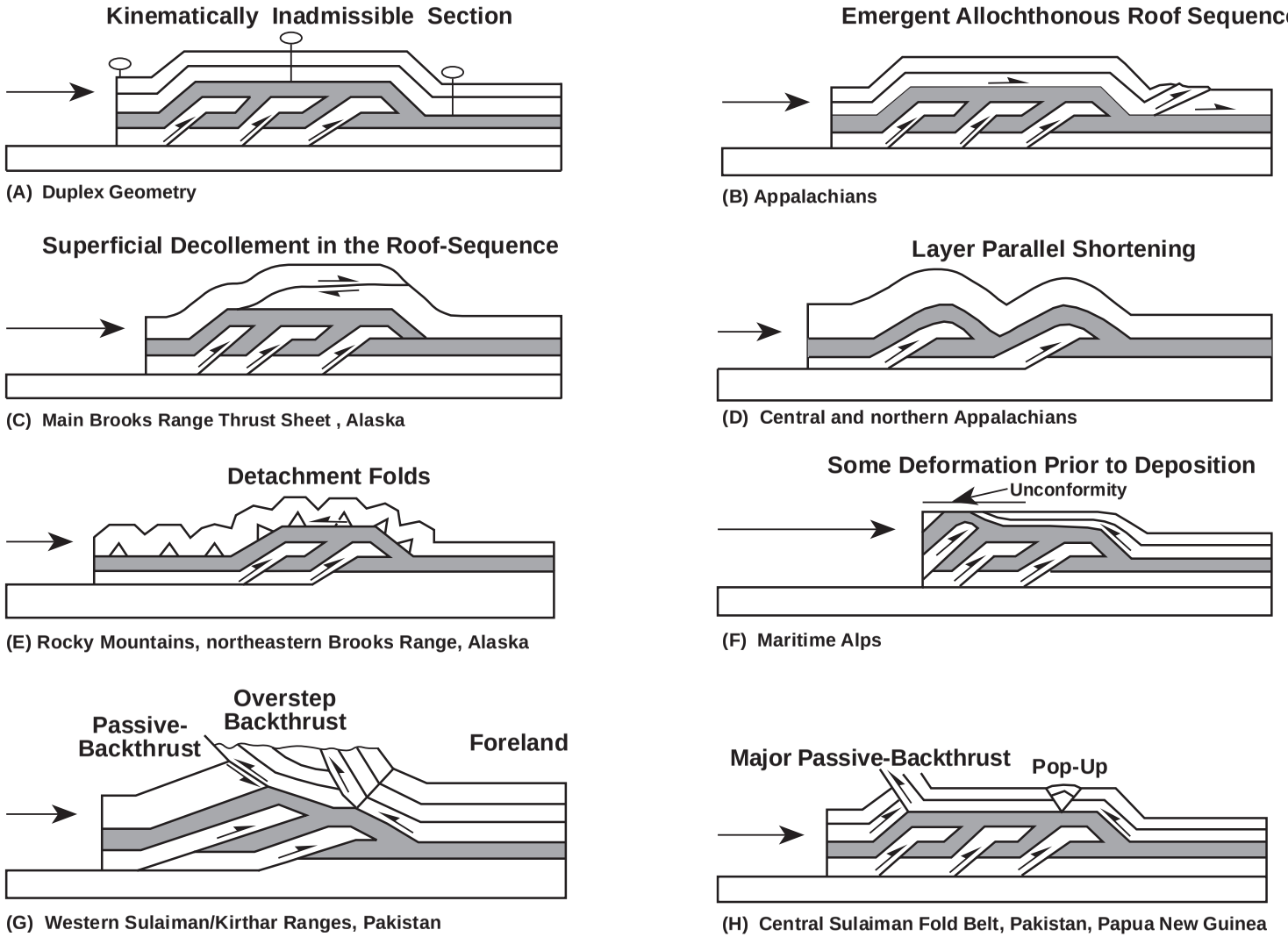


Figure 4.20. Conceptual models for the structure of mountain fronts (modified from Jadoon *et al.* 1994).

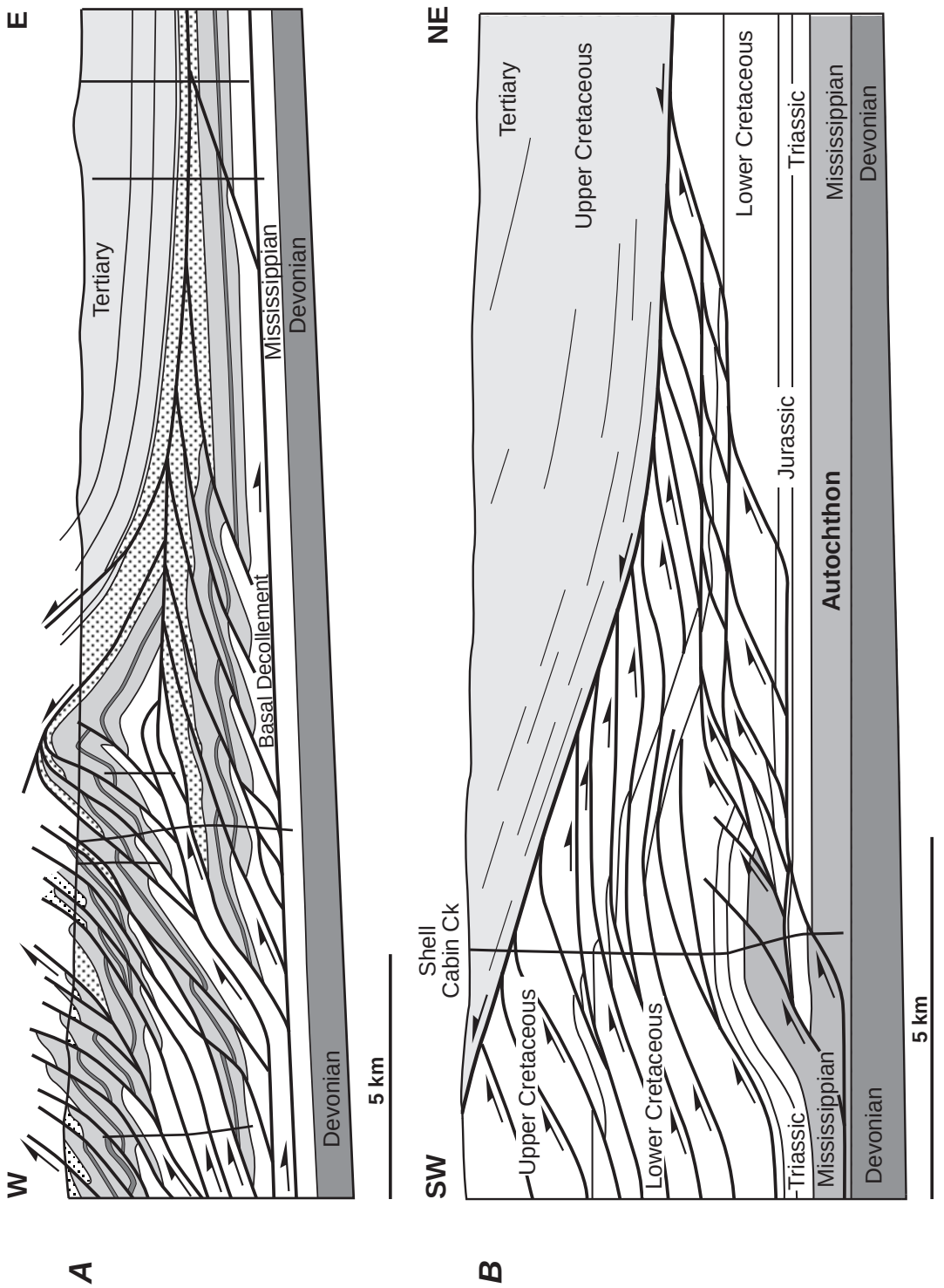


Figure 4.21. Cross sections illustrating the geometry of triangle zones in the Canadian Rocky Mountains. **A.** Highwood structure, southwest Alberta (modified from Mackay *et al.* 1996). **B.** Cabin Creek, Alberta (modified from Jones *et al.* 1996).

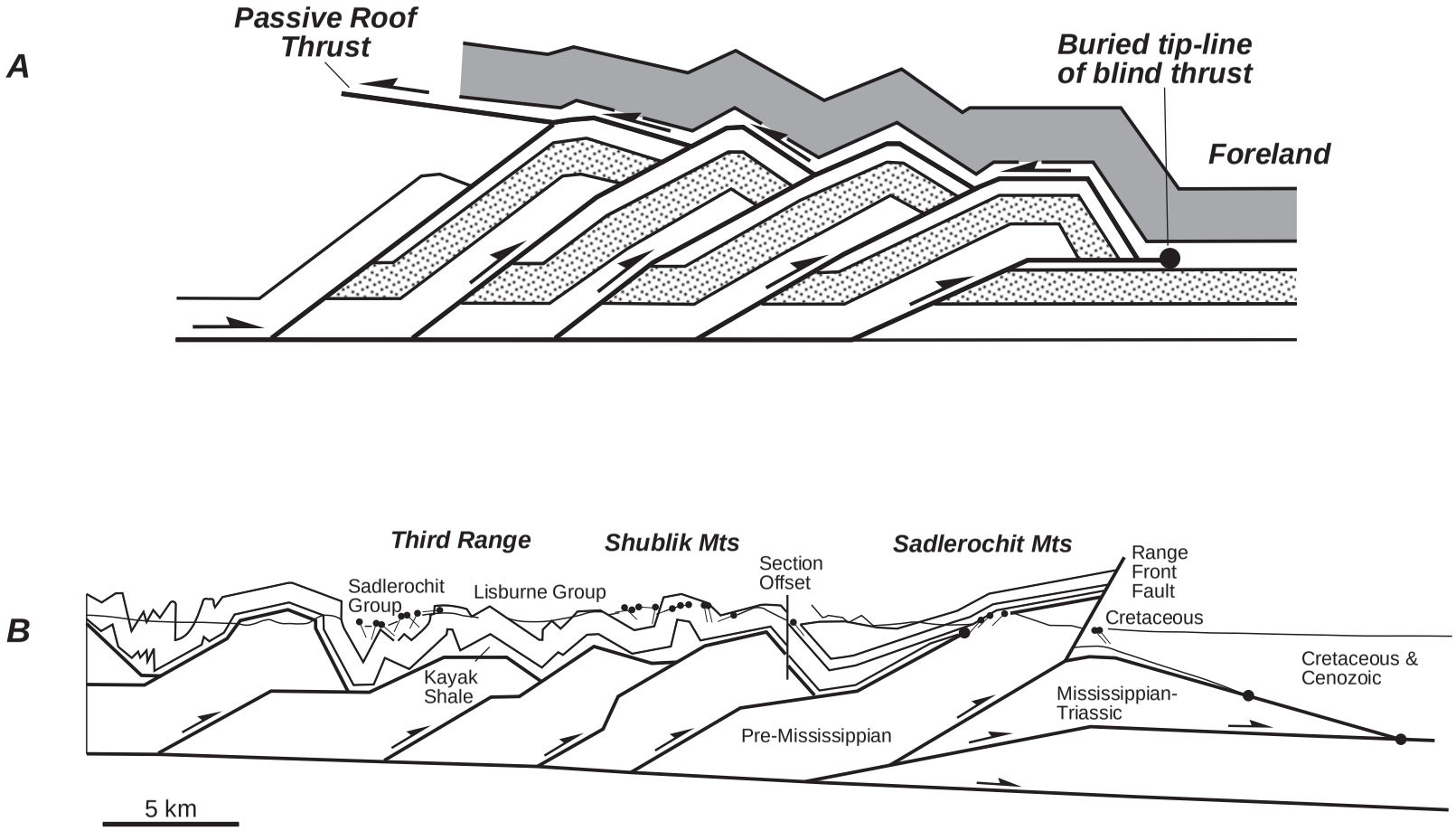


Figure 4.22. Passive roof thrust. **A.** Conceptual model (modified from Banks & Warburton, 1986; McClay, 1992). **B.** Cross-section showing a passive roof duplex in the eastern Brooks Range of Alaska (modified from Namson & Wallace, 1986;Wallace, 1993).

4.3.4 Basement-Involved Thrust Systems

The thrust systems described above (Fig. 4.9) are commonly developed when thrusting occurs upon sedimentary successions (e.g. Bally *et al*. 1966; Boyer & Elliot, 1982; McClay, 1992). However, orogenic belts typically have basement-involved thrust systems in which competent, rigid, crystalline basement thrust sheets (e.g Type C and Type F thrust sheets of Hatcher, 2004) are emplaced above less competent and dominantly thinner sediment-dominated thrust sheets (e.g. Coward, 1983; Erslev, 1991; Schmidt *et al*. 1993; Narr & Suppe, 1994; Mitra & Sussman, 1997; Mitra & Mount, 1998; Hatcher, 2004) (Figs. 4.6b, 4.6c, 4.10 & 4.23). This structural style is commonly referred to as 'thick-skinned' tectonics (e.g. Coward, 1983) (Fig. 4.23) in contrast with the 'thin-skinned' structural style typically described for the frontal and more external parts of fold and thrust belts, where deformation concentrates in the sedimentary cover and the underlying basement remains undeformed (e.g. Bally *et al*. 1966; Price, 1986) (Fig. 4.10).

Basement-involved thrust systems are characterized by steeply-dipping thrust faults that bring thick crystalline basement thrust sheets over their sedimentary cover forming tight, overturned and sheared footwall synclines and broad, uplifted hangingwall anticlines (e.g. Erslev, 1991; Narr & Suppe, 1994; Mitra & Sussman, 1997; Mitra & Mount, 1998) (Fig. 4.23). Basement-involved thrust systems occur dominantly in the hinterlands of orogenic belts (Fig. 4.10). Examples include the southern Alps in Italy and the Appalachians and Sevier thrust belts of the United States (e.g. Mitra & Sussman, 1997; Hatcher, 2004) (Fig. 4.23). Nevertheless, basement-involved thrust systems have been also recognized in foreland regions, such as the Laramide uplifts of the western United States (e.g. Erslev, 1991; Schmidt *et al*. 1993) and the Sierras Pampeanas of Argentina (Cristallini *et al*. 2004). In some cases the basement involved thrust systems are controlled by inversion of pre-existing basement extensional faults that underlie the developing fold and thrust belt (McClay, 2004) (Fig. 4.24).

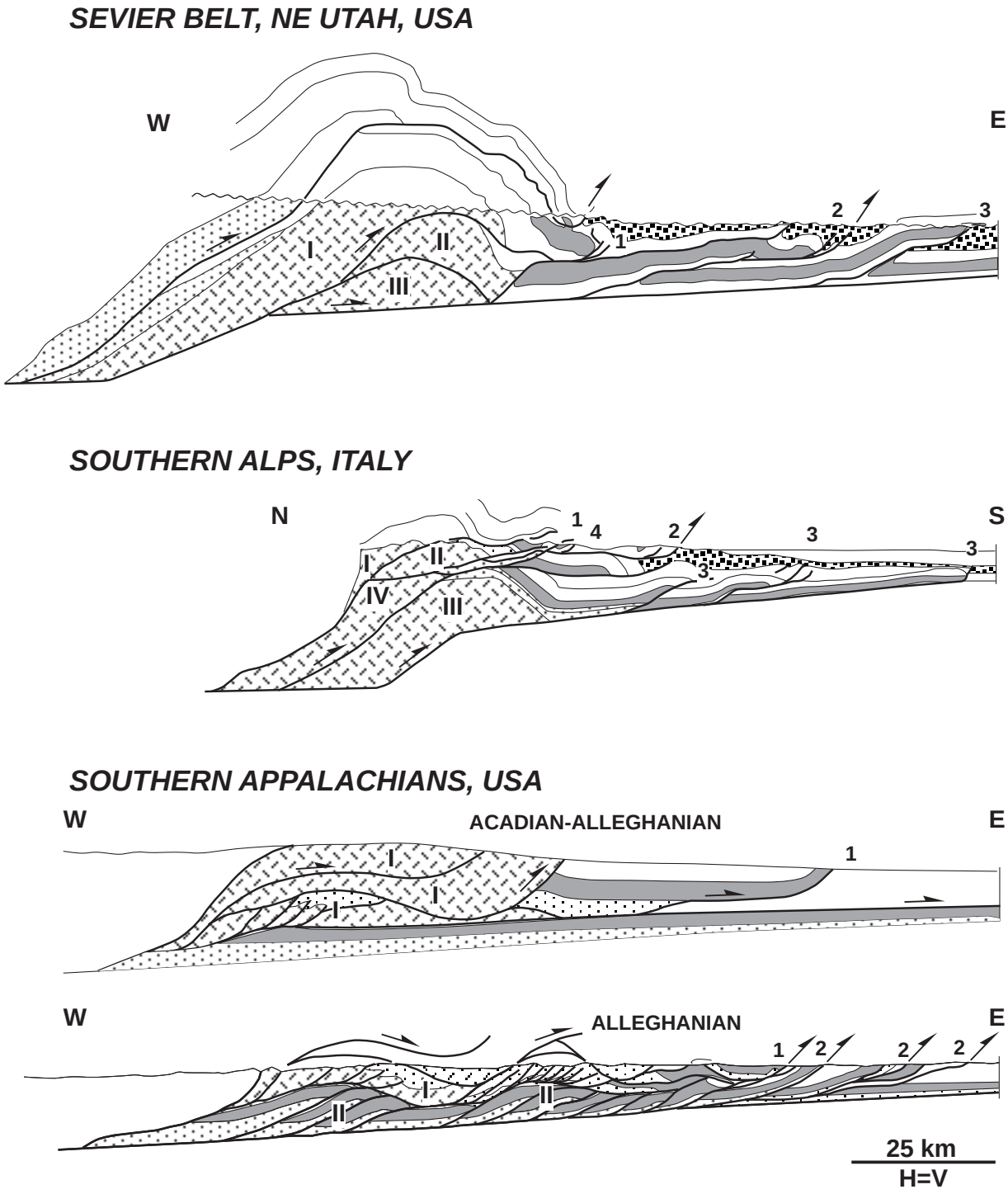


Figure 4.23. Examples of basement-involved thrust systems in orogenic belts (modified from Mitra & Sussman, 1997).

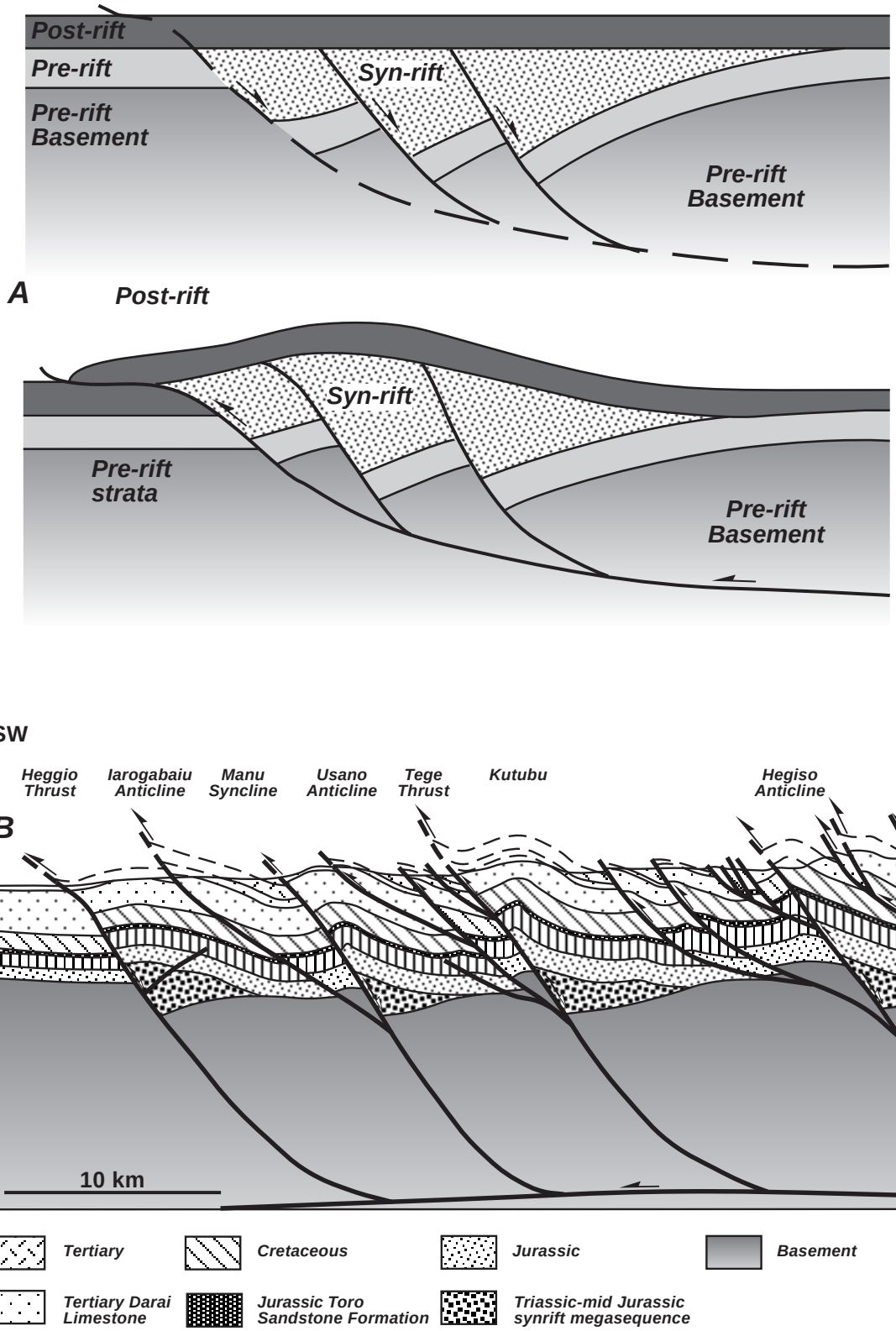


Figure. 4.24. Inversion structures and thrust systems. **A.** Idealized view of normal fault reactivation and basin inversion (modified from Butler, 1989). **B.** Cross section across the Central fold belt, Papua New Guinea (modified from Buchanan & Warburton, 1996).

4.4 3D THRUST SYSTEMS

Thrust systems (Figs. 4.9, 4.10 & 4.23) and their related fold structures do not extend indefinitely (Fig. 4.7) but rather are rarely cylindrical over large distances and commonly show along-strike terminations with complex three-dimensional geometries (e.g. Dahlstrom, 1970; Boyer & Elliot, 1982; Apotria *et al*. 1992; McClay, 1992; Wilkerson, 1992; Wilkerson *et al*. 1992; Pohn, 1998; Fermor, 1999; Price, 2001; Wilkerson *et al*. 2002; McClay *et al*. 2004*a*). Fault terminations are generally ascribed to loss of fault slip or displacement gradient and changes in fault geometry (Boyer & Elliot, 1982; Mitra, 1986; McClay, 1992; Apotria *et al*. 1992; Wilkerson *et al*. 2002).

4.4.1 Lateral Ramps, Tear Faults and Transverse Zones

Thrust faults commonly have complex three dimensional geometries with a frontal ramp perpendicular to the tectonic transport direction, which is bounded by two lateral/oblique ramps and/or tear faults (Boyer & Elliot, 1982; Butler, 1982; Hossack, 1983; Price & Cosgrove, 1990; McClay, 1992; Wilkerson *et al*. 2002), parallel or oblique to the tectonic transport direction (Figs. 4.25, 4.26 & 4.27). The term lateral ramp was introduced by Hossack (1981), Boyer & Elliot (1982), Butler (1982) and Hossack (1983) to describe a ramp that is parallel to the regional tectonic transport direction. Pohn (1998) expanded the term lateral ramp to refer a zone of structural disruption, controlled by faulting, folding, and possible intense fracturing, where *decollement* changes stratigraphic level along strike.

Woodward (1987) suggests that lateral ramps in the northern Absaroka thrust system (Fig. 4.5) are localized by facies changes that occur across the strike of the thrust belt. Lateral and oblique ramps may be also associated with basement buttressing (Apotria *et al*. 1992). Wilkerson *et al*. (2002) have proposed a number of criteria that either individually or combined can be used to support the interpretation of a lateral and/or oblique ramp. These include, steep fold plunges at thrust fault terminations, hanging-wall cut-off lines trending at high angles to the thrust fault strike, stratigraphic contacts trending at high angles to the thrust fault strike, abrupt stratigraphic separation near thrust fault terminations, and actual changes in thrust fault orientation (Wilkerson *et al*. 2002). Pohn (1998) suggested that along-strike abrupt changes in fold wavelength or fold terminations, change in the frequency of mapped faults at the surface, and

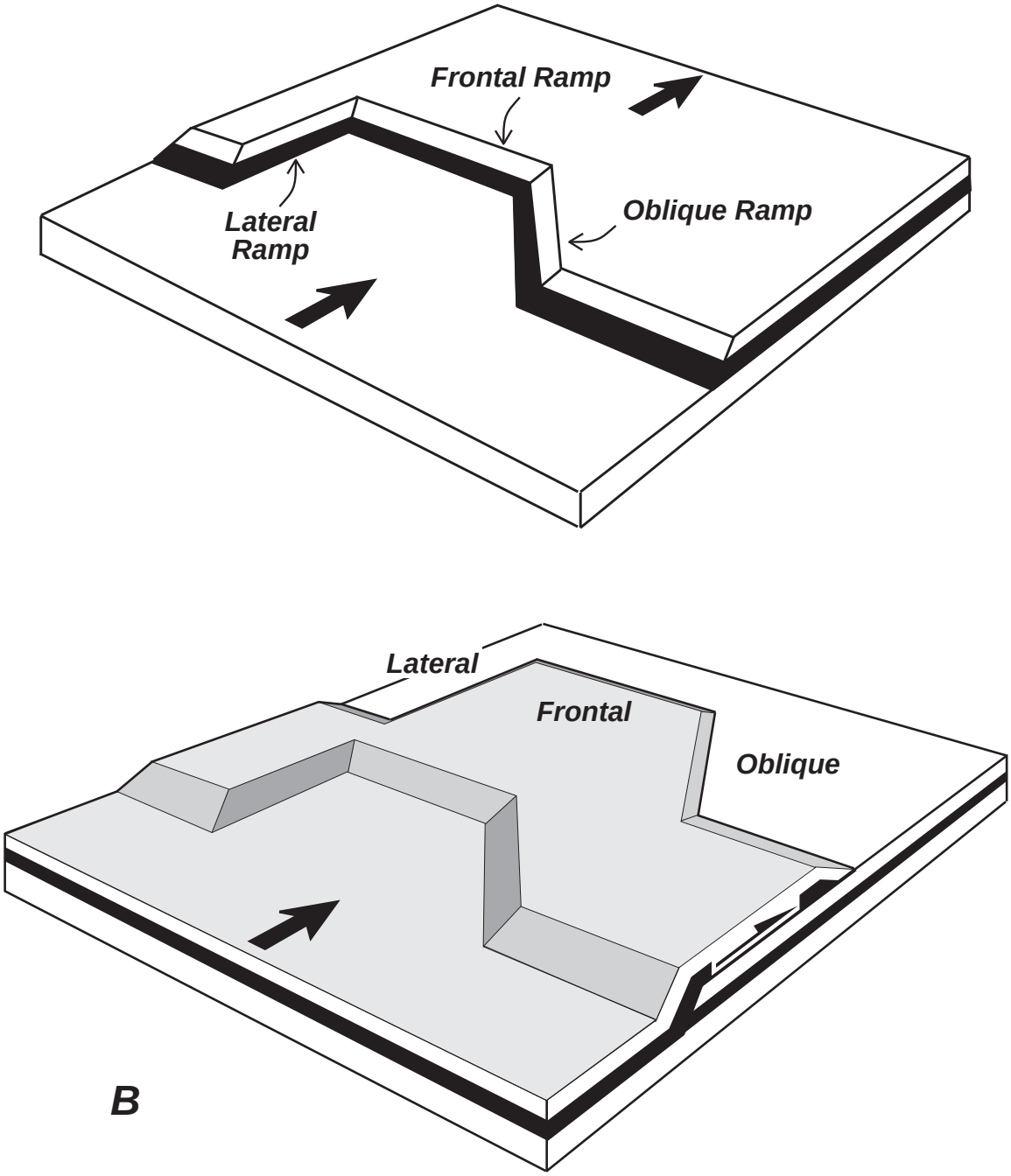


Figure 4.25. 3D thrust geometries (modified from McClay, 1992). **A.** 3D footwall ramp structures. **B.** Ramp-related hangingwall folds above frontal, oblique and lateral ramps. Solid arrows indicate the direction of tectonic transport.

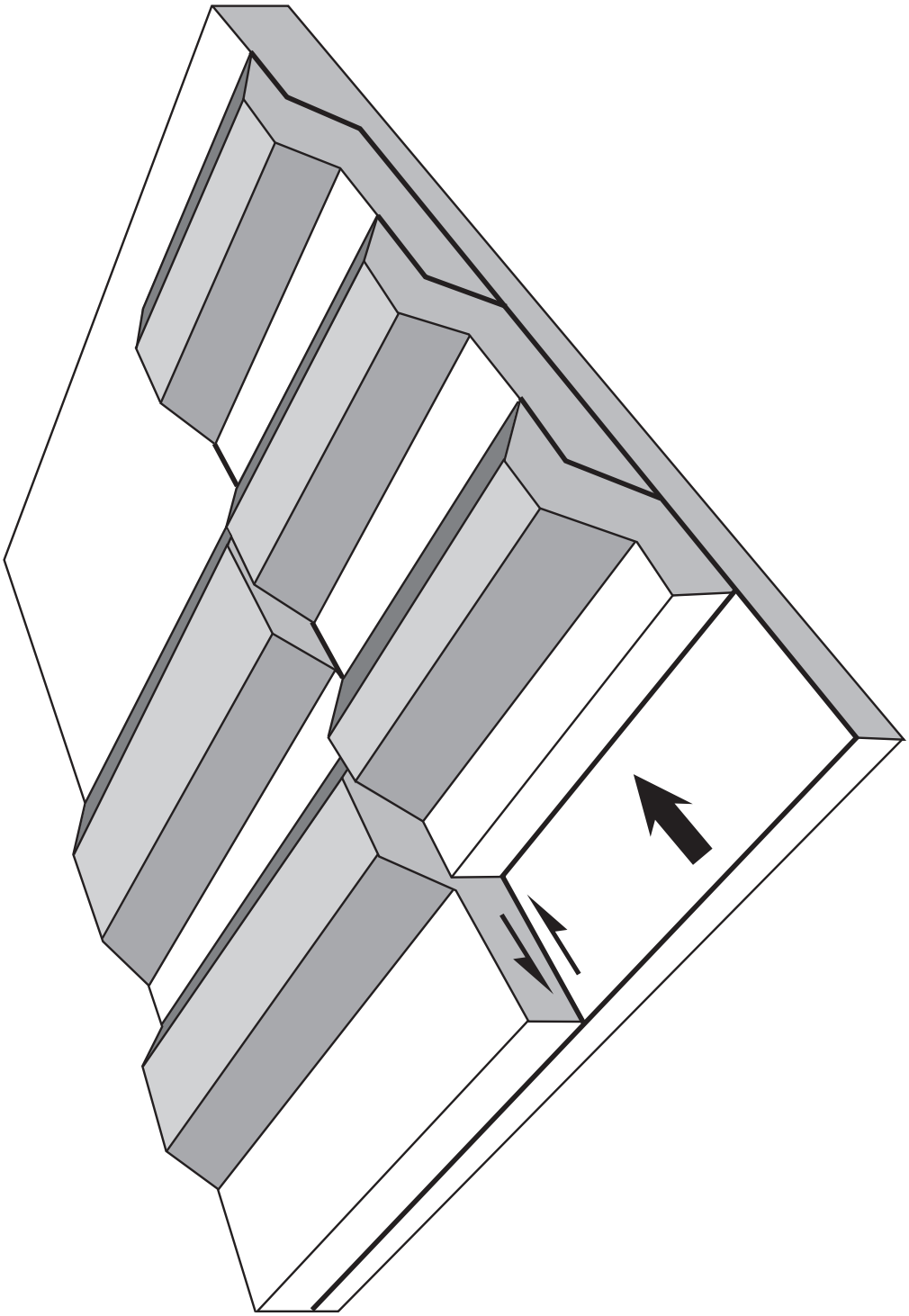


Figure 4.26. Strike-slip or transfer fault between foreland-propagating thrust faults (modified from McClay, 1992). Note transfer fault is parallel to the direction of tectonic transport.

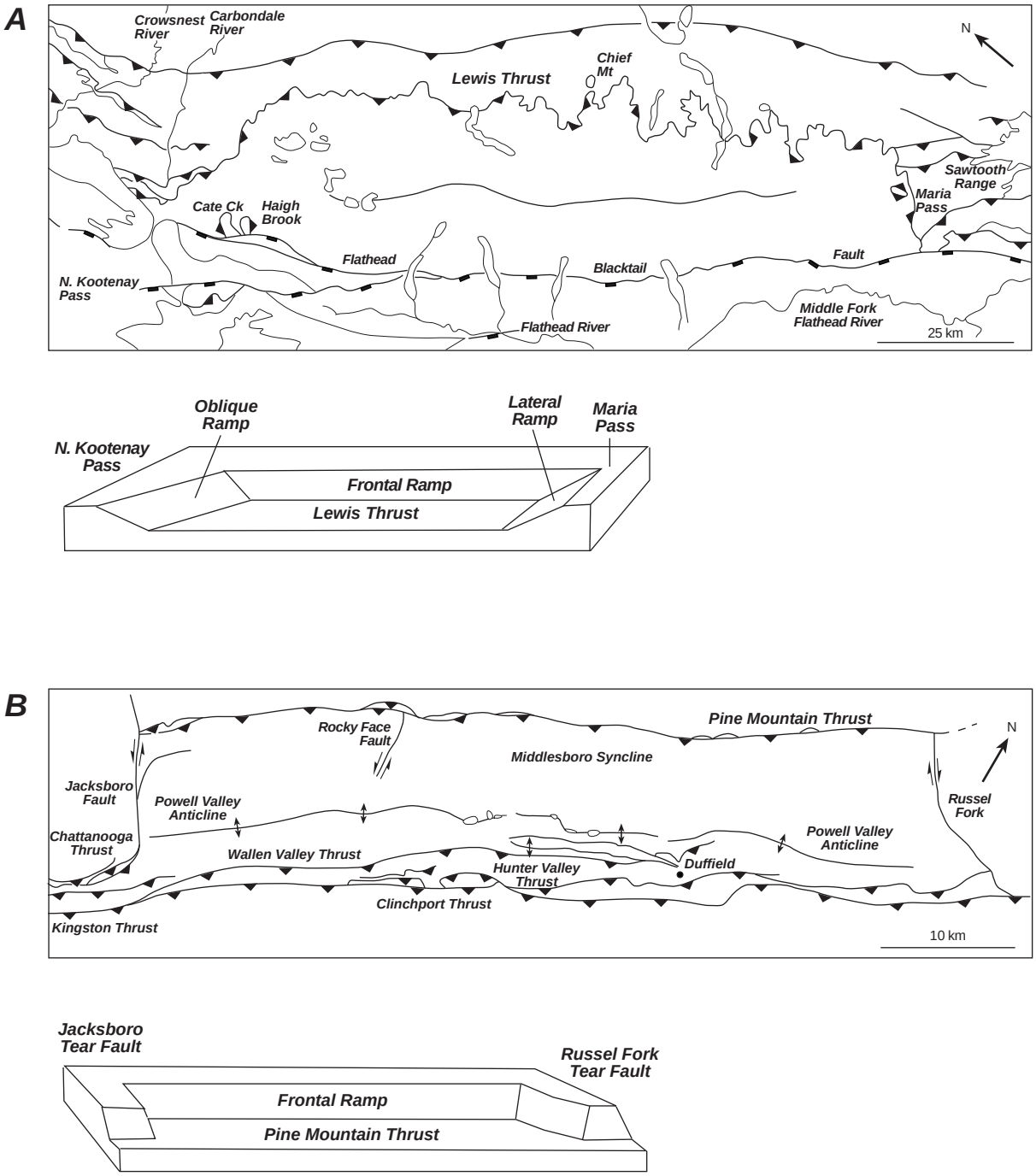


Figure 4.27. 3D geometry of thrust systems. **A.** Map of the Lewis thrust, Canadian Rocky Mountains. Note the frontal ramp that brings the fault up to the surface, the lateral ramp near Maria Pass, and the oblique ramp near North Kootenay Pass. **B.** Map of the Pine Mountain thrust, southern Appalachian Valley and Ridge province of the eastern United States. Tear faults mark the northeast and southwest terminations of the Pine Mountain thrust sheet. Schematic block diagram shows the footwall geometry of the Pine Mountain thrust. Note the frontal ramp of the Pine Mountain thrust is bounded by tear faults (modified from Twiss & Moores, 1992).

geomorphologic criteria as evidence for recognizing the subsurface presence of lateral and/or oblique ramps.

In the absence of footwall deformation the best evidence to support the presence of lateral ramp or oblique ramp is the direct measurement of changes in strike of the footwall surface (Wilkerson *et al*. 2002). Specifically, if fault segments change trend to become sub-parallel or slightly oblique to the transport direction after the removal of topographic effects, a lateral/oblique ramp, by definition exists (Apotria *et al*. 1992; Apotria, 1995; Wilkerson *et al*. 2002). This change in trend likely will also affect the overlying thrust sheet(s). As the hangingwall is folded over such a lateral/oblique footwall ramp, pre-existing structures may be rotated with respect to their regional orientations.

Folds and faults also may develop at a high angle to the overall direction of regional tectonic transport, commonly with fold axes parallel or sub-parallel to the strike of the lateral/oblique footwall ramp (Apotria, 1995). In addition, large hangingwall lateral/oblique ramps exhibit dramatic thickness changes, leading to the development of tear faults near transitions from a thicker hangingwall to a thinner hangingwall (e.g. Mount Head, Canada; Douglas, 1952). Dixon & Spratt (2002) have successfully used scale physical models to demonstrate how a thrust sheet accommodates itself to displacement over ramp systems consisting of two frontal-ramp segments linked by either tear faults or more gently-dipping lateral ramp structures. Lateral ramps have also been modelled successfully with sandbox analogue models (Calassou *et al*. 1993). Frontal ramps tend to intersect bedding at angles varying between 10° and 35°, with a maximum frequency near 20° (Fermor, 1999). Lateral ramps, in turn, may have any cut-off angle up to 90°, but the frequency distribution is not well constrained (Fermor, 1999).

During thrusting, local duplex development may result in lateral variations in thicknesses between the roof and floor thrusts. Elliot & Johnson (1980) show a series of cross faults that strike parallel to the direction of tectonic transport. These faults only offset the roof thrust without affecting the floor of the duplex, and are termed

hangingwall drop faults (Butler, 1982; Bégin & Spratt, 2002). These represent differential uplift caused by variable duplex thicknesses.

Simultaneous thrust sheet movement over frontal and lateral ramps gives rise to flat-topped anticlines and domes. These are referred to as culminations (Dahlstrom, 1970; Butler, 1982) and the limbs of these structures are termed culmination walls (Butler, 1982; McClay, 1992). The terms dorsal culmination wall, frontal culmination wall and lateral culmination wall are used to refer to the part of the culmination located above rear, frontal and lateral ramps, respectively (McClay, 1992). Culminations commonly have more complex geometries and oblique culmination walls are also developed. Interference frontal or dorsal and lateral culmination walls form corner folds (Alvarez Marrón, 1995) (Figs. 4.25, 4.28 & 4.29), which are oblique to the tectonic transport direction. Culminations laterally terminate abruptly with the development of doubly-plunging antiformal structures (Boyer & Elliot, 1982) (Fig. 4.30). Associated folds plunge in opposite directions off the ends of the culminations. Dahlstrom (1970) and Boyer & Elliot (1982) discuss the reasons why a duplex or a culmination occur in one place and not in another, invoking factors such as along-strike changes in lithostratigraphy and changes in ductility and stratigraphic thickness amongst others.

Erosion through culminations commonly forms windows (Boyer & Elliot, 1982**)** (Figs. 4.31, 4.32 & 4.33). Boyer & Elliot (1982) describe different window geometries depending on the geometry of thrust systems. Windows are typically spatially related to structural culminations, antiformal stacks and frontal and/or lateral ramps in depth (Boyer & Elliot, 1982; Pohn, 1998).

Thrust sheets can be segmented by tear faults or transfer faults (Fig. 4.26), that accommodate differential displacement of different parts of the sheet. Tear faults are steeply-dipping and oriented parallel or subparallel to the regional tectonic transport direction (e.g. McClay, 1992) (Fig. 4.26). Tear faults commonly occur in the hangingwall of thrust faults and accommodate different amounts of displacement either on different parts of the fault or between two thrust sheets (Figs. 4.26 & 4.27b). Examples of tear faults include the Jacksboro and Russel Fork tear faults of the Valley and Ridge Province of the southern Appalachians (Mitra, 1988) (Fig. 4.27b).

Figure 4.28. Block diagram showing interference of thrust related folds above frontal and lateral ramps. White arrows indicate direction of tectonic transport. Frontal folds are FF related to frontal footwall ramps and FH related to frontal hangingwall ramps. Lateral folds are LF related to lateral footwall ramps and LH related to lateral hangingwall ramps. Corner folds are CF and CH that are related to intersection of footwall and hangingwall ramps, respectively (modified from Alvarez-Marron, 1995).

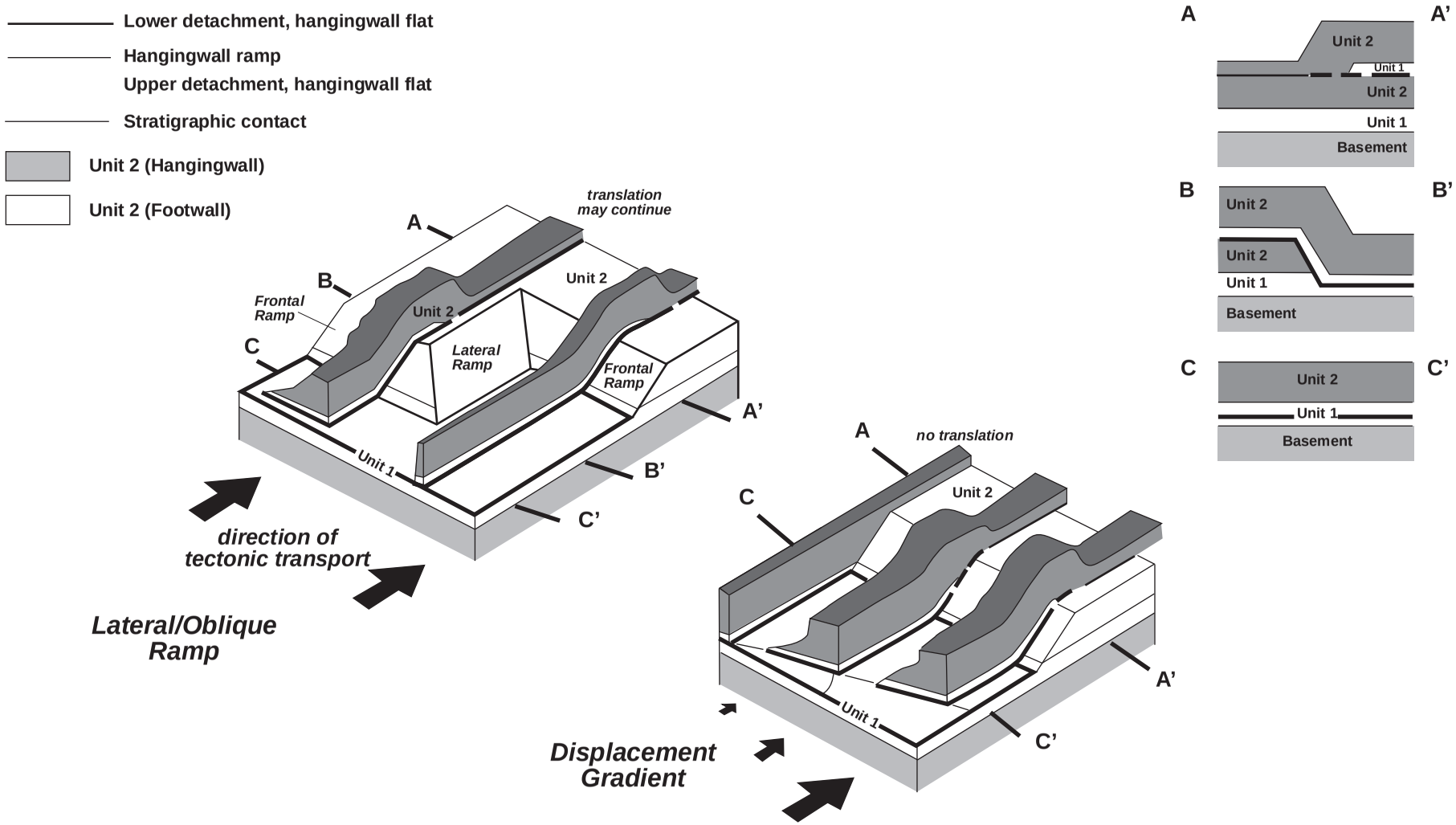


Figure 4.29. Schematic block diagrams illustrating the influence of transverse structures and displacement gradient on thrust displacement (modified from Thomas & Bayona, 2002).

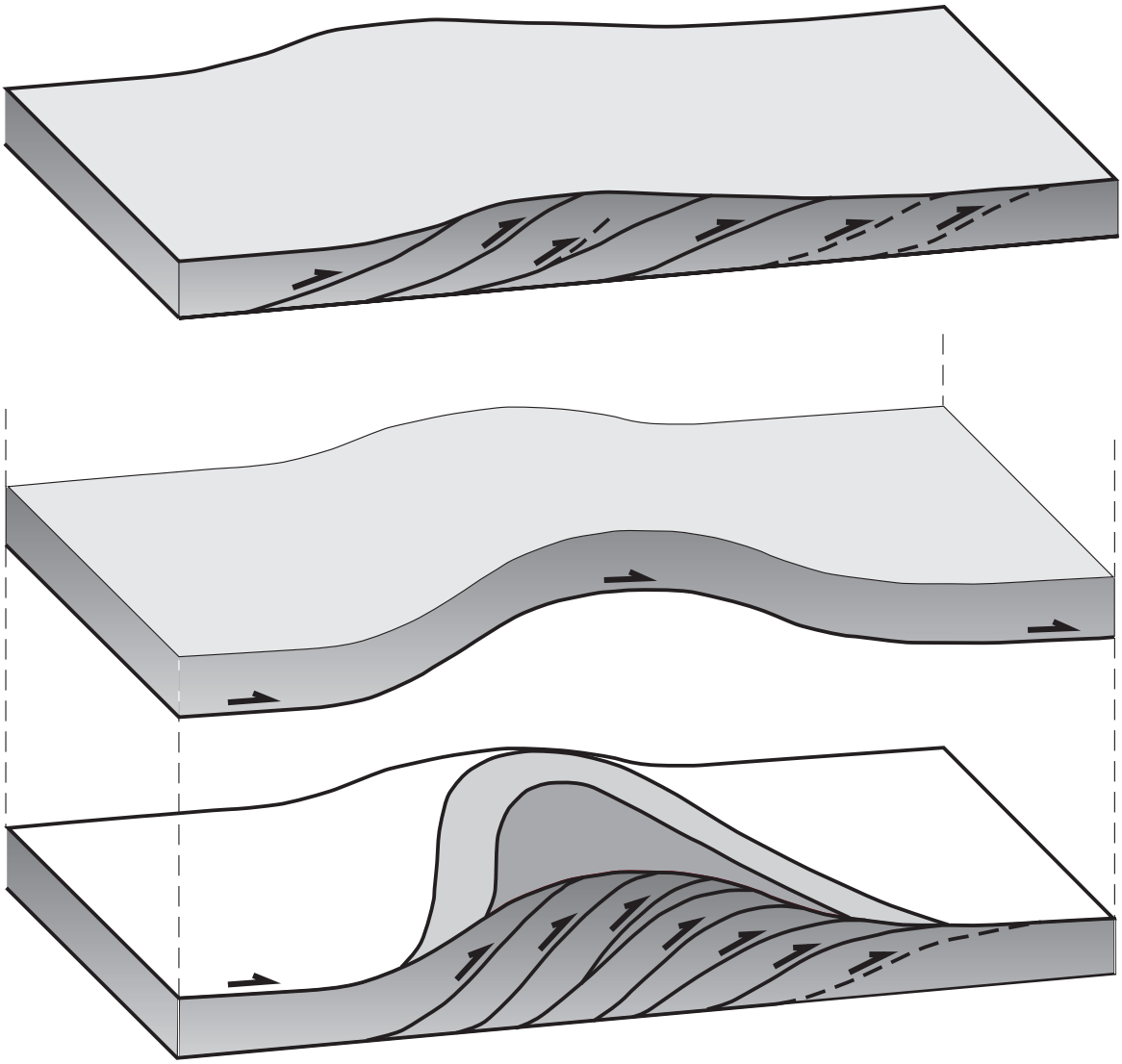


Figure 4.30. 3D duplex model and development of plunging culmination (modified from Fermor, 1999). Note that thickness of the duplex and displacement on link thrusts may change along strike.

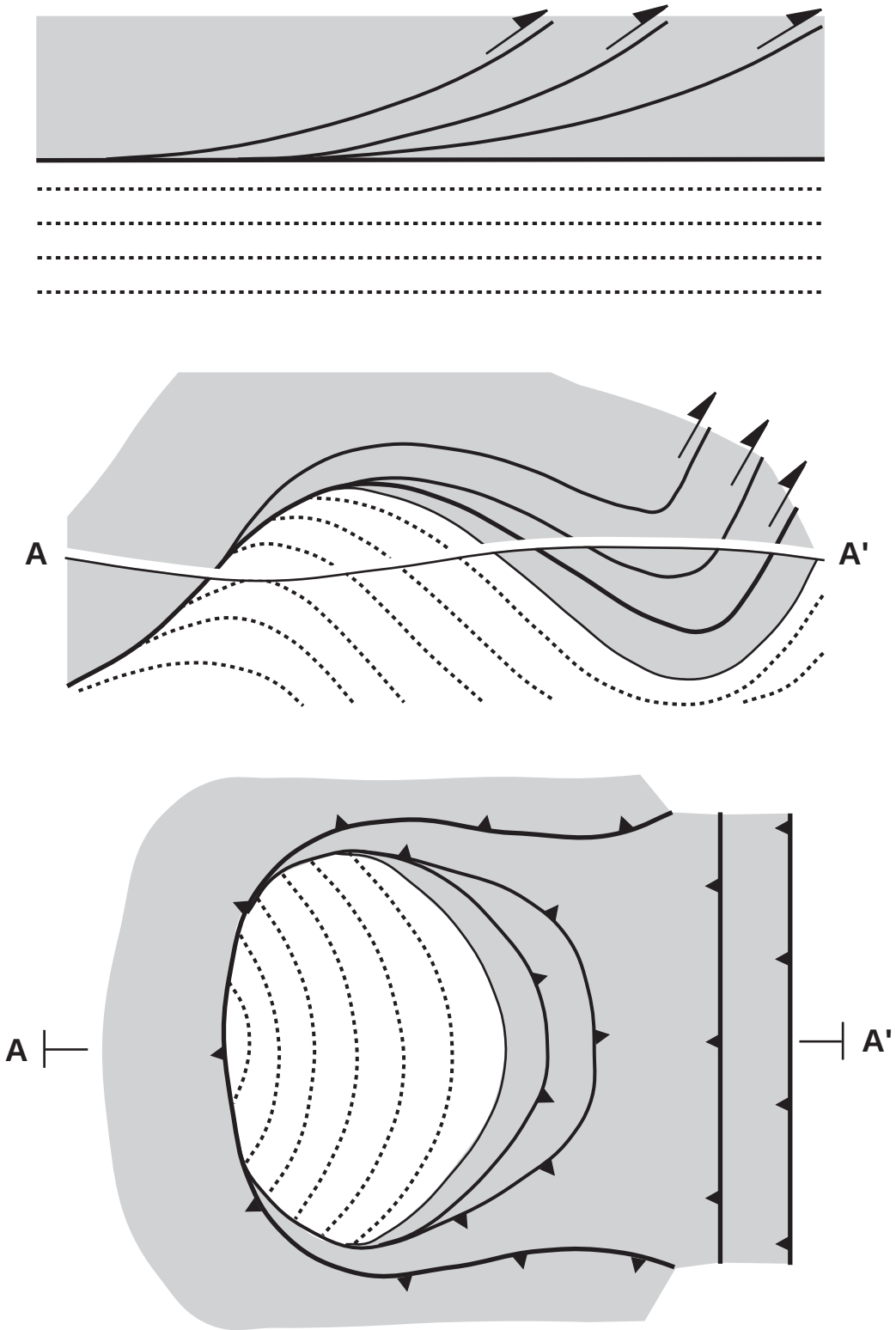


Figure 4.31. Characteristic map pattern of an eyelid window (modified from Boyer, 1978; Boyer & Elliot, 1982).

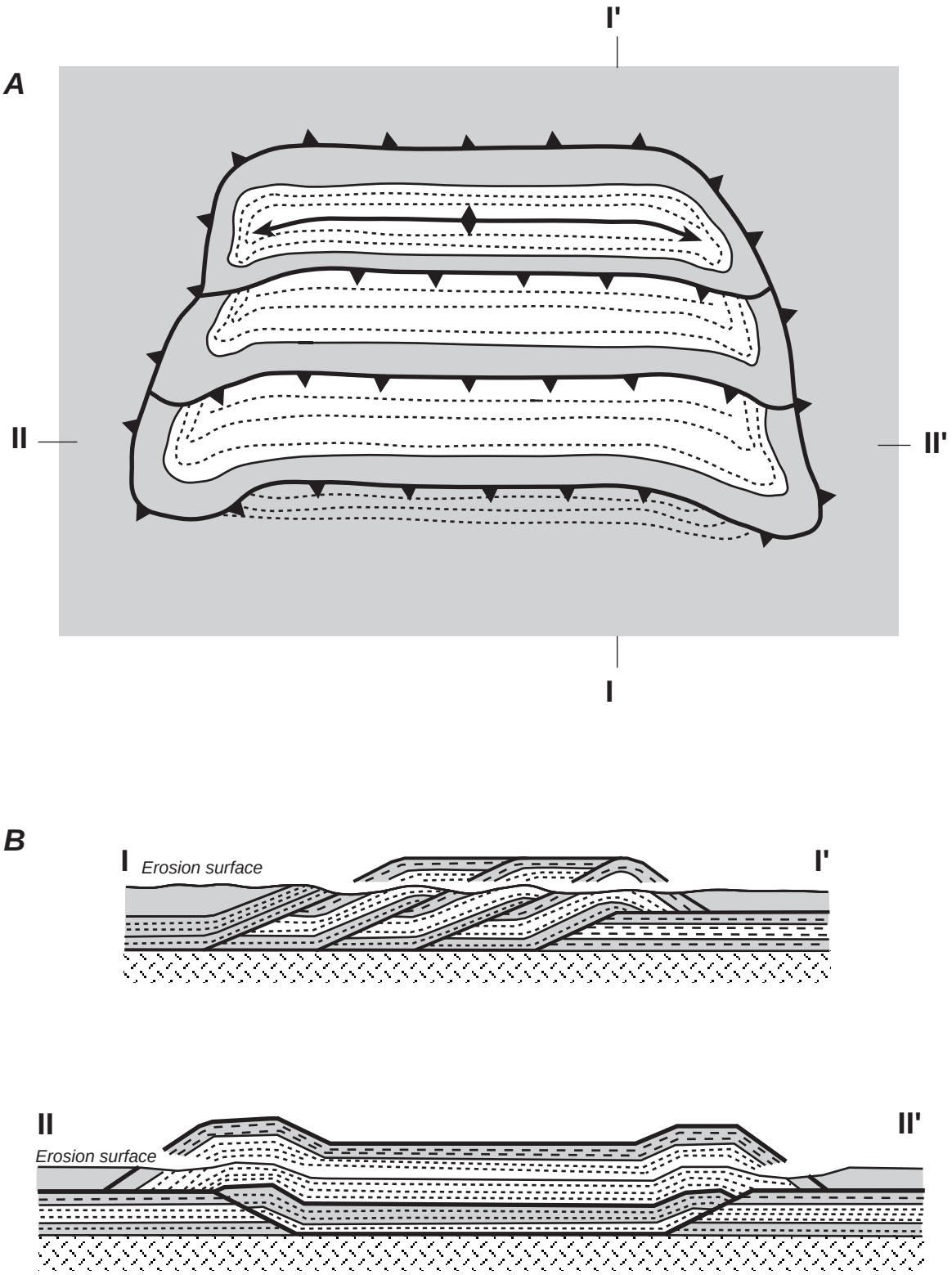


Figure 4.32. Window formed by erosion of a hinterland-dipping duplex (modified from Boyer, 1978; Boyer & Elliot, 1982). **A.** Outcrop pattern in map view. **B.** Cross section view. Anticline occurs at foreland side of window and overlies ramp in floor thrust. Other anticlines occur within each horse. Lateral termination of window may be lateral ramp in the floor thrust, with roof and floor thrusts rejoining along and across strike.

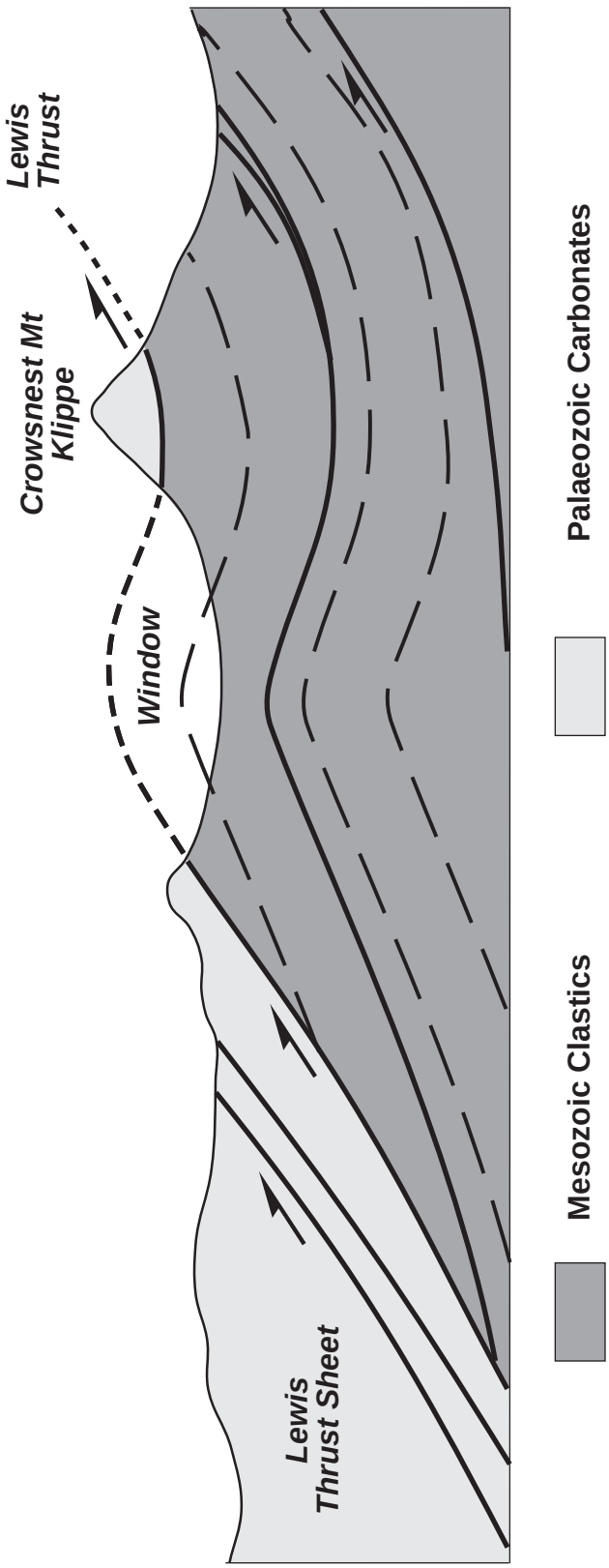


Figure 4.33. Schematic cross section through the Crowsnest Mountain area of the Canadian Rocky Mountains, illustrating klippe and window geometries (modified from McClay & Insley, 1986).

Transverse Zones

Transverse zones are those portions of fold and thrust belts in which the map-view traces of major thrust faults and fault-related folds change along-strike, commonly trending at a high angle to the regional structural grain of the fold and thrust belt (Wheeler, 1980; Pohn *et al*. 1985; Thomas, 1990). Transverse zones have also been referred to as incipient tear faults (Rich, 1934) or cross-strike structural discontinuities (Wheeler, 1978, 1980). Transverse zones are commonly broad diffuse zones of structural disruption that can originate during or subsequent to thrusting (Thomas, 1990). Thomas (1990), Thomas & Bayona (2002) and Bayona *et al*. (2003) propose underlying basement faults, basement-rooted faults in the cover strata, drape folds in the cover strata over basement faults, stratigraphic variations in the *decollement*, and a combination of stratigraphic variations and underlying basement structures as possible fundamental controls in the formation of transverse zones. Examples of transverse zones in fold and thrust belts have been described by Thomas (1990), Paulsen & Marshak (1997, 1998), Pohn (1998), Price (2001), Thomas & Bayona (2002), Bayona *et al*. (2003). Calassou *et al*. (1993), Schreurs *et al*. (2002), Dixon & Spratt (2004), and Spratt *et al*. (2004) have successfully used scaled physical modelling to study the development of transverse zones.

4.5 3D THRUST BELT GEOMETRIES

Orogenic belts and their external foreland fold and thrust belts are not linear features but rather commonly show plan-view arcuate geometries (Macedo & Marshak, 1999; Paulsen & Marshak, 1999; Marshak, 2004) (Figs. 4.1 & 4.34). The origin of thrust belt curvature has been subject of study for over the last two centuries (e.g. Rogers, 1858; Dana, 1866; Wegener, 1915; Argand, 1921, 1924; Carey, 1955; Marshak, 1988; 2004). Carey (1955) firstly introduced the term orocline to refer to a map-view curve in a mountain belt formed by physically bending of once straight structural trends. The origin of orogenic curves, nowadays referred to as a variety of terms such as salients, recesses, arcs, oroclines and syntaxes, has more recently been studied by Marshak (1988), Marshak *et al*. (1992), Macedo & Marshak (1999), Marshak (2004), Weil & Sussman (2004). Thrust belt curves are defined by topographic relief and along-strike variations in the bearing of the structural grain (e.g. fault and fold trends). Examples of fold and thrust belt curvature include the Jura Mountains in the western Alps, the

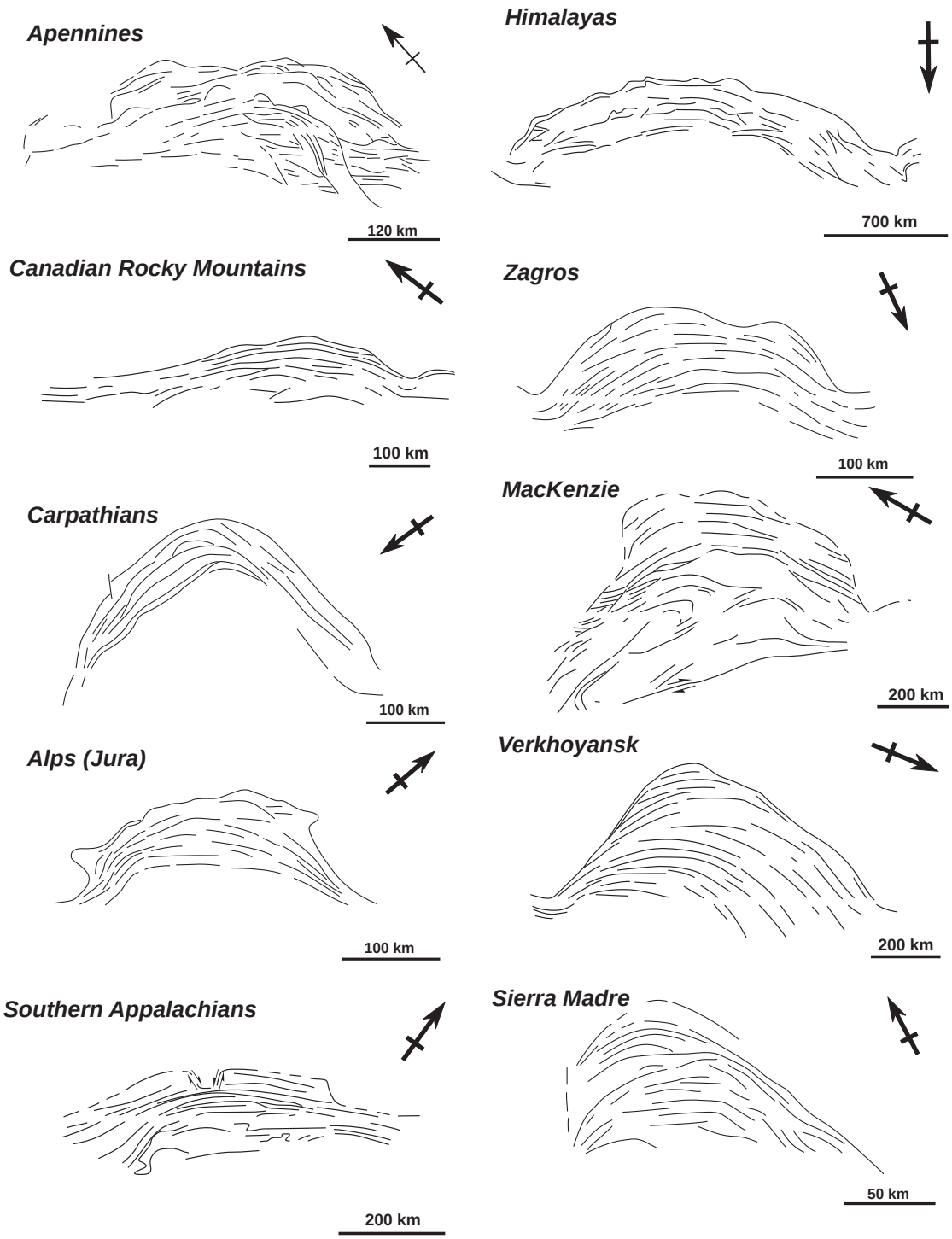


Figure 4.34. Examples of map view thrust belt geometries (modified from Macedo & Marshak, 1999; Marshak, 2004). Refer to Figure 4.1 for location of individual fold and thrust belts.

Zagros fold belt of Iran, and the southern Appalachians (Macedo & Marshak, 1999; Marshak, 2004) (Figs. 4.1, 4.8 & 4.34). The geometry of map-view curves in fold and thrust belts are very diverse, varying from symmetric, asymmetric, parabolic, to irregular geometries (e.g. Macedo & Marshak, 1999; Marshak, 2004; Weil & Sussman, 2004). Many of these curves are fundamentally 'thin-skinned' and their presence does not require bending of the entire crust or lithosphere below (Marshak, 2004).

The regional progressive change in the structural trends of an orogenic belt is referred to map-view curve, regardless the origin of the change (Marshak, 1988; Macedo & Marshak, 1999; Marshak, 2004). A salient or antitaxial curve is a curve that is convex in the direction of tectonic transport, whereas a recess (syntaxial curve or syntaxis) is a curve that is concave in the direction of transport. A rotational curve or orocline (Carey, 1955) forms by progressive bending of once-straight structural trends as segments of the orogenic belt rotate about a vertical axis (e.g. Weil & Sussman, 2004). An example is the Alaskan orocline formed by Tertiary contraction of North America against Eurasia (Plafker & Berg, 1994; Glen, 2004) (Figs. 1.2, 2.1 & 2.2). Non-rotational curves initiate with a curved trajectory and therefore their formation does not involve rotation about a vertical axis (Marshak, 1988).

Macedo & Marshak (1999) and Marshak (2004) propose several factors that control and may contribute to the development of thrust belt curvature but conclude that in most cases orogenic curvature is controlled by inherited basin geometries. Several authors have noted the positions of map-view curves in fold and thrust belts correlate with pre-deformational characteristics of the pre-existing geometry of the sedimentary basin from which the curve formed (e.g. Aitken & Long, 1978; Macedo & Marshak, 1999; Marshak, 2004). Macedo & Marshak (1999) examined the geometry and geologic setting of many salients worldwide and noted that, in most cases, the apex of a given salient coincides with the predeformational depocentre in the sedimentary basin from which the fold and thrust belt formed. Fold and thrust belt curves whose position and geometry reflect characteristics of the pre-existing basin are called basin-controlled curves (Macedo & Marshak, 1999) (Fig. 4.35). Marshak (2004) argues that the majority of map-view curves in fold and thrust belts are basin-controlled. This relationship occurs because predeformational characteristics of the basin determine

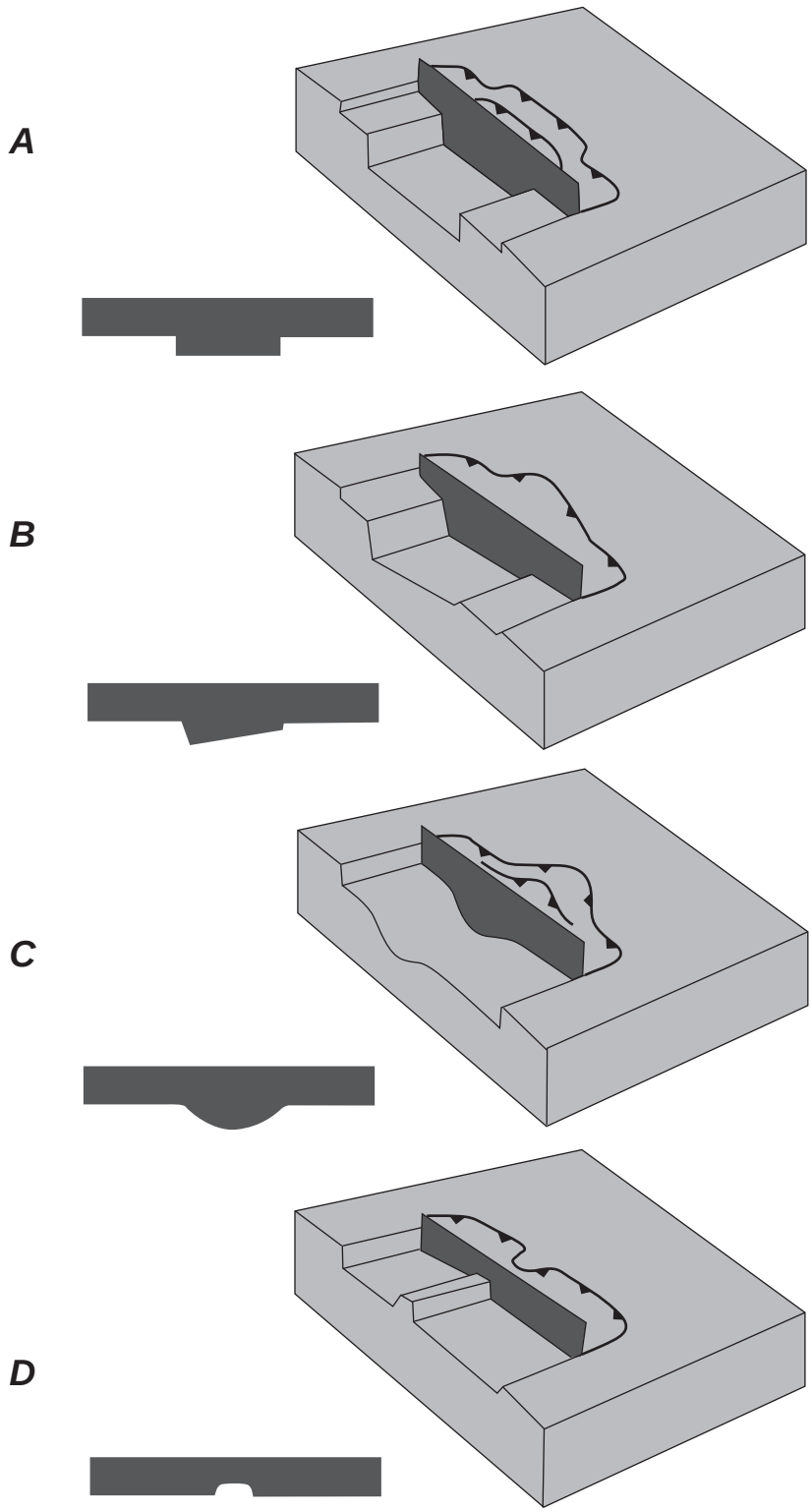


Figure 4.35. Schematic diagrams showing the control that pre-existing basin geometries exert in the geometry of thrust systems (modified from Macedo & Marshak, 1999; Marshak, 2004). **A.** Symmetric rift. **B.** Asymmetric rift. **C.** Spoon-shaped basin. **D.** Structural high.

the width of a fold and thrust belt for a given amount of shortening (Marshak, 2004). This relationship can be readily understood in the context of the critical taper theory of Davis *et al*. (1983), Dahlen, (1984), and Dahlen *et al.* (1984). Along-strike changes in the value of the critical taper angle, the slope of the basal detachment, or the thickness of the sedimentary wedge being deformed determine whether a given fold and thrust belt is narrow or wide (Marshak *et al*. 1992; Marshak & Wilkerson, 1992; Calassou *et al*. 1993; Boyer, 1995; Mitra, 1997; Macedo & Marshak, 1999; Marshak, 2004; McClay *et al.* 2004). Wider portions become salients and narrower areas recesses (Marshak, 2004). However not all curves are basin-controlled. Other curves are the result from irregularities on colliding margins. These include curves that resulted from indentation of rigid blocks (Tapponier & Molnar, 1976), those that reflect the presence of promontories and recesses to the foreland of the advancing thrust belt, or those resulting from the interaction of the fold and thrust belt with a buttress or basement high in the foreland (Marshak, 2004).

Other causes for thrust belt curvature formation are the interaction of a thrust belt with foreland obstacles or promontories, hinterland collision of an indenter, interaction with subsequent strike-slip faults, and warping of the downgoing (underthrust plate) (e.g. Macedo & Marshak, 1999; Marshak, 2004; Weil & Sussman, 2004). Not all curve-forming processes lead to oroclinal bending of a fold and thrust belt in that not all curves involve rotation of segments of the thrust belt around a vertical axis. Factor such as depth to detachment, rock strength, detachment strength, and detachment slope all affect the width of a fold and thrust belt for a given amount of displacement as predicted by the critical taper theory.

Along-strike changes in the depth, strength and slope of detachment, or along-strike changes in the strength of the thrust wedge, erosion and plutonism are another factors. (Macedo & Marshak, 1999; Marshak, 2004; Weil & Sussman, 2004). Other possible causes of curve formation are the intersection of nonparallel belts, curves formed in response to strike-slip faulting, curves reflecting the shape of a down-going slab, or simply curves that may be an artefact of the erosion of a regional-scale plunging folds oblique to the thrust front. Many volcanic arcs form map-view curves in response to the geometry of the subducting slab.

4.6 THRUST SEQUENCES

An issue debated amongst structural geologists for decades was whether thrust faults developed in a regular time sequence (Bally *et al*. 1966; Dahlstrom, 1970; Boyer & Elliot, 1982; Butler, 1987). It is nowadays admitted that thrust systems evolve through time differently depending on a large number of factors, including mechanical stratigraphy, thickness of thrust sheets, rate of uplift, erosion and sedimentary loading, and crustal inheritance amongst others (e.g. Beaumont, 1992, 2000; Storti *et al*. 2000; Burbank & Anderson, 2001). Understanding the way in that a foreland fold and thrust belt evolves through time is key to any structural study and is essential for cross section construction and basin reconstruction (Boyer & Elliot, 1982; Butler, 1987; Morley, 1988). The term thrust sequence refers to the order in which new thrust faults develop in a thrust belt. A first separation or classification of thrust sequences can be made based upon whether thrusts follow a particular order of emplacement (i.e. in-sequence thrusting) or they develop randomly (i.e. out-of-sequence thrusting) (Fig. 4.36).

4.6.1 In-Sequence Thrusting

Two end members of models of 'in-sequence' thrusting have been proposed. These are the 'forward-breaking' sequence or 'piggy-back' sequence (Bally *et al*. 1966; Dahlstrom, 1970; Boyer & Elliot, 1982; Butler, 1987), and the 'break-back' sequence (Butler, 1987).

'Forward-Breaking' or 'Piggy-Back' Sequence

The 'forward-breaking' or 'piggy-back' sequence (Fig. 4.36a) refers to the thrust sequence in which thrust faults develop sequentially from the hinterland to the foreland, and from the top to the bottom of the thrust belt or accretionary wedge (Bally *et al*. 1966; Dahlstrom, 1970; Boyer & Elliot, 1982; Butler, 1987) (Fig. 4.36a). In the 'forward-breaking' sequence, when younger thrust faults originate, overlying older thrust faults become inactive and are carried passively by underlying younger faults (Boyer & Elliot, 1982). The older and higher thrust sheets then become folded as a result of the fault bend folding and fault propagation folding (Suppe & Medwedeff, 1990) related to the displacement on underlying thrust systems (Figs. 4.11, 4.12, 4.13 & 4.14). The 'forward-breaking' or 'piggy-back' sequence appears to be dominant in most foreland fold and thrust belts and has become the most widely accepted nowadays.

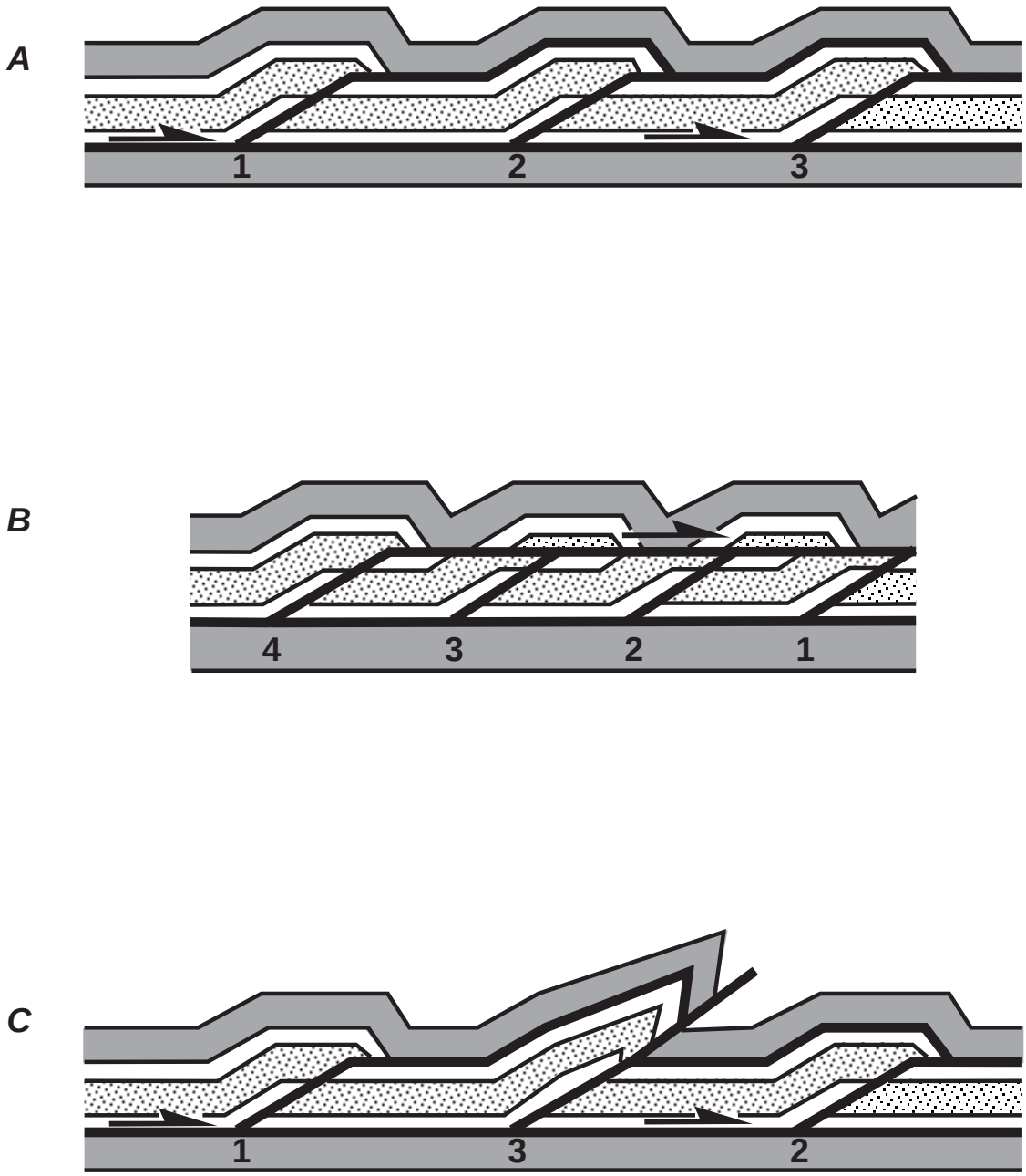


Figure 4.36. Thrust sequences (modified from McClay, 1992). **A.** Forward-breaking or piggy-back sequence. **B.** Break-back sequence. **C.** Out-of-sequence thrusting. Numbers indicate the sequential development of thrusts.

'Break-Back' Sequence

The 'break-back' sequence refers to the thrust sequence in which new and younger thrust faults nucleate in the hangingwalls of older thrusts and progressively propagate towards the hinterland (Butler, 1987; McClay, 1992). Examples of 'break-back thrusting' include the Pedraforca thrust systems of the Spanish Pyrenees (e.g. Martinez *et al*. 1986) (Figs. 4.36b & 4.37). Break-back sequences have been also referred to as out-of-sequence thrusts in the literature. However, the term 'out-of-sequence' thrusting should be more appropriately used to describe thrust sequences which do not conform to either a progressive forward-breaking or break-back sequence (McClay, 1992).

4.6.2 'Out-of-Sequence' Thrusting

Out-of-sequence thrusts, those which do not obey the 'in-sequence' propagation style, (e.g. Boyer, 1992; Morley, 1998; McClay, 1992) (Fig. 4.36c) are common features developed during the evolution of any fold and thrust belt and are nowadays believed to form part of the normal deformation sequence (Boyer, 1992). When out-of-sequence thrusting occurs in previously folded and/or faulted strata, younger-over-older structural relationships can be expected. In particular cases out-of-sequence thrusting may be very difficult to distinguish from gravity sliding (Morley, 1988). Examples of out-of-sequence thrusting can be found in the Moine thrust of northwest Scotland (Coward & McClay, 1981), and the Appalachians in the eastern United States (Boyer, 1992).

Morley (1988) recognizes two end members or types of out-of-sequence thrusting: one in which older in-sequence thrusts are reactivated along their entire length and another type in which completely new thrusts propagate through already deformed thrust sheets. Although considered to be developed randomly and following no order, out-of-sequence thrusting occurs a response to critical taper readjustment in an orogenic wedge and are part of a normal deformation sequence (Boyer, 1992). Out-of-sequence thrusting can be triggered by loss of taper either due to erosion or by elongation of the wedge by foreland propagation of the thrust front (Morley, 1988). If the model of Davis *et al*. (1983), Dahlen, (1984), and Dahlen *et al*. (1984) for the evolution of orogenic wedges is considered correct, then out-of-sequence is expected to occur with considerable frequency in all fold and thrust belts.

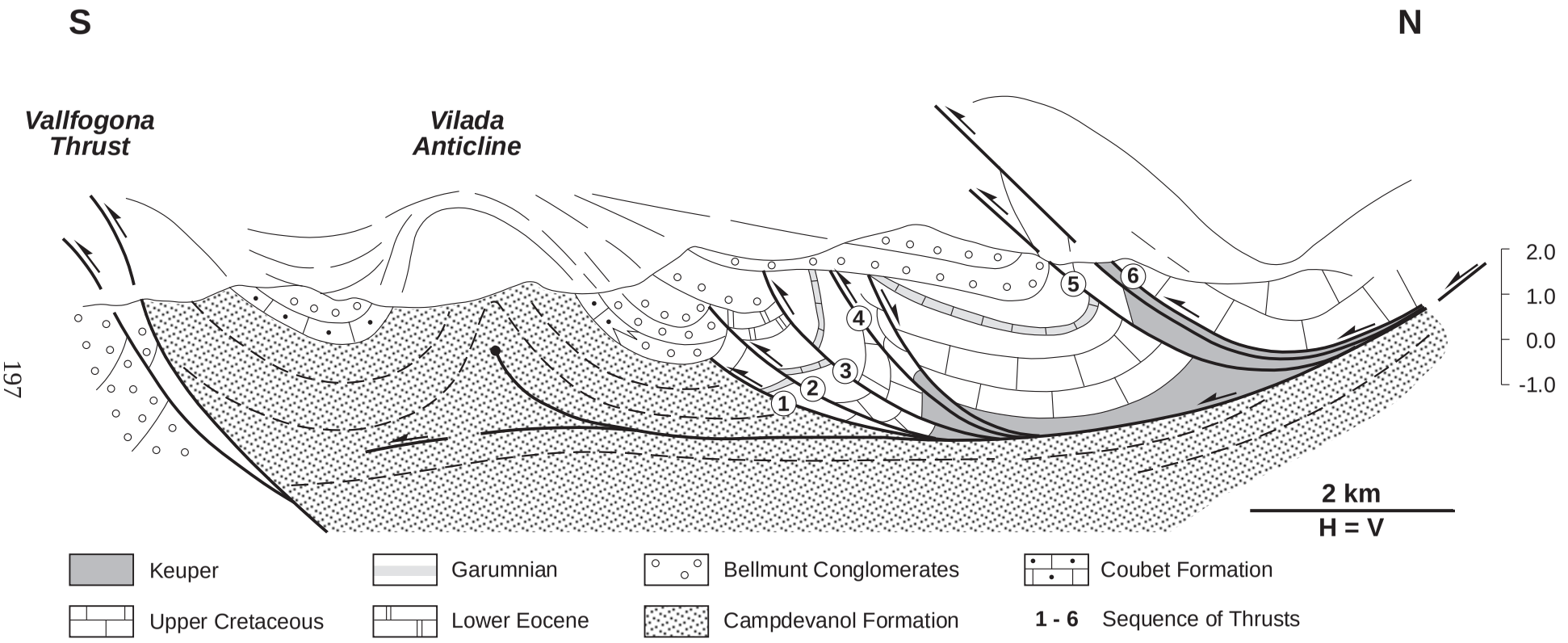


Figure 4.37. Break-back thrust sequence (modified from Martinez et *al.* 1986). Lower Pedraforca thrust sheet, southern Pyrenees, Spain. Numbers indicate relative ages of thrusting, with 1 being the oldest and 6 the youngest thrust fault.

Mitra & Sussman (1997) suggested that internal thrust sheets continue to shorten and thicken and are progressively uplifted in the internal parts of the fold and thrust belt concurrent with the advance of the external fold and thrust belt on to the foreland. Mitra & Sussman (1997) proposed that a new mechanism of late-stage thrusting, referred to as connecting splay duplexing, may be important in thickening the rear wedge and maintaining taper in the foreland fold and thrust belt as a whole.

4.6.3 Synchronous Thrusting

The widely accepted 'forward-breaking' or 'piggy-back' sequence (Fig. 4.38) and the paradigm that older thrust become inactive and are passively carried over lower and younger thrust systems have been challenged. Work by Boyer (1986*b*), Morley (1988), Boyer (1991, 1992), Tanner (1992), Price (2001) and, more recently, by Butler (2004) has revealed the significance of synchronous motion on several thrust faults in the development of thrust systems and the evolution of orogenic wedges. Synchronous thrusting (Fig. 4.38) implies that two or more thrusts may be active at one time and possibly involving 'in-sequence' and 'out-of-sequence' thrusting in order to maintain the critical taper according to the critical taper theory (e.g. Davis *et al*. 1983; Dahlen, 1984; Dahlen *et al*. 1984). Boyer (1992) argues that 'forward-breaking' or 'piggy-back' thrusting is incompatible with compelling new mechanical models for the development of thrust belts, which require synchronous thrusting, out-of-sequence thrusting, thrust reactivation and/or duplex underplating to maintain a critical taper. Synchronous thrusting accounts for the presence of stacks of imbricate thrust faults that typically occur on the crests or limbs of structural culminations (Fig. 4.18) and that are difficult to explain by simple conceptual 'piggy-back' thrusting (Boyer, 1992). The implication that 'out-of-sequence' thrusting should continue to occur in the interior of the wedge as it grows in width contradicts a basic presumption of the 'piggy-back' kinematic model (Price, 2001).

Synchronous thrusting has been successfully recreated in scaled physical models (e.g. Dixon & Liu, 1992; Storti *et al*. 2000; McClay & Whitehouse, 2004). Existing conceptual models for duplex development (e.g. Boyer & Elliot, 1982; Mitra, 1986) (Figs. 4.9a & 4.11) cannot adequately explain the wide range of duplex geometries observed in nature (Figs. 4.12, 4.13, 4.14, 4.15 & 4.16.). The markedly diverse

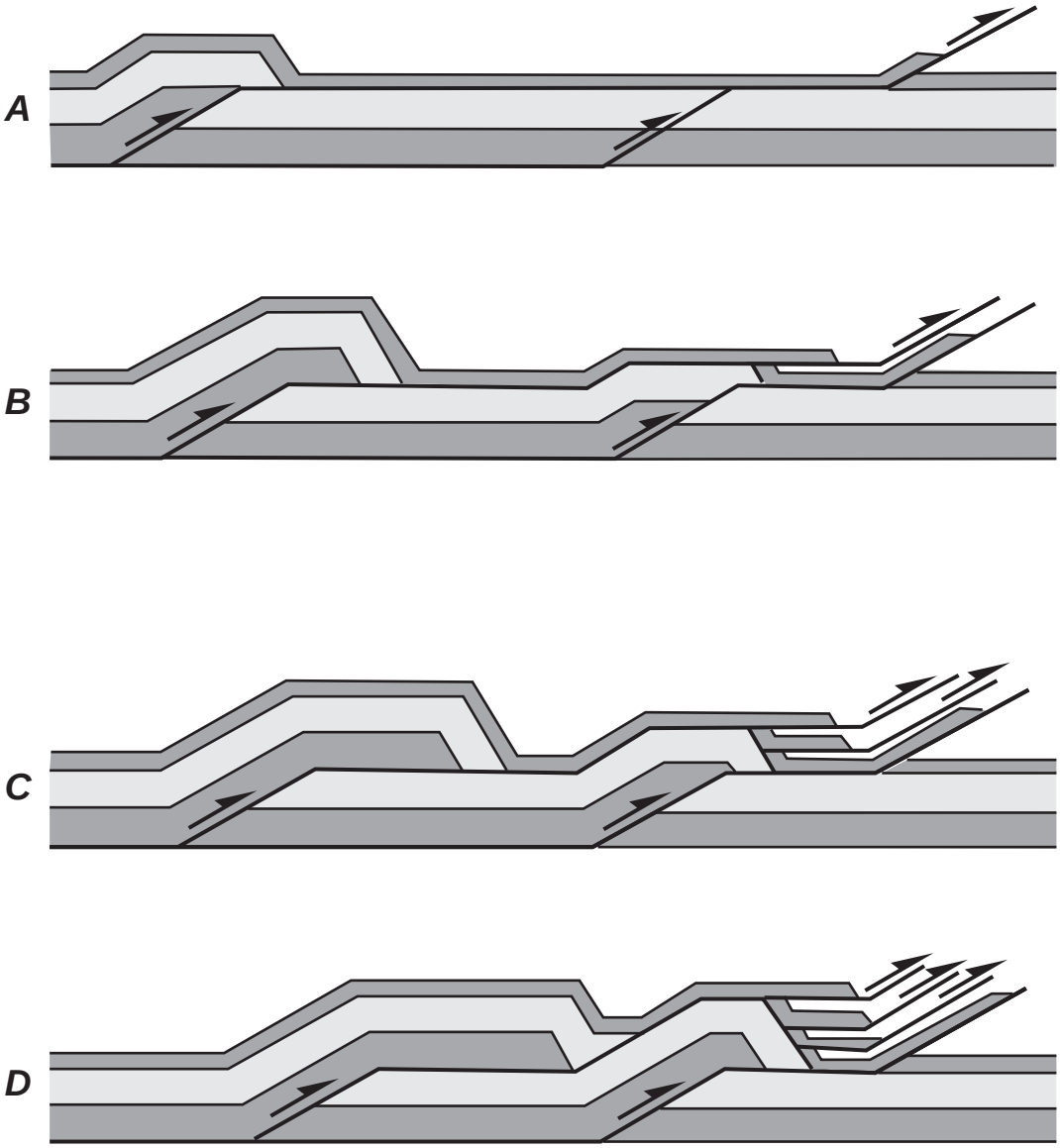


Figure 4.38. Synchronous thrust model (modified from Boyer, 1992).

geometry observed in duplex systems may account for a synchronous thrusting mechanism (McClay & Insley, 1986*a*; Boyer, 1992; Tanner, 1992). Butler (2004) examines some aspects on synchronous thrusting and argues that although thrusts may be active synchronously, they need not be active at the same rate.

A common criticism of the existing duplex model is that in order to produce a 'flat-topped' duplex (Fig. 4.11) the spacing and displacement of the horse-bounding thrust faults must have a precise and fixed relationship. Observed duplexes usually fail to match the conceptual models and in turn the size and spacing of thrust horses is often extremely irregular, and duplex geometry may vary from spaced ramp anticlines of the bumpy roof duplex to the overlapping imbricates of an antiformal stack (Mitra, 1986; McClay, 1992). These various geometries can be produced as a continuous process during synchronous thrusting. (Fig. 4.38). Duplexes generated by synchronous thrusting can be easily distinguished from the classic duplexes produced by footwall collapse towards the foreland. The former will have imbricate faults in the hangingwall of the roof thrust (Fig. 4.38) whereas the latter do not (Boyer, 1992) (Fig. 4.11).

Synchronous thrusting appears to be common in thrust belts that formed when oceanic crust was obducted onto a continental passive margin (Morley, 1988). Physical scaled modelling (Dixon, 2002; Dixon & Spratt, 2002) also evidences that passive margin architecture assisted by facies changes boundaries may give rise to a sequence of thrusting that does not necessarily obey the forward-breaking or piggy-back style.

4.7 SUMMARY

This chapter has reviewed some basic concepts on thrust tectonics and the geometry, dynamics, and kinematics of foreland fold and thrust belts. Some key points arising from this chapter are:

- Foreland fold and thrust belts are fundamental parts of the frontal and most external parts of orogenic belts.

- A thrust fault can be defined as a map-scale contractional fault that shortens a datum surface, usually bedding in upper crustal rocks or a regional foliation surface in more highly metamorphosed and strained rocks.

- Thrusts climb up stratigraphic section in the direction of thrust transport and propagate in the direction of movement and bring older rocks on top of younger rocks.

- Thrust faulting is kinematically linked to folding. Thrust fault-related folds include fault-propagation folds, fault-bend folds and fault detachment folds.

- Thrust faults commonly occur in families that form linked systems, referred as thrust systems, including duplexes, imbricate systems, and triangle zones.

- Thrust systems do not extend indefinitely but commonly terminate in lateral ramps, tear faults, or fault-related folds along fault tips.

- Fold and thrust belts commonly show an arcuate geometry in map view. Most curves are considered to be basin-controlled in that the fold and thrust belt inherits features of the pre-existing extensional basin.

- Thrust faulting develops in a sequential fashion, via in-sequence, out-of-sequence and/or synchronous thrusting.

CHAPTER 5

STRATIGRAPHY OF THE RED DOG DISTRICT

5.1 INTRODUCTION

5.2 NOMENCLATURE & RATIONALE OF DESCRIPTION

5.3 DEPOSITIONAL MEGASEQUENCES

5.4 STRATIGRAPHY OF THE ARCTIC ALASKA TERRANE

5.5 STRATIGRAPHY OF THE ANGAYUCHAM TERRANE

5.6 FORELAND BASIN STRATIGRAPHY

5.7 SUMMARY

CHAPTER 5 STRATIGRAPHY OF THE RED DOG DISTRICT

5.1 INTRODUCTION

This chapter describes the stratigraphy of the Red Dog district and sets a new tectonostratigraphic framework for the structural descriptions and analyses presented in Chapters 6 and 7. Previous studies in the Red Dog district and adjacent areas in the Brooks Range (e.g. Martin, 1970; Moore *et al*. 1986; Mayfield *et al*. 1988; Curtis *et al*. 1990; Ellersieck *et al*. 1990*a*; Mayfield *et al*. 1990; Young, 1992, 2000; Dumoulin *et al*. 2004; Young, 2004) have provided accurate lithostratigraphic descriptions and precise age constraints (cf. Chapter 3 and references therein), but have not set these stratigraphic relationships into a comprehensive tectonic context. Understanding the tectonostratigraphy of the Red Dog district is critical for the understanding of the geometry of the Palaeozoic basin in which the sediment-hosted Zn-Pb-Ag and barite deposits of the Red Dog district formed and the Mesozoic tectonic evolution of the area.

5.2 NOMENCLATURE AND RATIONALE OF DESCRIPTION

This section introduces the stratigraphic nomenclature used in this study. Stratigraphic nomenclature of the Red Dog district is complex (e.g. Dumoulin *et al*. 2004; Young, 2004; Figs. 5.1 & 5.2; cf. Chapter 3, Fig. 3.3a). The stratigraphy of the Red Dog district consists of Late Devonian to Early Cretaceous siliciclastic and carbonate strata together with felsic, intermediate, mafic and ultramafic intrusive and extrusive igneous rocks (Figs. 5.1 – 5.3) that were complexly thrust faulted and folded during the Mesozoic Brookian orogeny (cf. Chapter 2, Fig. 2.6).

The stratigraphy of the Red Dog district has been analysed using a sequence stratigraphic approach (e.g. Hubbard *et al*. 1985; Hubbard, 1988; Galloway, 1989; Williams, 1993; Emery & Myers, 1996; Miall, 1997). Sequence stratigraphy has long been used to analyse strata of the North Slope foreland basin and the underlying parautochthon (e.g. Hubbard *et al*. 1987; Moore *et al*. 1994; D. G. Roberts, 2005, *pers. comm.*) but has not been previously applied to their correlative strata in the fold and thrust belt of the Brooks Range due to the intense thrusting and folding.

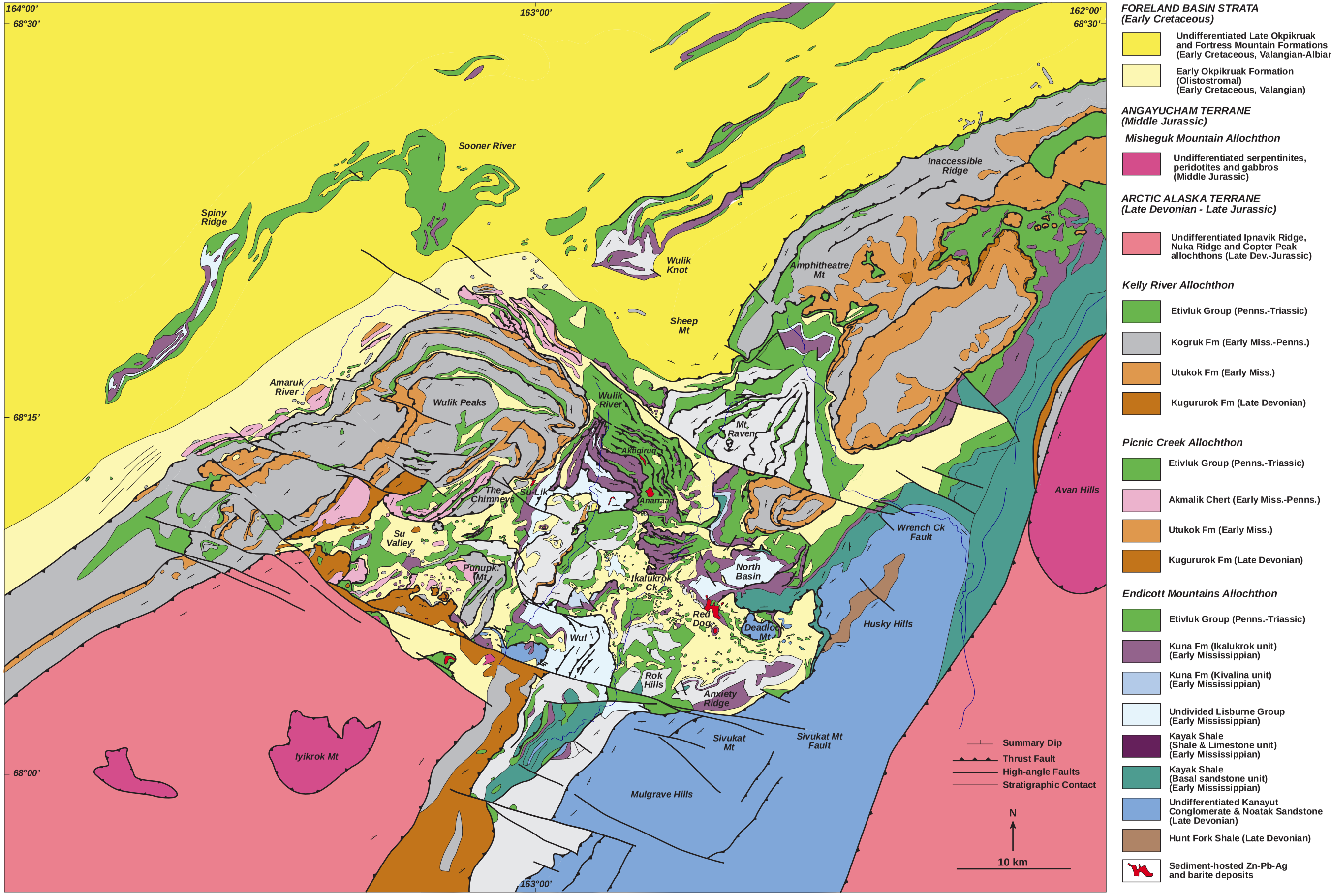


Figure 5.1. Geological map of the Red Dog district compiled from mapping by the author and Teck Cominco geological maps, published maps (Ellersieck *et al*. 1983, 1984, 1990*a*; Mayfield *et al*. 1984; Mayfield *et al.* 1990; Mull *et al.* 2000).

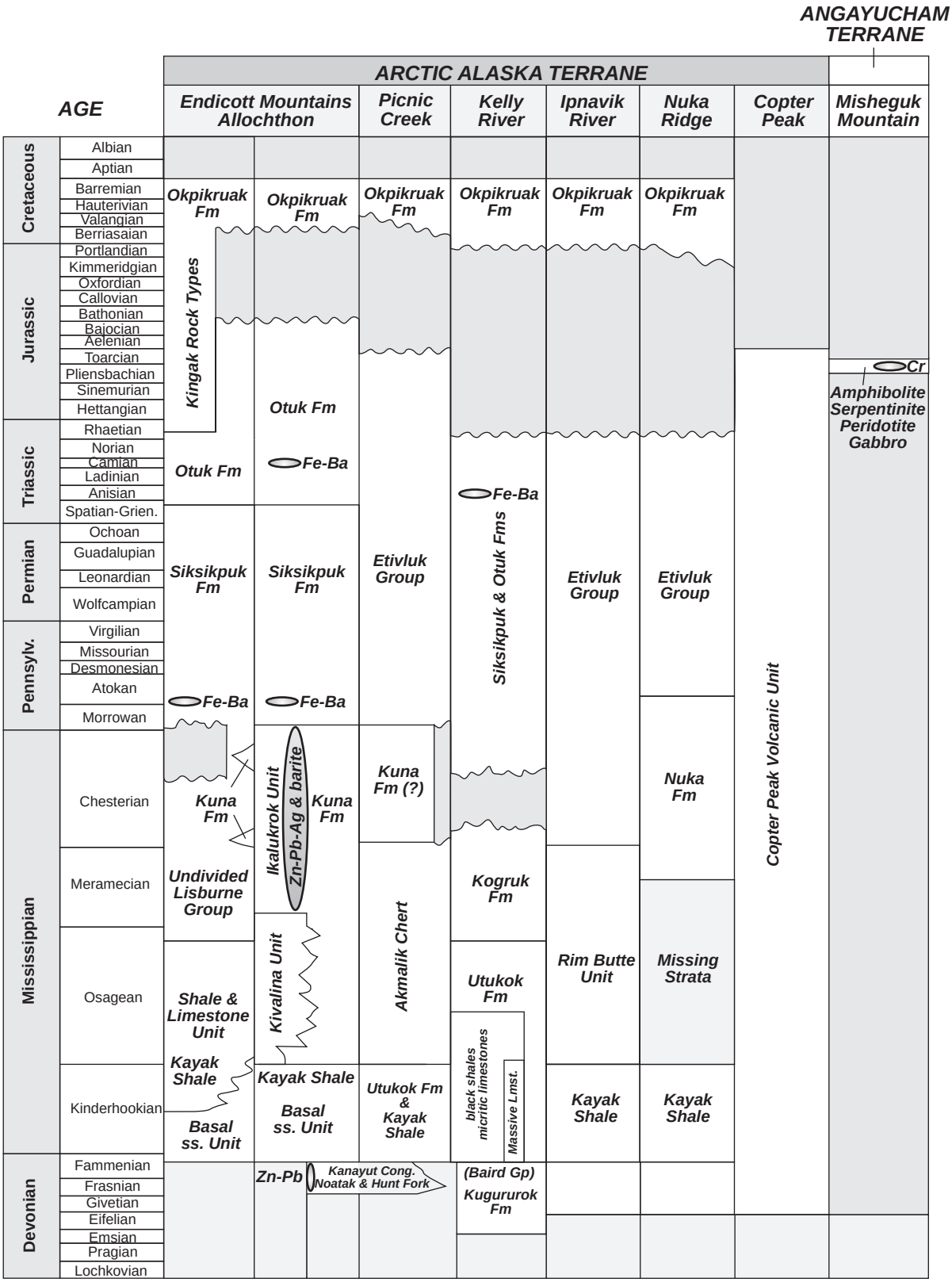


Figure 5.2. Summary chronostratigraphy of the Red Dog district (modified from Young, 2004). The stratigraphic position of the sediment-hosted Zn-Pb-Ag and barite deposits is shown.

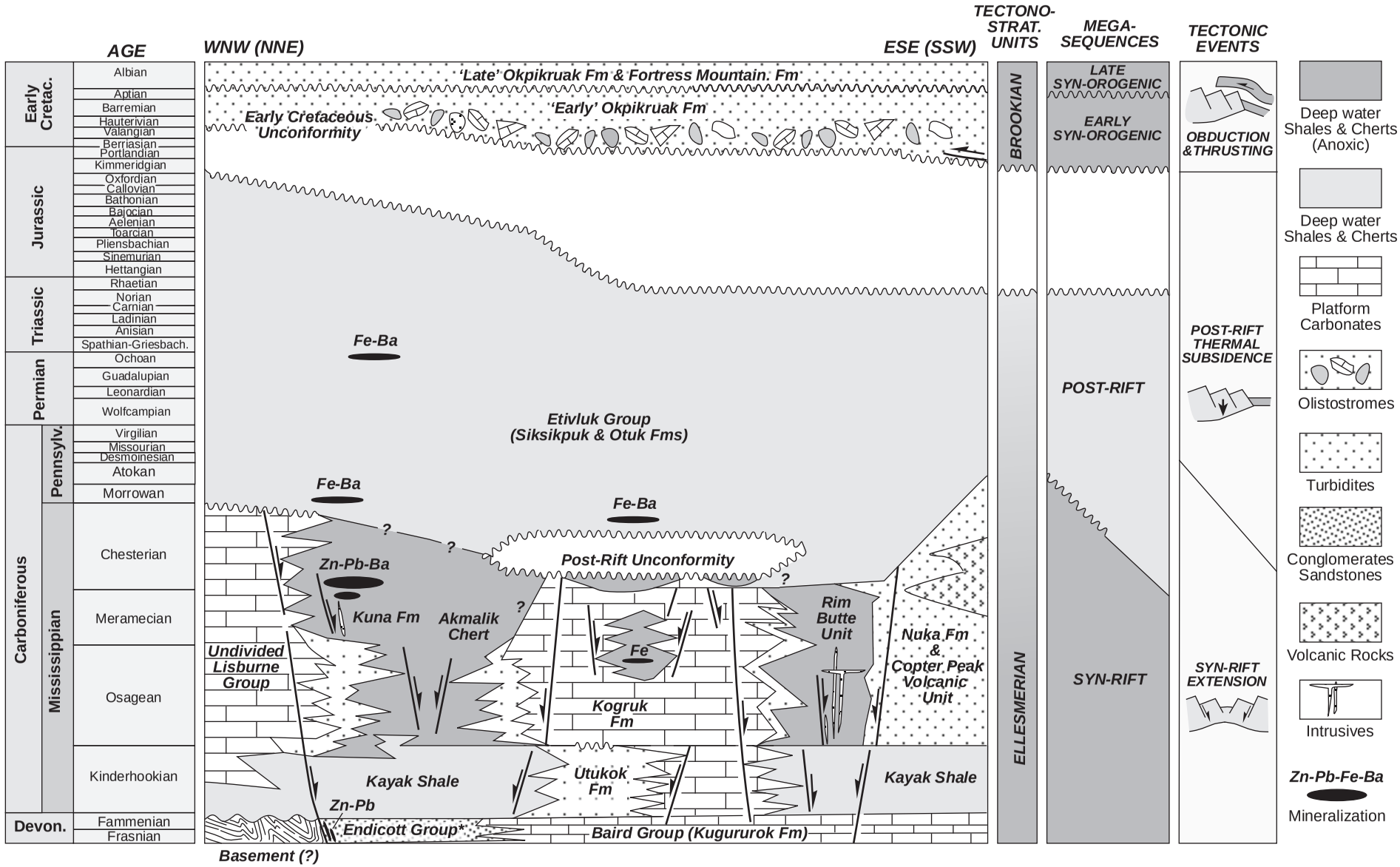


Figure 5.3. Chronostratigraphy of the Arctic Alaska terrane in the Red Dog district compiled from the results of this study. Age constraints based on Dumoulin *et al.* (2004), C. G. Mull (2004, *pers. comm.)*, and Young (2004). Note the Endicott Group* includes the Hunt Fork Shale, Noatak Sandstone, and Kanayut Conglomerate.

The stratigraphy of the Red Dog district has been subdivided into two main tectonostratigraphic units. From the oldest to the youngest these are the Ellesmerian and Brookian units (Fig. 5.3). This nomenclature is modified from that proposed by Lerand (1973), Hubbard *et al*. (1987) and Moore *et al*. (1994) for the undeformed portion of the Arctic Alaska terrane (i.e. Arctic Slope parautochthon or North Slope subterrane) (Fig. 2.3). In this study, the Ellesmerian and Brookian units have been further subdivided into depositional megasequences (Fig. 5.3) (cf. Hubbard *et al*. 1985) each reflecting a distinct tectonic event (e.g. syn-rift, post-rift, syn-orogenic), given the limitations that thrust faulting, folding on multiple detachment levels and syn-orogenic mass wasting processes have disrupted many of the original stratigraphic relationships.

Depositional megasequences can be subdivided into smaller units referred to as sequences. In the fold and thrust belt of the western Brooks Range including the Red Dog district, the term 'sequence' has been historically used to refer to the allochthonous thrust sheets and/or their internal imbrications (e.g. Martin, 1970; Moore *et al*. 1986; Mayfield *et al*. 1988; Ellersieck *et al*. 1990*a*). In this work the term 'sequence' is used in its original stratigraphic sense (e.g. Mitchum, 1977) and refers to a genetically related succession of strata bounded by unconformities or their laterally correlative conformities.

The stratigraphic descriptions presented in this chapter are based on field logging of selected stratigraphic successions together with the study of diamond drill cores from over 25 NQ-size exploration drill holes, 62 thin sections (30 μm), 25 polished sections, and 635 hand specimens. Stratigraphic thicknesses presented here are approximate, as units may significantly vary in thickness from one locality to another due to facies changes and structural thickening or thinning. Stratigraphic successions and contacts are commonly incomplete due to poor exposure (e.g. concealed by tundra cover or frost shattered) and complex thrust faulting, folding, extensional faulting, and gravity sliding. In addition, sedimentary features are locally overprinted by widespread diagenetic silicification and dolomitization, as well as by penetrative cleavage fabrics.

In the stratigraphic descriptions presented in this chapter, emphasis has been placed on interpretations of facies associations, sedimentary environments and depositional trends,

which have implications for the structural analyses presented in Chapters 6 and 7. Particular focus is placed on the stratigraphy of the Endicott Mountains allochthon, which hosts the sediment-hosted Zn-Pb-Ag and barite deposits of the Red Dog district. Focus is also placed in the syn-orogenic strata, key to the understanding of the tectonostratigraphic evolution of the area. Interpretations of depositional environments are based on models outlined by Bouma (1962), Wilson (1975), Bouma *et al*. (1985), Reineck & Singh (1980), Ahr (1989), Pickering *et al*. (1989), Miall (1992), Reading (1996), Bosence (1998), Leeder (1999), Nichols (1999), Tucker (2001), Bosence (2005). Carbonate rocks are classified after Dunham (1962) and age constraints are primarily based on palaeontological constraints from Dumoulin *et al*. (2004) and Young (2004).

5.3 DEPOSITIONAL MEGASEQUENCES

This section defines and describes the tectonostratigraphic and depositional megasequences of the Red Dog district of the Red Dog district (Fig. 5.3).

5.3.1 Ellesmerian Stratigraphy (Late Devonian – Late Jurassic)

The Ellesmerian stratigraphy consists of Late Devonian to Late Jurassic siliciclastic and carbonate strata that record sedimentation during continental rifting and development of the ancient continental passive margin of Arctic Alaska (Arctic Alaska terrane) (Fig. 5.3). In addition to sedimentary rocks, the Ellesmerian unit also contains felsic, intermediate, and mafic intrusive and extrusive igneous rocks that locally intrude and/or are interbedded with sedimentary rocks (Fig. 5.3). Total thickness of the Ellesmerian unit typically ranges from 700 m to 1500 m.

The Ellesmerian unit is here subdivided into two depositional megasequences. These are the Syn-rift and Post-rift megasequences (Fig. 5.3). The syn-rift—post-rift megasequence boundary has been established based on regional lithostratigraphic and chronostratigraphic correlations with other areas of the Brooks Range (cf. Chapter 2, Fig. 2.11) and identification of a 'break-up unconformity' (cf. Falvey, 1974) and its inferred correlative conformities.

Syn-Rift Megasequence (Late Devonian – Pennsylvanian-Permian)

The Syn-rift Megasequence consists of Late Devonian to Pennsylvanian strata of the Baird, Endicott and Lisburne groups as well as the Nuka Formation (Fig. 5.3). These stratigraphic units consist of siliciclastic, carbonate, and basinal pelagic strata (Fig. 5.3) that were deposited in fluvial, deltaic, estuarine, platform, and slope to basin sedimentary environments. The Syn-rift Megasequence records evidence for mechanical fault-related subsidence, lithospheric thinning, as well as locally elevated heat flow and magmatism.

In the Red Dog district, the base of the Syn-rift Megasequence is regionally faulted and pre-rift basement rocks are not exposed. Pre-rift rocks, however, occur approximately 75 km west of the study area, in the Lisburne Hills (cf. Chapter 2, Fig. 2.15), where Early Mississippian Ellesmerian strata unconformably overlie Ordovician and Silurian

basement metamorphic rocks (e.g. Moore *et al*. 2002; Young, 2002, *pers. comm.*; T. E. Moore, 2004, *pers. comm.*).

Post-Rift Megasequence (Pennsylvanian—Late Jurassic)

The Post-rift Megasequence consists of a condensed succession of Pennsylvanian to Jurassic (?) pelagic strata (Fig. 5.3). The Post-rift Megasequence is regionally continuous (Fig. 5.3) and relatively uniform in thickness and lithostratigraphy. This contrasts markedly with the abrupt facies changes that characterize the Syn-rift Megasequence (e.g. Lisburne Group) (Figs. 5.1, 5.3 – 5.14). The Syn-rift—Post-rift Megasequence boundary (Fig. 5.3) has been established on the basis of stratigraphic observations in the Red Dog district together with regional lithostratigraphic and chronostratigraphic correlations with other areas of the Brooks Range (e.g. Mull *et al*. 1982, 1987*b*; Mayfield *et al*. 1988; Crowder, 1990; Moore *et al*. 1994; Dumoulin *et al*. 2004; Young, 2004).

The Post-rift Megasequence in the Red Dog district consists of the Pennsylvanian to Jurassic Etivluk Group (Fig. 5.3). The Etivluk Group of the Red Dog district is here interpreted as a distal equivalent of transgressive fluvial deltaic siliciclastics of the Sadlerochit Group (e.g. Moore *et al*. 1994; Young, 2004) that unconformably overlies the Lisburne Group in the Arctic Slope parautochthon north of the Red Dog district (e.g. Crowder *et al*. 1990; Moore *et al*. 1994; Young, 2004) (cf. Chapter 2, Fig. 2.11). This unconformity, traditionally referred to as the 'Permian unconformity' (e.g. Moore *et al*. 1994; Young, 2004), is here interpreted as the 'break-up' or post-rift unconformity (e.g. Falvey, 1974) (Fig. 5.3). In the Red Dog district, the Etivluk lies unconformably to conformably on strata of the Lisburne Group (Fig. 5.3). The conformable contact between the Lisburne and Etivluk groups possibly is interpreted as the correlative conformity to the 'break-up' unconformity (Fig. 5.3). Conformable contacts between syn-rift and post-rift megasequences are common of distal, deeper parts, of passive margins, where sedimentation is typically continuous (e.g. Wilson *et al*. 2001; D. G. Roberts, 2002, *pers. comm.)*

5.3.2 Brookian Stratigraphy (Early Cretaceous)

The Brookian tectonostratigraphic unit has been subdivided into two depositional megasequences, here referred to as the early and late syn-orogenic megasequences (Fig. 5.3). These megasequences are described in detail in Section 5.6.

In many areas, the distinction between thrust sheets *sensu stricto* and thrust sheets that have been incorporated into syn-orogenic strata via gravity sliding and/or complex thrust tectonics is problematic. Major thrust sheets overlie, underlie or apparently grade to olistoliths and olistostrome deposits. Many of the allochthonous rocks, including thrust sheets that contain the sediment-hosted Zn-Pb-Ag and barite deposits of the Red Dog district, show equivocal relationships and are involved in olistostromes. Each allochthonous thrust sheet, gravity slide sheet, or block contains an incomplete to complete distinct lithostratigraphic succession.

5.4 STRATIGRAPHY OF THE ARCTIC ALASKA TERRANE

The Arctic Alaska terrane is here subdivided into six allochthonous thrust sheets that show distinct stratigraphic successions (Fig. 5.2). Stratigraphic correlations from allochthon to allochthon indicate that stratigraphic units were deposited contiguously and coevally in a continental margin prior to the Brookian orogeny (Figs. 5.2 & 5.3).

5.4.1 Stratigraphy of the Endicott Mountains Allochthon

The Endicott Mountains allochthon consists of three lithostratigraphically distinct thrust plates, which are the Wolverine Creek, Red Dog and Key Creek plates, in ascending structural order (Figs. 5.4 – 5.7). These plates regionally show equivocal relationships with syn-orogenic strata of the Brookian unit (Fig. 5.1). The Brookian unit is described separately in section 5.6. The stratigraphy of the Endicott Mountains allochthon consists of the Endicott and Lisburne Groups (Syn-rift Megasequence) as well as the Etivluk Group (Post-Rift Megasequence) (Figs. 5.2 & 5.3).

Endicott Group (early Late Devonian – Early Mississippian)

The Endicott Group of the Endicott Mountains allochthon in the Red Dog district consists of Late Devonian to Early Mississippian non-marine to deep-marine siliciclastic and carbonate strata (Figs. 5.3-5.7). The Endicott Group is subdivided into four distinct formations. These are, from the oldest to the youngest, the Hunt Fork Shale, the Noatak Sandstone, the Kanayut Conglomerate, and the Kayak Shale (Figs. 5.2, 5.3, 5.7, 5.8, 5.9 & 5.10). The Hunt Fork Shale, Noatak Sandstone, and Kanayut Conglomerate units define an upward-shallowing marine to fluvial-deltaic succession deposited during a marine regression, whereas the Kayak Shale marks the onset of a regional transgressive event (Figs. 5.4 & 5.7).

Hunt Fork Shale (early Late Devonian, Frasnian – Fammenian)

The Hunt Fork Shale is the oldest stratigraphic unit of the Red Dog district (Figs. 5.1 – 5.3). It consists of approximately 100 to 200 m of brown-, grey- and greenish-weathering very fine-grained sandstones that are rhythmically interbedded with grey- to greenish grey-weathering siltstones and shales (Figs. 5.7 & 5.8a). Sandstones and siltstones are cm-bedded (Fig. 5.8a) and typically show parallel laminations. Fossils include rare rhynchonellid brachiopods. In the Red Dog district, the Hunt Fork Shale is

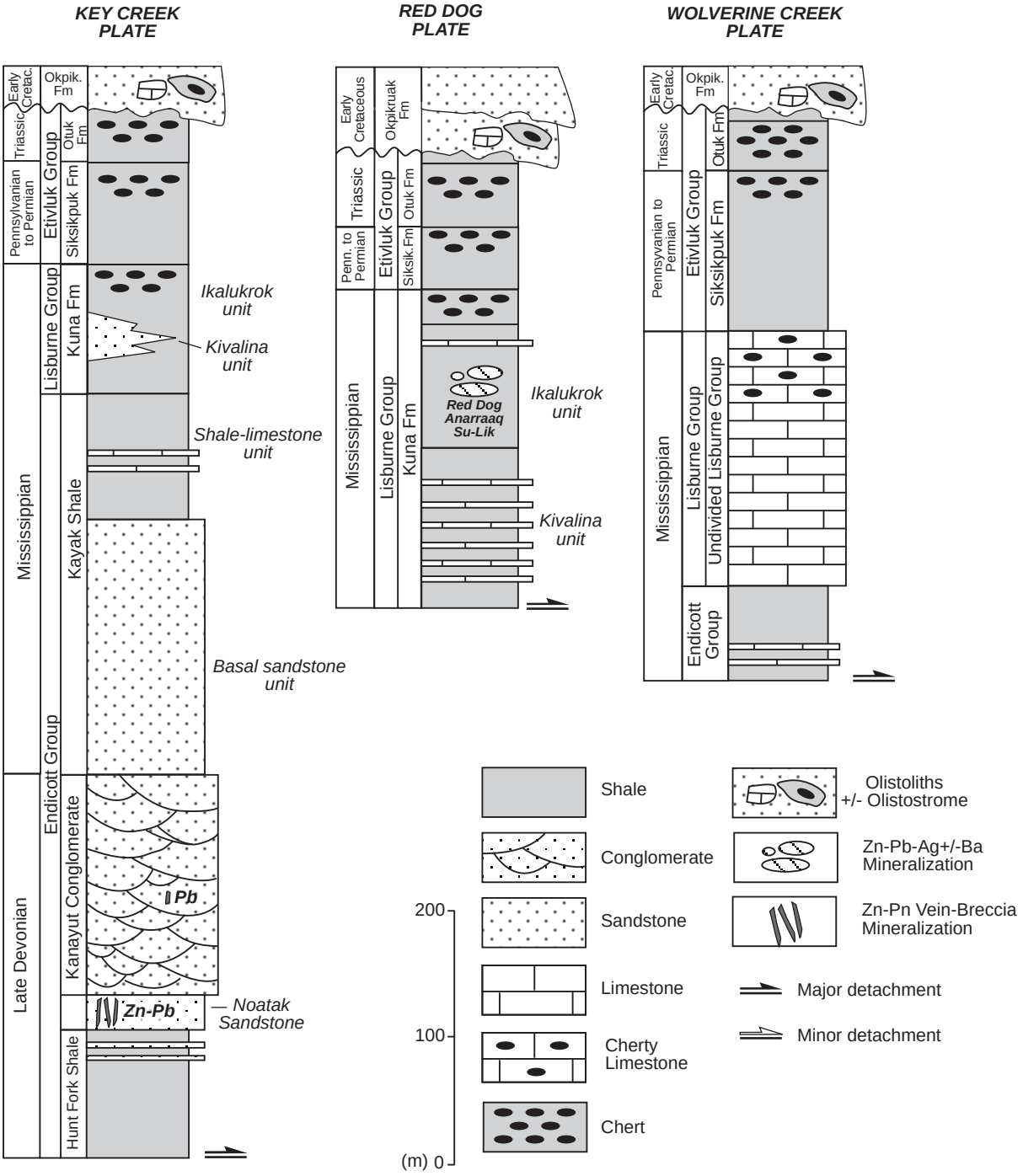


Figure 5.4. Summary stratigraphy of the Endicott Mountains allochthon.

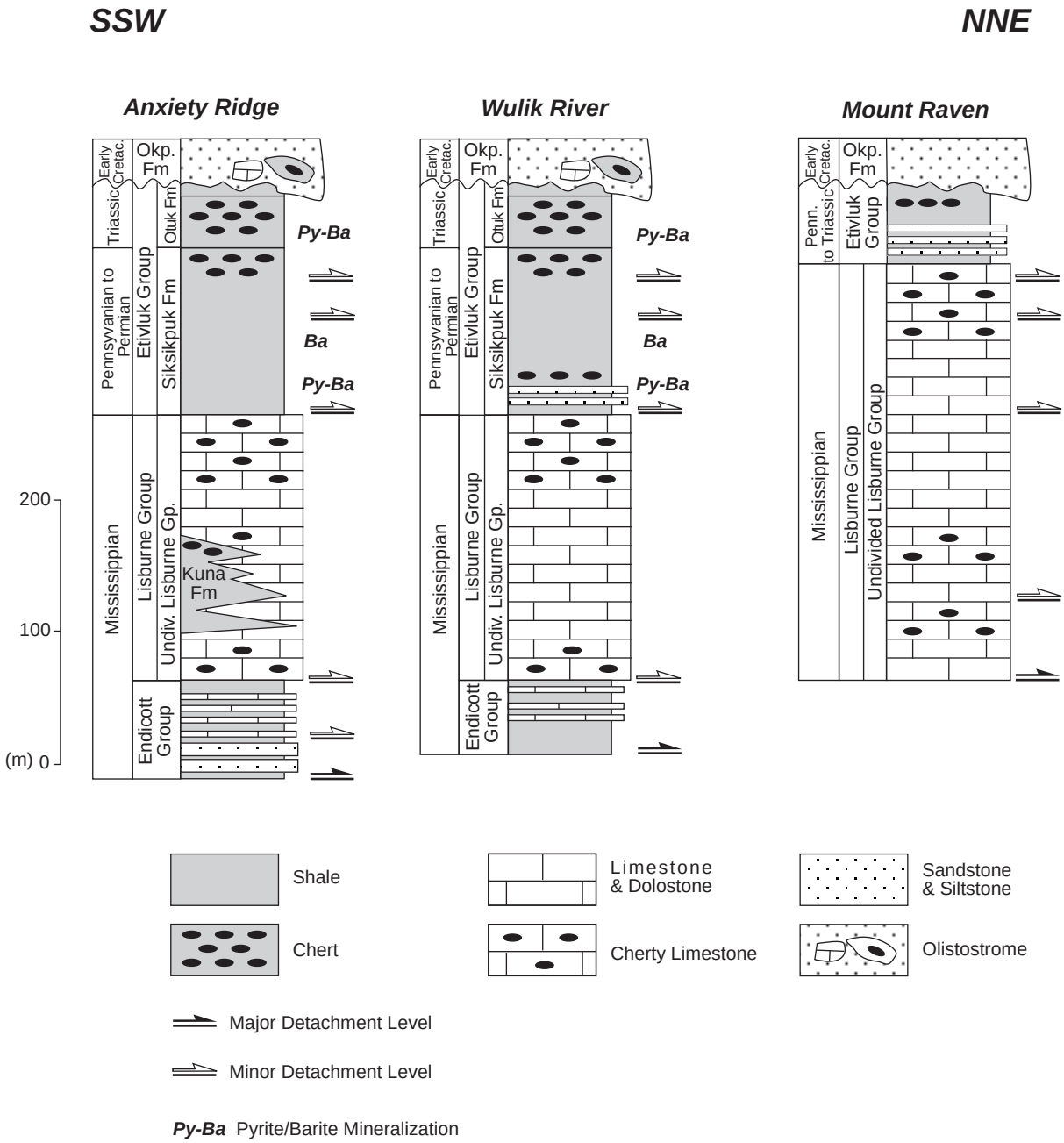


Figure 5.5. Summary stratigraphy of the Wolverine Creek plate. Compiled from stratigraphic successions from the Anxiety Ridge, Rok Hills and Mount Raven areas. Note NNE-shallowing facies of the Lisburne and Etivluk groups.

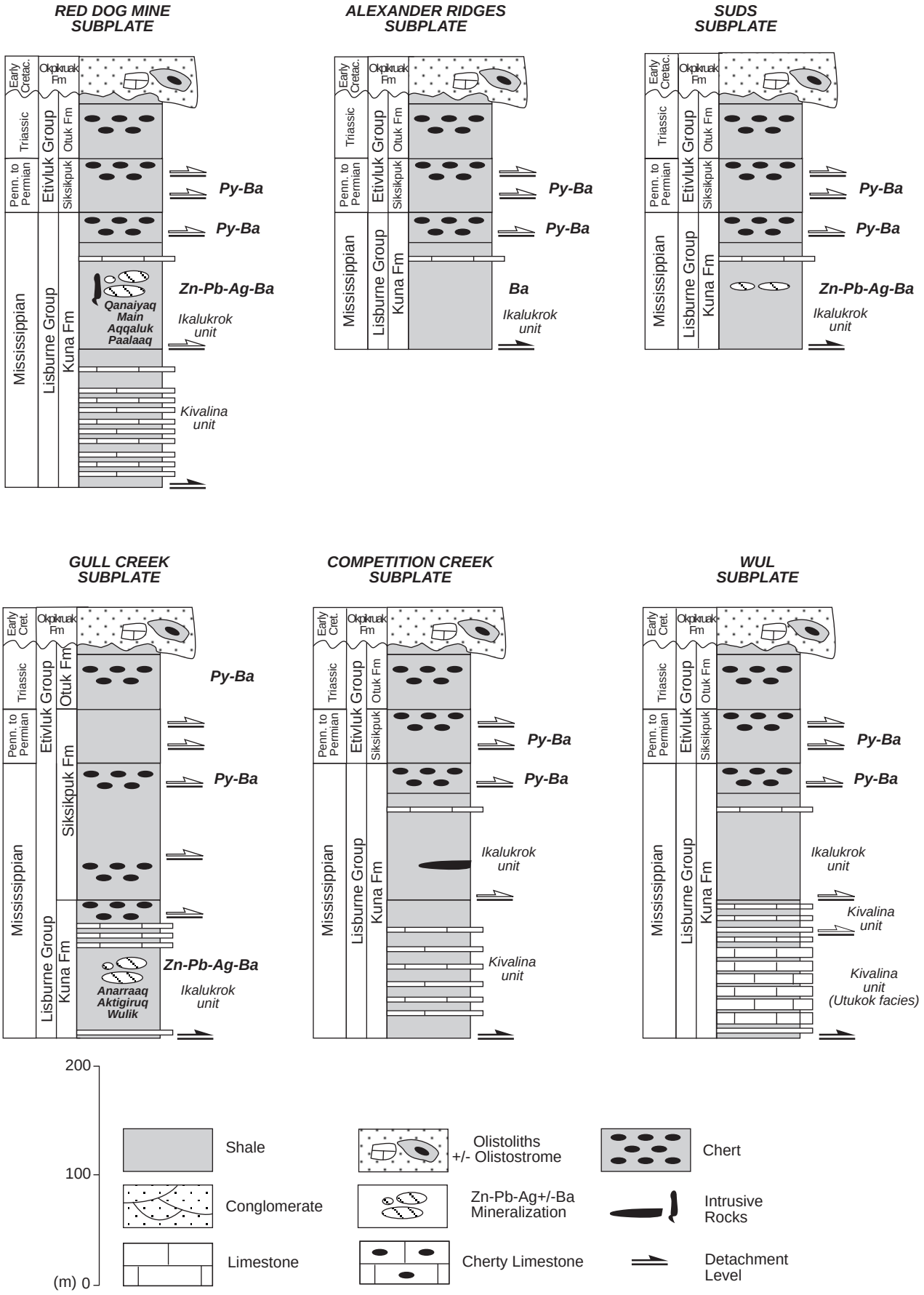


Figure 5.6. Summary stratigraphy of the Red Dog plate and contained thrust subplates of the Endicott Mountains plate.

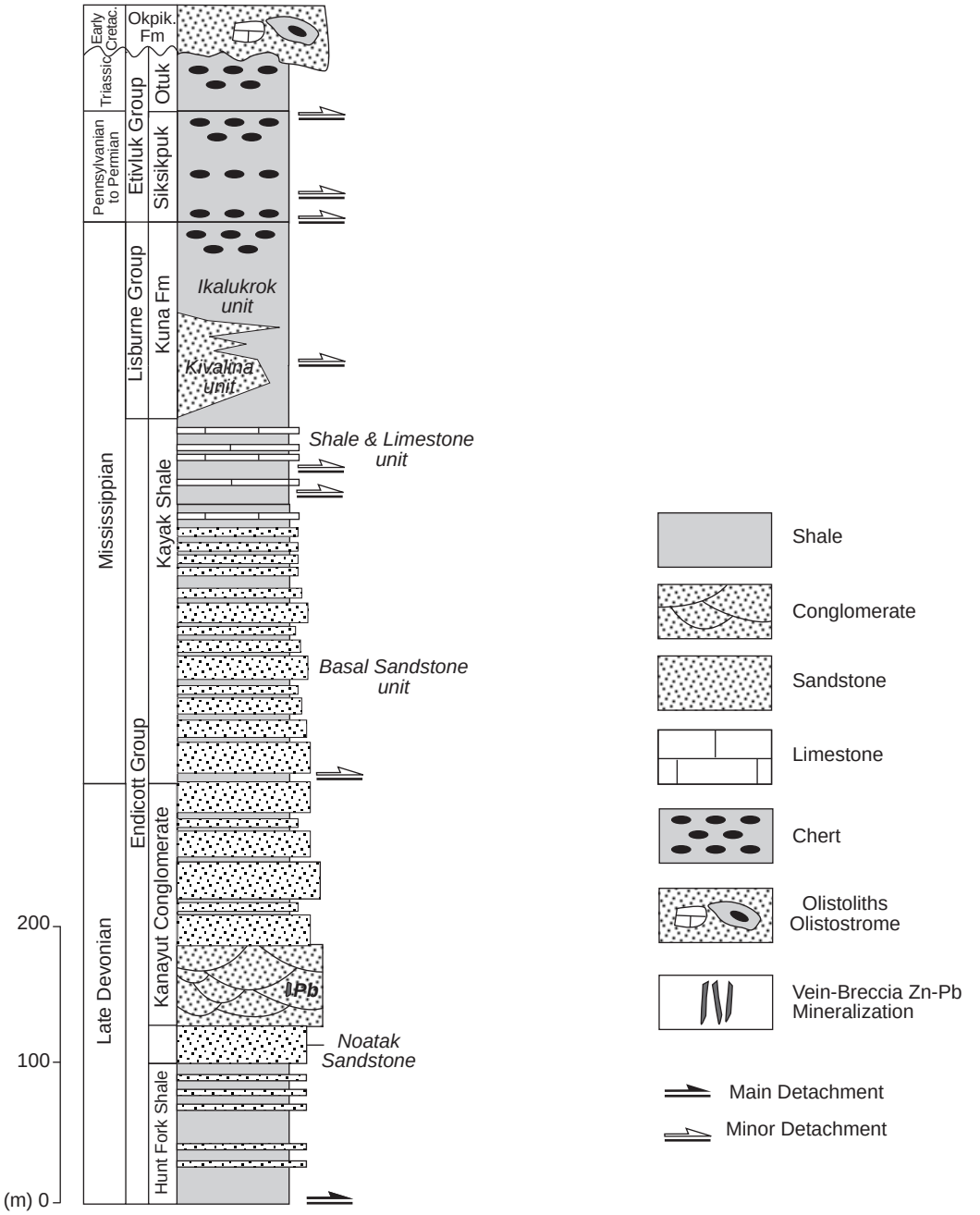


Figure 5.7. Summary stratigraphy of the Key Creek plate of the Endicott Mountains allochthon. Note sediment-hosted Zn-Pb vein-breccia mineralization in the Noatak Sandstone of the Endicott Group.

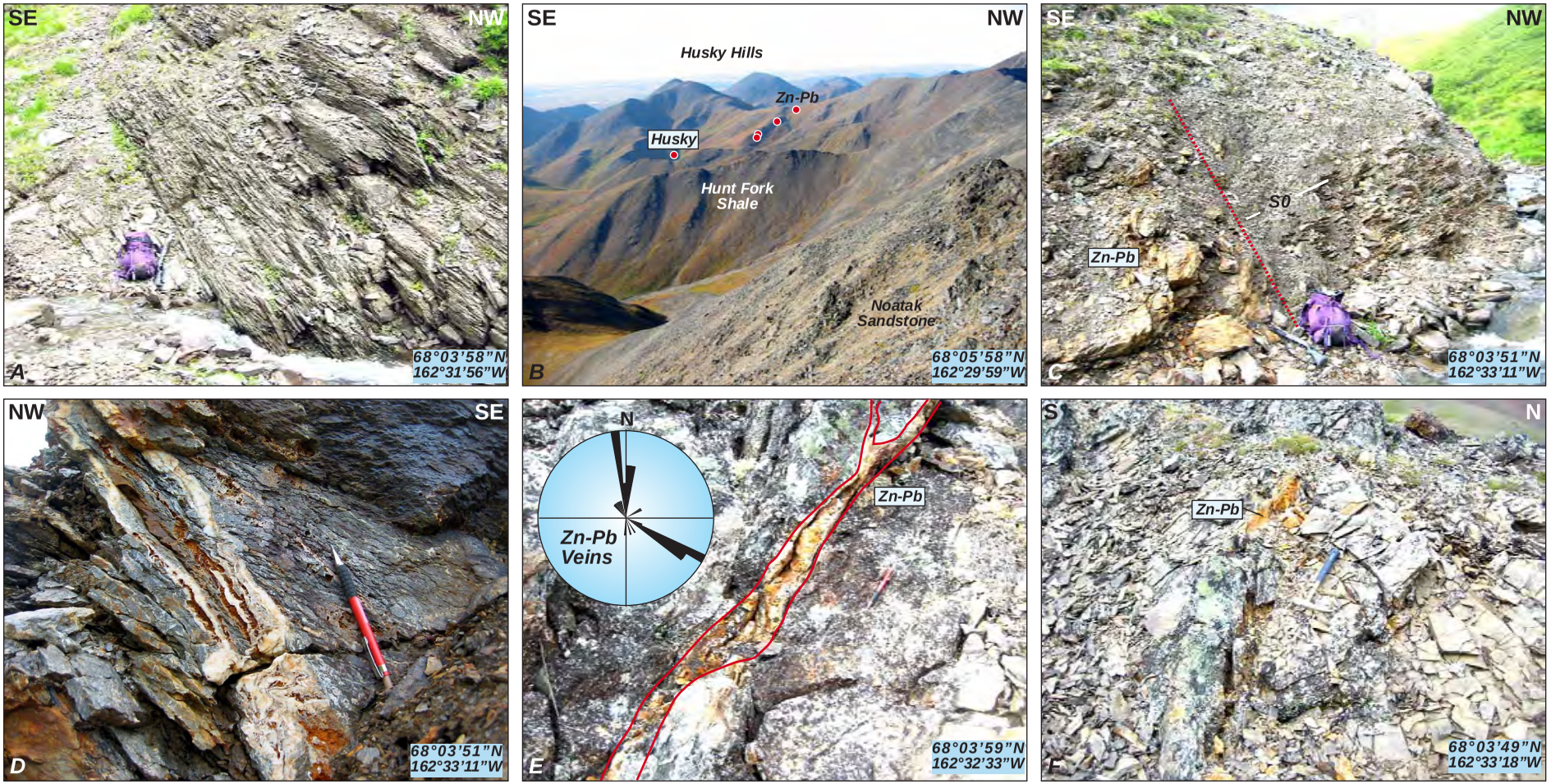


Figure 5.8. Sedimentary features of the Hunt Fork Shale and the Noatak Sandstone of the Endicott Group. **A.** Hunt Fork Shale outcrop showing laminated shales interbedded with siltstones and very fine-grained sandstones. Husky Hills. **B.** View of the Noatak Sandstone (foreground) and the Hunt Fork Shale (background). Husky Hills. Topographic relief is approximately 200 m. The location of the Zn-Pb Husky showing and other occurrences are shown with solid circles. **C.** Husky Zn-Pb vein-breccia in the Noatak Sandstone. Note the mineralized zone crosscuts bedding at a high angle. **D.** Detail of Zn-Pb vein associated to quartz. **E.** Previously unreported Zn-Pb-bearing veins in the Noatak Sandstone. Husky Hills. **F.** Zn-Pb vein in micaceous platy sandstones of the Noatak Sandstone, Husky Hills.

solely exposed in the Husky Hills (Figs. 5.1 & 5.8a, b), approximately 12 km east of the Red Dog mine (Fig. 5.1). Based on the facies associations and the relationship with the overlying stratigraphic units (Fig. 5.7), the Hunt Fork Shale is here interpreted as having been deposited in an open marine environment with limited and fluctuating clastic input, possibly a pro-delta setting (e.g. Reading, 1996; Leeder, 1999).

Noatak Sandstone (Late Devonian, Fammenian)

The Noatak Sandstone consists of approximately 20 to 100 m of thin- to medium-bedded coarse- to fine-grained quartzose to calcareous sandstones interbedded with brown-weathering, medium- to fine-grained platy micaceous (muscovite) sandstones and siltstones (Figs. 5.4, 5.7 & 5.8b) that conformably overlie the Hunt Fork Shale (Figs. 5.3, 5.7 & 5.8b). Fossils are locally abundant and include rhynchonellid brachiopods and plant fossils. Bioturbation is common throughout the unit. Sedimentary structures include trough cross-bedding, parallel and planar cross laminations, as well as locally abundant centimetric red- to bright orange-weathering ferroan carbonate (siderite and ankerite) and iron concretions.

The Noatak Sandstone contains sediment-hosted Zn-Pb vein-breccia mineralization (Figs. 5.2, 5.3, 5.7 & 5.8b – f). This includes the previously reported 'Husky' showing (latitude 68°03'51"N, longitude 162°33'11"W) (L. E. Young, 2002, *pers. comm.*; K. D. Kelley, 2004, *pers. comm.*) (cf. Chapter 3, Fig. 3.5; Fig. 5.8c, d) and four previously unreported Zn-Pb vein-breccia occurrences (Fig. 5.8e, f), located approximately 1 km north, north-northeast and northwest of Husky. Vein-breccia mineralization consists of sulphide-bearing veins (Fig. 5.8c –f) and disseminated sulphides hosted in fine- to coarse-grained sandstones (Fig. 5.7). Sulphide minerals, in decreasing order of abundance, include fine-grained galena, sphalerite, pyrite, and chalcopyrite. These typically occur associated with quartz and diffuse zones of ferroan carbonate alteration (Fig. 5.8c – f). Veins are centimetric to decimetric single segment planar to multiple segment veins with varying degrees of connectivity and lengths of a 20 cm to tens of metres (Fig. 5.8c – f). Lateral extent-to-thickness ratios typically range from 1:20 to 1:50. Veins are systematically oriented (upon restoration of bedding to the horizontal) forming well-defined N- to NNE-trending and WNW-ESE- to NW-SE-trending sets that crosscut bedding at moderate to steep angles (50° to 90°), averaging 70° (Fig. 5.8c

– f). These veins are possibly genetically and spatially related to syn-rift extensional faults (Fig. 5.3). Vein breccia mineralization in the Endicott Group is also possibly related to sulphide veins and associated sediment-hosted Zn-Pb-Ag and barite deposits of the Kuna Formation in the Red Dog Creek area (Fig. 5.3).

Kanayut Conglomerate (Late Devonian – Early Mississippian?, Fammenian – Kinderhookian)

The Kanayut Conglomerate consists of approximately 100 to 300 m of thinning-, fining- and shallowing-upward cycles of pebbly conglomerates, microconglomerates, microconglomeratic quartzites, quartzites, quartzitic sandstones, siltstones, mudstones, and shales (Fig. 5.9) that conformably overlie the Noatak Sandstone (Figs. 5.4 & 5.7). Individual cycles are approximately 20 to 50 m thick. The Kanayut Conglomerate is extensively exposed in the Husky Hills, Mulgrave Hills and Deadlock Mountain areas, in the eastern part of the Red Dog district (Fig. 5.1).

In spite of the name of the unit, conglomerates are rare in the Kanayut Conglomerate unit of the Red Dog district, where sandstones make approximately 80% of the total thickness of the unit (Fig. 5.9). Conglomeratic facies are restricted to decimetric to metric beds of poorly-sorted polymictic conglomerates and microconglomerates that contain pebble to coarse-grained sand angular to well-rounded clasts of milky quartz, black chert, shale, as well as greenish grey to maroon mud rip-up intraclasts. This contrasts with the Kanayut Conglomerate described elsewhere in the Brooks Range, which consists dominantly of conglomerates (e.g. Mull, 1982; Moore *et al*. 1994; Handschy, 1998*b;* L. E. Young, 2002, *pers. comm.*). Pebbly conglomerates and microconglomerates exhibit medium to large-scale trough and planar cross-bedding (Fig. 5.9d). Fossilized wood, impressions of plant fragments, and other unidentified carbonaceous material are locally abundant. Wood fossils and mud rip-up intraclasts are abundant at the base of individual shallowing-upward cycles and are here interpreted as lag deposits (cf. Leeder, 1999; Nichols, 1999).

Sandstones range from thin- to medium-bedded, poorly-sorted, coarse-grained immature ferruginous sandstone to medium- to thick-bedded mature coarse- to fine-grained quartzarenites and quartzites (Fig. 5.9a – c). Sandstones typically occur



Figure 5.9. Sedimentary features of the Kanayut Conglomerate. **A** and **B.** Shallowing- and fining-upward cycles of microconglomerates, sandstones, and shales. Topographic relief is approximately 90 and 75 m, respectively. **C.** Planar-bedded quartzites and quartzitic sandstones. **D.** Planar cross-bedding in fine- to coarse-grained sandstones. Deadlock Mountain. Rose diagram of unidirectional palaeocurrents (N=10). **E.** Kanayut Conglomerate in drill core. Note iron-rich coarse-grained sandstones (top) and grey quartzitic sandstones (bottom). **F.** Maroon to red-weathering mudstones interbedded with medium- to fine-grained sandstones. Deadlock Mountain. Topographic relief is approximately 25 m.

forming metric to decametric sheet-like bodies (Fig. 5.9a - c). Sedimentary structures include cm- to m-scale planar cross bedding (Fig. 5.9d) as well as current ripple marks and laminations. *Liesegangen* bands and rings are locally abundant in ferruginous quartzites and quartzitic sandstones. Parallel laminations and parting lineations are common in mature fine- to medium-grained sandstones and indicate deposition under a high-energy flow regime (e.g. Miall, 1992). Sandstones and quartzites of the Kanayut Conglomerate are characterized by overgrowth epitaxial silica and iron-rich silica cements and generally has a low porosity.

The top of individual fining-upward cycles typically consists of approximately 1 to 10 m of maroon to greenish-grey fissile shales interbedded with thinning- and fining-upward, m- to cm-thick, medium- to fine-grained sandstone beds, and quartzitic sandstones (Fig. 5.9f). Shales contain rare, poorly defined rootlets that occur as casts or bleached zones, possibly after oxidized organic matter. Shales in the Kanayut Conglomerate are interpreted as possible paleosoles (cf. Miall, 1992). Mineralization in the Kanayut Conglomerate consists of rare disseminated fine-grained galena grains and possible vein-breccia mineralization in coarse- to fine-grained sandstones that occur approximately 10 km south of the Red Dog mine.

The facies associations described above indicate that the Kanayut Conglomerate was possibly deposited in a fluvial setting, encompassing channel to flood plain environments during a regressive event (cf. Reading, 1996; Leeder, 1999; Nichols, 1999). The dominant sheet-like bodies (Fig. 5.9a – c) suggest that the Kanayut Conglomerate of the Red Dog district may have resulted largely from overbank flow on the distal part of distributary fluvial systems. The orientation of planar cross bedding foresets (Fig. 5.9d), imbricated clasts and crude clast a-axis alignment indicate SW-directed palaeocurrents (Fig. 5.9d) after restoring bedding to the horizontal. The Kanayut Conglomerate is here interpreted as having been deposited on a NW-SE-trending fault-controlled hangingwall sub-basin (cf. Bosence, 1988; Nichols, 1999) during early rifting of the ancient continental margin of Arctic Alaska (Fig. 5.3).

Kayak Shale (Early Mississippian, Kinderhookian – Osagean)

The Kayak Shale of the Endicott Mountains allochthon consists of approximately 110 to 275 m of siliciclastic and carbonate strata that conformably overlie the Kanayut Conglomerate and underlie and interfinger with platform carbonates and/or deep-water strata of the Lisburne Group (Figs. 5.3, 5.4, 5.7 & 5.10). The Kayak Shale is here subdivided into two informal units. From the oldest to the youngest, these are the Basal Sandstone unit and the Shale and Limestone unit (Figs. 5.4, 5.7 & 5.10). In the Endicott Mountains allochthon, the Basal Sandstone unit occurs solely in the Key Creek plate (Figs. 5.4 & 5.7), whereas the Shale and Limestone unit is locally present at the base of the Wolverine Creek and Red Dog plates.

Basal Sandstone Unit (Kinderhookian)

The Basal Sandstone unit consists of 100 to 200 m of thin-bedded fine-grained quartzitic sandstones and highly-bioturbated siltstones and shales (Fig. 5.10a – c) that conformably overlie the Kanayut Conglomerate (Figs. 5.4 & 5.7). Sedimentary structures include planar cross stratification, current and oscillation ripple marks, as well as distinctive flaser, lenticular, and wavy bedding (Fig. 5.10b, c). Fossils include locally abundant rhynchonellid brachiopods. Bioturbation, including dwelling burrows *Skolithos* sp. and other unidentified ichnofossils, is common throughout the unit. Facies associations indicate that the Basal Sandstone unit was possibly deposited in a tidal to shallow marine setting in transgressive conditions (cf. Reineck & Singh, 1980; Nichols, 1999), possibly reflecting increasing syn-rift subsidence at this time. Previous workers in the Red Dog district (e.g. Moore *et al*. 1986; Curtis *et al*. 1990; Ellersieck *et al*. 1990*a*; Cominco American Exploration Inc. 2001, *pers. comm.*; Kennecott Exploration, 2002, *pers. comm.*) have misidentified or assigned the Basal Sandstone unit to the Late Devonian Noatak Sandstone (cf. Chapter 3, Fig. 3.3b).

Shale and Limestone Unit (Kinderhookian)

The Shale and Limestone unit consists of approximately 10 to 125 m of laminated non-calcareous black shales together with minor thin-bedded to laminated, brown to buff-weathering fossiliferous limestones and impure limestones that conformably overlie the Basal Sandstone unit (Figs. 5.2-5.4, 5.6 & 5.10d-f). The Shale and Limestone unit grades laterally and vertically with the Kivalina unit of the overlying Kuna Formation

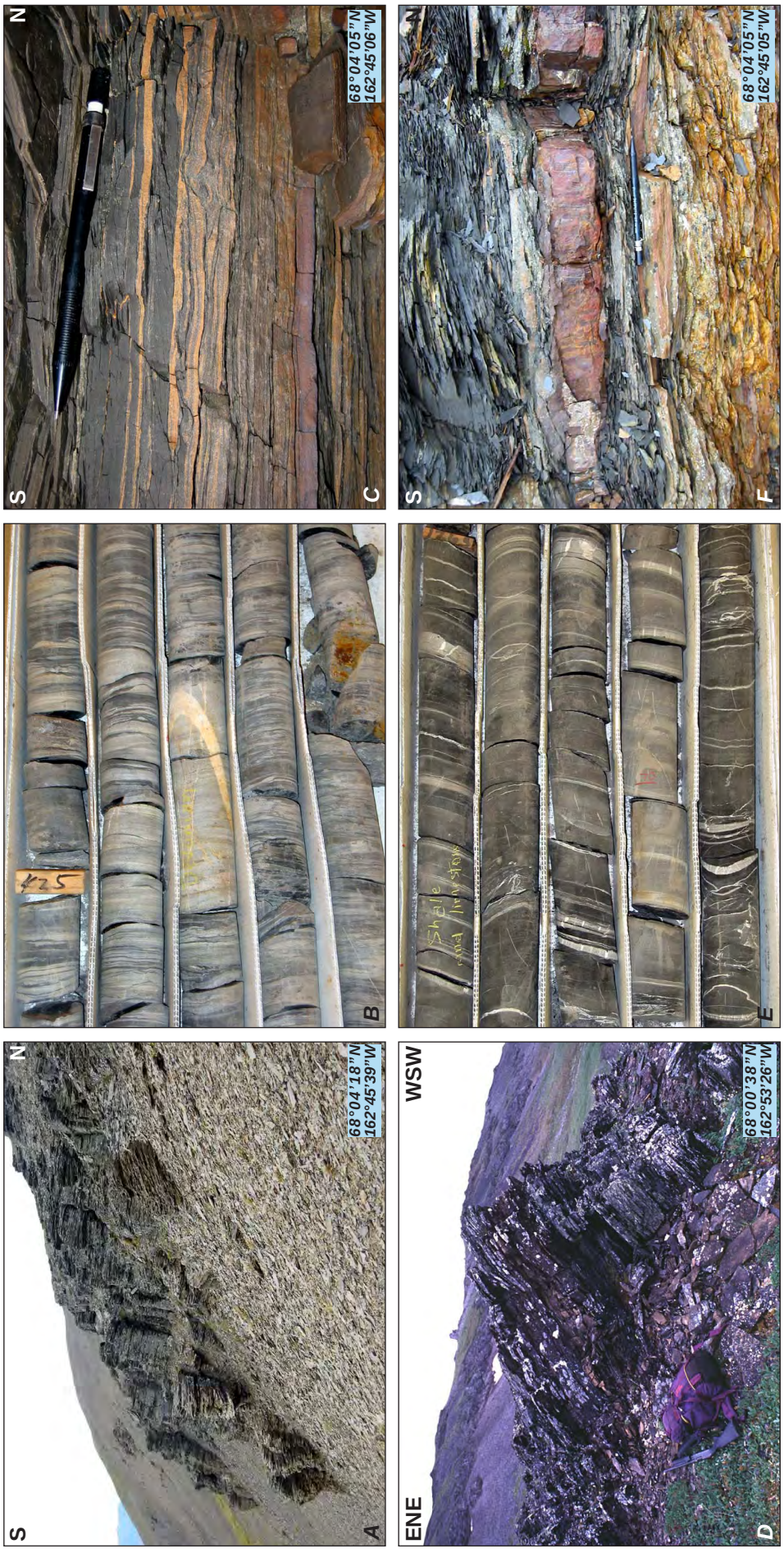


Figure 5.10. Sedimentary features of the Kayak Shale. **A.** Basal Sandstone unit. Kayak Hills. Note well-bedded sandstones. **B.** Basal Sandstone unit in core. Note interbedded sandstones and shales and ripple laminations. Core diameter is approximately 5 cm. **C.** Basal Sandstone unit outcrop showing flaser to lenticular bedding and laminations. Kayak Hills. **D.** Shale and Limestone unit outcrop. Note flaggy limestone in rubble pile. Anxiety Ridge. **E.** Shale and Limestone unit in drill core. Note non-calcareous black shales interbedded with centimetric layers of grey limestone. Core diameter is approximately 5 cm. **F.** Septarian concretions in black shale of the Shale and Limestone unit. Kayak Hills.

(Fig. 5.3). Black shales locally contain grey- to buff-weathering carbonate lenses and nodules up to 10 cm in diameter as well as reddish brown- to yellow-weathering ellipsoidal to oblate septarian, iron, and iron sulphide concretions that typically vary in size from 5 to 20 cm in diameter (Fig. 5.10e, f). Concretions typically coalesce to form 1 to 5 cm-thick discontinuous layers (Fig. 5.10f). Septarian concretions show typical radial to polygonal quartz veins and are commonly cored by disseminated pyrite and/or sphalerite grains. Orange-weathering fossiliferous flaggy calcareous layers (Fig. 5.10d, e) contain abundant shallow water bioclasts, including crinoids, flat sheets of encrusting bryozoans, and lesser rhynchonellid brachiopods. These deposits are here interpreted as distal turbidites with incomplete Bouma sequences (Tc—Td) (e.g. Bouma, 1962; Bouma *et al*. 1985) that re-deposited shallow-water fauna assemblages into a deeper water environment. Bioturbation is rare and typically limited to calcareous intervals. Flaggy calcareous layers typically show a distinctive satiny dull grey manganese coating. Based on the facies associations, the Shale and Limestone unit is interpreted as having been deposited in an outer platform or slope to basin sedimentary environment.

Lisburne Group (Early Mississippian – Pennsylvanian)

The Lisburne Group of the Endicott Mountains allochthon consists of Mississippian to Pennsylvanian fine-grained siliciclastic strata of the Kuna Formation and platform carbonates of the undivided Lisburne Group (Figs. 5.2 – 5.7). The Kuna Formation and the undivided Lisburne Group are interpreted as having been deposited coevally and contiguously and grade laterally and vertically amongst them (Figs. 5.3 – 5.7).

Kuna Formation (Early Mississippian – Late Mississippian, Osagean – Chesterian)

The Kuna Formation consists of approximately 100 to 250 m of black shales, cherts, minor limestones (mudstones to grainstones), calcarenites, calcareous sandstones, sandstones, and siltstones that conformably overlie the Shale and Limestone unit of the Kayak Shale (Figs. 5.3 – 5.7). The Kuna Formation can be subdivided into two informal members or units. From the oldest to the youngest these are the Kivalina and Ikalukrok units (Figs. 5.4 – 5.7).

Kivalina Unit (Early Mississippian, Osagean)

The Kivalina unit consists approximately of 50 to 150 m of dark grey to black calcareous to non-calcareous shales interbedded with fine-grained grey calcarenites, buff-weathering coarse-grained limestones (grainstones) and fine-grained micaceous sandstones and siltstones that gradationally overlie the Kayak Shale of the Endicott Group (Figs. 5.4 – 5.7 & 5.11). Black shales (Fig. 5.11a – d) are calcareous throughout the unit, only becoming weakly- to non-calcareous near the contact with the underlying Kayak Shale. Fossils include abundant crinoid ossicless and fragments of encrusting bryozoans, rhynchonellid brachiopods, and ostracods. Bioturbation is locally abundant. Fine- to coarse-grained bioclastic layers range in thickness from 0.5 cm to 8 cm thick (Fig. 5.11a – d) and are here interpreted as distal turbidites with incomplete Bouma sequences (Td—Te) (e.g. Bouma, 1962; Bouma *et al*. 1985). Shale-to-calcarenite ratios typically range from 1:5 to 1:20. Field mapping and drill-hole data suggest that the Kivalina unit turbidites become finer to the northeast. Sedimentary structures in the Kivalina unit include common graded bedding and parallel laminations, which are typically disrupted by well-developed, closely-spaced (1 to 5 mm) bedding-parallel irregular stylolites with flaser residue seams. The local high contents in detrital carbonate grains (*ca.* 90%) and re-deposited shallow water fauna indicate that turbidites possibly derived from adjacent carbonate platforms (Fig. 5.3). Turbidites locally have a high content (*ca.* 30%) in quartz, mica (muscovite) and other non-calcareous detritus, possibly derived from an unrecognized basement source. Possible sources include older syn-rift strata of the Endicott Group (e.g. Kanayut Conglomerate) or unidentified basement rocks that were potentially exposed during syn-rift extensional faulting.

The Kivalina unit also contains a distinctive shallower-water facies that consists of buff-weathering medium- to thick-bedded packstones, grainstones, and mudstones (Fig. 5.11e, f). These strata are restricted to a 35 km^2 area (Wul area), approximately 11 km southwest of the Red Dog mine (Figs. 5.1 & 5.7e, f). This facies contains winnowed assemblages of shallow water fossils, including colonial corals with dimensions of up to 35 cm x 25 cm, well-preserved large flat sheets of encrusting bryozoans (5 to 10 cm in diameter), and crinoids. This facies is lithologically and faunally equivalent to some limestones of the Shale and Limestone unit of the Kayak Shale and similar to parts of the coeval Utukok Formation. These strata were deposited with limited amounts of

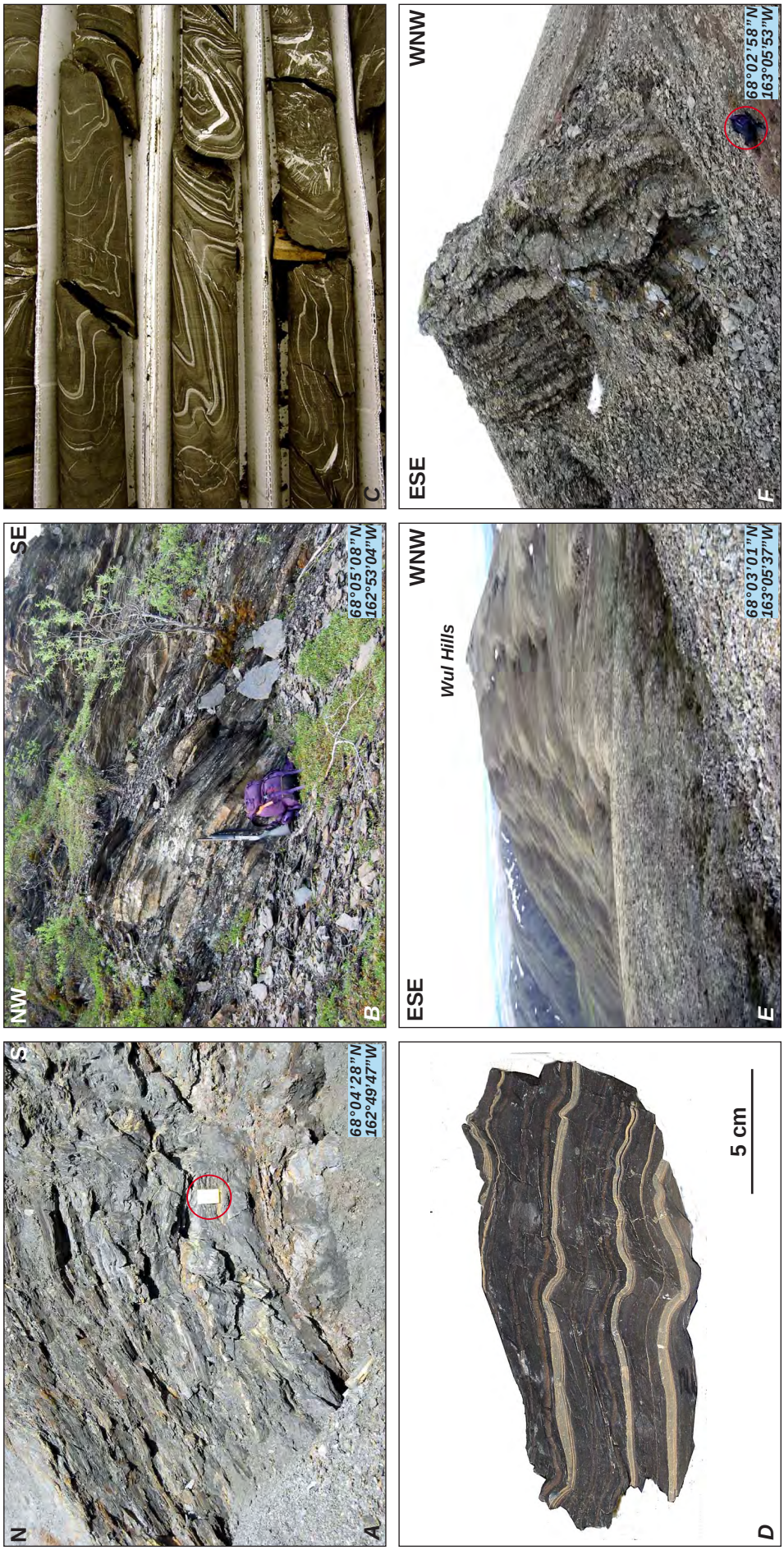


Figure 5.11. Sedimentary features of the Kivalina unit of the Kuna Formation. **A.** Kivalina unit outcrop showing thin-layered black shales and buff-weathering calcarenites. 950' bench level, east pit wall, Red Dog mine. 20 cm-long notebook is encircled for scale. **B.** Kivalina limestones and shales. Note platy and flaggy limestones. North Basin **C.** Kivalina unit in drill core. Note thin grey-weathering calcarenite layers. **D.** Kivalina unit hand specimen. **E.** Kivalina unit rubble outcrops showing shallow-water facies . Wul Hills. Topographic relief is approximately 50 m. **F.** Detail of shallow water facies of the Kivalina unit in the Wul Hills. Backpack is encircled for scale.

sedimentary transport, possibly reflecting deposition in a fault-controlled topographic high.

Ikalukrok Unit (Early to Late Mississippian, Osagean – Chesterian)

The Ikalukrok unit consists of approximately 25 to 125 m of black and dark to light grey shales together with varying amounts of calcareous to lithic turbidites, black cherts, and mudstones that conformably overlie the Kivalina unit (Figs. 5.4, 5.7 & 5.12). The Ikalukrok unit hosts the sediment-hosted Zn-Pb-Ag and barite deposits of the Red Dog district (Figs. 5.2 & 5.3) and can be subdivided into two informal sub-units, here referred to as the lower and upper Ikalukrok units.

Lower Ikalukrok Unit (Osagean)

The lower Ikalukrok unit consists of 10 to 100 m of massive to laminated, non-resistant, organic-rich, sooty and locally bituminous grey to black shales (Fig. 5.12a, b) that show varying degrees of silicification. Black shales are typically recessive weathering and form mottled rubble outcrops that weather grey, yellow, metal blue, reddish and whitish grey (Fig. 5.12a). The lower Ikalukrok unit also contains sparse grey to brownish fine-grained lithic sandstones, calcareous siltstones and grey-weathering micritic fetid flaggy limestones (Fig. 5.12c – e). These intervals are interpreted as distal turbidites with incomplete Bouma sequences (Tb/Tc – Te) (e.g. Bouma, 1962; Bouma *et al*. 1985) that deposited shallow water fauna (e.g. crinoids) into a deeper water setting.

Ikalukrok turbidites are commonly banded to laminated and more locally massive, becoming more abundant towards the top of the unit. Turbidites typically range in thickness from a few cm (Fig. 5.12c) to beds as thick as 5 m. Turbidite composition varies greatly from one turbidite to another and also vertically and/or laterally within a single turbidite. Sedimentary structures include current ripples and parallel laminations with locally well-developed parting lineations (Fig. 5.12d). Calcareous turbidites and micritic limestones exhibit abundant diagenetic bedding-parallel square waveform stylolites. Turbidites in the Ikalukrok unit (Fig. 5.12c, d) are coarser-grained and significantly thicker than the distal turbidites of the underlying Kivalina unit (Fig. 5.11c, d), but show a lower depositional frequency, possibly indicating a decrease in fault-related subsidence in the Osagean.

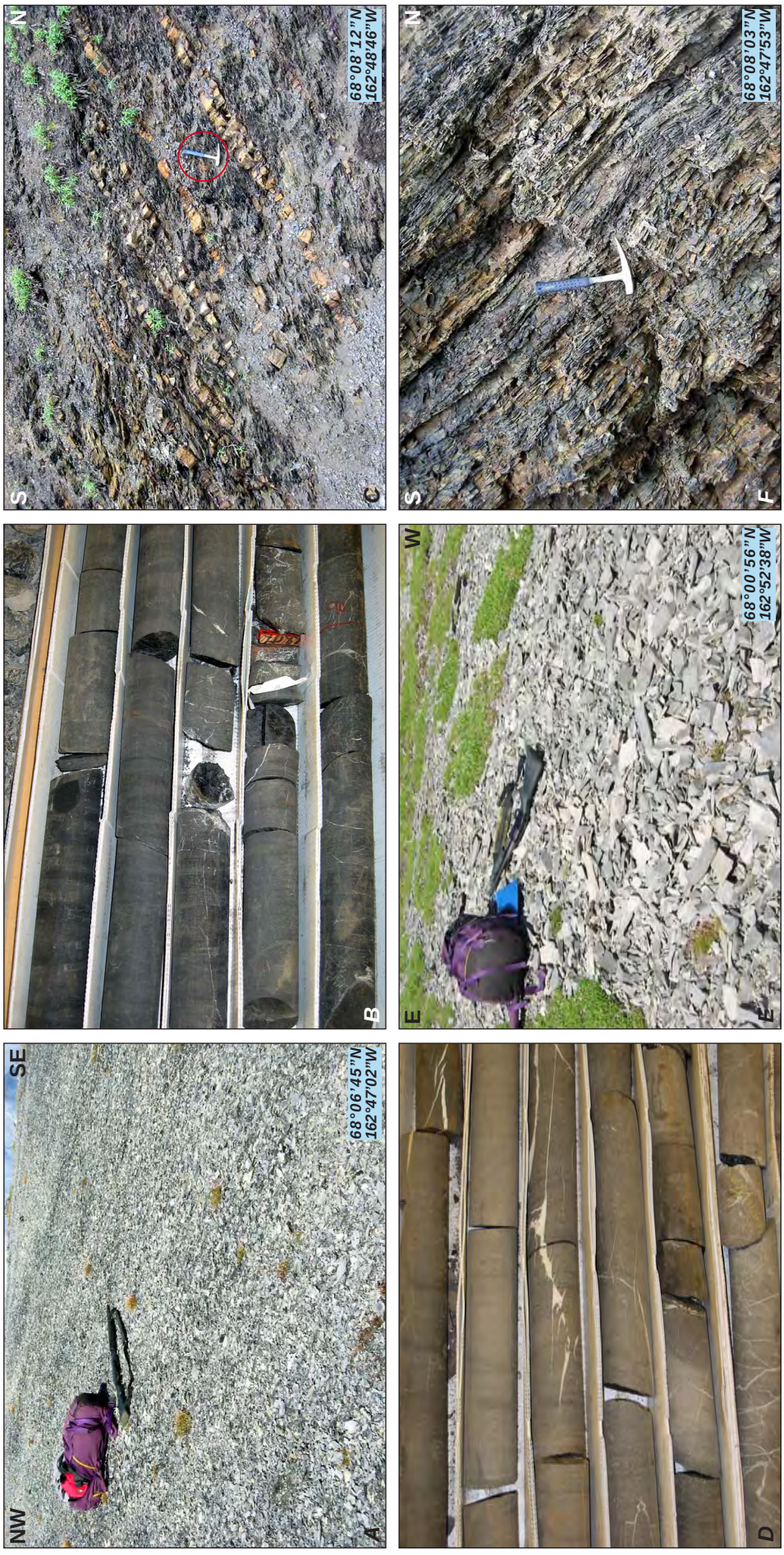


Figure 5.12. Sedimentary features of the Ikalukrok unit of the Kuna Formation. **A.** Ikalukrok unit rubble outcrop showing black and grey shales. North Basin. **B.** Ikalukrok unit black shales in drill core. Core diametre is approximately 5 cm. **C.** Ikalukrok unit outcrop showing black shales and buff-weathering calcareous turbidites. Shear Creek. **D.** Ikalukrok unit turbidites in drill core. Note parallel laminations and colour banding related to compositional changes. Core diameter is approximately 5 cm. **E.** Rubble outcrop showing characteristic platy grey-weathering micritic limestones. Anxiety Ridge. **F.** Thin-bedded to laminated Ikalukrok unit black cherts in the Shear Creek area.

Interbedded with black shales and spatially related with calcareous turbidites are rare 1 to 10 cm thick bedding-parallel veins of non-radial fibrous calcite perpendicular to the vein walls. These are interpreted as early diagenetic structures that possibly developed similarly to 'cone-in-cone' structures (cf. Tucker, 2001) under high pore fluid pressure conditions. These bedding parallel veins may have implications for fluid flow in the Ikalukrok unit, possibly acting as bedding-parallel fluid pathways during the Osagean.

Fossils in the lower Ikalukrok unit are rare, and consist largely of conodont assemblages (cf. Dumoulin *et al*. 2004). The lower Ikalukrok unit also contains previously undescribed macrofossils with large straight shells (?) (up to 1 m long) with circular section (5 to 15 cm in diameter) and cm- to dm-spaced coiled annulations. These fossils are here interpreted as possible ammonoids, possibly similar to *Orthoceras* sp. (e.g. Easton, 1960).

The lower Ikalukrok unit (Fig. 5.12a – e) is rich in organic matter and locally bituminous and rich in hydrocarbons. Hydrocarbons include locally abundant brittle black pyrobitumen and audible natural gas shows detected in exploration drill core. Gas in the Ikalukrok unit typically occurs in fractured black shales and turbidites (Fig. 5.12a-d) at one or more reservoirs at average depths of 700 m.

Upper Ikalukrok Unit (Osagean ? – Chesterian)

The upper Ikalukrok unit consists of approximately 5 to 30 m of thin- to thick-bedded planar- to irregularly-bedded, conchoidal-fractured, vitreous black cherts that are locally interbedded with black to brownish-weathering mudstones and siliceous mudstones (Fig. 5.12f). Whitish millimetric to centimetric grey- to whitish grey recessive-weathering laminae and layers are possibly silicified relict carbonate layers. Fossils include sparse radiolaria, which are locally closely packed into aggregates that define diffuse and irregular and discontinuous mm- to cm-thick layers. Sedimentary structures include locally abundant parallel laminations (Fig. 5.12f). The uppermost Ikalukrok unit contains conspicuous centimetric to decimetric convex-upward fluid and/or gas escape mounds (?) that are possibly related to syn-sedimentary hydrothermal activity in the Chesterian. These structures are possibly coeval with the formation of the sediment-hosted Zn-Pb-Ag and barite deposits of the Red Dog district.

Field mapping and drill hole data suggest that the Ikalukrok unit regionally thickens to the northwest, although this pattern may have been partly inherited from Mesozoic thrust faulting, folding, and/or gravity sliding. The Kuna Formation is here interpreted as having been deposited in a deep-water basinal environment, below the storm wave level. The preservation of carbonate material in the Ikalukrok unit indicates that depth of deposition did not exceed the calcite compensation depth (approximately 4 km for Present Day oceans) (e.g. Leeder, 1999; Tucker, 2001). The abundance of organic-rich black shales indicates deposition in an anoxic environment largely under starved conditions with fluctuating input of turbidites.

Sediment-Hosted Zn-Pb-Ag and Barite Mineralization in the Kuna Formation

The Ikalukrok unit of the Red Dog plate is regionally mineralized and hosts the sediment-hosted Zn-Pb-Ag and barite deposits at Red Dog, Su-Lik, Anarraaq, and Aktigiruq as well as a number of minor low-grade Zn-Pb occurrences and showings (cf. Chapter 3, Fig. 3.5; Figs. 5.2 & 5.3). Mineralization in the Ikalukrok unit consists of decametric to hectometric strata-bound lenses of massive to disseminated sulphides and barite (Fig. 5.13). Sulphide minerals include sphalerite, galena, pyrite, and marcasite (Fig. 5.13a – c). Associated minerals include widespread silica (quartz) as well as lesser strontianite and calcite. Sulphides occur in a wide range of textural associations that vary from deposit to deposit and also within a single deposit. These include massive, laminated, brecciated, veined, and colloform sulphide textures. Sphalerite textures and colours are highly variable. Common sphalerite varieties are red-brown and honey to yellow coarse-grained (Fig. 5.13a) and tan and cream fine-grained (Fig. 5.13c). Fine-grained varieties are commonly interstitial to pyrite and possibly post-date the generation of coarse-grained sphalerite. Pyrite occurs most commonly as a coarse-grained green brass variety that commonly forms nodules (Fig. 5.13d). Framboidal and zoned ocelar pyrite textures are locally developed. Sphalerite and pyrite locally form colloform growths. Galena occurs dominantly as a fine-grained bluish to coarse-grained silver varieties. Disseminated galena crystals (0.5 to 1 mm size) in black shale are common in the proximity of major Zn-Pb-Ag deposits. Pyrobitumen is locally abundant interstitially to sulphides, dominantly in pyrite and sphalerite and also associated to quartz veins.

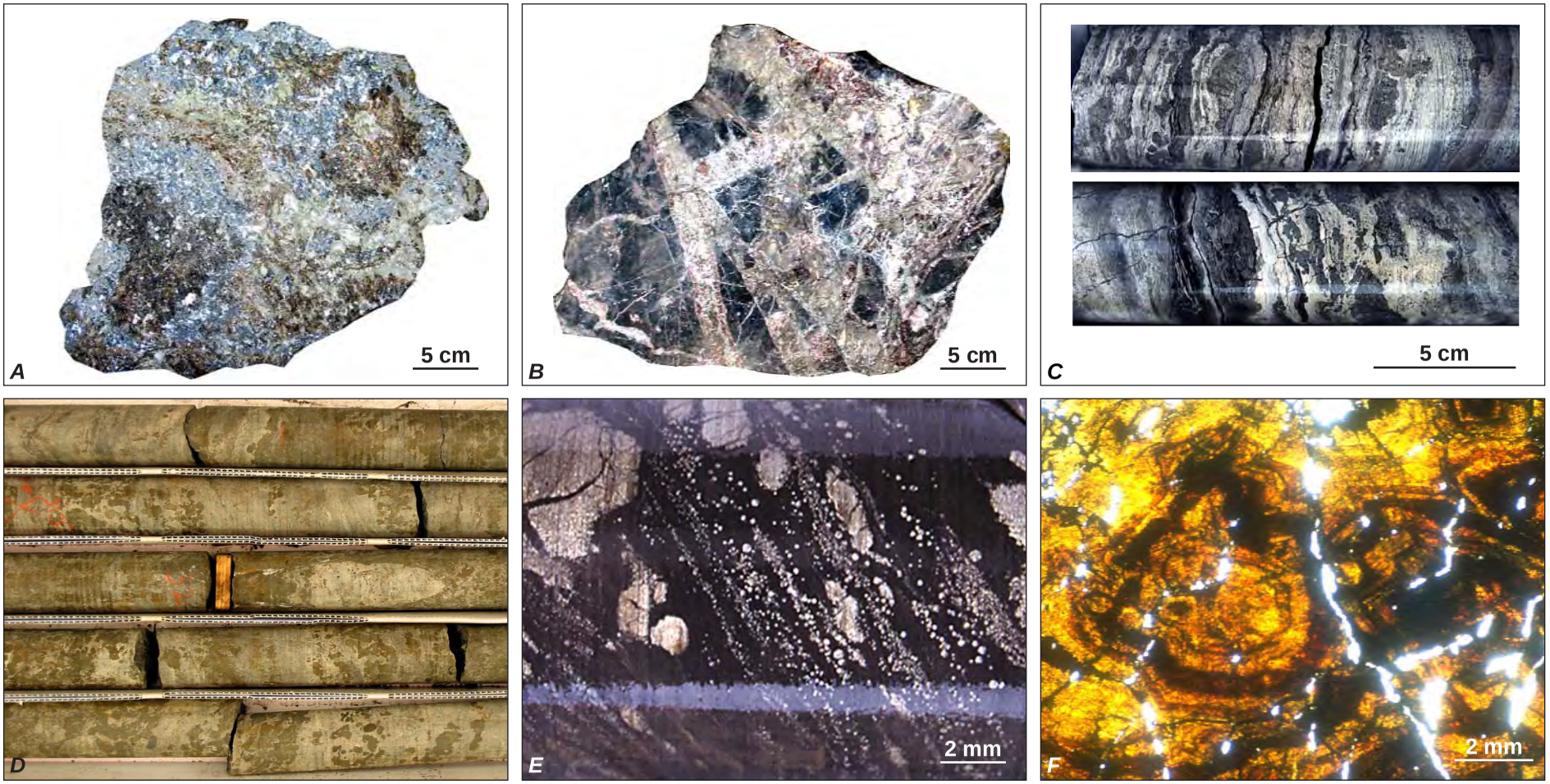


Figure 5.13. Sediment-hosted Zn-Pb-Ag and barite mineralization in the Kuna Formation. **A.** Hand specimen of coarse-grained massive sulphides from the Main deposit. **B.** Vein ore. Note sphalerite and pyrite veins hosted in Ikalukrok silicified shales and cherts. Sample from the east pit wall of the Red Dog mine. **C.** Drill core showing laminated to layered sulphides from the Anarraaq-Aktigiruq areas. **D.** Drill core showing massive sulphides from the Aktigiruq deposit. Sulphides consist dominantly of nodular brass pyrite with interstitial fine-grained cream sphalerite. **E.** Disseminated pyrite in black shales. **F.** Photomicrograph showing zoned sphalerite crystals.

The Zn-Pb-Ag deposits of the Red Dog district have been commonly referred to shale-hosted (e.g. Schmidt, 1997*a*; Kelley & Jennings, 2004). This study uses the general term 'sediment-hosted' in that the host lithologies are not restricted to shale but encompass a larger range of lithotypes, including black shales, calcareous and lithic siltstones and sandstones, limestones, calcareous radiolarites (?), and cherts. Mineralization is typically hosted in a grey- to bluish grey fine-grained silica matrix (e.g. deposits at Red Dog) and/or in carbonate (e.g. Aktigiruq, Anarraaq). Deposits hosted in black shales silica rock are heavily silicified whereas those hosted in carbonate show moderate to little silicification.

Ores show equivocal textures indicative of both syn-sedimentary and replacement origins. Sulphides may locally be replacing calcareous and/or lithic turbidites of the lower part of the Ikalukrok unit (Fig. 5.7). Lithic to medium-grained calcareous turbidites are locally mineralized with fine-grained green brass pyrite that appears to replace carbonate. Replacement occurs in individual grains that form discontinuous or diffuse layers. Pyrite locally replaces barite strings. Associated with mineralization are sparse to concentrated cylindrical structures approximately 2 to 6 mm in diameter, and up to 10 cm in length that occur exclusively in barite, sulphide-bearing barite and silica rock (Fig. 5.13c). Associated with the tube structures are millimetric spherical to ellipsoidal structures (faecal pellets ?). Tubes show equivocal relationship to bedding surfaces and are parallel, oblique and perpendicular to stratification. These may represent evidence of hydrothermal vent fauna similar to annelid cf. *Alvinella* documented in sulphide vents in modern oceanic environments (e.g. Goodfellow *et al*. 1993; L. Anderson, 2003, *pers. comm*.).

Oxidation of the mineralized Ikalukrok unit results in the formation of iron-rich gossan (Fig. 5.14f), which typically consists of a distinct bright-orange to reddish brown poorly consolidated ferricrete precipitate (jarosite) and amber yellow to ochre limonite (Fig. 5.14e). Gossan occurs in the Alvinella (latitude 68°08'58"N, longitude 162°52'24"W) and Ferric Creek areas (latitude 68°04'39"N, longitude 163°12'53"W), located 9 km northwest and 15 km west-southwest of the Red Dog mine, respectively. Gossan at Alvinella is associated with galena, sphalerite and pyrite showings. This study has identified a previously unreported gossan showing in black shales of the lower



Figure 5.14. Sediment-hosted Zn-Pb-Ag and barite mineralization. **A.** W-looking view of the Qanaiyaq deposit showing a distinctive vegetation kill zone related to sulphide and barite showings. Topographic relief is approximately 100 m. **B.** Massive barite. 975' bench level, east pit wall, Red Dog mine. Geological hammer for scale. **C.** Detail of exploration drill core showing barite nodules in silicified limestone. Anarraaq deposit. **D.** Worm tube structures in sulphide-bearing silica rock. 875' bench level, east pit wall, Red Dog mine. **E.** Gossan in the Alvinella area, Ikalukrok Creek. Note grey-weathering massive sulphides (foreground) and red-weathering jarosite and limonite (background). **F.** Previously unreported gossan in Ikalukrok black shales in the upper Wulik River area.

Ikalukrok unit in the upper Wulik River area, approximately 25 km northwest of the Red Dog mine, (latitude 68°15'46"N, longitude 163°01'49"W) (Fig. 5.14f). At this locality, gossan is spatially related to previously reported barite and Zn-Pb showings (L. E. Young, 2002, *pers. comm.;* cf. Young, 2004). Barite mineralization in the Ikalukrok unit locally results in distinctive vegetation kill zones.

Igneous Rocks in the Kuna Formation

The Kuna Formation contains at least three altered felsic to mafic igneous intrusives in strata of the Kivalina and Ikalukrok units. Intrusives have intermediate to mafic compositions and typically have a phaneritic 'salt-and-pepper' texture with sub-equal distribution of melanocratic (dominantly pyroxene) and leucocratic minerals (quartz and plagioclase). Intrusives appear to be spatially related to veined ore facies but also occur in non-mineralized strata (e.g. Kivalina unit). Intrusives occur in the Red Dog Main deposit, 1 km north of the Main deposit (latitude 68°04'57"N, longitude 163°01'58"W) and also 11 km to the northwest in the Kivalina unit north of the Competition Creek (latitude 68°09'28"N, longitude 163°01'58"W) (Fig. 5.1).

Undivided Lisburne Group (Early – Late Mississippian, Osagean – Chesterian)

The term undivided Lisburne Group is informally introduced in this study to refer to platform carbonate strata that conformably overlie the Kayak Shale in the Endicott Mountains allochthon (Figs. 5.1 – 5.5 & 5.15). The undivided Lisburne Group is characteristic of the Wolverine Creek plate (Figs. 5.4 & 5.5). Elsewhere in the Brooks Range, strata correlative to the undivided Lisburne Group of the Red Dog district are subdivided into the Alapah, Wahoo, and Wachsmuth limestone units (e.g. Bowsher & Dutro, 1957; Brosgé *et al*. 1962; Moore *et al*. 1994; Dumoulin *et al*. 1997; Young, 2004) (cf. Chapter 2, Fig. 2.11), which cannot be readily distinguished in the Red Dog district. In the Red Dog district, strata of the undivided Lisburne Group were previously assigned to the Kogruk Formation (e.g. Moore *et al*. 1986; Young, 1992, 2000; Dumoulin *et al*. 2004; Young, 2004) (cf. Chapter 3, Figs. 3.2a, b & 3.3a). This is here considered inappropriate in that the Kogruk Formation was formally defined to refer to lithostratigraphically distinct platform carbonates of the Lisburne Group that overlie the Utukok Formation in the Kelly River allochthon (e.g. Sable & Dutro, 1961; C. G. Mull, 2004, *pers. comm.*) (Figs. 5.2 & 5.3).

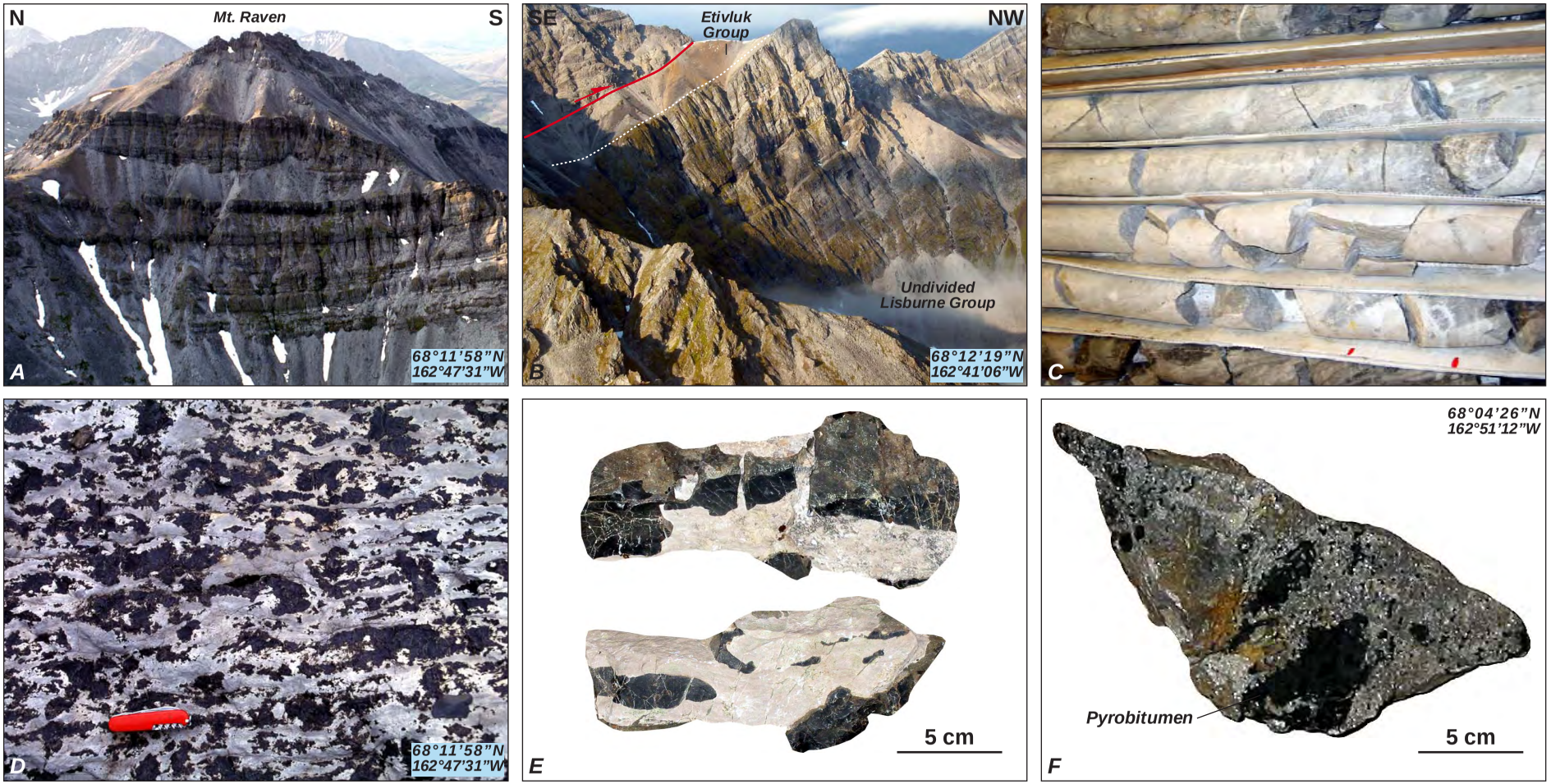


Figure 5.15. Sedimentary features of the undivided Lisburne Group. **A.** E-looking oblique aerial view of platform carbonates of the undivided Lisburne Group at Mount Raven. Topographic relief is approximately 500 m. **B.** Well-bedded limestones and cherty limestones near Wolverine Creek. Topographic relief is approximately 300 m. **C.** Undivided Lisburne Group in drill core. Core diameter is approximately 5 cm. **D.** Top view of bedding surface showing irregular chert nodules. Rok Hills. **E.** Hand specimens showing textural relationships between limestone and chert. **F.** Hand specimen of coarse-grained sucrosic dolostone showing pyrobitumen in intercrystalline and 'vuggy' porosity.

The undivided Lisburne Group consists of fossiliferous limestones (dominantly graded and well-sorted grainstones and packstones), cherty limestones, dolostones, as well as black cherts and mudstones that conformably overlie the Kayak Shale of the Endicott Group (Figs. 5.1 & 5.15). Fossils are locally abundant and include widespread crinoids, colonial and solitary rugose corals (*Zaphrentis* sp.), gastropods, as well as articulated spiriferid and rhynchonellid brachiopods. Bedded to nodular black cherts are abundant in the lower and uppermost parts of the unit (Fig. 5.15d, e). Chert nodules are rounded, warty to irregular and commonly define centimetric irregular patches (Fig. 5.15d). These typically coalesce to form irregular discontinuous parallel layers that concentrate along preferred stratigraphic horizons and weather out of the limestone. Most of the chert and dolomite possibly resulted from early diagenetic alteration. Relict textures are locally present in dolostones, whereas possible fenestral textures (e.g. Tucker, 2001), bird-eyes, and evaporites (?) occur towards the top of the unit. The uppermost part of the undivided Lisburne Group contains 10 to 50 m of black cherts, mudstones, and phosphatic black shales. These strata are equivalent to the Tupik Formation of Sable & Dutro (1961), which is here included with the undivided Lisburne Group.

Limestones and dolostones of the undivided Lisburne Group locally interfinger with coeval black shales, micritic limestones and dolomitized (?) micritic limestones of the Ikalukrok unit of the Kuna Formation (Fig. 5.3). Regional stratigraphic patterns indicate that facies changes between the undivided Lisburne Group and the Kuna Formation possibly occurred along north-northeast—south-southwest and west-northwest—east-southeast directions (Present Day coordinates). This transition is exposed from latitude 68°00’31”N longitude 162°54’20”W to latitude 68°01’25”N longitude 162°44’71”W in the Anxiety Ridge area, approximately 6 km south of the Red Dog mine (Fig. 5.1). Spatially related with facies changes between the undivided Lisburne Group and the Kuna Formation are sedimentary breccias and rudstones that occur at least at one locality, approximately 12 km south-southeast of the Red Dog mine (*ca*. latitude 68°01’17”N, longitude 162°46’12”W). Similar sedimentary breccias and rudstones occur in the Wulik Knot area, approximately 35 km northwest of the Red Dog mine (G. C. Broadbent, 2002, *pers. comm.*). Sedimentary breccias and proximal deposits are here interpreted as basin margin deposits.

The undivided Lisburne Group locally has a high effective porosity (*ca.* 6-12%) and is regionally rich in organic matter and hydrocarbons. Hydrocarbons in the undivided Lisburne Group typically occur as brittle black pyrobitumen that fills or lines 'vuggy', intercrystalline, and/or fracture porosity in micro-sucrosic to sucrosic grey- and whitish grey-weathering dolostones (Fig. 5.15f). Vugs typically consist of rarely interconnected molds of crinoids and brachiopods (?), locally as large as 5 cm in diameter. Hydrocarbons also occur in flattened and aligned discontinuous layer parallel laminae that resemble laminoid fenestrae textures (cf. Tucker, 2001). Intercrystalline porosity is here interpreted to have been enhanced by dolomitization, possibly during diagenetic alteration.

Based on facies associations and depositional trends, the undivided Lisburne Group is interpreted as having been deposited in a SSW- to SW-facing carbonate platform to slope setting (e.g. Ahr, 1989), possibly a subsiding margin platform (e.g. Bosence, 2005) that sourced the turbidites of the Kuna Formation (Figs. 5.3 & 5.11). Sedimentary breccias and a possible link with turbidites of the lower Ikalukrok unit suggest that platform margins were moderately steep and possibly fault-controlled (Fig. 5.3). The uppermost facies suggest restricted circulation in a deep-water setting and mark the onset of post-rift thermal subsidence and platform drowning.

Etivluk Group (Pennsylvanian — Late Jurassic)

The Etivluk Group of the Endicott Mountains allochthon consists of approximately 135 to 285 m of dominantly siliceous pelagic rocks together with minor carbonate and siliciclastic strata that conformably to disconformably (?) overlie strata of the Lisburne Group (Figs. 5.2 – 5.7). The Etivluk Group is widely exposed in the Red Dog district (Fig. 5.1) and occurs in all structural plates of the Endicott Mountains allochthon (Figs. 5.3 –5.7). The Etivluk Group of the Endicott Mountains allochthon is subdivided into the Siksikpuk and Otuk Formations (Figs. 5.4 – 5.7).

Siksikpuk Formation (Pennsylvanian – Lower Triassic, Morrowan – Griensbachian)

The Siksikpuk Formation consists of 35 to 135 m of cherts, shales, and mudstones (Fig. 5.16a – f) that conformably, paraconformably, disconformably, or unconformably (?) overlie the Kuna Formation and the undivided Lisburne Group (Fig. 5.2). The

Siksikpuk Formation is subdivided into three informal distinct units or members, referred to as the lower, middle and upper Siksikpuk units (Fig. 5.16a – f).

Lower Siksikpuk Unit

The lower Siksikpuk unit consists of approximately 5 to 40 m of distinctive thin- to medium-bedded bright orange- to grey-weathering cherts, grey to whitish mudstones, shales, and minor brown-weathering dolostones (Fig. 5.16a, b). This unit is equivalent to the 'orange cherty unit' of Moore *et al.* (1986) and Young (1989, 2000) (Fig. 3.3b). The lower Siksikpuk unit locally contains rare brown –weathering irregular to rounded calcareous and/or dolomitic nodules in silicified mudstones. Mineralization in the lower Siksikpuk unit includes locally abundant iron sulphides and barite. Iron sulphides occur as irregular to rounded (botroydal) pyrite-marcasite nodules (mm to 12 cm in diameter). The distinctive orange- to yellow-weathering colour that characterizes the lower Siksikpuk unit in outcrop (Fig. 5.16a, b) is interpreted to result from oxidation of iron sulphides. Barite occurs as disseminated laths, layers of laths and nodules, needles, rosettes, and beds.

The lower Siksikpuk Formation is interpreted as having been deposited in an open marine setting, possibly a pro-delta setting. Regional mapping indicates that the lower Siksikpuk unit is coarser-grained to the northeast where it includes approximately 5 to 20 m of siltstones that conformably to disconformably overlie the Lisburne Group. The lower Siksikpuk unit contains rare pyrobitumen in fracture porosity near the contact with the underlying Ikalukrok unit.

Middle Siksikpuk Unit

The middle Siksikpuk unit consists of approximately 20 to 45 m of distinctive massive to laminated brick red, maroon, grey, and greenish grey shales and rare cm-thick grey chert layers that conformably overlie the lower Siksikpuk unit (Fig. 5.16a, c). The middle Siksikpuk unit contains discontinuous, irregularly distributed and diffuse nodular greenish grey patches (Fig. 5.17d) and rounded to elongated (compacted and/or sheared) spots that are interpreted to result from reduction, possibly during early diagenesis. Maroon colours are prevalent and interpreted to predate reduction. Fossils in the middle Siksikpuk unit include sparse radiolaria that are commonly haematized.

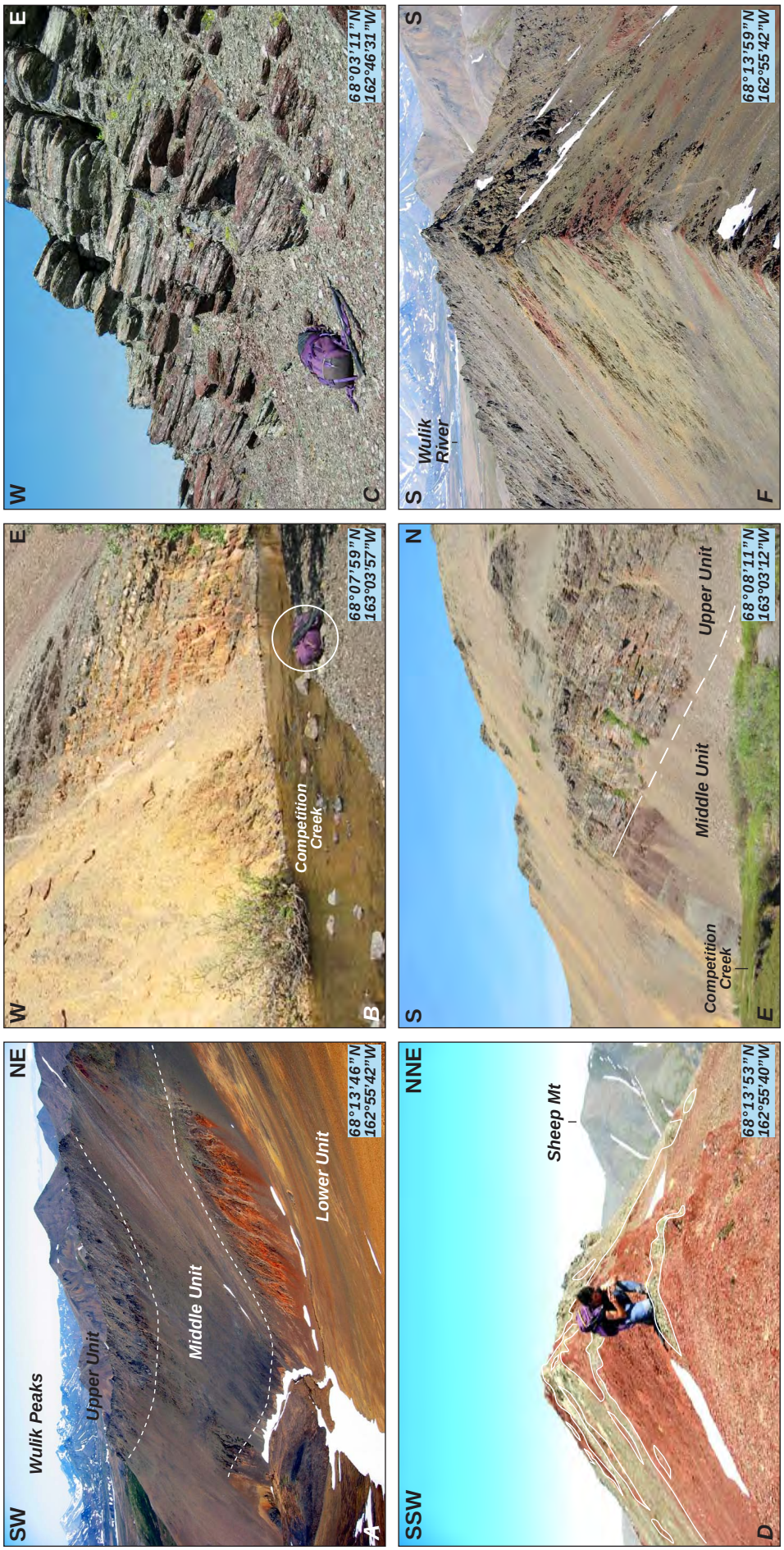


Figure 5.16. Sedimentary features of the Siksikpuk Formation. **A.** NW-looking view of the Siksikpuk Formation showing the lower, medium and upper units. Topographic relief is approximately 100 m. **B.** Lower Siksikpuk unit. Note distinctive orange-weathering colour related to oxidation of pyrite. Competition Creek. Backpack is encircled for scale. **C.** Middle Siksikpuk unit. Laminated maroon to red and greenish grey shales near Deadlock Mountain. **D.** Greenish grey irregular patches in maroon shale near Sheep Mountain. **E.** Well-bedded cherts of the upper Siksikpuk unit conformably overlie maroon and greenish grey shales of the middle Siksikpuk unit. Competition Creek. Topographic relief is approximately 20 m. **F.** Upper Siksikpuk unit chert near the Wulik River. Topographic relief is approximately 25 m.

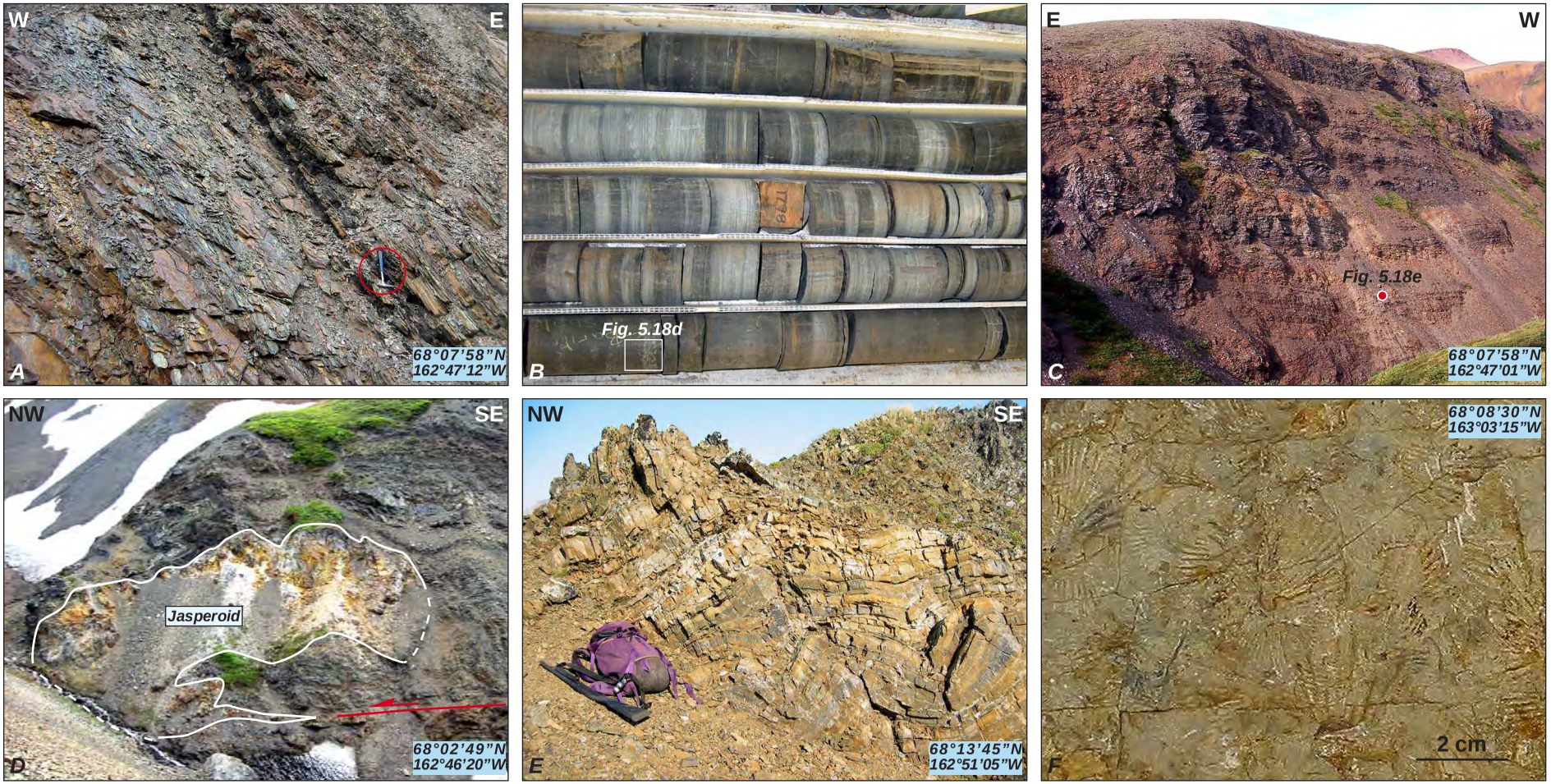


Figure 5.17. Sedimentary features of the Otuk Formation. **A.** Laminated and colour-banded shales of the lower Otuk unit. Shear Creek. Geological hammer encircled for scale. **B**. Lower Otuk unit in drill core. Note distinctive centimetric black and greenish grey colour bands and pyrite layers and laminae. **C.** Well-bedded cherts of the middle Otuk unit. Shear Creek. Topographic relief is approximately 75 m. **D.** White to amber yellow strata-bound massive jasperoid in cherts of the middle Otuk unit near Deadlock Mountain. Topographic relief is approximately 10 m. **E.** Buff-weathering dolomites and cherty dolomites of the upper Otuk unit near Wolverine Creek. Note distinctive colour banding. **F.** Top view of *Monotis* sp. impressions on cherty dolomite bedding surface near the Wulik River.

Radiolaria locally form aggregates that define 1 to 5 cm-thick discontinuous and irregular layers.

Mineralization in the middle Siksikpuk unit includes locally abundant disseminated milimetric to centimetric barite laths, layers of laths, needles, rosettes, rounded to irregular nodules and lesser pyrite nodules that commonly range in size from 1 to 5 cm in diameter (Fig. 5.18a). Quartz and calcite veins are also locally common and chlorite typically occurs coating fracture surfaces (Fig. 5.18b, c).

Upper Siksikpuk Unit

The upper Siksikpuk unit consists of approximately 10 to 50 m of dominantly discontinuous irregular, wavy to nodular, medium- to thick-bedded, greenish grey variegated argillaceous cherts that conformably overlie the middle Siksikpuk unit (Fig. 5.16a, e, f). Fossils in the upper Siksikpuk unit include sparse haematized radiolaria, which are locally closely packed into aggregates that define cm-thick discontinuous and irregular layers. Mineralization in the upper Siksikpuk unit includes locally abundant botroydal pyrite and/or marcasite that form nodules up to 10 cm in diameter.

Otuk Formation (Lower Triassic – Middle-Late Jurassic, Spatian – Bajocian)

The Otuk Formation consists of approximately 100 to 150 m of shales, cherts, dolostones, cherty dolostones, and minor silicified limestones that conformably overlie the Siksikpuk Formation (Figs. 5.1 & 5.17). The Otuk Formation is subdivided into three informal units, here referred to as the lower, medium and upper units (Fig. 5.17). These are in part equivalent to the shale, chert, and limestone members of the Otuk Formation of Mull *et al*. (1982) and Young (2004).

Lower Otuk Unit

The lower Otuk unit consists of approximately 25 to 50 m of thin-bedded to laminated, colour-banded light-grey, greenish-grey, and black shales together with minor thin-bedded to laminated black and grey cherts, and rare grey silicified limestones and dolostones (Fig. 5.17a, b). Colour bands typically range in thickness from a few mm to 20 cm (Fig. 5.17b). The base of the lower Otuk unit is regionally deformed and occurs as strongly sheared black and greenish-grey shales and mudstones with sheared pyrite

beds and nodules. This is equivalent to the 'transitional subunit' of the upper Siksikpuk Formation of Young (2000) or the 'transition facies' of Young (2004). Fossils in the lower Otuk unit include rare centimetric bone fragments in phosphatic shales, possibly equivalent to cf. *Ichthyosaur* reported by Tailleur *et al*. (1973) and Churkin *et al*. (1979) in correlative Late Triassic strata of the central Brooks Range.

Mineralization in the lower Otuk unit includes regionally abundant pyrite and barite. Pyrite occurs as continuous planar parallel layers and laminae that range in thickness from less than 1 mm to 5 cm (Fig. 5.17b). Less commonly, pyrite forms thicker massive layers up to 15 cm thick. Barite typically occurs as disseminated laths, layers of laths, needles, or rounded to irregular nodules. Barite rosettes and nodules typically range in size from a few mm to up to 10 cm in diameter (Fig. 5.18f) and locally form irregular layers of closely packed aggregates that are particularly abundant in the proximity of major sediment-hosted Zn-Pb-Ag deposits of the Red Dog district (e.g. east pit Red Dog mine). Less commonly barite forms decimetric to metric coarse-to fine-grained massive to laminated (?) beds (Figs. 5.17b, e & 5.18d – f) with thickness-to-lateral extent ratios that range from 1:5 to 1:10.

Middle Otuk Unit

The middle Otuk unit consists of approximately 20 to 50 m of variegated grey, greenish grey, acqua-marine, turquoise, bluish or black cherts and mm- to cm-bedded to laminated green to greenish-grey shales that conformably overlie the lower Otuk unit (Figs. 5.1 & 5.17c, d). The middle Otuk unit also locally contains rare unfossiliferous grey-weathering silicified limestone and dolostone layers and/or nodules near the contact with the overlying upper Otuk unit. Fossils include sparse radiolaria that locally form irregular layers. Chert layers (5 to 10 cm thick) are planar parallel bedded and typically quartz-veined perpendicular to bedding. Chert layers are typically colour-banded and have dark blue to dark grey centres bounded by a diffuse mm- to cm-thick whitish- to bluish-weathering rind in the upper and lower bedding surfaces (Fig. 5.17c). Shale layers are 0.5 to 1 cm thick. Shale-to-chert ratios typically range from 1:5 to 1:10. The central part of the middle Otuk unit contains a regional marker horizon that consists of 1 to 2.5 m of laminated to thin-bedded black to bluish chert with minor sooty pyritic black shales.

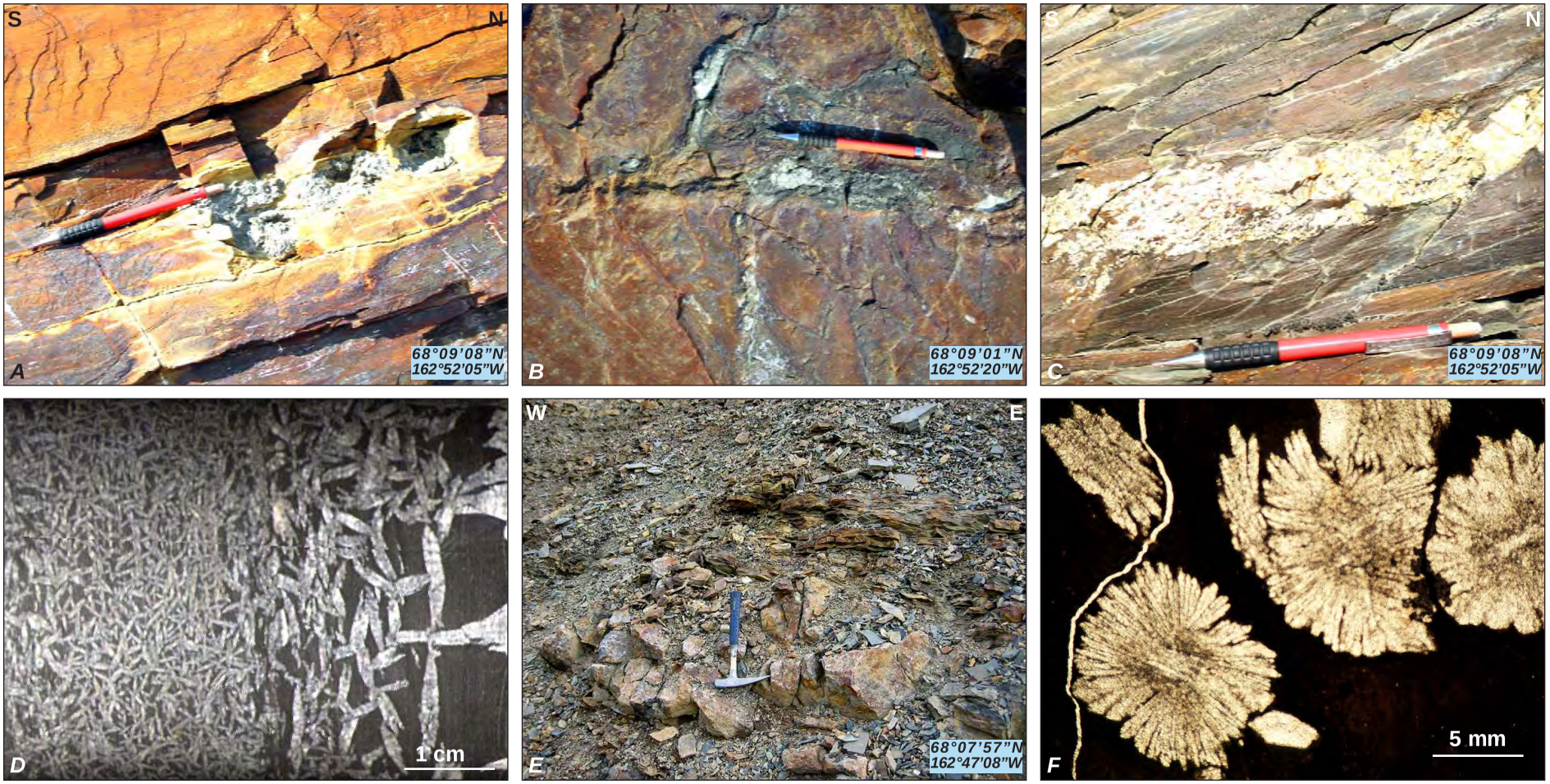


Figure 5.18. Mineralization in the Etivluk Group. **A.** Recessive-weathering dull grey pyrite nodules in bright orange-weathering cherts and shales of the lower Siksikpuk unit. Ikalukrok Creek. Note nodules coalesce to form a discontinuous bedding parallel layer. **B.** Pyrite veins in undifferentiated chert of the Siksikpuk Formation. Ikalukrok Creek. Note vein offset. **C.** Layer of coarse-grained barite laths in shales of the middle Siksikpuk Formation. Ikalukrok Creek. Note c-axes of laths are oriented parallel to bedding. **D.** Layer of fine- to coarse-grained barite laths in black shale of the lower Otuk unit. Way up is to the left. **E.** 50 cm-thick massive barite bed in laminated shales of the lower Otuk Formation. Shear Creek. **F.** Photomicrograph showing barite rosettes in black shales of the lower Otuk unit. Plane polarized light. Sample from 1125' bench level, east pit wall, Red Dog mine.

The middle Otuk unit locally contains irregularly-distributed but regionally abundant speckled and highly resistant red, vermillion, purple, amber to ochre yellow, yellowish white, violet, or grey strata-bound to rarely discordant massive siliceous 'jasperoid' bodies that occur in strongly folded and thrust faulted intervals (Fig. 5.17c, d). Jasperoid is typically 1 to 5 m thick and is commonly intensely brittle fractured with development of one or more sets of closely-spaced (1 to 5 cm) joints. Thickness-to-lateral extent ratios commonly range from 1:2 to 1:5. Jasperoid is here interpreted to result from escape of silica-rich fluids during the incipient stages of the Brookian orogeny (Fig. 5.17d). This is here interpreted as evidence for high pore fluid pressure. Mineralization in the middle Otuk unit consists of rare pyrite and/or marcasite that are locally abundant near the base of the unit forming centimetric layers, millimetric laminae, and pyrite and/or marcasite nodules (1 to 5 cm in diameter).

Upper Otuk Unit

The upper Otuk unit consists approximately of 10 to 50 m of thin- to thick-bedded grey- to buff-weathering dolostones, cherty dolostones, silicified limestones, and cherts (Fig. 5.17e) that conformably overlie the middle Otuk unit. Dolostones and cherty dolostones (5 to 10 cm thick) are typically colour-banded with dark grey to greenish grey centres that grade into a 0.5 to 5 cm-thick cream to buff diffuse alteration rinds in the upper and lower bedding surfaces (Fig. 5.17e). Bedding surfaces are planar parallel to wavy parallel, and only locally irregular with development of bedding-parallel well-spaced (5 to 20 cm) irregular to waveform stylolitic surfaces of possible diagenetic origin. Fossils include regionally abundant impressions on bedding surfaces of Late Triassic radially-ribbed pectinid pelecypods *Monotis* sp. and cf. *Halobia* (Fig. 5.17f) that locally form coquinoid beds. Mineralization in the upper Otuk unit consists of rare dark green amorphous malachite and azurite (?) that occur in fractures and/or as a thin coating on dolostone and/or cherty dolostone bedding surfaces. On the basis of the lithofacies and *in situ* biogenic shell accumulations, the upper Otuk unit is here interpreted as having been deposited below storm wave base, possibly in an outer shelf environment.

Conformably (?) overlying the upper Otuk unit are locally 1 to 10 m of recessive-weathering maroon, purplish-red, greenish or greenish grey mudstones. These strata are

equivalent to the 'Ipewick unit' of Crane & Wiggins (1976) or 'Ipewik Formation' of Moore *et al*. (1986) (cf. Chapter 3, Fig. 3.3), which is here included with the Otuk Formation. The 'Ipewick unit' of Crane & Wiggins (1976) or 'Ipewik Formation' of Moore *et al*. (1986) was never formally defined in accordance with the Code of Stratigraphic Nomenclature and does not meet the criteria for valid formation definition (C. G. Mull, 2004, *pers. comm.*). The uppermost Etivluk Group also locally contains up to 10 m of laminated non-calcareous dark grey to black organic-rich shales, here assigned to the Kingak Shale (cf. Young, 2004).

5.4.2 Stratigraphy of the Picnic Creek Allochthon

The Picnic Creek allochthon of the Red Dog district consists of two thrust plates that contain strata of the Baird, Endicott, Lisburne and Etivluk groups (Figs. 5.2 & 5.19). These are the Puzzle Creek and Amaruk River plates. These show varying degrees of stratal disruption and show equivocal stratigraphic and structural relationships with Early Cretaceous syn-orogenic strata of the Brookian unit.

Baird Group (Late Devonian)

The Baird Group of the Picnic Creek allochthon consists of approximately 20 to 50 m of grey- to white-weathering grainstones and packstones of the Kugururok Formation (Fig. 5.19).

Kugururok Formation (Late Devonian, Frasnian – Fammenian)

The Baird Group of the Picnic Creek allochthon consists of approximately 20 to 50 m of grey- to white-weathering grainstones and packstones of the Kugururok Formation. The base of the unit is a thrust fault.

Endicott Group (Early Mississippian, Kinderhookian)

The Endicott Group of the Picnic Creek allochthon consists of mixed carbonate and siliciclastic strata here assigned to the Kayak Shale. The Endicott Group appears to grade into strata of the Baird Group, possibly suggesting a lithostratigraphic link between the Endicott Mountains and Picnic Creek allochthons.

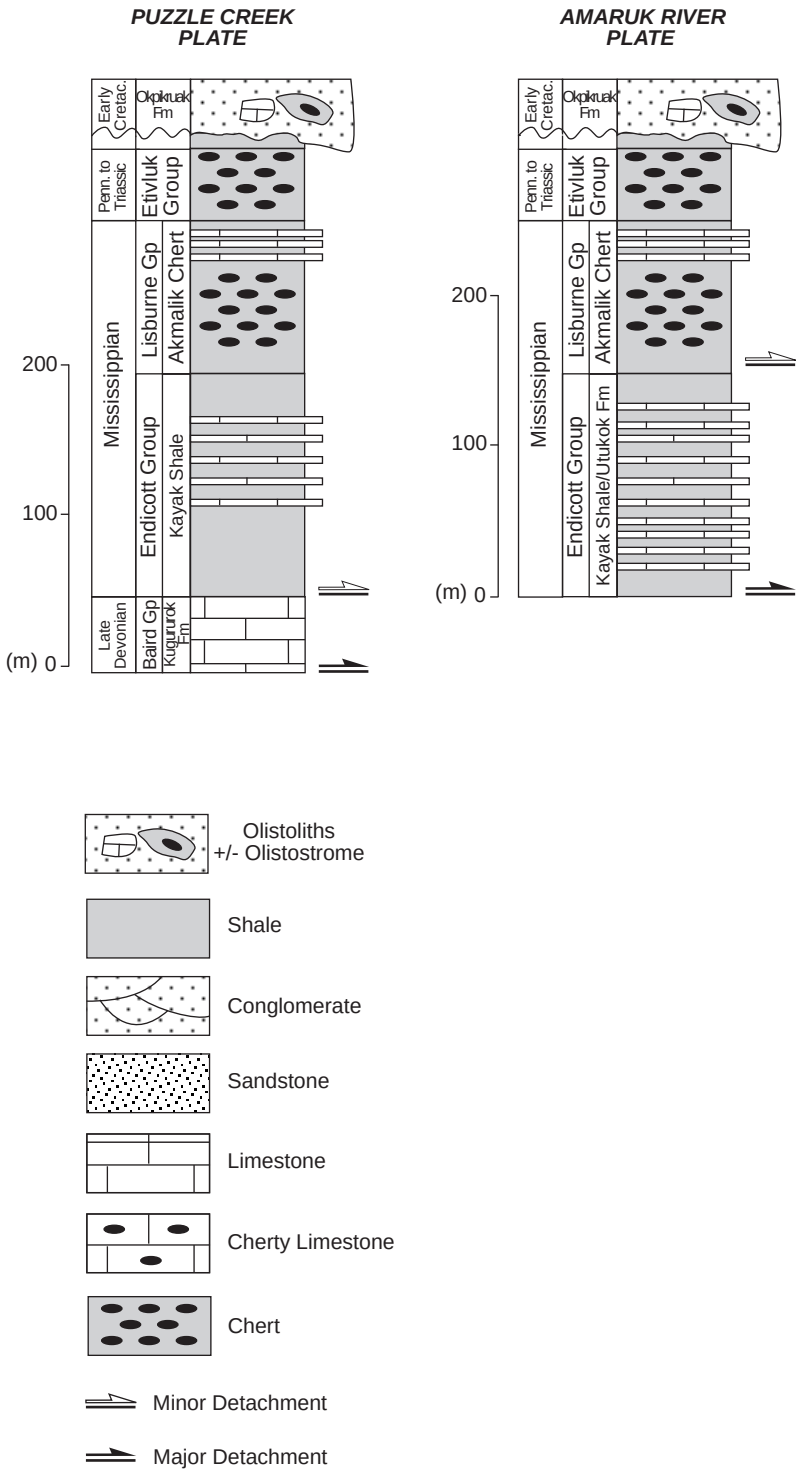


Figure 5.19. Summary stratigraphy of the Picnic Creek allochthon.

Kayak Shale

The Kayak Shale of the Picnic Creek allochthon consists of 20 to 75 m of shales and carbonate layers. Which are lithostratigraphically and faunally similar to the Kayak Shale of the Endicott Group. Fossils include locally abundant crinoids and brachiopods.

Lisburne Group (Early Mississippian – Late Mississippian)

In the Red Dog district, strata of the Lisburne Group in the Picnic Creek allochthon consist of unnamed deep-water siliciclastic and carbonate strata. These are here assigned to the Akmalik Chert (cf. Mull *et al*. 1987*b*), which forms the Lisburne Group of the Picnic Creek allochthon elsewhere in the Brooks Range. In the Red Dog district, these rocks have been previously assigned to Kogruk Formation (Teck Cominco, 2002, *pers. comm*.)

Akmalik Chert (Early Mississippian – Late Mississippian, Osagean – Chesterian)

The Akmalik Chert of the Red Dog district consists of approximately 50 to 100 m of rhythmically bedded and laminated black cherts, shales, grey-weathering limestones and dolomitic limestones (Figs. 5.1, 5.2 & 5.20a – e). Layer thickness typically ranges from 2 to 5 cm and are planar parallel bedded (Fig. 5.20b, c). Sedimentary structures include graded bedding, abundant parallel laminations (Fig. 5.20c), and possible soft deformation structures. In the Red Dog district, the Akmalik Chert also contains grey to whitish recessive-weathering layers and laminae (Fig. 5.20b) that possibly represent silicified former carbonate beds. The upper part of the Akmalik Chert consists dominantly of thin-bedded to laminated grey-weathering limestone, dominantly micritic limestones, grainstones, and black shales (Fig. 5.20e). This contrasts with the Akmalik Chert at its type locality in the central Brooks Range (cf. Mull *et al*. 1987*b*), where it consists almost exclusively of black cherts (C. G. Mull, 2004, *pers. comm.*). The Akmalik Chert is here interpreted as having been deposited in a deep-water setting with limited clastic input, represented by distal turbidites with incomplete Bouma sequences (Td—Te) (e.g. Bouma, 1962; Bouma *et al*. 1985). Turbidites were possibly derived from adjacent carbonate platforms (e.g. Kogruk Formation) (Fig. 5.3).

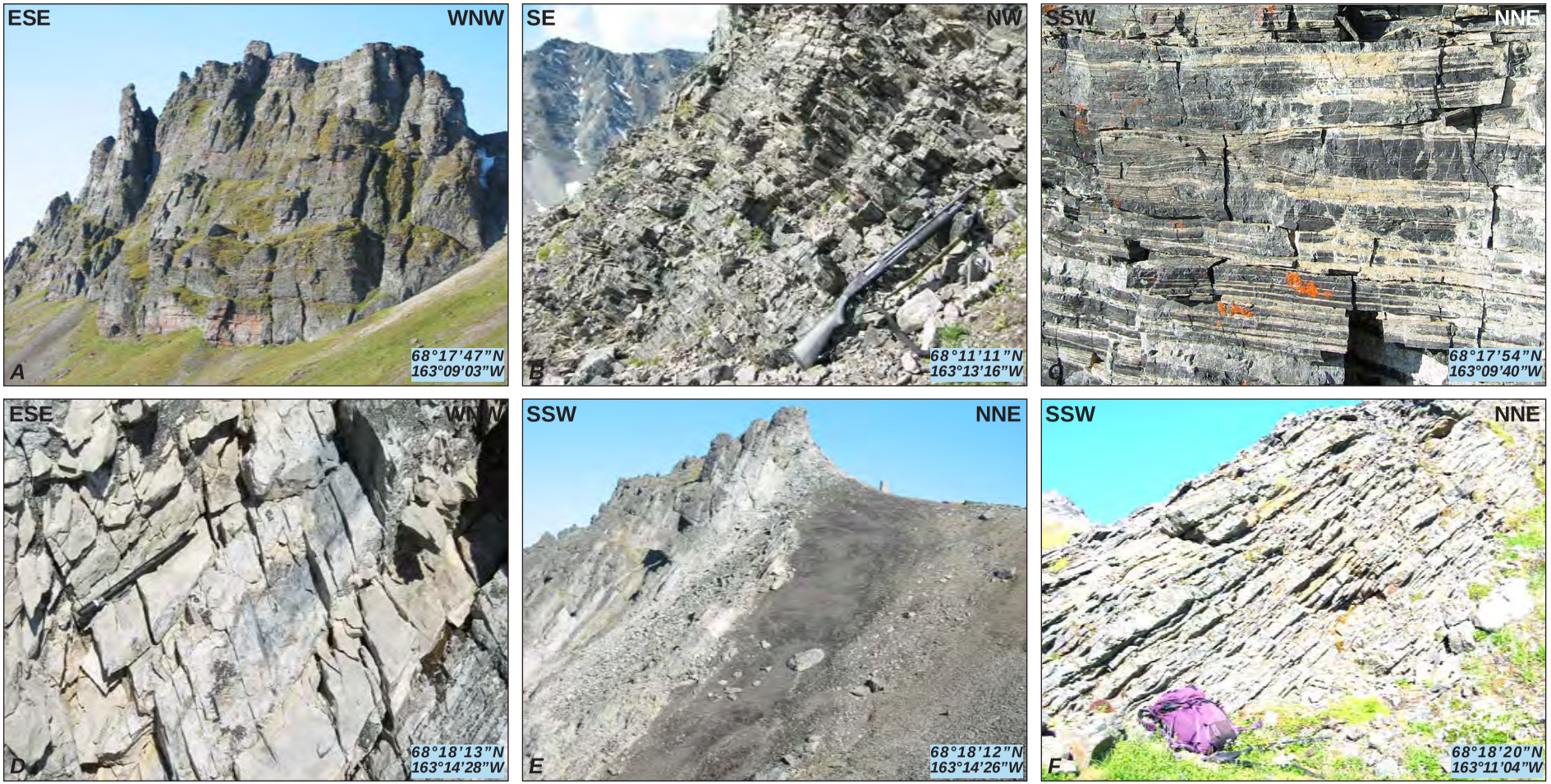


Figure 5.20. Sedimentary features of the Akmalik Chert. **A.** SSW-looking view of well-bedded black cherts of the Akmalik Chert north of the Wulik Peaks. Topographic relief is approximately 75 m. **B.** View of thin-layered black cherts and grey-weathering carbonates in the Chimneys area. Shotgun is approximately 90 cm long. **C.** Detail of interbedded black cherts and grey-weathering grainstones. Note soft-sediment deformation features. **D.** Grey-weathering dolostones and black cherts. **E.** Interbedded grey-weathering grainstones and black cherts overlie recessive weathering black shales. Thickness of outcrop is approximately 15 m. **F.** Detail of condensed cherts of the Etivluk Group of the Picnic Creek allochthon.

Etivluk Group (Chesterian – Bajocian)

The Etivluk Group of the Picnic Creek allochthon consists of approximately 8 to 20 m of wavy to planar bedded thin to thick bedded cherts, grey to green cherts cherts and minor shales (Fig. 5.20f). Layer thickness typically ranges from 5 to 15 cm (Fig. 5.20f). Fossils include sparse radiolaria. The Siksikpuk and Otuk Formations cannot be readily distinguished (Fig. 5.20f). The unit suggests condensation and deposition under starved conditions. The uppermost Etivluk Group contains 1 to 4 m of recessive-weathering maroon to purplish-red mudstones.

5.4.3 Stratigraphy of the Kelly River Allochthon

The Kelly River allochthon of the Red Dog district consists of strata of the Baird, Lisburne and Etivluk Groups (Figs. 5.2 & 5.21). These occur in five lithostratigraphically distinct thrust plates (Fig. 5.21). The Kelly River allochthon consists of strata of the Syn-rift (Baird and Lisburne groups) and Post-rift (Etivluk Group) megasequences (Fig. 5.3). In the Red Dog district the Kelly River allochthon consists of at least five distinct stratigraphic successions that are preserved in individual thrust plates of limited lateral extent (Fig. 5.1). In ascending structural order these are, the Iyichoruk Mountain, Kelly, Amphitheatre Mountain, Wulik Peaks and Chimneys plates (Fig. 5.21). These consist dominantly of platform carbonates of the Lisburne Group. The Kelly River allochthon shows varying degrees of structural disruption and locally grades into Early Cretaceous syn-orogenic olistostrome (Fig. 5.2).

Baird Group (Late Devonian, Frasnian to Fammenian)

The Baird Group in the Red Dog district consists solely of Late Devonian platform strata of the Kugururok Formation (Figs. 5.21 & 5.22). The Baird Group is regionally faulted and its basal contact with older (basement ?) rocks is not exposed.

Kugururok Formation (Fammenian)

The Kugururok Formation of the Kelly River allochthon consists of approximately 10 to 100 m of thin-bedded to massive grey-, bluish grey-, and yellowish-weathering fossiliferous limestones (dominantly packstones, grainstones, and wackestones) together with minor dolostones and mudstones (Fig. 5.22a – c). Fossils are locally abundant, including solitary rugose corals and encrusting bryozoans. The Kugururok

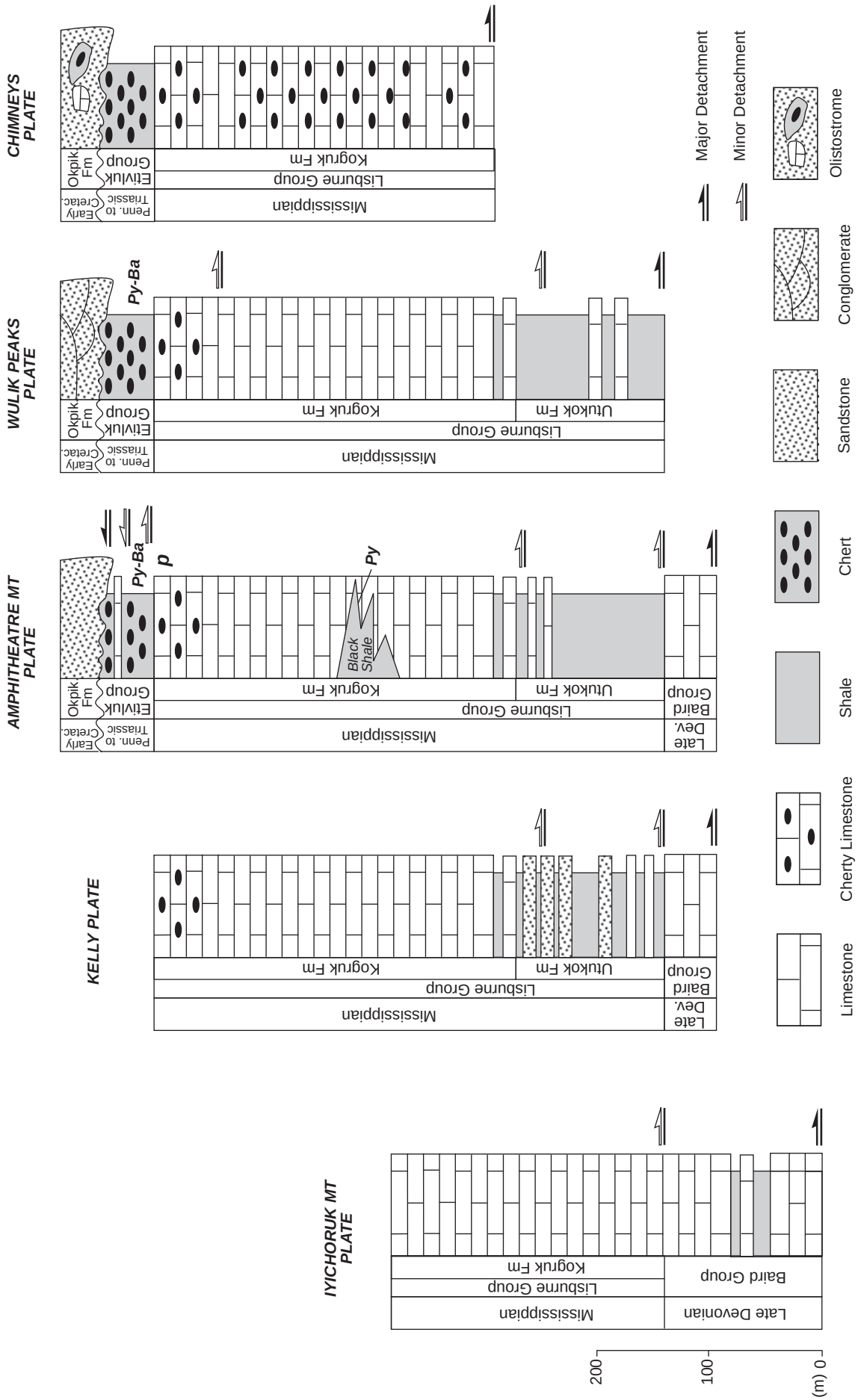


Figure 5.21. Summary stratigraphy of the Kelly River allochthon.

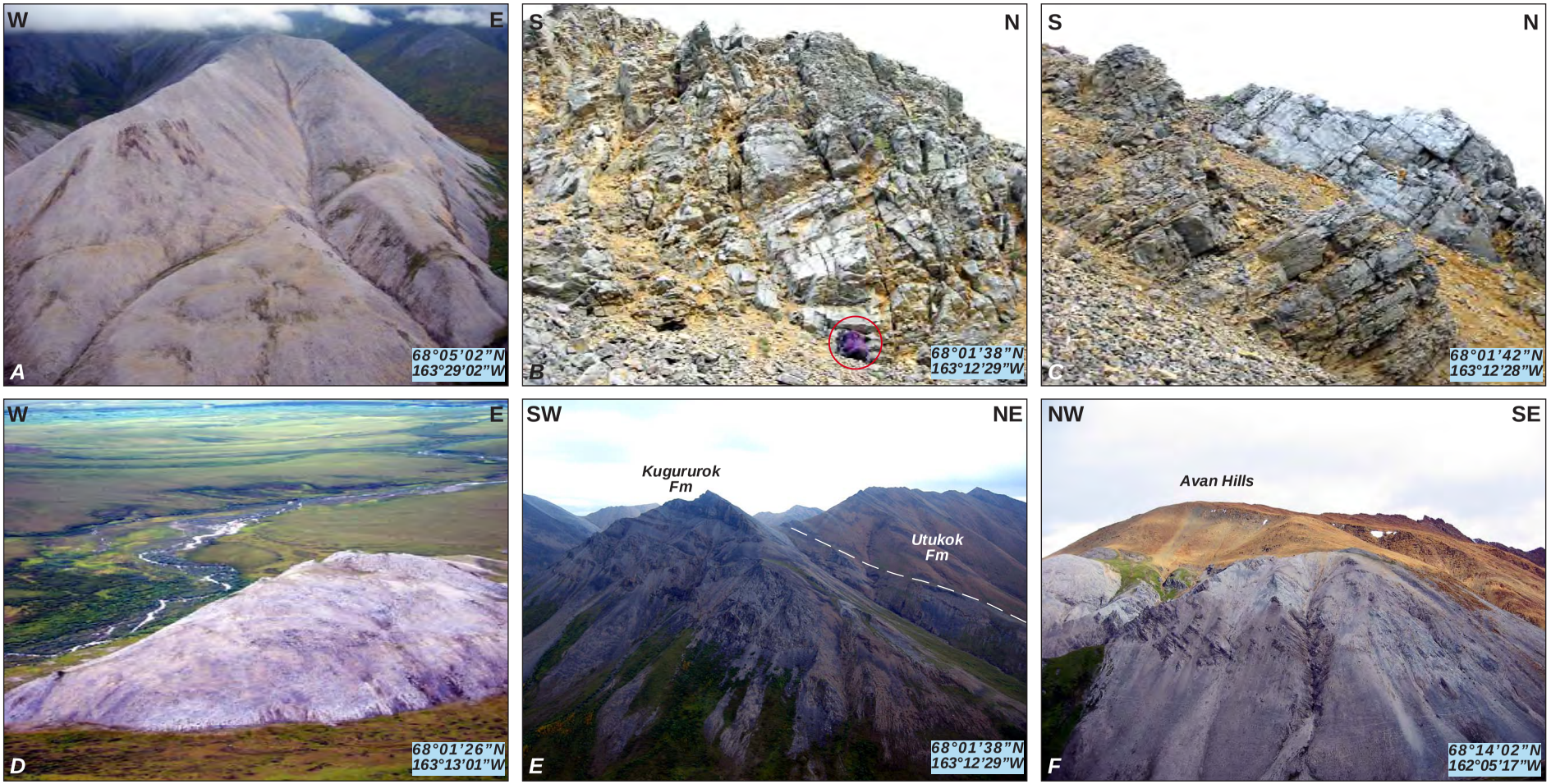


Figure 5.22. Sedimentary features of the Baird Group. **A.** Grey-weathering limestones of the Kugururok Formation near Punuphakhroak Mountain. Topographic relief isapproximately 50 m. **B.** Kugururok Formation grainstones arranged in shallowing- and thining-upwards cycles. Wulik Peak. Backpack is encircled for scale. **C.** Well-bedded fossiliferous wackestones (foreground) and well-bedded to massive packstones (background). Wulik Peak. Thickness is approximately 10 m. **D.** Typical Kugururok Formation rubble outcrop. Near Wulik Peak. Outcrop is approximately 100 m across. **E.** Grey-weathering limestones of the Kugururok Formation underlies orange-weathering strata of the Utukok Formation. Wrench Creek. Topographic relief is approximately 200 m. **F.** Well-bedded grey-weathering limestones of the Kugururok Formation underlie orange-weathering ultramafic rocks. Avan Hills. Topographic relief is approximately 150 m.

Formation is locally organic-rich and contains solid hydrocarbons in the form of pyrobitumen that occurs in intercrystalline porosity. The Kugururok Formation is here interpreted as a fault-block carbonate platform (cf. Bosence, 1998, 2005) that possibly developed on the footwall area of an extensional fault block isolated from siliciclastic supply (Fig. 5.3).

Lisburne Group (Early Mississippian – Late Mississippian)

The Lisburne Group of the Kelly River allochthon consists of carbonate and siliciclastic strata of the Utukok and Kogruk formations. The Lisburne Group is present in all the structural plates of the Kelly River allochthon (Fig. 5.21).

Utukok Formation (Early Mississippian, Osagean)

The Utukok Formation consists dominantly of approximately 10 to 200 m of orange- to grey-weathering fossiliferous impure flaggy limestones (dominantly bioclastic grainstones and wackestones), and shales that conformably overlie the Kugururok Formation of the Baird Group (Figs. 5.2, 5.3, 5.21 & 5.23). The Utukok Formation comprises a large range of lithologies that also include calcareous quartzites, quartzose sandstones, ferruginous sandstones, calcareous sandstones, sandy limestones, and black shales (Fig. 5.23). Sedimentary structures include parallel and cross laminations and possible hummocky stratification. Fossils (Fig. 5.23d) include abundant crinoid, solitary corals and bryozoan bioclasts. Bioturbation is locally abundant and includes bedding-parallel overlapping U-shaped feeding burrows (cf. *Zoophycos*). The Utukok Formation possibly derived from adjacent carbonate platforms (e.g. Kugururok and/or Kogruk formations) (Fig. 5.3). Thickness of carbonate layers varies from 3 to 10 cm approximately. The wide range of lithologies suggests that the Utukok Formation of the Red Dog was deposited in platform to basin settings. The local abundance of quartz and mica in the Utukok Formation suggests that an unrecognized basement source was possibly locally exposed during the Osagean. Possible sources include Syn-rift siliciclastic strata of the Endicott Group or pre-rift basement rocks.

Kogruk Formation (Early Mississippian – Late Mississippian, Osagean – Chesterian)

The Kogruk Formation consists approximately of 200 to 600 m of medium- to thick-bedded white- to grey-weathering fossiliferous limestones (packstones, poorly-sorted

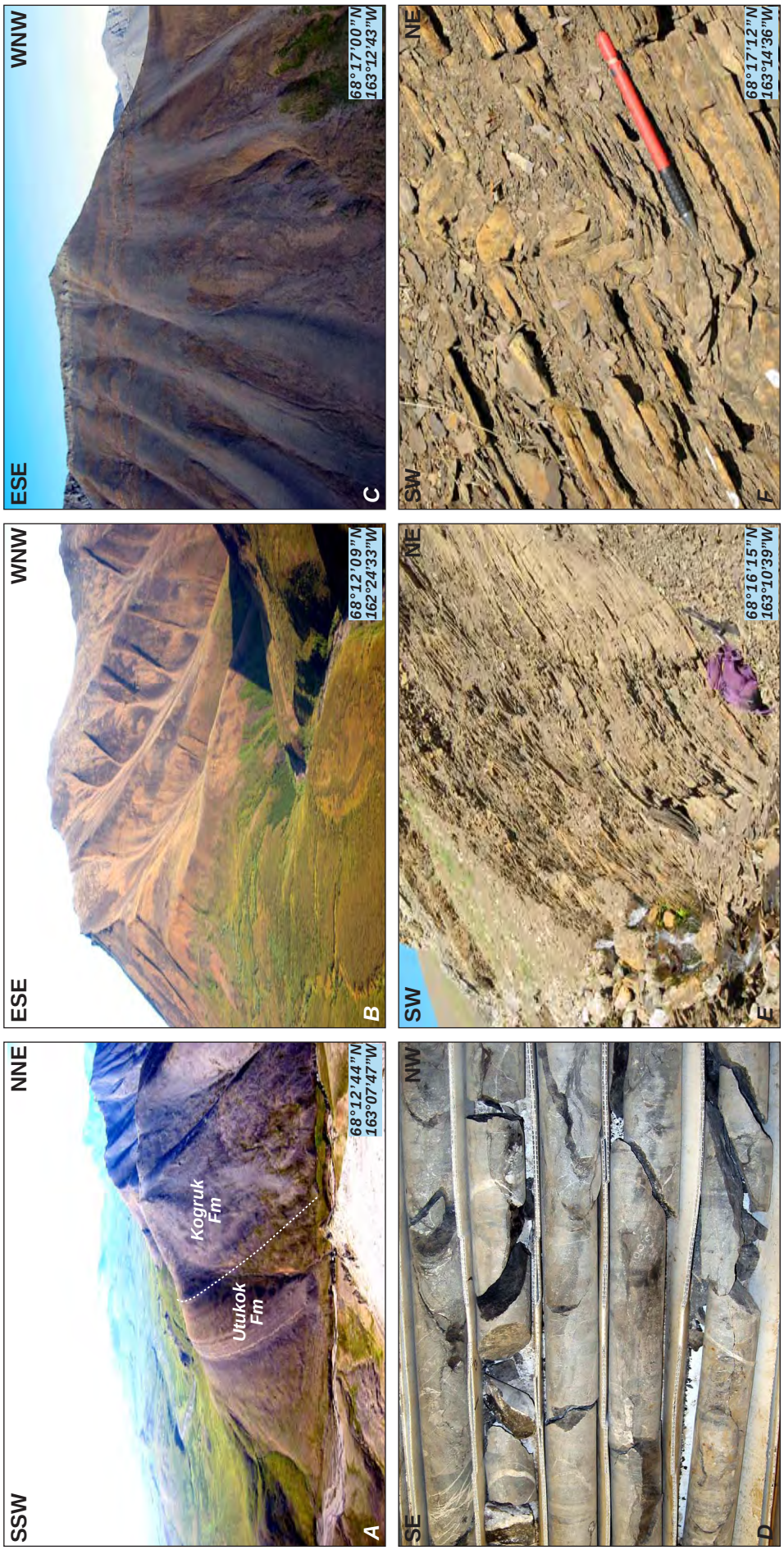


Figure 5.23. Sedimentary features of the Utukok Formation. **A.** Orange-weathering limestones and shales of the Utukok Formation are conformably overlain by grey-weathering limestones of the Kogruk Formation. Topographic relief is approximately 250 m. **B.** Orange-weathering limestones, shales, and calcareous quartzites of the Utukok Formation near Kelly River. Topographic relief is approximately 200 m. **C.** Orange-weathering shales and grainstones of the Utukok Formation in the Wulik Peaks. **D.** Fossiliferous grey limestones in drill core. Note abundant crinoid bioclasts. **E.** Platy micritic limestones, calcarenites, and shales north of the Wulik Peaks. **F.** Detail of shaly limestones near the Wulik River.

wackestones and grainstones) together with locally abundant black cherts, minor mudstones and dolostones that conformably to locally unconformably overlie the Utukok Formation (Figs. 5.2, 5.3, 5.21 & 5.24). Fossils include colonial and solitary rugose corals (*Zaphrentis* sp.), crinoids, spiriferid brachiopods, ostracods, and lesser encrusting bryozoans. The Kogruk Formation also contains locally pyritic black shales (Fig. 5.24e) that resemble strata of the coeval lower Ikalukrok unit of the Kuna Formation (Fig. 5.12). Chert in the Kogruk Formation typically occurs as well- to irregularly-bedded centimetric to metric layers and nodules (Fig. 5.24b, f). Sedimentary textures (Fig. 5.24f) indicate that cherts of the Kogruk Formation resulted largely or entirely from diagenetic alteration.

Previously unreported unconformities occur locally in the Kogruk and Utukok formations (Fig. 5.25a). These are here interpreted as onlap terminations (e.g. Mitchum *et al*. 1977; Cartwright *et al*. 1993) of planar-bedded limestones on to irregular erosive surfaces in the Utukok Formation (Fig. 5.25b). Onlap terminations possibly represent the response of the platforms to syn-rift subsidence. These relationships are possibly correlative with unconformities documented in platform carbonate strata of the Lisburne Group, elsewhere in the Brooks Range (e.g. Schoennagel, 1977; J. A. Dumoulin, 2003, *pers. comm.*).

The uppermost Kogruk Formation locally contains approximately 10 to 50 m of medium- to thin-bedded and locally laminated dark-grey limestones, nodular to bedded black cherts as well as phosphate-rich black shales and mudstones. These strata are equivalent to the Tupik Formation of Sable & Dutro (1961) (cf. Chapter 2, Fig. 2.11), which is here included with the Kogruk Formation. These strata are interpreted as having been deposited in a deep-water environment and overlie in a sharp planar conformable (?) contact shallow water carbonates (Fig. 5.3). This contact is here interpreted to record the onset of drowning of the carbonate platforms of the Lisburne Group. Platform drowning may have resulted from a rapid sea level rise, imminent post-rift thermal subsidence, or a combination of both processes. This facies is locally absent below post-rift strata of the Etivluk Group, which suggests the presence of a depositional hiatus or a disconformity (Fig. 5.3).

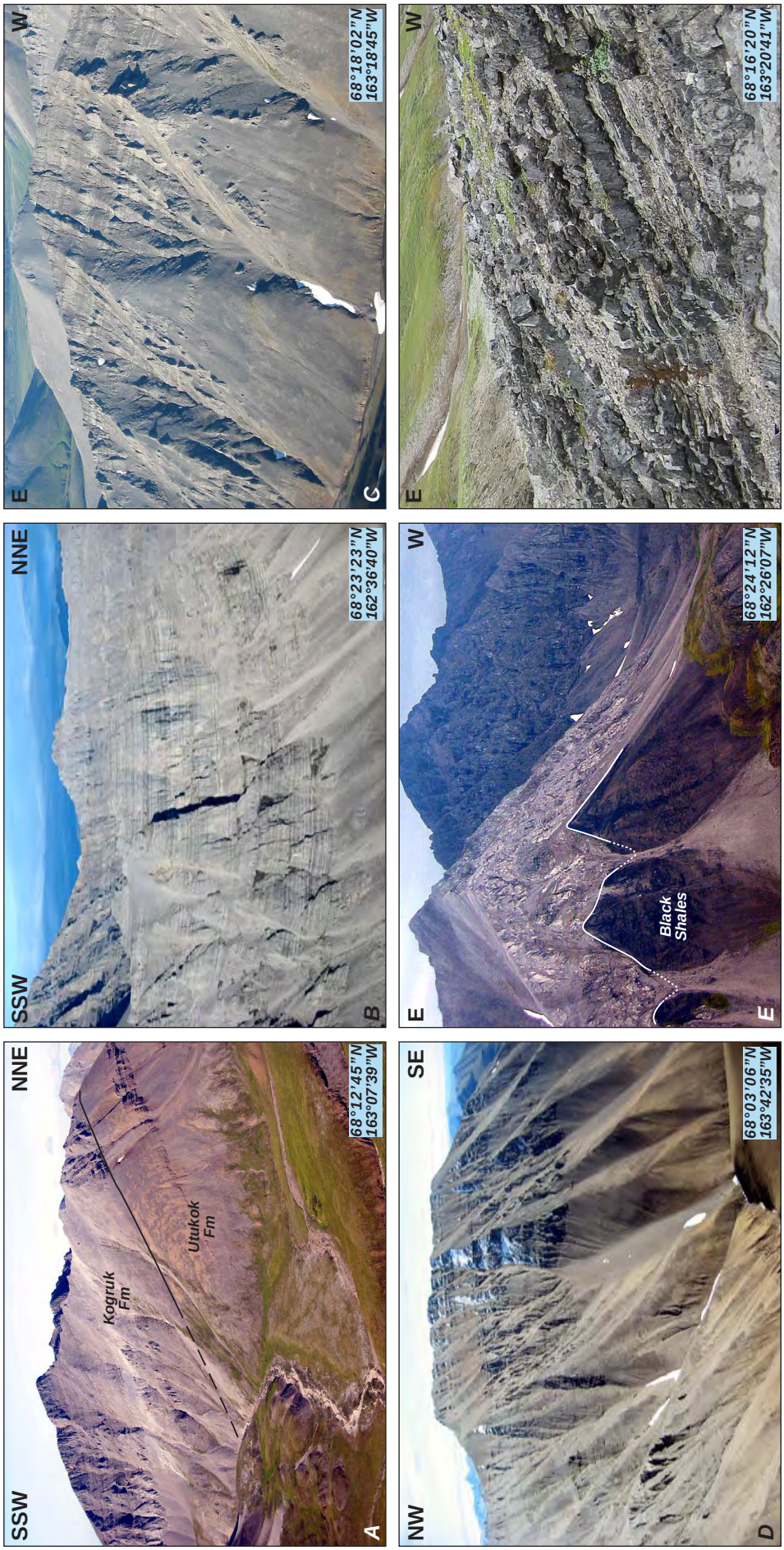


Figure 5.24. Sedimentary features of the Kogruk Formation. **A.** Grey-weathering limestones of the Kogruk Formation conformably overlie distinctive orange-weathering limestones and shales of the Utukok Formation. Wulik Peaks area. Topographic relief is approximately 500 m. **B.** Interbedded grey-weathering limestones and black cherts near Amphitheatre Mountain. Topographic relief is approximately 150 m. **C.** Grey-weathering limestones. Wulik Peaks. Topographic relief is approximately 100 m. **D.** Limestones Topographic relief is approximately 500 m. **E.** Pyritic black shales interbedded with grey-weathering limestones. **F.** Detail of chert replacement textures in limestone. Northern Wulik Peaks. Outcrop is approximately 1.5 m high.

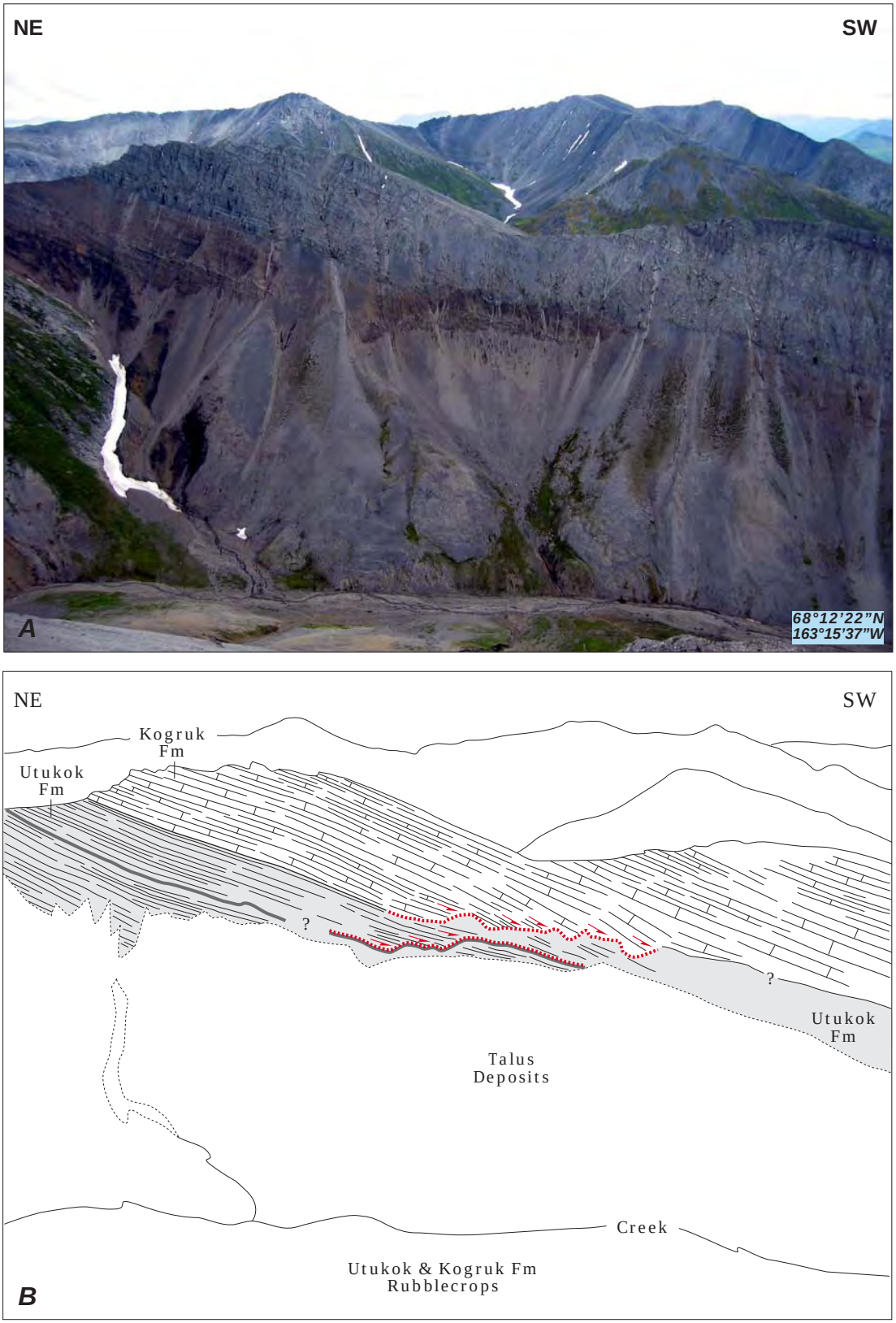


Figure 5.25. Local unconformities in the Utukok and Kogruk formations of the Lisburne Group. **A.** SE-looking view of Mississippian strata of the Lisburne Group. Orange-weathering impure limestones and shales of the Utukok Formation are overlain by well-bedded grey grainstones and packstones of the Kogruk Formation **B.** Line-drawing interpretation of the outcrop showing unconformity surfaces (dashed red lines). Marker bed (grey thick line) is shown for reference. Note onlap terminations of the Kogruk and Utukok formations on to unconformity surfaces. Topographic relief is approximately 150 m. Lik Camp lies approximately 2 km north of this locality.

The Kogruk Formation is here interpreted as having been deposited in a carbonate platform, possibly a subsiding margin platform (e.g. Bosence, 2005) that evolved from a fault-block platform carbonates of the Kugururok Formation (Fig. 5.3).

Etivluk Group (Pennsylvanian – Jurassic)

The Etivluk Group of the Kelly River allochthon consists of a condensed succession of variegated cherts and shales similar to that of the Endicott Mountains allochthon. The Etivluk Group can be locally subdivided into the Siksikpuk and Otuk Formations (Fig. 5.26).

Siksikpuk Formation (Pennsylvanian – Lower Triassic, Morrowan – Griensbachian)

The Siskikpuk Formation (Fig. 5.26) consists of 10 to 30 m of maroon to vermillion red shales that underlie cherts of the Otuk Formation. Shales are locally mineralized with barite laths and centimetric pyrite and marcasite nodules.

Otuk Formation (Lower Triassic – Middle-Late Jurassic, Spatian – Bajocian)

The Otuk Formation of the Kelly River allochthon (Fig. 5.26), although condensed, contains the same stratigraphic units described for the Endicott Mountains allochthon.

Lower Unit

It consists of black to greenish grey shales and minor chert. Shales are locally phosphatic and are mineralized with sparse to locally abundant barite laths and centimetric to decimetric pyrite nodules.

Middle Unit

It contains variegated cherts and rare grey-weathering silicified limestone beds. A marker horizon consisting of black shales occurs in the central part of the unit. Mineralization is locally abundant and includes rounded pyrite nodules, up to 15 cm in diameter, that locally form irregular and discontinuous layers.

Upper Unit

The upper unit consists of approximately 10 to 40 m of dolostones and well-bedded to wavy-bedded cherty dolostones with locally abundant impressions of *Monotis* sp.

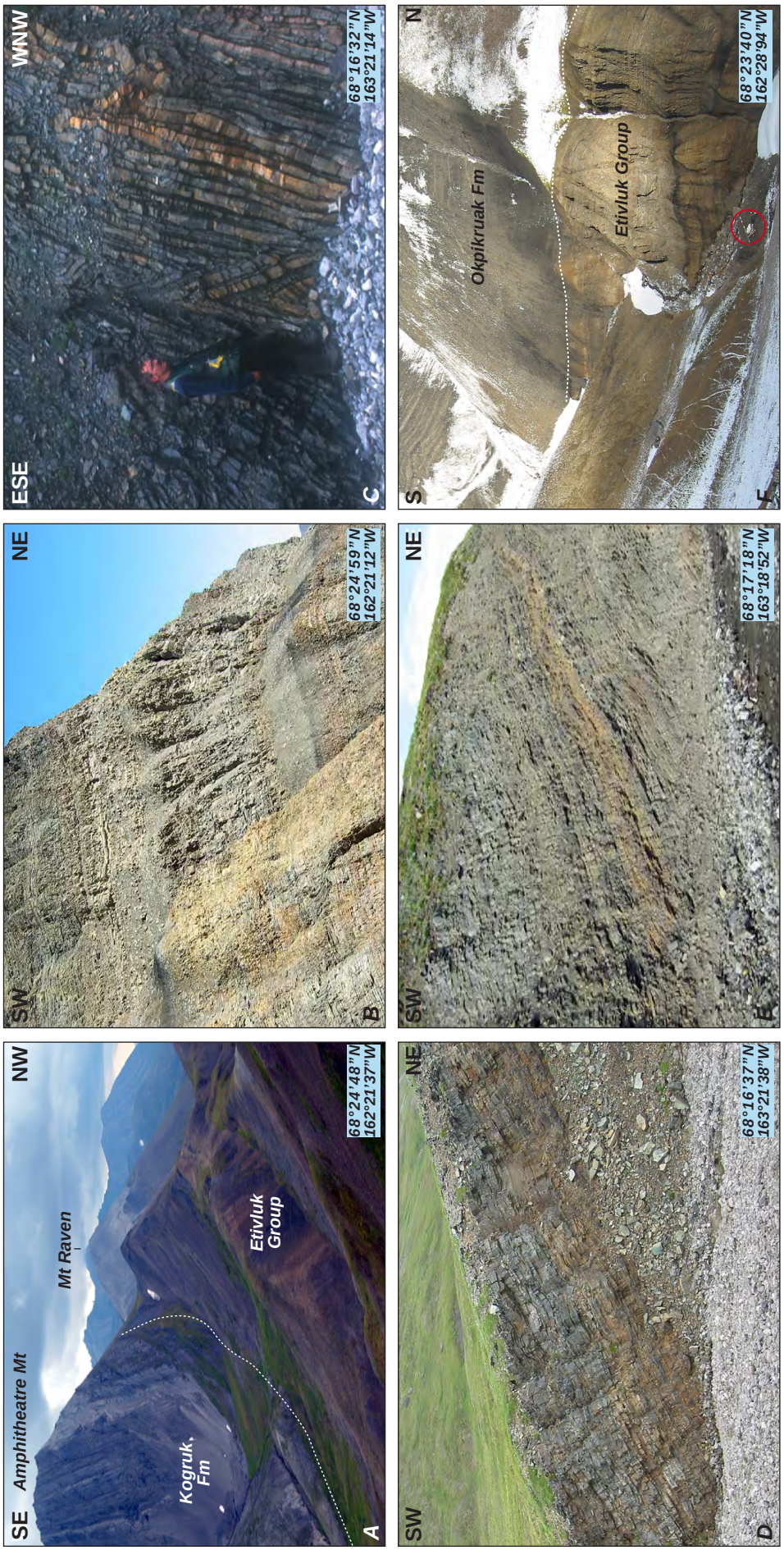


Figure 5.26. Sedimentary features of the Etivluk Group of the Kelly River allochthon. **A.** Buff-weathering shales and cherts of the Siksikpuk Formation conformably overlie grey-weathering well-bedded platform carbonates of the Kogruk Formation. Amphitheatre Mountain. Topographic relief is approximately 200 m. **B.** Well-bedded variegated cherts of the middle Otuk unit. Note black shales and cherts of the marker horizon in the lower right corner of the photograph. **C.** Detail of Otuk Formation cherts in the Wulik Peaks area. Brooks Range geologist Lorne Young for scale. **D.** Cherts of the Otuk Formation. Wulik Peaks. **E.** Buff-weathering dolomite and cherty dolomite of the upper Otuk unit near Wolverine Creek. Note distinctive colour banding. **F.** Cherts and shales of the Otuk Formation underlie turbidites of the Okpikruak Formation. Inaccessible Ridge. Helicopter is encircled for scale.

Centimetric to decimetric layers of grey-weathering dolostone and/or silicified limestone occur near the top of the unit.

5.4.4 Stratigraphy of the Ipnavik River Allochthon

The Ipnavik River allochthon (Fig. 5.27) is locally exposed in the Red Dog district (Fig. 5.2) and consists of Syn-rift strata of the Lisburne Group and Post-rift strata of the Etivluk Group.

Lisburne Group (Early – Late Mississippian)

The Lisburne Group of the Ipnavik River allochthon consists of unnamed deep-water strata here assigned to the Rim Butte unit (cf. Dumoulin *et al*. 1993, 2004) (Figs. 5.2 & 5.3).

Rim Butte Unit (Early – Late Mississippian, Kinderhookian – Meramecian)

The Rim Butte unit consists of approximately 50 to 100 m of black cherts and siliceous mudstones that are rhythmically interbedded with grey-weathering micritic limestones (Figs. 5.1, 5.15 & 5.27). Fossils include sparse radiolaria. Facies associations suggest that the Rim Butte unit was deposited in a slope to basin environment. The Rim Butte unit contains rare metric mafic sills.

Etivluk Group (Pennsylvanian – Jurassic)

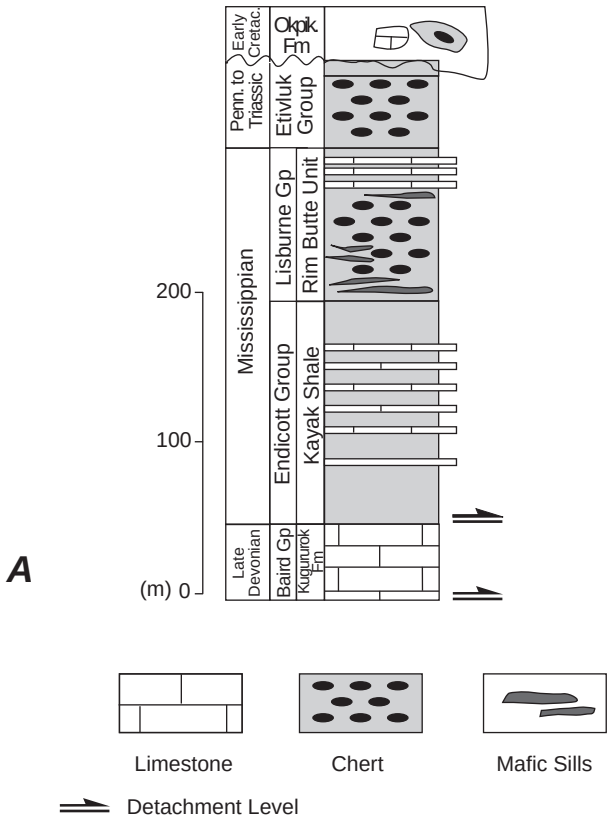
The Etivluk Group of the Ipnavik River allochthon consists of poorly exposed variegated cherts and shales that conformably overlie the Rim Butte unit (Fig. 5.27b).

5.4.5 Stratigraphy of the Nuka Ridge Allochthon

The Nuka Ridge allochthon occurs as isolated thrust sheets that show equivocal relationships with the Okpikruak Formation. In the Red Dog district strata assigned to the Nuka Ridge allochthon occur in large olistoliths in strata of the Brookian unit.

Nuka Formation (Early Mississippian – Pennsylvanian)

The Nuka Formation consists dominantly of grey and brown to reddish medium to thick-bedded coarse- to fine-grained poorly-sorted clast-supported microconglomerates, coarse- to fine-grained immature sandstones, arkoses, arkosic sandstones, calcareous



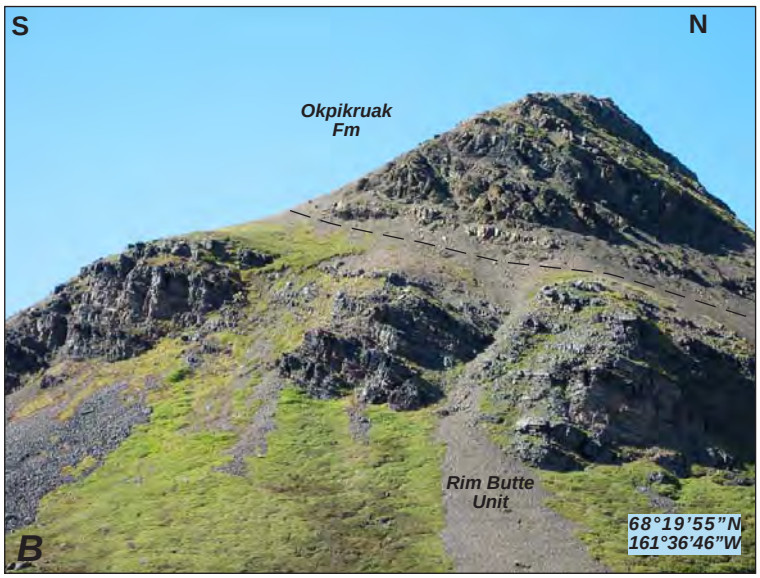


Figure 5.27. Summary stratigraphy of the Ipnavik River allochthon. **A.** Summary stratigraphic column. **B.** Field photograph showing well-bedded cherts of the Rim Butte unit unconformably overlain by the Okpikruak Formation.

arkosic sandstones, and arkosic (?) limestones that conformably (?) overlie strata of the Baird Group and/or the Kayak Shale (Figs. 5.1, 5.15 & 5.28a). Arkosic sandstones typically contain distinctive unaltered and little transported sub-euhedral K-feldspar (microcline) grains together with angular to well-rounded milky quartz, black chert grains and sparse fine-grained authigenic glauconite (Fig. 5.28b). The Nuka Formation in the Red Dog district is dominantly exposed as olistoliths in early syn-orogenic strata of the Brookian Megasequence. Fossils in the Nuka Formation are locally abundant and include crinoid and rhynchonellid brachiopod fragments. Facies associations indicate that the Nuka Formation was deposited in a proximal shallow-water environment. The elevated content in K-feldspar, quartz, and mica suggests provenance from a felsic granitic source, possibly basement rocks exposed in the distal part of the rifted continental margin (e.g. rift shoulder).

5.4.6 Stratigraphy of the Copter Peak Allochthon

The Copter Peak allochthon consists largely of Late Devonian to Jurassic intermediate to mafic extrusive igneous rocks together with variable amounts of interbedded shallow water limestones and pelagic strata (Figs. 5.2, 5.3 & 5.29) that are poorly exposed in the Red Dog district (Fig. 5.1). In the Red Dog district, these include syn-rift Ellesmerian strata of the Baird Group and basalts of the Copter Peak volcanic unit (Fig. 5.3).

Baird Group (Late Devonian, Frasnian – Fammenian)

The Baird Group of the Copter Peak allochthon consist of platform carbonates here assigned to the Kugururok unit that are locally interstratified with basaltic rocks of the Copter Peak volcanic unit (Fig. 5.30).

Kugururok Formation (Late Devonian, Frasnian – Fammenian)

The Kugururok Formation of the Copter Peak allochthon consists dominantly of grey-weathering platform carbonates, including glauconitic impure limestone, locally rich in K-feldspar (microcline). The Kugururok Formation is locally intruded by mafic sills (Fig. 5.30a). Mafic sills occur at two localities 1 km southwest of Punupkahkroak Mountain (latitude 68°04’35”N, longitude 163°23’06”W and latitude 68°05’32”N, longitude 163°23’33”W) (Fig. 5.1) and also at several localities east of the Avan Hills (Fig. 5.30). Sills consists of 1 to 2 m-thick leucocratic to brownish-weathering

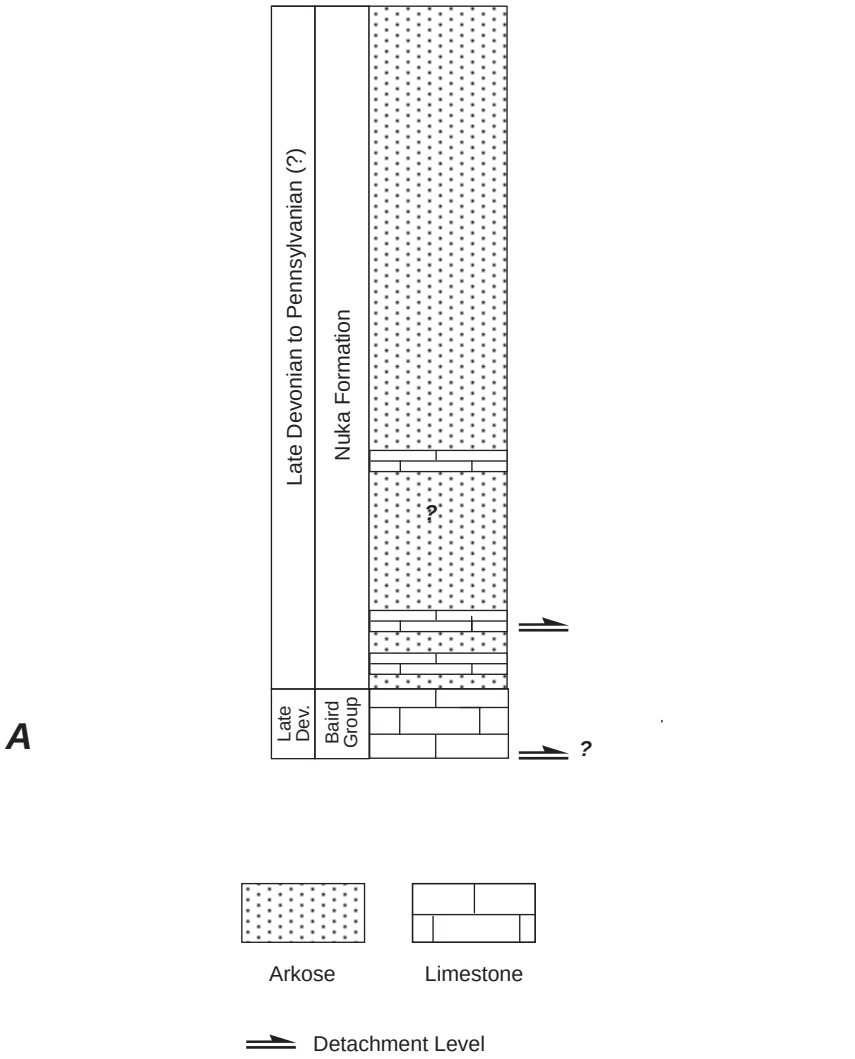


Figure 5.28. Summary stratigraphy of the Nuka Ridge allochthon. **A.** Interpretive stratigraphic column constructed from isolated outcrops (not to scale). **B.** Hand specimen of arkose of the Nuka Formation. Note K-feldspar clasts.

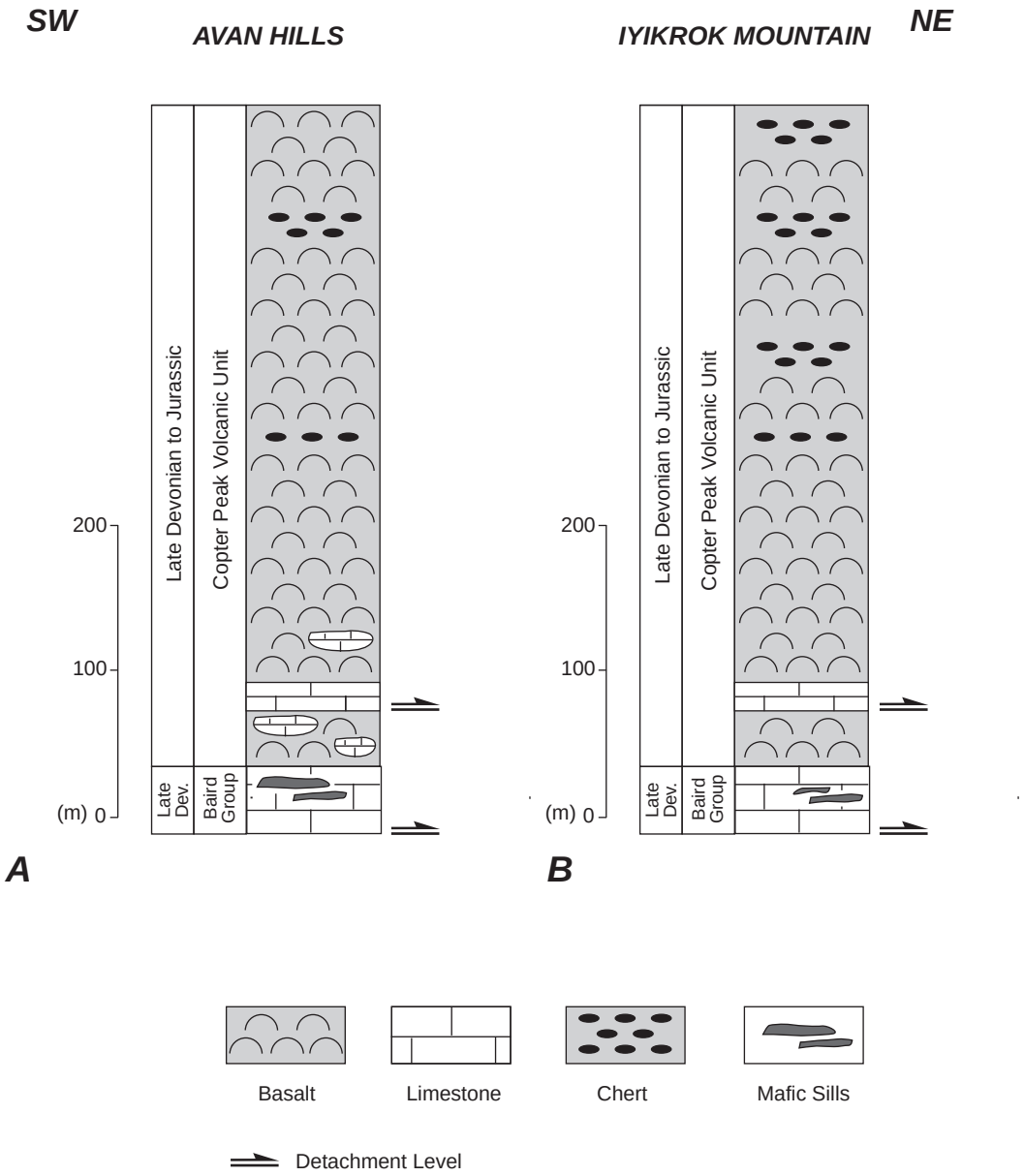


Figure 5.29. Summary stratigraphy of the Copter Peak allochthon compiled from observations near Iyikrok Mountain (A) and the Avan Hills (B).

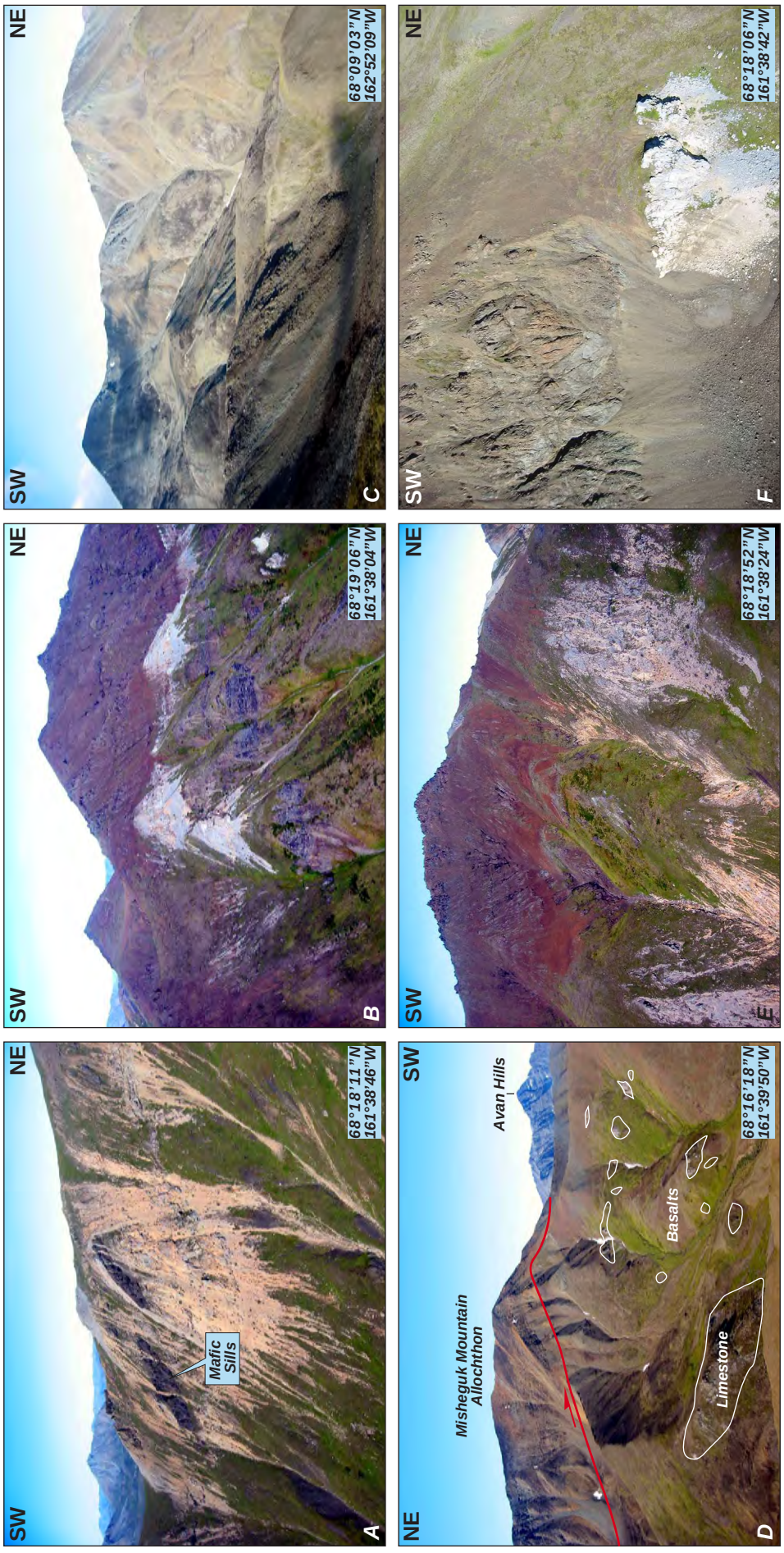


Figure 5.30. Sedimentary features of the Copter Peak allochthon. **A.** Grey-weathering arkosic limestones with metric brown-weathering mafic sills. Note pinky salmon colours in limestone associated to altered feldspar. Topographic relief is approximately 75 m. **B.** Basalts overlying platform carbonates. Topographic relief is approximately 150 m. **C.** Grey to reddish-weathering basalts of the Copter Peak volcanic unit. Topographic relief is approximately 200 m. **D.** Basalts with isolated limestone blocks. Topographic relief is approximately 200 m. **E.** Red-weathering basalts overlie grey-weathering arkosic limestone. Avan Hills. Topographic relief is approximately 100 m. **F.** Detail of relationship between grey-weathering limestone and volcanic rocks. Note melange-like texture in the volcanic rocks. Topographic relief is approximately 25 m.

melanocratic diorite with ophitic texture composed of plagioclase and aegirine-augite clinopyroxene. Sills are bedding parallel and show well developed millimetric to centimetric chilled margins. Sills typically occur spatially related to pink salmon-weathering arkosic limestones. These strata were previously assigned to the Nuka Ridge allochthon (e.g. Curtis *et al*. 1990; Moore *et al*. 1994), to the Ipnavik River allochthon (e.g. Mayfield *et al*. 1990), and the Kelly River allochthon (e.g. Moore *et al*. 1986; Young, 2004).

Copter Peak Volcanic Unit (Late Devonian – Late Jurassic)

The Copter Peak volcanic unit (Figs. 5.2, 5.3, 5.29 & 5.30) is informally introduced in this study to refer to unnamed volcanic rocks of the Copter Peak allochthon. These consist of grey, greenish- and reddish-weathering, fine-grained and dominantly aphyric to porphyritic basalts (Fig. 5.30) with rare amphibole euhedral to sub-euhedral hornblende phenocrysts (approximately 1 mm in size). Basalts are sparsely amygdaloidal and vesicular and show intergranular, intersertal, or ophitic to sub-ophitic textures. Alteration is common and includes abundant chlorite, calcite, chalcedony, albite, and epidote. Basalts are locally interstratified with layered to massive grey-weathering limestone and grey- to pink-weathering arkosic limestones of the Kugururok Formation of the Baird Group (Figs. 5.30). Locally, limestones occur as isolated metric to decametric blocks included in basaltic lavas (Fig. 5.30d). These carbonate rocks were previously assigned to the Nuka Formation of the Nuka Ridge allochthon (e.g. Curtis *et al*. 1990) (cf. Chapter 2, Fig. 2.11). Basaltic rocks include documented ages that span from Late Devonian to Early Jurassic (e.g. Moore *et al*. 1994; Young, 2004) (Fig. 5.2). Basalts of the Copter Peak volcanic unit were previously interpreted as seamounts of the Angayucham terrane (Moore *et al*. 1994; Young, 2004) that were accreted to the continental margin of the Arctic Alaska terrane during the Brookian orogeny (cf. Chapter 2, Fig. 2.6). Stratigraphic relationships and age relationships suggest that the Copter Peak volcanic unit formed from basaltic flows that were locally interstratified with carbonate platform strata in the distal part of the ancient continental margin of Arctic Alaska (Fig. 5.3).

5.5 STRATIGRAPHY OF THE ANGAYUCHAM TERRANE

In the Red Dog district, the Angayucham terrane consists of a relatively undisrupted and ordered igneous succession of Middle Jurassic ultramafic, mafic, and felsic igneous rocks together with minor metamorphic rocks that are preserved in the Misheguk Mountain allochthon (Figs. 5.2 & 5.31). The Angayucham terrane structurally overlies continental margin strata of the Arctic Alaska terrane.

5.5.1 Igneous Stratigraphy of the Misheguk Mountain Allochthon

The Misheguk Mountain allochthon in the Red Dog district consists of Jurassic felsic to ultramafic rocks and minor metamorphic rocks (Figs. 5.2, 5.31, 5.32 & 5.33). The Misheguk Mountain allochthon is exposed in the Iyikrok Mountain and Avan Hills areas, 35 km southwest and 36 km northeast of the Red Dog mine, respectively (Fig. 5.1). The Misheguk Mountains allochthon is here subdivided into four units. From the base to the top of the allochthon these are, the metamorphic sole unit, isotropic ultramafic unit, layered ultramafic unit, and layered gabbro unit (Fig. 5.31).

Metamorphic Sole Unit (Middle Jurassic)

The metamorphic sole unit consists of 2 to 10 m of metamorphic rocks, dominantly amphibolites that are exposed at the base of the Misheguk Mountain allochthon in the Iyikrok Mountain area (Fig. 5.31). The metamorphic sole unit has not been identified in the Avan Hills covered during this study (Fig. 5.31) but has been reported and described by Harris (1992, 1998, 2004) further east. The base of the unit is a regional thrust fault (Fig. 5.31).

Isotropic Ultramafic Unit (Middle Jurassic)

The base of the ultramafic unit consists approximately of 3 to 20 m of recessive-weathering dark green to black serpentinites with distinctive tectonic foliation and waxy lustre (Fig. 5.32a). Serpentinites consist dominantly of chrysotile and lizardite with rare relics of porphyroclastic-textured harzburgites and finely disseminated magnetite. Serpentinites are overlain by approximately 750 to 1.5 km of peridotites (Fig. 5.32). Peridotites are dun orange-weathering chromite-bearing serpentinized dunites and wherlites that show a distinctive ‘elephant-skin’ texture (Fig. 5.32b, d-f). Serpentinization typically ranges from 10 to 80% and occurs as a gently- to

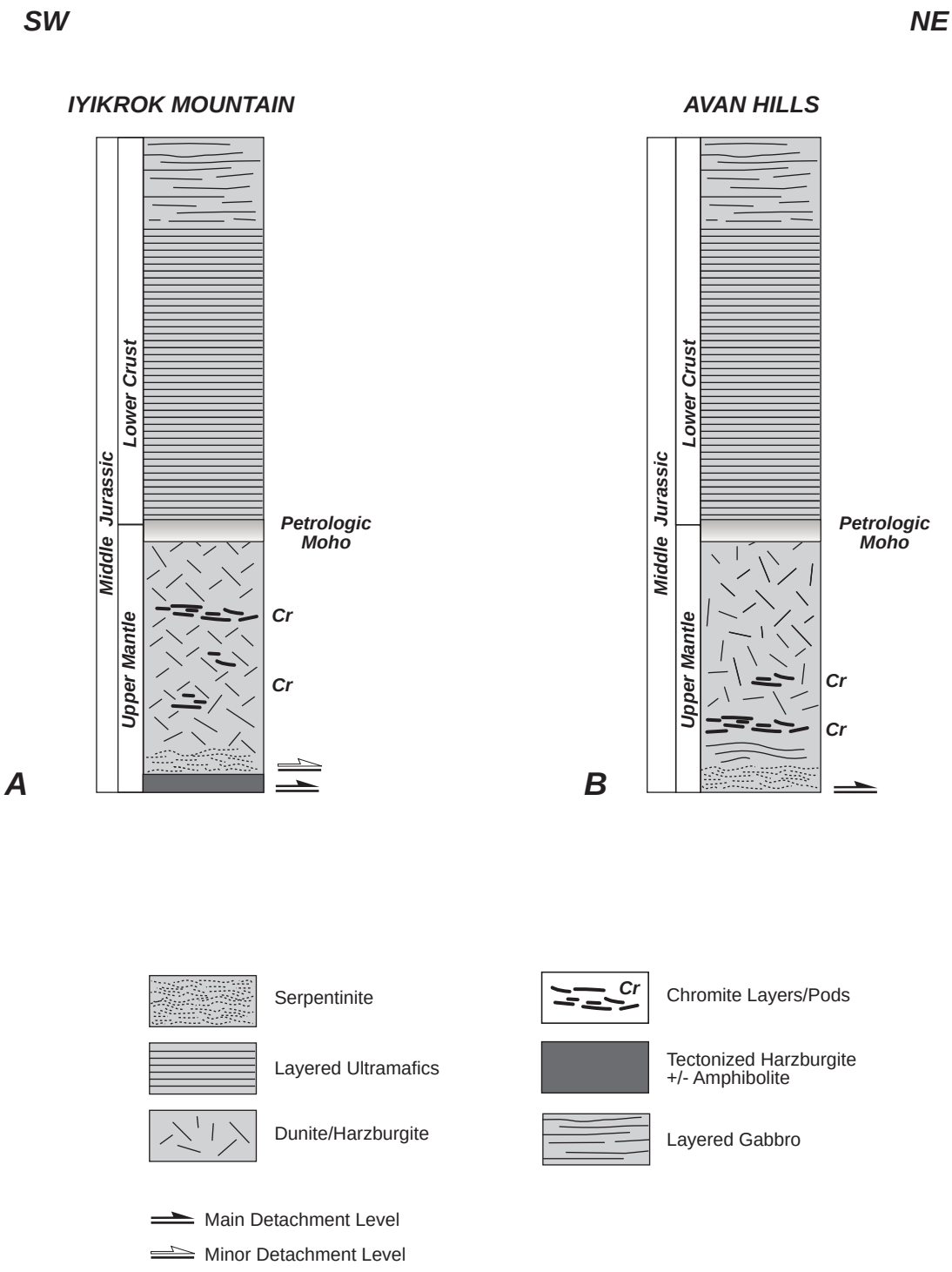


Figure 5.31. Summary igneous stratigraphy of the Misheguk Mountain allochthon. **A.** Iyikrok Mountain. **B.** Avan Hills. Approximate position of the petrologic Moho is shown schematically. Note chromite mineralization near the base of the allochthon. Columns not to scale.

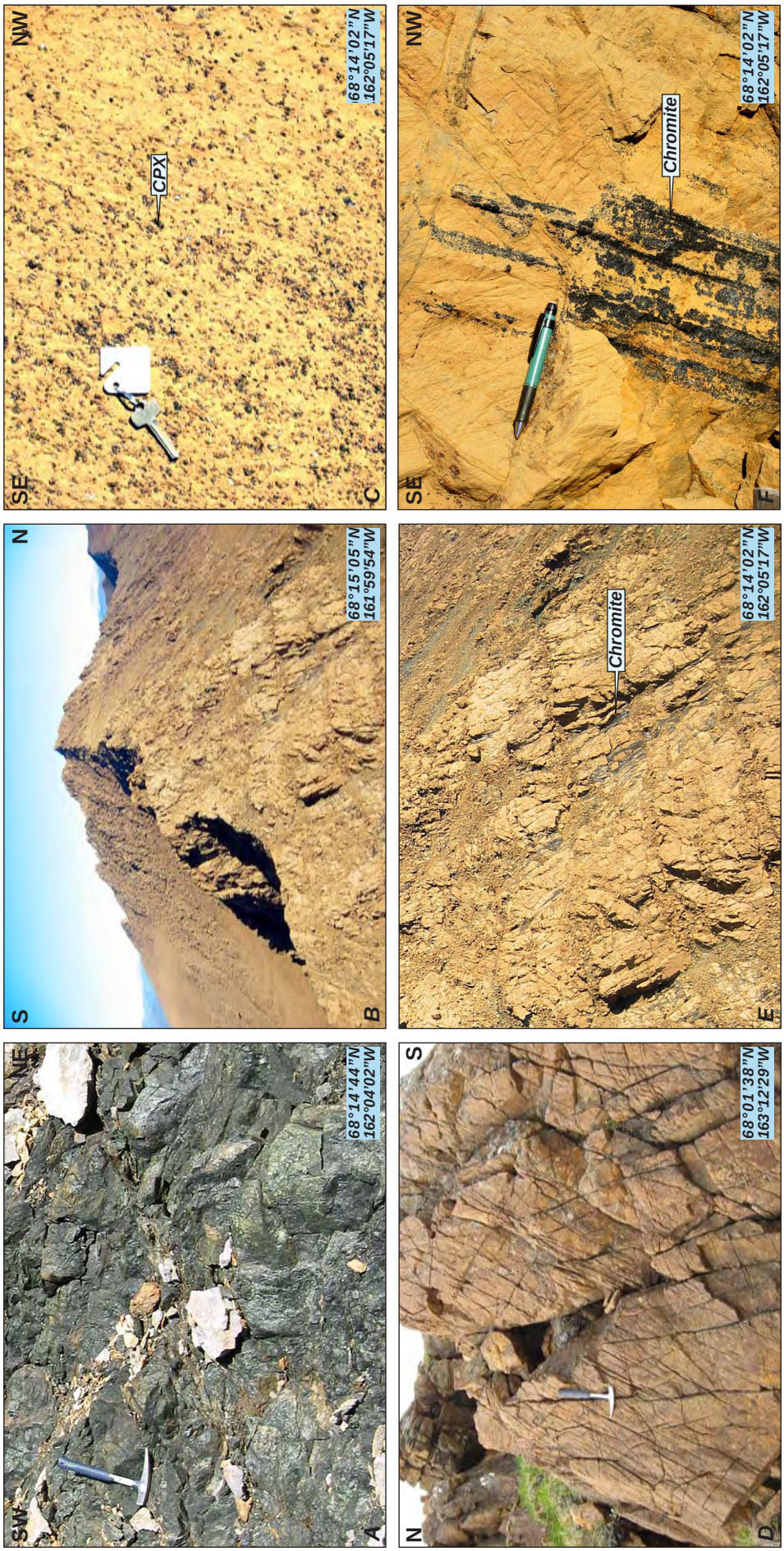


Figure 5.32. Rock units of the Angayucham Terrane. **A.** Dark green tectonized serpentinites. **B.** W-looking oblique aerial view of orange-weathering serpentinized dunites. Avan Hills. Topographic relief is approximately 200 m. **C.** Porphyritic texture with green clinopyroxene phenocrysts in serpentinized olivine matrix. Avan Hills. **D.** Brown-weathering unserpentinized peridotite. Iyikrok Mountain. **E.** Serpentinized dunites with metric irregular chromitite layers and pods. Avan Hills. Field of view is approximately 25 m. **F.** Disseminated and layered chromite in serpentinized dunite. Note well developed 'elephant-skin' texture in the dunite host. Avan Hills.

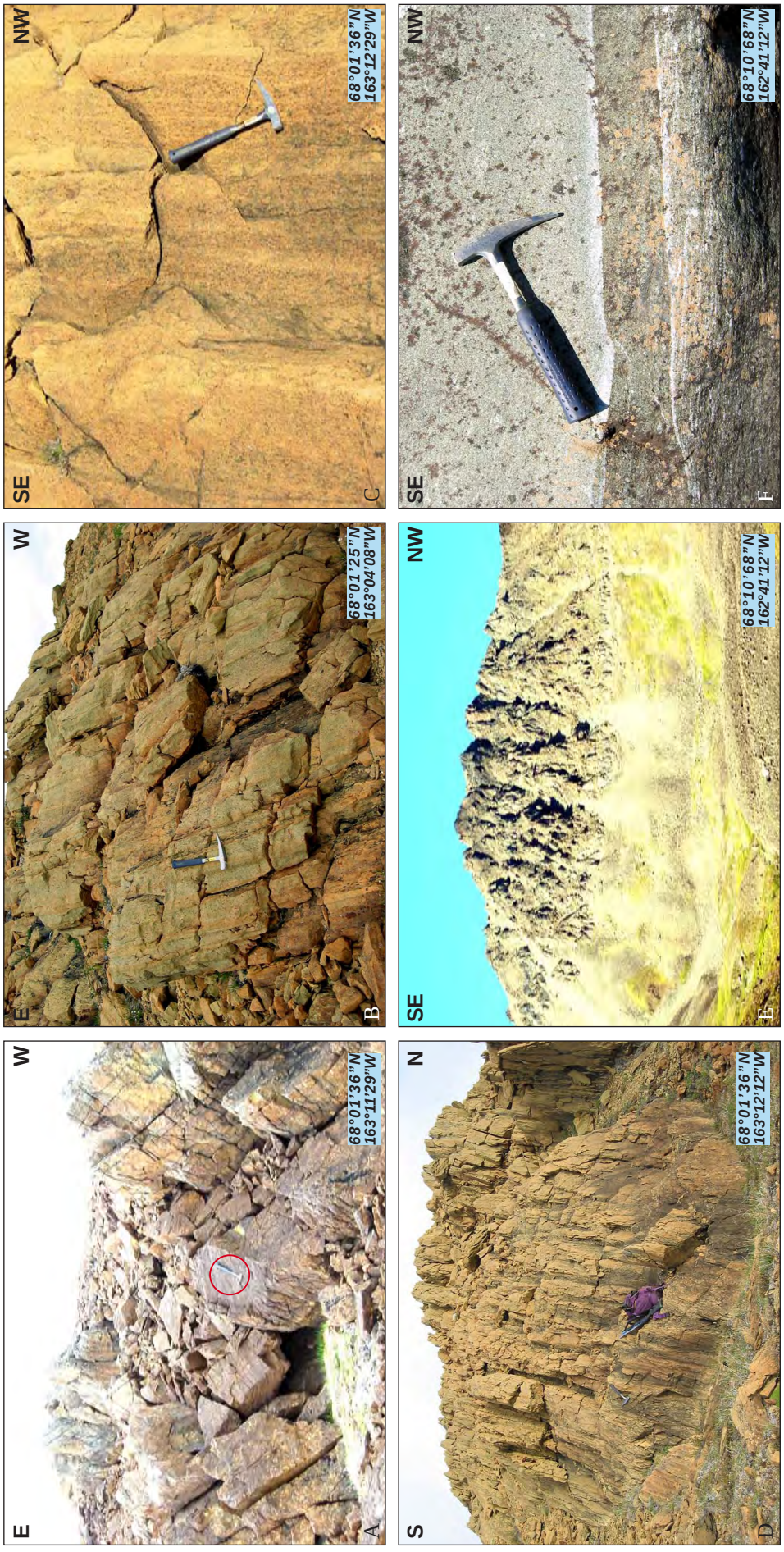


Figure 5.33. Rock units of the Angayucham terrane. **A.** Partly to non-serpentinized dunites near Iyikrok Mountain. Geological hammer encircled for scale. **B.** Layered dunites and pyroxenites at Iyikrok Mountain. **C.** Ultramafic cumulates at Iyikrok Mountain. **D.** Banded dunites and pyroxenites at Iyikrok Mountain. **E.** Layered gabbros near the Avan Hills. Topographic relief is approximately 100 m. **F.** Detail of layered gabbro near the Avan Hills.

sub-horizontally-dipping halo in the basal part of the unit. This halo is oriented highly oblique to steeply-dipping fabrics and magmatic layering. Serpentinized and partially serpentinized dunites typically show mesh texture with olivine relicts. Unserpentinized dunites have allotriomorphic to granular (gabbroic) textures and are locally porphyritic and rich in pyroxene. Pyroxene occurs as emerald green euhedral to sub-euhedral orthopyroxene (augite-enstatite series) and clinopyroxene (diopside-augite series) phenocrysts (1mm to 0.5 cm in diameter) that weather out of the matrix of orange-weathering severely serpentinized olivine (Fig. 5.32c). Clinopyroxene becomes more abundant towards the base of the unit. Overlying the serpentinized dunites are weakly- to non-serpentinized brown-weathering dunites (Fig. 5.32d).

Dunites are extensively mineralized with chromite, which becomes more abundant towards of the base of the unit (Fig. 5.32f). Chromite typically occurs as disseminated (3 to 5%) fine-grained metallic black grains and polycrystalline, rounded aggregates. These form highly resistant discontinuous parallel grainy layers and irregularly distributed pods of chromitite that weather out of the serpentinized dunite host (Fig. 5.32e). Associated minerals include magnetite and iddingsite. Individual chromite grains are 0.2 to 1.5 mm in size. Individual chromite layers range from 2 to 10 cm in thickness (Fig. 5.32e), whereas pods and lenses occur in clusters that range in size from a few centimetres to 1 m (Fig. 5.32e). Chromite is possibly of cumulate origin.

Associated to the ultramafic unit are rare centimetric to metric granitoid intrusions and planar pegmatite dykes with centimetric chilled margins. These intrusives are possibly late in origin and largely post-date crystallization of the unit. The isotropic ultramafic unit is here interpreted as highly depleted peridotites that resulted from partial melting in the upper mantle.

Layered Ultramafic Unit (Middle Jurassic)

Overlying the ultramafic unit are 700 to 2000 m of ultramafic cumulates that consist of varying amounts of clinopyroxene, olivine, and Ca-plagioclase that form conspicuous cumulate textures. Magmatic layering is defined by varying olivine-to-pyroxene ratios (1:2 to 1:10) and changes in grain size, which form graded cumulates with cyclic mineral and phase layering (Fig. 5.33f). Layer thickness typically ranges from 5 mm to

20 cm. Layer thickness and grain size decreases upwards. Clinopyroxene is dominant and locally forms distinctive centimetric layers of emerald green orthopyroxenite and websterite.

Layered Gabbro Unit (Middle Jurassic)

The layered ultramafic unit is overlain by at least 1000 m of layered gabbros. These consist of varying amounts of Ca-plagioclase, clinopyroxene, orthopyroxene, and amphibole (hornblende), which form alternating centimetric to metric melanocratic norite and leucocratic nortite to anorthosite layers with phaneritic granular to aphanitic textures (Fig. 5.33f). Layer thickness and grain size appears to decrease upwards. Layering contacts are typically sharp and characterized by pervasive layer-parallel shear fabrics and mineral flow lineations that have partly or entirely disrupted the original cumulate textures (Fig. 5.33f).

5.5.2 Tectonic Affinity of the Angayucham Terrane

The mineral parageneses and mineralization described above (Figs. 5.31 – 5.33) indicate an oceanic upper mantle to lower crust affinity for the rocks of the Angayucham terrane. Ultramafic rocks of the Angayucham terrane are believed to have crystallized in Middle Jurassic time (e.g. Moore *et al*. 1994; Harris, 1998, 2004; Young, 2004) and are here interpreted as having formed off the Late Devonian to Jurassic rifted ancient continental margin of Arctic Alaska as part of an ophiolite that possibly formed in a supra-subduction setting (cf. Hawkins, 2003; Pearce, 2003). The base of the layered ultramafic unit is here interpreted as the upper mantle to lower crust transition (i.e petrologic Moho) (Fig. 5.31). The crystallization sequence of the ultramafic rocks of the Angayucham terrane is characteristic of supra-subduction zone ophiolites (e.g. Gass, 1990; Hawkins, 2003; Pearce, 2003). This is also supported by the presence of podiform chromite mineralization (Fig. 5.33), which typically forms from highly depleted residua in supra-subduction zone ophiolites (e.g. Coleman, 1971, 1977; Boudier & Nicolas, 1985; Roberts, 1992; Dilek, 2003; Moores, 2003).

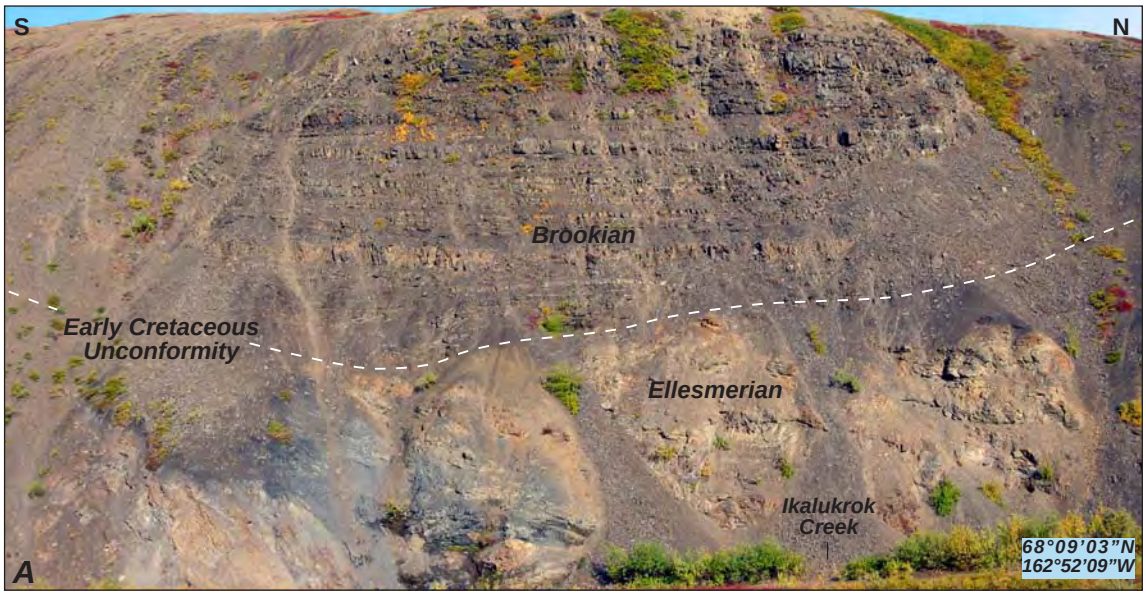
5.6 FORELAND BASIN STRATIGRAPHY

The Brookian stratigraphic unit in the Red Dog district consists of Early Cretaceous syn-orogenic deep marine strata deposited during the Brookian orogeny on the advancing western Brooks Range fold and thrust belt and also in the adjacent North Slope foreland basin (Figs. 2.4 & 2.5). The Brookian unit is separated from the Ellesmerian strata by the Early Cretaceous unconformity (Figs. 5.3 & 5.34). The Early Cretaceous unconformity is commonly an angular unconformity and more locally a disconformity (Fig. 5.34a). The Brookian stratigraphy is interpreted as having been deposited in a deep-marine environment, below the effect of the storm-wave base or surface currents. This implies that the Early Cretaceous unconformity is the result of submarine erosion, probably related to sedimentation on submarine canyons or channels. The Brookian unit is extensively exposed in the study area and makes up approximately 60% of the exposures of the study area. This section provides the first detailed descriptions of the syn-orogenic strata of the Red Dog district and the western Brooks Range.

The Brookian stratigraphy has been further subdivided into two distinct megasequences. From the oldest to the youngest, these are the early and late Syn-orogenic Megasequences (Fig. 5.3). The early Syn-orogenic Megasequence consists of the early Okpikruak Formation (Fig. 5.3). The late Syn-orogenic Megasequence consists of the late Okpikruak and the Fortress Mountain formations (Fig. 5.3). The 'early' and 'late' syn-orogenic megasequences defined in this study broadly correlate with the phases of *flysch* and *molasse* deposition used in the analysis of many orogenic belts (e.g. Allen *et al*. 1986). The terms 'early' and 'late' syn-orogenic are however preferred in that the terms *flysch* and *molasse* imply genetic relationships that may not be certainly applicable to the syn-orogenic strata of the Red Dog district and the Brooks Range.

5.6.1 Early Syn-orogenic Megasequence (Late Jurassic ? - Early Cretaceous)

The early Syn-orogenic Megasequence consist of large volumes of deep marine clastic strata that record deposition of the earliest syn-orogenic strata of the western Brooks Range fold and thrust belt in the Red Dog district. The Early Syn-orogenic Megasequence contains abundant olistoliths and internally coherent decametric to kilometric disrupted thrust sheets or gravity slide sheets of older strata of the Syn-rift



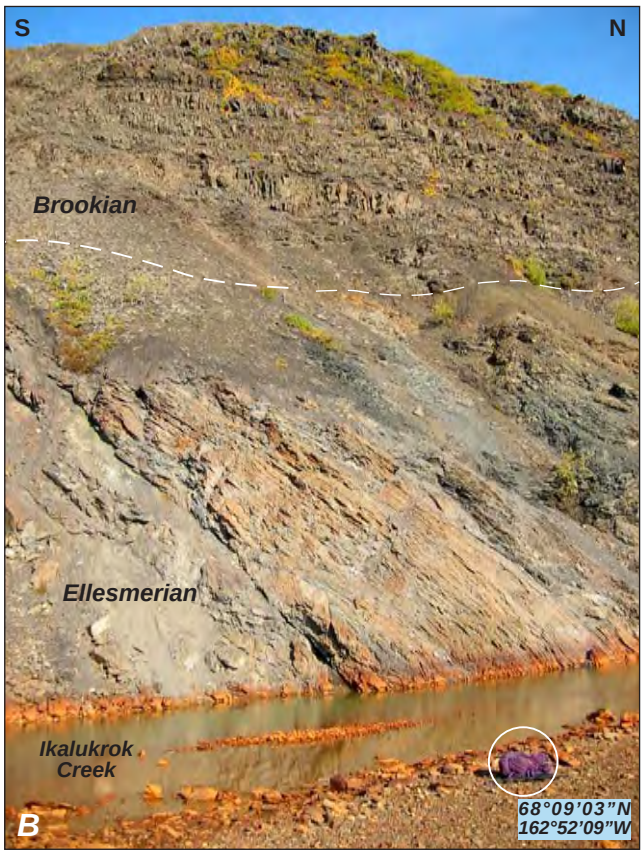


Figure 5.34. Early Cretaceous unconformity. **A.** W-looking photomosaic showing strata of the Brookian unit unconformably overlying the Ellesmerian unit. Field of view is approximately 50 m. Topographic relief is approximately 25 m. Alvinella, Ikalukrok Creek. **B.** Detail of angular unconformity. Subhorizontally-dipping strata of the Okpikruak Formation lie unconformably on steeply-dipping strata of the Etivluk Group. Unconformity angle is approximately 30°. Note bright-orange precipitate gossan (jarosite) along creek bed, related to oxidation of nearby massive sulphide showings (also see Fig. 5.14e). Alvinella, Ikalukrok Creek. Backpack is encircled for scale.

and Post-rift megasequences of the Ellesmerian unit (Fig. 5.3). The basal Megasequence boundary is the Early Cretaceous unconformity (Figs. 5.3 & 5.34). The upper boundary of the Megasequence is commonly marked by a thrust fault that separates the syn-orogenic strata from older and pre-orogenic Ellesmerian stratigraphy. The early Syn-orogenic sequence comprises the early Okpikruak Formation.

Early Okpikruak Formation (Late Jurassic – Early Cretaceous, Berriasaian - Valangian)

The early Okpikruak Formation consists of conglomerates, microconglomerates, sandstones, greywackes, siltstones, shales, mudstones, and rare bioclastic calcarenites (Fig. 5.35). These form turbidites and olistostromes that unconformably to disconformably overlie strata of the Ellesmerian Megasequence (Figs. 5.3 & 5.34). The early Okpikruak Formation lies more commonly unconformably on Permian and Triassic strata of the Etivluk Group (Figs. 5.3 & 5.35a), specifically on the upper or middle units of the Siksikpuk and Otuk formations, respectively. However, the Okpikruak Formation locally unconformably overlies older strata, including the Mississippian Ikalukrok unit of the Kuna Formation. This suggests high rates of submarine erosion and incision during syn-orogenic deposition. The early Okpikruak Formation can be subdivided into proximal and distal facies.

Proximal Facies

The proximal facies of the early Okpikruak Formation is characterized by gravity-driven deposits, including olistostromes and turbidites (Figs. 5.35 & 5.36). In the Red Dog district, olistostromes occur as chaotic sedimentary deposits that consist of mappable distinct, older rock fragments, blocks, and/or sheets (olistoliths) emplaced in a poorly-sorted fine- to coarse-grained sedimentary matrix. Olistostromes are interpreted as having been deposited by thrust-related mass-wasting and gravity sliding processes in a deep marine environment. These deposits are here interpreted as A1 facies of Pickering *et al.* (1989). The distinctive feature of olistostrome in the Red Dog district is the occurrence of metric to kilometric chaotic and lithostratigraphically distinct blocks or olistoliths that occur at the same stratigraphic level within the early Okpikruak Formation (Fig. 5.36). Olistostromes show no true bedding, except for large clasts or olistoliths of previously bedded and consolidated sediment (Fig. 5.36).

Figure 5.35. Sedimentary features of the early Okpikruak Formation. **A.** Coarse-grained sandstone and shale disconformably overlie distinctive maroon to red-weathering mudstone (Ipewik-type facies) of the Etivluk Group. North of Wulik Peaks. Backpack encircled for scale. **B.** Detail of sandstone and shale forming turbidite cycles. Wulik Peaks. **C.** Conglomerate unconformably overlying medium-to fine-grained sandstone. Near Lik Camp. **D.** Turbidite channels. Ikalukrok Creek. Backpack encircled for scale. **E.** Polymictic conglomerate. Note rounded igneous clasts and dominantly angular sedimentary clasts. Punukphakroak Mountain. 10 cm long gun shell encircled for scale. **F.** Polymictic conglomerate with abundant clasts derived from the middle and upper units of the Otuk Formation near the Wulik Peaks.

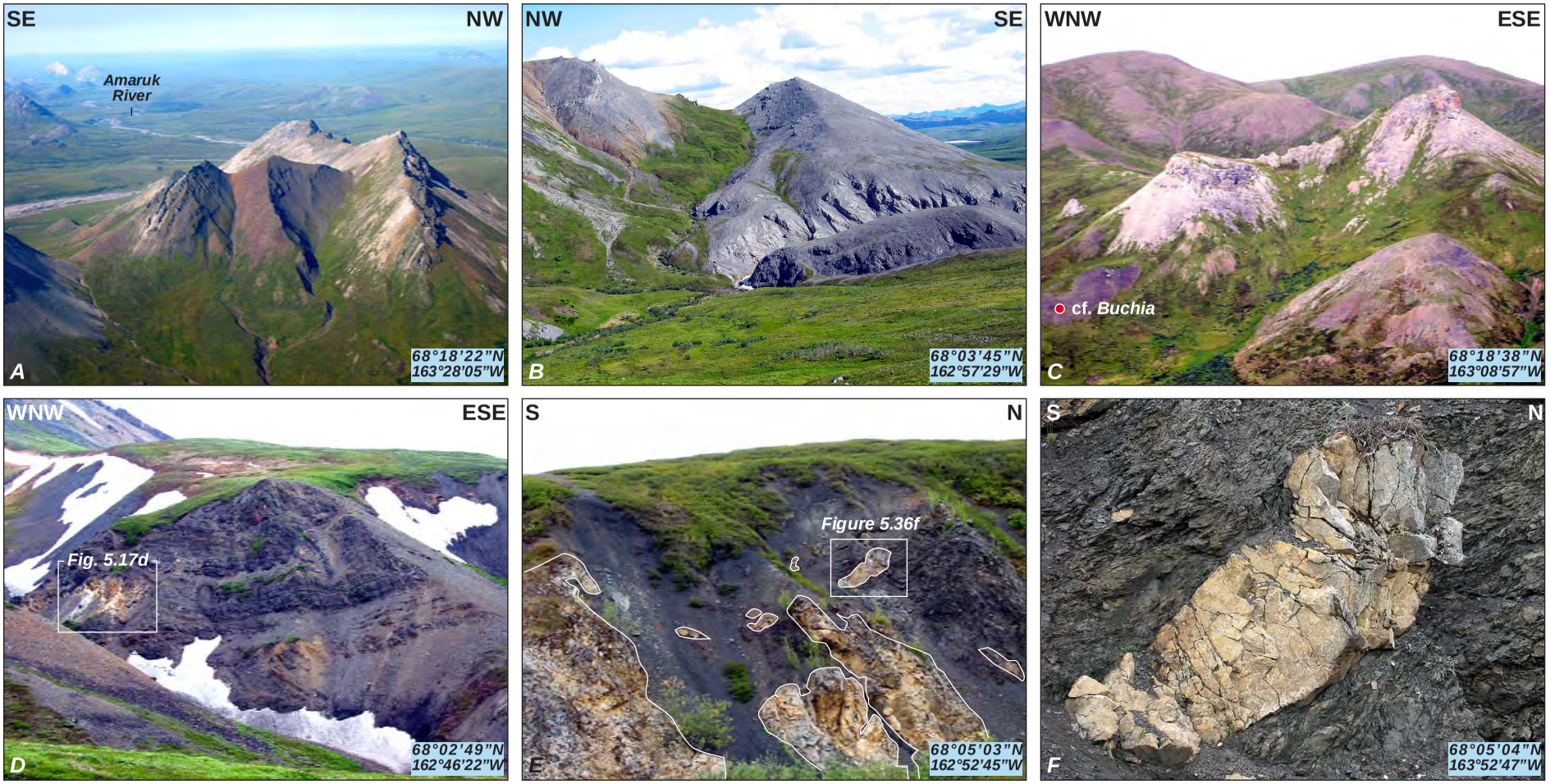


Figure 5.36. Sedimentary features of the Okpikruak Formation olistostrome. **A.** SSW-looking oblique aerial view of sheet-like olistoliths of Akmalik Chert in red-weathering coarse-grained sandstone of the Okpikruak Formation. Near headwaters of Amaruk River. Topographic relief is approximately 75 m. **B**. Exotic Kinderhookian limestone olistolith in Okpikruak Formation. Olistolith is approximately 300 m across. Near Lik Camp. **C.** Kogruk Formation olistoliths in Okpikruak Formation mudstone, sandstone, and conglomerate. The location for cf. *Buchia* is shown. Topographic relief is approximately 50 m. North of Wulik Peaks. **D.** Otuk Formation olistolith in Okpikruak Formation shale. Note internal deformation. Near Deadlock Mountain. Topographic relief is approximately 20 m. **E.** Olistolith of pyrobitumen-bearing dolostone and limestone of the undivided Lisburne Group in Okpikruak Formation shales. North Basin. Topographic relief is approximately 20 m. **F.** Detail of olistoliths shown in **E**.

Previous studies in the Red Dog district (e.g. Moore *et al*. 1986; Curtis *et al*. 1990; Ellersieck *et al*. 1990*a*; Mayfield *et al*. 1990) have interpreted these large blocks as thrust sheet klippen and/or windows of older strata on the Okpikruak Formation.

The regional distribution of olistostrome and the volume and size of olistoliths in the Red Dog district gradually decreases to the northeast and northwest. Olistoliths are particularly abundant in the area comprised between the Wrench Creek and Sivukat Mountain faults, specifically along Su Valley, approximately 20 km west-northwest of the Red Dog mine, and also along the Amaruk River, approximately 45 km northwest of the Red Dog mine. Olistostromes and olistoliths in the Okpikruak Formation become rare north of the Wrench Creek fault. Larger olistoliths occur as blocks and sheets that are commonly internally deformed (Fig. 5.36). Internal deformation shows evidence for syn-sedimentary and tectonic origin. Tectonic deformation includes folding and thrust faulting that pre-date, are synchronous with, and/or post-date the incorporation of the olistoliths into the early Okpikruak Formation matrix. Evidence for syn-sedimentary deformation includes widespread distorted bedding and layer-parallel extension, including necking, boudinage, and shear fractures. Outcrop-scale syn-sedimentary 'surge zones' with extensional trailing edges and contractional leading edges also locally occur.

Olistoliths are very diverse in size, shape, and lithology (Figs. 5.35 & 5.36). Olistolith size typically ranges from metric blocks (Fig. 5.36f) to sheets with areal dimensions of up to 5 km^2 (Fig. 5.36a-c, e). Olistolith shape commonly ranges from isometric (Fig. 5.36d), lens-like (Fig. 5.36f), sheet-like (Fig. 5.36a) to irregular (Fig. 5.36e). Hectometric olistoliths are typically derived from more competent units (e.g. Kogruk Formation platform carbonates of the Kelly River allochthon). Metric olistoliths typically consist of cherts and shales (e.g. Siksikpuk and Otuk Formation of the Endicott Mountains allochthon). Olistoliths are commonly hosted in mudstones and shales, or more locally in inversely- to normal-graded, poorly- to well-sorted and dominantly

matrix-supported polymictic conglomerate and medium- to thick-bedded, well- to poorly-sorted, coarse- to fine-grained sandstone and shale (Figs. 5.35c, e, f & 5.36e, f). Larger olistoliths have preferred orientations and appear to follow the regional structural patterns. Smaller olistoliths are locally oriented parallel to tectonic fabrics in the Okpikruak Formation host. Clast supported monomictic conglomerates with angular to sub-angular chert clasts are also common. These are here interpreted as locally derived deposits. Olistoliths and clasts commonly form 30% to 40% of the total volume of olistostromal deposits. Most conglomerates are poorly sorted and lack stratification, grading, or preferred clast orientation (Fig. 5.35e). Crude c-axis clast imbrication is locally developed in better-sorted conglomeratic beds (Fig. 5.35c). Clast composition varies significantly and includes angular to well-rounded clasts of igneous (ultramafic, mafic, and intermediate extrusive and intrusive rocks), metamorphic, and sedimentary rocks (Figs. 5.35c, e, f). This indicates significant spatial variations in the available sources during syn-orogenic sedimentation. Sedimentary clasts include widespread angular to rounded chert clasts derived from the middle and upper units of the Otuk Formation (Fig. 5.35f) and carbonate clasts derived from the Lisburne Group (Fig. 5.35e). These latter include widespread olistoliths of grey-weathering limestone derived from the Kogruk Formation and pyrobitumen-bearing dolostones derived from the undivided Lisburne Group (Fig. 5.36e). This latter relationship has implications for regional fluid flow during the Brookian orogeny. Metamorphic clasts include schist and orthogneiss. Identified igneous clasts include basalt, granite, peridotites, serpentinized peridotites, diorites, and gabbros and are dominantly matrix supported, but locally allow point contacts. Matrix varies from coarse-grained (coarse sand) to fine-grained (silt and mud size).

Olistoliths are particularly abundant in the vicinity of the Red Dog mine (within a 5 km radius), where laterally discontinuous thrust sheet remnants of the Red Dog plate of the Endicott Mountains allochthon are spatially related with at least 130 metric to hectometric olistoliths that can be identified from surface mapping. At least 26 of these olistoliths consist of strata of the Ikalukrok unit. Olistoliths are rare to absent in the northern part of the Red Dog district (Fig. 5.1).

Facies distribution and structure of deposits suggest that olistostrome deposition involved a variety of transport mechanisms. The presence of hectometric to kilometric sheet-like bodies of Early Mississippian to Triassic strata included in Early Cretaceous Okpikruak Formation (Fig. 5.36a, b) suggests sliding of large coherent units with varying degrees of dismemberment. The sheet-like geometry of many olistoliths (Fig. 5.36a) indicates that detachment or sliding occurred along the bedding surfaces, possibly the same detachment units upon which thrusting occurred. The abundance of irregularly-shaped olistoliths (Fig. 5.36b – f) suggest rock fall processes, whereas less ordered deposits (Fig.5.35b – f) indicate transport via slumping, high density debris flows, low-density turbidite currents or some combination of these three mechanisms (Fig. 5.37). The local presence of intraformational conglomerates provides evidence for syn-orogenic reworking of the Okpikruak Formation. Pressure marks in matrix-supported conglomerate clasts indicate reworking of syn-orogenic strata.

The source for some olistostromes can be inferred from correlations with lithostratigraphic units contained in thrust sheet Red Dog district and/or adjacents areas of the western Brooks Range. However, many clasts and/or olistoliths are exotic and derived from lithostratigraphic units that are not presently preserved in the thrust sheets. This implies that a large volume of Ellesmerian strata of the ancient passive margin was eroded during thrust sheet emplacement and incorporated into syn-orogenic strata during the Brookian orogeny.

Distal Facies

The distal facies of the early Okpikruak Formation is generally fine-grained and consists dominantly of olive green to buff-weathering, medium- to thin-bedded, coarse- to fine-grained micaceous (muscovite) sandstones and well-sorted sheet-like sandstones and siltstones and satiny brownish grey to black bioturbated mudstones and shales that form thinning- and fining-upward cycles that form complete to incomplete Bouma sequences, (Ta – Td) and (Tb – Td), respectively (e.g. Bouma, 1962; Bouma *et al*. 1985) (Fig. 5.35b – d). These are locally arranged in metric-thick fining-up cycles with locally well-developed channel geometries. Sand-to-mud ratios typically range from 3:1 to 1:5. Sandstones consist dominantly of quartz, however greenish-weathering sandstones litharenite to sub-litharenite facies are locally abundant and rich in

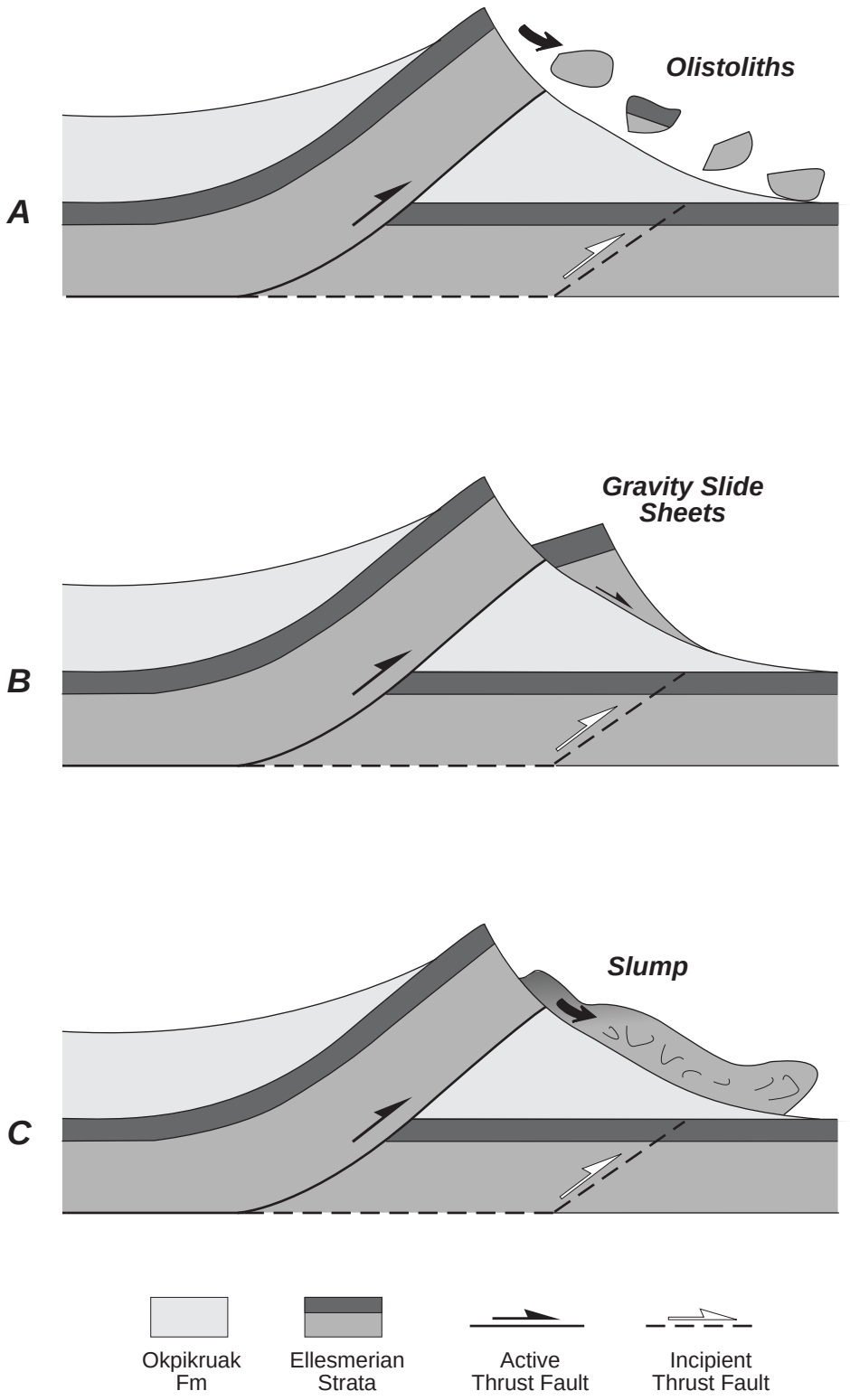


Figure 5.37. Synoptic diagram showing mechanisms of deposition of mass-wasting deposits of the Okpikruak Formation. **A.** Rock fall. Olistoliths are incorporated into the Okpikruak Formation matrix. **B.** Gravity slide sheet. Coherent slide sheets are detached from an advancing thrust sheet and incorporated into syn-orogenic strata. Note glide surface cuts down section. **C.** Deposition slumping, debris flow and turbidity currents. Note internal deformation of the transported mass.

chloritized volcanic rock fragments and altered feldspar (Ca-Plagioclase). Sedimentary structures include parallel and cross laminations, low amplitude ripple marks, flutes, normal to inverse graded bedding, and locally abundant parting lineations. Palaeocurrents indicate local sediment-transport directions to the north, northwest, and east after upon correction restoration to the horizontal for structural deformation.

Fossils in the Okpikruak Formation of the western Brooks Range are rare and have solely been reported at one locality (cf. Chapter 3; Curtis *et al*. 1990). A new fossil locality was discovered during the course of this study approximately 35 km northwest of the Red Dog mine (latitude 68°19'06"N, longitude 163°09'23"W) (Fig. 5.36c). Fossils consist of unidentified rounded-shelled forms, approximately 1 to 5 cm in diameter, that occur in brownish to black mudstone rubble outcrops. These fossils are possibly correlative to Early Cretaceous (Valangian) cf. *Buchia* reported by Curtis *et al*. (1990) and *Buchia* sp. identified by Curtis *et al*. (1990) southwest of Misheguk Mountain. Bioturbation in the Okpikruak Formation is locally abundant and consists of dendritic traces, cf. *Dendrites* and cf. *Nereites*.

The proximal and distal facies of the early Okpikruak Formation are here interpreted to reflect proximal deposition in a deep-water fan (e.g. Pickering *et al*. 1989), possibly developed at the front of the advancing thrust sheets. The early Okpikruak Formation is here interpreted as the precursor of the North Slope foreland basin.

5.6.2 Late Syn-orogenic Megasequence (Early Cretaceous)

The late Syn-orogenic Megasequence records Early Cretaceous deep marine late syn-orogenic sedimentation at the front of the Brooks Range foreland fold and thrust belt (Figs. 5.3 & 5.38). The late Syn-orogenic Megasequence comprises strata of the late Okpikruak and Fortress Mountain formations (Figs. 5.3 & 5.38) and is interpreted to record the transition from mass-wasting deposition to relatively stable sedimentation. The Late Syn-orogenic Megasequence is interpreted to be part of the North Slope foreland basin and is not assigned to any allochthon. The mass-wasting deposits that characterize much of the Early Syn-orogenic Megasequence (Figs. 5.3 & 5.36) are rare to absent in the Late Syn-orogenic Megasequence (Fig. 5.38).

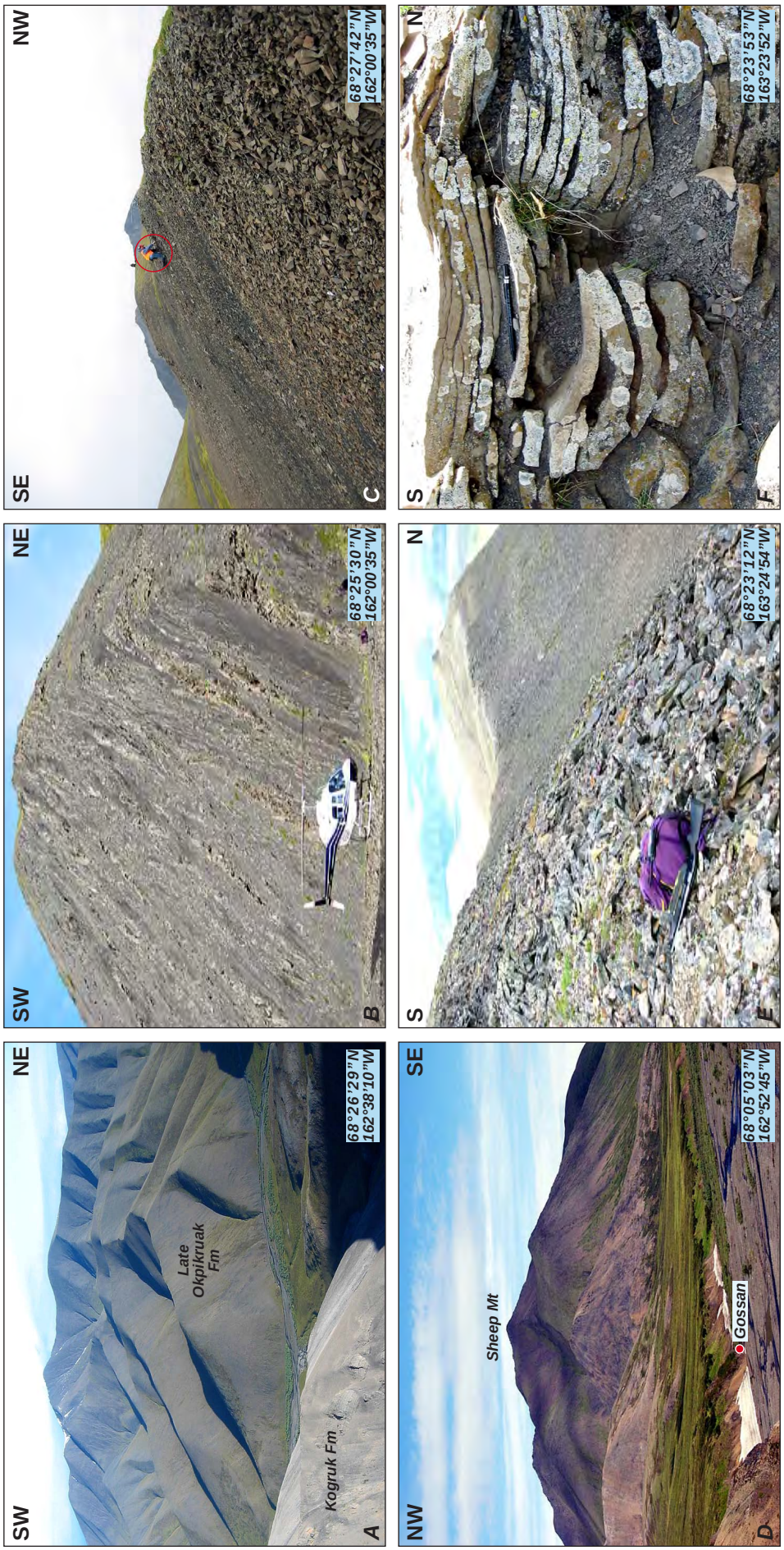


Figure 5.38. Sedimentary features of the late Okpikruak Formation and the Fortress Mountain Formation. **A.** N-looking aerial view of extensive outcrops of the Late Okpikruak Formation northeast of Amphitheatre Mountain. Topographic relief is approximately 75 m. **B.** Turbidites near Amphitheatre Mountain. Helicopter for scale. **C.** Typical late Okpikruak Formation rubble outcrop. U. S. Geological Survey geologist Thomas Moore encircled for scale. **D.** Extensive outcrops of fine- to coarse-grained sandstones of the Okpikruak Formation in the Sheep Mountain area. **E.** Fortress Mountain Formation rubble outcrop northwest of the SoonerRiver. **E.** Dish structures in fine- to medium-grained sandstone of the late Okpikruak Formation near the Sooner River.

Late Okpikruak Formation (Early Cretaceous, Valangian – Aptian)

The late Okpikruak Formation consists of rhythmically-bedded, coarse- to fine-grained, well-sorted mature sandstones and shales that are typically arranged in thinning- and fining-upward turbidite cycles with incomplete Bouma sequences (Tb-Te) (e.g. Bouma, 1962; Bouma *et al*. 1985) (Fig. 5.38). The total thickness of the late Okpikruak Formation is unknown, possibly exceeding 2 km. Sedimentary structures include locally abundant current and climbing ripples, convolute bedding, pillar, and dish structures (Fig. 5.38f). Fluid escape structures are here interpreted as indicators of high rates of sedimentation, rapid deposition, and high pore fluid pressure (cf. Pickering *et al*. 1989). The Late Okpikruak unit was previously assigned to the partly Albian Fortress Mountain Formation (Mayfield *et al*. 1990*a*), but C. G. Mull (2004, *pers. comm.*), based on regional mapping and palaeontological data (cf. Mull, 1995; Mull *et al*. 2000), has suggested that much of the Fortress Mountain Formation mapped by Mayfield *et al*. (1990) is actually Okpikruak Formation of Valangian age. The late Okpikruak Formation is here interpreted as having been deposited in a submarine fan environment (e.g. Pickering *et al*. 1989).

Fortress Mountain Formation (Early Cretaceous, Aptian – Albian)

The Fortress Mountain Formation consists dominantly of conglomerates, sandstones and shales that unconformably (?) overlie the late Okpikruak Formation (Fig. 5.1). These are interpreted as turbidites with complete (Ta – Te) to incomplete (Tb – Te) Bouma sequences (e.g. Bouma, 1962; Bouma *et al*. 1985). The Fortress Mountain Formation is also locally arranged in thickening- and coarsening-upward cycles. Possible growth strata were identified at two localities northwest of Sheep Mountain and northwest of the Sooner River. Sedimentary structures include cross-bedding, climbing ripples, flute casts, convolute bedding and dish structures. Fluid escape structures are here interpreted as indicators of high rate of sedimentation and high pore fluid pressure during deposition. Fine- to coarse-grained sandstones contain rare pyrobitumen in fracture porosity. Facies associations indicate that the Fortress Mountain Formation was deposited in a submarine fan setting with overlapping lobe deposits (cf. Pickering *et al*. 1989).

5.7 SUMMARY

This chapter has described the stratigraphy of the Red Dog district and has erected a new tectonostratigraphic framework. Key points arising from this chapter are:

- The stratigraphy of the Red Dog district consists of Late Devonian to Early Cretaceous clastic and carbonate sedimentary rocks together with felsic, intermediate, mafic, and ultramafic extrusive and intrusive igneous rocks that were deposited in the ancient continental margin of Arctic Alaska and were subsequently complexly thrust and folded during the Brookian orogeny. These are preserved in two terranes, the Arctic Alaska and Angayucham terranes.

- The stratigraphy of the Arctic Alaska terrane in the study area is subdivided into two main units that record two major events. These are the Ellesmerian and Brookian units, which are separated by the Early Cretaceous unconformity. The Ellesmerian and Brookian units are intensely disrupted by thrust faulting and folding and are incorporated into a series of regional thrust sheets or allochthons.

- The Ellesmerian unit records deposition during rifting and development of the continental margin of Arctic Alaska from the Late Devonian to the Jurassic. The Ellesmerian unit can be subdivided into the Syn-rift and Post-rift depositional megasequences.

- Stratigraphic differences from one allochthon to another are more common in strata of the Syn-rift Megasequence (Endicott and Lisburne groups) whereas post-rift strata is relatively continuous and uniform in all structural units. The Zn-Pb-Ag and barite deposits of the Red Dog district are hosted in deep water facies of the Lisburne Group (late syn-rift) of the Endicott Mountains allochthon.

- The Brookian unit can be subdivided into the Early and Late syn-orogenic Megasequences, which record Early Cretaceous syn-orogenic sedimentation related to the Brookian orogeny. The Early syn-orogenic Megasequence is characterized by turbidites and olistostromes that locally show equivocal structural and stratigraphic relationships with the allochthonous thrust sheets.

- The Angayucham terrane is unrelated to the Arctic Alaska terrane and consists exclusively of mafic and ultramafic rocks that have all the characteristics of the lower part of a supra-subduction zone ophiolite.

CHAPTER 6

STRUCTURAL ANALYSIS OF THE RED DOG DISTRICT

6.1 INTRODUCTION

6.2 STRUCTURAL NOMENCLATURE & HIERARCHY

6.3 ARCTIC ALASKA TERRANE

6.4 ANGAYUCHAM TERRANE

6.5 STRUCTURE OF THE THRUST FRONT

6.6 WRENCH CREEK AND SIVUKAT MOUNTAIN FAULTS

6.7 THRUST SYSTEMS AND KINEMATIC ANALYSES

6.8 SUMMARY

CHAPTER 6 STRUCTURAL ANALYSIS OF THE RED DOG DISTRICT

6.1 INTRODUCTION

This chapter presents a structural analysis of the Red Dog district. Previous regional studies in the Red Dog district and adjacent areas of the western Brooks Range (e.g. Martin, 1970; Moore *et al*. 1986; Mayfield *et al*. 1988; Curtis *et al*. 1990; Ellersieck *et al*. 1990*a*; Mayfield *et al*. 1990; Young, 1992, 2004) have established the main structural relationships (cf. Chapter 3 and references therein), but have not integrated these observations into a coherent tectonic model. These previous studies were largely of reconnaissance style and primarily focused on the characterization of the stratigraphic successions and their regional stacking order. This chapter presents the first detailed structural analysis of in the Red Dog district and the western Brooks Range and sets a new structural framework for the area.

6.2 STRUCTURAL NOMENCLATURE AND HIERARCHY

This section introduces the structural nomenclature used in this study, which differs significantly from that of previous work (cf. Chapters 2 & 3; e.g. Martin, 1970; Mull, 1982; Moore *et al*. 1986; Mayfield *et al*. 1988; Young, 1992, 2004). Structural nomenclature of the Red Dog district is complex (e.g. Young, 2004; Chapters 2 & 3 and references therein). The structural nomenclature and hierarchy used in this research is presented in Figure 6.1.

6.2.1 Structural Units

The highest hierarchical unit of the study area is the terrane (*sensu* Jones *et al*. 1981; Jones 1983; Howell *et al*. 1985). The Red Dog district contains two terranes. In ascending structural order these are the Arctic Alaska and Angayucham terranes (Fig. 6.1). The Arctic Alaska and Angayucham terranes are separated by a major fault zone, here referred to as the Angayucham thrust (Fig. 6.1). The subdivision of the Arctic Alaska terrane into subterranes, as previously proposed by Jones *et al*. (1987), Moore *et al*. (1992, 1994) and Young (2004) is here considered inappropriate in that the subterrane terminology obscures the fact that these structural units are thrust sheets that share the same tectonostratigraphy and tectonic evolution.

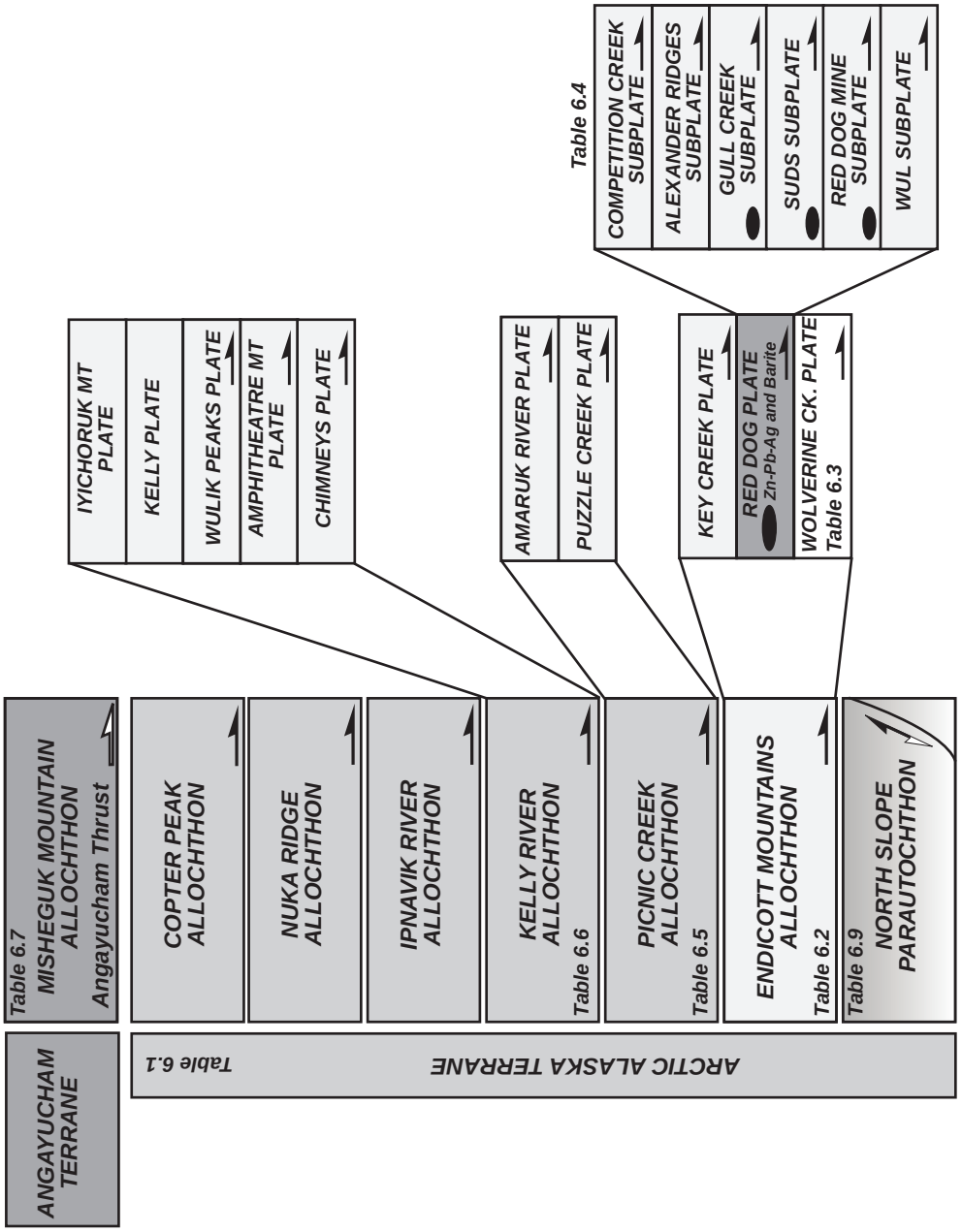


Figure 6.1. Structural hierarchy of the Red Dog district compiled from the results of this study and Mull (1982), Moore *et al.* (1986), Mayfield *et al.* (1988), Moore *et al.* (1994), Teck Cominco American Exploration Inc. (2002, *pers. comm.*), Young (2004). Note the structural position of the Zn-Pb-Ag and barite deposits the Red Dog district.

This study has subdivided the two terranes into a series of lithostratigraphically distinct units referred to as allochthons (Fig. 6.1). For the purposes of this study, an allochthon is defined as a thrust sheet of regional extent that has been transported 10's to 100's of km from its original palaeogeographic location by thrust faulting and/or gravity sliding, and is structurally and tectonostratigraphically coherent and distinct from the coeval overlying and underlying allochthon units.

The allochthons of the Red Dog district are complexly deformed (cf. Chapter 5, Fig. 5.1) by thrust faulting and related folding, extensional faulting and one or more penetrative cleavage fabrics. Allochthons locally show uncertain stratigraphic and structural relationships with syn-orogenic strata of the Brookian unit (cf. Chapter 5, Fig. 5.1). Individual allochthons of the Artic Alaska terrane typically contain one or more distinct Late Devonian or Early Mississippian through Early Cretaceous stratigraphic successions (cf. Chapter 5, Fig. 5.2) that are interpreted as having been deposited coevally and contiguously (cf. Chapter 5, Fig. 5.3). Allochthons typically show internal imbrications that in the Red Dog district and western Brooks Range have been historically referred to as 'sequences' (e.g. Martin, 1970; Moore *et al*. 1986; Mayfield *et al*. 1988; Young, 1992). The term 'sequence' was used as an informal lithostratigraphic classification (e.g. Martin, 1970; Moore *et al*. 1986; Mayfield *et al*. 1988; Young, 1992) and has no structural meaning. In this study the term 'sequence' is replaced by the term 'plate' or 'thrust plate' (Fig. 6.1). Sequence names of prior authors (e.g. Martin, 1970; Moore *et al*. 1986; Mayfield *et al*. 1988; Young, 1992) are retained (e.g. Key Creek sequence of Curtis *et al*. 1983 becomes the Key Creek plate in this study). Thrust plates are also internally imbricated into smaller units, referred to as thrust subplates (Fig. 6.1). Thrust subplates can be also further subdivided into smaller units informally referred to as thrust imbricates or thrust panels.

The Arctic Alaska terrane in the Red Dog district consists of six allochthons that contain Late Devonian to Early Cretaceous strata of the Ellesmerian and Brookian tectonostratigraphic units (cf. Chapter 5, Figs. 5.1, 5.2 & 5.3). In ascending structural order these are, the Endicott Mountains, Picnic Creek, Kelly River, Ipnavik River, Nuka Ridge, and Copter Peak allochthons (Fig. 6.1; Table 6.1). The Copter Peak allochthon was previously assigned to the Angayucham terrane (e.g. Mull, 1982; Moore *et al*.

	Structural Trends	Detachmen Level(s)	Structural Thickness	Tectonic Transport Direction	Mineralization
Copter Peak Allochthon	NE-SW-trending	Kugururok Fm	0 to 1 km	Northwest	-
Nuka Ridge Allochthon	NE-SW-trending	Nuka Fm	0 to 100 m	Northwest	-
Ipnavik River Allochthon	NE-SW-trending	Kugururok Fm	0 to 100 m	Northwest	-
Kelly River Allochthon	NE-SW-trending	Kugururok Fm Utukok Fm	200 m to 3 km	West-northwest to north-northeast	Barite and pyrite in Etivluk Group
Picnic Creek Allochthon	NE-SW-trending	Kugururok Fm, Kayak Shale Akmalik Chert	250 m to 1 km	West-northwest to north-northeast	Barite and pyrite in Etivluk Group
Endicott Mountains Allochthon	NE-SW- to WNW-ESE-trending	Hunt Fork Shale, Kayak Shale Kuna Fm & Undivided Lisburne Group	1 to 6 km	West-northwest to north-northeast	Sediment-hosted Zn-Pb-Ag and barite deposits

Table 6.1. Summary structural features of the allochthons of the Arctic Alaska terrane.

1986, 1994; Young, 2004), but is here included in the Arctic Alaska terrane on basis of regional field, tectonostratigraphic and age relationships (cf. Chapter 5, Figs. 5.2, 5.3, 5.29 & 5.30).

In the Red Dog district, the Endicott Mountains allochthon of Mull (1982) has been historically referred to as the Brooks Range allochthon ('Brooks Range sequence' of Martin, 1970; Moore *et al*. 1986; Mayfield *et al*. 1988; Young, 1989, 1992; Teck Cominco American Inc. 2001) (cf. Chapters 2 & 3). For the sake of consistency with the nomenclature already in use elsewhere in the Brooks Range, the term Endicott Mountains allochthon is used (Fig. 6.1; Table 6.1). The Wolverine Creek allochthon of Moore *et al*. (1986) or Wolverine Creek sequence of Young (1992) is here included with the Endicott Mountains allochthon (Fig. 6.1; Table 6.1).

The allochthons of the Red Dog district are separated from the North Slope parautochthon by a well developed thrust front. In this study, the term thrust front is used in its geomorphostructural sense (cf. Morley, 1986). The deformation front is interpreted to extend into the North Slope foreland basin. The term North Slope parautochthon is here used to refer to autochthonous to parautochthonous strata of the Arctic Alaska terrane that underlie the allochthons of the Arctic Alaska and Angayucham terranes (Fig. 6.1) as well as syn-orogenic strata of the North Slope foreland basin. This structural unit was previously referred to as the Arctic Slope parautochthon (Karl & Mull, 1993) or as the North Slope terrane or subterrane (e.g. Moore *et al*. 1992, 1994). Elevation of the North Slope parautochthon to the terrane or subterrane category is here considered inappropriate in that parautochthonous strata that underlie the North Slope foreland basin share the same geological history and tectonostratigraphy with the allochthonous thrust sheets of the Arctic Alaska terrane.

6.3 ARCTIC ALASKA TERRANE

This section describes the structure of the Arctic Alaska terrane in the Red Dog district. The Arctic Alaska terrane forms the bulk of exposures in the study area and consists of six tectonostratigraphically distinct allochthons (Figs. 6.1 & 6.2a – f; Table 6.1; cf. Chapter 5, Fig. 5.1). In this study, particular focus is placed upon the Endicott Mountains allochthon, which hosts all known sediment-hosted Zn-Pb-Ag and barite deposits of the Red Dog district (Figs. 6.1 & 6.2a).

6.3.1 Endicott Mountains Allochthon

The Endicott Mountains allochthon is the most extensive allochthon unit of the Red Dog district (cf. Chapter 5, Fig. 5.1; Fig. 6.2a, b). It is thrust northwestward over the North Slope parautochthon and internally imbricated into three tectonostratigraphically distinct thrust plates that show markedly different structure and structural styles. In ascending structural order these are, the Wolverine Creek, Red Dog, and Key Creek plates (cf. Chapter 5, Figs. 5.4 – 5.7; Figs. 6.1, 6.2a; Table 6.2).

Wolverine Creek Plate

The Wolverine Creek plate is the lowermost allochthonous structural unit of the Red Dog district (Fig. 6.1). It is imbricated into a series of antiformally-folded NE-SW- to WNW-ESE-trending and WNW- to NNE- and SE-verging thrust subplates that crop out in two NE-SW-trending Mount Raven and Wulik River structural windows (Figs. 6.2a, b, 6.3 & 6.4; Table 6.3).

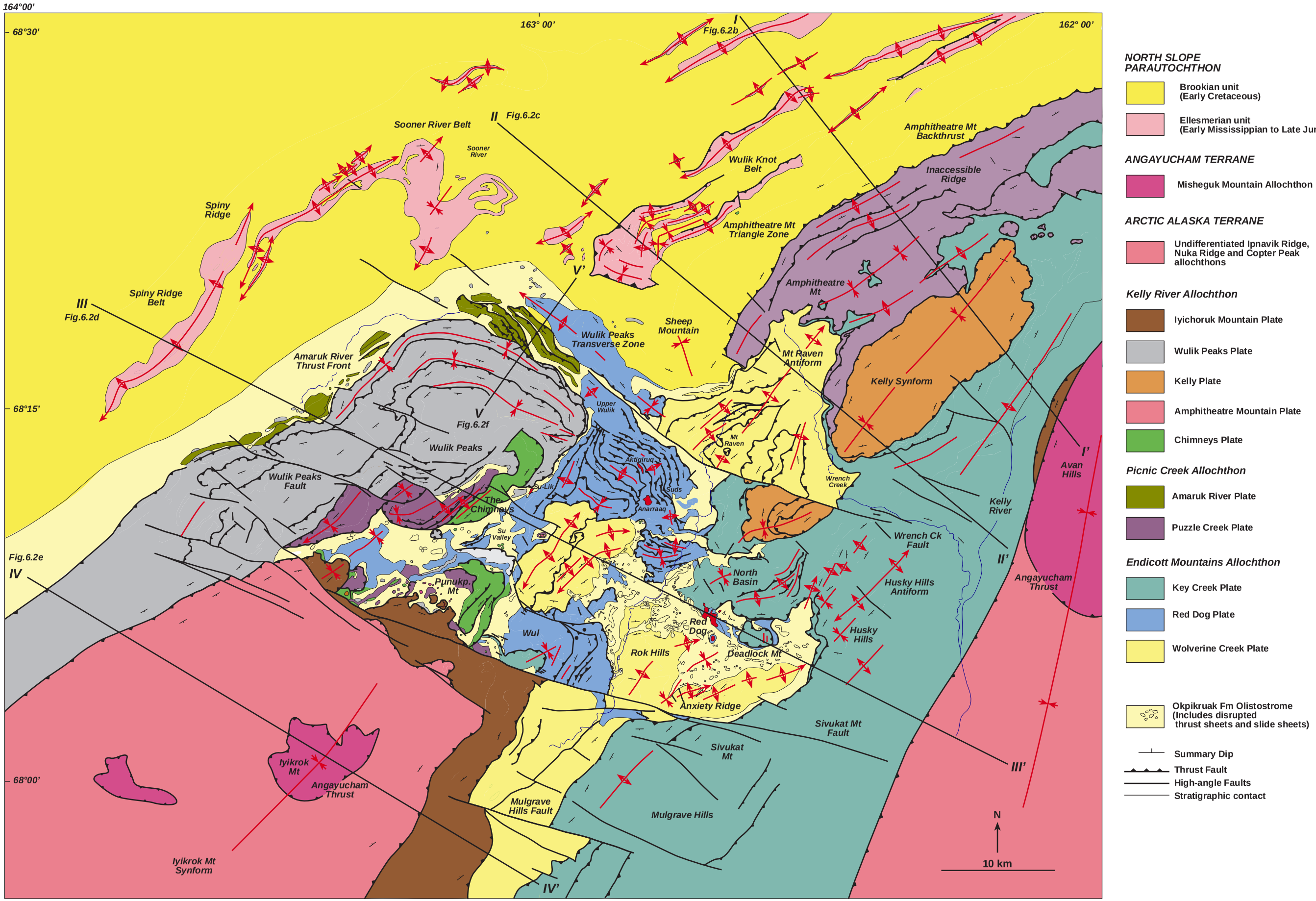


Figure 6.2a. Structural map of the Red Dog district compiled from the results of this study.

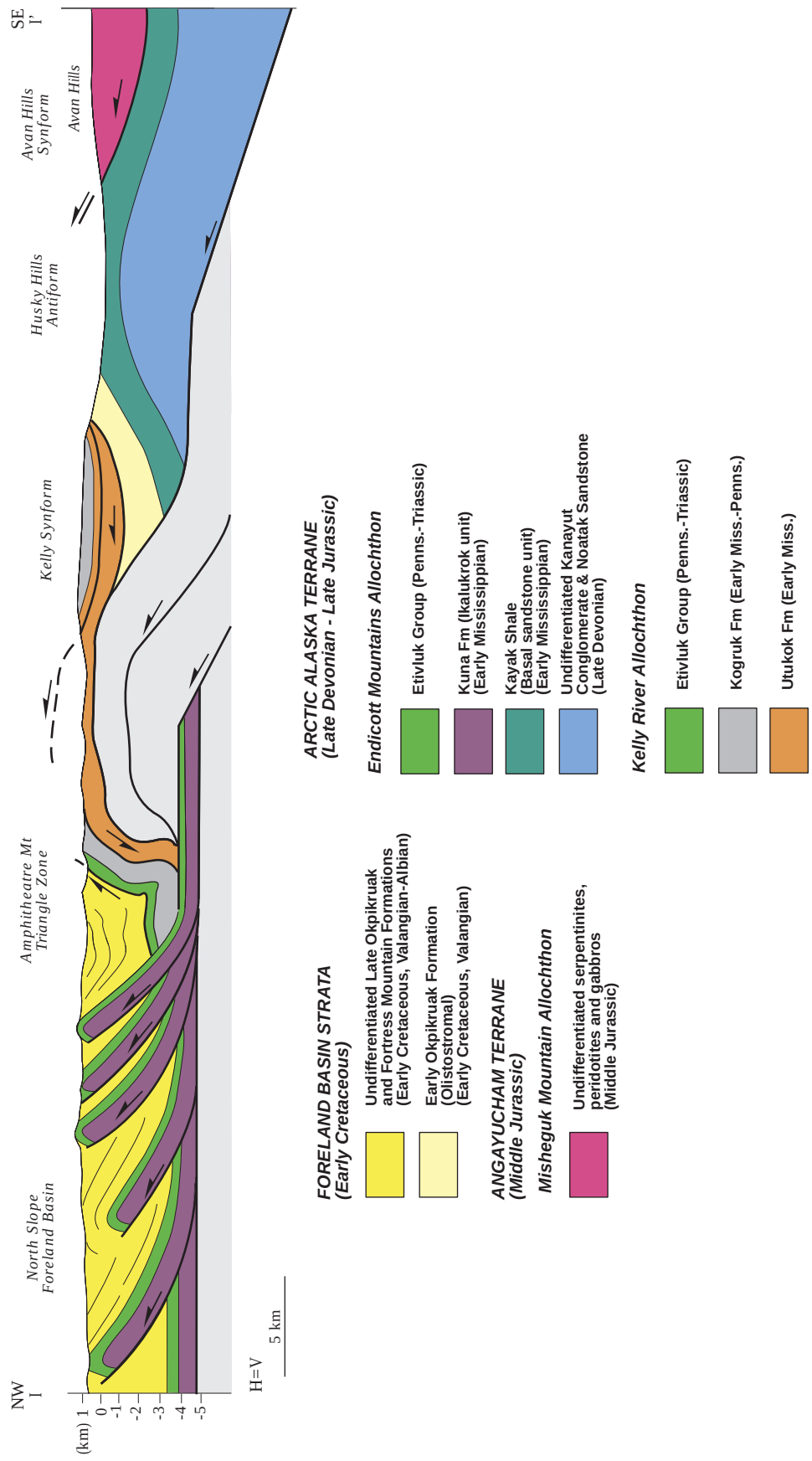


Figure 6.2b. Cross section I-I' across the Red Dog district. Refer to Figure 6.2a for location.

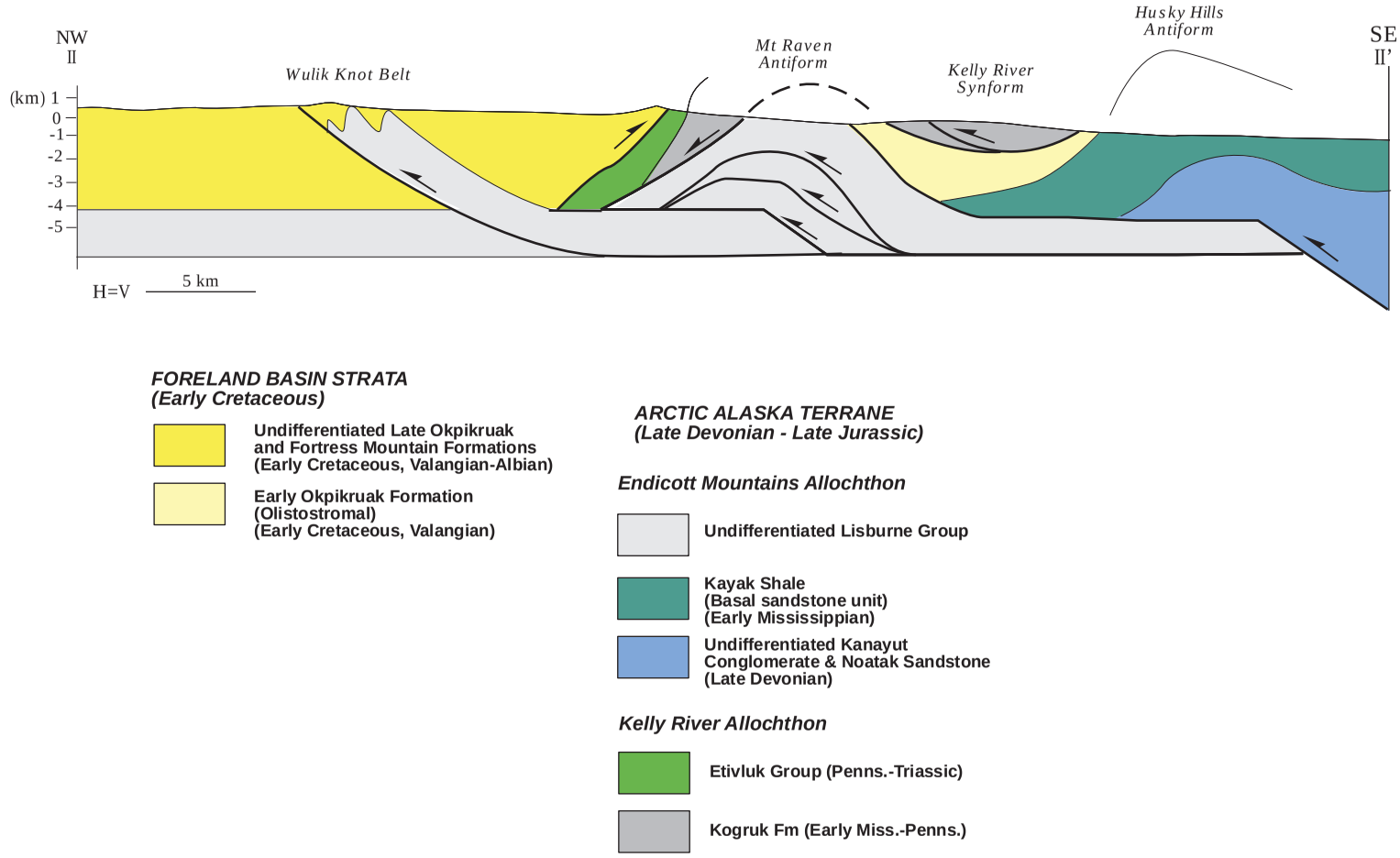


Figure 6.2c. Cross section II-II' across the Red Dog district. Refer to Figure 6.2a for location.

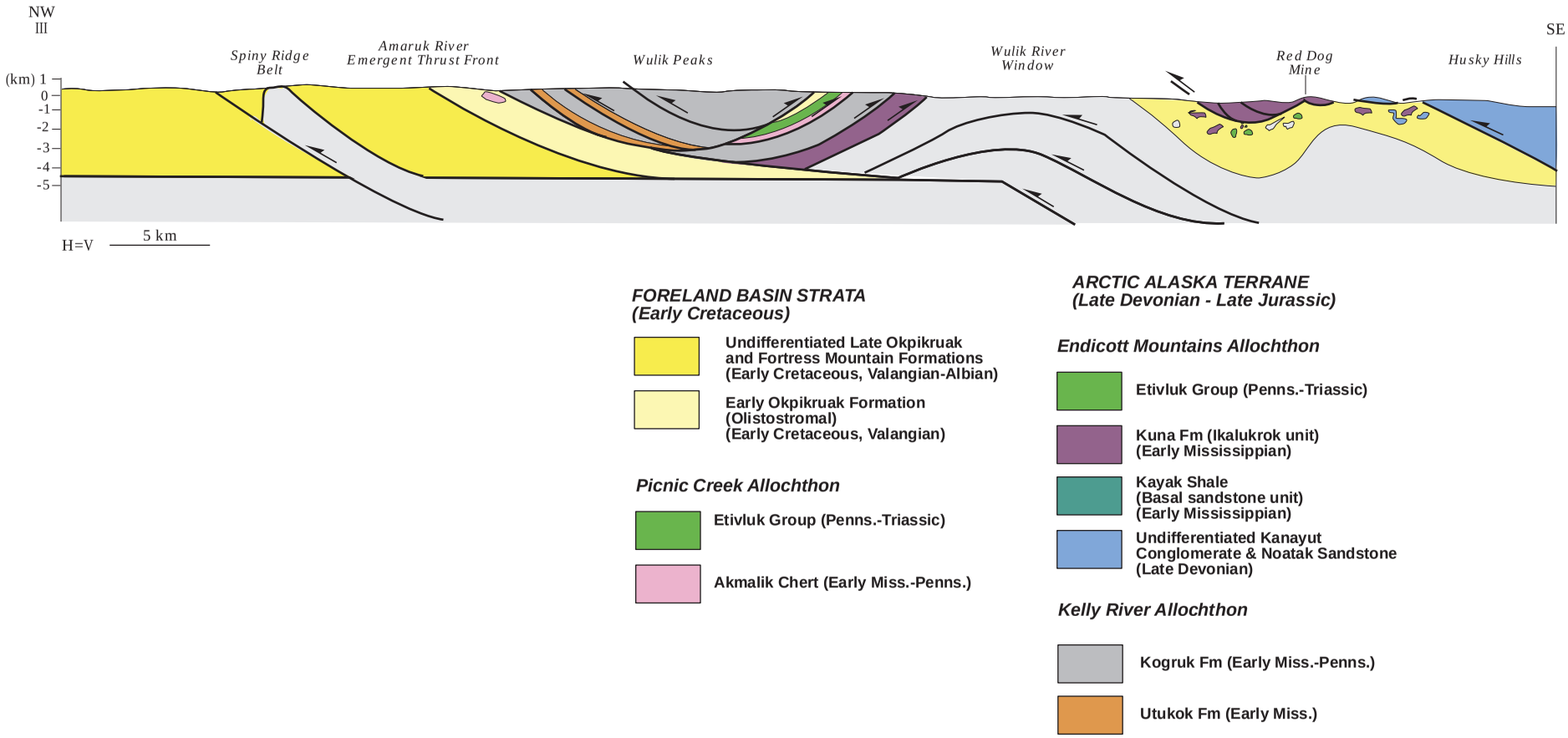


Figure 6.2d. Cross section III-III' across the Red Dog district. Refer to Figure 6.2a for location.

Figure 6.2e. Regional cross section. Refer to Figure 6.2a for location.

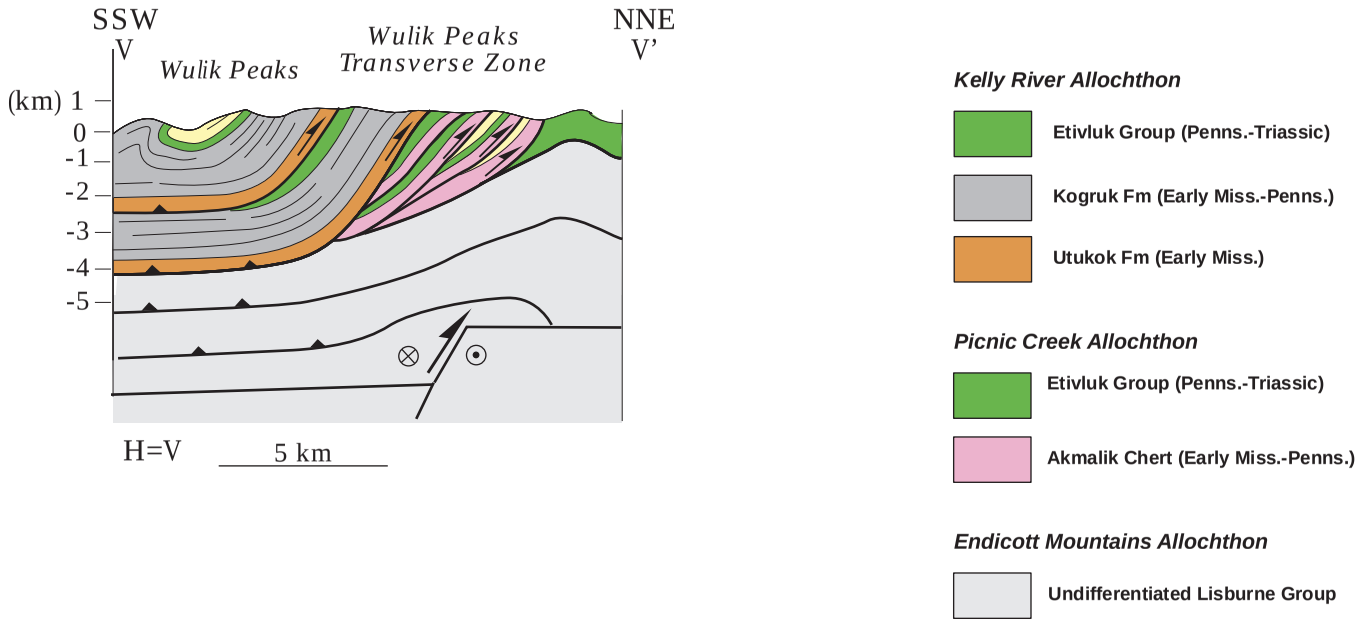


Figure 6.2f. Cross section V-V' across the Red Dog district. Refer to Figure 6.2a for location.

	Structural Trends	Detachment Level	Structural Styles	Tectonic Transport Direction	Mineralization
Key Creek Plate	NE-SW-trending SE- to NW-dipping	Hunt Fork Shale (Late Devonian)	Antiformal stacks Fault-propagation folds	West-northwest to northwest	Zn-Pb vein-breccia (Endicott Group)
Red Dog Plate	WNW- to NW-trending SSW- to SW-dipping	Kuna Formation (Early Mississippian)	Imbricate thrust systems, detachment folds, disruption grading into olistostrome	West-northwest to north-northeast	Zn-Pb-Ag & barite deposits (Kuna Fm)
Wolverine Creek Plate	NE-SW-trending SE- to NW-dipping	Kayak Shale and Und. Lisburne Group (Early Mississippian)	Antiformal stacks	West-northwest to northwest	?

Table 6.2. Summary structural features of the Key Creek, Red Dog and Wolverine Creek plates of the Endicott Mountains allochthon in the Red Dog district.

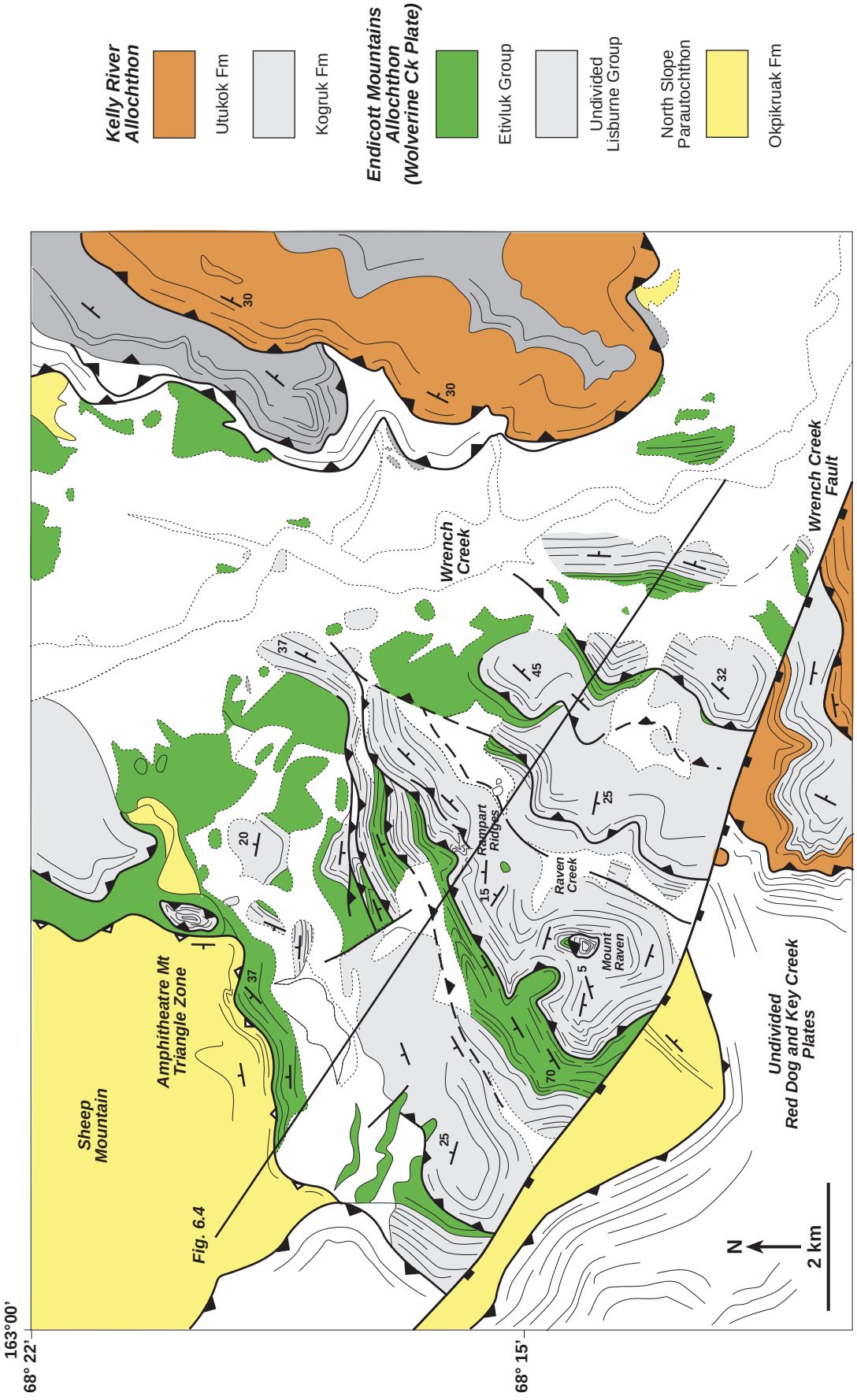


Figure 6.3. Summary structural map of the Mount Raven window.

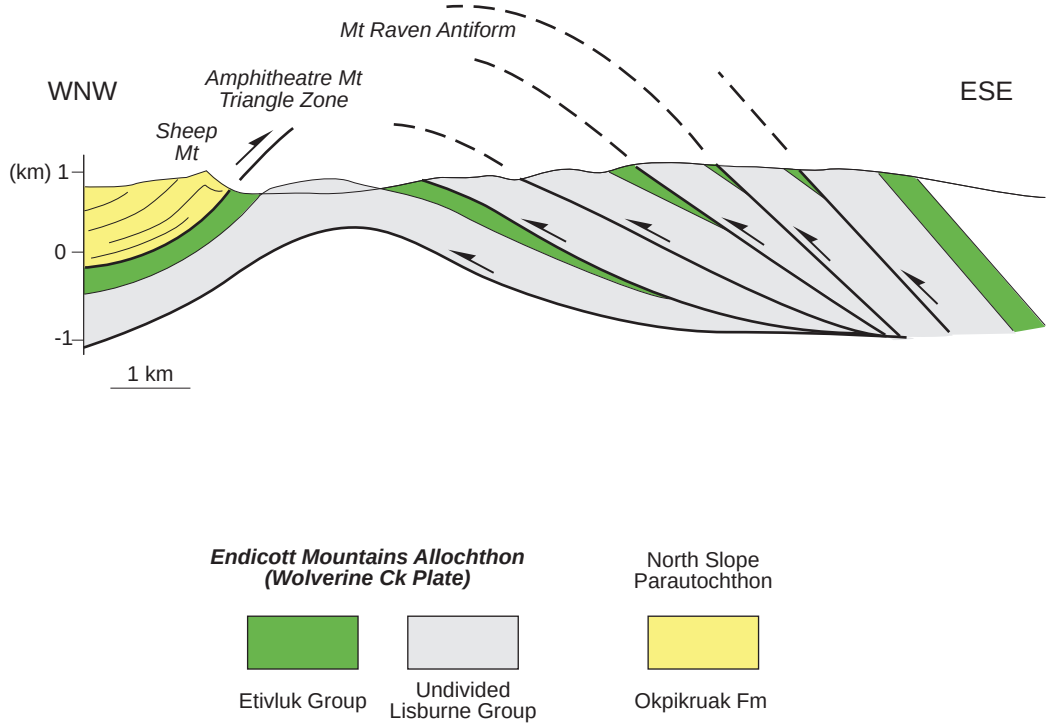


Figure 6.4. WNW-ESE-trending cross section across the Mount Raven window showing the structure of the Mount Raven antiform. Note antiformally-stacked thrust sheets.

	Structural Trends	Structural Styles	Associated Syn-orogenic Strata	Tectonic Transport Direction	Tectonostratigraphy
Mount Raven Window	NE-SW-trending SE- to NW-dipping	Antiformal Stacks, Fault-propagation folds	Okpikruak Fm detached above the Amphitheatre Mt triangle zone	Northwest	Carbonate Platform
Wulik River Window	WNW-ESE- to NW-SE-trending SSW- to SW-dipping	Imbricate thrust systems, fault-propagation folds	Olistostromal. Olistoliths derived from the Wolverine Creek, Red Dog and Key Creek plates	Northwest to north-northeast	Carbonate Platform and Slope to Basin

Table 6.3. Summary structural features of the Mount Raven and Wulik River windows.

Mount Raven Window

The Mount Raven window is located approximately 20 km north-northwest of the Red Dog mine (Fig. 6.2a). It is approximately 15 km long, 5 to 10 km wide and exposes part of a major NNE-SSW-trending, NNE-plunging, and WNW-verging antiformal culmination, here named the Mount Raven antiform (Figs. 6.2a – c & 6.3). The Mount Raven window is the highest topographic feature and the northernmost structural culmination of the western Brooks Range fold and thrust belt in the Red Dog district.

To the north, northeast and east, the Mount Raven antiform plunges gently (10° to 20°) beneath the Kelly and Amphitheatre Mountain plates of the Kelly River allochthon (Figs. 6.2a & 6.3). To the south, the Mount Raven antiform is offset by the WNW-ESE-trending Wrench Creek fault, which juxtaposes the Wolverine Creek plate against the downthrown Red Dog and Key Creek plates of the Endicott Mountains allochthon as well as the Kelly plate of the Kelly River allochthon (Figs. 6.2a & 6.3). To the northwest, the Mount Raven antiform is underthrust by syn-orogenic strata of the North Slope foreland basin (Figs. 6.2a & 6.3) forming a well-developed NE-SW-trending triangle zone. This structure, here named the Amphitheatre Mountain triangle zone (Fig. 6.2a), defines the thrust front of the western Brooks Range fold and thrust belt in the northern part of the Red Dog district (Fig. 6.4) and is described in detail in Section 6.5.

The Mount Raven antiform consists of at least four major NNE-SSW-trending, WNW-verging and WNW- to ESE-dipping, antiformally-stacked thrust subplates and a series of smaller imbrications that can be identified from surface mapping (Figs. 6.2a, 6.3 & 6.4). These thrust subplates are arranged in a well-developed antiformal stack (Figs. 6.4 – 6.9). The floor thrust of the antiformal stack locates in the uppermost Shale and Limestone unit of the Kayak Shale or at the base of the overlying undivided Lisburne Group (cf. Chapter 5, Figs. 5.4 & 5.5; Figs. 6.3 & 6.4). The roof thrust is located in the upper part of the Etivluk Group, near the base of the Otuk Formation. Individual thrust horses consist of strata of the undivided Lisburne Group and the Siksikpuk Formation of the Lisburne Group. Thicknesses of individual horses typically

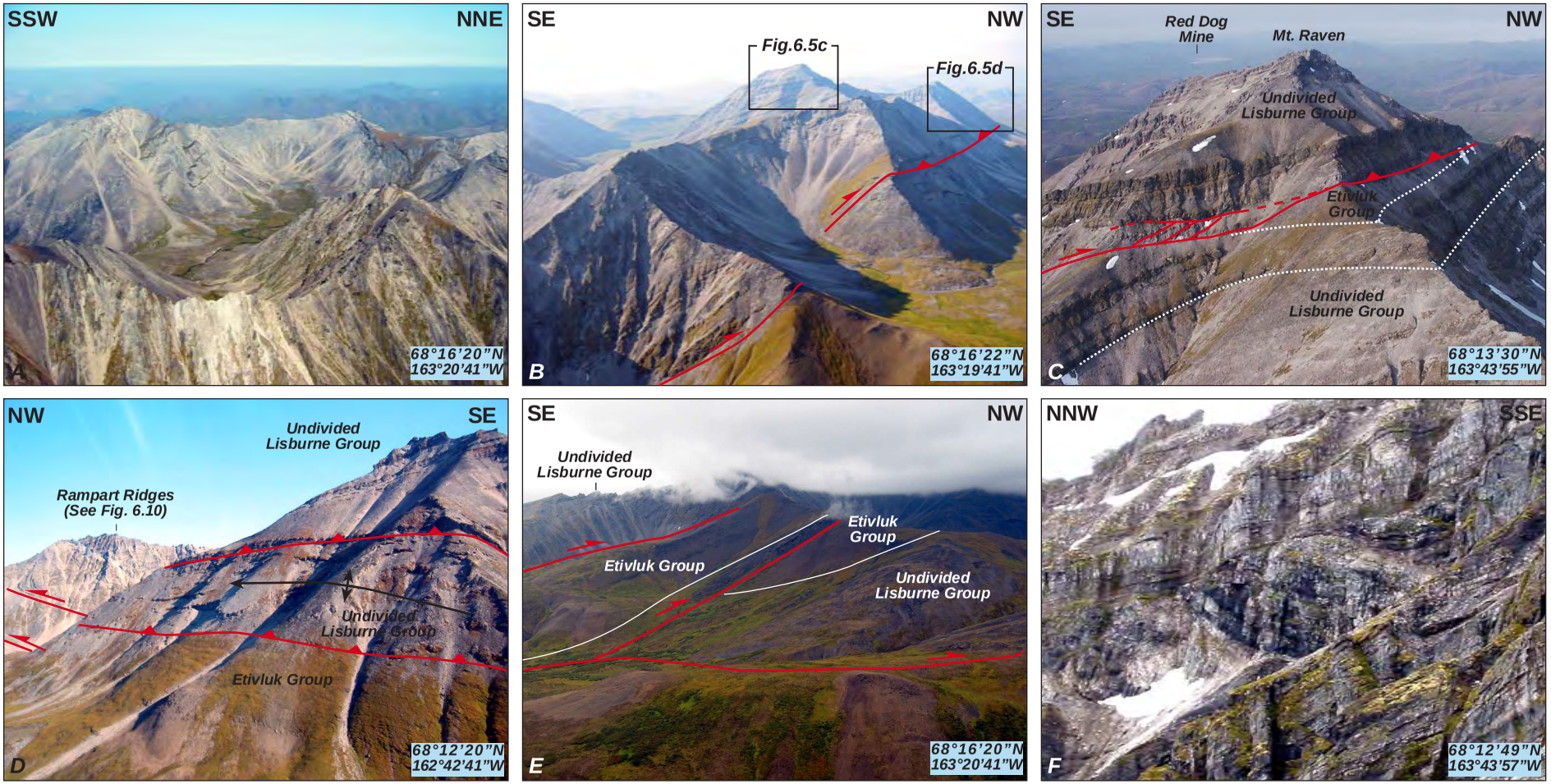


Figure 6.5. Structural features of the Mount Raven antiform. **A. W**NW-looking aerial oblique view of the Mount Raven window. Topographic relief is approximately 700 m. **B.** SW-looking view of ESE-dipping thrust sheets of the eastern limb of the Mount Raven antiform. Topographic relief is approximately 500 m. **C.** Detail of thrust fault at Mount Raven. Topographic relief is approximately 200 m. **D.** Detail of thrust faults and fault-related folds near Mount Raven. Topographic relief is approximately 250 m. **E.** Detail of thrust horses repeating strata of the undivided Lisburne Group and the Etivluk Group. **F.** Detail of outcrop-scale footwall duplex structure. Topographic relief is approximately25 m.

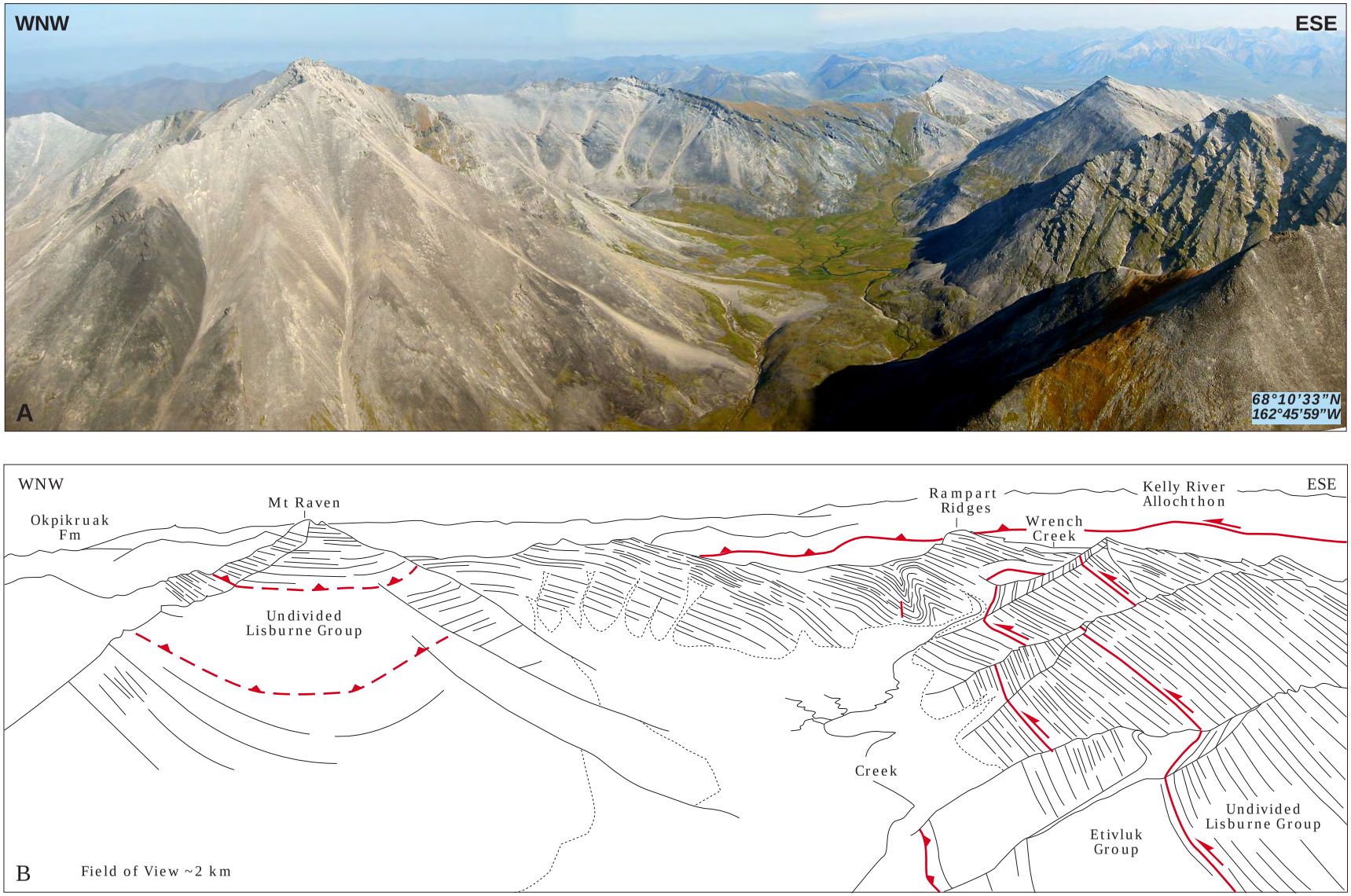


Figure 6.6. Mount Raven antiform. **A.** NE-looking oblique aerial photomosaic showing the eastern limb of the Mount Raven antiform. Field of view is approximately 2 km in the foreground. **B.** Line drawing structural interpretation. Note ESE-dipping, WNW-verging thrust repetitions of the undivided Lisburne Group. The Kelly River allochthon lies in the background.

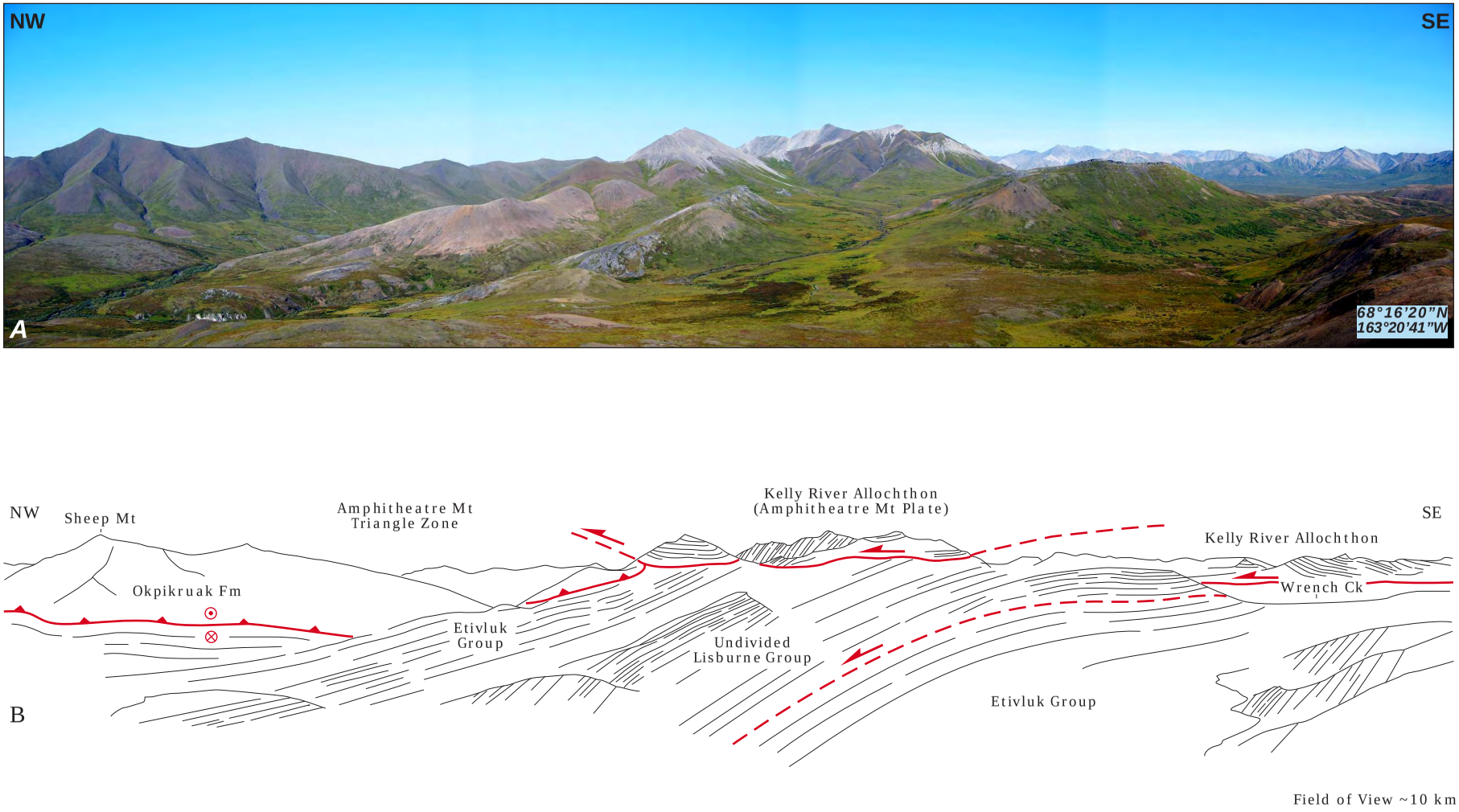


Figure 6.7. Mount Raven antiform. **A.** N-looking panoramic view of the western front limb of the Mount Raven antiform. **B.** Line-drawing structural interpretation of A showing WNW- to NW-dipping and NW-verging thrust sheets. Field of view is approximately 10 km. Topographic relief is approximately 700 m at Sheep Moutain.

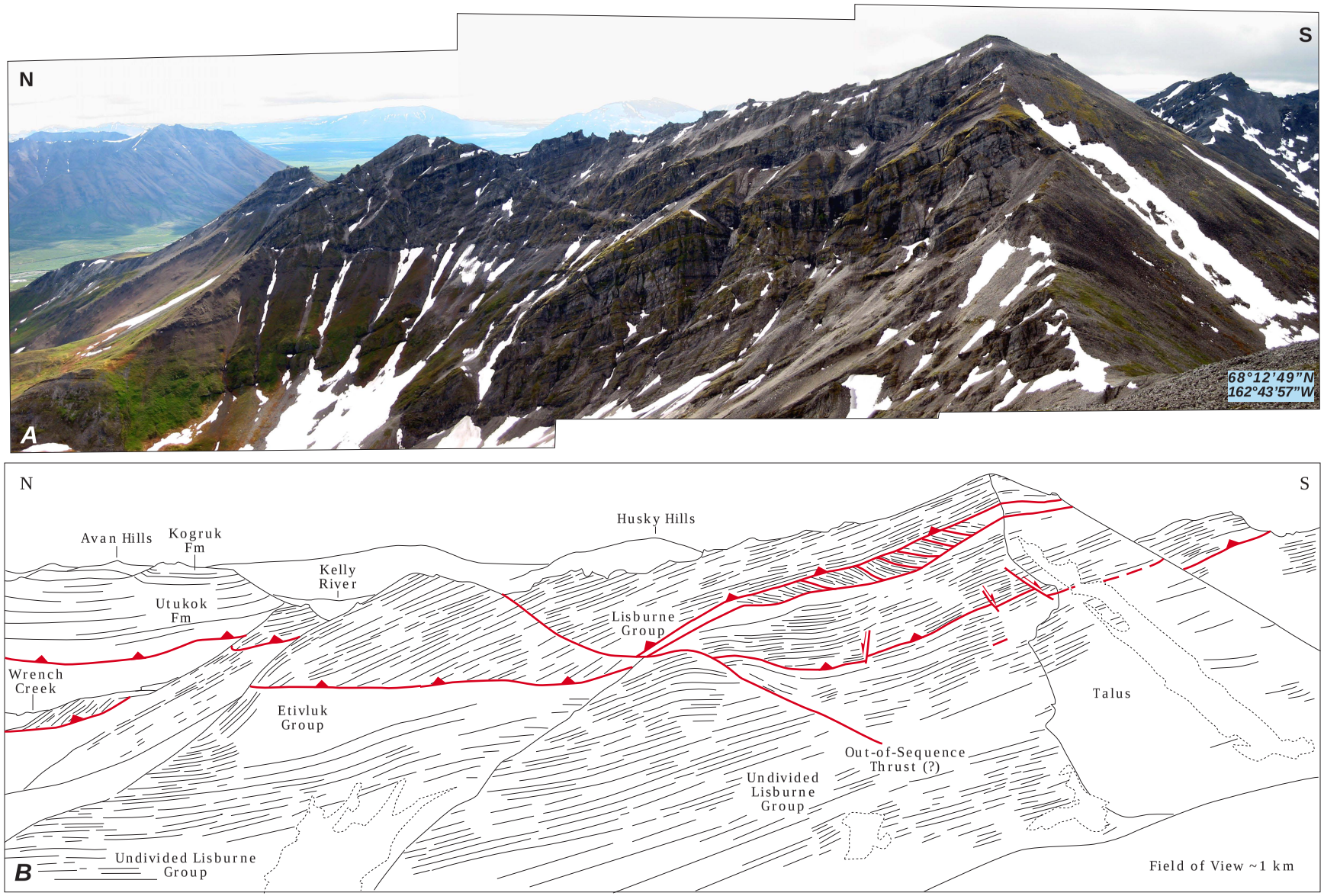


Figure 6.8. Plunging termination of the Mount Raven antiform. **A.** ESE-looking photomosaic showing the NNE-plunging termination of the Mount Raven antiform. Field of view is approximately 1 km. Topographic relief is approximately 300 m. **B.** Line-drawing structural interpretation of A. Note stacked thrust sheets of the Wolverine Creek plate dip gently to the north-northeast below the Kelly plate of the Kelly River allochthon (in the background).



Figure 6.9. Field sketches illustrating the structural styles of the Wolverine Creek plate of the Endicott Mountains allochthon in the Mount Raven window. **A.** S-looking up-plunge view of the Mount Raven antiform. Note antiformally folded thrust sheets of strata of the undivided Lisburne Group. Topographic relief is approximately 600 m. **B.** W-looking view of stacked WNW-transported thrust sheets. Topographic relief is approximately 100 m. **C.** S-looking view of E-dipping stacked thrust sheets of the eastern limb of the Mount Raven antiform. Topographic relief is approximately 500 m.

range from 200 to 600 m. The total structural thickness of the Wolverine Creek plate in the Mount Raven antiform is approximately 6 km.

The wavelength of the Mount Raven antiform varies from 15 to 20 km and the antiform limbs generally dip between 35º to 50º. The northwestern limb of the Mount Raven antiform exposes two NW-dipping thrust horses, whereas the southeastern limb exposes as many as four repetitions. Individual link thrusts are approximately 2 to 10 km in length. At surface, thrust fault dips ranges from 30° to the west-northwest to approximately 50° to the east-southeast. The NNE-plunging termination of the Mount Raven antiform shows NNE-plunging stacked fault-bend folds, with hangingwall cut-off angles that typically range from 35° to 40°. Thrust sheets are locally offset by WNW-ESE- to NW-SE-trending and NNE- to SSW-downthrown late extensional faults with inferred vertical throws of metres to tens of metres.

Intra-thrust subplate shortening is dominantly accommodated by thrust fault-related folds, minor imbrications, and well-developed cleavage fabrics. Thrust fault-related folds typically occur as asymmetric to locally recumbent northwest-vergent fault-propagation folds that are locally offset by low displacement out-of-sequence thrust faults (Figs. 6.5 & 6.10). Fold wavelength ranges from 50 to 500 m. Hangingwall and footwall cut-off angles typically range from 20° to 35°. Fault-related folds are well exposed approximately 2 km north of Mount Raven (Figs. 6.5 & 6.10).

Thrust faults occur as discrete zones that locally show associated metric to decametric hinterland-dipping footwall duplexes with smooth floor and roof thrust surfaces and planar to sigmoidal link thrusts (Fig. 6.5d). Footwall duplexes are typically 10 to 15 m long and 2 to 5 m thick. The number of thrust horses for individual duplexes commonly ranges from 5 to 10. Duplexes are typically developed in thin-layered, planar parallel-bedded dolostones, limestones and shales of the undivided Lisburne Group in the immediate footwall to major thrust faults (Fig. 6.5e) typically being from 10 to 20 m long.

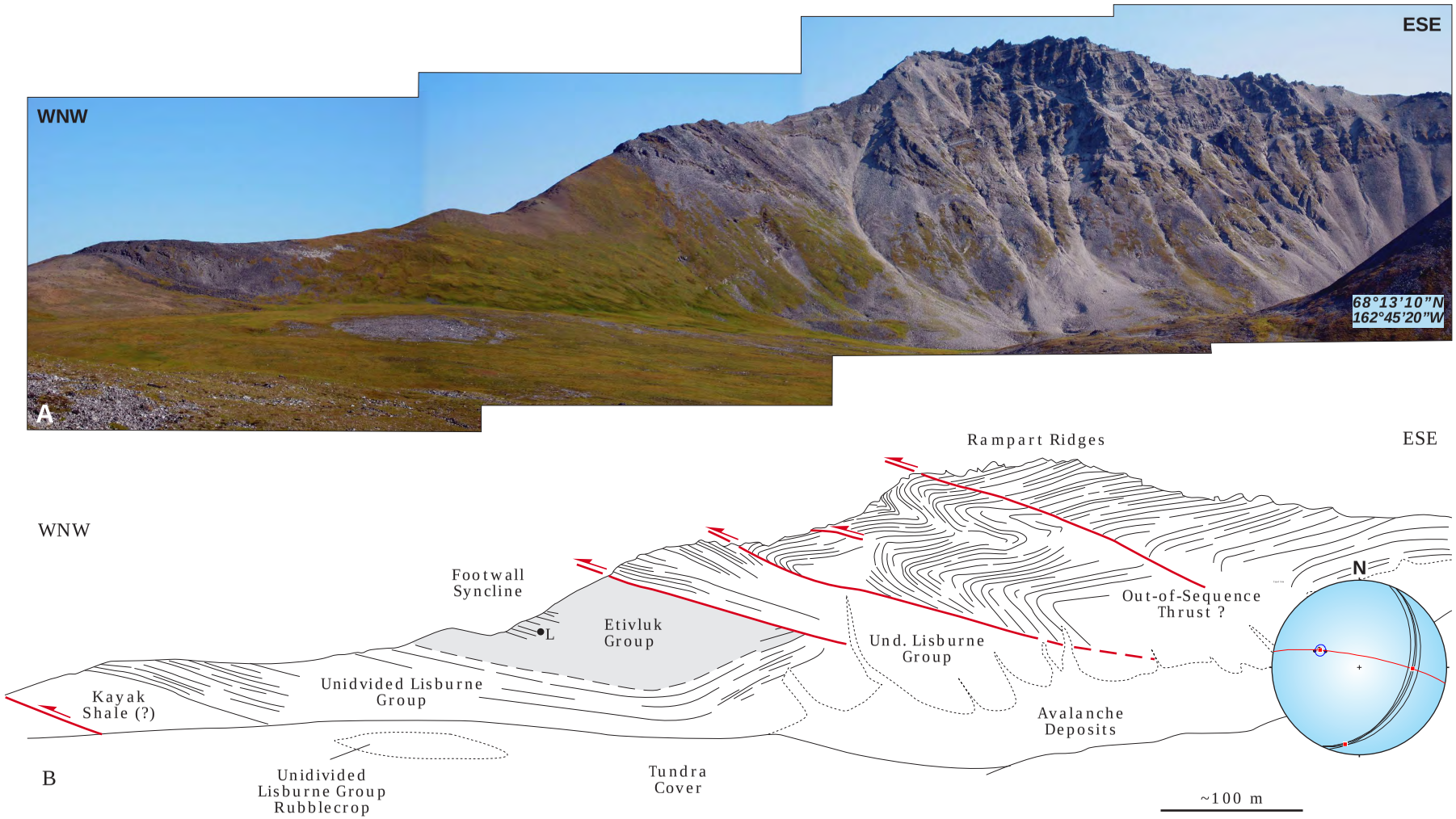


Figure 6.10. Structural styles of the Wolverine Creek plate near Mount Raven. **A.** NNE-looking photomosaic showing thrust faults and fault-related folds in the Rampart Ridges. Field of view is approximately 1 km and topographic relief is 600 m. **B.** Line-drawing structural interpretation of A and lower hemisphere stereographic projection of slaty cleavage (N=5) in shales and siltstones of the Etivluk Group at locality L.

Link thrust fault angles show a maximum dip of ~ 45º in the central part of the duplex decreasing progressively towards the leading and trailing edges of the duplex. Duplex thickness typically ranges from 1 to 10 m approximately.

Associated with northwest vergent thrust faults and fault-related folds are a series of ESE-dipping continuous to spaced cleavage fabrics. These occur as a disjunctive smooth and irregular fracture to pressure solution cleavage in limestones, cherty limestones and dolostones of the undivided Lisburne Group or as a rough to continuous slaty cleavage in shales and siltstones of the Etivluk Group. Tabular to irregular pencil cleavage is typically developed near minor fold hinges in shales and siltstones of the Etivluk Group.

Thrust fault orientation, fault-related fold asymmetries, the arrangement of cut-off lines and points, together with the orientation of minor fold axes and the attitude of the regional cleavage in the Mount Raven antiform indicate a consistent west-northwest to northwest tectonic transport direction (Fig. 6.11). Kinematic indicators in the floor and roof thrusts show a consistent northwest tectonic transport direction, whereas slip vectors for individual thrust horses are typically widely scattered with marked north-northwest to north-northeast components. This is interpreted to indicate three dimensional accommodation slip on the NNE-plunging termination of the Mount Raven antiform.

Wulik River Window

The Wulik River window is located immediately northwest, west, and south of the Red Dog mine (Fig. 6.2a). It is best exposed in the footwall of the Sivukat Mountain fault but is also exposed along a narrow NE-SW-trending corridor that extends along the western margin of the Mulgrave Hills (Fig. 6.2a) and further south to the Chukchi Sea coast. The thrust sheets of the Wolverine Creek plate south of the Sivukat Mountain fault were previously assigned to the structurally higher Key Creek plate (Teck Cominco American, 2001, *pers. comm.*; Young, 2004). The antiformal duplex that characterizes the Wolverine Creek plate in the Mount Raven window is in the Wulik River window replaced by a complex arrangement of NW-verging and SE-dipping stacked thrust subplates that are partly concealed by a succession of early syn-orogenic

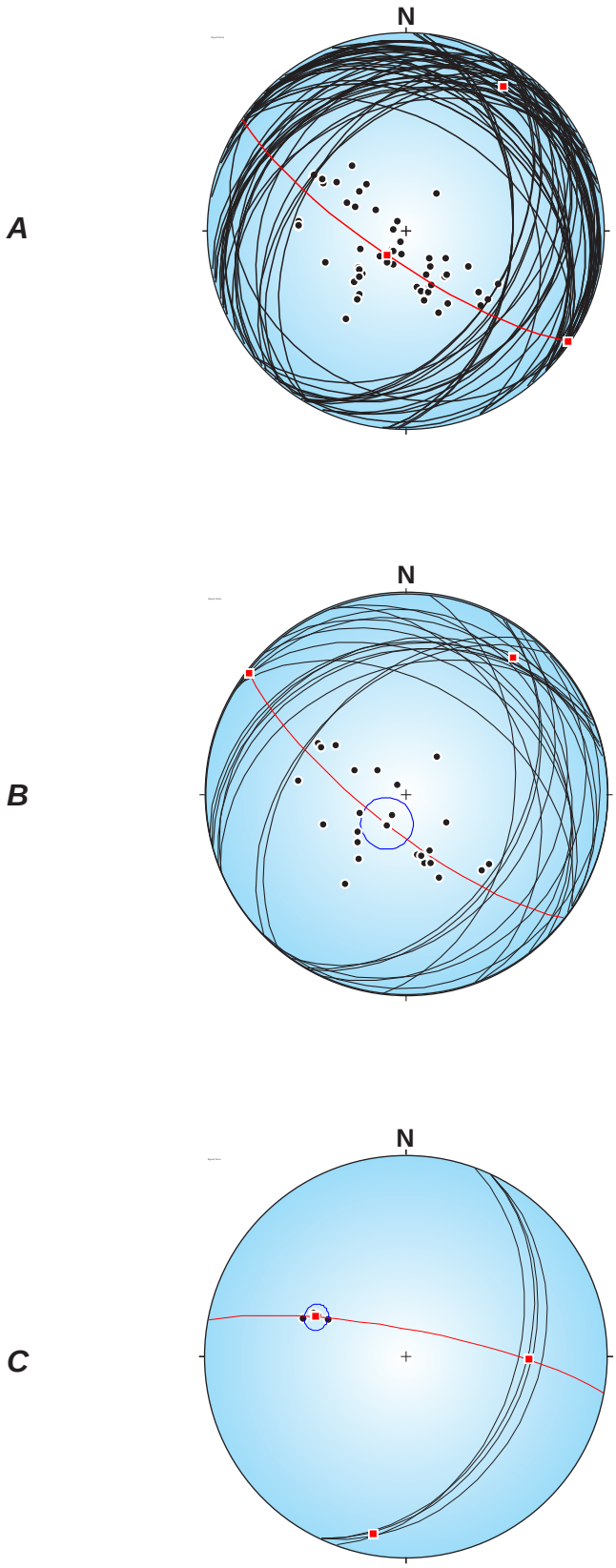


Figure 6.11. Lower hemisphere equal area stereographic projections of structural data from the Mount Raven antiform. **A.** Great circles and poles to bedding from the undivided Lisburne Group (N=72). Mean fold axis =12°/036°. **B.** Great circles and poles to thrust fault surfaces (N=25). **C.** Great circles and poles to slaty cleavage in strata of the Etivluk Group (N=4).

olistostromal strata of the Okpikruak Formation, including widespread olistoliths and locally well developed olistostromal mélange. These thrust sheets form a poorly defined NNE- and SSW-doubly-plunging antiformal culmination. The Wulik River window is bounded to the south by the WNW-ESE-trending Sivukat Mountain fault. Individual thrust sheets are typically 300 to 600 m thick. Thrust subplates are detached in strata of the Shale and Limestone unit of the Kayak Shale (cf. Chapter 5, Fig. 5.5). The structure consists of large fault-propagation folds with steeply-dipping to overturned front limbs and gently-dipping long back limbs. Syn-orogenic olistolith-bearing strata of the Okpikruak Formation typically lies unconformably on the back limb of the anticlines.

The Okpikruak Formation locally shows well-developed scaly fabrics and soft-sediment deformation structures that are best developed in olistostromal and olistolith-bearing strata. Outcrop-scale elongate olistoliths show a preferred orientation, parallel to phacoidal fabrics in highly deformed Okpikruak Formation shales (cf. Chapter 5, Fig. 5.36f). Olistoliths typically range in size from outcrop-scale metric blocks (cf. Chapter 5, Fig. 5.36e) to blocks of *ca.* 1 km^2. These were previously interpreted as klippen or windows (e.g. Moore *et al.* 1986; Young, 1992; Teck Cominco American Inc. Exploration, 2001, *pers. comm.*).

The Wolverine Creek plate of the Wulik River window is well exposed in Anxiety Ridge, located approximately 5 km south of the Red Dog mine (cf. Chapter 5, Fig. 5.1; Fig. 6.2a). The Anxiety Ridge exposes an approximately 11 km-long and 2 km-wide belt of Mississippian to Early Cretaceous strata. The structure of Anxiety Ridge consists of dominantly NW- to NNW-verging and SE- to ENE-plunging stacked fault related folds. Progressively older strata are exposed to the ESE. These fold structures are ESE-plunging to doubly-plunging structures with moderately to gently-dipping fold axial surfaces, which commonly show box-like geometries (Figs. 6.12 – 6.15). The thrust fault flooring the anticline is concealed by extensive early Okpikruak Formation. To the north, thrust panels of the Anxiety Ridge are unconformably overlain by a thick succession (>1 km ?) of syn-orogenic strata of the Early Cretaceous Okpikruak Formation, which extends northwards for approximately 5 km to the Red Dog mine area. The contact between the Lisburne Group and the Okpikruak Formation

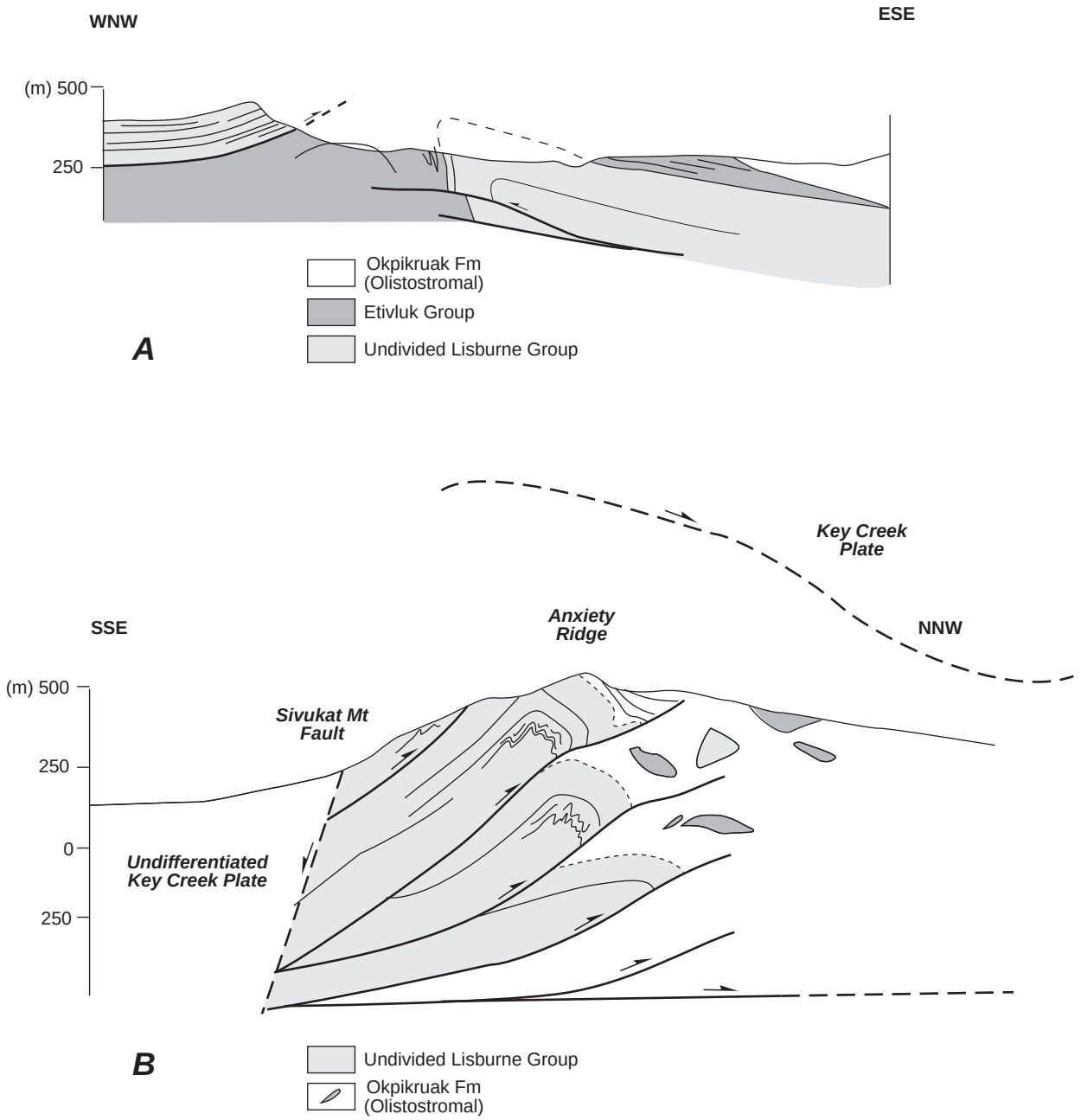


Figure 6.12. Cross sections illustrating the structural styles of the Wolverine Creek plate in the Wulik River window. **A.** Wulik River area. **B.** Anxiety Ridge.

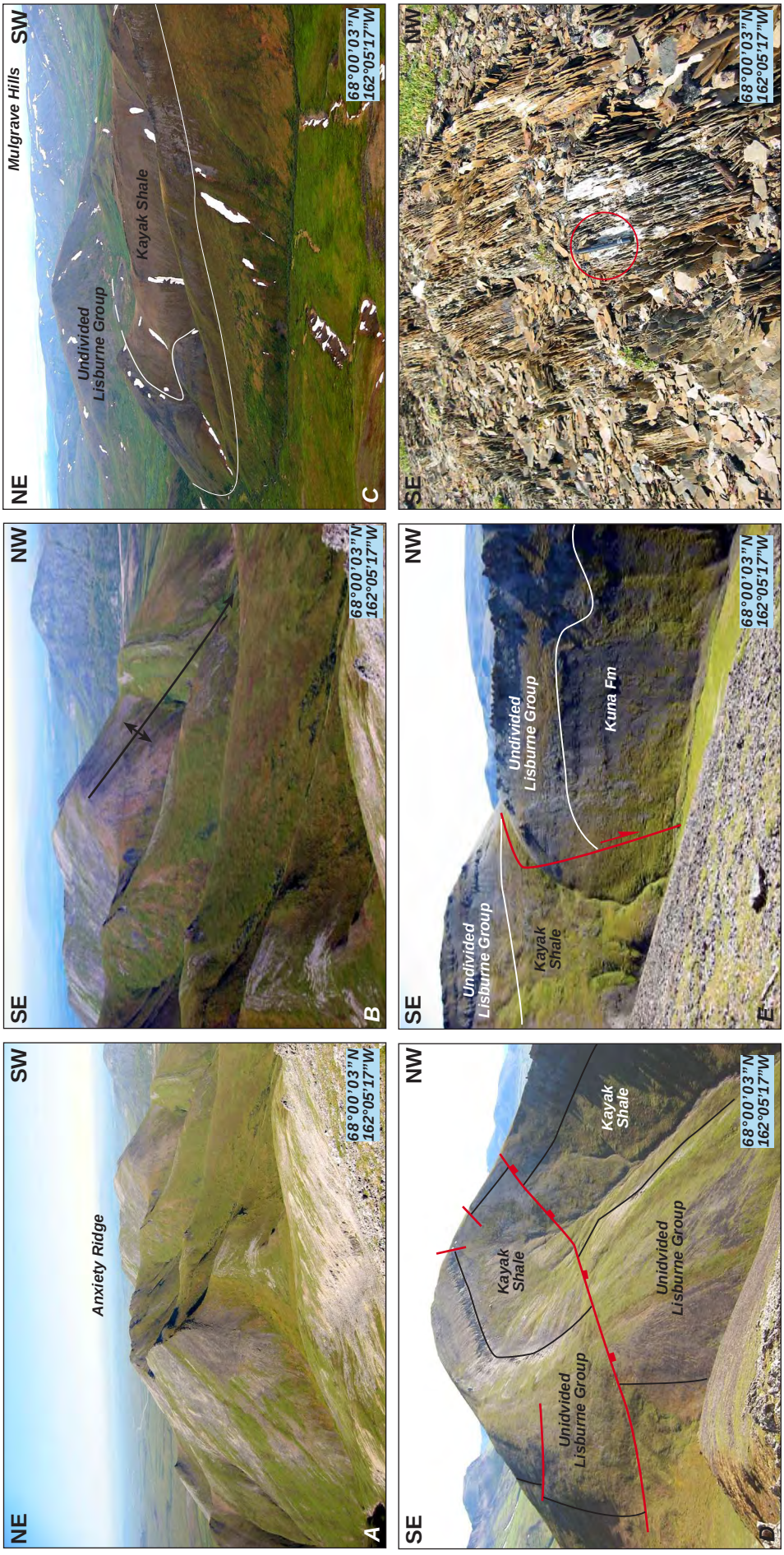


Figure 6.13. Structural features of the Wulik River window in the Anxiety Ridge area. **A.** SW-looking view of fault-related folds. Topographic relief is approximately 250 m. **B.** Detail of ENE-plunging anticline. Topographic relief is approximately 200 m. **C.** Detail of ENE-WSW-plunging fault-related fold cored by the Kayak Shale. **D.** Detail of extensional faults in fault-related anticline. Topographic relief is approximately 200 m. **E. Detail of** extensional fault. Topographic relief is approximately 25 m. **F.** Detail of well-developed continuous cleavage in strata of the Kayak Shale.

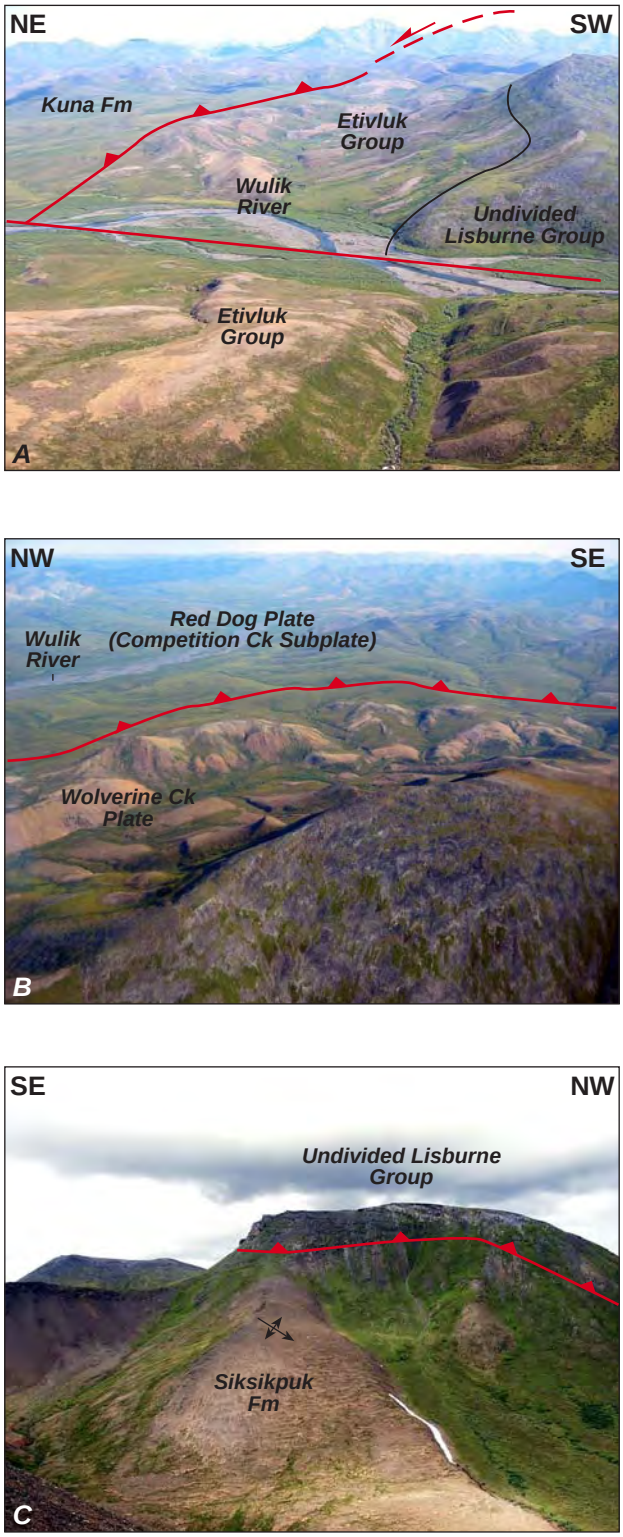


Figure 6.14. Structural features of the Wulik River window in the Wulik River area. **A.** NW-looking view of the Wulik River window. Field of view is approximately 1 km. Topographic relief is approximately 500 m. **B.** NE-looking view of antiformal culmination. **C.** View of SE-verging thrust fault bringing platform carbonates of the Lisburne Group over strata of the Siksikpuk Formation. Topographic relief is approximately 200 m.

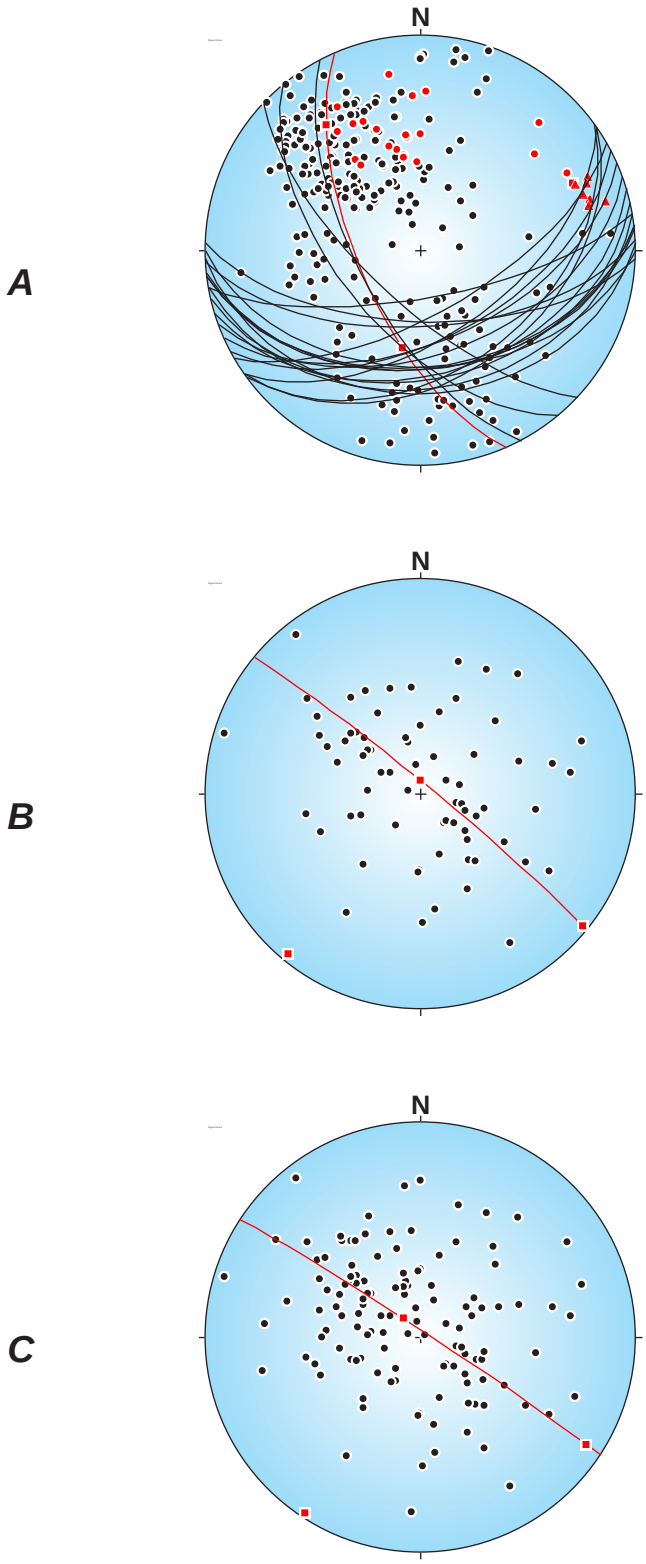


Figure 6.15. Lower hemisphere equal area stereographic projection of structural data from the Wulik River window. **A.** Great circles and poles to bedding (solid black circles) (N=175), poles to cleavage surfaces (red solid circles (N=30) and minor fold axes (red triangles) (N=10) **B.** Poles to bedding in the Wulik River area (N=98). **C.** Poles to bedding in the Rok Hills area (N=75).

as a thrust fault (Mayfield *et al.* 1990*a*; Teck Cominco American Inc. Unpublished). Folds at the Anxiety Ridge are offset by a series of northerly-trending dip-slip and oblique-slip extensional faults with lengths of a few metres to 500 m and inferred vertical throws of several tens of metres.

Red Dog Plate

The Red Dog plate is the thinnest and most discontinuous thrust plate of the Endicott Mountains allochthon in the Red Dog district (Figs. 6.2a, 6.4, 6.16 & 6.17). It hosts the sediment-hosted Zn-Pb-Ag and barite deposits of the Red Dog district (cf. Chapter 5, Figs. 5.5, 5.13 & 5.14; Fig. 6.1). It consists of WNW-ESE- to NE-SW-trending, discontinuous thrust remnants that are typically preserved in the core of regional synforms developed on the dorsal and frontal walls of structural culminations of the Wolverine Creek plate (i.e. Mount Raven and Wulik River windows) (Fig. 6.2a). Total thickness of the Red Dog plate significantly varies from area to area, being absent to *ca.*1 km thick. The Red Dog plate shows varying degrees of structural disruption and appears to grade laterally into syn-orogenic olistostrome and olistostromal melange (cf. Chapter 5, Fig. 5.1; Fig. 6.2a). The Red Dog plate is detached in the Kivalina or Ikalukrok units of the Kuna Formation (cf. Chapter 5, Fig. 5.6). In this study, the Red Dog plate has been subdivided into six distinct thrust subplates that show markedly different lithostratigraphy and structure. In inferred ascending structural order these are here referred to as the Wul, Red Dog Mine, Suds, Gull Creek, Alexander Ridges and Competition Creek thrust subplates (Figs. 6.1 & 6.16; Table 6.4).

Wul Subplate

The Wul subplate is restricted to the Wul area, located approximately 15 km southwest of the Red Dog mine, in the immediate footwall of the Sivukat Mountain fault (Fig. 6.16). The Wul subplate consists of at least four thrust sheets that structurally overlie the Wolverine Creek plate to the west, north and east. To the south, it is offset by the WNW-ESE-trending Sivukat Mountain fault and juxtaposed against the Kelly River allochthon (Fig. 6.16). The Wul subplate is detached in shales and limestones of the Kivalina unit of the Kuna Formation (cf. Chapter 5, Fig. 5.6) and is structurally repeated on three major thrust imbrications that can be identified from surface mapping (Fig. 6.16). Total structural thickness of the Wul subplate is approximately 1 km. The

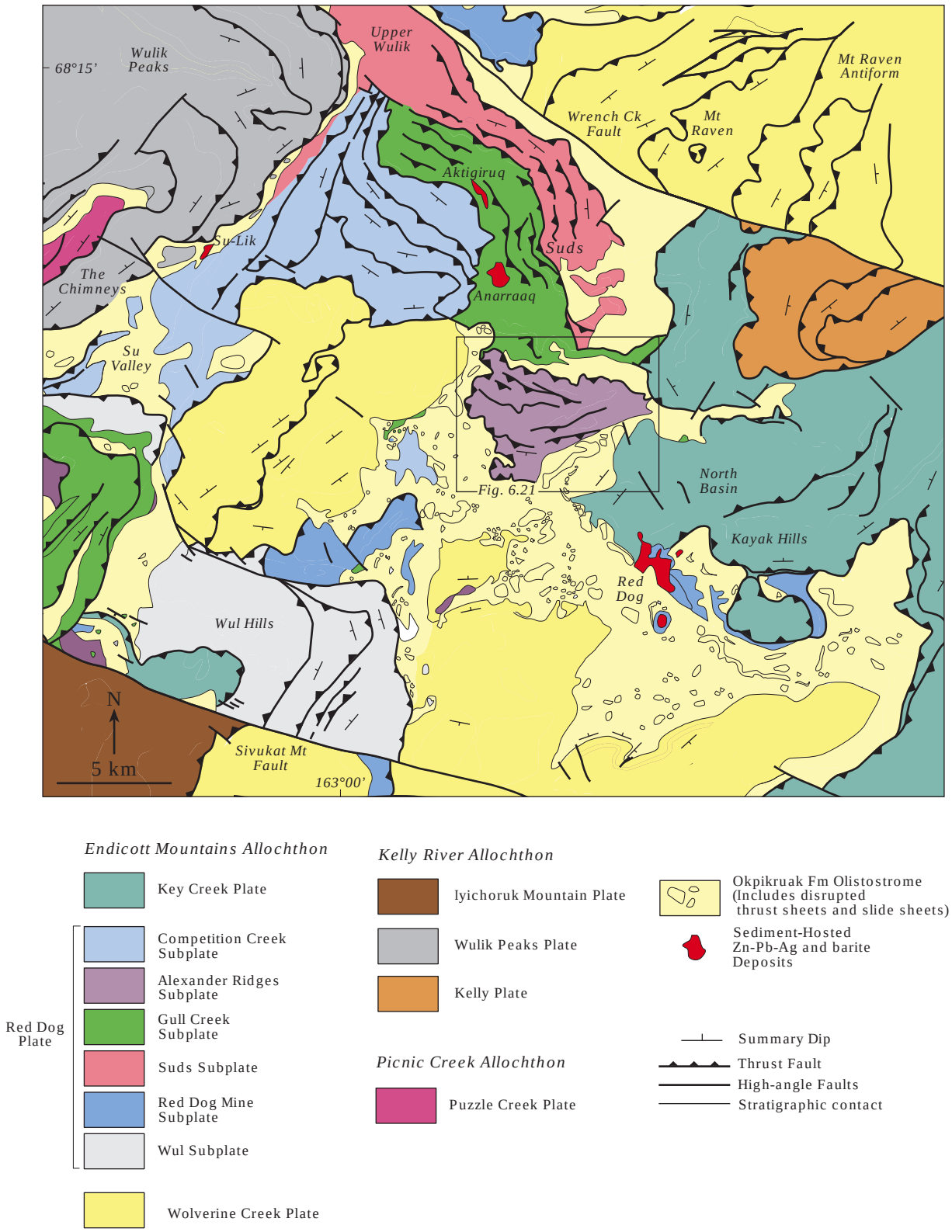
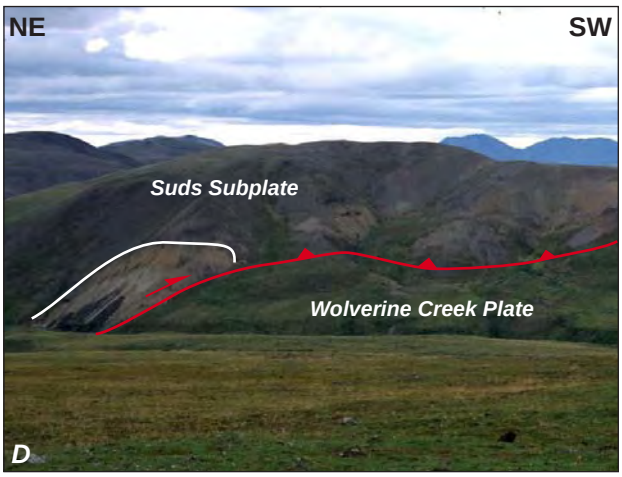


Figure 6.16. Simplified structural map of the central part of the Red Dog district showing the distribution of thrust subplates of the Red Dog plate of the Endicott Mountains allochthon. Note thrust subplates are largely discontinuous and spatially related to early syn-orogenic olistostromes of the Okpikruak Formation.





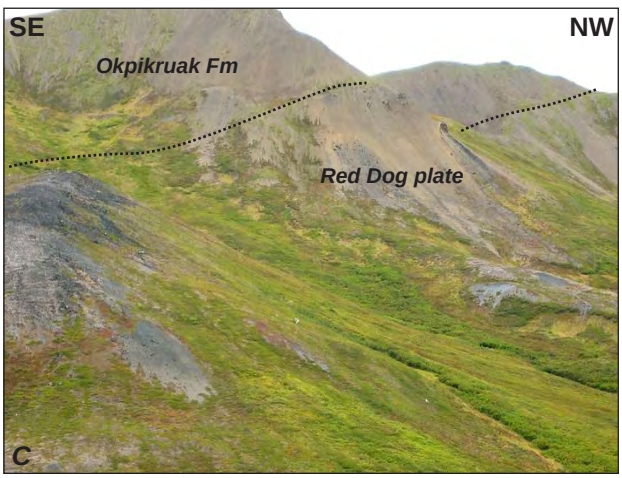


Figure 6.17. Structural features of the Red Dog plate. **A.** Imbricate thrust faults. Topographic relief is approximately 250 m. **B.** Thrust fault-related folds at the base of the Red Dog plate. Topographic relief is approximately 75 m. **C.** Thrust imbricate of the Red Dog plate unconformably overlain by olistostrome of the Okpikruak Formation. Topographic relie is approximately 50 m in the foreground.

	Structural Trends	Detachmen Level(s)	Structural Thickness	Tectonic Transport Direction	Mineralization
Competition Creek Subplate	NE-SW-trending	Kivalina and Ikalukrok units (Kuna Fm)	0 to 1 km	North-northeast to southeast	-
Alexander Ridges Subplate	NE-SW-trending	Ikalukrok unit (Kuna Fm)	500 m	North to north-northeast	-
Gull Creek Subplate	NE-SW-trending	Ikalukrok unit (Kuna Fm)	1 km	Northwest	Anarraaq and Aktigiruq deposits
Suds Subplate	NE-SW-trending	Ikalukrok unit Lower Siksikpuk unit	600 m	North to northeast	Zn-Pb and barite showings
Red Dog Mine Subplate	NE-SW-trending	Kivalina and Ikalukrok units (Kuna Fm)	100 to 600 m	West-northwest to north-northeast	Qanaiyaq, Main, Aqqaluk and Paalaaq Deposits
Wul Subplate	NE-SW- to WNW-ESE-trending	Kivalina unit (Kuna Fm)	700 m to 1 km	Northwest to southeast	-

Table 6.4. Summary structural features of the thrust subplates of the Red Dog plate of the Endicott Mountains allochthon.

structural style of the Wul subplate is controlled by large sub-horizontally to gently-dipping (5° to 10°) thrust faults. Intra-thrust subplate shortening is largely accommodated by thrust faulting and homogeneous strain with cleavage development (Fig. 6.5). Cleavage consists of anastomosing to wavy fabrics that are locally refracted through competent units (Fig. 6.5). Cleavage forms continuous to discontinuous wavy cleavage domains that form an irregular network of lenticular and elongated microlithons. Locally, the anastomosing cleavage is deformed by a later well-developed crenulation cleavage. The cleavage is offset by outcrop-scale gently- to moderately-dipping SE-verging thrust faults. Kinematic indicators and the arrangement of branch lines indicate a southeast tectonic transport direction.

Red Dog Mine Subplate

The Red Dog Mine subplate is a series of unnamed thin and discontinuous thrust panels that host the sediment-hosted Pb-Zn-Ag and barite deposits of the Red Dog Creek area (Fig. 6.16). The Red Dog Mine subplate occurs in the immediate footwall of the Key Creek plate, exposed in the Deadlock Mountain and North Basin areas (Figs. 6.12 – 6.14). This thrust subplate is highly discontinuous and typically shows uncertain structural and stratigraphic relationships with the Okpikruak Formation. Total thickness of the subplate ranges from approximately 100 to 350 m. The Red Dog mine subplate overlies olistolith-bearing shales and sandstones of the Wolverine Creek plate. Within it thrust faults, detachment folds (Fig. 6.18) and transported detachment folds occur. The detailed structure of the Red Dog mine subplate and its sediment-hosted Zn-Pb-Ag deposits is described in Chapter 7.

The Red Dog Mine subplate is detached in Early Mississippian shales of the Ikalukrok unit and/or thin-bedded calcareous turbidites of the Kivalina unit of the Kuna Formation. This basal detachment is a 1 to 100 m thick fault zone with well-developed mélange textures.

Surface mapping and drill hole data indicate that the Red Dog Mine subplate ranges from 350 m to less than 50 m in thickness, becoming increasingly disrupted to the east and west where it grades into syn-orogenic olistostromal strata of the Okpikruak Formation. Olistoliths occur along a narrow, approximately 0.5 to 1.5 km wide, NW-

Figure 6.18. Detachment folds in the Red Dog plate. **A.** W-looking photomosaic of the Red Dog plate. Field of view is approximately 500 m. Topographic relief is approximately 50 m. **B.** Line-drawing structural interpretation of A. Note N-verging strongly asymmetric detachment folds. Lower-hemisphere stereographic projection of great circles and poles to cleavage (solid circles, N=25), minor fold axes (red triangles, N=20), and bedding-cleavage intersection lineations (solid squares, N=25).

trending belt in the immediate footwall of the Zn-Pb-Ag deposits (cf. Chapter 5, Fig. 5.1). Olistoliths consist of isolated metric to decametric isometric to sheet-like blocks of the undivided Lisburne Group, the Kuna, Siksikpuk, and Otuk formations (see Chapter 7).

Suds Subplate

It is thrust on top of the Wolverine Creek plate and overlain by the Gull Creek subplate. The Suds subplate extends to the northwest in the Upper Wulik River area, where it is structurally overlain by imbricate thrust panels of the Picnic Creek allochthon and unconformably overlain by a thick section of syn-orogenic strata of the Okpikruak Formation. The Suds subplate of the Red Dog district is regionally mineralized and includes Zn-Pb showings at Alvinella (cf. Chapter 5, Figs. 5.14e & 5.34b).

Gull Creek Subplate

The structure of the Gull Creek subplate is characterized by WNW-ESE- to NW-SE-trending and dominantly SSW-dipping thrust faults and associated fault-propagation and detachment folds (Fig. 6.19). The Gull Creek subplate is detached in Early Mississippian strata of the Ikalukrok unit of the Kuna Formation (cf. Chapter 5, Fig. 5.6). The Gull Creek plate is thrust on top of the Suds subplate and is structurally overlain by the Alexander Ridges and the Competition Creek subplates to the east and west, respectively (Fig. 6.16). This subplate is also characterized by well developed cleavage fabrics (Fig. 6.20). The Gull Creek subplate contains the Anarraaq and Aktigiruq sediment-hosted Zn-Pb-Ag deposits, which are described in Chapter 7.

Alexander Ridges Subplate

The Alexander Ridges subplate is exposed approximately 6 km northwest of the Red Dog mine (Figs. 6.2a & 6.21). It forms a 15 km^2 thrust remnant that consists of at least five imbrications that can be identified from surface mapping (Figs. 6.2a & 6.21). Thrust panels consist of E-W- to WNW-ESE-trending, SSW-dipping and N- to NNE-verging thrust faults (Figs. 6.21 – 6.23). The Alexander Ridges subplate is detached in Early Mississippian black shales of the lower Ikalukrok unit of the Kuna Formation (cf. Chapter 5, Fig. 5.6). To the southeast the Alexander Ridges subplate is unconformably

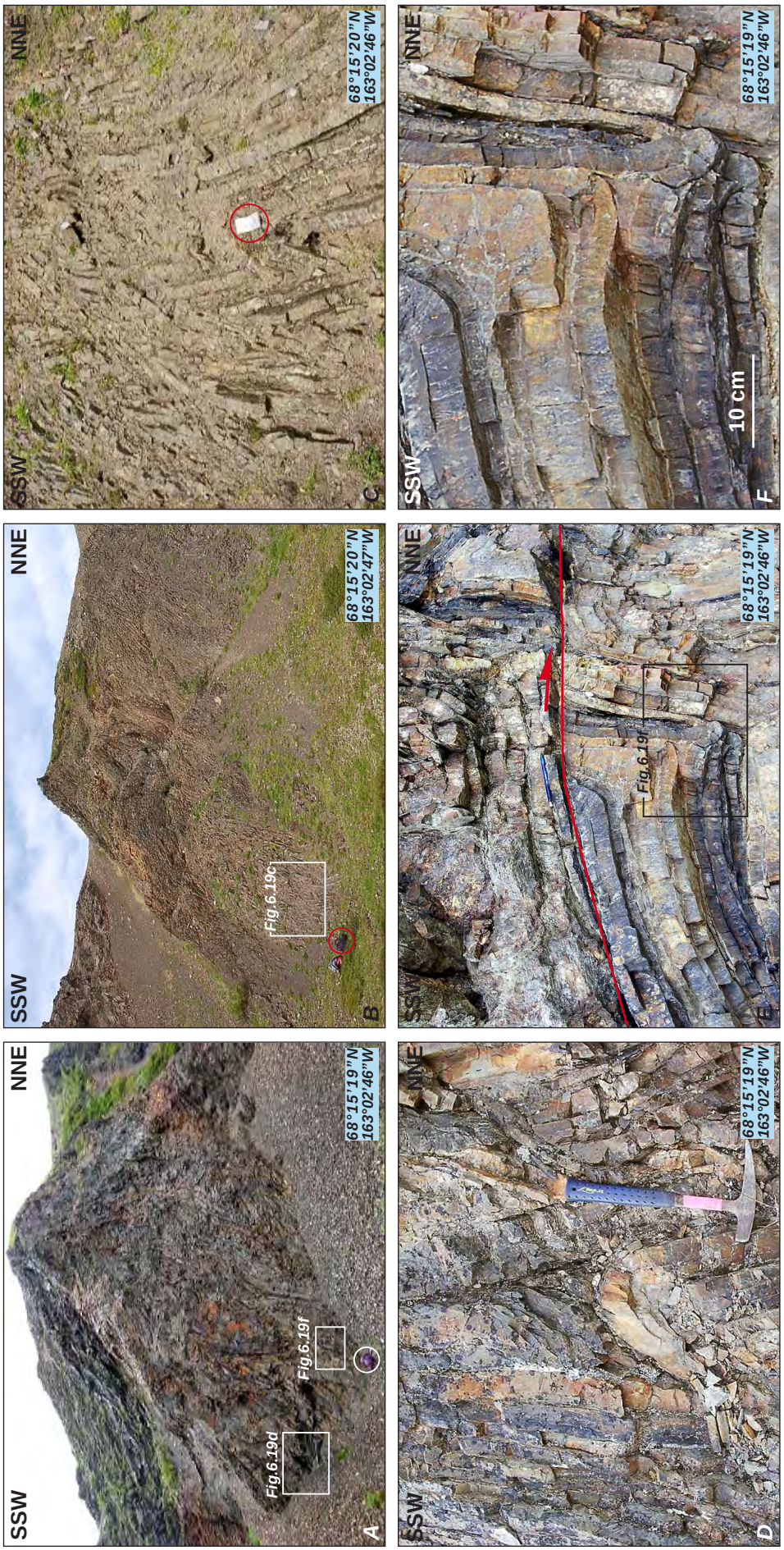


Figure 6.19. Details of detachment folds in the Etivluk Group of the Red Dog plate. **A.** WNW-looking view of detachment folds in well-bedded cherts of the middle unit of the Otuk Formation. Line length balancing of outcrop indicates 215% of shortening. Backpack is encircled for scale. **B.** Detail of WNW-plunging detachment folds in the middle unit of the Otuk Formation. Backpack is encircled for scale. **C.** Detail of NNE-verging, WNW-plunging symmetric to asymmetric detachment folds in cherts of the middle Otuk unit. Compass is encircled for scale. **D.** Detail of asymmetric detachment fold showing cleavage fan. **E.** Detail of fold hinge showing saddle reef structure filled with silica. Pencil for scale. **F.** Detail of saddle reef structure.

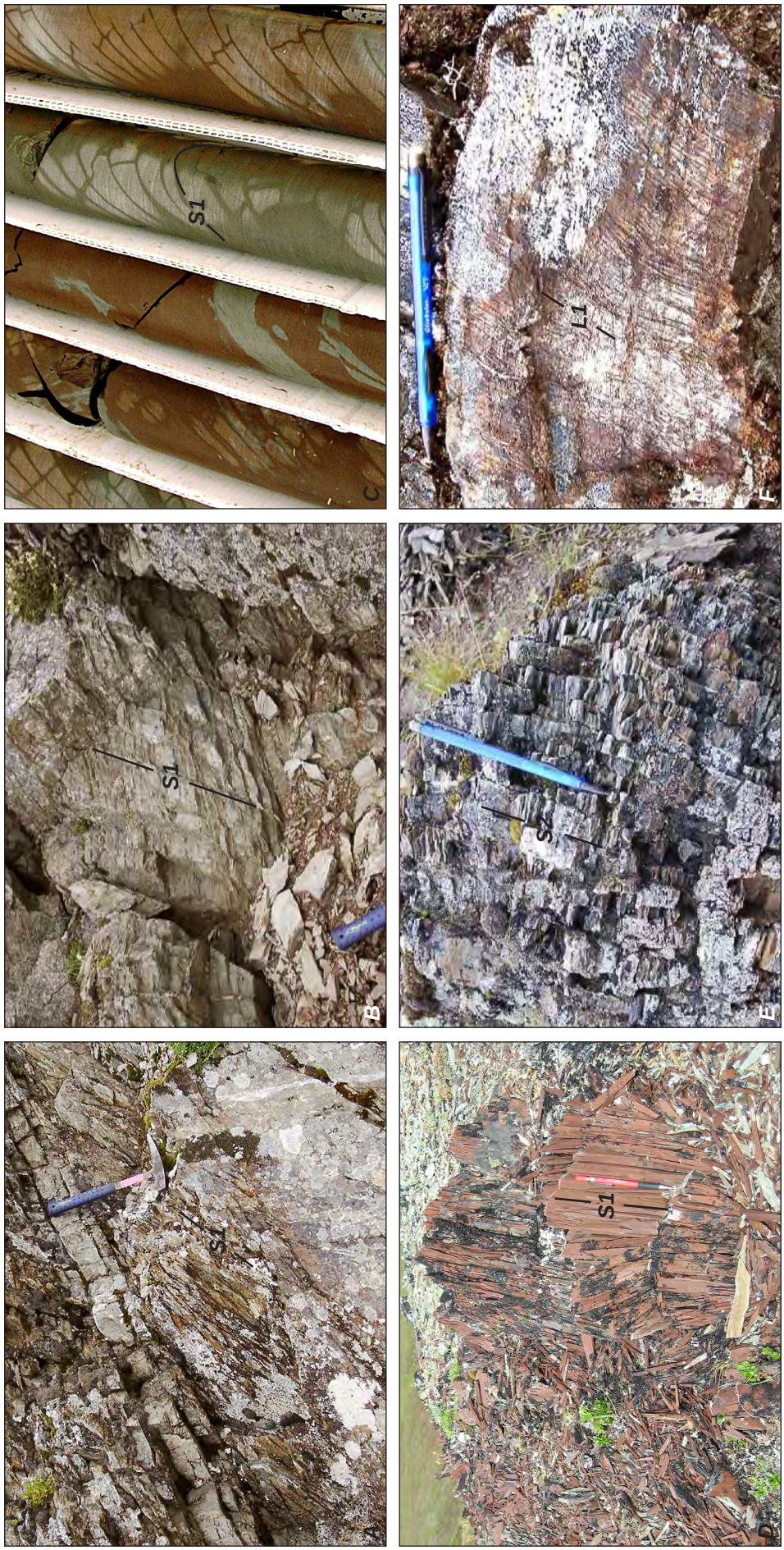


Figure 6.20. Cleavage fabrics in the Red Dog plate. **A.** Refracted cleavage in cherts and shales of the Siksikpuk Formation. Geological hammer for scale. **B.** Spaced cleavage in cherts and shales of the upper unit of the Siksikpuk Formation. **C.** Detail of drill core showing cleavage in shales of the middle unit of the Siksikpuk Formation. Core diameter is approximately 5 cm. **D.** Pencil cleavage in shales of the middle unit of the Siksikpuk Formation. **E.** Detail of crenulation cleavage in shales of the middle unit of the Siksikpuk Formation. **F.** Detail of intersection lineation in the lower unit of the Siksikpuk Formation.

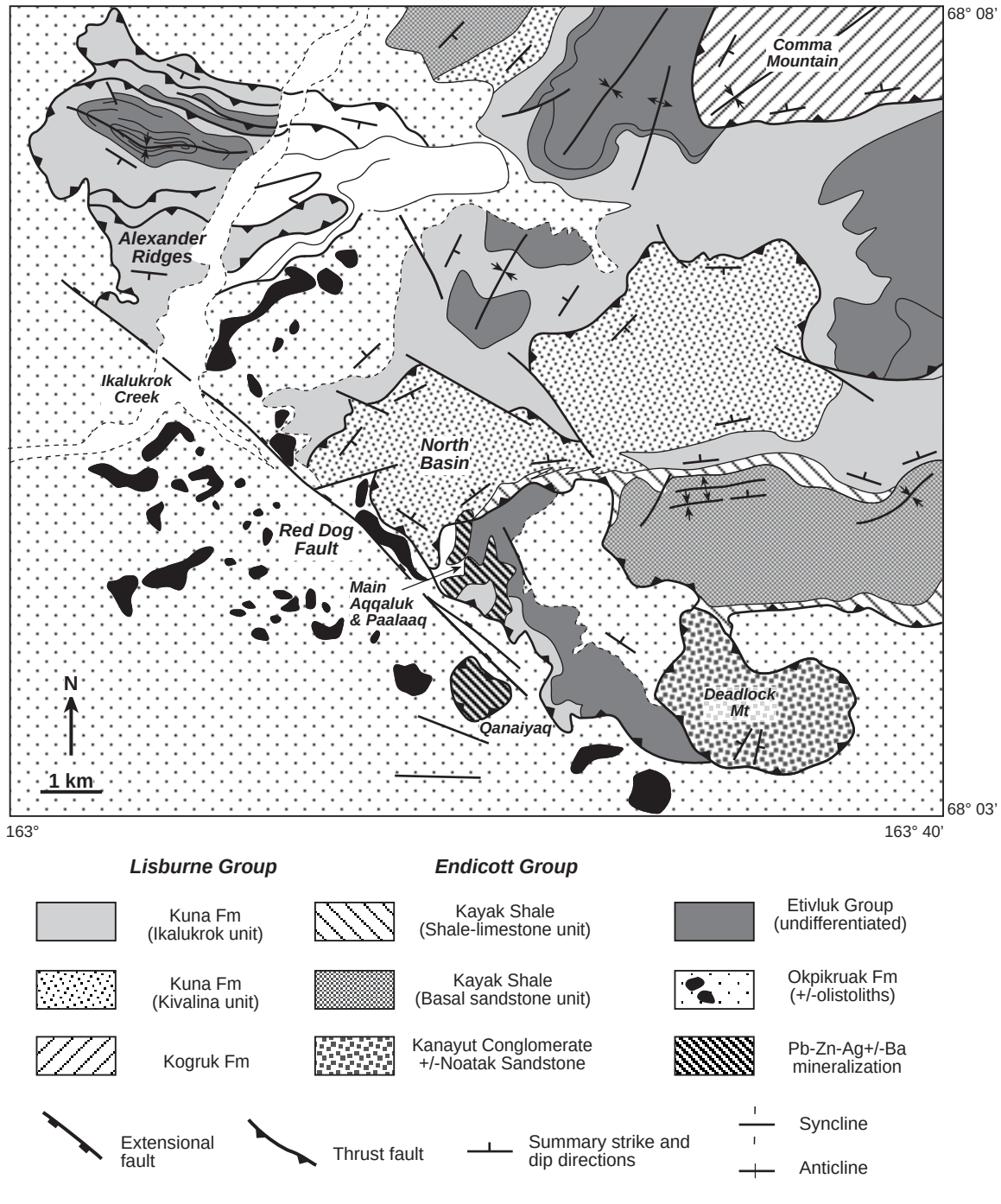


Figure 6.21. Structural map of the Red Dog area including the Alaxander Ridges plate of the Red Dog plate.

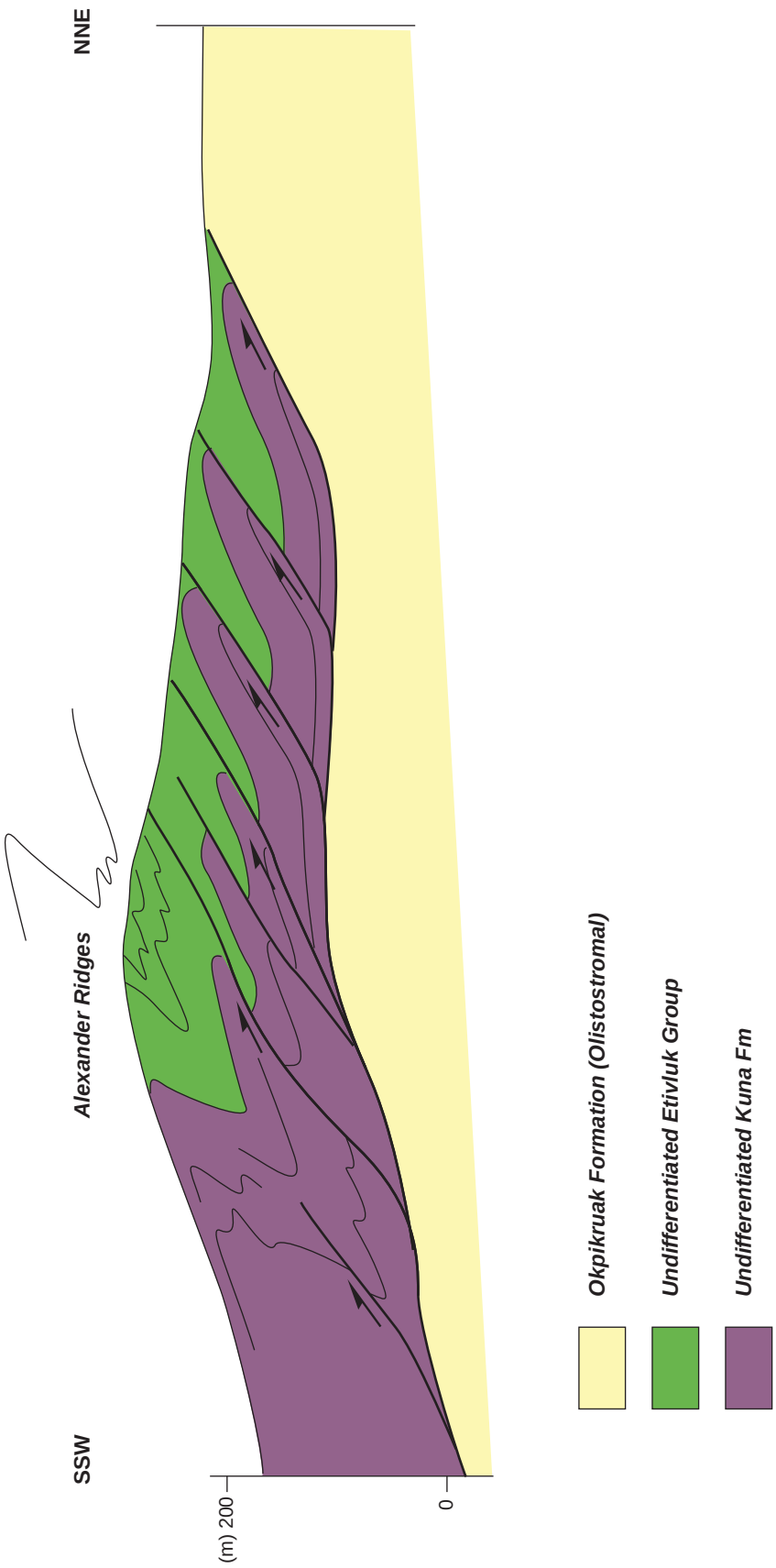


Figure 6.22. Schematic field cross section showing thrust fault imbricates in the Alexander Ridges subplate.



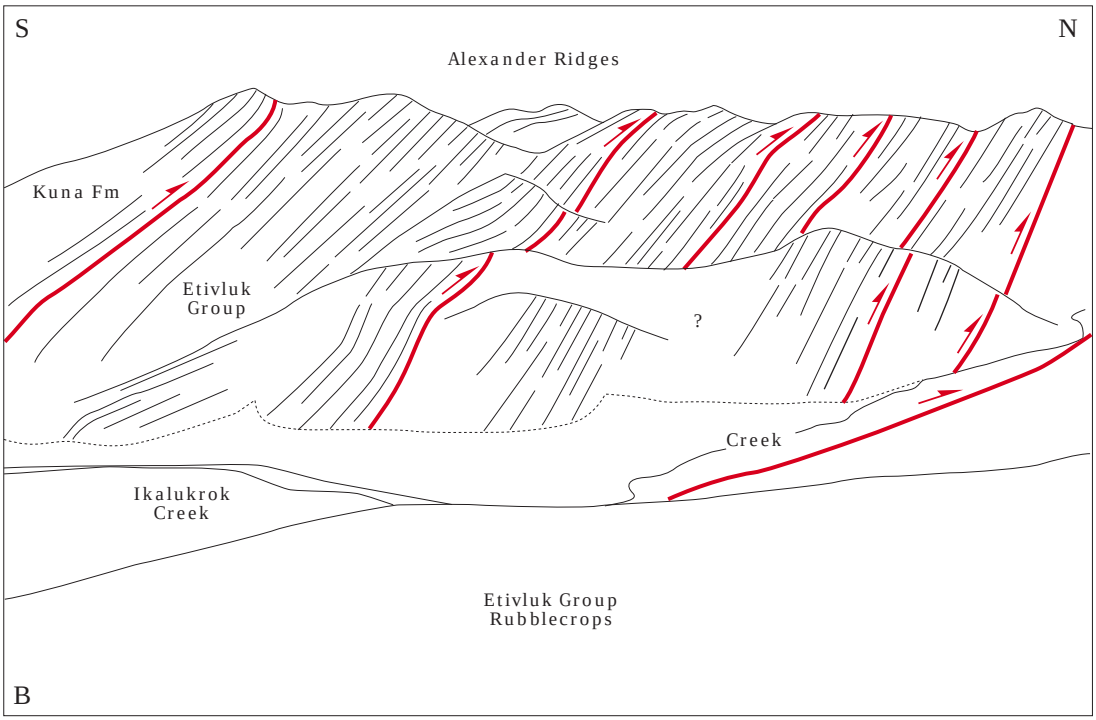


Figure 6.23. Alexander Ridges subplate. **A.** W-looking view of the Alexander Ridges. Dark-weathering strata are black shales and cherts of the Ikalukrok unit of the Kuna Formation. Buff-weathering strata are cherts and shales of the Siksikpuk Formation of the Etivluk Group. Topographic relief is approximately 200 m. **B.** Line-drawing structural interpretation of A showing S-dipping, N-verging thrust imbrications.

overlain by early syn-orogenic strata of the Okpikruak Formation (Fig. 6.21). To the south it lies directly on top of Early Cretaceous strata of the Wolverine Creek plate, whereas to the north and northeast it overlies the Gull Creek subplate of the Red Dog plate (Fig. 6.21) Mineralization in the Alexander Ridges subplate includes massive and bedded barite in strata of the Ikalukrok unit (Fig. 6.21).

Competition Creek Subplate

The Competition Creek subplate occurs approximately 16 km northwest of the Red Dog mine (Fig. 6.16). It is poorly exposed and consists solely of strata of the Kuna Formation (cf. Chapter 5, Fig. 5.6), which form at least three dominantly WNW-ESE-trending and folded imbricate thrust planes that can be inferred by surface mapping and drill hole data (Fig. 6.16). The two southernmost thrust panels are detached in shales of the Kivalina unit of the Kuna Formation, whereas the northernmost thrust panel is detached in the Ikalukrok unit (Figs. 6.16 & 5.1). The Competition Creek subplate structurally overlies distinct plates and subplates of the Endicott Mountains allochthon. To the south, the Competition Creek subplate overlies the Wolverine Creek plate. To the north, the Competition Creek subplate structurally overlies a thick section of folded and faulted strata of the Etivluk Group of the underlying Gull Creek subplate (Fig. 6.16). To the southwest the Competition Creek subplate structurally overlies discontinuous thrust subplates that are here interpreted to be part of an olistostrome (Fig. 6.16). The dominant WNW-ESE-trending structural grain of the Competition Creek subplate is offset by a series of NNE-SSW-trending, WNW-dipping, and ESE-verging thrust faults that are detached in the Kivalina or Ikalukrok units of Kuna Formation (Fig. 6.2a; cf. Chapter 5, Fig. 5.1).

Key Creek Plate

The Key Creek plate is the structurally highest unit of the Endicott Mountains allochthon in the Red Dog district and overlies the Red Dog and Wolverine Creek plates (Figs. 6.1 & 6.2a). It is exposed in the Husky Hills and the Deadlock Mountain – North Basin areas, and also along a poorly-exposed NE-SW-trending belt that extends for approximately 63 km along the Mulgrave Hills (Fig. 6.2a) into the Chukchi Sea Coast. The Key Creek plate has a marked NE-SW-trending structural grain (Fig. 6.2a) defined by large thrust faults and associated thrust fault-related folds. This structural grain is

offset by a series of regional WNW-ESE- to NW-SE-trending high-angle late extensional faults, including the Wrench Creek, Sivukat Mountain and Mulgrave faults (Fig. 6.2a). Structural thickness of the Key Creek plate in the Red Dog district is estimated to range from 2 to 5 km.

Husky Hill Antiform

In the Husky Hills, located approximately 12 km east of the Red Dog mine (Fig. 6.2a), the Key Creek plate exposes a major NNE-SSW- to NE-SW-trending, WNW- to NW-verging, doubly-plunging antiform that extends for approximately 45 km along-strike and has a wavelength of ~10 km (Figs. 6.2a, 6.24 & 6.25). The fold axial surface of the Husky Hills antiform dips 40° to 65° to the southeast and east-southeast. Interlimb angles typically range from 42° to 95°. The NNE-plunging termination of the Husky Hills antiform is aligned with the NNE-plunging culmination of the Mount Raven antiform and broadly coincides with the eastern tip of the Wrench Creek fault (Fig. 6.2a). The SSW-plunging termination of the Husky Hills antiform broadly coincides with the eastern tip of the Sivukat Mountain fault.

The Husky Hills antiform is cored by and detached in strongly cleaved Late Devonian strongly cleaved phyllites, shales and siltstones of the Hunt Fork Shale (cf. Chapter 5, Figs. 5.1, 5.4 & 5.7) that are only exposed in the central Husky Hills (Figs. 6.26 & 6.27). The Hunt Fork Shale appears to be increasingly deformed towards the base of the unit, suggesting the presence of a major thrust fault at depth.

Further west, the basal thrust of the Key Creek plate progressively ramps up through the Kanayut Conglomerate and reaches an upper detachment in the Early Mississippian Kayak Shale. The strata of the Key Creek plate are polyharmonically folded and locally detached along the stratigraphic contact between the incompetent Kayak Shale and the more competent Kanayut Conglomerate and Noatak Sandstone units (Fig. 6.28). Folds in the Kayak Shale are typically symmetric to asymmetric and have wavelengths that vary from 1 to 10 m and high amplitudes that commonly range from 3 to 10 m. Parasitic detachment folds in the Kayak Shale are disharmonic to polyharmonic with interlimb angles of approximately 30° to 45°. The dip of the frontal limb ranges from gently-dipping upright through vertical to moderately-dipping overturned. The Husky

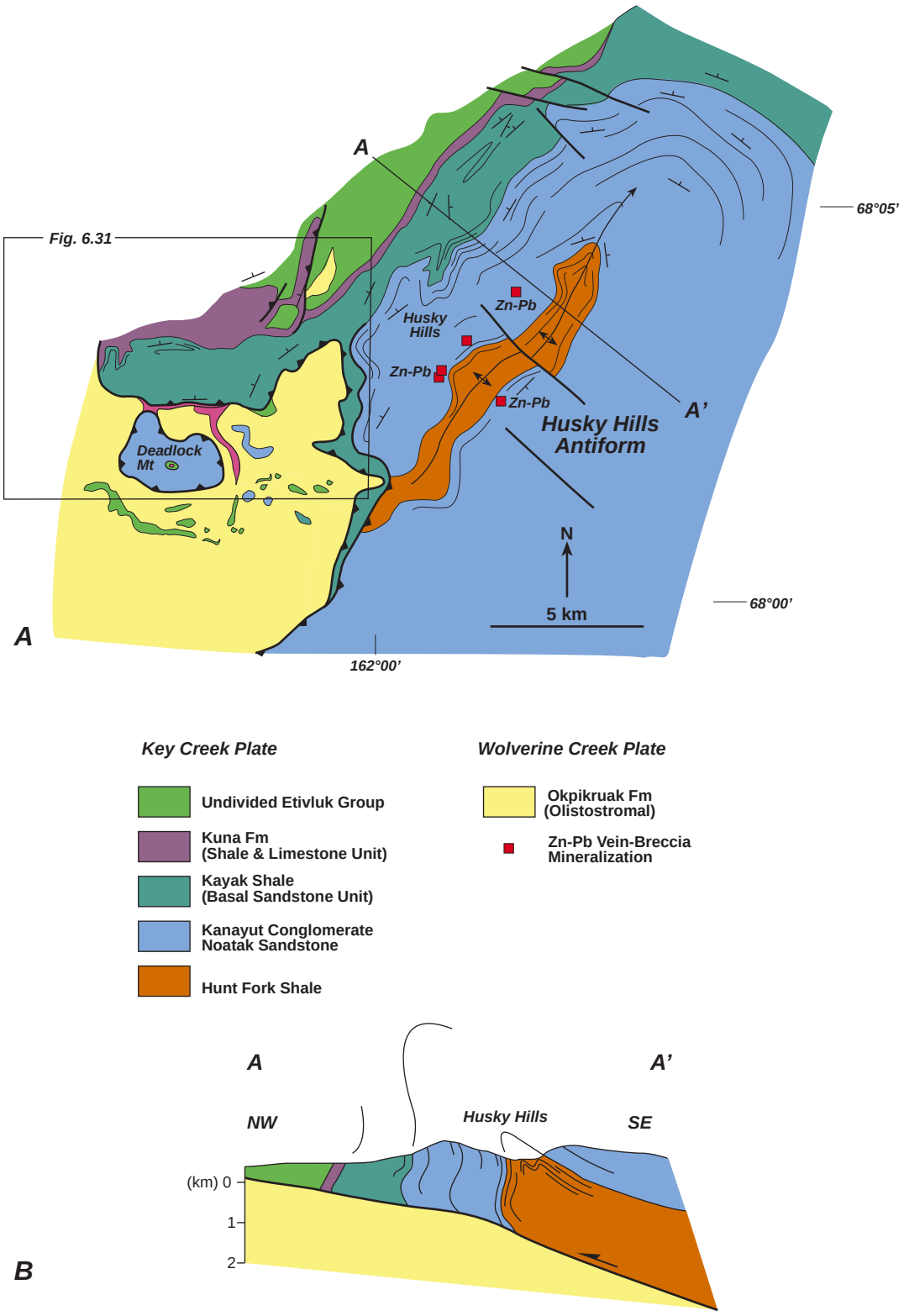


Figure 6.24. Key Creek plate. **A.** Simplified structural map of the Husky Hills and Deadlock Mountain areas showing the structure of the Husky Hills antiform and the location of Zn-Pb vein-breccia mineralization. **B.** Cross section across the Husky Hills antiform.

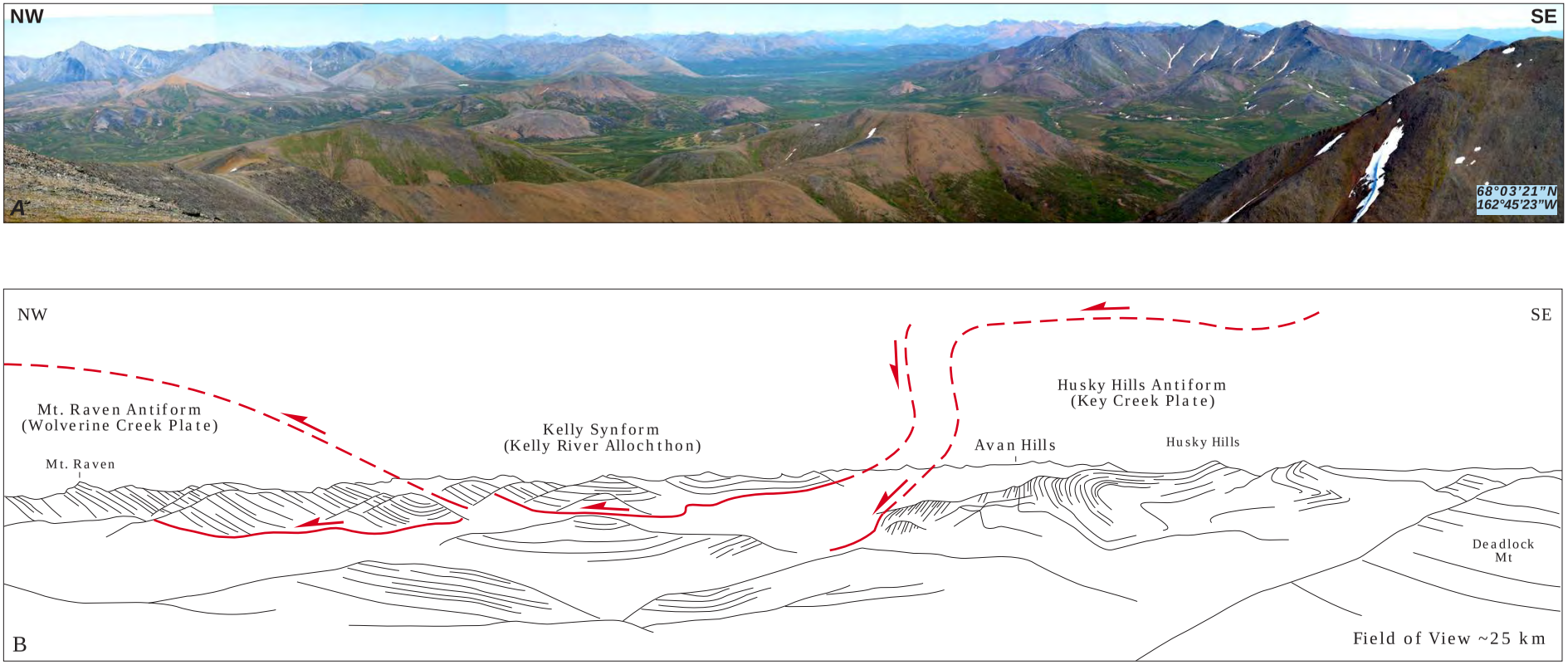


Figure 6.25. Structural relationships of the Key Creek plate. **A.** N-looking photomosaic showing the Key Creek plate. Field of view is approximately 25 km. Topographic relief is approximately 500 m in the Husky Hills. **B.** Line-drawing structural interpretation of A. Note the Kelly River synform and the Mount Raven antiform ahead of the Husky Hills antiform. The Red Dog mine is located approximately 1 km northwest of the point of view.

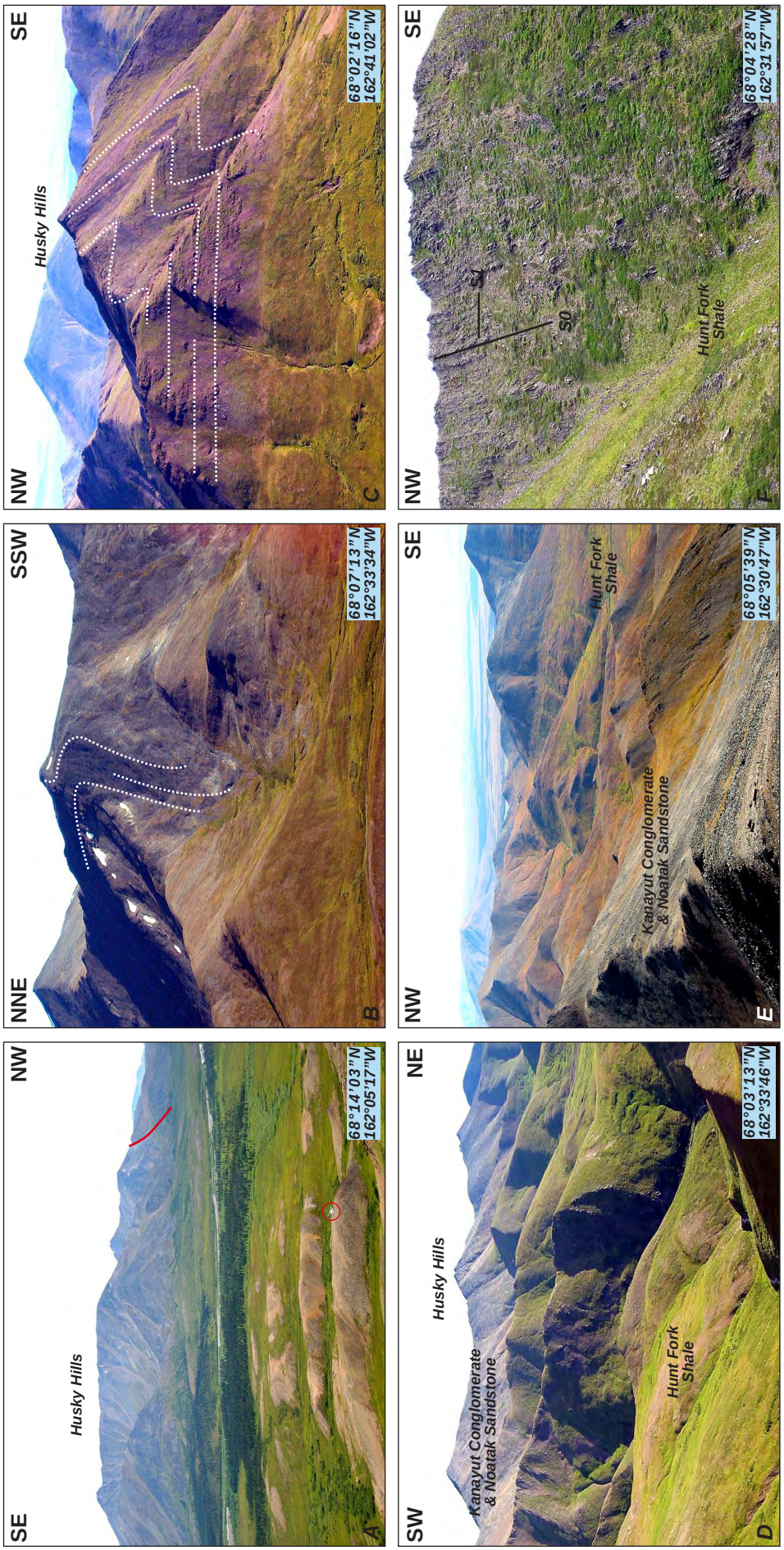


Figure 6.26. Structural features of the Husky Hills antiform in the Husky Hills area. **A.** S-looking view of the Husky Hills showing the frontal part of the Key Creek plate. Helicopter encircled for scale. **B.** Detail of anticline-syncline pair. Topographic relief is approximately 200 m. **C.** Detail of NW-verging asymmetric syncline in strata of the Kanayut Conglomerate. Topographic relief is approximately 200 m. **D & E.** Details of the NNE-plunging termination of the Husky Hills antiform. Topographic relief is approximately 300 and 200 m, respectively. **F.** Bedding-cleavage relationships (S0 & S1) in strata of the Hunt Fork Shale in the front limb of the Husky Hills antiform. Outcrop is approximately 25 m high.

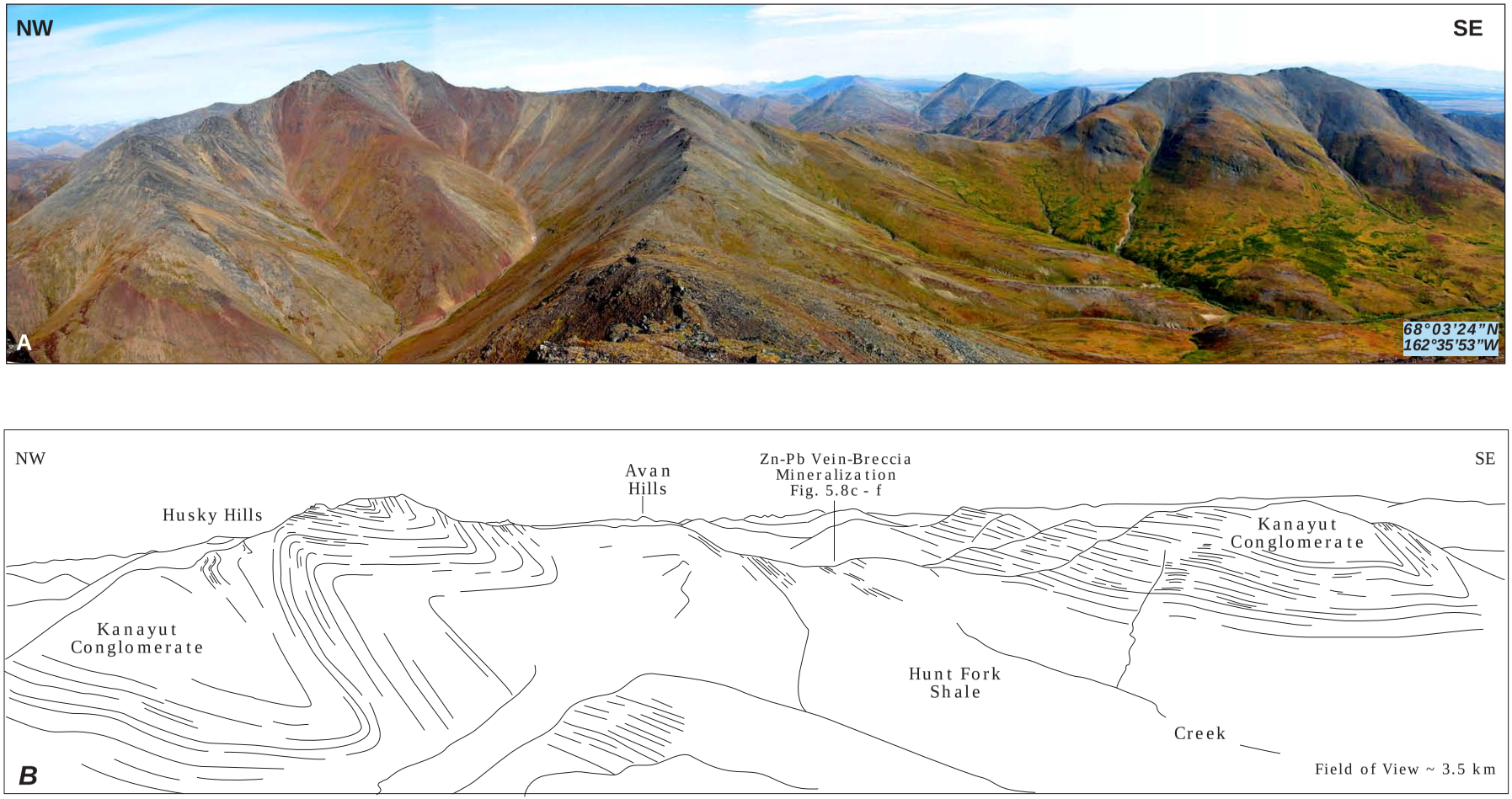


Figure 6.27. Structural styles of the Husky Hills antiform. **A.** NE-looking photomosaic showing the structure of the Husky Hills antiform in the Husky Hills. Topographic relief is approximately 500 m. Field of view is approximately 3.5 km. **B.** Line-drawing structural interpretation of A, showing the geometry of the Husky Hills antiform. Note strongly asymmetric anticline cored by the Hunt Fork Shale. The location of vein-breccia Zn-Pb mineralization is shown.

Figure 6.28. Husky Hills antiform. **A.** NE-looking photomosaic. Topographic relief isapproximately 500 m. Field of view is approximately 1.5 km. **B.** Line-drawing structural interpretation of A showing the NE-plunging termination of the Husky Hills antiform. Note polyharmonic folding associated with competence contrasts between the Kanayut Conglomerate and the Kayak Shale.

Hills antiform is interpreted to be underlain by a major ESE-dipping and WNW-verging thrust fault (Fig. 5.24b). The Husky Hills antiform shows a consistent SE-dipping regional axial planar slaty cleavage that is best developed in strata of the Hunt Fork Shale (Fig. 6.26f; cf. Chapter 5, Fig. 5.8a) and fine-grained strata of the Kanayut Conglomerate, the Noatak Sandstone and the Kayak Shale (cf. Chapter 5, Fig. 5.8a & d). Pencil cleavage is developed in the vicinity of fold hinge zones in the Kayak Shale. Kinematic indicators, including cleavage, orientation and asymmetry of folds, outcrop-scale thrust faults and stepped slickenside surfaces, slickenfibre lineations, indicate a west-northwest to northwest regional tectonic transport direction (Fig. 6.29).

The Husky Hills antiform is offset by a series of WNW-ESE-trending, NNE- to SSW-dipping high-angle, late extensional faults that are perpendicular to the trace of the antiform. Fault spacing typically ranges from 100 m to 1 km. NNE-SSW-trending and WNW- to ESE-dipping extensional faults are also present in the crest of the antiform. These are parallel to slightly oblique to the axial trace of the Husky Hills antiform and have moderately low displacements, commonly in the range of 5 to 25 metres. These are possible outer-arc extensional faults associated with the development of the Husky Hills antiform.

The Deadlock Mountain thrust is interpreted as a regional-scale frontal ramp along which the Endicott Mountains allochthon climbed from a lower detachment in Late Devonian incompetent shales and siltstones of Hunt Fork Shale ramped up through the competent Noatak Sandstone and Kanayut Conglomerate units and reached a higher detachment in Early Mississippian incompetent shales the Shale and Limestone unit of the Kayak Shale. This ramp is complexly folded by imbrication and duplexing on the underlying Wolverine Creek plate.

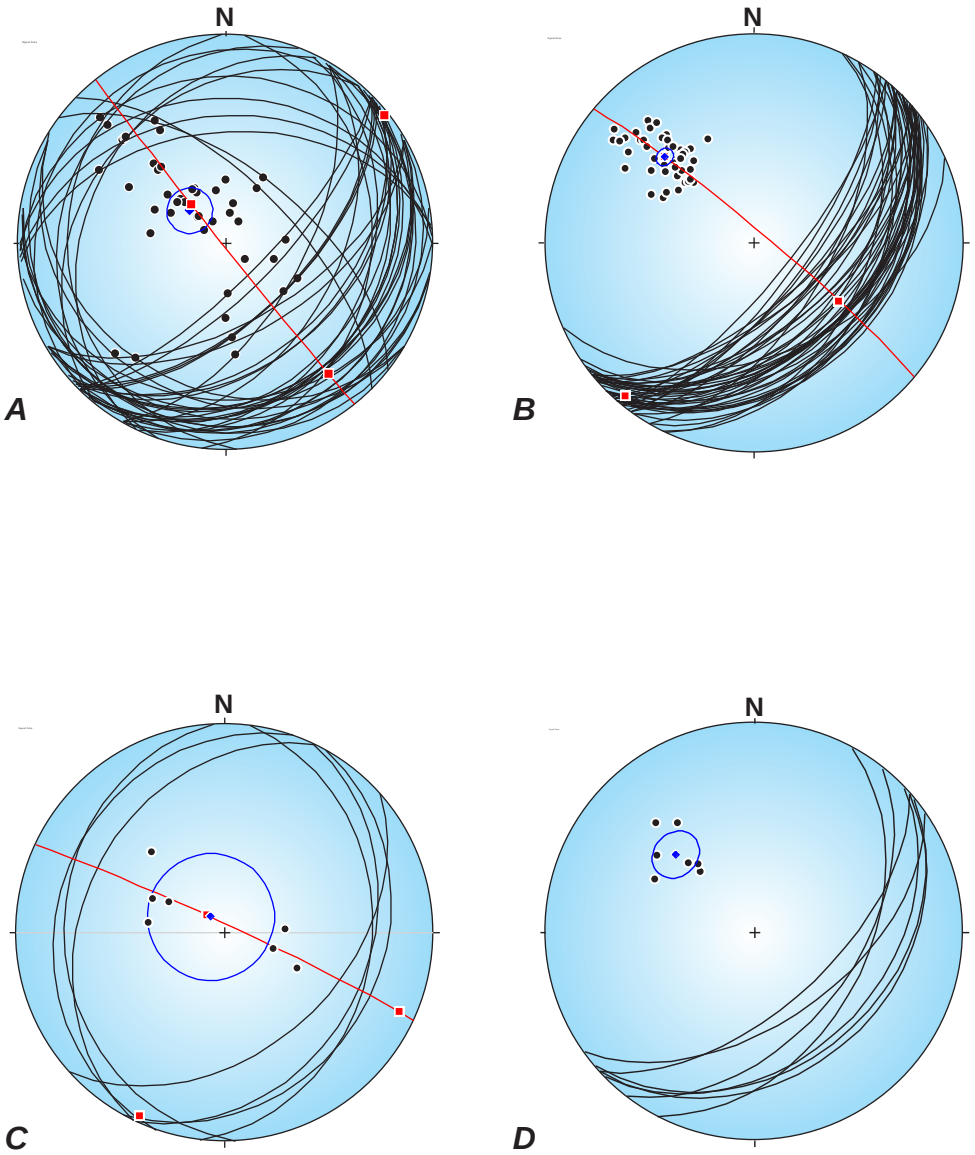


Figure 6.29. Lower hemisphere equal area stereographic projection of structural data from the Key Creek plate of the Endicott Mountains allochthon in the Husky Hills area. **A.** Great circles and poles to bedding in the Kanayut Conglomerate in the northern Husky Hills (N=50). Fold axis=1°/51°. **B.** Great circles and poles to cleavage in the northern Husky Hills (N=51). Mean pole=40°/314°. **C.** Great circles and poles to bedding in the Kanayut Conglomerate in the southern Husky Hills (N=10). Fold axis=3°/205°. **D.** Great circles and poles to cleavage in the Hunt Fork Shale in the south-central Husky Hills (N=7). Mean 45°/314°.

Husky Hills Vein-Breccia Mineralization

Sediment-hosted vein-breccia Zn-Pb mineralization (cf. Chapter 5, Fig. 5.7b – f) occurs in the front and back limbs of the Husky Hills antiform. Zn-Pb-bearing veins dominantly crosscut bedding surfaces at high angles, with cut-off angles that range from 60° to 90° (Figs. 6.24a & 6.30a; cf. Chapter 5, Fig. 5.7c, e, f). Veins are WNW-ESE to NNW-trending (Fig. 6.30b) and are oriented perpendicular to sub-perpendicular and parallel to sub-parallel to the fold axial trace of the Husky Hills antiform. Veins are offset by SE-dipping, NW-verging outcrop-scale thrust faults and deformed by fault-related folds and by well developed spaced to continuous penetrative cleavage (cf. Chapter 5, Fig. 5.7d).

Based on the evidence presented above and in Chapter 5 (Fig. 5.7), vein-breccia mineralization is here interpreted to pre-date deformation of the Brookian orogeny and the development of the Husky Hills antiform. The high cut-off angles to bedding indicate that veins possibly formed in an extensional setting as predicted by fault dilatancy models (e.g. Garven, 1985; Sibson, 1990, Person & Garven, 1994; Strayer *et al*. 2001; Garven *et al*. 2003; Sibson, 2004) (Fig. 6.30c). Vein-breccia mineralization are here interpreted to have been formed by metal-bearing hydrothermal fluids, which filled dilation zones or damage zones in the vicinity of WNW-ESE- to NNE-SS-trending extensional faults of the ancient continental margin in the Palaeozoic. Subordinate bedding-parallel Zn-Pb-bearing veins are here interpreted to have resulted from sulphide remobilization during Palaeozoic basin inversion (?) or Mesozoic Brookian contraction.

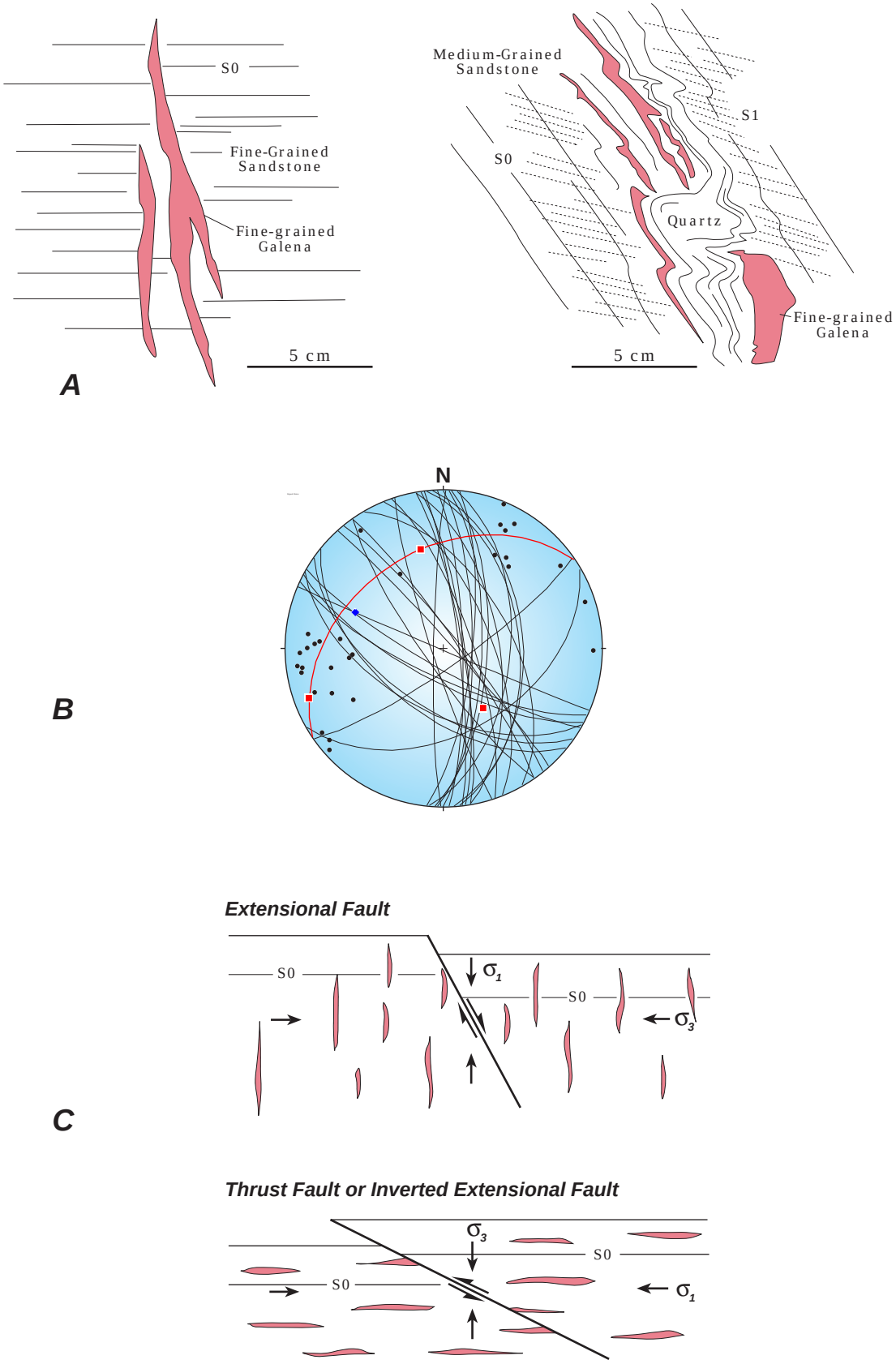


Figure 6.30. Husky Hills vein-breccia mineralization. **A.** Field sketches showing the relationships between galena veins and bedding. **B.** Lower hemisphere stereographic projection of Zn-Pb veins (N=32) in the Noatak Sandstone, Husky Hills. **C.** Conceptual models showing the relationships between vein orientation and stress fields (modified from Sibson, 1990).

Deadlock Mountain and North Basin Areas

Deadlock Mountain, located approximately 2 km southeast of the Red Dog mine (Figs. 6.1 & 6.31), exposes a 4 km^2-klippe of Late Devonian to Early Mississippian syn-rift strata of the Endicott Group of the Key Creek plate. The Key Creek plate at Deadlock Mountain is floored by a subhorizontally-dipping thrust fault, here named the Deadlock Mountain thrust (Figs. 6.31 – 6.33). The Deadlock Mountain thrust is a folded regional hangingwall ramp, in which the basal thrust of the Key Creek plate climbs from Late Devonian strata to early Mississippian strata of the Kayak Shale. The thrust cuts up section and generally dips to the northwest and north such that progressively younger units are exposed to the north and northwest (Figs. 6.31 – 6.33). The Deadlock Mountain thrust fault places Late Devonian to Early Mississippian strata of the Endicott Group on top of olistolith-bearing conglomerates, sandstones and shales of the Okpikruak Formation and older strata of the underlying Red Dog plate. Thrust fault-related folds are well exposed along the east face of Deadlock Mountain (Figs. 6.34 & 6.35). These occur as NNE-SSW-trending and WNW-vergent gently inclined to recumbent fault-related folds developed in the Kanayut Conglomerate of the Endicott Group above a footwall and hangingwall thrust ramp (Figs. 6.34 & 6.35). The axial surface of this fold structure is gently inclined (~10°) to the east-southeast to sub-horizontal. Hangingwall cut-off angles range from 45° to 90º. Folding is accompanied by a well-developed and consistent ESE-dipping axial planar spaced to continuous cleavage, which is best developed in maroon shales and siltstones of the Kanayut Conglomerate (Fig. 6.36).

Coarse- to medium-grained sandstones of the Kanayut Conglomerate show bedding surfaces coated with chlorite fibre lineations parallel to the slip direction of WNW-ENE flexural slip movement on bedding surfaces indicate west-northwest—east-northeast flexural slip on bedding surfaces. Fibre lineations orthogonal to slightly oblique to the trend of the fold axial surface and are consistent with the attitude of the ESE-dipping regional cleavage and other kinematic indicators. Minor, parasitic and disharmonic folding is common in more thinner-bedded layers and more incompetent levels.

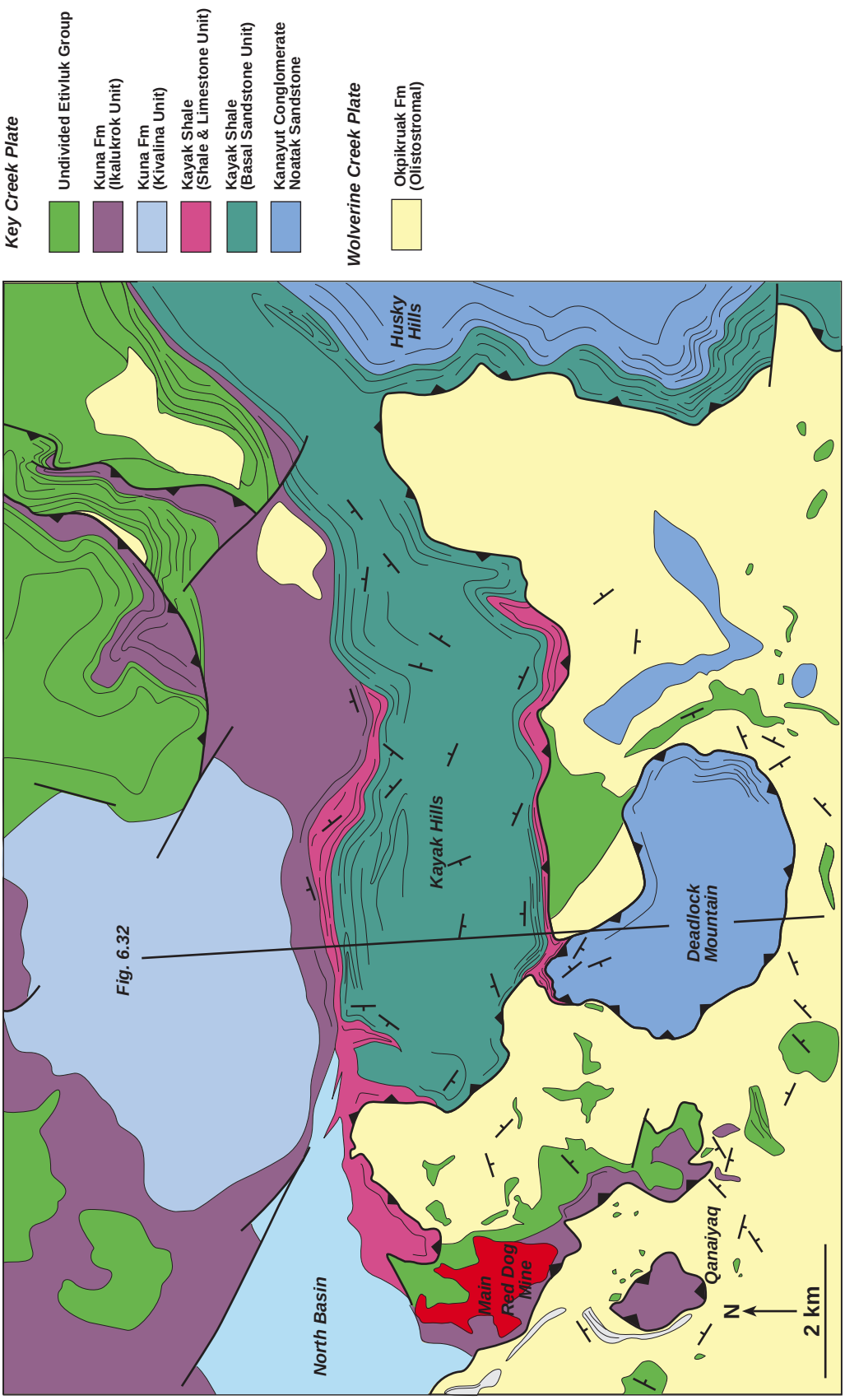


Figure 6.31. Simplified geologic map showing the structure of the Key Creek plate in the Deadlock Mountain and North Basin areas. Line of cross-section is shown.

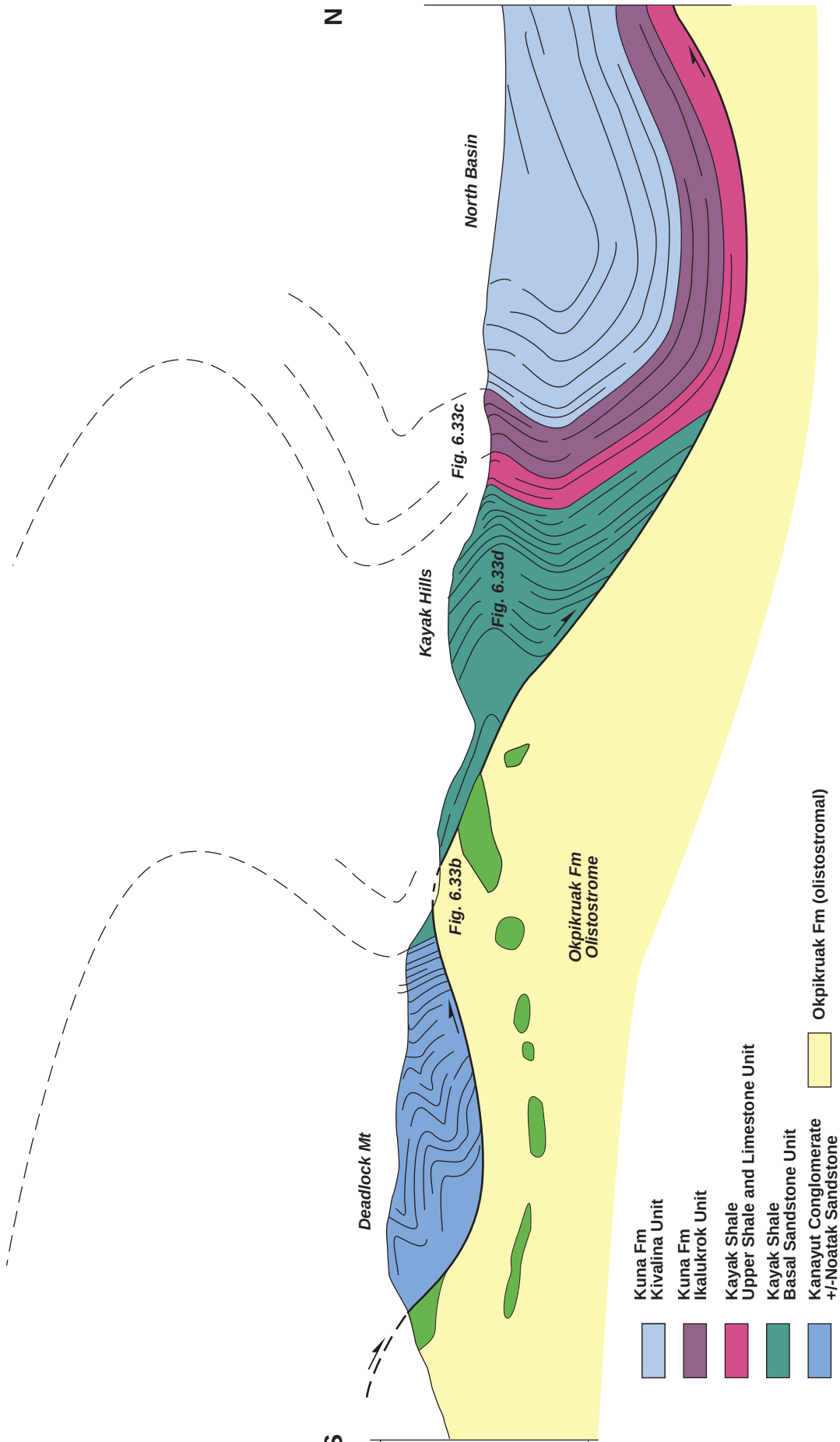


Figure 6.32. S-N cross section showing the structure of the Key Creek plate in the Deadlock Mountain and North Basin areas. No vertical exaggeration. Folded Deadlock Mountain thrust is interpreted to reflect imbrication on the underlying Wolverine Creek plate. Refer to Figure 6.31 for location of cross section.

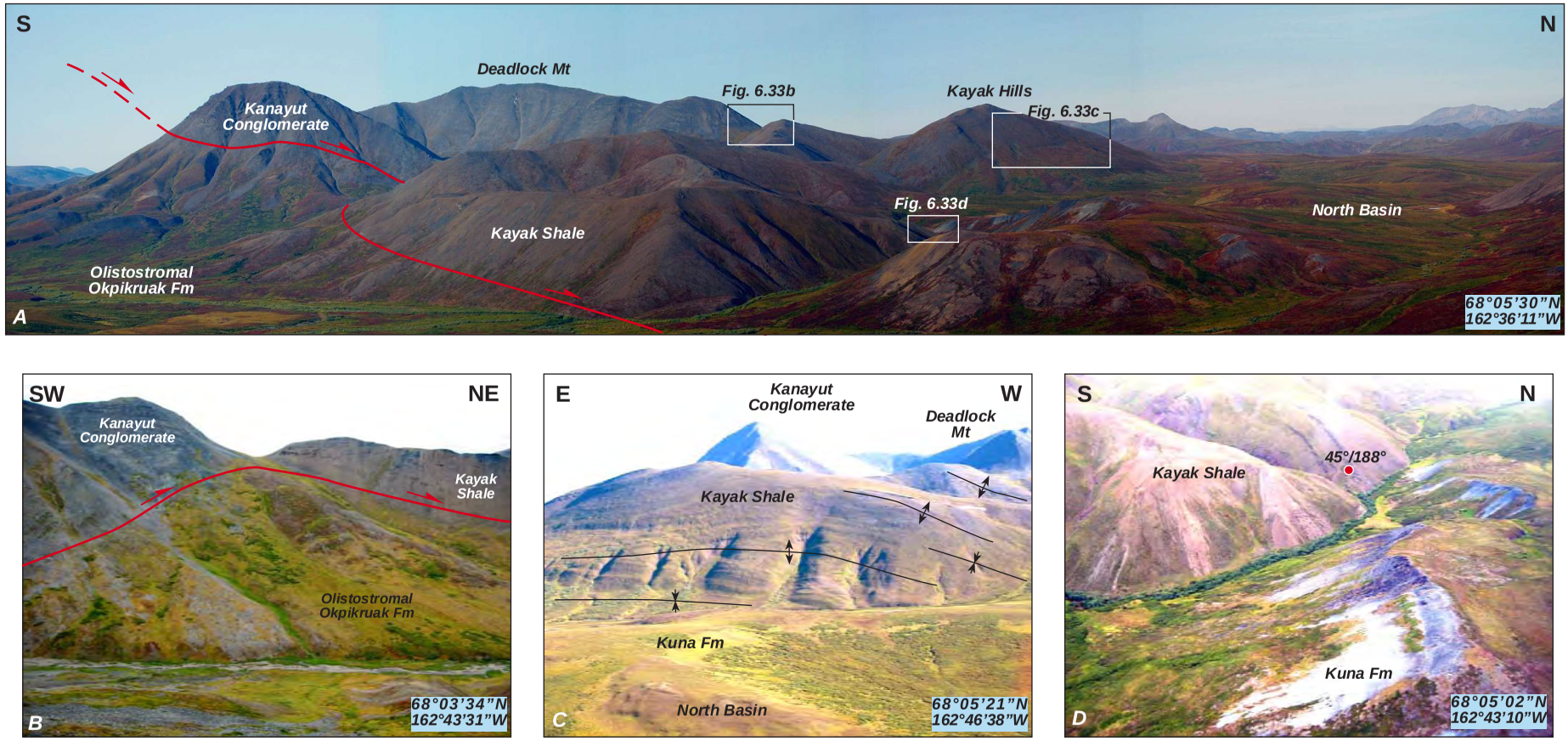


Figure 6.33. Structural features of the Key Creek plate in the Deadlock Mountain area. **A.** W-looking photomosaic of the Key Creek plate viewed from the Husky Hills. Field of view is approximately 3 km. Topographic relief is approximately 800 m. **B.** Detail showing the Deadlock Mountain thrust. Topographic relief is approximately 350 m. See cross section in Figure 6.32. **C.** S-looking view of E-W-trending detachment folds in the Basal Sandstone unit of the Kayak Shale. Topographic relief is approximately 600 m. **D.** Detail of N-dipping stratigraphic contact between the Kayak Shale and the Kuna Formation in the North Basin area. Topographic relief is approximately 25 m. Contact is steeply dipping to locally overturned.

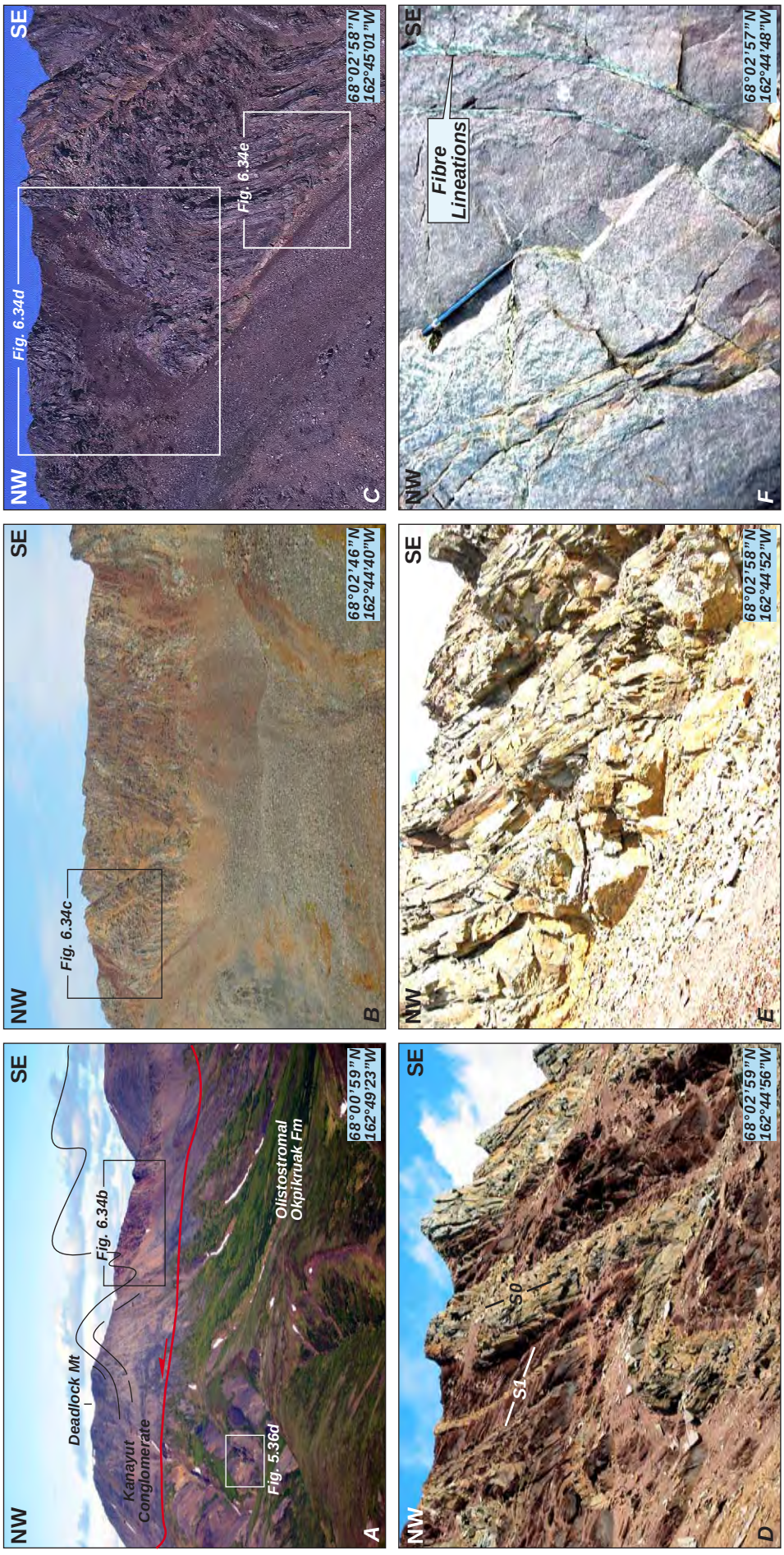


Figure 6.34. Detailed structural features of the Key Creek plate in the Deadlock Mountain area. **A.** NE-looking view of the Key Creek plate in the Deadlock Mountain area. Note klippen of Kanayut Conglomerate thrust on top of olistolith-bearing strata of the Okpikruak Formation. Topographic relief is approximately 500 m. **B.** Detail of inclined fault-related folds in the immediate hangingwall of the Deadlock Mountain thrust. Topographic relief is approximately 50 m. **C.** Detail of anticline shown in B showing well-developed axial planar cleavage in folded sandstones and maroon shales. **D.** Detail of axial planar slaty cleavage in mudstones and shales of the Kanayut Conglomerate. **E.** Detail of asymmetric syncline in medium- to coarse-grained sandstones of the Kanayut Conglomerate. Outcrop is approximately 5 m high. **F.** Chloritized flexural slip surfaces in medium-grained sandstones of the Kanayut Conglomerate. Pencil for scale.

Figure 6.35. Field sketch showing the structure of the Key Creek plate along the northwest face of Deadlock Mountain. Note inclined fault-related fold in Late Devonian strata of the Kanayut Conglomerate.

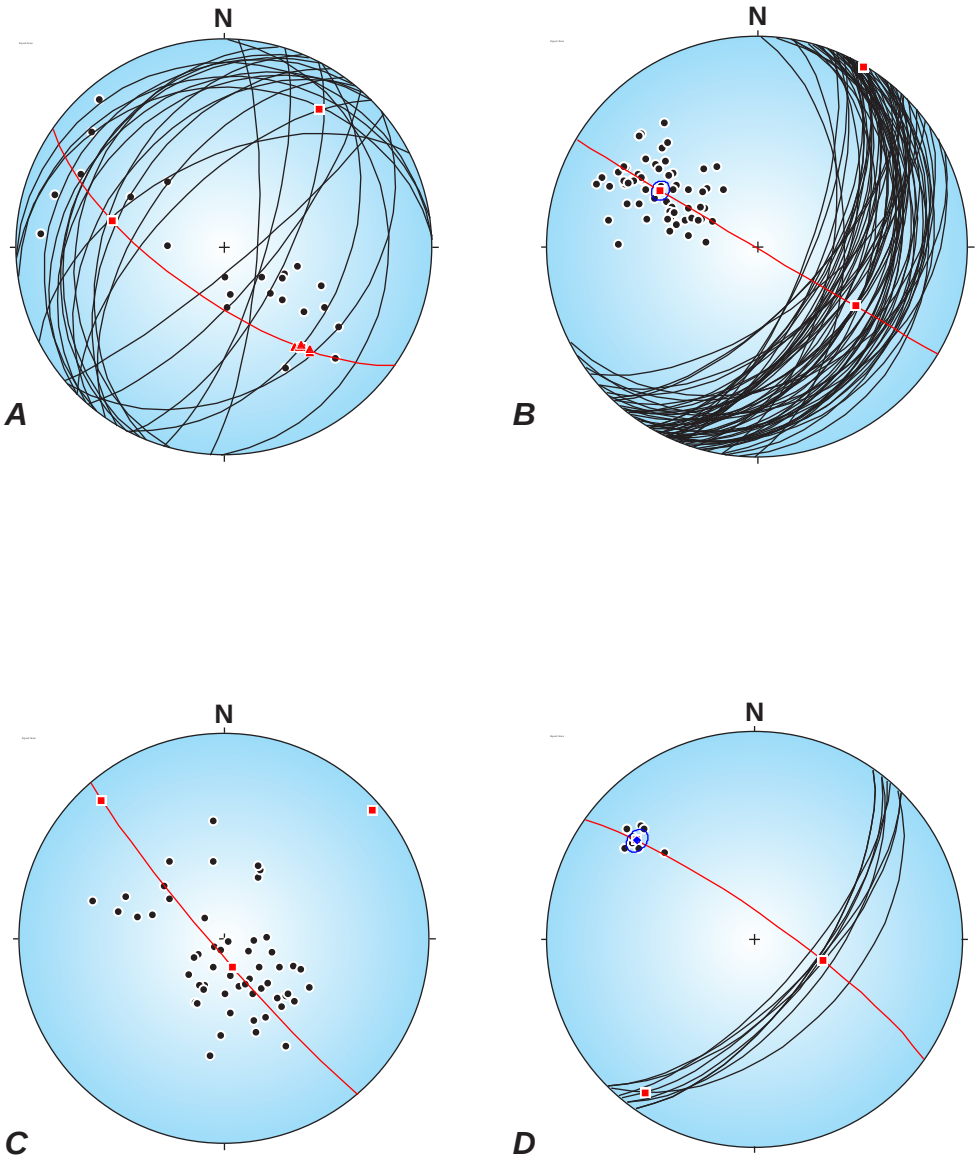


Figure 6.36. Structural data from the Key Creek plate in the Deadlock Mountain area. **A.** Great circles and poles to bedding (N=25) in the Kanayut Conglomerate at Deadlock Mountain. Fold axis = 34°/201°. Solid triangles are slicken fibres on slip surfaces. **B.** Great circles and poles to cleavage (N=70) in the Kanayut Conglomerate at Deadlock Mountain. Mean pole 45°/300°. **C.** Great circles and poles to bedding (N=58) in the Basal Sandstone unit of the Kayak Shale in the Kayak Hills. **D.** Great circles and poles to cleavage (N=9) in the Kayak Shale north of Deadlock Mountain. Mean pole= 27°/310°.

The contact between the Kayak Shale and the Kuna Formation is moderately north dipping to overturned. The Kayak Shale in the Deadlock Mountain area (Fig. 6.34c) shows a structural style similar to that observed in the Husky Hills (Fig. 6.28a, b), with WNW-ESE- to NE-SW-trending asymmetric to symmetric short-wavelength and high-amplitude folds. The Key Creek plate extends to the north of the Red Dog mine forming a broad synform (Fig. 6.2a). Thrust sheets exposed in this area were previously assigned to the Red Dog plate (Teck Cominco American Inc. 2001, *pers. comm.*; Young, 2004). The structural styles of the Key Creek plate in this area are controlled by a complex arrangement of closely-spaced (10 to 100 m) thrust faults, detachment folds and transported detachment folds (Fig. 6.37). Folds are strongly asymmetric and typically show long and gently-dipping backlimbs and steep upright to overturned front limbs. The strata are deformed on multiple detachment levels, including the Ikalukrok, middle Siksikpuk, and lower Otuk units. Fold wavelength typically ranges from 5 to 25 m and fold amplitude varies from 3 to 10 m. Interlimb angles vary from 35° to 60°. Folds locally show evidence for flattening including bulbous hinges. Associated with these folds is a consistent SE-dipping slaty cleavage

6.3.2 Picnic Creek Allochthon

The Picnic Creek allochthon of the Red Dog district consists of two distinct thrust plates, here referred to as the Amaruk River and Puzzle Creek plates (Table 6.5). These are exposed north, west and east of the Wulik Peaks and also in the immediate footwall to the Sivukat Mountain fault, 15 km west of Red Dog (Fig. 6.2a). The main structural features of the Amaruk River and Puzzle Creek plates of the Picnic Creek allochthon are summarized in Table 6.5 and described in detail below.

Amaruk River Plate

The Amaruk River thrust plate occurs along the western and northern margins of the Wulik Peaks (Fig. 6.2a) and is spatially associated with the Wulik Peaks plate of the Kelly River allochthon. It occurs as discontinuous WNW-ESE- to NE-SW-trending and SSW- to SE-dipping thrust remnants that are spatially related to olistostromal melange of the Okpikruak Formation and olistoliths derived from the Kelly River and Nuka Ridge allochthons. Sheet-like olistoliths have preferred orientations and are internally imbricated by thrust faults which are consistent with the regional trends (Figs. 6.2a &

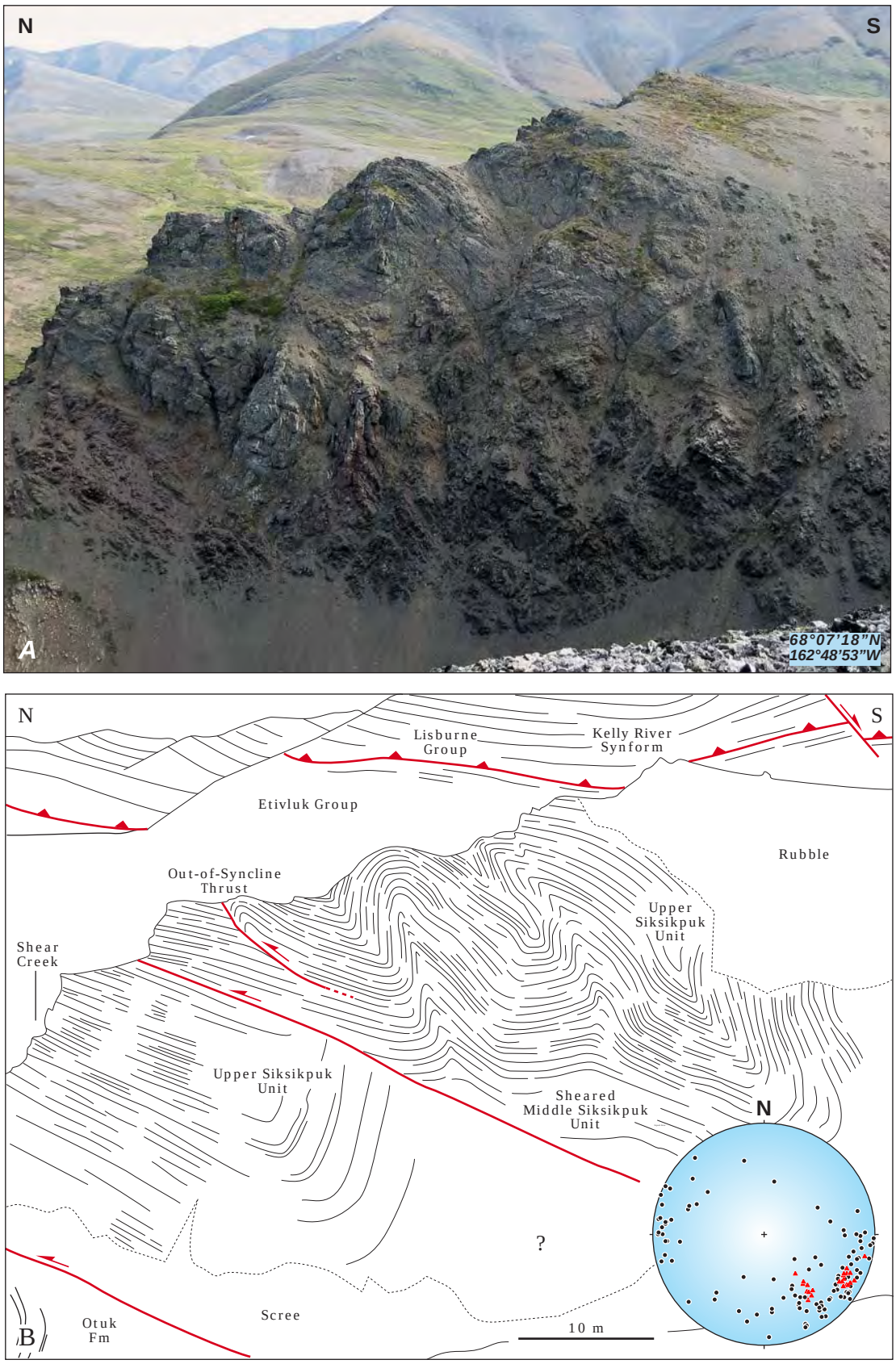


Figure 6.37. Detachment folds in the Key Creek plate. **A.** W-looking view of NNE-verging strongly asymmetric detachment folds in the Siksikpuk Formation near Shear Creek. Topographic relief is approximately 50 m. **B.** Line-drawing structural interpretation of A. Lower hemisphere equal area stereographic projection of minor fold axes (black circles) (N=110) and bedding-cleavage intersection lineations (red triangles, N=20). The Kelly River allochthon lies in the background.

	Tectonic Transport Direction	Structural Trends	Detachment Level(s)	Structural Styles	Thickness
Amaruk River Plate	North to north-northeast	WNW-ESE-trending SSW-downthrown	Kayak Shale Akmalik Chert	Imbricate Thrust Systems, Fault-propagation and detachment folds	1 km
Puzzle Creek Plate	Southeast	WNW-ESE-trending SSW-downthrown	Baird Group, Kayak Shale Akmalik Chert	Imbricate Thrust Systems, Fault-propagation and detachment folds	1 to 1.5 km

Table 6.5. Summary structural features of the Amaruk River and Puzzle Creek plates of the Picnic Creek allochthon.

6.38; cf. Chapter 5, Fig. 5.1). This suggests that olistoliths were possibly deformed during and after they were incorporated into the syn-orogenic strata.

Individual thrust subplates of the Amaruk River plate are detached in the Kayak Shale of the Endicott Group and the partly coeval Utukok Formation of the lower part of the Lisburne Group (cf. Chapter 5, Fig. 5.19). The thrust panels are approximately 300 to 500 m thick dominantly WNW-ESE-trending and dip 45°- 60° degrees to the south-southwest and display complex arrays of thrust faults, locally forming en-echelon. North of the Wulik Peaks, the Amaruk River plate forms WNW-ESE-trending thrust sheets that are thrust on top or included within the Okpikruak Formation. Outcrop-scale duplexes typically occur at the base of individual thrust subplates. These occur as single and multi-bed hinterland-dipping duplexes that locally are sub-horizontally stacked forming multi-story hinterland-dipping duplexes (cf. Wallace *et al*. 1997).

Puzzle Creek Plate

The Puzzle Creek plate in the Chimneys area (Fig. 6.2) consists of three NE-SW-trending and SE-verging thrust subplates that are thrust over the Kelly River and Endicott Mountains allochthons (Figs. 6.2a, 6.39 – 6.42; cf. Chapter 5, Fig. 5.1). The total thickness of the Puzzle Creek plate in the Chimneys area is estimated in approximately 0.5 to 1 km. Thrust subplates are detached in the Kugururok Formation, the Kayak Shale and/or at the base of the Akmalik Chert (cf. Chapter 5, Fig. 5.19). The Puzzle Creek was previously assigned to the Ipnavik River allochthon (e.g. Mayfield *et al*. 1990*a*). The Picnic Creek allochthon exposed at the Punupkahkroak Mountain area (Fig. 6.2a) is very similar stratigraphically and structurally to the Picnic Creek allochthon of the Chimneys area and is here interpreted to be part of the Puzzle Creek plate. At Punupkhakroak Mountain, the Picnic Creek allochthon consists of isolated remnants of Lisburne and Etivluk strata that rest on syn-orogenic conglomerates, sandstones, and shales of the Okpikruak Formation. These are here interpreted as olistoliths and gravity slides that were incorporated into the Okpikruak Formation.

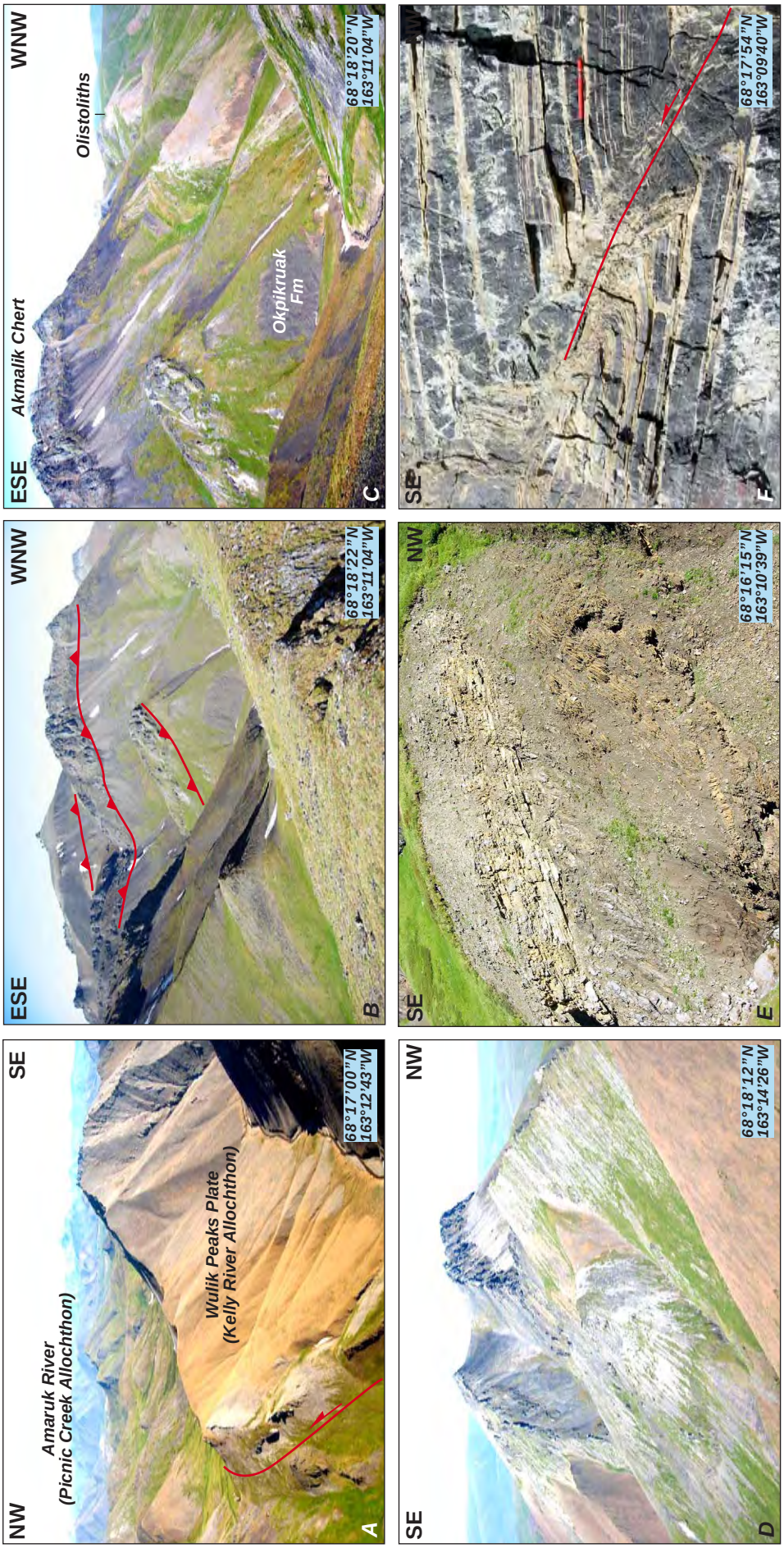


Figure 6.38. Structural features of the Amaruk plate of the Picnic Creek allochthon. **A.** E-looking view of north of the Wulik Peaks showing the Wulik Peaks plate of the Kelly River allochthon thrust over the Amaruk River plate of the Picnic Creek allochthon. **B.** SW-looking view of NNE-transported thrust subplates of the Amaruk River plate. Topographic relief is approximately 500 m. **C.** Detail of the frontal part of the Amaruk plate showing thrust subplates structurally overlying olistoliths derived from the Wulik Peaks plate of the Kelly River allochthon. **D.** Detail of SSW-dipping thrust subplates of the Amaruk plate. **E.** Outcrop-scale multi-story duplexes at the base of thrust subplate. Outcrop is approximately 15 m. **F.** Detail of outcrop-scale fault-propagation fold in strata of the Akmalik Chert. Pencil for scale.

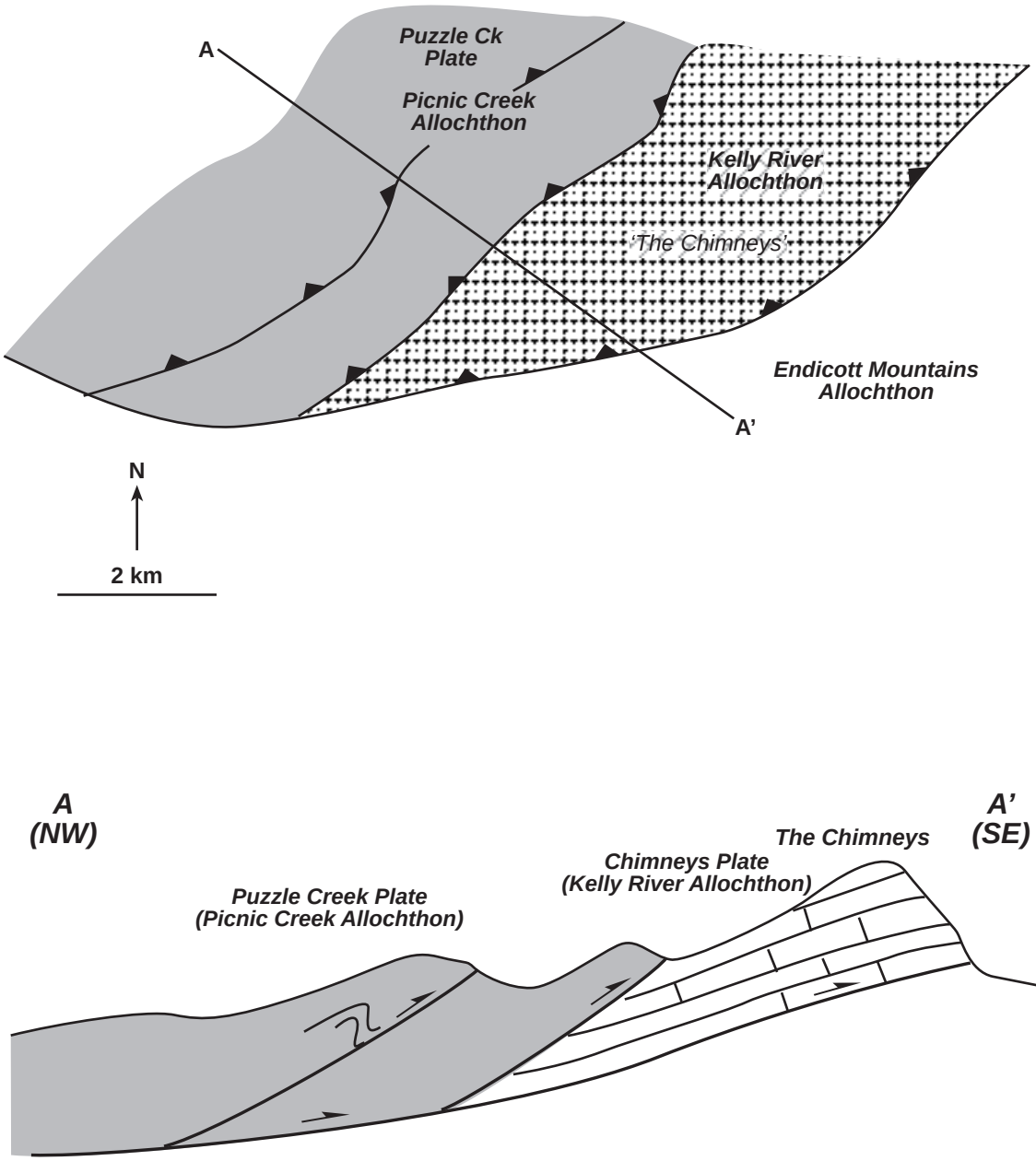


Figure 6.39. Schematic map and cross-section of the Chimneys area.



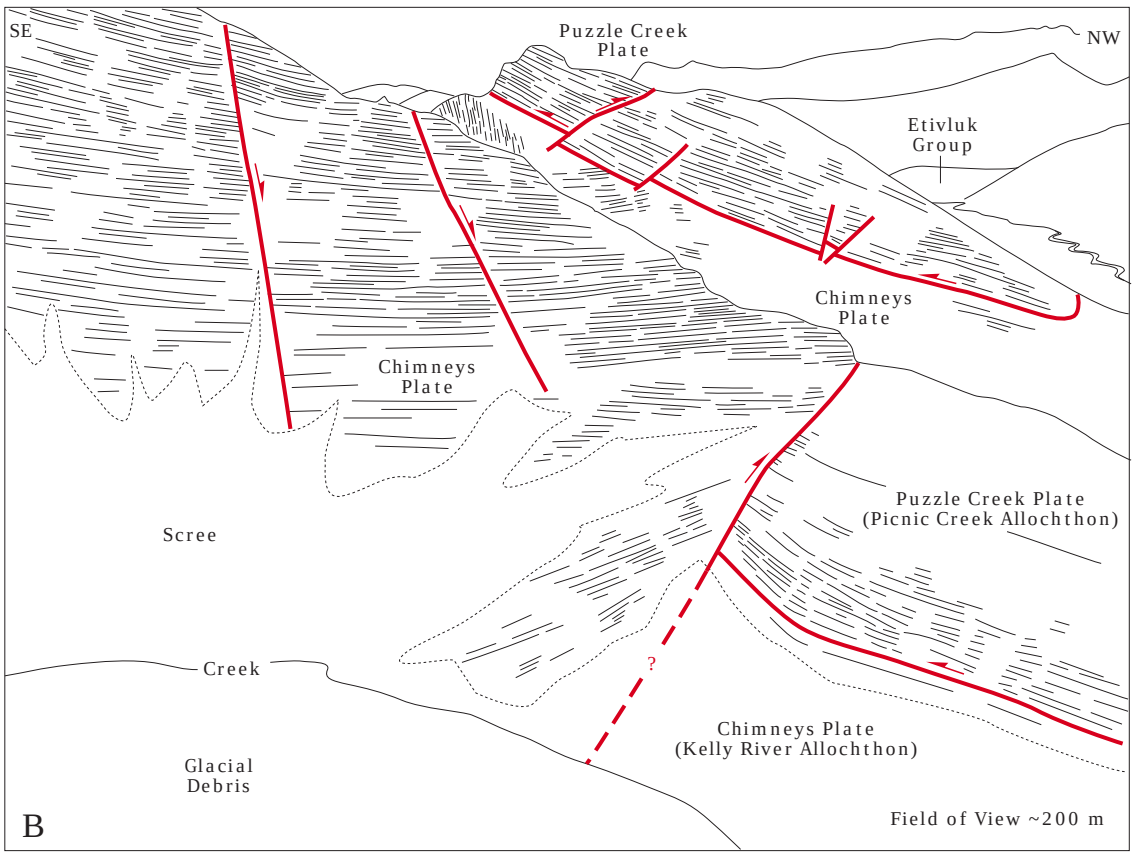


Figure 6.40. Structural relationships in the Chimneys area. **A.** S-looking view of the Chimneys area. Topographic relief is approximately 400 m. **B.** Line drawing interpretation of A showing the Puzzle Creek plate of the Picnic Creek allochthon structurally overlying Lisburne Group strata of the Chimneys plate of the Kelly River allochthon.

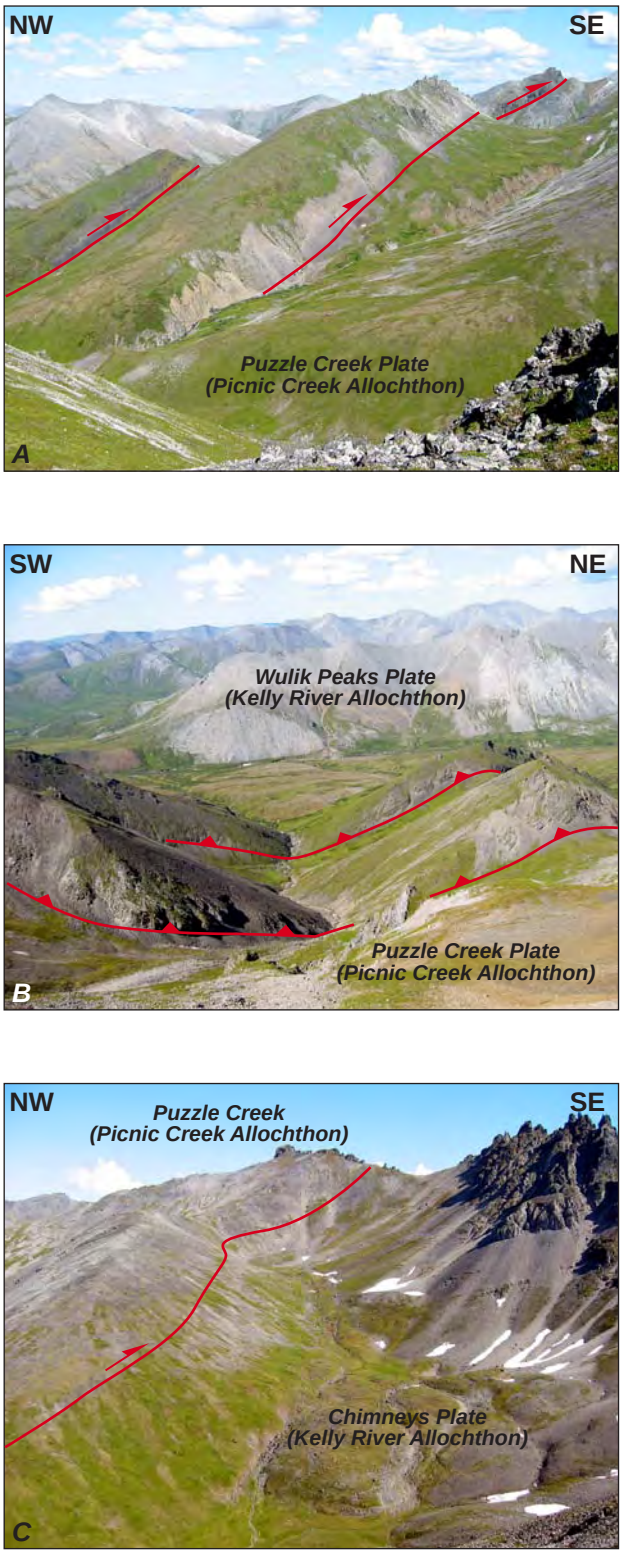


Figure 6.41. Structural features of the Puzzle Creek plate. **A.** View of imbricated thrust subplates of the Puzzle Creek plate northwest of the Chimneys. Topographic relief is approximately 250 m. The Wulik Peaks plate of the Kelly River allochthon lies in the background. **B.** Detail of imbricate thrust faults. Topographic relief is approximately 200 m. **C.** Detail of the Puzzle Creek plate structurally overlying the Chimneys plate of the Kelly River allochthon. Topographic relief is approximately 300 m.

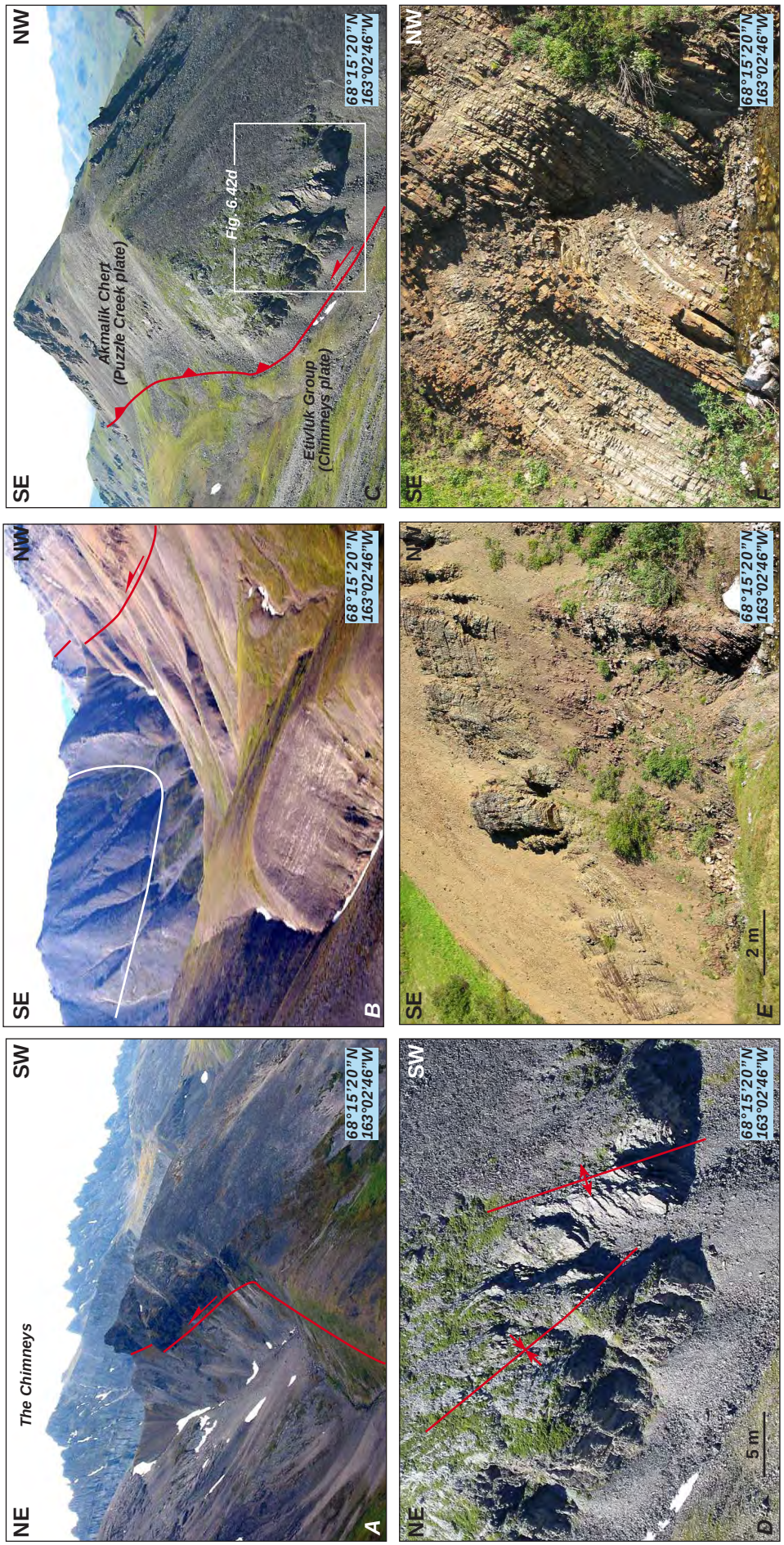


Figure 6.42. Evidence of SE-verging thrusting in the Chimneys area. **A.** Footwall cut-off indicating tectonic transport to the southeast. Topographic relief is approximately 300 m. **B.** SE-verging asymmetric footwall syncline. Topographic relief is approximately 250 m. **C.** SE-verging thrust sheets with SE-verging fault-related folds. Topographic relief is approximately 50 m. **D.** Detail of C, showing asymmetric SE-verging folds in strata of the Akmalik Chert. **E & F.** Details of SE-verging folds in strata of the Siksikpuk Formation in the Chimneys plate of the Kelly River allochthon.

6.3.3 Kelly River Allochthon

The Kelly River allochthon is widely exposed in the Red Dog district (Figs. 6.2a & 5.1) where it is typically preserved in the core of NE-SW-trending broad regional synforms developed at the frontal and dorsal walls of structural culminations in the Endicott Mountains allochthon (e.g. Mount Raven and Husky Hills antiforms) (Figs. 6.2a, 6.4 & 6.25). The Kelly River allochthon forms the thrust front of the western Brooks Range fold and thrust belt in the Red Dog district (Fig. 6.2a). In this study, the Kelly River allochthon has been subdivided into five tectonostratigraphically distinct, internally imbricated and regionally folded thrust plates (Figs. 6.1 & 6.2a; cf. Chapter 5, Fig. 5.21). In inferred ascending structural order these are the Chimneys, Amphitheatre Mountain, Wulik Peaks, Kelly, and Iyichoruk Mountain thrust plates (Figs. 6.1, 6.2a; Table 6.6; cf. Chapter 5, Fig. 5.21). Some thrust plates (e.g. Amphitheatre Mountain, Wulik Peaks) are spatially restricted (Fig. 6.2a) and therefore their structural positions relative to other plates of the allochthon are interpretive. In addition, some thrust plates (e.g. Chimneys plate) are locally disrupted and involved in syn-orogenic olistostromes.

The Kelly River allochthon of the Red Dog district is detached in the Late Devonian Kugururok Formation (cf. Chapter 5, Figs. 5.1 & 5.21) in the structurally higher thrust plates (e.g. Kelly, and Amphitheatre Mountain plates) and in the Early Mississippian Utukok and/or Kogruk Formations (cf. Chapter 5, Figs. 5.1 & 5.21) in structurally lower thrust plates (e.g. Wulik Peaks and Chimneys plates). The thrust plates are emplaced over the Picnic Creek and the Endicott Mountains allochthons, or directly onto parautochthonous syn-orogenic strata of the foreland basin (Fig. 6.2a). The structural features of the thrust plates of the Kelly River allochthon are summarized in Table 6.6 and described in detail below.

	Structural Trends	Detachment Level	Tectonic Transport Direction	Structural Thickness	Associated Syn-orogenic Strata
Iyichoruk Mt Plate	NE-SW-trending SE- to NW-dipping	Kugururok Fm	Northwest	0.5 to 1 km	None
Kelly Plate	NE-SW-trending SE- to NW-dipping	Kugururok Fm Utukok Fm	Northwest	1.5 km	None
Wulik Peaks Plate	NE-SW- to WNW-ESE-trending SE- to SSW-dipping	Utukok Fm	Northwest to north-northeast	2.5 km	Turbidites & Olistostromes
Amphitheatre Mt Plate	NE-SW-trending SE- to NW-dipping	Utukok Fm	Northwest	2 km	None
Chimneys Plate	NE-SW-trending NW-dipping	Kogruk Fm	Southeast	0.9 km	None

Table 6.6. Summary structural features of the thrust plates of the Kelly River allochthon.

Chimneys Plate

The Chimneys plate of the Kelly River allochthon is restricted to the Chimneys and Punupkhakroak Mountain areas, located approximately 22 km northwest and 15 km west-southwest of Red Dog mine, respectively (Fig. 6.2a). The Chimneys plate consists largely of NE-SW-trending, gently to NW- to sub-horizontally-dipping and SE-verging thrust sheets. The Chimneys plate structurally overlies olistostrome of the Okpikruak Formation of the Red Dog plate and is structurally overlain by imbricated thrust subplates of the Puzzle Creek plate of the Picnic Creek allochthon (Fig. 6.43). Fold asymmetries, vergence, regional dip, thrust fault topology, and well-exposed cut-off relationships indicate a southeast tectonic transport direction (Fig. 6.42). The Chimneys plate is spatially related to olistoliths derived from the Endicott Mountains, Picnic Creek, Kelly River and Nuka Ridge allochthons and with polymictic intraformational conglomerate of the Okpikruak Formation. The Chimneys plate grade laterally into olistoliths and gravity slide sheets (Fig. 6.2a; cf. Chapter 5, 5.1).

Amphitheatre Mountain Plate

The Amphitheatre Mountain plate is spatially restricted to the northern part of the Red Dog district (Fig. 6.2a; cf. Chapter 5, Fig. 5.21) and only occurs north of the Wrench Creek fault. It is preserved along the crest and western limb of the Mount Raven antiform and forms the thrust front of the western Brooks Range fold and thrust belt north of the Wrench Creek fault (Fig. 6.2a).

The Amphitheatre Mountain plate is detached in Late Devonian limestones of the uppermost Kugururok Formation (cf. Chapter 5, Figs. 5.1 & 5.21) and/or near the base of the Utukok Formation. It consists of at least four antiformally-stacked thrust subplates that define a folded NE-SW-trending duplex structure, named the Amphitheatre Mountain duplex. The floor and roof thrusts are located at the base of the Utukok formation and at the base of the Okpikruak Formation, respectively. The roof thrust of the duplex structure dips to the northwest beneath a thick succession of syn-orogenic strata of the Okpikruak Formation. This defines the Amphitheatre Mountain triangle zone, described in detail in Section 6.5. Thrust horses of the Amphitheatre Mountain duplex are internally deformed and show NE-SW-trending and

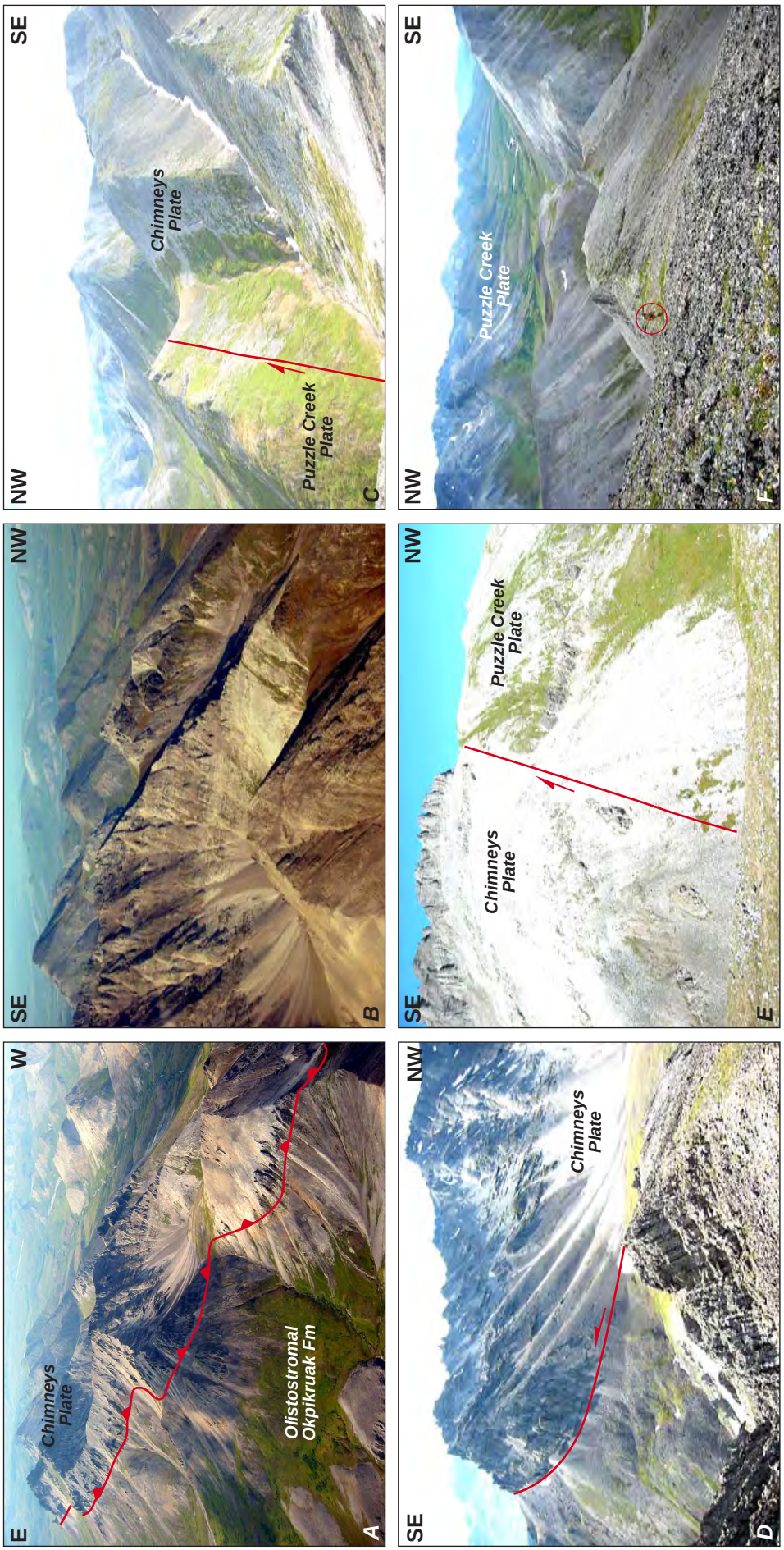


Figure 6.43. Structural features of the Chimneys plate. **A.** S-looking oblique aerial view of NW-dipping, SE-verging thrust sheet of the Chimneys plate. Topographic relief is approximately 250 m. **B.** S-looking view of structural relationships in the Chimneys area. The Puzzle Creek plate of the Picnic Creek allochthon structurally overlies the Chimneys plate. Topographic relief is approximately 300 m. **C.** Thrust fault contact between the Puzzle Creek and Chimneys plate. Topographic relief is approximately 150 m. **D.** SE-verging thrust sheets. Topographic relief is approximately 200 m. **E.** High angle reverse fault. Topographic relief is approximately 100 m. **F.** SW-looking view of the Chimneys and Puzzle Creek plate. Rio Tinto geologist Graeme Broadbent is encircled for scale.

NW-verging asymmetric thrust fault-related folds with gently-dipping back limbs and upright to overturned front limbs (Fig. 6.44).

Wulik Peaks Plate

The Wulik Peaks plate is restricted to the Wulik Peaks area, located approximately 20 km northwest of the Red Dog mine (Fig. 6.2a). It forms the thrust front south of the Wrench Creek fault. The Wulik plate is internally imbricated into four to six NNE-SSW- to WNW-ESE-trending and ESE- to SSW-dipping thrust subplates that can be identified from surface mapping (Figs. 6.2a & 5.1). The structural thickness of the Wulik Peaks plate is approximately 3 km. The Wulik Peaks is exposed on both sides of the Sivukat Mountain fault. In the footwall of the Sivukat Mountain fault, the Wulik Peaks plate shows uncertain structural relationships with the Picnic Creek allochthon and olistostromes. In the hangingwall of the Sivukat Mountain fault the Wulik Peaks plate is structurally overlain by the Copter Peak and Misheguk Mountain allochthons.

The Wulik Peaks plate is detached in Early Mississippian strata of the Utukok Formation (cf. Chapter 5, Fig. 5.21) with local development of metric to decametric intraformational duplexes.

The Wulik Peaks plate has a complex structure with two well defined leading edges that form angles of 116° to 140°. This deflection in the structural trends, here named the Wulik Peaks transverse zone, is described in detail in Section 6.5. The Wulik Peaks plate regionally dips gently to the southeast, except in its northern part. Along its northeastern edge it is thrust on top of olistostromal strata of the Okpikruak Formation. To the east, it overlies both the Red Dog plate of the Endicott Mountains allochthon and the Chimneys plate of the Kelly River allochthon. To the west the Wulik Peaks plate is thrust over a laterally discontinuous thrust sheets and olistoliths of the Amaruk plate of the Picnic Creek allochthon and a thick succession of olistostromal syn-orogenic strata of the Okpikruak Formation (Figs. 6.2a & 5.1). Thrust subplates are approximately 900 m thick and display variable structural trends from NE-SW- to WNW-ESE. Individual thrust faults identified by surface mapping can be traced along strike for distances as large as 32 km and have estimated displacements of a few hundreds of metres to approximately 2 km.

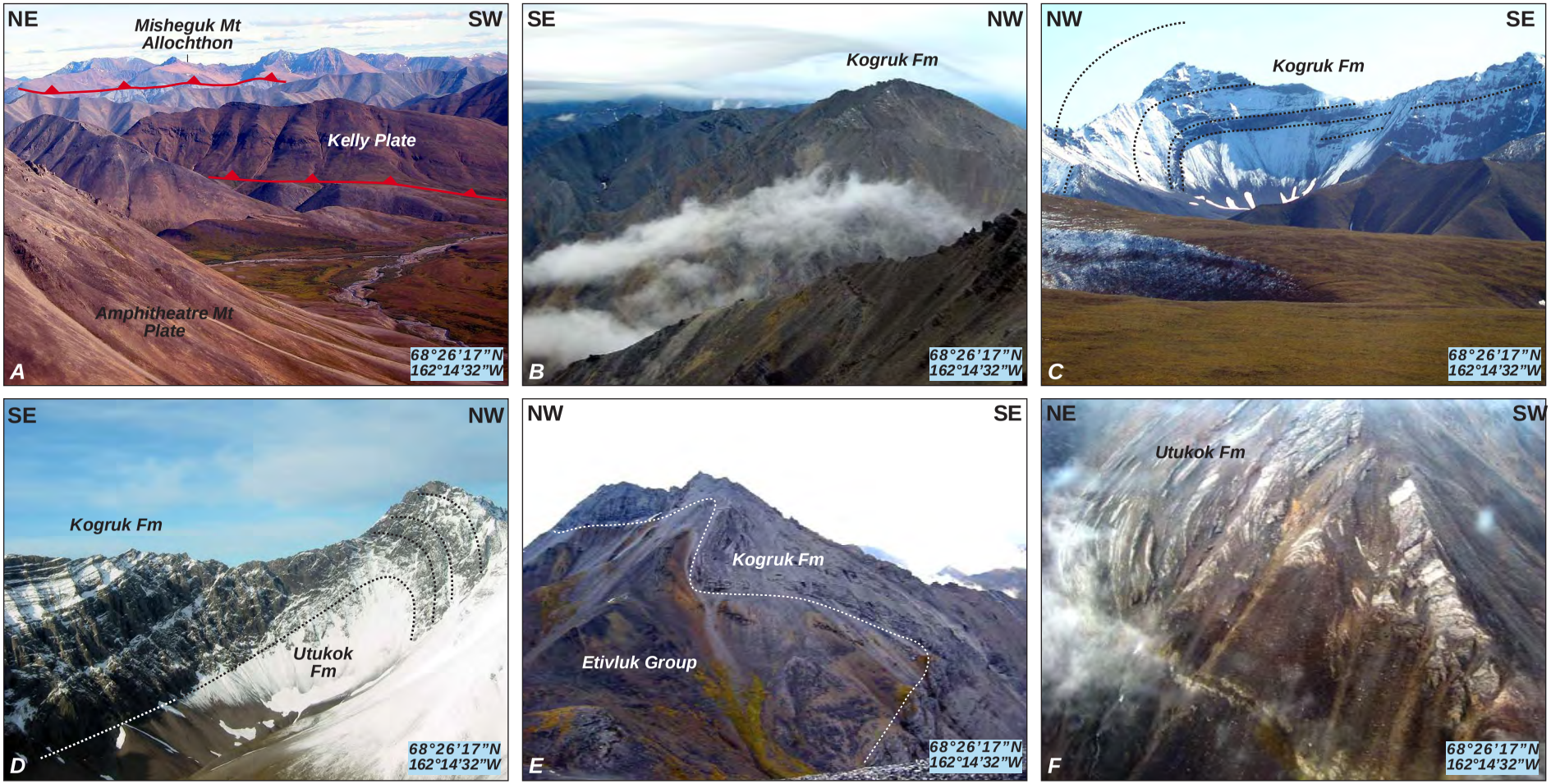


Figure 6.44. Structural features of the Amphitheatre Mountain plate. **A.** SE-looking view showing the thrust fault contact between the Kelly and Amphitheatre Mountain plates. The Misheguk Mountain allochthon lies in the background. Topographic relief is approximately 500 m. **B.** SW-looking view of NW-dipping thrust sheets of the Amphitheatre Mountain plate along the thrust front. Topographic relief is approximately 400 m. **C.** Fault propagation fold in platform carbonates of the Kogruk Formation along the thrust front. Field of viw is approximately 1.5 km. **D.** Detail of fault-propagation cored by the Utukok Formation. Topographic relief is approximately 75 m. **E.** Recumbent fold along the thrust front. Topographic relief is approximately 100 m. **F.** Detail of NE-plunging fault-related fold in strata of the Utukok Formation. Topographic relief is approximately 25 m.

Thrust sheets are gently dipping (20° to 35°) to the southeast along the NE-SW-trending leading edge and progressively curve and become steeply-dipping (45° to 65°) the south-southwest along the WNW-ESE-trending leading edge. This is clearly shown in map view, with apparent thinning of the thrust sheets to the north and northeast. This pattern is also accentuated by the presence of NNW- to NNE-trending moderately- to steeply-dipping, NNW- to NNE-trending dip-slip and dextral oblique slip extensional faults that cause along-strike extension of the WNW-ESE-trending leading edge.

Thrust sheets show fault-related folds, typically asymmetric hangingwall anticlines and footwall synclines. Footwall synclines commonly show overturned and moderately sheared back limbs and are cored by conglomerates of the Okpikruak Formation. Intraformational detachments in strata of the Lisburne and Etivluk Group typically give rise to symmetric to strongly asymmetric folds and faulted detachment folds.

The WNW-ESE-trending leading edge has larger fold wavelength and amplitudes. These folded thrusts are here interpreted to have resulted from amplification folding of pre-existing thrust faults. This occurred in relation with the development of the Wulik Peaks transverse zone. Folded thrusts are also deformed by subsequent NW-dipping, SE-verging backthrusts that have tilted the folded thrusts to the northwest.

Along the WNW-ESE-trending leading edge, thrust faults are locally folded into tight upright and asymmetric WNW-trending and NNE-verging asymmetric to symmetric anticline-syncline pairs (Figs. 6.45 – 6.47) with interlimb angles of 35° to 50°. Folds plunge moderately (20° to 40°) and have ~1 km wavelength. The fold axial traces are sub-vertical to steeply-dipping to the south-southwest. The folded thrust faults have been subsequently tilted and refolded by a younger SE-verging backthrust that dips gently, approximately 30°, to the northwest and brings the Kelly River allochthon on top of syn-orogenic olistostrome and discontinuous thrust subplates of the Red Dog plate of the Endicott Mountains allochthon. The SE direction of tectonic transport on this NW-dipping thrust fault is constrained by the regional dip, the occurrence of asymmetric metric folds in the immediate hanging wall of the thrust fault, map patterns, branch line arrangements, and along-strike structural correlations with other SE-vergent thrust sheets such as those observed in the Chimneys plate of the Picnic Creek

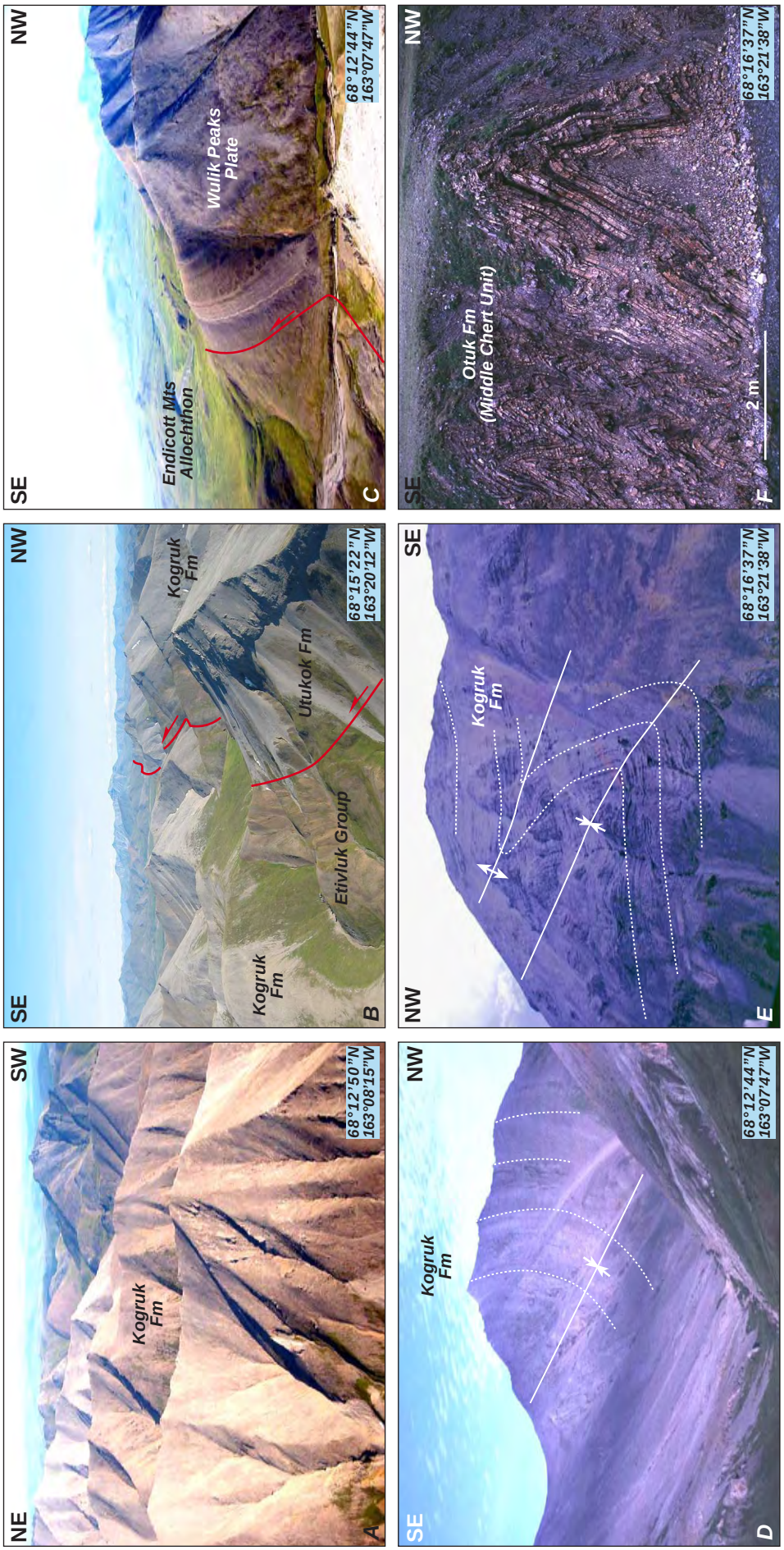


Figure 6.45. Structural features of the Wulik Peaks plate. **A.** WNW-looking view of imbricate thrust faults along the northwest leading edge of the Wulik Peaks plate. Dark-weathering thrust imbricates of the Amaruk River plate of the Picnic Creek allochthon lie in the background. Topographic relief is approximately 500 m. **B.** ESE-looking view of NNE-verging thrust sheets of the Wulik Peaks plate. Topographic relief is approximately 300 m. **C.** SW-looking view of SE-verging thrust fault bringing the Wulik Peaks plate over olistostromal strata of the Endicott Mountains allochthon. Topographic relief is approximately 300 m. **D.** Detail of syncline in strata of the Kogruk Formation. Topographic relief is approximately 250 m. **E.** Detail of NW-verging asymmetric folds in the Kogruk Formation. Topographic relief is approximately 150 m. **F.** Detail of symmetric to asymmetric detachment folds in well-bedded cherts of the middle chert unit of the Otuk Formation.

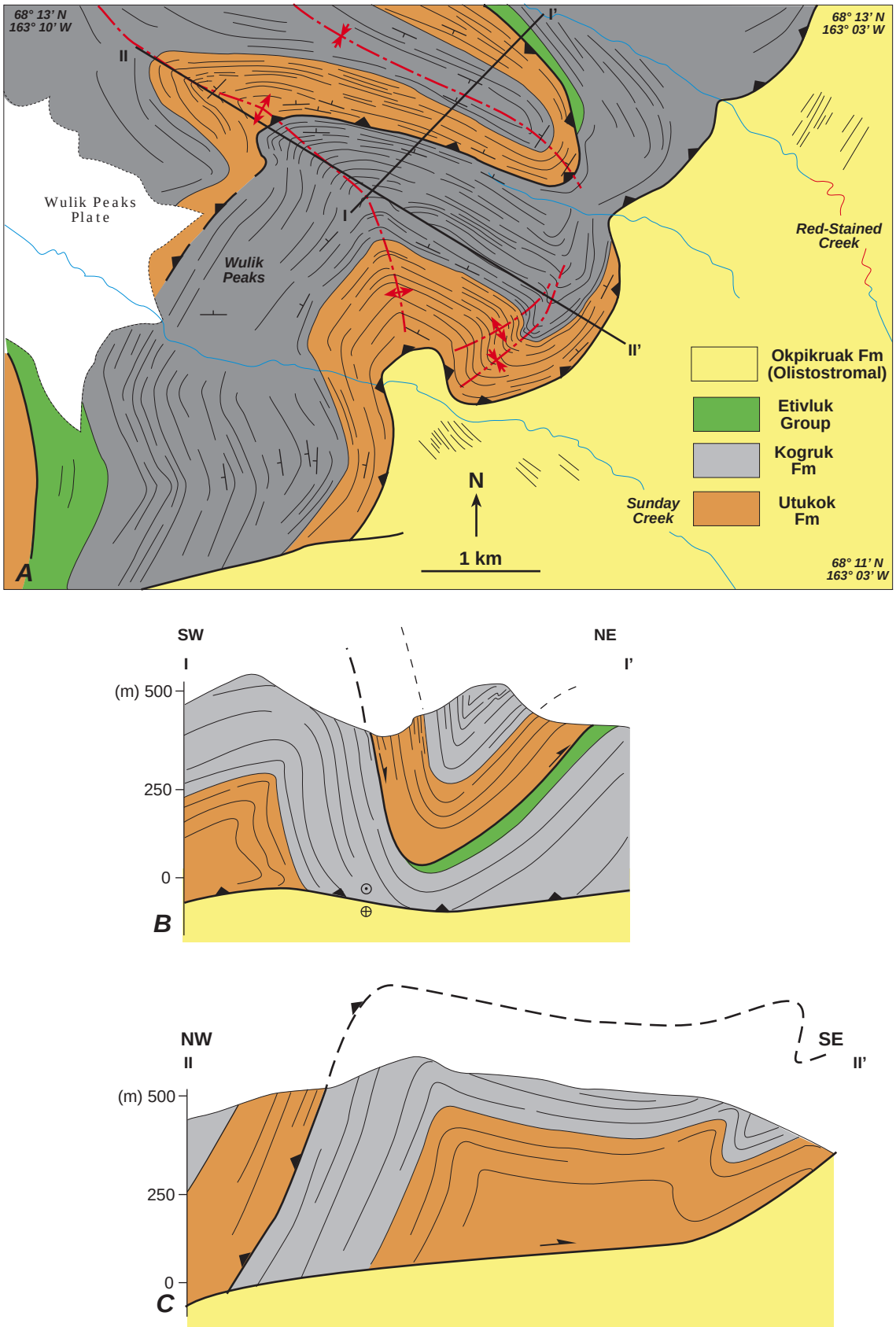


Figure 6.46. Folded thrust faults in the Wulik Peaks plate of the Kelly River allochthon. **A.** Detailed structural map of the northeastern margin of the Wulik Peaks plate of the Kelly River allochthon showing folded thrust faults transported on a NW-dipping, SE-verging backthrust. **B & C.** Cross sections. Refer to A for location of individual sections.

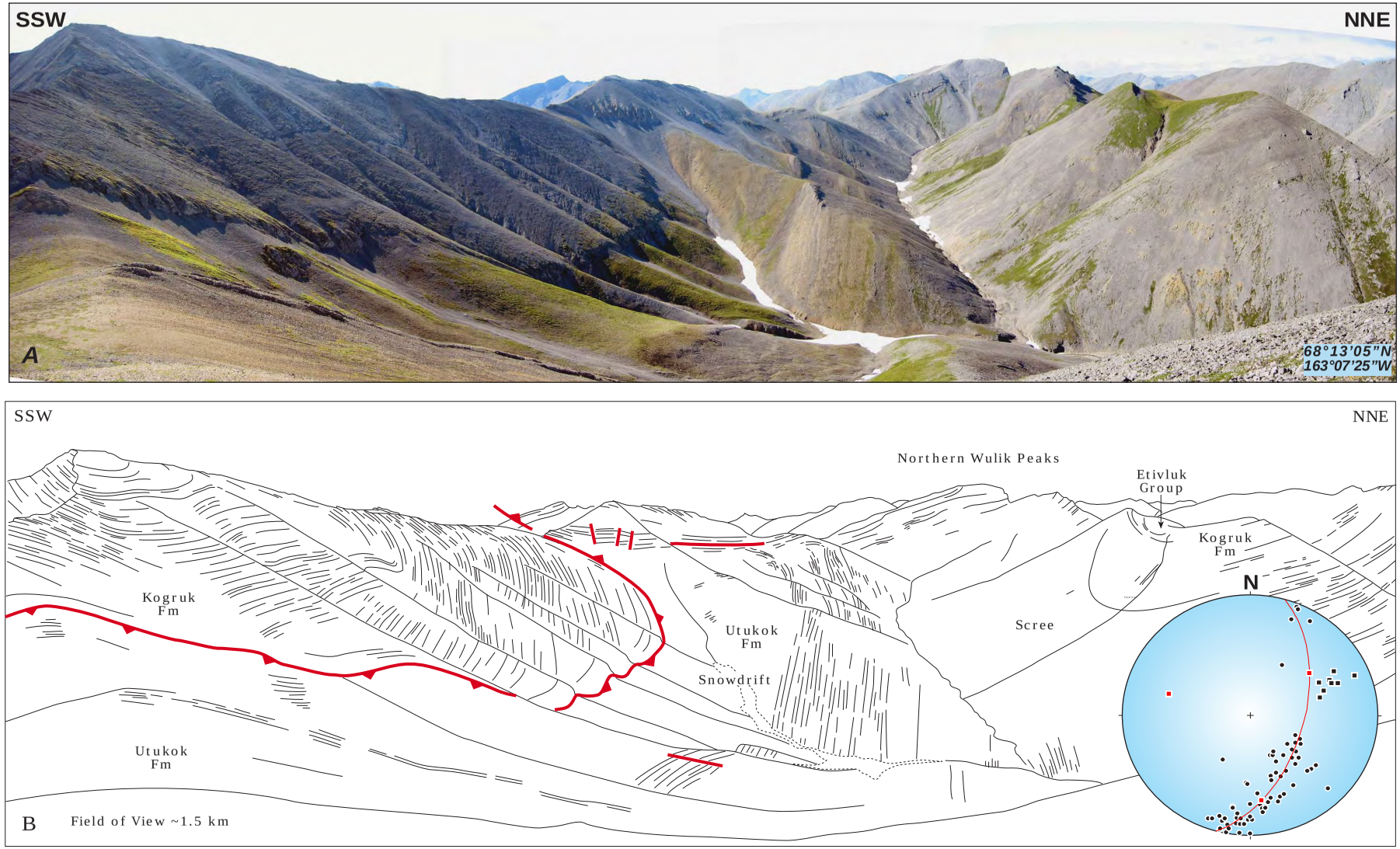


Figure 6.47. Folded thrust in the Wulik Peaks plate of the Kelly River allochthon. **A.** W-looking photomosaic. Field of view is approximately 1.5 km. **B.** Line-drawing structural interpretation and lower hemisphere stereographic projection showing poles to folded thrust fault (solid circles) (N=71) and joints in the Kogruk Formation (N=4).

allochthon in the Chimneys area. The fold axial traces run parallel to sub-parallel to the regional NW tectonic transport direction and are strongly oblique to the dominant NE-SW structural grain of the De Long Mountains.

Kelly Plate

The Kelly plate of the Kelly River allochthon is exposed in the footwall and hangingwall of the Wrench Creek, approximately 20 km north of the Red Dog mine (Fig. 6.2a). It consists exclusively of strata of the Kugururok, Utukok and Kogruk formations (cf. Chapter 5, Fig. 5.21). The Kelly plate is internally imbricated and consists of at least three NNE- to NE-trending and WNW- to NW-verging thrust subplates (Figs. 6.48 & 6.49). These are arranged in a regional hinterland-dipping duplex that has been folded into a NE-SW-trending regional scale broad open synform developed between the Husky Hills and Mount Raven antiforms (Figs. 6.2a, b & 6.48). This synform, named the Kelly River synform (Fig. 6.2a), has a minimum wavelength of 10 km and extends for ~30 km along strike. Thrust horse spacings and thicknesses are commonly irregular, possibly reflecting original depositional thickness changes. The floor thrust is located near the base of the Utukok Formation. Metric-scale fault slivers of grey-weathering limestones of the Kugururok Formation are preserved at the base of the plate. The roof thrust (not exposed) is inferred to occur at the top of the Kogruk Formation.

The Kelly plate structurally overlies the Key Creek and Wolverine Creek plates of the Endicott Mountains allochthon to southeast side and is thrust on top of the Amphitheatre Mountain plate to the northwest (Fig. 6.2a, b). Outcrop-scale kinematic indicators and well-exposed cut-off relationships indicate a northwest tectonic transport direction.

Iyichoruk Mountain Plate

The Iyichoruk Mountain plate (Figs. 6.1 & Fig. 6.2a, c) is a newly identified thrust plate of the Kelly River allochthon in the Red Dog district. The Iyichoruk Mountain plate occurs as a series of poorly exposed synformal thrust remnants that consist largely of Late Devonian and Early Mississippian platform carbonates of the Baird and Lisburne groups (cf. Chapter 5, Fig. 5.21). The Iyichoruk Mountain plate crops out south of

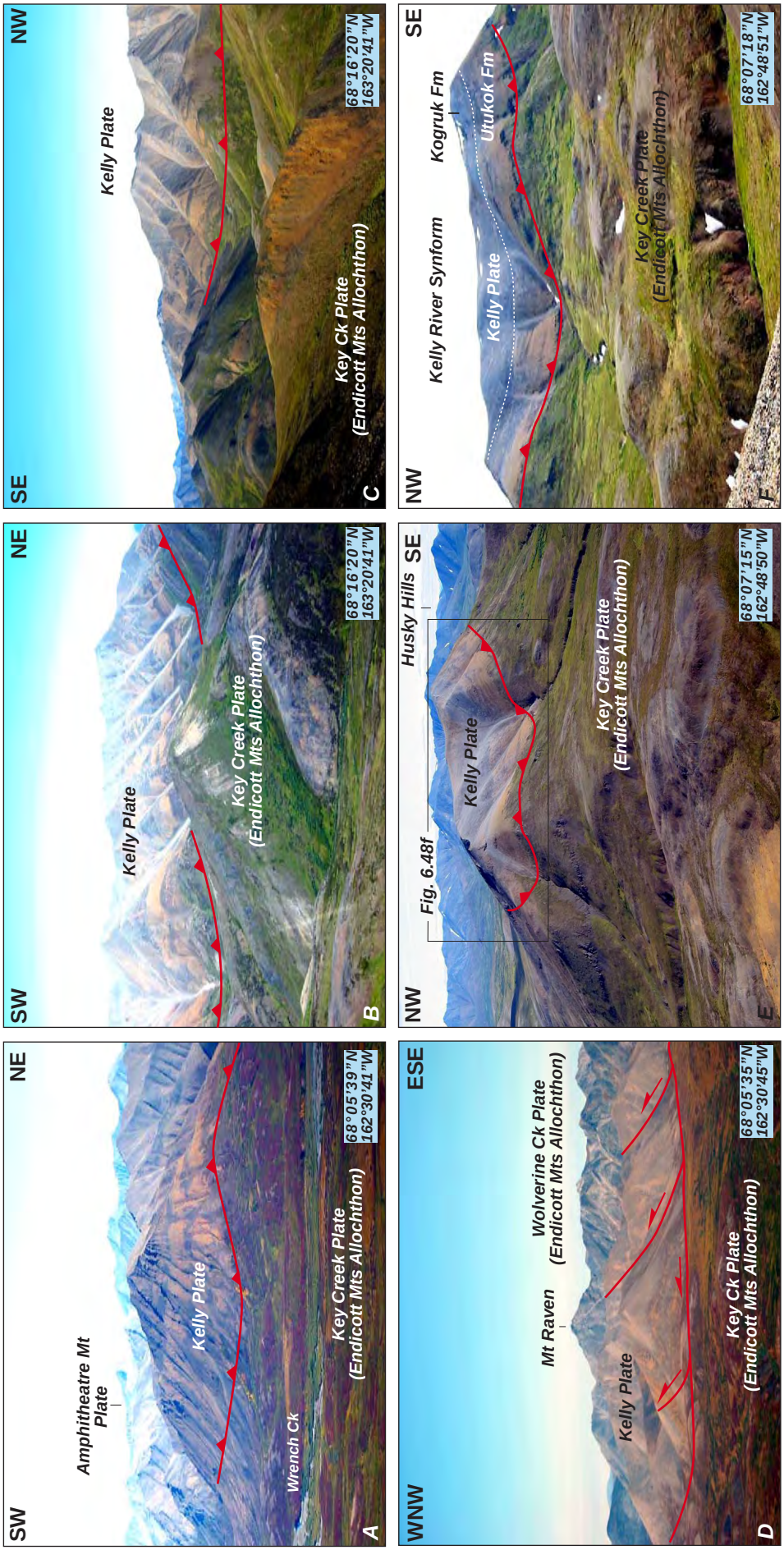


Figure 6.48. Structural features of the Kelly plate of the Kelly River allochthon. **A.** NW-looking view of the Kelly plate from the Husky Hills. Note the Kelly plate structurally overlies the Key Creek plate of the Endicott Mountains allochthon. Topographic relief is approximately 350 m. **B & C.** Details of the eastern limb of the Kelly plate. Topographic relief is approximately 300 m. **D.** NNE-looking view of thrust horses of the Kelly plate in the hangingwall of the Wrench Creek fault. Topographic relief is approximately 500 m. **E.** SW-looking view of klippen of the Kelly plate. Topographic relief is approximately 250 m. **F.** Detail of the Kelly plate in the Kelly synform. Topographic relief is approximately 250 m.

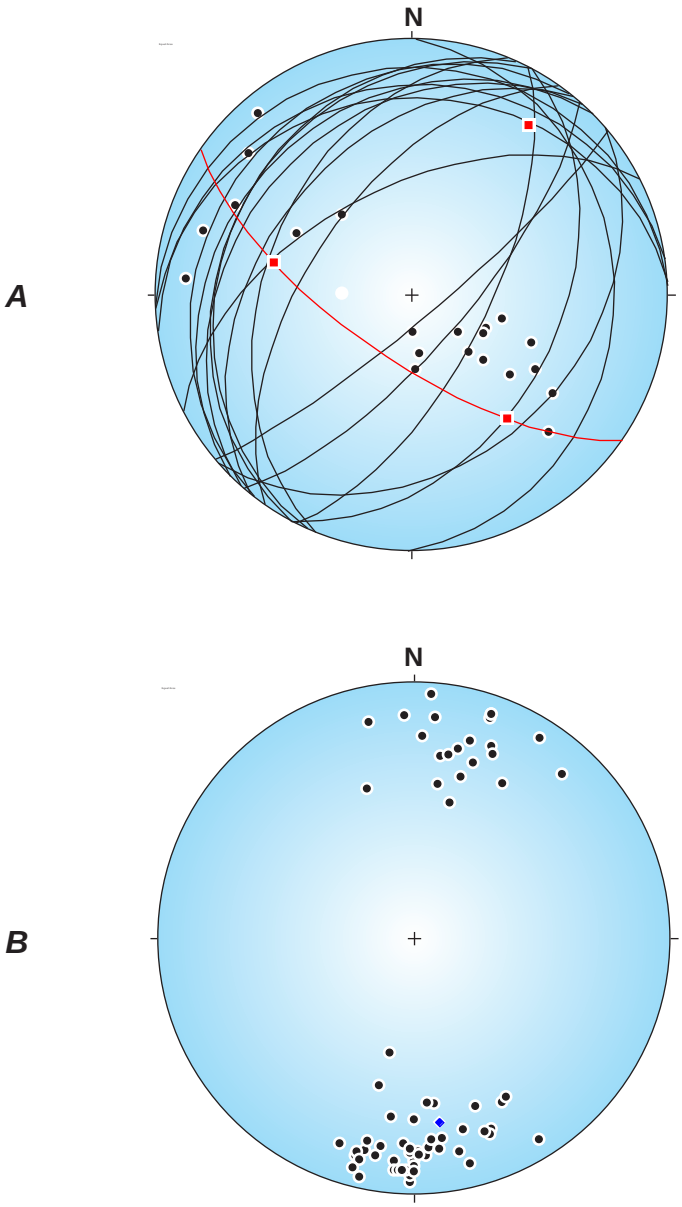


Figure 6.49. Lower hemisphere equal area stereographic projection of structural data from the Kelly plate of the Kelly River allochthon. **A.** Great circles and poles to bedding in strata of the Kogruk Formation (N=23). **B.** Minor fold axes in strata of the Utukok Formation (N=68).

Punupkhakroak Mountain and along a poorly-exposed NE-SW-trending corridor (Fig. 6.2a) that extends to south into the Chukchi Sea Coast. The Iyichoruk Mountain plate overlies the Chimneys plate in the footwall to the Sivukat Mountain Fault (Fig. 6.2a). In turn, in the hangingwall of the Sivukat Mountain fault, the Iyichoruk plate rests directly on top the Endicott Mountains allochthon (Fig. 6.2a). South of the Sivukat Mountain fault, the Iyichoruk plate is structurally overlain by the Copter Peak allochthon (Fig. 6.2a). Kinematic indicators show NW- to SE-tectonic transport directions.

The Iyichoruk Mountain plate is also locally exposed northeast of the Red Dog mine, in the immediate footwall of the Misheguk Mountain allochthon of the Angayucham terrane (Fig. 6.2a). The Iyichoruk Mountain plate is here interpreted to be the structurally equivalent to the Eli plate of the Kelly River allochthon (Eli sequence of Mayfield *et al.* 1988), which is exposed approximately 50 km east of the Red Dog mine.

6.3.4 Ipnavik River and Nuka Ridge Allochthons

In the Red Dog district, the Ipnavik River and Nuka Ridge allochthons are locally exposed, approximately 40 km northeast and also 30 km southwest of the Red Dog mine (Figs. 6.2a, 6.50). The Ipnavik River and Nuka Ridge allochthons also locally occur as scattered rubble outcrops in the hangingwall to the Sivukat Mountain fault (Fig. 6.2a) and along a poorly-exposed NE-SW-trending and 90 km-long broad corridor that extends from northeast of the Red Dog mine to the Chukchi Sea coast to the south (Fig. 6.50). The lack of intact or continuous exposures has prevented detailed structural analysis of these units

6.3.5 Copter Peak Allochthon

In the Red Dog district, the Copter Peak allochthon occurs east, west and north of the Husky Hills antiform and also in the immediate hangingwall of the Sivukat Mountain fault, approximately 30 km northeast and also 40 km southwest of the Red Dog mine, respectively (Figs. 6.2a & 6.50). The Copter Peak allochthon is preserved in two NE-SW-trending regional broad open synforms developed in the frontal and dorsal walls of the Husky Hills antiform (Figs. 6.2a & 6.50). The Copter Peak allochthon is locally disrupted forming a complexly deformed assemblage or melange that consists of highly

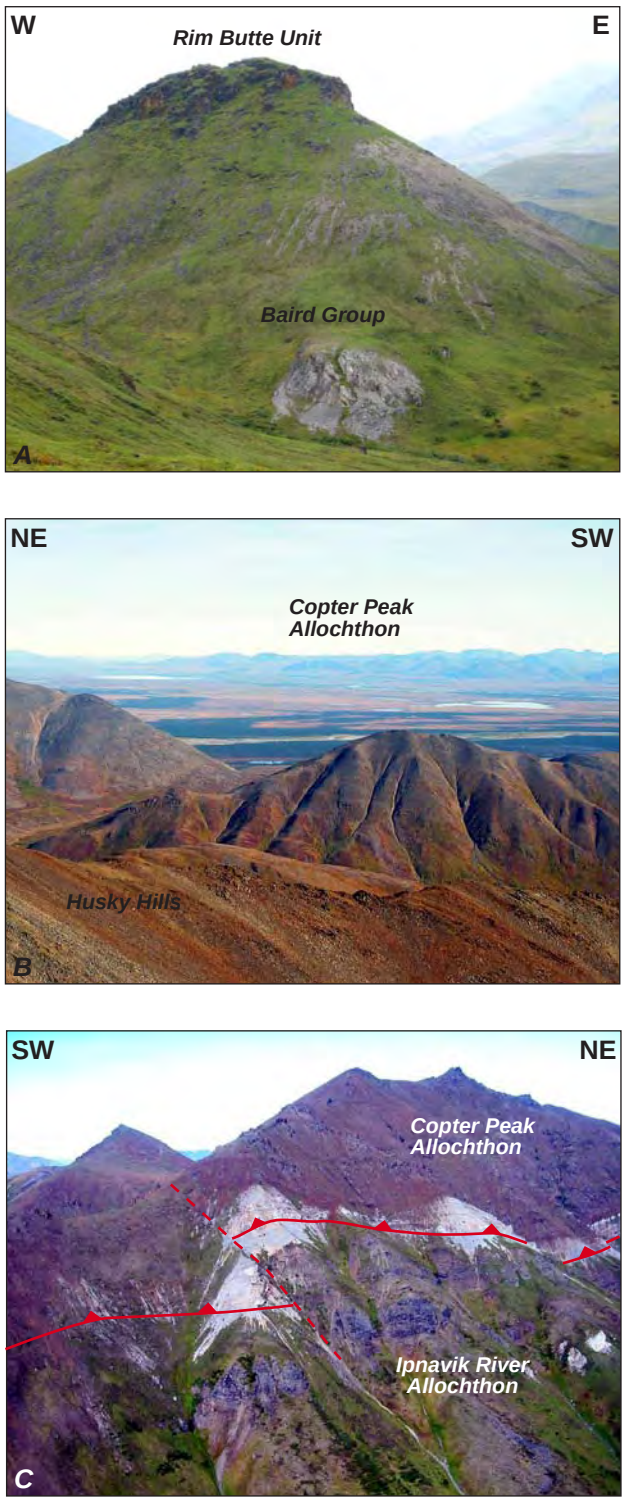


Figure 6.50. Structural features of the higher allochthons. Outcrop is approximately 20 m high. **A.** N-looking view of thrust sheet remnant of the Ipnavik River allochthon south of the Sivukat Mountain fault. **B.** SE-looking view of poorly-exposed thrust sheets of the Copter Peak allochthon east of the Husky Hills. Topographic relief is approximately 100 m. **C.** NW-looking view of sub-horizontally stacked thrust sheets of the Copter Peak and Ipnavik River allochthons near the Avan Hills.Topographic relief is approximately 150 m.

deformed basalts of the Copter Peak volcanic unit and platform carbonates of the Kugururok Formation along with cherts and shales of the Etivluk Group (cf. Chapter 5, Fig. 5.30d, f).

Northeast and east of the Red Dog mine, the Copter Peak allochthon is thrust on top of the Endicott Mountains allochthon and is overlain by the Misheguk Mountain allochthon (Fig. 6.2a, e). Southwest of the Red Dog mine, the Copter Peak allochthon is thrust on top of the Wulik Peaks plate of the Kelly River allochthon and is overlain by the Misheguk Mountain allochthon (Fig. 6.2a). The lack of intact outcrop has prevented detailed structural analysis of this unit. The Copter Peak allochthon is overlain by the Angayucham terrane (Fig. 6.1), which is described below.

6.4 ANGAYUCHAM TERRANE

The Angayucham terrane in the Red Dog district consists solely of the Misheguk Mountain allochthon (Figs. 6.1 & 6.2a; cf. Chapter 5, Figs. 5.1 & 5.2), which structurally overlies the allochthons of the Arctic Alaska terrane (Figs. 6.1 & 6.2a, b, e; cf. Chapter 5, Fig. 5.1). The main structural features of the Misheguk Mountain allochthon in the Red Dog district are summarized in Table 6.7 and described in detail below.

6.4.1 Misheguk Mountain Allochthon

The Misheguk Mountain allochthon in the Red Dog district consists of ultramafic to felsic igneous rocks (cf. Chapter 5, Figs. 5.31 – 5.33) that are contained in two NE-SW-trending Type C crystalline thrust sheet (Hatcher & Hooper, 1992; Hatcher, 2004) remnants, approximately 2 to 5 km thick. These are preserved in the core of two regional synforms, here named the Avan Hills and Iyikrok Mountain synforms (Figs. 6.2a, b, e & 6.51). The Avan Hills and Iyikrok Mountain synforms are developed in the NNE-plunging termination as well as in the frontal and dorsal walls of the Husky Hills antiform (Figs. 6.2a, b, e, 6.28, 6.52 & 6.53). The Misheguk Mountain allochthon in the Red Dog district is exposed in the Avan Hills and Iyikrok Mountain areas, located approximately 36 km northeast and 37 km southwest of the Red Dog mine, respectively (Fig. 6.2a; cf. Chapter 5, Fig. 5.1). These are equivalent to the Iyikrok Mountain and Avan Hills plutons of Martin (1970) or complexes of Moore *et al.* (1994), Patton *et al.* (1994) and Young (2004) (cf. Chapter 2, Fig. 2.16).

Avan Hills

The Avan Hills expose a NE-SW-trending, doubly-plunging, and NW-verging broad regional synformal klippen north of the Wrench Creek fault along the NNE-plunging termination of the Husky Hills antiform (Figs. 6.2a, b, 6.54 & 6.55). The Misheguk Mountain allochthon at this locality overlies the allochthons the Arctic Alaska terrane. It has a marked NE-SW-trending structural grain defined by gently to steeply SE-dipping magmatic layering and tectonic foliations (cf. Chapter 5, Figs. 5.31 – 5.33) that are locally oblique to the base of the allochthon (Fig. 6.52). The base of the allochthon is the Angayucham thrust (Figs. 6.51, 6.52 a, b, d), which marks the suture between the continental Arctic Alaska and Angayucham terranes (Figs. 6.1 & 6.2a, b).

	Main Structures	Structural Trends	Detachment Level	Tectonic Transport Direction	Mineralization
Misheguk Mountain Allochthon	Angayucham Thrust Shear Fabrics	NE-SW-trending SE- to NW-dipping	Angayucham Thrust Serpentinites and serpentinized peridotites (Petrologic Moho)	Top to the northwest	Podiform and disseminated chromite

Table 6.7. Summary structural features of the Misheguk Mountain allochthon in the Red Dog district.

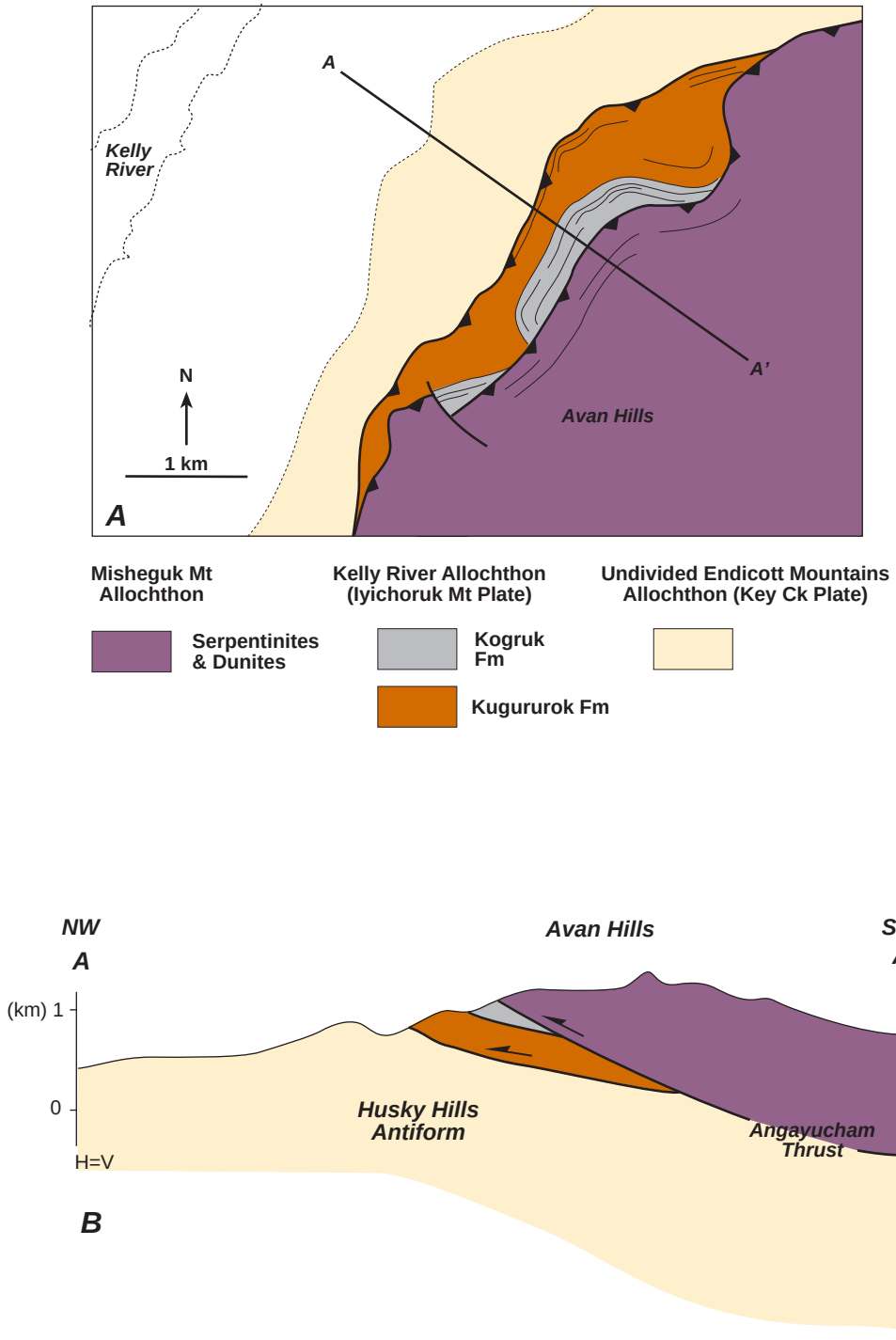


Figure 6.51. Misheguk Mountain allochthon. **A.** Simplified structural map of the western margin of the Avan Hills showing the Angayucham thrust and the relationship with the underlying Kelly River allochthon. **B.** NW-SE-trending schematic cross section. Refer to A for location.

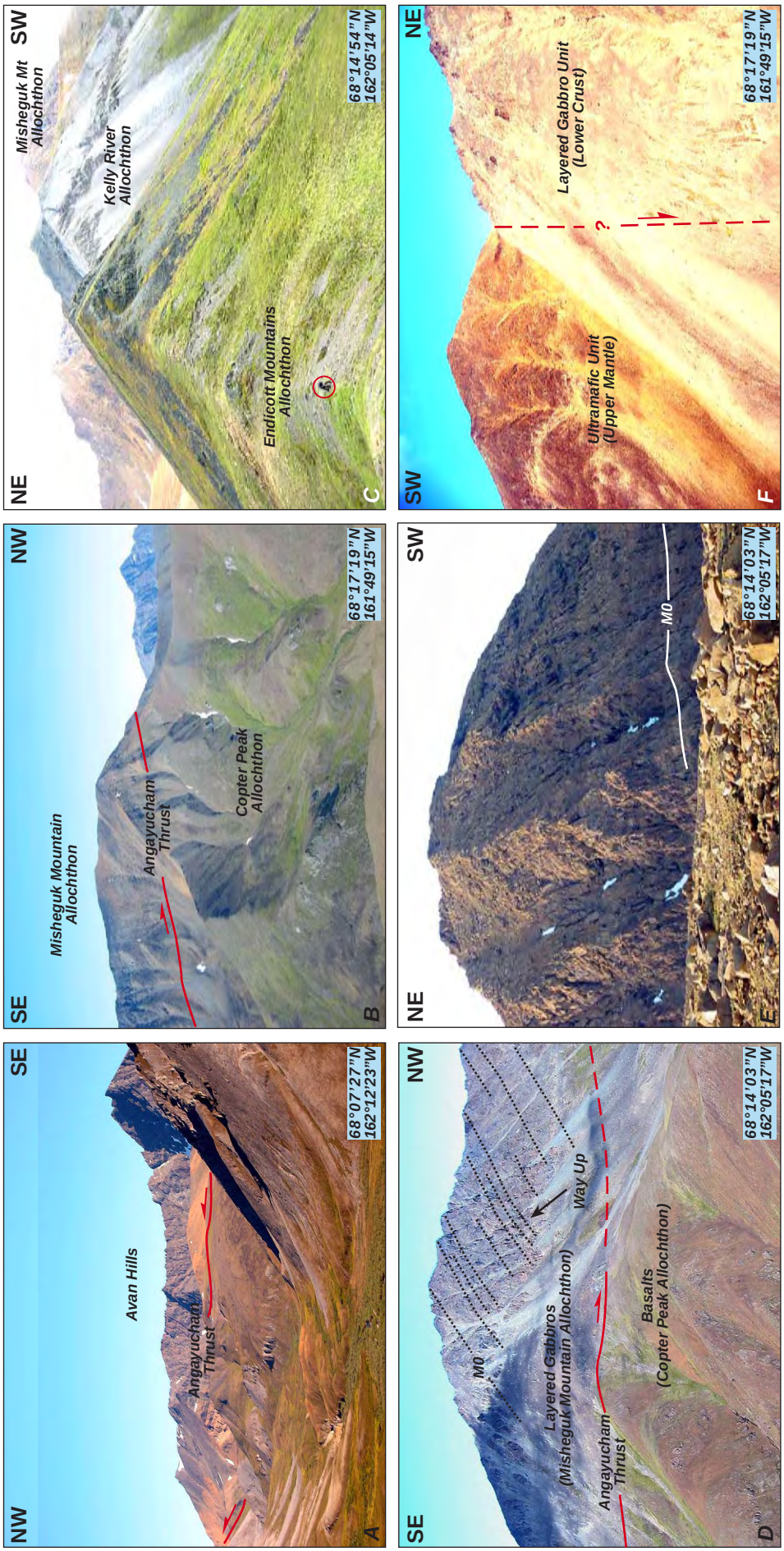


Figure 6.52. Structural features of the Misheguk Mountain allochthon. **A.** General view of the Misheguk Mountain allochthon in the Avan Hills area. Note sub-horizontal thrust stacking and orange-weathering serpentinized halo at the base of the allochthon. Topographic relief is approximately 700 m. **B.** View of the Misheguk Mountain allochthon overlying the Copter Peak allochthon. Topographic relief is approximately 500 m. **C.** View of thrust stacking patterns in the Avan Hills. Topographic relief is approximately 600 m. Geologist is encircled for scale. **D.** View of lower crust layered gabbros structurally overlying the Copter Peak allochthon. Note the Angayucham thrust cuts down-section in the direction of tectonic transport. Topographic relief is approximately 300 m. **E.** NW-looking view of layered ultramafic rocks . Note magmatic layering (M0) and with a well-developed N- to NW- dipping joints. Topographic relief is approximately 400 m. **F.** NW-looking view of extensional fault juxtaposing upper mantle dunites against lower crust gabbros. Topographic relief is approximately 100 m.

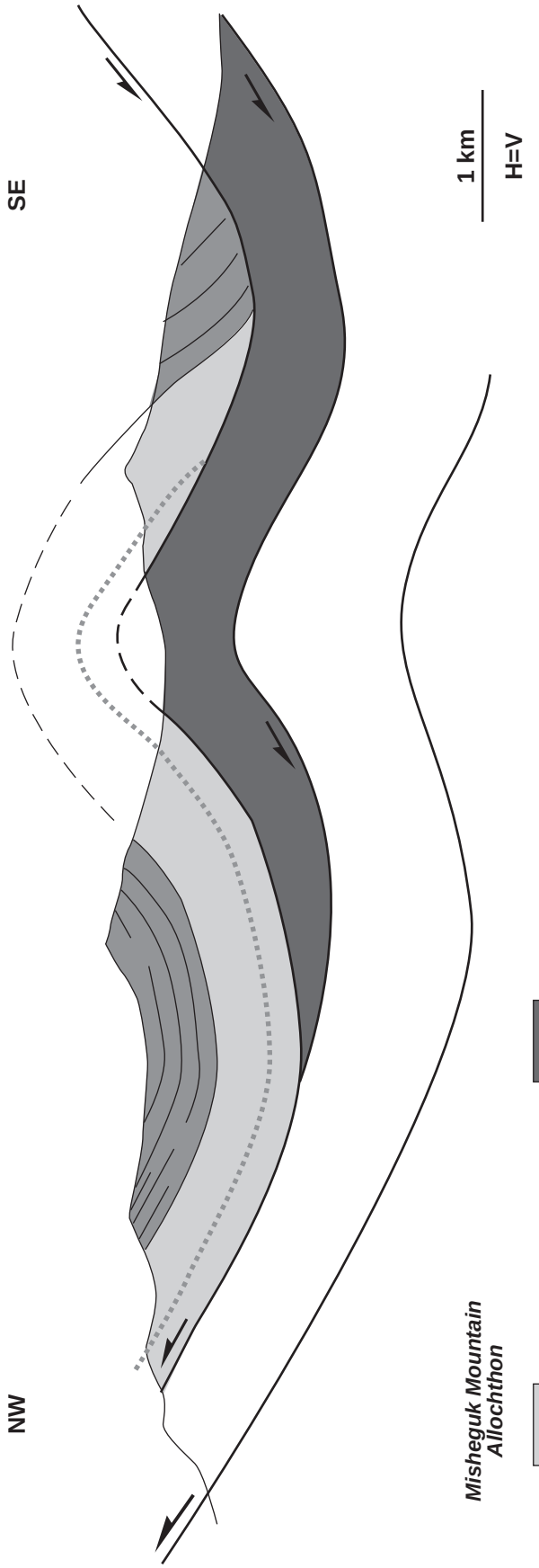


Figure 6.53. Schematic field cross section showing structural relationships in the Avan Hills area. Misheguk Avan Hills structurally overlie the Copter Peak and Kelly River allochthons. Note Angayucham thrust cuts downsection in the direction of tectonic transport both in the hangingwall and footwall.

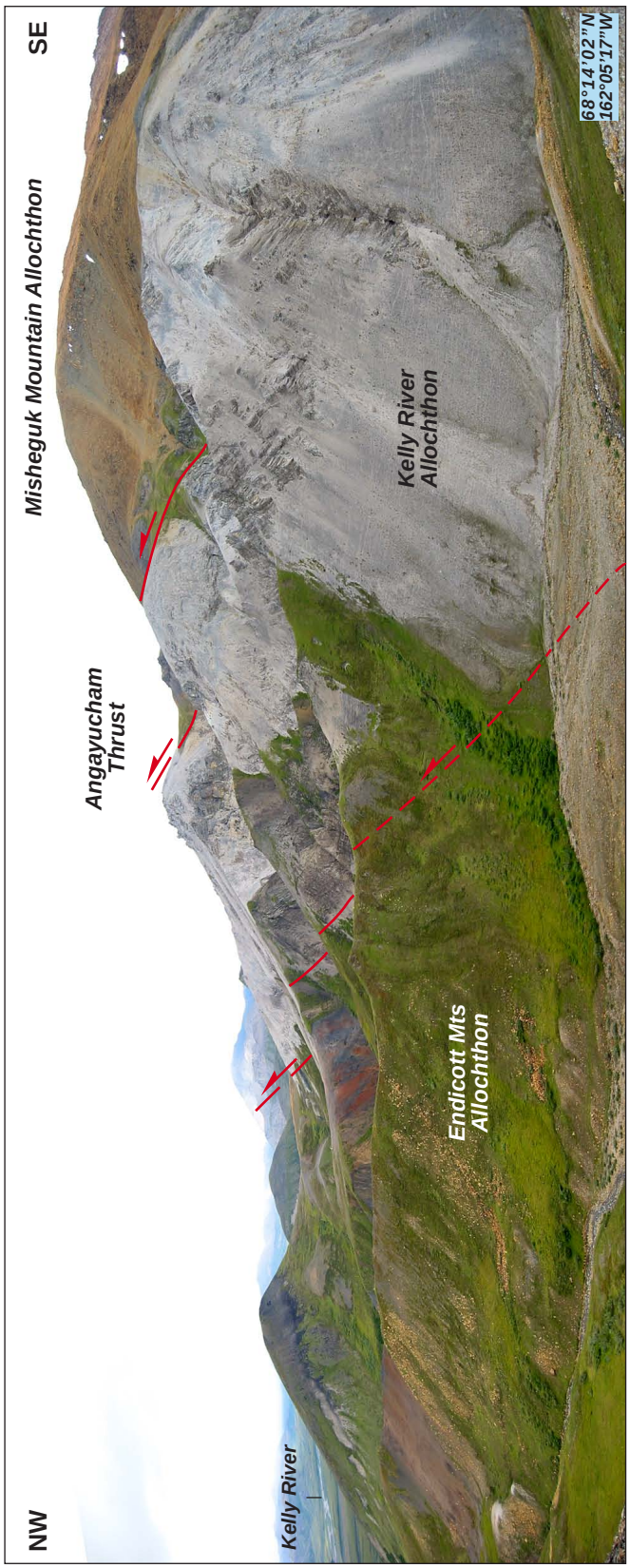


Figure 6.54. NE-looking photomosaic showing the Angayucham thrust and allochthon stacking patterns in the western margin of the Avan Hills. Jurassic dark green-weathering serpentinite and orange-weathering dunites of the Misheguk Mountain allochthon structurally overlie grey-weathering Mississippian carbonates of the Kelly River allochthon (40°/125°). Note structural thinning of the Kelly River allochthon below the Angayucham thrust. The Kelly River allochthon overlies poorly exposed strata of the Key Creek plate of the Endicott Mountains allochthon. Field of view is approximately 1 km. Topographic relief is approximately 500 m.

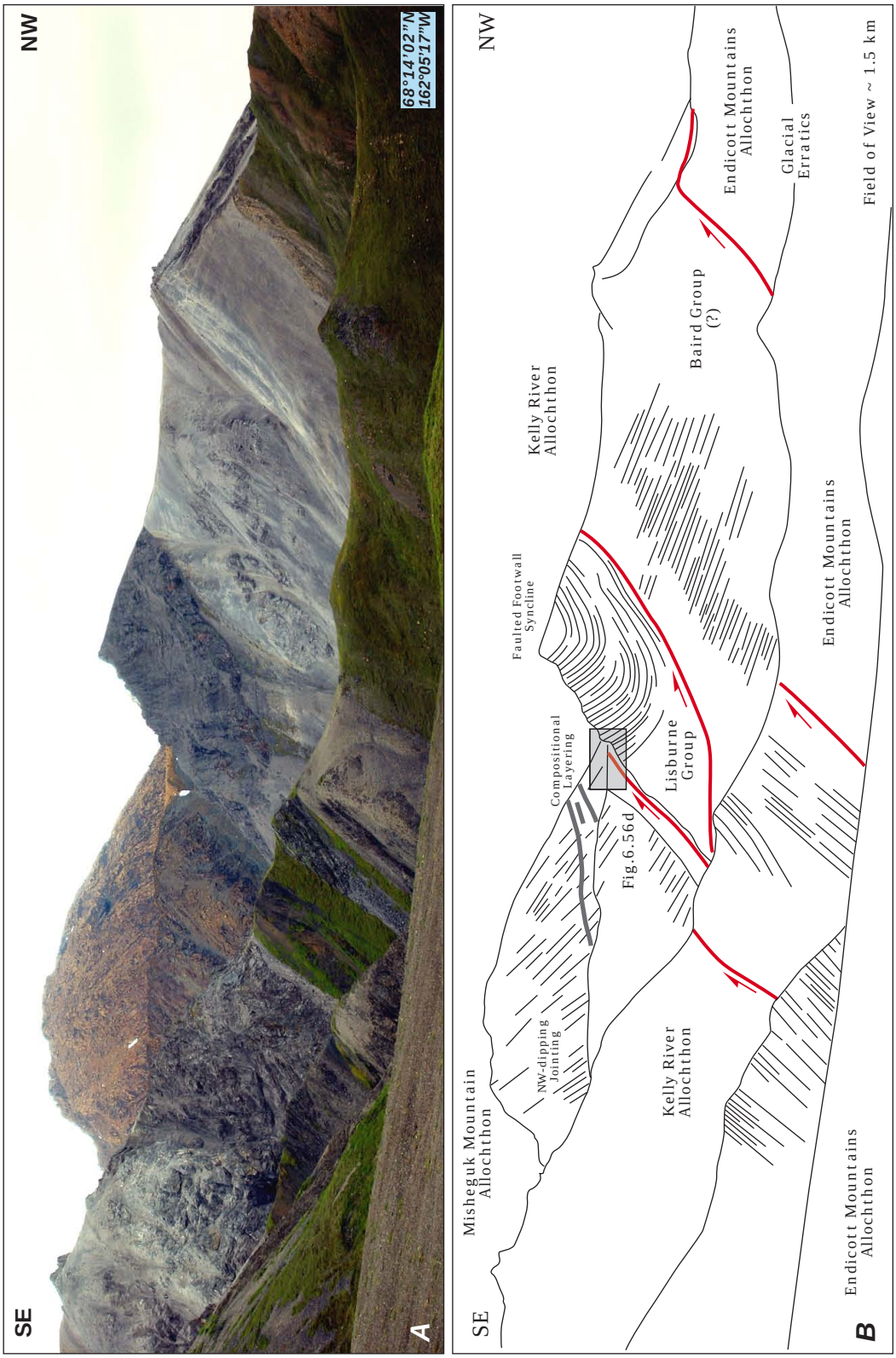


Figure 6.55. Structural relationships in the Avan Hills area. **A.** SW-looking panoramic view of the allochthon stack in the western part of the Avan Hills. Field of view is approximately 1.5 km. Topographic relief is approximately 600 m. **B.** Line-drawing structural interpretation of A.

Angayucham Thrust

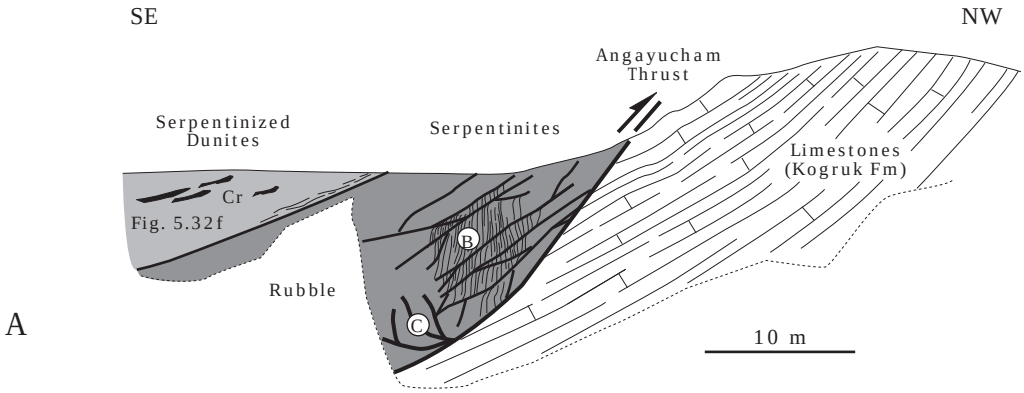
The Angayucham thrust is a regional-scale fault that brings Middle Jurassic upper mantle serpentinized peridotites and lower crust gabbros (Figs. 6.2a, 6.51 – 6.56; cf. Chapter 5, Figs. 5.1 & 5.32a) on top of structurally thinned Late Devonian to Early Mississippian platform carbonates of the Kelly River allochthon (Figs. 6.51 – 6.56). The Angayucham thrust is well exposed along the western margin of the Avan Hills (Fig. 6.2a) where it occurs as an approximately 5 to 10 m thick, recessive-weathering and gently to moderately (20° to 50°) SE-dipping planar hangingwall flat fault zone that consists of satiny black to dark green magnetite-bearing serpentinites (Fig. 6.56a - f; cf. Chapter 5, Fig. 5.32a). Serpentinites in the fault zone are highly tectonized and show poorly- to well-developed schistose phacoidal fabrics, defined by a variably spaced (1 mm to 2 cm) anastomosing foliation that encloses symmetric to asymmetric striated lithons of less deformed serpentinite (Figs. 6.56e, f & 6.57a, b). These serpentinites are here interpreted as *LS*-tectonites with poorly- to well-developed *S*-*C* foliations (cf. Ramsay & Huber, 1987*a*; Passchier & Trouw, 1998) (Figs. 6.56e, f & 6.57a, b). *S* planes are dominantly steeply-dipping to the southeast (Figs. 6.56e, f, 6.57 & 6.58) and *C* surfaces dip moderately to gently, forming a series of stacked shear bands (Fig. 6.57b). Spacing of *C* surfaces typically ranges from 1 to 7 cm.

Serpentinites along the Angayucham thrust are here interpreted to have resulted from low-grade dynamothermal metamorphism and recrystallization of fine- to coarse-grained dunites (cf. Chapter 5, Figs. 5.30 & 5.31). A diffuse zone of buff- to brown-weathering ferroan carbonate typically occurs along the fault zone, extending into the immediate footwall (Fig. 6.56d, e). This possibly resulted from syn-orogenic fluid flow along the Angayucham thrust and alteration of the underlying platform carbonates.

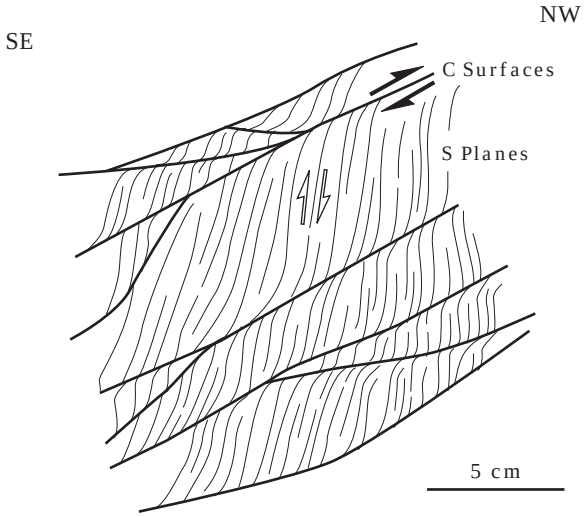
Sense of shear indicators in the Angayucham thrust show a regional top to the northwest tectonic transport direction (Figs. 6.56e, f, 6.57 & 6.58). This is consistent with the regional tectonic transport directions determined for the allochthons of the underlying Arctic Alaska terrane (Figs. 6.11, 6.29 & 6.36). Shear bands in the Angayucham thrust are locally crosscut by a series of NE-SW-trending and dominantly NW-dipping high-angle, planar to listric brittle extensional faults that locally merge with the Angayucham



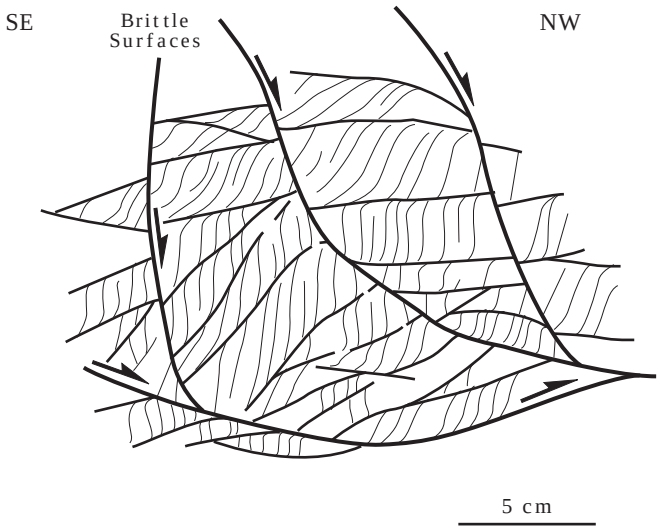
Figure 6.56. Structural features of the Angayucham thrust. **A.** Orange-weathering Jurassic dunites of the Misheguk Mountain allochthon structurally overlie grey-weathering Devonian to Mississippian platform carbonates of the Kelly River allochthon. Topographic relief is approximately 700 m. **B.** NE-looking view of the Angayucham thrust. Topographic relief is approximately 350 m. **C.** W-looking view of the Angayucham thrust. Topographic relief is approximately 10 m. Note folded grey-weathering limestones in the immediate footwall. **D.** Detail of the Angayucham thrust. Orange weathering serpentinized dunites and dark green-weathering serpentinites overlie grey-weathering platform carbonates of the Lisburne Group. U. S. Geological Survey geologist Chris Potter for scale. **E.** Detail of the Angayucham thrust. Dark green serpentinites structurally overlie relatively undisrupted Mississippian limestones. Note zone of iron carbonate alteration along fault zone. Geological hammer encircled for scale. **F.** Detail of tectonized serpentinites with well developed pachoidal texture and *S-C* shear fabrics. Kinematic indicators show a top to northwest tectonic transport direction. Geological hammer for scale.



A



B



C

Figure 6.57. Field sketches of structural relationships and tectonic fabrics in the Angayucham thrust in the Avan Hills area. **A.** Sketch showing the Angayucham thrust. **B.** Detail of the fault zone showing ductile shear bands with well developed, locally anastomosing, *C* surfaces and *S* planes. **C.** Detail of shear bands offset by late (?) brittle extensional fault. Note extensional faults locally merge into *C* surfaces.

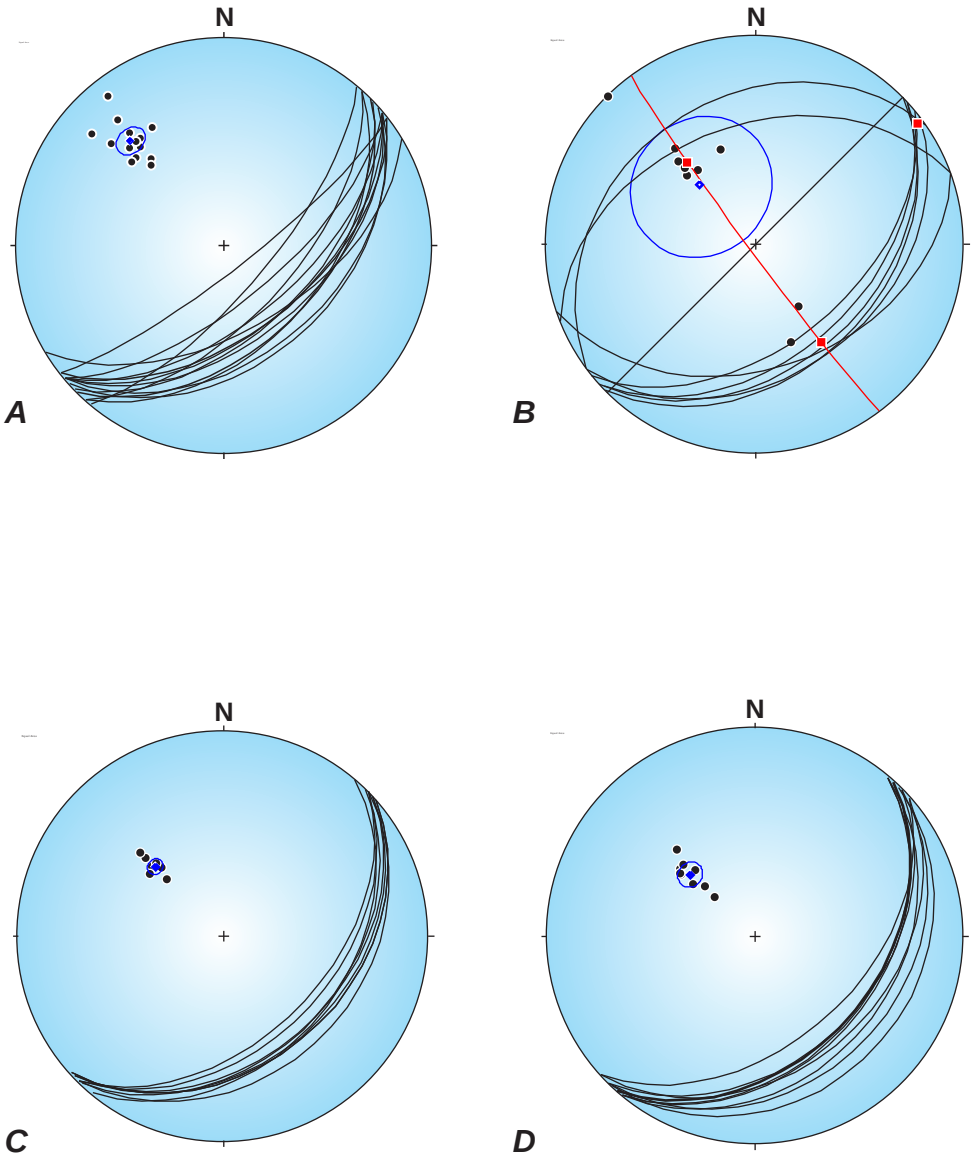


Figure 6.58. Lower hemisphere equal area stereographic projection of structural data from the Misheguk Mountain allochthon in the Avan Hills. **A.** Great circles and poles to foliation in tectonized serpentinites in the Angayucham thrust (N=10). **B.** Great circles and poles to bedding in strata of the Kelly River and Endicott Mountains allochthons in the immediate footwall to the Angayucham thrust (N=10). **C.** Great circles and poles to foliation in ultramafic rocks of the Misheguk Mountain allochthon. N=10. **D.** Great circles and poles to layer-parallel shear fabrics in layered gabbros (N=15).

thrust (Fig. 6.57c). These are interpreted as possible evidence for brittle reactivation of the Angayucham thrust as a detachment low-angle extensional fault.

Deformation of the ultramafic succession in the immediate hangingwall of the Angayucham thrust includes the development of rare mylonites and proto-mylonites. These show rare porphyroclastic textures with a bimodal distribution of ortho- and clinopyroxene porphyroclasts in a strongly serpentinized orange-weathering dunite matrix with olivine relicts and well-developed mesh texture. Porphyroclasts typically show poorly- to well-developed σ structures, which indicate deformation under relatively low shear strain rates (cf. Hibbard, 1995; Passchier & Trouw, 1998). Microstructures and deformation features observed in thin section include cataclasis, intergranular and transgranular cracks, recrystallization, undulatory extinction, deformation lamellae, and locally well-developed serrated grain boundaries. These microstructures are here interpreted to have resulted from early plastic deformation during obduction followed by brittle deformation during final emplacement of the allochthon. Layer-parallel shear fabrics are more common in the layered gabbro unit (cf. Chapter 5, Fig. 5.33f), which locally shows centimetric to decimetric intrafolial folds (e.g. Ramsay & Huber, 1987*a*) with poorly-defined sub-horizontal to sub-vertical axial surfaces that are parallel to slightly oblique the magmatic layering.

In addition to shear fabrics, massive and layered ultramafic rocks show well-developed sets of irregularly-spaced (10 cm to 10 m), N- to NW-dipping joints (Figs. 6.52e & 6.55) oriented sub-perpendicular to perpendicular to the magmatic layering (M0) and tectonic foliation (F1). This fabric commonly cuts slightly oblique across the compositional magmatic layering. The compositional layering is dominantly NE-SW-trending and moderately to steeply dipping to the southeast. It contains discrete poorly- to well- defined, irregularly-spaced zones laterally discontinuous centimetric zones of layer-parallel shear and flattening (cf. Chapter 5, Fig. 5.33f), together with shear zones in serpentinized dunites.

Intra-allochthonous thrust repetition and folding are rare and shortening is dominantly accommodated by penetrative fabrics. The progressive increase of clinopyroxene towards the base of the allochthon and the continuity of the basal serpentinization halo

(Fig. 6.52a) suggests that the Misheguk Mountain allochthon is not internally imbricated and was possibly emplaced as a single coherent thrust sheet.

Stacking Patterns

Stacking patterns and cut-off relationships suggest that the Angayucham thrust cuts down-section in the direction of tectonic transport both in the hangingwall and footwall (Figs. 6.52d & 6.56). This causes structural thinning and omission of structural levels in such way that successively lower allochthons are exposed in the footwall of the Angayucham thrust. In the western margin of the Avan Hills, the Copter Peak, Ipnavik River, Kelly River, and Picnic Creek allochthons are absent or structurally thinned below the Misheguk Mountain allochthon (Figs. 6.2a, b, 6.52c, 6.54, 6.55, 6.56 a – d). The Kelly River allochthon in the footwall of the Angayucham thrust is structurally thinned to 100 to 500 m (Figs. 6.52c, 6.53 – 6.55), which contrasts with the Kelly River allochthon further west, where it attains inferred structural thicknesses of 1 to 3 km (e.g. Amphitheatre Mountain area) (Fig. 6.2a, b). Structural separation along the Angayucham thrust is estimated to range approximately from 1 to 5 km.

The Misheguk Mountain allochthon shows a series of NW-SE-trending, NE- to SW-dipping, vertical to moderately-dipping extensional faults that locally juxtapose upper mantle serpentinized dunites against lower crust layered gabbros (Fig. 6.52f). Fault spacing varies from 100 m to 1 km approximately and inferred vertical throws range from approximately 100 m to 1 km. These NW-SW-trending extensional faults can be interpreted as late extensional faults that post-date emplacement of the Misheguk Mountain allochthon. A plausible alternative interpretation is that NW-SE-trending faults are pre-existing Jurassic extensional faults that were transported on the Angayucham thrust during the emplacement of the Misheguk Mountain allochthon in Late Jurassic to Early Cretaceous. Extensional faults in the Misheguk Mountain allochthon interpreted to pre-date emplacement of the allochthon have been described by Harris (2004) in the Misheguk Mountain ultramafic complex, approximately 36 km east-northeast of the Avan Hills (cf. Chapter 2, Figs. 2.14 & 2.18a, b).

Iyikrok Mountain

The Misheguk Mountain allochthon at Iyikrok Mountain is preserved in two synformal klippen that are underlain by the Angayucham thrust and structurally overlie poorly exposed basalts and platform carbonates of the Copter Peak allochthon (Figs. 6.2a, e & 6.59). The Misheguk Mountain allochthon at Iyikrok Mountain has a marked NNE- to NNW-trending, steeply-dipping (50° to 70°) structural grain defined by magmatic layering that is locally highly oblique to the Angayucham thrust (Figs. 6.59 & 6.60). This contrasts with the shallow- to moderately-dipping magmatic layering and tectonic fabrics observed in the Misheguk Mountain allochthon of the Avan Hills (Figs. 6.52 – 6.57). Serpentinized dunites and fine-grained layers of orthopyroxenite are locally penetratively deformed and show a continuous foliation (F1) (Fig. 6.59e) that is slightly oblique to the compositional layering (M0) (Fig. 6.59f).

Based on the structural features and relationships described above (Figs. 6.51 – 6.60) together with the rock assemblages and mineralization documented in Chapter 5 (Section 5.5; Figs. 5.31 – 5.33), the Misheguk Mountain allochthon is interpreted as part of a Tethyan- or Mediterranean-type ophiolite (cf. Moores, 1982; Dilek, 2003) that was obducted onto the continental Arctic Alaska terrane in Middle – Late Jurassic to Early Cretaceous time. The exposure of the petrologic Moho in the immediate hangingwall of the Angayucham thrust (Fig. 6.53; cf. Chapter 5, Fig. 5.31) indicates that the Misheguk Mountain allochthon was possibly detached at or near the plastic – brittle transition between the upper mantle and the lower crust. The regional continuity of the allochthon and the lack of intra-allochthonous repetition suggest that Misheguk Mountain allochthon was possibly emplaced as a coherent and relatively intact thrust sheet.

The Misheguk Mountain allochthon possibly formed above a NE-SW-trending suprasubduction zone, in the proximity of the Arctic Alaska terrane. The presence of intrafolial folds in lower crustal rocks and recrystallization textures (e.g. orthopyroxene-rich layers) are consistent with deformation at high temperature in a ductile flow regime. These features are typically ascribed to shearing of juvenile, hot, oceanic lithosphere (e.g. Nicolas, 1985; Dilek, 2003; Pearce, 2003). Regional map and thrust stacking patterns, show that the Angayucham thrust cuts down section in the direction

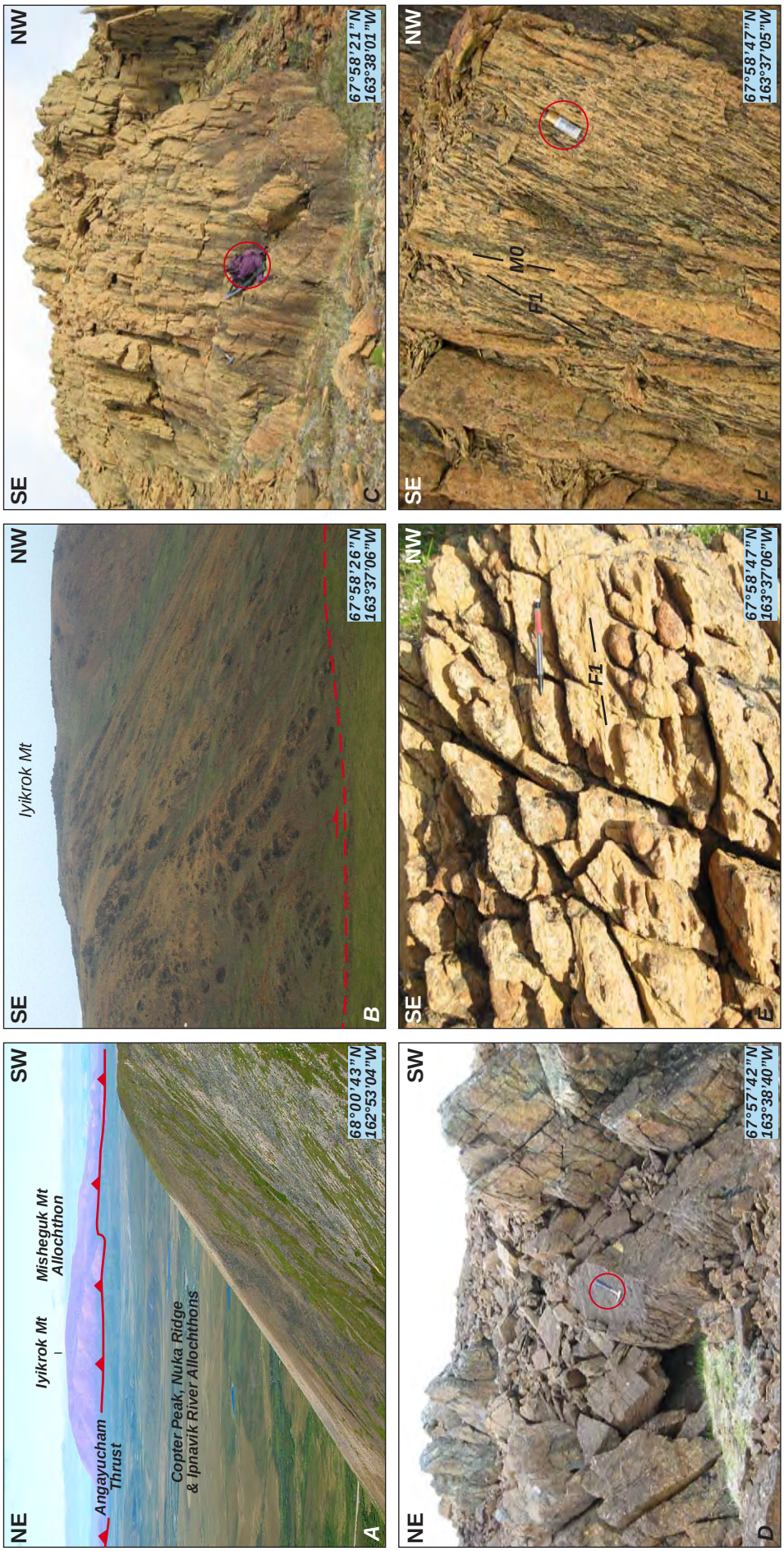


Figure 6.59. Structural features of the Misheguk Mountain allochthon in the Iyikrok Mountain area. **A.** S-looking view of Iyikrok Mountain from Anxiety Ridge. Relief is formed by dunites and gabbros. Lowlands consist of poorly exposed basalts of the Copter Peak allochthon. Topographic relief at Iyikrok Mountain is approximately 200 m. **B.** Dunites near the base of the allochthon. Topographic relief is approximately 50 m. **C.** Detail of steeply-dipping cumulate fabrics near the base of the allochthon. Backpack is encircled for scale. **D.** Detail of SW-dipping dunites. Geological hammer is encircled for scale. **E.** Pervasive foliation (M0) and poorly- to well developed mineral lineation in serpentinized dunite. Pencil for scale. **F.** Penetrative foliation (F1) in serpentinized dunite. Note foliation is oblique to magmatic layering (M0). 8 cm-long shotgun shell is encircled for scale.

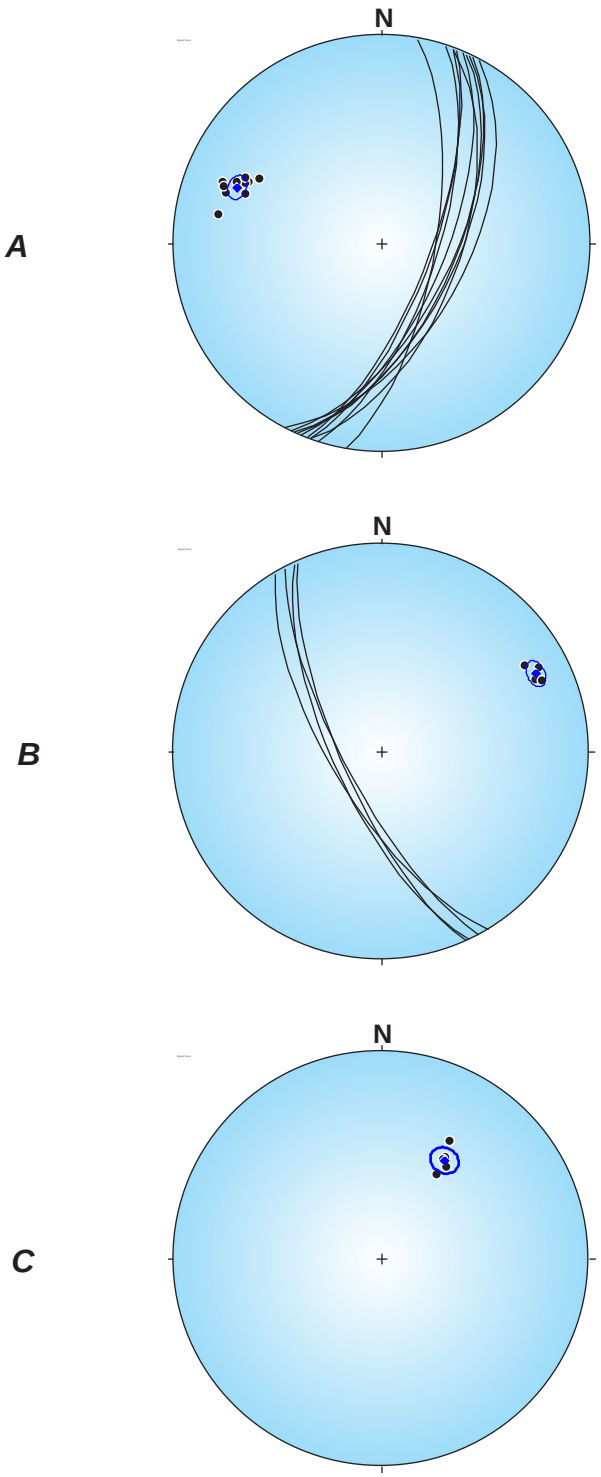


Figure 6.60. Lower hemisphere equal area stereographic projection of structural data from the Misheguk Mountain allochthon at Iyikrok Mountain. **A.** Great circles and poles to foliation (F1) in serpentinized dunite (N=10). **B.** Great circles and poles to magmatic layering (M0) in the layered ultramafic unit (N=5). **C.** Minor fold axes in serpentinized dunites (N=5).

of tectonic transport causing structural thinning and omission of structural levels. This suggests that following obduction, the Angayucham thrust was possibly reactivated as a syn-orogenic low-angle extensional fault. Other possible explanations for the geological relationships in the area include synchronous thrusting, out-of-sequence thrusting, or a combination of these processes.

6.5 STRUCTURE OF THE THRUST FRONT

The allochthons of the Arctic Alaska and Angayucham terranes in the Red Dog district terminate in a NE-SW- to WNW-ESE-trending and NW- to SE-dipping thrust front that separates the allochthonous thrust sheets and early syn-orogenic strata of the fold thrust belt from the North Slope parautochthon and foreland basin (Figs. 6.2a – f & 6.4). Previous regional studies in the area (e.g. Moore *et al*. 1986; Young, 1992; Young, 2004) considered all exposed Ellesmerian strata as far-travelled allochthonous thrust sheets (Figs. 2.14a, b & 3.5) and did not identify the thrust front.

The thrust front of the western Brooks Range fold and thrust belt in the Red Dog district is a complex composite structure whose geometry, vergence, orientation, position, structural styles, and tectonostratigraphic evolution vary significantly along strike (Fig. 6.2a – f). The thrust front was studied along and across strike for approximately 118 km, from the southwest end of the Wulik Peaks to the Inaccessible Ridge area in the northeast (Fig. 6.2a) and is here divided into three distinct segments. From northeast to southwest these are here named the Amphitheatre Mountain triangle zone, the Wulik Peaks transverse zone and the Amaruk River emergent thrust front (Figs. 6.2a & 6.61). The Amphitheatre Mountain triangle zone and the Amaruk River emergent thrust front are markedly NE-SW-trending and are shifted 17 to 25 km respect to each other by the WNW-ESE- to NW-SE-trending Wulik Peaks transverse zone (Figs. 6.2a & 6.61). The main structural features of the thrust front in the Red Dog district are summarized in Table 6.8 and described in detail below.

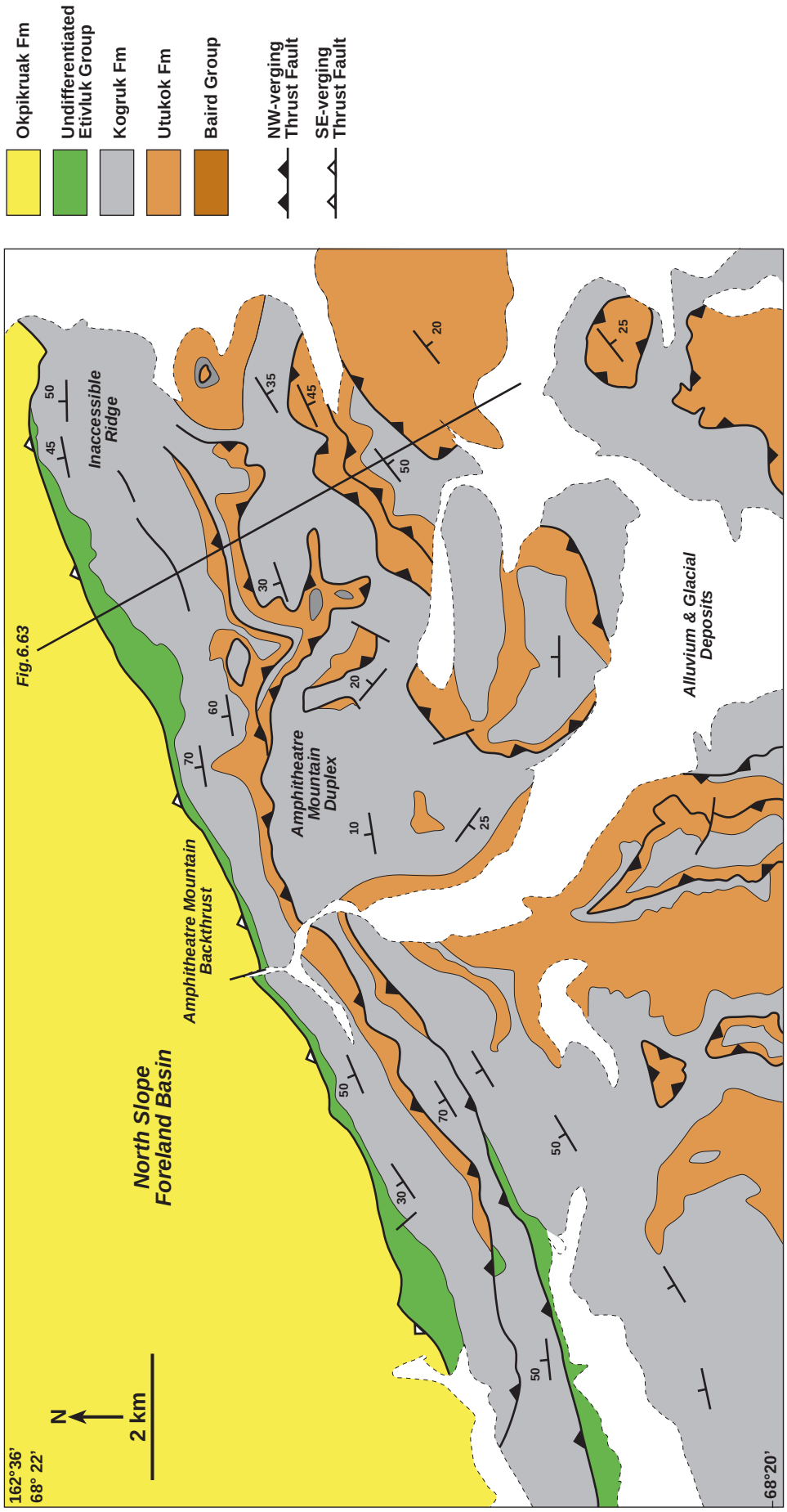


Figure 6.61. Simplified structural map of the Inaccessible Ridge area showing the Amphitheatre Mountain triangle zone (geology is compiled and modified from Curtis *et al.* 1990).

	Thrust Front Type	Structural Trends	Dip	Associated Structures	Associated Syn-orogenic Strata	Tectonic Transport Direction
Amphitheatre Mt Triangle Zone	Buried	NW-SE-trending SE- to NW-dipping	15 - 90° locally overturned	Mount Raven Antiform. Antiformal stacks with detachment folds above the upper detachment	Turbidites (Bouma sequences) with rare olistoliths	West-northwest to northwest Southeast above the upper detachment
Wulik Peaks Transverse Zone	Emergent	WNW-ESE- to NW-SE-trending SE- to NW-dipping	35 - 70°	WNW-ESE-trending Thrust faults and folded thrusts, NNW- to NNE- dip and oblique slip faults, Wrench Creek fault	Olistostromal. Olistoliths derived from the Kelly River, Picnic Creek and Endicott Mountains allochthons	North-northeast
Amaruk River Thrust Front	Emergent	NE-SW-trending SE-dipping	15 - 30°	Imbricate thrust faults	Olistostromal. Olistoliths derived from the Kelly River, Picnic Creek and Endicott Mountains allochthons	West-northwest to northwest

Table 6.8. Summary structural features of the thrust front of the Brooks Range fold and thrust belt in the Red Dog district.

6.5.1 Amphitheatre Mountain Triangle Zone

The term Amphitheatre Mountain triangle zone is introduced in this thesis to describe the structure of the thrust front of the western Brooks Range fold and thrust belt in the northern part of the Red Dog district (Fig. 6.2a – c & 6.61). The Amphitheatre triangle zone is a well-developed thin-skinned triangle zone (*sensu* Gordy *et al*. 1977; Jones, 1996) or type-II buried thrust front (cf. Morley, 1986) along which the allochthons of the Red Dog district terminate in a N- to NW-tapering wedge (Fig. 6.2a – c). The Amphitheatre Mountain triangle zone in the Red Dog district extends along strike for at least of 52 km, from the Mount Raven and Sheep Mountain areas into the Inaccessible Ridge area (Fig. 6.2a). Analyses of LANDSAT and MARS SLAR radar images together with the re-interpretation of map patterns from published geological maps (e.g. Mayfield *et al*. 1988, 1990; Moore *et al*. 1994; Mull *et al.* 2000) suggest that the Amphitheatre Mountain triangle zone is not restricted to the Red Dog district but possibly continues to the northeast into the west-central Brooks Range. The structural relationships documented in this study contrasts markedly with those of previous work (e.g. Mayfield *et al*. 1990; Young, 2004), in which the thrust front was interpreted as a SE-dipping, NW-verging thrust fault that emplaced the Kelly River allochthon over the Picnic Creek allochthon (cf. Chapter 3, Fig. 3.15).

In the Amphitheatre Mountain triangle zone, antiformally-stacked thrusts sheets of the Kelly River and the Endicott Mountains allochthons are underthrust by a thick succession (*ca.* 2 km) of syn-orogenic strata of the Okpikruak Formation (Figs. 6.61 – 6.63). The Amphitheatre Mountain triangle zone is developed on the Wolverine Creek plate in the Mount Raven area (Figs. 6.2a, b & 6.62a), and in the overlying Amphitheatre Mountain plate of the Kelly River allochthon further to the northeast (Figs. 6.2a, b & 6.62b).

In the Amphitheatre Mountain triangle zone, strata of the late Okpikruak Formation are detached from the underlying sedimentary succession on a S- to SE-verging, regional backthrust that acted as the roof thrust for underlying WNW- to NW-verging antiformal stacks in the Wolverine Creek plate of the Endicott Mountains allochthon (i.e. Mount Raven antiform) and the overlying Amphitheatre Mountain plate of the Kelly River

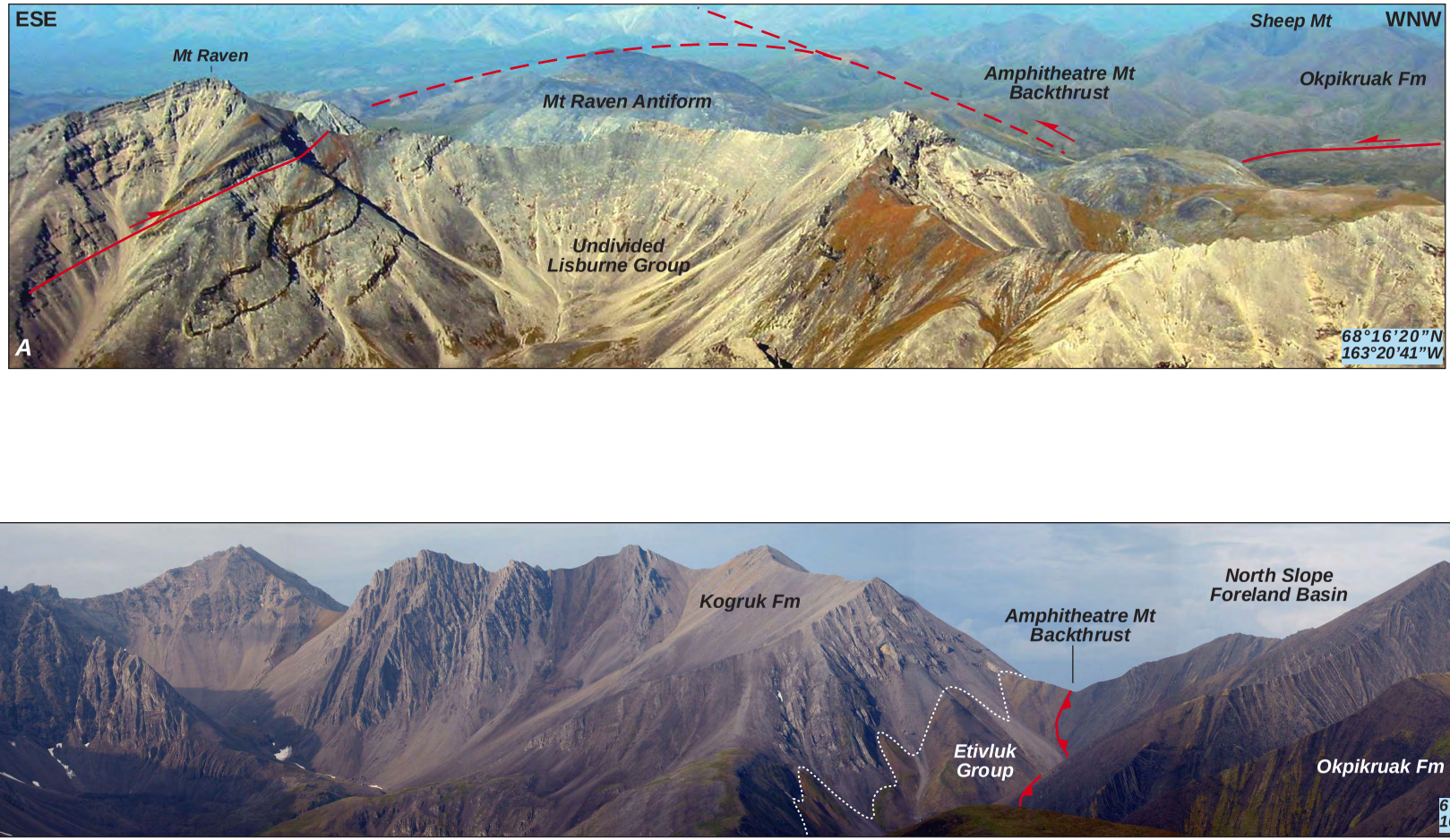


Figure 6.62. Amphitheatre Mountain triangle zone. **A.** SSW-looking oblique aerail photomosaic showing the Amphitheatre Mountain triangel zone in the Mount Raven area. Note the Mount Raven antiform. Field of view is approximately 2.5 km. **B.** SW-looking photomosaic of the Amphitheatre Mountain triangle zone in the Inaccessible Ridge area. Field of view is approximately 2.5 km and topographic relief is approximately 600 m.

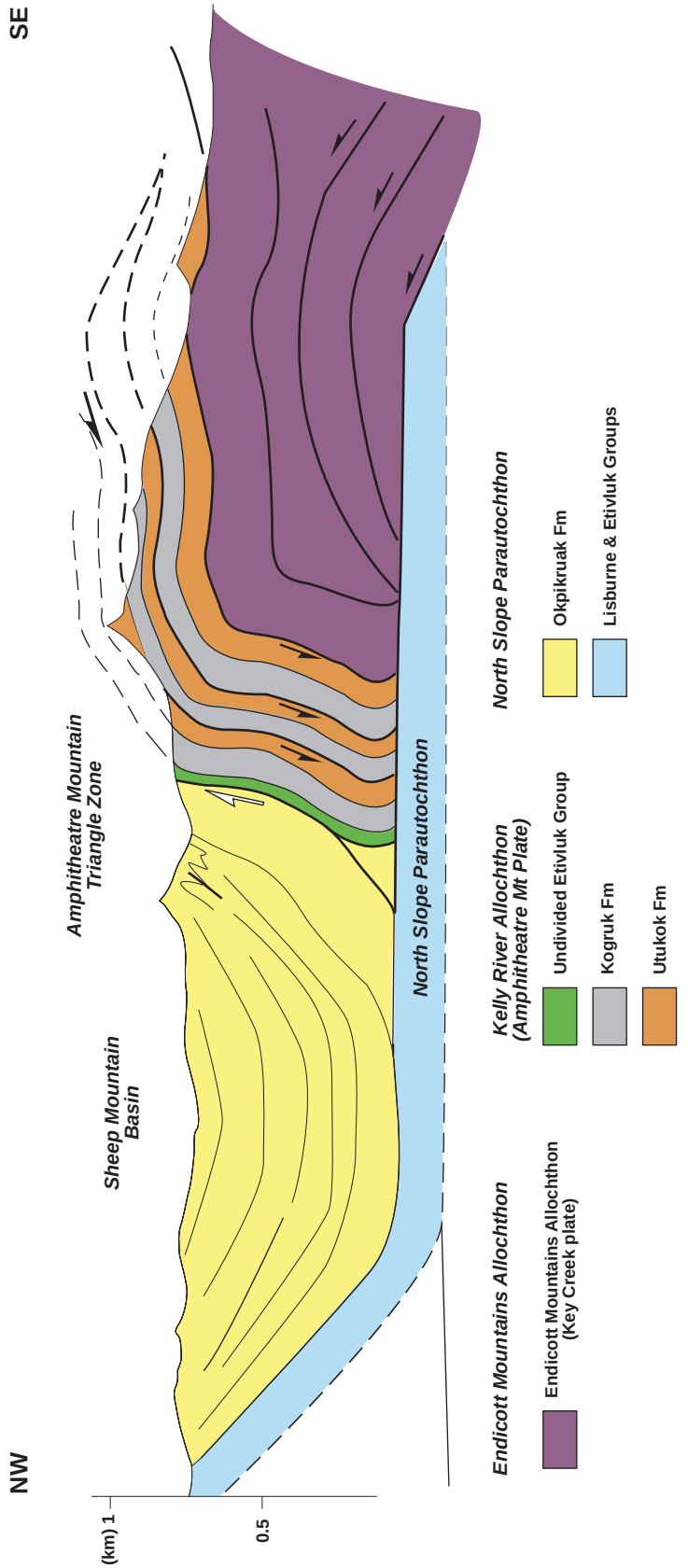


Figure 6.63. Northwest-southeast cross section showing the structure of the thrust front in the Inaccessible Ridge area. Note development of the Amphitheatre Mountain traingle zone.

allochthon (Figs. 6.61 – 6.64). This structure, here named the Amphitheatre Mountain backthrust, is described below.

Amphitheatre Mountain Backthrust

The Amphitheatre Mountain backthrust is a NW- to SE-dipping, SE-verging regional hangingwall and footwall flat thrust fault with no stratigraphic separation (Figs. 6.61 – 6.64). It is developed in incompetent shales of the uppermost Etivluk Group or at the base of the overlying Okpikruak Formation (Fig. 6.64a – c). The backthrust dips moderately to steeply (35 to 60°) to the north and northwest (Figs. 6.62b & 6.64a – d), and locally is folded and overturned, dipping gently to steeply to the southeast and south-southeast (Fig. 6.62b). Along-strike changes in the dip of the backthrust is here interpreted to reflect the non-cylindrical geometry of the Mount Raven antiform (Fig. 6.2a) possibly combined with differential progressive or renewed thrusting and folding on the underlying North Slope parautochthon. Locally, the folded backthrust has been rotated beyond its critical limit of stability and has been abandoned and breached by SE-dipping, NW-verging thrust faults (Fig. 6.7b). This interpretation is supported by structural relationships exposed approximately 2.5 km north-northwest of Mount Raven (Fig. 6.7a, b) and the presence in the syn-orogenic succession of olistoliths derived from the underlying Amphitheatre Mountain plate (Fig. 6.2a).

Subsidiary SE-verging detachments are locally developed in thin- and planar parallel-bedded cherts and shales of the lower and middle units of the Otuk Formation in the footwall of the backthrust (Fig. 6.64d & 6.65). Strata of the Otuk Formation locally show outcrop-scale intercutaneous wedges.

The structural style in the footwall of the Amphitheatre Mountain backthrust is characterized by antiformally-stacked thrust sheets of the Wolverine Creek plate of the Endicott Mountains allochthon and the Amphitheatre Mountain plate of the Kelly River allochthon (Figs. 6.44, 6.62, 6.63). These consist of NW- to SE-dipping, NW-verging thrust faults with fault-related folds and penetrative cleavage fabrics. Thrust horses in the immediate footwall of the triangle zone are overturned to steeply-dipping upright (Figs. 6.44 & 6.62a).

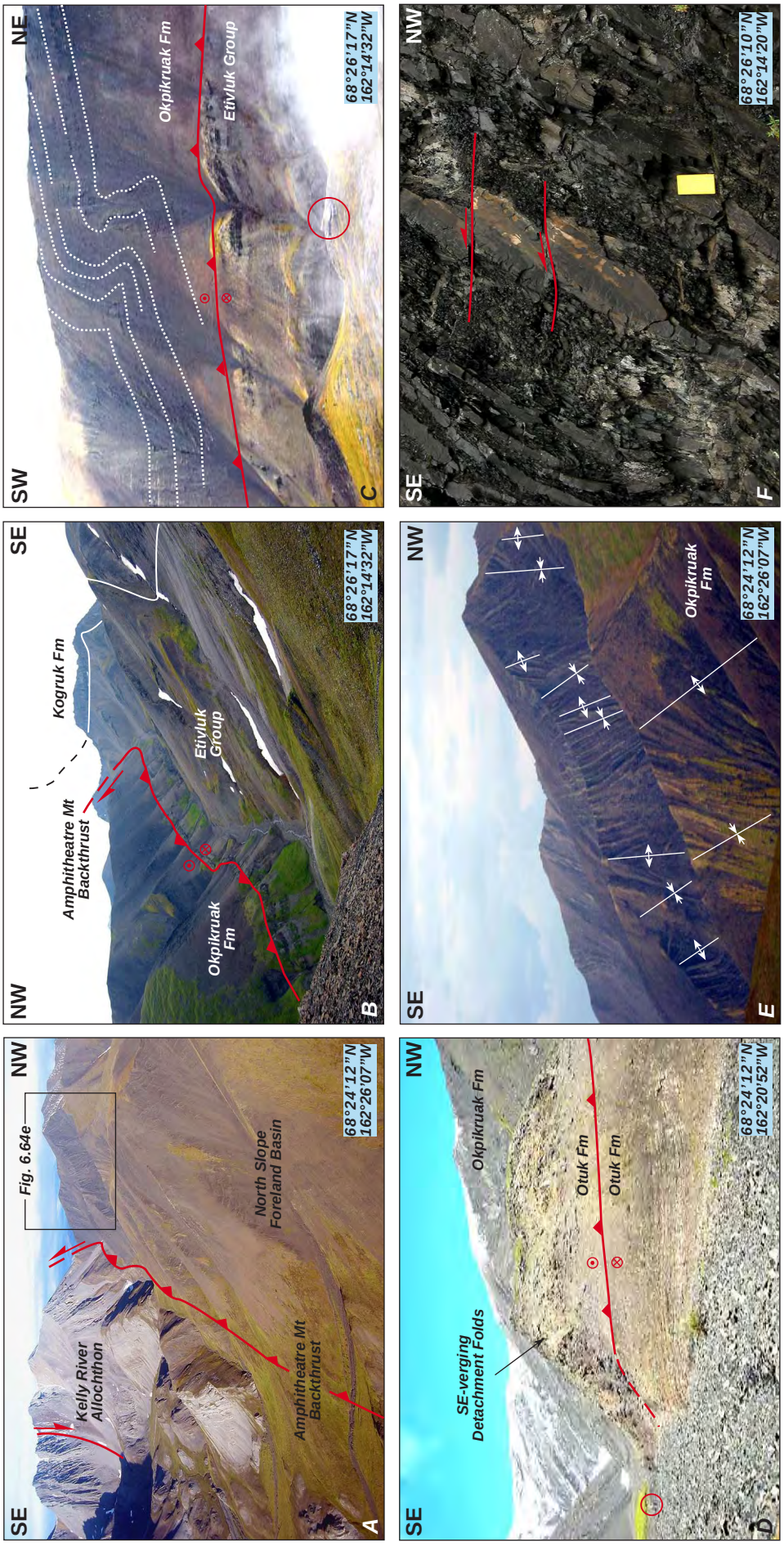


Figure 6.64. Structural features of the Amphitheatre Mountain triangle zone. **A.** SW-looking oblique aerial view of the Amphitheatre Mountain triangle zone in the Inaccessible Ridge area. Note NW-dipping thrust sheets of the Kelly River allochthon wedged underneath syn-orogenic strata of the Okpikruak Formation. Topographic relief is approximately 500 m. Field of view is approximately 2.5 km. **B.** Along-strike view of the Amphitheatre Mountain triangle zone. Topographic relief is approximately 250 m. **C.** Oblique view of SE-verging detachment folds in the Okpikruak Formation. Note detachment at the top of the Etivluk Group. Helicopter is encircled for scale. **D.** Intra-Etivluk Group detachment. U. S Geological Survey geologist Craig Johnson is encircled for scale. **E.** View of SE-verging detachment folds in the Okpikruak Formation. Topographic relief is approximately 350 m. **F.** Outcrop-scale thrust faults in frontal limb of anticline. Note well developed cleavage fabrics. 20 cm-long field notebook for scale.

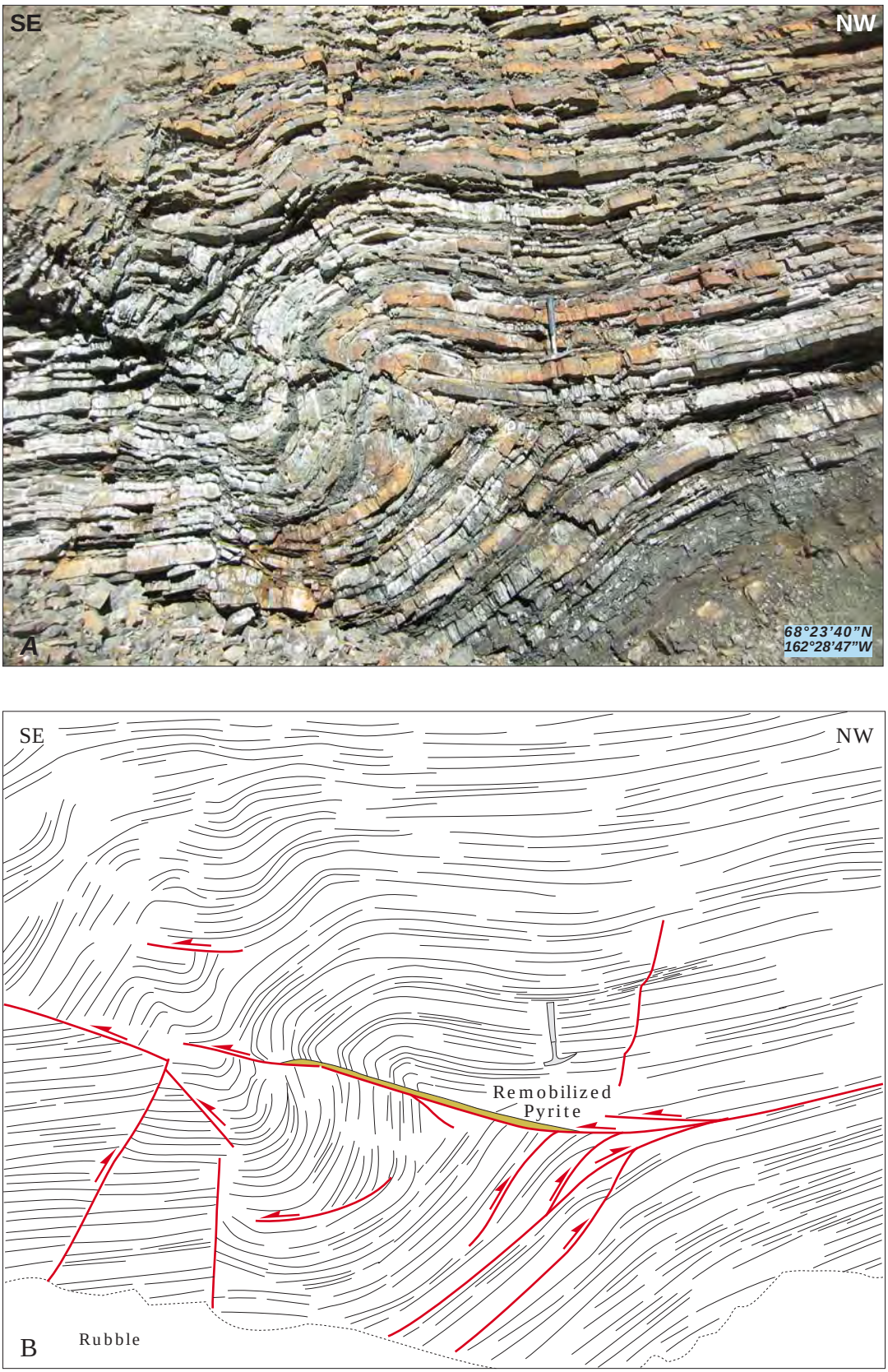


Figure 6.65. Detail of SE-verging detachment folds in the Amphitheatre Mountain triangle zone. **A.** Faulted detachment fold in pyrite-bearing shales and cherts of the Etivluk Group in the Amphitheatre plate of the Kelly River allochthon in the Inaccessible Ridge area. Geological hammer for scale. **B.** Line-drawing structural interpretation of A showing SE-verging asymmetric faulted detachment fold. Note footwall backthrusts and remobilization of pyrite along thrust fault surface.

The structural styles in the hangingwall of the Amphitheatre Mountain backthrust are characterized by NE-SW- to NNE-SSW-trending, symmetric to strongly asymmetric detachment folds in strata of the Okpikruak Formation (Figs. 6.62b, 6.64a, c, e & 6.66).

These detachment folds typically have short upright to overturned front limbs and gently- to steeply-dipping long back limbs (Figs. 6.62b, 6.64a, c, e & 6.66). Folds wavelengths commonly range from 5 to 30 m, interlimb angles that vary from 30° to 75°, and fold amplitudes on the order of 5 to 15 m. Fold axial surfaces dip gently to steeply (25° to 70°) to the north or northwest and are locally upright (Figs. 6.66 & 6.67).

SE-verging detachment folds are interpreted to have resulted from accommodation of excess bed length accumulated in the hangingwall of the Amphitheatre Mountain backthrust relative to the antiformally-stacked thrust sheets of the Kelly River and Endicott Mountains allochthon in the footwall (Fig. 6.68). Interlimb angles and outcrop-scale structures indicate that the detachment folds were locally amplified and flattened. Abrupt along-strike changes in fold wavelength, amplitude, vergence and asymmetry of the detachment folds are interpreted to reflect varying degrees of coupling between the Okpikruak Formation and underlying duplexes in the Endicott Mountains and Kelly River allochthons. SE-verging detachment folds are locally breached by gently to moderately NW-dipping (10° to 45°), SE-verging thrust faults and forelimb shear thrusts that accommodate centimetric to decametric displacement (Figs. 6.64e, f & 6.65b). These faults give rise to transported detachment folds and locally well developed decapitated fold geometries with hangingwall and footwall cut off angles that typically range from 60° to 90°. Associated with detachment folds are also well developed continuous to spaced cleavage fabrics (Fig. 6.64f).

6.5.2 The Wulik Peaks Transverse Zone

The term Wulik Peaks transverse zone (Figs. 6.62 & 6.69) is introduced in this thesis to refer to the section of the western Brooks Range fold and thrust belt in the Red Dog district in which major thrust faults, thrust fault-related folds and cleavage fabrics are deflected, trending at a high angle (74° to 90°) to the dominant NE-SW-trending regional structural grain (Figs. 6.2a & 5.1). The Wulik Peaks transverse zone is a

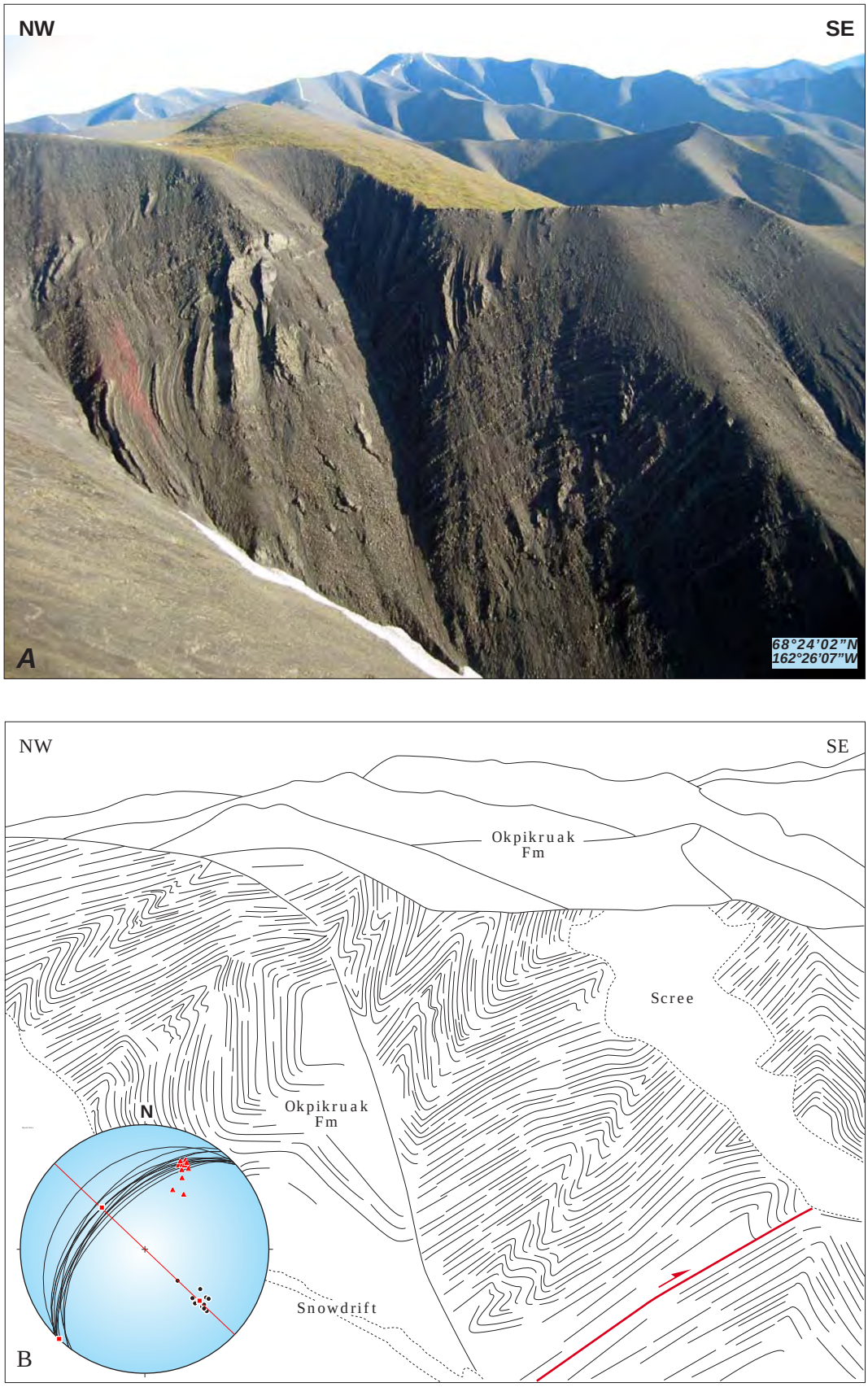


Figure 6.66. Structural styles in the hangingwall of the Amphitheatre Mountain backthrust. **A.** NE-looking view of SE-verging asymmetric detachment folds in turbidites of the Okpikruak Formation. Field of view and topographic relief is approximately 25 m. **B.** Line-drawing interpretation of A and lower hemisphere stereographic projection great circles and poles (solid circles) to fold axial surfaces (N=12) and minor fold axes (red triangles) (N=15).

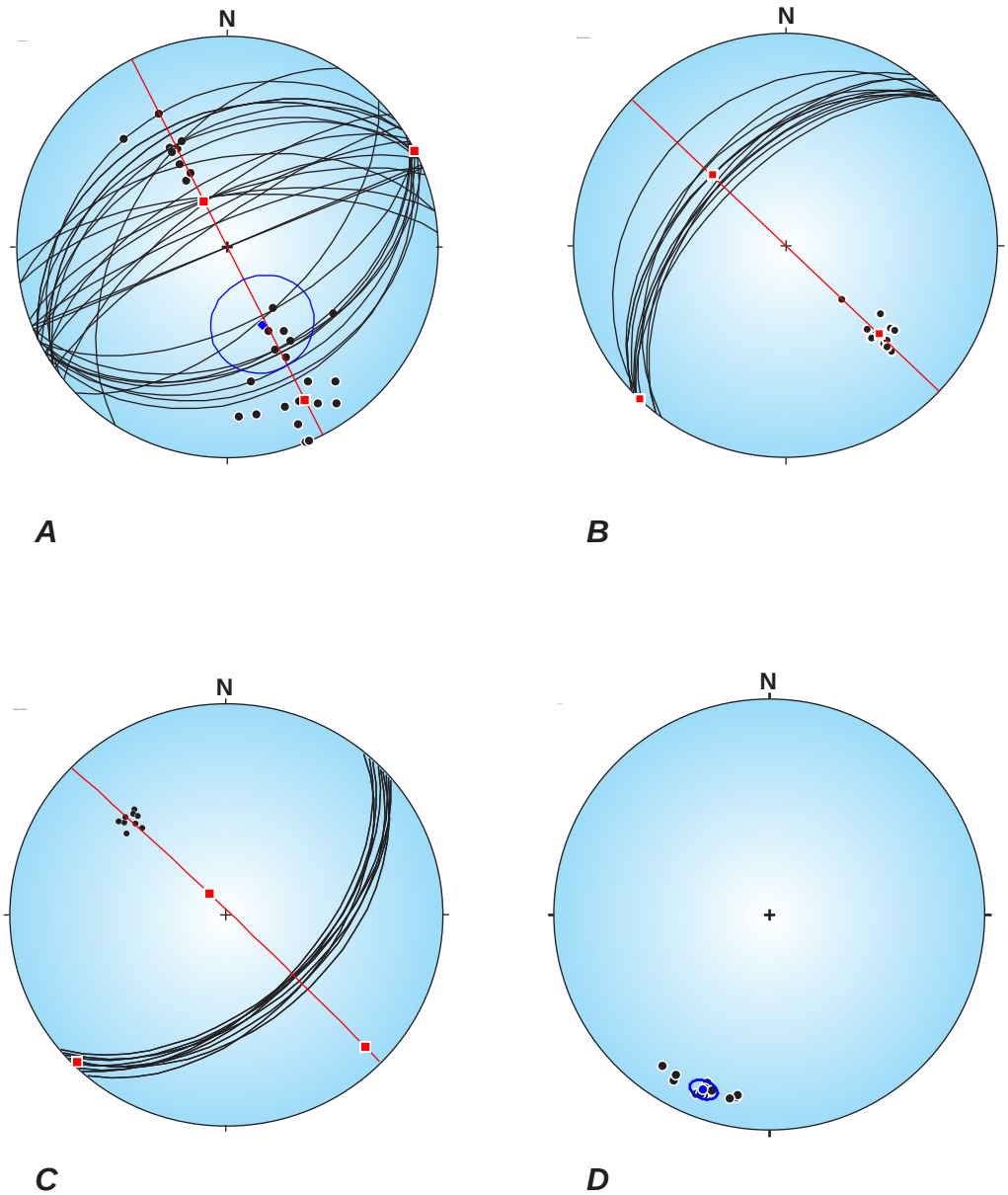


Figure 6.67. Lower hemisphere equal area stereographic projection of structural data from the Amphitheatre Mountain triangle zone. **A.** Great circles and poles to bedding (N=70) in strata of the Kogruk Formation of the Amphitheatre Mountain plate of the Kelly River allochthon. **B.** Great circles and poles to fold axial surfaces in strata of the Late Okpikruak Formation (N=12). **C.** Great circles and poles to fold axial surfaces in the Amphitheatre Mountain plate of the Kelly River allochthon (N=15). **D.** Minor fold axes in the Amphitheatre Mountain triangle zone in the Mount Raven and Sheep Mountain areas (N=15).

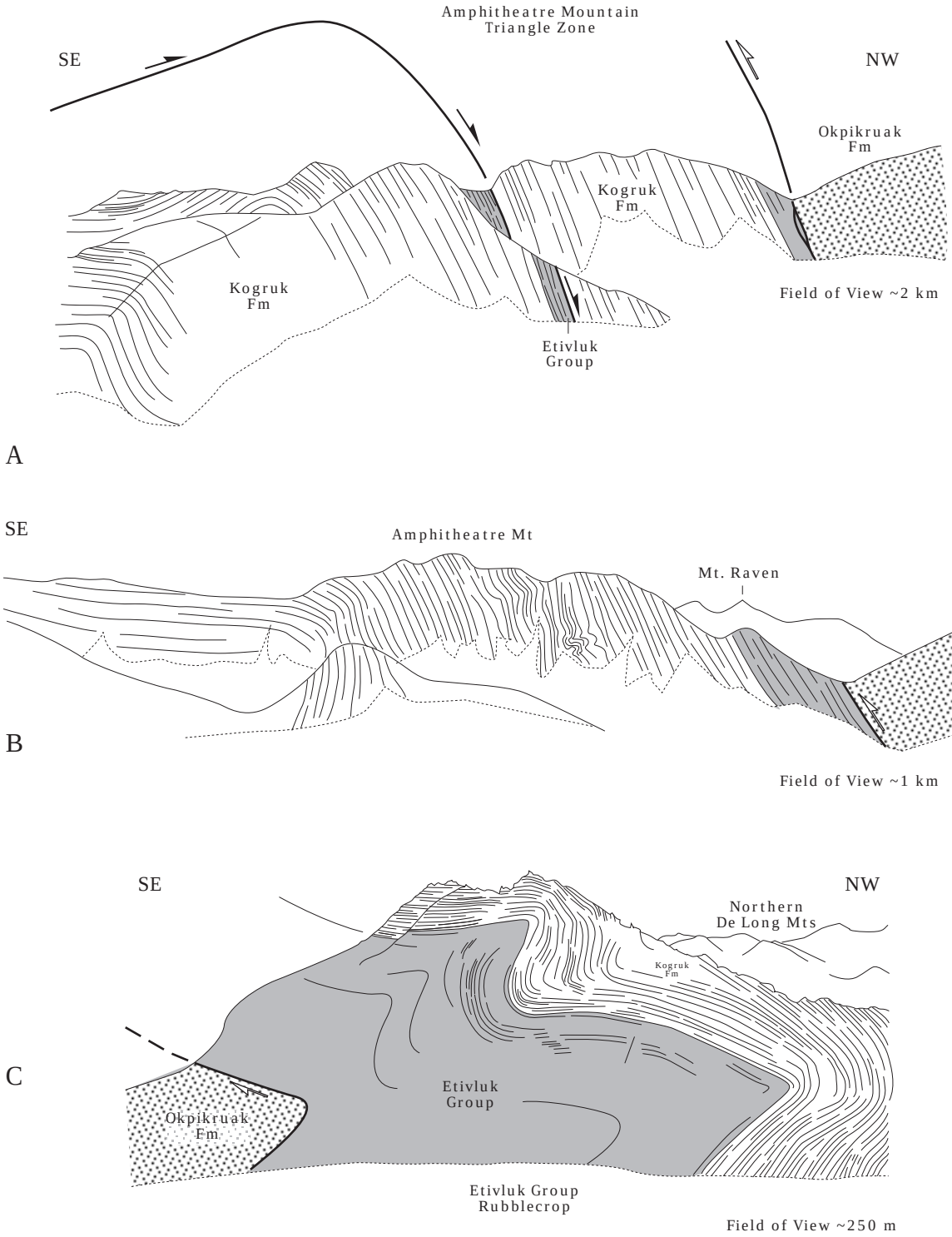


Figure 6.68. Field sketches illustrating the structure of the Amphitheatre Mountain triangle zone. **A.** Inaccessible Ridge. **B.** Amphitheatre Mountain. **C.** North of Inaccessible Ridge.

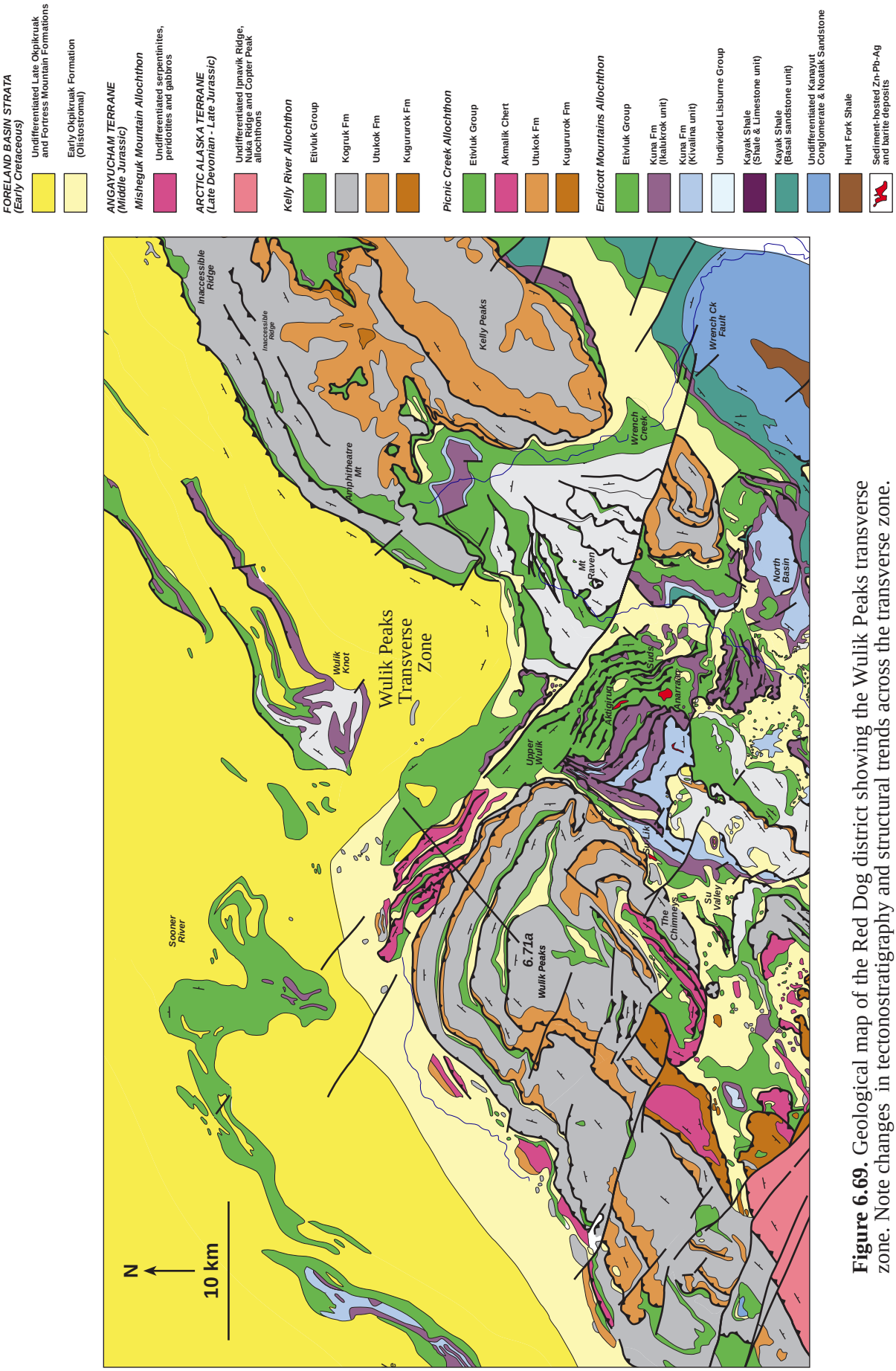


Figure 6.69. Geological map of the Red Dog district showing the Wulik Peaks transverse zone. Note changes in tectonostratigraphy and structural trends across the transverse zone.

regional-scale feature, approximately 50 km long and as much as 20 km wide that extends from the northwestern margin of the Wulik Peaks and the adjacent North Slope foreland basin in the northwest to the Wrench Creek area in the southeast (Fig. 6.2a). The Wulik Peaks transverse zone is a complex branching fault array (Fig. 6.2f) that consists of WNW-ESE- to NW-SE-trending, gently- to steeply-dipping and locally folded thrust faults, NNE- to NNW-trending and WNW- to ESE-downthrown high-angle dip slip and oblique slip faults along with complex detachment folds and penetrative cleavage fabrics (Figs. 6.70 – 6.72). The Wulik Peaks transverse zone is parallel to sub-parallel to the regional tectonic transport direction and is the locus of alignment and reversal of regional fold plunge terminations (e.g. Husky Hills and Mount Raven antiforms) (Figs. 6.2a & 5.1). Regional dip of thrust sheets suggests that the transverse zone dips 50° to 70° to the south-southwest. It involves at least the Endicott Mountains, Picnic Creek and Kelly River allochthons (Fig. 6.2a, f). This suggests that the development of the transverse zone was controlled by a deep-seated lateral ramp or tear fault in the North Slope parautochthon or in the underlying autochthonous basement.

The Wulik Peaks transverse zone forms a SSW-dipping and NNE-verging emergent thrust front that brings the Kelly River and Picnic Creek allochthons on top of olistostromal strata of the Late Okpikruak Formation (Figs. 6.2a & 6.70 – 6.72). Folded thrust faults (Figs. 6.47 & 6.48) along the transverse zone (Figs. 6.46 & 6.47) interpreted to have formed as a result of amplification associated with buttressing and development of the Wulik Peaks transverse zone. Map patterns, changes of fold amplitude and wavelength and increasing curvature of thrust sheets towards the northwest and the convergence of individual thrust faults into the trailing part of the transverse zone and the Wrench Creek fault (Figs. 6.2a & 5.1) suggest that local clockwise rotation about a vertical axis possibly occurred. Assuming that thrust faults of the Wulik Peaks plate originated as a continuous NE-SW-trending front (similar to that developed along the Amphitheatre Mountain triangle zone and the Amaruk River emergent thrust front) and based on map patterns, the amount of clockwise rotation is here estimated in approximately 63° to 55°. Thrust sheet dip appears to increase towards the leading edge of the transverse zone.

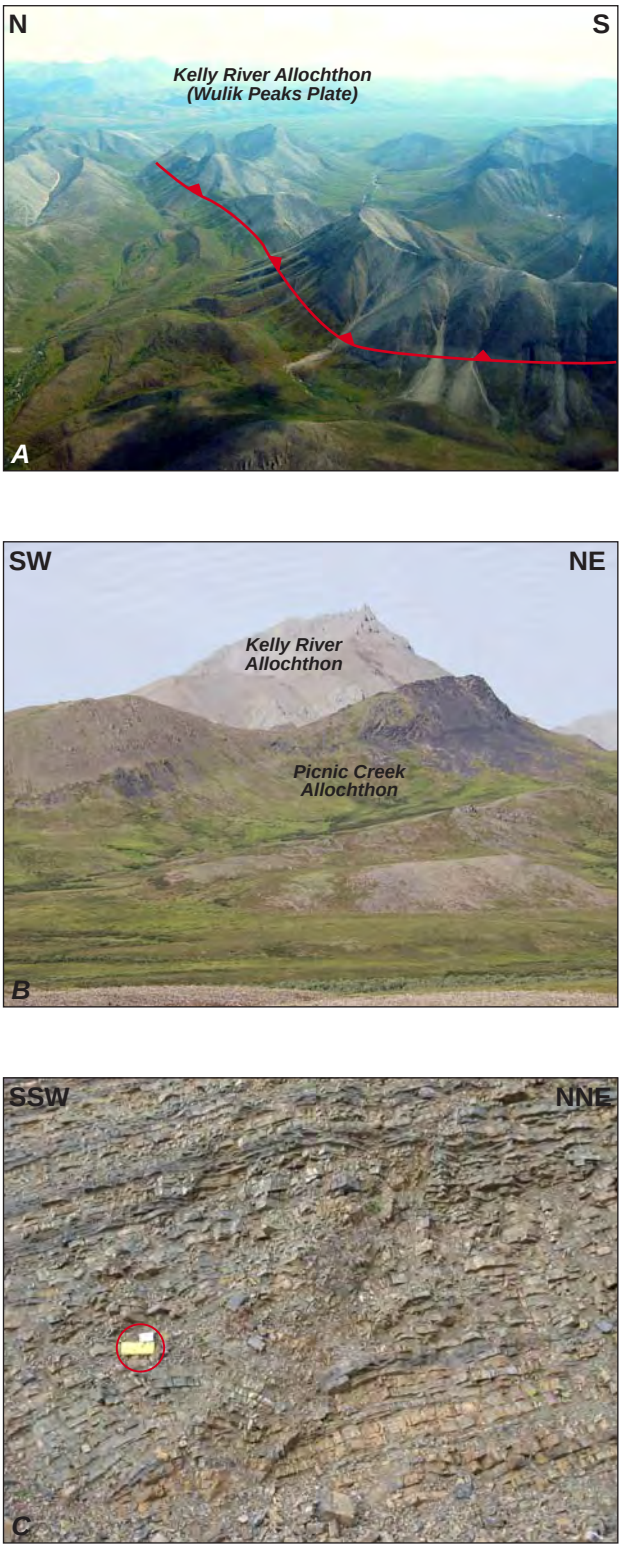
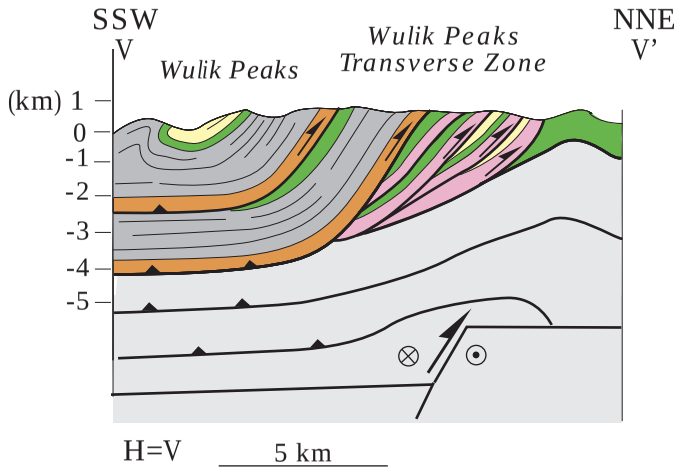


Figure 6.70. Structural features of the Wulik Peaks transverse zone. **A.** E-looking oblique aerial view of the deflection of thrust systems of the Wulik Peaks plate of the Kelly River allochthon. Topographic relief is approximately 200 m. **B.** NW-looking view of NNE-transported thrust sheets of the Kelly River and Picnic Creek allochthons along the Wulik Peaks transverse zone. Topographic relief is approximately 500 m. **C.** Detail of NNE-verging fault-propagation fold in well bedded cherts of the Otuk Formation, Wulik Peaks plate, Kelly River allochthon. 20 cm-long field notebook is encircled for scale.



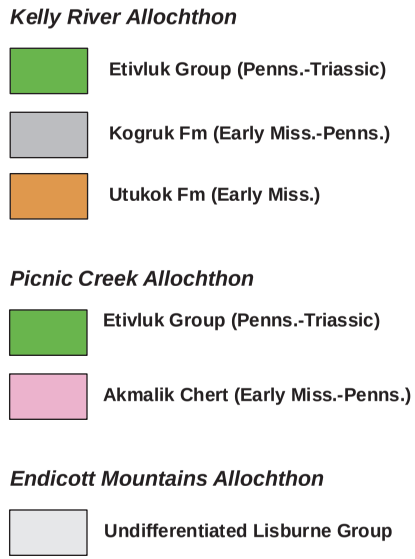


Figure 6.71a. Cross section across the Wulik Peaks transverse zone.

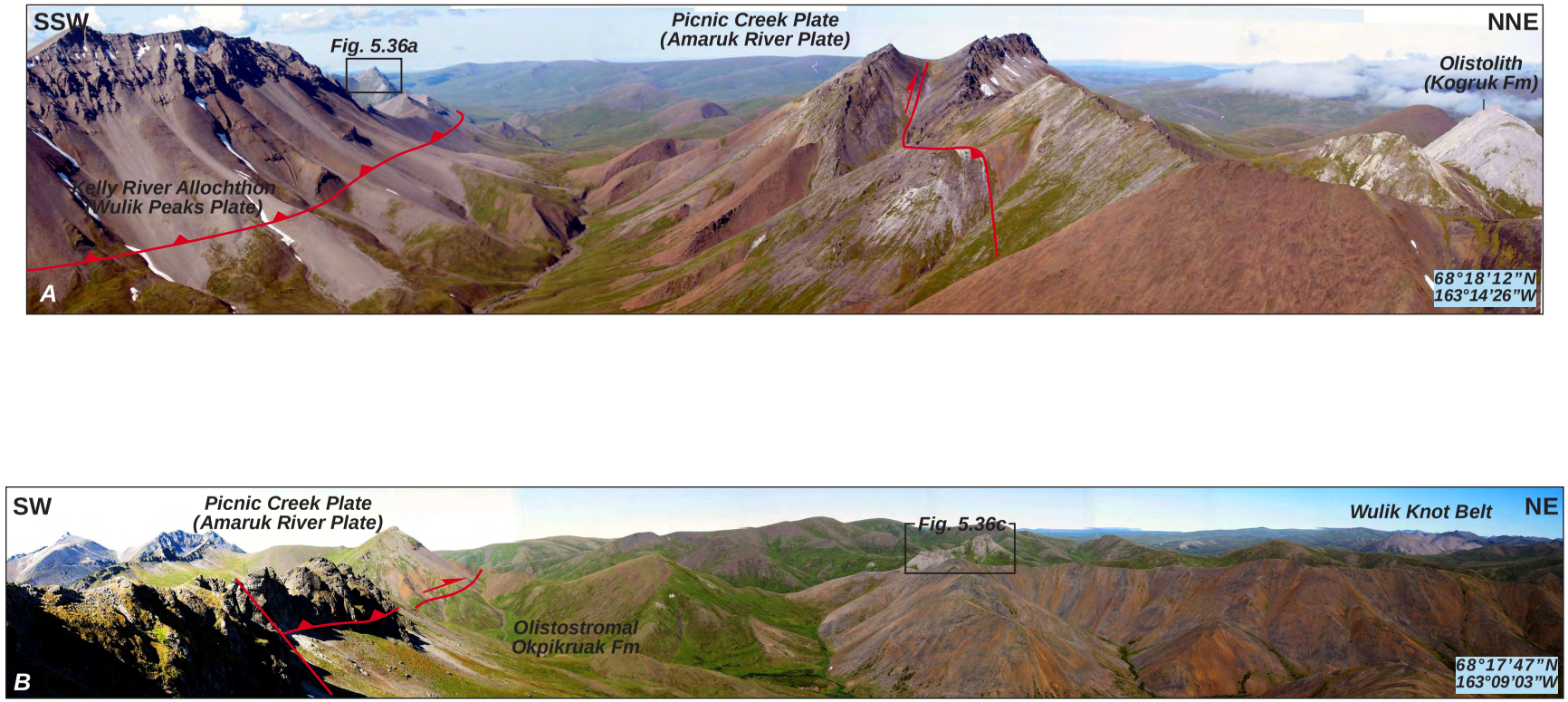


Figure 6.71b. Wulik Peaks transverse zone. **A.** WNW-looking photomosaic showing the lateral thrust systems of the Wulik Peaks transverse zone. Note the Kelly River and Picnic Creek allochthons are thrust on top of olistolith-bearing syn-orogenic strata. Topographic relief is approximately 500 m. **B.** NW-looking view of the Wulik Peaks transverse zone. Note emergent thrust front and olistoliths. Mesa-like relief in the background are long-wavelength detachment folds of the North Slope foreland basin. Topographic relief is approximately 150 m. Field of view is approximately 10 km.

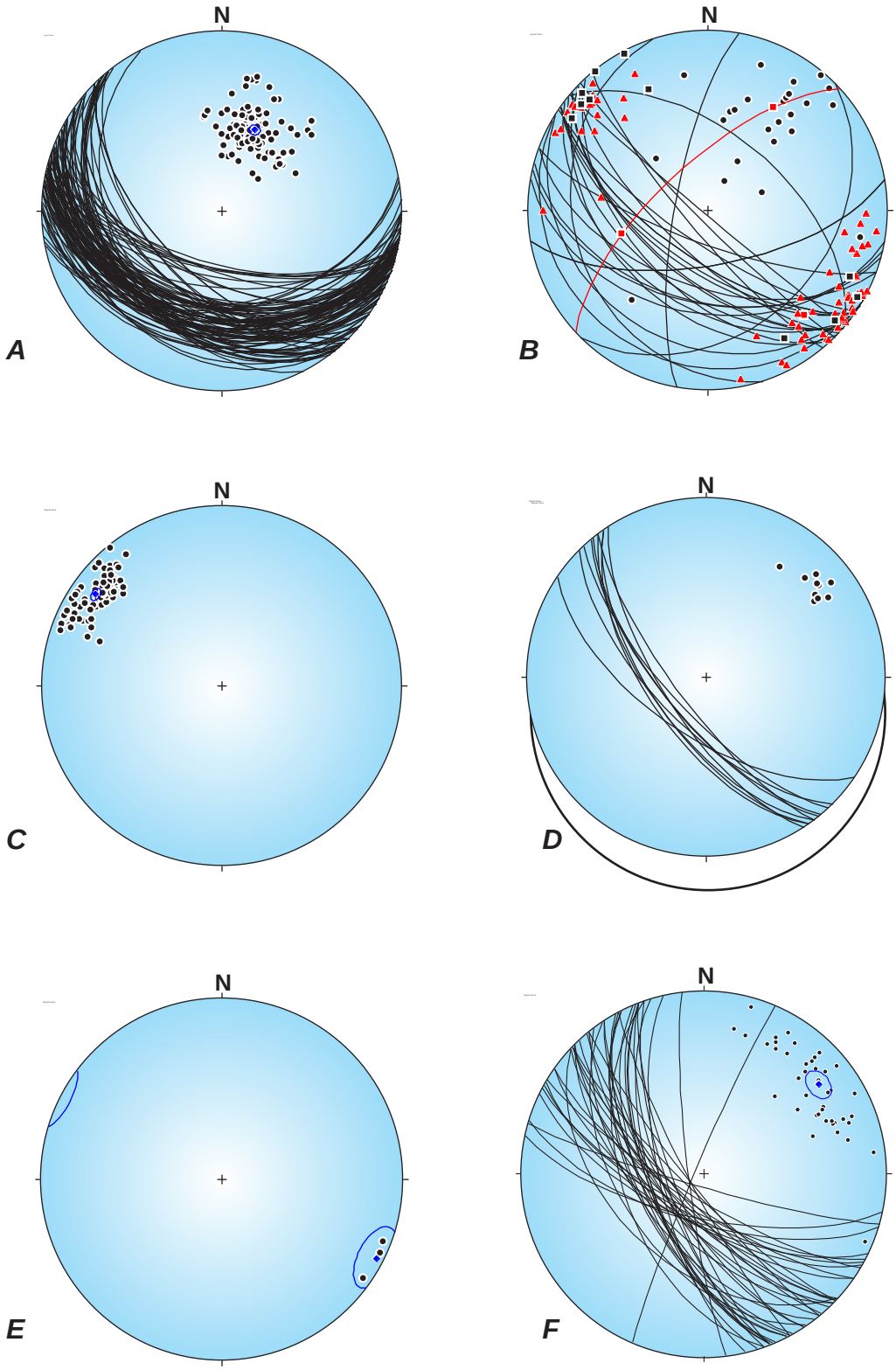


Figure 6.72. Lower hemisphere equal area stereographic projections of structural data from the Wulik Peaks transverse zone. **A.** Great circles and poles to bedding surfaces (N=100) from the Kelly River and Picnic Creek allochthons. **B.** Great circles and poles to cleavage (circles) (N=30), minor fold axes (triangles) (N=70) and cleavage-bedding intersection lineations (squares) (N=11) from the Endicott Mountains allochthon. Great circles and poles to thrust faults (N=20) in the Kelly River allochthon. **C.** Minor fold axes from the Endicott Mountains allocthon (N=75). **D.** Great circles and poles to high-angle reverse faults in the Amaruk River plate of the Picnic Creek allochthon (N=9). **E.** Pencil cleavage lineation in the Etivluk Group of the Kelly River allochthon (N=3). **F.** Great circles and poles to bedding in the Amaruk plate of the Picnic Creek allochthon in the Wulik Peaks transverse zone (N=50).

The WNW-ESE- to NW-trending structural grain of the Wulik Peaks transverse zone (Fig. 6.2a) is pervasively crosscut by NNW- to NNE-trending and dominantly SE-downthrown dip and oblique slip faults (Figs. 6.73 – 6.75). These are well exposed in NNE-verging thrust sheets of the Amaruk River plate of the Picnic Creek allochthon (Figs. 6.73 & 6.74) and the Wulik Peaks plate of the Kelly River allochthon (Fig. 6.75a). These faults are systematically arranged forming well-developed NNW- to NNE-trending 'horst-and-graben' structures (Figs. 6.73 & 6.74). Fault spacing ranges from approximately 10 to 100 m and inferred throws vary from 0.5 m to 25 m. Cumulative fault throws are of up to 200 m. The amount of extension is estimated to range from approximately 8 to 12%, based on simple line length restorations along a 2.5 km long WNW-ESE-trending section. These extensional faults are interpreted to record along-strike extension associated with the development of the Wulik Peaks transverse zone.

6.5.3 Amaruk River Emergent Thrust Front

The term Amaruk River emergent thrust front is introduced in this study to refer to the thrust front of the western Brooks Range southwest of the Wulik Peaks transverse zone (Fig. 6.2a, d, e, 6.75, 6.76d, e). The Amaruk River emergent thrust front is exposed along the western edge of the Wulik Peaks and the Amaruk River, approximately 35 km west-northwest of the Red Dog mine (Fig. 6.2a). In the Red Dog district, it extends for approximately 35 km, from the Wulik Peaks transverse zone to the southwest end of the Wulik Peaks. Analyses of LANDSAT and MARS SLAR images together with re-interpretation of map patterns from published geological maps (e.g. Mayfield *et al.* 1990) suggests that the Amaruk River emergent thrust front possibly continues for approximately 70 km to the southwest to the Chukchi Sea coast. Importantly, the Amaruk River emergent thrust front is shifted 17 to 25 km to the northwest into the North Slope parautochthon and foreland basin relative to the Amphitheatre Mountain triangle zone (Fig. 6.2a). The change in the position of the thrust front is interpreted to be associated with the development of the Wulik Peaks transverse zone and the Wrench Creek fault system.

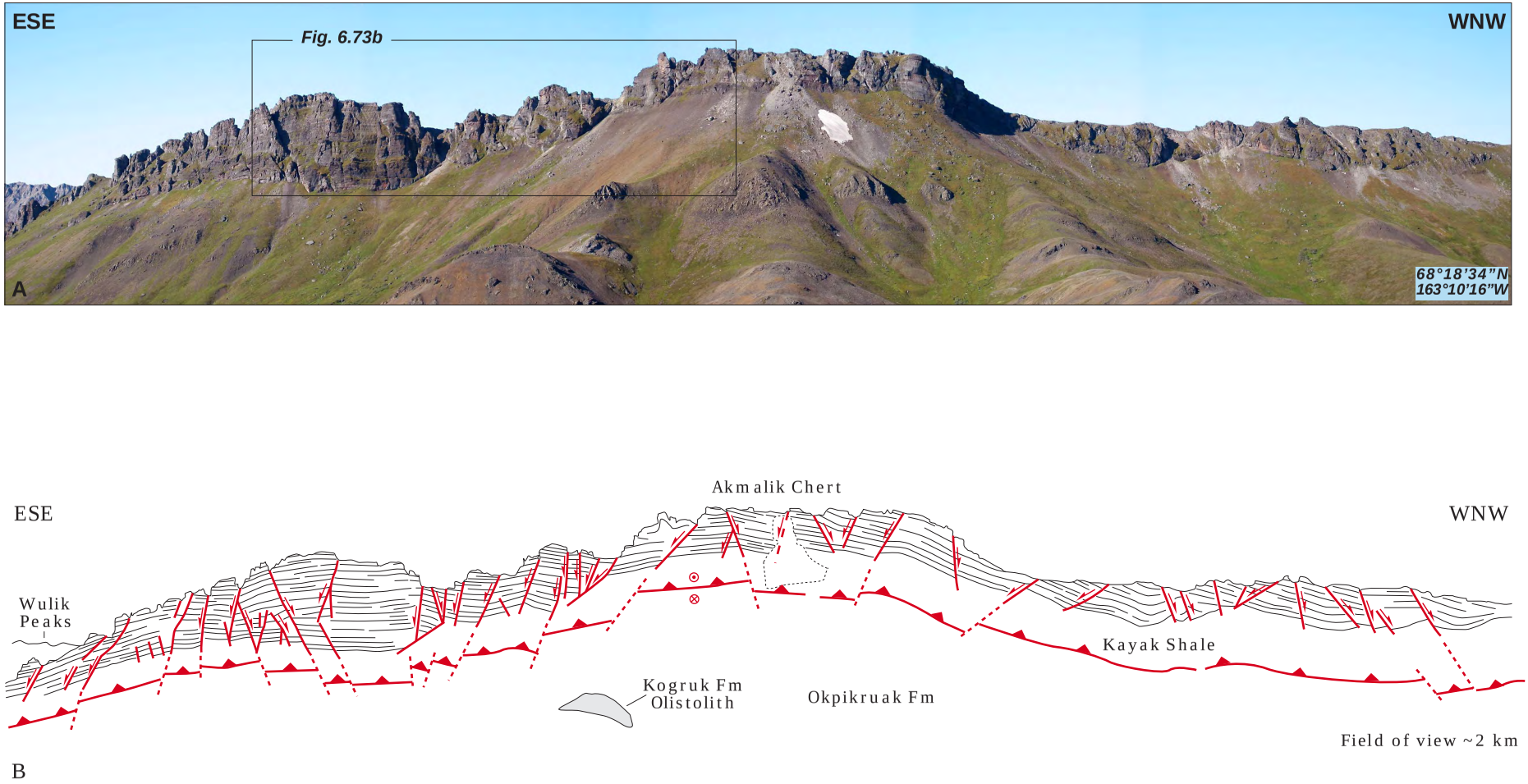


Figure 6.73a. Extensional faults associated with the Wulik Peaks transverse zone. **A.** SSW-looking photomosaic showing extensional faults in the leading edge of the Amaruk River plate of the Picnic Creek allochthon in the Wulik Peaks transverse zone. **B.** Line-drawing interpretation of A. Note extensional faults arranged in 'horst-and-graben' geometries. Fault throws range from 2 to 10 m. Fault spacing ranges from 10 to 25 m. Topographic relief is approximately 500 m and field of view is approximately 2 km. Note olistolith of the Kogruk Formation in the Okpikruak Formation in the footwall of the Amaruk River plate.



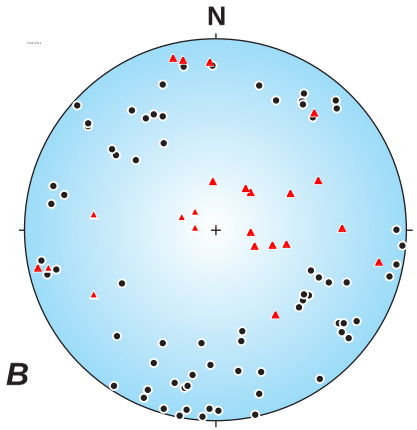


Figure 6.73b. Detail of extensional faults associated to the Wulik Peaks transverse zone. **A.** SSE-looking photomosaic showing NE-trending, SE-downthrown dip and oblique slip extensional faults in NNE-transported thrust sheets of the Amaruk River plate of the Picnic Creek allochthon. Topographic relief is approximately 100 m and field of view is approximately 750 m. Refer to Figure 6.73a for location. **B.** Lower hemisphere equal area stereographic projection of poles to extensional fault surfaces (black circles, N=120) and slickenline lineations (red triangles, N=30).

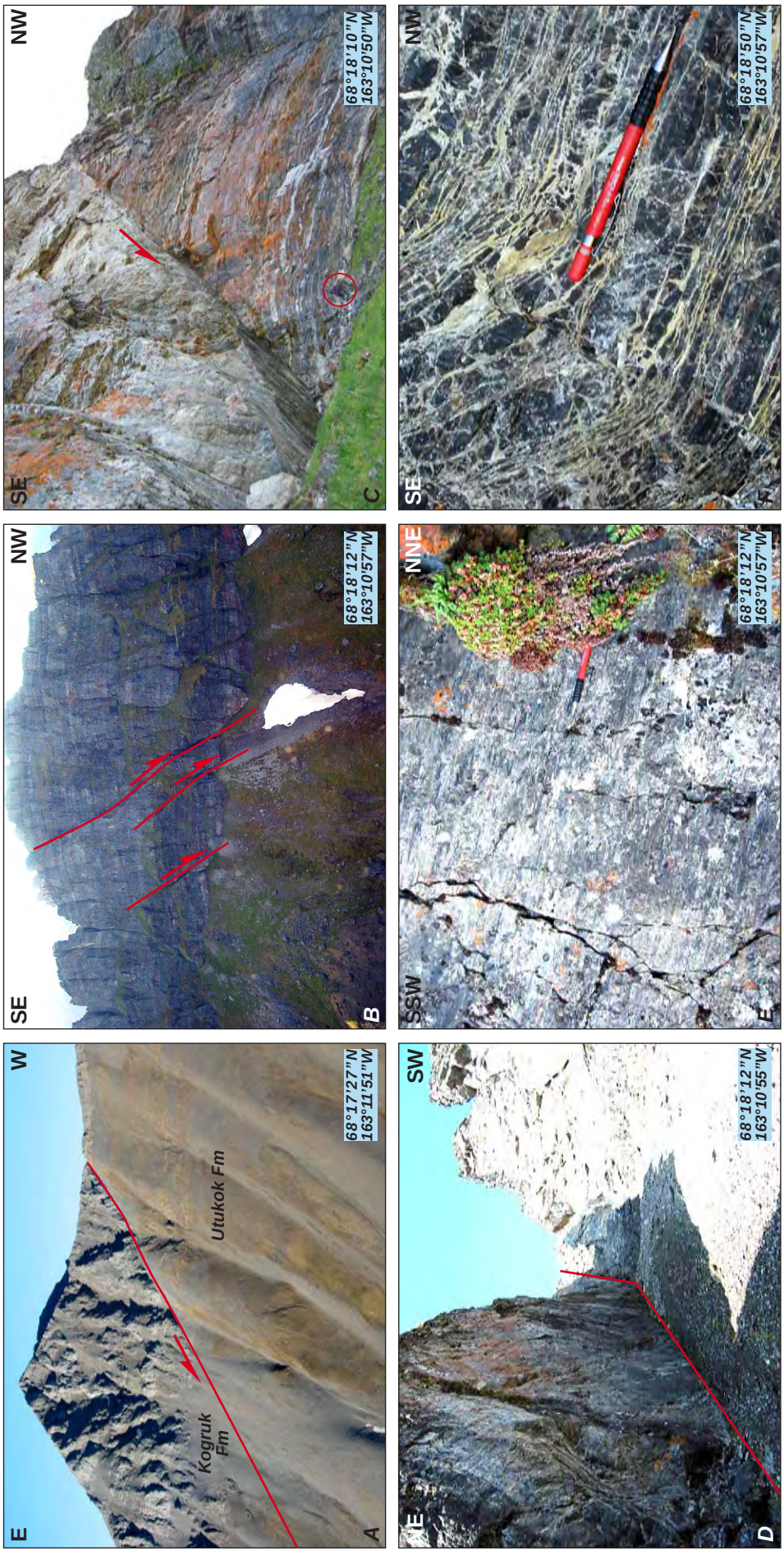


Figure 6.74. Detail of extensional faults along the Wulik Peaks transverse zone. **A.** Extensional fault in the Wulik Peaks plate of the Kelly River allochthon. Topographic relief is approximately 300 m. Field of view is approximately 500 m. **B.** Like-dipping faults in the Amaruk plate of the Picnic Creek allochthon. Topographic relief is approximately 25 m. **C.** Detail of dip-slip fault in the Akmalik Chert. Backpack is encircled for scale. **D.** Detail of oblique slip fault. Topographic relief is approximately 5 m. **E.** Detail of fault surface showing oblique-slip dextral displacement. Pencil for scale. **F.** Detail of fault rock. Pencil for scale.

Figure 6.75. NNE-looking oblique aerial view of the Amaruk River emergent thrust front. Note NW-verging thrust subplates of the Wulik Peaks plate of the Kelly River allochthon forming a well defined emergent thrust front. Field of view is approximately 2.5 km. Topographic relief is approximately 250 m.

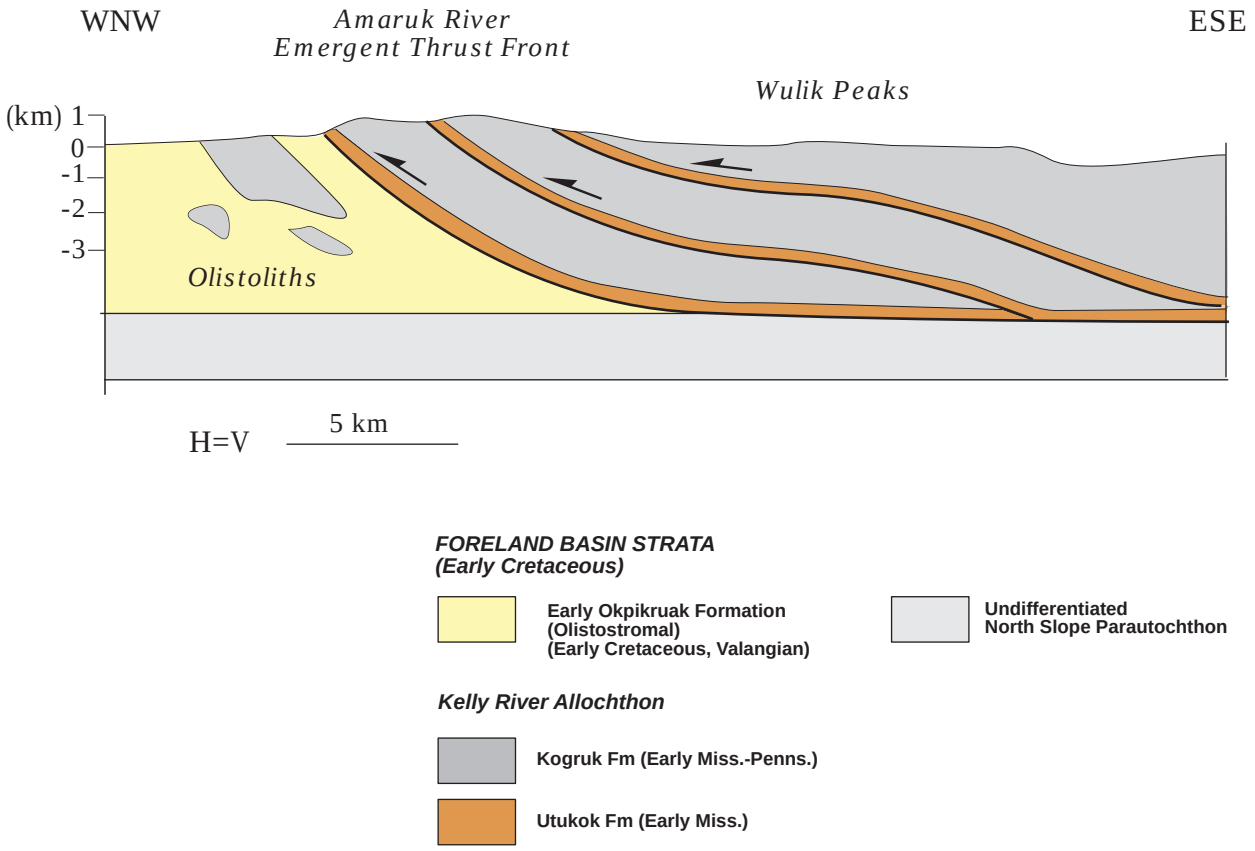


Figure 6.76. WNW-ESE-trending cross section showing the structure of the Amaruk River thrust front.

The structure of the Amaruk River emergent thrust front is characterized by gently to moderately SE-dipping (25° to 50°) and NW-verging thrust subplates of the Wulik Peaks plate and discontinuous thrust subplates of the Amaruk River plate of the Picnic Creek allochthon (Figs. 6.2a, d, e, 6.75 & 6.76). These form a strongly emergent thrust front (Type I emergent thrust front of Morley, 1986) that brings the allochthons of the Arctic Alaska and Angayucham terranes on top of a thick succession (>1 km?) of olistostromes and turbidites of the Okpikruak Formation (Figs. 6.2a, 6.75 & 6.76). Olistoliths along the emergent thrust front include metric to kilometric blocks and gravity slide sheets derived from the Picnic Creek, Kelly River, and Nuka Ridge allochthons (Fig. 6.38c; cf. Chapter 5, Figs. 5.1 & 5.36a, c). The olistostromal character of syn-orogenic strata along the Amaruk River emergent thrust front contrasts markedly with the turbidite sequences deposited on the buried thrust front of the Amphitheatre Mountain triangle zone (cf. Chapter 5, Fig. 5.38a, b).

6.5.4 Structure of the North Slope Parautochthon

The thrust front described above clearly does not represent the deformation front of the western Brooks Range fold and thrust belt in the Red Dog district. The detachment in which the thrust front was developed continues to the northwest beneath relatively undeformed Late syn-orogenic strata of the North Slope foreland basin, which locally reaches the surface in a series of uplifts or fold belts (Figs. 6.2a – f).

In the Red Dog district, the North Slope parautochthon is exposed in a series of narrow, linear to curved, NE-SW-trending and NW- to SE-verging antiformal culminations of Early Mississippian to Early Cretaceous strata that underlie the Wolverine Creek plate of the Endicott Mountains allochthon and are partly concealed by late syn-orogenic strata (Figs. 6.2a – f, 6.3, 6.77 & 6.78). These belts have lithostratigraphically affinity with the Endicott Mountains allochthon and were previously assigned to the Endicott Mountains and/or Picnic Creek allochthons (e.g. Mayfield *et al.* 1988; Curtis *et al.* 1990; Mayfield *et al.* 1990; Young, 2004). Evidence supporting the parautochthonous nature of these belts includes their position ahead of the thrust front (Fig. 6.2a) and their stratigraphic relationships with little deformed late syn-orogenic strata of the Okpikruak and Fortress Mountain formations (Figs. 6.2a, 6.78 & 5.1). In addition, the Etivluk Group of these belts contain Jurassic strata of the Kingak Shale, which is characteristic

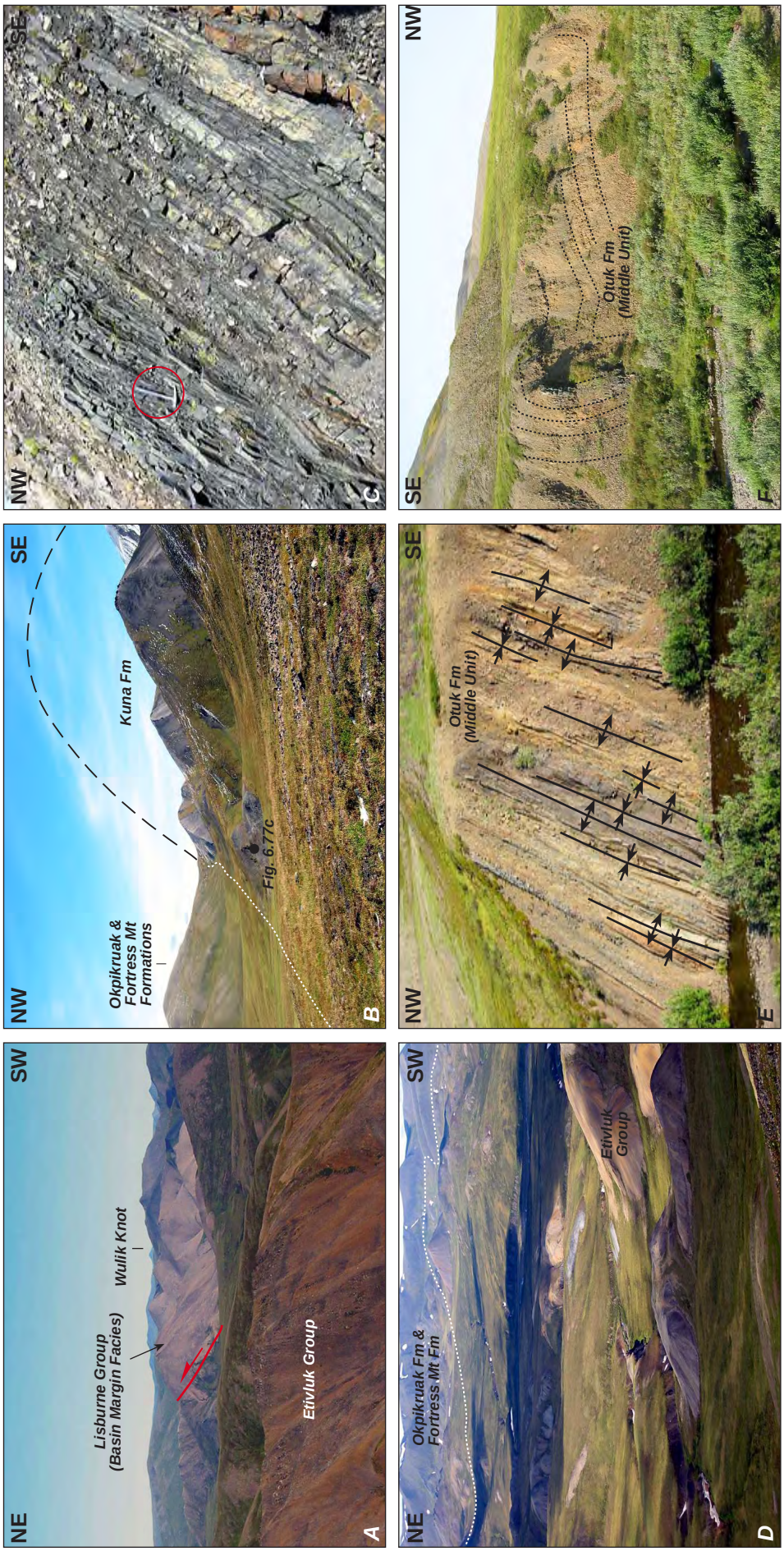


Figure 6.77. Structural features of the North Slope parautochthon in the Red Dog district. **A.** N-looking view of grey-weathering basin margin strata in the Wulik Knot area. Topographic relief is approximately 250 m. **B.** Antiformal culmination of strata of the Kuna Formation north of Inaccessible Ridge. Topographic relief is approximately 200 m. **C.** Detail of deep water strata of the Ikalukrok unit in the Wulik Knot belt. **D.** Window of strata of the Etivluk Group in the Sooner River area. The Okpikruak and Fortress Mountain formations lie in the background. Topographic relief is approximately 100 m. **E.** Detail of detachment folds with sub-vertical fold axes in the Spiny Ridge area. Field of view is approximately 15 m. **F.** Detail of SE-verging asymmetric fold in strata of the Otuk Formation in the Spiny Ridge area. Field of view is approximately 10 m.

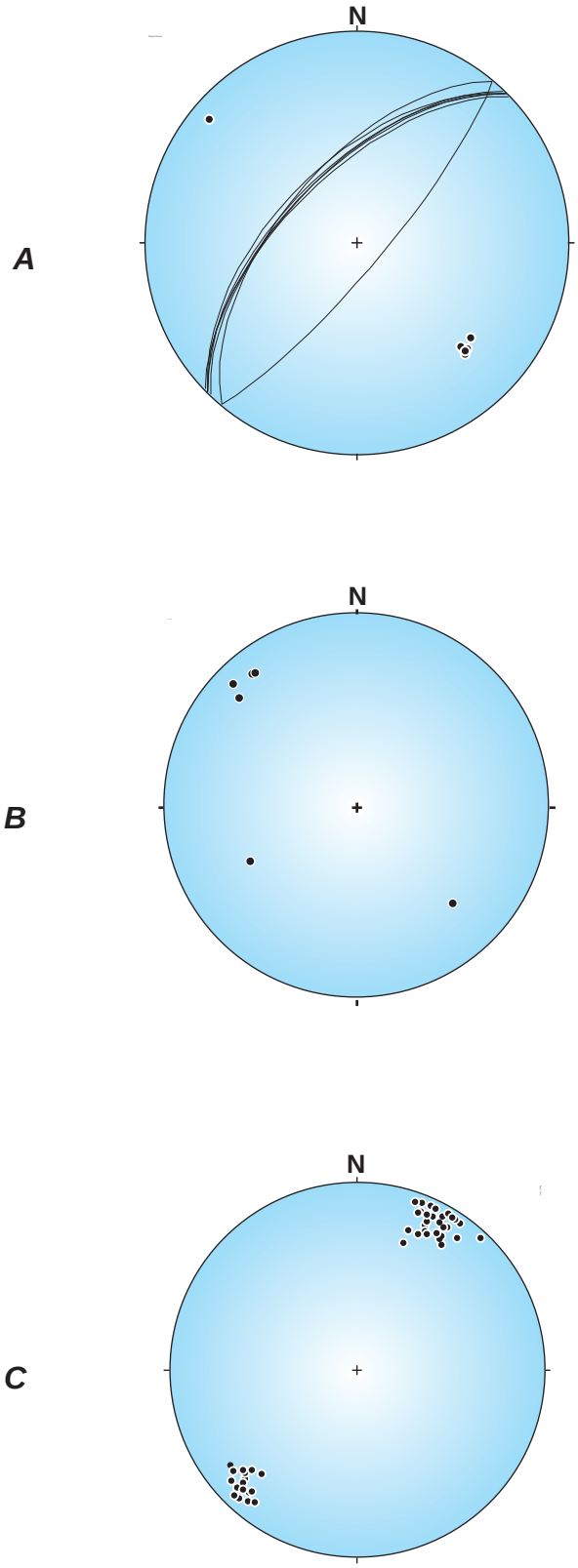


Figure 6.78. Lower hemisphere equal area stereopgraphic projections of structural data from the North Slope parautochthon. **A.** Great circles and poles to bedding in strata of the Kuna Formation in the Wulik Knot belt (N=7). **B.** Minor fold axes in Etivluk Group strata of the Sooner River belt (N=7). **C.** Minor fold axes in the Spiny Ridge belt (N=45).

of the North Slope parautochthon (e.g. Moore *et al*. 1994; Young, 2004). In this study, the outcropping North Slope parautochthon has been subdivided into three structurally and lithostratigraphically distinct domains. From northeast to southwest these are here named the Wulik Knot, Sooner River and Spiny Ridge belts (Fig. 6.2a – f). The main structural features of the parautochthonous belts are summarized in Table 6.9 and described in detail below.

Wulik Knot Belt

The Wulik Knot belt (Fig. 6.2a) consists of a series of discontinuous linear and narrow NE-SW- to WNW-ESE-trending uplifts of strata of the Lisburne and Etivluk groups, including the Kingak Shale. The Wulik Knot belt occurs north of the Wulik Peaks transverse zone and northwest of the Amphitheatre Mountain triangle zone (Fig. 6.2a – c). These belts extend for approximately 50 km, from the Wulik Knot area into the Inaccessible Ridge area (Fig. 6.2a). The Wulik Knot belt was previously assigned to the Picnic Creek allochthon (e.g. Mayfield *et al*. 1988; 1990*a*; Young, 2004). The Wulik Knot belt consists of at least six imbricates slices. Imbricate spacing typically ranges from 1 to 3 km (Fig. 6.2a). The structural styles of the Wulik Knot belt are characterized by NE-SW-trending and NW-verging, symmetric to asymmetric folds that are typically cored by strata of the Kuna Formation and the Etivluk Group (Figs. 6.77a – c & 6.78a). Fold wavelengths typically range from 10 to 200 m, and fold axial surfaces are upright to steeply-dipping (50 to 70°) to the southeast (Fig. 6.77a). These folds are partly concealed by late syn-orogenic strata of the Okpikruak and Fortress Mountain formations (Figs. 6.2a & 6.77b), which form a narrow an approximately 50 km long and 10 km wide NE-SW-trending synform, here named the Sheep Mountain synform (Fig. 6.2a – c). The back limb is gently- to steeply-dipping to locally overturned due to antiformally stacking of the underlying Kelly River and Endicott Mountains allochthons. The Sheep Mountain syncline is here interpreted as a piggy-back basin (cf. Ori & Friend, 1984; Allen *et al*. 1986) developed at the front of antiformally stacked thrust sheets of the Mount Raven antiform and transported on underlying thrust systems in the North Slope parautochthon. The basin fill consists of turbidite cycles and rare olistoliths typically confined to the basin margins.

	Structural Trends	*Structural Styles*	*Tectonic Transport Direction*	*Tectonostratigraphy*
Wulik Knot Belt	NE-SW- to WNW-ESE trending SE- to NW-dipping	Detachment Folds Fault-propagation folds	West-northwest to northwest Southeast above the upper detachment	Basin Margin Slope to basin
Sooner River Belt	WNW-ESE- to NW-SE-trending SSW- to SW-dipping	WNW-ESE-trending Thrust faults and folded thrusts, NNW- to NNE- dip and oblique slip faults, Wrench Creek fault	North-northeast	Slope to basin
Spiny Ridge Belt	NE-SW-trending SE-dipping	Imbricate thrust faults	West-northwest to northwest	Slope to basin

Table 6.9. Summary structural features of the Wulik Knot, Sooner River and Spiny Ridge belts of the North Slope parautochthon in the Red Dog district.

Strata of the Lisburne Group in the southern part of the Wulik Knot belt have lithostratigraphic affinity with a platform margin, including platform carbonates (Fig. 6.77a) and sedimentary breccias. These strata grade laterally and vertically to slope and basin strata of the Kuna Formation to the northeast and southwest (Figs. 6.77b, c & 5.1). Facies changes suggest that the southern part of the Wulik Knot belt and its projection into the thrust belt (i.e. Wulik Peaks transverse zone) are located along a pre-existing basement high.

Sooner River Belt

The Sooner River area, located approximately 45 km northwest of the Red Dog mine (Figs. 6.2a & 6.77d), exposes an approximately 5 km wide arcuate belt of poorly exposed and complexly deformed strata of the Lisburne and Etivluk groups (Fig. 6.77). The Sooner River belt is the projection of the Wulik Peaks transverse zone into the foreland basin (Fig. 6.2a). Local exposures show NNE- to SSW-plunging folds that are consistent with the patterns inferred from surface mapping (Fig. 6.78b). The lack of intact exposures and extensive tundra cover prevented detailed structural analysis of this area.

Spiny Ridge Belt

The Spiny Ridge uplift is located approximately 60 km west-northwest of the Red Dog mine and 10 to 15 km west of the Amaruk River emergent thrust front (Figs. 6.2a & 6.77e, f). The Spiny Ridge belt exposes a 21 km-long and 1 to 3.5 km wide NE-SW-trending belt of Early Mississippian to Early Cretaceous strata (Figs. 6.2a & 5.1). The Lisburne Group in the Spiny Ridge contains the Kivalina and Ikalukrok formations and has basinal affinity, similar to that of the Sooner River belt and the northern part of the Wulik Knot belt. This belt terminates abruptly in NE- and SW-plunging terminations (Fig. 6.2a) that are broadly aligned with the Wulik Peaks transverse zone, the NNE-plunging terminations of the Mount Raven and Husky Hills antiforms and the western tips of the Wrench Creek and Sivukat Mountain faults (Fig. 6.2a, b). The structural styles in the Spiny Ridge belt are characterized by NE-SW-trending detachment folds with multiple detachment levels and minor thrust faults (Figs. 6.77e, f & 6.78c). Fold wavelength typically ranges from 2 to 50 m. Fold asymmetries indicate a dominant southeast tectonic transport direction (Fig. 6.78) that is consistent with the asymmetry

of large folds in strata of the Fortress Mountain Formation further to the west. SE-verging thrust faults and folds (Fig. 6.77e) are superimposed on earlier WNW- to NW-verging detachment folds.

6.6 WRENCH CREEK AND SIVUKAT MOUNTAIN FAULTS

The dominant NE-SW-trending structural grain defined by the allochthons of the Arctic Alaska and Angayucham terranes of the Red Dog district is offset by a series of WNW-ESE- to NW-SE-trending, dominantly SSE- to SE-dipping, high-angle faults (Figs. 6.2a & 5.1). These faults occur at a range of scales that vary from outcrop-scale faults with lengths of a few tens of metres and metric vertical throws to extensional faults of regional extent. Regional-scale high-angle faults, which have lengths of up to 45 km and inferred vertical throws that exceed 1 km, are best represented by the Wrench Creek and Sivukat Mountain faults (Figs. 6.2a & 6.79). These faults are spatially related with the Wulik Peaks transverse zone (Fig. 6.2a) as well as major facies changes in strata of the Endicott Mountains allochthon and the North Slope parautochthon (e.g. Anxiety Ridge, Wul area, Wulik Knot). Other significant extensional faults include the Wulik Peaks and Mulgrave faults, which are first described in this study (Fig. 6.2a & 6.79).

The Wrench Creek and Sivukat Mountain faults occur as WNW-ESE- to NW-SE-trending lineaments and topographic edges that are readily visible in both conventional aerial photographs and satellite images (Figs. 6.79 & 6.80). The Wrench Creek and Sivukat Mountain faults define a bench-like topography that causes the De Long Mountains to progressively decrease in relief and elevation to the south-southwest, across the respective fault traces (Figs. 6.80 & 6.81). The drop in elevation and relief attains its maximum across the Sivukat Mountain fault, where the rugged relief of the De Long Mountains terminates abruptly (Figs. 6.79 & 6.80), giving way to a broad and heavily alluviated subdued lowland (Figs. 6.79 & 6.80) that extends to the southwest into the Chukchi Sea coast. The control on the Present Day topographic relief (i.e. fault-line scarps and terraced hill slopes) of the De Long Mountains suggest relatively recent fault activity. The main structural features of the Wrench Creek and Sivukat Mountain faults are summarized in Table 6.10 and described in detail below.

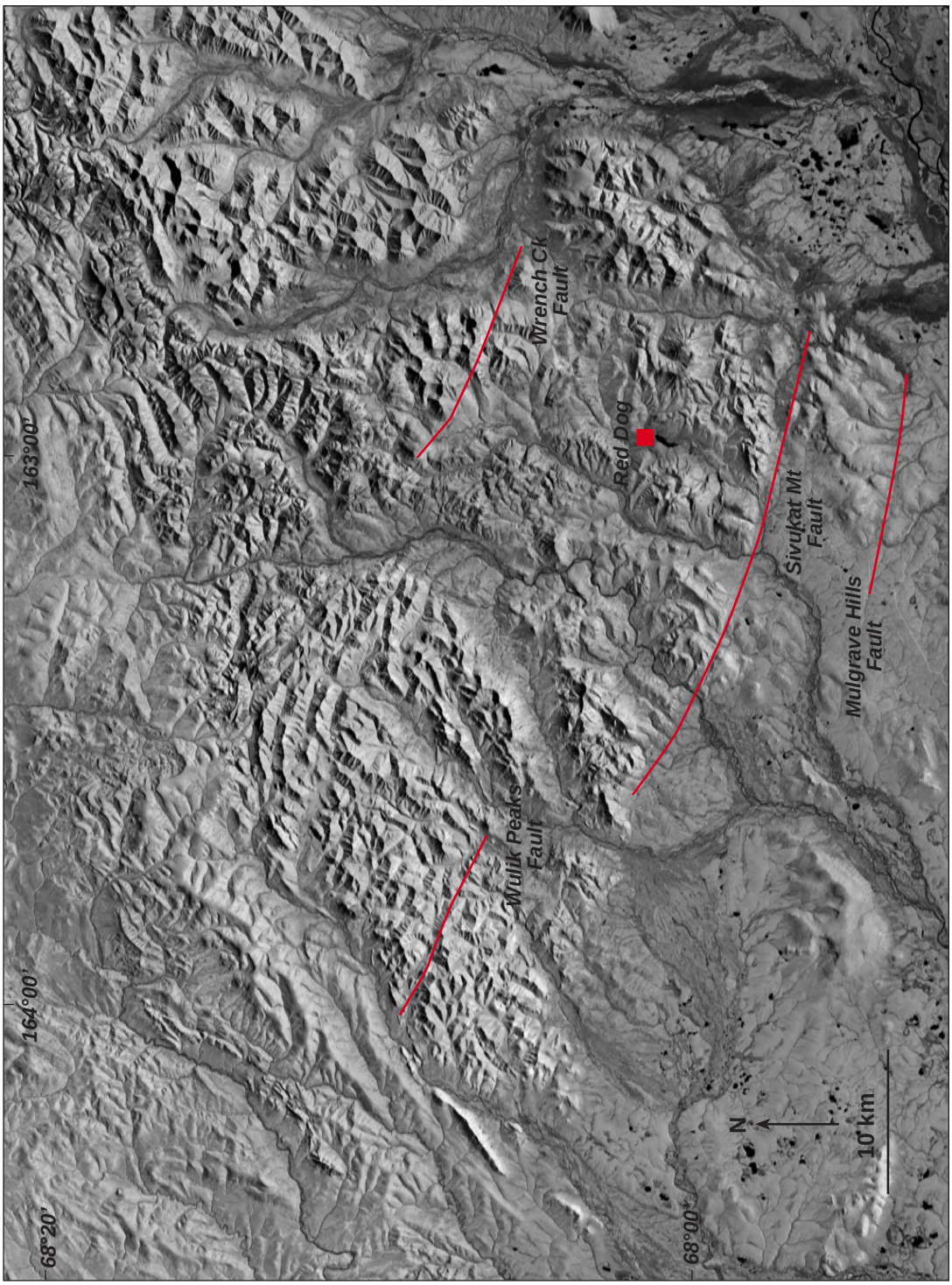


Figure 6.79. Landsat 5TM panchromatic (bands 7,5,4) of the central part of the Red Dog district showing the Wrench Creek and Sivukat Mountain faults. Note abrupt decrease in topographic relief southwestward across the Sivukat Mountain fault. The location of the Red Dog mine is shown.

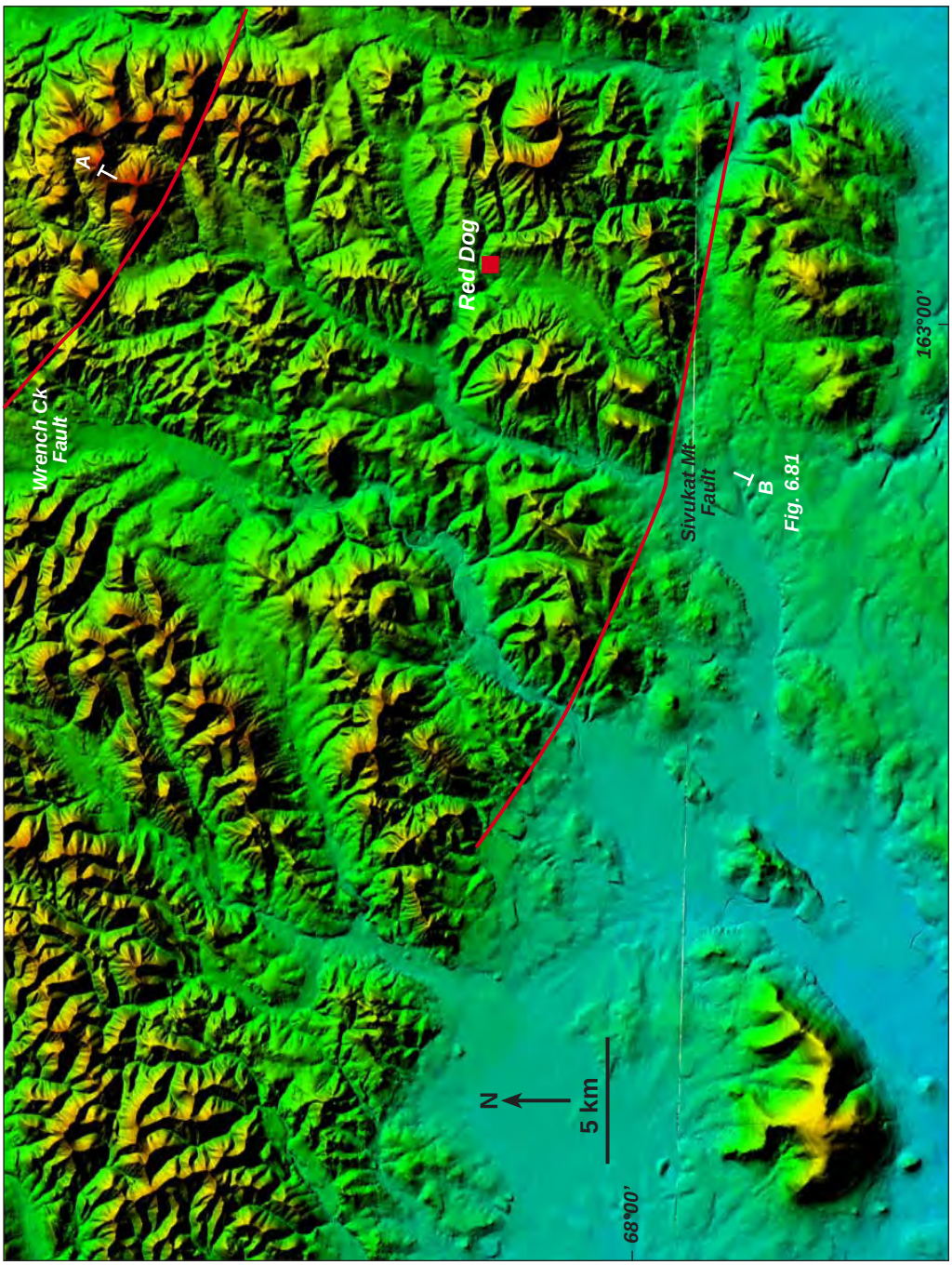


Figure 6.80. Digital elevation model (DEM) of the southern part of the Red Dog district. Note abrupt fault-line scarps with decrease in elevation and topografic relief across the Wrench Creek and Sivukat Mountain faults (DEM courtesy of Teck Cominco American Inc. Exploration). The location of the Red Dog mine is shown.

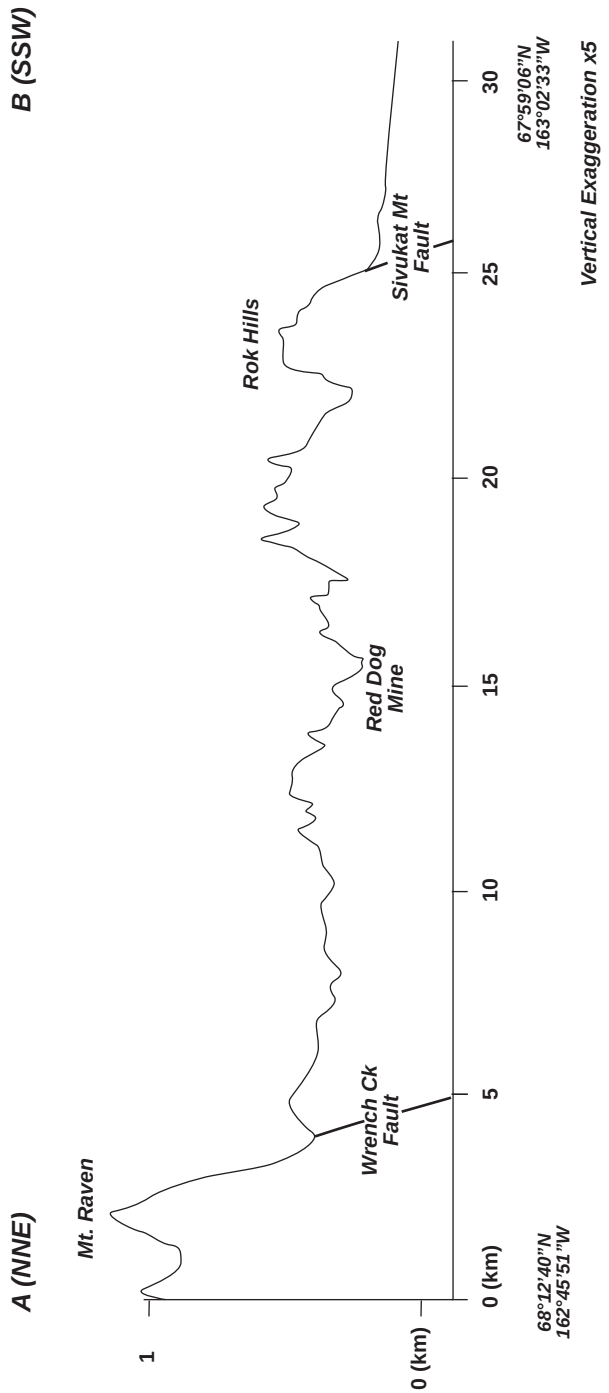


Figure 6.81. NNE-SSW-trending topographic profile across the Red Dog district showing the bench-like topography controlled by the Wrench Creek and Sivukat Mountain faults. Refer to Figure 6.80 for location of profile.

	Length	*Orientation*	*Associated Structures*	Inferred Vertical Throw	Inferred Dip
Wrench Creek Fault	35 km	WNW-ESE-trending SSW-downthrown	Wulik Peaks Transverse Zone	1 km	60° to 90°
Sivukat Mountain Fault	45 km	WNW-ESE-trending SSW-downthrown		1 to 1.5 km	60° to 90°

Table 6.10. Summary structural features of the Wrench Creek and Sivukat Mountain faults.

6.6.1 Wrench Creek Fault

The Wrench Creek fault is located approximately 15 km north of the Red Dog mine (Figs. 6.2a, 6.79 & 6.80). It is WNW-ESE-trending, SSW-downthrown and approximately 45 km long, extending from the NNE-plunging termination of the Husky Hills antiform in the east-southeast to the Wulik Peaks transverse zone in the west-northwest (Figs. 6.2a, 6.79 & 6.80). The actual fault surface is not exposed because of extensive tundra cover and talus deposits (Fig, 6.82). A significant vertical throw (1 to 3 km) is indicated by the juxtaposition of markedly different structural levels across the fault trace (Figs. 6.2a & 6.82). Inferred vertical displacement and structural separation across the fault trace decreases progressively to the west-northwest and east-southeast towards the fault tips. The Wrench Creek fault defines a prominent fault-line scarp, with a maximum drop in elevation of approximately 600 m in the vicinity of Mount Raven (Figs. 6.81 & 6.82).

The Wrench Creek fault is characterized by the lack of correlation of structural units across the fault trace (Figs. 6.2a & 5.1). The Wrench Creek fault offsets perpendicularly the fold axial trace of the Mount Raven antiform in the footwall of the fault (Fig. 6.2a) but parallels thrust faults and folds of the Red Dog plate of the Endicott Mountains allochthon in its hangingwall (Fig. 6.2a). The antiformal duplex defined by the Mount Raven antiform does not exist in the hangingwall of the Wrench Creek fault, where it is replaced by discontinuous emergent thrust sheets of the Red Dog and Wolverine Creek plates and Okpikruak Formation olistostrome (Figs. 6.2a & 5.1). The Wulik Peaks plate of the Kelly River allochthon, which is extensively exposed in the hangingwall of the Wrench Creek does not exist in its footwall (Figs. 6.2a & 5.1). Major tectonostratigraphic changes also occur across the trace of the Wrench Creek fault. The Wrench Creek fault is parallel to the regional tectonic transport direction and is spatially related with the deflection of structural trends along the Wulik Peaks transverse zone (Fig. 6.2a). These structural relationships suggest a possible genetic link between the Wrench Creek fault and the development of the Wulik Peaks transverse zone. The Wrench Creek fault possibly originated as a dextral tear fault in the North Slope parautochthon. Thrust sheets in the hangingwall of the Wrench Creek fault locally show evidence of structural thinning and convergence towards the Wrench Creek fault.



Figure 6.82. Structural features of the Wrench Creek fault. **A.** NNE-looking view of fault-line scarp along the Wrench Creek fault. Topographic relief is approximately 600 m. **B**. NNE-looking view showing the Wrench Creek fault. Topographic relief is approximately 600 m. **C.** NE-looking view showing offset of WNW-verging thrust subplates of the Wolverine Creek plate. Topographic relief is approximately 600 m. **D & E.** Along-strike view of the Wrench Creek fault east-southeast of Mount Raven. Topographic relief is approximately 200 m. **F.** Detail of outcrop-scale extensional fault in dolostones and cherts of the undivided Lisburne Group in the footwall of the Wrench Creek fault. Compass encircled for scale.

Map patterns, changes in structural separation across the fault and crosscutting relationships (Figs. 6.2a & 6.83) indicate that the final movement on the Wrench Creek fault postdates northwest to north-northeast emplacement of allochthons. The Wrench Creek fault offsets the Endicott Mountains allochthon and the Kelly plate of the Kelly River allochthons (Figs. 6.2a & 6.82). Present Day structural relationships indicate that the Wrench Creek fault was subsequently reactivated as an extensional fault. Evidence for extensional reactivation includes well-developed extensional fault-related folds (cf. McClay *et al.* 2001), and minor faults in the immediate hangingwall and footwall of the fault. Extensional fault-related folding occurs in the immediate footwall to the Wrench Creek fault (Fig. 6.82) as WNW-ESE-trending broad open monoclines developed in strata of the Lisburne Group (Fig. 6.84). Bedding surfaces in the immediate footwall to the Wrench Creek fault dip steeply to the south-southwest and are parallel to sub-parallel to the inferred fault surface. Frontal limbs are steeply-dipping (60°) to the south-southwest and back limbs are gently-dipping to the south-southwest. WNW-ESE-trending extensional fault-related folds form a complex regional fold pattern superimposed to the NNE-trending Mount Raven antiform.

Minor structures observed in the immediate footwall of the Wrench Creek fault include WNW-ESE- to NW-SE-trending and NNW- and SSE-dipping metric to decametric faults with dominant dip-slip and subordinate oblique-slip movement (Fig. 6.82f). These commonly form outcrop-scale like-dipping fault arrays downthrown to the south-southwest. Cut-off angles in the hangingwall and footwall typically vary from 45° to 70°. Associated with outcrop-scale extensional faults are planar parallel systematic to non-systematic, and dominantly antitaxial vein arrays with varying degrees of connectivity. Vein thickness typically ranges from hairline to individual veins as thick as 10 cm. Vein spacing varies from 0.5 cm to 10 cm approximately.

6.6.2 Sivukat Mountain Fault

The Sivukat Mountain fault is located approximately 5 km south of the Red Dog mine and 23 km south-southwest of the trace of the Wrench Creek fault (Figs. 6.2a, 6.79 & 6.80). It is an approximately 45 km long, WNW-ESE-trending, SSW-dipping high-angle planar fault that extends from Sivukat Mountain and the Husky Hills in the east, to the southern Wulik Peaks in the west. The Sivukat Mountain fault is a prominent

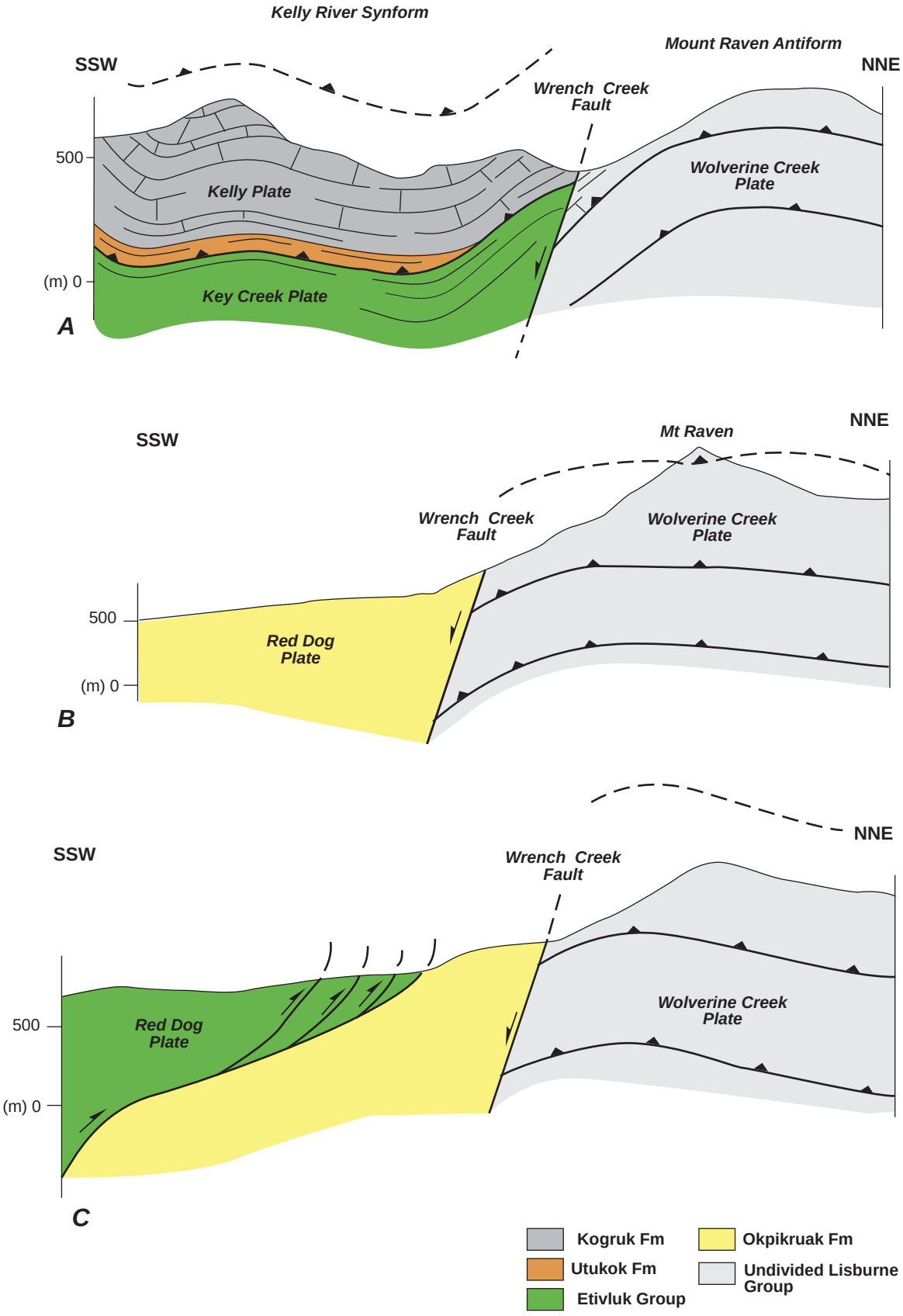


Figure 6.83. Cross sections across the Wrench Creek fault. Refer to Figure 6.2a for location of individual cross sections.

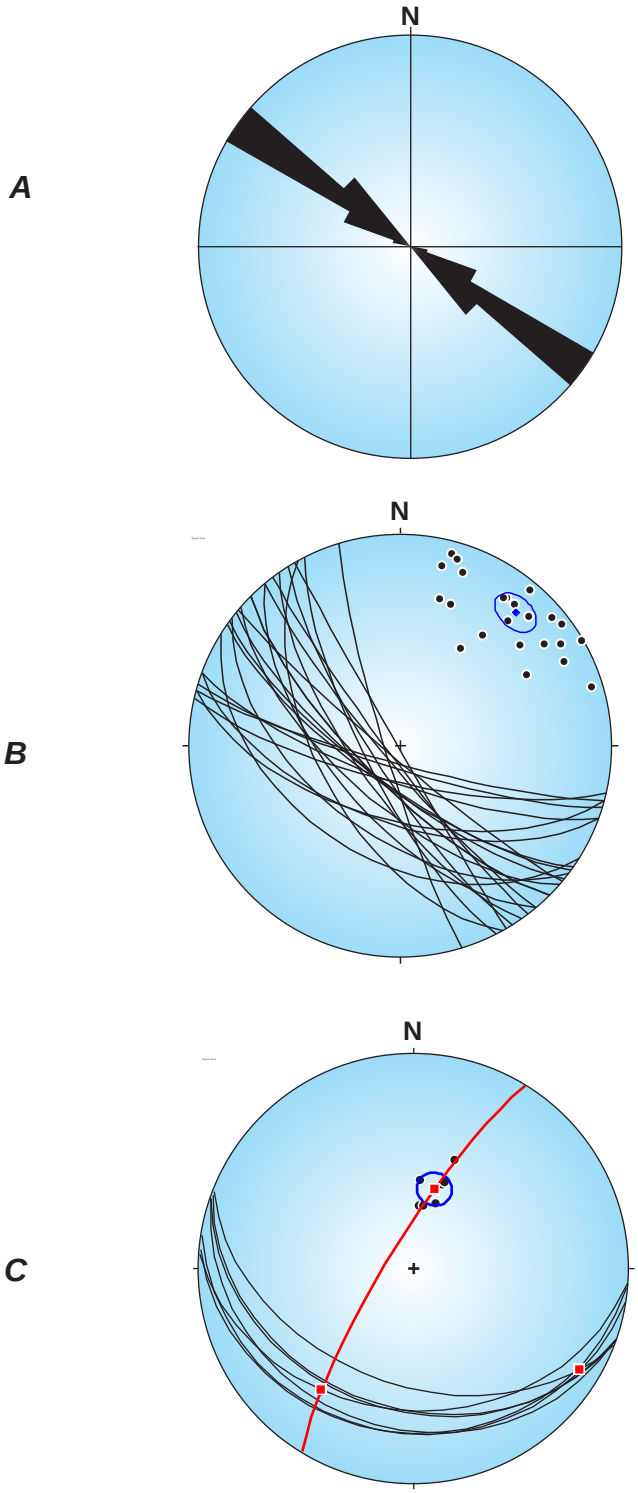


Figure 6.84. Rose diagram and lower hemisphere equal area stereographic projections of structural data from the Wrench Creek fault. **A.** Rose diagram showing orientation of lineaments in the Wrench Creek fault area (N=43). **B.** Great circles and poles to outcrop-scale extensional faults in the immediate footwall to the Wrench Creek fault (N=25). **C.** Great circles and poles to bedding in the immediate footwall to the Wrench Creek fault (N=8).

lineament with a well-developed fault-line scarp that causes an abrupt drop in elevation and topographic relief across the fault trace (Figs. 6.80 & 6.85). Fault-line scarps typically range from 8 to approximately 100 m.

The Sivukat Mountain juxtaposes the Kelly River and Copter Peak allochthons against the Endicott Mountains allochthon (Figs. 6.2a & 6.86). Cut-off angles in the hangingwall and footwall typically range from 20° to 60°. Map patterns show opposite apparent lateral offsets of 2 to 10 km that are here interpreted to reflect vertical throw of antiformally-folded allochthons across the Sivukat Mountain fault. The westernmost end of the Sivukat Mountain fault consists of a complex array of faults with numerous WNW-ESE-trending splays with inferred cumulative vertical throws of 100 m to 500 m (Fig. 6.2a).

Spatially and genetically related to the Sivukat Mountain fault are a series of WNW-ESE- to NW-SE-trending, SW-dipping like-dipping domino style outcrop-scale extensional faults that occur in the immediate footwall to the fault (Fig. 6.85a, b). Lineaments observed in aerial photographs suggest that similar structures possibly occur in the immediate hangingwall to the fault, however the lack of intact exposures and the extensive tundra cover has prevented further detailed analyses. Associated with these extensional faults are poorly to well-developed WNW-ESE-trending extensional fault-related folds that are superimposed to SE-verging thrust faults and associated folds (Fig. 6.85c). Minor faults dip moderately to steeply (50° to 60°) and are dominantly downthrown to the south-southwest. Fault spacing typically ranges from approximately 5 to 50 m, varying accordingly to the competency and thicknesses of the units involved. Vertical throws range from 2 to 20 m. Metric to decametric like-dipping fault blocks are interpreted to be part of the damage zone of the Sivukat Mountain fault. Associated with these faults are zones of planar and interconnected quartz and calcite veins and veinlets.

It is possible that the Sivukat Mountain fault originated as a dextral tear fault in the North Slope parautochthon that was subsequently reactivated as an extensional fault. Evidence for dextral movement includes the presence of NW- to NNW-trending outcrop-scale dextral strike-slip faults that are oriented 20° to 30° to the trace of the

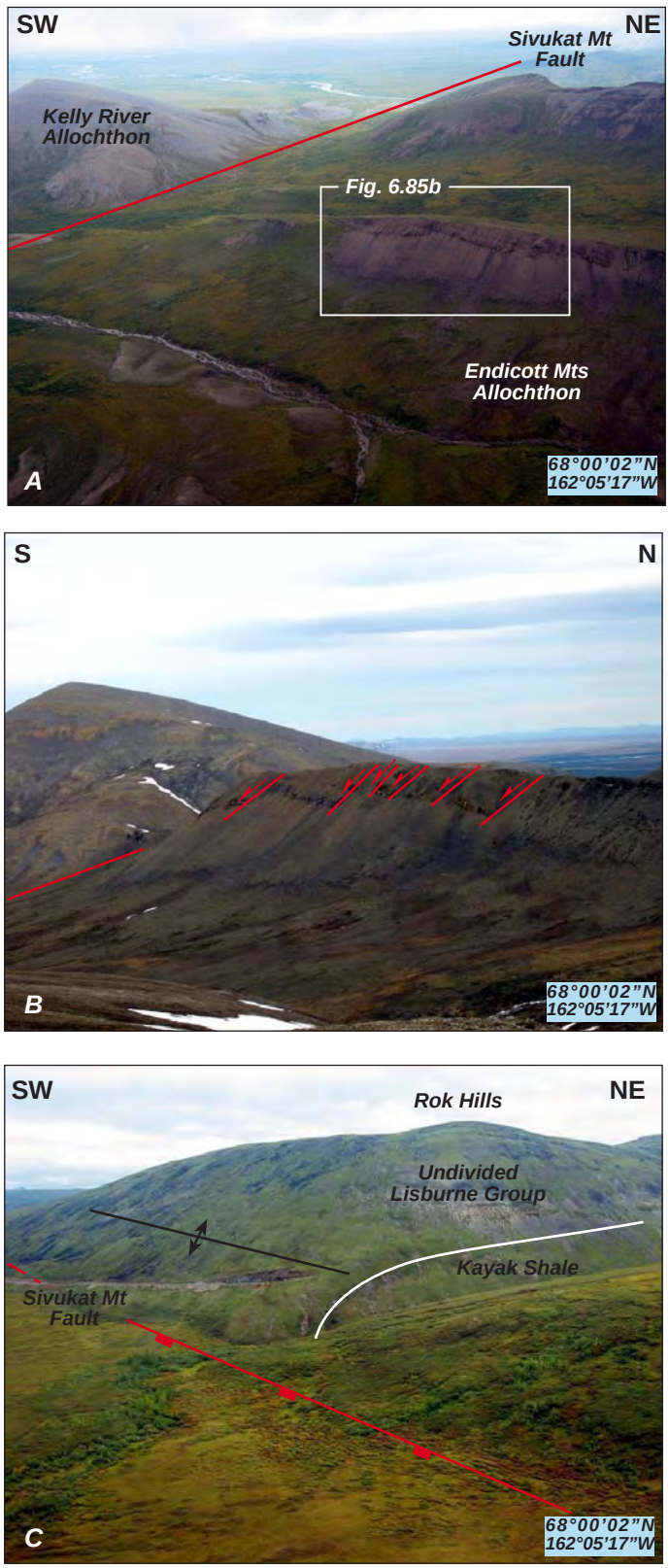


Figure 6.85. Structures associated with the Sivukat Mountain fault. **A.** WSW-looking oblique aerial view of the Sivukat Mountain in the Wul area. Fault juxtaposes the Endicott Mountains allochthon against the Kelly River allochthon. Topographic relief is approximately 150 m. **B**. SW-looking view of domino fault blocks in the immediate footwall of the Sivukat Mountain fault. Topographic relief is approximately 25 m. **C.** Extensional fault-related monoclinal fold in the footwall of the Sivukat Mountain fault in the Rok Hills. Topographic relief is approximately 100 m.

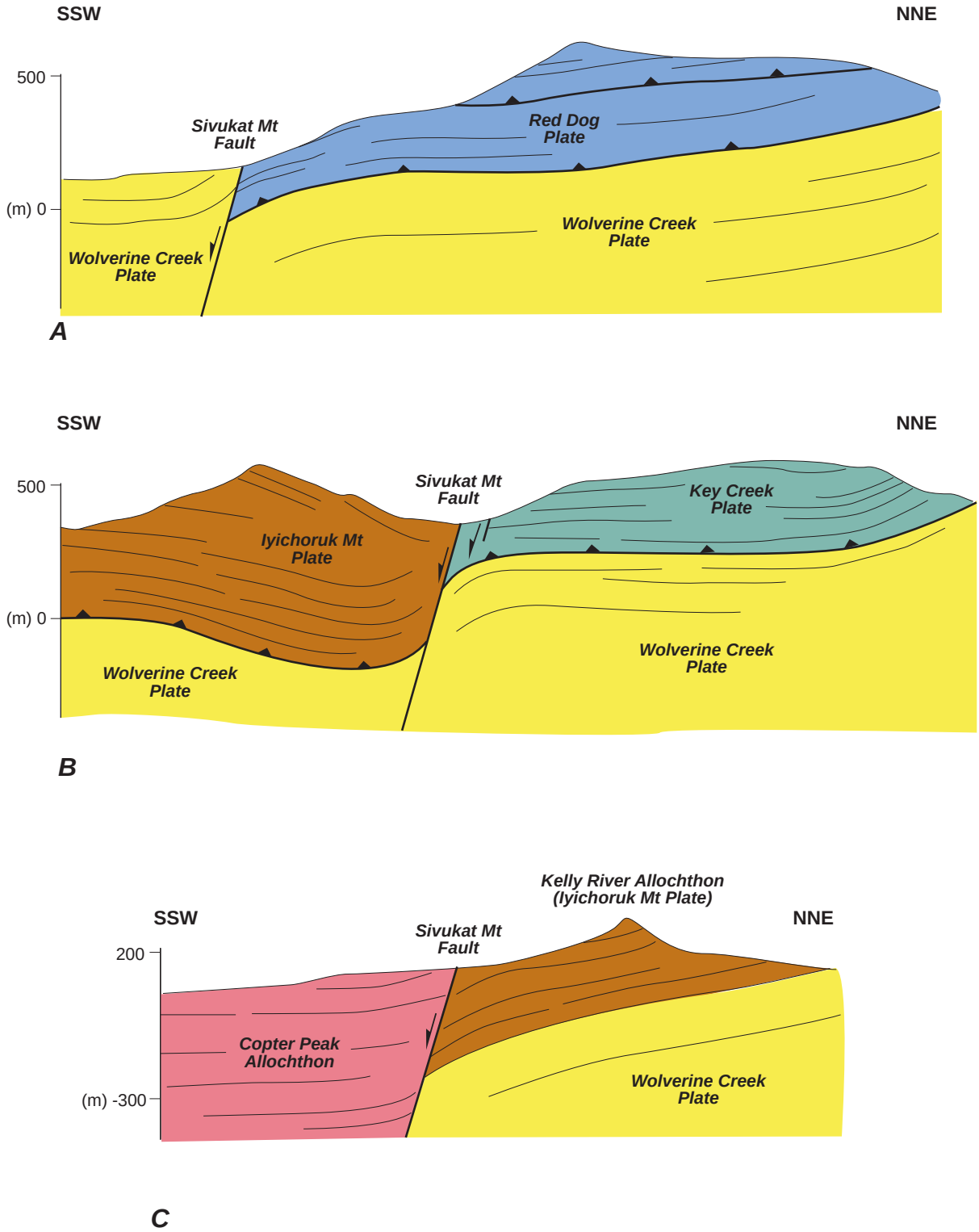


Figure 6.86. Cross sections across the Sivukat Mountain fault. Refer to Figure 6.2a for location of individual sections.

Sivukat Mountain fault (Fig. 6.87). These occur in the immediate footwall of the Sivukat Mountain fault and are here interpreted as possible R_1 Riedel shears (cf. Passchier & Trouw, 1994) associated with dextral movement on the Sivukat Mountain fault. Dextral movement is indicated by the asymmetry of the shear fabrics, vein-offsets, and the preferred orientation of *c*-axes of chert clasts in fault breccias (Fig. 6.87).

6.6.3 Other Late Extensional Faults

In addition to the Wrench Creek and Sivukat Mountain faults, this study has identified a series of previously unreported WNW-ESE- to NW-SE-trending lineaments, interpreted as potential late extensional faults. These include the Mulgrave Hills and Wulik Peaks faults (Fig. 6.79), which are possibly genetically and kinematically linked to the development of the Wrench Creek and Sivukat Mountain faults. These lineaments occur as WNW-ESE- to NW-SE-trending topographic edges and/or abrupt changes (Fig. 6.88) in the course of rivers and creeks. These lineaments are commonly tens of metres to 5 km long and have unknown amounts and sense displacement. WNW-ESE- to NW-SE-trending lineaments are not restricted to the allochthons of the fold and thrust belt but extend northwest of the thrust front into parautochthonous strata of the North Slope foreland basin. This indicates that late extensional faulting not only post-dates allochthon emplacement but also partly or entirely post-dates deposition of late syn-orogenic strata of the North Slope foreland basin. Outcrop-scale late extensional faults and associated jointing are widespread in the Red Dog district (Figs. 6.89 & 6.90).

Wulik Peaks Fault

The Wulik Peaks fault (Fig. 6.2a) consists of a 13 km-long array of WNW-ESE-to NW-SE-trending and SSW-downthrown high-angle dip-slip and oblique-slips faults that offset the Kelly River, Picnic Creek and Endicott Mountains allochthon in the Wulik Peaks area (Fig. 6.79). The Wulik Peaks fault is spatially related to local changes in the structural trends of the Wulik Peaks plate of the Kelly River allochthon and Amaruk River emergent thrust front (Figs. 6.2a & 5.1) and possibly originated as a tear fault that was subsequently reactivated as an extensional fault.

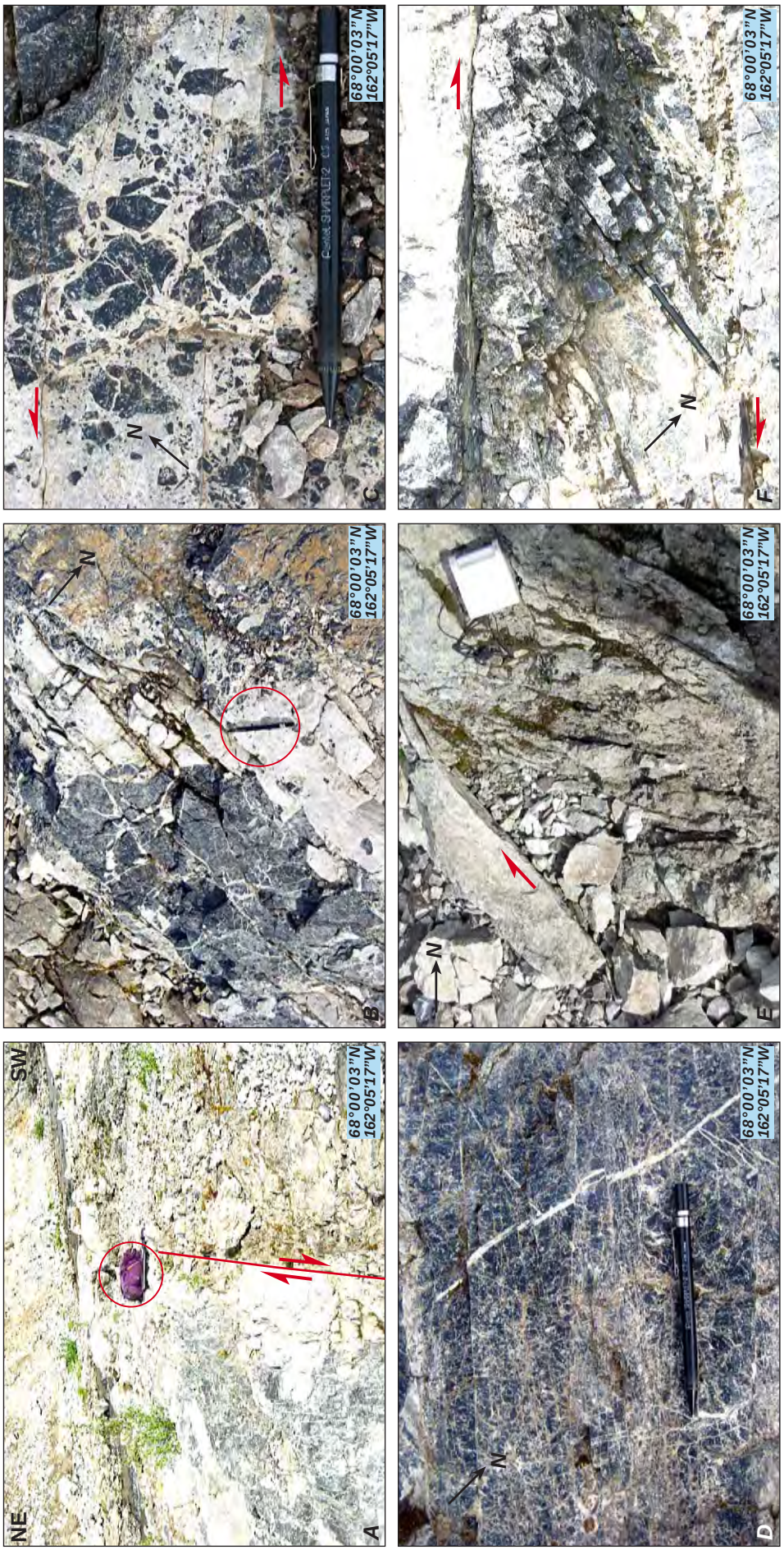


Figure 6.87. Outcrop-scale strike-slip structures in strata of the undivided Lisburne Group in the Rok Hills. **A.** N-looking view of outcrop-scale dextral strike-slip fault in cherty limestones of the undivided Lisburne Group. Backpack is encircled for scale. **B.** Top view of strike-slip fault zone showing veining and fault rock. Pencil for scale. **C.** Top view of strike-slip fault zone showing fault rock. Note rough alignment of black chert in grey-weathering carbonate matrix. **D.** Top view of fault rock showing intense veining. **E.** Top view of sidewall strike-slip duplex. Compass for scale. **F.** Top view of sidewall duplex. Pencil for scale.

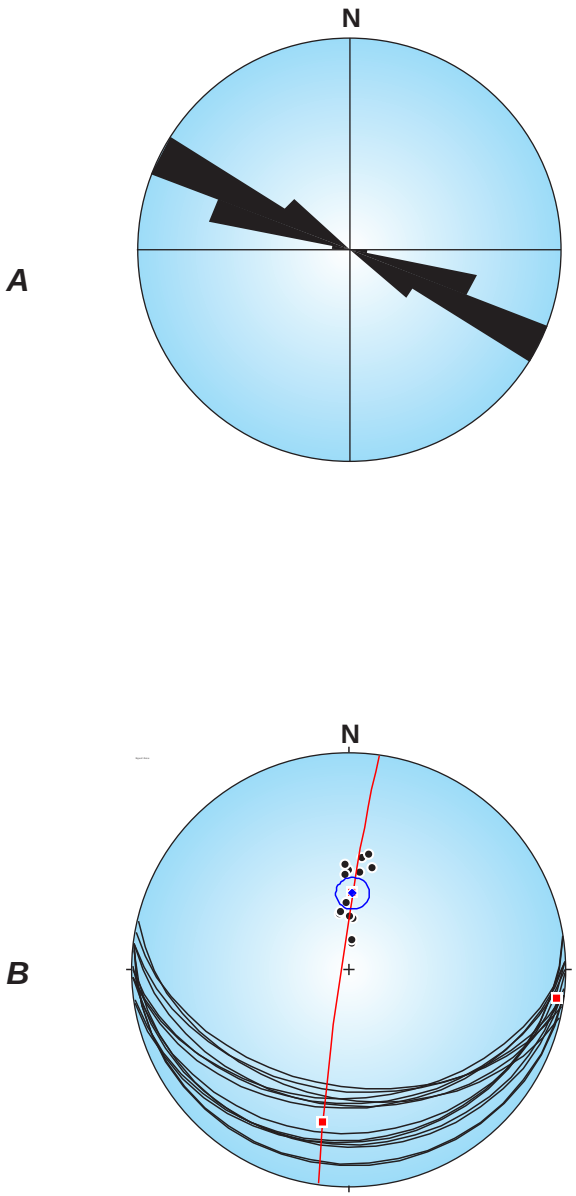


Figure 6.88. Structural data from the Sivukat Mountain fault. **A.** Rose diagram of lineaments and fault-line scarps associated with the Sivukat Mountain fault (N=42). **B.** Great circles and poles to bedding (N=16) in the undivided Lisburne Group in the immediate footwall to the Sivukat Mountain fault.

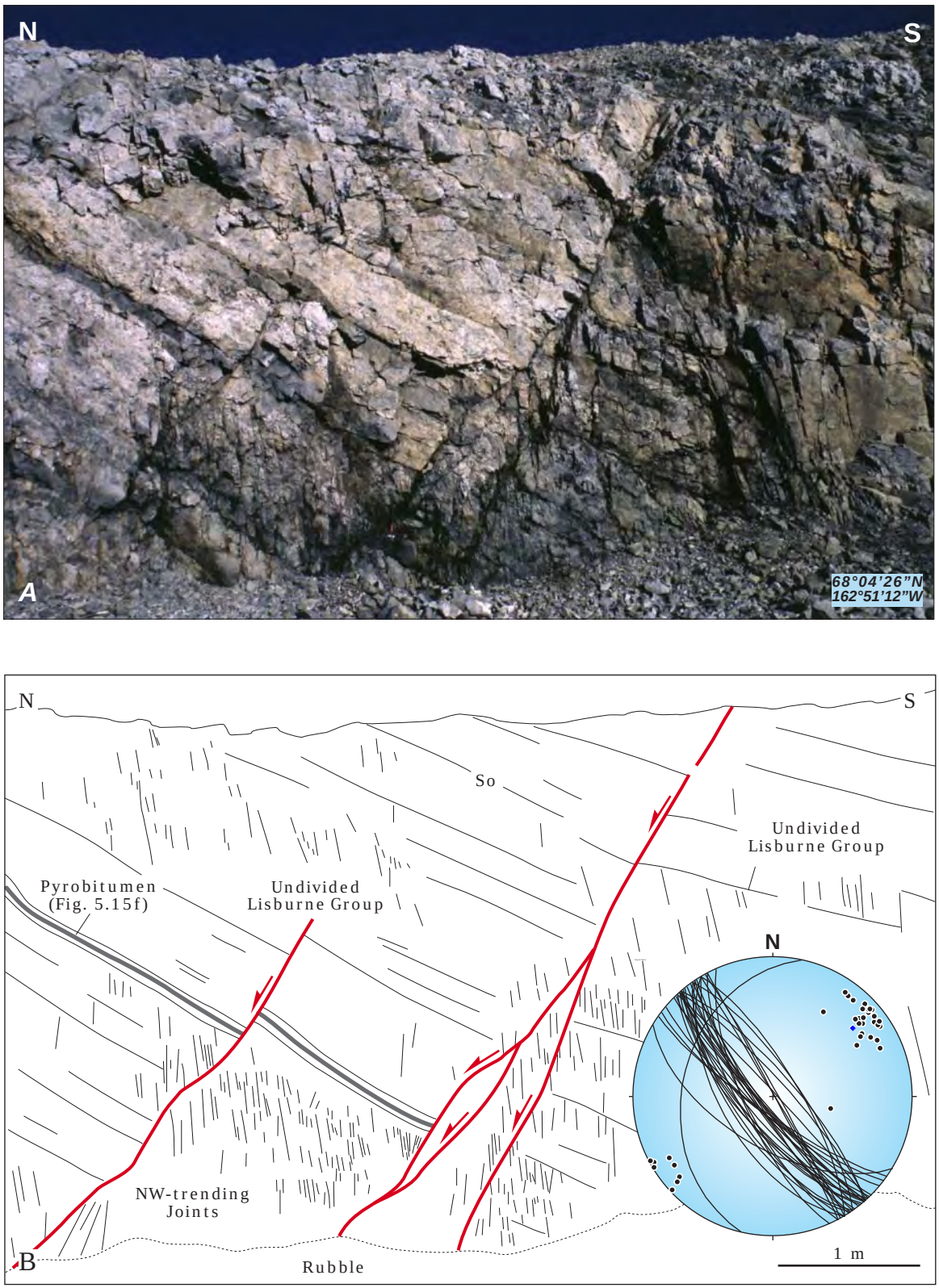


Figure 6.89. Outcrop-scale late extensional faults. **A.** Photograph of extensional faults in limestones, cherty limestones, and pyrobitumen-bearing dolostones of the undivided Lisburne Group in the Red Dog Creek. The outcrop is part of a large olistolith contained in shales and mudstones of the Okpikruak Formation (not shown). Topographic relief is approximately 5 m. **B.** Line-drawing interpretation of A and lower hemisphere equal area stereographic projection showing great circles and poles to fractures and faults (N=45).

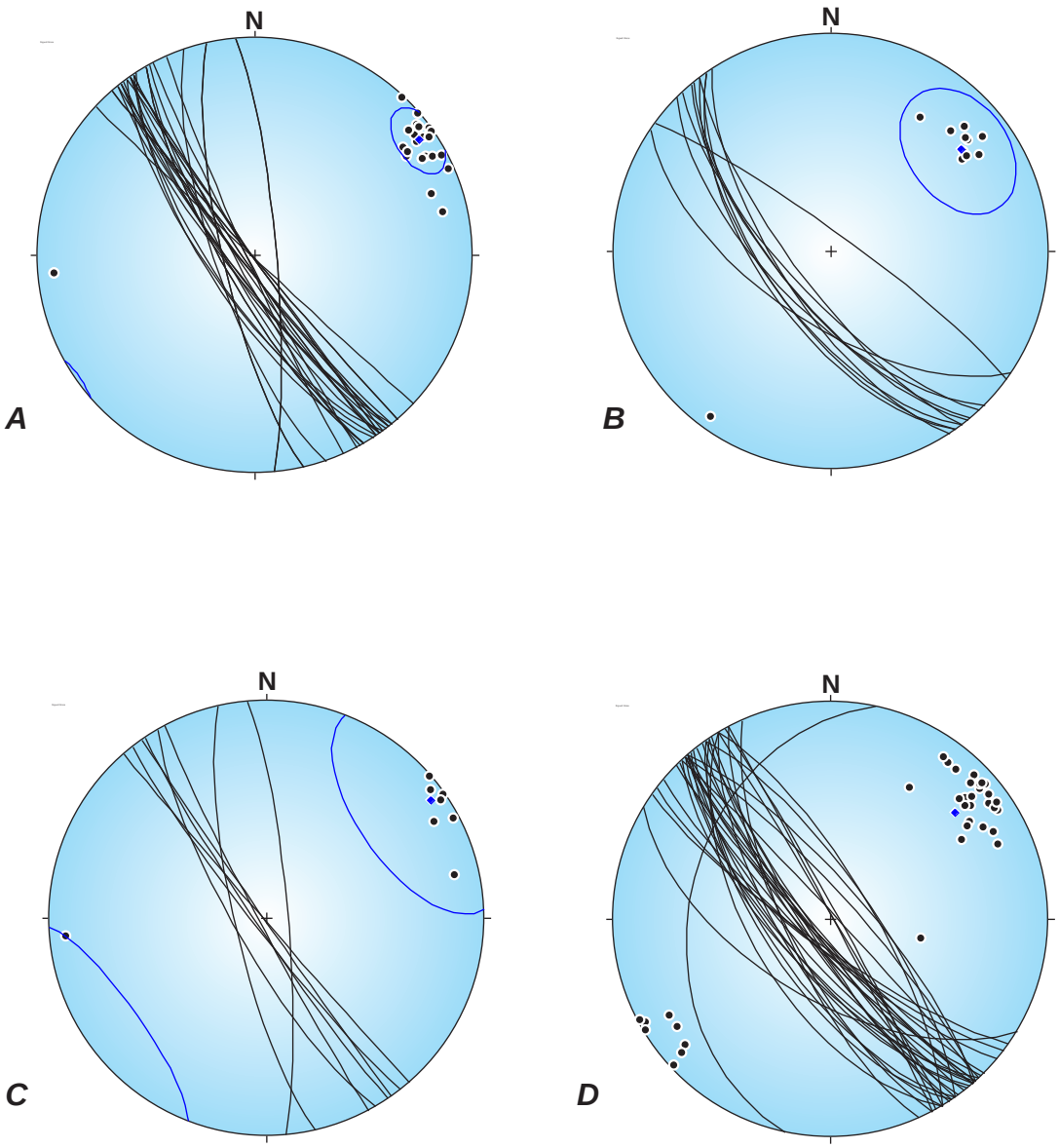


Figure 6.90. Lower hemisphere equal area stereographic projections of minor extensional faults and joints (great circles and poles) in strata of the undivided Lisburne Group of the Wolverine Creek plate in the footwall of the Sivukat Mountain fault. Rok Hills window. **A.** Anxiety Ridge (N=25). **B.** North Basin (N=20). **C.** Rok Hills (N=8). **D.** Red Dog Creek area (N=70).

Mulgrave Hills Fault

The Mulgrave Hills fault is a WNW-ESE-trending, 18 km-long, SSW-downthrown high angle extensional fault located approximately 12 and 30 km south-southwest of the Sivukat Mountain and the Red Dog mine, respectively (Fig. 6.79). The Mulgrave Hills fault forms a marked WNW-ESE-trending lineament that parallels the trace of the Sivukat Mountain fault and offsets the markedly NE-SW-trending structural grain defined by thrust faults and fault-related folds of the Key Creek plate of the Endicott Mountains allochthon.

6.7 THRUST SYSTEMS AND KINEMATIC ANALYSES

This section presents the key structural relationships described above.

6.7.1 Thrust Systems

Detachment Geometries

The Key Creek plate is detached in Late Devonian syn-rift incompetent shales and phyllites of the Hunt Fork Shale (cf. Chapter 5, Figs. 5.4, 5.7 & 5.8). The Key Creek plate is the lowest structural unit of the Red Dog district detached in Late Devonian strata. All structural units below the Key Creek plate (i.e. Red Dog and Wolverine Creek plates) are detached on Early Mississippian or younger strata (e.g. Kayak Shale, Kuna Formation) (cf. Chapter 5, Fig. 5.7). Allochthons are detached in Late Devonian strata of the Endicott or Baird groups. Within a single allochthon, thrust plates cut up-section in the direction of regional tectonic transport direction. Lower thrust plates are typically detached in Early Mississippian strata. Individual thrust faults apparently cut up section to the north-northeast along the Wulik Peaks transverse zone.

Allochthon Stacking Patterns

The structural hierarchy proposed in Figure 6.1 is generally preserved from area to area in the Red Dog district (Fig. 6.2a). Regional mapping, however, shows that allochthons are highly discontinuous and are commonly disrupted and involved in early syn-orogenic olistostromes (Figs. 6.2a & 5.1). The main allochthon units of the Red Dog district are the Endicott Mountains and Kelly River allochthons. In-sequence thrust stacking patterns are well developed north of the Wrench Creek fault and the Wulik

Peaks transverse zone, whereas to the south, the thrust stacking patterns are obscured by uncertain relationships between thrust sheets and early syn-orogenic olistostromal strata (cf. Chapter 5, Fig. 5.1).

Out-of-sequence relationships are locally developed. The most prominent out-of-sequence relationship in the Red Dog district is the presence of Jurassic ultramafic rocks of the Misheguk Mountain allochthon structurally overlying the Kelly River allochthon. In the Avan Hills the Misheguk Mountain allochthon lies structurally on top of the Kelly River and Endicott Mountains allochthons. This relationship suggests that displacement on the Angayucham thrust was synchronous with the emplacement of the underlying allochthons of the Arctic Alaska terrane. These relationships possibly resulted from a combination of synchronous thrusting and syn-orogenic low-angle extensional faulting.

6.7.2 Kinematic Analyses

Kinematic analyses were carried out to understand the motion of thrust systems in the Red Dog district. This is important because of the along-strike changes in the orientation of thrust systems (e.g. Wulik Peaks transverse zone). Structural data (*ca.* 9,000), including bedding, cleavage fabrics, bedding/cleavage intersection lineations, pencil cleavage lineations, minor fold axes, axial plane surfaces, foliations, shear fabrics, minor thrust faults, tear faults, extensional faults, slickenfibre and slickenline lineations, veins, joints, and tectonic stylolites, were systematically collected from all the exposed structural units covering an area of approximately 10,000 km^2. The regional tectonic transport of thrust sheets in the Red Dog district is indicated by the average trend of regional-scale structures such as terrane-, allochthon-, and thrust plate-bounding thrust faults the orientation of thrust fault-related folds and the attitude of the regional cleavage (Fig. 6.91). Because of the abundance of thin-bedded incompetent lithologies and the structural disruption of the area (cf. Chapter 5), small-scale structures such as minor fold axes are only indicators of local tectonic transport and do not necessarily reflect the dominant regional trends. In addition, many structural units in the area comprised between the Wrench Creek and Sivukat Mountain faults are incorporated into early syn-orogenic strata of the Okpikruak Formation.

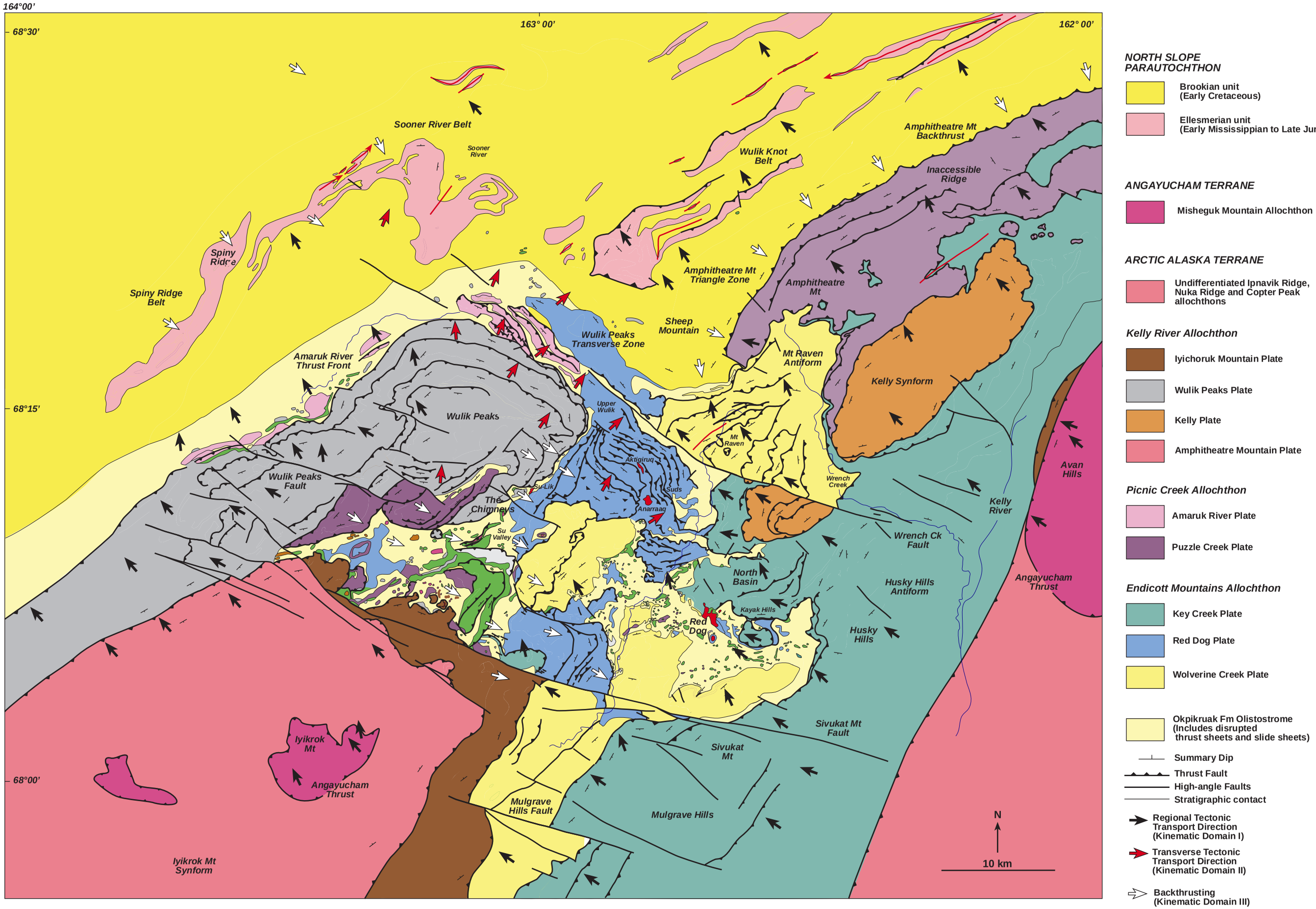


Figure 6.91. Summary tectonic transport direction map based on kinematic analyses carried out during this study.

The structural data were systematically analyzed and used to construct a synthetic tectonic transport direction map (Fig. 6.91). The Red Dog district can be subdivided into three homogeneous kinematic domains, here referred to as domains I, II and III (Fig. 6.91).

Domain I (WNW- to NW-directed Tectonic Transport)

Domain I reflects the west-northwest to northwest regional tectonic transport direction in the Red Dog district (Fig. 6.91). This is indicated by the dominant NE-SW- to NNE-SSW-trending orientation of allochthon-bounding thrust faults, major thrust fault-related folds and the consistent attitude of the regional cleavage. The kinematic domain I includes regional-scale structures such as the Husky Hills and Mount Raven antiforms and the Kelly synform.

Domain II (N- to NNE-directed Tectonic Transport)

Domain II largely correlates with the Wulik Peaks transverse zone and shows a north to north-northeast tectonic transport direction that is indicated by the orientation of major thrust faults, fault-related folds and cleavage attitude. North to north-northeast kinematic indicators are apparent and possibly reflect the rotation of NE-SW-trending thrust faults and related folds during the development of the Wulik Peaks transverse zone. Kinematic data in domain II locally shows widely scattered slip vectors with north-northeast marked components. This pattern is here interpreted to indicate accommodation slip at the edges of lateral ramps and/or plunging terminations of antiformally stacked thrust sheets.

Domain III (SE-directed Tectonic Transport)

Domain III is characterized by SE-directed thrust sheets and thrust fault-related folds that involve at least the Kelly River, Picnic Creek and Endicott Mountains allochthons in the western part of the Red Dog district (Fig. 6.91). SE-directed thrusting is well constrained by the regional dip of thrust sheets, the arrangement of the branch points and lines, well-exposed cut-offs as well as minor and large-scale fold asymmetries (Figs. 6.40 – 6.43). SE-verging thrust faults involving allochthonous thrust sheets are restricted to the south of the Wulik Peaks transverse zone. These SE-verging thrust faults are the projection to the southwest of the Amphitheatre Mountain triangle zone.

They possibly formed as a result of underthrusting of the allochthon stack. The processes that formed these structures were possibly similar to those that gave rise to the Amphitheatre Mountain triangle zone. The thrust faults possibly formed coevally with NW-verging thrusting that formed the Amaruk River thrust front to the northwest. An alternative hypothesis is that SE-verging structures are associated with the development of the Lisburne Hills – Herald Arch thrust belt to the west (cf. Chapter 2, Figs. 2.4, 2.14a & 2.16).

6.7.3 Thrust Sequences

Thrust sequences in the Red Dog district are difficult to determine because of the discontinuity of the structural units, the absence of restorable matching hangingwall-footwall relationships and the complex relationships between thrust sheets and early syn-orogenic strata. Valuable information on the kinematics of the thrust systems, however, can be obtained from indirect observations such as the spatial distribution and geometry of the thrust sheets, the detachment geometries, changes in structural relief, and the relationship between thrust sheets and olistoliths contained in syn-orogenic strata.

The allochthons of the Arctic Alaska terrane are regionally folded (e.g. Kelly synform) on underlying structural culminations and antiformal stacks (e.g. Mount Raven antiform) (Fig. 6.2). This suggests that thrusting possibly took place in a 'piggy-back' or 'forward-breaking' sequence (e.g. Boyer & Elliot, 1982; Butler, 1987; McClay, 1992). Individual thrust horses in antiformal stacks in Endicott Mountains allochthon (e.g. Mount Raven antiform) are progressively steeper towards the hinterland (Fig. 6.4). This is also consistent with back rotation and forward-breaking thrusting. These observations are also supported by the detailed analyses of the relationships between olistoliths and the thrust sheets from which they were derived. The presence of olistoliths derived from higher allochthons in the footwall of lower allochthons is consistent with a forward-breaking style of thrust propagation. The fact that successively lower thrust plates of a given allochthon are detached at higher structural levels (e.g. Endicott Mountains allochthon, Fig. 5.4) also supports a 'forward-breaking' sequence.

Examples of this relationship are well exposed along the Wulik Peaks transverse zone and the Amaruk River emergent thrust front, where Kogruk Formation olistoliths derived from the Wulik Peaks plate of the Kelly River allochthon lie on the footwall of the Amaruk River plate of the Picnic Creek allochthon (Figs. 5.1, 6.2a, 6.38 c). Out-of-sequence stacking patterns are associated with the Angayucham terrane. Out-of-sequence thrusting and/or low-angle extensional faulting accounts for the stacking of the Middle Jurassic ultramafic rocks of the Misheguk Mountain allochthon on top of Late Devonian to Mississippian strata of the Kelly River and Endicott Mountains allochthons.

6.8 SUMMARY

- The Red Dog district consists of two terranes. These are in ascending structural order the Arctic Alaska and Angayucham terranes.

- The Arctic Alaska terrane consists of the Endicott Mountains, Picnic Creek, Kelly River, Ipnavik River, Nuka Ridge and Copter Peak allochthons.

- The allochthons are internally imbricated into a series of lithostratigraphic distinct thrust plates and subplates. The structural styles are characterized by thrust faulting, detachment folding and late extensional faulting.

- Allochthons are regionally folded into a series of north-east striking and plunging regional antiforms and synforms. These antiforms are related to antiformal stacking of thrust sheets in the Key Creek and Wolverine Creek plates of the Endicott Mountains allochthon and/or the North Slope parautochthon.

- The Angayucham terrane is a NE-SW-trending and NW-verging type-C crystalline thrust sheet that was obducted on to the Arctic Alaska terrane. It is now preserved in the core of regional synforms developed at the front and back limbs of the Husky Hills antiform.

- The allochthons of the Arctic Alaska and Angayucham terranes in the Red Dog district terminate in a NE-SW- to WNW-ESE-trending thrust front. The thrust front is a complex composite structure whose orientation, vergence, position, and structural style vary along-strike. The thrust front can be divided into the NE-SW-trending Amphitheatre Mountain triangle zone, the WNW-ESE-trending Wulik Peaks transverse zone and NE-SW-trending Amaruk River emergent thrust front.

- The dominant northeast structural grain defined by the allochthons of the Red Dog district is offset by the WNW-ESE-trending and SSW-downthrown Wrench Creek and Sivukat Mountain extensional faults.

- The Wrench Creek and Sivukat Mountain faults are spatially related to the Wulik Peaks transverse zone and possibly originated as tear faults in the North Slope parautochthon during allochthon emplacement in the Early Cretaceous. These faults were subsequently reactivated as late extensional faults.

- Kinematic analyses indicate a regional west-northwest to northwest regional tectonic transport direction with local north to northeast tectonic transport along the Wulik Peaks transverse zone. SE-vergent thrusting is found in the western part of the district. Stacking patterns together with relationships between thrust sheets and early syn-orogenic strata suggest that the allochthons were largely emplaced in a forward-breaking sequence stepping to the northwest.

The structural evolution and the 3D geometries of thrust systems of the Red Dog district are reviewed in detail in Chapter 8.

CHAPTER 7

STRUCTURAL ANALYSIS OF THE SEDIMENT-HOSTED Zn-Pb-Ag AND BARITE DEPOSITS OF THE RED DOG DISTRICT

7.1 INTRODUCTION

7.2 DEPOSITS OF THE RED DOG CREEK AREA

7.3 DEPOSITS OF THE ANARRAAQ – WULIK AREA

7.4 DEPOSITS OF THE SU – LIK AREA

7.5 SUMMARY

CHAPTER 7 STRUCTURAL ANALYSIS OF THE Zn-Pb-Ag AND BARITE DEPOSITS OF THE RED DOG DISTRICT

7.1 INTRODUCTION

This chapter presents a structural analysis of the sediment-hosted Pb-Zn-Ag and barite deposits of the Red Dog district, focusing primarily on the deposits of the Red Dog Creek area. Previous research on the sediment-hosted Zn-Pb-Ag and barite mineralization of the Red Dog district focused on the ore characterization, geochemistry, and timing of mineralization of individual deposits (e.g. Lange *et al*. 1985; Moore *et al*. 1986; Young, 1989; Ayuso *et al*. 2004; Kelley *et al*. 2004*a*, *b*; Leach *et al*. 2004; Morelli *et al*. 2004; Slack *et al*. 2004; Chapter 3 and references therein). Existing structural information on the sediment-hosted Zn-Pb-Ag and barite deposits of the Red Dog district is scarce and commonly limited to outcrop-scale observations and interpretations based on patterns inferred from drill hole data (e.g. Moore *et al*. 1986; Sims, 1996; Edgerton, 1997*a*, *b*). These studies have proposed deposit-scale structural models that are not consistent with the regional structure, structural styles, and tectonostratigraphic relationships described in Chapters 5 and 6.

The sediment-hosted Zn-Pb-Ag and barite deposits of the Red Dog district occur in three areas - the Red Dog Creek, Anarraaq-Wulik and Su-Lik areas (Fig. 7.1). The Red Dog Creek area includes the Qanaiyaq (formerly known as Hilltop), Main, Aqqaluk, and Paalaaq deposits (Figs. 7.1 & 7.2). The deposits of Anarraaq-Wulik areas include the most recently discovered Anarraaq and Aktigiruq deposits (Fig. 7.1). The structural analysis presented in this chapter is based on field mapping, observations from drill cores from over 15 NQ-size exploration and mine drill cores, detailed 1:200 scale structural pit mapping in the Red Dog mine open pit, together with the study of 30 μm thin sections, 25 polished sections, and 200 hand specimens.

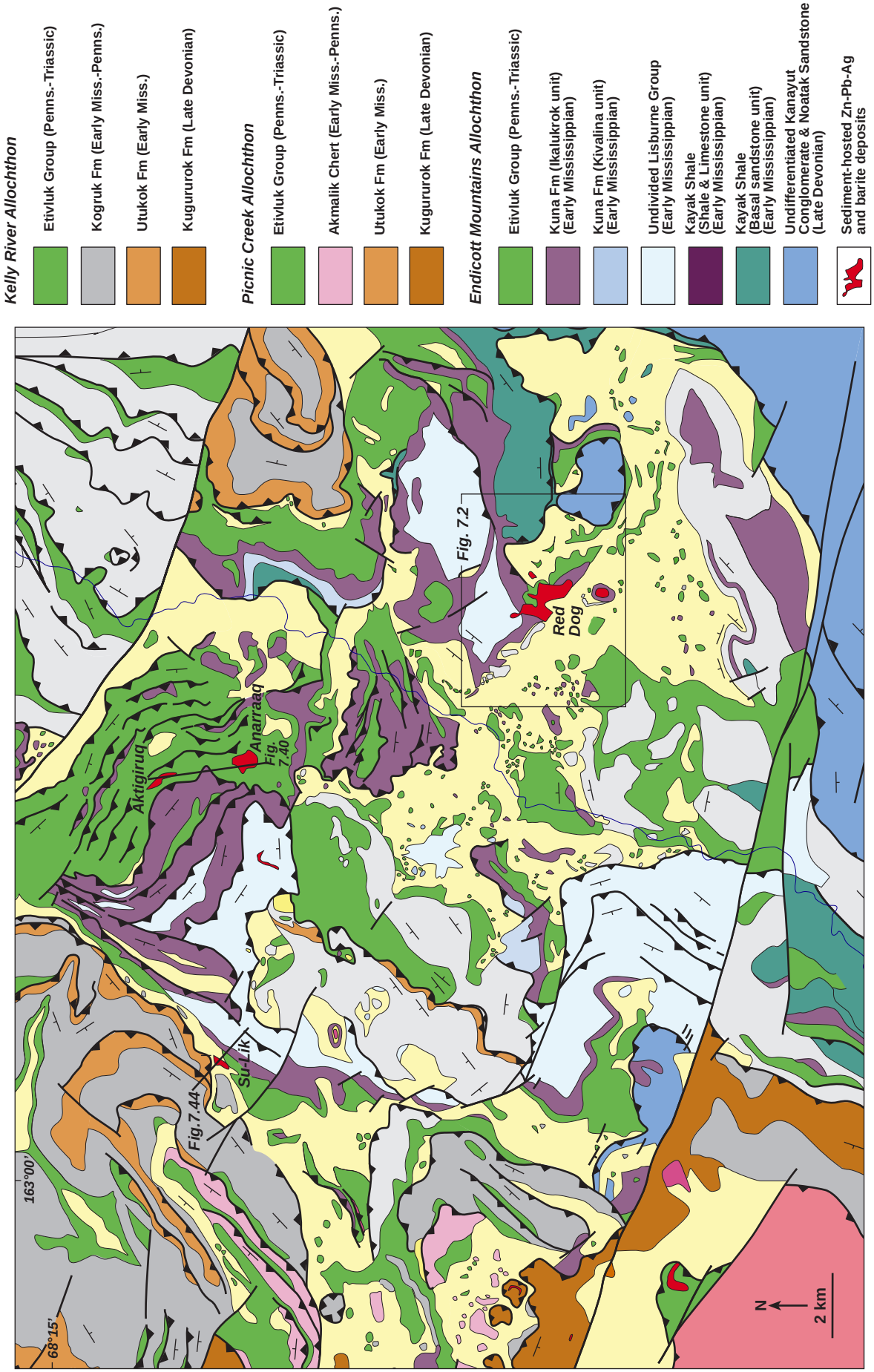


Figure 7.1. Geological map of the central part of the Red Dog district showing the location of the sediment-hosted Zn-Pb-Ag and barite deposits.

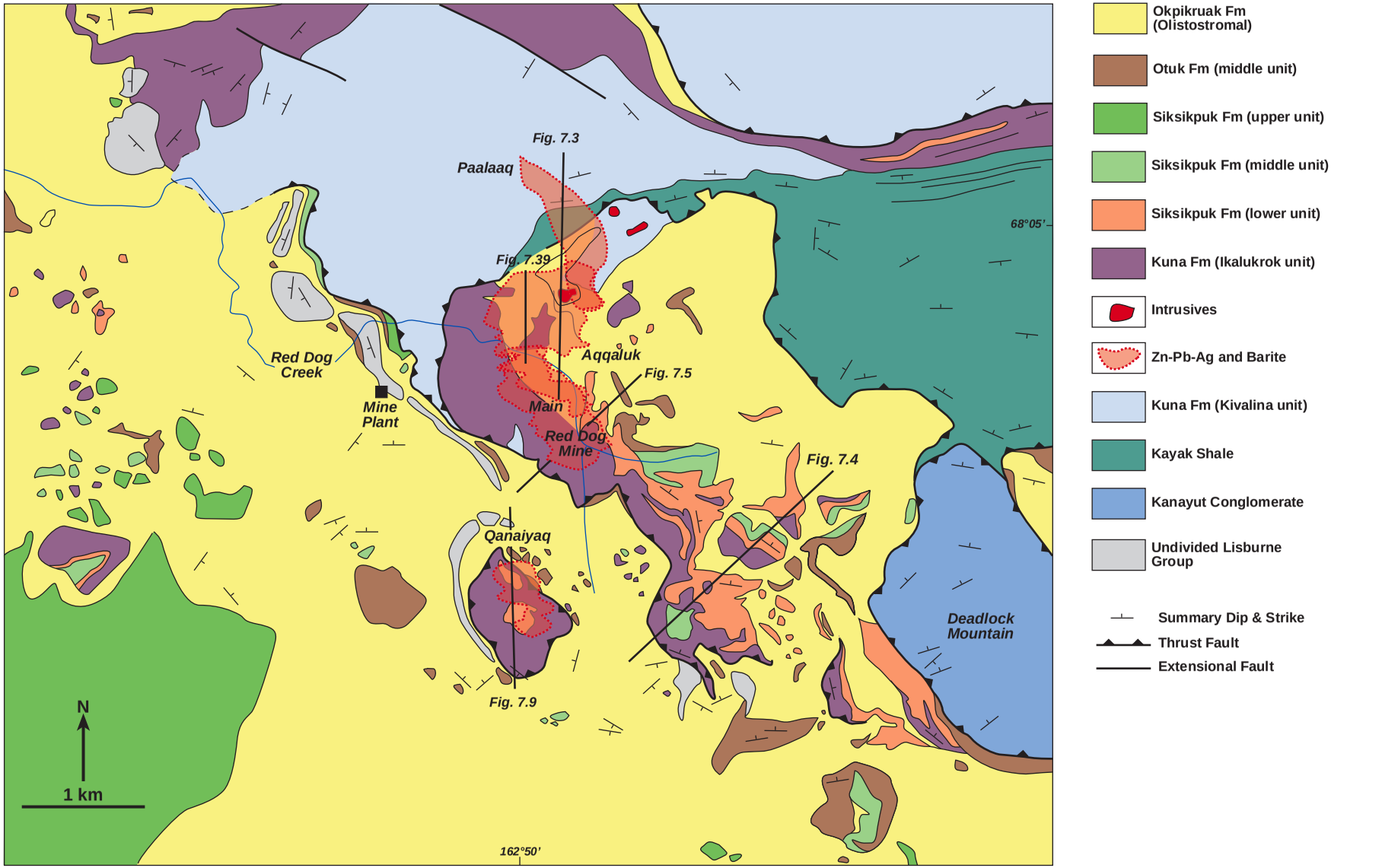


Figure 7.2. Geological map of the Red Dog Creek area, showing the Qanaiyaq, Main, Aqqaluk and Paalaaq deposits. Note discontinuity of the geological units and their relationship with the early Okpikruak Formation. Map compiled from field mapping by the author and published and unpublished maps by Teck Cominco American Inc. Exploration.

7.2 Zn-Pb-Ag-Barite Deposits of the Red Dog Creek Area

The sediment-hosted Zn-Pb-Ag and barite mineralization of the Red Dog Creek area consists of four structurally stacked orebodies that are contained in a NW-SE-trending, NE- to N-dipping array of discontinuous and highly disrupted thrust imbricates of the Red Dog plate of the Endicott Mountains allochthon (Figs. 7.1 – 7.5). This thrust subplate, here named the Red Dog Mine subplate (Fig. 7.2), occurs in the immediate footwall of the Key Creek plate and is exposed in the Deadlock Mountain and North Basin areas (i.e. Husky Hills antiform; cf. Chapter 6, Figs. 6.12 – 6.14; Figs. 7.1 – 7.3). The Red Dog Mine thrust subplate overlies, underlies or is contained in olistostromal syn-orogenic strata of the Okpikruak Formation of the Wolverine Creek plate (Figs. 7.2 – 7.5). The Red Dog Mine subplate is detached in Early Mississippian shales of the Ikalukrok unit and/or thin-bedded calcareous turbidites of the Kivalina unit of the Kuna Formation, which typically define a 1 to 100 m thick fault zone with well-developed mélange textures.

The four deposits of the Red Dog Creek area are hosted in black shales and silicified shales and mudstones of the Ikalukrok unit of the Kuna Formation (late Syn-rift Megasequence, cf. Chapter 5). The deposits are overlain by a 50 to 100 m thick barite cover, which locally extends into shales and cherts of the overlying Siksikpuk Formation (early Post-rift Megasequence, cf. Chapter 5).

As a result of the extensive tundra cover and sparseness of intact exposures in the area (Figs. 7.6 & 7.7), the structure of the deposits of the Red Dog Creek area can only be constrained by drill-hole data and exposures in the Red Dog mine open pit. Surface mapping and drill hole data indicate that the Red Dog Mine subplate ranges from 350 m to less than 50 m in thickness, with increased disruption to the east and west and grading into syn-orogenic olistostromal strata of the Okpikruak Formation (Figs. 7.1 & 7.2). Olistoliths occur along a narrow, approximately 0.5 to 1.5 km wide, NW-trending belt in the immediate footwall of the deposits (Fig. 7.2). This belt is interpreted as olistoliths and gravity slide sheets that occur at the same stratigraphic level in the Okpikruak Formation, recording an event of mass wasting during the advancement of the thrust front. These olistoliths consist of isolated metric to decametric size isolated

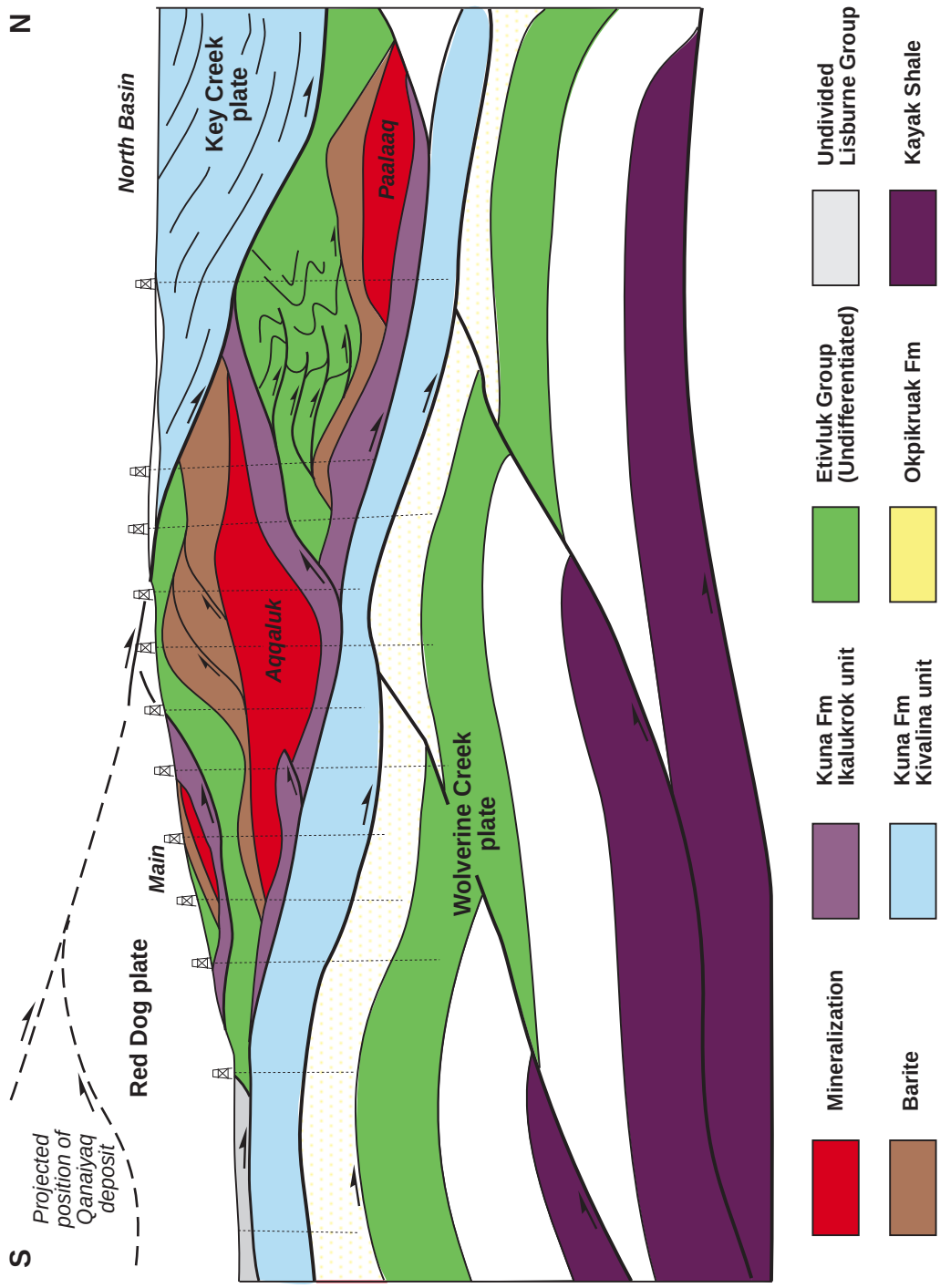


Figure 7.3. South-north cross section across the Red Dog area illustrating the arrangement of the Main, Aqqaluk and Paalaaq deposits. Section is based on drill hole data. Refer to Figure 7.2 for location.

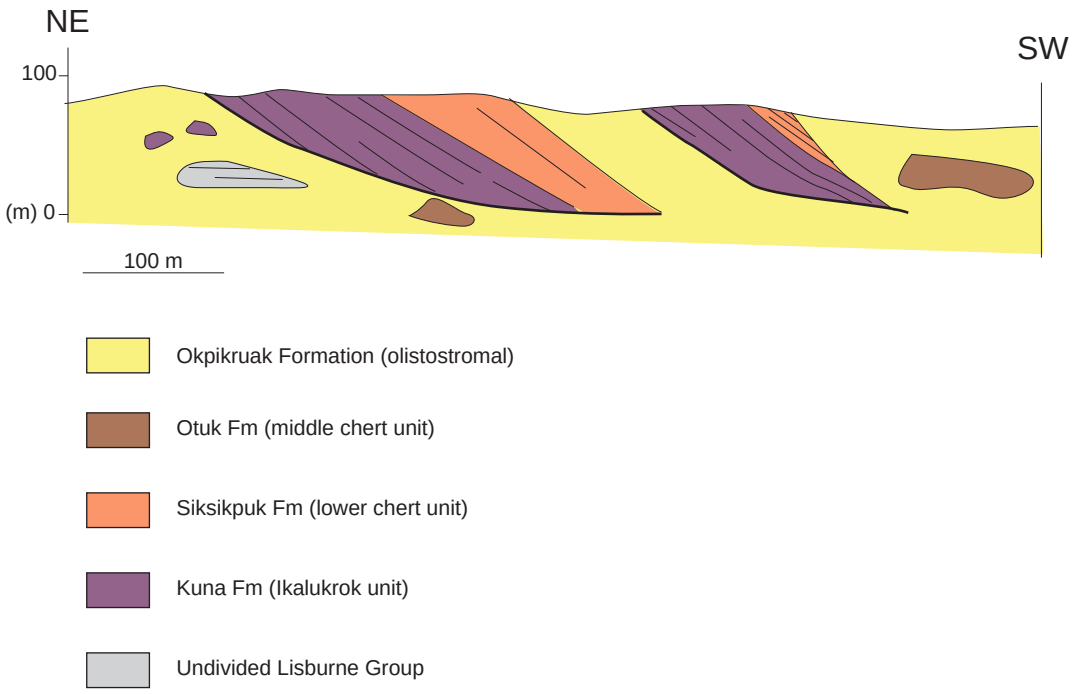


Figure 7.4. Southwest-northeast cross section across the Red Dog Creek area. Note discontinuity of the units and relationships with olistostromal strata of the syn-orogenic Okpikruak Formation. Refer to Figure 7.2 for location of section.

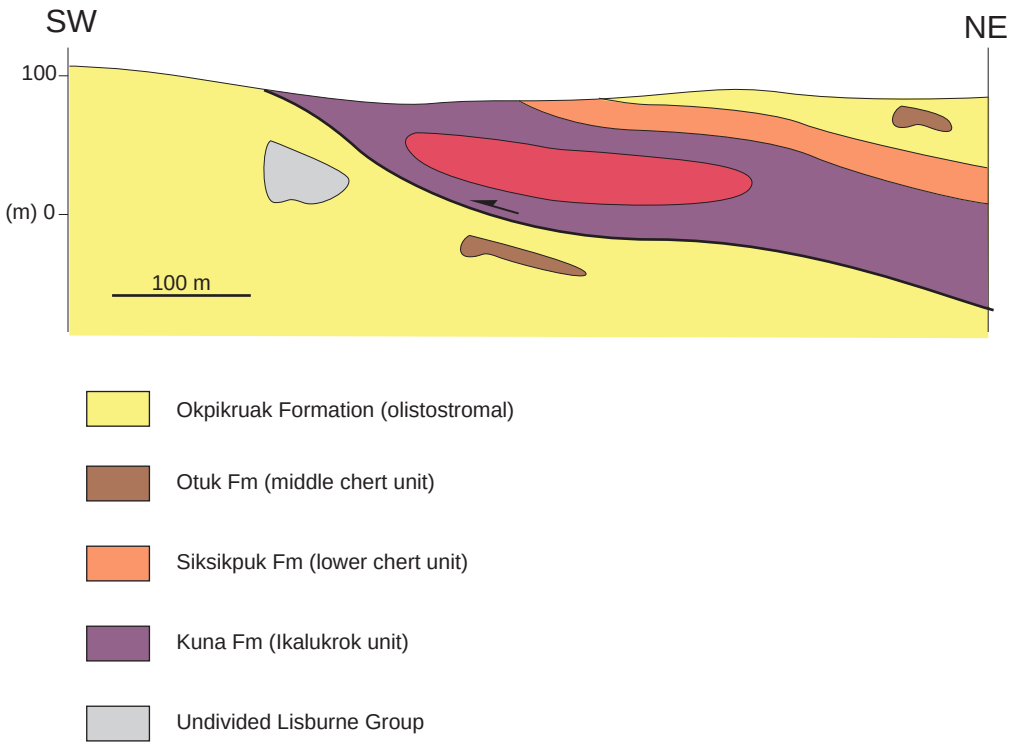


Figure 7.5. Southwest-northeast cross section across the Red Dog Creek area. Main deposit is shown schematically.

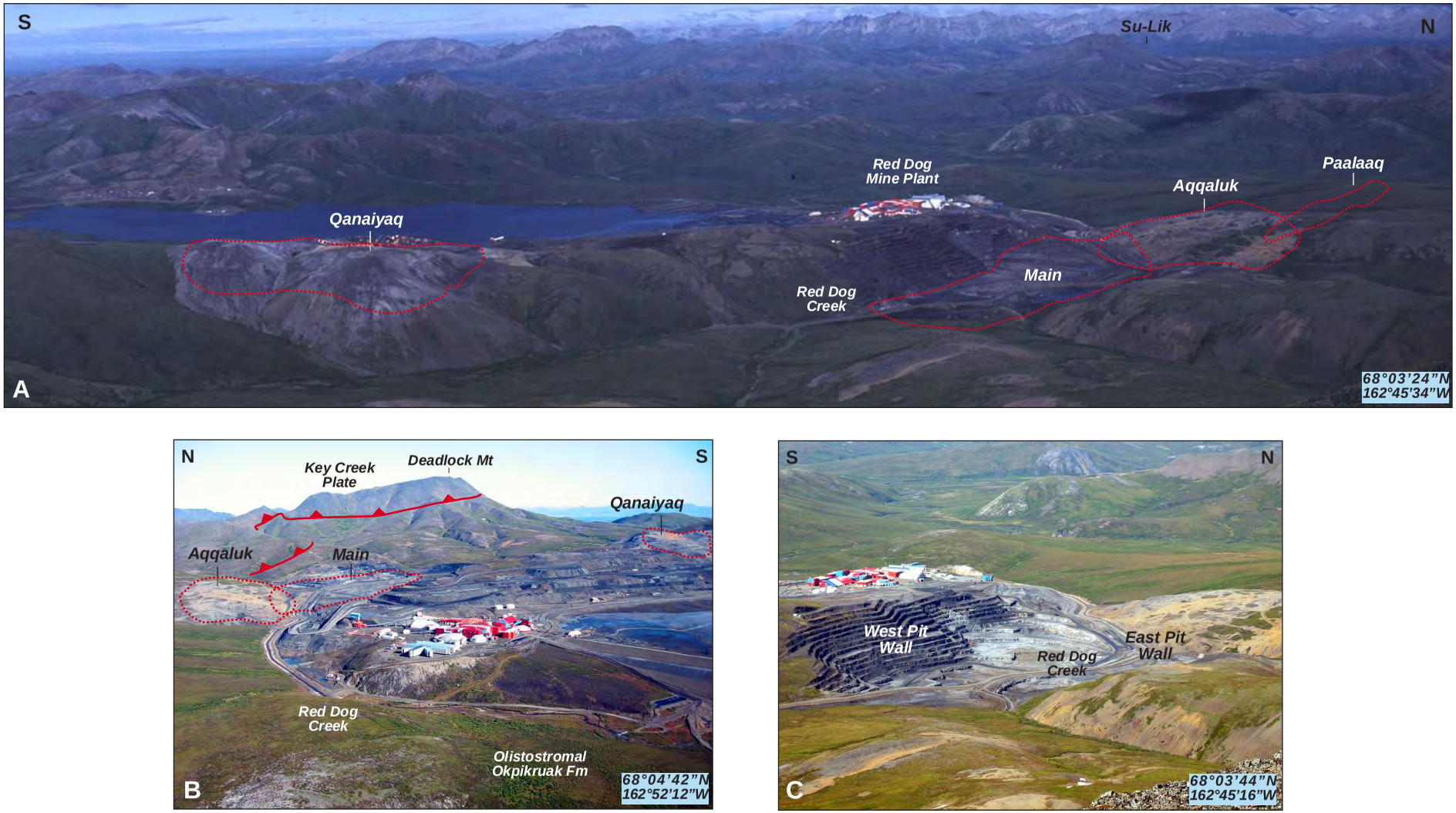


Figure 7.6. Sediment-hosted Zn-Pb-Ag and barite deposits of the Red Dog Creek area. **A.** W-looking photomosaic of the Red Dog Creek area showing the arrangement of the Red Dog deposits. View from the summit of Deadlock Mountain. Field of view is approximately 5 km. Topographic relief in the Red Dog mine is approximately 150 m. **B.** E-looking view of the Red Dog Creek area showing the arrangement of the Qanaiyaq, Main and Aqqaluk deposits. Note the Red Dog mine plant is built on a large olistolith of the undivided Lisburne Group. **C.** W-looking view of the Red Dog mine open pit. High wall is approximately 120 m high.

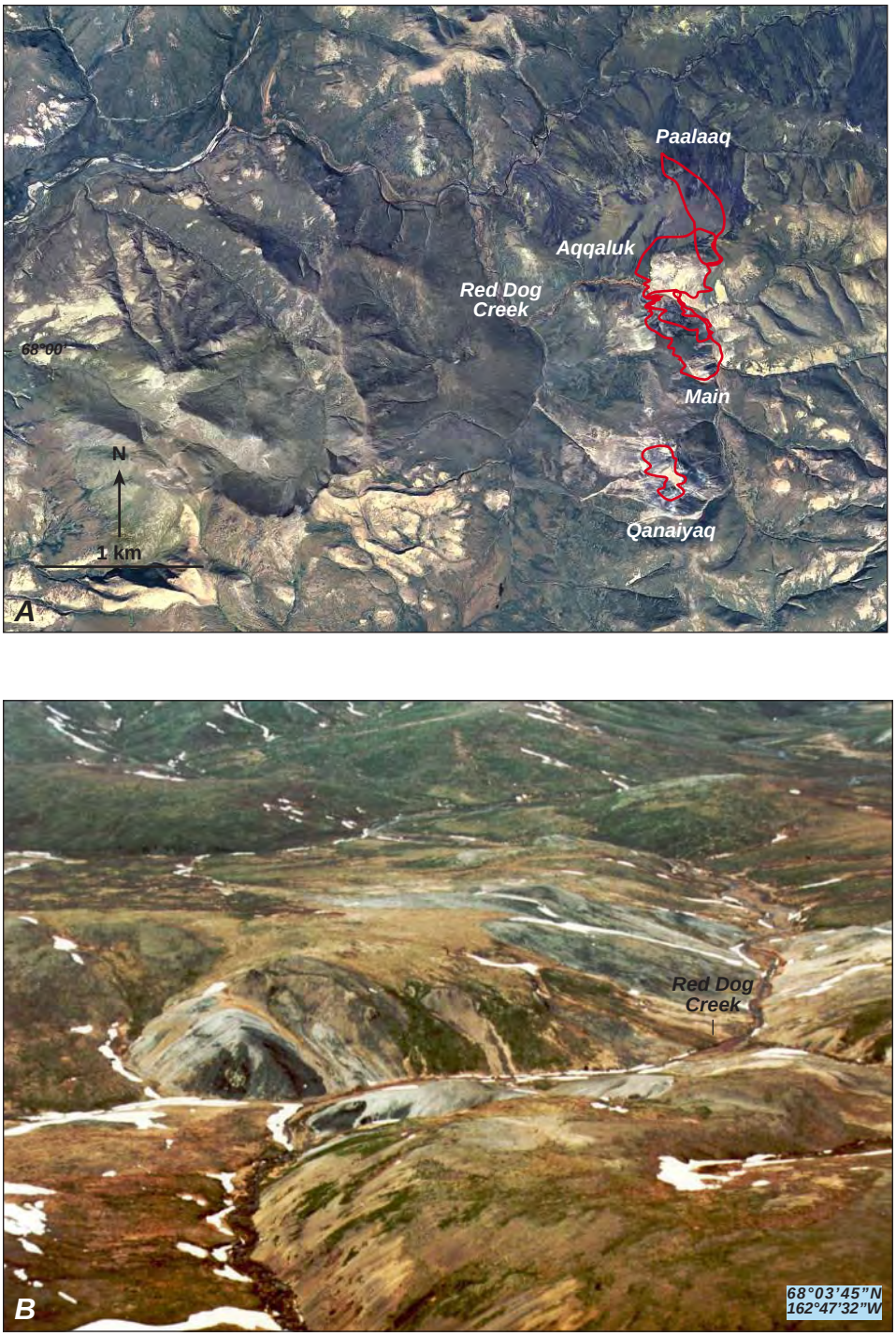


Figure 7.7. Pre-mining features of the Red Dog Creek area. **A**. Orthorectified aerial photograph of the Red Dog Creek area. Approximate outlines of the deposits are shown. Photograph taken July 1978. Note gossan and red staining in the Red Dog Creek. **B.** Oblique aerial photograph of the Red Dog Creek area (photograph courtesy of Teck Cominco American Inc.). Field of view is approximately 1 km and topographic relief is approximately 50 m.

blocks to sheet-like bodies of undivided Lisburne Group, the Kuna, Siksikpuk, and Otuk formations (Fig. 7.2). These olistoliths were previously interpreted as thrust klippen of the Red Dog plate or as windows of Ellesmerian strata on the Okpikruak Formation of the underlying Wolverine Creek plate (e.g. Moore *et al*. 1986; Young, 1989; Teck Cominco American Exploration, 2001 *pers. comm*.) (cf. Chapter 3, Fig. 3.15). This discontinuous belt was previously referred to as the 'attenuated subplate' (L. E. Young, 2002, *pers. comm*.).

This interpretation of these blocks is supported by locally well-exposed stratigraphic relationships in which metric to decametric size blocks of the Okpikruak Formation siltstones are enclosed in mudstones of the Okpikruak Formation. The olistostromal interpretation is also supported by the irregular relationships between outcrop patterns of the blocks and topography and consequently has important implications for exploration.

The four Red Dog Creek area deposits are, in descending structural order and from south to north, the Qanaiyaq, Main, Aqqaluk and Paalaaq deposits (Fig. 7.3). The Paalaaq, Aqqaluk and Main deposits overlap each other and are separated from the Qanaiyaq deposit by approximately 1 km (Fig. 7.1). The Qanaiyaq and Main deposits crop out (Fig. 7.2), whereas the Aqqaluk and Paalaaq deposits lie in the subsurface at depths of 50 to 500 m (Fig. 7.3). All these deposits occur largely as elongate stratiform lenses (Fig. 7.3) with their individual long axes broadly aligned in an approximately 3 km long trend that plunges to the north-northwest (Figs. 7.2 & 7.8). The deposits occur in an allochthonous, poorly-defined, northerly-dipping and verging duplex that has been folded by imbrication of underlying thrust systems, possibly of the Wolverine Creek plate. This Red Dog duplex is highly discontinuous and pinches out along-strike. The deposits of the Red Dog Creek area cannot be easily restored to their original palaeogeographic positions because their disrupted nature and uncertain stratigraphic positions. The structure of these deposits is described in descending structural stacking order from south to north.

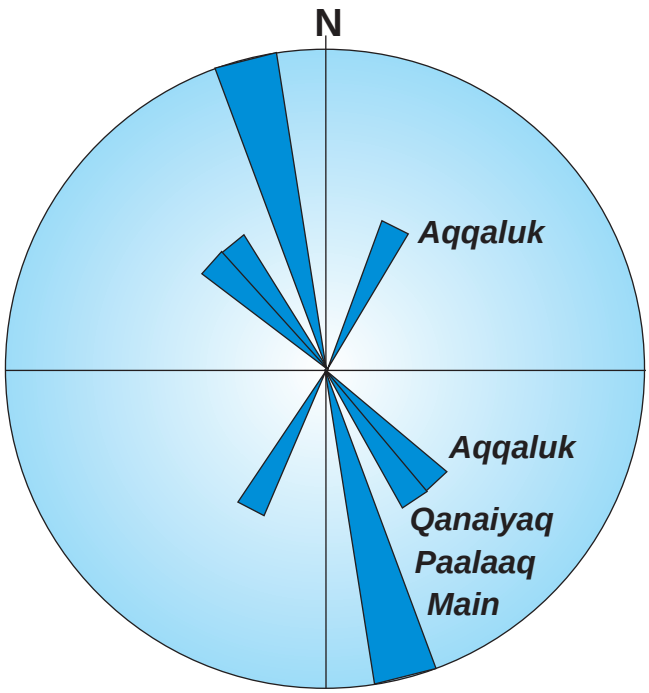


Figure 7.8. Rose diagram showing the orientation of the long axes of the deposits of the Red Dog Creek area based on drilling definition (N=35).

7.2.1 Qanaiyaq Deposit (formerly the Hilltop deposit)

The Qanaiyaq deposit is the southernmost, topographically highest and the smallest deposit in the Red Dog Creek area (Figs. 7.1 – 7.7). It is exposed in the hilltop area, approximately 750 m south of the main Red Dog mine (Fig. 7.2). The deposit is poorly exposed and occurs as highly-weathered rubble that forms a distinctive vegetation kill zone (*ca.* 1 km^2) associated with barite and massive sulphides (Figs. 7.2 & 7.3). At the Present Day, the Qanaiyaq deposit and its footwall are partly concealed by waste dumps and ore stockpiles from the Red Dog mine (Fig. 7.6). Drill hole data indicate that the Qanaiyaq deposit is approximately 50 to 100 m thick, 800 m long, and 200 to 600 m wide (Fig. 7.2). It is contained in a 0.8 km^2 flat-lying NNW-trending elongate and open synformal klippen (Fig. 7.3). Drill data indicate that the base of the deposit is shallow-dipping. The orebody is hosted in heavily silicified black shales of the Ikalukrok unit of the Kuna Formation that are underlain by thin slivers of the Kivalina unit (Fig. 7.9). Internal features of the orebody could not be readily determined in this study because the available drill core was highly weathered. The well-preserved sulphide textures observed in outcrop and locally in drill core indicate that the sulphide body is relatively undeformed. Vein-breccia mineralization and galena-rich horizons occur near the base of the deposit.

The immediate footwall of the Qanaiyaq deposit consists of metric to decametric size sheet-like olistoliths of the undivided Lisburne Group and metric size blocks of the Kuna, Siksikpuk and Otuk formations of the Etivluk Group (Fig. 7.9). At least 35 olistoliths were identified from surface mapping in the vicinity of the deposit. Additional olistoliths have been intercepted by exploration drilling near the deposit. These occur as isolated centimetric to metric intervals of Lisburne Group lithologies enclosed in the Okpikruak Formation. Because of the lack of intact surface exposures, no reliable kinematic data can be obtained from the Qanaiyaq deposit. Minor fold axes in the immediate footwall show scattered orientations, supporting the interpretation that footwall strata are largely olistostromal in character.



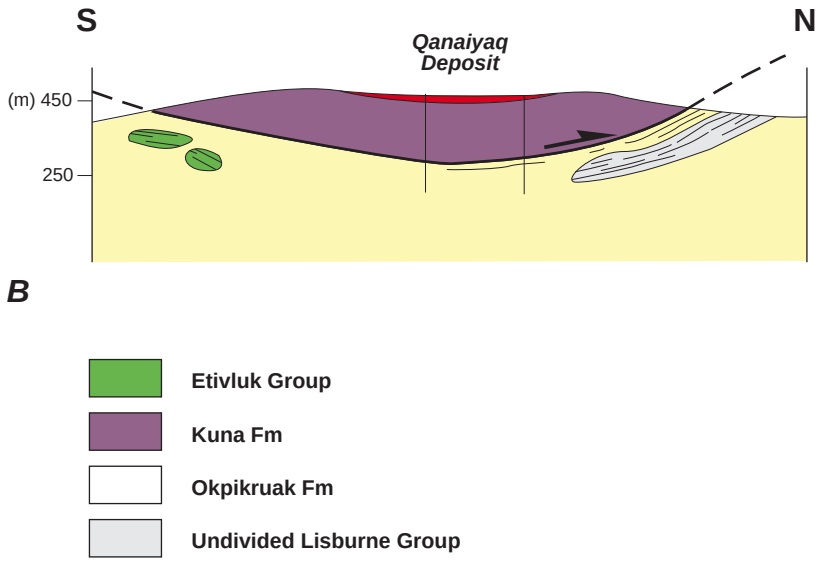


Figure 7.9. Qanaiyaq deposit. **A.** W-looking view of the Qanaiyaq deposit. Note vegetation kill zone and gossan associated with the presence of barite and sulphides. **B.** Cross section through the Qanaiyaq deposit. Note the Qanaiyaq deposit overlies olistoliths and Okpikruak Formation.

7.2.2 Main Deposit

The Main deposit lies approximately 750 m north of the Qanaiyaq deposit and is transected by the Red Dog Creek (Fig. 7.10). It is a N-trending, lens-shaped strata-bound orebody that has a length-to-width ratio of approximately 1:2. The Main deposit is approximately 1.5 km long, 100 to 1 km wide and approximately 135 m thick (Figs. 7.3 & 7.10). The deposit is contained in a laterally discontinuous remnant of the Red Dog Mine subplate (Figs. 7.1 & 7.2). To north the Main deposit is thrust over the Aqqaluk deposit (Figs. 7.2 & 7.3). To the west it is separated from the Okpikruak Formation by a complex deformation zone (Fig. 7.2) and to the east and south the deposit and overlying barren succession are partly or entirely concealed by syn-orogenic strata (Figs. 7.1 & 7.2).

The Main deposit is well exposed in the Red Dog mine open pit (Figs. 7.1, 7.2 & 7.10). Mining has removed most of the overlying Pennsylvanian to Early Cretaceous strata, partially exposing the mineralization (Fig. 7.10). The Red Dog mine open pit is elongate and trends north-south and has two main pit walls – and east wall and a west wall (Fig. 7.10). The east pit wall partly exposes the Main orebody and the overlying strata, whereas the west pit wall exposes the contact between the deposit and its footwall (Fig. 7.10). Structural analysis of the Main deposit involved the construction of a series of 1:200 scale bench structural maps (Enclosure II, Fig. 7.11). Each bench section was systematically staked at approximately 100 m-spaced intervals and stations were surveyed for future reference (Appendix I). Mapping of the west pit wall was limited to key localities because of bench wall instability. Bench mapping and bench-to-bench correlations were aided by using detailed panoramic photomosaics of individual bench walls (Fig. 7.12) as well as low-altitude high-resolution orthophotomosaic, pre-mining conventional aerial photographs, and oblique aerial photographs taken from a helicopter. Bench sections were plotted on a bench map and correlated to produce a map of the Red Dog mine pit (Fig. 7.11).

The stratigraphy of the Red Dog Mine subplate in the Red Dog mine is characteristic of the Red Dog plate of the Endicott Mountains allochthon (cf. Chapter 5, Fig. 5.6) (cf. Chapter 5, Figs. 5.11 – 5.14). However, identification of stratigraphic units in the Red

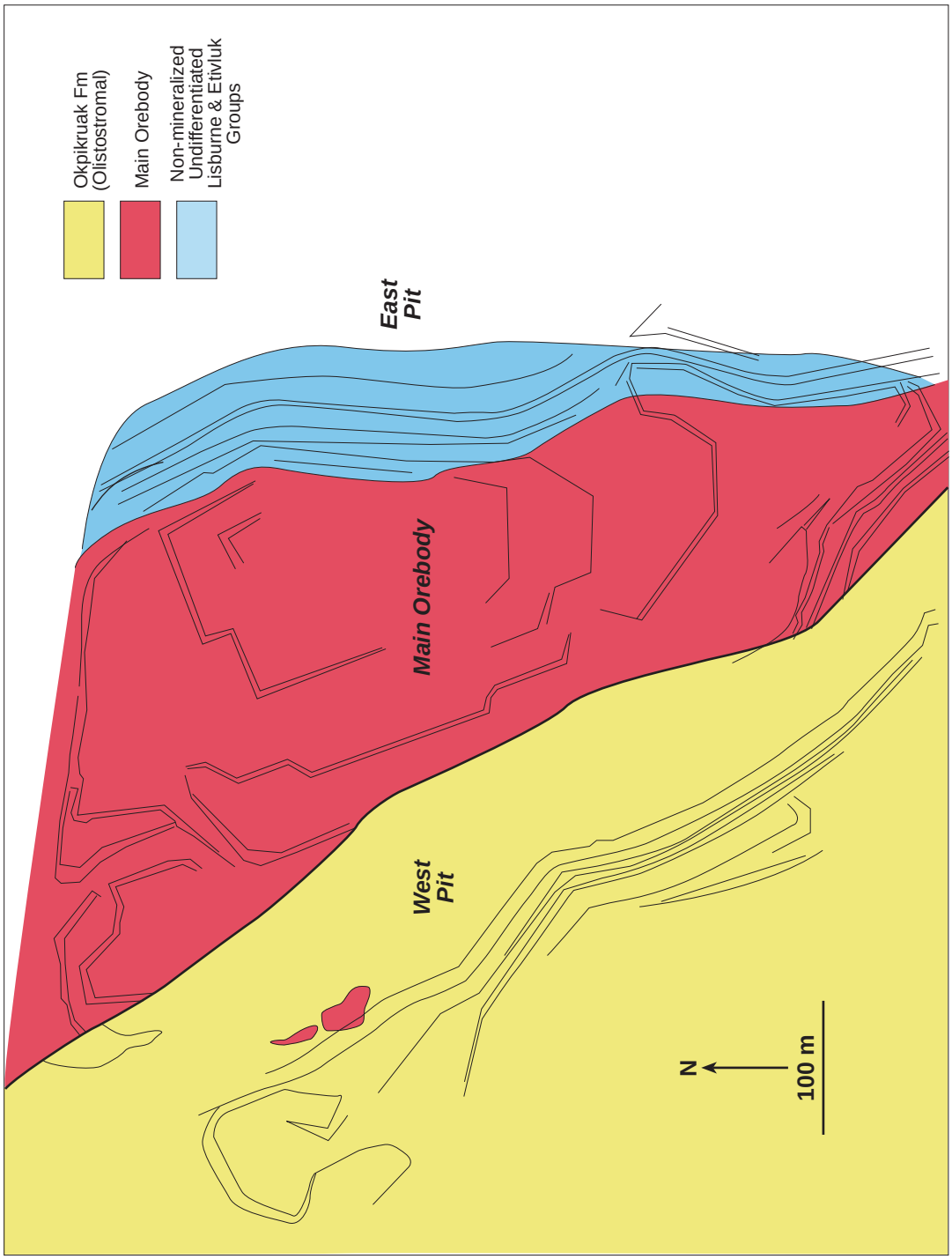


Figure 7.10. Schematic structural map of the Red Dog mine pit. Note the Main orebody is bounded by melange and olistostromal strata of the Okpikruak Formation to the west and overlain by non-mineralized strata to the west.

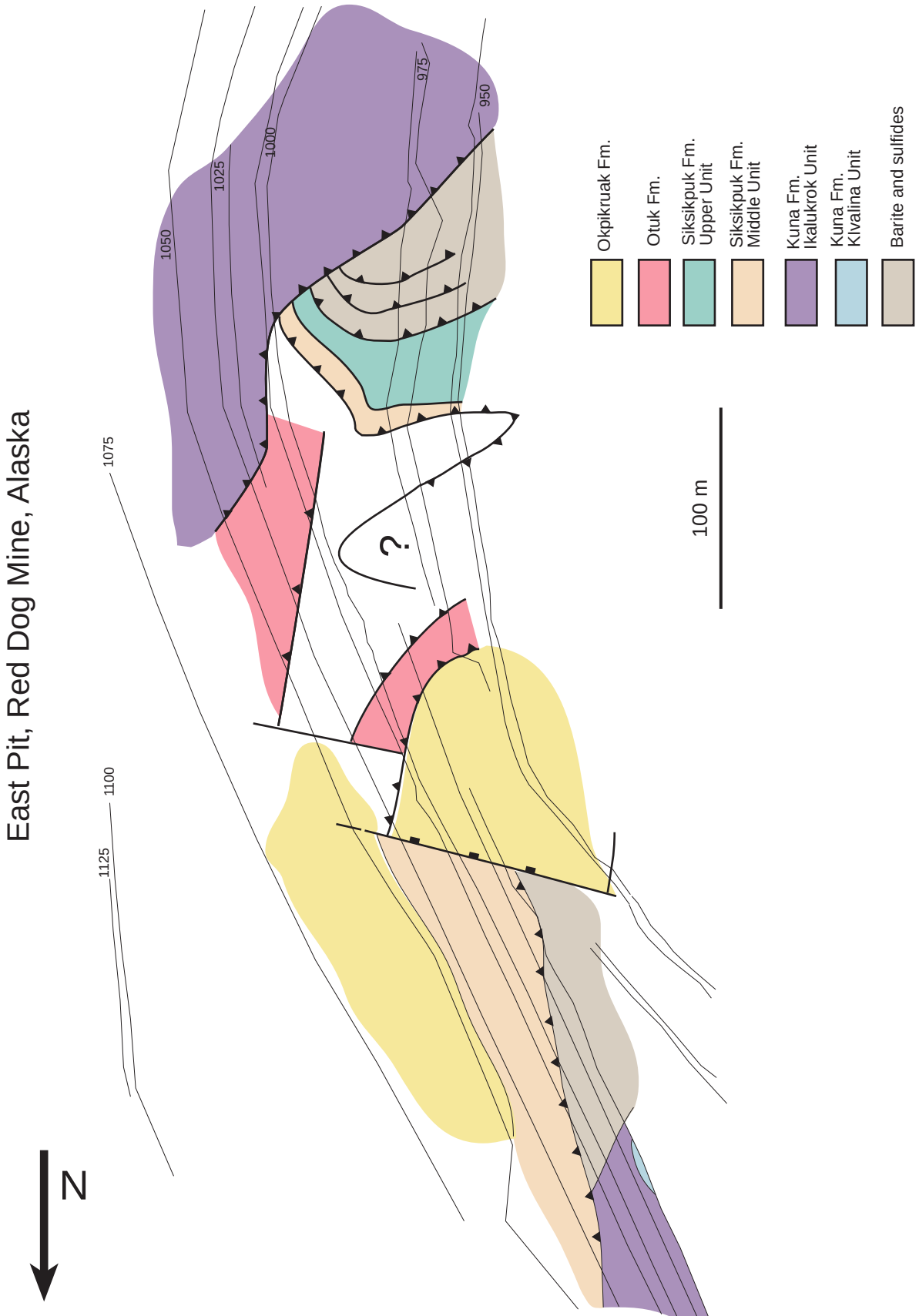


Figure 7.11. Summary structural map of the east pit of the Red Dog mine.



Figure 7.12. E-looking photomosaics of the east pit wall of the Red Dog mine. Individual bench walls are approximately 7 m high. **A.** July 2002. **B.** June 2001.

Dog mine open pit itself was hampered by the lack of natural surface weathering colours and textures. Bench walls in the Red Dog mine pit are typically coated with organic carbon due to the lack of surface oxidation (Fig. 7.12). In addition, blasting has caused some units (e.g. Siksikpuk and Otuk formations) to fracture intensely also hampering lithological identification. In addition much of the stratigraphy in the vicinity of the mineralization is strongly silicified, probably as a result of the development of an alteration halo around the orebodies as they were formed.

The geometry of the base of the deposit is interpreted from drill hole data. Bedding dips of 10 to 35° measured in vertical drill cores indicate that the deposit is relatively flat-lying to moderately dipping and in places gently to moderately folded. Thrust sheet dips of 5° to 20° (Enclosure II) in the east pit wall also indicate low overall dips for the deposit. At the deposit scale, fold wavelengths typically range from 200 to 500 m and fold amplitudes are on the order of 30 to 50 m. Deformation of sulphides near the base of the deposit is characterized by brecciation and veining together with alteration and replacement textures.

Thrust Systems in the Red Dog Open Pit

Thrust systems in the east pit of the Red Dog mine include individual thrust faults as well as duplexes that occur at a variety of scales, typically ranging from a few centimetres to hundreds of metres.

Thrust Faults

Thrust faults in the Red Dog mine occur as planar and low to moderately (20° to 45°) S- to NNE-dipping surfaces. Thrust faults range from knife-edge surfaces to fault zones as wide as 10 m (Fig. 7.13). The exact displacement for individual thrust faults cannot be readily determined because the corresponding footwalls are usually not exposed. Main thrust faults occur near the base of the Ikalukrok unit with secondary detachments at the base of the barite, and the Siksikpuk and Otuk formations (Figs. 7.13 – 7.17). Metre scale thrusts are commonly developed within stratigraphic units. A main thrust fault occurs in the southern part of the open pit, where the Ikalukrok unit is thrust over highly deformed strata of the Etivluk Group (Enclosure II; Fig. 7.15).

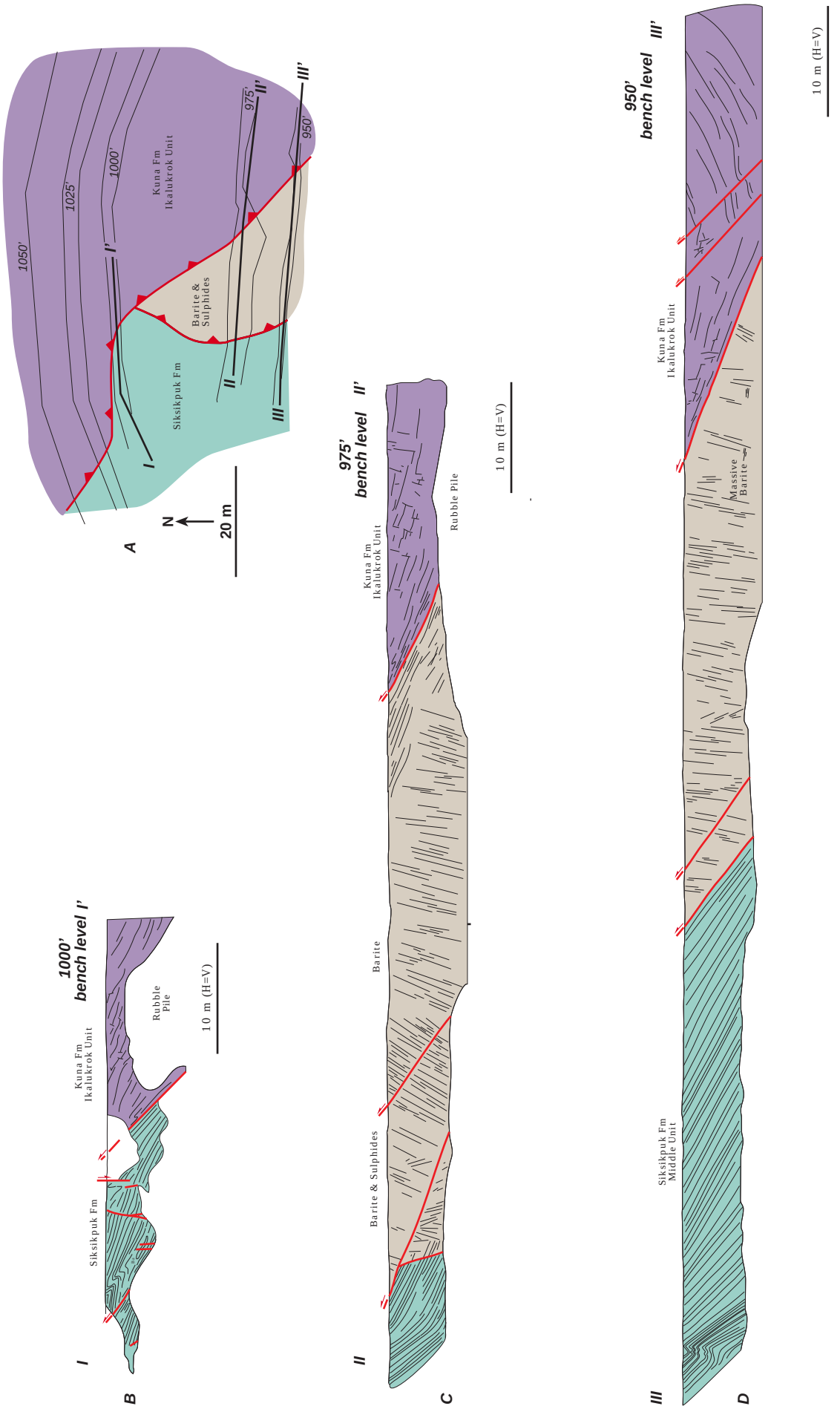


Figure 7.13. Examples of thrust faults in the Red Dog mine. **A.** Simplified geological map of the southern part of the east pit wall showing major thrust fault. **B, C & D.** Detailed cross sections. Refer to A for location of individual sections.

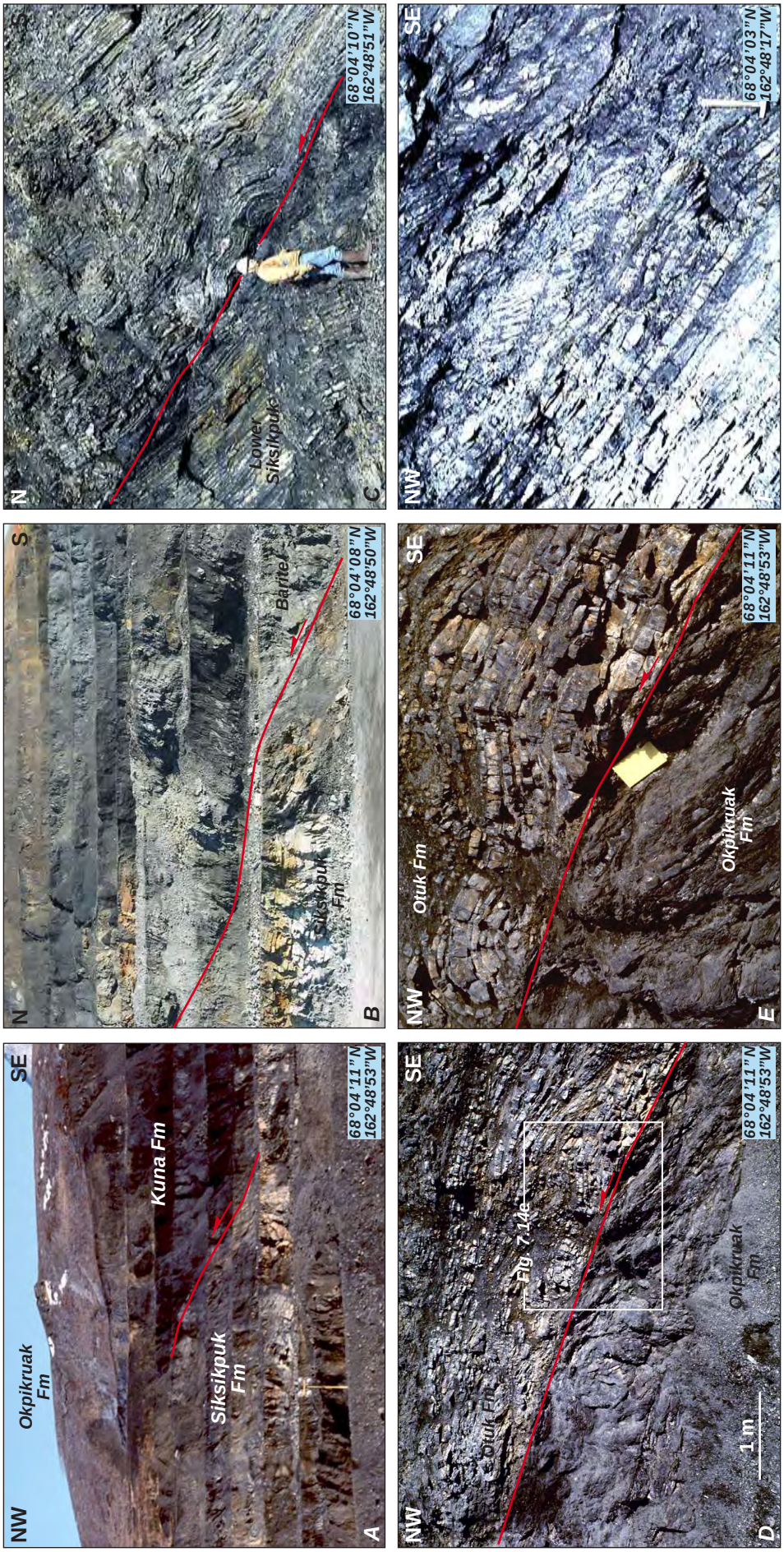


Figure 7.14. Thrust faults in the east pit. **A.** E-looking view of the east pit wall showing major thrust plates bringing black shales of the Ikalukrok unit of the Kuna Formation on top of the Etivluk Group. Individual bench walls are approximately 7 m high. **B.** E-looking view of thrust fault bringing barite over the Siksikpuk Formation. Bench walls are approximately 7 m high. **D.** Detail of shallow-dipping thrust fault in the Siksikpuk Formation. Teck Cominco geologist Scott Jennings for scale. **E.** Detail of thrust fault bringing well-bedded cherts of the Otuk Formation over of the Okpikruak Formation. 20 cm-long field note book for scale. **F.** Outcrop-scale footwall duplex in strata of the Siksikpuk Formation. Geological hammer for scale.

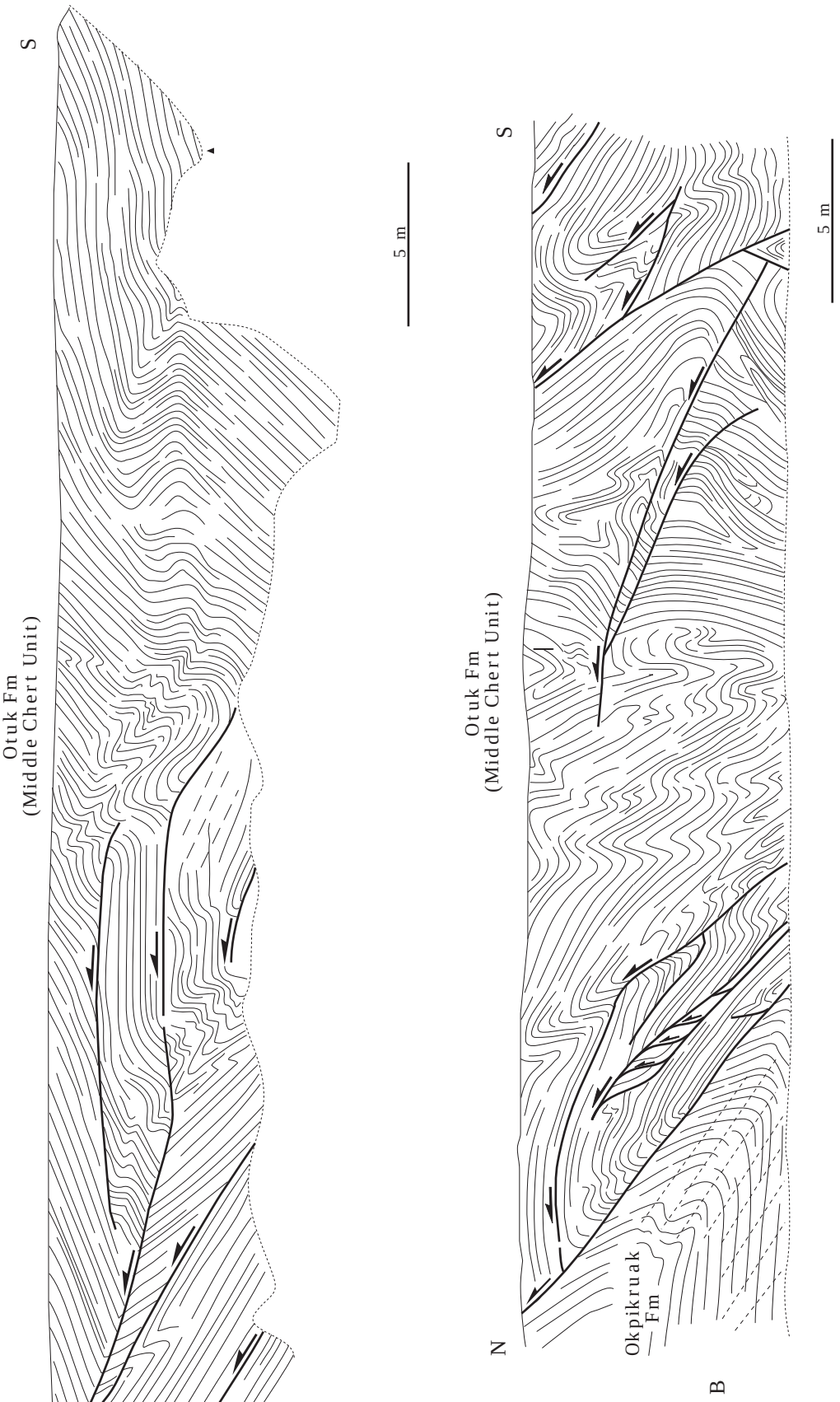


Figure 7.15. Sketches showing structural styles. **A.** Fault-related folds in well-bedded cherts and shales of the middle unit of the Otuk Formation. 1000' bench level, Red Dog mine east pit. **B.** Asymmetric detachment folds and thrust faults. 975' bench level, Red Dog mine east pit.

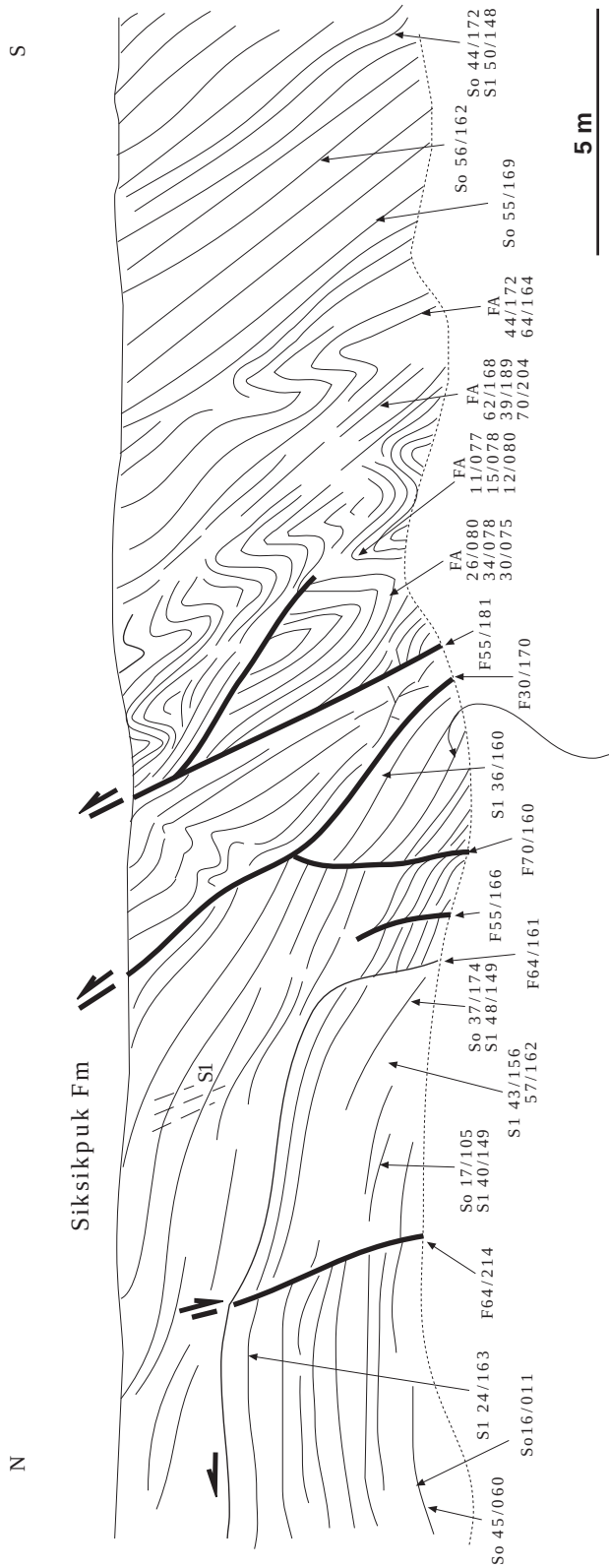


Figure 7.16. Field sketch showing thrust faults in strata of the Siksikpuk Formation, 975' bench level, east pit wall, Red Dog mine.

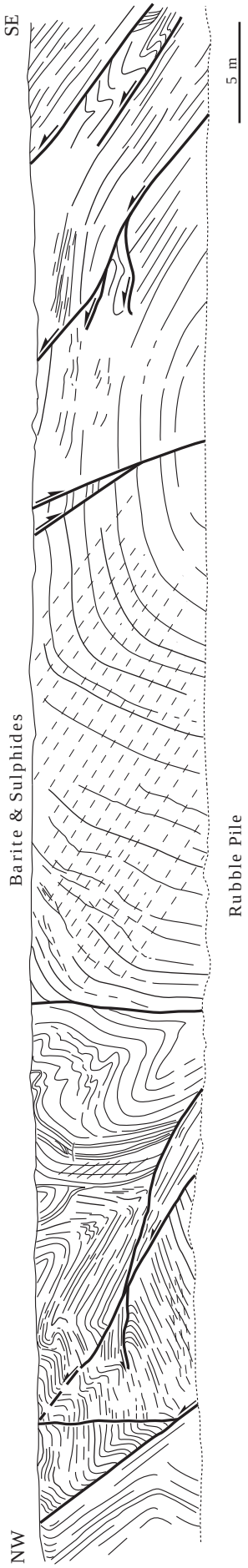


Figure 7.17. Detail bench section showing thrust faults and folds in barite and sulphides, 950' bench level, east pit wall, Red Dog mine.

The east pit wall was previously interpreted as the overturned limb of a folded thrust (e.g. O'Brien, 2001, *pers. comm.*; R. Robinson, 2003, *pers. comm.*). However fold asymmetries and bedding-cleavage relationships measured indicate that this structure is a right way up, southerly-dipping and north-vergent thrust sheet. Associated with thrust faults in the open pit are fault-propagation and detachment folds that in places display well-developed cleavage fabrics (Figs 7.13 – 7.18). Thrust-bedding cut-off angles typically range from 10° to 35°, although out-of-sequence thrusts locally show hangingwall and footwall cut-off angles as high as 60° (Figs. 7.13 – 7.17).

The thrust structures are offset by later NW-SE-trending extensional faults that will be described later in this chapter.

Duplexes

Outcrop-scale duplexes in the Red Dog open pit are typically developed in thinly-layered, parallel-bedded units, such as the lower Siksikpuk Formation and the middle Otuk Formation (Fig. 7.19; cf. Chapter 5, Fig. 5.3). These duplexes occur as decimetric to metric single- to multi-bed hinterland-dipping footwall duplexes and flexural slip duplexes. The duplexes are typically 2 to 7 m long and show length-to-thickness ratios of approximately 1:8 to 1:10 (Fig. 7.19). They have limited lateral extents (5 to 10 m) and usually cannot be correlated from bench to bench. Individual thrust horses are bounded by moderately SW-dipping sigmoidal link thrusts that merge asymptotically into the gently SW-dipping roof and floor thrusts (Fig. 7.19). Floor and roof thrust surfaces are typically developed in 1 to 3 cm thick incompetent shale horizons that have flexural-slip slicken-fibres and characteristic wispy fault gouges. The maximum link thrust fault angles typically occur in the central part of the duplex (at 45° to the floor thust) and progressively decrease towards the leading and trailing edges of the duplex (Fig. 7.19). Link thrust fault surfaces locally show slickenside fibre lineations. The floor and roof thrusts generally have smooth planar geometries and vertical separations between 0.5 to 1 m (Fig. 7.19). The number of duplex horses ranges from 7 to 20 and their spacing typically varies from 15 to 30 cm (Fig. 7.19).

Outcrop-scale duplexes are best developed in the southern part of the east pit where the Siksikpuk Formation is preserved in the footwall proximity of major thrust faults. Here

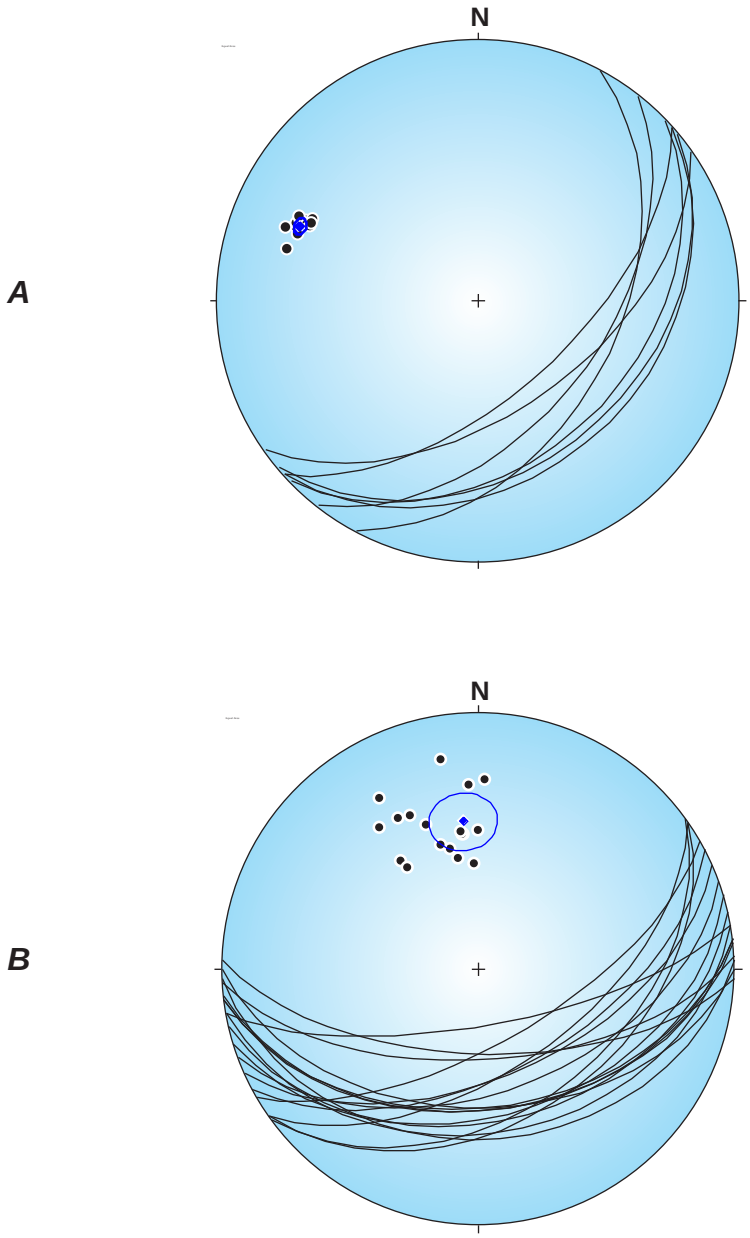


Figure 7.18. Lower hemisphere equal area stereographic projection of thrust faults in the east pit of the Red Dog mine. **A.** Great circles and poles to minor thrust faults in the 975' bench level (N=6). **B.** Great circles and poles to minor thrust faults in the 1000' bench level (N=17).

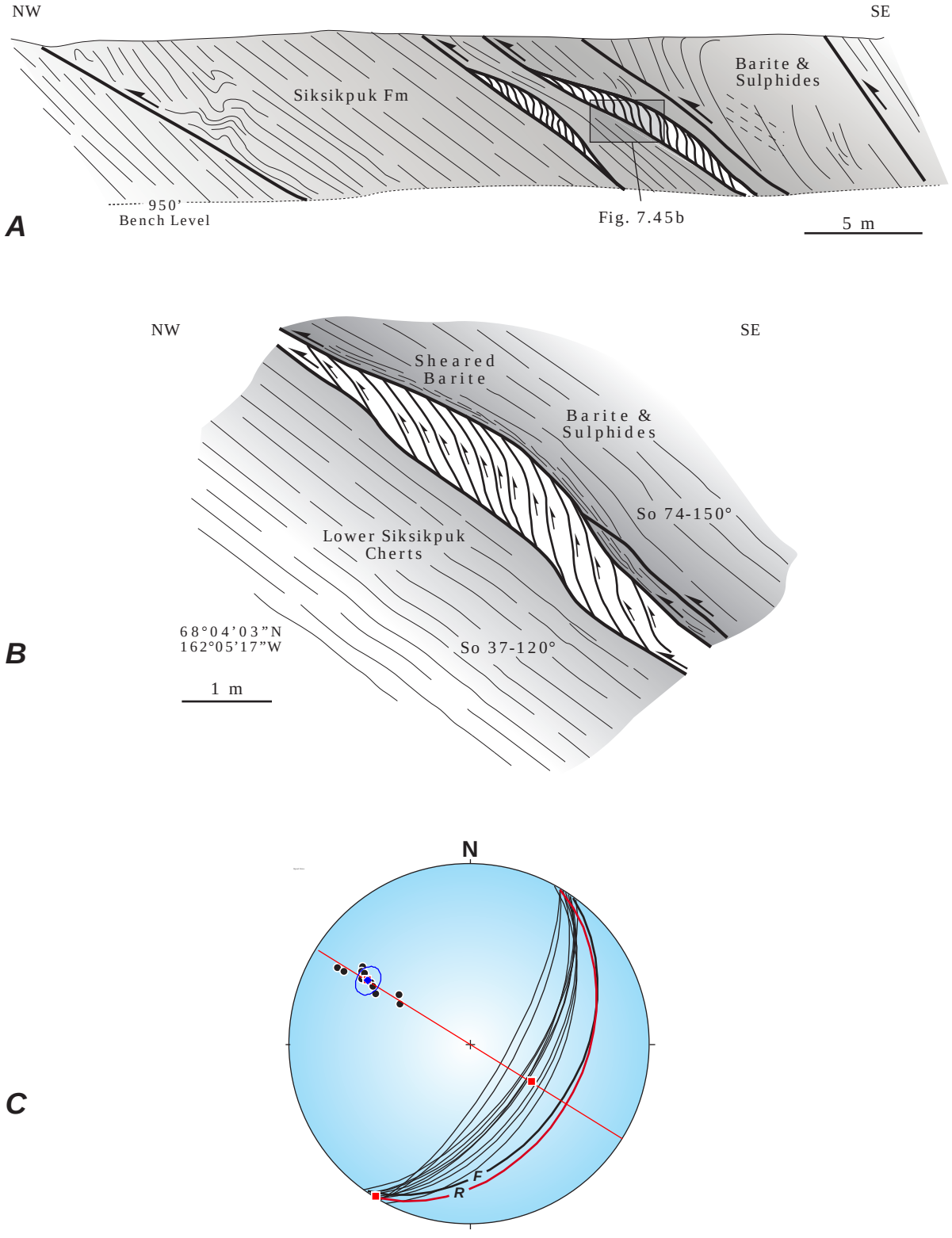


Figure 7.19. Duplex structures. **A.** Summary partial cross section of the 950' bench level, east pit wall of the Red Dog mine. Barite and sulphides are thrust over well-bedded cherts of the Siksikpuk Formation. Note SE-verging footwall duplexes developed below major thrust fault. **B.** Field sketch of duplex shown in B. **C.** Lower hemisphere equal area stereographic projection of outcrop-scale duplex structure in the 950' bench level. Poles to roof and floor thrusts, as well as link thrust faults. Roof thrust (R) (N=1), floor thrust (F) (N=1), link thrusts (N=12).

The floor and roof thrusts show consistent slip directions towards the northwest (Fig. 7.19), whereas slip vectors for individual thrust horses within the duplex are widely scattered (Fig. 7.19). The duplex structures of the Red Dog open pit are similar in dimensions, geometries, structural positions to other outcrop-scale duplex structures elsewhere in the district.

Folds in the Red Dog Open Pit

Folds exposed in the bench walls of the Red Dog open pit include fault-bend folds, fault-propagation folds, and detachment folds (Figs. 7.20 – 7.24). Strongly layered and well-bedded units (e.g. Otuk Formation) deform principally by bed-parallel flexural slip mechanisms whereas the Kivalina unit appears to deform both by bed-parallel slip as well as internal deformation that produces axial cleavages and inner arc contraction and outer arc extension. Chert layered units were deformed by flexural slip mechanisms.

Detachment Folds

Detachment folds typically occur in chert-rich units such as the lower Siksikpuk and the middle Otuk. They typically occur as NW- to NNE-trending symmetric to strongly asymmetric Type-E chevron folds (cf. Ramsay & Huber, 1987*a*) (Figs. 7.20 – 7.23). Asymmetric folds are typically grouped in metric to decametric scale trains with a NW- to NNE vergence with short overturned forelimbs and long, gently-dipping backlimbs (Figs. 7.21 & 7.22). Detachment folds are locally refolded with no consistent pattern evident. Simple bed-length balancing of fold profiles from individual bench walls indicate amounts of shortening that range from 50% to 260%. Minor fold axes display a wide distribution (Fig. 7.23).

Bedding parallel slickenlines and fold geometries indicate that the detachment folding was largely controlled by flexural slip. Fold interlimb angles typically range from 125° to 30°, average ~ 60°. Fold amplification and fold tightening is typically accommodated by minor bed-parallel thrust faults and/or development of bulbous carinate hinges (Fig. 7.22) with hinge zone thickening between chert and shale layers. These thickened hinges typically show quartz-filled saddle reef structures that locally contain up to 5 to 10% of disseminated pyrite and/or marcasite.



Figure 7.20. Detachment folds. **A.** Asymmetric detachment folds. 950' bench level Red Dog mine. **B.** Asymmetric detachment folds in the lower unit of the Otuk Formation. **C.** Refolded detachment fold in cherts of the lower unit of the Siksikpuk Formation. Note curved fold hinge. 20 cm-long notebook for scale.

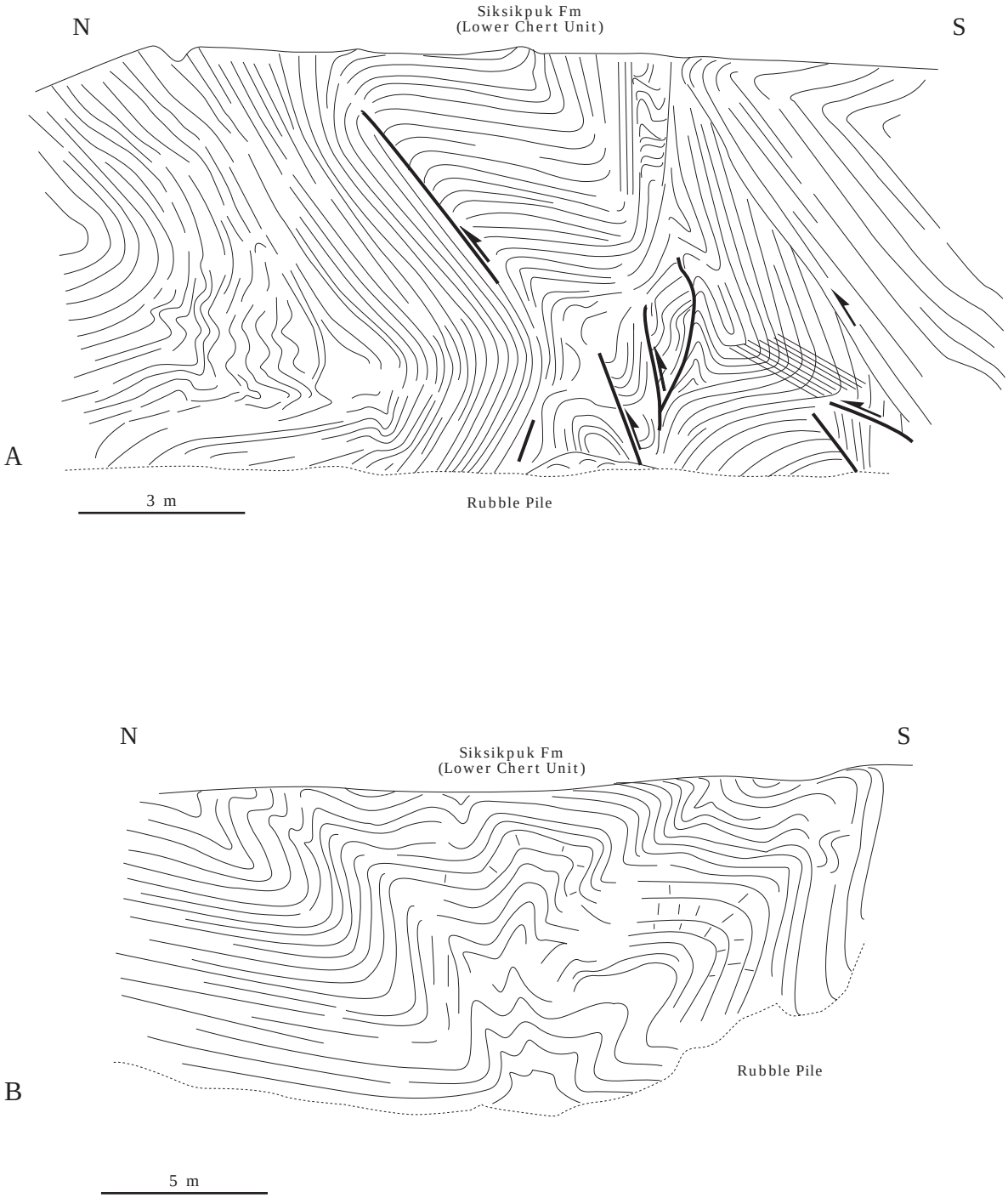


Figure 7.21. Field sketches of detachment folds. **A.** Detachment folds, 950' bench level, east pit wall. Note fold-accommodation thrust faults. **B.** Box fold in cherts of the lower Siksikpuk unit, 950' bench level Red Dog mine east wall.

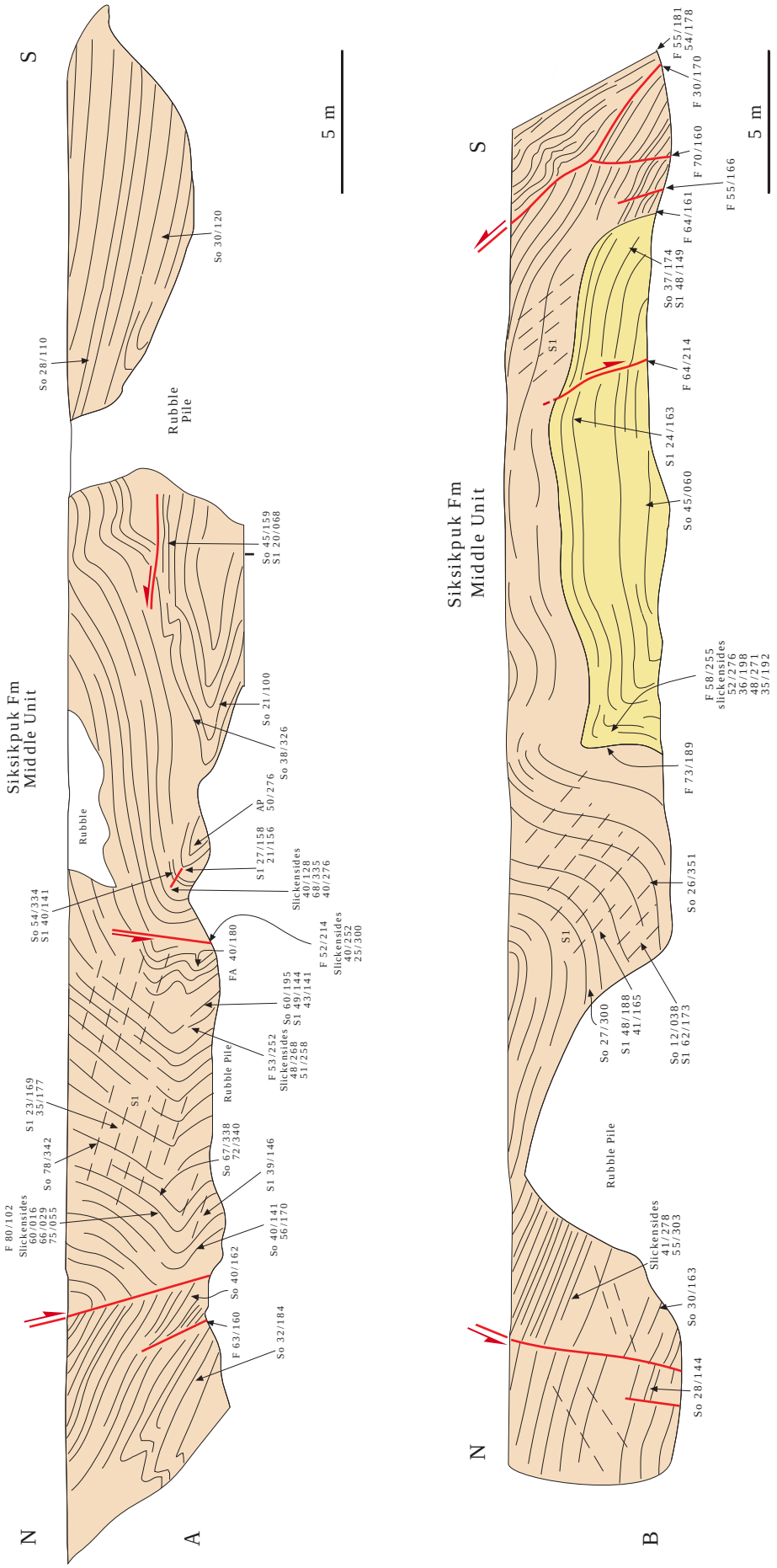


Figure 7.22. Detailed bench sections showing detachment folds in the Siksikpuk Formation. **A.** Recumbent fold in the middle shale unit of the Siksikpuk Formation. Note fold is offset by late extensional faults. **B.** Asymmetric folds in the Siksikpuk Formation, 975' bench level, east pit wall, Red Dog mine.

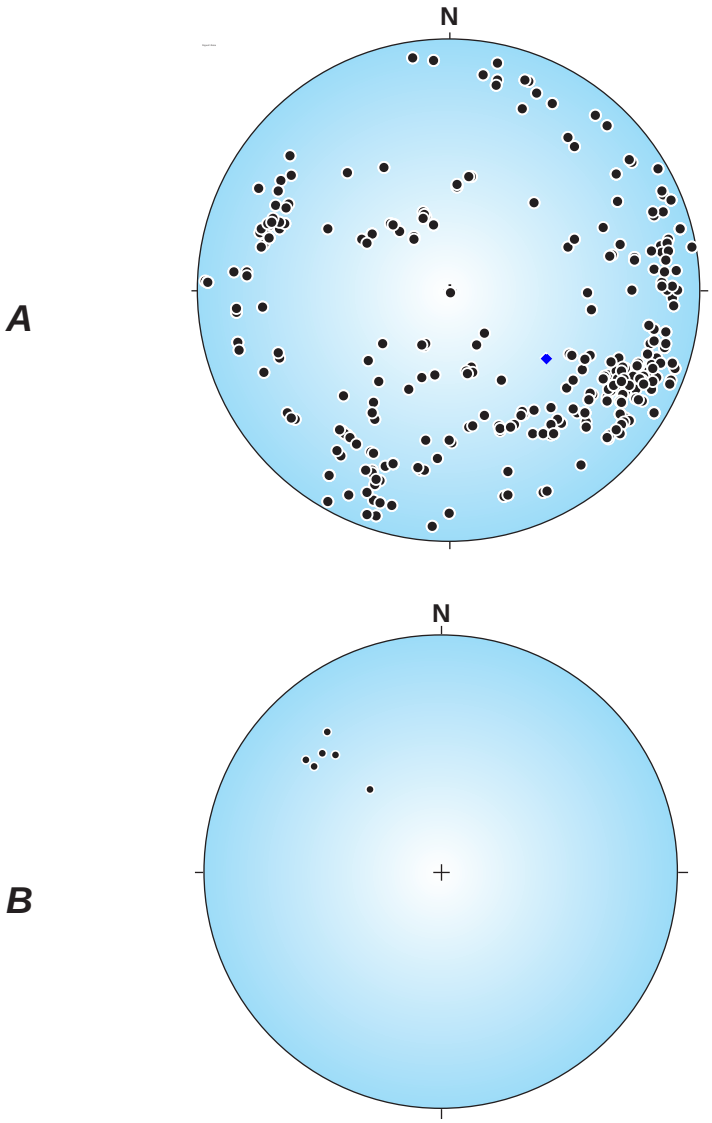


Figure 7.23. Lower hemisphere equal area stereographic projection of minor detachment fold axes in the east wall of the Red Dog mine open pit (N=396). Mean fold axis=51°/125°. **B.** Lower hemisphere equal area stereographic projection of minor fold axial surfaces (N=7).

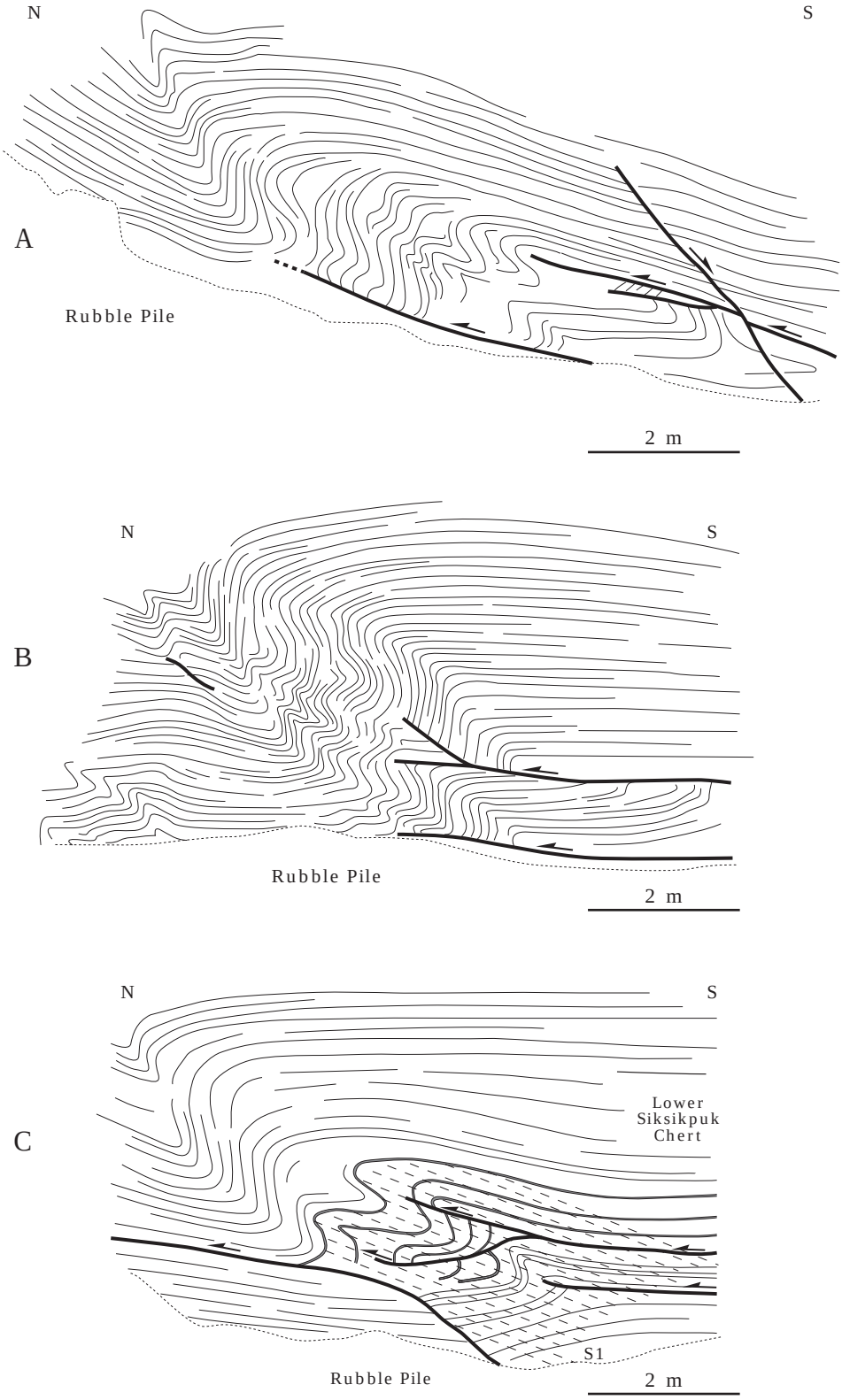


Figure 7.24. Field sketches showing examples of outcrop scale fault-related folds. **A**. Fault-propagation folds in the middle chert unit of the Otuk Formation, 1025' bench level, east pit wall. **B.** Fault-propagation folds in cherts and shales of the lower unit of the Siksikpuk Formation, 1000' bench level, east pit. **C.** Fault-propagation folds in cherts of the middle Otuk Formation in the 1050' bench level.

The detachment folds also have arrays of *en-echelon* shears veins and bedding-parallel shear veins – probably coeval with fold formation. Bedding-perpendicular quartz veins are typically rotated. Bedding-parallel fold accommodation faults are also found in some fold structures (Figs. 7.21 – 7.23). In addition chevron folds are commonly breached by younger subhorizontally-dipping, low-displacement (15 cm to 2 m) thrust faults with high (60° to 90°) cut-off angles that give rise to decapitated fold geometries (Fig. 7.22). Remobilized pyrite and/or marcasite are locally found along the thrust fault surfaces. Detachment folds wavelengths typically range from 1 to 20 m, with an average ~ 5 m. Slip surfaces with well-developed slicken-fibre lineations occur at the base of thicker beds in many of these folds.

Fault-Propagation Folds

Fault-propagation folds are typically developed in the Otuk Formation (Fig. 7.24). These typically have short, steep to overturned northern limbs and long, gently south-dipping back limbs. The associated thrust faults cut up-section through the front limb of these folds (Fig. 7.24). In places almost no footwall syncline is developed and the hangingwall fold structure is largely a transported fault-propagation fold (Fig. 7.24). These complex fault-propagation folds are best developed in the Lower Siksikpuk cherts and in the middle chert unit of the Otuk formation where flexural slip appears to be the main fold mechanism. Locally axial surface cleavages are associated with these folds (Fig. 7.24c).

Cleavage Fabrics in the Red Dog Open Pit

Cleavages are well developed in the Red Dog mine and include continuous or slaty cleavage, crenulation cleavage, and spaced cleavages (Figs. 7. 25 – 7.28). The cleavage fabrics in the Red Dog mine can be broadly correlated with regional cleavages described in Chapter 6 (cf. Chapter 6, Fig. 6.15).

Continuous (Slaty) Cleavage

In the Red Dog mine, continuous cleavage occurs as a well-developed slaty cleavage and rarely as a phyllitic schistosity. Slaty cleavage is well developed in shales of the Ikalukrok unit of the Kuna Formation, in the middle unit of the Siksikpuk Formation and in the lower unit of the Otuk Formation (Figs. 7.25 & 7.26).

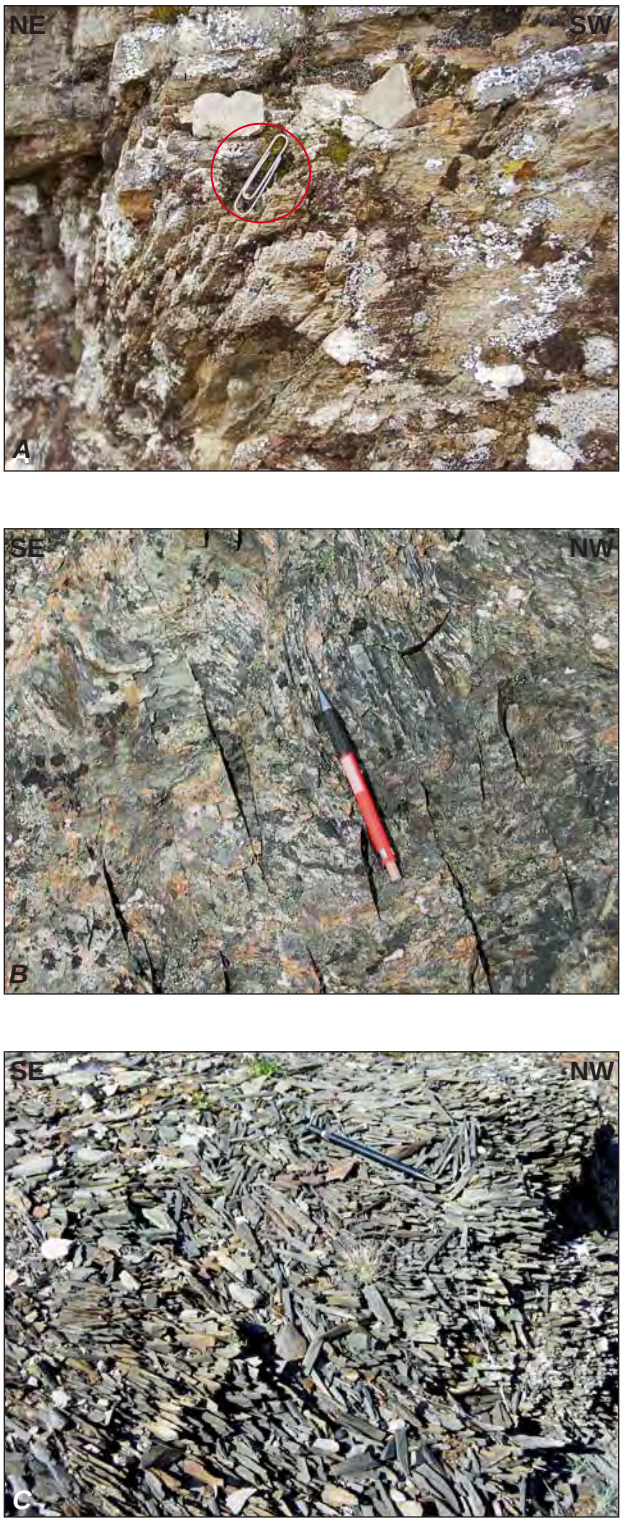


Figure 7.25. Cleavage fabrics in the east pit wall of the Red Dog mine. **A.** Detail of refracted cleavage in strata of the Siksikpuk Formation. 2 cm-long paperclip for scale. **B.** Cleavage fabrics in the lower unit of the Siksikpuk Formation. Pencil for scale. **C.** Pencil cleavage in shales of the middle unit of the Siksikpuk Formation. Pencil for scale.

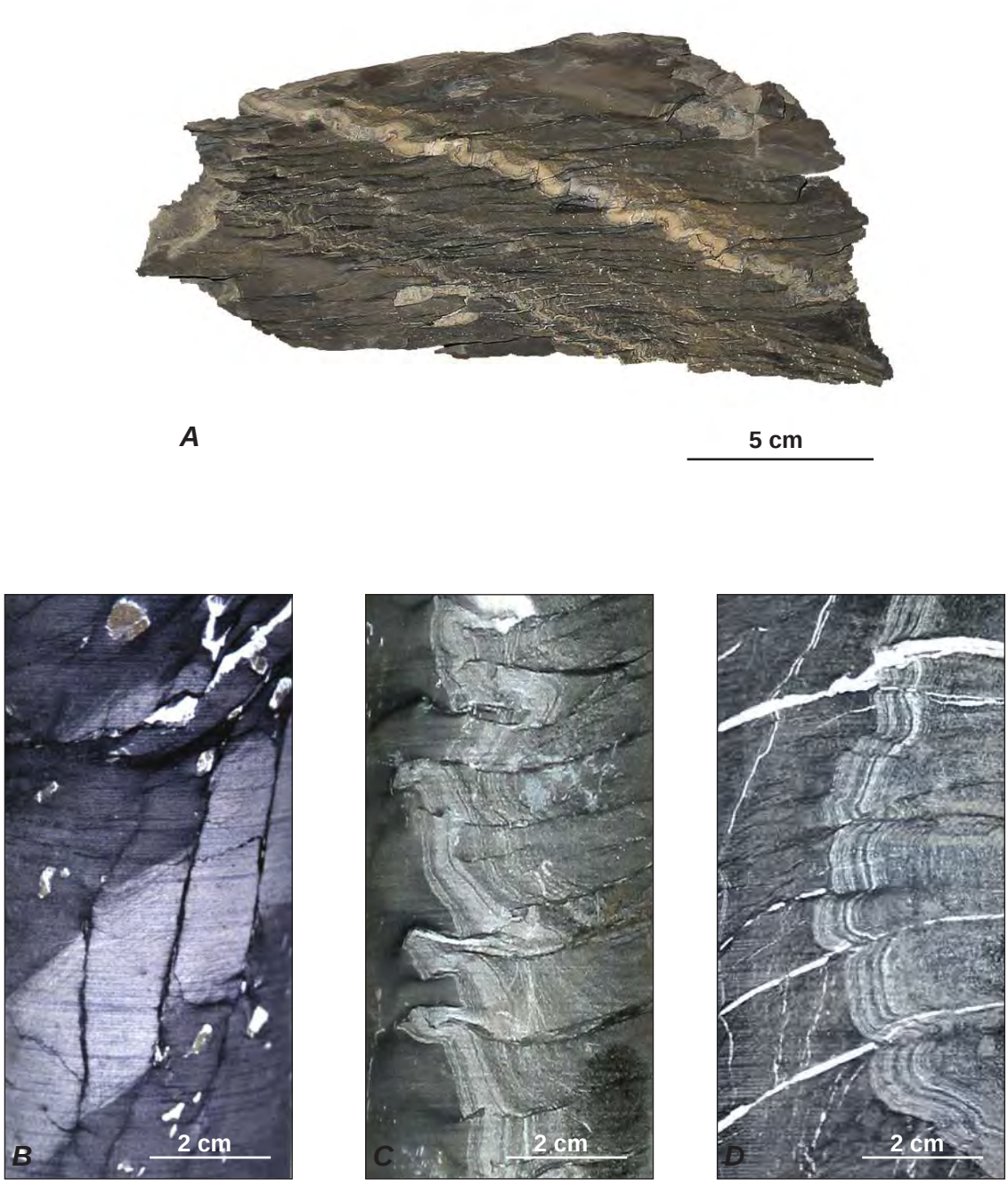


Figure 7.26. Detail of S2 cleavage fabrics in the Kivalina unit of the Kuna Formation. **A.** Hand-specimen showing spaced cleavage fabrics in black shales and calcarenites of the Kivalina unit. **B.** Photograph of drill core showing spaced cleavage. Note apparent extensional offset of layering related to loss of volume by pressure solution. **C.** Photograph of drill core showing well developed spaced cleavage seams in black shales and 'imbrications' in more competent grey-weathering calcarenite layers. **D.** Photograph of drill core showing spaced cleavage. Note calcite veins are preferentially developed along cleavage seams.

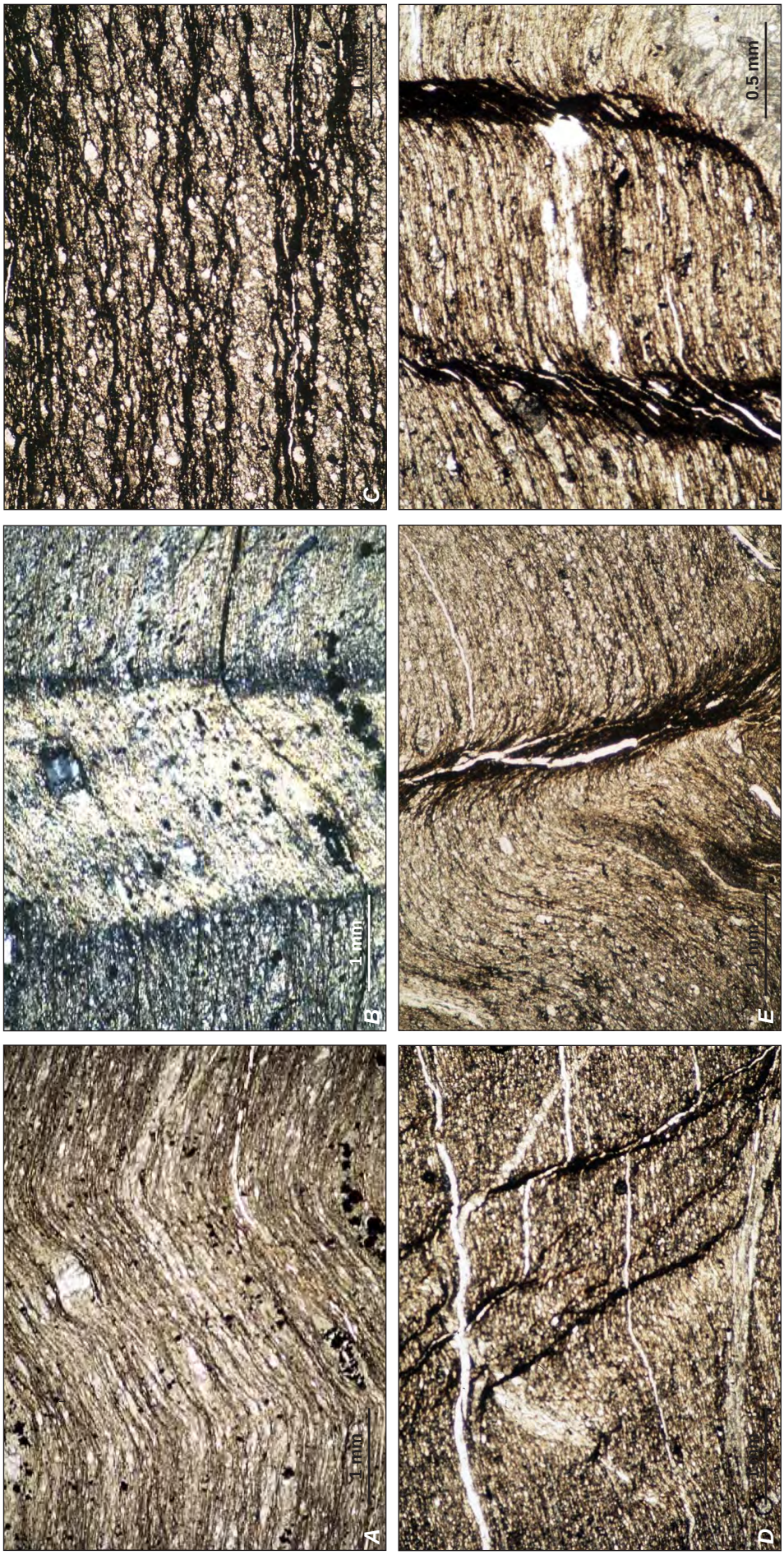


Figure 7.27. Photomicrographs showing cleavage fabrics in the east pit of the Red Dog mine. **A.** Strongly asymmetric zonal cleavage in baritic shales of the middle unit of the Siksikpuk Formation. Plane polarized light. **B.** View of A under cross polars. **C.** Anastomosing cleavage with well developed compositional domains. Note dark zones characterized by insoluble residues. Plane polarized light. **D.** View of pressure solution crenulation cleavage in calcarenites of the Kivalina unit. Plane polarized light. **E.** Asymmetric microfold associated with crenulation cleavage. Note quartz vein along cleavage seam. Plane polarized light. **F.** Detail of pressure solution cleavage seams. Plane polarized light.

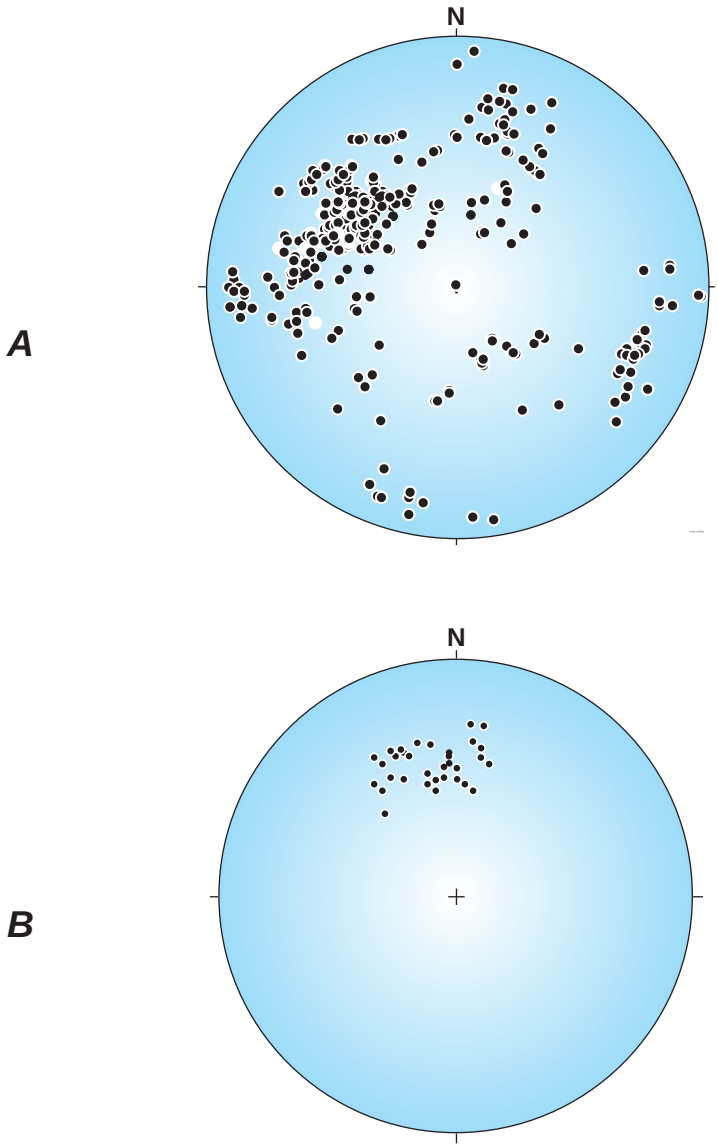


Figure 7.28. Lower hemisphere equal area stereographic projection of cleavage fabrics in the east pit wall of the Red Dog mine. **A.** Poles to slaty cleavage S1*a* in strata of the Siksikpuk and Otuk formations (N=393). **B.** Poles to S2 crenulation cleavage in strata of the Kivalina unit of the Kuna Formation (N=42).

Slaty Cleavage (S1a)

Slaty cleavage (S1*a*) is equivalent to the S1 regional cleavage documented in Chapter 6 (Figs. 6.15). In outcrop the S1*a* cleavage in the Siksikpuk Formation produces a 'wood fibre' texture but lacks the parting properties of typical slaty cleavages. In drill core, S1*a* cleavage occurs as well defined planar discontinuities that cause the cores to break into regularly spaced 'poker chips'. In thin section, the S1*a* cleavage is characterized by millimetre size elongate and lenticular microlithons of quartz and minor mica that are enveloped in discontinuous planar parallel to irregular anastomosing laminae rich in mica and/or heavy minerals (Fig. 7.27). Associated with the slaty cleavage are pressure shadows formed around disseminated pyrite grains. In zones of intense deformation the slaty cleavage (S1*a*) causes partial to complete bedding transposition. In places this slaty cleavage, especially in the middle Siksikpuk unit, has been in the past mistaken by workers in the area for bedding surfaces and/or laminations in core logging and field mapping. Clear grain size variations and radiolaria-rich layers must be used as bedding indicators. In the Ikalukrok and Kivalina units of the Kuna Formation S1*a* cleavage also occurs as a bedding-parallel stylolitic pressure solution cleavage (Fig. 7.26).

Disjunctive Cleavage

Disjunctive cleavage in the Red Dog mine occurs as spaced cleavage in competent siltstone and cherty lithologies and crenulation cleavages that are dominantly developed in calcareous shales and siltstones.

Spaced Cleavage (S1b)

Spaced cleavage is characteristic of thin- to medium-bedded and well-layered competent units (e.g. middle Otuk cherty shales and siltstones). S1*b* cleavage typically occurs as smooth parallel cleavage seams that where observed are perpendicular to sub-perpendicular to bedding with local refraction in less competent layers (Figs. 7.26 & 7.27). Cleavage spacing typically varies from 0.5 cm to ~10 cm. The S1*b* cleavage is interpreted to be equivalent to the S1*a* slaty cleavage. The spaced cleavage is preferentially developed around major fold hinges, where it forms poor to well-developed cleavage fans (Figs. 7.25 & 7.26).

Crenulation Cleavage (S2)

A crenulation cleavage is preferentially developed in the calcareous, thinly-layered to finely laminated shales and calcarenites of the Kivalina unit, of the middle Siksikpuk unit and locally in the Okpikruak Formation (Figs. 7.25 & 7.26). Crenulation cleavage occurs as a symmetric to strongly zonal, asymmetric high-angle pressure solution cleavage developed on top of a pre-existing bedding-parallel continuous slaty cleavage (S1*a*) (Fig. 7.27). The crenulation cleavage forms from pressure solution along the limbs of microfolds that vary from open and asymmetric to tight and symmetric (Fig. 7.27). The pressure solution cleavage seams are typically anastomosing, smooth to irregular and marked by accumulations of insoluble material along dissolution surfaces (Fig. 7.27). The middle Siksikpuk beds typically develop a markedly zonal asymmetric crenulation cleavage that shows zonal extinction patterns and reflectivity such that they resemble kink bands; this gives a banded appearance in outcrop associated with the domainal orientation of phyllosilicates.

The spacing of pressure solution cleavage seams typically ranges from 0.2 mm to 1 mm, in accordance with the microfold wavelengths and the amount of pressure solution shortening across them. Fold rodding lineations are produced by weathering out of minor fold hinges of the closely-spaced crenulation cleavages.

In the Kivalina unit, crenulation cleavage (S2) commonly causes apparent bedding/laminae offsets that typically range from 0.1 to 3 cm with an average ~0.5 cm, (Fig. 7.26). Millimetre to centimetre scale imbrications of calcarenite layers (Fig. 7.26) also occur. Calcite is preferentially remobilized along the main pressure solution cleavage seams (Fig. 7.27). Measurements from 10 ~1 m-thick core intervals give a volume loss by pressure solution in the Kivalina unit ranges from 5% to as much as 45%. The bulk strain accommodated by pressure solution cleavage development may account for the lack of observable mesoscopic folds in strata of the Kivalina unit.

Late Extensional Faults in the Red Dog Open Pit

Pit wall mapping during the course of this research identified a series of previously unrecognised NW-trending, SW-downthrown, high-angle planar late extensional faults faults. These are well exposed in the east pit wall of the Red Dog mine (Figs. 7.29 –

7.31). These extensional faults are dominantly parallel or slightly oblique to the bench walls of the Red Dog open pit (Fig. 7.10) being difficult to identify except where bench collapse has exposed polished fault surfaces. They are generally steeply dipping (Fig. 7.31) and fault-bedding cut-off angles typically range from 60° to 90°.

The extensional fault zones vary from knife-edge surfaces to approximately 20 cm- to 1 m thick fault breccias and gouges. Fault surfaces are planar to wavy and are locally refracted across changes in stratigraphy. Slickenlines, slicken-fibre lineations, and grooving indicate at least two episodes of movement (Figs. 7.29 & 7.31) with local development of 5 sets of fault slip lineations. These indicate an earlier oblique-slip motion and a later dip-slip reactivation.

These extensional faults exposed in the Red Dog open pit are the youngest structures. They post-date the thrust deformation and emplacement of the allochthons of the Red Dog district, offsetting the Main orebody as well as offsetting early syn-orogenic strata of the Okpikruak Formation. These NW-SE-trending extensional faults may be related to the Wrench Creek and Sivukat Mountain faults (Chapter 6). In addition to the extensional faults identified in the open pit a series of WNW-ESE- to NW-SE-trending lineaments extend from the Red Dog mine to the Sivukat Mountain fault (Fig. 7.6).

The vertical throws on these extensional faults in the open pit commonly range from only a few centimetres to 75 m or more. Typically associated with the large extensional faults are zones of closely-spaced planar joints and/or veins filled with quartz. Centimetre to decimetre thick fault gouges are locally developed in more incompetent lithologies such as the Ikalukrok unit.

Sulphide Deformation Features in the Red Dog Open Pit

Rocks exposed in the mineralized sections of the Red Dog open pit include –

a) Massive sulphides (>70% sulphides) consisting of fine to medium-grained banded pyrite, sphalerite and galena;
b) Semi-massive sulphides (40-70% sulphides) consisting of banded to laminated fine-grained pyrite, sphalerite and galena with interbedded silicified black shales cherts and in places barite;

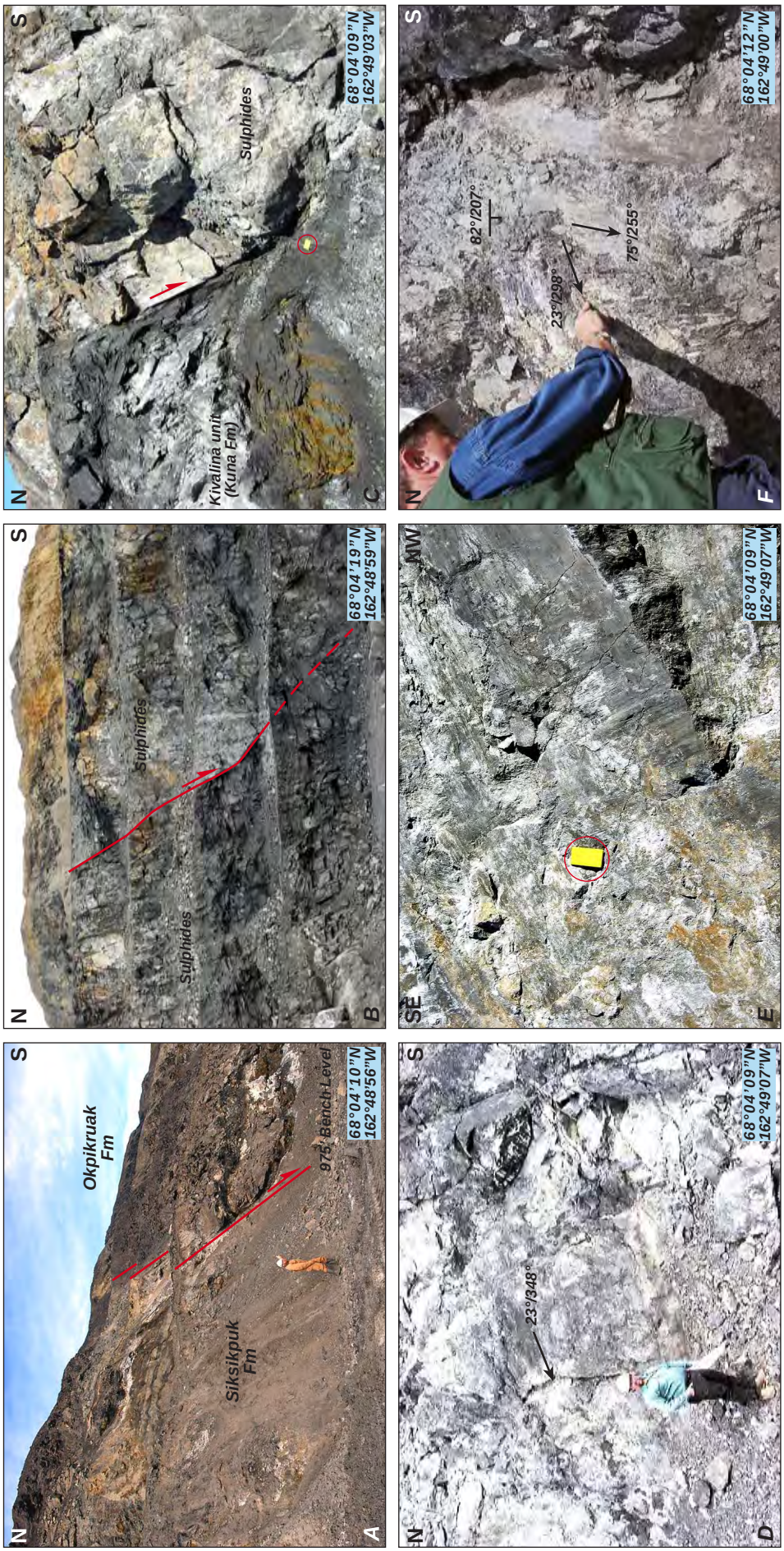


Figure 7.29. Extensional faults in the east pit wall of the Red Dog mine. **A.** E-looking oblique view of late extensional fault. Fault juxtaposes Early Cretaceous Okpikruak Formation (hangingwall) against Pennsylvanian strata of the Siksikpuk Formation. Teck Cominco geologist Scott Jennings for scale. **B.** E-looking view of high-angle extensional fault in the northeast pit. Bench walls are 7 m high. **C.** E-looking view of high angle extensional fault. Fault juxtaposes veined silica rock (hangingwall) against Early Mississippian strata of the Kivalina unit of the Kuna Formation. Note kinematic indicators in the footwall to the fault. Bench wall is 7 m high. 950' bench level. **D.** E-looking view of fault surface. Note slickenfibres and grooving. Geologist Neil O'Brien for scale. 950' bench level. **E.** Detail of NW-trending fault surface. Note two orthogonal generations of slickenlines. 20 cm-long notebook encircled for scale. **F.** Detail of extensional fault. Ken McClay for scale. 950' bench level.

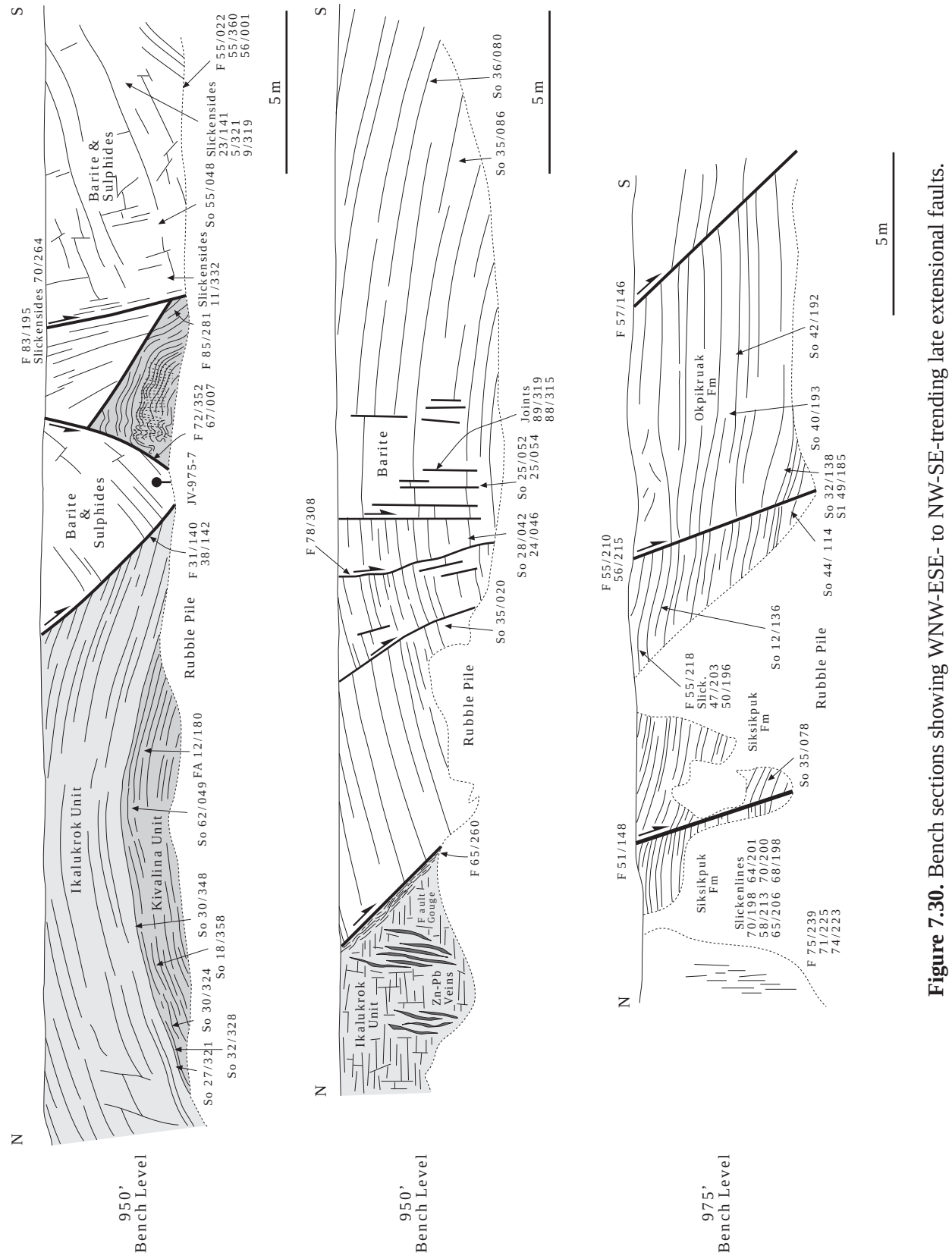


Figure 7.30. Bench sections showing WNW-ESE- to NW-SE-trending late extensional faults.

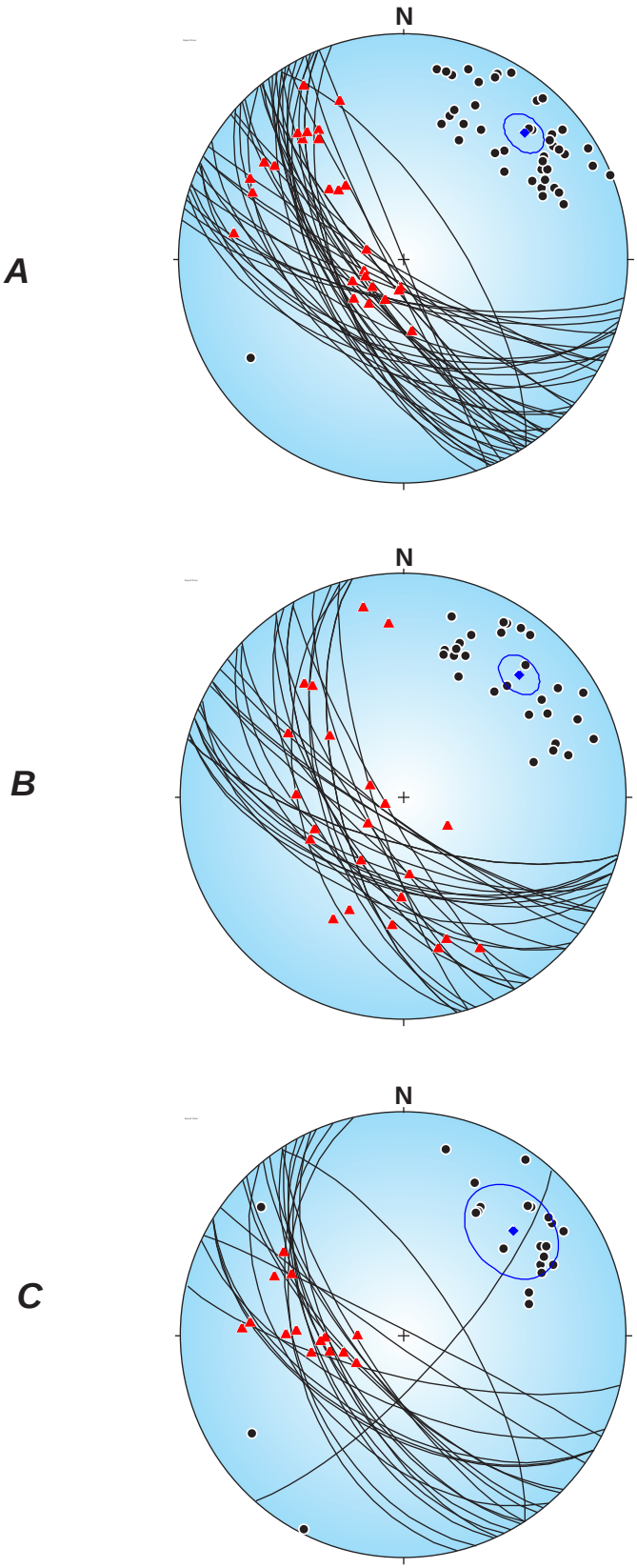


Figure 7.31. Lower hemisphere equal area stereographic projection of late extensional faults in the Red Dog mine. **A.** Great circles and poles to extensional faults (solid circles) (N=50) and slickenline lineations (solid triangles) (N=25). 925' bench, east pit Red Dog mine. Note two families of slickenline lineations, a dip slip and oblique slip. Mean fault surface= 68°/224°. **B.** 950' extensional faults. Great circles and poles to extensional faults (solid circles) (N=31) and slickenline lineations (solid triangles) (N=22) **C.** Great circles and poles to extensional faults (solid circles) (N=25) and slickenline lineations (solid triangles) (N=13). 1025' bench level, east pit wall.

c) Sulphide-bearing silica rock (<40% sulphides) – a whitish grey rock consisting of fine-grained to medium-grained euhedral quartz crystals with disseminated and semi-massive sulphides;
d) Sulphide and silica veined silicified Ikalukrok shales;
e) Vein-breccia mineralization consisting of coarse-grained sphalerite cross-cutting brecciated silicified shales and cherts;
f) Massive and banded barite.

Massive Sulphides and Semi-Massive Sulphides

The massive and semi massive sulphide mineralization show well-preserved delicate sulphide textures (e.g. pyrite and marcasite overgrowths, framboidal and colloform pyrite) indicating that the mineralization was not strongly deformed. Well-preserved textures including 'buckshot' sphalerite and disseminated galena are also present in the massive and banded sulphides. Where they are deformed the sulphides are sheared on millimetre to centimetre scale shear surfaces. Sulphide microstructures include deformation twins in coarse-grained sphalerite, indented pyrite framboids and pressure solution seams in semi-massive layered sulphides. Elongated worm tubes in silica rock and sulphide-bearing barite indicate high amounts of strain near the footwall of the Main deposit in the vicinity of the west pit (Fig. 7.32).

Sulphide Vein-Breccias and Sulphide Veins

Coarse-grained sphalerite and galena veins and vein-breccia mineralization are common in the lower part of the Main deposit (Figs. 7.32 & 7.33a, b). Zn-Pb veins occur in the Ikalukrok unit and also locally in the Kivalina unit (Fig. 7.33a). Zn-Pb vein-breccia mineralization and Zn-Pb veins are restricted to the syn-rift strata and do not extend into the Etivluk Group. Sulphide veins occur at the base, margins, and also within the main zone of massive mineralization. The vein and breccia systems that occur at the base of the Main deposit (Fig. 7.33a, b) may possibly be part of a vent or feeder zone (cf. Goodfellow *et al*. 1993) (cf. Chapter 3, Fig. 3.14).

Zn-Pb Vein-Breccias

Zn-Pb vein-breccias typically consist of centimetre to tens of centimetre sized angular equiaxed to elongate clasts of silicified black shales of the Ikalukrok unit separated by

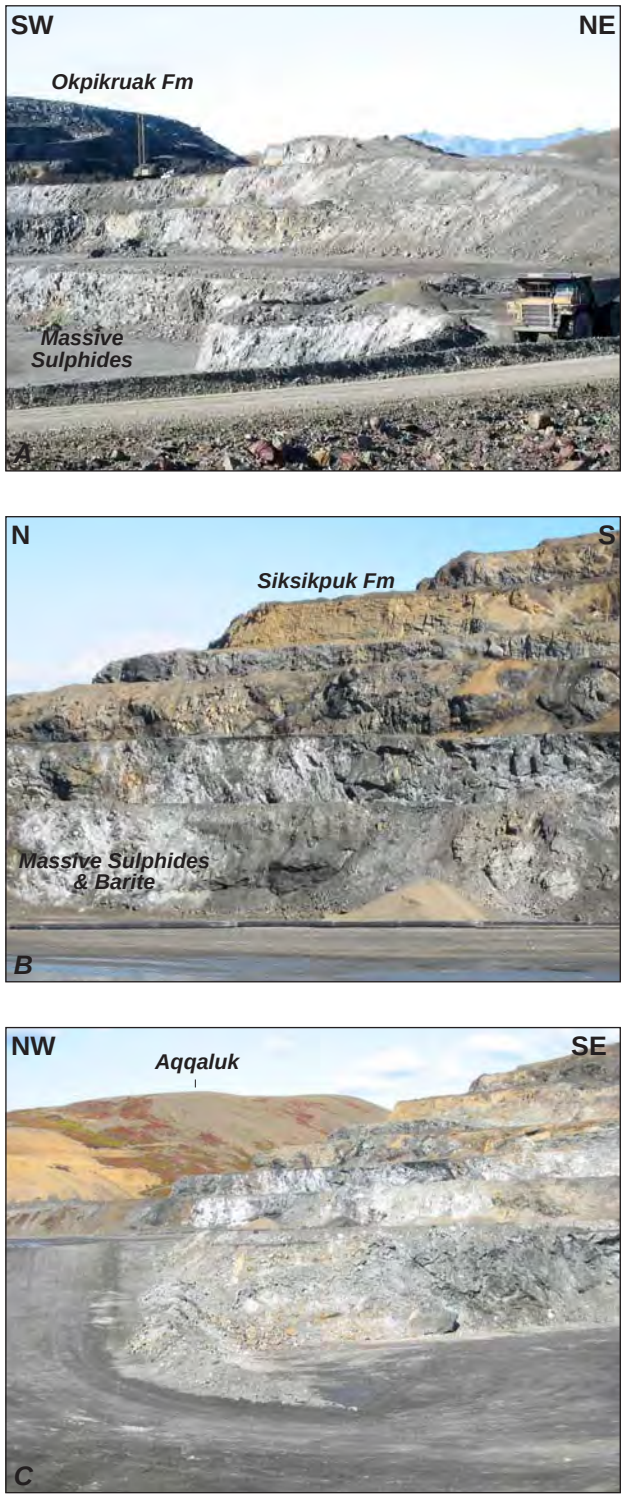


Figure 7.32. Main deposit. **A.** NW-looking view of massive sulphides. Bench walls are approximately 7 m high. **B.** View of the contact between sulphides and barite and the overlying Siksikpuk Formation. Bench walls are approximately 7 m high. **C.** Detail of massive sulphides. Bench walls are approximately 7 m high. The Aqqaluk lies in the background.

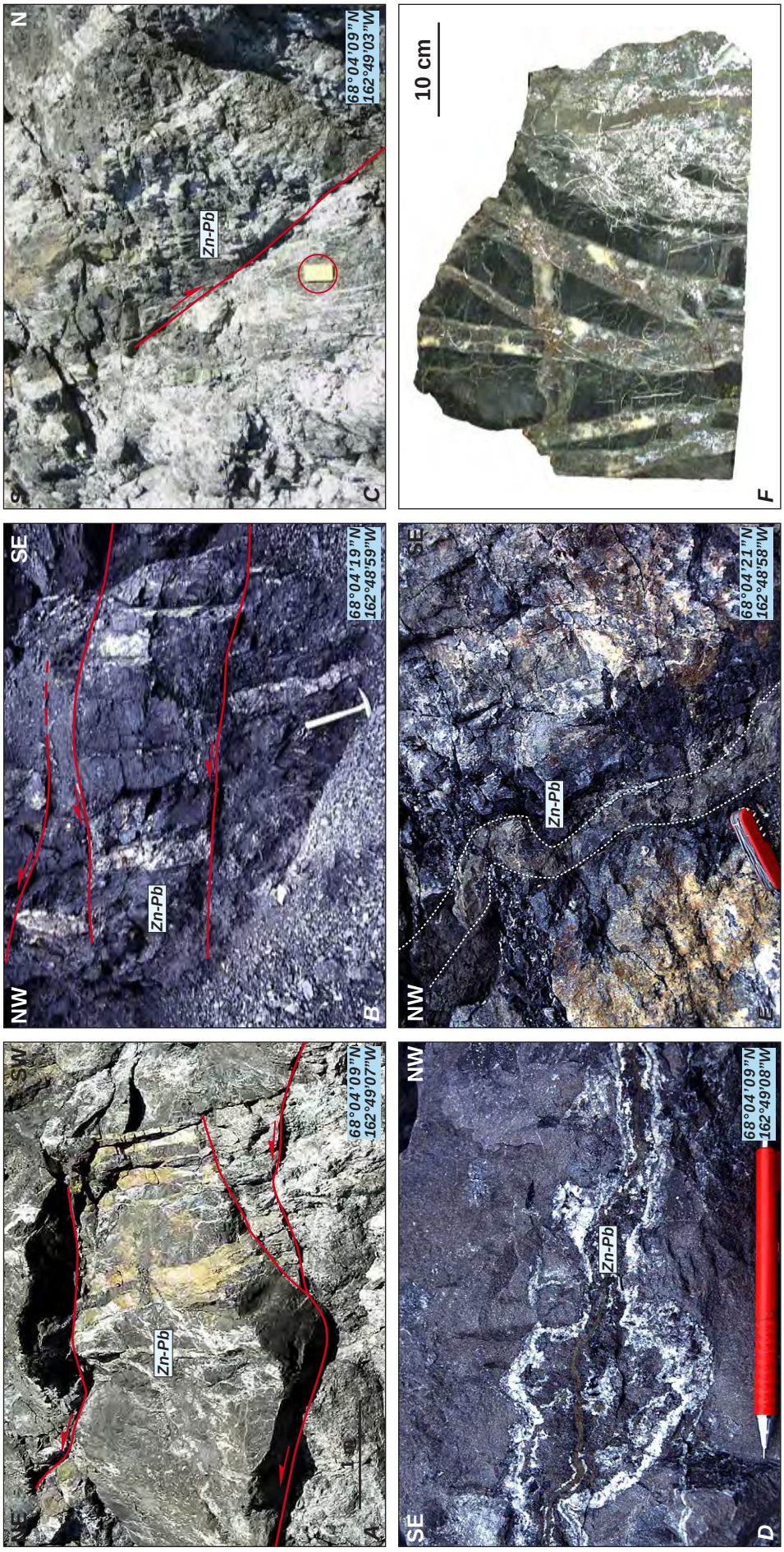


Figure 7.33a. Sulphide veins. **A.** Planar sphalerite veins in silica rock. 950' bench level, east pit wall. Note veins are offset by subhorizontally-dipping thrust faults. **B.** Sulphide veins in silicified black shales of the Ikalukrok unit. 975' bench level, east pit wall. Note metric offset along thrust faults. **C.** Vertical to sub-vertical veins in massive sulphides. 925' bench level, east pit wall. Note late extensional fault. 20 cm-long notebook is encircled for scale. **D.** Irregular symmetric vein in brecciated sulphides. 875' bench level, east pit wall. Note quartz in the vein margins. **E.** Pyrite vein in sulphide-bearing silica rock. 8 cm-long pocket knife for scale. **F.** Photograph of polished section showing veins brown red sphalerite. Note different cross cutting sets. Sample from the 925' bench level, east pit wall.

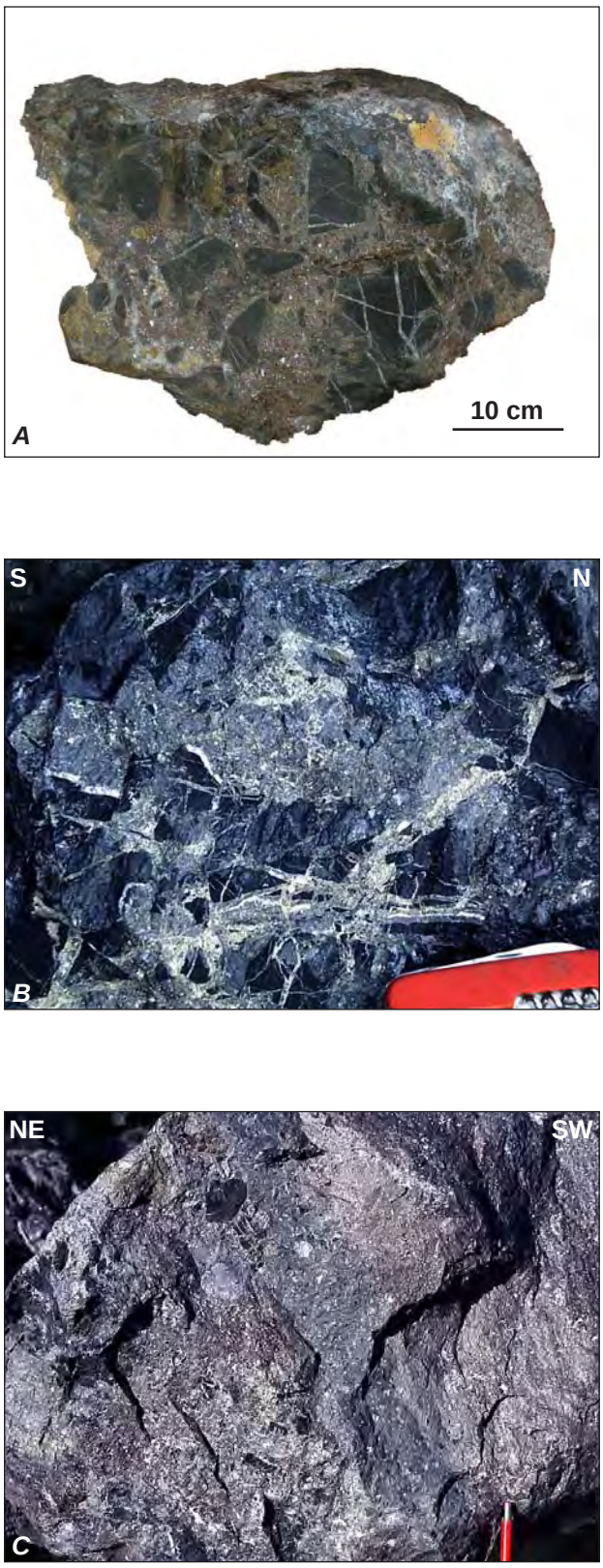


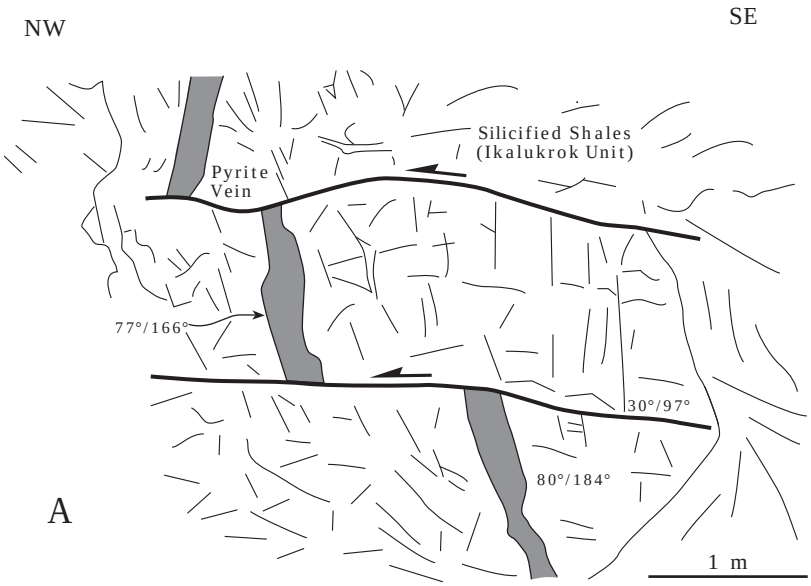
Figure 7.33b. Breccia ore. **A.** Hand specimen of mineralized breccia. **B.** Vein-breccia mineralization. Note angular clasts. 10 cm-long pocket knife for scale. **C.** Sulphide breccia with angular and rounded clasts. Pencil for scale.

multistage veins of fine- to coarse-grained, cream to red-brown sphalerite and yellow to green brassy pyrite (Fig. 7.33b). The angular clasts are themselves internally veined by single to multiple sets of hairline to 0.2 cm narrow pyrite ± sphalerite veins (Fig. 7.33b). Some clasts are mineralized with disseminated 'buckshot' sphalerite and framboidal pyrite. Cockade structures are commonly developed (cf. Hibbard, 1995). Mosaic and crackle breccia textures are also locally developed at the borders of the main zones of brecciation. Vein breccias also contain a fine-grained tan sphalerite in some places. Zones of vein-breccias grade laterally into non-brecciated silicified shales and poorly laminated to banded sulphides. The degree of brecciation apparently decreases to the north of the Main deposit grading laterally into poorly banded sulphides. The Vein breccia bodies are locally moderately to steeply dipping and trend north to northwest. Sulphide only breccias also occur and consist of rounded to sub-angular sphalerite rich fragments in a sulphide matrix (Fig. 733b).

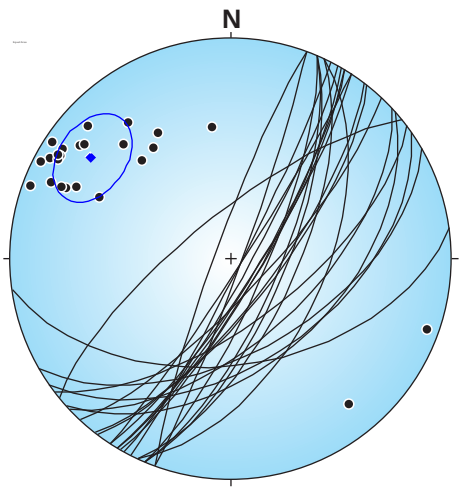
Sulphide-Quartz Veins

Sulphide - quartz veins in the Red Dog open pit mainly occur in the Ikalukrok units of the Kuna Formation, in the sulphide orebody and locally in the Kivalina unit. Pyrite veins associated with steeply-dipping felsic intrusives were also noted, that cropped out (and also found in drill core) in the southeast end of the mine pit before they were mined out in 2001.

The main gangue mineral in these veins is quartz but calcite and dolomite occur locally where the veins crosscut the Kivalina unit. The sulphide-quartz veins are dominantly NNE trending and steeply ESE- to WNW-dipping (Fig. 7.34). The veins vary from planar, parallel sided to irregular shaped, and typically vary in width from hairline fractures to veins as thick as 1 m. The veins crosscut bedding, sulphide-bearing silica rock and massive sulphides at high angles (60° - 90°) to the bedding or enveloping surfaces. Vein densities range from ~5 to ~25 veins per metre and vein spacings typically range from ~10 cm to ~5 m (Fig. 7.33a). Zones of closely spaced veins form high-grade ore that is mined. Pyrite and quartz veins commonly crosscut clasts of host rocks that are themselves veined by fine-grained sphalerite. Barite veins, although less common, also occur locally and may include hairline to 1 cm thick laminae of sphalerite, galena and/or pyrite.



A



B

Figure 7.34. Sulphide veins. **A.** Field sketch of NNE-trending sulphide veins offset by subhorizontally-dipping thrust faults. Thrust fault displacement ranges from 75 cm to 1 m. **B.** Lower hemisphere equal area stereographic projection of sulphide veins (N=25) in silicified black shales of the Ikalukrok unit of the Kuna Formation. Mean vein=67°/126°.

The sulphides in the veins range from monomineralic pyrite, sphalerite or marcasite to mixtures of coarse-grained red brown sphalerite, fine-grained galena, marcasite, pyrite and quartz (Fig. 7.33a). Polymineralic veins are dominantly planar parallel, single segment veins with multiple generations of coarse-grained brown to red-brown sphalerite, fine-grained pyrite and marcasite, fine-grained galena, milky quartz, chalcedony, and barite (Fig. 7.33a). Commonly associated with late quartz crystals in the central part of these veins are disseminated blebs (0.5 to 2%) of brittle black pyrobitumen that locally forms well-defined trails parallel to the vein margins. Barite also locally occurs in the centre of the veins.

The sulphide-quartz veins are locally cut by low-angle (10° to 30°) thrust faults, and folded by thrust-fault related folds (Fig. 7.33a). In places they are also transected by pressure solution cleavage seams.

Massive and Banded Barite

The massive barite massive cap that overlies the main sulphide orebody is commonly folded into centimetre to metre scale disharmonic and polyharmonic folds marked by fine-grained pyrite laminae. Local pressure solution textures occur in barite and sulphide-bearing barite and a planar spaced pressure solution cleavage in barite rich intervals also occurs. Barite shows evidence of plastic deformation and recrystallization.

West Wall in the Red Dog Open Pit

The west pit wall of the Red Dog mine exposes the contact of the massive and semi-massive sulphides of the Main deposit and the footwall consisting of highly deformed strata of the Okpikruak Formation (Figs. 7.35 & 7.36). The contact is a NW- to N-trending and E- to SE- dipping highly deformed mélange zone cut by complex fault systems (Fig. 7.37).

The Okpikruak Formation in the west wall of the open pit is an olistostromal unit that has been deformed into a complex mélange zone at the base of the orebody. This belt of highly deformed and disrupted strata forms a narrow belt, approximately 20 to 300 m wide with pinched-out wedges of sandstones of the Okpikruak formation and shales of

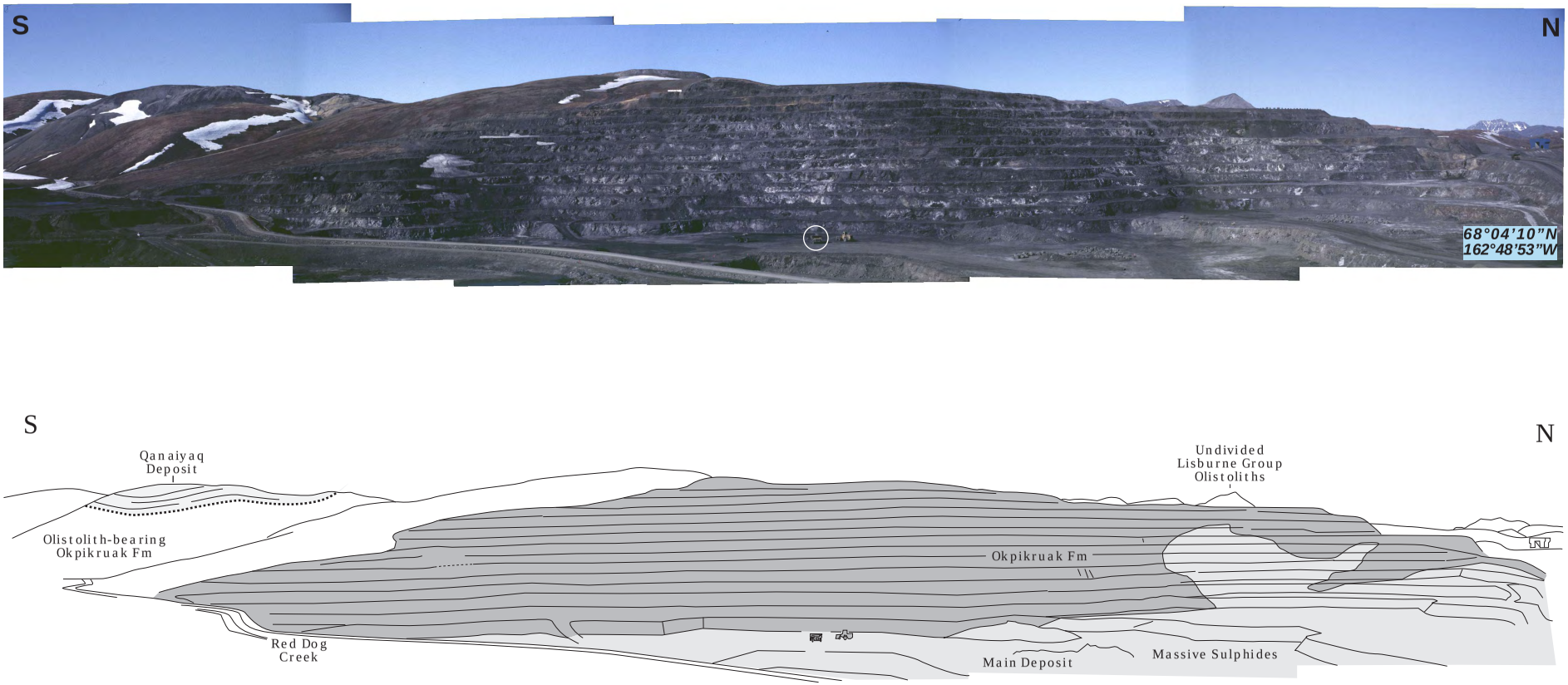


Figure 7.35. W-looking photomosaic of the west pit wall of the Red Dog mine. The Qanaiyaq deposit lies in the left in the background. Topographic relief is approximately 200 m. Field of view is approximately 1km Individual bench walls are approximately 7 m high. 80 Tn truck is encircled for scale.

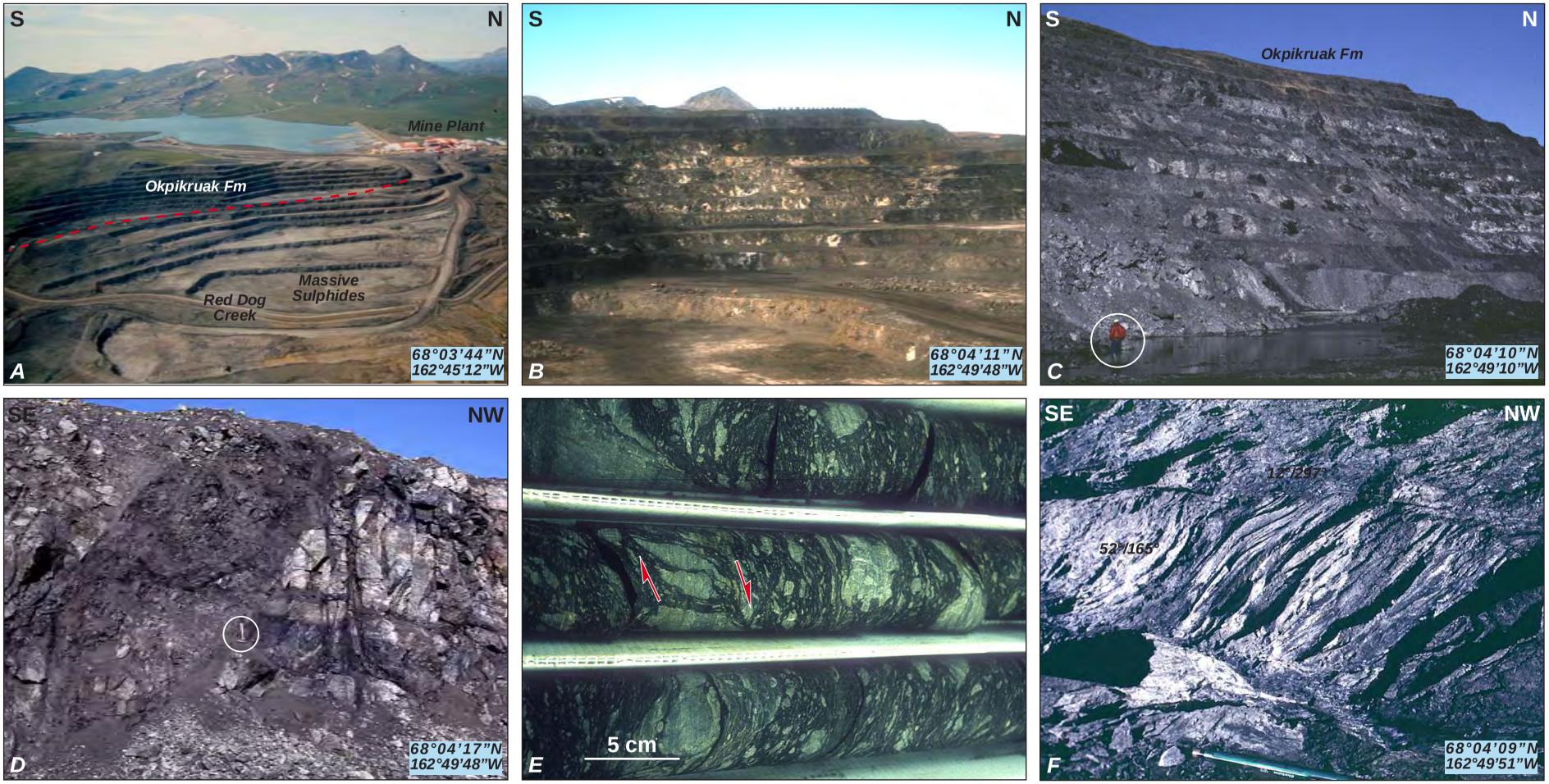


Figure 7.36. Structural features in the west pit wall. **A.** W-looking oblique aerial view of the Red Dog mine showing the contact between massive sulphides and the Okpikruak Formation along the west pit wall. Individual bench walls are approximately 7 m high. **B.** W-looking view showing the contact between the Main orebody and the Okpikruak Formation. Individual bench walls are approximately 7 m high. **C.** Detail of the west pit wall. Note collapse of benches. Ken McClay for scale. **D.** Detail of fault zone in massive sulphides. Geological hammer is encircled for scale. **E.** Detail of drill core showing melange and shear fabrics in the Okpikruak Formation in the footwall of the Main deposit. **F.** Detail of shear bands in shales of the Okpikruak Formation in the 975' bench level. Pencil for scale.

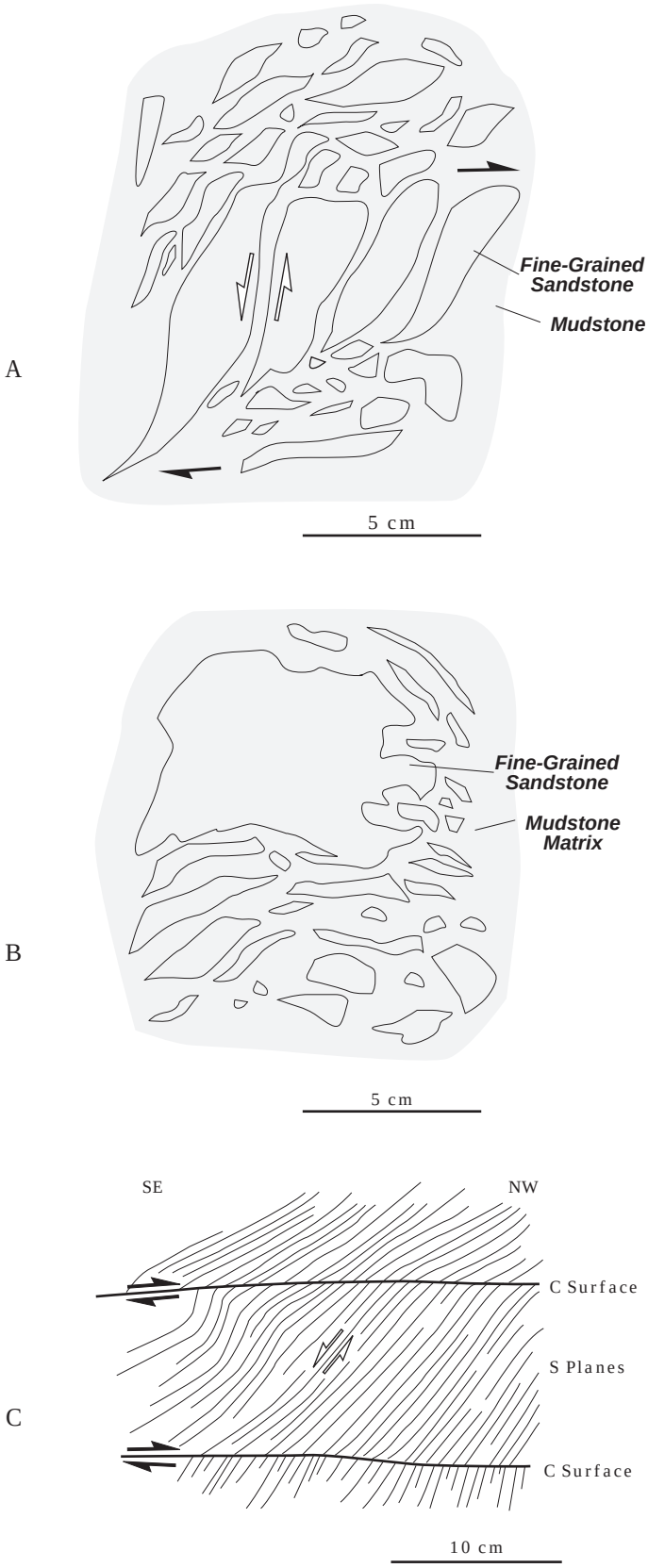


Figure 7.37. Details of deformation features in Okpikruak Formation melange in the 975' bench level of the Red Dog mine. **A.** Detail of shear fabrics. **B.** Soft-sediment deformation features. **C.** Detail of S-C fabrics in mudstones of the Okpikruak Formation.

the Etivluk Group. The disrupted zone grades laterally and vertically into olistostromes and well-bedded siliciclastic strata of the Okpikruak Formation.

This Okpikruak mélange consists of deformed, boudinaged and sheared centimetre to tens of metre sized fragments of Okpikruak sandstones as well as cherts of the Siksikpuk Formation and Otuk formations (Fig. 7.36). Fragment composition indicates provenance from both the Red Dog plate (e.g. Ikalukrok unit) and the Wolverine Creek plate (e.g. undivided Lisburne Group). The fine-grained mélange matrix shows a distinctive phacoidal scaly cleavage with polished carbonaceous surfaces (Fig. 7.36e) dominantly parallel to the margins of elongate mélange blocks. Contacts between the mélange matrix and coherent rock fragments are discrete brittle planar fault surfaces or show progressively disruption, grading into the deformed Okpikruak Formation. Many of the fragments and blocks display polished surfaces and 10 to 20% are internally brecciated showing intricate networks of millimetre to centimetre brittle fractures and microfractures that are infilled with quartz and/or Okpikruak Formation matrix. Folds in the west pit wall are rare and typically occur as poorly defined metre-scale rootless fold hinges, possibly indicating soft sediment deformation (Fig. 7.38).

The scaly cleavage in the mélange system is interpreted to be the result of strong simple shear deformation of poorly consolidated sediment under high pore fluid pressure conditions. The presence of veins filled with fine-grained sandstone, irregular-shaped fragements lacking internal structure together with deformed fragments with elongated necks or tails, diffuse grain boundaries, and rootless fold hinges indicate deformation of poorly-consolidated water-saturated sediments.

7.2.3 Aqqaluk Deposit

The Aqqaluk deposit is located immediately north of the Main deposit (Figs. 7.2 & 7.3). It is NNE- to NW trending lens-shaped strata-bound body. The southern distal margin of the mineralization is poorly exposed and is concealed by rubble outcrops of massive barite and shales of the Siksikpuk Formation. Drill hole data suggest that the Aqqaluk deposit has a wedge geometry and is approximately 100 to 200 m thick, and 650 to 870 m wide. The deposit is preserved in a southerly-dipping and northerly-verging thrust sheet (Fig. 7.39). The base of the deposit is a tectonic mélange in strata of the Kivalina

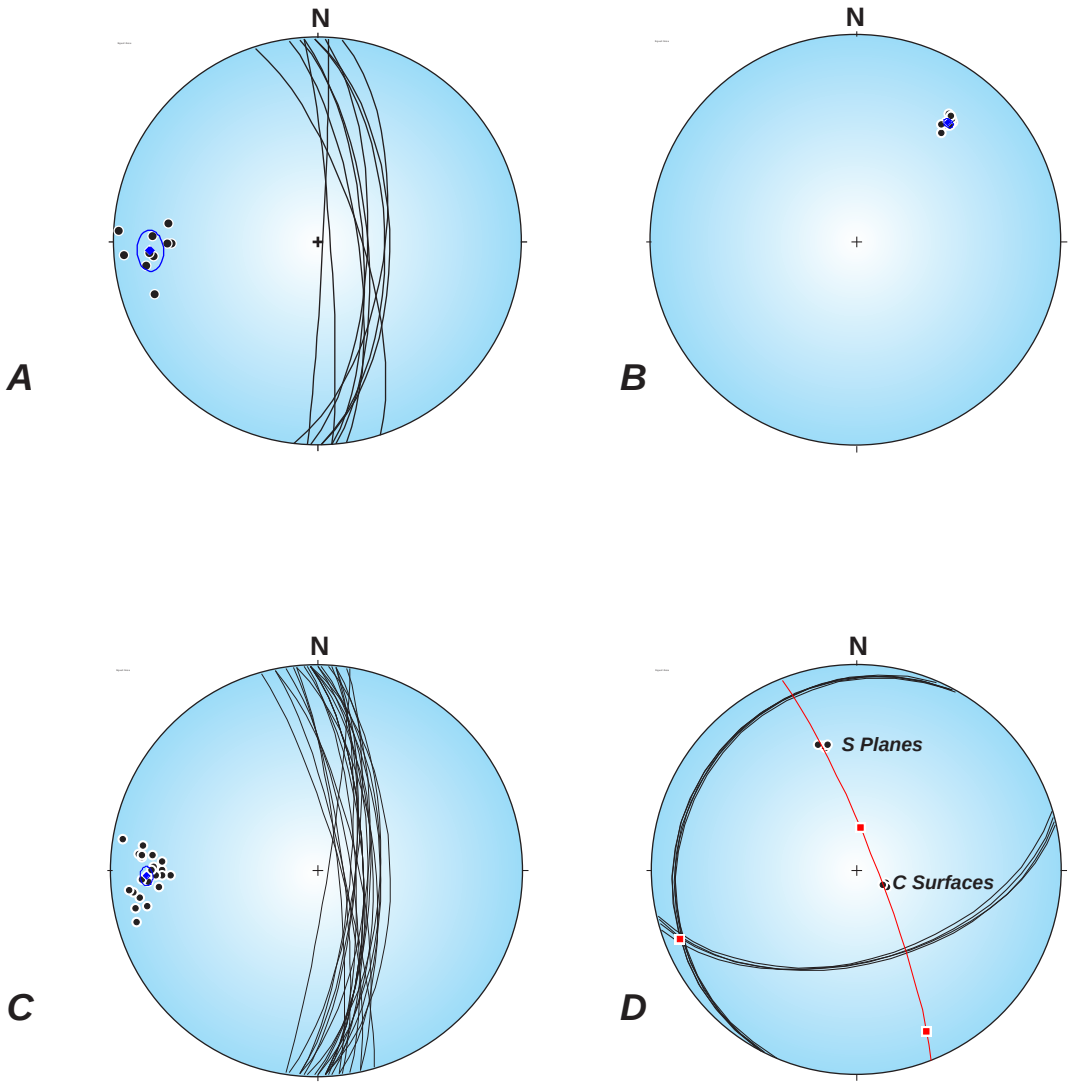


Figure 7.38. Lower hemisphere equal area stereographic projection of structural data from the west pit wall of the Red Dog mine. **A.** Great circles and poles to the contact between the Main deposit and Okpikruak Formation melange (N=10). **B.** Minor fold axis in strata of the Okpikruak Formation (N=6). **C.** Great circles and poles to extensional faults (N=25). **D.** Great circles and poles to shear fabrics in strata of the Okpikruak Formation (N=7).

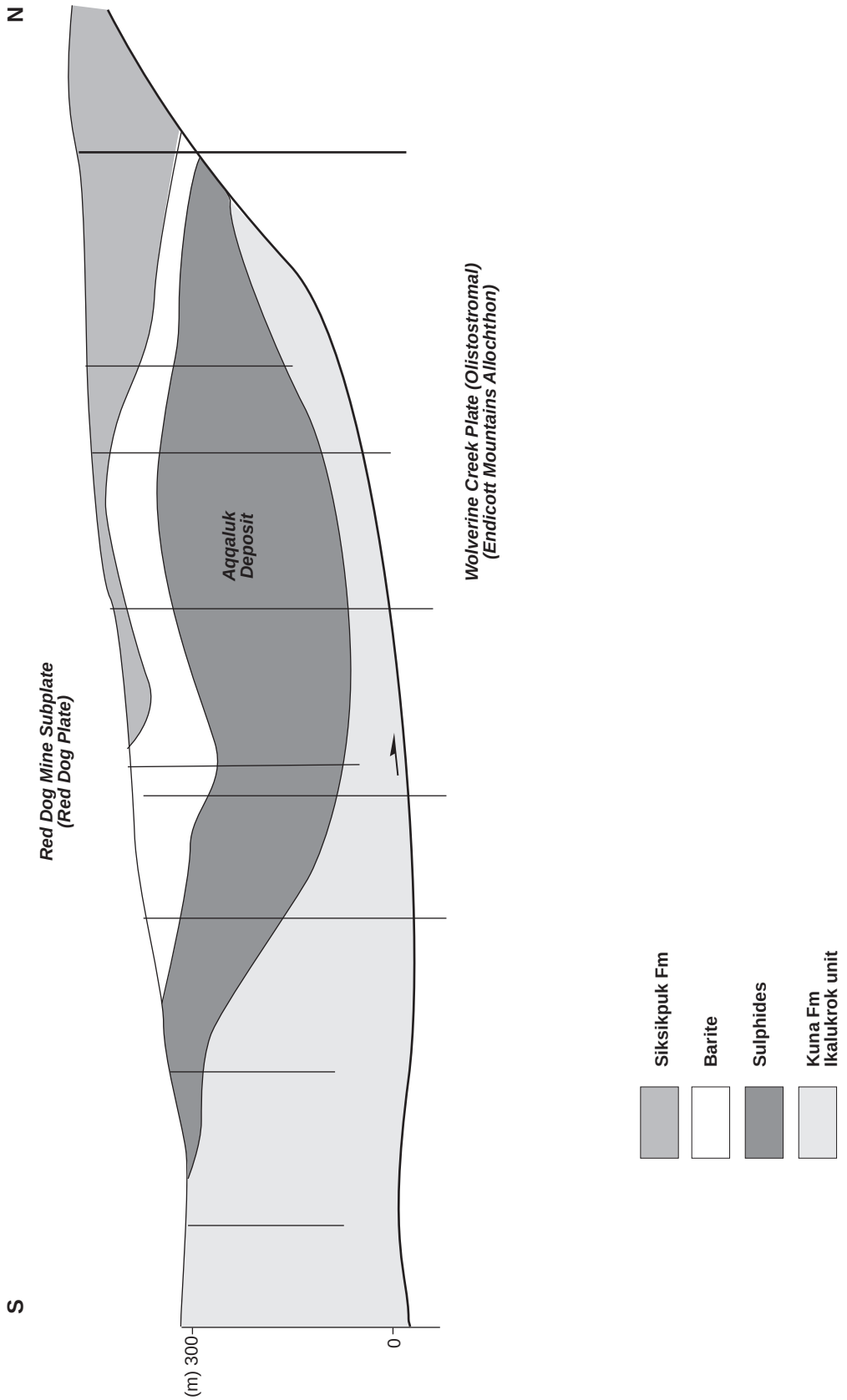


Figure 7.39. S-N Cross section across the Aqqaluk deposit. Refer to Figure 7.2 for location of section.

and Ikalukrok units of the Kuna Formation and the Okpikruak Formation. It overlies olistostromal strata that include olistoliths of the undivided Lisburne Group (Fig. 7.39).

7.2.4 Paalaaq Deposit

The Paalaaq deposit occurs north of the Aqqaluk deposit in the North Basin area (Figs. 7.1 & 7.2). Information on the structure of the Paalaaq deposit comes solely from limited drill hole data (4 holes) (Figs. 7.3 & 7.39). The Paalaaq deposit occurs in the footwall of the Key Creek plate (Fig. 7.3). It is overlain by a thick succession of structurally thickened Kivalina unit of the Key Creek plate. The Paalaaq deposit is NNE-trending and gently N-dipping (20° to 30°). It is detached in strata of the Kivalina and Ikalukrok units of the Kuna Formation.

7.3 DEPOSITS OF THE ANARRAAQ – WULIK AREA

These deposits are contained in two separate thrust subplates of the Red Dog plate of the Endicott Mountains allochthon 10 to 15 km north – north-northwest of the Red Dog mine (Figs. 7.1 & 7.40). The basal thrust dips to the north and northeast and thrust panels are SW-dipping (Figs. 7.40 & 7.41). The irregular thrust surface is possibly related to imbrication on underlying thrust ramps in the Wolverine Creek plate (Fig. 7.41). The deposits of the Anarraaq and Wulik areas occur north of Rok window in the hangingwall of the Wrench Creek fault and occur at depths of 600 to 800 m.

7.3.1 Anarraaq Deposit

The Anarraaq deposit is located approximately 10 km north-northwest of the Red Dog mine. Exploration drill hole data indicate the deposit is a strata-bound lens approximately 500 m long, 400 m wide and approximately 100 m thick (Teck Cominco. *pers. comm.*, 2002). It lies approximately 700 m below surface. Information about the Anarraaq deposit comes from drill hole data and from micro-gravity surveys.

This deposit is contained in a series of SSE- to SE-dipping thrust sheets that form a complex array of WNW-ESE- to NW-SE-trending thrust faults and folds, and overlies the Wolverine Creek plate of the Endicott Mountains allochthon (Figs. 7.1 & 7.41). The deposit is overlain by a structurally thickened succession of the Siksikpuk and Otuk formations, mainly exposed as rubble outcrop.

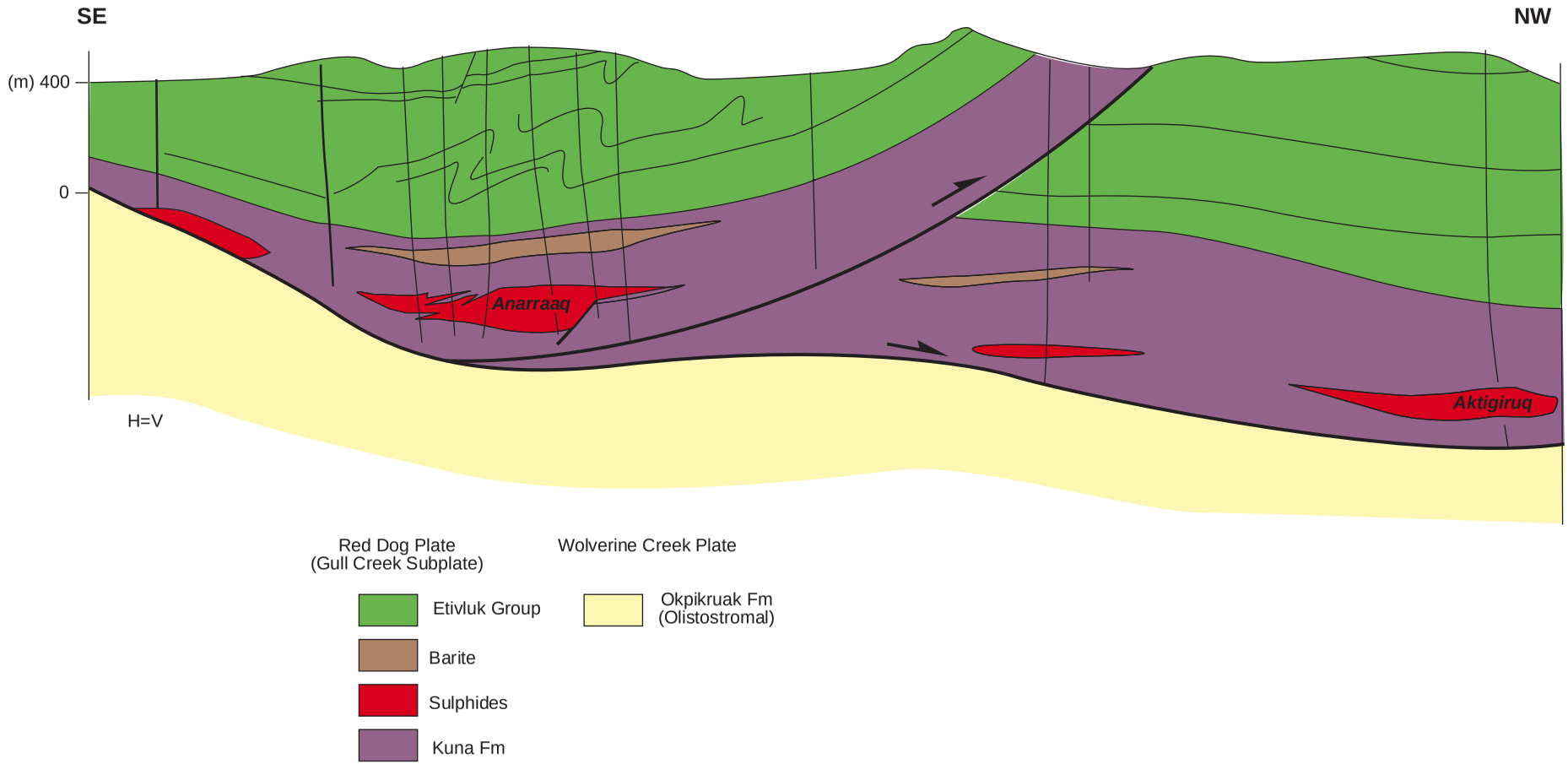


Figure 7.40. Southeast-northwest cross section showing the structure of the Anarraaq and Aktigiruq deposits.

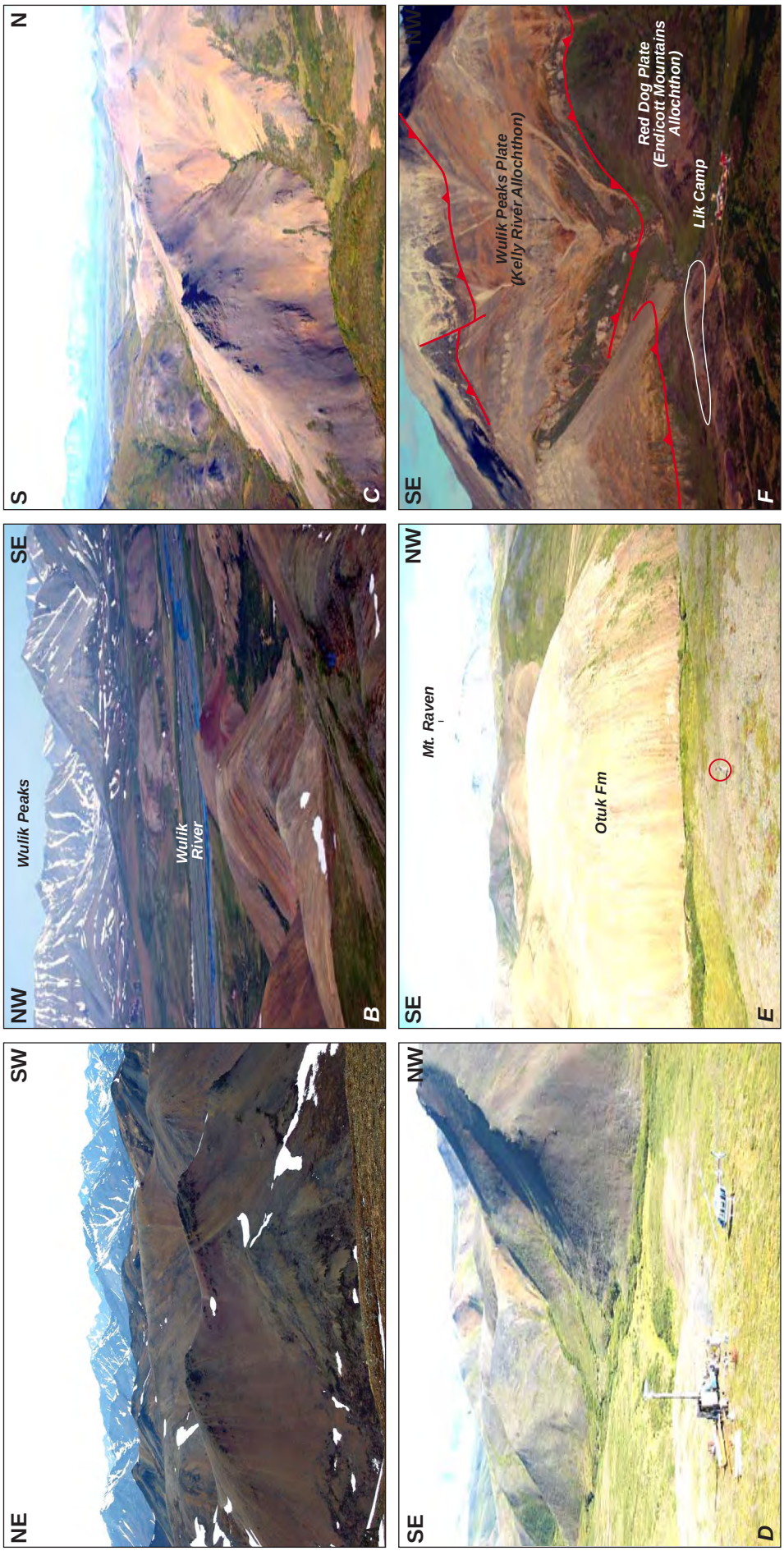


Figure 7.41. Structural features of the Anarraaq and Aktigiruq areas. **A.** S-looking view of NE-transported thrust sheets of the Gull Creek subplate of the Red Dog plate. Topographic relief is approximately 250 m. **B.** W-looking view of the Aktigiruq-Wulik area showing Etivluk Group rubble outcrops. The Wulik Peaks plate of the Kelly River allochthon lies in the background. **C.** View of thrust sheets in the Gull Creek subplate. **D.** View of the Aktigiruq deposit area. Drill rig and helicopter for scale. **E.** View of the Aktigiruq area showing a thick succession of strata of the Etivluk Group. Teck Cominco geologist Brigitte Dejou is encircled for scale. **F.** View of the Su and Lik deposits area. Note the Wulik Peaks plate of the Kelly River allochthon in the background.

It occurs in a synformal area that has an associated 2.9 mgal gravity anomaly (A. R. King, 2001, *pers. comm*.). The deposit is hosted by silicified black shales, mudstones and calcareous turbidites of the Ikalukrok unit. The Gull Creek subplate is detached in the lower part of the Ikalukrok unit, near the contact with the underlying Kivalina unit (Fig. 7.41). The deposit is thrust on top of highly tectonized strata of the Okpikruak Formation. It is overlain by a barite cap similar to that present in the deposits of the Red Dog Creek area. However, unlike in the deposits of the Red Dog Creek area, where barite directly rests on top of the sulphides, barite in the Anarraaq area is separated from the sulphides by approximately 20 to 100 m of unmineralized black shales (Fig. 7.41). The deposit is spatially related to abundant calcareous and lithic turbidites. Drill core data show that the deposit is flat-lying. The mineralization at Anarraaq consists of coarse-grained sphalerite facies as well as fine-grained laminated pyrite and light coloured sphalerite laminae (Fig. 7.42). The Anarraaq deposit lacks the vein-breccia ore facies that characterize the lower sections of the Red Dog mine area deposits.

Above the Anarraaq deposit the overlying Siksikpuk and Otuk formations appear to be structurally thickened, folded and deformed (Fig. 7.43) above a relatively undeformed Kuna Formation. This is indicated by folds observed in drill core as well as changes in the bedding-cleavage relationships in drill core. It is possible that the top of the sulphides and/or the barite bodies acted as a detachment surface during regional thrust deformation. The style of folding in the cross-sections is inferred from the drill cores though the deposit is similar to that observed in surface sections.

7.3.2 Aktigiruq Deposit

The Aktigiruq deposit lies approximately 1 km north of the Anarraaq deposit and lies 600 to 900 m below surface (Figs. 7.1 & 7.41). The Aktigiruq deposit occurs in the Gull Creek subplate of the Red Dog plate of the Endicott Mountains allochthon (Fig. 7.1). The Aktigiruq deposit is interpreted to occur at the same structural level as the Anarraaq deposit. At the present Day only a few exploration drill holes have penetrated this mineralized zone and it is not well defined. Three mineralized areas have been outlined. The Aktigiruq deposit is a strata-bound, flat-lying lens in Mississippian black shales of the Kuna Formation. It has no coarse-grained sphalerite or vein-breccia facies.

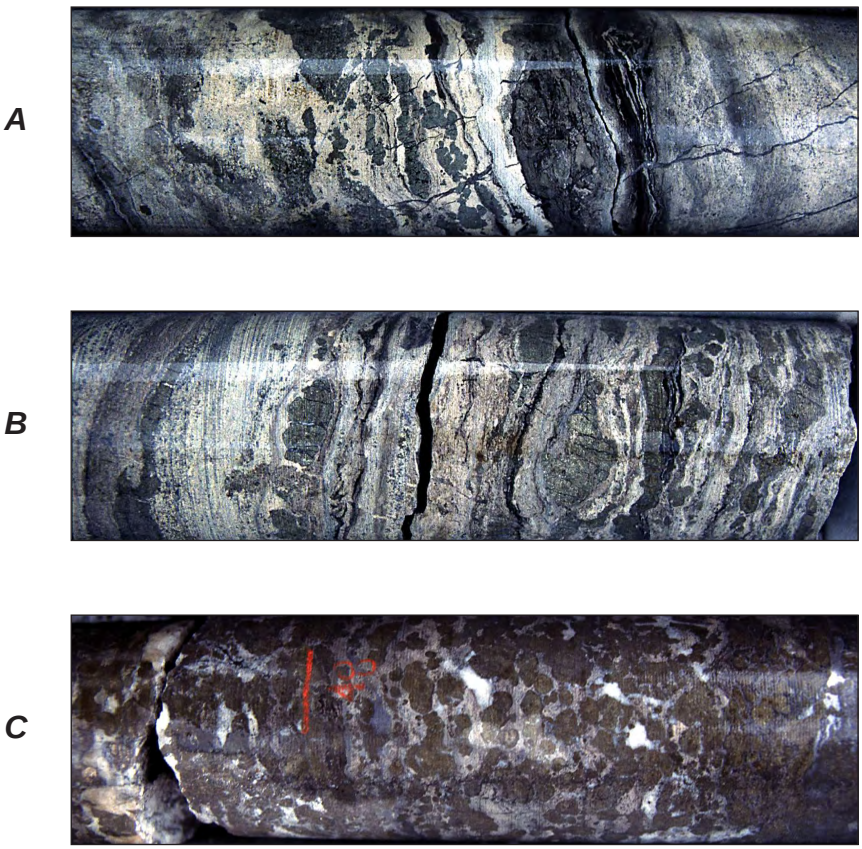


Figure 7.42. Photographs of exploration drill core from the Anarraaq deposit showing banded to laminated sulphides (A & B) and nodular sulphide textures (C). Drill core diameter is approximately 5 cm.

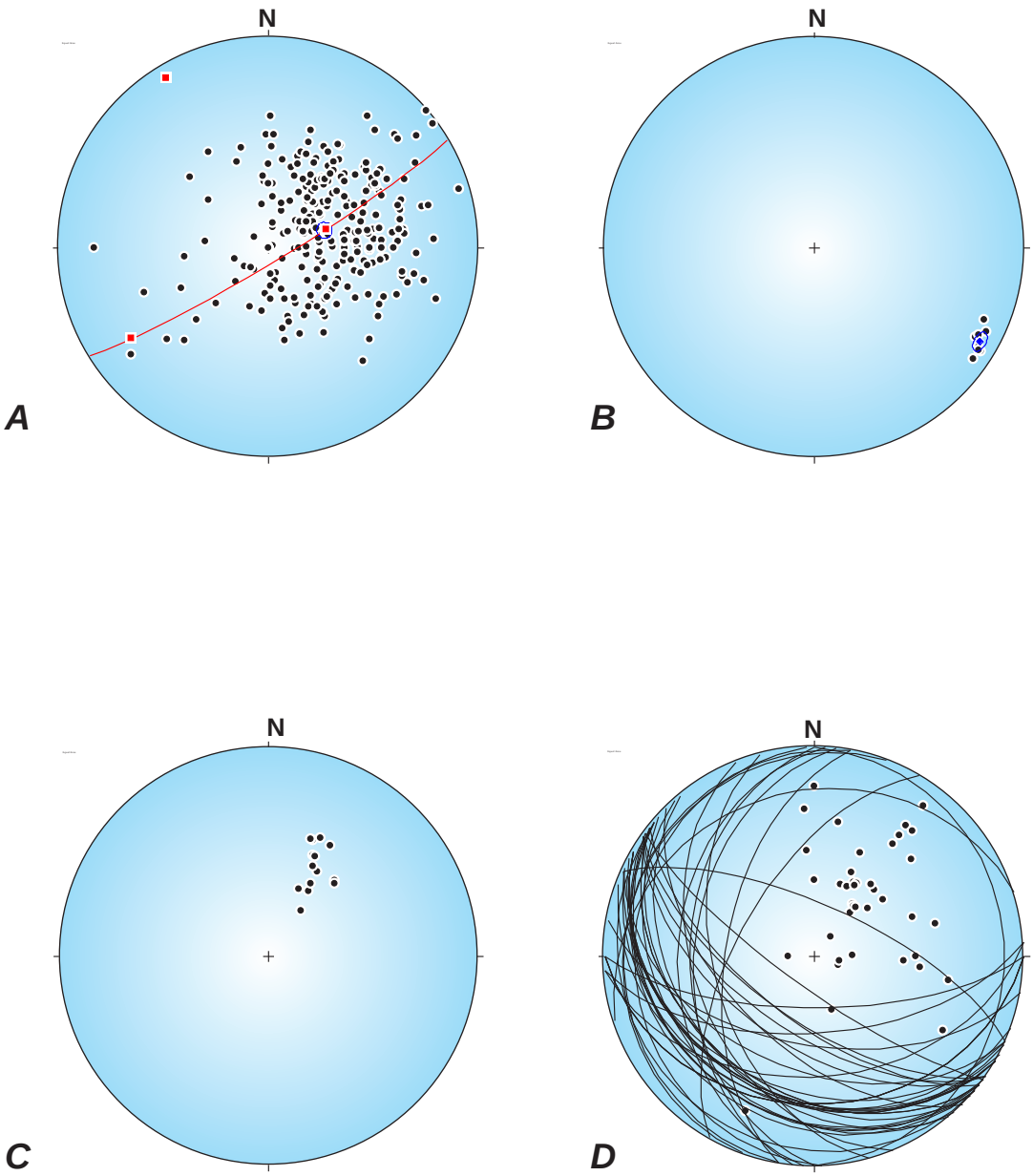


Figure 7.43. Lower hemisphere equal area stereographic projection of structural data from the Anarraaq area. **A.** Poles to bedding in strata of the Siksikpuk and Otuk Formations in the Anarraaq area (N=317). Fold axis=6°/328°. **B.** Minor fold axes in strata of the Otuk Formation (N=8). **C.** Poles to cleavage surfaces in strata of the Etivluk Group (N=15). **D.** Great circles and poles to outcrop-scale thrust faults (N=45).

Unlike the deposits at Red Dog and Anarraaq, barite is not present at Aktigiruq. Sulphides show well-preserved primary depositional textures (laminated, ocelar, and nodular textures) indicating that the sulphides are not significantly deformed. The sulphides consist of cream-buff coloured fine-grained sphalerite, fine-grained galena and iron sulphides (pyrite and marcasite). Ore facies are nodular, irregularly bedded to finely-laminated. The base of the deposit appears to be transitional, grading from finely-laminated sulphide layers into black shales with disseminated galena and sphalerite. The mineralization is overlain by a structurally-thickened and imbricated succession of cherts, and shales of the Siksikpuk and Otuk formations, and black shales, cherts and calcareous strata of the upper part of the Ikalukrok unit deformed in multiple detachment levels with associated detachment folds. The Aktigiruq deposit occurs in the structural footwall of the Anarraaq deposit (Fig. 7.41). The base of the Gull Creek thrust subplate is a thrust fault that places the Ikalukrok unit of the Kuna Formation on top of the Okpikruak Formation of the underlying Wolverine Creek plate (Fig. 7.41).

7.4 DEPOSITS OF THE SU – LIK AREA

The Su and Lik deposits lie approximately 21 km northwest of the Red Dog mine (Fig. 7.1). The Su and Lik are NE-SW-trending and lie approximately 200 m below surface (Fig. 7.44). Mapping in the area indicates that the Su and Lik deposits lie in a NE-SW-trending, NW-dipping and SE-verging discontinuous thrust remnant of the Red Dog plate of the Endicott Mountains allochthon. Transport on a NW-dipping and SE-verging thrust sheet possibly accounts for the relatively shallow depths at which the deposits occur, compared with deeper deposits further to the east (e.g. Anarraaq, Aktigiruq). The Su and Lik deposits are spatially related to olistostromal strata of the Okpikruak Formation, including mud-supported debris flow deposits and decametric to hectometric size olistoliths and gravity slide sheets. They occur in the immediate footwall to moderately to the steeply NW-dipping, SE-verging thrust plates and olistoliths of the Chimneys plate of the Kelly River allochthon and the Puzzle Creek plate of the Picnic Creek allochthon (Fig. 7.1).

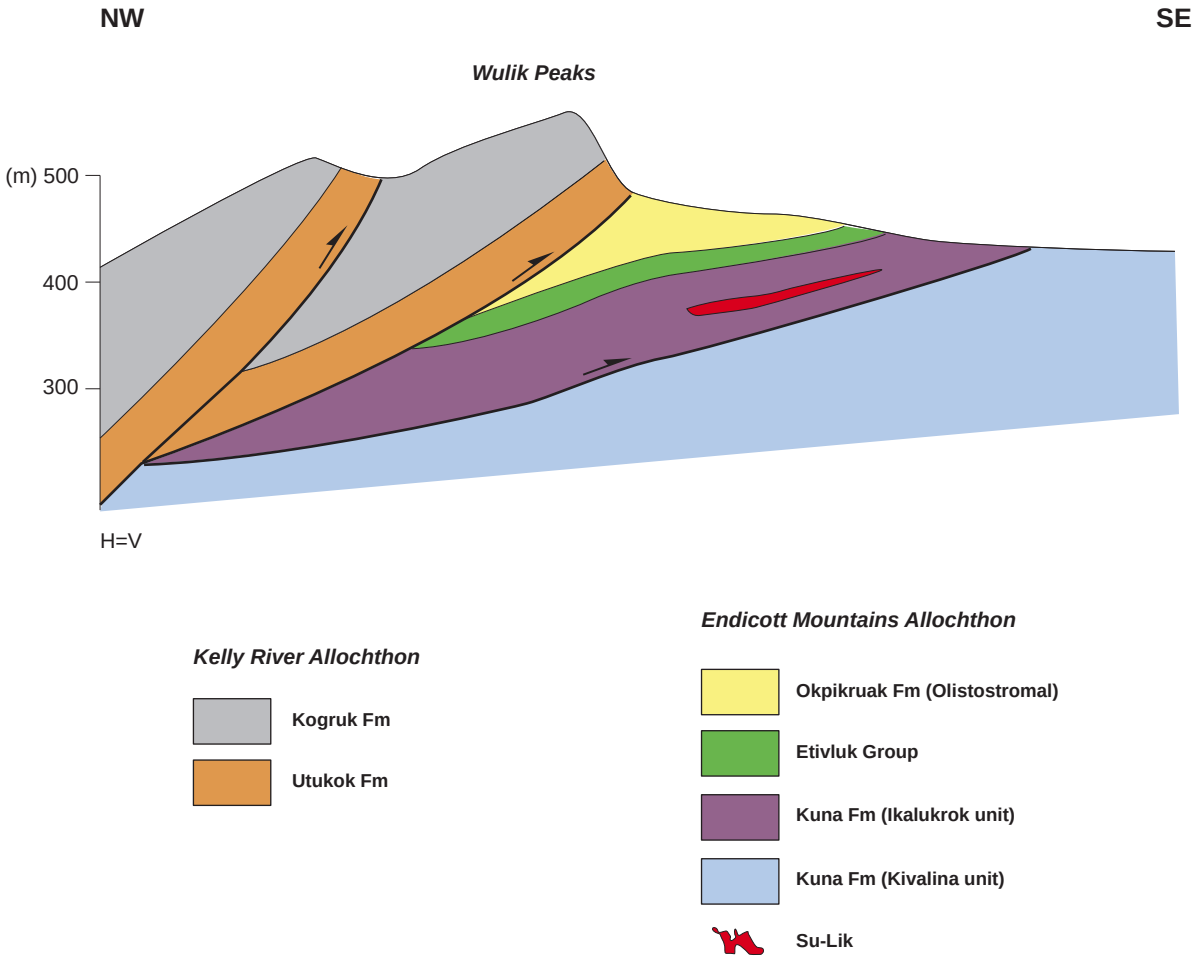


Figure 7.44. Cross section across the Su-Lik deposits. Refer to Figure 7.1 for location of cross section.

7.5 SUMMARY

The structural mapping and analysis of the sediment-hosted Zn-Pb-Ag and barite deposits of the Red Dog district has shown that:

- The known sediment-hosted Zn-Pb-Ag and barite mineralization in the Red Dog district occurs in three main areas - the Red Dog Creek area, the Anarraaq-Wulik, and Su-Lik areas. All known sulphide deposits are hosted in black shales, silicified mudstones and turbidites of the Ikalukrok unit of the Kuna Formation and are typically contained within thrust bounded sheets.

- Mineralization in the Red Dog Creek area consists of four thrust-stacked deposits. From south to north and from structurally highest to lowest these are the Qanaiyaq, Main, Aqqaluk and Paalaaq deposits. These deposits are contained in discontinuous and structurally disrupted thrust sheet remnants of the Red Dog mine thrust subplate. The Red Dog mine subplate is interpreted to be a disrupted olistostromal unit that was thrust into and incorporated blocks of the Early Cretaceous Okpikruak Formation.

- The sulphide and overlying massive barite deposits together with their overlying strata are deformed by NW to NE vergent thrust faults, duplexes, fault-related folds and well-developed penetrative fabrics. Primary sulphide depositional textures are however well-preserved in the deposits indicating relatively little internal deformation of the orebodies. A series of late (possible Tertiary age) NW-trending high-angle extensional faults offset the deposit and host rocks. These extensional faults post-date the emplacement and folding of the thrust sheets.

- The Anarraaq and Aktigiruq deposits are contained at the base of the Gull Creek subplate of the Red Dog plate of the Endicott Mountains allochthon.

- The Su and Lik deposits are contained in a NE-SW-trending, NW-dipping and SE-verging discontinuous thrust sheet that overlies olistostromal strata of the Okpikruak Formation.

The results of the structural analysis of the mineralization in the Red Dog district are integrated with the regional structural analysis in Chapter 8 and the implications for the tectono-stratigraphic evolution of the district, for mineralization models and for exploration strategies are discussed in detail.

CHAPTER 8

DISCUSSION

8.1 INTRODUCTION

8.2 TECTONOSTRATIGRAHIC ANALYSIS OF THE RED DOG DISTRICT

8.3 STRUCTURAL ANALYSIS OF THE RED DOG DISTRICT

8.4 TECTONIC EVOLUTION OF THE WESTERN BROOKS RANGE

8.5 IMPLICATIONS FOR THE FORMATION OF RED DOG TYPE MINERALIZATION AND FOR EXPLORATION IN THE RED DOG DISTRICT

8.6 SUMMARY

CHAPTER 8 DISCUSSION

8.1 INTRODUCTION

This chapter presents a discussion of the results of the structural and stratigraphic analyses of the Red Dog district (Chapters 5, 6 & 7) in relation to existing research on the Red Dog district and the Brooks Range (Chapters 2 & 3). The discussion is divided into four main sections. Section 8.2 summarizes the tectonostratigraphic analysis of the Red Dog district. Section 8.3 discusses the structural analysis and tectonic evolution of the Red Dog district. Section 8.4 discusses a new tectonostratigraphic model and the implications for the tectonic evolution of the western Brooks Range. Section 8.5 addresses the implications of the results of this study for the understanding of the tectonic controls on the mineralization of the Red Dog district and for the exploration of sediment-hosted Zn-Pb-Ag and barite deposits in the Red Dog district and elsewhere in the western Brooks Range.

8.2 TECTONOSTRATIGRAPHY OF THE RED DOG DISTRICT

8.2.1 Introduction

The Red Dog district of the western Brooks Range consists of two major allochthonous terranes, the Arctic Alaska and the Angayucham terranes (Figs. 8.1 & 8.2). These form part of a telescoped Devonian through Jurassic continental passive margin that is now preserved in seven stacked allochthon sheets bounded by regional, sub-horizontal thrust systems (Figs. 8.3 – 8.5). These were thrust northwestwards onto the passive margin of northern Alaska during the Middle to Late Jurassic - Late Cretaceous Brookian orogeny, forming a NE-SW- to WNW-ESE-trending and WNW-vergent, thin-skinned foreland fold and thrust belt. The Arctic Alaska terrane of the western Brooks Range consists of the lower six allochthons formed by the telescoping of proximal and distal sedimentary sections of the southern passive margin of the ancestral Alaskan continent. The seventh and uppermost thrust sheet consists of the ophiolite Misheguk Mountain allochthon of the Angayucham terrane (Figs 8.1 & 8.2). This is interpreted to have formed as Middle Jurassic oceanic crust south of the ancestral passive margin and subsequently obducted northwestwards onto the telescoped passive margin during the Brookian orogeny.

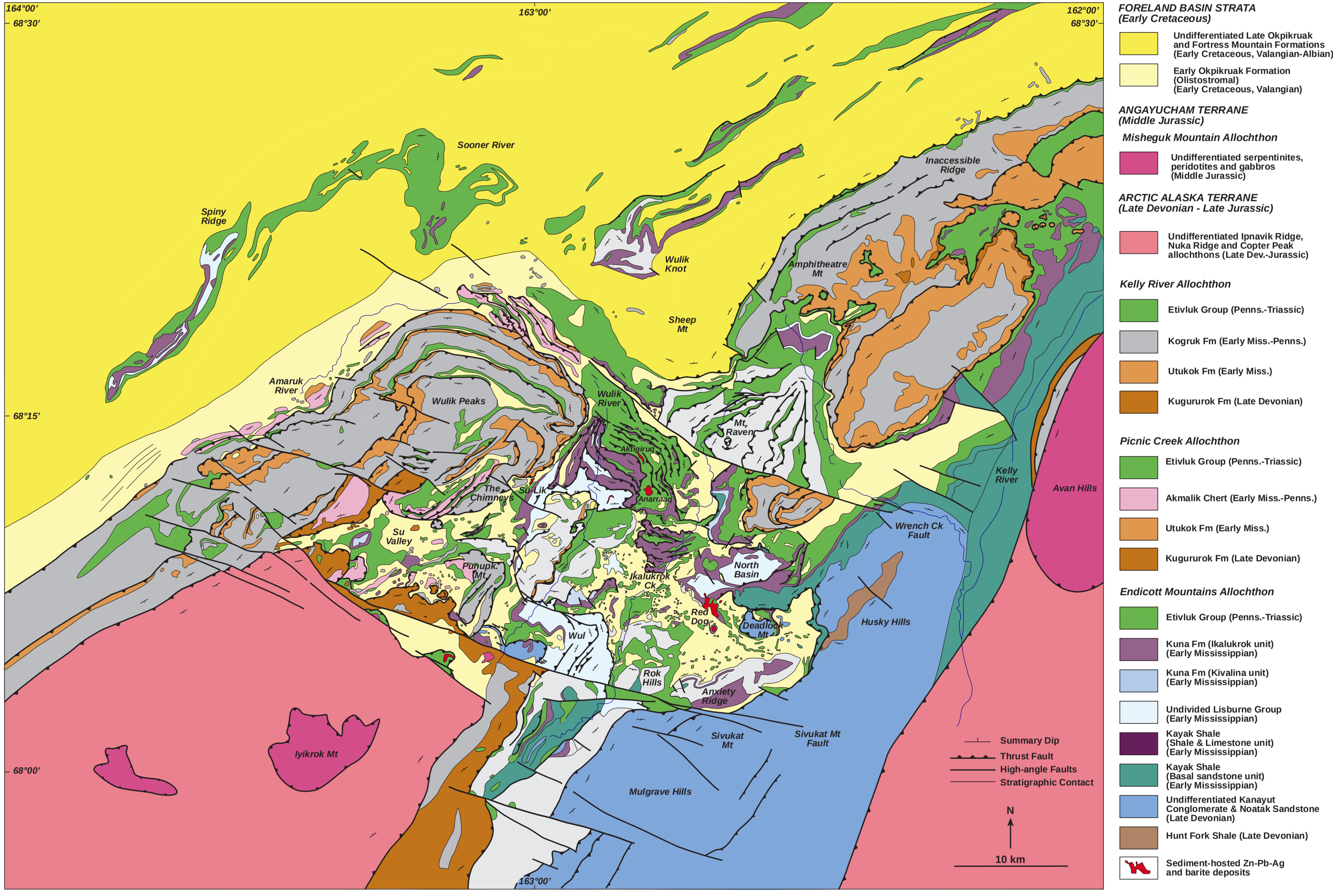


Figure 8.1. Geological map of the Red Dog district compiled from mapping by the author and Teck Cominco geological maps, published maps (Ellersieck *et al.* 1983, 1984, 1990*a*; Mayfield *et al.* 1984; Mayfield *et al.* 1990; Mull *et al.* 2000).

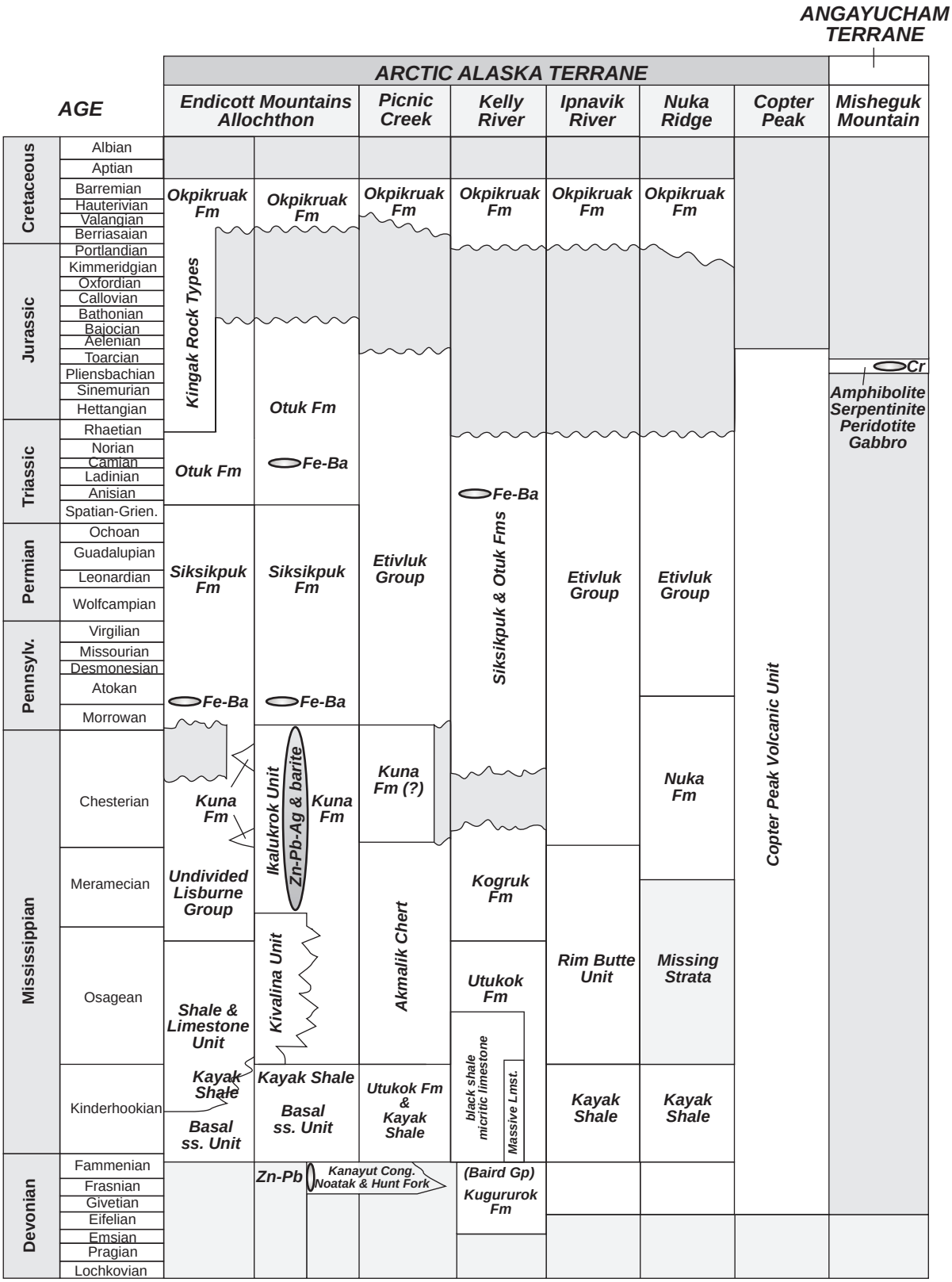


Figure 8.2. Summary chronostratigraphy of the Red Dog district (modified from Young, 2004). The stratigraphic position of the sediment-hosted Zn-Pb-Ag and barite deposits is shown.

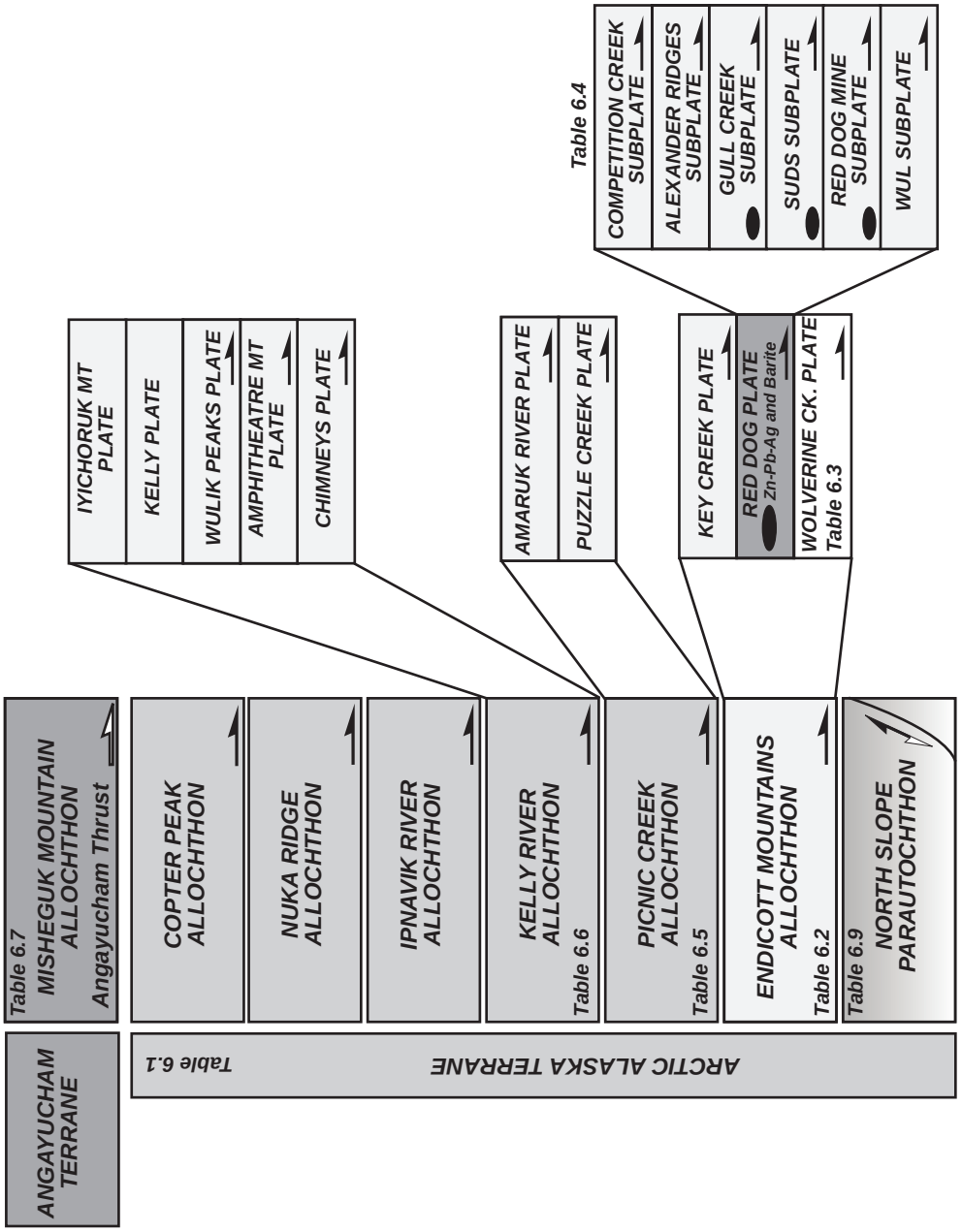


Figure 8.3. Structural hierarchy of the Red Dog district compiled from the results of this study and Mull (1982), Moore *et al.* (1986), Mayfield *et al.* (1988), Moore *et al.* (1994), Teck Cominco American Exploration Inc. (2002, *pers. comm.*), Young (2004). Note the structural position of the Zn-Pb-Ag and barite deposits the Red Dog district.

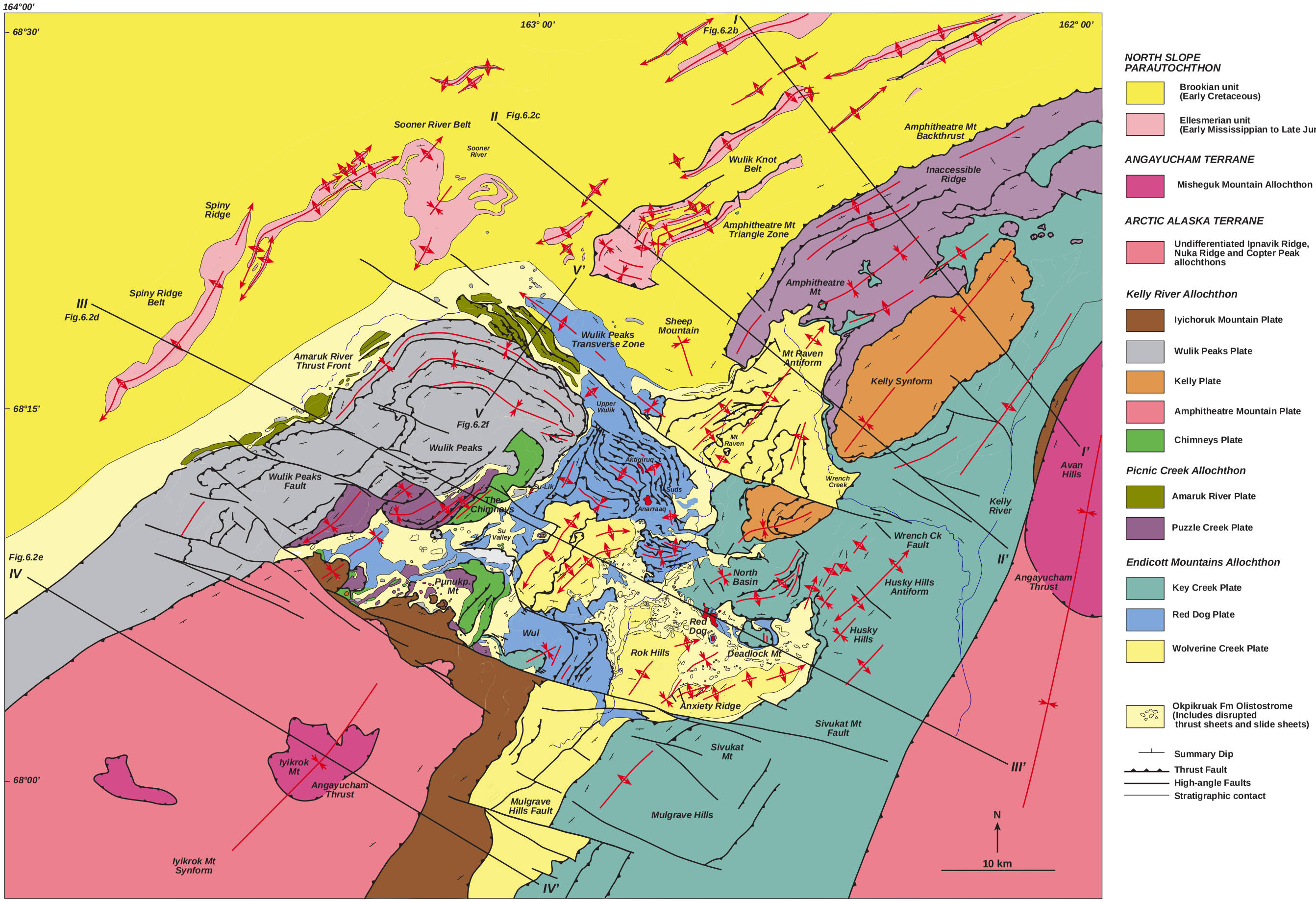


Figure 8.4. Structural map of the Red Dog district compiled from the results of this study.

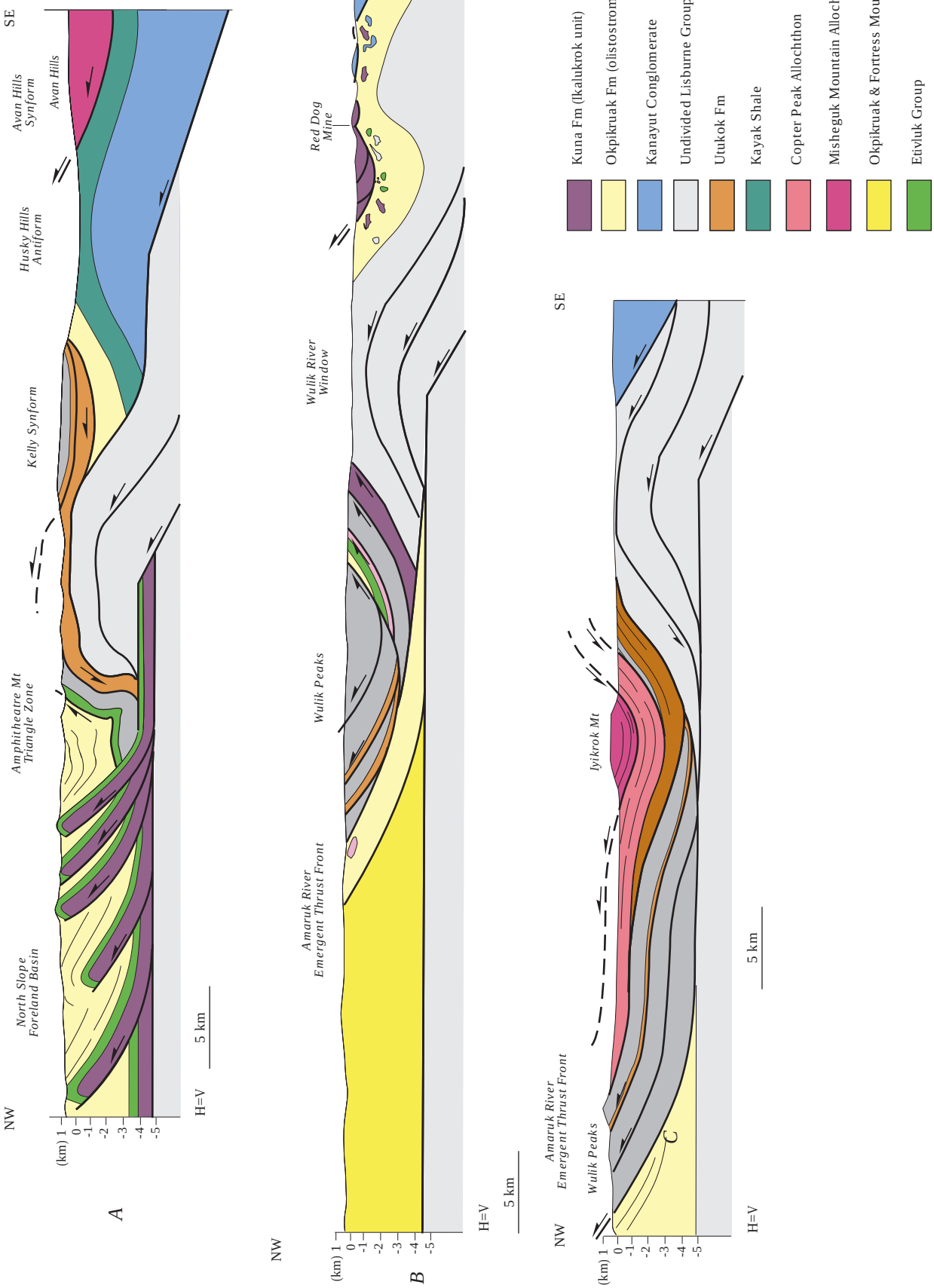


Figure 8.5. Summary regional cross sections across the Red Dog district. Refer to Figure 8.4 for location of individual sections.

Detailed regional and detailed stratigraphic and structural analyses of the complex fold and thrust belt of the Red Dog district has lead to a new stratigraphic interpretation and a new structural interpretation of the region. Key aspects are discussed below.

8.2.2 Tectonostratigraphy of the Red Dog District

The greater part of the Red Dog district consists of sedimentary successions of the Arctic Alaska terrane (Fig. 8.6). To the southwest and northeast these units are overthrust by the ophiolite of the Misheguk Mountain allochthon of the Angayucham terrane (Fig. 8.7).

The strata of the Arctic Alaska terrane can be subdivided into two regionally significant tectonostratigraphic units. These are the Ellesmerian and Brookian units, which in turn can be further subdivided into megasequences that result from distinct tectono-sedimentary events (Fig. 8.6).

The Ellesmerian Unit

The Ellesmerian unit consists of two distinct unconformity bounded rift-related megasequences that are interpreted to have formed on the southern margin of the ancestral Alaskan continent. These are –

1) Syn-Rift megasequence consisting of the Late Devonian through Late Mississippian strata deposited at during the rifting of the passive margin.

2) The Post-Rift megasequence consisting of Pennsylvanian though Late Jurassic strata deposited during the thermally induced subsidence of the sag phase of the passive margin.

No pre-rift strata are exposed in the Red Dog district. They are exposed in the Doonerak window in the central Brooks Range (Mull et al. 1997).

The syn-rift meagsequence consists of early rift continental to marine sediments of the Endicott Group and the distal platform carbonates of the Baird Group (Kugururok Formation). These are overlain in the extensional fault-controlled rift basins by marine successions of the Kayak Shale, the Utukok Formation and the Kuna Formation, the Akmalik Chert and Rim Butte units (Fig. 8.6). The deep marine black shales of the

Kuna formation hosts the Zn-Pb-Ag-Barite mineralization of the Red Dog district. The footwall of the main rift fault blocks consist of platform carbonates of the Kogruk formation and undivided Lisburne Group carbonate-rich strata. The rift basin interpretation for these marine clastic successions is similar to that for other black clastic rift basins along the western margin of ancestral north America such as the Mid-Late Palaeozoic Selwyn Basin and Kechika Trough (Abbott et al. 1986; McClay 1991; Goodfellow, 1998, 1999, Nelson et al. 2002). The strong post-depositional deformation and thrusting has obliterated the direct evidence for Late Devonian – Mississippian extensional faulting in the Red Dog district but geophysical data (gravity and magnetics) together with facies analyses and the interpretation of reactivated basement structures all point towards a dominantly extensional fault regime along the southern margin of ancestral Alaska at this time (cf. Young, 2004).

In the parautochthon to the north of the Red Dig district regional seismic sections (e.g. Fig. 8.7) show evidence of Late Mississippian age inversion of Late Devonian Early Mississippian age extensional faults. It is likely that during this time enhanced hydrothermal fluid circulation generated by regional contraction and focused by the rift fault systems produced the widespread barite and Zn-Pb-Ag-Fe mineralization as evidenced by the pervasive textural evidence for sub-surface replacement of particularly carbonatic turbidites in the Red Dog district (e.g. Kelly et al. 2004) (see also section 8.5).

The post-rift megasequence consists of the generally fine-grained siliciclastic strata of the Etivluk Group, which includes the Siksikpuk and Otuk formations. These are interpreted to have been deposited under relatively quiet conditions of post-rift thermal subsidence although to the north seismic evidence indicates that basin margin fault systems were being reactivated and inverting at this stage (Fig. 8.7).

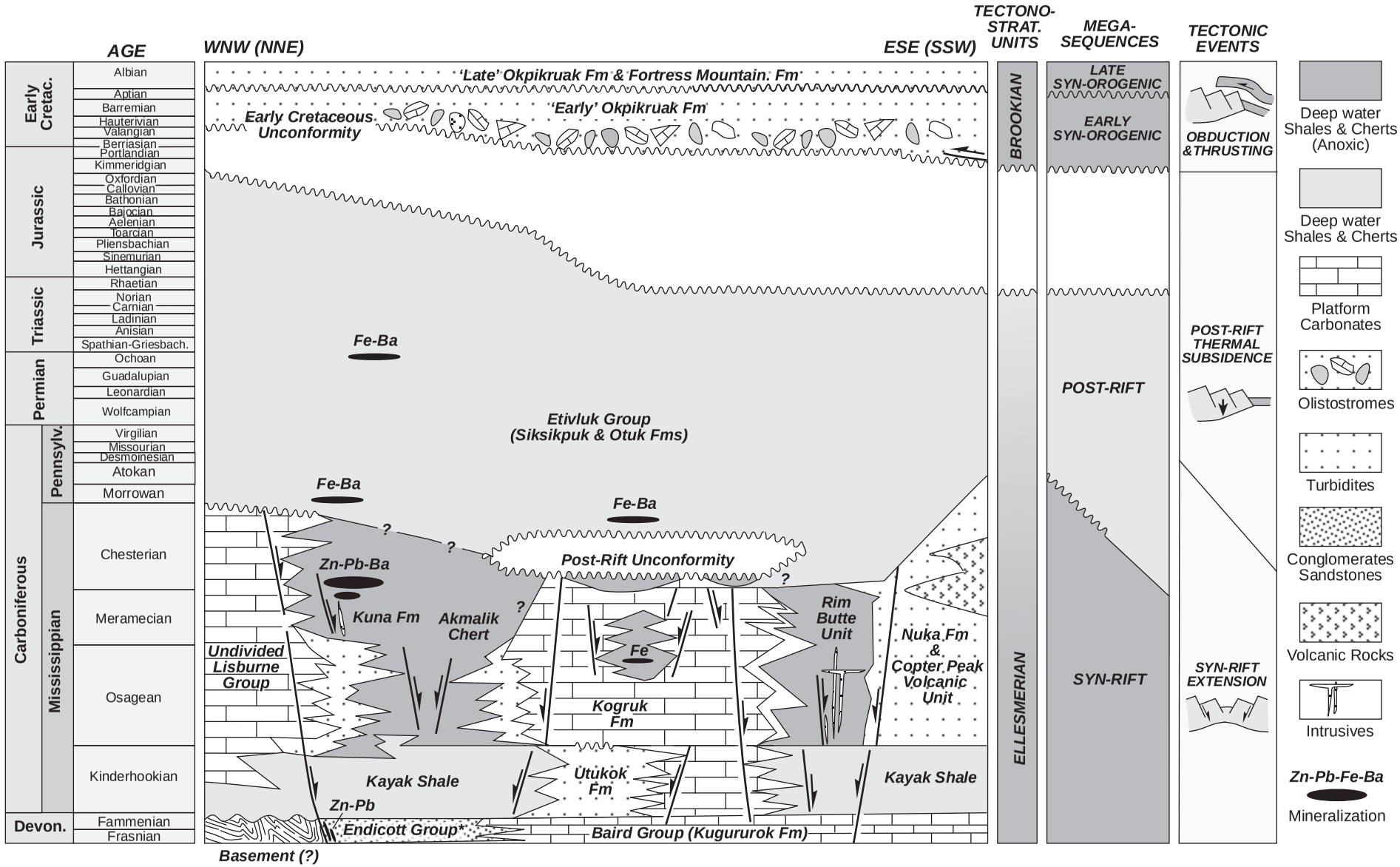


Figure 8.6. Chronostratigraphy of the Arctic Alaska terrane in the Red Dog district compiled from the results of this study. Age constraints based on Dumoulin *et al.* (2004), C. G. Mull (2004, *pers. comm.)*, and Young (2004). Note the Endicott Group* includes the Hunt Fork Shale, Noatak Sandstone, and Kanayut Conglomerate.

The Brookian Unit

The syn-contractional Brookian unit can be subdivided into the Early and Late Brookian megasequences (Fig. 8.6). In the Red Dog district the Early Brookian Megasequence consists of the Late Cretaceous Optikruak formation that is interpreted to have formed in an unstable deep marine environment in the proximal foredeep as the allochthon sheets formed largely by telescoped Ellesmerian sequences were emplaced northwestwards over the passive margin. This megasequence is characterized by deep marine strata including turbidites and significant olistostromes. The Late Brookian Megasequence in the Red Dog district consists of 'Late Okpikruak' and Fortress Mountain formations (Fig. 8.6). These are dominantly deep water successions that infilled the foredeep as the Brookian orgen developed and the major allochthon sheets were emplaced onto the passive margin.

The present day structural complexities of the Red Dog district prevent the detailed reconstruction of the tectonostratigraphic relationships in the Red Dog district but in the parautochthon of the foreland basin to the north some of these features are clearly shown in regional seismic lines (Fig. 8.7). The syn-rift and syninversion (early-syncontraction) mega-sequences occur in the lower part of the seismic section and the late syn-contraction northward vergent and prograding foreland basin infill sequences are shown in the upper part of the section (Fig. 8.7). These sequences can be correlated to the south into the Red Dog district to give the broad tectonostratigraphic correlation shown in Figure 8.6. The plan view dispositions in individual allochthons and thrust plates are summarized in the synoptic evolutionary model diagram at the end of this chapter.

The development of olistostromal units within the early syn-contractional Optikruak section is particularly important as these occur in key allochthon sheets and in particular in the mineralized Red Dog plate (Fig. 8.3). Incorporation of gravity slide blocks into the Red Dog plate has produced complex and confusing outcrop relationships in the vicinity of the Red Dog mine and has hampered both the structural interpretation and exploration for new mineralization. Figure 8.8 summarizes examples of how tectonically induced instabilities generated by an advancing thrust front into a deep water marine setting leads to the formation of mass wasting and gravity slide deposits –

olistostromes (cf. Abbate et al. 1970; Davis and Hyndman, 1989; Fowler, 2003; Medialdea et al. 2004). It is envisaged that in the Red Dog district as the northwest vergent allochthons were emplaced, individual thrust plates such as the Red Dog plate (Fig. 8.3) became emergent at the sea floor generating mass wastage deposits (olistoliths) that became incorporated and carried forward by the thrust plate. Spectacular examples of such mass wastage deposits are illustrated in 3D seismic images from offshore Brunei (McGilvery and Cook, 2003).

Misheguk Mountain allochthon of the Angayucham terrane

The Misheguk Mountain allochthon of the Angayucham terrane consists of Middle Jurassic upper mantle to lower crust ultramafic to basic and felsic igneous rocks. These include serpentinites, chromite-bearing serpentinized dunites, layered dunites and pyroxenites and layered gabbros (Fig. 8.9). The Angayucham terrane preserves the lower part of a typical ophiolite succession (e.g. Harris, 1997, 2004) interpreted to have formed as oceanic crust to the south of the southern passive margin and obducted northwestwards during the Brookian orogeny. This structural interpretation is discussed in more detail in section 8.3 below.

Zn-Pb-Ag-Barite Mineralization in the Red Dog District

This new tectonostratigraphic framework places the Zn-Pb-Ag-Barite mineralization of the Red Dog district within the late syn-rift megasequence of the Ellesmerian unit. The mineralization is structurally confined to the Red Dog plate of the Endicott Mountains allochthon. The implications for this and the tectonostratigraphy of the Red Dog plate are discussed in detail in section 8.5.

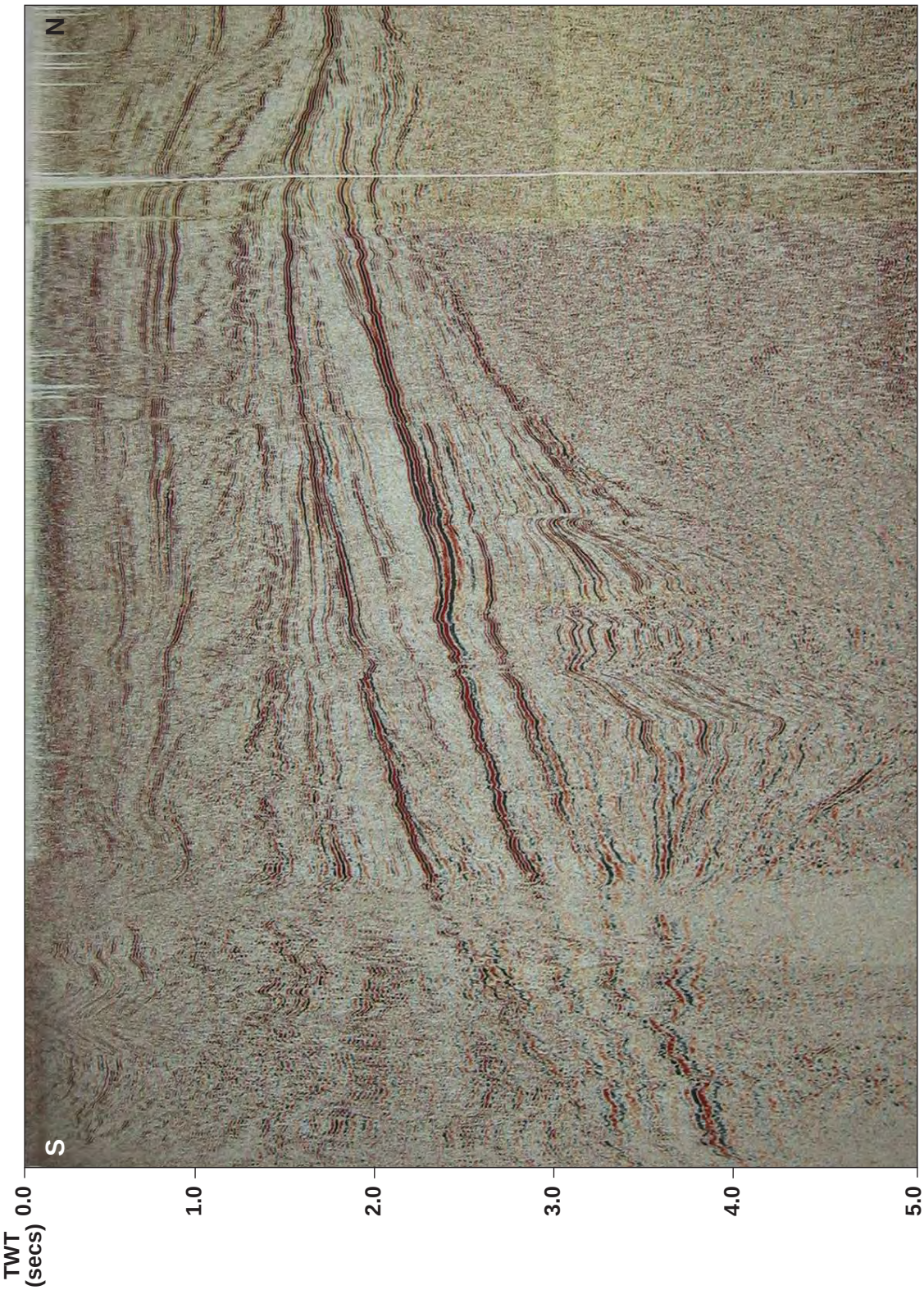


Figure 8.7.A. Regional seismic line across the North Slope parautochthon and foreland basin (seismic data courtesy of BP Exploration, 2005).

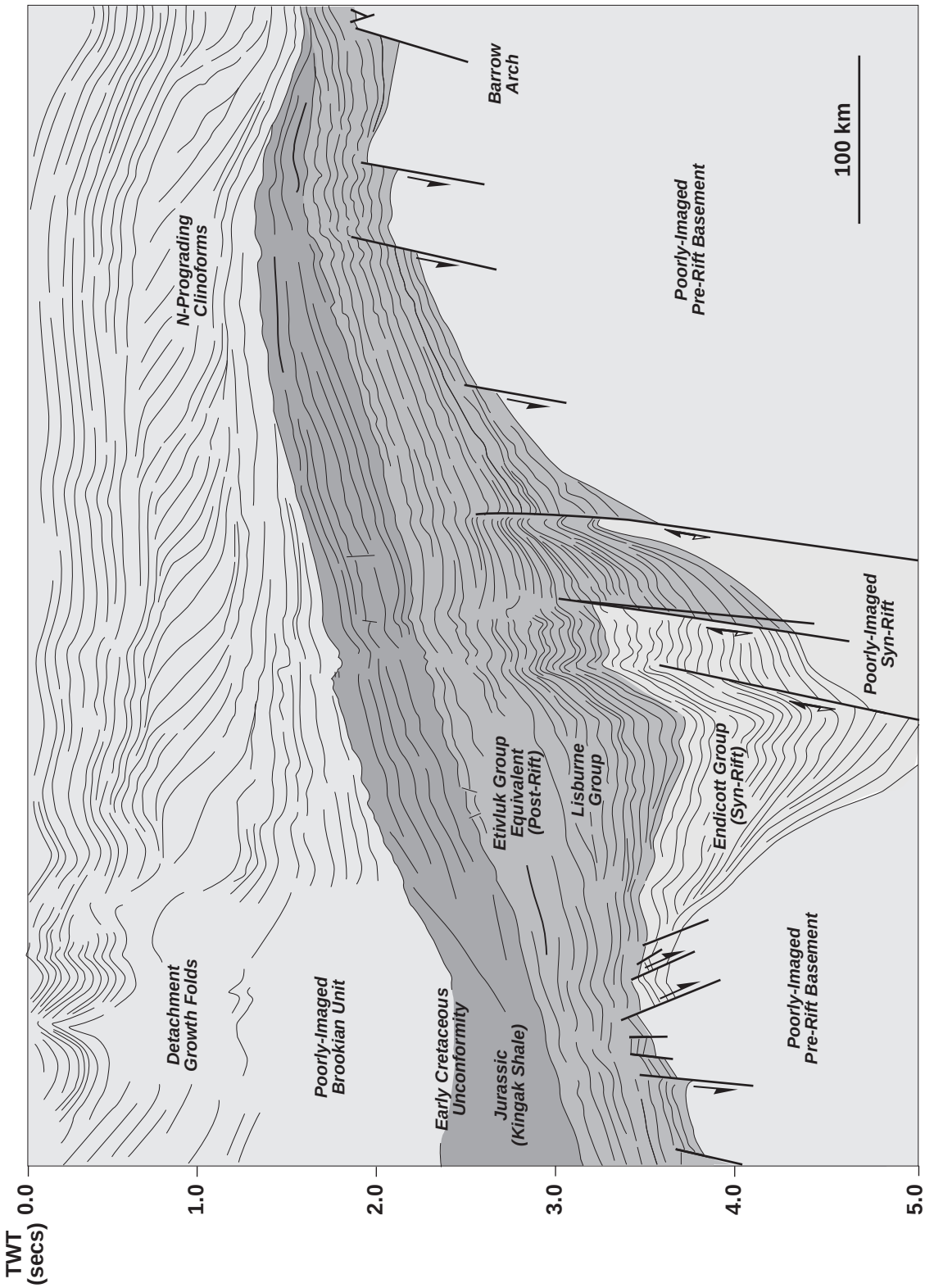


Figure 8.7B. Regional seismic line across the North Slope parautochthon and foreland basin (seismic data courtesy of BP Exploration, 2005).

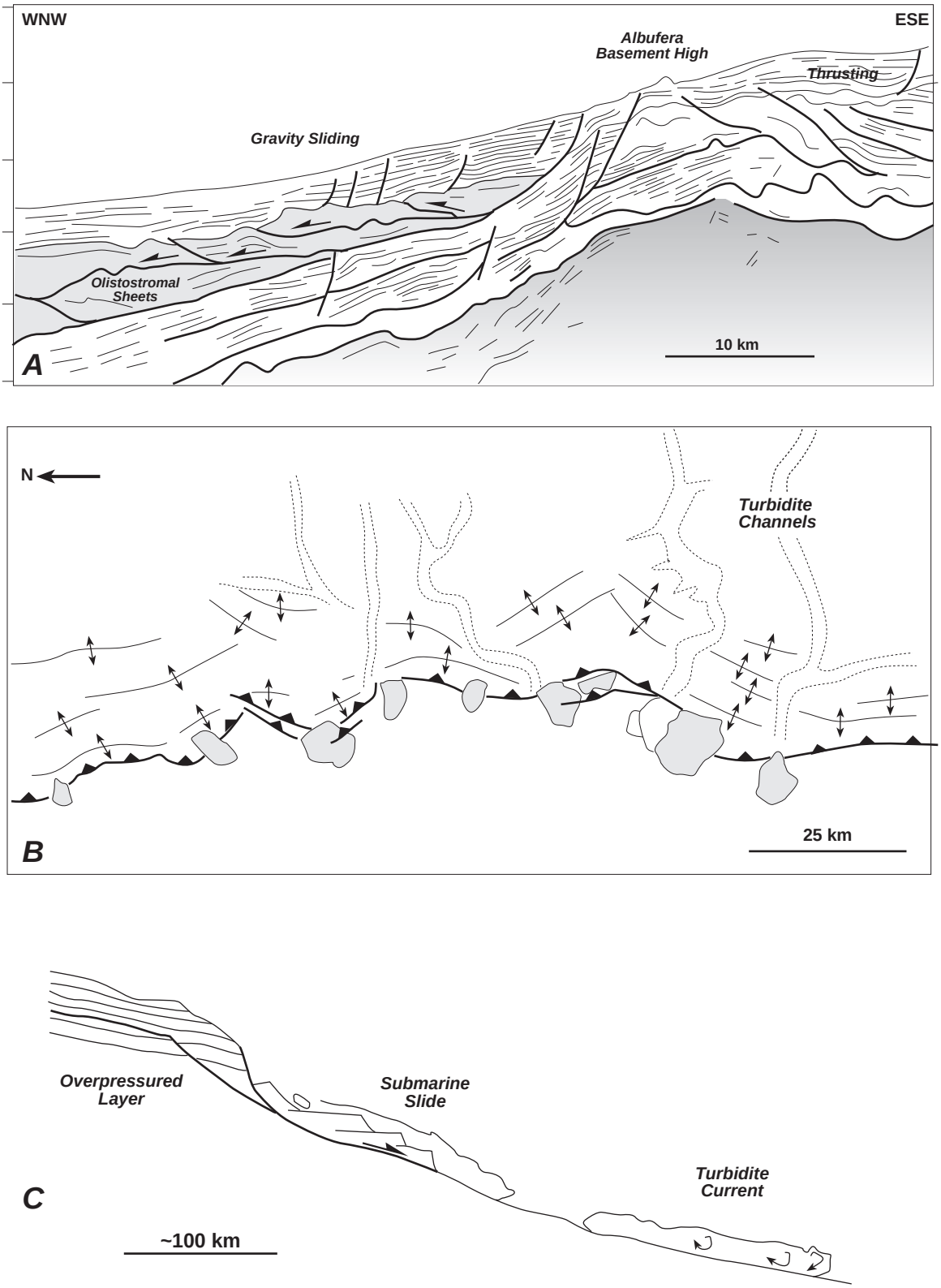


Figure 8.8. Gravity sliding in submarine settings. **A.** Line-drawing interpretation of seismic line across the Gibraltar Arc olistostrome complex (modified from Medialdea *et al.* 2004). **B.** Simplified map of the Cascadia accretionary prism showing the relationships between active thrust faults, mass-wasting deposits and turbidite channels (modified from Davis & Hyndman, 1989). **C.** Conceptual model for submarine gravity sliding in continental margins (modified from Fowler, 2003).

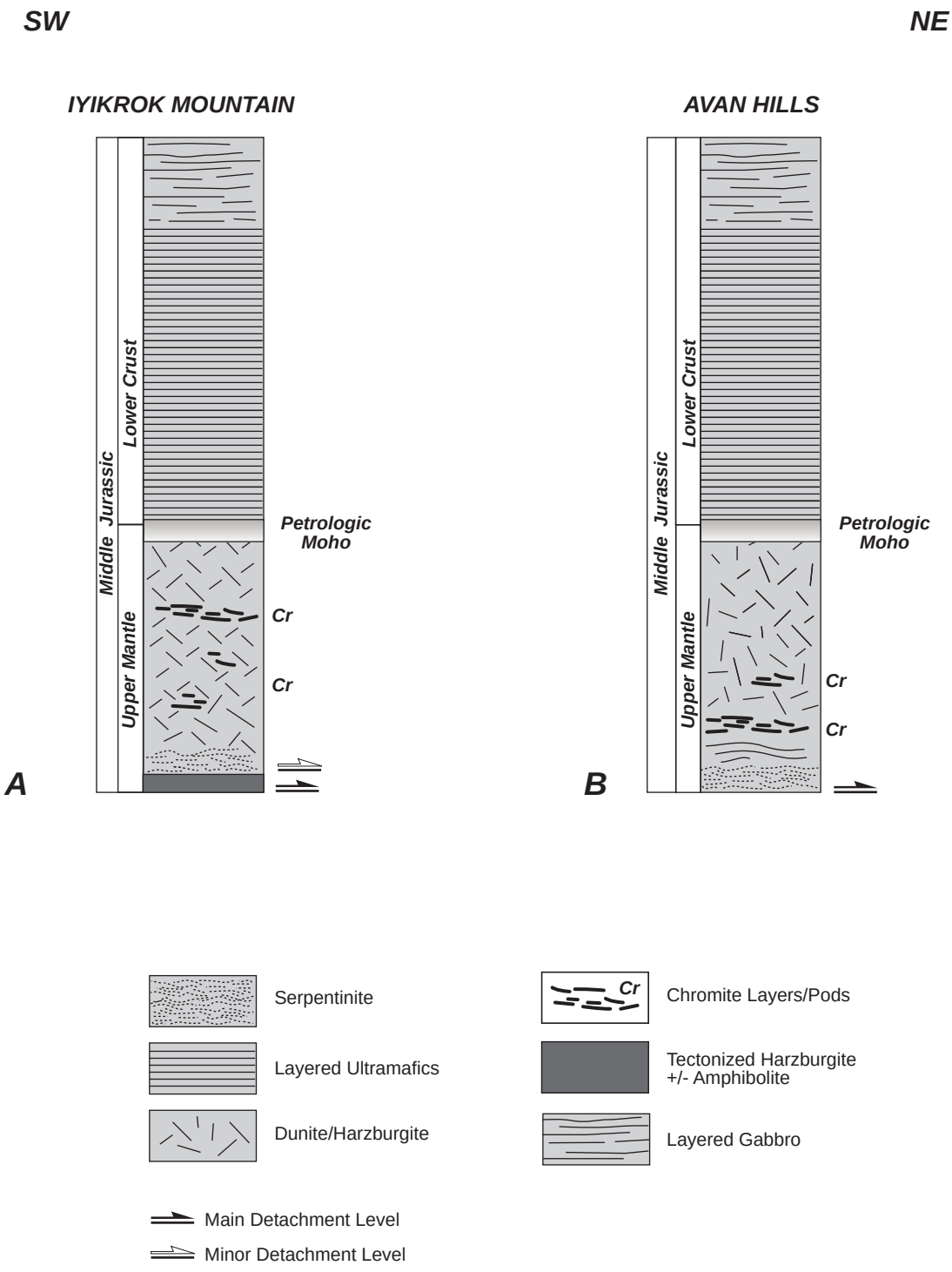


Figure 8.9. Summary igneous stratigraphy of the Angayucham terrane. **A.** Iyikrok Mountain. **B.** Avan Hills. Approximate position of the petrologic Moho is shown schematically. Note chromite mineralization near the base of the allochthon. Columns not to scale.

8.3 STRUCTURAL ANALYSIS OF THE RED DOG DISTRICT

8.3.1 Introduction

In this section the detailed structural interpretation of the Red Dog district and of the Red Dog mine are discussed. Structural analysis combined with the reinterpretation of the tectonostratigraphy has enabled the tectonic sequences to be analysed and a new structural model to be developed.

8.3.2 Tectonic Events in the Red Dog District, Northwestern Brooks Range

Six key tectonic events or tectonic phases have been identified in the Red Dog district in this study and as well as from regional geological maps and remotely sensed data and literature reviews. These are:

Phase D1 NW-SE Extensional Faulting - Late Devonian - Mississippian

The first recorded deformation event in the Red Dog district consists of Late Devonian to Early - Late Mississippian syn-rift extensional faulting. Because of the structural disruption caused by the Brookian orogeny, this event is inferred from facies associations and regional stratigraphic patterns (cf. Chapter 5) together with available regional geophysical data across the North Slope parautochthon (Fig. 8.7) (e.g. Decker & Karl, 1977; Geoterrex Ltd. 1981; Kirschner *et al*. 1983; Bird, 1986; Kirschner & Rycerski, 1988; Mauch, 1989; Bird & Molenaar, 1992; Barnes *et al*. 1994; Godson, 1994; Saltus & Simmons, 1997; Connard *et al*. 1999; Saltus *et al*. 1999, 2001*a*, 2002, 2005; Klemperer *et al*. 2002; Sherwood *et al*. 2002).

Phase D2 Post-Rift Inversion and Thermal Subsidence - Late Mississippian to Middle Jurassic

In the Red Dog district the end of the rift phase extension and the onset of the post rift phase is difficult to determine from the stratigraphic relationships in the disrupted allochthon sheets. The seismic line across the parautochthon however clearly indicates that contraction of the ancestral margin probably began in the Late Mississippian with inversion of the rift fault systems (Fig. 8.7) and continued into the Jurassic as the main phase of ophiolite emplacement and formation of allochthons began. Post-rift

stratigraphic units record a generalized deepening of the basin, drowning of carbonate platforms, and decreasing clastic input (cf. Chapter 5, Fig. 5.3).

The sediment-hosted Zn-Pb-Ag and barite deposits as well as the Zn-Pb vein-breccia mineralization probably formed at this time in the in late syn-rift – early inversion in the Late Mississippian (Chesterian).

Phase D3 Ophiolite Obduction - Late Jurassic – Early Cretaceous

Late Jurassic to Early Cretaceous collision and NW-vergent obduction of oceanic lithosphere on to the Arctic Alaska terrane resulting in the emplacement of the Angayucham terrane and Misheguk Mountain allochthon. Ductile deformation fabrics and a tectonic foliation formed at this time.

Phase D4 NW directed thrusting - Early Cretaceous to Late Cretaceous?

Phase 4 involved NW-directed thrusting and emplacement of the main allochthon thrust sheets. Thrusting was accompanied by mass wasting of the advancing emergent thrust front to form olistostromes some of which were incorporated into the thrust sheets. The Wulik Peaks transverse zone formed at this time, possibly involving clockwise rotation of thrust sheets accompanied by fault-related folding, minor strike-slip faulting and development of penetrative cleavage fabrics (S1 & S2). Low angle detachment extensional faulting and final emplacement of the Misheguk Mountain allochthon possibly took place in Middle Cretaceous. Coeval with thrusting, low angle extensional faulting and brittle fragmentation of the Angayucham thrust took place.

Phase D5 SE vergent thrusting - Late Cretaceous – Paleocene

This phase involved Tertiary SE-verging thrusting and thrust fault-related folding. This phase is best seen in the Lisburne Hills – Herald Arch fold and thrust belt to the northeast of the Brooks Range but may have also affected the mountain front detachment folds to the southwest of the Wulik peaks trensverse zone and also locally may have produced southeast vergent ‘back’ thrusts.

Phase D6 NNE-SSW-trending Extension - Eocene – Present Day

Phase 6 consists of NNE-SSW to NE-SW extension and possibly oblique-slip reactivation of the WNW-ESE- to NW-SE-trending Wrench Creek and Sivukat Mountain faults and related structures (e.g. Mulgrave Hills fault). Phase D6 extensional faults offset D4 and D5 structures.

8.3.3 Fold and Thrust Belt Structures in the Red Dog District

In the Red Dog district the western Brooks Range fold and thrust belt consists of seven dominantly northeast-southwest trending sub-horizontal thrust sheets that are vertically stacked on top of each other (Figs. 8.4 & 8.5). The dominant NE-SW fold and thrust trend is interrupted by a prominent NW-trending transverse zone, the Wulik Peaks transverse zone, that offsets the thrust front and locally produces a northwest structural grain (Figs 8.1 & 8.4). The fold and thrust belt contains a number of regional northeast trending antiforms (e.g. Mount Raven antiform) and synforms that are interpreted to be related to duplexes in underlying thrust sheets (Fig. 8.5). Individual allochthons are internally deformed by folds and imbricate thrust faults. This internal allochthon deformation subdivides them into individual, stratigraphically distinct thrust plates and sub-plates (Fig. 8.3). Syn-orogenic strata (Fig. 8.7) date the onset of this main Brookian orogenic contractional phase as beginning in the Early Cretaceous and possibly extending into the Tertiary. The NW-trending late extensional faults such as the Wulik and Sivukat Mountain fault system formed in the Tertiary and control a dominant topographic grain in the Present Day topography.

Thrust Systems and Allochthon Stacking Patterns

In ascending structural order the allochthons are the Endicott Mountains, Picnic Creek, Kelly River, Ipnavik River, Nuka Ridge, Copter Peak and Misheguk Mountain allochthons (Fig. 8.3). Each allochthon preserves a distinct part of the ancient continental margin (Chapter 5). The allochthons are detached in Late Devonian to Early Mississippian strata and are internally imbricated into a series of tectonostratigraphically coherent thrust plates and subplates that vary from 500 to 3 km thick (Fig. 8.5 & Enclosure 2).

The allochthons are regionally folded into a series of regional NE-SW-trending antiforms and synforms with wavelengths of 15 to 30 km (Fig. 8.5). Higher allochthons are preserved in the core of regional synforms (e.g. Kelly River synform). Antiformal stacking or duplexing at lower structural levels has produced the regional antiforms (e.g. Mount Raven antiform). The allochthons of the Arctic Alaska terrane are structurally overlain by the Misheguk Mountain allochthon of the Angayucham terrane. The Misheguk Mountain allochthon is interpreted to be a type-C crystalline thrust sheet (cf. Hatcher, 2004) that was obducted on to the Arctic Alaska terrane. The base of the Angayucham terrane is the Angayucham thrust, a regional NE-SW-trending thrust fault that cuts down-section.

Angayucham Terrane

It has been recently proposed that the ultramafic rocks of the western Brooks Range, including the Misheguk Mountain allochthon of the Red Dog district, are not allochthonous thrust sheets but rooted intrusions (e.g. Saltus *et al.* 2001*a, b*; T. Hudson, 2002, *pers. comm.*; Saltus *et al.* 2003) (cf. Chapter 2, Fig. 2.16). Structural relationships in the Red Dog district indicate that the Angayucham terrane is a fault-bounded, allochthonous thrust sheet (Chapter 6, Figs. 6.51 – 6.60). Evidence includes the well-exposed fault contacts (i.e. Angayucham thrust) (Figs. 6.51 – 6.57) and the structural position of the Angayucham terrane above continental margin strata of the Arctic Alaska terrane (Fig. 8.5c). The presence of a metamorphic sole (e.g. Harris, 2004), upper mantle and lower crust assemblages, and chromite mineralization are unequivocal elements of typical ophiolite systems. These features are consistent with the relative age of ultramafic rock crystallization and cooling of the metamorphic sole (e.g. Harris, 1997; 2004). The geochemical affinity of the Angayucham terrane, transitional between mid-ocean ridge basalts and volcanic arcs (cf. Harris, 1992; Moore *et al*. 1994), is consistent with ophiolites that form in supra-subduction zone settings (e.g. Harris, 1998; Hawkins, 2003; Pearce, 2003; Harris, 2004). All these observations are consistent with the models proposed by earlier workers (e.g. Roeder & Mull, 1978; Harris, 1997) for an ophiolitic origin of these units.

The contact between the Angayucham and Arctic Alaska terranes is characterized by structural thinning and omission of structural levels below the Angayucham thrust (e.g. Avan Hills and Iyikrok Mountain) (Figs. 8.5c & 8.9). On the western margin of the

Avan Hills, the entire Copter Peak, Nuka Ridge, Ipnavik River, Kelly River, and Picnic Creek allochthons are absent below the Misheguk Mountain allochthon (Fig. 8.5c; cf. Chapter 6, Fig. 6.2b-f). Structural thinning below ophiolite thrust sheets is not unique to the Red Dog district but has been widely documented in other orogenic belts. Examples include the Semail ophiolite of Oman (e.g. Searle, 1985; Hanna, 1990, Robertson & Searle, 1990; Robertson *et al.* 1990; Searle & Cox, 1999), the Coast Range ophiolite of California (Platt, 1986, 1993) and ophiolite allochthons of the Variscan Iberian Massif (e.g. Martinez-Catalán *et al*. 2002). Structural thinning below ophiolites in orogenic belts is commonly ascribed to late orogenic and/or post-orogenic collapse and extension (e.g. Hanna, 1990; Dewey *et al*. 1993; Martinez-Catalán *et al*. 2002), synchronous or out-of-sequence thrusting (e.g. Morley, 1988), or alternatively to syn-orogenic extension driven by internal thickening of the orogenic wedge (e.g. Platt, 1986, 1993) (Fig. 8.10).

It is possible that final emplacement of the Angayucham terrane was controlled by syn-orogenic extension related to structural thickening in the internal part of the orogen as predicted by the models of Platt (1986, 1993) (Fig. 8.11) and Brown (2004). Evidence for significant structural thickening includes basement-involved thrusting documented along the southern Brooks Range and within the thrust belt (e.g. Doonerak window, Chapter 2, Fig. 2.5) (e.g. Moore *et al*. 1994; Young, 2004). Middle Cretaceous N-dipping extensional faults associated to exhumation of HP – LT metamorphic rocks of the Schist Belt in (cf. Chapter 2, Figs. 2.4, 2.5) have been documented by Gottschalk (1990) and Miller & Hudson (1991). Syn-orogenic low-angle extensional faulting possibly accounts for the anomalous Present Day position of the Misheguk Mountain allochthon in the Red Dog district, which presently lies in the frontal and most external part of the fold and thrust belt on the southwestern flank of the western Brooks Range in the Red Dog district (Figs. 5.1 & 6.2a).

Structure of the Thrust Front

In the Red Dog district, the western Brooks Range fold and thrust belt terminates in a NE-SW- to WNW-ESE-trending and NW- to SE-dipping thrust front that separates allochthonous thrust sheets and early syn-orogenic strata of the fold thrust belt from the North Slope parautochthon and foreland basin (Figs. 6.2 a-f, 8.5).

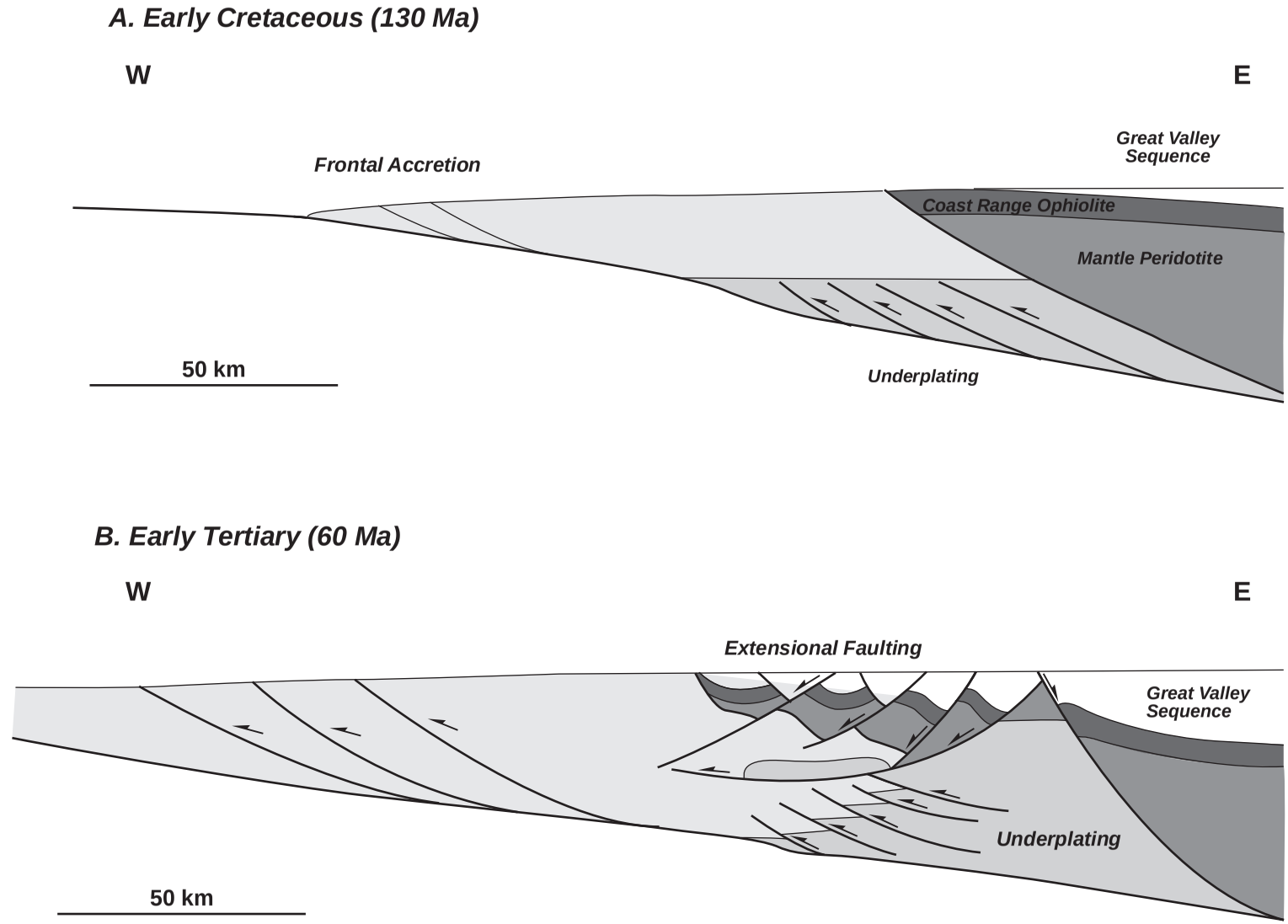


Figure 8.10. Tectonic evolution of the Franciscan Complex and the Coast Range ophiolite, California. **A.** Early Cretaceous underthrusting and obduction of the Coast Range ophiolite. **B.** Early Tertiary. The leading edge of the Coast Range ophiolite is involved in extensional faulting in response to underplating and desestabilization of the orogenic wedge. The ophiolite was original juxtaposed on to sedimentary wedge along a Late Jurassic thrust fault. The Present Day contacts are low-angle detachment extensional faults that formed at a later stage and which brought the high-level ophiolitic rocks against deeper structural levels causing the omission of units (modified from Platt, 1990)

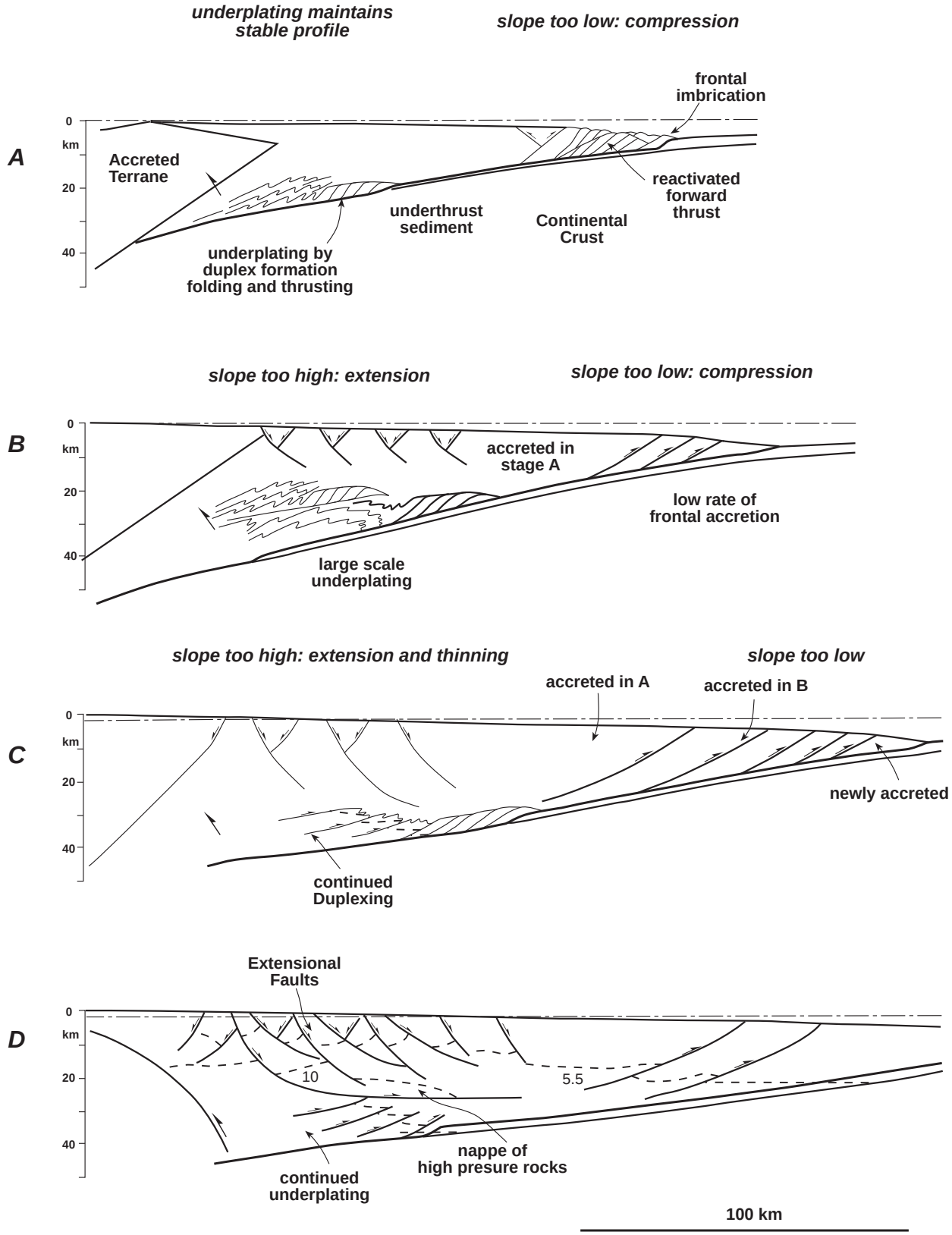


Figure 8.11. Synoptic evolutionary model of an accretionary wedge. Note development of extensional faults in response to changes in taper (modified from Platt, 1986; Brown, 2004).

The thrust front in the Red Dog district is a complex composite structure that varies significantly along strike (cf. Chapter 6, Figs. 6.2 a-f, 6.61 - 69). The thrust front is subdivided into three distinct segments. From northeast to southwest these are the NE-SW-trending Amphitheatre Mountain triangle zone, the WNW-ESE-trending Wulik Peaks transverse zone, and the NE-SW-trending Amaruk River emergent thrust front (Fig. 6.66). The Amaruk River thrust front thrust front occurs as a NE-SW-trending and NW-verging emergent thrust front that is shifted by the Wulik Peaks transverse zone 21 to 25 km to the northwest relative to the Amphitheatre triangle zone (Figs 8.1 & 8.4). The relationships of the thrust front structures to the Wulik Peaks transverse zone are illustrated in detail below.

This thrust front of the western Brooks Range fold and thrust belt formed during the Early Cretaceous Valangian based on *Buchia* cf. found in a new fossil locality in olistolith-bearing syn-orogenic strata along the thrust front by the author. Recently published models (e.g. O'Sullivan *et al.* 1997; Moore *et al*. 2004, 2005) have proposed that the thrust front developed in the Paleocene (*ca.* 60 Ma). The Amphitheatre Mountain triangle zone of the Red Dog district is comparable in geometry and structural position to triangle zones identified in the central Brooks Range (e.g. Moore *et al*. 1997*b*, 2005).

Kinematic Indicators and Directions of Tectonic Transport

Regional and detailed kinematic analyses throughout the Red Dog district indicate an overall regional west-northwest to northwest tectonic transport direction with local north to north-northeast thrust sheet transport restricted to the Wulik Peaks transverse zone (Fig. 8.12). Figure 8.13 shows summary structural data from either side of the Wuliks peaks transverse zone (Figs. 8.13a,b & e,f) where the fold axes indicate northeast or southwest plunges and where the main faults, bedding and cleavage surfaces show a dominant NE-SW structural grain. In contrast structural data within of immediately adjacent to the transverse zone show NW-SE structural trends.

Prior of the recognition of the Wulik Peaks transverse zone in this study and De Vera *et al*. (2004), the occurrence of northeast-southwest and west-northwest east-southeast to northwest-southeast thrust fault and fold trends in the Red Dog district was traditionally

interpreted in terms of two superposed, orthogonal and unrelated tectonic events (e.g. Moore *et al*. 1986; Young, 1989, 1992; Sims, 1996, Edgerton, 1997; L. E. Young, 2002, *pers. comm*.). NW-SE-trending structures of the Red Dog district were previously ascribed to the ENE-directed compressional event was interpreted to be related to the emplacement of the Lisburne Hills-Herald Arch thrust belt west of the Red Dog district (Fig. 2.16). The influence of this event on the Brooks Range can be seen in the westernmost part of the North Slope foreland basin, where Late Cretaceous strata are wedged and complexly refolded. However, no superposition or cross-cutting relationships between WNW-transported and NNE-transported structures have been observed in the Red Dog district.

Unlike the dominant NE-SW-trending thrust faults, which have a regional extent, WNW-ESE-trending thrust structures are localized and restricted to the Red Dog district (Figs. 8.1 & 8.4). This NW-SE trending zone has been called the Wulik Peaks transverse zone in this thesis.

The Wulik Peaks Transverse Zone

The Wulik Peaks transverse zone is a approximately 70 km long and 20 km wide regional WWN-ESE- to NW-SE-trending along-strike discontinuity in the dominant northeast-southwest structural trend of the Brooks Range fold and thrust belt in the Red Dog district (Fig. 8.4). The Wulik Peaks transverse zone consists of a complex branching array of WNW-ESE- to NW-SE-trending gently- to steeply-dipping thrust faults, NNE- to NNW-trending high-angle extensional faults together with complex folds and penetrative cleavage fabrics that strike at 74° to 90° to the dominant NE-SW-trending structural grain of the rest of the Red Dog district. The Wulik Peaks transverse involves the North Slope parautochthon and the Endicott Mountains, Picnic Creek and Kelly River allochthons. Regional dips of the thrust sheets suggests that the transverse zone dips from 38° to 65° to the southwest.

The Wulik Peaks transverse zone controls the geometry and position of the thrust front of the western Brooks Range foreland fold and thrust belt (cf. Chapter 6, Figs. 6.61 – 6.69).

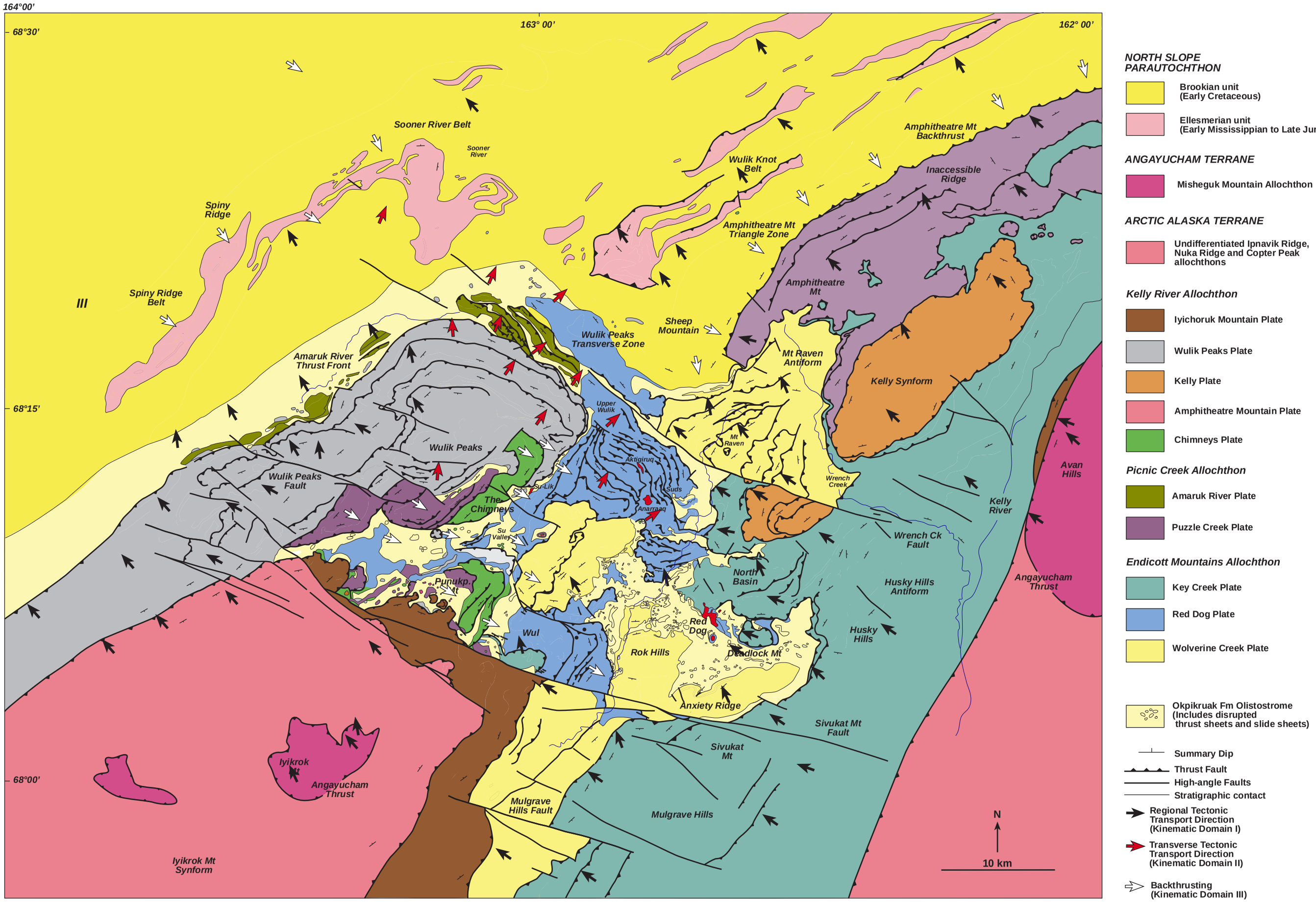


Figure 8.12. Summary tectonic transport map of the Red Dog district compiled from the results of this study.

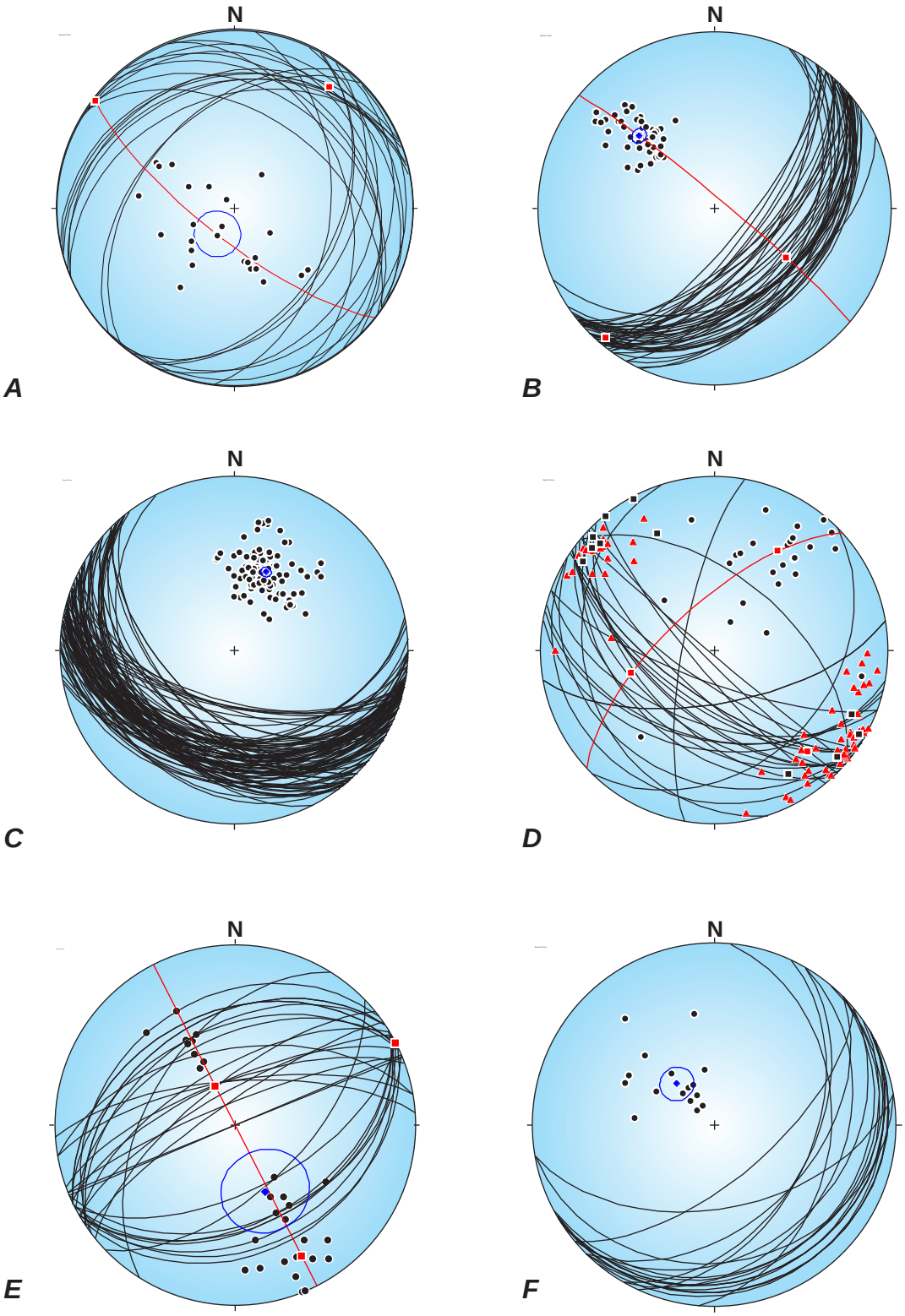


Figure 8.13. Summary lower hemisphere equal area stereographic projections of structural data from the Red Dog district. **A.** Great circles and poles to thrust fault surfaces (N=25). **B.** Great circles and poles to cleavage in the Husky Hills antiform (N=51). **C.** Great circles and poles to bedding surfaces (N=100) from the Kelly River and Picnic Creek allochthons. **D.** Great circles and poles to cleavage (circles) (N=30), minor fold axes (triangles) (N=70) and cleavage-bedding intersection lineations (squares) (N=11) from the Endicott Mountains allochthon. **E.** Great circles and poles to bedding (N=70) in strata of the Kogruk Formation of the Amphitheatre Mountain plate of the Kelly River allochthon. **F.** Poles and great circles to thrust faults along the Amaruk River emergent thrust front (N=20).

North of the transverse zone, the thrust belt terminates in a Type II buried thrust front (cf. Morley, 1986) that forms a well-developed antiformal stack and triangle zone (i.e. Mount Raven antiform, Amphitheatre Mountain triangle zone) (Fig. 6.66). South of the Wulik Peaks transverse zone the thrust front is controlled by an emergent thrust front (i.e. Amaruk River emergent thrust front) (Fig. 6.69). This pattern of along-strike change in the structure and position of the thrust front across transverse zones has been identified in other fold and thrust belts. Examples include the southern Urals (e.g. Perez-Estaún *et al*. 1997; Brown *et al.* 1998, 1999) (Fig. 8.14), the Pyrenees (e.g. López-Blanco, 2002; Larrasoaña *et al*. 2003), the Taiwan thrust belt (e.g. Motherau *et al*. 2000; Lacombe *et al.* 2003), the northern Potwar Plateau and Salt Range of Pakistan (e.g. Morley, 1986; Jaswal *et al*. 1997; Grelaud *et al*. 2002), the Outer Albanides (e.g. Roure *et al*. 2004), the MacKenzie fold and thrust belt (e.g. Vann *et al*. 1986; Gabrielse, 1991), and the Moroccan Rif (Morley, 1986) (Figs 8.15 & 8.16). In many cases these changes in thrust front strikes and positions are inferred to reflect the influences of basement faults at angles to the main thrust front trends.

Basement Structures of the Wulik Peaks Transverse Zone

Structural, stratigraphic, and geophysical data indicate that the Wulik Peaks transverse zone reflects the influence of older inherited basement structures.

Regional Bouguer gravity and aeromagnetic maps of northern Alaska (e.g. Decker & Karl, 1977; Geoterrex Ltd. 1981; Barnes *et al*. 1994; Godson, 1994; Saltus & Simmons, 1997; Connard *et al*. 1999; Saltus *et al*. 1999, 2001a, 2002, 2005) together with petroleum industry seismic and well data (e.g. Kirschner *et al*. 1983; Bird, 1986; Oldow et al. 1987; Kirschner & Rycerski, 1988; Mauch, 1989; Bird & Molenaar, 1992; Kirschner, 1994a, b; Cole *et al*. 1997; Moore *et al.* 1997; Klemperer *et al*. 2002; Sherwood *et al.* 2002; D. G. Roberts, 2005, *pers. comm*.) show a consistent pattern of WNW-ESE- to NNW-trending regional basement highs and lows that underlie most of the Brooks Range, the North Slope foreland basin, and the northern Chukchi Sea (Figs. 8.17a & 8.17b). These features, which include the Umiat, Ikpikpuk, Meade basins and the Hanna trough (e.g. Grantz & May, 1981; Grantz *et al*. 1991; Moore *et al*. 1994; Kelley & Brosgé, 1995; Sherwood *et al*. 2002; Young, 2004) (Fig. 8.18; Chapter 2, Fig. 2.16), have been interpreted as Late Devonian to Jurassic rift structures.

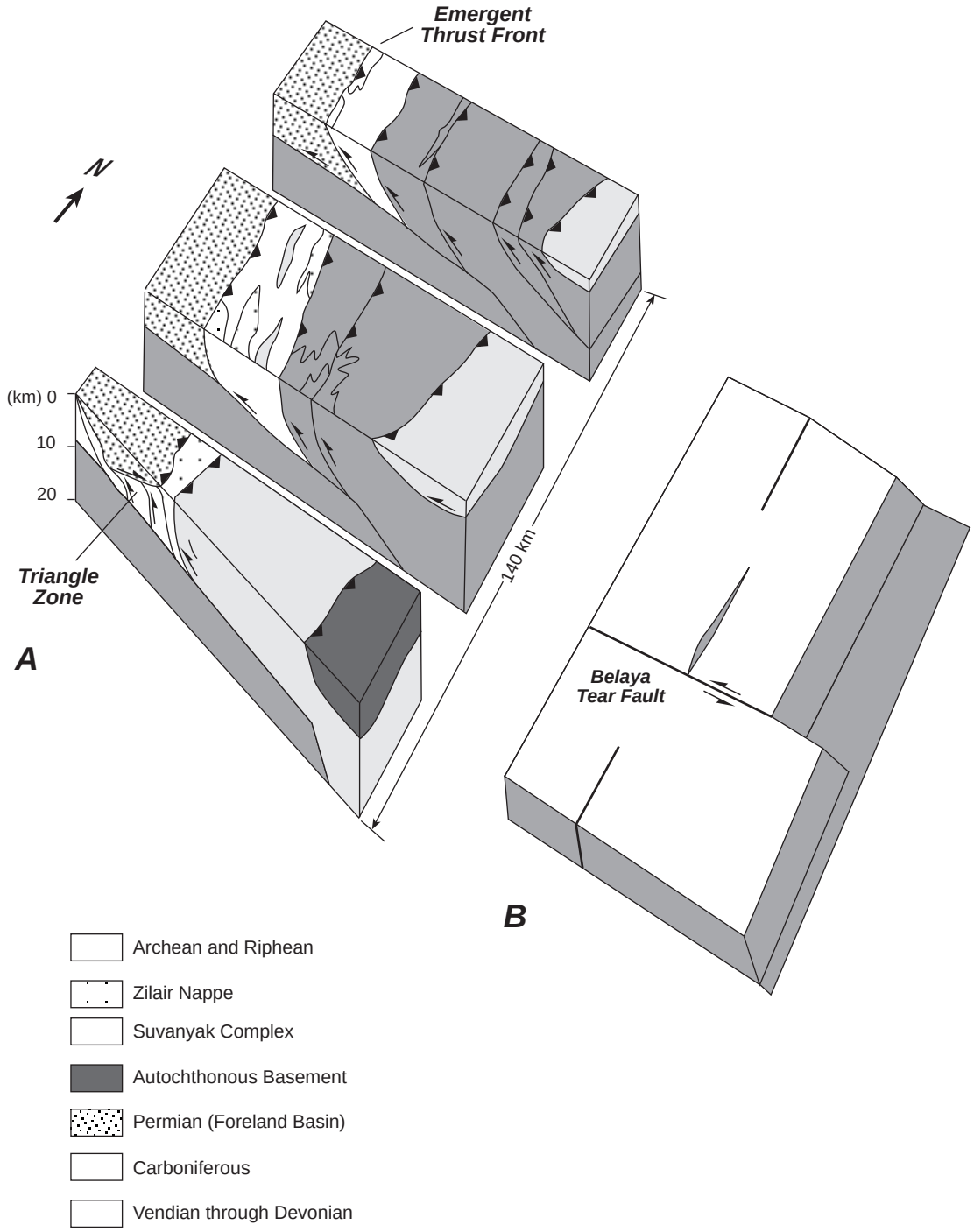


Figure 8.14. A. Block diagram illustrating map and cross sectional view of along-strike strutcural changes in the Belaya transverse zone, southern Urals foreland fold and thrust belt. **B.** Block diagram illustrating the inferred basement geometry and the location of the Belaya basement tear fault (modified from Perez-Estaun *et al.* 1997). Note change from a well developed emergent thrust front (north) to a triangle zone (south) across the Belaya transverse zone.

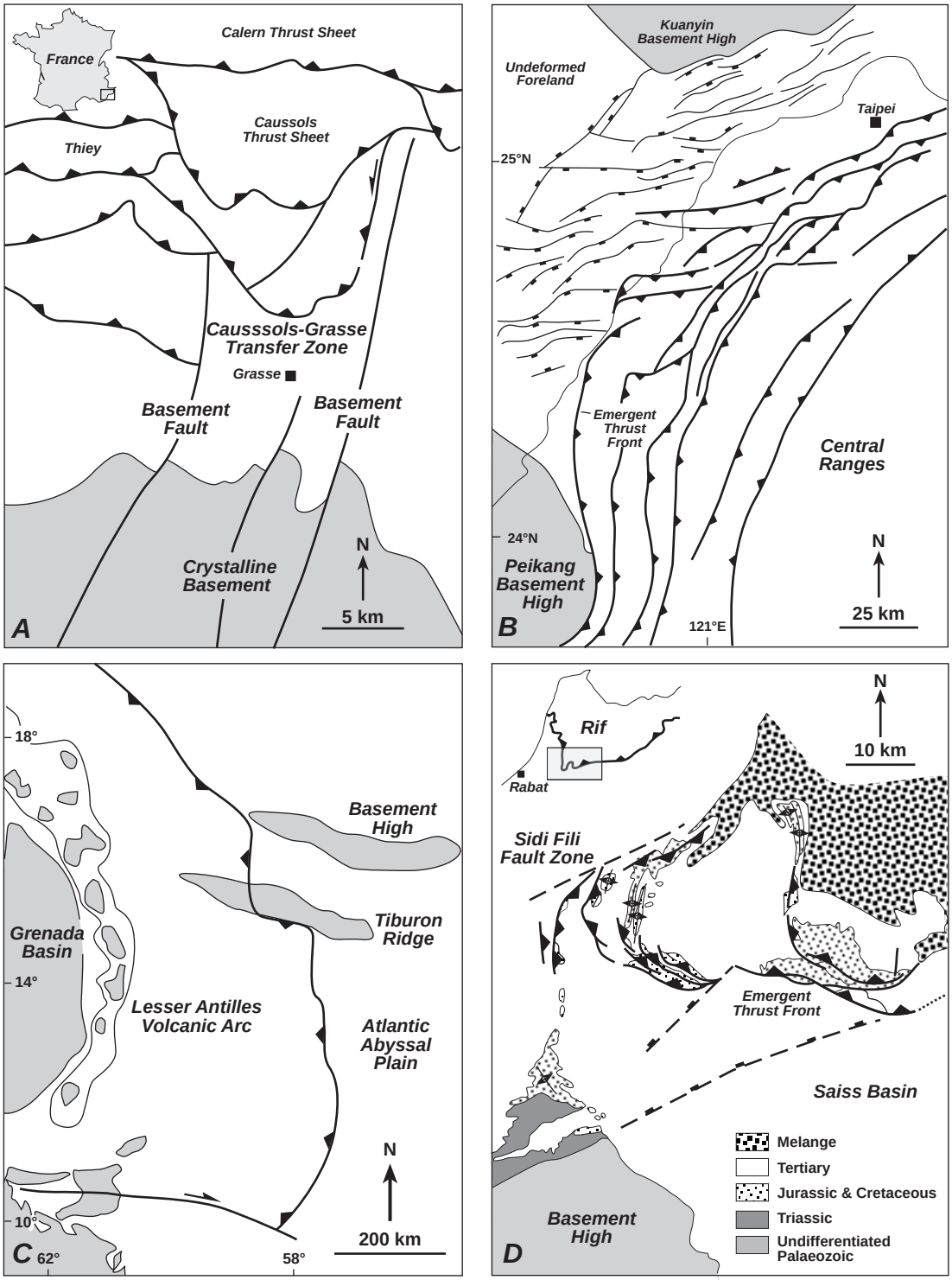


Figure 8.15. A. Simplified map of the Caussols-Grasse transfer zone of southern France (modified from Calassou *et al*. 1993). **B.** Simplified structural map of the Taiwan fold and thrust belt. Note development of transverse zones associated to pre-existing basement extensional faults (modified from Lacombe *et al*. 2002). **C.** Simplified fault map of the Barbados accretionary prism. Note along-strike change in the thrust front related to basement highs (modified from Calassou *et al*. 1993). **D.** Simplified fault map of the Moroccan Rif showing the control of basement structure in the geometry of the thrust front (modified from Morley, 1986).

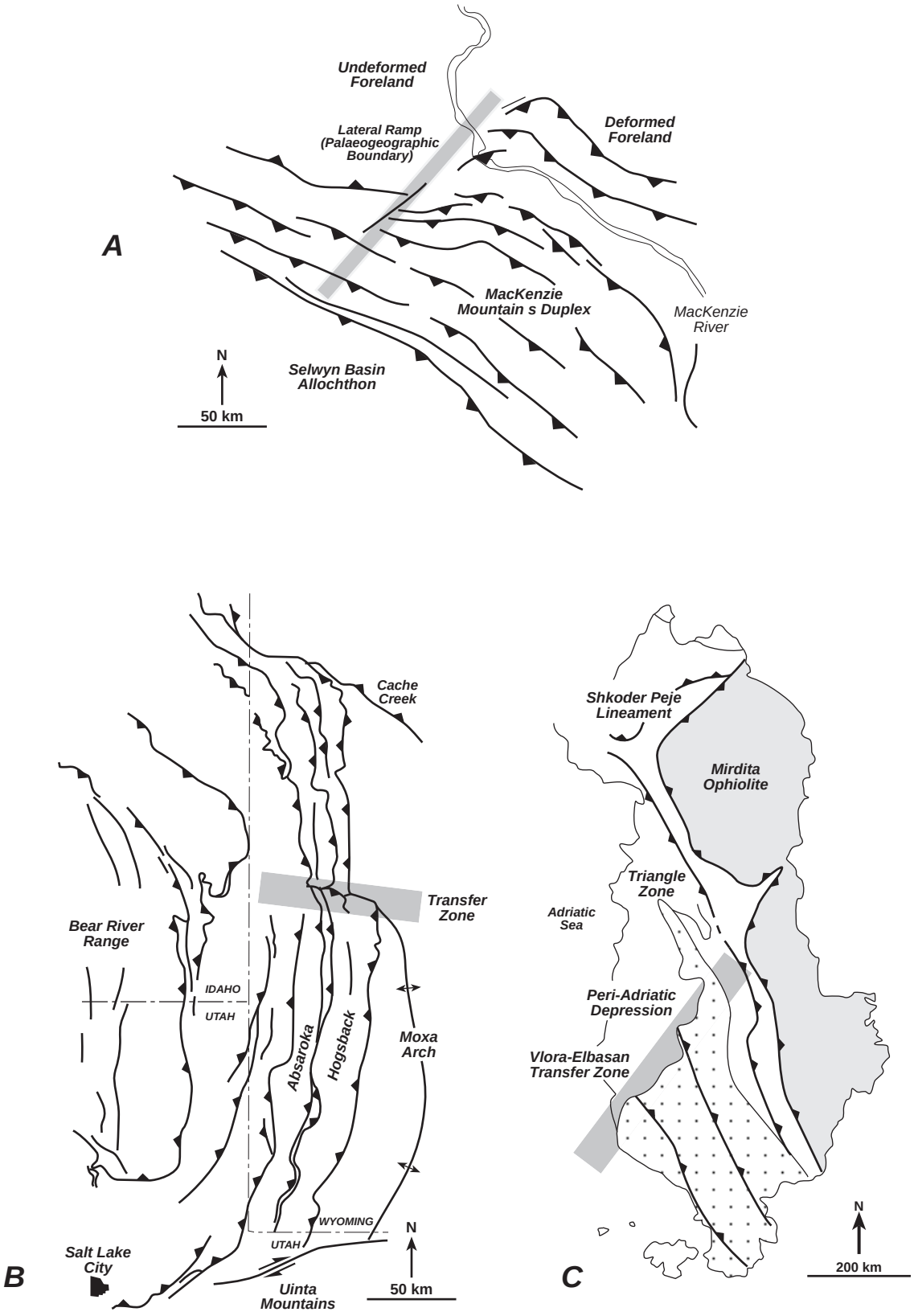


Figure 8.16. Examples of transverse zones in fold and thrust belts. **A.** Simplified fault map of the MacKenzie thrust belt of the Northwest Territories, Canada (modified from Vann e*t al.* 1986). Note along-strike change in the position of the thrust front and change from an emergent thrust to the east to a triangle zone in the west. **B.** Simplified map showing a transfer zone in the Wyoming-Idaho-Utah thrust belt (modified from Hatcher, 2004). **C.** Simplified map of the Outer Albanides showing the Vlora-Elbasan transverse zone (modified from Roure *et al.* 2004).

These basins strike at moderate to high angles (60° to 90°) to the dominant NE-SW-trending structural grain of the Red Dog district and are consistently oriented parallel to sub-parallel to the WNW-ESE-trending Wulik Peaks transverse zone (Fig. 8.18).

Whereas pre-existing basins have been well studied in the central North Slope (Kirschner & Rycerski, 1988; Mauch, 1989; Bird & Molenaar, 1992) no data have been published for their counterparts in the western Brooks Range, including the Red Dog district. Limited gravity, aeromagnetic and controlled-source audio-magnetotelluric surveys across the Red Dog district (e.g. Tailleur, 1970; Decker & Karl, 1977; Geoterrex Ltd. 1981; Young, 1992; Saltus & Simmons, 1997; Connard *et al.* 1999; Saltus *et al*. 1999; Young, 2002, *pers. comm*.) indicate that the Wulik Peaks transverse zone is underlain by an approximately 80 km long and 20 km wide regional WNW-ESE- to NW-SE-trending magnetic positive anomaly (200 to 300 nT) (Fig. 8.19). This feature, here named the Sooner River arch, is interpreted as an extensional fault-controlled basement high that extends from the Red Dog district to the northwest into the northern Chukchi Sea (Fig. 8.20).

Present Day seismicity patterns also indicate the presence of underlying WNW-ESE- to NW-SE-trending basement structures along the Wulik Peaks transverse zone. Seismicity maps of northwestern Alaska (e.g. Fujita *et al.* 1990; Page *et al.* 1991; Klemperer *et al*. 2002; Alaska Earthquake Information Centre, 2005) show Present Day earthquake epicentres with magnitudes of 4.5 to 5.5, and depths of 15 to 45 km (cf. Klemperer *et al.* 2002) along the Wulik Peaks transverse zone. Earthquake epicentres plot on the NNE-plunging terminations of the Mount Raven and Husky Hills antiforms, as well as along the Mulgrave and Wulik Peaks faults, forming poorly to well-defined WNW-ESE- to NW-SE-trending clusters. Although many of these earthquakes are too small to yield reliable focal mechanism solutions, it is suggested that the Present Day seismicity results from reactivation of the same basement fault systems that controlled the development of the ancient continental margin of Arctic Alaska in the Palaeozoic and the development of the Wulik Peaks transverse zone during the Mesozoic Brookian orogeny.

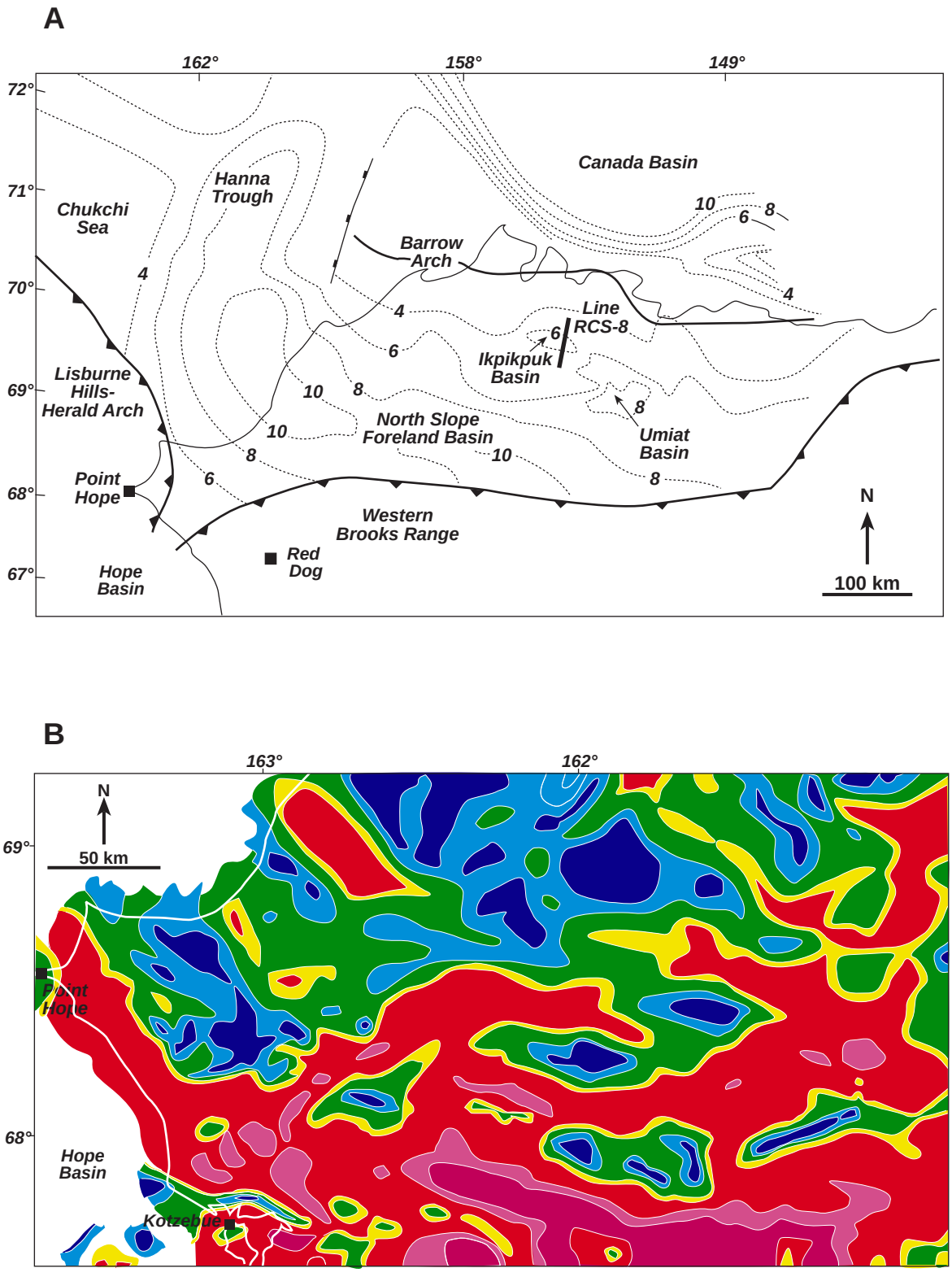


Figure 8.17. A. Structure contour map of the North Slope foreland basin showing depth (in km) to basement. Contours generated from seismic and well data. (modified from Bird, 1988; Bird & Molenaar, 1992; Grantz & May, 1983). **B.** Bougueur gravity gradient contour map (10 km upward continued) of northwestern Alaska. Note NW-SE-trending basement fabrics deeply buried beneath strata of the North Slope foreland basin (modified from Teck Cominco Alaska Inc. database). Lows are cool colours whereas highs are red colours.

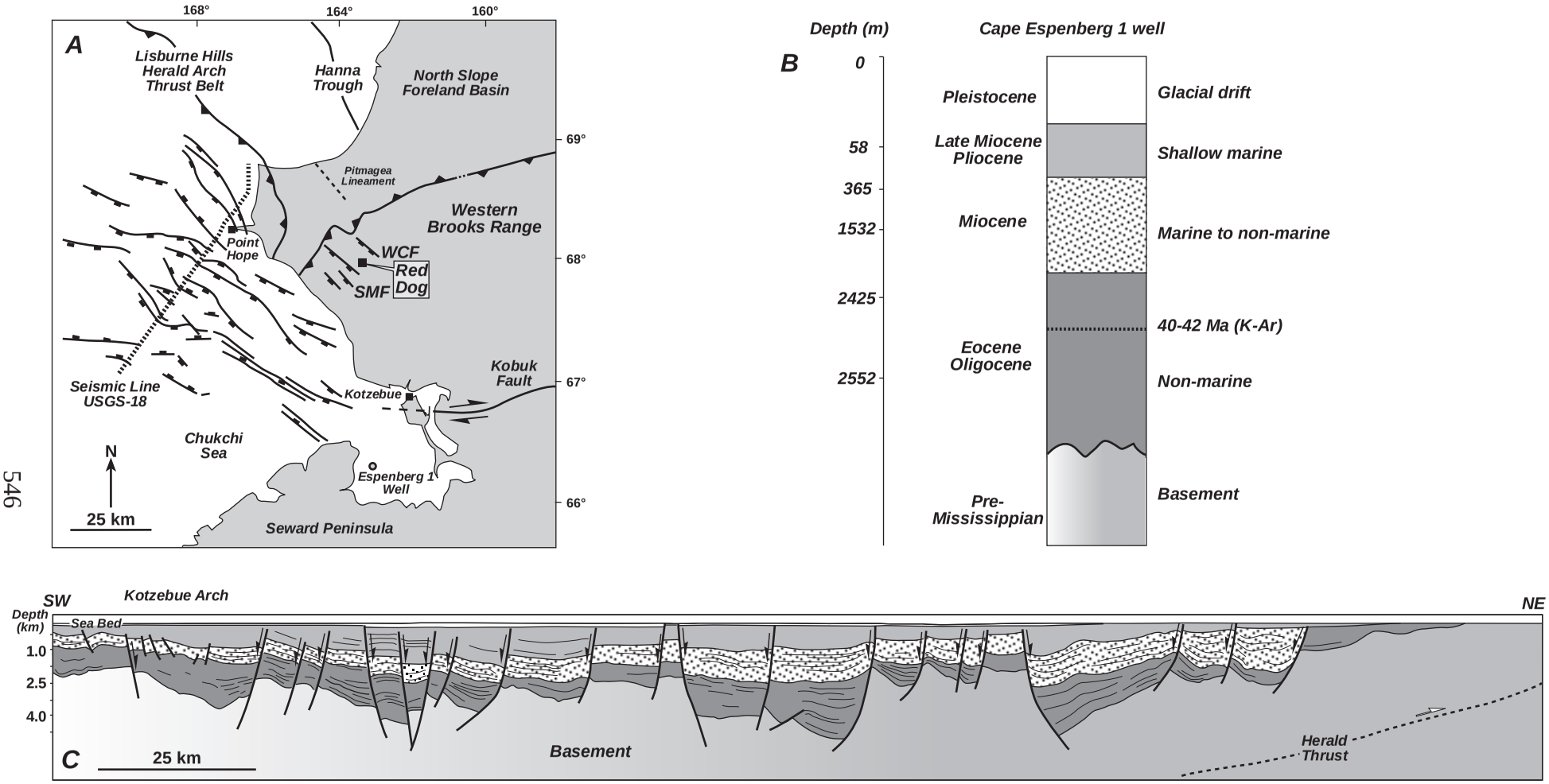


Figure 8.18. Hope basin. **A.** Simplified fault map of the Hope Basin (modified from Tolson, 1987; Elswick & Toro, 2003).The location of the Red Dog mine and the Wrench Creek (WCF) and Sivukat Mountain (SMF) are shown. **B.** Generalized stratigraphic column of the Hope basin from the Cape Espenberg 1 well. Refer to A for location (modified from Tolson, 1987; Decker *et al*. 1988; Elswick & Toro, 2004). **C.** Interpretation of seismic line USGS-18 (reinterpreted from Elswick & Toro, 2003). Refer to A for location of section.

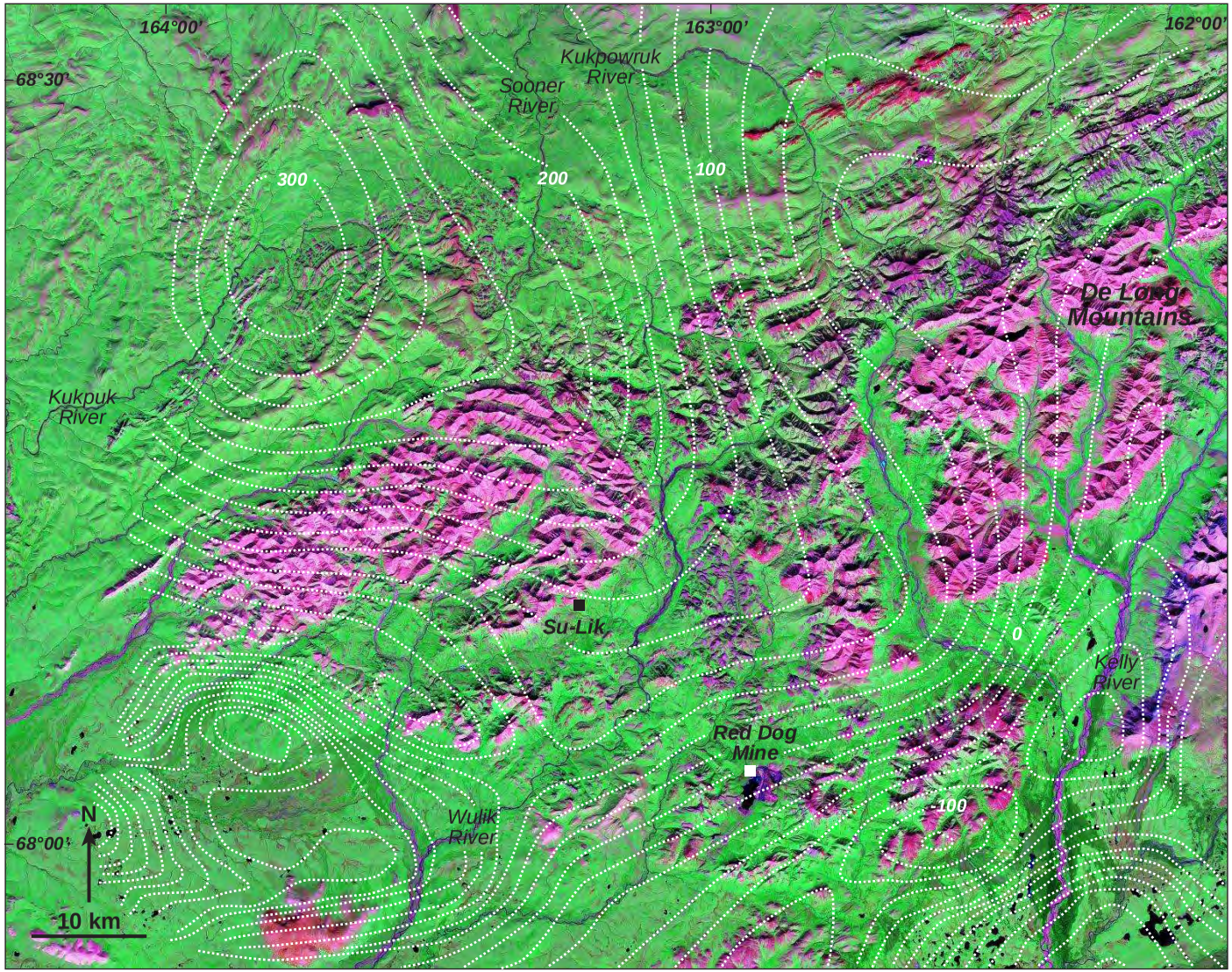


Figure 8.19. Landsat 7 TM image (spectral bands 7,4,2) of the Red Dog district overlain by contours (nT) of magnetic data upwardly continued 10 km to emphasize basement features. Note the direct correlation between positive magnetic anomaly in the Sooner River area and the Wulik Peaks transverse zone and the Wrench Creek and Sivukat Mountain faults (satellite imagery from National Aeronautics and Space Administration, 2005; Magnetic anomaly contours from Saltus & Simmons, 1997; Connard *et al.* 1999; Saltus *et al.* 1999).

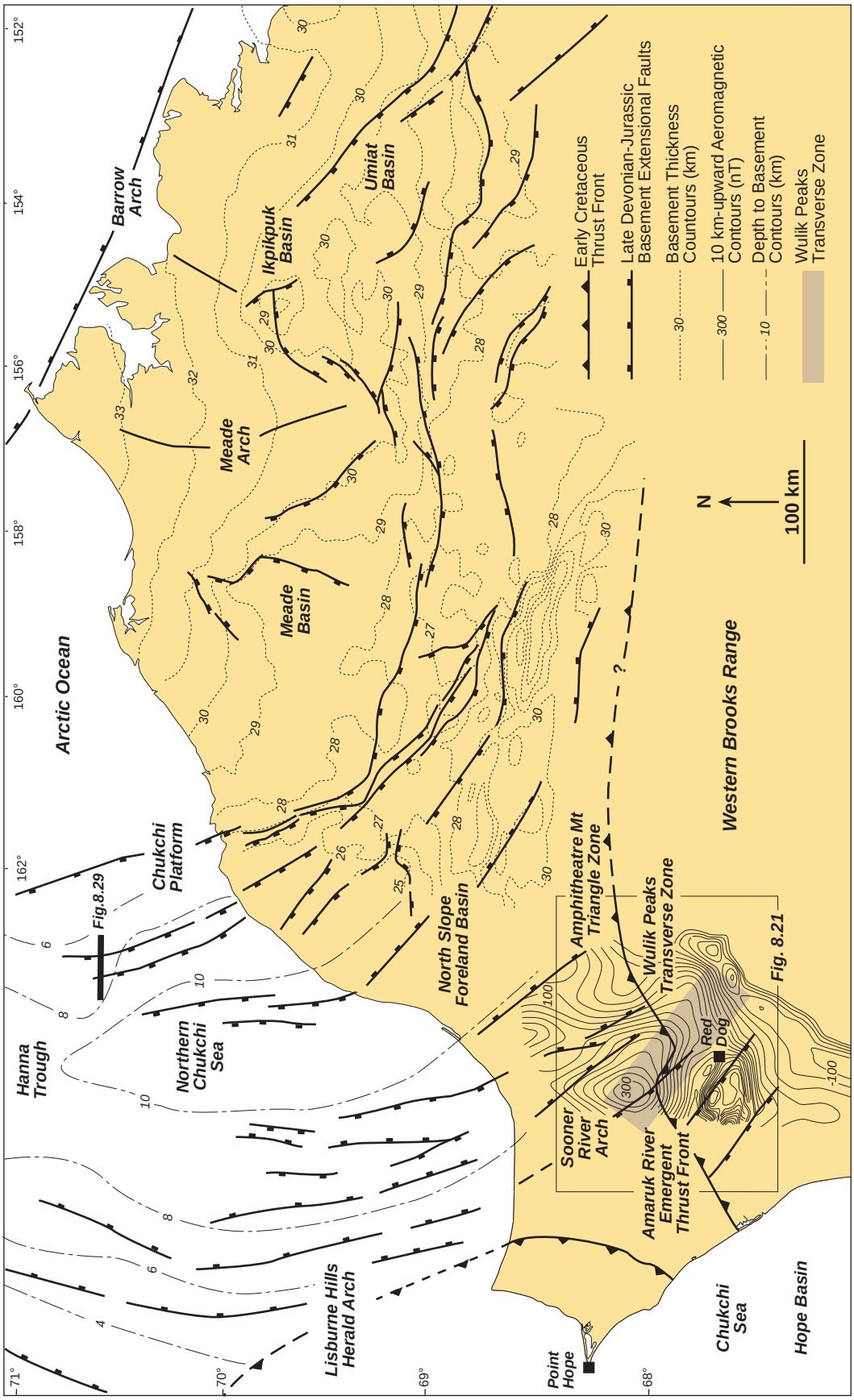


Fig. 8.20. Map of the northern Alaska showing the relationship between Late Devonian to Jurassic basement extensional faults and the Wulik Peaks transverse zone (compiled and interpreted from Decker & Karl, 1977; Geoterrex Ltd. 1981; Bird, 1988; Barnes *et al.* 1994; Godson, 1994; Saltus & Simmons, 1997; Connard *et al.* 1999; Saltus *et al.* 1999, 2001*a*, 2002, 2005). Depth to basement contours are based on seismic surveys and well data. The location of the Red Dog mine is shown.

Stratigraphic Changes Across the Wulik Peaks Transverse Zone

In the Red Dog district, NNE- and WNW-trending facies changes with NNE-shallowing facies (Chapter 5) and SW- to S-directed palaeocurrents suggest that the geometry of the pre-existing continental margin was possibly controlled by NW-SE- to NW-SW-trending extensional faults. This is also consistent with the WNW-ESE- to NW-SE-trending systematic orientation of Zn-Pb vein-breccia mineralization in syn-rift strata of the Endicott Group (cf. Chapter 5, Fig. 5.10; Chapter 6). Parautochthonous basin margin facies (e.g. Anxiety Ridge, Wulik Knot) are interpreted to have been deposited on the hangingwall of major extensional fault blocks that were spatially related to the the Wulik Peaks transverse zone (Figs. 5.1 & 8.1).

The stratigraphic patterns in the Red Dog district are also consistent with stratigraphic relationships documented elsewhere in the Brooks Range. Young (2004) has suggested that sedimentation across the Brooks Range was largely controlled by N- to NW-trending extensional faults. Kelley & Brosgé (1995) identified a series of *en echelon* WNW-ESE-trending depocentres of Late Devonian to Mississippian syn-rift strata. This is also consistent with regional SW- to S-directed palaeocurrents in the Kanayut Conglomerate (e.g. Churkin & Trexler, 1980; Nilsen, 1981; Moore & Nilsen, 1984; Handschy, 1998*b*). Regional lithofacies distribution of the Lisburne Group along the Brooks Range and North Slope parautochthon defines a series of well-defined WNW-ESE- to NW-SE-trending belts (e.g. Armstrong & Mamet, 1978; Dumoulin *et al*. 1997; Sherwood *et al*. 2002; L. E. Young, 2002, *pers. comm.*).

Wrench Creek and Sivukat Mountain Faults

The Wrench Creek and Sivukat Mountain faults are WNW-ESE- to NW-SE-trending, SSW-downthrown high-angle extensional faults that postdate the emplacement of the allochthons of the Arctic Alaska and Angayucham terranes (Figs. 8.1 & 8.4). The faults are approximately 45 km long and have inferred vertical throws of approximately 1 to 3 km (Chapter 6). They are interpreted to have developed above the oblique ramp system underlying the Wulik Peaks transverse zone and were later reactivated as dip to oblique slip extensional faults or may have possibly originated as thrust-related tear faults in the North Slope parautochthon. Evidence for the latter interpretation includes the lack of

structural correlation across the faults. The Mount Raven antiform does not exist south of the Wrench Creek fault, whereas the Wulik Peaks plate of the Kelly River allochthon is not present north of the Wrench Creek fault (Fig. 8.5).

Timing of Late Extensional Faulting

The absolute timing of late extensional movement on the Wrench Creek and Sivukat Mountain faults cannot be readily determined because of the lack of preserved post-Early Cretaceous strata. A minimum age for these structures is only constrained by Valangian strata that are offset by the Wrench Creek fault. Extensional reactivation of the Wrench Creek and Sivukat Mountain faults may be ascribed to NE-SW-trending regional extension associated with the opening of the NW-SE- to WNW-ESE-trending Hope basin. The Hope basin is an approximately 800 km-long Cenozoic extensional basin that spans the Chukchi Sea (cf. Chapter 2, Figs. 2.4 & 2.16; Fig. 8.18) (Klemperer *et al*. 2002). Opening of the Hope basin is constrained by middle Eocene (40-42 Ma K-Ar ages) early syn-rift strata (e.g. Tolson, 1987; Decker *et al*. 1988; Klemperer *et al*. 2002). The WNW-ESE- to NW-SE-trending Wrench Creek and Sivukat Mountain faults are similar in size and are oriented parallel to sub-parallel to the extensional faults of the Hope basin (Fig. 8.18) (cf. Elswick, 2003; Elswick & Toro, 2003) (Fig. 8.18).

A diffuse belt of Present Day seismicity that extends from the Hope basin into the Red Dog district (e.g. Tolson 1987; Decker *et al*. 1988; Fujita *et al*. 1990; Page *et al*. 1991; Moll-Stalcup, 1994; Plafker *et al*. 1994; Mackey *et al*. 1997; Klemperer *et al*. 2002; Alaska Earthquake Information Centre, 2005) indicates that extensional faulting has continued into the Present Day. Present Day stress trajectories, determined from earthquake focal mechanism solutions (e.g. Fujita *et al*. 1990; Page *et al*. 1991; Plafker *et al*. 1994, Reinecker *et al*. 2004) indicate a NW-SE-trending maximum horizontal component of stress, compatible with northeast-southwest extension on the Wrench Creek and Sivukat Mountain faults. These observations are also consistent with the models of Hudson & Plafker, (1978), Biswas *et al*. (1986) and Page *et al*. (1991), who have suggested that Present Day regional stresses in western Alaska are dominantly controlled by regional extension.

The Wrench Creek and Sivukat Mountain faults have well-developed fault-line scarps (Figs. 6.61 – 6.69) that cause the rugged topography of the Brooks Range (cf. Chapter

1, Fig. 1.2; cf. Chapter 6) to dramatically decrease in the Red Dog district. In addition, the presence of numerous widely spaced clusters of H- and S-charged springs spatially related with mapped faults (e.g. Young, 1992) may be interpreted as permissive evidence of relatively recent fault activity.

Structural Analysis of the Red Dog Mine

In the vicinity of the Red Dog mine and locally to the north the Red Dog style mineralization is structurally restricted to the Red Dog plate of the Endicott Mountains allochthon (Chapters 5 & 7). The Red Dog plate is internally imbricated and stacked with folding and thrusting of the deposits.

The best exposures of deposit scale structures are found in the Red Dog open pit (Chapter 7 & Enclosure 3). Detailed mapping shows that the main Red Dog deposit is complexly folded and thrusted (Enclosure 3). Complex thrust fault-related folds – both detachment and transported fault-propagation folds are well developed (Chapter 7; Enclosure 3). Several SW dipping thrust faults also occur in the open pit. Fold axes and inferred tectonic transport directions are highly variable with both NW directed movement as well as NNE directed movement (Enclosure 3). This is interpreted to reflect the proximity to the Wulik Peaks transverse zone where both directions of thrust and fold vergence are to be expected (see discussion above). Vein and silicified sulphide units display relatively little internal deformation with pervasive strains being developed in the enveloping stratigraphy. The barite bodies above the deposit show penetrative deformation fabrics in places but trace fossils are also preserved in baritic units.

In addition to the pervasive 'Brookian' deformation a new set of late NW trending extensional faults has also been mapped in the Red Dog open pit (Chapter 7). These are interpreted to be part of the Tertiary age Wrench Creek and Sivukat Mountain extensional fault system.

The complex stratigraphy of the Red Dog plate (Chapter 5) with the inclusion of olistolith blocks in the Optikruak formation may be explained by an evolutionary model

where emergent thrust structures within the foredeep basin generate unstable slopes that then collapse producing mass wastage deposits and slide and slump units (Fig. 8.21). Mass wastage deposits of this type have been imaged in 3D seismic surveys offshore Brunei where active tectonic thrusting and folding occurs at the Present Day (McGilvrey & Cook, 2003).

8.3.4 Tectonostratigraphic Model for the Evolution of the Red Dog District

The structural and stratigraphic analysis of the Red Dog district carried out in this research project have been combined to produce a synoptic model for the evolution of this part of the western Brooks Range (Fig. 8.22). Inherited Late Devonian – Early Mississippian basement faulting in two orientations – one NE-SW trending defining the overall structure of the southern passive margin of ancestral Alaska, combined with a second NW-SE trending basement fault fabric producing segmentation of the margin, controlled the geometries of the allochthons and thrust sheets in the Red Dog district. Sedimentary facies variations of both the syn-rift and post-rift successions also reflect these two inherited structural elements (Chapter 5) (Fig. 8.22). In particular the NW trending Sooner River Arch was a long-lived basement high that controlled both the syn-rift architecture and also the early inversion history as well as the later Brookian thrust structures. As a result two dominant structural trends were formed – a regional NE-SW dominant thrust and fold belt system compatible with the rest of the western Brooks Range as well as the Wulik Peaks transverse zone with a NW orientation (Figs. 8.1, 8.4 & 8.22). The Wulik Peaks transverse zone is an SW dipping oblique-lateral ramp that generated rotation, folding, local extension and strike-slip faulting along its length during the dominant NW vergent Brookian thrusting (Fig. 8.22).

Figure 8.23 is a simplified synoptic diagram of the Wuliks Peak transverse zone showing the probable clockwise rotation of the thrust sheets and the synchronous development of both strike-slip and extensional faults along the transverse oblique to lateral ramp system. Similar geometries have been inferred by Paulsen & Marshak (1999) and Marshak (2004) for inversion of basement involved extensional faults (Fig. 8.24). In the Red Dog district the detachment geometries of the Endicott Mountains allochthon is inferred to have been controlled by the pre-existing basin geometry controlled by Late Devonian – Early Mississippian extensional faults (Fig. 8.25).

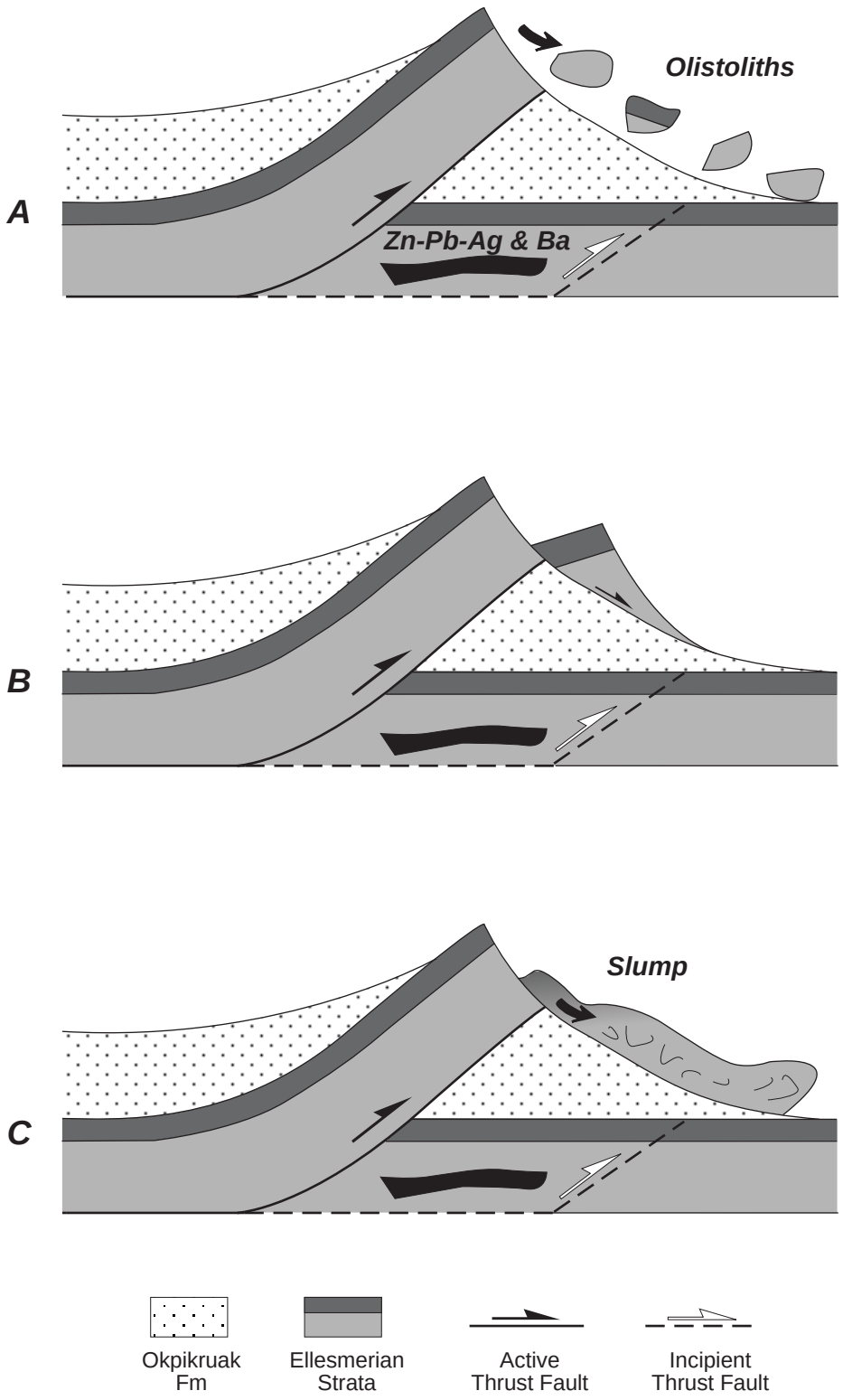


Figure 8.21. Synoptic diagram showing possible mechanisms of deposition of mass-wasting into the Okpikruak Formation above the Red Dog plate. **A.** Rock fall. Olistoliths are incorporated into the Okpikruak Formation matrix. **B.** Gravity slide sheet. Coherent slide sheets are detached from an advancing thrust sheet and incorporated into syn-orogenic strata. Note glide surface cuts down section. **C.** Deposition slumping, debris flow and turbidity currents. Note internal deformation of the transported mass.

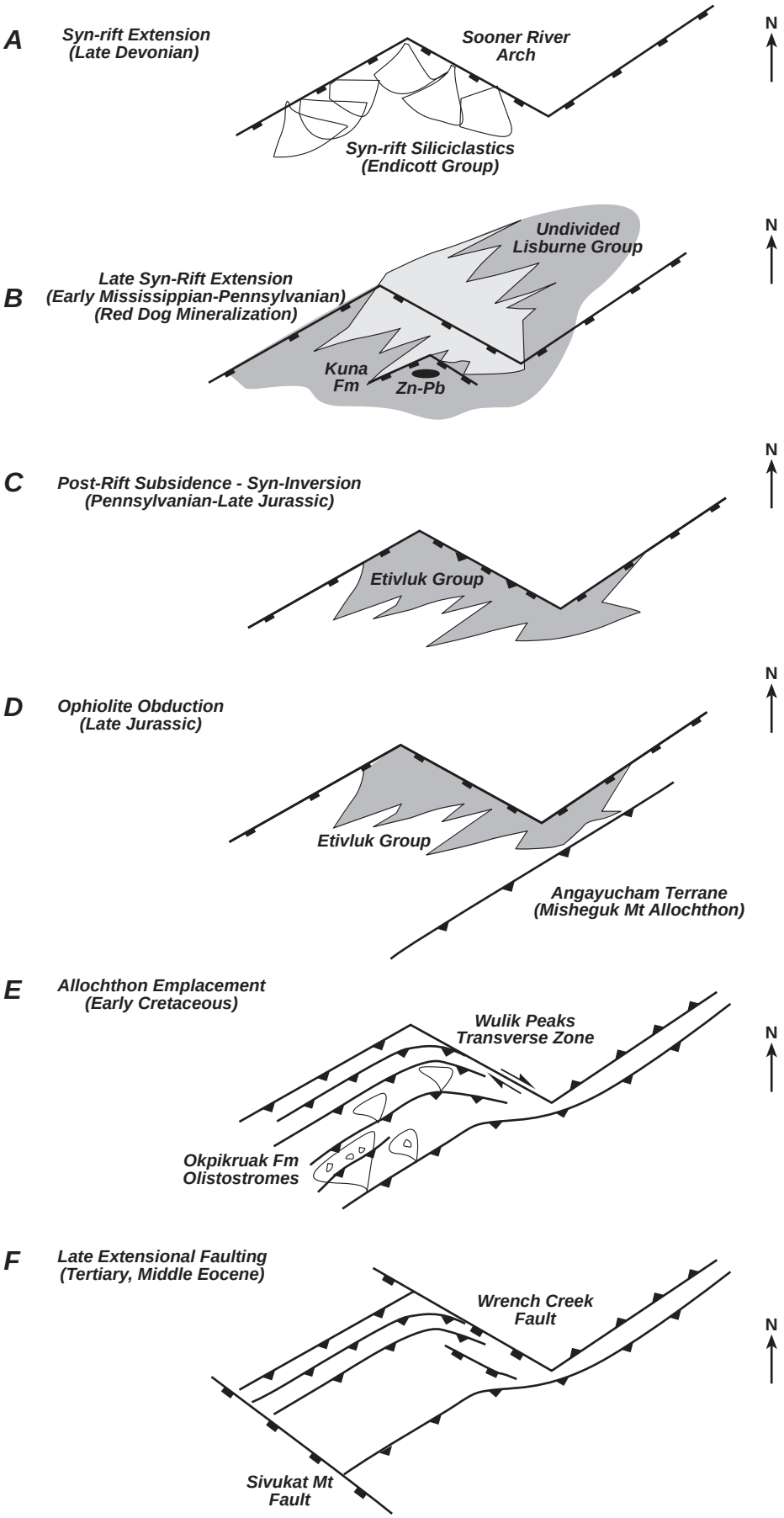


Figure 8.22. Simplified synoptic diagram illustrating key tectonostratigraphic events in the evolution of the Red Dog district.

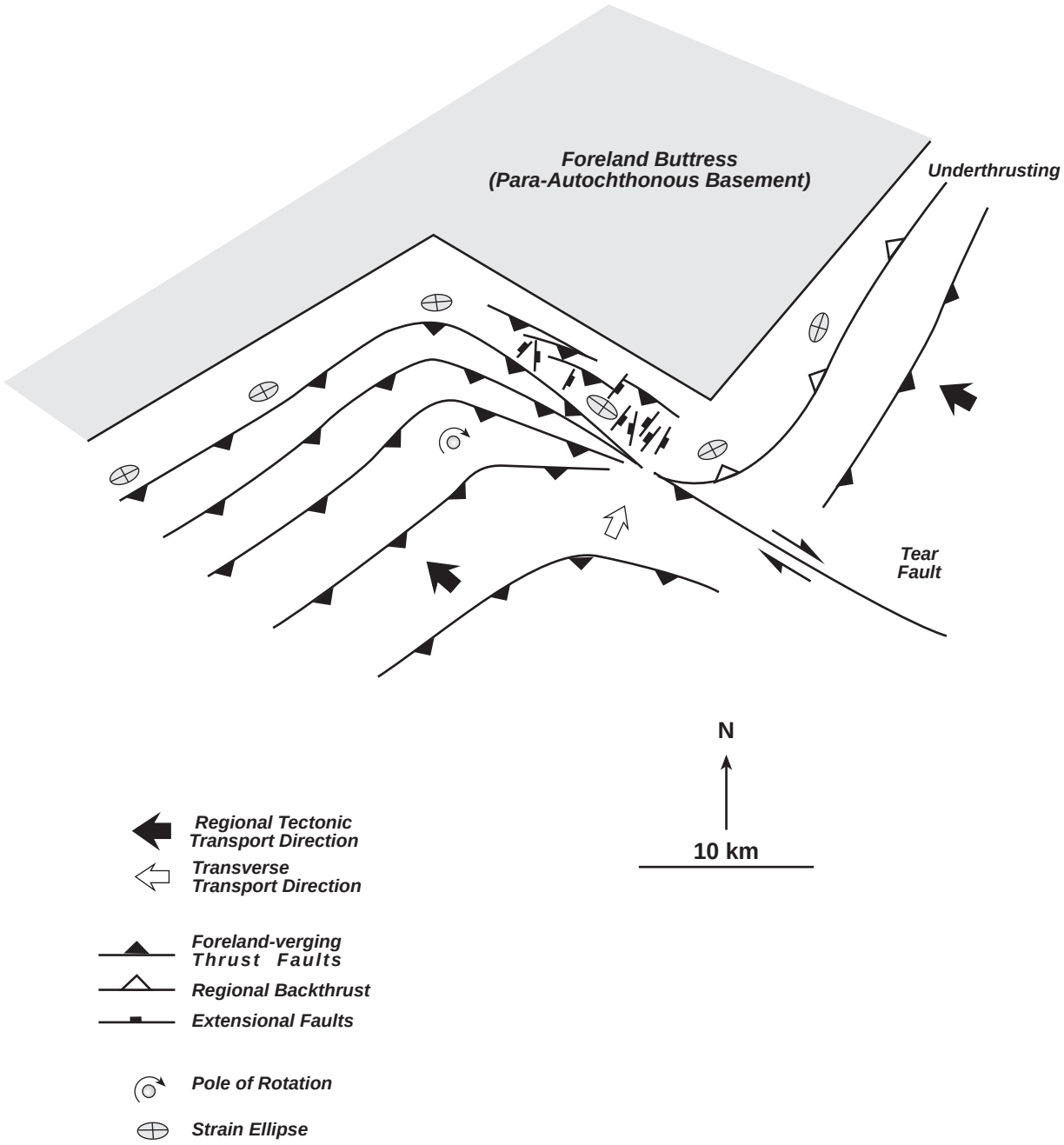


Figure 8.23. Simplified synoptic diagram showing the main structural relationships in the Wulik Peaks transverse zone. Hypothetical strain ellipses are shown.

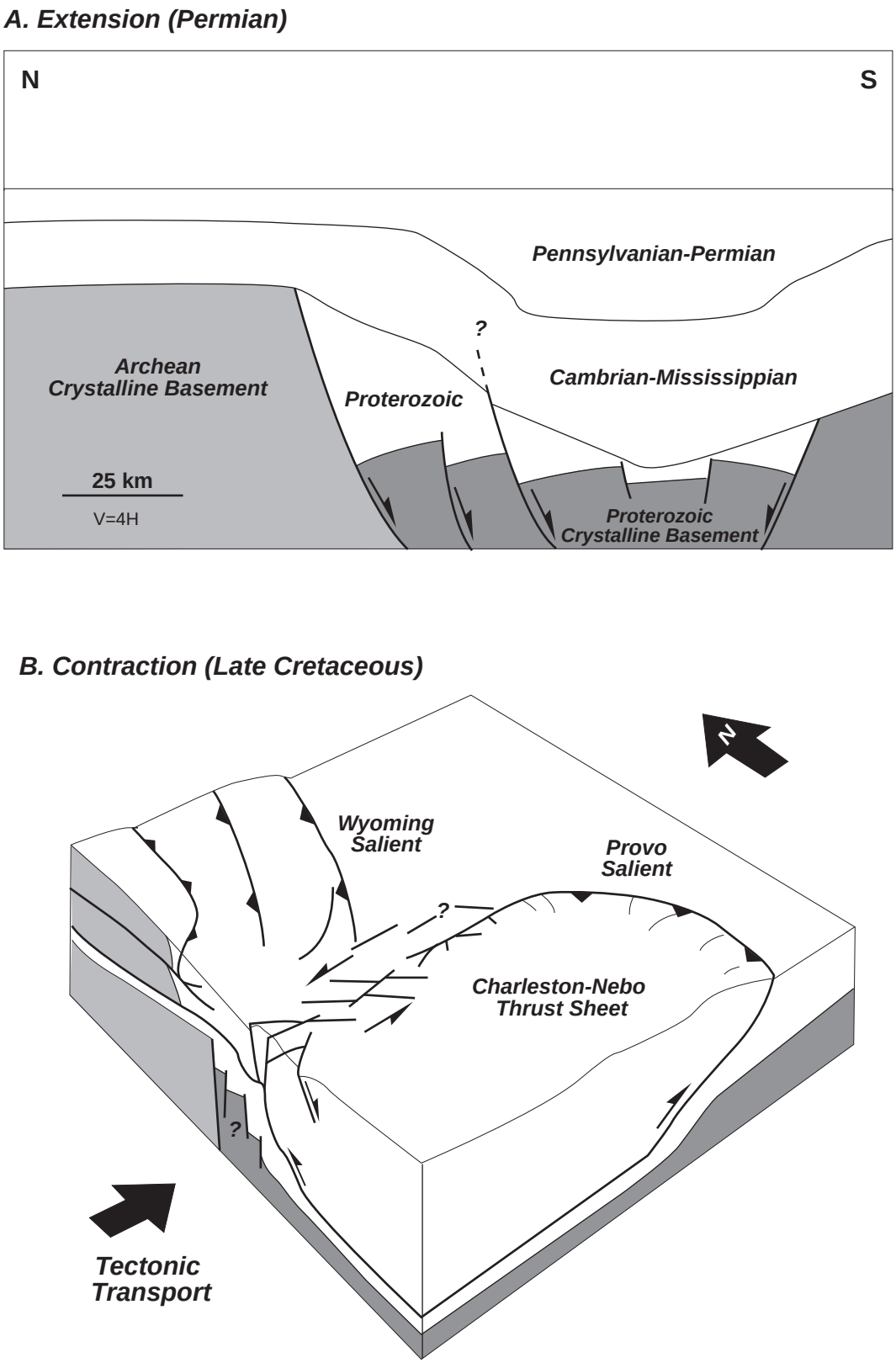


Figure 8.24. Transverse zone in the Uinta recess of the United States (modified from Paulsen & Marshak,1999; Marshak, 2004). **A**. Schematic cross-section showing the basin geometry prior to thrusting. **B.** 3D synoptic diagram showing transverse zone associated with structural inheritance of the asymmetric pre-existing basement high shown in A. Note that the southern part formed over an abruptly deepening basin, evolved into a tear fault while the northern segment, formed over a gently tapering basin, did not but rather formed a gently curved salient.

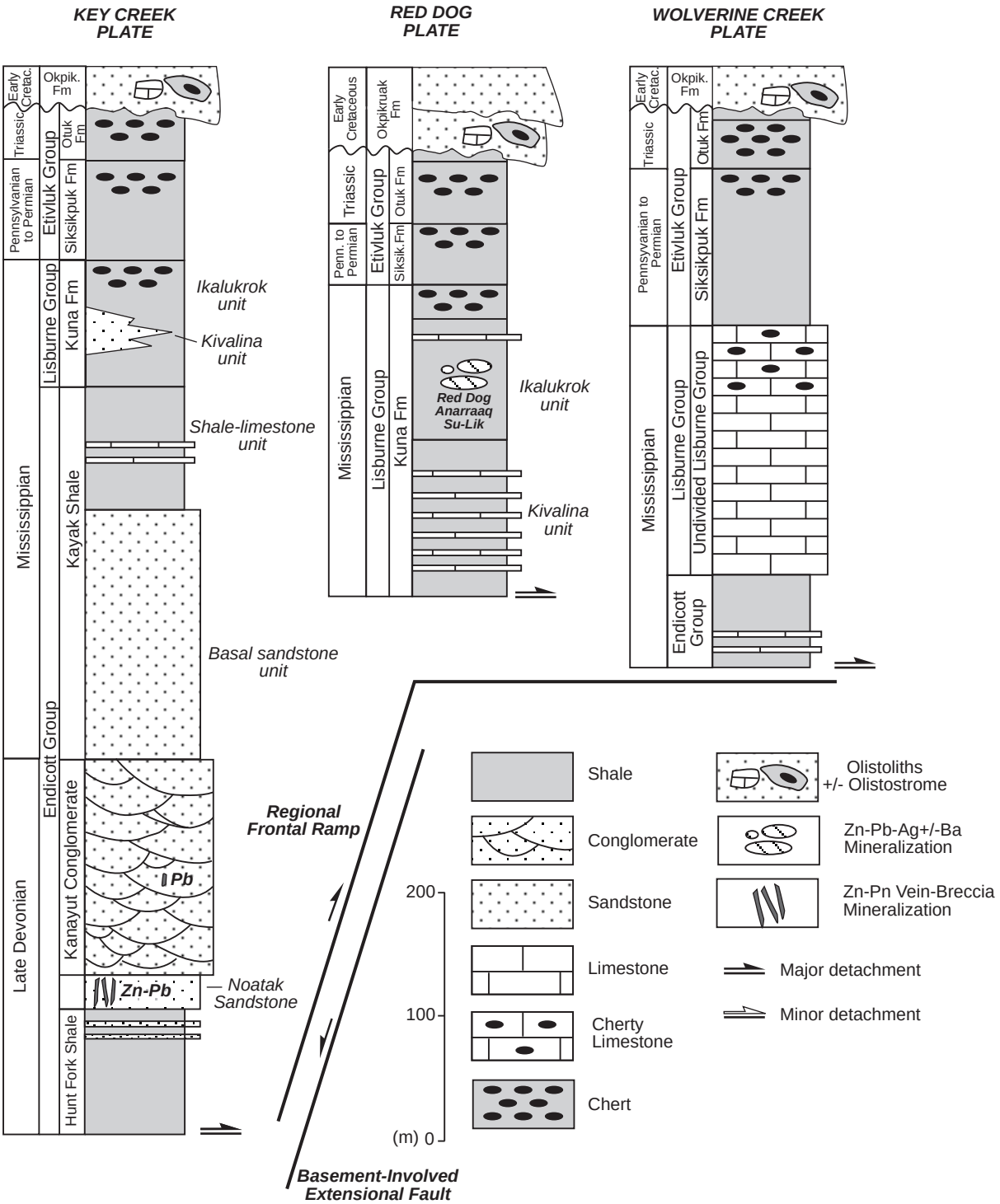


Figure 8.25. Summary stratigraphy of the Key Creek, Red Dog, and Wolverine Creek plates of the Endicott Mountains allochthon showing detachment geometry controlled by pre-existing basin fault geometry.

A synoptic model for the progressive evolution for the Wulik Peaks transverse zone during the major Brookian contractional deformation is shown in Figure 8.26. Figure 8.27 shows a schematic 3D block diagram of the Wulik Peaks transverse zone resulting from thrusting across a pre-existing basement fault controlled lateral ramp.

8.4 TECTONIC EVOLUTION OF THE WESTERN BROOKS RANGE

The results of this tectono-stratigraphic analysis of the Red Dog district have important implications for the tectonic evolution of the western Brooks Range. The dominant regional orientation of the major folds and thrusts in the northwestern Brooks Range is a gently arcuate NE-SW trend (Figs. 8.1 & 8.4). The dominant tectonic transport direction for the Brookian allochthon thrust sheets is from southeast to northwest (Fig. 8.12). In this thesis only one major regional phase of thrusting, folding and associated cleavage development has been found. Along strike changes in structural grain across the Wulik Peaks transverse zone are interpreted to reflect the influence of pre-existing basement fabrics on thrust architectures (see discussion below). Contrary to previous models the result from this study do not support two different phases of shortening in the western Brooks Range (e.g. Moore *et al*. 1986; Young, 1989, 1992; Sims, 1996, Edgerton, 1997). The structural patterns seen on Landsat images (Fig. 8.28) show a complexly folded 'interference zone between the Lisburne Hill thrust belt and the mountain front of the northwestern Brooks Range. In this thesis these are interpreted to be two different age and largely unrelated fold-thrust belts.

8.4.1 Transverse Zones and Basement Structural Inheritance

Typical thin-skinned fold and thrust belts (e.g. the Canadian Rocky Mountains and the Appalachians) generally produce gently arcuate fold and thrust trends along strike with well documented structural styles of thrust and fold systems (see review in Chapter 4) (e.g. Bally *et al*. 1966; Dahlstrom, 1969, 1970; Boyer & Elliot, 1982; Boyer, 1986; Mitra, 1986; Butler, 1989; Woodward *et al*. 1989; McClay, 1992, 2004).

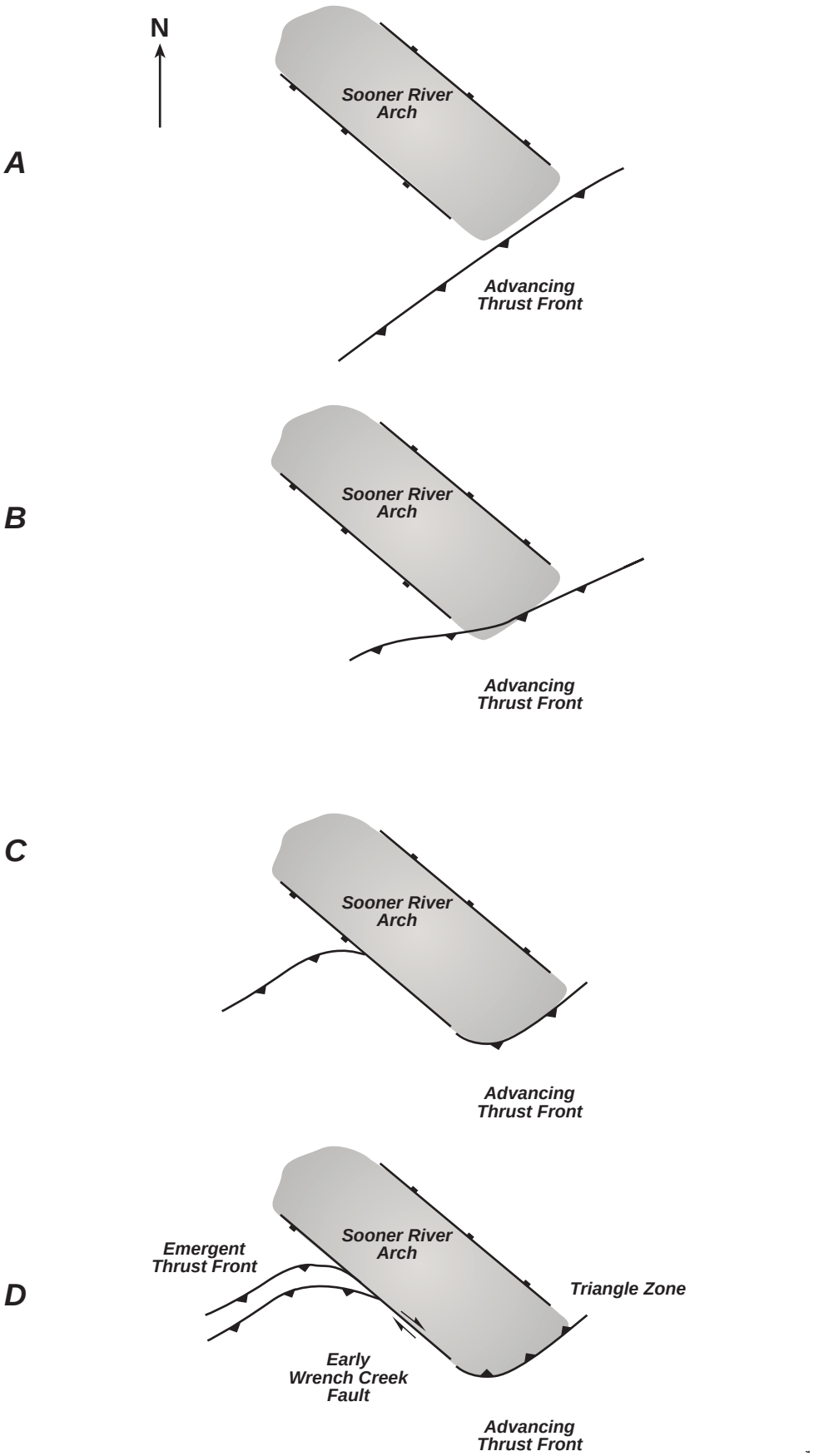


Figure 8.26. Synoptic model illustrating the development of the Wulik Peaks transverse zone.

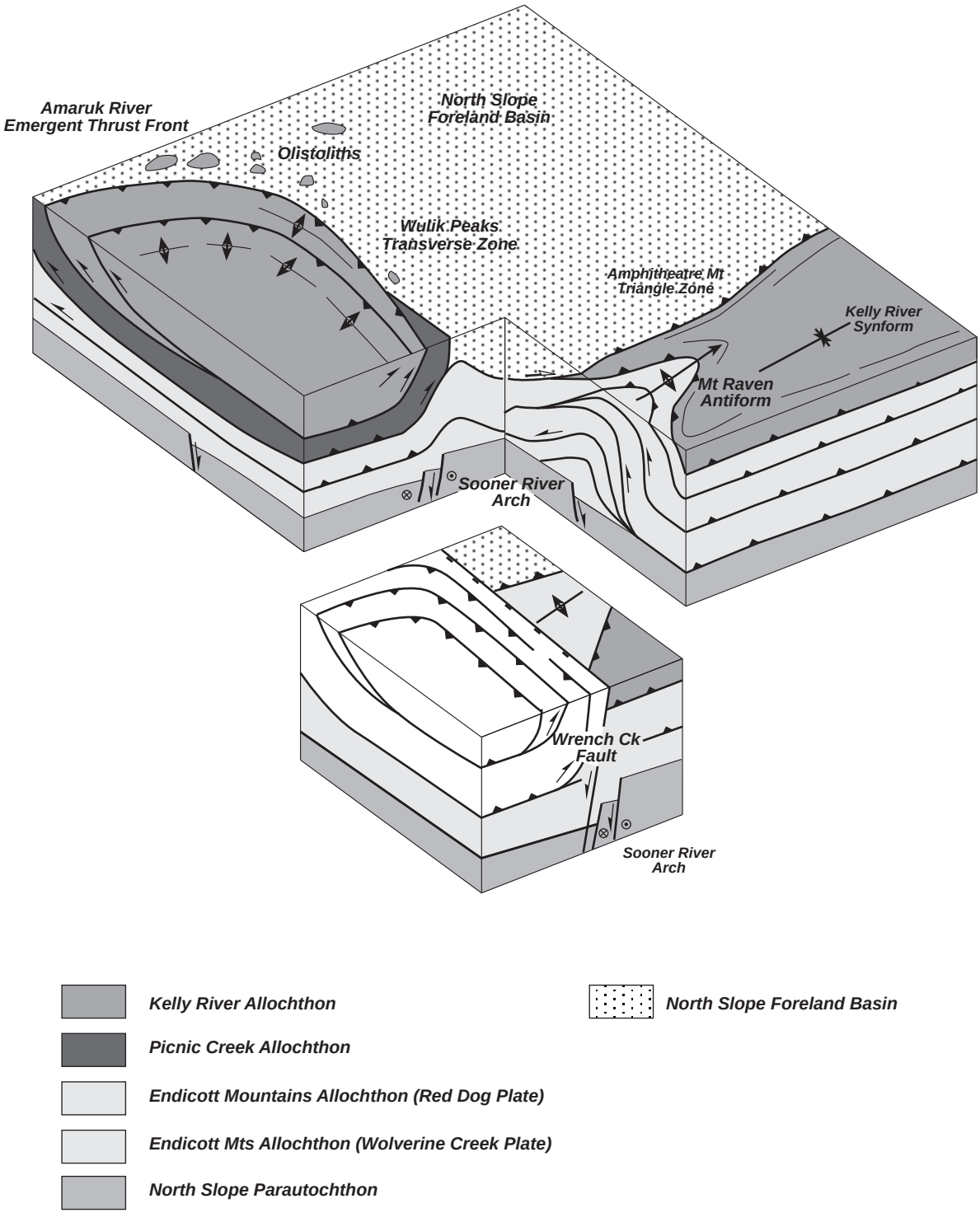


Figure 8.27. Synoptic 3D diagram showing the structure of the Wulik Peaks transverse zone.

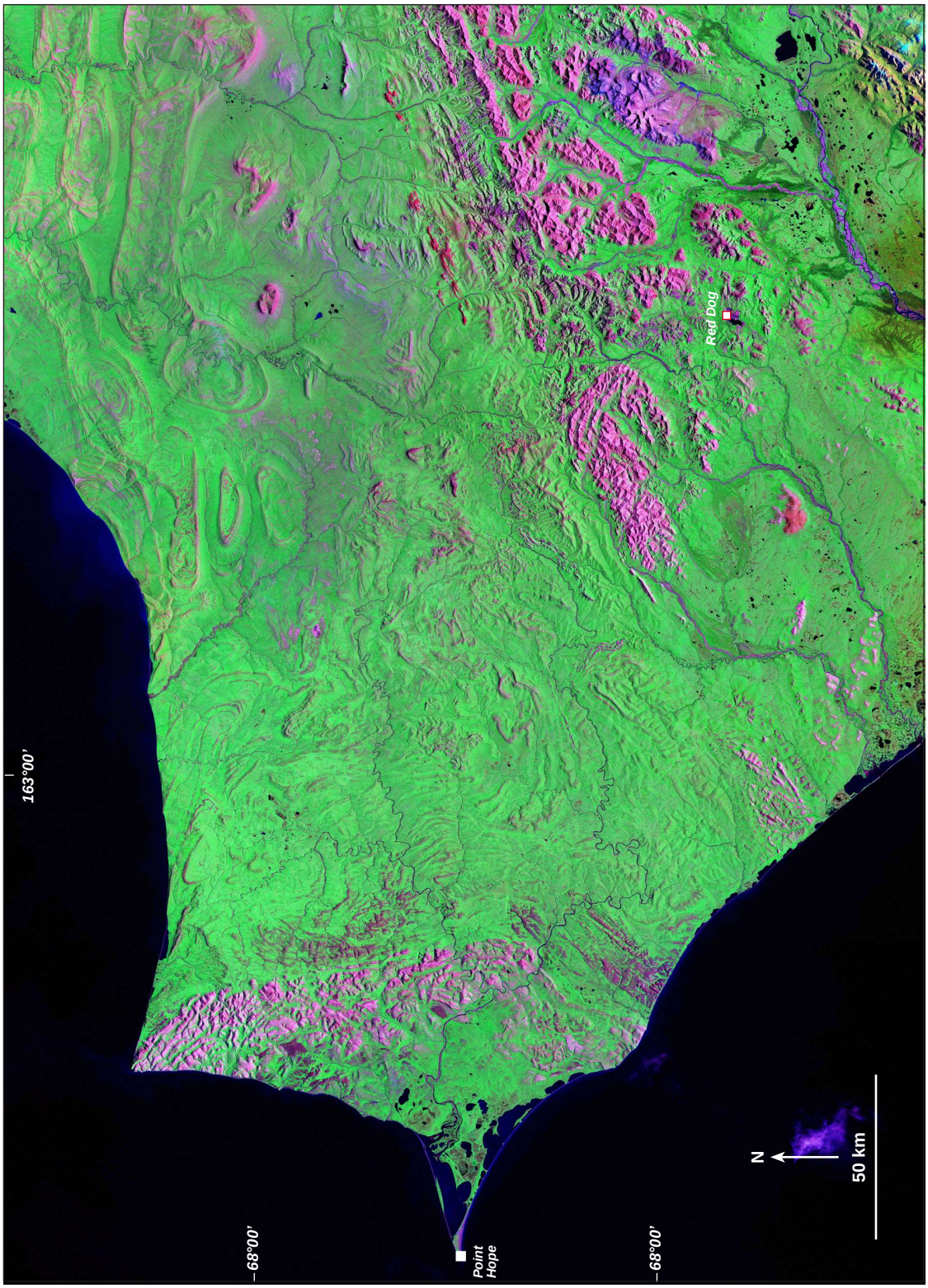


Figure 8.28A. Landsat image (spectral bands 3,4,7) of northwesternmost Alaska showing the relationship between the western Brooks Range and the Lisburne Hills-Herald Arch thrust belts (imagery from National Aeronautic and Space Administration, 2005). The location of the Red Dog district is shown.

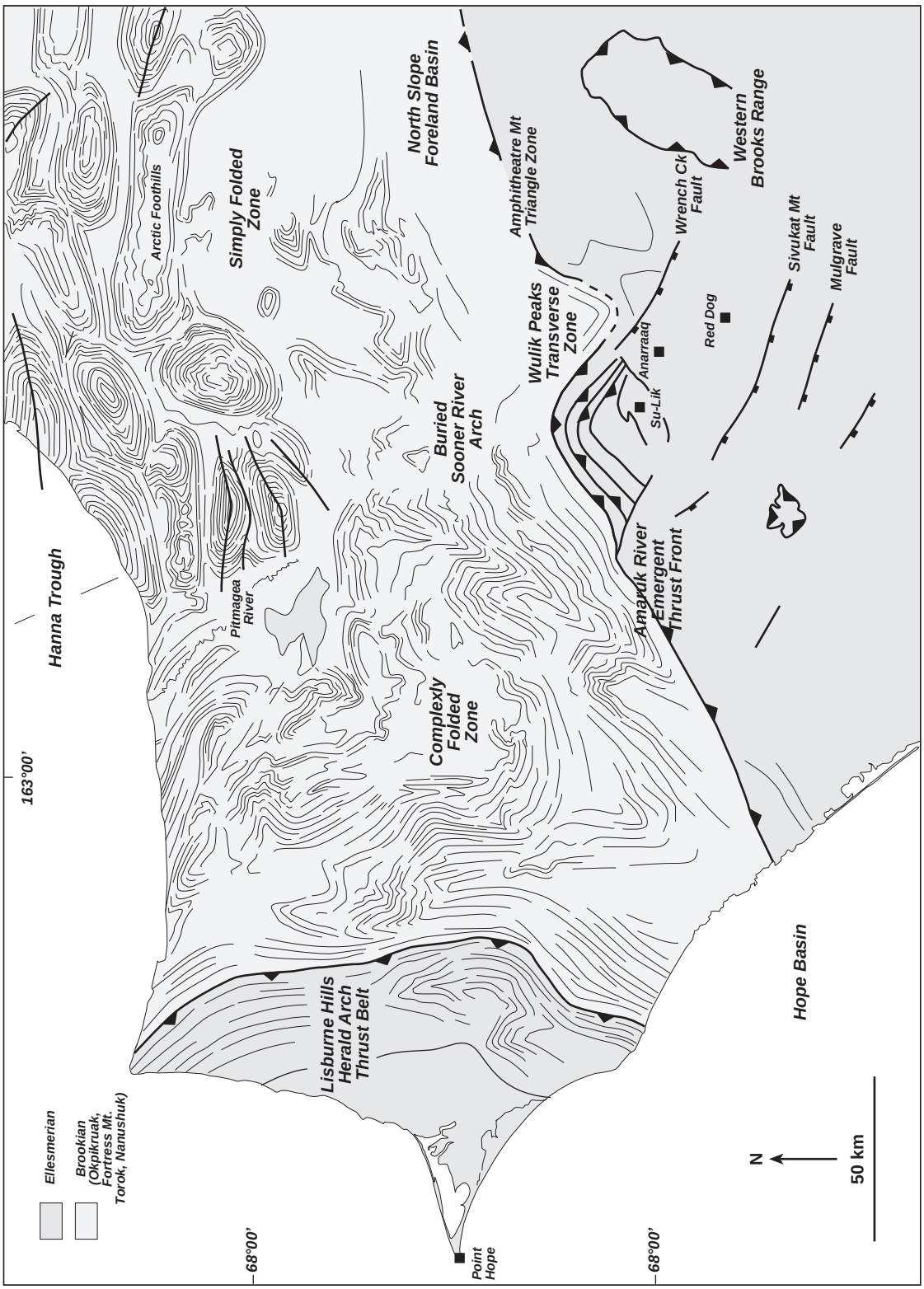


Figure 8.28B. Line-drawing interpretation of landsat image shown in Figure 8.28A.

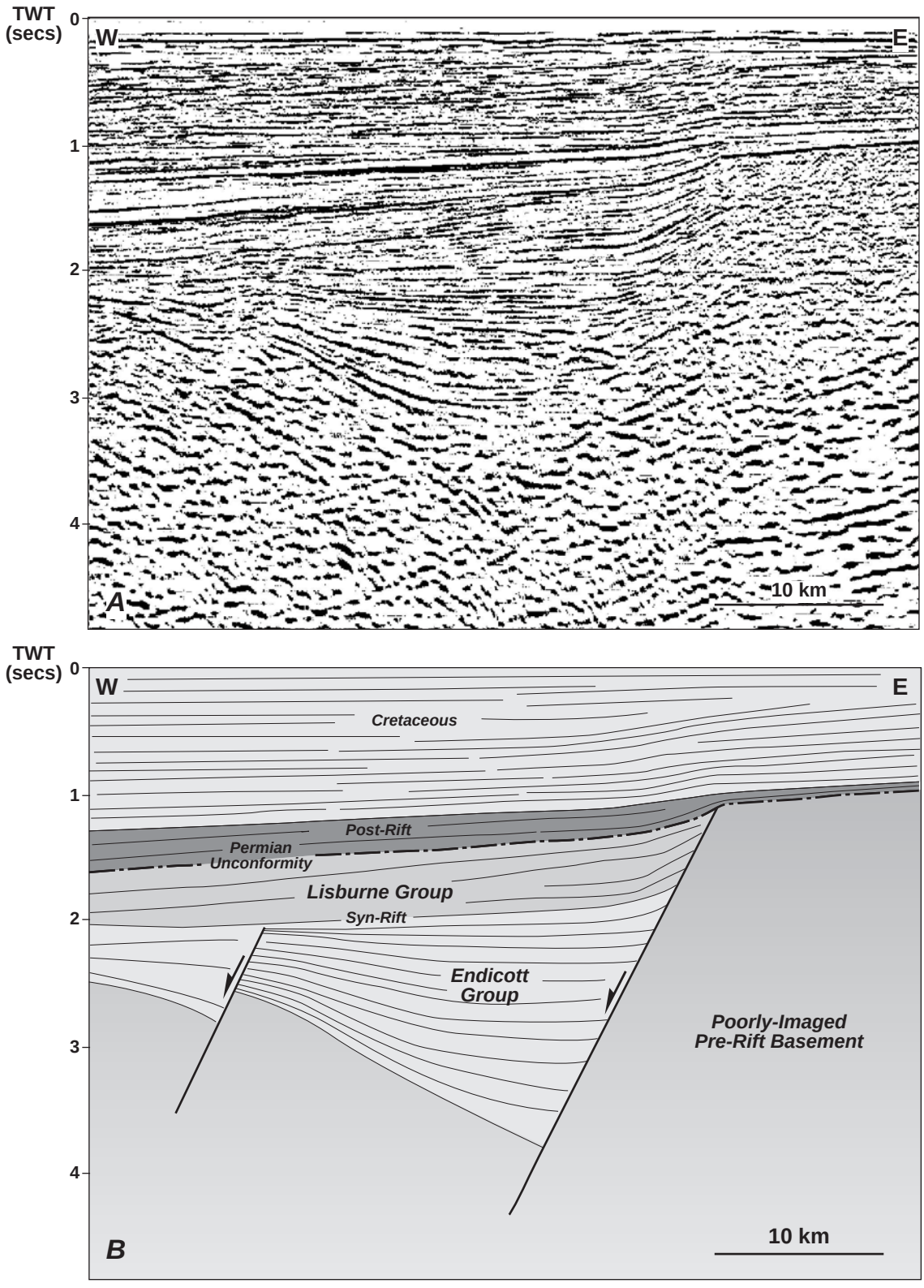


Figure 8.29. Late Devonian to Jurassic rift structures. **A.** Detail of seismic line across the Hanna Trough, Chukchi Sea (from Sherwood *et al*. 2002). **B.** Line-drawing structural interpretation showing a N-trending half-graben structure in the Hanna Trough-Chukchi Sea platform.

However more complex geometries are developed where thrusting involves basement fault systems and where continental margins are segmented along strike and particularly where contraction is oblique to the orientation of the margin.

Continental passive margins typically contain pre-rift, syn-rift and post-rift megasequences (e.g. Hubbard *et al*. 1985) (Figs. 8.6 & 8.29) that are controlled by three-dimensional rift and passive margin fault systems (e.g. Coletta *et al*. 1988; Milani & Davison, 1988; Ebinger, 1989; McClay & Khalil, 1998). During subsequent inversion and shortening these basement-involved fault systems combined with extensional fault-controlled facies variations may be expected to exert significant local controls on later contractional structures and thrust geometries.

Structural control by pre-existing basement-involved extensional faults on the development of thrust systems is not unique to the Red Dog district but has been described for many other fold and thrust belts – e.g. in the Appalachians (Thomas, 1977; Woodward *et al*. 1988; Thomas, 1990; Pohn, 1998; Thomas & Bayona, 2002; Bayona *et al*. 2003; Surles & Thomas, 2004; Thomas, 2004); in the Taiwan thrust belt (e.g. Mouthereau *et al*. 2002) (Fig. 8.15b); in the western and southern Alps (e.g. Butler, 1989; Coward *et al*. 1991; Butler, 1992; Welbon & Butler, 1992, Schönborn, 1992; Calassou *et al*. 1993; Wissing & Pfiffner, 2003) (Fig. 8.15a); in the Variscan orogenic belt (e.g. Öncken *et al*. 2000; Lacquement *et al*. 2005); in the southern Urals (e.g. Pérez-Estaún *et al*. 1997; Brown *et al*. 1999) (Fig. 8.14); in the Moroccan Rif (Morley, 1986) (Fig. 8.15d); in the Outer Albanides (e.g. Roure *et al*. 2004) (Fig. 8.16c); in the Bolivian Andes (Hinsch *et al*. 2002) and in the Zagros of Iran (e.g. Sepehr & Cosgrove, 2004). The influence of 3D basin geometries on the development of thrust systems has been also successfully reproduced in scaled analogue models (e.g. Calassou *et al*. 1993; Macedo & Marshak, 1999; Marshak, 2004; McClay *et al*. 2004).

In the Red Dog district lithostratigraphic changes in the syn-rift megasequence (Chapter 5), along-strike changes in the detachment units (Fig. 8.25) and underlying basement extensional faults (Fig. 8.29) all contributed to the development of the Wulik Peaks transverse zone (Figs. 8.26 & 8.27). Similar controls may be expected for other potential transverse zones if they exist elsewhere in the Brooks Range.

8.4.2 Inherited Basement-Involved Faults and Lateral/Oblique Ramps

Geometric and kinematic models together with scaled analogue models of deformation at oblique and lateral ramps (e.g. Apotria *et al*. 1992; Wilkerson *et al*. 1992; Calassou *et al*. 1993; Apotria, 1995; Pohn, 1998; Macedo & Marshak, 1999; Wilkerson, 1992; Wilkerson *et al.* 2002; Schreurs *et al*. 2003; Marshak, 2004) show that thrust faults in the cover sequence become strongly deflected and rotated around lateral of highly oblique ramp structures (cf. Fig 8.26). The models predict that deflection of thrust faults and tectonic transport directions increases with dip of the oblique or lateral ramp. A steeply-dipping lateral or oblique ramp may cause buttressing, and is most likely to generate significant local rotation in the cover thrust systems. Local tear faults and extensional faults may also develop (Fig. 8.23). Northwestward directed thrusting against the Sooner River arch (Fig. 8.23) would give rise to the prominent Wulik Peaks transverse zone with expected local clockwise rotation of individual thrust sheets. Palaeomagnetic studies (e.g. Apotria *et al*. 1992; Jolly & Sheriff, 1992; Dinarés *et al*. 1992; Apotria, 1995; Bayona *et al*. 2003) would be needed to confirm the exact amounts of vertical axis rotation in the Wulik Peaks transverse zone.

Buttressing along the Sooner River arch may have also enhanced underthrusting and the development of the Amphitheatre Mountain triangle zone (Figs. 8.4 & 8.5) as has been documented for other fold and thrust belts (e.g. Mugnier *et al*. 1997; Couzens-Schultz *et al*. 2003). Differential syn-orogenic sedimentation across the transverse zone may have enhanced this effect (cf. Boyer, 1992; Mitra, 1994; Marshak, 2004).

Tear faulting and buttressing-related thrust sheet rotations in fold and thrust belts commonly cause tangential extension with the development of graben structures perpendicular / sub-perpendicular to transverse zones or form strike-slip faults parallel to the structural grain of the thrust belt (e.g. McKenzie & Jackson, 1983; Apotria, 1995; Macedo & Marshak, 1999; Hindle *et al*. 2000; Lickorish *et al*. 2002; Lacombe *et al.* 2003; Kwon & Mitra, 2004; Marshak, 2004) (Figs. 8.4 & 8.23). Similar effects may be expected in other transverse zones in the Brooks Range.

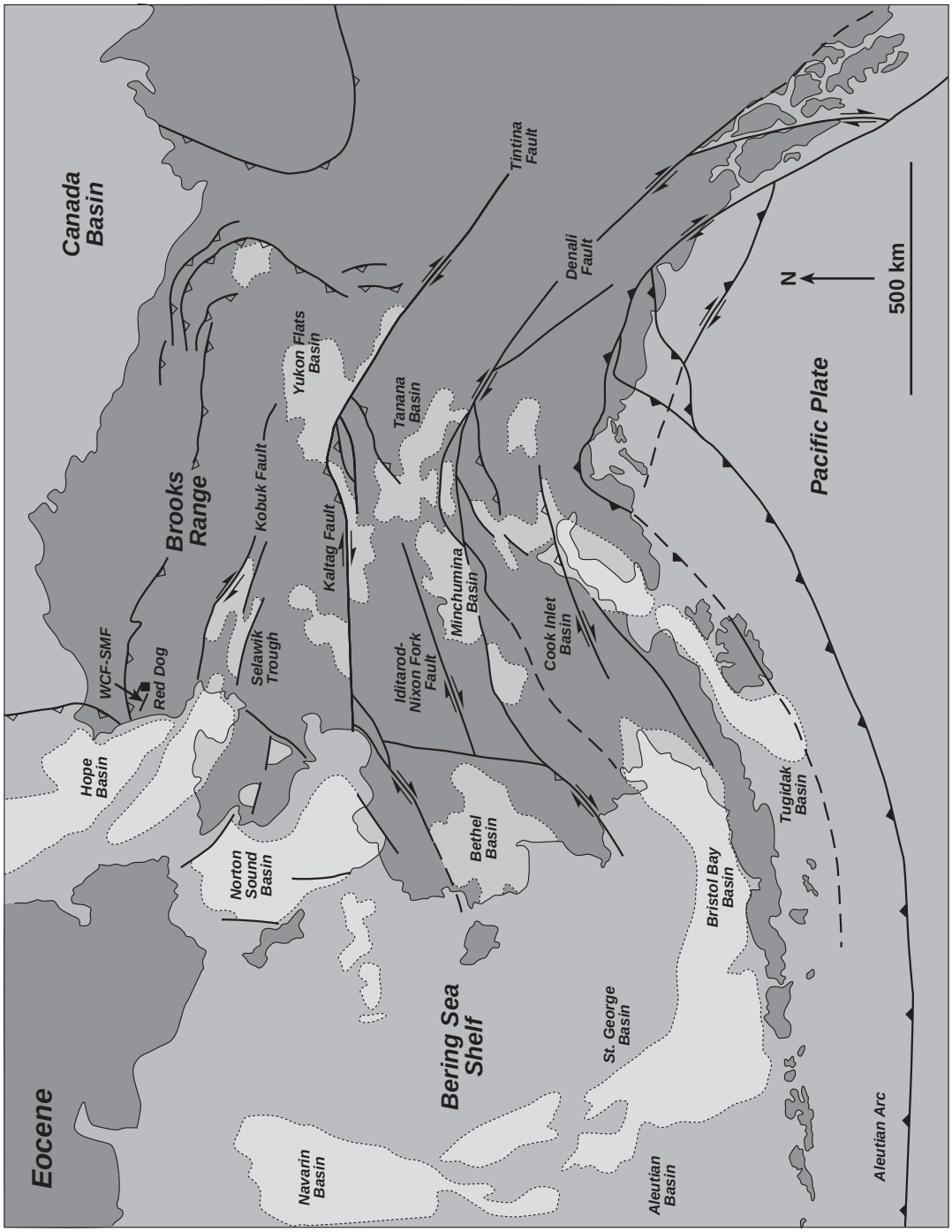
8.4.3 Tertiary Regional Strike-Slip Faults Systems and Tertiary Extensional Fault Systems

The Wrench Creek and Sivukat Mountain faults and the Tertiary basins of northwestern Alaska occur in a region of major dextral strike-slip faults (e.g. Kobuk & Denali fault systems; Fig. 8.30) (Schultz & Aydin, 1990; Kirschner, 1994*a*). Some models propose that NW-SE-trending Hope basin is related to Eocene transtension at the trailing edge of the Kobuk fault (e.g. Tolson, 1987; Worrall, 1991; Kirschner, 1994*a*, *b*) whereas Elswick & Toro (2003) suggested that these Tertiary extensional basins formed as a result of Early Tertiary extensional collapse of the Lisburne Hills-Herald Arch thrust belt. The Kobuk fault accommodates approximately 30 km of dextral displacement (Avé Lallemant *et al*. 1998) and it is unlikely to have generated the 800 km long Hope basin. In this thesis the NW trending Sivukat Mountain and Wrench Creek faults, are interpreted to have formed from renewed reactivation of old crustal fault systems (e.g. Wulik Peaks transverse zone) to accommodate Cenozoic to Present Day counter-clockwise rotation and extrusion of northwest Alaska (Plafker and Berg, 1994).

8.5 Implications for Zn-Pb-Ag Barite Mineralization of the Red Dog District

8.5.1 Introduction

The Zn-Pb-Ag- Barite deposits of the Red Dog district are hosted in the Red Dog plate of the Endicott Mountains allochthon (Figs. 8.1 & 8.4). The deposits are preserved in duplex structures that have a floor thrust in the Kuna Formation and a roof thrust at the base of the overlying Key Creek plate (Fig. 8.5b). These sediment-hosted Zn-Pb-Ag and barite deposits are hosted in black shales, mudstones, and lithic to calcareous turbidites of the Ikalukrok unit of the Kuna Formation of the Red Dog plate of the Endicott Mountains allochthon (Fig. 8.6). Additional minor Zn-Pb mineralization occurs as mineralized veins and breccias in syn-rift siliciclastics of the Noatak Sandstone and Kanayut Conglomerate of the Endicott Group in the Key Creek plate of the Endicott Mountains allochthons.



Figur 8.30. Tectonic map of Alaska showing the spatial relationship between regional-scale curved strike-slip faults and sedimentary basins in the Eocene. The location of Red Dog and the Wrench Creek (WCF) and Sivukat Mountain faults (SMF) is shown (modified from Kirschner, 1994; Plafker & Berg, 1994).

8.5.2 Structural Controls on Red Dog Mineralization

The Red Dog mine sub-plate consists of a series of discontinuous thrust sheet remnants (Figs. 8.1 & 8.4; Enclosure 1) that show equivocal stratigraphic and structural relationships with early syn-orogenic olistostromal strata of the Okpikruak Formation. It is structurally overlain by the Key Creek plate (Fig. 8.5c). The Red Dog plate is interpreted to having been thrust into the foredeep basin where the Okpikruak formation was being deposited and where olistoliths were also forming such that these were syn-tectonically incorporated into the Red Dog plate and its sub-plates (Fig. 8.21). This resulted in a complex stratigraphy in these thrust units that has hampered exploration in the area. The Red Dog mine sub-plate is detached in strata of the Kivalina or Ikalukrok units of the Kuna Formation (Fig. 8.5b).

The deformation of the mineralized units is characterized by thrust faults, duplexes, and detachment and fault-propagation folds (Enclosure 3). Thrust faults and thrust-related folds are offset by late NW-SE-trending and SW- to NE-downthrown late extensional faults (Fig. 8.5b; Enclosure 3). These are probably linked to the extension on the Wrench Creek and Sivukat Mountain fault systems.

Direct structural control on the position of the Red Dog mineralization is not apparent from the field exposures or in the Red Dog open pit due to the intense thrusting and folding focused around the orebodies (Chapter 7; Figs. 8.5b; Enclosure 3). The vein breccia ore that was originally exposed in the bottom of Red Dog creek as observed before mining operations began has traditionally been interpreted as a feeder or basal stockwork zone (Moore et al. 1986; Kelley et al. 2004). There is no direct hard evidence for syn-sedimentary extensional fault control on the mineralization in the Red Dog district. However the close spatial association of the mineralization in the Red Dog district with the Wulik Peaks transverse zone (Fig. 8.31) strongly suggests that there was the underlying basement high strongly controlled the hydrothermal fluid circulation in the district. (cf. SEDEX models by Goodfellow, 1998,1999). Similar extensional fault and basement control has been proposed for many SEDEX like deposits along the North American Cordillera (e.g. Fig. 8.32; Nelson et al. 2002) and for other stratabound sulphide deposits in extensional basins (Fig. 8.33).

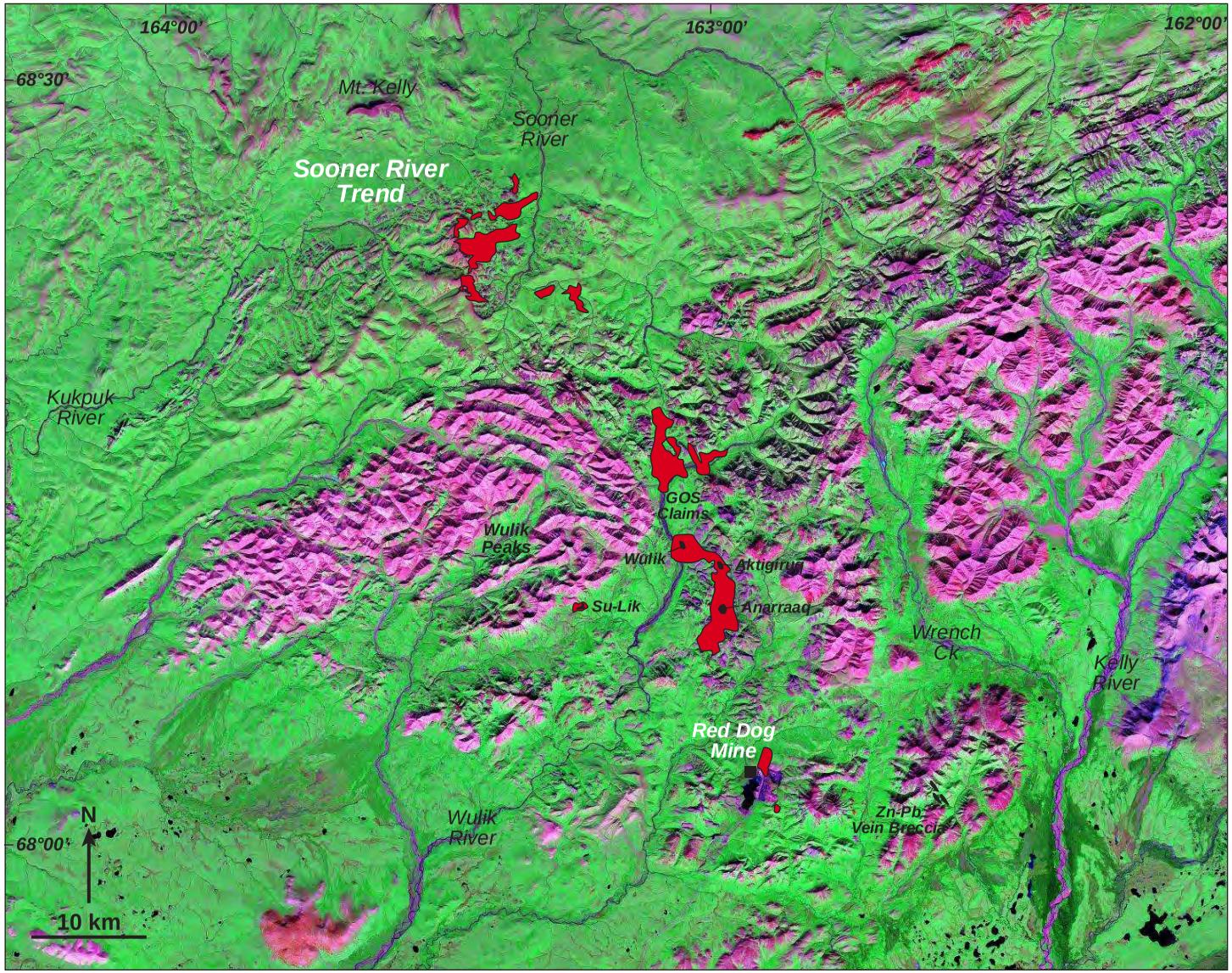


Figure 8.31. Landsat 7 TM image (spectral bands 7,4,2) of the Red Dog district the Sooner River trend. Major gravity anomalies (>1.7 mgal) are shown in red. Note the northwesterly alignment of the sediment-hosted Zn-Pb-Ag and barite deposits of the Red Dog district broadly following the Wulik Peaks transverse zone (imagery from National Aeronautics and Space Administration, 2005).

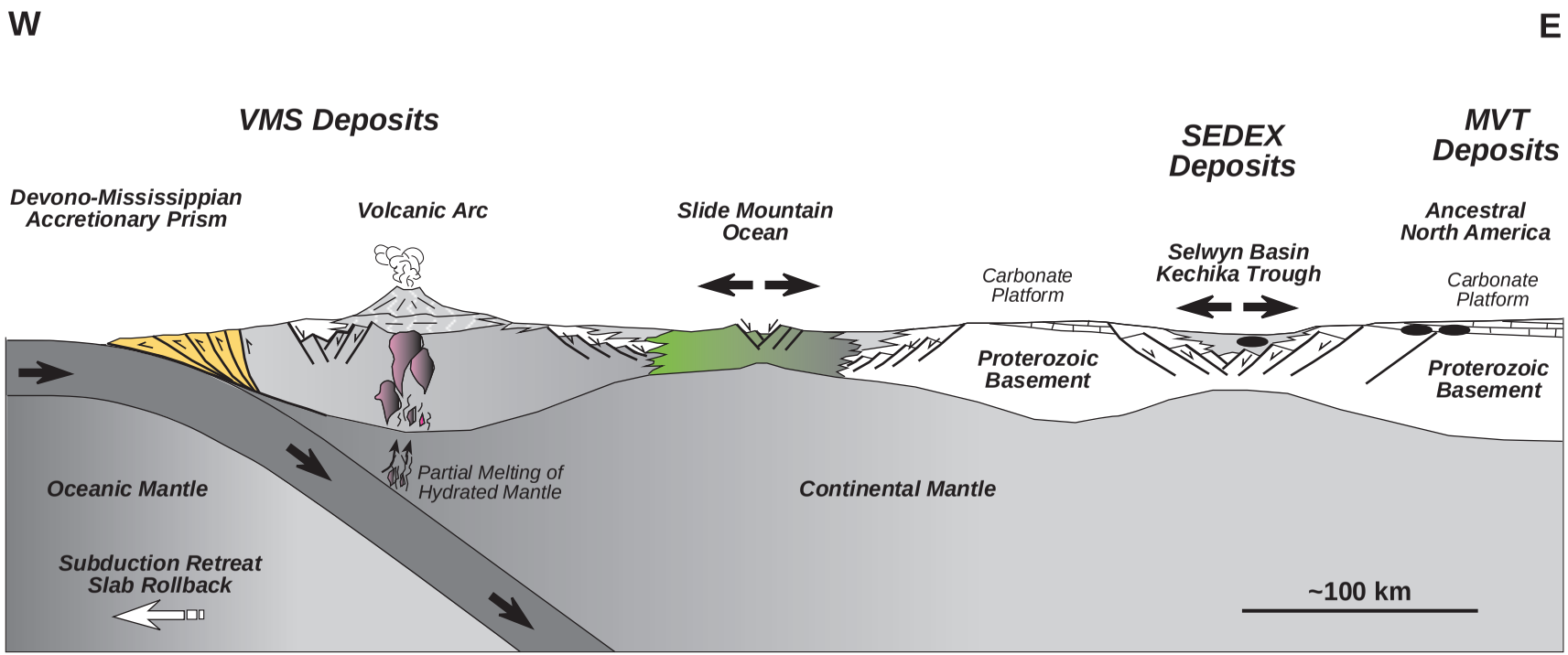


Figure 8.32. Schematic diagram showing the tectonic setting of SEDEX, Volcanic Massive Sulphide (VMS) and Mississippi Valley-Type (MVT) deposits of the Canadian Cordillera in Late Devonian to Early Mississippian time (modified from Nelson *et al.* 2002).

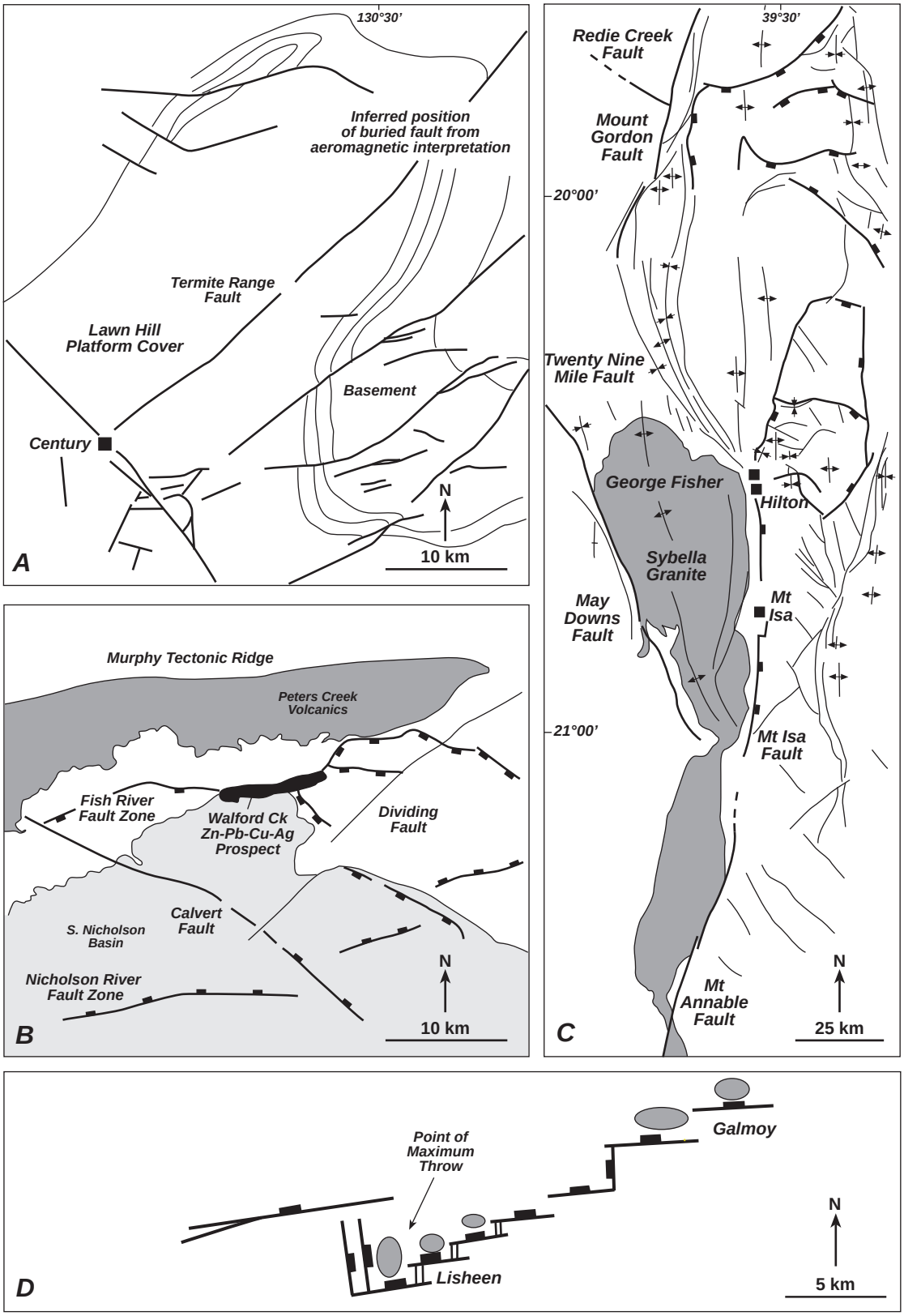


Figure 8.33. Extensional fault systems and location of sediment-hosted Zn-Pb-Ag and barite deposits. **A.** Schematic fault map showing the relationship between the Century deposit and the Termite Range fault. **B.** Simplified map of the Walford Creek prospect showing the spatial relationship between mineralization and the intersection of the Fish River and Dividing faults. **C.** Summary fault map of the Isa Valley showing the structural positiom of the Mount Isa, Hilton,and George Fisher deposits (modified from Betts *et al*. 2003). **D.** Simplified fault map of the Lisheen and Galmoy areas of Ireland showing the spatial relationship between extensional faults and mineralization (modified from Hitzman, 1999).

8.5.3 Tectonostratigraphic Model for the Formation of Red Dog District Mineralization

The new interpretation of the tectonostratigraphy of the Red Dog plate as a complex of mineralized units and tectonically incorporated syn-orogenic strata and olistoliths of the Okpikruak Formation (Fig. 8.21) has very important implications for the tectonostratigraphic model of the formation of the Red Dog deposits as well as for exploration in the Red Dog district. Previously considered barren olistolith-bearing early syn-orogenic strata of the Okpikruak Formation (Fig. 8.1) should not be disregarded for exploration as they may well be underlain by disrupted olistostromal elements of the prospective Red Dog plate. Ore deposits have been discovered in olistoliths incorporated into syn-orogenic successions in other fold and thrust belts. Examples include ore-bearing olistostromes and allochthonous Sb-Hg deposits of the Alay Range in the southern Tien Shan (e.g. Belousov, 2002) and Cu-Co deposits in disrupted thrust sheets of the Fungurume Group in the Pan-African Lufilian fold and thrust belt (Zambian Copperbelt) (e.g. Wendorff, 2003, 2005, *in Press*).

Mineralization and Basin Geometry

The loci of mineralization centres in the Red Dog district are broadly aligned along the WNW-ESE- to NW-SE-trending Wulik Peaks transverse zone (Fig. 8.31). The Wulik Peaks transverse zone is interpreted to reflect an underlying basement high – the Sooner Arch (Figs. 8.26 & 8.27) that appears to have controlled the loci of the Zn-Pb-Ag-Barite mineralization in the Red Dog district. Sediment-hosted Zn-Pb deposits are known to occur associated with extensional faults, particularly at the intersection of fault systems (e.g. McClay, 1991; Goodfellow *et al*. 1993; Goodfellow, 1999; Betts *et al*. 2003) (Fig. 8.33, Chapter 3, Section 3.5) and these typically define regional prospective trends that follow extensional fault-controlled basin margins. Examples include the Selwyn basin and Kechika Trough (e.g. Gordey *et al.* 1982; McClay & Bidwell, 1987; McClay *et al*. 1989; McClay, 1991; Goodfellow, 1998; Nelson *et al*. 2002), Sullivan (e.g. Goodfellow, 1998), the Irish and northeastern Australian deposits (e.g. Large & Hitzman, 1986; Hitzman, 1999; Betts *et al*. 2003) and modern environments such as the Middle Valley in the northern Juan de Fuca Ridge and the Red Sea (e.g. Goodfellow *et al.* 1993).

Figure 8.34 is a summary tectonostratigraphic model showing the likely structural controls on Red Dog style mineralization in the district during the Late Mississippian. In this thesis it is proposed that mineralization occurred during the early stages of post-rift development when the main basin bounding faults began to invert (cf. Fig. 8.7). Inversion enhanced and focused fluid flow along the main fault systems allowing sub-surface replacement of calcareous turbidites and carbonate units in the Kuna formation, slicification an barite formation (in some cases at the sea floor acting as a cap rock to the mineralization below). It is beyond the scope of this thesis to discuss fully the mineralization models and isotopic signatures of the mineralization and the reader is referred to the papers in Kelley & Jennings (2004) for more detailed discussion of the Red Dog mineralizing processes.

8.5.4 Implications for Exploration in the Red Dog District and in the Western Brooks Range

For the last 25 years, exploration for sediment-hosted Zn-Pb-Ag and barite deposits in the Red Dog district has been based on the allochthon model of Moore *et al*. (1986), with the subsequent modifications by Young (1989), Jennings *et al*. (1998), Jennings & King (2002), King *et al.* (2002), and Young (2004) (cf. Chapter 3). This model is based on the assumption that the allochthons of the Red Dog district are regionally continuous 'Rocky Mountain style' thrust sheets consisting of Late Devonian or Early Mississippian to Early Cretaceous strata (e.g. Moore *et al*. 1986). Exploration mapping and drilling in the district have traditionally used the Okpikruak Formation as a regional marker unit to identify the base of the prospective Red Dog plate (e.g. Moore *et al*. 1986; Young, 1989; Jennings *et al.* 1998; King *et al*. 2002; Young, 2004).

The orientation, location, as well as the structural and tectonostratigraphic patterns associated with the Wulik Peaks transverse zone (Chapter 6, Section 6.5) may provide clues to the location of basin margins and buried extensional faults in the North Slope parautochthon that could have localized other sediment-hosted Zn-Pb deposits deposits.

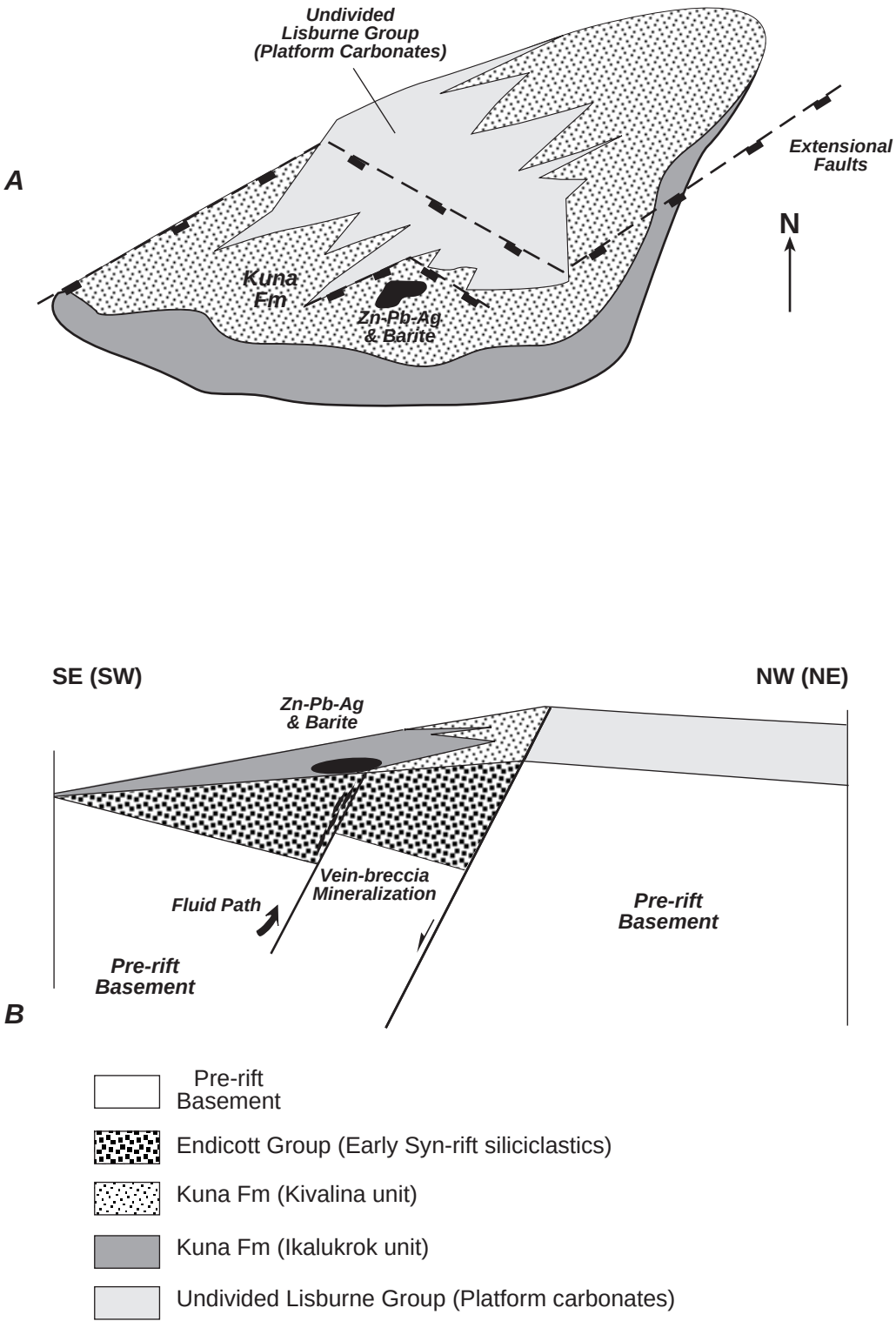


Figure 8.34. Schematic model for the structural control on the Red Dog deposits. **A.** Simplified map view of the Red Dog basin showing the relationship between basin margin structures and Zn-Pb-Ag and barite deposits. **B.** Schematic cross section showing the relationship between extensional faults and the Zn-Pb-Ag and barite deposits. Not to scale.

The WNW-ESE- to NW-SE-trending late extensional faults (Figs. 8.1 & 8.4; Enclosure 3) have important implications for the exploration and exploitation of sediment-hosted Zn-Pb-Ag deposits in the Red Dog district. These regional faults such as the Sivukat Mountain and Wrench Creek faults downthrow to the south-southwest and this together with decreasing structural relief to the southwest, increases the depth to prospective rocks of the Endicott Mountains allochthon. Favourable stratigraphy may lie locally at relatively shallow depths due to development of underlying structural culminations or alternatively on the footwall blocks of these regional extensional fault systems.

WNW-ESE- to NW-SE-trending late extensional faults in the vicinity of the Red Dog mine (see Chapter 7) have segmented the ore bodies with throws that range from order of 1 to 100 m. Late extensional faults also have implications for current exploitation and pit wall stability of the Red Dog mine. The west pit wall of the Red Dog mine approximately parallels a complex NW-SE-trending fault array that separates the Main deposit from highly tectonized strata of the Okpikruak Formation. The high slope angle (45°, 1:1 stripping ratio) of the west pit of the Red Dog mine combined with the favourable orientation of the faults and joints (Chapter 7) account for recent collapse of bench walls. The west pit wall, where structures strike approximately 20° to the pit wall, is susceptible to planar and translational failures. In contrast the east pit wall, areas of intersection between late extensional faults and thrust faults are prone to wedge failure. Continued mapping of orientation, dip, frequency and distribution of extensional faults and fractures in the Red Dog mine pit would result in savings and improvement of safety. Bench-parallel fault-controlled drainages and springs should be carefully mapped and monitored as they mark potentially hazardous work areas, particularly during the spring thaw.

8.6 SUMMARY

The discussion presented above has reviewed the stratigraphic and structural evolution of the Red Dog district of the western Brooks Range. A new tectonostratigraphy has been developed and a new tectonic model for the Red Dog district has been erected combining this work with previously published data. The principal results and key conclusions of this thesis are presented in the following Chapter 9.

CHAPTER 9

CONCLUSIONS

9.1 INTRODUCTION

9.2 TECTONOSTRATIGRAPHY OF THE RED DOG DISTRICT

9.3 REGIONAL STRUCTURE OF THE RED DOG DISTRICT

9.4 Zn-Pb-Ag AND BARITE MINERALIZATION OF THE RED DOG DISTRICT

9.5 SUGGESTIONS FOR FUTURE RESEARCH

CHAPTER 9 *CONCLUSIONS*

9.1 INTRODUCTION

The research presented in this thesis has resulted in a new structural interpretation and a new tectonostratigraphy for the Red Dog district, western Brooks Range of Alaska. This has lead to a new tectonostratigraphic interpretation and evolutionary model for the Zn-Pb-Ag and barite mineralization of the Red Dog district. The stratabound / stratiform mineralization is confined to the Red Dog thrust plate of the Endicott Mountains allochthon of the Arctic Alaska terrane of northern Alaska (Chapter 7). The mineralization appears to be structurally controlled by the major WNW-trending Wulik Peaks transverse zone within the dominant NE-SW-trending thin-skinned fold and thrust belt of the western Brooks Range. This new tectonostratigraphic model for the world-class Red Dog Zn-Pb-Ag and barite mineralization has import implications for exploration for new deposits within the Red Dog district as well as elsewhere in the Brooks Range of northern Alaska.

The Red Dog district records a remarkable history of Late Devonian to Present Day structural inheritance of both NE-SW trending and WNW-ESE- to NW-SE-trending long-lived fault systems. Late Devonian to Late Mississippian extensional faults associated with rifting and passive margin development of the Arctic Alaska terrane controlled the contraction of the passive margin during the Brookian orogeny that formed the western Brooks Range in this region. The WNW-ESE-trending faults were also later reactivated by Middle Eocene to Present Day extension.

The detailed conclusions resulting from the research presented in this thesis are summarized below.

9.2 TECTONOSTRATIGRAPHY OF THE RED DOG DISTRICT

The Red Dog district of the western Brooks Range consists of two major allochthonous terranes, the Arctic Alaska and the Angayucham terranes. These form part of a telescoped Devonian through Jurassic continental passive margin and oceanic crust that are now preserved in seven stacked allochthon sheets bounded by regional sub-

horizontal thrust systems. These were thrust northwestwards onto the passive margin of northern Alaska in the Mid-Late Jurassic - Late Cretaceous Brookian orogeny, forming a NE-SW- to WNW-ESE-trending and WNW-vergent thin-skinned foreland fold and thrust belt. The Arctic Alaska terrane of the western Brooks Range consists of the lower six allochthons formed by the telescoping of proximal and distal sedimentary sections of the southern passive margin of the ancestral Alaskan continent. The seventh and uppermost thrust sheet consists of the Misheguk Mountain allochthon of the Angayucham terrane. This is interpreted to have formed as Middle Jurassic oceanic crust south of the ancestral passive margin and subsequently obducted northwestwards onto the telescoped passive margin during the Brookian orogeny.

Detailed regional mapping of the complex fold and thrust belt of the Red Dog district has lead to a new stratigraphic interpretation and a new structural interpretation of the region. Key conclusions are:

- The greater part of the Red Dog district consists of sedimentary successions of the Arctic Alaska terrane. To the south and southwest of the area these units are overthrust by the ophiolitic units of the Misheguk Mountain allochthon of the Angayucham terrane.

- The strata of the Arctic Alaska terrane can be subdivided into two regionally significant tectonostratigraphic units. These are the Ellesmerian and Brookian units, which can be further subdivided into depositional megasequences that result from distinct tectonic events.

- The Ellesmerian unit consists of two distinct unconformity bounded rift-related Megasequences that are interpreted to have formed on the southern margin of ancient Arctic Alaska.

These are:

1) Syn-rift Megasequence consisting of the Late Devonian though Late Mississippian strata deposited at during the rifting of the passive margin.

2) The Post-rift Megasequence consisting of Pennsylvanian through Late Jurassic strata deposited during the thermally induced subsidence of the sag phase of the passive margin.

- No pre-rift strata are exposed in the Red Dog district. Pre-rift rocks occur west of the Red Dog district in the Lisburne Hills – Herald Arch thrust belt.

- The syn-rift Megasequence consists of early rift continental to marine sediments of the Endicott Group and the distal platformal carbonates of the Baird Group (Kugururok Formation). These are overlain in the rift basins by marine successions of the Kayak Shale, the Utukok Formation and the Kuna Formation and Rim Butte units. The deep water black shales of the Kuna Formation host the Zn-Pb-Ag-Barite mineralization of the Red Dog district. The footwall of the main rift fault blocks consist of platform carbonates of the Kogruk Formation and the undivided Lisburne Group. Early inversion of basin bounding fault systems may have begun in the late syn-rift and the transitional period into the post-rift.

- The post-rift Megasequence consists of generally fine-grained siliciclastic strata of the Etivluk Group, including the Siksikpuk and Otuk formations.

- The syn-orogenic Brookian unit can be subdivided into the Early and Late Brookian megasequences. In the Red Dog district the Early Brookian Megasequence consists of the Early Cretaceous Okpikruak Formation that is interpreted to have formed in an unstable deep marine environment in the proximal foredeep as the allochthon sheets formed largely by telescoped Ellesmerian sequences were emplaced northwestwards over the passive margin. This depositional megasequence consists of turbidites and olistostromes. The Late Brookian Megasequence in the Red Dog district consists of 'Late Okpikruak' Formation and the Fortress Mountain Formation. These are dominantly deep marine successions that infilled the foredeep as the Brookian orogen developed and the major allochthon sheets were emplaced northwestwards onto the passive margin.

- The Misheguk Mountain allochthon of the Angayucham terrane consists of Middle Jurassic upper mantle to lower crust ultramafic to mafic and felsic igneous rocks. These

include serpentinites, chromite-bearing serpentinized dunites, layered dunites and pyroxenites and layered gabbros. The Angayucham terrane preserves the lower part of a typical ophiolite succession that formed south of the Arctic Alaska terrane and was obducted during the Brookian orogeny. The basal contact of this unit is extensional in character probably reflecting extensional collapse of the thrust wedge system.

❑ This new revised tectonostratigraphy places the sediment-hosted Zn-Pb-Ag and barite mineralization of the Red Dog district within the late syn-rift megasequence of the Ellesmerian unit. The mineralization is structurally confined to the Red Dog plate within the Endicott Mountains allochthon.

9.3 REGIONAL STRUCTURE OF THE RED DOG DISTRICT

Key tectonic events in the Red Dog district identified in this study and also derived from remotely sensed data and the study of regional geological maps are:

1) Late Devonian (Frasnian and possibly older) to Late Mississippian (Chesterian) NE-SW-directed extension producing a series of NW-SE-trending rift basins along the margin of ancient Arctic Alaska. Earl inversion in the parautochthon occurs around this time and appears transitional into the post-rift period.

2) Post-rift subsidence from the Late Mississippian (Chesterian) to the Late Jurassic..

3) Late Jurassic ophiolite obduction and emplacement of the Misheguk Mountain allochthon of the Angayucham terrane. Initiation of the Brookian orogeny.

4) Late Jurassic – Early Cretaceous Brookian orogeny with NW-vergent thrusting in the northwestern Brooks Range. Thrusting and telescoping of the originally extended passive margin forming seven distinct thrust bounded allochthons.

5) Paleocene southeast vergent thrusting in the Lisburne Hills – Herald Arch thrust belt further to the northwest of the Red Dog district (possible but uncertain effects in the Red Dog district).

6) Eocene to Present Day late northwest trending extensional faulting.

- In the Red Dog district the western Brooks Range fold and thrust belt consists of seven dominantly northeast-southwest trending sub-horizontal thrust sheets (allochthons) that are vertically stacked. The dominant NE-SW fold and thrust trend is interrupted by a prominent NW trending transverse zone, the Wulik Peaks transverse zone, that offsets the thrust front and locally produces a northwest structural trend. The fold and thrust belt contains a number of regional northeast trending antiforms (e.g. Raven Peak antiformal stack) and synforms that are probably related to duplexes in underlying thrust sheets. Individual allochthons are internally deformed by folds and imbricate thrusts. This internal allochthon deformation subdivides them into individual, stratigraphically distinct thrust plates and sub-plates. Syn-orogenic strata date the onset of this Brookian orogenic contractional phase as beginning in the Late Cretaceous and continuing into the Tertiary. NW-trending late extensional faults such as the Wrench Creek fault and Sivukat Mountain fault system formed in the Tertiary.

- In ascending structural order the allochthons are the Endicott Mountains, Picnic Creek, Kelly River, Ipnavik River, Nuka Ridge, Copter Peak and Misheguk Mountain allochthons. Each allochthon preserves a distinct part of the ancient continental margin. The allochthons are detached in Late Devonian to Early Mississippian strata and are internally imbricated into a series of tectonostratigraphically coherent thrust plates and subplates that vary from 500 to 3 km thick.

- The allochthons are regionally folded into a series of regional NE-SW-trending antiforms and synforms with wavelengths of 15 to 30 km. Higher allochthons are preserved in the core of regional synforms (e.g. Kelly River synform). Antiformal stacking or duplexing at lower structural levels has produced the regional antiforms (e.g. Mount Raven antiform).

- The allochthons of the Arctic Alaska terrane are structurally overlain by the Misheguk Mountain allochthon of the Angayucham terrane. The Misheguk Mountain allochthon is a type-C crystalline thrust sheet that was obducted on to the Arctic Alaska terrane. The base of the Angayucham terrane is the Angayucham thrust, a regional NE-

SW-trending thrust fault that cuts down-section and its is now preserved in a series of regional synforms.

- Regional and detailed kinematic analyses throughout the Red Dog district indicate an overall regional west-northwest to northwest tectonic transport direction with local north to north-northeast thrust sheet transport restricted to the Wulik Peaks transverse zone.

- The Wulik Peaks transverse zone is an approximately 70 km long and 20 km wide regional WWN-ESE- to NW-SE-trending along-strike discontinuity in the dominant NE-SW structural trend of the Brooks Range fold and thrust belt in the red Dog district. The Wulik Peaks transverse zone consists of a complex branching array of WNW-ESE- to NW-SE-trending gently- to steeply-dipping thrust faults, NNE- to NNW-trending high-angle extensional faults together with complex folds and penetrative cleavage fabrics that strike at 74° to 90° to the dominant NE-SW-trending structural grain of the rest of the Red Dog district. The Wulik Peaks transverse zone developed in strata of the North Slope parautochthon, and the Endicott Mountains, Picnic Creek and Kelly River allochthons. Regional dips of the thrust sheets suggests that the transverse zone dips from 38° to 65° to the southwest. The along-strike changes in the geometries of the thrust system were probably enhanced by differential syn-orogenic sedimentation across this transverse zone.

- Structural, stratigraphic, and geophysical data suggest that the along-strike changes in the geometry and position of the thrust front and the development of the Wulik Peaks transverse zone resulted from the inheritance in the Early Cretaceous from Late Devonian to Jurassic WNW-ESE- to NW-SE-trending extensional faults of the ancient continental margin. The Sooner River arch is a basement high that represents the onshore extension in the western Brooks Range of the western flank of the NNW-SSE- to NW-SE-trending Hanna Trough.

- The Red Dog district exposes distinct along-strike variations and internal geometries of the thrust front of the western Brooks Range fold and thrust belt. From northeast to southwest these are the Amphitheatre Mountain triangle zone, the Wulik Peaks transverse zone (summarized above) and the Amaruk River emergent thrust front.

- The thrust front in the Amphitheatre Mountain triangle zone is controlled by a NE-SW-trending antiformal stack (i.e. Mount Raven antiform) and associated triangle zone (i.e. Amphitheatre Mountain triangle zone) that evolved as a buried thrust front.

- The Amaruk River thrust front is a NE-SW-trending and NW-verging emergent thrust front that is shifted 21 to 25 km to the northwest relative to the Amphitheatre triangle zone.

- The Wrench Creek and Sivukat Mountain faults are WNW-ESE- to NW-SE-trending, SSW-downthrown high-angle extensional faults that postdate allochthon emplacement. The faults are approximately 45 km long and have inferred vertical throws of approximately 1 to 3 km. The Wrench Creek fault and Sivukat Mountain faults exert a fundamental control on the Present Day topography of the Red Dog district. They developed above the oblique ramp system underlying the Wulik Peaks transverse zone and were later reactivated as dip to oblique slip extensional faults. This late extensional faulting is possibly genetically linked to middle Eocene to Present Day

- Regional thrust stacking patterns and relationships with syn-orogenic strata indicate that thrust sheets were largely emplaced in a 'forward-breaking' sequence.

- In the vicinity of the Red Dog mine and locally to the north the Red Dog style mineralization is structurally restricted to the Red Dog plate of the Endicott Mountains Allochthon. The Red Dog plate is internally imbricated and stacked with folding and thrusting of the deposits.

- The loci of mineralization in the Red Dog district are broadly aligned along the Wulik Peaks transverse zone possibly indicating that this exerted a fundamental tectonic control on the mineralization.

- Recognition of the Wulik Peaks transverse zone provides clues to the location of now-buried extensional faults in the North Slope parautochthon that could have localized other sediment-hosted Zn-Pb-Ag deposits.

9.4 Zn-Pb-Ag-BARITE MINERALIZATION OF THE RED DOG DISTRICT

- The Zn-Pb-Ag and barite deposits of the Red Dog district are hosted in the Red Dog plate of the Endicott Mountains allochthon. The deposits are preserved in duplex structures that have a floor thrust in the Kuna Formation and a roof thrust at the base of the overlying Key Creek plate. These sediment-hosted Zn-Pb-Ag and barite deposits are hosted in black shales, mudstones, and lithic to calcareous turbidites of the Ikalukrok unit of the Kuna Formation of the Red Dog plate of the Endicott Mountains allochthon. Additional minor Zn-Pb mineralization occurs as mineralized veins and breccias in syn-rift siliciclastics of the Noatak Sandstone and Kanayut Conglomerate of the Endicott Group in the Key Creek plate of the Endicott Mountains allochthons.

- The Red Dog Mine thrust subplate consists of a series of discontinuous thrust sheet remnants that show equivocal stratigraphic and structural relationships with early syn-orogenic olistostromal strata of the Okpikruak Formation. It is interpreted to having been thrust into the foredeep basin where the Okpikruak Formation was being deposited and where olistoliths were also forming such that these were syn-tectonically incorporated into the Red Dog plate and its sub-plates. The Red Dog mine subplate is detached in strata of the Kivalina or Ikalukrok units of the Kuna Formation.

- The deformation of the mineralized units is characterized by thrust faults, duplexes, and detachment and fault-propagation folds. Thrust faults and thrust-related folds are offset by late NW-SE-trending and SW- to NE-downthrown late extensional faults. These are probably linked to the extension on the Wrench Creek and Sivukat Mountain fault systems.

- The west pit wall of the Red Dog mine exposes a major fault zone consisting of highly-tectonized syn-orogenic strata of the Okpikruak Formation.

- The new interpretation of the tectonostratigraphy of the Red Dog Plate as a complex of mineralized units and tectonically incorporated syn-orogenic sediments and olistoliths of the Optikruak Formation has very important implications for exploration in the Red Dog district. Previously considered barren Okpikruak Formation may well be underlain by disrupted olistostromal elements of the Red Dog plate.

9.5 SUGGESTIONS FOR FUTURE RESEARCH

This section briefly outlines possibilities for future research in the Red Dog district in order to improve the tectonostratigraphic and structural understanding as well as that for the development of mineralization in the Red Dog district. In particular the development of a better model and understanding of the stratigraphic and structural controls on the mineralization would greatly aid further exploration for sediment-hosted Zn-Pb-Ag and barite deposits in the Red Dog district.

- Detailed structural and stratigraphic analyses of parautochthonous sections (e.g. Mount Raven antiform, Wulik Knot and Spiny Ridge belts) would provide further constraints on the pre-contraction basin geometries, palaeogeographies and the location of basin margin structures that could have localized sediment-hosted Zn-Pb-Ag and barite deposits.

- Detailed structural and stratigraphic studies of syn-orogenic strata of the Okpikruak formation, focusing on the development of olistostromes and their relationships to the development of the fold and thrust belt, are required in order to test the tectonostratigraphic models developed in this thesis as well as aid the unravelling of the structure of the Red Dog thrust plate that contains the Zn-Pb-Ag and barite mineralization.

- Further structural studies of the Wulik Peaks transverse zone involving both detailed mapping and section construction as well as geophysical studies (high resolution gravity and magnetics) are required to delineate the basement fault systems that control the development of the transverse zone. Palaeomagnetic studies will also be needed to determine the amount of thrust sheet rotation about a sub-vertical axis within and adjacent to the Wulik Peaks transverse zone.

- Regional structural analysis of the frontal thrust systems of other areas of the western Brooks Range may locate other potential basement controls on the fold and thrust belt geometries.

- Acquisition of high-resolution aeromagnetic surveys and/or seismic data would provide valuable constraints into the basement structure of the Red Dog district.

- Gravimetric surveys in areas covered by syn-orogenic strata of the Okpikruak Formation (previously not considered a target for exploration) may locate blind mineralization within the disrupted Red Dog plate.

- Integration of existing apatite and zircon fission track data (e.g. U. S. Geological Survey) with the model proposed in this study would provide additional constraints on the absolute timing of deformation and thermal history of the Red Dog district.

- Integration of the structural model proposed in this research with on-going and future fluid flow modelling studies by the U. S. Geological Survey and Teck Cominco may lead to a better understanding of the tectono-stratigraphic environment during emplacement of the mineralization.

- Continued detailed bench mapping in the Red Dog open pit and the mapping of the Aqqaluk deposit will lead to a better understanding of the effects of deformation and thrusting on the distribution of mineralization with the resultant implications for exploration in the district.

LIST OF REFERENCES

ABBATE, E., BORTOLOTTI, V. & PASSERINI, P. 1970. Olistostromes and olistoliths. *Sedimentary Geology*, **4**, 521-557.

ABBOTT. J. G., GORDEY, S. P. & TEMPELMAN-KLUIT, D. J. 1986. Setting of sediment-hosted stratiform lead-zinc deposits in Yukon and northeastern British Columbia. *In*: MORIN, J. A. (ed). Mineral deposits of the Northern Cordillera, *Canadian Institute of Mining and Metallurgy Special Volume*, **37**, 1-18.

AHR, W, M. 1989. Sedimentary and tectonic controls on the development of an Early Mississippian carbonate ramp. Sacramento Mountains area, New Mexico. *In*: CREVELLO, P. D., WILSON, J. L., SARG, J. F. & READ, J. F. (eds). Controls on carbonate platform and basin development. *Society of Economic Paleontologists and Mineralogists Special Publication*, **44**, 203-212.

AITKEN, J. D. & LONG, D. G. F. 1978. MacKenzie tectonic arc-reflection of early basin configuration?. *Geology*, **6**, 626-629.

ALASKA EARTHQUAKE INFORMATION CENTRE, 2005. Seismicity maps. University of Alaska, Fairbanks. http://www.giseis.alaska.edu/Seis/ (visited 10th September 2005).

ALLEN, P. A., HOMEWOOD, P. W. & WILLIAMS, G. D. 1986. Foreland basins: An introduction. *In*: ALLEN, P. A. & HOMEWOOD, P. W. (eds). Foreland basins. *International Association of Sedimentologists Special Publication*, **8**, 3-12.

ALLERTON, S. 1998. Geometry and kinematics of vertical-axis rotations in fold and thrust belts. *Tectonophysics*, **299**, 15-30.

ALONSO, J. L. 1987. Sequence of thrusts and displacement transfer in the superposed duplexes of the Esla Nappe Region (Cantabrian Zone, NW Spain). *Journal of Structural Geology*, **9**, 969-983.

ALVAREZ-MARRÓN, J. 1995. Three-dimensional geometry and interference of fault-bend folds: Examples from the Ponga Unit, Variscan belt, NW Spain. *Journal of Structural Geology*, **17**, 549-560.

ALVAREZ-MARRÓN, J., MCCLAY, K. R., HARAMBOUR, S., ROJAS, L. & SKARMETA, J. 1993. Geometry and evolution of the frontal part of the Magallanes foreland thrust and fold belt (Vicuña area), Tierra del Fuego, Southern Chile. *American Association of Petroleum Geologists Bulletin*, **77**, 1904-1921.

AMATO, J. M., TORO, J. & MOORE, T. E. 2004. Origin of the Bering Sea salient. *In*: SUSSMAN, A. J. & WEIL, A. B. (eds). Orogenic curvature: integrating paleomagnetic and structural analyses. *Geological Society of America Special Paper*, **383**, 131-144.

ANDERSON, A. V. & WALLACE, W. K. 1990. Middle Devonian to Lower Mississippian clastic depositional cycles southwest of Bathtub Ridge, northeastern Brooks Range, Alaska. *Geological Association of Canada and Mineralogical Association of Canada Program with Abstracts*, **15**, A2.

APOTRIA, T. G. 1995. Thrust sheet rotation and out-of-plane strains associated with oblique ramps: an example from the Wyoming salient, USA. *Journal of Structural Geology*, **17**, 647-662.

APOTRIA, T. G., SNEDDEN, W. T, SPANG, J. H. & WILTSCHKO, D. V. 1992. Kinematic models of deformation at an oblique ramp. *In:* MCCLAY, K. R. (ed). Thrust Tectonics, *Chapman & Hall, London*, 141-154.

ARGAND, E. 1911. Les nappes de recouvrement des Alpes Pennines et leurs prolongement structuraux. Matériaux Géologique Suisse, 31.

ARGAND, E. 1924. La tectonique de l'Asia (Tectonics of Asia), translated by CAROZZI, A. V. 1974. *Hafner Press, New York*, 218p.

ARMSTRONG, A. K. 1974. Carboniferous carbonate depositional models, preliminary lithofacies and paleotectonic maps, Arctic Alaska. *American Association of Petroleum Geologists Bulletin*, **58**, 621-645.

ARMSTRONG, A. K. & BIRD, K. J. 1976. Carboniferous environments of deposition and facies, Arctic Alaska. *In*: MILLER, T. P. (ed). Symposium on recent and ancient sedimentary environments in Alaska. *Alaska Geological Society Symposium Proceedings*, A1-A16.

ARMSTRONG, A. K. & MAMET, B. L. 1977. Carboniferous microfacies, micro-fossils and corals, Lisburne Group, Arctic Alaska. *U. S. Geological Survey Professional Paper*, **849**, 114 p.

AUTHEMAYOU, C., BELLIER, O., CHARDON, D., MALEKZADE, Z. & ABASSI, M. 2005. Role of the Kazerun fault system in active deformation of the Zagros fold-and-thrust belt (Iran). *Comptes Rendus Geosciences*, **337**, 539-545.

AVÉ LALLEMANT, H. G., GOTTSCHALK, R. R., SISSON, V. B. & OLDOW, J. S. 1998. Structural analysis of the Kobuk fault zone, north-central Alaska. *In*: OLDOW, J. S. & AVÉ LALLEMANT, H. G. (eds). Architecture of the central Brooks Range fold and thrust belt, Arctic Alaska. *Geological Society of America Special Paper*, **324**, 261-268.

AYDIN, A. 2000. Fractures, faults, and hydrocarbon entrapment, migration, and flow. *Marine and Petroleum Geology*, **17**, 797-814.

AYUSO, R. A., KELLEY K. D., LEACH, D. L., YOUNG, L. E., SLACK, J. F., WANDLESS, G., LYON, A. A. M. & DILLINGHAM, J. L. 2004. Origin of the Red Dog Zn-Pb-Ag deposits, Brooks Range, Alaska: evidence from regional Pb and Sr isotope sources. *In*: Kelley K. D. & JENNINGS S. (eds). A Special Issue devoted to barite and zinc-lead-silver deposits in the Red Dog district, western Brooks Range northern Alaska. *Economic Geology*, **99**, 1533-1553.

BABY, P., HERAIL, G., SALINAS, R. & SEMPERE, T. 1992. Geometry and kinematic evolution of passive roof duplexes deduced from cross-section balancing: example from foreland thrust system of the southern Bolivian Subandean zone. *Tectonics*, **11**, 523-536.

BAINES, S. J., BURLEY, S. D. & GIZE, A. P. 1991. Sulphide mineralization and hydrocarbon migration in North Sea oilfields. *In*: PAGEL, M. & LEROY, J. L. (eds). Source, transport and deposition of metals. *Rotterdam, Balkema*, 507-510.

BALLY, A. W. 1983. Seismic expression of structural styles. *American Association of Petroleum Geologists. Studies in Geology*, Series 15, Volume 3.

BALLY, A. W., GORDY, P. L. & STEWART, G. A. 1966. Structure, seismic data and orogenic evolution of southern Canadian Rocky Mountains. *Bulletin of Canadian Petroleum Geology*, **14**, 337-381.

BANKS, C. J. & WARBURTON, J. 1986. 'Passive-roof' duplex geometry in the frontal structures of the Kirthar and Sulaiman mountain belts, Pakistan. *Journal of Structural Geology*, **8**, 229-238.

BARNES, D. F. & TAILLEUR, I. L. 1970. Preliminary interpretation of geophysical data from the lower Noatak River basin, Alaska. *U. S. Geological Survey Open-File Report*, **70-18**, 15p. scale 1:250,000.

BARNES, D. F., MARIANO, J., MORIN, R. L., ROBERTS, C. W. & JACHENS, R. C. 1994. Incomplete isostatic gravity map of Alaska. *In*: PLAFKER, G. & BERG, H. C. (eds). The Geology of Alaska. Boulder, Colorado, Geological Society of America, The Geology of North America, v-G-1. Plate 9. 1 sheet with text. Scale 1: 2.500.000.

BAYONA, G., THOMAS, W. W. & VAN DER VOO, R. 2003. Kinematics of thrust sheets within transverse zones: a structural and paleomagnetic investigation in the Appalachian thrust belt of Georgia and Alabama. *Journal of Structural Geology*, **25**, 1193-1212.

BEAUMONT, C. 1981. Foreland basins. *Royal Astronomical Society Geophysical Journal*, **65**, 291-329.

BEAUMONT, C., FULLSACK, P. & HAMILTON, J. 1992. Erosional control of active compressional orogens. *In*: MCCLAY, K. R. (ed). Thrust Tectonics, *Chapman & Hall, London*, 1-18.

BEAUMONT, C., MUÑOZ, J. A., HAMILTON, J. & FULLSACK, P. 2000. Factors controlling the Alpine evolution of the central Pyrenees inferred from a comparison of observations and geodynamical models. *Journal of Geophysical Research*, **105**, 8121-8145.

BECK, M., COX, A. & JONES, D. L. 1980. Penrose Conference Report: Mesozoic and Cenozoic microplate tectonics of western North America. *Geology*, **8**, 454-456.

BEGIN, N. J. & SPRATT, D. A. 2002. Role of transverse faulting in along-strike termination of Limestone Mountain Culmination, Rocky Mountain thrust-and-fold-belt, Alberta, Canada. *Journal of Structural Geology*, **24**, 689-707.

BELL, T. H. 1991. The role of thrusting in the structural development of the Mount Isa mine and its relevance to exploration in the surrounding region. *Economic Geology*, **86**, 1602-1625.

BELOUSOV, V. I. 2002. Ore-clastic olistostromes, ore clasts, and allochthonous Antimony-Mercury deposits in the Alay Range, southern Tien Shan. *Lithology and Mineral Resources*, **37**, 251-265.

BERG, H. C., JONES, D. L. & CONEY, P. J. 1978. Map showing tectonostratigraphic terranes of southeastern Alaska and adjacent areas. *U. S. Geological Survey Open-File Report*, **78-1085**, 2 sheets, scale 1:1,000,000.

BERNSTEIN, L. R. & COX, D. P. 1986. Geology and sulfide mineralogy of the number one orebody, Ruby Creek copper deposit, Alaska. *Economic Geology*, **81**, 1675-1689.

BETTS, P. G. & LISTER, G. S. 2002. Developing a geodynamically indicated targeting strategy for shale-hosted massive sulphide Pb-Zn-Ag mineralization in the western fold belt of the Mount Isa terrane. *Australian Journal of Earth Sciences*, **49**, 985-1010.

BETTS, P. G., GILES, D. & LISTER, G. S. 2003. Tectonic environment of shale-hosted massive sulfide Pb-Zn-Ag deposits of Proterozoic northeastern Australia. *Economic Geology*, **98**, 557-576.

BIRD, K. J. 1982. Rock-unit reports of 228 wells drilled on the North Slope, Alaska. *U. S. Geological Survey Open-File Report*, **82-278**, 106p.

BIRD, K. J. 1988. Structure-contour and isopach maps of the National Petroleum Reserve in Alaska. *In*: GRYC, G. (ed). Geology and exploration of the National Petroleum Reserve in Alaska, 1974 to 1982. *U. S. Geological Survey Professional Paper*, **1399**, 355-377.

BIRD, K. J. & MOLENAAR, C. M. 1987. Stratigraphy. *In*: BIRD, K. J. & MAGOON, L. B. (eds). Petroleum Geology of the northern part of the Arctic National Wildlife Refuge, northeastern Alaska. *U. S. Geological Survey Bulletin*, **1778**, 37-59.

BISWAS, N. N., AKI, K., PULPAN, H. & TYGAT, G. 1986. Characteristics of regional stresses in Alaska and neighbouring areas. *Geophysical Research Letters*, **13**, 177-180.

BLUM, J. D., BLUM, A. E., DAVIS, T. E. & DILLON, J. T. 1987. Petrology of cogenetic silica-saturated and –oversaturated plutonic rocks in the Ruby geanticline of north-central Alaska. *Canadian Journal of Earth Sciences*, **24**, 159-169.

BLYTHE, A. E., BIRD, J. M. & OMAR, I. G. 1996. Deformational history of the central Brooks Range, Alaska: results from fission-track and $^{40}Ar/^{39}Ar$ analyses. *Tectonics*, **15**, 440-455.

BLYTHE, A. E., MURPHY, J. M. & O'SULLIVAN, P. B. 1997. Tertiary cooling and deformation in the south-central Brooks Range: evidence from zircon and apatite fission-track analyses. *Journal of Geology*, **105**, 583-599.

BOAK, J. L., TURNER, D. L., WALLACE, W. K. & MOORE, T. E. 1985. K-Ar ages of allochthonous mafic and ultramafic complexes and their metamorphic aureoles, western Brooks Range, Alaska (abs). *Alaskan and West Coast Geology and Mineral Resources , American Association of Petroleum Geologists Abstracts with Programs*, Anchorage, May 22-24. p. 37.

BOGDANOV, N. A. & TILMAN, S. M. 1964. Similarities in the development of the Paleozoic structure of Wrangell Island and the western part of the Brooks Range (Alaska). *In*: Soreshchanie po Problem Tektoniki: Moskva, Nauka, Skladchatye oblasti Evrazil, Matenaly, p. 219–230.

BOLDREEL, L. O. & ANDERSEN, M. S. 1993. Late Paleocene to Miocene compression in the Faero-Rockall area. *In*: PARKER, J. R. (ed). Petroleum geology of northwest Europe. *Geological Society of London*, 1025-1034.

BOMBOLAKIS, E. G. 1994. Applicability of critical-wedge theories to foreland belts. *Geology*, **22**, 535-538.

BOOTH, G. G. 1983. Geology of the Red Dog lead-zinc deposit, De Long Mountains, Alaska (abs). *Northwest Mining Association Annual Meeting, Abstracts Volume*. unpaginated.

BOSENCE, D. W. J. 1998. Stratigraphic and sedimentological models of rift basins. *In*: PURSER, B. H. & BOSENCE, D. W. J. (eds). Sedimentation and Tectonics of rift bains: Red sea-Gulf of Aden. *Chapman & Hall, London*. 9-25.

BOSENCE, D. W. J. 2005. A genetic classification of carbonate platforms based on their basinal and tectonic settings in the Cenozoic, *Sedimentary Geology*, **175**, 49-72.

BOTT, M. H. P. 1992. The stress regime associated with continental break-up. *In*: STOREY, B. C., ALABASTER, T. & PANKHURST, R. J. (eds). Magmatism and the causes of continental break-up. *Geological Society of London Special Publication*, **68**, 125-136.

BOUDIER, F. & NICHOLAS, A. 1985. Harzburgite and lherzolite subtypes in ophiolitic and oceanic environments. *Earth and Planetary Science Letters*, **76**, 84-92.

BOUMA, A. H. 1962. Sedimentology of some Flysch deposits: a graphic approach to facies interpretation. *Elsevier*, 168pp.

BOUMA, A. H., NORMAK, W. R. & BARNES, N. E. 1985. Submarine fans and related turbidite systems. *Springer Verlag, New York*, 351p.

BOWSHER, A. L. & DUTRO, J. T. Jr. 1957. The Paleozoic section in the Shainin Lake area, central Brooks Range, Alaska. *U. S. Geological Survey Professional Paper*, **303-A**, 1-39.

BOX, S. E. 1985. Early Cretaceous orogenic belt in northeastern Alaska: Internal organization, lateral extent, and tectonic interpretation. *In*: HOWELL, D. G. (ed). Tectonostratigraphic terranes of the circum-Pacific region: *Circum-Pacific Council of Energy and Mineral Resources, Earth Science Series*, **1**, 137-145.

BOX, S. E. 1987. Late Cretaceous or younger SW-directed extensional faulting: Cosmos Hills, Brooks Range, Alaska. *Geological Society of America Abstracts with Programs*, v.19, n.6, p. 361.

BOYER, S. E. 1986*a*. Styles of folding within thrust sheets: examples from the Appalachian and Rocky Mountains of the USA and Canada. *Journal of Structural Geology*, **8**, 325-339.

BOYER, S. E. 1986*b*. Geometric evidence for simultaneous, rather than sequential, movement on major thrusts: implications for duplex development. *Geological Society of America Abstracts with Programs*, **18**, 549.

BOYER, S. E. 1992. Geometric evidence for synchronous thrusting in the southern Alberta and northwest Montana thrust belts. *In*: MCCLAY, K. R. (ed). Thrust Tectonics, *Chapman & Hall, London*, 377-390.

BOYER, S. E. 1995. Sedimentary basin taper as a factor controlling the geometry and advance of thrust belts. *American Journal of Science*, **295**, 1220-1254.

BOYER, S. E. & ELLIOT, D. 1982. Thrust systems. *American Association of Petroleum Geologists Bulletin*, **66**, 1196-1230.

BRANDON, M. T. 1989. Deformational styles in a sequence of olistostromal melanges, Pacific Rim Complex, western Vancouver Island, Canada. *Geological Society of America Bulletin*, **101**, 1520-1542.

BRISKEY, J. A. 1986. Sedimentary exhalative Zn-Pb deposit. *In*: COX, D. P. & SINGER, D. A. (eds.). Mineral deposit models. *U. S. Geological Survey Bulletin*, **1693**, 379p.

BROADBENT, G. C. 1995. The Century discovery, northwest Queensland. Is exploration ever complete?. *The Australasian Institute of Mining and Metallurgy Publication Series*, **9/95**, 81-86.

BROADBENT, G. C., MYERS, R. E. & WRIGHT, J. V. 1998. Geology and origin of the shale-hosted Zn-Pb-Ag mineralization at the Century deposit, northwest Queensland. Australia. *Economic Geology*, **93**, 1264-1294.

BROADBENT, G. C., ANDREWS, S. J. & KELSO, I. J. 2002. A decade of new ideas: geology and exploration history of the Century Zn-Pb-Ag deposit, northwestern Queensland, Australia. *Society of Economic Geologists Special Publication*, **9**, 119-140.

BROOKS, A. H. 1906. The geography and geology of Alaska with a section on climate by Cleveland Abbe, Jr. *U. S. Geological Survey Professional Paper*, **45**, 327p.

BROSGÉ, W. P., DUTRO, J. T. JR., MANGUS, M. D. & REISER, H. N. 1962. Paleozoic sequence in the eastern Brooks Range, Alaska. *American Association of Petroleum Geologists Bulletin*, **46**, 2174-2198.

BROSGÉ, W. P., NILSEN, T. H., MOORE, T. E. & DUTRO, T. JR. 1988. Geology of the Upper Devonian and Lower Mississippian (?) Kanayut Conglomerate in the central and eastern Brooks Range. *In*: GRYC, G. (ed). Geology and exploration of the National Petroleum Reserve in Alaska, 1974 to 1982. *U. S. Geological Survey Professional Paper*, **1399**, 299-317.

BROWN, D., JUHLIN, C., ALVAREZ-MARRÓN, J., PÉREZ ESTAÚN, A. & OSLIANSKI, A. 1998. Crustal-scale structure and evolution of an arc-continent collision zone in the southern Urals, Russia. *Tectonics*, **17**, 158-171.

BROWN, D., ALVAREZ-MARRÓN, J., PÉREZ ESTAÚN, A., PUCHKOV, V. & AYALA, C. 1999. Basement influence on foreland thrust and fold belt development: an example from the southern Urals. *Tectonophysics*, **308**, 459-472.

BROWN, D., JUHLIN, C., ALVAREZ-MARRÓN, J., PÉREZ ESTAÚN, A., GOROZHANINA, Y. & PUCHKOV, V. 2004. The structure of the south Urals foreland fold and thrust belt at the transition to the Precaspian Basin. *Journal of the Geological Society of London*, **5**, 813-822.

BROWN, R. L. 2004. Thrust-belt accretion and hinterland underplating of orogenic wedges – an example from the Canadian Cordillera. *In*: MCCLAY, K. R. (ed). Thrust tectonics and hydrocarbon systems. *American Association of Petroleum Geologists Memoir*, **82**, 53-66.

BRUYNZEEL, J. W., GULDENZOPH, E. C. & PICKARD, J. E. 1982. Petroleum exploration of NPRA, 1974-1981. Final Report: Houston, Tetra Tech, Inc. report 8200, 3 volumes, 5 boxes of geophysical maps. National Geophysical Data Centre, Boulder, Colorado, 80303.

BULL, S. W. & RAWLINGS, D. J. 1998. A tectono-stratigraphic review of the northern Australian Proterozoic zinc belt. *In*: HOLM, O., PONGRATZ, J. & MCGOLDRICK, P. J. (eds). Basins, fluids and Zn-Pb ores. University of Tasmania National Key Centre, 1-13.

BUNDTZEN, T. K., SWAINBANK, R. C., DEGGEN, J. R. & MOORE, J. L. 1990. Alaska's mineral industry, 1989. *Alaska Division of Geological and Geophysical Surveys Special Report*, **44**, 100p.

BURBANK, D. W. & ANDERSON, R. S. 2001. Tectonic geomorphology, *Blackwell Science*, 274p.

BUTLER, R. W. H. 1982. The terminology of structures in thrust belts. *Journal of Structural Geology*, **3**, 239-245.

BUTLER, R. W. H. 1983. Balanced cross-sections and their implications for the deep structure of the northwest Alps. *Journal of Structural Geology*, **5**, 125-137.

BUTLER, R. W. H. 1987. Thrust sequences. *Journal of the Geological Society of London*, **144**, 619-634.

BUTLER, R. W. H. 1989. The influence of pre-existing basin structure on thrust system evolution in the western Alps. *In*: COOPER, M. A. & WILLIAMS, G. D. (eds). Inversion Tectonics. *Geological Society of London Special Publication*, **44**, 105-122.

BUTLER, R. W. H. 1992. Structural evolution of the western Chartreuse fold and thrust system, NW French Subalpine chains. *In*: MCCLAY, K. R. (ed). Thrust Tectonics. *Chapman & Hall, London*, 287-298.

BUTLER, R. W. H. 2004. The nature of 'roof thrusts' in the Moine thrust belt, NW Scotland: implications for the structural evolution of thrust belts. *Journal of the Geological Society of London*, **5**, 849-859.

CALASSOU, S., LARROQUE, C. & MALAVIEILLE, J. 1993. Transfer zones of deformation in thrust wedges: An experimental study. *Tectonophysics*, **221**, 325-344.

CAMPBELL, R. H. 1961. Thrust faults in the southern Lisburne Hills, northwest Alaska. *U. S. Geological Survey Professional Paper*, **424-D**, 194-196.

CAMPBELL, R. H. 1967. Areal geology in the vicinity of the Chariot site, Lisburne Peninsula, northwest Alaska. *U. S. Geological Survey Professional Paper*, **395**, 71p.

CAREY, S. W. 1955. The orocline concept in geotectonics. *Proceedings of the Royal Society of Tasmania*, **89**, 255-289.

CAREY, S. W. 1958. The tectonic approach to continental drift. *In*: CAREY, S. W (ed). Continental drift, a symposium. *Hobart University of Tasmania*, 177-355.

CARNE, R. C. & CATHRO, R. J. 1982. Sedimentary exhalative (SEDEX) zinc-lead-silver deposits, northern Canadian Cordillera. *Canadian Institute of Mineralogy and Metallurgy*, **75**, 66-78.

CARTWRIGHT, J. A., HADDOCK, R. C. & PINHEIRO, L. M. 1993. The lateral extent of sequence boundaries. *In*: WILLIAMS, G. D. & DOBB, A. (eds). Tectonics and seismic sequence stratigraphy. *Geological Society of London Special Publication*, **71**, 15-34.

CASAVANT, R. & MILLER, S. 1999. Is the western Brooks Range on the move? Poster abstract. GeoDaze, 1999, Tucson, Arizona, unpaginated.

CHAPMAN, L. H. 2004. Geology and mineralization styles of the George Fisher Zn-Pb-Ag deposit, Mount Isa, Australia. *Economic Geology*, **99**, 233-255.

CHAPMAN, R. M., DETTERMAN, R. L. & MANGUS, M. D. 1964. Geology of the Killik-Etivluk rivers region, Alaska. *U. S. Geological Survey Professional Paper*, **303-F**, 325-407.

CHAPPLE, W. M. 1978. Mechanics of thin-skinned fold-and-thrust belts. *Geological Society of America Bulletin*, **89**, 1189-1198.

CHÁVEZ-CABELLO, G., COSSÍO-TORRES, T. & PETERSON-RODRÍGUEZ, 2004. Change of the maximum principal stress during the Laramide Orogeny in the Monterrey salient, northeast Mexico. *In*: SUSSMAN, A. J. & WEIL, A. B. (eds). Orogenic curvature: integrating paleomagnetic and structural analyses. *Geological Society of America Special Paper*, **383**, 145-159.

CHURKIN, M., NOKLEBERG, W. N. & HUIE, C. 1979. Collision deformed Palaeozoic continental margin, western Brooks Range, Alaska. *Geology*, **7**, 379-383.

CHURKIN, M. JR., CARTER, C. & TREXLER, J. JR. 1980. Collision deformed Paleozoic continental margin of Alaska: a foundation for microplate accretion. *Geological Society of America Bulletin*, **91**, 648-654.

CHURKIN, M. & TREXLER, J. JR. 1980. Circum-Arctic plate accretion-Isolating part of a Pacific Plate to form the nucleus of the Arctic. *Earth and Planetary Science Letters*, **49**, 356-362.

CHURKIN, M. & TREXLER, J. JR. 1981. Continental plates and accreted oceanic terranes in the Arctic. *In*: NAIRN, A. E. M. CHURKIN, M. JR. & STEHLI, F. G. (eds). The ocean basin and margins. Volume 5: The Arctic Ocean. *New York, Plenum Press*, 1-20.

COAKLEY, B. J. & WATTS, A. B. 1991. Tectonic controls on the development of unconformities: the North Slope, Alaska. *Tectonics*, **10**, 101-130.

COBIELLA-REGUERA, J. L. 2005. Emplacement of Cuban ophiolites. *Geologica Acta*, **3**, 273-294.

COLE, F., BIRD, K. J., TORO, J., ROURE, F., O'SULLIVAN, P. B., PAWLEWICZ, M. & HOWELL, D. G. 1997. An integrated model for the tectonic development of the frontal Brooks Range and Colville Basin 250 km west of the Trans-Alaska Crustal Transect. *Journal of Geophysical Research*, **102**, 20,685-20,708.

COLEMAN, R. G. 1971. Plate tectonic emplacement of upper mantle peridotites along continental edges. *Journal of Geophysical Research*, **76**, 1212-1222.

COLEMAN, R. G. 1977. Ophiolites, *New York, Springer-Verlag*, 229p.

COLLETA, B., LETOUZEY, J. & PINEDO, R. 1991. Computerized X-ray tomography analysis of sandbox models: Examples of thin-skinned thrust systems. *Geology*, **19**, 1063-1067.

CONEY, P. J. 1989. Structural aspects of suspects terranes and accretionary tectonics in western North America. *Journal of Structural Geology*, **11**, 107-125.

CONEY, P. J., JONES, D. L. & MONGER, J. W. H. 1980. Cordilleran suspect terranes. *Nature*, **299**, 329-333.

CONEY, P. J. & JONES, D. L. 1985. Accretion tectonics and crustal structure in Alaska. *Tectonophysics*, **119**, 265-283.

CONNARD, G. G., SALTUS, R. W., HILL P. L., CARLSON L. & MILICEVIC, B. 1999. Alaska Digital Aeromagnetic Database Description. *U. S. Geological Survey Open-File Report*, **99-0503**.

COOPER, D. J. W. 1988. Structure and sequence of thrusting in deep-water sediments during ophiolite emplacement in the south-central Oman Mountains, *Journal of Structural Geology*. **10**, 473-485.

COSGROVE, J. W. 1976. The formation of crenulation cleavage. *Journal of the Geological Society of London*, **132**, 155-178.

COUZENS-SCHULTZ, B. A., VENDEVILLE, B. C. & WILTSCHKO, D. V. 2003. Duplex style and triangle zone formation: insights from physical modelling. *Journal of Structural Geology*, **25**, 1623-1644.

COVEY, M. 1986. Evolution of foreland basins to steady state. *International Association of Sedimentologists Special Publication*, **8**, 77-90.

COWAN, D. S. 1985. Structural styles in Mesozoic and Cenozoic melanges in the western Cordillera of North America. *Geological Society of America Bulletin*, **96**, 451-462.

COWARD, M. P. 1983. Thrust tectonics, thin skinned or thick skinned, and the continuation of thrusts to deep in the crust. *Journal of Structural Geology*, **5**, 113-123.

COWARD, M. P., GILLCRIST, R. & TRUDGILL, B. 1991. Extensional structures and their tectonic inversion in the western Alps. *In*: ROBERTS, A. M., YIELDING, G. & FREEMAN, B. (eds). The geometry of normal faults. *Geological Society of London Special Publication*, **56**, 93-112.

COX, D. P. & SINGER, D. A. 1986. Mineral deposits models. *U. S. Geological Survey Bulletin*, **1693**, 379 p.

CRAIG, J. R. & VAUGHAN, D. J. 1994. Ore microscopy and ore petrography (2nd Edition). *John Wiley & Sons, New York*, 434p

CRANE, R. C. 1980. Comment on: Collision-deformed Paleozoic continental margin, western Brooks Range, Alaska. *Geology*, **8**, 354-355.

CRANE, R. C. 1987. Cretaceous olistostrome model, Brooks Range, Alaska, *In*: TAILLEUR, I. & WEIMER, P. (eds). Alaskan North Slope geology; Pacific Section, *Society of Economic Paleontologists and Mineralogists and Alaska Geological Society*, **1**, 433-440.

CRANE, R. C. & WIGGINS, V. D. 1976. The Ipewick Formation, a significant Jurassic-Neocomian map unit in the northern Brooks Range fold belt. *American Association of Petroleum Geologists, 51st Annual Meeting, Program and Abstracts*, p.25-26.

CRISTALLINI, E. O., COMINGUEZ, A. H., RAMOS, V. A., MERCERAT, E. D. 2004. Basement double-wedge thrusting in the northern Sierras Pampeanas of Argentina (27°S)-constraints from deep seismic reflection. *In*: MCCLAY, K. R. (ed). Thrust Tectonics and Petroleum Systems. *American Association of Petroleum Geologists Memoir*, **82**, 67-92.

CROWDER, R. K. 1990. Permian and Triassic sedimentation in the northeastern Brooks Range, Alaska: deposition of the Sadlerochit Group. *American Association of Petroleum Geologists Bulletin*, **74**, 1351-1370.

CURTIS, J. B. 2002. Fractured shale-gas systems. *American Association of Petroleum Geologists Bulletin*, **86**, 1921-1938.

CURTIS, S. M., ELLERSIECK, I., MAYFIELD, C. F. & TAILLEUR, I. L. 1984. Reconnaissance geologic map of the southwestern Misheguk Mountain quadrangle, Alaska. *U. S. Geological Survey Miscellaneous Investigations Series Map*, **I-502**. scale 1:63,360.

CURTIS, S. M., ELLERSIECK, I., MAYFIELD, C. F. & TAILLEUR, I. L. 1990. Reconnaissance geologic map of the De Long Mountains A-1 and B-1 quadrangles and part of the C-1 quadrangle, Alaska. *U. S. Geological Survey Miscellaneous Investigations Series Map*, **I-1930**. scale 1:63,360, 42p.

DAHLEN, F. A. 1984. Non cohesive critical Coulomb wedges: an exact solution. *Journal of Geophysical Research*, **81**, 10125-10133.

DAHLEN, F. A. 1990. Critical taper model of fold-and-thrust belts and accretionary wedges. *Annual Review of Earth and Planetary Sciences*, **18**, 55-99.

DAHLEN, F. A., SUPPE, J. & DAVIS, D. M. 1984. Mechanics of fold-and-thrust belts and accretionary wedges: Cohesive Coulomb theory. *Journal of Geophysical Research*, **89**, 10087-10101.

DAHLEN, F. A. & SUPPE, J. 1988. Mechanics growth, and erosion of mountain belts. *In*: CLARK, S. P. JR., BURCHFIEL, B. C. & SUPPE, J. (eds). Processes in continental lithospheric deformation. *Geological Society of America Special Paper*, **218**, 161-178.

DAHLEN, F. A. & BARR, T. D. 1989. Brittle frictional mountain building, 1, Deformation and mechanical energy budget. *Journal of Geophysical Research*, **94**, 3906-3922.

DAHLSTROM, C. D. A. 1969. Balanced cross sections. *Canadian Journal of Earth Sciences*, **6**, 743-757.

DAHLSTROM, C. D. A. 1970. Structural geology in the eastern margin of the Canadian Rocky Mountains. *Bulletin of Canadian Petroleum Geology*, **18**, 332-406.

DANA, J. D. 1866. A textbook of geology. *Theodore Bliss, Philadelphia*, 354p.

DAVIDSON, S. G., ANASTASIO, D. J., BEBOUT, G. E., HOLL, J. E. & HEDLUND, C. A. 1998. Volume loss and metasomatism during cleavage formation in carbonate rocks. *Journal of Structural Geology*, **20**, 707-726.

DAVIS, T. P. 2004. Mine-scale structural controls on the Mount Isa Zn-Pb-Ag and Cu orebodies. *Economic Geology*, **99**, 543-559.

DAVIS, D., SUPPE, J. & DAHLEN, F. A. 1983. Mechanics of fold-and-thrust belts and accretionary wedges. *Journal of Geophysical Research*, **94**, 10,347-10,354.

DAVIS, D. & ENGELDER, T. 1985. The role of salt in fold-and-thrust belts. *Tectonophysics*, **119**, 67-89.

DAVIS, D. & VON HUENE, R. 1987. Inferences on sediment strength and fault friction from structures at the Aleutian Trench. *Geology*, **15**, 517-522.

DAVIS, E. E. & HYNDMAN, R. D. 1989. Accretion and recent deformation of sediments along the northern Cascadia subduction zone. *Geological Society of America Bulletin*, **101**, 1465-1480.

DAVIS, G. H. & REYNOLDS, S. J. 1984. Structural geology of rocks and regions. *John Wiley & Sons*, 776p.

DECKER, J. E. & KARL, S. M. 1977. Preliminary aeromagnetic map of the Brooks Range and Arctic Slope, Alaska. *U. S. Geological Survey Open-File Report*, **77-166-E**. scale 1:1,000,000.

DE PAOR, D. G. 1988. Balanced sections in thrust belts. Part I: Construction. *American Association of Petroleum Geologists Bulletin*, **72**, 73-90.

DE VERA, J., MCCLAY, K. R. & KING, A. R. 2004. Structure of the Red Dog district, western Brooks Range, Alaska. *In*: Kelley K. D. & JENNINGS S. (eds). A Special Issue devoted to barite and zinc-lead-silver deposits in the Red Dog district, western Brooks Range northern Alaska. *Economic Geology*, **99**, 1415-1454.

DEWEY, J. F. 1976. Ophiolite obduction. *Tectonophysics*, **31**, 93-120.

DEWEY, J. F. 1988. Lithospheric stress, deformation and tectonic cycles: the disruption of Pangea and the closure of the Tethys. *In*: AUDLEY-CHARLES, M. G. & HALLAM, A. (eds). Gondwana and Tethys. *Geological Society of London Special Publication*, **37**, 23-40.

DEWEY, J. F. 2003. Ophiolites and lost oceans: rifts, ridges, arcs, and/or scrapings?. *In*: DILEK, Y. & NEWCOMB, S. (eds). Ophiolite concept and the evolution of geological thought. Boulder, Colorado. *Geological Society of America Special Paper*, **373**, 153-159.

DEWEY, J. F. & BIRD, J. M. 1970. Mountain belts and the new global tectonics. *Journal of Geophysical Research*, **75**, 2625-47.

DEWEY J. F., RYAN P. D. & ANDERSEN T. B. 1993. Orogenic uplift and collapse, crustal thickness, fabrics and metamorphic changes: the role of eclogites. *Geological Society of London Special Publication*, **76**, 325-343

DIEGEL, F. A. 1986. Topological constraints on imbricate thrust networks, examples from the Mountain City window, Tennessee, USA. *Journal of Structural Geology*, **8**, 269-280.

DILEK, Y. 2003. Ophiolite concept and its evolution. *In*: DILEK, Y. & NEWCOMB, S. (eds). Ophiolite concept and the evolution of geological thought. Boulder, Colorado. *Geological Society of America Special Paper*, **373**, 1-16.

DILLON, J. T. 1989. Structure and stratigraphy of the southern Brooks Range and northern Koyukuk basin near the Dalton Highway. *In*: MULL, C. G. & ADAMS, K. E. (eds). *Dalton Highway, Yukon River to Prudhoe Bay*, Alaska Division of Geological and Geophysical Surveys Guidebook 7, v.2, 157-187.

DINARÉS, J., MCCLELLAND, E. & SANTANACH, P. 1992. Contrasting rotations within thrust sheets and kinematics of thrust tectonics as derived from paleomagnetic data: an example from the Southern Pyrenees. *In*: MCCLAY, K. R. (ed). Thrust Tectonics, *Chapman & Hall, London*, 265-275.

DIXON, J. M. 2004. Physical (centrifuge) modelling of fold-thrust shortening across carbonate bank margins: timing, vergence and style of deformation. *In*: MCCLAY, K. R. (ed). *American Association of Petroleum Geologists Bulletin*, **82**, 227-242.

DIXON, J. M. & SUMMERS, J. M. 1985. Recent developments in centrifuge modelling of tectonic processes: equipment, model construction techniques and rheology of model materials. *Journal of Structural Geology*, **7**, 83-102.

DIXON, J. M. & LIU, S. 1992. Centrifuge modelling of the propagation of thrust faults. *In*: MCCLAY, K. R. (ed). Thrust Tectonics, *Chapman & Hall, London*, 53-70.

DIXON, J. M. & SPRATT, D. A. 2004. Deformation at lateral ramps and tear faults: centrifuge models and examples from the Canadian Rocky Mountain Foothills. *In*: MCCLAY, K. R. (ed). *American Association of Petroleum Geologists Bulletin*, **82**, 243-262.

DOUGLAS, R. J. W. 1952. Preliminary map, Waterton, Alberta. *Geological Survey of Canada Paper*, **51-22.**

DUMOULIN, J. A. & HARRIS, A. 1987. Lower Paleozoic carbonate rocks of the western Brooks Range. *In*: TAILLEUR, I. & WEIMER, P. (eds). Alaskan North Slope geology. Bakersfield, California. *Society of Economic Paleontologists and Mineralogists, Pacific Section, and Alaska Geological Society*, Book **50**, 311-336.

DUMOULIN, J. A. & HARRIS, A. 1992. Devonian-Mississippian carbonate sequence in the Maiyumerak Mountains, western Brooks Range, Alaska. *U. S. Geological Survey Open-File Report*, **92-3**, 83p.

DUMOULIN, J. A., HARRIS, A. & SCHMIDT, J. M. 1993. Deep-water lithofacies and conodont faunas of the Lisburne Group, western Brooks Range, Alaska. *In:* DUSEL-BACON, C. & TILL, A. B. (eds). Geologic studies in Alaska by the U. S. Geological Survey, 1992. *U. S. Geological Survey Bulletin*, **2068**, 12-30.

DUMOULIN, J. A., WATTS, K. T. & HARRIS, A. G. 1997. Stratigraphic contrasts and tectonic relationships between Carboniferous successions in the Trans-Alaska Crustal Transect corridor and adjacent areas, northern Alaska. *Journal of Geophysical Research*, **102**, 20,709-726.

DUMOULIN, J. A. & HARRIS, A. 1999. Carboniferous and related rocks in the Red Dog area. *In*: U. S. Geological Survey and Cominco Research Study at Red Dog. 1998 Results. Unpublished Report, 6-29.

DUMOULIN, J. A., YOUNG, L. E. & BLOME, C. D. 2001. Sedimentologic and paleontologic constraints on setting and age of the Red Dog Zn-Pb-Ag massive sulfide deposit, western Brooks Range, Alaska. *Geological Society of America Abstracts with Programs, A-272*.

DUMOULIN, J. A., HARRIS, A., BLOME, C. D. & YOUNG, L. E. 2004. Depositional settings, correlation, and age of Carboniferous rocks in the western Brooks Range. *In*: KELLEY K. D. & JENNINGS

S. (eds). A Special Issue devoted to barite and zinc-lead-silver deposits in the Red Dog district, western Brooks Range northern Alaska. *Economic Geology*, **99**, 1355-1384.

DUMOULIN, J. A., BURRUSS, R. C., LILLIS, P. G. & PARRIS, T. M. 2005. New field and geochemical evidence on the nature and extent of the Lisburne Petroleum system (northern Alaska). Geological Society of America Cordilleran Section, 101st Annual Meeting, April 29-May 1, 2005. *Abstracts with Programs*, **37**, n.4 .

DUTRO, J. T., BROSGÉ, W. P., LANPHERE, M. A. & REISER, H. N. 1976. Geologic significance of Doonerak structural high, central Brooks Range, Alaska. American Association of Petroleum Geologists, **60**, 952-961.

DUTRO, J. T. 1980. Comment on 'Collision-deformed Paleozoic continental margin, western Brooks Range, Alaska'. *Geology*, **8**, 355-356.

DUTRO, J. T. JR. 1981. Geology of Alaska bordering the Arctic Ocean. *In:* NAIRN, A. E. M., CHURKIN, M. JR. & STEHLI, F. G. (eds.). The ocean basins and margins, v. 5: The Arctic Ocean: *New York, Plenum Press*, 21–36.

EARDLEY, A. J. 1948. Ancient Arctica. *Journal of Geology*, **56**, 409-436.

EASTON, W. H. 1960. Invertebrate Paleontology, *New York, Harper*, 701 p.

EBINGER, C. J. 1989. Geometric and kinematic development of border faults and accommodation zones, Kivu-Rusizi Rift, Africa. *Tectonics*, **8**, 117-137.

EBINGER, C. J., PETIT, C. & BUROV, E. 2002. Causes and consequences of litospheric extension: the ups and downs of continental rifts. Sedimentation of continental rifts. *Society of Economic Paleontogists and Mineralogists Special Publication*, **73**, 11-23.

EDGERTON, D. G. 1997*a*. Geologic Models of sediment-buffered hydrothermal vents: a case study of the Red Dog Zn-Pb-Ag orebody, western Brooks Range, Alaska. PhD Thesis, University of Texas at Austin. Austin. 209p.

EDGERTON, D. G. 1997*b*. Reconstruction of the Red Dog Zn-Pb-Ba orebody, Alaska: implications for the environment during the mineralizing event. *Canadian Journal of Earth Sciences*, **34**, 1581-1602.

EINAUDI, M. T. & HITZMAN, M. W. 1986. Mineral deposits of northern Alaska. *Economic Geology*, **81**, 1583-1590.

ELLERSIECK, I. & MAYFIELD, C. F. 1983. The western Brooks Range, Alaska: Too much crust. *Geological Society of America Abstract with Programs*, 16, p. 281.

ELLERSIECK, I., TAILLEUR, I. L., MAYFIELD, C. F. & CURTIS, S. M. 1979. A new find of upper Cretaceous or Tertiary sedimentary rocks in the Noatak Valley. *In*: JOHNSON, K. M. & WILLIAMS, J. R. (eds). U. S. Geological Survey in Alaska. Accomplishments during 1978. *U. S. Geological Survey Circular, **804-B***. B13.

ELLERSIECK, I., CURTIS, S. M., MAYFIELD, C. F. & TAILLEUR, I. L. 1983. Reconnaissance geologic map of the De Long Mountains A2 and B2 quadrangles, and part of C2 quadrangles, Alaska: *U. S. Geological Survey Open-File Report*, **83-184**, scale 1:63.360, 53p. 2 sheets.

ELLERSIECK, I., CURTIS, S. M., MAYFIELD, C. F. & TAILLEUR, I. L. 1984. Reconnaissance geologic map of the south-central Misheguk Mountain quadrangle, Alaska: *U. S. Geological Survey Miscellaneous Investigations Series*. Map **I-1504**, scale 1:63.360, 53p. 2 sheets.

ELLERSIECK, I., CURTIS, S. M., MAYFIELD, C. F. & TAILLEUR, I. L. 1990*a*. Reconnaissance geologic map of the De Long Mountains A2 and B2 quadrangles, and part of C2 quadrangles, Alaska: *U. S. Geological Survey Miscellaneous Investigations Series*. Map **I-1931**, scale 1:63.360, 53p. 2 sheets.

ELLERSIECK, I., TAILLEUR, I. L. & MULL, C. G. 1990*b*. Explanation to accompany reconnaissance geologic map of the Story Creek area, National Petroleum Reserve, Alaska. *U. S. Geological Survey Open-File Report*, **90-533**, 21p.

ELLIOT, D. 1976. The motion of thrust sheets. *Journal of Geophysical Research*, **81**, 949-963.

ELLIOT, D. 1983. The construction of balanced cross sections. *Journal of Structural Geology*, **5**, p. 101.

ELLIOT, D. & JOHNSON, M. R. W. 1980. Structural evolution in the northern part of the Moine Thrust Belt, NW Scotland. *Transactions of the Royal Society of Edinborough: Earth Science*, **71**, 69-96.

ELSWICK, V. L. 2003. Seismic interpretation and structural evolution of the Hope Basin, Alaska. M.Sc. Thesis. Morgantown University, West Virginia, 43 p.

ELSWICK, V. L. & TORO, J. 2003. Seismic interpretation and structural evolution of the Hope Basin, Alaska. *Geological Society of America Abstracts with Programs*. Seattle November 2-5 2003. 9-21.

ERSLEV, E. A. 1991. Trishear fault-propagation folding. *Geology*, **19**, 617-620.

ESHELBY, J. D. 1973. Dislocation theory for geophysical applications. *Philosophical Transactions of the Royal Society*. **A274**, 331-338.

ESTABROOK, C. H., STONE, D. B. & DAVIES, J. N. 1998. Seismotectonics of northern Alaska. *Journal of Geophysical Research*, **93**, 12.026-12.040.

FALVEY, D. A. 1974. The development of continental margins in plate tectonic theory. *Australian Exploration Journal*, **14**, 95-106.

FERMOR, P. R. 1999. Aspects of the three-dimensional structure of the Alberta Foothills and Frontal ranges. *Geological Society of America Bulletin*, **111**, 317-346.

FERMOR, P. R. & PRICE, R. A. 1987. Multiduplex structure along the base of the Lewis thrust sheet in the southern Canadian Rockies. *Bulletin of Canadian Petroleum Geology*, **35**, 159-185.

FERMOR, P. R. & MOFFAT, I. W. 1992. Tectonics and structure of the western Canada foreland basin. *In*: MCQUEEN, R. W. & LECKIE, D. A. (eds). Foreland basins and fold belts. *American Association of Petroleum Geologists Memoir*, **55**, 81-105.

FOLEY, J. Y., MARDOCK, C. L., DAHLIN, D. C. & O'CONNOR, W. K. 1992. Reconnaissamce investigations of chromite deposits and platinum-group metals in the western Brooks Range, northwest Alaska. *U. S. Bureau of Mines Report*, **80-92**, 67 p.

FOLGER, P. F. & SCHMIDT, J. M. 1986. Geology of the carbonate-hosted Omar copper prospect, Baird Mountains, Alaska. *Economic Geology*, **81**, 1690-1695.

FORREST, K. 1983. Geologic and isotopic studies of the Lik deposit and the surrounding mineral district, De Long Mountains, western Brooks Range, Alaska. Ph.D Thesis. University of Minnesota, Minneapolis, 161p.

FORREST, K. & SAWKINS, F. J. 1987. Geologic setting and mineralization of the Lik deposit: implications for the tectonic history of the western Brooks Range. *In*: TAILLEUR, I. & WEIMER, P. (eds). Alaskan North Slope Geology, Bakersfield, California, *Society of Economic Paleontologists and Mineralogists, Pacific Section*, v.**1**, 295-305.

FUJITA, K. & NEWBERRY, J. T. 1982. Tectonic evolution of northeastern Siberia and adjacent regions. *Tectonophysics*, **89**, 337-357.

FUJITA, K., COOK, D. B., HASEGAWA, H., FORSYTH, D. & WETMILLER, R. 1990. Seismicity and focal mechanisms of the Arctic region and the North American plate boundary in Asia. . *In*: GRANTZ, A.,

JOHNSON, L. & SWEENEY, J. F. (eds). The Arctic Ocean Region. Boulder Colorado, Geological Society of America, The Geology of North America. v. L, 79-100.

GABRIELSE, H. 1991. Structural styles. Chapter 17. *In*: GABRIELSE, H. & YORATH, C. J. (eds). Geology of the Cordilleran Orogen in Canada. *Geological Survey of Canada. Geology of Canada*, **4**, 571-675.

GABRIELSE, H. & YORATH, C. J. 1991. Tectonic Synthesis. *In*: GABRIELSE, H. & YORATH, C. J. (eds). Geology of the Cordilleran Orogen in Canada. *Geological Survey of Canada. Geology of Canada*, **4**, 677-705.

GACCETA, J. D. & CHURCH, S. E. 1989. Lead isotope data base for sulfide occurrences in Alaska. *U. S. Geological Survey Open-File Report*, **89-688**, 60p.

GALLOWAY, W. E. 1989. Genetic stratigraphic sequences in basin analysis. Architecture and genesis of flooding-surface bounded depositional units. *American Association of Petroleum Geologists Bulletin*, **73**, 125–142.

GAMMOND, J. F. 1994. Normal faulting and tectonic inversion driven by gravity in a thrusting regime. *Journal of Structural Geology*, **16**, 1-9.

GARVEN, G. 1985. The role of regional fluid flow in the genesis of the Pine Point deposit, western Canada sedimentary basin. *Economic Geology*, **80**, 307-324.

GARVEN, G., RAFFENSPERGER, J. P., DUMOULIN, J. A., BRADLEY, D. A., YOUNG, L. E., KELLEY, K. D. & LEACH, D. L. 2003. Coupled heat and fluid flow modelling of the carboniferous Kuna Basin, Alaska: implications for the genesis of the Red Dog Pb-Zn-Ag-Ba ore district. *Journal of Geochemical Exploration*, **78-79**, 215-219.

GASS, I. G. 1990. Ophiolites and oceanic lithosphere. *In*: MALPAS, J., MOORES, E. M., PANAYIOTOU, A. & XENOPHONTOS, C. (eds). Ophiolites: Oceanic crustal analogues. Cyprus Geol. Surv. Dept, Nicosia, Cyprus, pp. 231– 234.

GEISER, P. A. 1988. The role of kinematics in the construction and analysis of geological cross sections in deformed terranes. *In*: MITRA, G. & WOJTAL, S. (eds). Geometries and mechanisms of thrusting, with special reference to the Appalachians, *Geological Society of America Special Paper*, **222**, 47-76.

GEOTERREX LTD. 1981. Interpretation report. Airborne electromagnetic survey. Bat-ringer input system: Unpublished Cominco American Internal Report, 173p.

GLEN, J. M. G. 2004. A kinematic model for the southern Alaska orocline based on regional fault patterns. *In*: SUSSMAN, A. J. & WEIL, A. B. (eds). Orogenic curvature: integrating paleomagnetic and structural analyses. *Geological Society of America Special Paper*, **383**, 161-172.

GODSON, R. H. 1994. Composite magnetic anomaly map of Alaska and adjacent offshore areas. *In*: PLAFKER, G. & BERG, H. C. (eds). The Geology of Alaska. Boulder, Colorado, Geological Society of America, The Geology of North America, v-G-1. Plate 10. 1 sheet. Scale 1: 2.500.000.

GOODFELLOW, W. D. 1998. Sediment-hosted Zn-Pb-Ag deposits of North America. Proceedings of a symposium on 'Basins, fluids and Zn-Pb ores'. *Centre for Ore Deposit Research*, University of Tasmania, June 1998. 59-91.

GOODFELLOW, W. D. 1999. SEDEX deposits: Geology, genesis and exploration. Alaska Miners Association. Short Course volume notes. 84p *Unpublished*

GOODFELLOW, W. D. & BLAISE, B. 1988. Sulphide formation and hydrothermal alteration of hemipelagic sediment, Middle Valley, Northern Juan de Fuca Ridge. *Canadian Mineralogist*, **26**, 675-696.

GOODFELLOW, W. D. & FRANKLIN, J. N. 1994. Geology, mineralogy and geochemistry of massive sulfides in shallow cores, Middle Valley, Juan de Fuca Ridge. *Economic Geology,* **88**, 2037-2068.

GOODFELLOW, W. D., LYDON, D. W. & TURNER, R. J. W. 1993. Geology and genesis of stratiform sediment-hosted (SEDEX) zinc-lead-silver sulfide deposits. *In*: KIRKHAM, R. V., SINCLAIR, W. D., THORPE, R. I. & DUKE, J. M. (eds). Mineral deposit Modelling. *Geological Association of Canada Special Paper*, **40**, 201-251.

GORDY, P. L., FREY, F. R. & NORRIS, D. K. 1977. Geological guide for the CSPG 1977 Waterton Glacier Park Field Conference, Calgary. *Canadian Society of Petroleum Geologists*, 93 p.

GORDEY, S. P., ABBOTT, J. G. & ORCHARD, M. J. 1982. Devono-Mississippian Earn Group and younger strata in east-central Yukon. *Geological Survey of Canada Paper* **82-1B**, 93-100.

GOTTSCHALK, R. R. 1990. Structural evolution of the Schist belt, south-central Brooks Range fold and thrust belt, Alaska. *Journal of Structural Geology*, **12**, 453-469.

GOTTSCHALK, R. R. JR. & OLDOW, J. S. 1988. Low–angle normal faults in the south-central Brooks Range fold and thrust belt, Alaska. *Geology*, **16**, 395-399.

GOTTSCHALK, R. R. & SNEE, L. W. 1998. Tectonothermal evolution of metamorphic rocks in the south-central Brooks Range, Alaska: Constraints from $^{40}Ar/^{39}Ar$ geochronology. *In*: OLDOW, J. S. & AVÉ LALLEMANT, H. G. (eds). Architecture of the central Brooks Range fold and thrust belt, Arctic Alaska. *Geological Society of America Special Paper,* **324**, 225-251.

GOTTSCHALK, R. R., OLDOW, J. S. & AVÉ LALLEMANT, H. G. 1998. Geology and Mesozoic structural history of the south-central Brooks Range, Alaska. *In*: OLDOW, J. S. & AVÉ LALLEMANT, H. G. (eds). Architecture of the central Brooks Range fold and thrust belt, Arctic Alaska. *Geological Society of America Special Paper,* **324**, 195-223.

GRANTZ, A. 1966. Strike-slip fault in Alaska. *U. S. Geological Survey Open-File Report,* **267**, 82p.

GRANTZ, A., HOLMES, M. L. & KOSOSKI, B. A. 1975. Geologic framework of the Alaskan continental terrace in the Chukchi and Beaufort seas. *In*: YORATH, C. J., PARKER, E. R. & GLASS, D. J. (eds). Canada's continental margins and offshore petroleum exploration. *Canadian Society of Petroleum Geologists Memoir*, **4**, 669-700.

GRANTZ, A. & MAY, S. D. 1979. Geology and tectonic development of the continental margin north of Alaska. *Tectonophysics*, **59**, 263-291.

GRANTZ, A. & MAY, S. D. 1983. Rifting history and structural development of the continental margin north of Alaska. *In*: WATKINS, J. S. & DRAKE, C. L. (eds). Studies in continental margin geology. *American Association of Petroleum Geologists Memoir*, **34**, 77-100.

GRANTZ, A. & MAY, S. D. 1988. Regional geology and petroleum potential of the United States Chukchi shelf north of Point Hope. *In*: GRYC, G. (ed). Geology and exploration of the National Petroleum Reserve in Alaska, 1974 to 1982. *U. S. Geological Survey Professional Paper,* **1399**, 209-229.

GRANTZ, A., EITTREIM, S. & WHITNEY, O. T. 1981. Geology and physiography of the continental margin north of Alaska and implications for the origin of the Canada basin. *In*: NAIRN, A. E. M., CHURKIN, M. JR. & STEHLI, F. G. (eds). The ocean basin and margins. Volume 5: The Arctic Ocean. *New York, Plenum Press*, 439-492.

GRANTZ, A., MAY, S. D. & HART, P. E. 1990. Geology of the Arctic continental margin of Alaska. *In*: GRANTZ, A., JOHNSON, L. & SWEENEY, J. F. (eds). The Arctic Ocean Region. Boulder Colorado, Geological Society of America, The Geology of North America. v. L, 257-288.

GRANTZ, A., MOORE, T. E. & ROESKE, S. M. 1991. A-3 Gulf of Alaska to Arctic Ocean. Boulder, Colorado, Geological Society of America Centennial Continent/Ocean Transect n15, 72p, 3 sheets, scale 1:500.000.

GRANTZ, A., MAY, S. D. & HART, P. E. 1994. Geology of the Arctic continental margin of Alaska. *In*: PLAFKER, G. & BERG, H. C. (eds). Geology of Alaska: Boulder, Colorado. Geological Society of America, The Geology of North America, v. G–1, p. 17–48.

GRELAUD, S., SASSI, W., DE LAMOTTE, D. F., JASWALL, T. & ROURE, F. 2002. Kinematics of eastern Salt Range and south Potwar basin (Pakistan): a new scenario. *Marine and Petroleum Geology*, **19**, 1127-1139.

GROSHONG, R. H. JR. & USDANSKY, S. I. 1988. Kinematic models of plane-roofed duplex styles. *Geological Society of America Special Paper*, **222**, 197-206.

GRYC, C., PATTON, W. W. JR. & PAYNE, T. G. 1951. Present Cretaceous stratigraphic nomenclature of northern Alaska. *Washington Academy of Science Journal*, **41**, 159-167.

GUSTAFSON, L. B. & WILLIAMS, N. 1981. Sediment-hosted stratiform deposits of copper, lead and zinc. *In*: SKINNER, B. J. (ed). Economic Geology Seventy-Fifth Anniversary Volume. *Economic Geology Publishing Company*. El Paso, Texas, 139-178.

GUTSCHER, M. A., KUKOWSKI, N., MALAVIELLE, J. & LALLEMAND, S. 1996. Critical behaviour of thrust wedges: insights from high basal friction sandbox experiments. *Geology*, **24**, 135-138.

HACKER, B. R., MOSENFELDER, J. L. & GNOS, E. 1996. Rapid emplacement of the Oman ophiolite: thermal and geochronologic constraints. *Tectonics*, **15**, 1230-1247.

HALGEDAHL, S. L. & JARRARD, R. D. 1987. Paleomagnetism of the Kuparuk River Formation from oriented drill core-evidence for rotation of the Arctic Alaska plate. *In*: TAILLEUR, I. & WEIMER, P. (eds). Alaskan North Slope geology. *Society of Economic Geologists, Pacific Section, and Alaska Geological Society*, **2**, 581-617.

HALLAM, A. 1984. Pre-Quaternary sea-level changes. *Annual Review of Earth and Planetary Sciences*, **12**, 205-243.

HAMILTON, J. M., BISHOP, D. T., MORRIS, H. C. & OWENS, O. E. 1982. Geology of the Sullivan orebody, Kimberley, B. C. Canada. *In*: HUTCHINSON, R. W., SPENCER, C. D. & FRANKLIN, J. M. (eds). Precambrian Sulphide Deposits. *Geological Association of Canada Special Paper*, **25**, H. S. Robinson Memorial Volume. P. 597-665.

HAMILTON, J. M., DELANEY, G. D., HAUSER, R. L. & RANSOM, P. W. 1983. Geology of the Sullivan deposit, Kimberley, British Columbia, Canada. *In*: SANGSTER, D. F. (ed). Sediment-hosted stratiform lead-zinc deposits. *Mineralogical Association of Canada Short Course Handbook*, **8**, 31-83.

HAMILTON, J. M., MCEACHERN, R. G. & OWENS, O. E. 2001. A History of Geological Investigations at the Sullivan Deposit. *In*: LYDON, J. W., HOY, T., SLACK, J. F. & KNAPP, M. (eds). The Geological Environment of the Sullivan Deposit British Columbia. *Geological Association of Canada, Mineral Deposits Division, Special Publication*, **1**, 4-12.

HANCOCK, K. D. 1990. Ultramafic Associated Chrome and Nickel Occurrences in British Columbia. *British Columbia Ministry of Energy, Mines and Petroleum Resources, Open File* **1990 - 27**, 62p.

HANDSCHY, J. W. 1998*a*. Regional stratigraphy of the Brooks Range and North Slope, Arctic Alaska. *In*: OLDOW, J. S. & AVE LALLEMANT, H. G. (eds). Architecture of the central Brooks Range fold and thrust belt, Arctic Alaska. *Geological Society of America Special Paper*, **324**, 1-8.

HANDSCHY, J. W. 1998*b*. Sedimentology and paleogeographic significance of Upper Devonian and Lower Mississippian clastic rocks, Endicott Mountains Allochthon, central Brooks Range, Alaska. *In*: OLDOW, J. S. & AVE LALLEMANT, H. G. (eds). Architecture of the central Brooks Range fold and thrust belt, Arctic Alaska. *Geological Society of America Special Paper*, **324**, 9-32.

HANDSCHY, J. W. 1998*c*. Spatial variation in structural style, Endicott Mountains allochthon, central Brooks Range, Alaska. *In*: OLDOW, J. S. & AVE LALLEMANT, H. G. (eds). Architecture of the central

Brooks Range fold and thrust belt, Arctic Alaska. *Geological Society of America Special Paper*, **324**, 33-50.

HANKS, C. L. 1990. Balanced cross sections of the Aichilik River and Okpilak batholith regions, northeastern Brooks Range, Alaska. *Alaska Division of Geological and Geophysical Surveys Public Data File* ,**90-2A**, 12 p., scale 1:125.000, 2 sheets.

HANKS, C. L. 1993*a*. The Cenozoic structural evolution of a fold-and-thrust-belt, northeastern Brooks Range, Alaska. *Geological Society of America Bulletin*, **105**, 287-305.

HANKS, C. L. 1993*b*. Rapid evaluation of regional geometry and shortening of a fold-and-thrust belt: an example from the northeastern Brooks Range, Alaska. *American Association of Petroleum Geologists Bulletin*, **77**, 19-28.

HANNA, S. S. 1990. The alpine deformation of the central Oman Mountains. *In*: ROBERTSON, A. H. F., SEARLE, M. P. & RIES, A. C. (eds). The geology and tectonics of the Oman region. *Geological Society of London Special Publication*, **49**, 341-359.

HARBERT, W., FREI, L., JARRARD, R., HALGEDAHL, S. & ENGEBRETSON, D. 1990. Paleomagnetic and plate tectonic constraints on the evolution of the Alaskan-eastern Siberian Arctic. *In*: GRANTZ, A., JOHNSON, L. & SWEENEY, J. F. (eds). The Arctic Ocean region. Boulder, Colorado, Geological Society of America, The Geology of North America, v. L. 567-592.

HARDY, S., POBLET, J., MCCLAY, K. R. & WALTHAM, D. 1996. Mathematical modelling of growth strata associated with fault-related fold structures. *Geological Society of London Special Publication*, **99**, 265-282.

HARLAND, W. B., ARMSTRONG, R. L., COX, A. V., CRAIG, L. E., SMITH, A. G. & SMITH, D. G. 1990. A geologic time scale, 1989 edition. *Cambridge University Press: Cambridge*, p.1-263.

HARRIS, R. A. 1988. Origin, emplacement and attenuation of the Misheguk Mountain allochthon, western Brooks Range, Alaska. *Geological Society of America Abstracts with Programs*, **20**, A112.

HARRIS, R. A. 1992. Peri-collisional extension and the formation of Oman-type ophiolites in the Banda arc and Brooks Range. *In*: PARSON, L. M., MURTON, B. J. & BROWNING, P. (eds). Ophiolites and their modern analogues. *Geological Society of London Special Paper*, **60**, 301-325.

HARRIS, R. A. 1998. Origin and tectonic evolution of the metamorphic sole beneath the Brooks Range ophiolite, Alaska, *In*: OLDOW, J. S. & AVE LALLEMANT, H. G. (eds). Architecture of the central Brooks Range fold and thrust belt, Arctic Alaska. *Geological Society of America Special Paper*, **324**, 293-312.

HARRIS, R. A. 2004. Tectonic evolution of the Brooks Range ophiolite, northern Alaska. *Tectonophysics*, **392**, 143-163.

HARRIS, R. A., STONE, D. B. & TURNER, D. L. 1987. Tectonic implications of plaeomagnetic and geochronologic data from the Yukon-Koyukuk province, Alaska. *Geological Society of America Bulletin*, **99**, 362-375.

HARRIS, R. A., MOORE, T. E., WIRTH, K., MULL, C. G. & MCBRIDE, J. 2003. Rooted Brooks Range ophiolite. Implications for Cordilleran terranes: comment and reply. *Geology*, **31**, 91-92.

HATCHER, R. D. JR. 1989. Tectonic synthesis of the U. S. Appalachians. *In*: HATCHER, R. D. Jr., THOMAS, W. A. & VIELE, G. W. (eds). The Appalachian-Ouachita Orogen in the United States. Boulder, Colorado, Geological Society of America. The Geology of North America, v. **F-2**, 511-535.

HATCHER, R. D. JR. 2004. Properties of thrusts and upper bounds for the size of thrust sheets. *In*: MCCLAY, K. R. (ed). Thrust Tectonics and Petroleum Systems. *American Association of Petroleum Geologists Memoir*, **82**, 19-30.

HATCHER, R. D. JR. & HOOPER, R. J. 1992. Evolution of crystalline sheets in the internal parts of mountain chains. *In*: MCCLAY, K. R. (ed.). Thrust Tectonics. *London, Chapman & Hall*, 217-233.

HATCHER, R. D. JR., OSBERG, P. H., ROBINSON, P. & THOMAS, W. A. 1990. Tectonic map of the U. S. Appalachians. Geological Society of America, The Geology of North America, v. **F-2**, Plate 1, scale 1:2.500.000.

HAWKINS, J. W. 2003. Geology of supra-subduction zones – implications for the origin of ophiolites. *In*: DILEK, Y. & NEWCOMB, S. (eds). Ophiolite concept and the evolution of geological thought. *Geological Society of America Special Paper*, **373**, 227-268.

HECKEL, P. H. 1986. Sea-level curve for the Pennsylvanian eustatic marine transgressive-regressive depositional cycles along mid-continent outcrop belt, North America. *Geology*, **14**, 330-334.

HELWIG, J. 1974. Eugeosynclinal basement and a collage concept of orogenic belts. *In*: DOTT, R. H. & SHAVER, R. H. (eds). Modern and ancient geosynclinal sedimentation. *Society of Paleontologists and Mineralogists Special Publication*, **19**, 359-380.

HERRON, E. M., DEWEY, J. F. & PITMAN, W. C. 1974. Plate tectonics model for the evolution of the Arctic. *Geology*, **2**, 377–380.

HEUBECK, C. 1992. Sedimentology of large olistoliths, Southern Cordillera Central, Hispaniola. *Journal of Sedimentary Research*, **62**, 474-482.

HIBBARD, M. J. 1995. Petrography to petrogenesis. *Prentice Hall, New Jersey*, 586 p.

HILL, K. C., KEETLEY, J. T., KENDRICK, R. D. & SUTRIYONO, E. 2004. Structure and hydrocarbon potential of the New Guinea fold belt. *In*: MCCLAY, K. R. (ed). Thrust tectonics and hydrocarbon systems. *American Association of Petroleum Geologists Memoir*, **82**, 505-525.

HILLHOUSE, J. W. & GROMMÉ, S. 1988. Cretaceous Remagnetization of Paleozoic sedimentary rocks in the Brooks Range, Alaska. *In*: GRYC, G. (ed). Geology and exploration of the National Petroleum Reserve in Alaska, 1974 to 1982. *U. S. Geological Survey Professional Paper*, **1399**, 633-641.

HILLHOUSE, J. W. & COE, R. S. 1994. *In*: PLAFKER, G. & BERG, H. C. (eds). The Geology of Alaska. Geological Society of America, The Geology of North America, v. **G-1**. 812-979.

HINSCH, R, KRAWCZYK, C. M., GAEDICKE, C., GIRAUDO, R. & DEMURO, D. 2002. Basement control on oblique thrust sheet evolution: seismic imaging of the active deformation front of the Central Andes in Bolivia. *Tectonophysics*, 355, 23-39.

HINDLE, D., BESSON, O. & BURKHARD, M. 2000. A model of displacement and strain for arc-shaped mountain belts applied to the Jura arc. *Journal of Structural Geology*, **22**, 1285-1296.

HITZMAN, M. W. 1986. Geology of the Ruby Creek copper deposit, southwestern Brooks Range, Alaska. *Economic Geology*, **81**, 1644-1674.

HITZMAN M. W. 1999. Extensional faults that localize Irish syndiagenetic Zn-Pb deposits and their later compressional fate. *In*: MCCAFREY K., LONERGAN, L. & WILKINSON, J. (eds.). Fractures, Fluid Flow and Mineralization. *Geological Society of London Special Publication*, **155**, 233-245.

HITZMAN, M. W. & LARGE, D. 1986. A review and classification of the Irish carbonate-hosted base metal deposits. *In*: ANDREW, C. J., CROWE, R. W. A., FINLAY, S., PENNELL, W. M. & PYNE, J. F. (eds). Geology and Genesis of Mineral Deposits in Ireland. *Irish Association for Economic Geology*, 217-238.

HITZMAN, M. W., PROFFETT, J. M. JR., SCHMIDT, J. M. & SMITH, T. E. 1986. Geology and mineralization of the Ambler district, northwest Alaska. *Economic Geology*, **81**, 1592-1618.

HITZMAN, M. W., REDMOND, P. B. & BEATY, D. W. 2002. The Carbonate-Hosted Lisheen Zn-Pb-Ag Deposit, County Tipperary, Ireland. *Economic Geology*, **97,** 1627-1655.

HORSFIELD, W. T. 1977. An experimental approach to basement controlled faulting. *Geologie in Mijnbouw*, **56**, 363-370.

HOSSACK, J. R. 1979. The use of balanced cross-sections in the calculation of orogenic contraction: a review. *Journal of the Geological Society, London*, **136**, 705-711.

HOSSACK, J. R. 1981. Sequence of hanginwall imbrication in the Valdres Thrust, Djuptjernskampen, Norway. Abstract. *Journal of Structural Geology*, **3**, 188.

HOSSACK, J. R. 1983. A cross-section through the Scandinavian Caledonides constructed with the aid of branch-line maps. *Journal of Structural Geology*, **5**, 103-111.

HOWELL, D. G., JONES, D. L. & SCHERNER, E. R. 1985. Tectonostratigraphic terranes of the circum-Pacific region. *In*: HOWELL, D. G. (ed). Tectonostratigraphic terranes of the circum-Pacific region. Houston, Texas, *Circum Pacific Council for Energy and Mineral Resources, Earth Sciences Series*, **1**, 3-30.

HOWELL, D. G., BIRD, K. J., HUAFU, L. & JOHNSON, M. J. 1990. Tectonics and petroleum potential of the Brooks Range Fold and Thrust Belt-A progress report. *In*: DWIGHT, C. B. & FORD, A. B. (eds). Geological studies in Alaska by the U. S Geological Survey, 1990. *U. S. Geological Survey Bulletin*, **1999**, 112-126.

HSÜ, K. J. 1974. Melanges and their distinction from olistostromes. *In*: DOTT, R. H. JR & SHAVER, R. H. (eds). Modern and ancient geosynclinal sedimentation. *Society of Economic Palaeontologists and Mineralogists Special Publication*, **19**, 321-333.

HUBBARD, R. J. 1988. Age and significance of sequence boundaries on Jurassic and Early Cretaceous rifted continental margins. *American Association of Petroleum Geologists Bulletin*, **72**, 49-72.

HUBBARD, R. J., PAPE, J. & ROBERTS, D. G. 1985. Depositional sequence mapping as a tecthnique to establish tectonic and stratigraphic framework and evaluate hydrocarbon potential on a passive continental margin. *In*: BERG, O. R. & WOOLVERTON, D. Seismic stratigraphy II. *American Association of Petroleum Geologists Memoir*, **39**, 79-91.

HUBBARD, R. J., EDRICH, S. P. & RATTEY, R. P. 1987. Geologic evolution and hydrocarbon of the Arctic Alaska microplate. *Marine and Petroleum Geology*, **4**, 2-34.

HUBBERT, M. K. & W. W. RUBEY, 1959. Role of fluid pressure in mechanics of overthrust faulting. *Geological Society of America Bulletin*, **70**, 115-166.

HUDSON, T. & PLAFKER, G. 1978. Kigluaik and Bendeleben faults, Seward Peninsula. *In*: JOHNSON, K. M. (ed). The United States Geological Survey in Alaska Accomplishments during 1977. *U. S. Geological Survey Circular*, **772-B**, 47-50.

HUTCHISON, C. S. 1983. Economic deposits and their tectonic settings. *MacMillan Education Ltd, London*, 365p.

JADOON, I. A., LAWRENCE, R. B. & LILLIE, R. J. 1994. Seismic data, geometry, evolution, and shortening in the active Sulaiman fold-and-thrust belt of Pakistan, southwest of the Himalayas. *American Association of Petroleum Geologists Bulletin*, **78**, 758-774.

JAMISON, W. R. 1987. Geometric analysis of fold development in overthrust terranes. *Journal of Structural Geology*, **9**, 207-219.

JASWAL, T. M., LILLIE, R. J. & LAWRENCE, R. D. 1997. Structure and evolution of the northern Potwar deformed zone, Pakistan. *American Association of Petroleum Geologists*, **81**, 308-328.

JENNINGS, S. & KING, A. R. 2002. Geology, exploration history and future discoveries in the Red Dog district, western Brooks Range, Alaska. *In*: COOKE, D. R. & PONGRATZ, J. (eds). Giant ore deposits: characteristics, genesis, and exploration: Hobart, Tasmania. *Centre for Ore Deposit Research Special Publication*, **4**, 151-160.

JENNINGS, S., YOUNG, L. E, PLAHUTA, J. T. 1998. The key to new discoveries at Red Dog. *In:* WALTON, G. & JAMBOR J. (eds). Pathways '98 Extended Abstracts Volume: British Columbia and Yukon Chamber of Mines, Society of Economic Geologists, Vancouver, Canada. 111-113.

JENNINGS, S., YOUNG, L. E., PLAHUTA, J. T., KROLAK, T. E. & COULTER G. A. 1998. New discoveries at Red Dog Zn-Pb deposit, Alaska. Society of Economic Mineralogists, Orlando, Transactions v. 304.

JOHNSON, C. A., KELLEY, K. D. & LEACH, D. 2003. Stable isotopic evidence that barite deposits in the western Brooks Range, Alaska mark the sites of Mississippian methane seeps. *Geological Society of America Annual Meeting Programs with Abstracts*, **155-3**.

JOHNSON, C. A., KELLEY, K. D. & LEACH, D. L. 2004. Sulfur and oxygen isotopes in barite deposits of the Western Brooks Range, Alaska, and implications for the origin of the Red Dog massive sulfide deposits. *In*: KELLEY, K. D. & JENNINGS S. (eds). A Special Issue devoted to barite and zinc-lead-silver deposits in the Red Dog district, western Brooks Range northern Alaska. *Economic Geology*, **99**, 1435-1448.

JOHNSON, J. G., KLAPPER, G. & SANDBERG, C. A. 1985. Devonian eustatic fluctuations in Euramerica. *Geological Society of America Bulletin*, **96**, 567-587.

JOHNSTON, S. T. 2001. The great Alaskan terrane wreck: Reconciliation of paleomagnetic and geologic data in the northern Cordillera. *Earth and Planetary Science Letters*, **193**, 259-272.

JOLLY, A. D. & SHERIFF, S. D. 1992. Paleomagnetic study of thrust sheet motion along the Rocky Mountain front in Montana. *Geological Society of America Bulletin*, **104**, 779-785.

JONES, D. L. 1983. Recognition, character, and analysis of tectonostratigraphic terranes in western North America. *In*: HASHIMOTO, M. & UYEDA, S. (eds). Accretion tectonics in the Circum-Pacific regions. *Boston, D. Reidel Publishing Company*. 21-36.

JONES, D. L., SILBERING, N. J., CONEY, P. J. & PLAFKER, G. 1981. Tectonostratigraphic terrane map of Alaska, Part 3: Summary descriptions of terranes. *U. S. Geological Survey Open-File Report*, **81-792**, 2 sheets, scale 1:2.000.000. 20p.

JONES, D. L., SILBERING, N. J., CONEY, P. J. & PLAFKER, G. 1987. Lithotectonic map of Alaska (west of the 141st meridian). *U. S. Geological Survey Miscellaneous Field Studies*, Map **MF-1874A**, scale 1:2,500,000, 1 sheet.

JONES, P. B. 1980. Evidence from Canada and Alaska on plate tectonic evolution of the Arctic Ocean basin. *Nature*, **285**, 215-217.

JONES, P. B. 1996. Triangle zone geometry, terminology and kinematics. *Bulletin of Canadian Petroleum Geology*, **44**, 139-152.

KARL, S. M. 1991. Arc and extensional basin geochemical and tectonic affinities for the Maiyumerak basalts in the western Brooks Range. *In*: BRADLEY, D. C. & FORD, A. B. (eds). Geologic Studies in Alaska by the U. S. Geological Survey in 1990. *U. S. Geological Survey Bulletin*, **1999**, 141-145.

KARL, S. M. & LONG, C. L. 1990. Folded Brookian thrust faults: Implications of three Geological/Geophysical transects in the Western Brooks Range, Alaska. *Journal of Geophysical Research*, **95**, 8581-8592.

KARL, R. W. & BIRD, J. M. 1992. Chronology of ophiolite crystallization, detachment, and emplacement: evidence from the Brooks Range, Alaska. *Geology*, **20**, 75-78.

KARL, S. M. & MULL, C. G. 1993. Appeal for non-proliferation of escalating terrane nomenclature. *In*: DUSEL-BACON, C. & TILL, A. B. (eds). Geologic studies in Alaska by the U. S Geological Survey, 1992. *U. S. Geological Survey Bulletin*, **2068**, 71-78.

KEARY, P. & VINE, F. J. 1996. Global Tectonics. 2nd Edition, *Blackwell Science*, 333 p.

KELLEY, J. S. & BROSGé, W. P. 1995. Geologic framework of the central Brooks Range: Regional relations and an alternative to the Endicott Mountains Allochthon. *American Association of Petroleum Geologists Bulletin*, **79**, 1087-1116.

KELLEY, J. S., SHERWOOD, K. W. & BANET, A. C. 1998. Angular unconformity separating Baird Group and Lisburne Group, western Brooks Range, Alaska (abs). *In*: KARL, S. M. (ed). The Alaska Geological Society 1998 Science and Technology Conference, "Cutting Edge in Alaska". Anchorage, Alaska, April 16th, 1998, unpaginated.

KELLEY, K. D. 2001. Evolution of trace element compositions in sphalerite and pyrite through time in the Zn-Pb-Ag shale-hosted Red Dog deposits, western Brooks Range, Alaska. *Geological Society of America Abstracts with Programs*, A-272.

KELLEY, K. D. & MULL, C. G. 1995. Maps showing areas of potential for mineral resources in the Killik River quadrangle, Brooks Range, Alaska. *U. S. Geological Survey Miscellaneous Field Studies*, Map **MF-2225-A**, scale 1:250.000.

KELLEY, K. D. & JENNINGS, S. 2004. A Special issue devoted to barite and zinc-lead-silver deposits in the Red Dog district, western Brooks Range, northern Alaska. *In*: Kelley K. D. & JENNINGS S. (eds). A Special Issue devoted to barite and zinc-lead-silver deposits in the Red Dog district, western Brooks Range northern Alaska. *Economic Geology*, **99**, Preface.

KELLEY, K. D., SEAL, R. R. II, SCHMIDT. J. M., HOOVER, D. B. & KLEIN, D. P. 1995. Sedimentary exhalative Zn-Pb-Ag deposits. *In*: DU BRAY, E. A. (ed). Preliminary Compilation of Descriptive Geoenvironmental Mineral Deposit Models. *U. S. Geological Survey Open-File Report*, **95-831**, 272.

KELLEY, K. D., TAYLOR, C. D. & CIEUTAT, B. A. 1997. Zinc-lead-silver mineral occurrences in the Howard Pass Quadrangle, Brooks Range, Alaska. *In*: DUMOULIN, J. A. & GRAY, J. E. (eds). Geologic studies in the Alaska by the U. S. Geological Survey in 1995. *U. S. Geological Survey Professional Paper*, **1574**, 101-110.

KELLEY, K. D., LEACH, D. L. & JOHNSON, C. A. 2000. Sulfur-, Oxygen-, and Carbon-isotope studies of the Ag-Pb-Zn vein-breccia occurrences, sulfide-bearing concretions, and barite deposits in the north-central Brooks Range, with comparisons to shale-hosted stratiform massive sulfide deposits. *In*: KELLEY, K. D. & GOUGH, L. P. (eds). Geologic Studies in Alaska by the U. S. Geological Survey, 1998. *U. S. Geological Survey Professional Paper*, **1615**, 189-201.

KELLEY, K. D., DUMOULIN, J. A. & JENNINGS, S. 2004*a*. The Anarraaq Zn-Pb-Ag and barite deposit, northern Alaska: Evidence for replacement of carbonate by barite and sulphides. *In*: KELLEY, K. D. & JENNINGS S. (eds). A Special Issue devoted to barite and zinc-lead-silver deposits in the Red Dog district, western Brooks Range northern Alaska. *Economic Geology*, **99**, 1577-1591.

KELLEY, K. D., LEACH, D. L., JOHNSON, C. A., CLARK, J. L., FAYEK, M., SLACK, J. F., ANDERSON, V. M., AYUSO, R. A. & RIDLEY, W. I. 2004*b*. Textural, compositional, and sulfur isotope variations of sulfide minerals in the Red Dog Zn-Pb-Ag deposits, Brooks Range, Alaska: Implications for Ore Formation. *In*: KELLEY, K. D. & JENNINGS S. (eds). A Special Issue devoted to barite and zinc-lead-silver deposits in the Red Dog district, western Brooks Range northern Alaska. *Economic Geology*, **99**, 1509-1532.

KING, A. R., LEACH, D. L., KELLEY, K. D., CLARK, J. L., YOUNG, L. E., SLACK, J. F., DE VERA, J. & AYUSO, R. A. 2002. A summary of ongoing research in the Red Dog district and possible applications to exploration. *In*: LARGE, R. R. (ed). Stratiform Zn-Pb-Ag deposits and geological environments with emphasis on the Australian and North American giants. *Society of Economic Geologists – Prospectors and Developers Association of Canada. Workshop, Toronto, March, 2002*. 6p.

KIRSCHNER, C. E. 1994*a*. Interior basins of Alaska. *In*: PLAFKER, G. & BERG, H. C. (eds). The Geology of Alaska. Boulder, Colorado, Geological Society of America, The Geology of North America, v-**G-1**. 469-493.

KIRSCHNER, C. E. 1994*b*. Map showing sedimentary basins in Alaska. *In*: PLAFKER, G. & BERG, H. C. (eds). The Geology of Alaska. Boulder, Colorado, Geological Society of America, The Geology of North America, v-**G-1**. Plate 7. 1 sheet. Scale 1: 2.500.000.

KIRSCHNER, C. E. & RYCERSKI, B. A. 1988. Petroleum potential of representative stratigraphic and structural elements in the National Petroleum Reserve. *In*: GRYC, G. (ed). Geology and exploration of the National Petroleum Reserve in Alaska, 1974 to 1982. *U. S. Geological Survey Professional Paper*, **1399**, 191-208.

KIRSCHNER, C. E., GRYC, G. & MOLENAAR, C. 1983. Regional seismic lines in the National Petroleum Reserve in Alaska. *In*: BALLY, A. W. (ed). Seismic expression of structural styles. Volume 1. *American Association of Petroleum Geologists Studies in Geology Series*, **15**, 1.2.5-1—1.2.5-14.

KLEMPERER, S. L., MILLER, E. L., GRANTZ, A., SCHOLL, D. W. & THE BERING-CHUKCHI WORKING GROUP. 2002. Crustal structure of the Bering and Chukchi shelves: Deep-seismic reflection profiles across the North American continent between Alaska and Russia. *In*: MILLER, E. L., GRANTZ, A. & KLEMPERER, S. L. (eds). Tectonic evolution of the Bering shelf, Chukchi Sea-Arctic margin and adjacent landmasses. Boulder Colorado, *Geological Society of America Special Paper*, **360**, 1-24.

KOEHLER, G. F. & TIKKANEN, G. D. 1991. Red Dog, Alaska: discovery and definition of a major zinc-lead-silver deposit. *Economic Geology Monograph*, **8**, 268-274.

KOONS, P. O. 1990. Two-sided orogens: collision and erosion from sandbox to the southern Alps, New Zealand. *Geology*, **18**, 679-682.

KOONS, P. O. 1994. Three-dimensional critical wedge: tectonics and topography in oblique collisional orogens. *Journal of Geophysical Research*, **99**, 12301-12315.

KORSCH, R. J. 1983. Franciscan-Knoxville problem: relationship between an accretionary prism and adjacent fore-arc basin. *American Association of Petroleum Geologists Bulletin*, **67**, 29-40.

KOYI, H. 1995. Mode of internal deformation in sand wedges. *Journal of Structural Geology*, **17**, 293-300.

KREBS, W. 1981. The geology of the Meggen ore deposit, *In*: WOLD, K. H. (ed). Handbook of strata-bound and stratiform ore deposits, Part III: *Amsterdam, Elsevier*, 509-549.

KUHN, D. 2002. Fold and thrust belt structures and strike-slip faulting at the SE margin of the Salar de Atacama basin, Chilean Andes. *Tectonics*, **21**, 8-17.

KURTAK, J. M., HICKS, R. W., WERDON, M. B., MEYER, M. P. & MULL, C. G. 1995. Mineral investigations in the Colville mining district and southern Nature Petroleum Reserve in Alaska. *U. S. Bureau of Mines Open-File Report*, **8-95**, 217pp.

KWON, S. & MITRA, G. 2004. Strain distribution, strain history, and kinematic evolution associated with the formation of arcuate salients in fold-thrust belts: the example of the Provo salient, Sevier orogen, Utah. *In*: SUSSMAN, A. J. & WEIL, A. B. (eds). Orogenic curvature: integrating paleomagnetic and structural analyses. *Geological Society of America Special Paper*, **383,** 205-223.

LACOMBE, O., MOUTHEREAU, F., ANGELIER, J., CHU, H. T. & LEE, J. C. 2003. Frontal belt curvature and oblique ramp development at an obliquely collided irregular margin: Geometry and kinematics of the NW Taiwan fold-thrust belt. *Tectonics*, **22**, 9-16.

LACQUEMENT, F., AVERBUCH, O., MANSY, J. L., SZANIAWSKI, R. & LEWAQNDOWSKI, M. 2005. Transpressional deformations at lateral boundaries of propagating thrust-sheets: the example of the

Meuse Valley Recess within the Ardennes Variscan fold-and-thrust belt (N France – S Belgium). *Journal of Structural Geology, In Press.*

LANE, L. S. 1997. Canada Basin, Arctic Ocean: Evidence against a rotational origin. *Tectonics*, **16**, 363-387.

LANGE & NOKLEBERG, 1987. Geologic setting, petrology, and geochemistry of stratiform sphalerite-galena-barite deposits, Red Dog Creek and Drenchwater areas, northwestern Brooks Range, Alaska: a discussion. *Economic Geology*, **82**, 1079-1081.

LANGE, I. M., NOKLEBERG, W. J., PLAHUTA, J. T., KROUSE, H. R., DOE, B. R. & ULDIS, J. 1981. Isotopic geochemistry of stratiform zinc-lead-barium deposits, Red Dog creek and Drenchwater creek areas, northwestern Brooks Range, Alaska. Proceedings of the Symposium on Mineral Deposits of the Pacific Northwest, Geological Society of America, Cordilleran Section Meeting at Corvallis, Oregon. March 20th-21st, 1980. *U. S. Geological Survey Open-File Report*, **81-355**, 2-16.

LANGE, I. M , NOKLEBERG, W. J., PLAHUTA, J. T., KROUSE, H. R. & DOE, B. R. 1985. Geologic setting, Petrology, and geochemistry of stratiform sphalerite-Galena-Barite Deposits, Red Dog Creek and Drenchwater Creek areas, northwestern Brooks Range, Alaska. *Economic Geology*, **80**, 1896-1926.

LARGE, D. E. 1980. Geological parameters associated with sediment-hosted, submarine exhalative Pb-Zn deposits: an empirical model for mineral exploration. *Geologisches Jahrbuch*, **40**, 59-129.

LARGE, D. E. 1983. Sediment-hosted massive sulfides lead-zinc deposits. *In*: SANGSTER, D. F. (ed). *Mineralogical Association of Canada Short Course Handbook*, **8**, 175-250.

LARGE, D. E. 2001. Sediment-hosted lead-zinc deposits: 20 years of progress. *Geological Society of America Abstracts with Programs*, A-272.

LARGE, R. R. 2003. The formation of giant stratiform sediment-hosted Zn-Pb-Ag deposits. *Geological Society of America Annual Meeting Abstracts with Programs* Seattle, November 2–5, 2003 Paper No. 1-7.

LARGE, R. R., BULL, S. W., COOKE, D. R. & MCGOLDRICK, P. J. 1998. A genetic model for the HYC deposit, Australia: based on the regional sedimentology, geochemistry, and sulfide-sediment relationships. *Economic Geology*, **93**, 1345–1368.

LARRASOAÑA, J. C., PARES, J. M., MILLAN, H., DEL VALLE, J. & PUEYO, E. L. 2003. Paleomagnetic, structural, and stratigraphic constraints on transverse fault kinematics during basin inversion: The Pamplona fault (Pyrenees, north Spain). *Tectonics*, **22**, 10-22.

LAUBSCHER, H. P. 1986. The eastern Jura: relationships between thin-skinned and basement tectonics, local and regional. *Geologische Rundschau*, **75**, 535-553.

LAWTON, D. C., SPRATT, D. A. HOPKINS, J. C. 1994. Tectonic wedging beneath the Rocky Mountain foreland basin, Alberta, Canada. *Geology*, **22**, 519-522.

LAWVER, L. A. & SCOTESE, C. R. 1990. A review of tectonic models for the evolution of the Canada basin. *In*: GRANTZ, A., JOHNSON, L. & SWEENEY, J. F. (eds). The Arctic Ocean region: Boulder, Colorado, Geological Society of America, The Geology of North America, V. L, 593-618.

LEACH, D. L. & SANGSTER, D. F. 1993. Mississippi Valley-type lead-zinc deposits. *In*: KIRKHAM, R. V., SINCLAIR, W. D., THORPE, R. I. & DUKE, J. M. (eds). Mineral deposit Modelling. *Geological Association of Canada Special Paper*, **40**, 289-314.

LEACH, D. L., MARSH, E., EMSBO, P., ROMBACH, C. S., KELLEY, K. D. & ANTHONY, M. 2004. Nature of hydrothermal fluids at the shale-hosted Red Dog Zn-Pb-Ag deposits, Brooks Range, Alaska. *In*: KELLEY, K. D. & JENNINGS, S. (eds). A Special Issue devoted to barite and zinc-lead-silver deposits in the Red Dog district, western Brooks Range northern Alaska. *Economic Geology*, **99**, 1449-1480.

LEE M. J. & WILKINSON, J. J. 2002. Cementation, hydrothermal alteration, and Zn-Pb mineralization of carbonate breccias in the Irish Midlands: Textural evidence from the Cooleen Zone, near Silvermines, County Tipperary. *Economic Geology*, **97**, 653-662

LEFFINGWELL DE, E. K. 1919. The Canning River region, northern Alaska. *U. S. Geological Survey Professional Paper*, **109**, 251p.

LEGG, G. W. 1983. National Petroleum Reserve in Alaska. Geological report, Lisburne test well no.1. Husky Oil NPR Operations Inc. 161p.

LEPAIN, D. L., CROWDER, R. K. & WALLACE, W. K. 1994. Early Carboniferous transgression on a passive continental margin: Deposition of the Kekiktuk Conglomerate; northeastern Brooks Range, Alaska. *American Association of Petroleum Geologists Bulletin*, **78**, 679-699.

LERAND, M. 1973. Beaufort Sea. *In*: MCCROSSAN, R. G. (ed). The future petroleum provinces of Canada; their geology and potential. *Canadian Society of Petroleum Geologists Memoir*, **1**, 315-386.

LEWCHUK, M. T., LEACH, D., SYMONS, D. & ELMORE, R. 2001. Paleomagnetic dating of mineralization at Red Dog and the Mesozoic tectonic history of the Brooks Range, Alaska. *Geological Society of America Abstracts with Programs*, A-272.

LEWCHUK M. T., FOUCHER J. & ELMORE, R. D. 2004. Paleomagnetism of the Mesozoic Asik Mountain mafic complex in northern Alaska: implications for the tectonic history of the Arctic Composite terrane. *In*: KELLEY, K. D. & JENNINGS S. (eds). A Special Issue devoted to barite and zinc-lead-silver deposits in the Red Dog district, western Brooks Range northern Alaska. *Economic Geology*, **99**, 1345-1354.

LICKORISH, W. H., FORD, M., BUERGISSER, J. & COBBOLD, P. R. 2002. Arcuate thrust systems in sandbox experiments; a comparison to the extensional arcs of the western Alps. *Geological Society of America Bulletin*, **114**, 1089-1107.

LIND, I. L. 1993. Stylolites in chalk from Leg 130, Ontong java Plateau. *In*: BERGER, W. H. (ed). *Proceedings of the Ocean Drilling Program, Scientific Results*, **130**, 445-451.

LIU, S. & DIXON, J. M. 1991. Centrifuge modelling of thrust faulting: structural variation along-strike in fold-thrust belts. *Tectonophysics*, **188**, 39-62.

LIU, H., MCCLAY, K. R. & POWELL, D. 1992. Physical models of thrust wedges. *In*: MCCLAY, K. R. (ed). Thrust Tectonics. *Chapman & Hall, London*, 71-82.

LONSDALE, P. F., BISCHOFF, J. L., BURNS, M. V., KASTNER, M. & SWEENEY, R. E. 1980. A high temperature hydrothermal deposit on the sea bed at a Gulf of California spreading center. *Earth and Planetary Science Letters*, **49**, 8-20.

LÓPEZ-BLANCO, M. 2002. Sedimentary response to thrusting and fold growing on the SE margin of the Ebro basin (Paleogene, NE Spain). *Sedimentary Geology*, **146**, 133-154.

LUJÁN, M., STORTI, F., BALANYÁ, J. C., CRESPO-BLANC, A. & ROSSETTI, F. 2003. Role of décollement material with different rheological properties in the structure of the Aljibe thrust imbricate (Flysch Trough, Gibraltar Arc): an analogue modelling approach. *Journal of Structural Geology*, **25**, 867-881.

LYDON, J. W. 1983. Chemical parameters controlling the origin and deposition of sediment-hosted stratiform lead-zinc deposits. *In*: SANGSTER, D. F. (ed). Short course in sediment-hosted stratiform lead-zinc deposits. *Mineralogical Association of Canada, Short Course Handbook*, **8**, 175-250.

LYDON, J. W. 1995. Sedimentary exhalative sulphides (SEDEX). *In*: ECKSTRAND, O. R., SINCLAIR, W. D. & THORPE, R. I. (eds). Geology of Canadian Mineral Deposit Types, *Geological Survey of Canada*, **8**, 130-152.

LYDON, J. W., GOODFELLOW, W. D. & JONASSON, I. R. 1985. Stratiform baritic deposits of the Selwyn basin: Geology, geochemistry and genesis. Conference of stratiform sediment-hosted Pb-Zn deposits. Abstracts Volume, Stanford University, Ore Deposits Research Group.

MACEDO, J. & MARSHAK, S. 1999. Control on the geometry of fold-thrust belt salients. *Geological Society of America Bulletin*, **111**, 1808-1822.

MACINTYRE, D. G. 1991. Sedex-sedimentary-exhalative deposits. *In*: MCMILLAN, W. J. (ed). Ore deposits, tectonics and metallogeny in the Canadian Cordillera. British Columbia. *Ministry of Energy, Mines and Petroleum Resources Paper,* **1991-4**, 25-70.

MACKAY, P. A., VARSEK, J. L., KUBLI, T. E., DECHESNE, R. G., NEWSON, A. C. & REID, J. P. 1996. Triangle zones and tectonic wedges: and introduction. *Bulletin of Canadian Petroleum Geology*, **44**, 1-5.

MALAVIEILLE, J. 1984. Modélisation expérimentale des chevauchements imbriqués: application aux chaînes de montagnes. *Bulletin de la Societé Geologique de France*, **7**, 129-138.

MARSHAK, S. 1988. Kinematics of orocline and arc formation in thin-skinned orogens. *Tectonics*, **7**, 73-86.

MARSHAK, S. 2004. Salients, recesses, arcs, oroclines, and syntaxes: A review of ideas concerning the formation of map-view curves in fold-thrust belts. *In:* MCCLAY, K. R. (ed). *American Association of Petroleum Geologists Memoir*, **82**, 133-158.

MARSHAK, S. & WILKERSON, M. S. 1992. Effect of overburden thickness on thrust-belt geometry and development. *Tectonics*, **11**, 560-566.

MARSHAK, S., WILKERSON, M. S. & HSUI, A. T. 1992. Generation of curved fold-thrust belts: insight from simple physical and analytical models. *In:* MCCLAY, K. R. (ed). Thrust Tectonics. *Chapman & Hall, London*. 83-92.

MARTIN, A. J. 1970. Structure and tectonic history of the western Brooks Range, De Long mountains, northern Alaska. *Geological Society of America Bulletin*, **81**, 3605-3622.

MARTíNEZ, A., VERGES, J. & MUÑOZ, J. A. 1986. Secuencias de propagacion del sistema de cabalgamientos de la terminacion oriental del manto del Pedraforca y relacion con los conglomerados sinorogénicos. *Acta Geologica Hispanica*, **23**, 119-128.

MARTíNEZ CATALÁN, J. R., DíAZ GARCíA, F., ARENAS, R., ABATI, J., CASTINEIRAS, P., GONZÁLEZ CUADRA, P., BARREIRO, J. G., RUBIO PASCUAL, F. J. 2002. Thrust and detachment systems in the Ordenes complex (northwestern Spain): Implications for the Variscan-Appalachian geodynamics. *In*: MARTíNEZ CATALÁN, J. R., HATCHER, R. D. JR., ARENAS, R. & DIAZ GARCIA, F. (eds.). Variscan-Appalachian dynamics: The building of the late Paleozoic basement. *Geological Society of America Special Paper*, **364**, 163-182.

MARQUÉS, F. O. & COBBOLD, P. R. 2002. Topography as a major factor in the development of arcuate thrust belts: insights from sandbox experiments. *Tectonophysics*, **348**, 247-268.

MARQUÍNEZ, J. L. 1989. Mapa geológico de la Región del Cuera y Picos de Europa (Cordillera Cantábrica, NW de España). *Trabajos de Geología, Universidad de Oviedo*, **18**, 137-144.

MAUCH, E. A. 1989. Stratigraphic and structural interpretation of selected seismic lines, Ikpikpuk-Umiat Basin, National Petroleum Reserve, Alaska. *In*: BALLY, A. W. (ed). Atlas of seismic stratigraphy. *American Association of Petroleum Geologists.* Studies in Geology, **27**, v. 3.

MAYFIELD, C. F. 1980. Comment on 'Collision-deformed Paleozoic continental margin, western Brooks Range, Alaska'. *Geology*, **8**, 357-359.

MAYFIELD, C. F., TAILLEUR, I. L., MULL, C. G. & SABLE, E. G. 1978. Bedrock geologic map of the south half of the National Petroleum Reserve in Alaska. *U. S. Geological Survey Open-File Report,* **78-70B**. scale 1:1.000.000.

MAYFIELD, C. F., TAILLEUR, I . L. & ELLERSIECK, I. 1983. Stratigraphy, Structure, and palinspastic synthesis of the western Brooks Range, northwestern Alaska. *U. S. Geological Survey Open-File Report,* **830-799**, 61 p.

MAYFIELD, C. F., CURTIS, S. M., ELLERSIECK, I. & TAILLEUR, I. L. 1984. Reconnaisance geological map of southeastern Misheguk Mountain Quadrangle, Alaska. *U. S. Geological Survey Miscellaneous Investigations Series,* Map **I-1503**, scale 1:63.360. 2 sheets.

MAYFIELD, C. F., TAILLEUR, I. L. & ELLERSIECK, I. 1988. Stratigraphy, Structure, and palinspastic synthesis of the western Brooks Range, Northwestern Alaska. *In*: GRYC, G. (ed). Geology and exploration of the National Petroleum Reserve in Alaska, 1974 to 1982. *U. S. Geological Survey Professional Paper,* **1399**, 143-186.

MAYFIELD, C. F., CURTIS, S. M., ELLERSIECK, I., & TAILLEUR, I. L. 1990. Reconnaissance geologic map of the De Long Mountains A-3 and B-3 quadrangles and parts of the A-4 and B-4 quadrangles, Alaska. *U. S. Geological Survey Miscellaneous Investigations Series,* Map **I-1929**, scale 1:63.360. 2 sheets.

MAYNARD, J. B. 1983. Geochemistry of sedimentary ore deposits. Springer Verlag, New York, 305p.

MAYNARD, J. B. 1991. Shale-hosted deposits of Pb, Zn, and Ba: Syngenetic deposition from exhaled brines in deep marine basins. *In*: Force, E. R. (ed). Sedimentary and Diagenetic Mineral Deposits: A Basin Analysis Approach to Exploration. *Society of Economic Geologists*, El Paso, 177-187.

MCCAFFREY, R. & ABERS, G. A. 1991. Orogeny in arc-continent collision: The Banda Arc and western New Guinea. *Geology*, **19**, 563-566.

MCCLAY, K. R. 1977. Pressure solution and cobble creep in rocks. *Journal of the Geological Society of London*, **134**, 57-70.

MCCLAY, K. R. 1981. What is a thrust? What is a nappe? *In*: MCCLAY, K. R. & PRICE, N. J. (eds). Thrust and Nappe Tectonics. *Geological Society of London Special Publication*, **9**, 7-12.

MCCLAY, K. R. 1983*a*. Structural evolution of the Sullivan Fe-Pb-Zn-Ag orebody, Kimberley, British Columbia, Canada. *Economic Geology*, **78**, 1398-1424.

MCCLAY, K. R. 1983*b*. Deformation of stratiform lead-zinc deposits. *In*: SANGSTER, D. F. (ed). Sediment-hosted stratiform lead-zinc deposits. *Mineralogical Association of Canada. Short Course Handbook*, **8**, 283-309.

MCCLAY, K. R. 1990. Extensional fault systems in sedimentary basins. A review of analogue model studies. *Marine and Petroleum Geology*, **7**, 206-233.

MCCLAY, K. R. 1991. Deformation of stratiform Zn-Pb (-barite) deposits in the northern Canadian Cordillera. *Ore Geology Reviews*, **6**, 435-462.

MCCLAY, K. R. 1992. Glossary of thrust tectonics terms. *In:* MCCLAY, K. R. (ed). Thrust Tectonics. *Chapman & Hall, London*, 419-433.

MCCLAY, K. R. 2004. Thrust tectonics and hydrocarbon systems; Introduction. *In*: MCCLAY, K. R. (ed). Thrust Tectonics and Petroleum Systems. *American Association of Petroleum Geologists Memoir*, **82**, xi-xxii.

MCCLAY, K. R. & COWARD, M. P. 1981. The Moine thrust zone: An overview. *In*: MCCLAY, K. R. & PRICE, N. (eds). Thrust and Nappe Tectonics. *Geological Society of London Special Publication*, **9**, 241-260.

MCCLAY, K. R. & INSLEY, M. W. 1986*a*. Duplex structures in the Lewis thrust sheet, Crowsnest Pass, Rocky Mountains, Alberta, Canada. *Journal of Structural Geology*, **8**, 911-922.

MCCLAY, K. R. & INSLEY, M. W. 1986*b*. Structure and mineralization of the Driftpile Creek area, northeastern British Columbia (94E/16,94F/14,94K/4,94L1). *British Columbia Ministry Energy Mines and Petroleum Resources Paper*, **1986**, 343-350.

MCCLAY, K. R. & BIDWELL, G. E. 1987. Geology of the Tom Deposit, MacMillan Pass, Yukon Territory. *In*: MORIN, J. A. (ed). Mineral deposits of the Northern Cordillera. *Canadian Institute of Mineralogy & Metallurgy Special Volume*, **37**, 100-114.

MCCLAY, K. R. & KHALIL, S. 1998. Extensional hard linkages, eastern Gulf of Suez, Egypt. *Geology*, **26**, 563-566.

MCCLAY, K. R. & WHITEHOUSE, P. S. 2004. Analogue Modelling of doubly vergent thrust wedges. *In*: MCCLAY, K. R. (ed). Thrust Tectonics and Petroleum Systems. *American Association of Petroleum Geologists Memoir*, **82**, 187-210.

MCCLAY, K. R. & INSLEY, M. W. & ANDERTON, R. 1988. Tectonics and mineralization of the Kechika Trough, Gataga area, northeastern British Columbia. *Geological Survey of Canada Paper*, **88-1A**, 1-12.

MCCLAY, K. R., INSLEY, M. W. & ANDERTON, R. 1989. Inversion of the Kechika trough, northeastern British Columbia, Canada. *In:* COOPER, M. A. & WILLIAMS, G. D. (eds). Inversion Tectonics. *Geological Society of London Special Publication*, **44**, 235-257.

MCCLAY, K. R., WHITEHOUSE, P. S., AMILIBIA, A., DE VERA, J. & DJEBBAR, T. 2004*a*. 4D evolution of fault systems in sedimentary basins: a review. *Petroleum Exploration Society of Australia*. 2nd Eastern Australian Basins Symposium, Adelaide, 20th-22nd September. p. 1-26.

MCCLAY, K. R., WHITEHOUSE, P. S., DOOLEY, T. & RICHARDS, M. 2004*b*. 3D evolution of fold and thrust belts formed by oblique convergence. *Marine and Petroleum Geology*, **21**, 857-877.

MCCONNELL, R. G. 1887. Report of the geological structure of a portion of the Rocky Mountains, accompanied by a section measured near the 51st parallel. *Geological Survey of Canada Annual Report*, **1886**, 1D-41D.

MCELROY, R., CATER, J., ROBERTS, I., PECKHAM, A. & BOND, M. 1990. The structure and stratigraphy of SE Zanskar, Ladakh Himalaya. *Journal of the Geological Society of London*, **147**, 989-997.

MCGILVERY, T. A., & COOK, D.L., 2003. The influence of local gradients on accommodation space and linked depositional elements scross a stepped slope profile, offshore Brunei. In Roberts, H.H., Rosen, N.C., Fillon, R.H., & Anderson, J.B. (eds), GCS-SEPM Foundation 23rd Annual Bob F Perkins Research Conference Prodeedings, 23 – 55.

MCGOLDRICK, P. J., BULL, S. W., COOKE, D. R. & LARGE, R. R. 1998. Northern Australian Proterozoic stratiform sediment-hosted (SEDEX) Zn-Pb-Ag deposits. Basin, fluids and Zn-Pb ores Symposium Proceedings. *Centre for Ore Deposit Research*, University of Tasmania, June, 1998. 15-27.

MCKENZIE, D. P. & JACKSON, J. A. 1983. The relationship between strain rates, crustal thickening, palaeomagnetism, finite strain and fault movements within a deforming zone. *Earth and Planetary Science Letters*, **65**, 182-202.

MCWHAE, J. R. 1986. Tectonic history of northern Alaska, Canadian Arctic, and Spitsbergen regions since Early Cretaceous. *American Association of Petroleum Geologists Bulletin*, **70**, 430-450.

MEDIALDEA, T., VEGAS, R., SOMOZA, L., VÁZQUEZ. J. T., MALDONADO, A., DÍAZ-DEL-RÍO, V., MAESTRO, A., CÓRDOBA, D. & FERNÁNDEZ-PUGA, M. C. 2004. Structure and evolution of the

"Olistostrome" complex of the Gibraltar Arc in the Gulf of Cádiz (eastern Central Atlantic): evidence from two long seismic cross-sections. *Marine Geology*, **209**, 173-198

MENZIES, M. A., KLEMPERER, S. L. EBINGER, C. J. & BAKER, J. 2002. Characteristics of volcanic rifted margins. *In*: MENZIES, M. A., KLEMPERER, S. L. EBINGER, C. J. & BAKER, J. Volcanic rifted margins. *Geological Society of America Special Paper*, **362**, 1-14.

METZ, P. A. 1980. Comment on 'Collision-deformed Paleozoic continental margin, western Brooks Range, Alaska'. *Geology* , **8**, 360-361.

MIALL, A. D. 1992. Alluvial deposits. *In*: WALKER, R. G. & JAMES, N. P. (eds). Facies models. *Geological Association of Canada*, 119-142.

MIALL, A. D. 1997. The geology of stratigraphic sequences. *Springer Verlag, Berlin-Heidelberg*, 433p.

MILANI, E. J. & DAVISON, I. 1988. Basement control and transfer tectonics in the Reconcavo-Tucano-Jatoba rif, Brazil. *Tectonophysics*, **154**, 41-70.

MILLER E. L. 1987. Dismemberment of the Brooks Range orogenic belt during middle Cretaceous extension. *Geological Society of America Abstracts with Programs*, **19**, p.432.

MILLER, E. L. & HUDSON, T. L. 1991. Mid-Cretaceous extensional fragmentation of a Jurassic-Early Cretaceous compressional orogen, Alaska. *Tectonics*, **10**, 781-796.

MILLER, E. L. & HUDSON, T. L. 1993. Reply to comment on 'Mid-Cretaceous extensional fragmentation of a Jurassic-Early Cretaceous compressional orogen, Alaska'. *Tectonics*, **12**, 1082-1086.

MILLER, T. P. 1994. Geothermal resources of Alaska. *In*: PLAFKER, G. & BERG, H. C. (eds). The Geology of Alaska, Geological Society of America The Geology of North America series v. G-1, p. 979-987.

MITCHUM, R. M. JR. 1977. Seismic stratigraphy and global changes of sea level, Part 1: Glossary of terms used in seismic stratigraphy. *In*: PAYTON, C. E. (ed). Seismic Stratigraphy - Applications to Hydrocarbon Exploration. *American Association of Petroleum Geologists Memoir*, **26**, 205-212.

MITRA, G. 1994. Strain variation in thrust sheets across the Sevier fold-and-thrust belt (Idaho-Utah-Wyoming): implications for section restoration and wedge taper evolution. *Journal of Structural Geology*, **16**, 585-602.

MITRA, G. 1997. Evolution of salients in a fold-and-thrust belt: the effects of sedimentary basin geometry, strain distribution and critical taper. *In*: SENGUPTA, S. (ed). Evolution of geological structures in micro-to macro-scales. *London, Chapman & Hall*, 83-92.

MITRA, G. & SUSSMAN, A. J. 1997. Structural evolution of connecting splay duplexes and their implication for critical taper: an example based upon geometry and evolution of the Canyon range culmination, Sevier Belt, central Utah. *Journal of Structural Geology*, **19**, 503-522.

MITRA, S. 1986. Duplex structures and imbricate thrust systems: geometry, structural position, and hydrocarbon potential. *American Association of Petroleum Geologists Bulletin*, **70**, 1087-1112.

MITRA, S. 1988. Three-dimensional geometry and kinematic evolution of the Pine Mountains thrust system, southern Appalachians. *American Association of Petroleum Geologists Bulletin*, **100**, 72-95.

MITRA, S. 1990. Fault-propagation folds: Geometry, kinematic evolution, and hydrocarbon traps. *American Association of Petroleum Geologists Bulletin*, **74**, 921-945.

MITRA, S. 2002. Fold-accommodation faults. *American Association of Petroleum Geologists Bulletin*, **86**, 671-693.

MITRA, S. & BOYER, S. 1986. Energy balance and deformation mechanisms of duplexes. *Journal of Structural Geology*, **8**, 291-304.

MITRA, S. & MOUNT, V. S. 1998. Foreland-involved basement structures. *American Association of Petroleum Geologists Bulletin*, **82**, 70-109.

MOLENAAR, C. M. 1988. Depositional history and seismic stratigraphy of Lower Cretaceous rocks in the National Petroleum Reserve in Alaska and adjacent areas. . *In*: GRYC, G. (ed). Geology and exploration of the National Petroleum Reserve in Alaska, 1974 to 1982. *U. S. Geological Survey Professional Paper*, **1399**, 593-621.

MOLENAAR, C. M., EGBERT, R. M. & KRYSTINIK, L. F. 1988. Depositional facies, petrography, and reservoir potential of the Fortress Mountain Formation (lower Cretaceous), central North Slope. Alaska. *In*: GRYC, G. (ed). Geology and exploration of the National Petroleum Reserve in Alaska, 1974 to 1982. *U. S. Geological Survey Professional Paper*, **1399**, 257-280.

MOLL-STALCUP, E. J., BREW, D. A. & VALLIER, T. L. 1994. Latest Cretaceous and Cenozoic magmatism in mainland Alaska. *In*: PLAFKER, G. & BERG, H. C. (eds). The Geology of Alaska. Boulder, Colorado, Geological Society of America, The Geology of North America, v-G-1. 589-619.

MON, R., MONALDI, C. R. & SALFITY, J. A. 2005. Curved structures and interference fold patterns associated with lateral ramps in the Eastern Cordillera, Central Andes of Argnetina. *Tectonophysics*, **399**, 173-179.

MONGER, J. W. H. & NOKLEBERG, W. J. 1996. Evolution of the northern North America Cordillera: generation, fragmentation, displacement and accretion of successive North American plate-margin arcs. *In*: COYNER, A. R. & FAHEY, P. L. (eds). Geology and ore deposits of the American Cordillera. *Geological Society of Nevada Symposium Proceedings*, Reno/Sparks, Nevada, April 1995. 1133-1152.

MOORE, D. W., YOUNG, L. E., MODENE, J. S. & PLAHUTA, J. T. 1986, Geologic setting and genesis of the Red Dog zinc-lead-silver deposit, western Brooks Range, Alaska. *Economic Geology*, **81**, 1696-1727.

MOORE, T. E. 1992. The Arctic Alaska super terrane, *In*: BRADLEY, D. C. & DUSEL-BACON, C. (eds). Geologic studies in Alaska by the U. S Geological Survey, 1991. *U. S Geological Survey Bulletin*, **2041**, 238-244.

MOORE, T. E. & NILSEN, T. H. 1984. Regional variations in the fluvial Upper Devonian and Lower Mississippian(?) Kanayut Conglomerate, Brooks Range, Alaska. *Sedimentary Geology*, **38**, 465-497.

MOORE, T. E. & POTTER, C. J. 2003. Structural Plays in Ellesmerian Sequence and Correlative Strata of the National Petroleum Reserve, Alaska. *U. S. Geological Survey Open-File Report*, **03-253**, 58p.

MOORE, T. E., NILSEN, T. H. & BROSGÉ, W. P. 1989. Sedimentology of the Kanayut Conglomerate. *In*: MULL, C. G. & ADAMS, K. E. (eds.). Dalton Highway, Yukon River to Prudhoe Bay, Alaska. *Alaska Department of Natural Resources, Division of Geological and Geophysical Surveys*, v. **2**, 219-252.

MOORE, T. E., WALLACE, W. K., BIRD, K. J., KARL, S. M., MULL, C. G. & DILLON, J. T. 1992. Stratigraphy, structure and geologic synthesis of northern Alaska. *U. S. Geological Survey Open-File Report*, **92-330**, 283p.

MOORE, T. E., WALLACE, W. K., BIRD, K. J., KARL, S. M., MULL, C. G. & DILLON, J. T. 1994. Geology of northern Alaska, *In*: PLAFKER, G. & BERG, H. C. (eds). The Geology of Alaska. Boulder, Colorado, Geological Society of America, The Geology of North America, v-G-1, 49-140.

MOORE T. E., HEMMING, S. & SHARP, W. D. 1997*a*. Provenance of the Carboniferous Nuka Formation, Brooks Range, Alaska: a multicomponent isotope provenance study with implications for age of cryptic crystalline basement. *In*: DUMOULIN, J. A. & GRAY, J. E. (eds). Geologic Studies in Alaska by the U. S. Geological Survey, 1995. *U. S. Geological Survey Professional Paper*, **1574**, 173-194

MOORE, T. E., WALLACE, W. K., MULL, C. G., ADAMS, K. E., PLAFKER, G. & NOKLEBERG, W. J. 1997*b*. Crustal implications of bedrock geology along the Trans-Alaska Crustal Transect (TACT) in the Brooks Range, northern Alaska. *Journal of Geophysical Research*, **102**, 20.645-20.684.

MOORE, T. E., DUMITRU, T. A., ADAMS, K. E., WITEBSKY, S. N. & HARRIS, A. G. 2002*a*. Origin of the Lisburne Hills- Herald Arch thrust belt: Stratigraphic, structural, and fission track evidence from the Cape Lisburne area, northwestern Alaska. *In*: MILLER, E. L., GRANTZ, A. & KLEMPERER, S. L. Tectonic evolution of the Bering shelf, Chukchi Sea-Arctic margin and adjacent landmasses. Boulder Colorado, *Geological Society of America Special Paper*, **360**, 77-109.

MOORE, T. E., POTTER, C. J. & O'SULLIVAN, P. B. 2002*b*. Superposed coaxial orogens in the Brooks Range fold-and-thrust belt, Alaska. *Geological Society of America Abstracts with Programs*, Denver 27th-30th October.

MOORE, T. E., POTTER, C. J. & O'SULLIVAN, P. B. 2004*a*. The Brooks Range, Alaska: the consequence of four distinct tectonic events. *Geological Society of America Abstracts with Programs*, v. 36, 5, p.270. Denver 7-10 October.

MOORE, T. E., POTTER, C. J. & O'SULLIVAN, P. B., SHELTON, K. L. & UNDERWOOD, M. B. 2004*b*. Two stages of deformation and fluid migration in the west-central Brooks Range fold and thrust belt, northern Alaska. *In*: SWENNEN, R., ROURE, F. & GRANATH, J. W. *American Association of Petroleum Geologists Hedberg Series*, **1**, 157-186.

MOORE, T. E., POTTER, C. J. & O'SULLIVAN, P. B. 2005. Frontal triangle zones of the Brooks Range fold and thrust belt, northern Alaska; regional framework. *American Association of Petroleum Geologists Annual Convention*, Calgary June 19th-22nd.

MOORES, E. M. 1982. Origin and emplacement of ophiolites. *Reviews of Geophysics and Space Physics*, **20**, 735-760.

MOORES, E. R. 2003. A personal history of the ophiolite concept. *In*: DILEK, Y. & NEWCOMB, S. Ophiolite concept and the evolution of geological thought. *Geological Society of America Special Paper*, **373**, 17-29.

MORIN, R. L. & MOORE, T. E. 1996. Gravity models of the Siniktanneyak mafic-ultramafic complex, western Brooks Range, Alaska-evidence for thrust emplacement of Brooks Range ophiolites. *In*: MOORE, T. E. & DUMOULIN, J. A. (eds). Geologic studies in Alaska by the U. S. Geological Survey, 1994. *U. S. Geological Survey Bulletin*, **2152**, 101-110.

MORLEY, C. K. 1986. A classification of thrust fronts. *American Association of Petroleum Geologists Bulletin*, **70**, 12-25.

MORLEY, C. K. 1988. Out-of-sequence thrusting. *Tectonics*, **7**, 539-561.

MORLEY, C. K. 1989. Basin inversion in the Osen-Røa thrust sheet, southern Norway. *In:* COOPER, M. A. & WILLIAMS, G. D. (eds). Inversion Tectonics. *Geological Society of London Special Publication*, **44**, 259-273.

MOUTHEREAU, F., DEFFONTAINES, B., LACOMBE, O. & ANGELIER, J. 2002. Variations along strike of the Taiwan thrust belt: basement control on structural style, wedge geometry, and kinematics. *In*: BYRNE, T. B. & LIU, C. S. (eds). Geology and geophysics of an arc-continent collision, Taiwan, Republic of China. Boulder, Colorado. *Geological Society of America Special Paper*, **358**, 35-58.

MUGNIER, J. L., BABY, P., COLLETA, B., VINOUR, P., BALE, P. & LETURMY, P. 1997. Thrust geometry controlled by erosion and sedimentation: A view from analogue models. *Geology*, **25**, 427-430.

MULL, C. G. 1979. Nanushuk Group deposition and the late Mesozoic structural evolution of the central and western Brooks Range and Arctic Slope. *In*: AHLBRANDT, T. S. (ed). Preliminary geologic, petrologic, and paleontologic results of the Nanushuk Group rocks, North Slope, Alaska. *U. S. Geological Survey Circular*, **794**, 5-13.

MULL, C. G. 1980. Comment on 'Collision-deformed Paleozoic continental margin, western Brooks Range, Alaska'. *Geology*, **8**, 361-362.

MULL, C. G. 1982. Tectonic evolution and structural style of the Brooks Range, Alaska: an illustrated summary. *In*: POWERS, R. B. (ed). Geological studies of the Cordilleran thrust belt.Volume 1, *Rocky Mountain Association of Geologists*. 1-45.

MULL, C. G. 1985. Cretaceous tectonics, depositional cycles, and the Nanushuk Group, Brooks Range and Arctic Slope, Alaska. *In*: HUFFMAN, A. C. JR. (ed). Geology of the Nanushuk Group and related rocks, North Slope, Alaska. *U. S. Geological Survey Bulletin*, **1614**, 7-36.

MULL, C. G., DILLON, J. T. & ADAMS, K. E. 1986. The Doonerak fenster, central Brooks Range, Alaska. *Alaska Division of Geological and Geophysical Surveys Report of Investigations*, 87-08.

MULL, C. G. 1989. Generalized geologic map of the Brooks Range and Arctic Slope, Alaska. *In*: MULL, C. G. & ADAMS, K. E. (eds). Guidebook to bedrock geology along the Dalton Highway, Yukon River to Prudhoe Bay, Alaska. Alaska Division of Geological and Geophysical Surveys Guidebook 7, sheet 1, scale 1:2,850,000.

MULL, C. G. 1995. Generalized geologic map of the De Long Mountains quadrangle, western Brooks Range, Alaska. *Division of Geological and Geophysical Surveys*. scale 1:250,000. 1 sheet.

MULL, C. G., TAILLEUR, I. L., MAYFIELD, C. F. & PESSEL, G. H. 1976. New structural and stratigraphic interpretations, central and western Brooks Range and Arctic Slope. *In*: Cobb, E. H. (ed). The United States Geological Survey in Alaska: Accomplishments during 1975. *U. S. Geological Survey Circular*, **733**, 24-26.

MULL, C. G., TAILLEUR, I. L., MAYFIELD, C. F., ELLERSIECK, I. & CURTIS, S. 1982. New Upper Paleozoic and Lower Mesozoic stratigraphic units, central and western Brooks Range, Alaska. *American Association of Petroleum Geologists Bulletin*, **66**, 348-362.

MULL, C. G., CROWDER, K., ADAMS, K. E., SIOK, J. P., BODNAR, D. A., HARRIS, E. E. & ALEXANDER, R. A. 1987*a*. Stratigraphy and structural setting of the Picnic Creek allochthon, Killik River quadrangle, central Brooks Range, Alaska: a summary. *In*: TAILLEUR, I. L. & WEIMER, P. (eds). Alaskan North Slope Geology: *Society of Economic Paleontologists and Mineralogists, Pacific Section, and Alaska Geological Society, Bakersfield, California* , **50**, 649-662.

MULL, C. G., ROEDER, D. H., TAILLEUR, I . L. PESSEL, G. H., GRANTZ, A. & MAY, S. D. 1987*b*. Geologic sections and maps across Brooks Range and Arctic Slope to Beaufort Sea. *Geological Society of America Map and Chart Series,* **MC-28S**, scale 1:500,000.

MULL, C. G., HARRIS, A. G. & CARTER, J. L. 1997. Lower Mississippian (Kinderhookian) biostratigraphy and lithostratigraphy of the western Endicott Mountains, Brooks Range, Alaska. *In*: DUMOULIN, J. A. & GRAY, J. E. (eds). Geologic Studies in Alaska by the U. S. Geological Survey in 1995. *U. S. Geological Survey Professional Paper*, **1574**, 221-242.

MULL, C. G., HARRIS, E. E., REIFENSTUHL, R. R. & MOORE, T. E. 2000. Geologic map of the Coke Basin-Kukpowruk River area. De Long Mountains D-2 and D-3 quadrangles, Alaska. *Division of Geological and Geophysical Surveys, Report of Investigations,* **2000-2**, 1 sheet, scale 1:63,360.

MULUGUETA, G. 1988. Modelling the geometry of Coulomb thrust wedges. *Journal of Structural Geology*, **10**, 847-859.

MULUGUETA, G. & KOYI, H. 1987. Three-dimensional geometry and kinematics of experimental piggy-back thrusting. *Geology*, **15**, 1052-1056.

MULUGUETA, G. & KOYI, H. 1992. Episodic accretion and strain partitioning on a model sand wedge. *Tectonophysics*, **202**, 319-333.

MUÑOZ, J. A. 1992. Evolution of a continental collision belt: ECORS Pyrenees crustal balanced cross-section. *In*: MCCLAY, K. R. (ed). Thrust Tectonics. *Chapman & Hall, London*, 235-246.

MURCHEY, B., JONES, D. L., HOLDSWORTH, B. K. & WARDLAW, B. R. 1988. *In*: GRYC, G. (ed). Geology and exploration of the National Petroleum Reserve in Alaska, 1974 to 1982. *U. S. Geological Survey Professional Paper*, **1399**, 697-724.

MUTTER, J. C. 1985. Seaward dipping reflectors and the continent-ocean boundary at passive continental margins. *Tectonophysics*, **114**, 117-131.

NAMSON, J. S. & WALLACE, W. K. 1986. A structural transect across the northeastern Brooks Range. *Geological Society of America Abstracts with Programs*, **18**, n2. p.163.

NARR, W. & SUPPE, J. 1994. Kinematics of basement-involved compressive structures. *American Journal of Science*, **294**, 802-860.

NATIONAL GEOPHYSICAL DATA CENTRE (NGDC), 2005.
http://www.ngdc.noaa.gov/mgg/image/images.html. (visited 10th January 2005).

NATIONAL AERONAUTICS AND SPACE ADMINISTRATION (NASA), 2005.
https://zulu.ssc.nasa.gov/mrsid/ (visited 10th January 2005).

NAYLOR, M. A., MANDL, G. & SIJPESTEIN, C. H. K. 1986. Fault geometries in basement induced wrench faulting under different initial stress states. *Journal of Structural Geology*, **8**, 737-752.

NELSON, K. 2001. Cominco to develop shallow gas leases north of Red Dog mine. *Petroleum News*, vol. 6, n. 7.

NELSON, S. W. 1980. Comment on 'Collision-deformed Paleozoic continental margin, western Brooks Range, Alaska'. *Geology*, **8**, 364-366.

NELSON, B. K., NELSON, S. W. & TILL, A. B. 1993. Nd- and Sr-isotope evidence for Proterozoic and Paleozoic crustal evolution in the Brooks Range, Northern Alaska. *Journal of Geology*, **101**, 435-450.

NELSON, J., PARADIS, S., CHRISTENSEN, J. & GABITES, J. 2002. Canadian cordilleran Mississippi Valley-type deposits: A case for Devonian-Mississippian back-arc hydrothermal origin. *Economic Geology*, **97**, 1013-1036.

NEWBERRY, R. J., DILLON, J. T. & ADAMS, D. D. 1986. Regionally metamorphosed, calc-silicate-hosted deposits of the Brooks Range, northern Alaska. *Economic Geology*, **81**, 1728-1752.

NEWMAN, G. W., MULL, C. G. & WATKINS, N. D. 1979. Northern Alaska paleomagnetism, plate rotation, and tectonics. *In*: SISSON, A. (ed) The relationship of plate tectonics to Alaskan geology and resources. Anchorage, Alaska Geological Society Symposium, 6th, Proceedings, 16-19.

NILSEN, T. H. 1981. Upper Devonian and Lower Mississippian redbeds, Brooks Range, Alaska. *In*: SMIALL, A. D. (ed). Sedimentation and tectonics in alluvial basins. *Geological Association of Canada Special Paper*, **23**, 187-218.

NILSEN, T. H. & MOORE, T. E. 1982*a*. Fluvial-facies model for the Upper Devonian and Lower Mississippian (?) Kanayut Conglomerate, Brooks Range, Alaska. *In*: ASHTON, F. E. & BALKWILL, H. R. (eds). Arctic geology and geophysics. *Canadian Society of Petroleum Geologists Proceedings of the Third International Symposium on Arctic Geology*, 1-12.

NILSEN, T. H. & MOORE, T. E. 1982*b*. Sedimentology and stratigraphy of the Kanayut Conglomerate, central and western Brooks Range, Alaska-report of the 1981 field season. *U. S. Geological Survey Open-File* Report, **82-674**, 64p.

NILSEN, T. H. & MOORE, T. E. 1984. The Kanayut Conglomerate in the westernmost Brooks Range, Alaska. *In*: COONRAD, W. L. & ELLIOT, R. L. (eds). The United States Geological Survey in Alaska. Accomplishments during 1981. *U. S. Geological Survey Circular*, **868**, 12-16.

NOKLEBERG, W. J. & WINKLER, G. R. 1978. Stratiform zinc-lead mineralization, Drenchwater Creek area, Howard Pass quadrangle, western Brooks Range, Alaska. *In*: JOHNSON, K. M. (ed). The U. S. Geological Survey in Alaska: Accomplishments during 1977. *U. S. Geological Survey Circular*, **772-B**, B17-B19.

NOKLEBERG, W. J. & WINKLER, G. R. 1982. Stratiform zinc-lead deposits in the Drenchwater Creek area, Howard Pass Quadrangle, northwestern Brooks Range, Alaska. *U. S. Geological Survey Professional Paper*, **1209**, 22pp.

NOKLEBERG, W. J., JONES, D. L. & SILBERING, N. J. 1985. Origin and tectonic evolution of the Maclaren and Wrangellia terranes, eastern Alaska Range, Alaska. *Geological Society of America Bulletin*, **96**, 1251-1270.

NOKLEBERG, W. J., BREW, D. A., GRYBECK, D., YEEND, W., BUNDTZEN, T. K., ROBINSON, M. S. & SMITH, T. E. 1994. Metallogeny and major mineral deposits of Alaska. *In*: PLAFKER, G. & BERG, H. C. (eds). The Geology of Alaska. Boulder, Colorado, Geological Society of America, The Geology of North America, v-**G-1**. 855-903.

NOKLEBERG, W. J., PARFENOV, L. M., MONGER, J. W. H., BARANOV, B. V., BYALOBZHESKY, S. G., BUNDTZEN, T. K., FEENEY, T. D., FUJITA, K., GORDEY, S. P., GRANTZ, A., KHANCHUK, A. I., NATALIN, B. A., NATAPOV, L. M., NORTON, I. A., PATTON, W. W. JR., PLAFKER., G., SCHOLL., D. W., SOKOLOV, S. D., SOSUNOV, G. M., STONE, D. B., TABOR, R. W., TSUKANOV, N. V. & VALLIER., T. L. 1997. Summary Circum-North Pacific tectonostratigraphic terrane map. *Geological Survey of Canada Open File*, **3428** / *U. S. Geological Survey Open File Report*, **96-727**. 1 sheet.

NOKLEBERG, W. J., BUNDTZEN, T. K., EREMIN, R. A., RATKIN, V. A., DAWSON, K. M., SHPIKERMAN, V. I., GORYACHEV, N. A., BYALOBZHESKY, S. G., FROLOV, Y. F., KHANCHUK, A. I., KOCHL, R. D., MONGER, J. W. H., POZDEEV, A. I., ROZENBLUM, I. S., RODIONOV, S. M., PARFENOV, L. M., SCOTESE, C. R. & SIDOROV, A. A. 2003. Metallogenesis and tectonics of the Russian Far East, Alaska, and the Canadian Cordillera. *U. S. Geological Survey Open-File Report*, **03-434**, 378p.

NORTHWEST ALASKA NATIVE ASSOCIATION & COMINCO LTD. 2000 Shared values, common goals, exceptional results. The Red Dog mine history. U*npublished*. 28 p.

OLDOW, J. S., AVÉ LALLEMANT, H. G., JULIAN, F .E. & SEIDENSTICKER, C. M. 1987. Ellesmerian (?) and Brookian deformation in the Franklin Mountains, northeastern Brooks Range, Alaska, and its bearing on the origin of the Canada Basin. *Geology*, **15**, 37-41.

OLDOW, J. S., BALLY, A. W., AVÉ LALLEMANT, H. G. & LEEMAN, W. P. 1989. Phanerozoic evolution of the North American Cordillera. *In*: BALLY, A. W. & PALMER, A. R. (eds). The Geology of North America-An Overview. Boulder, Colorado, Geological Society of America, The Geology of North America, **A-619**, 139-232.

ÖNCKEN, O., PLESCH, A., WEBER, J., RICKEN, W. & SCHRADER, S. 2000. Passive margin detachment during arc-continent collision (Central European Variscides). *In*: FRANKE, W., HAAK, V., ÖNCKEN, O. & TANNER, D. (eds). Orogenic processes: qualification and modelling in the Variscan Belt. *Geological Society of London Special Publication*, **179**, 199-216.

ORI, G. G. & FRIEND, P. F. 1984. Sedimentary basins formed and carried piggyback on active thrust sheets. *Geology*, **12**, 475-478.

O'SULLIVAN, P. B. 1999. Apatite and zircon fission track thermochronology studies. *In*: U. S. Geological Survey and Cominco Research Study at Red Dog, 1998 Results. *Unpublished Report*, 66-79.

O'SULLIVAN, P. B., GREEN, P. F., BERGMAN, S. C., DECKER, J., DUDDY, I. R., GLEADOW, A. J. W. & TURNER, D. L. 1993. Multiple phases of Tertiary uplift and erosion in the Arctic National Wildlife Refuge, Alaska, revealed by apatite fission track analysis. *American Association of Petroleum Geologists Bulletin*, **77**, 359-385.

O'SULLIVAN, P. B., MURPHY, J. M. & BLYTHE, A. E. 1997. Late Mesozoic and Cenozoic thermotectonic evolution of the central Brooks Range and adjacent North Slope foreland basin, Alaska: In cluding fission track results from the Trans-Alaska Crustal Transect (TACT). *Journal of Geophysical Research*, **102**, 20,821-20,845.

O'SULLIVAN, P. B., MOORE, T. E. & MURPHY, J. M. 1998. Tertiary uplift of the Mount Doonerak antiform, central Brooks Range, Alaska: Apatite fission-track evidence from the Trans-Alaska crustal transect. *In*: OLDOW, J. S. & AVE LALLEMANT, H. G. (eds). Architecture of the central Brooks Range fold and thrust belt, Artic Alaska. *Geological Society of America Special Paper*, **324**, 179-194.

O'SULLIVAN, P. B., KELLEY, K. D. & JENNINGS, S. 2000. Post-mineralization thermotectonic evolution of the region of the Red Dog Pb-Zn-Ag mine, northwest Alaska. *Geological Society of Australia Abstracts*, v. **58**, 255-257.

O'SULLIVAN, P. B. & WALLACE, W. K. 2002. Out-of-sequence, basement involved structures in the Sadlerochit Mountains region of the Arctic National Wildlife Refuge, Alaska: Evidence and implications from fission-track thermochronology. *Geological Society of America Bulletin*, **114**, 1356-1378.

PAGE, R. A., BISWAS, N. N., LAHR, J. C. & PULPAN, H. 1991. Seismicity of continental Alaska. *In*: SLEMMONS, D. B., ENGDAHL, E. R., ZOBACK, M. D. & BLACKWELL, D. D. (eds). Neotectonics of North America. Boulder, Colorado. Geological Society of America, Decade Map Volume 1.

PALLISTER, J. S. & CARLSON, C. 1988. Bedrock geologic map of the Angayucham Mountains, Alaska: U. S. Geological Survey Miscellaneous Field Studies Map MF–2024, scale 1:63,360.

PALLISTER, J. S., BUDAHN, J. R. & MURCHEY, B. L. 1989. Pillow basalts of the Angayucham terrane- oceanic plateau and island crust accreted to the Brooks Range. *Journal of Geophysical Research*, **94**, 15,901-15,923.

PARNELL, J., HONGHAN, C., MIDDLETON, T. & CAREY, P. 2000. Significance of fibrous mineral veins in hydrocarbon migration: fluid inclusion studies. *Journal of Geochemical Exploration*, **69-70**, 623–627.

PASSCHIER, C. W. & TROUW, R. A. J. 1998. Microtectonics. *Springer-Verlag Berlin, Heidelberg*, 289p.

PATTON, W. W. JR. 1956. New and redefined formations of Early Cretaceous age, Mesozoic sequence in the Colville River region, northern Alaska. *American Association of Petroleum Geologists Bulletin*, **40**, 219-223.

PATTON, W. W. JR. 1957. A new Upper Paleozoic formation, central Brooks Range, Alaska, Areal geology. Exploration of Naval Petroleum Reserve n4 and adjacent areas, northern Alaska, 1944-53. *U. S. Geological Survey Professional Paper*, **303-B**, 41-45.

PATTON, W. W. JR. & HOARE, J. M. 1968. The Kaltag fault, west-central Alaska. *U. S. Geological Survey Professional Paper*, **600D**, 147-153.

PATTON, W. W. JR. & TAILLEUR, I. L. 1977. Evidence in the Bering Strait region for differential movement between North America and Eurasia. *Geological Society of America Bulletin*, **88**, 1298-1304.

PATTON, W. W. JR. & BOX, S. E. 1989. Tectonic setting of the Yukon-Koyukuk basin and its borderlands, western Alaska. *Journal of Geophysical Research*, **94**, 15,807-15,820.

PATTON, W. W. JR., BOX, S. E. & GRYBECK, D. J. 1994. Ophiolites and other mafic-ultramafic complexes in Alaska. *In*: PLAFKER, G. & BERG, H. C. (eds). The Geology of Alaska. Boulder, Colorado, Geological Society of America, The Geology of North America, v-**G-1**. 671-686.

PAULSEN, T. & MARSHAK, S. 1997. Structure of the Mount Raymond transverse zone at the southern end of the Wyoming salient, Sevier fold-thrust belt, Utah. *Tectonophysics*, **280**, 199-211.

PAULSEN, T. & MARSHAK, S. 1999. Origin of the Uinta recess, Sevier fold-thrust belt, Utah: Influence of basin architecture on fold-thrust belt geometry. *Tectonophysics*, **312**, 203-216.

PAYNE, T. G. 1955. Mesozoic and Cenozoic tectonic elements of Alaska. *U. S. Geological Survey Miscellaneous Geologic Investigations,* Map **I-84**, scale 1:5,000,000.

PEACH, B. N., HORNE, J., GUNN, W., CLOUGH, C. T., HINXMAN, L. W. & TEALL, J. J. H. 1907. The geological structure of the north-west Highlands of Scotland. *Geological Survey of Great Britain Memoir*.

PEARCE, J. A. 2003. Supra-subduction zone ophiolites: the search for modern analogues. *In*: DILEK, Y. & NEWCOMB, S. (eds). Ophiolite concept and the evolution of geological thought. *Geological Society of America Special Paper*, **373**, 269-293.

PÉREZ-ESTAÚN, A., BASTIDA, F., ALONSO, J. L., MARQUÍNEZ, J., ALLER, J., ALVAREZ-MARRÓN, J., MARCOS, A. & PULGAR, J. A. 1988. A thin-skinned tectonic model for an arcuate fold and thrust belt: Cantabrian Zone. *Tectonics*, **7**, 517-537.

PÉREZ-ESTAÚN, A., ALVAREZ-MARRÓN, J., BROWN, D., PUCHKOV, V., GOROZHANINA, Y. & BARYSHEV, V. 1997. Along-strike structural variations in the foreland thrust and fold belt of the southern Urals, *Tectonophysics*, **276**, 265-280.

PERKINS, W. G. 1997. Mount Isa lead-zinc orebodies: replacement lodes in a zoned syndeformational copper-lead-zinc system. *Ore Geology Reviews*, **12**, 61-110.

PERKINS, W. G. 1998. Timing of formation of stratiform fine-grained pyrite: post-diagenetic cleavage replacement at Mount Isa?. *Economic Geology*, **93**, 1153-1164.

PERKINS, W. G. & BELL, T. H. 1998. Stratiform replacement lead-zinc deposits: a comparison between Mount Isa, Hilton and McArthur River. *Economic Geology*, **93**, 1190-1212.

PERSON, M. A. & GARVEN, G. 1994. A sensitivity study of the driving forces on fluid flow during continental rift evolution: *Geological Society of America Bulletin*, **106**, 461-475.

PICKERING, K., HISCOTT, R. & HEIN, F. 1989. Deep Marine Environments. *Unwin Hyman, London*, 416p.

PINI, G. A. 1999. Tectonosomes and olistostromes in the Argille Scagliose of the northern Appennines, Italy. *Geological Society of America Special Paper*, **335**, 1-70.

PLAFKER, G. & BERG, H. C. 1994. Overview of the geology and tectonic evolution of Alaska. *In*: PLAFKER, G. & BERG, H. C. (eds). The Geology of Alaska. Boulder, Colorado, Geological Society of America, The Geology of North America, v-**G-1**. 989-1022.

PLAFKER, G., GILPIN, L. M. & LAHR, J. C. 1994. Neotectonic map of Alaska. *In*: PLAFKER, G. & BERG, H. C. (eds). The Geology of Alaska. Boulder, Colorado, Geological Society of America, The Geology of North America, v-**G-1**. Plate 12.

PLAHUTA, J. T. 1978. Geologic map and cross section of the Red Dog prospect, De Long Mountains, northwestern Alaska. *U. S. Bureau of Mines Open File Report*, **65-78**, 11p.

PLAHUTA, J. T. & ROBINSON, J. D. 1979. Zinc-lead-barite mineralization in upper Paleozoic marine sedimentary rocks at the Red Dog deposit, De Long Mountains, Alaska. *84th Northwest Mining Association Annual Congress, Spokane, Proceedings*, 20 p.

PLANKE, S., SYMONDS, P. A., ALVESTAD, E. & SKOGSEID, J. 2000. Seismic volcanostratigraphy of large-volume basaltic extrusive complexes on rifted margins. *Journal of Geophysical Research*, **105**, 19,335-19,351.

PLATT, J. P. 1986. Dynamics of orogenic wedges and the uplift of high-pressure metamorphic rocks. *Geological Society of America Bulletin*, **97**, 1037-1053.

PLATT, J. P. 1993. Exhumation of high-pressure rocks: a review of concepts and processes. *Terra Nova*, **5**, 119-133.

POBLET, J. & MCCLAY, K. R. 1996. An analysis of single layer detachment folding. *American Association of Petroleum Geologists*, **80**, 1085-1109.

POBLET, J., BULNES, M., MCCLAY, K. R. & HARDY, S. 2004. Plots of crestal structural relief and fold area versus shortening: a graphical technique to unravel the kinematics of thrust-faulted folds. *In*: McClay, K. R. (ed). Thrust tectonics and Petroleum Systems. *American Association of Petroleum Geologists Memoir*, **82**, 372-299.

POHN, H. A. 1998. Lateral ramps in the folded Appalachians and in overthrust belts worldwide-A fundamental element of thrust-belt architecture. *U. S. Geological Survey Bulletin*, **2163**. p. 63.

POHN, H. A. & COLEMAN, J. L. JR. 1991. Fold patterns, lateral ramps and seismicity in central Pennsylvania. *Tectonophysics*, **186**, 133-149.

POHN, H. A. & MOLNIA, B. F. 1992. Structural analysis of side-looking airborne radar data from the western Brooks Range, *EOS Transactions, American Geophysical Union*, **73**, 288.

POHN, H. A., DEWITT, W. JR. & SCHULTZ, A. P. 1985. Disturbed zones, lateral ramps and their relationship to the structural framework of the central Appalachians. Eastern Section. *American Association of Petroleum Geologists*, Guidebook, **3**, 62p.

PORTER, S. C. 1966. Stratigraphy and deformation of Paleozoic section at Anaktuvuk Pass, central Brooks Range. *American Association of Petroleum Geologists Bulletin*, **50**, 952-980.

POTTER, C. J. & MOORE, T. E. 2005. Gas and oil plays related to frontal thrusts and folds of the Brooks Range foothills and Arctic Coastal Plain, central North Slope, Alaska. Cordilleran Section - 101st Annual Meeting. *Geological Society of America Abstracts with Programs*, **37**, No. 4, Paper No. 40-2.

POTTER, C. J., MOORE, T. E. & O'SULLIVAN, P. 2002. Tertiary frontal structures of the Brookian orogen beneath the arctic coastal plain and offshore northern Alaska. *Geological Society of America Abstracts with Programs*, Denver 27th-30th October.

POTTER, C. J., GROW, J. A., PERRY, W. J., MOORE, T. E., O'SULLIVAN, P. B., PHILLIPS, J. D. & SALTUS, R. W. 2004. Tertiary thrust systems and fluid flow beneath the Beaufort Coastal Plain (1002 Area), Arctic National Wildlife Refuge, Alaska, USA. *In*: SWENNEN, R., ROURE, F. & GRANATH, J. W. *American Association of Petroleum Geologists Hedberg Series*, **1**, 187-214.

PRICE, N. J. & COSGROVE, J. W. 1990. Analysis of geological structures. Chapter 7, Overthrust and thrust nappes. *Cambridge University Press, Cambridge*. 502p.

PRICE, R. A. 1973. Large-scale gravitational flow of supra-crustal rocks, southern Canadian Rockies. *In*: DE JONG, K. A. & SCHOLTEN, R. (eds). Gravity and tectonics. *New York, Wiley & Sons*, 491-502.

PRICE, R. A. 1981. The Cordilleran foreland thrust and fold belt in the southern Canadian Rocky Mountains. *In*: MCCLAY, K. R. & PRICE, N. J. (eds). Thrust and nappe tectonics. *Geological Society of London Special Publication*, **9**, 427-448.

PRICE, R. A. 1986. The southeastern Canadian Cordillera: thrust faulting, wedging and delamination of the lithosphere. *Journal of Structural Geology*, **8**, 239-254.

PRICE, R. A. 1988. The mechanical paradox of large overthrusts. *Geological Society of America Bulletin*, **100**, 1898-1908.

PRICE, R. A. 1990. The mechanical paradox of large overthrusts. Alternative interpretation, reply. *Geological Society of America Bulletin*, **102**, 529-532.

PRICE, R. A. 2001. An evaluation of models for the kinematic evolution of thrust and fold belts; structural analysis of a transverse fault zone in the Front Ranges of the Canadian Rockies north of Banff, Alberta. *Journal of Structural Geology*, **23**, 1079-1088.

PRICE, R. A. & FERMOR, P. R. 1985. Structure section of the Cordilleran foreland fold and thrust belt west of Calgary, Alberta. *Geological Survey of Canada Paper*, **84-14**, 1 sheet.

PRICE, R. A. & MONGER, J. W. H. 2003. A transect of the southern Canadian Cordillera from Calgary to Vancouver. *Fieldtrip Guide Book. Geological Association of Canada. Cordilleran Section*. 165p.

RAMOS, V. A., ZAPATA, T., CRISTALLINI, E. & INTROCASO, A. 2004. The Andean thrust system-latitudinal variations in structural styles and orogenic shortening. *In*: MCCLAY, K. R. (ed). Thrust Tectonics and Petroleum Systems. *American Association of Petroleum Geologists Memoir*, **82**, 31-51.

RAMSAY, J. G. 1974. The development of chevron folds. *Geological Society of America Bulletin*, **85**, 1741-1754.

RAMSAY, J. G. 1980. The crack-seal mechanism of rock deformation. *Nature*, **284**, 135-139.

RAMSAY, J. G. & HUBER, M. I. 1987*a*. The techniques of modern structural geology. Volume 1.Strain Analysis. *Academic Press, London*, 307p.

RAMSAY, J. G. & HUBER, M. I. 1987*b*. The techniques of modern structural geology. Volume 2. Folds and fractures. *Academic Press, London*, 391p.

READING, H. G. 1996. Sedimentary environments. Processes, facies, and stratigraphy. *Blackwell Science*, 688p.

REINECK, H. E. & SINGH, I. B. 1980. Depositional sedimentary environments. *New York, Springer Verlag*, 549p.

REINECKER J., HEIDBACH O., TINGAY M., CONNOLLY P. & MÜLLER B. 2004. The 2004 release of the World Stress Map. www.world-stress-map.org. (visited 10th January 2005).

RICCI LUCCHI, F. 1987. Semi-allochthonous sedimentation in the Apenninic thrust belt. *Sedimentary Geology*, **50**, 119-134.

RICH, J. L. 1934. Mechanics of low-angle overthrust faulting as illustrated by Cumberland thrust block, Virginia, Kentucky, and Tennessee. *American Association of Petroleum Geologists Bulletin*, **18**, 1584-1596.

RICHARD, P. D. & COBBOLD, P. R. 1990. Experimental insights into partitioning of fault motions in continental convergent wrench zones. *Annales Tectonicae*, **4**, 35 - 44.

RICHARDSON, A. N. & BLUNDELL, D. J. 1996. Continental collision in the Banda Arc. *In*: HALL, R. & BLUNDELL, D. (eds). Tectonic evolution of southeast Asia. *Geological Society of London Special Publication*, **106**, 47-60.

RICKWOOD, F. K. 1970. The Prudhoe Bay field. *In*: ADKISON, W. L. & BROSGÉ, M. M. (eds). Proceedings of the geological seminar on the North Slope of Alaska. *American Association of Petroleum Geologists Pacific Section*, p. L1-L11.

ROBERTS, S. 1992. Influence of the partial melting regime on the formation of ophiolite chromitite. *In*: PARSON, L. M., MURTON, B. J. & BROWNING, P. (eds). Ophiolites and their modern analogues. *Geological Society of London Special Publication*, **60**, 203-217.

ROBERTSON, A. H. F. 2004. Development of concepts concerning the genesis and emplacement of Tethyan ophiolites in the Eastern Mediterranean and Oman regions. *Earth Science Reviews*, **66**, 331-387.

ROBERTSON, A. H. F. & SEARLE, M. P. 1990. The northern Oman Tethyan continental margin: stratigraphy, structure, concepts and controversies. *In*: ROBERSTON, A. H. F., SEARLE, M. P. & RIES, A. C. The geology and tectonics of the Oman region. *Geological Society of London Special Publication*, **49**, 3-25.

ROBERTSON, A. H. F., KEMP, A. E. S., REX, D. C. & BLOME, C. D. 1990. Sedimentary and structural evolution of a continental margin transform lineament: the Hatta Zone, northern Oman Mountains. *In*: ROBERSTON, A. H. F., SEARLE, M. P. & RIES, A. C. The geology and tectonics of the Oman region. *Geological Society of London Special Publication*, **49**, 285-305.

ROBINSON, P. T., MALPAS, J. & XENOPHONTOS, C. 2003. The Troodos massif of Cyprus: its role in the evolution of the ophiolite concept. *In*: DILEK, Y. & NEWCOMB, S. (eds). Ophiolite concept and the evolution of geological thought. *Geological Society of America Special Paper*, **373**, 295-308.

ROCKWELL, D. W. 1978. Preliminary draft of interim report on review and analysis of seismic and subsurface data from the foothills belt and adjoining portion of the coastal plain sector of the National Petroleum Reserve in Alaska. *Stewart Folk Company Inc. Houston, Technical Memo*, 33p.

ROEDER, D. & MULL, C. G. 1978. Tectonics of Brooks Range ophiolites, Alaska. *American Association of Petroleum Geologists Bulletin*, **62**, 1696-1713.

ROEDER, D. & CHAMBERLAIN, R. L. 1995. Structural geology of Sub-Andean fold and thrust belt in northwest Bolivia. *In*: TANKARD, A. J.

ROEDER, D. & BOYER, S. 2001. Fold-thrust belts: Petroleum potential, global setting, Geodynamics. *American Association of Petroleum Geologists Programs with Abstracts*, Denver, 3rd June 2001.

ROGERS, H. D. 1858. The Geology of Pennsylvania, v. 2, 1045p. J. B. Lippincot, Philadelphia.

ROMBACH, C. S. & LAYER, P. W. 2004. Geochronology of the western and central Brooks Range, Alaska: Implications for the geologic evolution of the Anarraaq and Red Dog Zn-Pb-Ag deposits. *In*: KELLEY, K. D. & JENNINGS, S. (eds). A Special Issue devoted to barite and zinc-lead-silver deposits in the Red Dog district, western Brooks Range northern Alaska. *Economic Geology*, **99**, 1307-1322.

ROURE, F., HOWELL, D. G., GUELLEC, S. & CASERO, P. 1990. Shallow structures induced by deep-seated thrusting. *In*: Letouzey (ed). Petroleum and tectonics of mobile belts. *Technip Editions, Paris*, 15-30.

ROURE, F., NAZAJ, S., MUSHKA, K., FILI, I., CADET, P. & BONNEAU, M. 2004. Kinematic evolution and petroleum systems-An appraisal of the Outer Albanides. *In*: MCCLAY, K. R. (ed). Thrust Tectonics and Petroleum Systems. *American Association of Petroleum Geologists Memoir*, **82**, 485-504.

RUSSEL, M. J. 1983. Major sediment-hosted exhalative zinc-lead deposits: fomation from hydrothermal convection cells that deepen during crustal extension.

RUSSEL, R. H., ROBINSON, J. D. & VAN BLARICOM, R. 1978. The Noatak Project. Cominco American Inc. 1977. *Unpublished Internal Annual Report.*

RUTTER, E. H. 1976. The kinetics of rock deformation by pressure solution. *Philosophical Transactions of the Royal Society of London*, **A283**, 203-219.

SABLE, E. G. & DUTRO, J. T. JR. 1961. New Devonian and Mississippian formations in the De Long Mountains, northern Alaska. *American Association of Petroleum Geologists Bulletin*, **45**, 585-593.

SABLE, E. G., DUTRO, J. T., MANGUS, M. D. & MORRIS, R. H. 1981. Geology of the Kukpowruk-Nuka Rivers region, northwestern Alaska. *U. S. Geological Survey Open-File Report*, **81-1078**, 240p.

SAFARICZ, M. & DAVISON, I. 2005. Pressure solution in chalk. *American Association of Petroleum Geologists Bulletin*, **89**, 383-401.

SALTUS, R.W. & SIMMONS G. C. 1997. Composite and Merged Aeromagnetic Data for Alaska: A Website for Distribution of Gridded Data and Plot Files. *U. S. Geological Survey Open-File-Report 97-520*. http://pubs.usgs.gov/of/1997/ofr-97-0520/

SALTUS, R.W. & BIRD, K. J. 2003. Digital depth horizon compilations of the North Slope and adjacent Arctic regions. *U. S. Geological Survey Open-File Report*, **03-230**, 21p.

SALTUS, R. W, HUDSON, T. L. & CONNARD, G. G. 1999. A new magnetic view of Alaska. *GSA Today*, **9**, 1-6.

SALTUS, R. W., HUDSON, T. L. & PHILLIPS, J. D. 2001*a*. Basement geophysical interpretation of the National Petroleum Reserve Alaska (NPRA), northern Alaska.
U. S. Geological Survey Open-File Report, **01-0476**.

SALTUS, R. W., HUDSON, T. L, KARL, S. M. & MORIN, R. L. 2001*b*. Rooted Brooks Range ophiolite; Implications for Cordilleran terranes. *Geology*, **29**, 1151-1154.

SALTUS, R. W., HUDSON, T. L., PHILLIPS, J. D., KULANDER, C., DUMOULIN, J. A. & POTTER, C. 2002. Basement geology of the National Petroleum Reserve Alaska (NPRA), northern Alaska. *U. S. Geological Survey Open-File Report*, **02-0127**.

SALTUS, R. W., HUDSON, T. L., KARL, S. M. & MORIN, R. L. 2003. Rooted Brooks Range ophiolite: implications for Cordilleran terranes. Comments to Reply. *Geology*, **31**, 91-92.

SALTUS, R.W., PHILLIPS, J. D. & POTTER, C. J. 2005. Gravity and aeromagnetic data analysis, central North Slope, Alaska – historical perspective and contemporary implications. Cordilleran Section, 101st Annual Meeting (April 29–May 1, 2005). Paper No. 40-10.

SANGSTER, D. F. 1983. Short course in sediment-hosted stratiform lead-zinc deposits. *Mineralogical Association of Canada, Short Course Handbook*, **8**, 251-282.

SANGSTER, D. F. 1990. Mississippi Valley-type and Sedex zinc-lead deposits: a comparative examination. Transactions of the IMM section B, **99**, 21-40.

SANGSTER, D. F. & LEACH, D. L. 1995. Evidence for a genetic link between SEDEX and MVT deposits. *In*: LEACH, D. L. & GOLDHABER, M. B. (eds). Extended abstracts. International conference on Carbonate-Hosted Lead-Zinc deposits. St. Louis, Missouri, June 1-4. 260-263.

SAUNDERS, W. B. & RAMSBOTTOM, W. H. C. 1986. The mid-Carboniferous eustatic event. *Geology*, **14**, 208-212.

SAWKINS, F. J. 1976. Metal deposits related to intracontinental hotspot and rifting environments. *Journal of Geology*, **84**, 653-671.

SCHEDL, A. & WILTSCHKO, D. V. 1987. Possible effects of pre-existing basement topography on thrust fault ramping. *Journal of Structural Geology*, **9**, 1029-1037.

SCHMIDT, J. M. 1986. Stratigraphic setting and mineralogy of the Arctic volcanogenic massive sulfide prospect, Ambler district, Alaska. *Economic Geology*, **81**, 1619-1643.

SCHMIDT, J. M. 1997*a*. Shale-hosted Zn-Pb-Ag and barite deposits of Alaska. *In*: GOLDFARB, R. J. & MILLER, L. D. (eds). Mineral deposits of Alaska. *Economic Geology Monograph*, **9**, 35-65.

SCHMIDT, J. M. 1997*b*. Strata-bound carbonate-hosted Zn-Pb and Cu deposits of Alaska. *In*: GOLDFARB, R. J. & MILLER, L. D. (eds). Mineral deposits of Alaska. *Economic Geology Monograph*, **9**, 90-119.

SCHMIDT, J. M. 2000. Geology and geochemistry of Zn-Pb-Ag vein-breccias at Whoopee Creek, Alaska. *In*: KELLEY, K. D. & GOUGH, L. P. (eds). Geologic studies in Alaska by the U. S. Geological Survey. *U. S. Geological Survey Professional Paper*, **1615**, 203-221.

SCHMIDT, J. M. & ZIERENBERG, R. A. 1989. Reconstruction of primary features and isotopic evidence for multiple sulfur sources at the Red Dog zinc-lead-silver deposit, Noatak district, Alaska. *In*: SCHINDLER, K. S. (ed). U. S. Geological Survey Research on Mineral Resources-1989 Programs with Abstracts. 5th Annual McKelvey Forum on Mineral and Energy Resources. *U. S. Geological Survey Circular*, **1035**. unpaginated.

SCHMIDT, C. J., CHASE, R. & ERSLEV, E. A. 1993. Laramide basement deformation in the Rocky Mountain foreland of the western United States. *Geological Society of America Special Paper*, **280**, 365 p.

SCHOENNAGEL, F. A. 1967. Mississippian unconformities in northern Alaska related to Antler tectonic pulses. *American Association of Petroleum Geologists Bulletin*, **61**, 435-447.

SCHÖNBORN, G. 1992. Kinematics of a transverse zone in the southern Alps, Italy. *In*: MCCLAY, K. R. (ed). Thrust Tectonics. *Chapman & Hall, London*. 299-310.

SCHRADER, F. C. 1902. Geological section of the Rocky Mountains in northern Alaska. *Geological Society of America Bulletin*, **13**, 233-252.

SCHREURS, G., HÄNNI, R. & VOCK, P. 2002. Analogue modelling of transfer zones in fold and thrust belts: a 4-D analysis. *In*: SCHELLART, W. P. & PASSCHIER, C. (eds). Analogue modelling of large-scale tectonic processes. *Journal of the Virtual Explorer*, **6**, 43-49.

SCHULTZ, R. A. & AYDIN, A. 1990. Formation of interior basins associated with curved faults in Alaska. *Tectonics*, **9**, 1387-1407.

SEARLE, M. P. 1985. Sequence of thrusting and origin of culminations in the northern and central Oman Mountains. *Journal of Structural Geology*, **7**, 129-143.

SEARLE, M. P. & COX, J. 1999. Tectonic setting, origin and obduction of the Oman ophiolite. *Geological Society of America Bulletin*, **111**, 104-122.

SENGÖR, A. M. C. 2003. The repeated rediscovery of melanges and its implications for the possibility and the role of objective evidence in the scientific enterprise. *In*: DILEK, Y. & NEWCOMB, S. (eds). Ophiolite concept and the evolution of geological thought. *Geological Society of America Special Paper*, **373**, 385-445.

SEPEHR, M. 2004. The tectonic significance of the Kazerun fault zone, Zagros fold-thrust belt, Iran. Ph.D. Thesis. Imperial College, University of London. 215p.

SEPEHR, M. & COSGROVE, J. 2004. Structural framework of the Zagros fold-thrust belt, Iran. *Marine and Petroleum Geology*, **21**, 829-843.

SHAW, J. H., CONNORS, C. & SUPPE, J. 2005. Seismic interpretation of contractional fault-related folds. *American Association of Petroleum Geologists Atlas, Studies in Geology*, **53**, 156.

SHERWOOD, K. W., JOHNSON, P. P., CRAIG, J. D., ZERWICK, S. A., LOTHAMER, R. T., THURSTON, D. K. & HURLBERT, S. B. 2002. Structure and stratigraphy of the Hanna Trough, U. S. Chukchi Shelf, Alaska. *In*: MILLER, E. L., GRANTZ, A. & KLEMPERER, S. L. (eds). Tectonic Evolution of the Bering Shelf-Chukchi Sea-Arctic Margin and Adjacent Landmasses. *Geological Society of America Special Paper*, **360**, 39-66.

SIBSON, R. H. 1990. Conditions for fault-valve behavior. *In*: KNIPE, R. J. & RUTTER, E. H. (eds). Deformation mechanisms, rheology and tectonics. *Geological Society of London*, 15-28.

SIBSON, R. H., MOORE, J. M. & RANKIN, A. H. 1975. Seismic pumping - a hydrothermal fluid transport mechanism. *Journal of the Geological Society of London*, **131**, 653-659.

SILBERING, N. J. & JONES, D. L. 1984. Lithotectonic terrane maps of the North American Cordillera. *U. S. Geological Survey Open-File Report*, **84-523**, 3 sheets.

SILBERING, N. J., JONES, D. L., CONEY, P. J., BERG, H. C. & PLAFKER, G. 1994. Lithotectonic terrane map of Alaska and adjacents parts of Canada. *In*: PLAFKER, G. & BERG, H. C. (eds). The Geology of Alaska. Boulder, Colorado, Geological Society of America, The Geology of North America, v-**G-1**, Plate 3, 1 sheet with text. Scale 1:2,500,000.

SIMS, D. B. 1996. The relationship of ore and structural geology at the Red Dog Zn-Pb-Ag deposit, western Brooks Range, Alaska. *PhD Thesis. University of Arizona, Tucson*, 142 p.

SIOK, J. P. 1989. Stratigraphy and petrology of the Okpikruak Formation at Cobblestone Creek, northcentral Brooks Range. *In*: MULL, C. G. & ADAMS, K. E. (eds). Dalton Highway, Yukon River to Prudhoe Bay, Alaska. Bedrock geology of the eastern Koyukuk basin, central Brooks Range and east-central Arctic Slope. *Alaska Division of Geological & Geophysical Surveys Guidebook*, **7**, 285-292.

SLACK, J. F., DUMOULIN, J. A., HARRIS, A. G., BLOME, C. D. & YOUNG, L. E. 2004. Depositional settings, correlation, and age of Carboniferous rocks in the western Brooks Range, Alaska: Provenance, deposition, and metallogenic significance. *In*: KELLEY, K. D. & JENNINGS, S. (eds). A Special Issue devoted to barite and zinc-lead-silver deposits in the Red Dog district, western Brooks Range northern Alaska. *Economic Geology*, **99**, 1385-1414.

SLOSS, L. L. 1963. Sequences in the cratonic interior of North America. *Geological Society of America Bulletin*, **74**, 93-114.

SMITH, D. G. 1987. Late Paleozoic to Cenozoic reconstructions of the Arctic. *In*: TAILLEUR, I. & WEIMER, P. (eds). Alaskan North Slope geology: Bakersfield, California, *Society of Economic Paleontologists and Mineralogists, Pacific Section, and Alaska Geological Society*, Book 50, v. **1 & 2**, p. 785–795.

SMITH, P. S. 1913. The Noatak-Kobuk region. *U. S. Geological Survey Bulletin*, **536**.

SMITH, P. S. 1939. Areal geology of Alaska. *U. S. Geological Survey Professional Paper*, **192**, 100 p.

SNELSON, S. & TAILLEUR, I. L. 1968. Large-scale thrusting and migrating Cretaceous foredeeps in the western Brooks Range and adjacent regions of northwestern Alaska (abs). *American Association of Petroleum Geologists Bulletin*, **52**, p. 567.

SOLIE, D. N. & MULL, C. G. 1991. Kikiktat Mountain klippe- a link between the Copter Peak and Nuka Ridge allochthons, northcentral Brooks Range, Alaska. *In*: REGER, R. D. (ed). Short Notes on Alaskan Geology 1991. *State of Alaska, Department of natural Resources, Division of Geological and Geophysical Surveys Professional Report*, **111**, 77-88.

SOTO, R., STORTI, F., CASAS, A. M. & FACCENNA, C. 2003. Influence of along-strike pre-orogenic sedimentary tapering on the internal architecture of experimental thrust wedges. *Geological Magazine*, **140**, 253-264.

SPRATT, D. A., DIXON, J. M. & BEATTIE, E. T. 2004. Changes in structural style controlled by lithofacies contrast across transverse carbonate bank margins: Canadian Rocky Mountains and scaled physical models. *In*: MCCLAY, K. R. (ed). *American Association of Petroleum Geologists Memoir*, **82**, 263-280.

STERNE, E. J., ZANTOP, H. & REYNOLDS, R. C. 1984. Clay mineralogy and carbon-nitrogen geochemistry of the Lik and Competition Creek zinc-lead-silver prospects, De Long Mountains, Alaska. *Economic Geology*, **79**, 1406-1411.

STOCKMAL, F. S., BEAUMONT, C. & BOUTILIER, R. 1986. Geodynamic models of convergent margin tectonics: transition from rifted margin to overthrust belt and consequences for foreland basin development. *American Association of Petroleum Geologists Bulletin*, **70**, 181-190.

STORTI, F. & MCCLAY, K. R. 1995. Influence of syntectonic sedimentation on thrust wedges in analogue models. *Geology*, **23**, 999-1002.

STORTI, F., SALVINI, F. & MCCLAY, K. R. 2000. Synchronous and velocity-partitioned thrusting and thrust polarity reversal in experimentally produced, doubly-vergent thrust wedges: Implications for natural orogens. *Tectonics*, **19**, 378-396.

STRAYER, L. M., HUDLESTON, P. J. & LORIG, L. J. A numerical model of deformation and fluid-flow in an evolving thrust wedge. *Tectonophysics*, **335**, 121-145.

SUPPE, J. 1980. Imbricated structure of western foothills belt, south-central Taiwan. *Petroleum Geology of Taiwan*, **17**, 1-16.

SUPPE, J. 1983. Geometry and kinematics of fault-bend folding. *American Association of Petroleum Geologists Bulletin*, **64**, 916-926.

SUPPE, J. 1985. Principles of structural geology. *Prentice Hall, New Jersey*, 537p.

SUPPE, J. & MEDWEDEFF, D. A. 1990. Geometry and kinematics of fault propagation folding, *Eclogae Geologicae Helveticae*, **83**, 409-454.

SURLES, M. & THOMAS, W. A. 2004. Orthogonal basement fault systems and diachronous Ouachita-Appalachian thrusting around the Black Warrior basin, Alabama and Mississippi. *Geological Society of America Abstracts with Programs*, **36**, 5.

SWEENEY, J. F. 1982. Arctic Alaska, a two-stage displaced terrane. Proceedings. 33rd Alaska Science Conference, Fairbanks, Alaska. *American Association for the Advancement of Science*, p. 146.

SZUMIGALA, D. J. & SWAINBACK, R. C. 2001. Alaska's mineral industry 2000: A summary. Information Circular 47, Alaska Division of Geological and Geophysical Surveys, 15p.

TAILLEUR, I. L. 1969. Rifting speculation of the geology of Alaska's North Slope. *Oil & Gas Journal*, **67** v.39. 128-130.

TAILLEUR, I. L. 1970. Lead, zinc, and barite-bearing samples from the western Brooks Range, Alaska. *U. S. Geological Survey Open-File Report*, **70-319**, 16p.

TAILLEUR, I. L. 1973. Probable rift origin of Canada Basin, Arctic Ocean. *In*: PITCHER, M. G. (ed). Arctic geology. *American Association of Petroleum Geologists Memoir*, **19**, 526-535.

TAILLEUR, I. L. & SABLE, E. G. 1963. Nuka Formation of Late Mississippian to Late Permian age, new formation in northern Alaska. *American Association of Petroleum Geologists Bulletin*, **47**, 632-642.

TAILLEUR, I. L. & BROSGÉ, W. P. 1970. Tectonic history of northern Alaska, *In*: ADKISON, W. L. & BROSGÉ, M. M. (eds). Proceedings of the geological seminar on the North Slope of Alaska. Los Angeles, *American Association of Petroleum Geologists*, p. E1-E19.

TAILLEUR, I. L., KENT, B. H. JR. & REISER, H. N. 1966. Outcrop geology maps of the Nuka-Etivluk region, northern Alaska. *U. S. Geological Survey Open-File Report*, **66-128**, scale 1:63,360, 7 sheets.

TAILLEUR, I. L., BROSGÉ, W. P., & REISER, H. N. 1967. Palinspastic analysis of Devonian rocks in northwestern Alaska. *In*: OSWALD, D. H. (ed.). International Symposium of the Devonian System. Calgary, Canada, *Alberta Society of Petroleum Geologists*. p. 1345-1361.

TANNER, P. W. G. 1992. The duplex model: Implications from a study of flexural-slip duplexes, *In:* MCCLAY, K. R. (ed). Thrust Tectonics. *Chapman & Hall, London*, 201-208.

TAPPONIER, P. & MOLNAR, P. 1976. Slip-line field theory and large-scale continental tectonics. *Nature*, **264**, 319-324.

TAVARNELLI, E. 1999. Normal faults in thrust sheets, pre-orogenic extension, post-orogenic extension, or both?. *Journal of Structural Geology*, **21**, 1011-1018.

TECK COMINCO LTD. 2001. Press Release. http://www.teckcominco.com/news/01-archive/01-29-tc.htm

TECK COMINCO LTD. 2005.
http://www.teckcominco.com/operations/reddog/production.htm

THOMAS, W. A. 1977. Evolution of Appalachian-Ouachita salients and recesses from reentrants and promontories in the continental margin. *American Journal of Science*, **277**, 1233-1278.

THOMAS, W. A. 1990. Controls on location of transverse zones in thrust belts. *Eclogae Geologicae Helvetiae*, **83**, 727-744.

THOMAS, W. A. 2004. Genetic relationship of rift-stage crustal structure, terrane accretion, and foreland tectonics along the southern Appalachian-Ouachita orogen. *Journal of Geodynamics*, **37**, 549-563.

THOMAS, W. A. & BAYONA, G. 2002. Palinspastic restoration of the Anniston Transverse Zone in the Appalachians thrust belt, Alabama. *Journal of Structural Geology*, **24**, 797-826.

THOMAS, W. A., ASTINI, R. A. & BAYONA, G. 2002. Ordovician collision of the Argentine Precordillera with Gondwana, independent of Laurentian Taconic orogeny. *Tectonophysics*, **345**, 131-152.

TILL, A. B. 1992. Detrital blueschists-facies metamorphic mineral assemblages in Early Cretaceous sediments of the foreland basin of the Brooks Range, Alaska, and implications for orogenic evolution. *Tectonics*, **11**, 1207-1223.

TILL, A. B. & SNEE, L. W. 1995. $^{40}Ar/^{39}Ar$ evidence that formation of blueschists in continental crust was synchronous with foreland fold and thrust belt deformation, western Brooks Range, Alaska. *Journal of Metamorphic Geology*, **13**, 41-60.

TILL, A. B., SCHMIDT, J. M. & SNELSON, S. W. 1988, Thrust involvement of metamorphic rocks, southwestern Brooks Range, Alaska. *Geology*, **10**, 930-933.

TILL, A. B., BOX, S. E., ROESKE, S. M. & PAPPERTON, W. W. 1993. Comment on "Mid-Cretaceous fragmentation of a Jurassic-Early Cretaceous compressional orogen, Alaska". *Tectonics*, **12**, 1076-1081.

TOLSON, R. B. 1987. Structure, stratigraphy, tectonic evolution and petroleum source potential of the Hope Basin, southern Chukchi Sea, Alaska. Ph.D Thesis. Stanford University, 261p.

TUCKER, M. E. 2001. Sedimentray petrology, 3rd edition. *Blackwell Science*. 262 p.

TWISS, R. J. & MOORES, E. M. 1992. Structural geology. *New York, W.H. Freeman*, 532 pp.

VANN, I. R., GRAHAM, R. H. & HAYWARD, A. B. 1986. The structure of mountain fronts. *Journal of Structural Geology*, **8**, 215-227.

VERA, J. A. (ed). 2004. Cordillera Bética y Baleares. *In*: VERA, J. A. (ed). Geología de España. *Sociedad Geologica de Espana, Instituto Geologico y Minero de España*, Madrid, 346-464.

VOGL, J. J. 2002. Late-orogenic backfolding and extension in the Brooks Range collisional orogen, northern Alaska. *Journal of Structural Geology*, **24**, 1753-1776.

VON HUENE, R., BOURGOIS, J., MILLER, J. & PAUTOT, G. 1989. A large tsunamonic landslide and debris flow along the Peru trench. *Journal of Geophysical Research*, **94**, 1703-1714.

WALDRON, J. W. F., TURNER, D. & STEVENS, K. M. 1988. Stratal disruption and development of melange, western Newfoundland: effect of high fluid pressure in an accretionary terrane during ophiolite emplacement. *Journal of Structural Geology*, **10**, 861-873.

WALLACE, W. K. 1993. Detachment folds and a passive-roof duplex: Examples from the northeastern Brooks Range, Alaska. *In*: SOLIE, D. N. & TANNIAN, F. (eds). Short Notes on Alaskan Geology 1993. *Alaska Division of Geological and Geophysical Surveys Geologic Report*, **113**, 81-99.

WALLACE, W. K. & ENGEBRETSON, D. C. 1984. Relationships between plate motions and Late Cretaceous to Paleogene magmatism in southwestern Alaska. *Tectonics*, **3**, 295-315.

WALLACE, W. K. & HANKS, C. L. 1990. Structural provinces of the northeastern Brooks Range, Arctic National Wildlife Refuge, Alaska. *American Association of Petroleum Geologists Bulletin*, **74**, 1100-1118.

WALLACE, W. K. & HOMZA, T. X. 2004. Detachment folds versus fault-propagation folds, and their truncation by thrust faults. *In*: MCCLAY, K. R. (ed). Thrust Tectonics and Hydrocarbon Systems. *American Association of Petroleum Geologists Memoir*, **82**, 331-362.

WALLACE, W. K., MOORE, T. E. & PLAFKER, G. 1997. Multistory duplexes with forward-dipping roofs, north-central Brooks Range, Alaska. *Journal of Geophysical Research*, **102**, 20,773-20,796.

WALSH, J. J. & WATTERSON, J. 1988. Analysis of the relationship between the displacements and dimensions of faults. *Journal of Structural Geology*, **10**, 238-247.

WARBURTON, J. 2004. Passive roof duplex model and its application in fold belt exploration in Pakistan. *In*: Continental Tectonics: discussion meeting in memory of the life and work of Mike Coward. 27th-28th May 2004. *Geological Society of London*. Unpaginated.

WARNER, M. C. 1998. Geochemical characterization of sedimentary organic matter and hydrothermal petroleum in the black-shale hosted Zn-Pb deposit at Red Dog mine, western Brooks Range, Alaska. Ph.D Thesis. Bloomington, University of Indiana, 216p.

WASHINGTON, P. A. 1990. The mechanical paradox of large overthtrusts: alternative interpretation. *Geological Society of America Bulletin*, **102**, 529-532.

WEGENER, A. 1915. Die Entstehung der kontinente und ozeane. Vieweg, brawnschweig.

WEIL, A. B. & SUSSMAN, A. J. 2004. Classifying curved orogens based on timing relationships between structural development and vertical axis rotations. *In*: SUSSMAN, A. J. & WEIL, A. B. (eds). Orogenic curvature: integrating paleomagnetic and structural analyses. *Geological Society of America Special Paper*, **383**, 1-15.

WELBON, A. I. & BUTLER, R. W. H. 1992. Structural styles in thrust belts developed through rift basins: a view from the western Alps. *In*: LARSEN, R. M., BREKKE, B. T., LARSEN, B. T. & TALLERAAS, E. (eds). Structural and tectonic modelling and its applications to petroleum geology. *Norwegian Petroleum Society Special Publication*, **1**, 469-479.

WENDORFF. M. 2003. Stratigraphy of the Fungurume Group - evolving foreland basin succession in the Lufilian fold-thrust belt, Neoproterozoic-Lower Palaeozoic, Democratic Republic of Congo. *South African Journal of Geology*, **106**, 17-34.

WENDORFF. M. 2005. Sedimentary genesis and lithostratigraphy of Neoproterozoic megabreccia from Mufulira, Copperbelt of Zambia. *Journal of African Earth Sciences*, *In Press*.

WENTWORTH, C. M., BLAKE, JR, M. C., JONES, D. L, WALTER, A. W. & ZOBACK, M. D. 1984. Tectonic wedging associated with emplacement of the Franciscan assemblage, California Coast ranges. Field Trip Guidebook Pacific Section. *Society of Economic Paleontologists and Mineralogists*, **43**, 163-173.

WERDON, M. B. 1996. Drenchwater, Alaska- Zn-Pb-Ag mineralization in a mixed black shale-volcanic environment. *In*: COYNER, A. R. & FAHEY, P. L. (eds). Geology and ore deposits of the American Cordillera. *Geological Society of Nevada Symposium, Reno/Sparks, Nevada, April 1995, Symposium Proceedings*, **3**, 1341-1354.

WERDON, M. B. 1999. Geologic setting of Mississippian vein-breccias at the Kady Zn-Pb-Cu-Ag prospect: Plumbing system for a failed SEDEX deposit?. *In*: KELLEY, K. D. (ed). Geologic studies in Alaska by the U. S Geological Survey, 1997. *U. S. Geological Survey Professional Paper*, **1614**. 5-34.

WERDON, M. B., NEWBERRY, R. J., BURNS, L. E. & MULL, C. G. 1996. Probabilistic estimate of mineral resources in the Colville mining district, Alaska. *Alaska Division of Geological and Geophysical Surveys Report of Investigations*, **96-5**, 33pp.

WERDON M. B., LAYER, P. W. & NEWBERRY, R. J. 2004. $^{40}Ar/^{39}Ar$ dating of Zn-Pb-Ag mineralization in the northern Brooks Range, Alaska. *In*: KELLEY, K. D. & JENNINGS, S. (eds). A Special Issue devoted to barite and zinc-lead-silver deposits in the Red Dog district, western Brooks Range northern Alaska. *Economic Geology*, **99**, 1323-1343.

WHEELER, R. L. 1978. Cross-strike structural discontinuities: possible exploration tool in detached forelands. *Geological Society of America Abstracts with Programs*, **10**, 4, 201.

WHEELER, R. L. 1980. Cross-strike structural discontinuities: possible exploration tool for natural gas in the Appalachian over-thrust belt. *American Association of Petroleum Geologists Bulletin*, **64**, 2166-2178.

WHEELER, J. O. & MCFEELY, P. 1991. Tectonic assemblage map of the Canadian Cordillera and adjacent parts of the United States of America. *Geological Survey of Canada*, Map **1712A**, scale 1:2,000,000.

WILBUR, S. C., SIOK, J. P. & MULL, C. G. 1987. A comparison of two petrographic suites of the Okpikruak Formation: A point count Analysis. *In*: TAILLEUR, I. L. & WEIMER, P. (eds). Alaskan North Slope Geology. Bakersfield, California, Pacific Section, *Society of Economic Paleontologists and Mineralogists*, Book **50**, 441-448.

WILKERSON, M. S. 1992. Differential transport and continuity of thrust sheets. *Journal of Structural Geology*, **14**, 749-751.

WILKERSON, M. S., MARSHAK, S. & BOSWORTH, W. 1992. Computerized tomographic analysis of displacement trajectories and three-dimensional fold geometry above oblique thrust ramps. *Geology*, **20**, 439-442.

WILKERSON, M. S., APOTRIA, T. & FARID, T. 2002. Interpreting the geologic map expression of contractional fault-related fold terminations: lateral/oblique ramps versus displacement gradients. *Journal of Structural Geology*, **24**, 593-607.

WILKINSON, J. J., EYRE, S. L. & BOYCE, A. J. 2005. Ore-forming processes in Irish-type carbonate-hosted Zn-Pb deposits: evidence from mineralogy, chemistry, and isotopic composition of sulfides at the Lisheen mine. *Economic Geology*, **100**, 63–86.

WILLETT, S. D. 1992. Dynamic and kinematic growth and change of a Coulomb wedge. *In*: MCCLAY, K. R. (ed). Thrust Tectonics. *Chapman & Hall, London*, 19-32.

WILLETT, S. D., BEAUMONT, C. & FULLSACK, P. 1993. Mechanical model for the tectonics of doubly-vergent compressional orogens. *Geology*, **21**, 371-374.

WILLHOUSE, J. W. & COE, R. S. 1994. Paleomagnetic data from Alaska. *In*: PLAFKER, G. & BERG, H. C. (eds). The Geology of Alaska. Boulder, Colorado, Geological Society of America, The Geology of North America, v-G-1. 671-686, 797-812.

WILLIAMS, G. D. 1993. Tectonics and seismic sequence stratigraphy: an introduction. *In*: WILLIAMS, G. D. & DOBB, A. (eds.). Tectonics and seismic sequence stratigraphy. *Geological Society of London Special Publication*, **71**, 1-13.

WILSON, R. C. L., MANATSCHAL, G. & WISE, S. 2001. Rifting along non-volcanic passive margins: stratigraphic and seismic evidence from the Mesozoic successions of the Alps and western Iberia. *In*: WILSON, R. C. L., WHITMARSH, R. B., TAYLOR, B. & FROITZHEIM, N. Non-volcanic rifting of continental margins: a comparison of evidence from land and sea. *Geological Society of London Special Publication*, **187**, 429-452.

WIRTH, K. R. & BIRD, J. M. 1992. Chronology of ophiolite crystallization, detachment, and emplacement: Evidence from the Brooks Range, Alaska. *Geology*, **20**, 75-78.

WIRTH, K. R., BIRD, J. M., HARDING, D. J. & HEIZLER, M. T. 1993. Age and evolution of western Brooks Range ophiolites, Alaska-results from $^{40}Ar/^{39}Ar$ thermochronometry. *Tectonics*, **12**, 410-432.

WISSING, S. B. & PFIFFNER, O. A. 2003. Numerical models for the control of inherited basin geometries on structures and emplacement of the Klippen nappe (Swiss Prealps). *Journal of Structural Geology*, **25**, 1213-1227.

WISSINGER, E. S., LEVANDER, A. R., OLDOW, J. S., FUIS, G. S. & LUTTER, W. J. 1998. Seismic profiling constraints on the evolution of the central Brooks Range, Alaska. *In*: OLDOW, J. S. & AVE LALLEMANT, H. G. (eds). Architecture of the central Brooks Range fold and thrust belt, Arctic Alaska. *Geological Society of America Special Paper*, **324**, 269-291.

WITHJACK, M. O., SCHLISCHE, R. W. & OLSEN, P. E. 1998. Diachronous rifting, drifting, and inversion on the passive margin of central eastern North America: An analog for other passive margins. *American Association of Petroleum Geologists Bulletin*, **82**, 817-835.

WOLFENDEN, E., EBINGER, C., YIRGU, G., RENNE, P. & KELLEY, S. 2005. Evolution of a volcanic rifted margin: southern Red Sea, Ethiopia. *Geological Society of America Bulletin*, **117**, In Press.

WOODWARD, N. B. 1987. Geological applicability of critical-wedge thrust belt models. *Geological Society of America Bulletin*, **99**, 827-832.

WOODWARD, N. B., WALKER, K. R. & LUTZ, C. T. 1988. Relationships between early Paleozoic facies patterns and structural trends in the Saltville thrust family, Tenessee Valley and Ridge, southern Appalachians. *Geological Society of America Bulletin*, **100**, 1758-1769.

WOODWARD, N. B., BOYER, S. E. & SUPPE, J. 1989. Balanced geological cross-sections. *American Geophysical Union Short Course in Geology*, **6**, 132p.

WORRALL, D. M. 1991. Tectonic history of the Bering Sea and the evolution of Tertiary strike-slip basins of the Bering Shelf. *Geological Society of America Special Paper*, **257**, 120p.

WRIGHT HORTON JR., J. & RAST, N. 1989. Melanges and olistostromes in the U. S. Appalachians. *Geological Society of America Special Paper*, **228**, 276 p.

YOUNG, L. E. 1989. Geology and genesis of the Red Dog deposit. Western Brooks Range, Alaska. *Canadian Institute of Mining Bulletin*, **82**, 57-67.

YOUNG, L. E. 1992. The Wolverine Creek sequence-evidence for an allochthon below the Brooks Range allochthon, western Brooks Range, Alaska: State of Alaska, Department of Natural Resources, *Division of Geological and Geophysical surveys Report of Investigations*, **92-4**, 19p.

YOUNG, L. E. 2000. A guide to mapping and core logging for the Red Dog-Noatak Project region. *Cominco American Inc. Exploration Internal File. Unpublished*, 41p.

YOUNG, L. E. 2004. A geologic framework for mineralization in the western Brooks Range. *In*: KELLEY, K. D. & JENNINGS, S. (eds). A Special Issue devoted to barite and zinc-lead-silver deposits in the Red Dog district, western Brooks Range northern Alaska. *Economic Geology*, **99**, 1281-1306.

YOUNG, L. E. & MOORE, D. W. 1987. Geologic setting, petrology, and geochemistry of stratiform sphalerite-galena-barite deposits, Red Dog Creek and Drenchwater Creek areas- a discussion. *Economic Geology*, **82**, 1077-1079.

YOUNG, L. E., ST. GEORGE, P. & BOULEY, B. A. 1997. Porphyry copper deposits in relation to the magmatic history and palinspastic restoration of Alaska. *In*: GOLDFARB, R. J. & MILLER, L. D. (eds). Mineral deposits of Alaska. *Economic Geology Monograph*, **9**, 306-333.

ZHAO, W. L., DAVIS, D. M., DAHLEN, F. A. & SUPPE, J. 1986. Origin of convex accretionary wedges: evidence from Barbados. *Journal of Geophysical Research*, **91**, 10,246-10,258.

ZIEGLER, P. A. 1988. Laurussia—the Old Red Continent. *In*: MCMILLAN, N. J., EMBRY, A. F. & GLASS, D. J. (eds). Devonian of the world, Volume I. Regional syntheses. *Canadian Society of Petroleum Geologists Memoir*, **14**, 15-48.

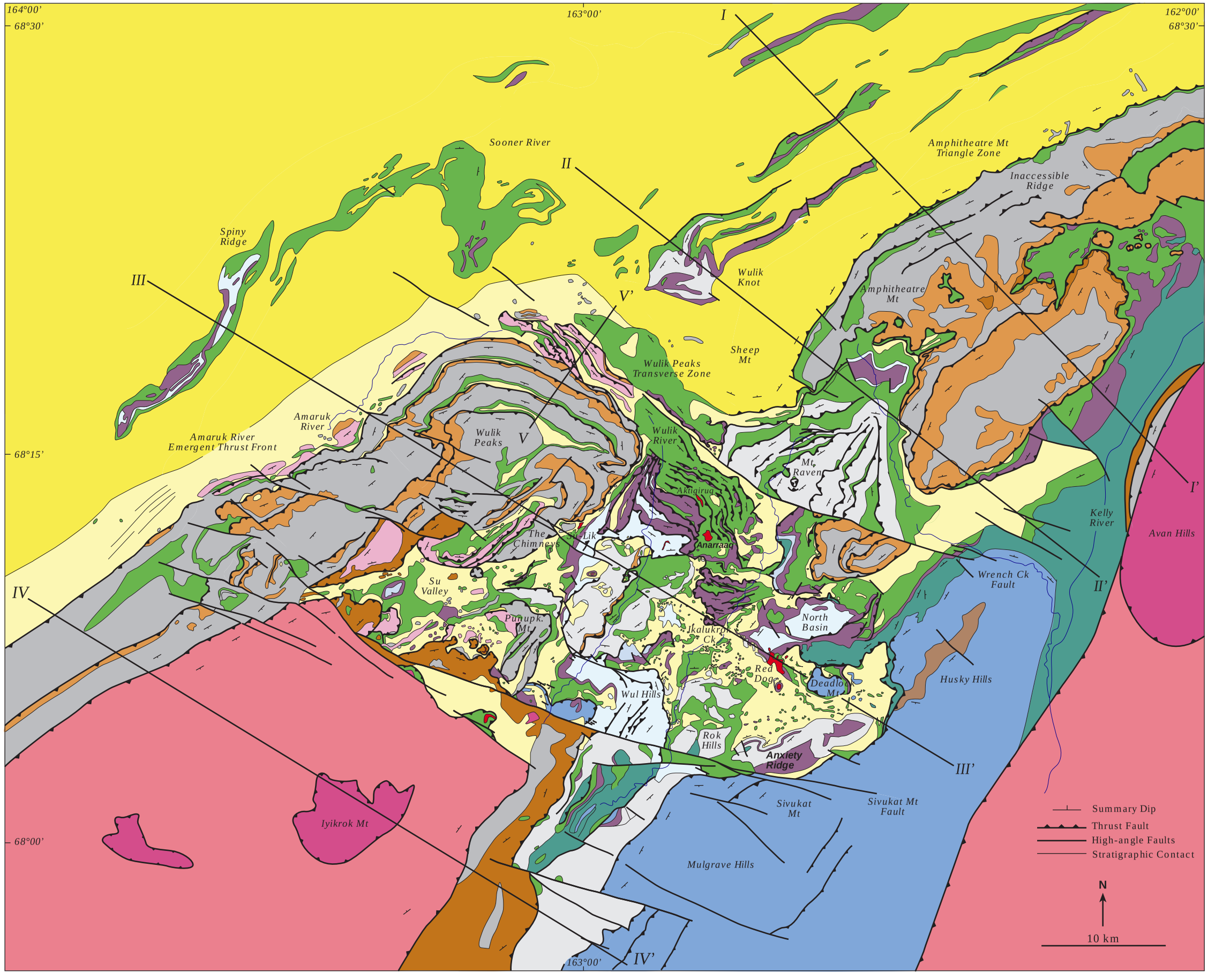
ZIEGLER, P. A., VAN WEES, J. D. & CLOETINGH, S. 1998. Mechanical controls on collision-related compressional intraplate deformation. *Tectonophysics*, **300**, 103-129.

ZWEIGEL, P. Arcuate accretionary wedge formation at convex plate margin corners: results of sandbox analogue experiments. *Journal of Structural Geology*, **20**, 1597-1609.

Appendix 1. Coordinates of station points in the east pit wall of the Red Dog mine. Coordinates are referred to Alaska State Plane, Zone 7 coordinate system used in The Red Dog mine operations.

Bench Level	*Station ID*	*East*	*North*	*Elevation (ft)*	*Elevation (m)*
950	JV 950-1	588303.838	143266.365	949.509	289.410
950	JV 950-2	588322.908	143564.698	951.264	289.945
950	JV 950-3	588331.744	143689.773	950.789	289.800
950	JV 950-4	588281.844	143985.048	950.862	289.823
950	JV 950-5	588233.142	144177.49	952.967	290.464
950	JV 950-6	588091.483	144350.855	951.222	289.932
975	JV 975-1	588392.379	143373.521	976.704	297.699
975	JV 975-2	588415.175	143673.083	975.199	297.241
975	JV 975-3	588348.102	143963.326	974.555	297.044
975	JV 975-4	588321.124	144057.445	977.429	297.920
975	JV 975-5	588380.946	144081.646	990.119	301.788
975	JV 975-6	588245.942	144347.944	975.657	297.380
975	JV 975-7	588118.159	144618.393	974.541	297.040
975	JV 975-8	588043.258	144781.88	974.784	297.114
1000	JV 1000-1	588576.658	143522.504	1002.281	305.495
1000	JV 1000-2	588542.899	143758.289	1001.047	305.119
1000	JV 1000-3	588419.406	144096.067	1001.358	305.214
1000	JV 1000-4	588290.108	144366.649	998.586	304.369
1000	JV 1000-5	588164.44	144638.991	1002.692	305.621
1025	JV 1025-1	588600.217	143772.378	1026.937	313.010
1025	JV 1025-2	588497.427	144053.197	1026.868	312.989
1025	JV 1025-3	588364.937	144322.053	1023.888	312.081
1025	JV 1025-4	588237.244	144593.378	1025.368	312.532
1025	JV 1025-5	588125.345	144830.817	1026.206	312.788
1050	JV 1050-1	588642.673	143791.599	1046.396	318.942
1050	JV 1050-2	588531.884	144069.786	1051.686	320.554
1050	JV 1050-3	588399.373	144337.124	1051.477	320.490
1050	JV 1050-4	588320.993	144476.105	1051.368	320.457

GEOLOGICAL MAP OF THE RED DOG DISTRICT (ENCLOSURE 1)



FORELAND BASIN STRATA
(Early Cretaceous)

- Undifferentiated Late Okpikruak and Fortress Mountain Formations (Early Cretaceous, Valangian-Albian)
- Early Okpikruak Formation (Olistostromal) (Early Cretaceous, Valangian)

ANGAYUCHAM TERRANE
(Middle Jurassic)

Misheguk Mountain Allochthon

- Undifferentiated serpentinites, peridotites and gabbros (Middle Jurassic)

ARCTIC ALASKA TERRANE
(Late Devonian - Late Jurassic)

- Undifferentiated Ipnavik Ridge, Nuka Ridge and Copter Peak allochthons (Late Dev.-Jurassic)

Kelly River Allochthon

- Etivluk Group (Penns.-Triassic)
- Kogruk Fm (Early Miss.-Penns.)
- Utukok Fm (Early Miss.)
- Kugururok Fm (Late Devonian)

Picnic Creek Allochthon

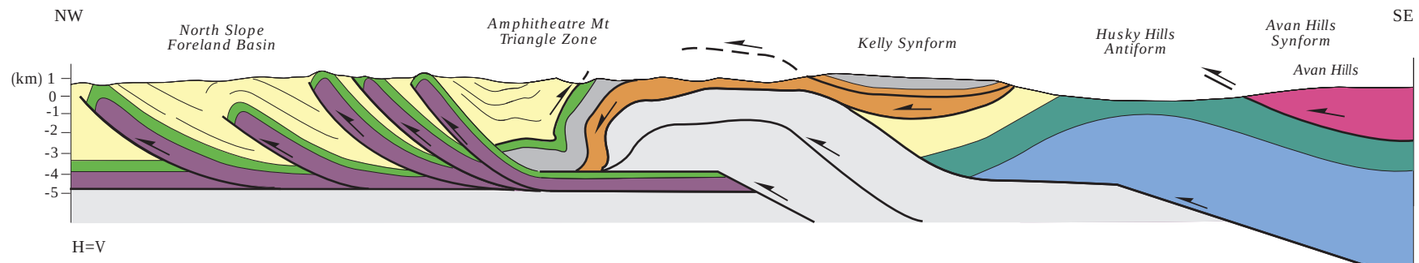
- Etivluk Group (Penns.-Triassic)
- Akmalik Chert (Early Miss.-Penns.)
- Utukok Fm (Early Miss.)
- Kugururok Fm (Late Devonian)

Endicott Mountains Allochthon

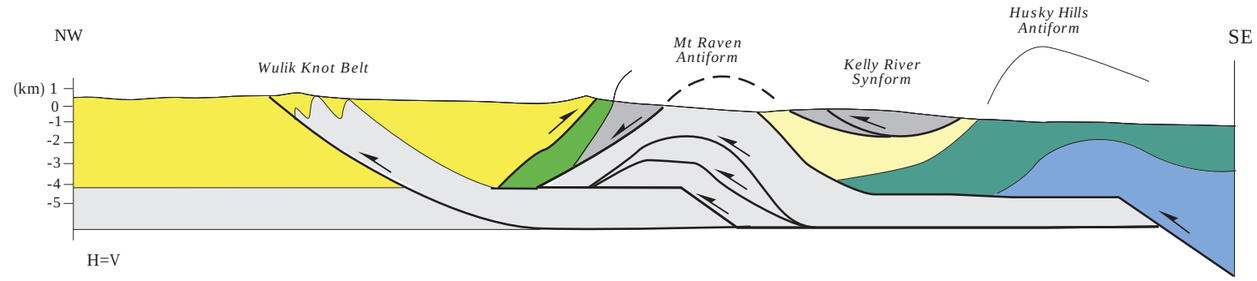
- Etivluk Group (Penns.-Triassic)
- Kuna Fm (Ikalukrok unit) (Early Mississippian)
- Kuna Fm (Kivalina unit) (Early Mississippian)
- Undivided Lisburne Group (Early Mississippian)
- Kayak Shale (Shale & Limestone unit) (Early Mississippian)
- Kayak Shale (Basal sandstone unit) (Early Mississippian)
- Undifferentiated Kanayut Conglomerate & Noatak Sandstone (Late Devonian)
- Hunt Fork Shale (Late Devonian)
- Sediment-hosted Zn-Pb-Ag and barite deposits

ENCLOSURE 2 - REGIONAL CROSS SECTIONS

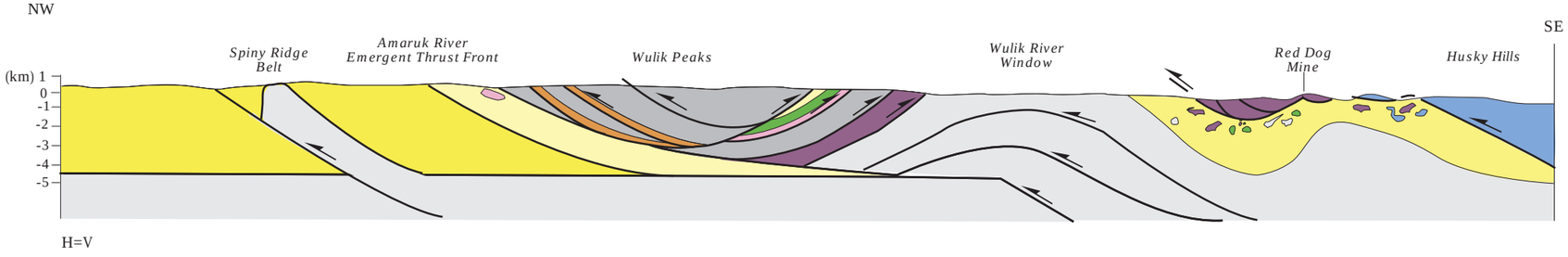
Cross Section I-I'



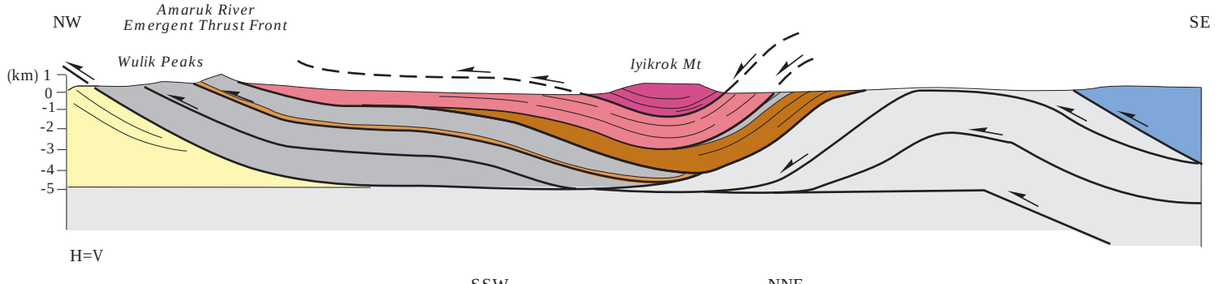
Cross Section II-II'



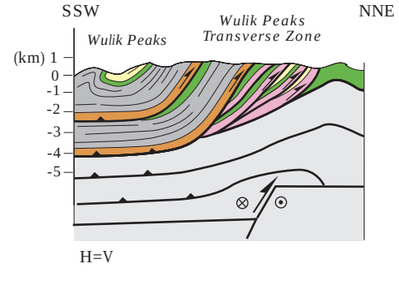
Cross Section III-III'



Cross Section IV-IV'



Cross Section V-V'



FORELAND BASIN STRATA (Early Cretaceous)

- Undifferentiated Late Okpikruak and Fortress Mountain Formations (Early Cretaceous, Valangian-Albian)
- Early Okpikruak Formation (Olistostromal) (Early Cretaceous, Valangian)

ANGAYUCHAM TERRANE (Middle Jurassic)

Misheguk Mountain Allochthon

- Undifferentiated serpentinites, peridotites and gabbros (Middle Jurassic)

ARCTIC ALASKA TERRANE (Late Devonian - Late Jurassic)

- Undifferentiated Ipnavik Ridge, Nuka Ridge and Copter Peak allochthons (Late Dev.-Jurassic)

Kelly River Allochthon

- Etivluk Group (Penns.-Triassic)
- Kogruk Fm (Early Miss.-Penns.)
- Utukok Fm (Early Miss.)

Picnic Creek Allochthon

- Etivluk Group (Penns.-Triassic)
- Akmalik Chert (Early Miss.-Penns.)

Endicott Mountains Allochthon

- Etivluk Group (Penns.-Triassic)
- Kuna Fm (Ikalukrok unit) (Early Mississippian)
- Kayak Shale (Basal sandstone unit) (Early Mississippian)
- Undifferentiated Kanayut Conglomerate & Noatak Sandstone (Late Devonian)
- Undifferentiated Lisburne Group

ENCLOSURE 3 Bench Sections Red Dog Mine East Pit

